THE JOURNAL OF PHYSICAL CHEMISTRY

VOLUME 67, NUMBER 11 NOVEMBER, 1963

NOTES

COMMUNICATIONS TO THE EDITOR

Note Editor's new address on page 1A

Statement required by the act of October 23, 1962; Section 4369, Title 39 United States Code, showing the ownership, management, and circulation of *The Journal of Physical Chemistry*, published monthly at 20th and Northampton Sts., Easton, Pa. 18043, for Volume 67, Number 11 (November), 1963.

1. The names and addresses of the publisher, editor, and managing editor are: *Publisher:* American Chemical Society, 1155 16th St., N.W., Washington, D. C. 20036; *Editor:* W. Albert Noyes, Jr., 1155 16th St., N.W., Washington, D. C. 20036; *Managing Editor:* None.

2. The owner is: American Chemical Society, 1155 16th St., N.W., Washington, D. C. 20036.

3. The known bondholders, mortgagees, and other security holders owning or holding 1 per cent or more of total amount of bonds, mortgages, or other securities are: None.

4. The average number of copies of each issue of this publication sold or distributed, through the mails or otherwise, to paid subscribers during the twelve months preceding the date shown above was: 5,371.

I certify that the above statements made by me are correct and complete.

Richard H. Belknap,
for the Publisher

AUTHOR INDEX

No. 29 in the ADVANCES IN CHEMISTRY SERIES

PHYSICAL PROPERTIES OF CHEMICAL COMPOUNDS—III

This handbook of basic data contains 456 full-page tables on 434 aliphatic compounds and 22 miscellaneous compounds and elements—all carefully worked out by R. R. Dreisbach of The Dow Chemical Co.

It is a sequel to **PHYSICAL PROPERTIES—II** (Advances No. 22), which covers 476 organic straight-chain compounds, and **PHYSICAL PROPERTIES—I** (Advances No. 15), which presents data on 511 organic cyclic compounds.

This series provides you with a breadth of data that you can get in no other way. For each compound 15 physical properties are given: purity—freezing point—vapor pressure—liquid density—vapor density—refractive index—rate of change of boiling point with pressure—latent heat of fusion—latent heat of evaporation—critical values—compressibility—viscosity—heat content—surface tension—solubility. Parameters are also furnished for interpolating and extrapolating determined data for almost all the compounds. To get this information by ordinary means you would have to seek out many sources.

PHYSICAL PROPERTIES—III offers the extra advantage of a cumulative index to **all three volumes** (1443 compounds and elements). Use it and the earlier compilations to save yourself hours of laboratory time, and to answer questions quickly.

489 pages. Cloth bound. Price: $6.50

PHYSICAL PROPERTIES—II — 491 pages • cloth bound • price: $6.50
PHYSICAL PROPERTIES—I — 536 pages • cloth bound • price: $5.85

Order from:

Special Issues Sales/American Chemical Society/1155 Sixteenth Street, N.W./Washington 6, D.C.

THE JOURNAL OF
PHYSICAL CHEMISTRY

(Registered in U. S. Patent Office) (© Copyright, 1963, by the American Chemical Society)

VOLUME 67, NUMBER 11 NOVEMBER 15, 1963

HEAT CAPACITIES FROM 11 TO 305°K. AND ENTROPIES OF L-ARGININE·HCl, L-HISTIDINE·HCl, AND L-LYSINE·HCl[1]

BY ARTHUR G. COLE, JOHN O. HUTCHENS, AND J. W. STOUT

Departments of Chemistry and Physiology and the Institute for Study of Metals, University of Chicago, Chicago, Illinois

Received July 1, 1963

Heat capacities have been measured from 11 to 305°K. for L-arginine·HCl, L-histidine·HCl, and L-lysine·HCl. Values of $C_p°$, $S°$, $(H° - H_0°)/T$, and $-(F° - H_0°)/T$ are tabulated as a function of temperature from 10 to 310°K. The entropies ($S°_{298.15}$ in cal. deg.$^{-1}$ mole^{-1}) are 68.43 for L-arginine·HCl, 65.99 for L-histidine·HCl, and 63.21 for L-lysine·HCl.

The residues of three α-amino acids, each having a second basic group, occur naturally as constituents of proteins. While these are quantitatively most important in the basic proteins of cell nuclei, they are also a part of the structure of cytoplasmic proteins. Of these basic amino acids, only arginine has been studied previously from the standpoint of its thermal properties. Huffman, Fox, and Ellis[2] measured the heat of combustion of D-arginine, while Huffman and Ellis[3] measured its heat capacities from 90 to 298°K. We present here our data concerning the heat capacities from 11 to 305°K. for L-arginine·HCl, L-histidine·HCl, and L-lysine·HCl. Unfortunately, none of these substances have been burned to obtain an enthalpy of combustion.

Experimental

Amino Acids.—The three amino acid monohydrochlorides were provided by the late J. P. Greenstein of the National Institutes of Health. All three met the chromatographic criteria of purity and enzymatic tests for absence of the D-isomer previously described.[4] They were crystalline, as evidenced by microscopic examination in polarized light. Each was dried to constant weight *in vacuo* ($<10^{-6}$ mm.) in a system trapped with liquid nitrogen. No abnormal values of heat capacity were observed in the neighborhood of the ice point.

Experimental Methods and Calculations.—The methods for measuring heat capacities have been described in detail.[5] The calorimeter used was the one with six radial fins, and the thermometer was the one bearing the laboratory designation "H." Sample weights *in vacuo* were 81.008 g. for L-arginine·HCl, 68.656 g. for L-histidine.HCl, and 65.611 g. for L-lysine·HCl. In each case, the heat capacity of the empty calorimeter represented approximately 40% of the total heat capacity over most of the temperature range employed.

Results

The experimentally measured quantities ($\Delta H/\Delta T$) are listed in Table I for L-arginine·HCl in the chronological order in which they were obtained. From these, the thermal history of the amino acid can be deduced. Where ΔT for an individual experiment is not obvious from Table I, the limits previously described[4] apply. Equivalent data are given in Table II for L-histidine·HCl and in Table III for L-lysine·HCl. Calculations of curvature corrections for individual measurements below 50°K. indicated that none were

TABLE I

HEAT CAPACITY OF L-ARGININE·HCl IN CAL. DEG.$^{-1}$ MOLE^{-1}

[0°C. = 273.15°K.; mol. wt. $C_6H_{15}O_2N_4Cl$ = 210.68]

T, °K.	$\Delta H/\Delta T$	T, °K.	$\Delta H/\Delta T$	T, °K.	$\Delta H/\Delta T$
298.76	62.70	46.34	12.60	198.90	45.44
297.67	62.31	50.71	14.15	204.97	46.44
53.00	14.93	79.80	22.72	210.98	47.51
58.89	16.86	84.31	23.94	217.35	48.55
64.11	18.49	89.30	25.11	220.68	49.09
69.77	20.12	94.76	26.31	226.75	50.18
75.29	21.56	100.26	27.44	232.73	51.22
80.67	22.99	105.78	28.60	234.96	51.57
10.91	0.716	111.24	29.72	240.53	52.47
11.94	0.879	115.91	30.63	246.54	53.57
13.01	1.101	121.60	31.72	252.53	54.50
14.19	1.358	127.18	32.75	258.88	55.68
16.04	1.809	132.97	33.88	265.41	56.78
17.72	2.266	138.65	34.94	271.60	57.93
19.58	2.800	144.14	35.92	278.32	59.06
21.41	3.368	149.82	36.92	284.45	60.07
23.48	4.066	158.03	38.39	290.66	61.12
25.94	4.932	163.58	39.36	297.32	62.26
28.81	5.988	169.47	40.39	304.16	63.36
31.92	7.164	175.36	41.46	270.15	57.40
35.11	8.395	181.42	42.46	276.17	58.33
38.52	9.691	187.58	43.48	284.45	60.35
42.27	11.09	193.03	44.47	291.69	61.61

(1) The heat capacity studies reported here were entirely supported by the U. S. Atomic Energy Commission. Ancillary studies were supported by a grant from the National Institutes of Health and by the Wallace A. and Clara M. Abbott Memorial Fund of the University of Chicago. Support of the cryogenic facilities by the National Science Foundation is gratefully acknowledged.

(2) H. M. Huffman, S. W. Fox, and E. L. Ellis, *J. Am. Chem. Soc.*, **59**, 2144 (1937).

(3) H. M. Huffman and E. L. Ellis, *ibid.*, **59**, 2150 (1937).

(4) J. O. Hutchens, A. G. Cole, and J. W. Stout, *ibid.*, **82**, 4813 (1960).

(5) A. G. Cole, J. O. Hutchens, R. A. Robie, and J. W. Stout, *ibid.*, **82**, 4807 (1960).

TABLE II

HEAT CAPACITY OF L-HISTIDINE·HCl IN CAL. DEG.$^{-1}$ MOLE^{-1}

[0°C. = 273.15°K.; mol. wt. $C_6H_{10}O_2N_3Cl$ = 191.63]

T, °K.	$\Delta H/\Delta T$	T, °K.	$\Delta H/\Delta T$	T, °K.	$\Delta H/\Delta T$
301.66	60.95	169.79	38.62	11.39	0.615
57.85	16.37	175.56	39.59	12.39	0.778
63.17	17.94	181.39	40.51	13.61	1.031
68.66	19.44	186.87	41.30	15.01	1.361
74.34	20.86	192.77	42.32	16.54	1.783
79.50	22.13	198.76	43.26	18.22	2.286
84.26	23.29	204.60	44.24	20.17	2.907
89.54	24.48	210.24	45.13	22.38	3.667
94.67	25.49	220.93	46.90	24.78	4.498
100.03	26.54	226.90	47.83	27.22	5.451
105.55	27.59	233.12	48.75	29.87	6.477
111.17	28.66	239.37	49.82	32.85	7.637
116.88	29.70	245.78	51.07	36.25	8.938
120.85	30.39	251.42	51.76	40.08	10.38
126.52	31.36	258.10	52.93	44.31	11.91
132.14	32.39	264.72	54.14	48.90	13.53
137.74	33.34	271.13	55.21	54.09	15.20
143.34	34.23	277.70	56.17	267.25	54.25
148.89	35.17	284.24	57.27	272.70	55.34
152.92	35.83	290.99	58.37	279.44	56.33
158.60	37.01	297.86	59.68	285.97	57.53
164.14	37.68	305.29	60.69		

TABLE III

HEAT CAPACITY OF L-LYSINE·HCl IN CAL. DEG.$^{-1}$ MOLE^{-1}

[0°C. = 273.15°K.; mol. wt. $C_6H_{16}O_2N_2Cl$ = 182.66]

T, °K.	$\Delta H/\Delta T$	T, °K.	$\Delta H/\Delta T$	T, °K.	$\Delta H/\Delta T$
299.68	57.50	163.74	36.31	298.32	57.08
51.56	13.36	166.84	36.76	305.14	58.41
56.28	14.76	172.57	37.63	10.82	0.729
61.70	16.34	178.38	38.52	11.72	0.875
67.00	17.78	183.94	39.32	12.76	1.076
72.14	19.08	189.50	40.10	13.93	1.332
76.92	20.26	195.11	40.94	15.25	1.637
81.27	21.36	200.97	41.78	16.71	2.008
85.66	22.44	204.87	42.32	18.48	2.486
90.71	23.53	210.48	43.20	20.39	3.036
95.88	24.56	216.29	44.02	22.53	3.699
101.20	25.65	223.09	45.06	24.90	4.467
106.60	26.71	229.67	46.42	27.36	5.286
112.04	27.76	235.30	46.89	30.02	6.196
117.51	28.78	241.12	47.80	33.07	7.254
119.05	29.04	244.52	48.29	36.54	8.436
124.52	30.00	250.23	49.33	40.42	9.719
130.03	30.92	256.07	50.23	44.46	11.04
135.41	31.85	262.03	51.07	48.65	12.38
141.05	32.76	268.08	52.09	265.42	51.63
146.66	33.65	274.02	53.02	270.53	52.49
152.16	34.52	280.04	53.98	276.49	53.84
157.92	35.41	286.05	55.00	284.13	54.65
		291.95	56.00		

required within the limits of accuracy claimed. The values of $\Delta H/\Delta T$ are therefore equal to C_p at the stated temperatures.

The thermodynamic properties of L-arginine·HCl, derived from the data of Table I, are given in Table IV. Equivalent data for L-histidine·HCl and L-lysine·HCl are presented in Tables V and VI, respectively. The ice point was taken as 273.15°K. and 1 cal. = 4.1840 absolute joules.

From the values of $S°_{298.15}$ given in Tables IV–VI and the entropies of the elements,[6] we have calculated

(6) National Bureau of Standards Circular 500, "Selected Values of Chemical Thermodynamic Properties," U. S. Government Printing Office, Washington, D. C., 1952.

TABLE IV

THERMODYNAMIC PROPERTIES OF L-ARGININE·HCl IN CAL. DEG.$^{-1}$ MOLE^{-1}

T, °K.	$C_p°$	$S°$	$\frac{H° - H_0°}{T}$	$\frac{-(F° - H_0°)}{T}$
10	0.556	0.202	0.149	0.053
15	1.549	0.598	0.436	.162
20	2.928	1.226	0.880	.345
25	4.592	2.053	1.452	.601
30	6.432	3.052	2.128	.924
35	8.344	4.186	2.879	1.308
40	10.26	5.426	3.682	1.744
45	12.12	6.742	4.517	2.226
50	13.90	8.112	5.366	2.746
55	15.60	9.517	6.220	3.297
60	17.22	10.94	7.069	3.875
70	20.18	13.83	8.735	5.090
80	22.82	16.70	10.33	6.362
90	25.22	19.52	11.86	7.668
100	27.41	22.30	13.30	8.992
110	29.46	25.01	14.68	10.33
120	31.42	27.65	15.99	11.66
130	33.31	30.24	17.25	12.99
140	35.17	32.78	18.47	14.31
150	36.98	35.27	19.64	15.63
160	38.74	37.71	20.78	16.93
170	40.49	40.11	21.89	18.22
180	42.22	42.47	22.97	19.51
190	43.92	44.80	24.03	20.78
200	45.62	47.10	25.06	22.04
210	47.30	49.36	26.08	23.28
220	49.02	51.60	27.09	24.52
230	50.72	53.82	28.08	25.74
240	52.43	56.02	29.06	26.96
250	54.14	58.19	30.02	28.17
260	55.86	60.35	30.98	29.36
270	57.60	62.49	31.94	30.55
280	59.32	64.61	32.89	31.73
290	61.01	66.72	33.83	32.90
300	62.68	68.82	34.76	34.06
310	64.33	70.90	35.69	35.22
273.15	58.14	63.16	32.24	30.92
298.15	62.37	68.43	34.59	33.84
310.15	64.36	70.93	35.70	35.23

the entropies of formation of these compounds. They are ($\Delta S_f°_{298.15}$ in cal. mole^{-1} deg.$^{-1}$): −341.01 for L-arginine·HCl, −242.54 for L-histidine·HCl, and −300.46 for L-lysine·HCl.

Discussion

Huffman and Ellis[3] reported $S°_{298.1}$ for D-arginine to be 59.9 cal. mole^{-1} deg.$^{-1}$, or 8.5 cal. mole^{-1} deg.$^{-1}$ less than the value of $S°_{298.15}$ reported here for L-arginine·HCl. Strictly comparable data for hydrochlorides of other substances are lacking. In the following two cases, unfortunately, all available amino groups are converted to the hydrochloride, whereas in the case of L-arginine·HCl only one of the two basic groups is neutralized, leaving a zwitterionic substance with the consequent ability for strong ionic binding in the crystal. For glutamic acid, Huffman and Borsook[7] give $S°_{298.1}$ a value of 45.7 cal. mole^{-1} deg.$^{-1}$, while in this laboratory it was found to be 44.98 cal. mole^{-1} deg.$^{-1}$.[8] Huffman, Ellis, and Borsook[9] re-

(7) H. M. Huffman and H. Borsook, *J. Am. Chem. Soc.*, **54**, 4297 (1932).

(8) J. O. Hutchens, A. G. Cole, R. A. Robie, and J. W. Stout, *J. Biol. Chem.*, in press.

(9) H. M. Huffman, E. L. Ellis, and H. Borsook, *J. Am. Chem. Soc.*, **62**, 297 (1940).

TABLE V

THERMODYNAMIC PROPERTIES OF L-HISTIDINE·HCl IN CAL. DEG.$^{-1}$ MOLE^{-1}

T, °K.	$C_p°$	$S°$	$\frac{H° - H_0°}{T}$	$\frac{-(F° - H_0°)}{T}$
10	0.409	0.136	0.102	0.034
15	1.360	0.458	.343	.115
20	2.851	1.046	.777	.269
25	4.621	1.869	1.366	.503
30	6.522	2.879	2.066	.813
35	8.455	4.030	2.841	1.189
40	10.34	5.283	3.661	1.621
45	12.16	6.606	4.505	2.101
50	13.89	7.977	5.357	2.620
55	15.49	9.377	6.207	3.170
60	17.01	10.79	7.045	3.747
70	19.79	13.63	8.671	4.956
80	22.28	16.44	10.22	6.216
90	24.53	19.19	11.69	7.505
100	26.55	21.88	13.07	8.808
110	28.45	24.50	14.39	10.12
120	30.25	27.06	15.63	11.42
130	31.99	29.55	16.82	12.72
140	33.69	31.98	17.97	14.01
150	35.35	34.36	19.07	15.29
160	37.00	36.69	20.14	16.55
170	38.63	38.99	21.18	17.80
180	40.24	41.24	22.19	19.04
190	41.86	43.46	23.19	20.27
200	43.48	45.65	24.16	21.48
210	45.09	47.81	25.12	22.69
220	46.70	49.94	26.06	23.88
230	48.31	52.05	27.00	25.06
240	49.93	54.14	27.92	26.22
250	51.58	56.21	28.83	27.38
260	53.25	58.27	29.74	28.53
270	54.94	60.31	30.64	29.67
280	56.62	62.34	31.54	30.80
290	58.29	64.36	32.43	31.92
300	59.94	66.36	33.32	33.04
310	61.58	68.35	34.21	34.14
273.15	55.47	60.94	30.92	30.03
298.15	59.64	65.99	33.16	32.83
310.15	61.60	68.38	34.22	34.16

TABLE VI

THERMODYNAMIC PROPERTIES OF L-LYSINE·HCl IN CAL. DEG.$^{-1}$ MOLE^{-1}

T, °K.	$C_p°$	$S°$	$\frac{H° - H_0°}{T}$	$\frac{-(F° - H_0°)}{T}$
10	0.588	0.224	0.163	0.061
15	1.576	.633	.456	.177
20	2.922	1.264	.899	.366
25	4.497	2.082	1.458	.624
30	6.187	3.051	2.104	.946
35	7.905	4.134	2.810	1.323
40	9.587	5.300	3.553	1.747
45	11.22	6.524	4.315	2.209
50	12.82	7.789	5.086	2.704
55	14.37	9.084	5.860	3.225
60	15.85	10.40	6.631	3.768
70	18.57	13.05	8.146	4.904
80	21.06	15.69	9.606	6.088
90	23.36	18.31	11.01	7.301
100	25.42	20.88	12.35	8.530
110	27.36	23.39	13.63	9.768
120	29.21	25.85	14.85	11.01
130	30.96	28.26	16.02	12.24
140	32.60	30.62	17.15	13.47
150	34.19	32.92	18.23	14.69
160	35.75	35.18	19.28	15.90
170	37.27	37.39	20.29	17.10
180	38.74	39.56	21.27	18.29
190	40.19	41.69	22.23	19.46
200	41.65	43.79	23.17	20.63
210	43.12	45.86	24.08	21.78
220	44.60	47.90	24.98	22.92
230	46.11	49.92	25.86	24.05
240	47.64	51.91	26.74	25.17
250	49.19	53.89	27.61	26.28
260	50.77	55.85	28.47	27.38
270	52.38	57.79	29.32	28.47
280	54.00	59.73	30.18	29.55
290	55.68	61.65	31.03	30.62
300	57.42	63.57	31.88	31.69
310	59.24	65.48	32.73	32.75
273.15	52.88	58.40	29.59	28.81
298.15	57.10	63.21	31.72	31.49
310.15	59.27	65.51	32.74	32.76

ported $S°_{298.1}$ for glutamic acid·HCl to be 59.33, which is approximately 14 cal. mole^{-1} deg.$^{-1}$ greater than that of the parent amino acid. Huffman and Fox[10] found $S°_{298.1}$ to be 46.2 cal. mole^{-1} deg.$^{-1}$ for DL-ornithine; Huffman, Ellis, and Borsook[9] reported a value of 70.25 cal. mole^{-1} deg.$^{-1}$ for ornithine dihydrochloride. The difference is about 12 cal. mole^{-1} deg.$^{-1}$ per molecule of HCl.

Since the formation of a hydrochloride produces such different effects on the entropies of these three substances, it would appear that the estimates of other thermal properties, such as the heat of combustion of the hydrochlorides from data for the parent compounds, might be subject to large errors. Consequently, although Huffman, Fox, and Ellis[2] reported the heat of combustion of D-arginine, we have not felt sufficiently confident of the correction to be made for the addition of an HCl molecule to calculate a value for the enthalpy of formation of L-arginine·HCl. No enthalpy values are available for lysine or histidine, nor are there any previous reports of heat capacities for these substances.

(10) H. M. Huffman and S. Fox, *J. Am. Chem. Soc.*, **62**, 3464 (1940).

HEAT CAPACITY FROM 11 TO 300°K., ENTROPY, AND HEAT OF FORMATION OF DOLOMITE

BY J. W. STOUT AND RICHARD A. ROBIE

Institute for the Study of Metals, and Departments of Chemistry and Geology, University of Chicago, Chicago 37, Illinois

Received July 1, 1963

The heat capacity of dolomite, $CaMg(CO_3)_2$, has been measured over the temperature range from 11 to 300°K. Smoothed values of the heat capacity, entropy, enthalpy, and free energy are tabulated. At 298.15°K. the values of thermodynamic functions are $C_p^\circ = 37.65 \pm 0.10$ cal. deg.$^{-1}$ mole, $S^\circ = 37.09 \pm 0.10$ cal. deg.$^{-1}$ mole^{-1}, $H^\circ - H_0^\circ = 6210 \pm 16$ cal. mole^{-1}. From the high temperature dissociation equilibrium data of Graf and Goldsmith and the entropies of dolomite, $CaCO_3$ (calcite), and $MgCO_3$ (magnesite), $\Delta H^\circ_{298} = 2.94$ kcal. and $\Delta F^\circ_{298} = 2.70$ kcal. for the reaction $CaMg(CO_3)_2 = CaCO_3 + MgCO_3$.

Dolomite, of ideal composition $CaMg(CO_3)_2$, is a naturally occurring mineral of geological interest. It is also of considerable chemical interest as an example of an ordered compound of $CaCO_3$ and $MgCO_3$. The rate of formation of the thermodynamically stable dolomite from calcite and magnesite at temperatures below 300° is very slow,[1] even when the solids are in contact with water and CO_2, and the free energy change in this reaction at 298.15°K. is best determined from a knowledge of the enthalpy and entropy changes. In this paper we present the results of low-temperature heat capacity measurements from which the entropy of dolomite is calculated. By use of the heat capacity and entropy results and the data of Graf and Goldsmith[2] on the dissociation equilibrium in the dolomite–calcite system we obtain values for the heat and free energy of formation of dolomite from calcite and magnesite at 298.15°K.

Experimental

Apparatus.—The cryostat, calorimeter, and platinum resistance thermometer–heater used for the heat capacity measurements have been described[3] previously. The gold-plated copper calorimeter was without fins. Its internal volume was 151 cm.^{3} and its weight, including the resistance thermometer–heater, was 84.07 g. The resistance of the platinum thermometer–heater was 127.734 ohms at 273.15°K. and 0.1122 ohms at 10°K. The resistance of the thermometer–heater was measured at the triple-point temperature of water four times during the series of measurements described in this and the following paper.[4] The first two measurements were before and after the calibration of the thermometer–heater against a platinum thermometer which had been calibrated by the Bureau of Standards. The third measurement of the triple-point resistance was after completion of heat capacity measurements of the empty calorimeter and of talc, and the fourth after the completion of the heat capacity measurements of tremolite and dolomite. The extreme variation found in the triple-point resistance was 0.004 ohms, which corresponds to 0.008°K.

Dolomite Sample.—Because of the difficulty[1] of synthesizing crystalline dolomite in the quantity required for heat capacity measurements, a naturally occurring sample was used. The sample was crystals from Binnental, Switzerland, which were between 0.5 and 3 cm. in diameter. Each individual crystal was washed with water using a stiff toothbrush. The growth surfaces were cleaved off with a razor blade and discarded. The remaining material was in the form of glass-clear crystals ranging in size from 0.1 to 2 cm. This material was washed in boiling distilled water three times and then dried at 100°. The crystals were crushed in a porcelain mortar and the fraction passing a 10-mesh screen and not passing a 70-mesh screen was selected. This fraction was examined under an eight power binocular microscope and visible foreign material removed. A random sample of the material so obtained, which was used for the heat capacity measurements, was taken for chemical, microscopic, and X-ray analysis. Microscopic analysis with a petrographic microscope revealed no extraneous phases. The X-ray powder picture gave sharp lines characteristic of dolomite with no measureable difference in spacing from the most stoichiometric natural dolomite investigated by Graf and Goldsmith.[2]

The sample was analyzed chemically for calcium by precipitation of CaC_2O_4 and for magnesium by weighing $Mg_2P_2O_7$. CO_2 was determined by dissolving the dolomite crystals in standardized dilute aqueous HCl in a closed CO_2-free system, driving off the CO_2, and back titrating the unused acid with aqueous NaOH. Bureau of Standards samples of dolomite and of Na_2CO_3 were used to calibrate the analytical procedures. There was no undissolved residue when the sample was treated with aqueous HCl. Analyses for MnO, FeO, and SrO were made by spectrochemical analysis. The results of the analyses, in weight % of the various oxides, were: CaO, 30.77; MgO, 21.54; CO_2, 47.38; MnO, 0.10; FeO, 0.008; SrO, 0.017; total, 99.82. The analysis calculated for the formula $CaMg(CO_3)_2$ is: CaO, 30.41; MgO, 21.86; CO_2, 47.73.

The sample of dolomite used for the heat capacity measurements weighed 188.60 g. *in vacuo*.

Experimental Results

The experimentally measured values of heat capacity, $\Delta H/\Delta T$, corresponding to 184.42 g. [the formula weight of $CaMg(CO_3)_2$] of the dolomite sample, are listed in Table I. The measurements are listed in chronological order. The temperature T_{av} listed in Table I is the arithmetic mean of the initial and final temperatures of a measurement. The temperature rise in an individual measurement may be inferred from the temperature interval between successive measurements. No hysteresis or dependence of the heat capacity on thermal history was observed. The defined calorie, equal to 4.1840 joules, is used. The ice-point temperature is taken as 273.15°K. Certain values marked in Table I are "bad vacuum runs" taken to evaluate a correction[3] for temperature gradients within the calorimetric system and are of lower accuracy than the remaining points, whose accuracy has been previously discussed.[3]

Discussion

Thermodynamic Properties of $CaMg(CO_3)_2$.—In order to calculate the heat capacity and other thermodynamic properties of ideal dolomite it is necessary to make correction for the deviations from ideal stoichiometry in the sample actually measured. From the analysis given in the Experimental section one calculates that the sample measured may be represented by the empirical formula: $CaMg(CO_3)_2 + 0.0427CaCO_3 + 0.0027MnCO_3 + 0.0003SrCO_3 + 0.0002FeCO_3 + 0.0151Mg(OH)_2$. We have assumed that the excess magnesium oxide is present as brucite, $Mg(OH)_2$,

(1) D. L. Graf and J. R. Goldsmith, *J. Geol.*, **64**, 173 (1956).

(2) D. L. Graf and J. R. Goldsmith, *Geochim. Cosmochim. Acta*, **7**, 109 (1955).

(3) A. G. Cole, J. O. Hutchens, R. A. Robie, and J. W. Stout, *J. Am. Chem. Soc.*, **82**, 4807 (1960).

(4) R. A. Robie and J. W. Stout, *J. Phys. Chem.*, **67**, 2252 (1963).

TABLE I

HEAT CAPACITY, IN CAL. DEG.$^{-1}$, OF 184.42 G. OF DOLOMITE FROM BINNENTAL, SWITZERLAND

(0°C. = 273.15 °K.)

T_{av}, °K.	$\Delta H/\Delta T$	T_{av}, °K.	$\Delta H/\Delta T$	T_{av}, °K.	$\Delta H/\Delta T$
301.10	37.85	175.83	26.97	16.74	0.1441[a]
		181.53	27.61	18.90	0.2232
52.68	5.110	187.19	28.22	20.49	0.2998
57.37	6.133	193.00	28.84	22.51	0.4211
62.69	7.326	198.77	29.41	24.78	0.5910
67.95	8.519	204.37	29.98	27.51	0.8426
73.03	9.656	210.13	30.54	30.47	1.173
78.10	10.805	216.00	31.11	37.05	2.112
82.99	11.93	222.00	31.64	40.99	2.782
87.64	12.94	227.74	32.14	45.34	3.596
92.93	14.05	233.60	32.63	50.03	4.550
98.50	15.16	244.85	33.66		
103.96	16.23	250.55	34.11	33.75	1.607
109.21	17.22	256.44	34.60	17.69	0.1764
114.52	18.19	262.61	35.06		
120.04	19.14	268.60	35.57	238.31	33.07
125.41	20.06	274.46	36.01		
130.95	20.95	280.38	36.44	251.17	34.13[b]
136.56	21.83	286.44	36.89	257.01	34.64[b]
142.23	22.86	292.15	37.28	262.31	34.99[b]
147.89	23.47	297.89	37.70	268.88	35.55[b]
153.49	24.22			276.51	36.15[b]
159.12	24.95	11.64	0.0444	282.43	36.62[b]
164.66	25.66	13.10	0.0638	288.66	37.06[b]
170.20	26.31	15.00	0.0980		

[a] Point unreliable because of switch failure. [b] "Bad vacuum runs."

rather than as MgO. This assumption is reasonable from a geological point of view. Furthermore, the assumed presence of 0.14 wt. % of firmly bound water in the sample, together with the substances found by analysis, accounts for 99.96% by weight of the sample. Accordingly we converted the measured heat capacities to a basis of 189.95 g., the weight corresponding to the empirical formula given, and subtracted the heat capacity of 0.0151 $Mg(OH)_2$ given by the data of Giauque and Archibald.[5] This is equivalent to the assumption that $Mg(OH)_2$ is present as a separate phase.

From the microscopic and X-ray evidence it is probable that the $CaCO_3$, $MnCO_3$, $SrCO_3$, and $FeCO_3$ given in the empirical formula are present in solid solution in the dolomite phase. The low temperature heat capacity of $CaCO_3$ (calcite) has been measured by Anderson[6] between 57°K. and room temperature, and by Simon and Swain[7] from 15 to 80°K. Anderson[8] has also reported heat capacity measurements between 55°K. and room temperature of $MgCO_3$ (magnesite), $MnCO_3$, $SrCO_3$, and $FeCO_3$. Above 70°K. the heat capacity of dolomite is equal to the sum of the heat capacities of calcite and magnesite to within 1%, indicating that the partial molal heat capacities of $CaCO_3$ and $MgCO_3$ in dolomite are equal to the heat capacities of pure calcite and magnesite, respectively. Accordingly we have corrected our data above 70°K. by subtracting from the heat capacity of 189.95 g. of the measured material, the heat capacities of 0.0151-$Mg(OH)_2$ + 0.0427$CaCO_3$ + 0.0027$MnCO_3$ + 0.003-$SrCO_3$ + 0.0002$FeCO_3$.

(5) W. F. Giauque and R. C. Archibald, *J. Am. Chem. Soc.*, **59**, 561 (1937).
(6) C. T. Anderson, *ibid.*, **56**, 340 (1934).
(7) F. Simon and R. C. Swain, *Z. physik Chem.* (Leipzig), **B28**, 189 (1935).
(8) C. T. Anderson, *J. Am. Chem. Soc.*, **56**, 849 (1934).

Below 70°K. the heat capacity of dolomite becomes less than the sum of the heat capacities of calcite and magnesite, and below 35°K. it is less than the heat capacity of calcite alone. It is apparent that the partial molal heat capacity of $CaCO_3$ and $MgCO_3$ is less in dolomite than in the pure substances, and we have assumed that the partial molal heat capacities of all carbonates in dolomite are reduced below that of the respective pure substances by the same factor. Furthermore, no significant error is introduced by replacing the small amounts of $MnCO_3$, $SrCO_3$, and $FeCO_3$ by an equal number of moles of $CaCO_3$. Designate by $C_p(S)$ the heat capacity of 189.06 g. of material obtained by subtracting from the heat capacity of 189.94 g. of the measured sample the heat capacity of 0.0151 $Mg(OH)_2$, by $C_p(D)$ the heat capacity of pure dolomite corresponding to the formula $CaMg(CO_3)_2$, and by r the ratio of the heat capacity of magnesite to that of calcite. Values of r were obtained from the measured heat capacities of calcite[6,7] and the measurements and low temperature extrapolation by Anderson[8] for magnesite. Then

$$C_p(D) = \bar{C}_p(CaCO_3) + \bar{C}_p(MgCO_3) = (1 + r)\bar{C}_p(CaCO_3) \quad (1)$$

$$C_p(S) = 1.0459\bar{C}_p(CaCO_3) + \bar{C}_p(MgCO_3) = (1.0459 + r)\bar{C}_p(CaCO_3) \quad (2)$$

$$C_p(D) = (1 + r)(1.0459 + r)^{-1}C_p(S) \quad (3)$$

Equation 3 was used to calculate the heat capacity of dolomite below 70°K. Above 70°K. it is equivalent to the procedure described earlier for this temperature region.

Recent measurements of Kalinkina[9] have shown that $MnCO_3$ and $FeCO_3$ have anomalies in heat capacity arising from antiferromagnetic ordering of the magnetic moments at 29.4 and 30.6°K., respectively. No anomaly was observed in our sample of dolomite, indicating that the manganese impurity was probably present in a dilute solid solution which would not become antiferromagnetically ordered in the temperature range investigated.

The heat capacity of dolomite, corrected for impurities as described, is less than that of 184.42 g. of the measured sample by 0.8% at 10°K., 1.1% at 20°K., 0.8% at 50°K., 0.29% at 100°K., 0.16% at 200°K., and 0.12% at 300°K. Smoothed values of the heat capacity, entropy, enthalpy, and Gibb's free-energy function for $CaMg(CO_3)_2$ (dolomite) are listed in Table II. The values of the heat capacity have been corrected for curvature.

Heat of Formation of Dolomite. Thermal Dissociation of Dolomite.—The enthalpy change for the reaction

$$CaMg(CO_3)_2 \text{ (dolomite)} = CaCO_3 \text{ (calcite)} + MgCO_3 \text{ (magnesite)} \quad (4)$$

may be estimated from data on the temperature and pressure of CO_2 at the equilibrium between dolomite, a magnesian calcite, MgO, and CO_2 gas. The equilibrium in this dissociation reaction has been investi-

(9) I. N. Kalinkina, *Zh. Eksperim. i Teor. Fiz.*, **43**, 2028 (1962).

gated by Graf and Goldsmith,[2] Harker and Tuttle,[10] and Goldsmith and Heard.[11] The various data are in agreement. We shall make use of the measurements of Graf and Goldsmith which are in a range of pressure and temperature where the thermodynamic properties of CO_2 gas are known, and where the composition of the dolomite in equilibrium does not deviate seriously from the ideal composition. From the data for dolomite in the present paper and from the measurements of Anderson[6,8] one obtains for reaction 4, $\Delta S°_{298}(4) = 0.81 \pm 0.29$ cal. deg.$^{-1}$.

TABLE II

THERMODYNAMIC PROPERTIES OF DOLOMITE, $CaMg(CO_3)_2$

[1 mole = 184.42 g.; 0°C. = 273.15°K.]

T, °K.	$C_p°$, cal. deg.$^{-1}$ mole^{-1}	$S°$, cal. deg.$^{-1}$ mole^{-1}	$H° - H_0°$, cal. mole^{-1}	$\frac{(F° - H_0°)}{T}$, cal. deg.$^{-1}$ mole^{-1}
10	0.028	0.009	0.07	0.002
15	0.097	0.031	0.35	0.008
20	0.271	0.080	1.21	0.019
25	0.601	0.172	3.32	0.040
30	1.102	0.324	7.51	0.073
35	1.771	0.542	14.62	0.124
40	2.584	0.830	25.46	0.194
45	3.497	1.186	40.62	0.284
50	4.506	1.606	60.59	0.394
55	5.568	2.085	85.76	0.526
60	6.671	2.617	116.4	0.678
65	7.804	3.195	152.5	0.849
70	8.930	3.815	194.4	1.038
75	10.06	4.469	241.8	1.245
80	11.20	5.155	295.0	1.468
90	13.40	6.603	418.1	1.957
100	15.42	8.120	562.3	2.497
110	17.32	9.680	726.1	3.079
120	19.10	11.26	908	3.70
130	20.75	12.86	1108	4.34
140	22.30	14.45	1323	5.00
150	23.71	16.04	1553	5.69
160	25.02	17.61	1797	6.38
170	26.25	19.17	2053	7.09
180	27.40	20.70	2321	7.80
190	28.47	22.21	2601	8.52
200	29.49	23.70	2891	9.24
210	30.47	25.16	3191	9.97
220	31.41	26.60	3500	10.69
230	32.30	28.02	3819	11.41
240	33.16	29.41	4146	12.13
250	34.01	30.78	4482	12.85
260	34.83	32.13	4826	13.57
270	35.62	33.46	5178	14.28
280	36.37	34.77	5538	14.99
290	37.09	36.06	5905	15.69
300	37.77	37.33	6280	16.39
273.15	35.86	33.87	5291	14.50
298.15	37.65	37.09	6210	16.26
	±0.10	±0.10	±16	±0.04

The reaction

$$MgCO_3 \text{ (magnesite)} = MgO + CO_2 \text{ (gas)} \quad (5)$$

has been considered by Kelley and Anderson,[12] who obtain $\Delta H°_{298}(5) = 28.27$ kcal. by analysis of the dissociation data of Marc and Simek.[13] We have recalculated the value of $\Delta H°_{298}(5)$ from Marc and Simek's data, making use of the available entropy[14] and high temperature heat content[15] data and the thermodynamic properties[16,17] of CO_2 gas. At temperatures above 700°K. the heat capacity of $MgCO_3$ was assumed equal to that of $CaCO_3$ (calcite). We obtain $\Delta H°_{298}(5) = 28.15 \pm 0.05$ kcal. from the dissociation data of Marc and Simek.[13] Harker and Tuttle[10] have measured the dissociation equilibrium of $MgCO_3$ at higher temperatures. From their data at pressures below 1400 atm. CO_2 pressure, which lie in the range where thermodynamic data on CO_2 are available, we obtain $\Delta H°_{298}(5) = 28.03 \pm 0.25$ kcal. The errors listed for these values of $\Delta H°_{298}(5)$ are the standard deviations calculated from the variation among the individual measurements. Additional error will be introduced by the uncertainties in the entropy and high temperature heat content data. Considering these, we find $\Delta H°_{298}(5) = 28.14 \pm 0.18$ kcal. From this number, together with[14] $\Delta S°_{298}(5) = 41.78 \pm 0.24$ cal. deg.$^{-1}$ and the values[15] of $H° - H°_{298}$ and $S° - S°_{298}$ for $MgCO_3$, MgO, and CO_2, one may calculate $\Delta F°(5)$ at any temperature.

At the equilibrium involving dolomite, magnesian calcite, MgO, and CO_2, the free energy change in zero for the reactions

$$MgCO_3 \text{ (solid solution, } x) = MgO + CO_2 \text{ (gas)} \quad (6)$$

$$CaMg(CO_3)_2 \text{ (dolomite)} = CaCO_3 \text{ (solid solution, } x) + MgO + CO_2 \text{ (gas)} \quad (7)$$

Here x is the mole fraction of $MgCO_3$ in the magnesian calcite solid solutions. From $\Delta F(6) = 0$ one obtains

$$\Delta F(5) = \bar{F}_M - F_M(p) = \bar{H}_M - H_M(p) + RT \ln x \quad (8)$$

Here $\bar{F}_M$ and $\bar{H}_M$ are the partial molal free energy and enthalpy of $MgCO_3$ in the magnesian calcite solutions and $F_M(p)$ and $H_M(p)$ are molal free energy and enthalpy of pure $MgCO_3$ (magnesite). In the right third of eq. 8 the entropy of mixing valid for dilute solutions is assumed. At a temperature of 1173°K. the composition of the dolomite is[11] $Ca_{0.53}Mg_{0.47}CO_3$, and as the temperature is lowered the composition rapidly approaches the ideal $Ca_{0.5}Mg_{0.5}CO_3$. One may therefore with good approximation write

$$\bar{F}_M + \bar{F}_C = F_D(p) = F_M(p) + F_C(p) - \Delta F(4) \quad (9)$$

since, as the composition varies slightly from the ideal equimolal calcium–magnesium mixture, the variation of the partial molal free energy of $MgCO_3$ in the dolomite phase is, by the Gibbs–Duhem equation, almost exactly compensated by the variation of the partial molal free energy of $CaCO_3$ in this phase, so that the sum of the two remains equal to the free energy of dolomite of ideal composition. In eq. 9 the subscript C refers to $CaCO_3$ and D to $CaMg(CO_3)_2$. From $\Delta F(7) = 0$ and eq. 9 one obtains

$$\Delta H(4) + \bar{H}_C - H_C(p) = T\Delta S(4) - \Delta F(5) - RT \ln (1 - x) \quad (10)$$

(10) R. I. Harker and O. F. Tuttle, *Am. J. Sci.*, **253**, 209 (1955).

(11) J. R. Goldsmith and H. C. Heard, *J. Geol.*, **69**, 45 (1961).

(12) K. K. Kelley and C. T. Anderson, U. S. Bureau of Mines Bulletin No. 384, 1935, p. 25.

(13) R. Marc and A. Simek, *Z. anorg. Chem.*, **82**, 17 (1913).

(14) K. K. Kelley and E. G. King, U. S. Bureau of Mines Bulletin No. 592, 1961.

(15) K. K. Kelley, U. S. Bureau of Mines Bulletin No. 584, 1960.

(16) J. Hilsrenrath, *et al.*, U. S. National Bureau of Standards Circular 564, 1955, pp. 167–180.

(17) D. Price, *Ind. Eng. Chem.*, **47**, 1649 (1955).

TABLE III

ENTHALPY CHANGE IN REACTION $CaMg(CO_3)_2 = CaCO_3 + MgCO_3$ CALCULATED FROM DISSOCIATION EQUILIBRIUM DATA[a] OF GRAF AND GOLDSMITH[a]

T, °K.	P_{CO_2}, atm.	x, mole fraction	$\Delta F°(5)$, kcal.	$(P-1)\Delta V_S$, kcal.	$RT \ln f_{CO_2}$, kcal.	$\Delta F(5)$, kcal.	$\bar{H}_M - H_M(p)$, kcal.	$-RT \ln (1-x)$, kcal.	$T\Delta S(4)$, kcal.	$\Delta H(4)$, kcal.
1136	1361	0.257	−17.53	−0.55	17.21	−0.88	2.37	0.61	0.92	2.41
1069	681	0.178	−15.10	−0.28	14.33	−0.96	2.71	0.42	0.87	2.24
1076	544	0.183	−15.27	−0.22	13.87	−1.63	2.00	0.43	0.87	2.93
1013	245	0.138	−12.89	−0.10	11.30	−1.69	2.30	0.30	0.82	2.81
998	245	0.129	−12.32	−0.10	11.13	−1.29	2.78	0.27	0.81	2.37
953	66.3	0.105	−10.60	−0.03	7.97	−2.65	1.61	0.21	0.77	3.64
892	27.2	0.081	− 8.25	−0.01	5.87	−2.39	2.06	0.15	0.72	3.27
888	27.2	0.079	− 8.10	−0.01	5.84	−2.27	2.21	0.15	0.72	3.13
873	17.0	0.074	− 7.51	−0.01	4.92	−2.60	1.92	0.13	0.71	3.44
907	51.0	0.086	− 8.83	−0.02	7.10	−1.75	2.68	0.16	0.74	2.64
903	51.0	0.084	− 8.68	−0.02	7.07	−1.62	2.82	0.16	0.73	2.51
861	16.3	0.070	− 7.05	−0.01	4.78	−2.27	2.28	0.12	0.70	3.09
830	7.83	0.062	− 5.84	0.00	3.40	−2.45	2.14	0.11	0.67	3.23
830	6.81	0.062	− 5.84	0.00	3.17	−2.68	1.91	0.11	0.67	3.45
						Mean	2.27			2.94

[a] See text for description of column headings.

Furthermore

$$\Delta F(5) = \Delta F°(5) + RT \ln f_{CO_2} + (P-1)\Delta V_S \quad (11)$$

where f_{CO_2} is the fugacity of CO_2 gas calculated from the tables[16,17] of thermodynamic properties and ΔV_S is the difference in molar volumes of MgO and $MgCO_3$. From the compilation of Robie and Bethke[18] one finds $\Delta V_S = -16.77$ cm.^{3}. The variation of this quantity with pressure and temperature will be neglected. At room temperature the heat capacity of dolomite equals the sum of the heat capacities of magnesite and calcite to within 0.1% and we have assumed that $\Delta C_p = 0$ at higher temperatures for the formation of either dolomite or magnesian calcite solid solution from pure magnesite and calcite. Furthermore the work of Goldsmith, Graf, and Heard[19] has shown that the volume changes in forming dolomite or magnesian calcite solid solutions from magnesite and calcite are small. We therefore assume $\Delta H(4)$ and $\Delta S(4)$ to be independent of temperature and pressure from room temperature and atmospheric pressures to the highest temperatures and pressures employed in the dissociation equilibrium measurements.

In Table III are listed the equilibrium data of Graf and Goldsmith.[4] The last five measurements listed in Table III were made with magnesian calcite as starting material and the remaining measurements used dolomite as starting material. The mole fraction, x, of $MgCO_3$ in the magnesian calcite solid solutions is taken from the revised values of Graf and Goldsmith.[20] Goldsmith and Heard[11] obtain slightly smaller values of x at the higher temperatures. However, the error in the value of $\Delta H(4)$ calculated from eq. 10 arising from the uncertainty in x is negligible compared to the other experimental errors. Examination of the column headed $\bar{H}_M - H_M(p)$ in Table III, calculated by eq. 8, shows that within the rather large experimental error there is no significant trend with composition. We may therefore conclude that within the experimental errors of the dissociation data $\bar{H}_M - H_M(p)$ is independent of composition and therefore $\bar{H}_C - H_C(p)$ is zero. The values of $\Delta H(4)$ listed in the last column of Table III are calculated from eq. 10 with $\bar{H}_C - H_C(p)$ set equal to zero.

The standard deviation calculated from the variation of $\Delta H(4)$ in Table III is 0.12 kcal. Considering the additional errors arising from the errors in $\Delta S(4)$ and $\Delta F°(5)$ we conclude that from the dissociation data $\Delta H°_{298}(4) = 2.94 \pm 0.3$ kcal. A further error in this number may arise from the possibility that the MgO produced in the dolomite decomposition, because of small particle size, has a higher free energy than the normal material. This effect has been discussed by Giauque[21] for the case of MgO produced by the thermal decomposition of $Mg(OH)_2$ and Taylor and Wells[22] find that MgO so prepared may vary in enthalpy by nearly 1 kcal. Since no information is available on the particle size produced in the dolomite decomposition a correction cannot be made. If such an effect is present the value of $\Delta H°_{298}$ quoted above would be too large.

Aqueous Solubility of Dolomite, Magnesite, and Calcite.—The free energy of formation of dolomite from calcite and magnesite may be calculated from the solubilities of the three carbonates in aqueous solutions. Halla[23] has calculated $\Delta F°_{298}(4)$ from the solubilities of the three carbonates in water saturated with CO_2 at 1 atm. We shall repeat the calculation here since Halla erroneously used the mean ionic activity coefficient of an alkaline earth bicarbonate in aqueous solution rather than the cube of this number. The solubility of dolomite, magnesite, and calcite at 298°K. in aqueous solutions saturated with CO_2 at 1 atm. pressure has been measured by Yanat'eva.[24] In these solutions the only important ionic species are the alkaline earth metal ions and HCO_3^- ions and the ionic strength, μ, may be calculated from the molalities, m, reported by Yanat'eva. The ionic activity coefficients, γ, have been esti-

(18) R. A. Robie and P. M. Bethke, U. S. Geological Survey, Report TEI-822, 1962.

(19) J. R. Goldsmith, D. L. Graf, and H. C. Heard, *Am. Mineralogist*, **46**, 453 (1961).

(20) D. L. Graf and J. R. Goldsmith, *Geochim. Cosmochim. Acta*, **13**, 218 (1958).

(21) W. F. Giauque, *J. Am. Chem. Soc.*, **71**, 3192 (1949).

(22) K. Taylor and L. S. Wells, *J. Res. Natl. Bur. Std.*, **21**, 133 (1938).

(23) (a) F. Halla, *Z. physik. Chem.* (Frankfurt), **17**, 368 (1958); (b) *ibid.*, **21**, 349 (1959); (c) *ibid.*, **22**, 133 (1959); (d) *ibid.*, **25**, 267 (1960).

(24) O. K. Yanat'eva, *Izv. Akad. Nauk SSSR, Otd. Khim. Nauk.*, 1119 (1954); *Bull. Acad. Sci. USSR, Div. Chem. Sci.* (English Transl.), 977 (1954)

mated from the tables in Klotz.[25] The calculation is summarized as follows.

$$CaCO_3 \text{ (calcite)} + CO_2\ (P = 1) + H_2O = Ca^{+2} + 2HCO_3^- \quad (12)$$

$$m[Ca(HCO_3)_2] = 9.0 \times 10^{-3};\ \mu = 2.7 \times 10^{-2}$$

$$\gamma_{Ca^{+2}} = 0.56 \quad \gamma_{HCO_3^-} = 0.86$$

$$\Delta F^\circ_{298}(12) = -RT \ln (4)(9.0 \times (10^{-3})^3(0.56)(0.86)^2 = -RT \ln 1.21 \times 10^{-6}$$

$$MgCO_3 \text{ (magnesite)} + CO_2\ (P = 1) + H_2O = Mg^{+2} + 2HCO_3^- \quad (13)$$

$$m[Mg(HCO_3)_2] = 16.5 \times 10^{-3};\ \mu = 4.95 \times 10^{-2}$$

$$\gamma_{Mg^{+2}} = 0.52 \quad \gamma_{HCO_3^-} = 0.82$$

$$\Delta F^\circ_{298}(13) = -RT \ln (4)(16.5 \times 10^{-3})^3(0.52)(0.82)^2 = -RT \ln 6.3 \times 10^{-6}$$

$$CaMg(CO_3)_2 \text{ (dolomite)} + 2CO_2\ (P = 1) + 2H_2O = Ca^{+2} + Mg^{+2} + 4HCO_3^- \quad (14)$$

$$m[CaMg(HCO_3)_2] = 3.245 \times 10^{-3};\ \mu = 1.95 \times 10^{-2}$$

$$\gamma_{Ca^{+2}} = 0.60 \quad \gamma_{Mg^{+2}} = 0.62 \quad \gamma_{HCO_3^-} = 0.872$$

$$\Delta F^\circ_{298}(14) = -RT \ln (256)(3.245 \times 10^{-3})^6(0.60) \times (0.62)(0.872)^2 = -RT \ln 6.4 \times 10^{-14}$$

$$\Delta F^\circ_{298}(4) = \Delta F^\circ_{298}(14) - \Delta F^\circ_{298}(13) - \Delta F^\circ_{298}(12) = 2.83 \text{ kcal.}$$

$$\Delta H^\circ_{298}(4) = 2.83 + 0.24 = 3.07 \text{ kcal.}$$

This value of $\Delta H^\circ_{293}(4)$ is in good agreement with the value 2.94 kcal. which was calculated earlier from the dissociation measurements. However Halla[23b] has also calculated $\Delta F^\circ_{298}(4)$ from the measured solubilities at the two triple points where dolomite and calcite or magnesite, respectively, are in equilibrium with water saturated with CO_2 at 1 atm. pressure. He obtains $\Delta F^\circ_{298}(4) = 0.710$ kcal. from his measurements[26] and $\Delta F^\circ_{298}(4) = 1.017$ kcal. from the measurements of Yanat'eva.[27] The corresponding values of $\Delta H^\circ_{298}(4)$ are 0.95 and 1.26 kcal. In this calculation the neglect of ionic activity coefficients introduces negligible error since only the ratio of the activity coefficients of Ca^{+2} and Mg^{+2} is involved.

(25) I. M. Klotz, "Chemical Thermodynamics," Prentice-Hall, Inc., New York, N. Y., 1950, p. 332.

Conclusion

The disagreement between the values of $\Delta F^\circ_{298}(4)$ calculated from the solubility measurements leads one to suspect that true thermodynamic equilibrium may not be established in these measurements. This would also be expected from the hydrothermal synthesis results of Goldsmith and Graf.[1] The most reliable values of the enthalpy and free energy changes for the decomposition of dolomite into calcite and magnesite appear to be those calculated from the high temperature equilibrium data, namely $\Delta H^\circ_{298}(4) = 2.94$ kcal. and $\Delta F^\circ_{298}(4) = 2.70$ kcal. A direct calorimetric measurement of the enthalpy change in reaction 4, by measurement of the heats of solution of the various carbonates, would be valuable in establishing these numbers more precisely.

Acknowledgments.—We thank Prof. Fritz Laves for obtaining for us the sample of dolomite, Miss M. C. Batchelder for the chemical and spectrochemical analyses, Prof. J. O. Hutchens and Dr. A. G. Cole for stimulating discussions of the experimental measurements, and Prof. J. R. Goldsmith for advice on the dolomite decomposition. The partial support of this work by the Office of Naval Research and by the National Science Foundation is gratefully acknowledged.

(26) F. Halla, *Tschermaks mineral. petrog. Mitt.*, **48**, 271 (1936).

(27) O. K. Yanat'eva, *Zh. Obsch. Khim.*, **25**, 234 (1955); *J. Gen. Chem. USSR*, **25**, 217 (1955).

HEAT CAPACITY FROM 12 TO 305°K. AND ENTROPY OF TALC AND TREMOLITE

BY RICHARD A. ROBIE[1] AND J. W. STOUT

Institute for the Study of Metals, and Departments of Geology and Chemistry, University of Chicago, Chicago 37, Illinois

Received July 1, 1963

The heat capacities of talc, $Mg_3Si_4O_{10}(OH)_2$, and tremolite, $Ca_2Mg_5Si_8O_{22}(OH)_2$, have been measured between 12 and 305°K. Smoothed values of heat capacity, entropy, enthalpy, and free energy are tabulated. At 298.15° K. the values of the thermodynamic functions are: talc, $C_p^\circ = 76.89 \pm 0.23$ cal. deg.$^{-1}$ mole^{-1}, $S^\circ = 62.33 \pm 0.19$ cal. deg.$^{-1}$ mole^{-1}, $H^\circ - H_0^\circ = 11{,}205 \pm 34$ cal. mole^{-1}; tremolite, $C_p^\circ = 156.7 \pm 0.6$ cal. deg.$^{-1}$ mole^{-1}, $S^\circ = 131.2 \pm 0.5$ cal. deg.$^{-1}$ mole^{-1}, $H^\circ - H_0^\circ = 23{,}335 \pm 90$ cal. mole^{-1}. From the equilibrium data of Bowen and Tuttle and the entropy of talc, the heat of formation of talc from MgO, SiO_2, and H_2O (liq.) is calculated to be $\Delta H^\circ f_{298} = -43.6 \pm 1$ kcal.

The heat capacities of the minerals talc and tremolite were determined in order to provide basic thermochemical data necessary for understanding of the chemical equilibria involved in the formation of some common mineral assemblages. The thermodynamics of these minerals is also important in the field of ceramics.

(1) Theoretical Geophysics Branch, U. S. Geological Survey, Acorn Building, Silver Spring, Maryland.

Experimental

Apparatus.—The apparatus used to measure the heat capacities and the method of treating the data for heat exchange have been described previously.[2a] The calorimeter and resistance thermometer–heater are described in the preceding paper.[2b]

Sample of Talc, $Mg_3Si_4O_{10}(OH)_2$.—The sample of talc was obtained through the courtesy of Drs K. O. Bennington and Paul H. Reitan. It was in the form of a dense aggregate of small crystals 0.01 to 1.0 mm. in diameter. The material was chipped into small pieces using a hardened steel scribe point and sieved. Material passing a 20-mesh screen and retained on a 50-mesh screen was saved. Because talc is an exceedingly soft mineral, with a perfect basal cleavage (001), it was feared that crushing in a mortar might distort the crystals, as was pointed out by Gruner,[3] and we therefore did not grind the sample. This method of sample preparation gave rice-shaped particles each composed of possibly 100 or so small undistorted crystals. The sample was passed through a strong magnetic field to remove any iron introduced in the chipping operation and carefully hand sorted under a binocular microscope. The talc had a very faint greenish tint and the aggregate was translucent. Spectroscopic analysis of the material showed all nonessential elements except iron and aluminum to be less than 0.02% by weight. Three independent spectrographic analyses gave a considerably lower value for iron than the wet chemical analyses. We believe the spectrographic analysis to be more nearly correct and have modified the wet analysis (Table I) accordingly.

TABLE I

CHEMICAL ANALYSES[a] OF TALC AND TREMOLITE, WEIGHT %

	Talc, Murphy, North Carolina		Tremolite, Falls Village, N. Y.		
Oxide	Found	Calcd. for $Mg_3Si_4O_{10}(OH)_2$	Found		Calcd. for $Ca_2Mg_5Si_8O_{22}(OH)_2$
SiO_2	62.47	63.37	57.76		59.17
TiO_2	0.00		0.00		
Al_2O_3	.47		.51		
Fe_2O_3	n.d.		n.d.		
FeO	0.45[b]		0.11		
MnO	.00		.01		
MgO	31.76	31.88	25.21		24.81
CaO	0.00		12.96		13.80
Na_2O			0.43		
K_2O			.12		
P_2O_5			.01		
CO_2			.31	0.51[c]	
H_2O^+	4.70	4.75	2.13		2.22
H_2O^-	0.06		0.00		
	99.91	100.00	99.57		100.00

[a] Wet analysis: H. B. Wiik, Helsinki, Finland, unless otherwise specified. [b] Spectroscopic analysis: O. Joensuu, Miami University, Miami, Fla. [c] Independent carbon dioxide analysis: M. C. Batchelder, Institute for the Study of Metals, University of Chicago, Chicago, Ill.

Prior to filling the calorimeter, the sample was placed in an oven for 12 hr. at 115° to drive off any surface moisture. The calorimeter was filled with 198.12 g. (*in vacuo*).

Sample of Tremolite, $Ca_2Mg_5Si_8O_{22}(OH)_2$.—Tremolite presented greater difficulties in obtaining a pure single phase material of approximate stoichiometric composition. The sample, provided by Dr. Brian Mason of the American Museum of Natural History, consisted of a radial aggregate of needle-like tremolite crystals 1 to 4 mm. across and up to 2 cm. long, embedded in a matrix of calcite and dolomite. The tremolite–carbonate rock was crushed to pass 30 mesh and was then heated with dilute HCl over a steam bath until no more effervescence occurred. The acid was renewed frequently. The material was dried at 110° for 2 hr. and sieved; the fraction passing 75 mesh was discarded and the remaining fraction carefully hand-picked under a binocular microscope. The tremolite was crushed again and the acid treatment repeated. It was sieved and the material passing 100 mesh was discarded. Microscopic examination with a petrographic microscope showed that not all the carbonate phase had been removed, approximately 1%, by volume, remaining. It would have been possible to remove the bulk of the remaining carbonate by repeated crushings and acid leaching. This was not done since we wished to avoid the difficulties encountered with very fine grained samples. A random sample was selected for chemical analyses. Several independent determinations were made for CO_2 to accurately determine the carbonate impurity. The results of the analysis are given in Table I.

The sample was heated at 115° for 12 hr. prior to filling the calorimeter. The calorimeter was filled with 207.07 g. (*in vacuo*).

Experimental Results

In Table II are listed the experimentally measured values of the heat capacity of 379.29 g. of talc of the composition listed in Table I. The heat capacities of 812.4 g. of the tremolite whose analysis is given in Table I are listed in Table III. These data are uncorrected for curvature or impurities. The measurements are listed in chronological order. T_{av} listed in Tables II and III is the arithmetic mean of the initial and final temperatures of a measurement. The temperature rise in an individual measurement may be inferred from the temperature interval between successive measurements. No dependence of heat capacity on thermal history was observed. The defined calorie, 4.1840 j., is used. The ice-point temperature is taken as 273.15°K. The 1961 International Scale of Atomic Weights[4] is used. Certain values marked

TABLE II

HEAT CAPACITY IN CAL. DEG.$^{-1}$ OF 379.29 G. OF TALC FROM MURPHY, NORTH CAROLINA

[0°C. = 273.15°K.]

T_{av}, °K.	$\Delta H/\Delta T$	T_{av}, °K.	$\Delta H/\Delta T$
299.39	76.86	225.37	61.63
306.45	77.96	230.89	63.01
		236.24	64.28
81.33	14.71	238.53	64.87
		245.27	66.43
52.74	5.697	251.56	67.76
57.48	6.970	257.81	69.19
61.89	8.248	263.47	70.40
66.37	9.635	269.25	71.57
70.78	11.04	274.77	72.72
74.92	12.42	281.54	73.95
79.12	13.91	288.11	75.17
83.44	15.47	294.38	76.24
87.88	17.10	299.96	77.10
91.53	18.42		
95.61	19.90	11.85	0.1690
99.95	21.52	13.45	.2017
104.20	23.08	15.61	.2702
108.98	24.87	18.12	.3809
113.89	26.71	20.02	.4838
118.71	28.52	22.45	.6472
123.84	30.44	24.60	.8123
128.80	32.22	26.79	1.015
134.24	34.22	29.41	1.291
140.30	36.41	32.43	1.673
146.33	38.51	35.83	2.172
151.93	40.42	39.47	2.785
156.29	41.88	42.34	3.314
161.86	43.67	45.71	4.018
168.14	45.70		
174.44	47.69	45.73	4.017
180.54	49.51	49.71	4.933
186.28	51.22	53.71	5.944
190.45	52.39		
196.15	54.08		
202.23	55.71		
208.68	57.45		
214.91	59.08		
219.56	60.22		

(2) (a) A. G. Cole, J. O. Hutchens, R. A. Robie, and J. W. Stout, *J. Am. Chem. Soc.*, **82**, 4803 (1960); (b) J. W. Stout and R. A. Robie, *J. Phys. Chem.*, **67**, 2248 (1963).

(3) J. W. Gruner, *Z. Krist.*, **88**, 412 (1934).

(4) A. E. Cameron and E. Wichers, *J. Am. Chem. Soc.*, **84**, 4175 (1962).

TABLE III

HEAT CAPACITY IN CAL. DEG.$^{-1}$ OF 812.4 G. OF TREMOLITE FROM FALLS VILLAGE, NEW YORK

[0°C. = 273.15°K.]

T_{av}, °K.	$\Delta H/\Delta T$	T_{av}, °K.	$\Delta H/\Delta T$
304.22	158.9	254.99	141.1
		260.82	143.5
54.16	13.78	266.63	145.7
58.91	16.71	272.62	148.1
64.06	20.20	278.33	150.2
69.39	23.87	284.37	152.3
75.26	28.07	289.76	154.2
79.83	31.59	295.48	156.2
84.28	35.03	301.18	157.8
89.33	38.99		
94.53	42.99	249.17	138.7[a]
100.17	47.34	255.01	141.1[a]
105.79	51.76	260.85	143.5[a]
110.92	55.73	267.13	146.0[a]
116.34	59.96	273.40	148.6[a]
121.95	64.24	279.32	150.6[a]
127.41	68.36	289.13	153.9[a]
132.63	72.25	294.89	155.6[a]
138.26	76.33		
144.22	80.53	12.37	0.1878
149.98	84.53	13.61	.2376
155.38	88.21	15.49	.3450
161.13	92.02	17.64	.5089
167.02	95.74	20.28	.8161
172.64	99.24	21.79	1.030
178.88	103.0	24.08	1.428
184.86	106.5	26.68	1.973
190.75	109.8	29.80	2.784
196.46	113.0	33.38	3.887
202.20	116.0	36.91	5.171
208.24	119.2	40.57	6.673
214.22	122.2	50.31	11.57
220.03	125.0	54.93	14.25
225.82	127.9		
231.42	130.5	42.98	7.734
236.91	133.0	47.57	10.03
243.04	136.3		
249.12	138.6		

[a] "Bad vacuum runs."

in Table III are "bad vacuum runs" taken to evaluate a correction[2a] for temperature gradients within the calorimeter. These points are of lower accuracy than the remaining points, whose accuracy has been discussed previously.[2a]

Thermodynamic Properties

In order to calculate the heat capacity and other thermodynamic properties of talc and tremolite of ideal composition it is necessary to make correction for the deviations from the ideal of the compositions of the samples whose heat capacity was measured. From the analytical data in Table I, one calculates that 384.17 g. of the talc sample corresponds to the empirical formula

$$Mg_3Si_4O_{10}(OH)_2 + 0.0176\ FeAl_2O_4 + 0.006FeO + 0.004\ Mg(OH)_2 + 0.027MgO$$

It is probable that most of these impurities are actually present in solid solution in the talc structure, which for our sample would have the structural formula[5]

$$(Mg_{3.00}Fe_{0.02})\ (Si_{3.96}Al_{0.04})\ O_{10}\ (OH)_{1.99}$$

One may, however, approximately correct to the heat capacity of talc of ideal composition by subtracting from the heat capacity of 384.17 g. of sample the heat capacities of the remaining substances listed in the empirical formula. The substances listed were chosen because their low temperature heat capacities have been measured. References to the original heat capacity measurements are listed by Kelley and King.[6]

To check the magnitude of the possible error introduced by this method of correction, the heat capacity of $Mg_3Si_4O_{10}(OH)_2$ was compared with the sum of the heat capacities of $2MgO + 4SiO_2 + Mg(OH)_2$. The heat capacity of this sum is greater than the observed heat capacity of talc by 36% at 50°K., 11.4% at 100°K., and 2.6% at 300°K. The correction to the experimental data is 1.5% at 50°K. and 0.9% at 300°K. Accordingly the maximum error we should introduce in C_p by correcting in this fashion would be −0.3% at 50° and −0.1% at 100°K. Above 100°K. this method of correcting for impurities introduces negligible error. The error in the entropy at 298°K. will of course be much smaller since the entropy at 100°K. is only about 17% of $S°_{298}$.

TABLE IV

THERMODYNAMIC PROPERTIES OF TALC, $Mg_3Si_4O_{10}(OH)_2$

[1 mole = 379.289 g.; 0°C. = 273.15°K.]

T, °K.	$C_p°$, cal. deg.$^{-1}$ mole^{-1}	$S°$, cal. deg.$^{-1}$ mole^{-1}	$H° - H_0°$, cal. mole^{-1}	$-\frac{(F° - H_0°)}{T}$, cal. deg.$^{-1}$ mole^{-1}
10	0.078	0.027	0.204	0.007
15	.229	.084	.932	.022
20	.477	.182	2.65	.049
25	.841	.325	5.89	.089
30	1.352	.521	11.30	.144
35	2.031	.778	19.69	.216
40	2.866	1.102	31.88	.305
45	3.849	1.495	48.59	.415
50	4.996	1.959	70.63	.546
55	6.284	2.494	98.78	.698
60	7.686	3.100	133.7	.873
65	9.201	3.775	175.8	1.069
70	10.79	4.514	225.8	1.289
75	12.46	5.315	283.9	1.530
80	14.23	6.176	350.6	1.793
90	17.88	8.063	511.2	2.383
100	21.54	10.13	708.2	3.054
110	25.28	12.36	942.3	3.798
120	29.04	14.72	1214	4.608
130	32.72	17.19	1523	5.481
140	36.33	19.75	1868	6.409
150	39.80	22.38	2249	7.385
160	43.11	25.05	2663	8.406
170	46.33	27.76	3111	9.465
180	49.41	30.50	3590	10.56
190	52.35	33.25	4099	11.68
200	55.16	36.01	4636	12.83
210	57.84	38.77	5201	14.00
220	60.39	41.51	5793	15.18
230	62.85	44.25	6409	16.39
240	65.22	46.98	7049	17.61
250	67.52	49.69	7713	18.84
260	69.72	52.38	8399	20.07
270	71.82	55.05	9107	21.32
280	73.77	57.70	9835	22.57
290	75.56	60.32	10582	23.83
300	77.18	62.91	11346	25.09
273.15	72.45	55.89	9335	21.72
298.15	76.89 ± 0.23	62.33 ± 0.19	11205 ± 34	24.86 ± 0.07

In Table III are listed the thermodynamic quantities for talc of ideal composition $Mg_3Si_4O_{10}(OH)_2$, corrected as described previously for impurity.

(5) W. L. Bragg, "Atomic Structure of Minerals," Cornell University Press, Ithaca, N. Y., 1937, p. 200.

(6) K. K. Kelley and E. G. King, U. S. Bureau of Mines Bulletin No. 592, 1961.

On a plot of C_pT^{-2} *vs.* T for talc, the three lowest experimental points lie above a smooth curve passing through the higher temperature points and through zero at 0°K. with finite slope. We believe these points are high because of magnetic entropy associated with the ferrous ion impurity in the talc and are not representative of pure material. In calculating the thermodynamic functions listed in Table IV these points have been ignored and the extrapolation of the heat capacity was made with the smooth curve of C_pT^{-2} *vs.* T which joins smoothly to the experimental points at 20°K. and above.

From the analytical data one finds that 861.3 g. of the tremolite sample corresponds to the empirical composition $Ca_2Mg_5Si_8O_{22}(OH)_2$ + 0.061$MgCO_3$ + 0.023$Mg_3Si_4O_{10}(OH)_2$ + 0.0065Fe_2SiO_4 + 0.023$KAlSiO_3$ + 0.065$NaAlO_2$ + 0.0275Na_2SiO_3 + 0.122$MgSiO_4$ + 0.037MgO, and the heat capacities of the various substances listed were subtracted from that of 861.3 g. of our sample to give the heat capacity of tremolite of ideal composition. In Table V are listed the smooth values of the heat capacity and other thermodynamic functions for tremolite of ideal composition $Ca_2Mg_5Si_8O_{22}(OH)_2$.

TABLE V

THERMODYNAMIC PROPERTIES OF TREMOLITE, $Ca_2Mg_5Si_8O_{22}(OH)_2$

[1 mole = 812.410 g.; 0°C. = 273.15°K.]

T, °K.	$C_p°$, cal. deg.$^{-1}$ mole^{-1}	$S°$, cal. deg.$^{-1}$ mole^{-1}	$H° - H_0°$, cal. mole^{-1}	$\frac{(F° - H_0°)}{T}$, cal. deg.$^{-1}$ mole^{-1}
10	0.0946	0.034	0.25	0.0089
15	.283	.103	1.14	.0276
20	.713	.235	3.47	.0614
25	1.522	.474	8.91	.118
30	2.741	.853	19.38	.207
35	4.349	1.39	36.94	.336
40	6.319	2.10	63.47	.485
45	8.575	2.97	100.6	.733
50	11.24	4.01	150.0	1.007
55	14.12	5.21	213.3	1.334
60	17.27	6.57	291.7	1.713
65	20.65	8.09	386.4	2.144
70	24.09	9.74	498.2	2.627
75	27.66	11.53	627.5	3.160
80	31.45	13.43	775.2	3.742
90	39.24	17.59	1128	5.045
100	46.92	22.12	1559	6.523
110	54.69	26.95	2067	8.158
120	62.44	32.04	2653	9.934
130	69.96	37.34	3315	11.84
140	77.19	42.79	4051	13.86
150	84.17	48.36	4858	15.97
160	90.04	54.01	5734	18.17
170	97.26	59.71	6675	20.44
180	103.3	65.44	7678	22.79
190	109.0	71.18	8740	25.18
200	114.5	76.91	9858	27.63
210	119.7	82.63	11029	30.11
220	124.7	88.31	12251	32.62
230	129.5	93.96	13522	35.17
240	134.1	99.57	14841	37.74
250	138.6	105.1	16204	40.32
260	142.8	110.7	17612	42.92
270	146.8	116.1	19060	45.53
280	150.5	121.5	20547	48.15
290	153.9	126.8	22069	50.77
300	157.2	132.2	23624	53.40
273.15	148.1	117.8	19527	46.26
298.15	156.7 ± 0.6	131.2 ± 0.5	23335 ± 90	52.91 ± 0.21

Since the specific heats of most of the minerals considered do not differ much from one another, the error introduced by the impurity correction as described is appreciably less than the error in the analytical data on which it is based. We estimate that the errors arising from the impurity correction increase the error in the smoothed values of the heat capacity over the temperature range from 40 to 250°K. from the normal 0.2%[2a] to 0.3% for talc and 0.4% for tremolite.

The Heat of Formation of Talc.—Bennington[7] has obtained a value for the heat of formation, from the oxides, for the same sample of talc used in the heat capacity measurements reported here. His data are in marked disagreement with thermal weight loss studies[8] and with the high pressure equilibrium data of Bowen and Tuttle[9] for the reactions

$$Mg_3Si_4O_{10}(OH)_2 + Mg_2SiO_4 = 5MgSiO_3 + H_2O$$

and

$$Mg_3Si_4O_{10}(OH)_2 = 3MgSiO_3 + SiO_2 + H_2O$$

between 900 and 1100°.

In order to resolve this discrepancy the equilibrium data were subjected to a "third law" treatment[10] to check their internal consistency and to see if a resaonable value of $\Delta H°f$ could be obtained. For the equilibrium data we may write

$$\Delta F = 0 = \Delta F°_T + \int_0^P \Delta V_{solids}\, dP + RT \ln f_{H_2O}$$

The term due to the volume of the solid phases is small and may be approximated by $(P - 1)\Delta V°_{298}$ where $\Delta V°_{298}$ is the volume change at 298.15°K. and one atmosphere pressure. Subtracting $\Delta H°_{298}$ from both sides and rewriting we obtain

$$-\frac{\Delta H°_{298}}{T} = \Delta \frac{F°_T - H°_{298}}{T} + \frac{(P-1)\Delta V°_{298}}{T} + R \ln f_{H_2O}$$

The first term on the right-hand side was calculated from data listed in Kelley[5,11] and the entropy of $Mg_3Si_4O_{10}(OH)_2$ given above and approximating the heat capacity of $Mg_3Si_4O_{10}(OH)_2$ between 300 and 1200°K. by the relation

$$C_p = 84.58 + 41.68 \times 10^{-3}T - 17.96 \times 10^5 T^{-2}$$

This function fits the measured data for $Mg_3Si_4O_{10}(OH)_2$ within 10% at 100°K., 5% at 200°K., and 0.1% at 300°K., and its slope agrees well with the measured data near room temperature. Molar volumes for the solids were taken from a report by Robie and Bethke,[12] and the fugacity of H_2O from Holser's[13] tables. The results of these calculations are summarized in Tables VI and VII. Using the heats of formation of $MgSiO_3$ and Mg_2SiO_4 given by Torgeson and Sahama[14] and the heat of vaporization of water from the NBS tables,[15] leads to eight values for the heat of the reaction

$$3MgO + 4SiO_2 + H_2O\ (liq.) = Mg_3Si_4O_{10}(OH)_2$$

(7) K. O. Bennington, *J. Geol.*, **64**, 558 (1956).

(8) R. H. Ewell, E. N. Bunting, and R. F. Geller, *J. Res. Natl. Bur. Std.*, **15**, 551 (1935).

(9) N. L. Bowen and O. F. Tuttle, *Bull. Geol. Soc. Am.*, **60**, 439 (1949).

(10) G. N. Lewis and M. Randall, "Thermodynamics," 2nd Ed., revised by K. S. Pitzer and L. Brewer, McGraw-Hill Book Co., Inc., New York, N. Y., 1961, p. 178.

(11) K. K. Kelley, U. S. Bureau of Mines Bulletin No. 584, 1960.

(12) R. A. Robie and P. M. Bethke, U. S. Geol. Survey Report REI-822, 1962.

(13) W. T. Holser, *J. Phys. Chem.*, **58**, 316 (1954).

(14) D. R. Torgeson and Th. G. Sahama, *J. Am. Chem. Soc.*, **70**, 2156 (1948).

(15) F. D. Rossini *et al.*, U. S. Natl. Bur. Standards Circular 500, 1952.

TABLE VI

ΔH°_{298} FOR THE REACTION $Mg_3Si_4O_{10}(OH)_2 + Mg_2SiO_4 = 5MgSiO_3 + H_2O$ (g)[a]

T, °K.	P_{H_2O}, atm.	$\Delta(F^\circ_T - H^\circ_{298.16})$, kcal.	$(P-1)\cdot\Delta V^\circ_{298}$, cal.	f_{H_2O}, atm.	$\Delta H^\circ_{298.16}$, kcal.
897	408	−35.60	− 228	343	25.42
928	1021	−36.71	− 571	716	25.15
943	1531	−37.24	− 857	1010	25.14
952	2042	−37.56	−1144	1311	25.12
				Mean	25.21

[a] Equilibrium data of Bowen and Tuttle (see ref. 9).

TABLE VII

ΔH°_{298} FOR THE REACTION $Mg_3Si_4O_{10}(OH)_2 + 3MgSiO_3 + SiO_2 + H_2O$ (g)[a]

T, °K.	P_{H_2O}, atm.	$\Delta(F^\circ_T - H^\circ_{298.16})$, kcal.	$(P-1)\cdot\Delta V^\circ_{298}$, cal.	f_{H_2O}, atm.	$\Delta H^\circ_{298.16}$, kcal.
1034	408	−41.24	−193	368	29.29
1065	1021	−42.37	−484	860	28.55
1086	1531	−43.13	−726	1269	28.43
1099	2042	−43.59	−969	1678	28.34
				Mean	28.65

[a] See ref. 9.

with a mean value of −43.60 kcal. and a spread of 2.10 kcal. A 10% error in the assumed value of C_p of talc at 1000°K. would amount to 1.5 kcal. in these calculations.

Although these data leave much to be desired they are reasonably consistent, and combined with the fact that Bowen and Tuttle were able to convert a mixture $MgSiO_3$ and silica into talc at 1000 atm. H_2O pressure and 750°, are sufficient proof to conclude that Bennington's value of −35.53 kcal. is wrong. The crude value of $\Delta H^\circ f$ for $Mg_3Si_4O_{10}(OH)_2$ obtained above was recently confirmed by Barany[16] who made measurements of the heat of formation on a portion of our heat capacity sample. Barany's value, −44.89 ± 0.34 kcal., is to be preferred. From this heat of formation, the entropy of talc given in Table IV and entropies summarized in Kelley,[5] the free energy of formation of talc from the oxides is −40.95 kcal. at 298.15°K.

Acknowledgments.—We thank Drs. K. O. Bennington and Paul H. Reitan for the sample of talc, Dr. Brian Mason for the sample of tremolite, and H. B. Wilk, O. Joensuu, and Miss M. C. Batchelder for analyses. The partial support of this work by the Office of Naval Research and by the National Science Foundation is gratefully acknowledged.

(16) R. Barany, U. S. Bureau Mines Rept. Invest., 6251, 1963.

ELECTRON DIFFRACTION STUDY ON THE MOLECULAR STRUCTURE OF CHLORINE[1a]

BY SHUZO SHIBATA[1b]

Department of Chemistry, Shizuoka University, Shizuoka, Japan

Received September 6, 1962

The molecular structure of gaseous chlorine was determined by the sector-microphotometer method of electron diffraction. It was found that the Cl–Cl distance was 1.993 Å. and the root-mean-square amplitude of vibration was 0.051 Å. The anharmonicity of vibration was observed and estimated to be $a = 2.0$ Å.$^{-1}$, and the equilibrium distance was deduced to be 1.986 Å. These values are in good agreement with the data from the spectroscopic method. The error introduced in the observed atomic distance by the asymmetry of the gas jet is discussed.

Since the invention of the sector-microphotometer method, electron diffraction experiments have become much more precise. A method more rigorous than the conventional is now needed, especially in respect to neglect of nonnuclear scattering,[2a,b] failure of Born approximation,[2c] and anharmonicity of molecular vibration.[3] In this paper the anharmonicity problem was experimentally investigated through the study of the molecular structure of chlorine. Anharmonicity in chlorine is larger than in bromine and iodine. The asymmetry parameter of the molecular vibration could be estimated from the result obtained by electron diffraction as well as from spectroscopic data. On the other hand, corrections must be introduced for departures of the experimental measurement from the ideal conditions postulated in the equation of electron diffraction. In this paper the effect of the nozzle on the spreading of the gas and the asymmetry of the gas jet was investigated.

Experimental

Procedure.—The electron diffraction photographs[4] of chlorine were taken using an electron beam wave length, λ, of 0.053 Å. The camera distances, L, were 12.5 and 28.5 cm. The value of $2\pi/L\lambda$ was determined by the measurement of the transmission pattern of gold foil. An r^3-sector[5] with a beam trap was used. The beam trap was provided to prevent secondary electrons and X-rays from fogging the photograph. It was proved by a blank test that there was no extraneous scattering. When not rotating, the beam trap has a hole in the center which is used for sector centering. This hole closes during rotation. Two nozzles were used in the present experiment to investigate the "nozzle effect." One was a cigarette holder-type nozzle and the other was a drum-type nozzle. The shapes of these are shown in Fig. 6. The former has been used by many Japanese investigators. The chlo-

(1) (a) Presented at International Conference on Magnetism and Crystallography (1961), *J. Phys. Soc. Japan*. **17**, Supplement B-II, 34 (1962); (b) Department of Chemistry, University of Oslo, Blindern, Norway.

(2) (a) L. S. Bartell, L. O. Brockway, and R. H. Schwendeman, *J. Chem. Phys.*, **23**, 1854 (1954); (b) S. H. Bauer, *et al.*, have proposed a method: K. P. Coffin (Doctoral Thesis, Cornell University, 1951); (c) for example, V. Schomaker and R. Glauber, *Nature*, **170**, 290 (1952).

(3) L. S. Bartell, *J. Chem. Phys.*, **23**, 1219 (1955).

(4) The electron diffraction apparatus at Nagoya University was used; described at the annual meeting of the Chemical Society of Japan (1953) by Y. Morino, M. Kimura, and M. Iwasaki. Refer to M. Iwasaki, *Bull. Chem. Soc. Japan*, **32**, 205 (1959).

(5) The angular aperture of the brass sector was given by $\theta = cr^3$ with $r_{max} = 27.19$ mm. and $\theta_{max} = 5.40$ radians. S. Shibata, symposium on the diffraction of X-ray and electrons held in Osaka, Japan, November, 1956.

rine gas was kept at a pressure of 40 mm. in a 2-l. bottle and was injected into the diffraction chamber through the nozzle. The gas was then trapped by a cold trap containing liquid air. For each camera distance and each nozzle, one pair of the best photographs was selected from a large number of photographs for analysis. The density of these photographs was measured by a Riken B type microphotometer. The density of all the photographs used was under 0.25.

Analysis.—The density of the photograph was converted to intensity of the scattered electrons by Karle's method.[6] The total scattering intensities are shown in Fig. 1. These intensities were measured over the range of q from 10 to 100. The background I_B was smoothly drawn through the total intensity curve I_T. Then, the reduced intensity was obtained by the usual method.[7] The elimination of nonnuclear scattering was carried out by multiplying $[Z^2/(Z^2+Z)][\Sigma(Z-f)^2+ZS/(Z-f)^2]$ where for the coherent scattering factor, f, values calculated by Viervoll and Øgrim,[8] and for the incoherent scattering factor, S, values, calculated using Bewilogua's function,[9] were used. The qM and qM_c curves are shown in Fig. 2. The intensity curve in the inner region ($q = 10 \sim 25$) was obtained from measurement of longer camera distance photographs.

The atomic distance $r(q)$ was obtained from the intensity curve at every node and antinode. The values of $r(q)$ shows a tendency to decrease with increasing q values. This is due to the anharmonicity of vibration between chlorine atoms. If the potential of the vibration is represented by a Morse function

$$V(r) = D\{1 - \exp[-a(r - r_e)]\}^2 \qquad (1)$$

the theoretical intensity curve is expressed, as shown by Bartell[3]

$$qM_c = (c/r_e)\exp(-l^2\pi^2q^2/200) \times \sin\{(\pi q/10)[r_g(1) + \phi]\} \qquad (2)$$

where

$$\phi = -a\pi^2q^2/2400\ \alpha^2,\ \alpha = {}^1/_2l^2,\ c = (10/\pi)[Z^2/(Z^2+Z)]$$

The l is the root-mean-square amplitude and a is the asymmetry parameter. The asymmetry parameter, a, as well as the mean distance $r_g(1)$ can easily be estimated by using the preceding intensity function. The radial distribution function, $f(r)$, can be calculated by Fourier inversion of qM_c by use of an artificial damping factor $\exp(-b^2\pi^2q^2_{max}/100) = 0.1$. The theoretical intensity curve was used for the range of $q \leq 10$ which is necessary for the calculation of $f(r)$. The values of r and l were determined by the trial and error method. The $f(r)$ curve was calculated after redrawing of the background until the negative region of the curve was eliminated. The maximum height of the ghost was less than 2% of the height of the Cl–Cl peak. The final $f(r)$ curve is shown in Fig. 3. The asymmetry features can be seen when the peak is compared with a symmetric gaussian peak shown by the dotted lines in Fig. 3. The deviations are caused by the effect of anharmonicity of the molecular vibration. Taking into account the effect of anharmonic vibration, the radial distribution function[3] can be analytically expressed by

$$f(r) = A(1 + Bx + Cx^3)\exp(-Hx^2) \qquad (3)$$

where $x = r - r_e$, $B = [(a - r_e^{-1})/\gamma] + a(\gamma - 1)/2\gamma^2$, $C = a\alpha/3\gamma^3$, $H = \alpha/\gamma$, and $\gamma = 4b\alpha + 1$. It was shown that a for chlorine could be estimated from the data of the radial distribution curve as well as from the data of the intensity curve.

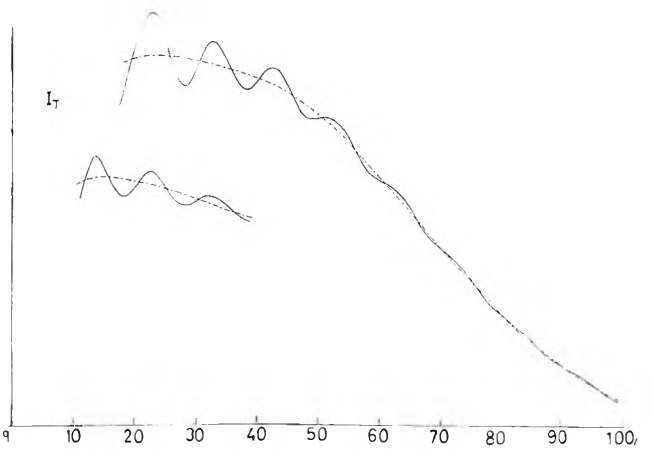

Fig. 1.—Total intensity curves and background intensity curves. The upper curve was obtained from the short camera distance photographs. The lower curve was obtained from the long camera distance photographs.

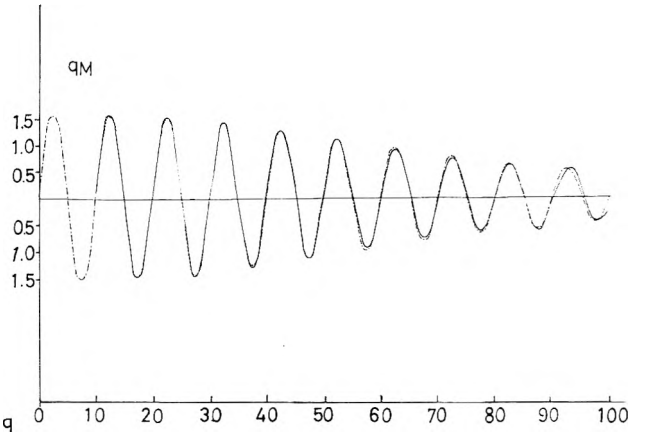

Fig. 2.—Frequency modulation of the intensity curve: ———, observed qM_c; — — —, observed qM; — · —, qM_c calculated with assumption of harmonic vibration.

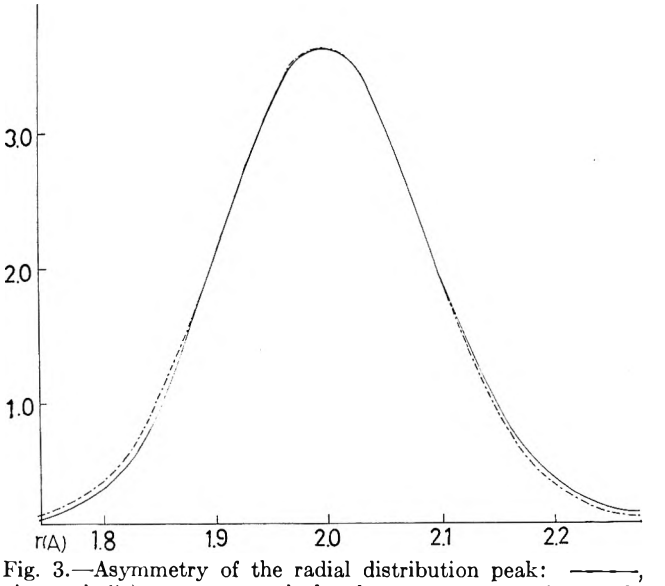

Fig. 3.—Asymmetry of the radial distribution peak: ———, observed $f(r)$; — · —, calculated symmetry gaussian peak.

Results and Discussion

1. $r_g(1)$.—The center of gravity of $P(r)/r$, $r_g(1)$, was obtained from the radial distribution curve $f(r)$ by use of the relation $\Sigma rf(r)/\Sigma f(r)$. Also $r_g(1)$ was evaluated from the extrapolation of $r(q)$ to $q = 0$ on the plot of $r(q)$ against q^2 which is shown in Fig. 4. The average value of $r_g(1)$ was 1.993 Å. From the measurement by the visual method, Pauling and Brockway[10] reported 2.009 ± 0.015 A. for the Cl–Cl distance of the gaseous chlorine molecule.[11]

(6) J. Karle and I. L. Karle, *J. Chem. Phys.*, **18**, 957 (1950).

(7) L. S. Bartell, L. O. Brockway, and R. H. Schwendeman, *ibid.*, **23**, 1854 (1955).

(8) H. Viervoll and O. Øgrim, *Acta Cryst.*, **2**, 277 (1949).

(9) L. Bewilogua, *Physik. Z.*, **32**, 740 (1931).

(10) L. Pauling and L. O. Brockway, *J. Chem. Phys.*, **2**, 867 (1934).

2. r_{RD}.—The position of the maximum of $f(r)$, r_{RD}, was estimated from the interpolation of r to $[\ln (f_0/f)]^{1/2} = 0$ on the graph of $[\ln (f_0/f)]^{1/2}$ plotted against r, where f_0 is the maximum of $f(r)$. Then, it was found that there exists the approximate relation[12]

$$[\ln (f_0/f)]^{1/2} = (H + B^2/2)^{1/2}[r - (r_e + B/2H)] \quad (4)$$

which is easily derived from eq. 3. On the other hand, the upper part of the $f(r)$ curve can be represented by a second-order equation, so r_{RD} was easily estimated by a relation obtained from $f'(r) = 0$. The average value of r_{RD} was 1.992 Å.

3. l.—The root-mean-square amplitude, l, was estimated from the inclination of $[\ln (f_0/f)]^{1/2}$ curve as determined by eq. 4.[13] On the other hand, the values of $\ln (qM_c)$ at every antinode of the intensity curve were plotted against the corresponding q^2. The value of l[14] was estimated from the inclination of $\ln (qM_c)$ on the graph. These values should be corrected for the gas spreading effect.[15] The average value l_e obtained was 0.051 Å. This value of l_e was slightly larger than the value of 0.044 Å.[16] at 298°K. calculated from the spectroscopic data ($w_e = 565$ cm.$^{-1}$).[17]

4. r_e.—The equilibrium distance was estimated from the $r_g(1)$ value by use of the relation

$$r_e = r_g(1) - 3\,al^2/2 + l^2/r_e \quad (5)$$

Also it was estimated from the r_{RD} value by use of

$$r_e = r_{RD} - (l^2/2)\,[3a - 2/r_e - a/(l^2 + 2b)] \quad (6)$$

which can be obtained from eq. 4.[12] The average r_e value was found to be 1.986 using $a = 2$, $l = 0.051$, $r_g(1) = 1.9928$, and $r_{RD} = 1.9917$ Å. with use of eq. 5 and 6.[18] The observed r_e value agrees with the spectroscopic value of 1.9890 Å.[19] The result obtained is shown in Table I. Recently Bartell, *et al.*,[20] obtained 1.983 Å. for r_e for the chlorine molecule. The data are shown in Table II with the spectroscopic data.

The mean displacement of the distance from r_e, $<\Delta r>$, which is $(r_g - r_e)$, is not zero because of the anharmonicity of vibration. This is approximately equal to $(3/2)al^2$ and is estimated to be 0.008 Å. using the observed l and a values.

5. a.—The asymmetry parameter was estimated by three methods. One of these methods is the intensity curve method where the value of a was evaluated from the inclination of the $r(q)$ *vs.* q^2 plot at every node and antinode. The results are shown in Fig. 4. The a was found to be 2.0 Å.$^{-1}$ by using a least squares on the data shown in the preceding plot. However, the error in a is large in this method and is equal to approximately the value of a itself. The error possibly arises from the finer gear slippage in the microphotometer, the correction of which is difficult.

The second method is the radial distribution method. The relation between $r_g(1)$ and r_{RD} is easily obtained from eq. 5 and 6 and is represented by

$$r_g(1) - r_{RD} = a/4\alpha\gamma \quad (7)$$

Therefore

$$a = [2(r_g(1) - r_{RD})/l^2](1 + 2b/l^2) \quad (8)$$

a was estimated to be 2.4 Å.$^{-1}$ by use of the observed values of $r_g(1)$, r_{RD}, and l.

The anharmonicity parameter can also be calculated from the dissociation energy by

$$a = (h^2/32\pi^2 l^4 \mu D)^{1/2} \coth(hcw/2kT) \quad (9)$$

where μ is the reduced mass and D is the dissociation energy. The value of a was found to be 1.7 Å.$^{-1}$ using $l = 0.051$ Å. (observed value), $D_o = 57.1$ kcal.[17] (spectroscopic data which was obtained from a measurement of a convergent limit), and wave number, w, which was calculated from the observed mean amplitude. The error was ±0.2 Å.$^{-1}$ in this method.

The asymmetry parameter, a, was calculated to be 2.0 Å.$^{-1}$ by two independent methods. For the calculation, the following equations were used after substituting $D_o = 57.3$ kcal.[21] (from a thermochemical measurement), $w = 565$ cm.$^{-1}$, [17] and vibrational constant $xw = 4$ cm.$^{-1}$ [17] (spectroscopic data which were obtained from a measurement of band heads)

$$a = (2\pi^2 c^2 w^2 \mu/D)^{1/2} \quad (10)$$

and

TABLE I

MOLECULAR PARAMETERS OF CHLORINE OBTAINED BY ELECTRON DIFFRACTION

$r_g(1) = 1.9928 \pm 0.0025$ Å.[a] $\quad l_e = 0.051 \pm 0.003$ Å.
$r_{RD} = 1.9917 \pm 0.0020$ Å. $\quad a = 2.0 \pm 0.4$ Å.$^{-1}$[b]
$r_e = 1.9862$ Å.

[a] The errors shown are the standard deviation from the average over four values obtained from four plates. For each plate two $r_g(1)$ values were obtained from the intensity curve and the radial distribution curve. These errors include the deviations in the values from each curve. The scale factor uncertainty in L and λ is about one part per thousand. [b] The error is the standard deviation from the average value obtained by the three methods.

TABLE II

COMPARISON OF DATA ON THE MOLECULAR STRUCTURE OF CHLORINE

Method	r_e, Å.	l_e, Å. (°K.)	a, Å.$^{-1}$
E.D.[a]	1.986	0.051 (298)	2.0
E.D.[b]	1.983	0.0446 (300)	
Spect.	1.988[c]	0.044 (298)	2.0
	1.989[d]		

[a] Present methods used. [b] See ref. 20. [c] See ref. 17. [d] See ref. 19.

(11) Collin reported 2.02 Å. from the X-ray analysis of crystalline chlorine; R. L. Collin, *Acta Cryst.*, **5**, 431 (1952).

(12) Equation 4 shows that the deviation of r_{RD} from r_e is given by $B/2H$, i.e., $(1/4\alpha)(3a - 2/r_e - a/\gamma)$.

(13) The mean amplitude obtained is l_f, which means $<(r - r_g(1))^2>^{1/2}$. Generally the notation of l means l_α in this paper.

(14) There are various definitions of mean amplitudes. The mean amplitude l here is l_e, which means $<(r - r_e)^2>^{1/2}$; see T. Morino, Y. Nakamura, and T. Iijima, *J. Chem. Phys.*, **32**, 643 (1960).

(15) As will be shown later, 0.0004 Å. was used for a cigarette holder-type nozzle and 0.0014 Å. was used for a drum-type nozzle.

(16) The correction for anharmonicity was very small and the correction to get from l_α to l_e was negligible. The effect of isotopic atom Cl^{37} on l was very small and was within experimental error.

(17) G. Herzberg, "Molecular Spectra and Molecular Structure, Diatomic Molecules," D. van Nostrand Co., Inc., Princeton, N. J., 1950. The value of r_e was recalculated by Prof. R. M. Badger from the data of A. Elliot, *Proc. Roy. Soc.* (London), **A123**, 623, 629 (1929); **A127**, 638 (1930).

(18) The correction for centrifugal stretching by rotation was omitted.

(19) W. G. Richards and R. F. Barrow, *Proc. Chem. Soc.*, 297 (1962).

(20) L. S. Bartell and K. Kuchitsu, presented at the International Conference on Magnetism and Crystallography, 1961, and L. S. Bartell, private communication, 1962.

(21) E. A. Moelwyn-Hughes, "Physical Chemistry," Pergamon Press, Ltd., London, 1957.

$$a = (8\pi^2\mu cx\omega/h)^{1/2} \quad (11)$$

It is not feasible at present to derive a reliable value of a from electron diffraction analysis, but it is interesting that the present results are in good agreement with those from spectroscopic experiments.

Instrumental Factors.—The effect of instrumental factors on the results was eliminated as far as possible in the following manner. The effect of the nozzle[22] used was checked with respect to the departures from the ideal condition of the electron diffraction experiment.

1. Background Intensity.—Two nozzles were used in the present experiment; one was a cigarette holder-type and the other was a drum-type nozzle. The observed background intensity, I_B, was compared with the theoretical background intensity when both the cigarette holder-type and the drum-type nozzles were used. The theoretical background intensity was calculated by

$$I_B = [\Phi(q, k, L)/q][(Z - f)^2 + ZS] \quad (12)$$

where $\Phi(q, k, L)$ is the correction term for the r^3 sector. As shown in Fig. 5 a better agreement between the observed background and the theoretical one was obtained when using the cigarette holder-type nozzle. The values of the theoretical and the observed background were set equal at $q = 40$. Then the maximum deviation of the observed from the theoretical background was about 3% in the outer region ($q > 25$).

2. Gas Spread.—For the cigarette holder-type nozzle the experimental background intensity was proportional to q^{-4}. This is the ideal feature. But in the case of the drum-type nozzle the intensity falls abruptly at $q \sim 50$ and the factor was found to be $q^{-4.7}$ in the range $q \sim 70$ to 100. This effect is due to screening of the scattering by a part of the nozzle. Making use of this effect, the gas spread near the drum-type nozzle was experimentally estimated from the observed background intensity. If the gas spread effect is represented by $(\pi/\sigma)^{1/2} \exp(-\sigma x^2)$ and the background function is approximated by $1/s^3$, then from the ratio of the experimental background to the theoretical background the value of σ was found to be 0.9. The feature of the gas spread is shown in Fig. 6. Then the correction[23] for mean amplitude l was estimated to be 0.0014 Å.

For the use of the cigarette holder-type nozzle, the features of gas spread also can be approximated by the gaussian function. The value of σ was assumed to be 3.0 which was obtained from Karle's data.[22] The value of 0.0004 Å. was corrected for apparent mean amplitude. Table III shows the experimental result obtained with use of both the cigarette holder type and the drum-type nozzle.

3. Movement of Scattering Center.—The $r_g(1)$ value obtained with the drum-type nozzle was about 0.003 Å. smaller than the $r_g(1)$ value obtained with the cigarette-type nozzle. This is due to the fact[24] that the asymmetry feature of the jet makes the gas distribution asymmetric along the electron beam. Therefore, it is necessary to make a correction for the atomic distances obtained with the drum-type nozzle. If the asymmetrical distribution of the gas spread is expressed by the function $(\pi/\sigma)^{1/2} \exp(-\sigma x^2)(1 + \rho x)$,[25] the apparent contraction[26] of the atomic distance

(22) The effect of a delocalized gas sample upon the atomic and molecular scattering curve was discussed by R. B. Harvey, F. A. Keidel, and S. H. Bauer, *J. Appl. Phys.*, **21**, 860 (1950), I. L. Karle and J. Karle, *J. Chem. Phys.*, **18**, 963 (1950), and L. S. Bartell, *J. Appl. Phys.*, **31**, 252 (1960).

(23) K. Kuchitsu, *Bull. Chem. Soc. Japan*, **32**, 748 (1959).

(24) This was suggested by Y. Marata of Tokyo University.

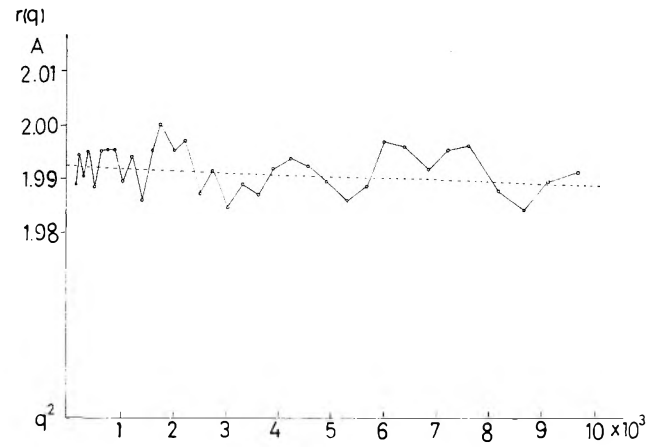

Fig. 4.—$r(q)$ plotted against q^2. The dotted line was obtained by a least square fitting.

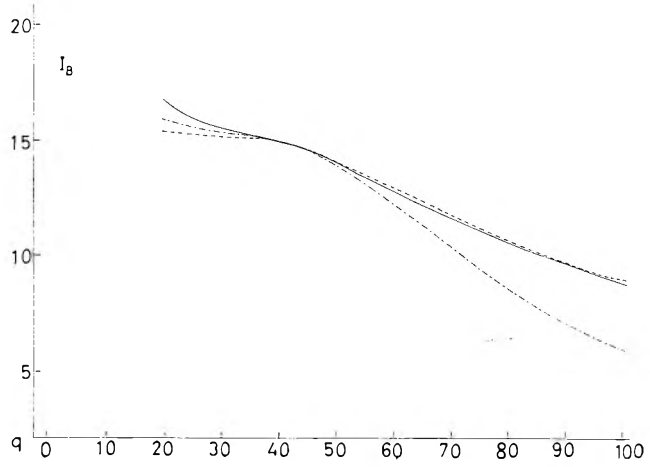

Fig. 5.—Experimental and theoretical background intensity curves: ———, for cigarette holder-type nozzle; — — —, for drum-type nozzle; ———, theoretical I_B.

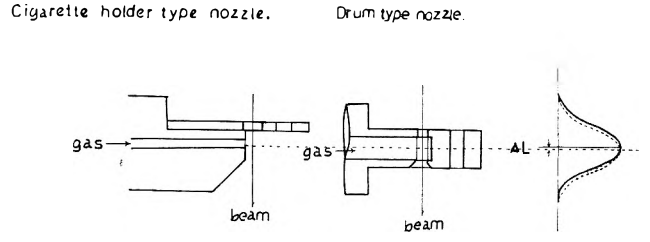

Fig. 6.—Two types of nozzles used. In the distribution curve of gas, ——— shows the actual spread and ——— shows the symmetric spread.

TABLE III

COMPARISON OF DATA OBTAINED WITH USE OF BOTH THE CIGARETTE HOLDER-TYPE AND THE DRUM-TYPE NOZZLE

Nozzle	$r_g(1)$, Å.	r_{RD}, Å.	l_c, Å.	Index of resolution
Cigarette holder-type	1.9933	1.9922	0.0518 (0.0514)	98%
Drum-type	1.9899 (1.9921)[a]	1.9889 (1.9911)[a]	0.0527 (0.0513)	96%

[a] The parenthesized numbers are the values corrected for the gas spread effect.

was estimated to be 0.0022 Å. using the observed value of 0.9.[27]

4. Beam Trap.—To see the benefits of using a beam trap, the experiment was carried out with the sector without the beam trap. The analysis of the photographs showed that the mean amplitude increased 0.002 Å. and index of resolution became 94%. But the value of $r_\rho(1)$ and r_{RD} were unchanged within the limits of experimental error.

Acknowledgment.—The author wishes to express his sincere gratitude to Professor Y. Morino for his kind advice. He is also indebted to Mr. O. Ohashi and Mr. I. Obara of Shizuoka University for their help in the analyses. This research was financially supported by the Scientific Grant from the Ministry of Education of Japan.

(25) The value of ρ was experimentally estimated to be 0.23.

(26) Due to the different form of this nozzle the correction is opposite to that proposed by Bartell (ref. 22).

(27) In this case the asymmetrical distribution was approximated by the symmetrical distribution with a shift of $\rho/2\sigma$.

DISPERSION CONDUCTIVITY THEORY APPLIED TO OXYGEN DIFFUSION IN BLOOD

BY IRVING FATT AND RICHARD C. LA FORCE

Department of Mineral Technology, University of California, Berkeley, California

Received November 16, 1962

A theory is developed for calculating steady-state diffusion flux through a dispersion in which the diffusion coefficient in the dispersed phase is dependent on the concentration of the diffusing species. The theory is based on semitheoretical conductivity equations for dispersed systems. The theory when applied to oxygen flux in blood agrees qualitatively with available experimental data. There is also agreement with a previous treatment of oxygen flux in blood where whole blood is approximated first by alternate layers of hemoglobin and plasma transverse to the diffusion path and then parallel to it. The oxygen flux calculated from the dispersion equations lies between the flux for transverse and parallel layers, indicating the reliability of the results.

Introduction

Steady-state diffusion flux of a molecular species through a dispersion is normally calculated from Fick's first law by use of an effective diffusion coefficient for the dispersed system. This diffusion coefficient is a function of the diffusion coefficient for the diffusing species in the dispersed and continuous phases and the volume fraction of dispersed phase. Theoretical equations relating effective diffusion coefficient to these system parameters are useful only for very small volume fractions of dispersed spheres. There are, however, many semitheoretical and empirical equations for the effective diffusion coefficient of dispersions. Meredith and Tobias[1] have given a summary of these equations. Many of these equations are useful for dispersions of nonspherical particles and for large volume fractions of dispersed phase.

None of the equations mentioned can be applied to dispersions in which the diffusion coefficient, in the dispersed or continuous phase, is a function of concentration of diffusing species, and yet the most common and important dispersed system, namely blood, is just such a dispersion. In a previous publication[2] we showed how to calculate upper and lower limits for the effective diffusion coefficient for oxygen in blood. In that paper we pointed out how an estimate of the oxygen transport could be made by first assuming all the hemoglobin to be in layers parallel to the direction of oxygen diffusion and then transverse to this direction. These two limiting solutions must bracket the exact solution, and, since they lie close together for oxygen partial pressures of physiological interest, they should, we believe, represent a good approximation to the exact answer.

We will show here that a semitheoretical equation given by Meredith and Tobias[1] for calculating diffusion in a simple dispersion can be used for dispersions containing a dispersed phase in which the diffusion coefficient is concentration dependent. We will use blood as an example of this kind of system and show that the effective diffusion coefficient calculated in this way lies between the limits we have previously determined. Furthermore, this calculated effective diffusion coefficient for oxygen in blood is in at least qualitative agreement with experimental data in the literature.

Theory

Blood is a dispersion of red blood cells in a homogeneous protein solution called the plasma. The red blood cells in man are biconcave disks, 7 μ in diameter and 2 μ thick. The cell is a membrane envelope filled with a hemoglobin solution. An effective diffusion coefficient for oxygen diffusion through blood cannot be calculated from the conventional equations for effective diffusion coefficients of dispersions because the diffusion coefficient for oxygen in hemoglobin solution depends upon the mean oxygen pressure. Our approach, therefore, is to divide a barrier of blood into many thin layers. Across each thin layer we assume a constant oxygen concentration for the purpose of calculating the effective oxygen diffusion coefficient. Integration over many thin layers gives the oxygen flux for a given oxygen pressure gradient and therefore yields the oxygen diffusion coefficient.

We have shown[3] that the oxygen flux per unit area through a thin barrier of hemoglobin solution is given by

$$J = \frac{D_A' a \Delta P}{\Delta x} + D_E \frac{\partial f(P)}{\partial P} \frac{\Delta P}{\Delta x} \qquad (1)$$

where J is the flux per unit area and ΔP a small oxygen

(1) R. E. Meredith and C. W. Tobias, "Advances in Electrochemistry and Electrochemical Engineering," Vol. 2, C. W. Tobias, Ed., Interscience Publishers, Inc., New York, N. Y., 1962, p. 15.

(2) R. C. La Force and I. Fatt, *Trans. Faraday Soc.*, **58**, 1451 (1962).

(3) I. Fatt and R. C. La Force, *Science*, **133**, 1919 (1961).

pressure differential across a barrier of thickness Δx. The diffusion coefficients for dissolved oxygen and oxyhemoglobin are D_A' and D_E, respectively, and the concentration of dissolved oxygen is equal to its partial pressure multiplied by the constant a. The concentration of oxyhemoglobin is not related to oxygen partial pressure by a constant, however, but by the factor $\partial f(P)/\partial P$ where $f(P)$ is the familiar hemoglobin–oxyhemoglobin dissociation curve.

From eq. 1 we may define a conductivity coefficient for oxygen flux as

$$D_A'a + D_E \frac{\partial f(P)}{\partial P} = k_d \qquad (2)$$

It is important to keep in mind that k_d is pressure dependent through the $\partial f(P)/\partial P$ term. An analogous coefficient for plasma is simply

$$D_A a = k_c \qquad (3)$$

We now consider whole blood to be a suspension of oblate spheroids of hemoglobin having conductivity k_d in plasma which has a conductivity k_c. For this calculation we assume that the red blood cell membrane is infinitely conductive to oxygen. We will later show the effect of the cell membrane if it has a finite oxygen conductivity.

Meredith and Tobias[1] have shown that an earlier equation of Bruggeman, based on an extension of Maxwell's treatment of the conductivity of a suspension of spheres, can be modified to give an expression for the conductivity of a dispersion of oblate spheroids of conductivity k_d dispersed in a continuous medium of conductivity k_c. We assume here that the red blood cell is approximately an oblate spheroid. Meredith's equation is

$$\phi = \frac{\left(\frac{k_m}{k_c} - \frac{k_d}{k_c}\right)\left(\frac{k_m}{k_c} + \alpha\frac{k_d}{k_c}\right)^{\gamma}}{\left(1 - \frac{k_d}{k_c}\right)\left(1 - \alpha\frac{k_d}{k_c}\right)^{\gamma}}\left(\frac{k_m}{k_c}\right)^{\beta} \qquad (4)$$

where k_m is the conductivity of the dispersion and ϕ the volume fraction of plasma. The volume fraction of oblate spheroids is $1 - \phi$. We shall use this result directly, making allowance for the fact that k_d is pressure dependent.

From microscopic observations and from electrical conductivity data on whole dog's blood[4] we can assume that the red blood cells are oblate spheroids with an axial ratio between 3 and 4.5. α, β, and γ were taken for convenience in calculation as 1.182, $-1/6$, and $-1/3$, respectively. The choice of these constants is somewhat arbitrary because we are using eq. 4 for particles, biconcave disks, and at particle concentrations for which this theoretical equation has not been checked against experimental data. However, the constants need only be known approximately because we are more interested here in the relation of oxygen conductivity of dispersion to oxygen pressure than in the absolute value of the conductivity. Meredith and Tobias[1] show that in the limiting case $k_d/k_c = 0$, and at $\phi = 0.50$ the electrical conductivity of a dispersion of spheres is only 20% greater than that of dog's blood. For $k_d/k_c \geq 1$, the situation existing for oxygen conductivity of a dispersion of red blood cells, the conductivity of a dispersion of nonspherical particles is

(4) H. Fricke, *Phys. Rev.*, **24**, 575 (1924).

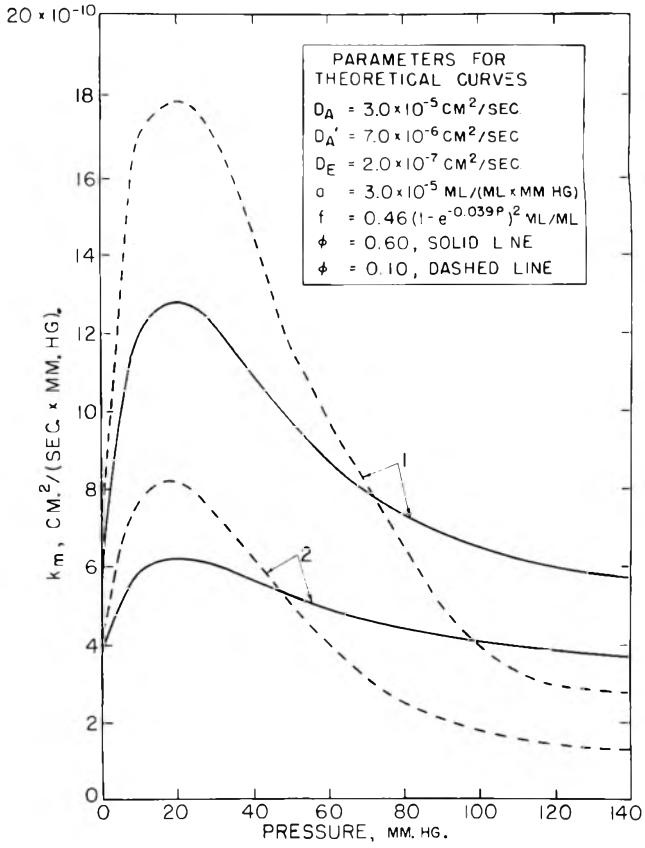

Fig. 1.—Conductivity of a dispersion as a function of pressure for whole blood: solid curves are for normal whole blood; dashed curves are for a paste of red cells; curves labeled 1 are for cells without membrane; curves labeled 2 are for cells with membrane.

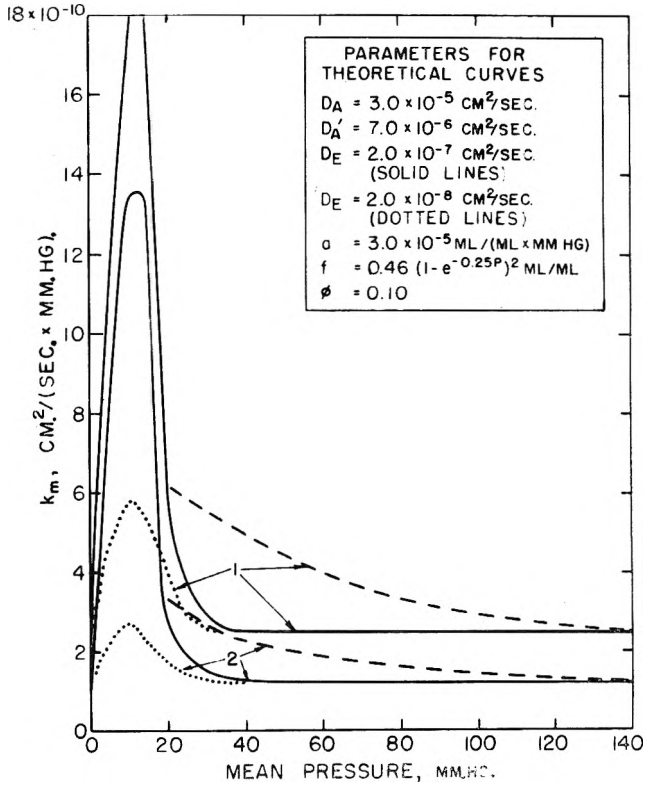

Fig. 2.—Conductivity of a red cell paste as a function of pressure calculated from eq. 4 and 8 compared to Scholander's data, dashed curve: curves labeled 1 are for cells without membrane; curves labeled 2 are for cells with membrane.

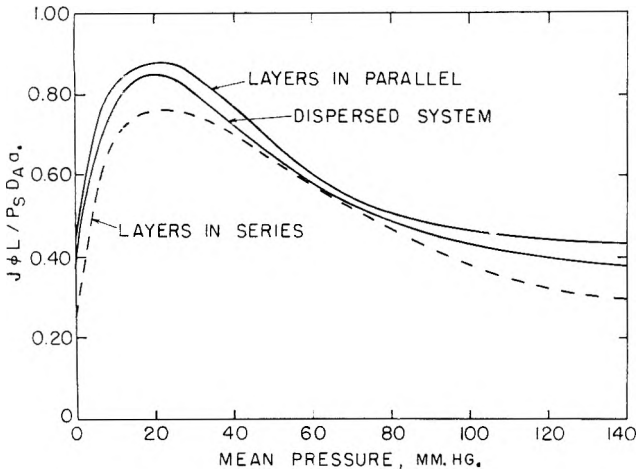

Fig. 3.—Dimensionless flux parameter as a function of mean pressure for a dispersion of hemoglobin with no cell membrane and with parameters shown in Fig. 1, for $\phi = 0.60$.

greater than that for spherical particles. However, the difference is not strongly dependent upon α, β, and γ because of the location of α in eq. 4 and because β and γ are fractional exponents.

Equation 4 must be evaluated by numerical techniques.

The values of k_d and k_c used in evaluating eq. 4 were calculated from eq. 2 and 3 using parameters which we presented in our previous work on oxygen transport in whole blood.[2] These parameters are reproduced here in the inserts of Fig. 1 and 2. Equation 4 was then solved by a trial and error procedure on a high-speed digital computer. As mentioned before, k_d will be pressure dependent because of the S-shaped dependence of $f(P)$ on P and k_m will, therefore, also be pressure dependent. We may numerically calculate the dependence of k_m on P by using, as suggested by Visser,[5] the following semiempirical expression for $f(P)$ to evaluate $\partial f(P)/\partial P$.

$$f(P) = 0.46(1 - e^{-0.039P})^2 \qquad (5)$$

The numerical coefficients in this equation give $f(P)$ for normal conditions in the human body. A plot of k_m *vs.* P for whole blood with $D_E = 2.0 \times 10^{-7}$ cm.^{2}/sec. and at body conditions is shown by the solid curves in Fig. 1. The dashed curves are for a cell volume fraction of 0.90 and demonstrate the effect of an increase in cell content. The effect of the choice of D_E will be discussed later.

Having k_m as a function of P, we can now calculate the oxygen flux J as a function of pressure drop $P_2 - P_1$ and layer thickness L for a layer of whole blood. The equation for steady-state conductivity under these conditions is

$$LJ = \int_{P_1}^{P_2} k_m \, dP \qquad (6)$$

Equation 6 may be evaluated from the curves in Fig. 1 by numerical integration. For convenience in calculation we have written eq. 6 in terms of a dimensionless flux parameter $J\phi L/P_s D_A a$ as follows.

$$\frac{J\phi L}{P_s D_A a} = \frac{\phi}{P_s D_A a} \int_{P_1}^{P_2} k_m \, dP \qquad (7)$$

(5) B. F. Visser and A. H. J. Maas, *Phys. Med. Biol.*, **3**, 264 (1959).

where $P_s = P_2 - P_1$. Some of our results will be presented in terms of this dimensionless flux.

The effect of the cell membrane on steady-state oxygen transport in whole blood may also be estimated. Data from studies[6] of oxygen diffusion through red blood cells indicate that the properties of the membrane surrounding the cell are such as to reduce oxygen flux through the cell to 40% of the flux in the absence of a membrane. Furthermore, oxygen flux in the membrane material depends only on oxygen pressure differential and not on mean oxygen pressure. Under these conditions the effect of the membrane on oxygen diffusion can be taken into account simply by multiplying k_d in eq. 4 by 0.40. Equation 4 now becomes

$$\phi = \left(\frac{\frac{k_m}{k_c} - \frac{0.40\,k_d}{k_c}}{1 - \frac{0.40\,k_d}{k_c}}\right)\left(\frac{\frac{k_m}{k_c} + \alpha\frac{0.40k_d}{k_c}}{1 + \alpha\frac{0.40k_d}{k_c}}\right)^{\gamma}\left(\frac{k_m}{k_c}\right)^{\beta} \qquad (8)$$

Equation 8 may also be evaluated by a trial and error procedure, thereby giving k_m for a suspension in plasma of oblate spheroids each containing a hemoglobin solution surrounded by a membrane. The effect of the membrane is to increase the resistance to the transport of oxygen through the spheroids. Figure 1 shows the effect of cell membrane on k_m for whole blood, $\phi = 0.60$, and for a red cell paste, $\phi = 0.10$, both at body conditions, and for $D_E = 2.0 \times 10^{-7}$ cm.^{2}/sec.

Discussion

Figure 1 shows that the effective conductivity of whole blood to oxygen is oxygen pressure dependent. k_m is at maximum where the slope is maximum on the S-shaped relation between oxygen content and pressure for hemoglobin. The effect of the cell membrane is to lower the conductivity, but the general shape remains the same. Note, however, that for $\phi = 0.60$ the ratio between k_m at high oxygen pressures, 140 mm. or above, to k_m at the peak is about 1.7 for cells with membranes and 2.2 for cells without membranes. This difference may offer a means for using experimental data to test the effect of the cell membrane. Unfortunately there is only one set of experimental data in the literature which can be used to test the theoretical curves in Fig. 1. Scholander[7] measured the ratio of oxygen to nitrogen flux at different air pressure gradients through a "paste" of washed, human red blood cells smeared on filter paper. The downstream side was always a "vacuum" (containing only water vapor). His flux ratio, presented in his Fig. 4, can be shown by a simple argument to be equivalent to our k_m multiplied by a constant. Let Scholander's ratio be J_{O_2}/J_{N_2}, then

$$\frac{J_{O_2}}{J_{N_2}} = \frac{k_m \Delta P_{O_2}}{k_{N_2} \Delta P_{N_2}} \qquad (9)$$

where k_{N_2} is the diffusion conductivity to nitrogen. But since at the downstream side $P_{O_2} = P_{N_2} = 0$

$$\frac{J_{O_2}}{J_{N_2}} = \frac{k_m P_{O_2}}{k_{N_2} P_{N_2}} \qquad (10)$$

(6) F. J. W. Roughton, "Progress in Biophysics and Biophysical Chemistry," Vol. 9, Pergamon Press, London, 1959, p. 55.

(7) P. F. Scholander, *Science*, **131**, 585 (1960).

For air $P_{O_2} = 0.25P_{N_2}$. For blood constituents k_{N_2} is not a function of pressure, therefore

$$\frac{J_{O_2}}{J_{N_2}} = \text{constant} \times k_m \qquad (11)$$

Scholander's paste was about 10% plasma,[8] $\phi = 0.10$, and the flux measurement was made at room temperature, about 25°, and in the absence of carbon dioxide. For these conditions the pH may rise to about 8 and the coefficient of P in eq. 5 is then about -0.25. A plot of the theoretical k_m from eq. 4 and 8 for these conditions is shown by the solid lines in Fig. 2 for $D_E = 2.0 \times 10^{-7}$ cm.²/sec., and by the dotted lines for $D_E = 2.0 \times 10^{-8}$ cm.²/sec. The effect of the increase in the coefficient of P in eq. 5 can be seen by comparing the dashed curves in Fig. 1 with the solid curves in Fig. 2. The increase in the coefficient does not greatly change the position of the curve on the vertical scale but does cause the peak to be sharper and the flat portion to be longer. For coefficients much larger than 0.25 the curve will tend to become flat over most of the pressure range with a sharp spike at about 15 mm.

Scholander's experimental data can be compared to our theoretical curves in Fig. 2 by matching theory and experiment at 140 mm. oxygen pressure to give the lower dashed curve in Fig. 2. All that can be said is that there is qualitative agreement.

If we assume that in Scholander's data the cell membrane does not hinder movement of oxygen, we can match his data at 140 mm. to our theoretical curve for cells without membrane. Scholander's data are then shown as the upper dashed curve in Fig. 2. Again there is qualitative agreement so that it is not possible from this treatment to evaluate quantitatively the effect of cell membrane on oxygen movement through the cell. There appears, however, to be somewhat better agreement between the experimental and theoretical curves when the theory includes a cell membrane, giving evidence that there is some effect due to the membrane.

Figure 3 shows the dimensionless flux parameter $J\phi L/P_s D_A a$ as a function of mean oxygen pressure, when the oxygen pressure gradient is 10 mm., for the dispersed system as calculated from eq. 4 and compares this curve with our previous results.[2] The flux parameter calculated here from integration of the Meredith–Tobias dispersion equation falls as it should between the curves for alternate layers of hemoglobin and plasma in series and in parallel.

One of the parameters of whole blood not yet well known is D_E, the diffusion coefficient of oxyhemoglobin in the hemoglobin solution found in the red blood cell. The comparison of Scholander's experimental data to theory using both $D_E = 2.0 \times 10^{-7}$ and 2.0×10^{-8} cm.²/sec. as shown in Fig. 2 does not permit a choice of D_E for whole blood. Additional diffusion data on whole blood, preferably a direct measurement of D_E, are needed.

Acknowledgment.—This study was supported by a U. S. Public Health Service Grant, No. H 6796, and the Miller Institute for Basic Research in Science. The authors wish to thank Dr. T. D. Mueller for programming eq. 4 and 8 for evaluation on a digital computer.

(8) P. F. Scholander, private communication.

KINETICS OF ION EXCHANGE IN THE CHELATING RESIN BIO-CHELEX 100. I. THE EXCHANGE OF THE ALKALINE EARTH IONS

BY CARLA HEITNER-WIRGUIN AND GEORGE MARKOVITS

Department of Inorganic and Analytical Chemistry, Hebrew University, Jerusalem, Israel

Received February 15, 1963

The exchange of the cations Ca, Sr, and Mg on the chelating resin Bio-chelex 100 in the hydrogen form was studied. The slow step which determines the rate of exchange of these ions is diffusion through the resin particle. The diffusion coefficients at two temperatures and the activation energies for the various cations were calculated.

Introduction

The chelating resin Bio-chelex 100 consists of a cross-linked polystyrene matrix with iminodiacetic acid, $R\text{–}N(CH_2COOH)_2$, as the functional group. In some preliminary experiments it was found that in acid solutions the resin can act as an anion exchanger at the nitrogen atom and thus may enable the study of chloro complexes. Sorption of copper chloride was studied at various concentrations of hydrochloric acid. It was shown that $CuCl_4^{2-}$ was sorbed rapidly at high concentrations of acid,[1] but very slowly in the absence of hydrochloric acid, *i.e.*, in weak acid and neutral solutions. It therefore appears that the sorption of copper proceeds by two different exchange reactions, the one an anion-exchange reaction in concentrated acid solutions and the other a very slow exchange by chelation. To explain these results, the kinetics of the exchange on the hydrogen form of the resin were studied. The cations used in this study were the alkaline earths which are known to give weak complexes with iminodiacetate in solution, and copper, which gives a very strong complex with the same anion. A kinetic study on the similar Dowex A-1 resin was effected by Turse and Rieman.[2] These authors worked with the sodium form of the resin, concluding that the slow step is the chemical exchange reaction for cations giving a chelate with the resin, while when nonchelating cations such as the alkaline ions were used, the slow step is diffusion through the particle. Schwarz[3] studied the kinetics of isotope exchange on the same Dowex A-1, Na form resin for the sodium and zinc ions in

(1) G. Markovits and C. Heitner-Wirguin, unpublished results.

(2) R. Turse and W. Rieman, III, *J. Phys. Chem.*, **65**, 1821 (1961).

(3) A. Schwarz, Thesis, Israel Institute of Technology, Haifa, 1962.

buffered solutions. He also concluded that in the case of sodium the slow step is the diffusion within the resin particles, while in the case of zinc the chemical exchange reaction is the rate-determining step. It is interesting to note that Schwarz[3] and Turse and Rieman[2] concluded that the rate-determining step is the chemical reaction for zinc and copper, although they could not obtain a linear plot for log $(1 - F)$ *vs.* t. Since the water content of the resin in the hydrogen and sodium form is different (resin volume[4] of Na^+, 1.00; H^+, 0.45), the kinetics of the exchange reactions on these two resin forms need not be identical.

Experimental

The resin used was Chelex 100 prepared by Bio-Rad Laboratories (analytical grade of the resin Dowex A-1) supplied in 50–100 mesh particles in the sodium form. The resin was converted to the hydrogen form by hydrochloric acid and washed with water until the effluents were free of chloride ions.

The capacity of the resin was determined by passing a sodium sulfate solution through samples of 0.25–0.50 g. of the resin. The hydrogen ions thus liberated were titrated with NaOH with phenolphthalein as indicator. This method gives one hydrogen ion per iminodiacetic group and the capacity found was 2.27 ± 0.02 meq. H^+/g. of an air-dried resin. The latter was analysed for nitrogen, and the following percentages were found: (a) for the hydrogen form 3.51; (b) for the sodium form 4.44. These results agree well with the determined hydrogen capacity of the resin.

The capacity of the resin as an anion exchanger was determined by equilibrium experiments with a series of solutions containing various concentrations of sulfuric acid. The sulfate concentration was determined from the equilibrium solutions, gravimetrically as $BaSO_4$. The equilibrium capacity found was about 0.4 meq. of SO_4^{2-}/g. of resin (in a 0.05 M H_2SO_4 solution).

Rates of exchange were determined in a modification of the limited bath technique.[5] Chloride salt solutions (50 ml., 1 M) of the cation or 250 ml. (0.01 M) were shaken in a thermostat until the desired temperature was reached, then 0.5 g. of Chelex 100 in the hydrogen form was added. After a given time the solutions were rapidly filtered with suction through a sintered glass funnel. On these solutions, separated at different intervals of time from various experiments, the necessary analyses were carried out to determine the extent of exchange. During these experiments the solutions were stirred vigorously (not less than 1200 r.p.m.)

Analytical Procedures.—The cations calcium, strontium, and magnesium were determined by titrations with MgEDTA using Eriochrome black as indicator.[6] Copper was determined complexometrically also, using the PAN indicator.[7]

Potentiometric titrations were carried out to ascertain that for every cation sorbed, two hydrogen ions were released. For control purposes, the cation determinations were carried out both on the solutions and on the resin (eluting the cation with nitric acid).

Particle Size of Resin.—The Chelex 100 was passed through appropriate sieves and two fractions could be separated. The radius of the particles in each fraction was determined by measuring the diameter of 100 beads on a micrometer microscope. These measurements were made on dry particles as well as on particles which had been immersed for 24 hr. in the appropriate electrolyte solution (concentration 1 M). As had been expected from the swelling data given by Dowex[4] (H^+, 0.45; Ca, 0.53), there were practically no changes in the size of the immersed particles, and the mean diameter measured was within the experimental error (about 4–5%).

Results and Discussion

As the limited bath technique was used, the equations developed by Boyd, *et al.*,[5] and improved by Reichenberg[8] were used.

The extent of reaction F is expressed as

$$F = \frac{\text{the amount of exchange at time } t}{\text{the amount of exchange at infinite time}}$$

The rate of exchange can be determined by three different steps.

(a) If the rate-determining step is diffusion through the ion-exchange particle, the following equations are valid.

$$F = 1 - \frac{6}{\pi^2} \sum_{n=1}^{\infty} \frac{\exp(-n^2 Bt)}{n^2}$$

where $B = \pi^2 D_1/r^2$, r = radius of the spherical particle, and D_1 = effective diffusion coefficient. A linear plot of Bt *vs.* t is obtained. Values of Bt for each F value are given by Reichenberg.[8]

(b) If the slow step is the diffusion through the liquid film at the resin particle boundary, then the equation reads

$$\log (1 - F) = -(R/2.303)t$$

where R is a constant defined by the parameters of the film and the diffusion coefficients of the ions through the liquid.

(c) If the rate-determining step is controlled by mass action

$$\log (1 - F) = \frac{S}{-2.303} (t)$$

where

$$S = K_1 m_{A^+} + k_2 m_{B^+}$$

It can be seen from the equations given in b and c that a plot of log $(1 - F)$ *vs.* t will be a straight line, the slope giving the constant R or S.

TABLE I

INFLUENCE OF CONCENTRATION ON THE EXTENT OF EXCHANGE OF $MgCl_2$

	F			$B \times 10^3$		
t, min.	1 M	0.75 M	0.5 M	1 M	0.75 M	0.5 M
5	0.21	0.20	0.225	8.60	7.72	9.2
10	.28	.29		8.00	8.61	9.3
15	.35	.345	17′−0.38	8.72	8.40	9.3
20	.40	.393		8.45	8.30	
45	.50	..	42′−0.52			7.9

Although the equations given by Boyd[5] were developed for the isotopic diffusion, it was later found by Dickel and Grimmeiss[8c] that the particle diffusion equation is valid for ion exchange at concentrations higher than 1 N, assuming that the composition of the external solution is constant (not time dependent).[8d] In the present case, this condition is obeyed, since the ion uptake by the resin at equilibria is very small in comparison with the total concentration (about 1×10^{-4} g.-ion) of divalent ion from a total of 5×10^{-2} g.-ion. As only a small part of the hydrogen ions on the resin are exchanged, the time dependent composition of the exchanger hardly changes either.

(4) "Dowex Chelating Resin A-1," The Dow Chemical Co., 1959.

(5) G. E. Boyd, A. W. Adamson, and L. S. Myers, Jr., *J. Am. Chem. Soc.*, **69**, 2836 (1947).

(6) (a) R. Pribil, "Complexonii in Chimia Analitica," Edit. Tehn. Bucureşti, 1961, pp. 254–255; (b) W. Biedermann and G. Schwarzenbach, *Chimia* (Aarau), **2**, 25 (1948).

(7) H. Flaschka and H. Abdine, *Chemist-Analyst*, **45**, 2 (1956).

(8) (a) D. Reichenberg, *J. Am. Chem. Soc.*, **75**, 589 (1953); (b) D. E. Conway, J. H. G. Green, and D. Reichenberg, *Trans. Faraday Soc.*, **50**, 511 (1954); (c) G. Dickel and H. Grimmeiss, *J. chim. phys.*, **55**, 269 (1958); (d) G. Dickel and E. Hübner, *Kolloid-Z.*, **179**, 60 (1961).

TABLE II

DIFFUSION COEFFICIENTS AND ENERGY OF ACTIVATION CALCULATED FOR THE EXCHANGE OF MCl_2 1 *M* ON CHELEX 100

M	Radius of particle, mm.	*B*, min.$^{-1}$ 30°	*B*, min.$^{-1}$ 50°	*D*, cm.^{2}/min. 30°	*D*, cm.^{2}/min. 50°	E_a, kcal./mole	Hydration no.
Mg^{2+}	0.134	8.43×10^{-3}	3.1×10^{-2}	1.15×10^{-7}	5.77×10^{-7}	12.8	12
Ca^{2+}	.134	1.49×10^{-2}	5.8×10^{-2}	2.72×10^{-7}	10.6×10^{-7}	14.8	10
Ca^{2+}	.171			2.77×10^{-7}			
Sr^{2+}	.134	1.69×10^{-2}	9.6×10^{-2}	3.17×10^{-7}	17×10^{-7}	17.2	10

Figure 1 represents the exchange of Ca, Sr, and Mg chlorides at two temperatures as a function of time. From the linearity of *Bt vs. t* (Fig. 2) the slow step for these cases should be diffusion through the particle. To check these results, additional experiments were done in which the radius of the particle and the concentration of the solutions were changed. From Fig. 2 it can be seen that the rate of exchange for calcium ions depends on the radius of the particle as can be expected for particle diffusion-controlled kinetics.

In Table I are represented the *F* and *B* values as a function of time for three different concentrations of $MgCl_2$ solutions. These values are within the limits of experimental error and show clearly that the rate of exchange is not dependent upon the concentration in solution. It has already been shown by Conway, *et al.*,[8] that even in the case of diffusion kinetics there is a very small increase in the rate of exchange with a decrease in concentration. This is due to the fact that the concentration affects the radius *r* of the swollen particles and probably also the diffusion coefficient D_1. Although in these experiments the concentrations chosen do not vary very much, the same tendency can be observed from the found *F* values.

The calculated values of the diffusion coefficients for three cations at two temperatures are presented in Table II. The good accordance of the diffusion coefficients calculated from experiments with two different particle sizes should be noted.

From the *D* values obtained at two temperatures, the energy of activation can be evaluated.[9]

$$\Delta\left[\ln\frac{\pi^2 D_1}{r^2} - \ln\frac{\pi^2 D_2}{r_2}\right] \Big/ \Delta\frac{1}{T} = -\frac{E_a}{R};$$

$$\frac{\Delta \ln \dfrac{D_1}{D_2}}{\Delta\dfrac{1}{T}} = -\frac{E_a}{R}$$

From these results it can be seen that the diffusion coefficients depend on the radius of the hydrated cation. The values found for the energy of activation for these reactions are unusually high compared with the values 5–10 kcal./mole obtained for the exchange of hydrogen by monovalent ions on strong cation exchangers.[8,9] This may be due to the low swelling of the resin. Experiments done at 0° showed that no exchange occurred under these conditions.

A series of kinetic measurements was also carried out for the same exchange reactions at low concentrations of the chloride salts. These results are summarized in Table III by evaluation of the three rate constants at different intervals of time. The values obtained for calcium show that it cannot be decided easily which step controls the exchange, since neither

(9) T. R. E. Kressman and J. A. Kitchener, *Discussions Faraday Soc.*, **4**, 90 (1949).

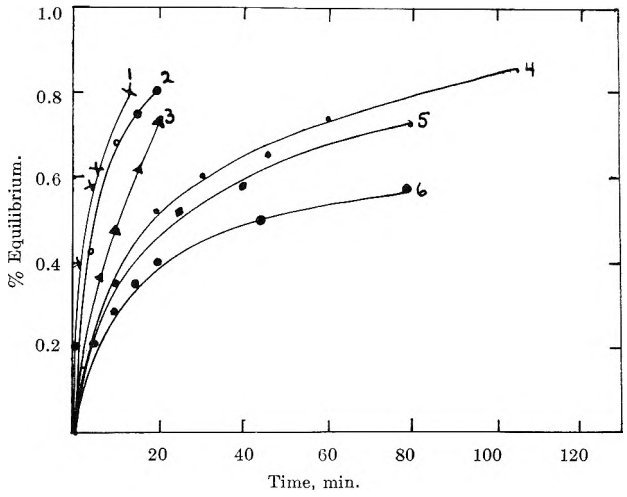

Fig. 1.—Rate of exchange adsorption of 1 *M* MCl_2 solutions: 1, Sr 50°; 2, Ca 50°; 3, Mg 50°; 4, Ca 30°; 5, Sr 26°; 6, Mg 30°.

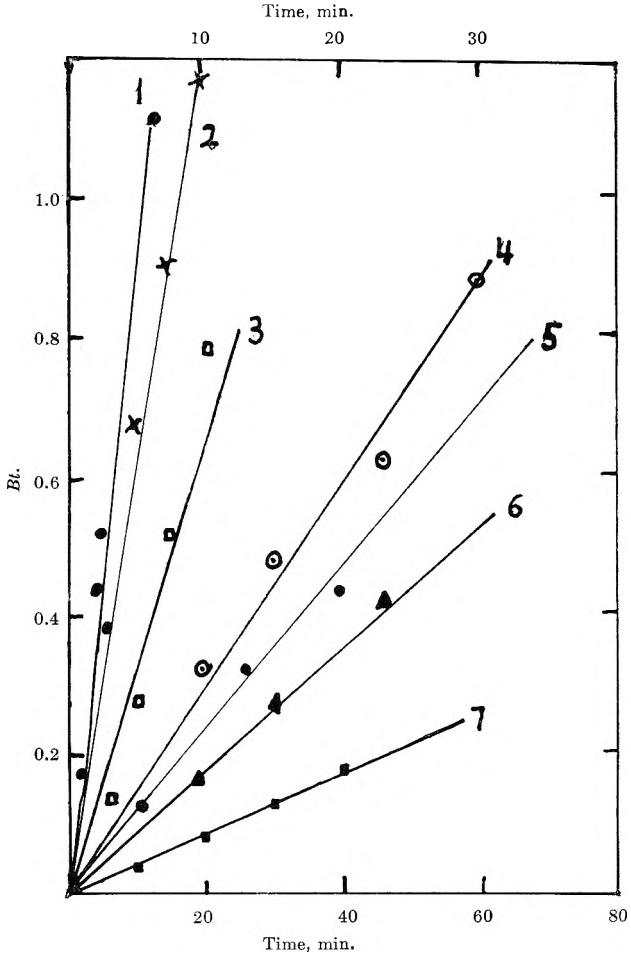

Fig. 2.—Plots of *Bt vs.* time of 1 *M* MCl_2 solutions using Chelex (r = 0.134 mm.): 1, Sr 50°; 2, Ca 50°; 3, Mg 50°; 4, Ca 30°; 5, Sr 26°; 6, Ca (r = 0.171 mm.) 30°; 7, Mg 30° (upper scale of time).

TABLE III

RATE CONSTANTS FOR THE THREE TYPES OF KINETICS EVALUATED FROM DILUTED SOLUTIONS OF MCl_2 (3×10^{-3} M)

Mg^{2+} 30°			Mg^{2+} 50°			Ca^{2+} 30°		
	$B \times 10^2$	$R(S) \times 10^2$		$B \times 10^2$	$R(S) \times 10^2$		$B \times 10^2$	$R(S) \times 10^2$
Min.	min.$^{-1}$	min.$^{-1}$	Min.	min.$^{-1}$	min.$^{-1}$	Min.	min.$^{-1}$	min.$^{-1}$
6	2.18	3.11	3	8.60	9.20	5	1.24	2.50
10	1.99	2.40	5	9.60	8.00	6	1.91	2.90
16	1.56	1.56	7	9.25	5.41	8	2.35	2.86
24	1.59	1.09	10	9.44	6.20	10	3.01	3.01
36	1.51	1.20	15	8.15	4.95	13	3.36	2.90
83	1.78	1.02				17	3.59	2.75
						20	4.15	2.84

B, R, nor S are true constants. In the case of magnesium, the results are much clearer, the B values being more constant than the R or S values. This relative constancy is even better shown at 50°, and it may be assumed that the diffusion through the particle controls the exchange also in diluted solutions. (However, experiments with $MgCl_2$ done with two different particle sizes showed no clear proportionality between B values and the square of the radii or between R values and the first power of the particle radii.)

From these results it can be concluded that in the case of the cations investigated, the rate-determining step is the diffusion through the particle. These results do not agree with those found for calcium and magnesium by Turse and Rieman.[2] They found that the rate-controlling step is a second-order chemical reaction. The main difference between the present study and that of Turse and Rieman[2] consists in the fact that the latter worked with the sodium form of the resin, where swelling is more than twice as strong as in the hydrogen form used here. The rate of exchange in their case is therefore much higher. It is possible that under their experimental conditions the diffusion through the swollen particle is much quicker, and therefore the chemical reaction determines the rate of exchange. Experiments similar to those reported here were also carried out with copper solutions. The exchange of copper is much slower than that of the alkaline earths, which might be explained by the different extent of ionic or covalent bond in the different complexes. The results for the kinetics of copper exchange as well as a complete discussion will be published separately.

THE THEORY OF ELECTRON SCATTERING FROM MOLECULES. II. MOLECULAR HYDROGEN[1a]

BY R. A. BONHAM AND T. IIJIMA[1b]

Department of Chemistry, Indiana University, Bloomington, Indiana

Received March 6, 1963

Expressions for the differential cross sections for the total electron scattering (including all inelastic processes) and the elastic electron scattering from molecular hydrogen have been derived. The total molecular intensity has been computed with both the Wang and Weinbaum molecular wave functions and the effect of the chemical bond on these calculations is discussed. The binding effects should contribute only small corrections to the usual interpretation of diffraction results for the case of H_2 unless extremely small angle scattering data were available.

The elastic differential scattering cross section for molecular hydrogen has been calculated by Massey,[2a] Massey and Mohr,[2b] Roscoe,[3] and McWeeny[4] using the first Born approximation and neglecting polarization and exchange effects. Unfortunately, the results presented in the first paper are too general to be readily applicable to the discussion at hand, while the second paper contains a number of small errors and is not sufficiently general to allow easy extension to other cases. The paper by McWeeny[4] is concerned only with the X-ray form factor of an H atom in an H_2 molecule in a fixed orientation in space. Also, Massey and Mohr's[2b] and Roscoe's[3] evaluations of the main term containing the effect of chemical binding were not exact.

We have calculated the total intensity of electrons scattered by molecules using the same approximations discussed previously and employing both the Wang wave function[5] and the Weinbaum wave function.[6] We have also succeeded in evaluating all but one of the necessary integrals in simple closed forms and it has been evaluated numerically.

1. General Theory

The general theory of electron scattering from molecules has already been discussed[7,8] and so will only be recapitulated here.

The total intensity of electrons scattered from a polyatomic molecule can be expressed as

$$I = (4/a^2r^2s^4) \sum_T g_T W_T \sum_V W_V < \psi_{VT}| \int d\Omega_0 \sum_{n=1}^{N} \sum_{m=1}^{N} \{Z_nZ_m - Z_nF_m^* - Z_mF_n + S_{nm}\} \exp[i\vec{s}\cdot\vec{r}_{nm}]| \psi_{VT} > \quad (1.0)$$

with

$$F_n = \sum_{i=1}^{Z_n} \int d\tau |\psi_e|^2 \exp[i\vec{s}\cdot\vec{r}_{in}] \quad (1.1)$$

and

$$S_{nm} = \sum_{i=1}^{Z_n} \sum_{j=1}^{Z_m} \int d\tau \, |\psi_e|^2 \exp[i\vec{s}\cdot(\vec{r}_{in} - \vec{r}_{jm})] \quad (1.2)$$

(1) (a) Contribution Number 1150 from the Chemical Laboratories of Indiana University; (b) the authors wish to thank the United States Air Force Office of Scientific Research and the United States Atomic Energy Commission for their financial support.

(2) (a) H. S. W. Massey, *Proc. Roy. Soc.* (London), **A129**, 616 (1930); (b) H. S. W. Massey and C. B. O. Mohr, *ibid.*, **A135**, 258 (1932).

(3) R. Roscoe, *Phil. Mag.*, **26**, 32 (1938).

(4) R. McWeeny, *Acta Cryst.*, **5**, 463 (1952).

(5) S. C. Wang, *Phys. Rev.*, **31**, 579 (1928).

(6) S. Weinbaum, *J. Chem. Phys.*, **1**, 593 (1933).

(7) T. Iijima, R. A. Bonham, and T. Ando, *J. Phys. Chem.*, **67**, 1472 (1963).

(8) L. S. Bartell, private communication.

These foregoing integrations are carried out over all the electronic coordinates, $\vec{r}_{nm}$ being an interatomic vector; ψ_e, the molecular wave function; $|\vec{s}|$, the usual scattering variable; $\vec{r}_{in}$, the vector between the ith electron and the nth nucleus; the W's, the usual Boltzmann weighting factors; ψ_{VT}, the vibrational wave function including centrifugal distortion effects, Z_n, the atomic number of the nth nucleus; $\int d\Omega_0$, the usual classical average over all orientations of the molecule; and g_T, the degeneracy of the Tth rotational state.

2. The Wang Wave Function for H_2

The aforementioned formulas can easily be applied to the Wang wave function for the H_2 molecule which can be written[5] in the general form

$$\psi_e = (1/N)[u_A(1)u_B(2) + u_A(2)u_B(1)] \quad (2.0)$$

where, if the u_A-values and u_B-values are normalized, the normalization factor N can be written as

$$N^2 = 2(1 + s_{AB}^2) \quad (2.1)$$

where s_{AB} is the overlap integral. If $u_A(1)$ and $u_B(2)$ have the forms $\exp[-Zr_{A1}]/\alpha$ and $\exp[-Zr_{B2}]/\alpha$ where α is the normalization constant for the u-values, the overlap integral can be written in terms of the bond length r_{AB} as[6]

$$s_{AB} = \exp[-Zr_{AB}](1 + Zr_{AB} + Z^2r_{AB}^2/3) \quad (2.2)$$

Substituting the square of eq. 2.0 into eq. 1.0, the F and S functions are found to reduce to

$$F_A = f_H(1 + \exp[-\vec{s}\cdot\vec{r}_{A1}]) + 2s_{AB}g_A \quad (2.3)$$

$$F_B = f_H(1 + \exp[+\vec{s}\cdot\vec{r}_{A1}]) + 2s_{AB}g_B \quad (2.4)$$

$$S_{AA} = S_{BB} = 1 \quad (2.5)$$

$$S_{AB} = N^2f_H^2(1 + \exp[-2i\vec{s}\cdot\vec{r}_{AB}]) + 2N^2g_Ag_B^* \quad (2.6)$$

and

$$S_{BA} = N^2f_H^2(1 + \exp[2i\vec{s}\cdot\vec{r}_{AB}]) + 2N^2g_A^*g_B \quad (2.7)$$

where

$$f_H = (1/N^2\alpha^2)\int d\tau \exp[-2Zr + i\vec{s}\cdot\vec{r}] = 8Z^4/[(1 + s_{AB}^2)(4Z^2 + s^2)^2] \quad (2.8)$$

$$g_A = (1/N^2\alpha^2)\int d\tau \exp[-Z(r + |\vec{r} + \vec{r}_{AB}|) + i\vec{s}\cdot\vec{r}] \quad (2.9)$$

and

$$g_B = \exp[i\vec{s}\cdot\vec{r}_{AB}]\,g_A \quad (2.10)$$

The last integral cannot be evaluated in closed form but the double integrals

$$\int d\Omega_0\, g_B = \int d\Omega_0\, g_A = (1/2)\exp[-Zr_{AB}]f_H \times \{(1 - 4Z^2/s^2)\sin sr_{AB}/sr_{AB} - (4Z/s^2r_{AB})\cos sr_{AB} + 4Z(1 + Zr_{AB} + s^2r_{AB}/2Z)/(s^2r_{AB})\} \quad (2.11)$$

can be.[9] The details of the evaluation of this integral are presented in Appendix I.

(9) We are indebted to Professor Marc Ross of the Indiana University Physics Department for pointing out this fact.

The total intensity for scattering for H_2 can now be written in the form

$$I = (4/a^2r^2s^4)\sum_T g_TW_T\sum_V W_V < \psi_{VT}|\int d\Omega_0\{[4 - 8f_H - 4s_{AB}(g_A + g_A^* + g_B + g_B^*) + 4N^2g_Ag_A^*] + [2 - 8f_H + 4N^2f_H^2]\cos[\vec{s}\cdot\vec{r}_{AB}]\}|\psi_{VT}> \quad (2.12)$$

which after averaging over all the rotations reduces to

$$I = (4/a^2r^2s^4)\{[4 - 8f_H - 16s_{AB}(\exp[-Zr_{AB}]f_H \times (2Z + 2Z^2r_{AB} + s^2r_{AB}/2)/(s^2r_{AB}))] + [2 - 8f_H + 4N^2f_H^2 - 16s_{AB}(\exp[-Zr_{AB}]f_H(1 - 4Z^2/s^2)/2)] \times (\sin[sr_{AB}]/(sr_{AB})) + 16s_{AB}(\exp[-Zr_{AB}] \times f_H(2Z/s^2r_{AB}))\cos[sr_{AB}] + 4N^2\int d\Omega_0\, g_Ag_A^*\} \quad (2.13)$$

We here omit the vibrational average $<\psi_{VT}|\ldots|\psi_{VT}>$, restricting the discussion to a rigid model of the molecule, because our purpose is to determine the effect of the binding electrons upon scattering intensity and because these effects appear only at small s-values where the effect of molecular vibration is not appreciable. The vibrational average of the dominant internuclear term, $\sin(sr_{AB})/sr_{AB}$, has been worked out by many authors.[10-12] The vibrational averages of other terms containing r_{AB} are safely given by replacing r_{AB} by $<r_{AB}>$, because the vibrational corrections to these terms are of higher order.

The last integral in eq. 2.13 is the only integral we have not been able to evaluate in a simple closed form, but we have evaluated it numerically, after reducing it to the form

$$\int d\Omega_0 g_Ag_A^* = (16\pi^2/N^4\alpha^4)\sum_{n=0}^{\infty}(2n + 1) \times \left[\int_0^{\infty} dr\, r^2\exp[-Zr]\,j_n(sr)\,(d/dZ)Z \times \begin{cases} j_n(iZr)\,h_n(iZr_{AB}) \\ j_n(iZr_{AB})\,h_n(iZr) \end{cases}\right]^2 \begin{matrix} r_{AB} > r > 0 \\ \infty > r > r_{AB} \end{matrix} \quad (2.14)$$

The functions $j_n(x)$ and $h_n(x)$ are the spherical Bessel functions of the first kind and the third kind,[13] and the details of the numerical integration are given in Appendix II. It is of interest to point out that in the limit as $s \to 0$, $\int d\Omega_0 g_Ag_A^*$ in eq. 2.14 has the value $s_{AB}^2/2(1 + s_{AB}^2)$.

3. The Weinbaum Function for H_2

The Weinbaum wave function for H_2 can be written as

$$\psi_e = (1/N')[\{u_A(1)u_B(2) + u_A(2)u_B(1)\} + \mu\{u_A(1)u_A(2) + u_B(1)u_B(2)\}] \quad (3.0)$$

where the factor μ determines the contribution of the ionic structures. After rather simple manipulation similar to that in section 2, the total intensity is found to be

(10) L. S. Bartell, *J. Chem. Phys.*, **23**, 1219 (1955).
(11) K. Kuchitsu and L. S. Bartell, *ibid.*, **35**, 1945 (1961).
(12) R. A. Bonham and J. L. Peacher, *ibid.*, **38**, 2319 (1963).
(13) Morse and Feshbach, "Methods of Theoretical Physics," Part II, McGraw-Hill Book Co., Inc., New York, N. Y., 1953, p. 1465.

$$I = (4/a^2r^2s^4) \sum_T g_T W_T \sum_V W_V < \psi_{VT} | \int d\Omega_0 \{[4 - 8f_H a_1 + 4f_H^2 N^2 a_2 - 4s_{AB}(g_A + g_A^* + g_B + g_B^*)a_4 + 4N^2 f_H(g_A + g_A^* + g_B + g_B^*)a_5 + 4N^2 g_A g_A^* a_6] + [2 - 8f_H a_1 + 4N^2 f_H^2 a_3] \cos [\vec{s}\cdot\vec{r}_{AB}]\} | \psi_{VT} > \quad (3.1)$$

corresponding to eq. 2.12. The factors a_1, a_2, . . . and a_6 are given as

$$a_1 = \gamma(1 + 2\mu s_{AB} + \mu^2)$$
$$a_2 = \gamma\mu^2$$
$$a_3 = \gamma$$
$$a_4 = \gamma(1 + 2\mu/s_{AB} + \mu^2)$$
$$a_5 = \gamma\mu$$
$$a_6 = \gamma(1 + \mu^2)$$

with $\gamma = 1/(1 + 4\mu s_{AB}/(1 + s_{AB}^2) + \mu^2)$. Equation 3.1 reduces to the results presented in section 2 when μ is zero.

4. The Case of Elastic Electronic Scattering

If a velocity analyzer is used with sufficient resolving power to separate electronic energy losses but not the associated vibrational and rotational energy losses,[14,15] then the intensity is given by the expression

$$I' = (4/c^2r^2s^4) \sum_T g_T W_T \sum_V W_V < \psi_{VT} | \int d\Omega_0 | \sum_{n=1}^{N} \{Z_n - F_n\} \exp [i\vec{s}\cdot\vec{r}_n]|^2 | \psi_{VT} > \quad (4.0)$$

Equation 4.0 can be readily reduced to the form

$$I' = (4/a^2r^2s^4) \sum_T g_T W_T \sum_V W_V < \psi_{VT} | \int d\Omega_0 \{[2 - 8f_H + 8f_H^2 + 16s_{AB}^2 g_A g_A^* - 4s_{AB}(g_A + g_A^* + g_B + g_B^*) + 8s_{AB} f_H(g_A + g_A^* + g_B + g_B^*)] + [2 - 8f_H + 8f_H^2] \cos [\vec{s}\cdot\vec{r}_{AB}]\} | \psi_{VT} > \quad (4.1)$$

the notation being the same as in section 2, and then into the form

$$I' = (4/c^2r^2s^4)\{[2 - 8f_H + 8f_H^2 - 16s_{AB}(\exp[-Zr_{AB}])f_H(1 - 2f_H)(2Z + 2Z^2 r_{AB} + s^2 r_{AB}/2)/(s^2 r_{AB})] + [2 - 8f_H + 8f_H^2 - 16s_{AB}(\exp[-Zr_{AB}])f_H(1 - 2f_H)(1 - 4Z^2/s)/2] \sin [sr_{AB}]/(sr_{AB}) + 16s_{AB}(\exp[-Zr_{AB}])f_H(1 - 2f_H)(2Z/s^2 r_{AB}) \times \cos [sr_{AB}] + 16s_{AB}^2 \int d\Omega_0 g_A g_A^*\}, \quad (4.2)$$

by making use of the integrals evaluated in section 2, and performing the rotational average. The corresponding expressions for the Weinbaum wave function can be obtained by replacing f_H by $a_1 f_H$ and s_{AB} by $a_4 s_{AB}$ in (4.1) and (4.2). The amplitude of $M(s)$, the *reduced* molecular intensity, is very nearly twice as great for the *elastic* scattering by H_2 as for the *total* scattering as discussed in section 2. While this is an exceedingly important point for H_2, the enhancement of $M(s)$ in the elastic case should not be so pronounced for molecules containing atoms of larger atomic number.

(14) J. Karle, *J. Chem. Phys.*, **35**, 963 (1961).
(15) D. A. Swick, *Rev. Sci. Instr.*, **31**, 525 (1960).

5. Numerical Calculations

Because the terms in eq. 2.14 for $n \geq 1$ result in terms involving the exponential integral which include both atomic (incoherent) contributions and molecular (coherent) contributions, it is impossible to define $M(s)$ rigorously in the usual manner. We have chosen to illustrate the effects of chemical binding by presenting the total intensity leveled by the conventional atomic scattering background function. Note that although the contribution of the $n = 1$ term in (2.14) is small in comparison to the $n = 0$ term, it is still exceedingly important, because the contribution from the $n = 0$ term is largely canceled by the other terms in eq. 2.13.

Scattering functions calculated for the hydrogen molecule from the expressions presented so far for both the total scattering (including both elastic and inelastic scattering) and the elastic scattering alone with both the Wang and the Weinbaum wave functions are shown in Fig. 1–5. They are compared with the curves for the case of negligible bonding distortion, *i.e.*, for the wave function

$$\psi_e = u_A(1)u_B(2) \quad (5.0)$$

As mentioned earlier, the division of the intensity functions by the atomic scattering background for the distortionless case allows a sensitive comparison of the various intensity curves in the small-s region.[16]

The bonding distortion has two aspects, the introduction of new terms in the electron distribution corresponding to covalent and partial ionic structure and a change in the value of the Z-parameter for the molecular wave functions. Fig. 1, 2, and 4 show the first effect, the curves for the distortionless case (eq. 5.0) having been calculated with the respective Wang and Weinbaum Z-values. In Fig. 3 and 5, the distortionless curves were calculated with the hydrogen-atom value, namely $Z = 1/a$, with a the Bohr radius.

The numerical values of the parameters used in the molecular wave functions are shown in Table I.[17]

TABLE I

THE VALUES OF THE MOLECULAR WAVE FUNCTION PARAMETERS USED IN THE CALCULATIONS

	Z	μ
Wang[a]	$1.166/a$	
Weinbaum[b]	$1.193/a$	0.256

a = 0.5292 Å. (the Bohr radius); r_{AB} = 0.7417 Å[c]

[a] See ref. 5. [b] See ref. 6. [c] See ref. 17.

The numerical procedures were checked by comparing the first term in the calculation of the expansion of $\int d\Omega_0 g_A g_A^*$ with the analytical result for $|\int d\Omega_0 g_A|^2$. The total intensity ratios were also checked by deriving expressions valid at $s = 0$ (see Appendix III for the details) for the total intensity ratios. These expressions were evaluated numerically, although they can be evaluated in a closed analytical form, and compared with the extrapolated values of the various intensity ratio curves.

(16) It should be mentioned that the assumption[7] $s_{if} = s$ should still hold good at $s = 0.1$ for 40-kv. electrons though the effects of polarization may be important in this region.
(17) G. Herzberg, "Molecular Spectra and Molecular Structure," D. Van Nostrand Co., New York, N. Y., 1950.

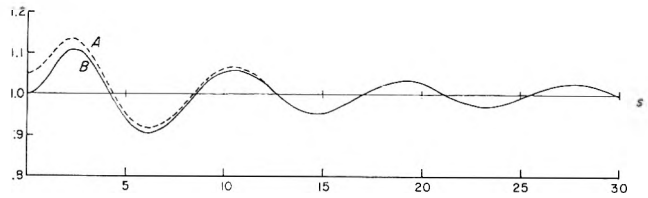

Fig. 1.—Total intensity of H_2 for total scattering leveled by the atomic scattering intensity of two independent hydrogen atoms. I: A, results for the Wang function leveled with the molecular Z-value; B, results for the independent atom model leveled with the molecular Z-value.

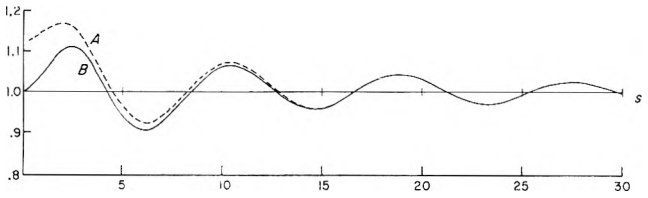

Fig. 2.—Total intensity of H_2 for total scattering leveled by the atomic scattering intensity of two independent hydrogen atoms. II: A, results for the Weinbaum function leveled with the molecular Z-value; B, results for the independent atom model leveled with the molecular Z-value.

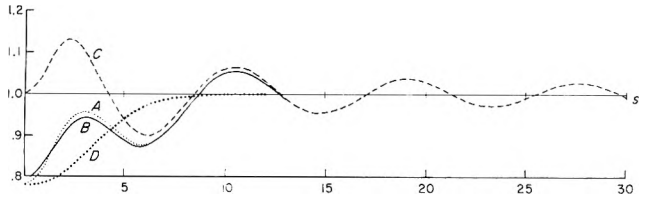

Fig. 3.—Total intensity of H_2 for total scattering leveled by the atomic scattering intensity of two independent hydrogen atoms. III: A, result for the Wang function leveled with the atomic Z-value; B, result for the Weinbaum function leveled with the atomic Z-value; C, result for the independent atom model leveled with the atomic Z-value; D, the approximate background which would have to be used to make the M(s) by A or B match the M(s) by C.

6. Conclusions

It is impossible to divide the contribution of chemical binding to the total intensity into coherent and incoherent parts. However, Fig. 3 and 5 show the predicted result for the leveled total intensity if the theoretical background by the independent atom theory is chosen as the leveling function. It is clear that the effects of binding could be largely eliminated by the proper drawing of the background function if the data were to extend to only $s = 5$ or so. The standard procedures of analysis of the data would introduce small errors into both the index of resolution and the mean amplitude of vibration because of the uncertainty in drawing the background. For the case of H_2, the least squares fitting of the experimental data would probably give a value for the index of resolution of 1.10~1.20 and a value for the mean amplitude smaller than the correct value by 0.002 Å. For larger molecules, it would appear that these corrections should be even smaller. It thus seems that the consideration of binding is not important in the routine structural analysis of larger molecules. In the event that scattering data for H_2 extending into $s \cong 1$ could be obtained, it might be possible to see the binding distortions discussed in this paper. The dotted line in Fig. 3 indicates the background which would have to be used to make the experimental M(s) match the theoretical M(s) given by the independent atom theory.

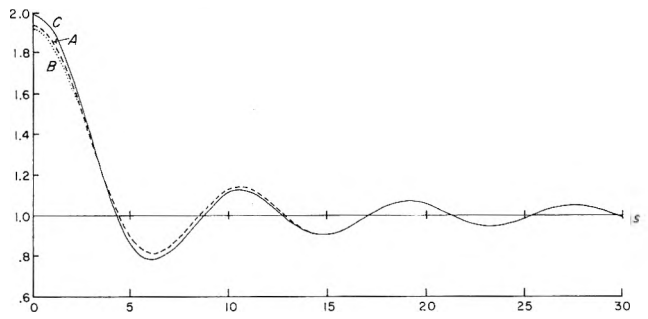

Fig. 4.—Total intensity of H_2 for elastic scattering leveled by the atomic scattering intensity of two independent hydrogen atoms. I: A, result for the Wang function leveled with molecular Z-value; B, result for the Weinbaum function leveled with molecular Z-value; C, result for the independent atom model leveled with molecular Z-value. (Note: Since the leveling function is not the same for A and B, because of the different values of the Z-parameter, these curves show the relative comparisons of A and C, and B and C, but not of A and B.)

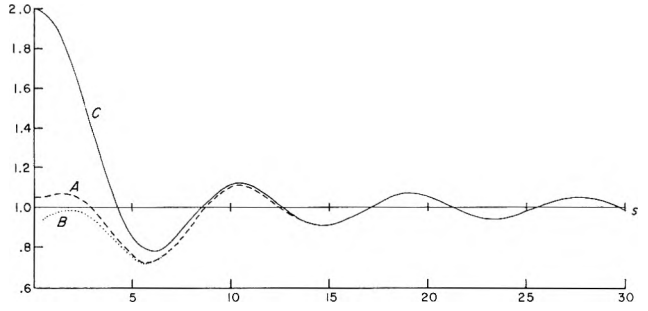

Fig. 5.—Total intensity of H_2 for elastic scattering leveled by the atomic scattering intensity of two independent hydrogen atoms. II: A, result for the Wang function leveled with atomic Z-value; B, result for the Weinbaum function leveled with atomic Z-value; C, result for the independent atom model leveled with atomic Z-value.

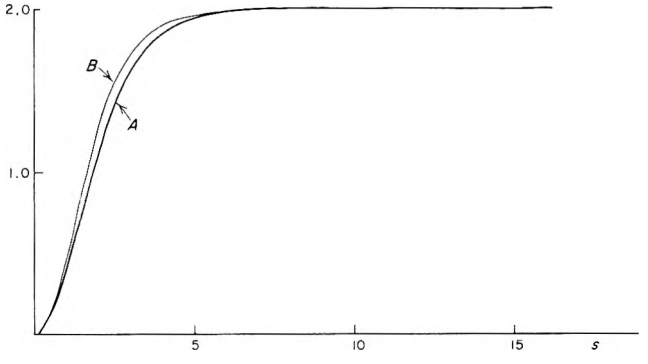

Fig. 6.—Inelastic scattering factor for H_2, *i.e.*, $(a^2r^2/4)[s^4I^{\text{TOTAL}} - s^4I^{\text{ELASTIC}}]$: A, by the Weinbaum function; B, by the independent atom model (where Z-value is that for an H atom, $1/a$).

Figure 5A shows the correct result for the intensity $H_2/2H$ given by Massey and Mohr.[2] The deviations between the results presented here and the earlier work are due mainly to the approximations used by Massey and Mohr in evaluating the terms g_A and $g_A{}^*g_A$.

We have shown elsewhere[18] that the error in using a Wang type variational wave function for H_2^+, rather than the exact one, introduces an uncertainty of 24% in the magnitude of the calculated correction on the average for the region $s = 1$ to 5. In Fig. 7 a comparison of the diagonal component of the first-order

(18) T. Iijima and R. A. Bonham, *J. Phys. Chem.*, in press.

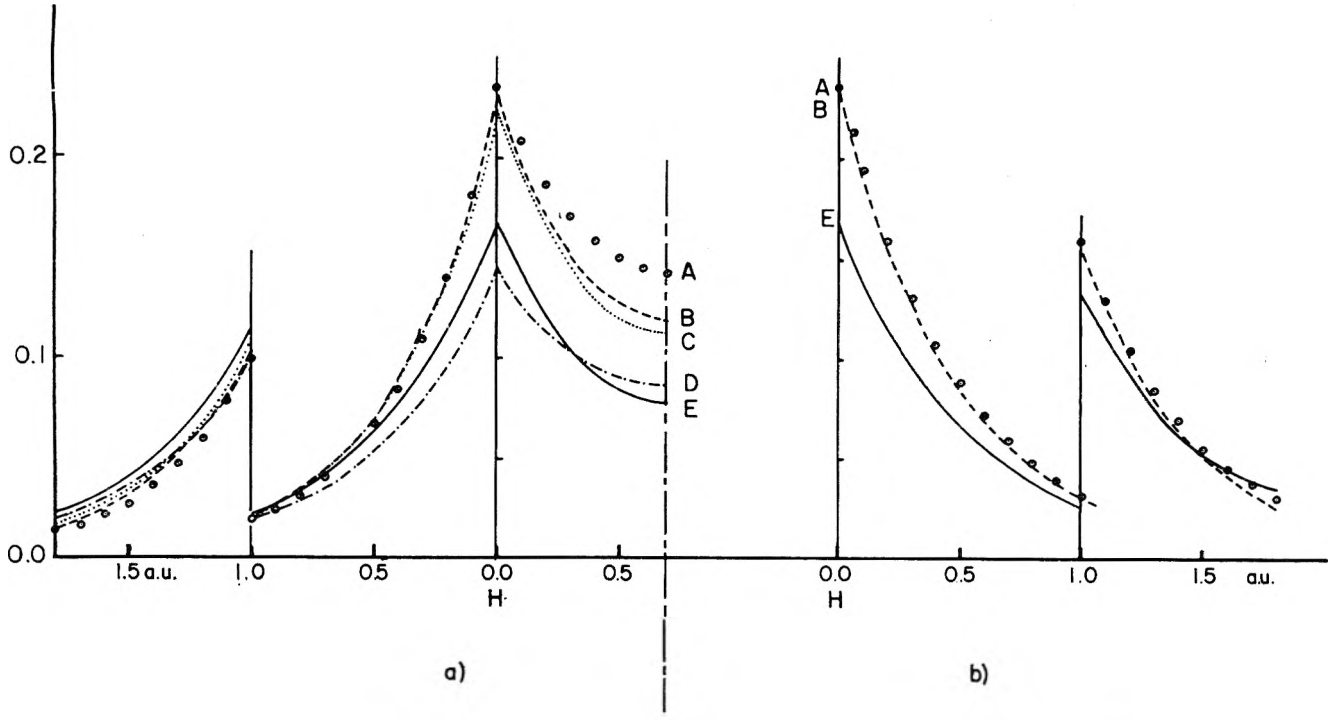

Fig. 7.—Diagonal component of first-order density matrices of the hydrogen molecule for various wave functions: (a) along the bond axis and (b) perpendicular to the bond axis at a nucleus (note that magnified portions have been multiplied by a factor of 5): A, Hagstrom (binding energy, 99% of observed value); B, Weinbaum (ionic) (86%); C, Wang (80%); D, Heitler–London (66%); E, two hydrogen atoms.

density matrices for the wave functions used in our calculations is made with a reasonably accurate wave function for H_2.[19] It seems apparent from Fig. 7 and our previous work on H_2^+ that the Weinbaum wave function should give at least 80% of the correction due to binding. The directions of the deviations between the accurate and approximate wave functions for H_2^+ and H_2 suggest that the use of a more exact wave function for H_2 in the calculations presented here would lead to an additional decrease of the total intensity at small scattering angles.

It is, of course, possible that polarization might introduce some uncertainties in our results at small angles. The neglect of exchange, on the other hand, should not affect these results as exchange should be important only at larger scattering angles.[20] The use of higher Born approximations has been discussed by Hoerni[21] and, although he neglected binding, it would appear that corrections due to higher terms in the Born series should be quite small for the case of molecular hydrogen.

The effect of binding on the inelastic scattering factor has been calculated by taking the difference between the intensities for the total scattering and elastic scattering cases. It appears that the cross section for total scattering is decreased more by binding than the cross section for the elastic scattering. This is reflected in the decrease in the inelastic scattering factor shown in Fig. 6. This is in agreement with the calculations of Roscoe.[22]

In Fig. 1, 2, and 4, the scattered intensity has been leveled by using the independent atom background function using the effective Z for the molecule. These results are compared with those of Fig. 3 and 5 and indicate that distortions in the scattering intensity due to changes in the effective Z-value are large and determine nearly all of the observed deviations due to binding.

The total scattering cross section inferred from the results in Fig. 1 and 2 indicate a relative increase in the cross section which is due to the presence of the cross terms, $u_A(1)u_B(1)$, in the electron density. This is more than offset, however, by the change in the effective Z-values which leads to a reduction in the physical size of the molecule as compared to the size of two spherical hydrogen atoms the same distance apart. Of course, the decomposition of the binding distortions and their identification with particular terms of the wave function is arbitrary. However, the general conclusion that the size of the molecule has decreased in the course of binding and is to blame for the observed changes seems to be valid. This can easily be understood by comparing the electron density of a single hydrogen atom with the density of a single electron in the hydrogen molecule (see Fig. 7). In the case of the molecule, the electron density is enhanced in the neighborhood of the bond and especially near the nuclei at the expense of decreasing the density on the sides of the nuclei away from the bond. This contraction of charge is considered to be more or less essential in the formation of the covalent bond.[23]

7. Acknowledgments.—The authors wish to thank Professors L. S. Bartell, Harrison Shull, Marc Ross, and Stanley Hagstrom for helpful comments. Thanks are also due the Indiana University Research Computing Center for the use of their facilities and Mrs. Connie Williams for her help in preparing the manuscript.

(19) S. Hagstrom, to be published.
(20) R. A. Bonham, *J. Chem. Phys.*, **36**, 3260 (1962).
(21) J. Hoerni, *Phys. Rev.*, **102**, 1530 (1956).
(22) R. Roscoe, *Phil. Mag.*, **31**, 349 (1941).
(23) K. Ruedenberg, *Rev. Mod. Phys.*, **34**, 326 (1962).

8. Appendix I

The Integral $\bar{g}_A = \int g_A d\Omega_0$

As has been presented in eq 2.9, the integral g_A is defined as

$$g_A = (1/N^2\alpha^2) \int \exp[-Zr] \exp[-Z|\vec{r} + \vec{r}_{AB}|] \times \exp[i\vec{s}\cdot\vec{r}]d\tau \quad (8.0)$$

where $\vec{r}$ is the vector from the nucleus A to a point in the volume element to be integrated over and $\vec{r}_{AB}$ is the vector from the nucleus B to A. The magnitude $|\vec{r} + \vec{r}_{AB}|$ is simply the distance between the nucleus B and the point specified by the vector $\vec{r}$. The second exponential term can be expanded in Legendre polynomials as

$$\exp[-Z|\vec{r} + \vec{r}_{AB}|] = \exp[-Z\sqrt{r^2 + r^2_{AB} + 2rr_{AB}\cos u}] = \sum_{n=0}^{\infty} (-1)^n(2n + 1)f_n(r,r_{AB})P_n(\cos u) \quad (8.1)$$

with[24]

$$f_n(r,r_{AB}) = (d/dZ)\bar{Z}j_n(ix)h_n(iy)$$
$$x = Zr,\ y = Zr_{AB},\ r_{AB} \geq r > 0$$
$$x = Zr_{AB},\ y = Zr,\ r > r_{AB} \quad (8.2)$$

Here u is the angle between the two vectors $\vec{r}$ and $\vec{r}_{AB}$. The phase factor can also be expanded in the series[24]

$$\exp[i\vec{s}\cdot\vec{r}] = \sum_{k=0}^{\infty} (2k + 1)\, i^k P_k(\cos\theta)\, j_k(sr) \quad (8.3)$$

where θ is the angle between $\vec{s}$ and $\vec{r}$. By letting the vector $\vec{s}$ be the polar axis, the directions of the vectors $\vec{r}$ and $\vec{r}_{AB}$ are expressed by means of polar coordinates (θ, ϕ) and (θ_0, ϕ_0), respectively. Then we have[25]

$$P_n(\cos u) = P_n(\cos\theta)P_n(\cos\theta_0) + 2\sum_{m=1}^{n}\{(n - m)!/(n + m)!\} P_n^m(\cos\theta)P_n^m(\cos\theta_0)\cos[m(\phi - \phi_0)] \quad (8.4)$$

and

$$d\tau = dr r^2\, d\theta \sin\theta\, d\phi$$

By using eq. 8.1, 8.3, and 8.4, eq. 8.0 can be reduced to

$$g_A = (4\pi/N^2\alpha^2) \int dr r^2 \exp[-Zr] \sum_{n=0}^{\infty} (-1)^n(2n + 1)i^n P_n(\cos\theta_0)\, f_n(r,r_{AB})\, j_n(sr) \quad (8.5)$$

after integration over θ and ϕ. By further averaging over the orientation of $\vec{r}_{AB}$ in space, $\bar{g}_A$ is obtained as

$$\bar{g}_A = (4\pi/N^2\alpha^2) \int dr r^2 \exp[-Zr]\, f_0(r,r_{AB})\, j_0(sr) \quad (8.6)$$

because the average of $P_n(\cos\theta_0)$ vanishes except for $n = 0$.

The radial integration of eq. 8.6, carried out analytically, leads to the final result

$$\bar{g}_A = (1/2)\exp[-Zr_{AB}]\, f_H[4Z(1 + Zr_{AB} + r_{AB}s^2/4Z)/s^2r_{AB} + (1 - 4Z^2/s^2)\sin sr_{AB}/sr_{AB} - (4Z/s)\cos sr_{AB}/sr_{AB}] \quad (8.7)$$

where f_H is given by eq. 2.8.

The integral g_B is given by eq. 8.0 with $-\vec{r}_{AB}$ in place of $+\vec{r}_{AB}$. Then the factor $(-1)^n$ in eq. 8.1 and 8.5 disappears, but this does not change eq. 8.7, since only the $n = 0$ term remains in either case after averaging over all orientations. We then have the result

$$\bar{g}_B = \bar{g}_A \quad (8.8)$$

9. Appendix II

The Integral $N^2 \int d\Omega_0 g_A g_A^*$

By means of eq. 8.5, we have

$$N^2 g_A g_A^* = (16\pi^2/N^2\alpha^4)[\int dr\, r^2 \exp[-Zr] \sum_{n=0}^{\infty} (2n + 1)\, i^n P_n(\cos\theta)_0\, f_n(r,r_{AB})\, j_n(sr)][\int dr\, r^2 \times \exp[-Zr] \sum_{k=0}^{\infty} (2k + 1)(-i)^k P_k(\cos\theta_0)\, f_k(r,r_{AB})\, j_k(sr)] \quad (9.0)$$

By averaging this over the orientation of $\vec{r}_{AB}$, the integral $N^2 \int g_A g_A^* d\Omega_0$ can be obtained as

$$N^2 \int d\Omega_0 g_A g_A^* = (16\pi^2/N^2\alpha^4) \sum_{n=0}^{\infty} (2n + 1) \times [\int dr\, r^2 \exp[-Zr]\, f_n(r,r_{AB})\, j_n(sr)]^2 \quad (9.1)$$

We evaluated this integral numerically, as only the first term of the summation over n can be integrated analytically. It is simply $N^2\bar{g}_A^2$.

The expansion coefficient $f_n(r, r_{AB})$ given by eq. 8.2 is successively generated by the following recursion formula

$$f_n(r, r_{AB}) = (2n + 1)H_n - I_n - J_n \quad (9.2)$$

with

$$H_n = -[(2n - 1)^2/xy]H_{n-1} + H_{n-2} + [(2n - 1)/x^2]I_{n-2} + [(2n - 1)/y^2]J_{n-2}$$

$$I_n = (2n + 1)H_n - (x/y)J_{n-1}$$

$$J_n = (2n + 1)H_n - (y/x)I_{n-1}$$

and

$$H_0 = (-1/xy)\exp[-y]\sinh x$$

$$I_0 = (-1/y)\exp[-y][(\sinh x)/x - \cosh x]$$

$$J_0 = (-1/x)\exp[-y](\sinh x)(1 + 1/y)$$

$$H_1 = [(1 + y)/xy^2]\exp[-y][(\sinh x)/x - \cosh x]$$

and with

$$x = Zr,\ y = Zr_{AB} \quad r_{AB} \geq r > 0$$
$$x = Zr_{AB},\ y = Zr \quad r \geq r_{AB}$$

The optimum values of r_{max} and Δr for the radial sum were found by comparing the term for $n = 0$ with the value calculated by the analytical expression for $N^2\bar{g}_A^2$. The values $r_{max} = 4.00$ Å. and $\Delta r = 0.05$ Å. were found to give a value correct to better than one part per ten thousand.

(24) *Cf.* reference 13, Chapter 11.
(25) *Cf.* reference 13, Chapter 10.

As shown in Table II, the contributions from terms for n higher than 3 or 4 were found to be negligibly small.

Although the results reported in this work are based on the value of this integral calculated by using the parameters listed in Table I, the integral was also evaluated for several other sets of parameter values as tabulated in Table III, in order that it might be of some help in future work.

TABLE II

THE CONTRIBUTIONS OF TERMS OF HIGHER n TO THE INTEGRAL $N^2 \int d\Omega_0 g_A g_A^*$

s	n_{max}	Value of $N^2 \int d\Omega_0 g_A g_A^*$ (Z = 1.166/a, r_{AB} = 0.7417 Å.)
0.5	0	0.14955
	1	.15127
	2	.15127
	3	.15127
3.0	0	.01673
	1	.02417
	2	.02519
	3	.02527
	4	.02527

TABLE III

VALUES OF THE INTEGRALS $N^2 \int d\Omega_0 g_A g_A^* \times 10^4$ A^3

Z	s = 0.5	1.0	1.5	2.0	2.5	3.0	3.5	4.0	4.5	5.0
					r_{AB} = 0.75 Å.					
1.6	1773	1305	815	450	229	111	52	26	11	5
2.0	1604	1302	935	606	364	206	112	59	31	16
2.4	1383	1186	925	664	445	281	170	99	57	32
2.8	1145	1016	836	642	464	318	209	132	81	49
					r_{AB} = 1.00 Å.					
1.6	1461	1054	636	335	161	73	32	13	6	2
2.0	1184	943	657	408	232	123	62	30	14	7
2.4	891	751	570	393	250	149	84	45	23	12
2.8	631	550	441	326	225	146	90	52	30	16
					r_{AB} = 1.25 Å.					
1.6	1134	799	464	232	104	43	17	7	3	1
2.0	797	662	418	247	132	65	30	13	6	2
2.4	508	419	308	203	122	68	35	17	9	4
2.8	299	256	199	141	92	50	32	17	9	4
					r_{AB} = 1.50 Å.					
1.6	830	570	317	149	62	23	8	3	1	0
2.0	474	376	243	136	68	31	13	5	2	1
2.4	261	211	149	94	53	27	13	6	2	1
2.8	127	106	80	54	33	19	10	5	2	1
					r_{AB} = 1.75 Å.					
1.6	574	383	203	89	34	12	4	1	0	0
2.0	284	211	130	69	32	13	5	2	1	0
2.4	124	98	67	40	21	10	4	2	1	0
2.8	50	41	30	19	11	6	3	1	1	0
					r_{AB} = 2.00 Å.					
1.6	378	244	123	50	18	5	2	0	0	0
2.0	155	112	66	33	14	5	2	1	0	0
2.4	56	43	28	16	8	3	1	1	0	0
2.8	18	15	10	6	3	2	1	0	0	0

10. Appendix III

The Intensity Ratio in the Limit $s \to 0$

The expressions of the scattered intensity in the limit $s \to 0$ are obtained by expanding the phase factors in eq. 1.1 and 1.2 in a power series in s, as

$$\lim_{s\to 0} I^T = (6/a^2r^2s^2) \int d\Omega_0 [\langle z_{1A}^2 \rangle + \langle z_{1A}z_{2B} \rangle] \quad (10.0)$$

for the total scattering, and

$$\lim_{s\to 0} I^E = (4/a^2r^2) \int d\Omega_0 [\langle z_{1A}^2 \rangle^2 + \langle z_{1A} \rangle^2 r_{AB}^2 \cos^2 \theta_0 + 2 \langle z_{1A}^2 \rangle \langle z_{1A} \rangle r_{AB} \cos \theta_0] \quad (10.1)$$

for the elastic scattering,[26] respectively, with

$$\langle z_{1A}^2 \rangle = \int d\tau_1 |\psi_e|^2 z_{1A}^2$$

$$\langle z_{1A} \rangle = \int d\tau_1 |\psi_e|^2 z_{1A}$$

and

$$\langle z_{1A}z_{2B} \rangle = \int d\tau_1 d\tau_2 |\psi_e|^2 z_{1A}z_{2B}$$

The z-axis is taken in the direction of the s-vector, *i. e.*

$$z_{1A} = \vec{r}_{1A} \cdot \vec{s} \quad (10.2)$$

and so on. The fact that the molecule is nonpolar, *i.e.*, the electron distribution has a center of symmetry, has greatly simplified eq. 10.0 and 10.1.

By carrying out the angular integration and averaging over the orientation of $\vec{r}_{AB}$ in space, and by using the Wang function, eq. 10.0 and 10.1 are reduced to

$$\lim_{s\to 0} I^T = (6/a^2r^2s^2)(4Z^3/3N^2)\{J + J(0420) + 2s_{AB}J(1410) - 4Z^3(J(0321)^2 + 2J(1311)^2)\} \quad (10.3)$$

$$\lim_{s\to 0} I^E = (4/a^2r^2)(16Z^6/9N^4)\{J^2 + J(0420)^2 + (4/5)J(0422)^2 + 2JJ(0420) + 4s_{AB}JJ(1410) + 4s_{AB}J(0420)J(1410) + (16s_{AB}/5)J(0422)J(1412) + 4s_{AB}^2J(1410)^2 + (16s_{AB}^2/5)J(1412)^2 + (9/5)r_{AB}^2[J(0321) + 2s_{AB}J(1311)]^2 - 2r_{AB}[J + J(0420) + 2s_{AB}J(1410) + (4/5)J(0422) + (8/5)s_{AB}J(1412)][J(0321) + 2s_{AB}J(1311)]\} \quad (10.4)$$

The integral $J(klmn)$ is defined as

$$J(klmn) = \int_0^\infty \exp[-kZr] f_n(mZ, r_{AB}, r) r^l dr$$

and J is

$$J = \int_0^\infty \exp[-2Zr] r^4 dr = (3/4Z^5)$$

The $J(klmn)$ values were integrated numerically in a manner similar to that mentioned in Appendix II.

The intensities for the distortionless case and for the independent atom model were obtained in a similar manner from the wave function given by eq. 5.0 as

$$\lim_{s\to 0} I_A^T = (6/a^2r^2s^2)(4Z^3/3)J \quad (10.5)$$

and

$$\lim_{s\to 0} I_A^E = (4/a^2r^2)(16Z^6/9)J \quad (10.6)$$

By eq. 10.3–10.6 the intensity ratios $\lim_{s\to 0} I^T/I_A^T$ and $\lim_{s\to 0} I^E/I_A^E$ were calculated for curve A in Fig. 1 and 3–5 and gave agreement to three significant figures with the extrapolated values.

(26) For the case where the molecule has a dipole moment, eq. 10.1 becomes $\lim_{s\to 0} I^T = 4\mu^2/3a^2r^2s^2$ where μ is the dipole moment of the molecule.

MERCURY-PHOTOSENSITIZED DECOMPOSITION OF ALIPHATIC HYDROCARBONS—RADICAL DETECTION WITH ETHYL-CARBON-14 RADICALS[1]

BY RICHARD A. HOLROYD AND GEORGE W. KLEIN

Radiation Research Laboratories, Mellon Institute, Pittsburgh, Pennsylvania

Received March 8, 1963

Ethyl-C^{14} radicals have been utilized as a scavenger to identify and measure the yields of the radicals produced in the mercury-photosensitized decomposition of propane, *n*-butane, isobutane, *n*-pentane, isopentane, neopentane, cyclopentane, *n*-hexane, 2-methylpentane, 2,2-dimethylbutane, and 2,3-dimethylbutane. This technique is ideal for this purpose since hydrogen atoms are available to generate the scavenger $C_2{}^{14}H_5$ radicals from ethylene-C^{14}, and high intensities prevail favoring combination reactions of radicals with $C_2{}^{14}H_5$ radicals. The relative quantum yields of the radicals (R) formed in the primary process are determined from the yields of labeled hydrocarbons, $RC_2{}^{14}H_5$. For example, in the case of 2-methylpentane the dissociation yields are 58% CH_3–$\dot{C}(CH_3)$–C_3H_7, 28% CH_3–$CH(CH_3)$–$\dot{C}H$–CH_2–CH_3, 14% CH_3–$CH(CH_3)$–CH_2–$\dot{C}H$–CH_3, and <1% isohexyl plus 2-methylpentyl. It is shown that in mercury sensitization of these hydrocarbons a tertiary hydrogen atom is 350 times, and a secondary hydrogen atom 65 times, more reactive than a primary hydrogen atom. Carbon–carbon bond cleavage does not occur. The quantum yields are close to unity for most hydrocarbons studied. Mercury sensitization of hydrocarbons is a source of a variety of secondary and tertiary alkyl radicals. In reacting with these radicals, $C_2{}^{14}H_5$ radicals will both disproportionate and combine. For example, $C_2{}^{14}H_5 + R \xrightarrow{k_4} RC_2{}^{14}H_5$ and $C_2{}^{14}H_5 + R \xrightarrow{k_5} C_2{}^{14}H_6 + R(-H)$. Where R is a secondary radical, k_5/k_4 is found to be between 0.20 and 0.27; where R is a tertiary radical, k_5/k_4 is from 0.54 to 0.74. A linear relationship is observed between log k_5/k_4 and ΔS, the difference in entropy of the products of these two reactions.

Introduction

Recent studies[2–5] of the mercury-photosensitized decomposition of aliphatic hydrocarbon vapors have indicated that the over-all primary process may be represented by reaction 1 although the exact mechanism

$$Hg^* + RH \longrightarrow R\cdot + H + Hg \qquad (1)$$

remains in doubt.[3] The relative frequency of formation of primary, secondary, and tertiary alkyl radicals has been determined only in a few cases. The purpose of the present study is to establish the identity of the radicals produced from various hydrocarbons and to determine their relative yields by using ethyl-C^{14} radicals as the scavenger.[6] This technique is ideally suited to the study of mercury-photosensitized reactions of hydrocarbons since hydrogen atoms are available to generate the scavenger $C_2{}^{14}H_5$ radicals from ethylene-C^{14} present in low concentrations, reaction 2, and high intensities prevail favoring radical combination reactions. Hydrogen abstraction from the hydrocarbon by

$$H + C_2{}^{14}H_4 \longrightarrow C_2{}^{14}H_5 \qquad (2)$$

$$H + RH \longrightarrow H_2 + R\cdot \qquad (3)$$

$$C_2{}^{14}H_5 + R\cdot \longrightarrow RC_2{}^{14}H_5 \qquad (4)$$

hydrogen atoms, reaction 3, also occurs but is necessarily suppressed by the presence of ethylene so that the radicals scavenged in reaction 4 are largely those produced by reaction 1. The relative yield of the labeled hydrocarbon $R_iC_2{}^{14}H_5$ measures the relative quantum yield of radical R_i.

Reaction 4 will be accompanied by the disproportionation reactions 5 and 5′.

$$C_2{}^{14}H_5 + R\cdot \longrightarrow C_2{}^{14}H_6 + R(-H) \qquad (5)$$

$$\longrightarrow C_2{}^{14}H_4 + RH \qquad (5')$$

A variety of secondary and tertiary radicals may be formed by sensitization of various hydrocarbons and the ratios k_5/k_4 for these radicals then are determined from the yields of the labeled hydrocarbon products. Such data on disproportionation reactions of ethyl radicals are unavailable at present except where *k* is either ethyl, isopropyl, or *t*-butyl.

Values for the ratio k_5'/k_4 cannot be obtained from this study since the products of reaction 5′ are identical with the initial reactants.

In addition to reactions 1 through 5, ethyl-C^{14} radicals and parent radicals, R, will react as in reactions 6–9. The presence of ethylene inhibits the

$$2C_2{}^{14}H_5 \longrightarrow C_4{}^{14}H_{10} \qquad (6)$$

$$\longrightarrow C_2{}^{14}H_4 + C_2{}^{14}H_6 \qquad (7)$$

$$2R\cdot \longrightarrow R_2 \qquad (8)$$

$$\longrightarrow RH + R(-H) \qquad (9)$$

occurrence of secondary reactions of hydrogen atoms with unsaturates formed in reaction 9. These secondary reactions in general are complicating factors in more conventional studies of the photosensitized decompositions of hydrocarbons.[4,5]

Results are presented here of a study of the photosensitized decomposition of propane, *n*-butane, isobutane, *n*-pentane, isopentane, neopentane, cyclopentane, *n*-hexane, 2-methylpentane, 2,2-dimethylbutane, and 2,3-dimethylbutane.

Experimental

The hydrocarbon and ethylene-C^{14} were added to a 220-ml. quartz reaction vessel, 5 cm. in diameter and 12 cm. long. The temperature of the cell was 25 ± 1° and the reactants were allowed to stand 15 min. prior to irradiation to ensure complete mixing. No stirrer was used. A low pressure mercury resonance lamp was placed 4 cm. from the front window of the reaction cell. A Corning 7910 filter was used to remove the 1849 Å. resonance line. The absorbed light intensity was approximately the same for all experiments. Cyclopentane, for which ϕ_H

(1) Supported in part by the U. S. Atomic Energy Commission; presented at the 144th National Meeting of the American Chemical Society, Los Angeles, Calif., April, 1963.

(2) R. A. Back, *Can. J. Chem.*, **37**, 1834 (1959).

(3) E. W. R. Steacie, "Atomic and Free Radical Reactions," 2nd Ed., Reinhold Publ. Corp., New York, N. Y., 1954.

(4) R. A. Back, *Trans. Faraday Soc.*, **54** 512 (1958).

(5) R. J. Cvetanovic, W. E. Falconer, and K. R. Jennings, *J. Chem. Phys.*, **35**, 1225 (1961).

(6) R. A. Holroyd and G. W. Klein, *J. Appl. Radiation Isotopes*, **13**, 493 (1962); *J. Am. Chem. Soc.*, **84**, 4000 (1962).

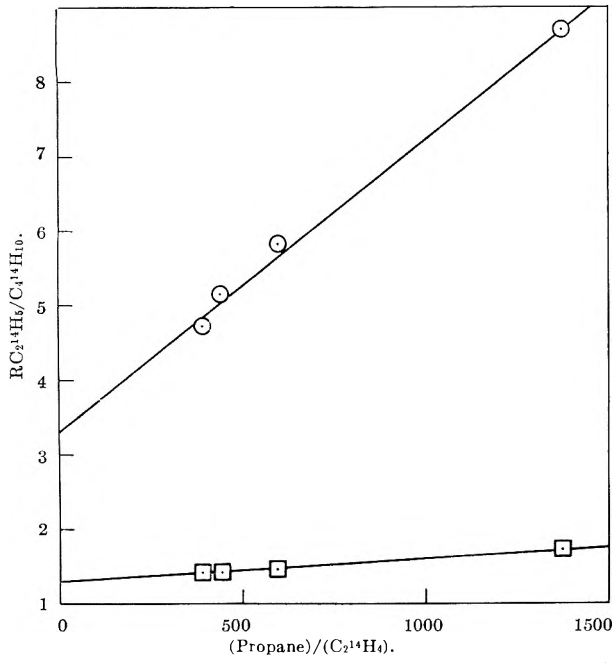

Fig. 1.—Propane. $RC_2{}^{14}H_5/C_4{}^{14}H_{10}$ *vs.* (propane)/($C_4{}^{14}H_4$): ⊙, $RC_2{}^{14}H_5$ is isopentane-C^{14}; ⊡, $RC_2{}^{14}H_5$ is *n*-pentane-C^{14}.

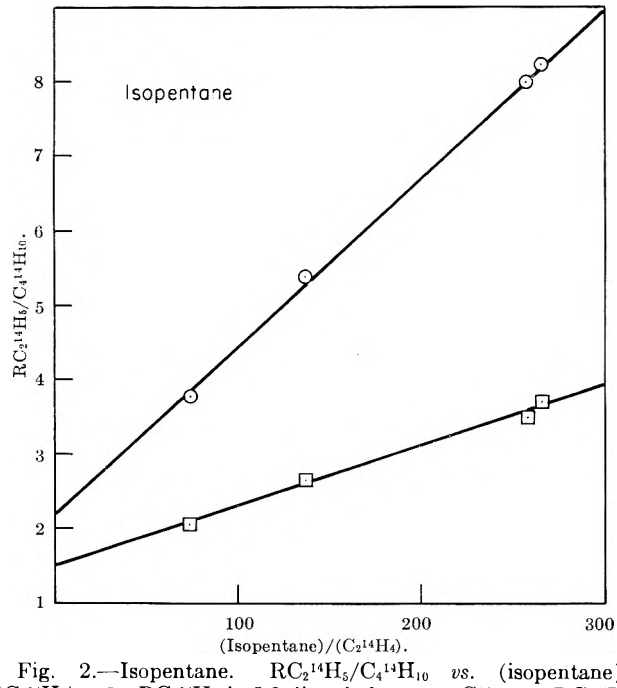

Fig. 2.—Isopentane. $RC_2{}^{14}H_5/C_4{}^{14}H_{10}$ *vs.* (isopentane)/($C_2{}^{14}H_4$): ⊙, $RC_4{}^{14}H_5$ is 3,3-dimethylpentane-C^{14}; ⊡, $RC_2{}^{14}H_5$ is 2,3-dimethylpentane-C^{14}.

= 0.8, was used as an actinometer.[7] The conversion in all runs was approximately 0.05% of the hydrocarbon and from 1 to 2% of the ethylene.

All hydrocarbons used were Phillips research grade and were purified previous to use by passage through a silica gel column to remove unsaturates. Only the first fraction eluted was used and in all cases the unsaturated impurity was <0.003 mole %. The ethylene-C^{14}, obtained from New England Nuclear Corp., was purified by gas chromatography and diluted with Phillips research grade ethylene to a specific activity of ~0.05 mc./mmole.

The concentration of the hydrocarbon in the cell was between 3 and 23 mmoles/l. The ethylene-C^{14} concentration was low enough so that quenching of Hg* by ethylene was minimal. The reaction mixture was analyzed by gas chromatography. A 40-ft. column was used, four-fifths of which was packed with 25% Dow-Corning silicone grease on celite and one-fifth of which contained specially prepared silica gel. Only the yields of the

(7) R. L. Strock and H. E. Gunning, *Can. J. Chem.*, **38**, 2295 (1960).

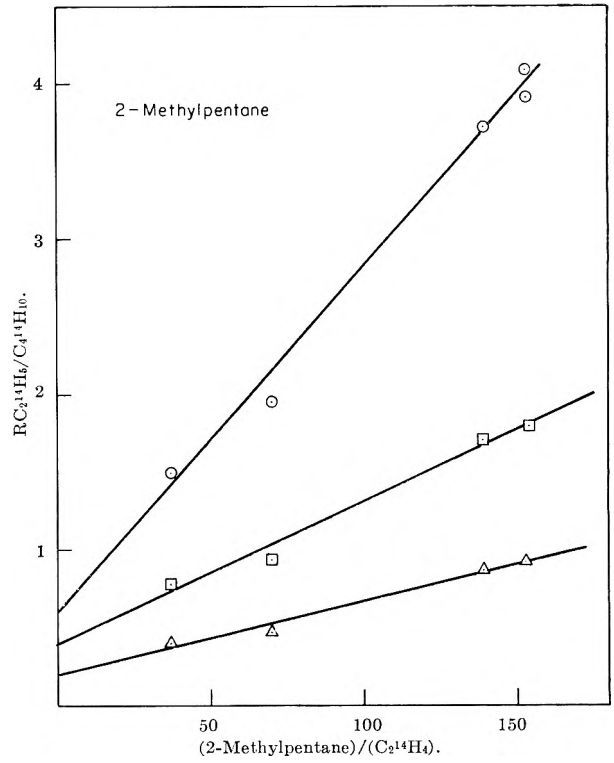

Fig. 3.—2-Methylpentane. $RC_2{}^{14}H_5/C_4{}^{14}H_{10}$ *vs.* (2-methylpentane)/($C_2{}^{14}H_4$): ⊙, $RC_2{}^{14}H_5$ is 3,3-dimethylhexane; ⊡, $RC_2{}^{14}H_5$ is 2-methyl,3-ethylpentane; △, $RC_2{}^{14}H_5$ is 2,4-dimethylhexane.

C^{14}-labeled products were determined. Detectable amounts of hydrogen and dimeric products were formed, but no quantitative measure of these yields was obtained. Further details of the analytical technique have been described elsewhere.[6] In most cases each labeled hydrocarbon was identified by addition of nonradioactive carrier to the sample for comparison of retention times. In a few cases carriers were not available and identification was inferred from the retention time only.

Results and Discussion

The results are summarized in Tables I through VI and in Fig. 1, 2, and 3. For all hydrocarbons studied the labeled products of the photosensitized decomposition were ethane-C^{14}, butane-C^{14}, and from one to three hydrocarbons formed by reaction of an ethyl-C^{14} radical with the parent radicals produced in reactions 1 and 3. Fragment radicals were not observed. This supports the generally accepted view that carbon–carbon bond cleavage does not occur.[3]

TABLE I

PROPANE

$C_2{}^{14}H_4$, μmoles/l.	(C_3H_8)/($C_2{}^{14}H_4$)	Rate, nanomoles/sec. C_2H_6	C_4H_{10}	*i*-C_5H_{12}	*n*-C_5H_{12}	k_5/k_4	k_3/k_2 × 10^3
17.6	389	...	0.305	1.14	0.127	..	1.6
12.0	438	0.288	.258	1.07	.107	0.23	1.6
11.5	595	.236	.217	1.05	.101	.20	1.5
14.9	1370	...	.119	0.916	.088	..	2.9

TABLE II

BUTANE

$C_2{}^{14}H_4$, μmoles/l.	(C_4H_{10})/($C_2{}^{14}H_4$)	Rate, nanomoles/sec. C_2H_6	C_4H_{10}	3-Methylpentane	*n*-Hexane	k_6/k_4
16.0	1350	0.183	~0.045	0.749	0.036	0.23
6.95	2750	.104	~0	.448	.021	.23
5.05	5150	.064	~0	.269	.0084	.24

No labeled products of molecular weight greater than that of $RC_2{}^{14}H_5$ were observed in any case. Therefore,

TABLE III

n-PENTANE

		Rate, nanomoles/sec.						
$C_2{}^{14}H_4$, μmoles/l.	$(C_6H_{12})/(C_2{}^{14}H_4)$	C_2H_6	C_4H_{10}	3-Methyl hexane	3-Ethyl pentane	*n*-Heptane	k_5/k_4	$k_3/k_2 \times 10^3$
106	75	0 421	0.521	0.831	0.608	0.031	0.25	3.8
55.2	285	298	.174	.631	.426	...	.26	4.2
74.5	268	.471	.368	1.02	.729	.11[a]	.24	3.4
41.9	477	25	.127	0.565	.391	.020	.25	3.4

[a] This experiment was done with the unfiltered light from the resonance lamp.

TABLE IV

ISOBUTANE

			Rate, nanomoles/sec					
C_4H_{10}, mmoles/l.	$C_2{}^{14}H_4$, μmoles/l.	$(C_4H_{10})/(C_2{}^{14}H_4)$	C_2H_6	C_4H_{10}	2,2-Dimethyl butane	2-Methyl pentane	k_5/k_4	$k_3/k_2 \times 10^3$
16.5	16.5	1000	0.106	0.0082	0.191	0.013	0.54	7.9
8.0	16.2	496	.178	.0226	.332	.023	.53	9.7
6.2	16.4	378	.233	.039	.415	.028	.55	8.8
4.9	~15.9	306	.351	...	.627	.044	.53	...
16.1	62.3	258	.305	.070	.544	.040	.54	8.9
15.9[a]	62.3	256	.362	.091	.637	.039	.55	7.8
15.8[a]	109.2	145	.420	.159	.734	.042	.54	7.9

[a] Low conversion.

TABLE V

NEOHEXANE

		Rate, nanomoles/sec.					
$C_2{}^{14}H_4$, μmoles/l.	$(C_6H_{14})/(C_2{}^{14}H_4)$	C_2H_6	C_4H_{10}	2,2-Dimethyl-hexane	3,3-Dimethyl-hexane and 2,2,3-trimethyl pentane	k_5/k_4	$k_3/k_2 \times 10^3$
25.8	276	0.322	0.346	0.029	1.36	0.21	2.1
14.1	504	.302	.277	.027	1.24	.22	1.5
84.8	84	.318	.590	.031	1.40	.18	1.8

TABLE VI

n-HEXANE, CYCLOPENTANE, NEOPENTANE, AND 2,3-DIMETHYLBUTANE

			Rate, nanomoles/sec.				
RH	$C_2{}^{14}H_4$, μmoles/l.	$(RH)/(C_2{}^{14}H_4)$	C_2H_6	C_4H_{10}	$RC_2{}^{14}H_5$	k_5/k_4	$k_3/k_2 \times 10^3$
n-Hexane	27.3	256	0.283	0.189	1.019[a]	0.27	4.0
n-Hexane	22.5	311	.285	.181	0.968[a]	.27	3.3
Cyclopentane	72.3	242	.236	.093	.841[b]	.27	8.5
Cyclopentane	45.8	317	.171	.055	.626[b]	.26	8.6
Neopentane	76.3	231	.025	> .116	.39[c]	< .03	..
Neopentane	14.8	1149	.050	> .141	.52[c]	..	..
Neopentane	3.0	1800	.077	> .093	.41[c]	..	..
2,3-Dimethylbutane	48 5	151	.214	.037	.298[d]	.71	18.0
2,3-Dimethylbutane	56 2	130	.287	.052	.448[d]	.63	21.0
2,3-Dimethylbutane	124	59	.432	.125	.585[d]	.71	22.0
2,3-Dimethylbutane	32	226	.164	.015	.219[d]	.74	23.0

[a] $RC_2{}^{14}H_5$ is the sum of 3-ethylhexane and 3-methylheptane. [b] $RC_2{}^{14}H_5$ is ethylcyclopentane. [c] $RC_2{}^{14}H_5$ is 2,2-dimethylpentane. [d] $RC_2{}^{14}H_5$ is 2,3,3-trimethylpentane.

radical addition reactions ($R \cdot + C_2{}^{14}H_4 \rightarrow$) were unimportant since these would lead to higher molecular weight products. Labeled *n*-hexane was fomed only in the case of butane where it is expected to be formed by reaction 4. Thus reaction 10 is unimportant since it would lead to the formation of labeled *n*-hexane

$$C_2{}^{14}H_5\cdot + C_2{}^{14}H_4 \longrightarrow C_4{}^{14}H_9\cdot \qquad (10)$$

in all systems.

The kinetic treatment of the data based on reactions 1 through 9 satisfactorily accounts for the experimental results. In the general case reaction 1 may produce several radicals: R_1, R_2, etc., of relative yields α_1, α_2, etc.; α_i is the fraction of dissociations which forms radical R_i. Similarly, reaction 3 may yield more than one radical: R_1, R_2, etc. It is asserted that the yields of labeled hydrocarbons $R_iC_2{}^{14}H_5$, are proportional to the yields of radicals, ϕ_{R_i},[8] formed in reactions 1 and 3.

(8) This assertion may be justified as follows: it is assumed that all radicals R, react only with other radicals and that the steady state approximation is valid. Then it has been shown (see ref. 6) that

$$\frac{\phi_{R_mC_2{}^{14}H_5}}{\phi_{R_nC_2{}^{14}H_5}} = \frac{\phi_{R_m}}{\phi_{R_n}} \times \frac{\sum_i \frac{a_i k_{ni}}{k_{nE}}(R_i)}{\sum_i \frac{a_i k_{mi}}{k_{mE}}(R_i)}$$

where k_{mi} is the specific rate constant (including both disproportionation and combination for reaction of radical R_m with radical R_i), a_i is a constant (= 1) except when two identical radicals are reacting (then $a_i = 2$), the subscript E refers to the $C_2{}^{14}H_5$ radical, and $\phi_{R_mC_2{}^{14}H_5}$ is the yield of labeled hydrocarbon formed from R_m. Thus a sufficient condition that the relative radical yields are determined is that the coefficients in the summations are equal; *i.e.*

$$a_i k_{ni}/k_{nE} = a_i k_{mi}/k_{mE}$$

This equality is true if the ratio, $k_{ij}{}^2/k_{ii}k_{jj}$, is a constant value for all radical pairs (R_i, R_j) in the system. This ratio is approximately given by the ratio of combination products

$$(R_iR_j)^2/(R_iR_i) \times (R_jR_j)$$

which has been shown to be about 4 for many radical pairs: *cf.* G. Porter,

It can also be shown that for each radical, R_i, the relationship

$$\frac{R_iC_2{}^{14}H_5}{C_4{}^{14}H_{10}} = A + B(RH)/(C_2{}^{14}H_4) \qquad (I)$$

should be obeyed. In (I), $A = 2\alpha_i(1 + k_7/k_6)/(1 + k_5/k_4 + k_5'/k_4)$, B is a constant, and α_i is the fraction of dissociations which forms R_i. In each case it was found that a plot of $R_iC_2{}^{14}H_5/C_4{}^{14}H_{10}$ *vs.* $(RH)/C_2{}^{14}H_4$ was linear (*cf.* Fig. 1, 2, and 3). The yield of $R_iC_2{}^{14}H_5$ in an individual experiment represents the combined yield of radicals R_i from the primary process and from reaction 3. However, from the intercepts (the value of $R_iC_2{}^{14}H_5/C_4{}^{14}H_{10}$ at infinite ethylene concentration) the values of α_i could be evaluated in each case. The disproportionation ratio, k_7/k_6, was assumed[9] to be 0.12; k_5/k_4 was evaluated from the data obtained here as described below. The term k_5'/k_4 was neglected since values for this ratio are unavailable for most of the radicals studied. An accurate determination of the relative yields would require including the contribution of reaction k_5'. However, it was found that in the present study neglecting this term does not affect the determination of relative radical yields to a significant extent.

It is impractical to use a very high ethylene-C^{14} concentration because of the high quenching cross section of ethylene. However, in some cases the amount of ethylene used was sufficient to scavenge 80% of the hydrogen atoms; thus reaction 3 was suppressed to a corresponding extent.

Values of k_3/k_2.—Rate constants for hydrogen atom abstraction by H atoms, k_3, were determined as the ratio k_3/k_2. These were calculated from eq. II.

$$\frac{\sum_i R_iC_2{}^{14}H_5(1 + k_5/k_4)}{1.12C_4{}^{14}H_{10}} = 2 + \frac{4k_3}{k_2}\frac{(RH)}{(C_2{}^{14}H_4)} \qquad (II)$$

This is obtained by rearranging eq. I and summing for all radical species. The value of k_5/k_4 is the value appropriate for each radical, R_i.

The individual ratios k_3/k_2, at 25°, are in reasonable agreement with data available in the literature. The average values of k_3/k_2 for propane, pentane, hexane, and neohexane are 1.9, 3.7, 3.7, and 1.8×10^{-3}, respectively (see Tables I, III, V, and VI). In these four hydrocarbons only secondary and primary hydrogen atoms are available for abstraction. In the case of butane, which should have a reactivity similar to these, a value of $k_3/k_2 = 2.2 \times 10^{-3}$ has been reported (obtained by combining the data of Cvetanovic[10] and Yang[11]).

The hydrocarbons with tertiary hydrogen atoms are much more reactive. For isobutane, the average value of k_3/k_2 at 25° is 8.6×10^{-3} (Table IV), in excellent agreement with the value of this ratio reported by Yang[12] of 8.4×10^{-3}. Similar values were obtained for isopentane ($k_3/k_2 = 10.6 \times 10^{-3}$), and for 2-methylpentane ($k_3/k_2 = 11.6 \times 10^{-3}$). As would be expected, k_3/k_2 for 2,3-dimethylbutane with two tertiary hydrogen atoms is 21×10^{-3}, about twice as great as for isopentane or isobutane.

Absolute Quantum Yields.—In order to calculate the absolute quantum yield of reaction 1, the absorbed light intensity and the rate of formation of H atoms must be known. The former was calculated to be 4.3 nanoeinsteins/sec., utilizing cyclopentane as an actinometer.[7] Since the experimental conditions were not changed, it was assumed this light intensity was constant throughout. The pressure of hydrocarbon was sufficient in all cases so that quenching of the excited mercury atoms was essentially complete. The yield of hydrogen atoms was derived from the total yield of scavenged hydrogen atoms, *i.e.*, $\phi_{C_2{}^{14}H_5}$. This is the sum of the yields of all labeled hydrocarbons.

$$\phi_{C_2{}^{14}H_5} = \phi_{C_2{}^{14}H_6} + 2\phi_{C_4{}^{14}H_{10}} + \sum_i \phi_{R_iC_2{}^{14}H_5}$$

From this ϕ_H is calculated by

$$\phi_H = \phi_{C_2{}^{14}H_5}\left(1 + \frac{k_3(RH)}{k_2(C_2{}^{14}H_4)}\right)$$

using the values of k_3/k_2 given in the tables.

Discussion of the Primary Processes

Propane.—In addition to $C_2{}^{14}H_6$ and $C_4{}^{14}H_{10}$ only two other labeled products are formed in propane, isopentane-C^{14} and *n*-pentane-C^{14}. The yield of the former is approximately 10 times that of *n*-pentane-C^{14} (Table I). The data are plotted according to eq. I in Fig. 1. From the intercepts it is found that $\alpha_{isopropyl} = 0.9$ and $\alpha_{n\text{-propyl}} = 0.1$ or the products of reaction 1 are 90% isopropyl and 10% *n*-propyl radicals. If this is expressed as a reactivity per hydrogen atom, the secondary hydrogen atoms are 27 times as reactive as the primary hydrogen atoms.

The values of α may be calculated from the data in Table I by an alternate approximate method without the use of eq. I. The relative yields of radicals produced in the system by both reactions 1 and 3 are given by the yields of isopentane-C^{14} and *n*-pentane-C^{14}, *i.e.*

$$\phi_{i\text{-Pr}}/\phi_{n\text{-Pr}} = \frac{\text{isopentane-C}^{14}\ (1.21)}{n\text{-pentane-C}^{14}\ (1.06)}$$

The fraction of the hydrogen atoms scavenged by ethylene is $\phi_{C_2{}^{14}H_6}/\phi_H$ and thus the fraction of the total radicals which are formed by reaction 3 is readily obtained. These radicals are expected to be mostly isopropyl radicals.[12] This method establishes a lower limit for $\alpha_{isopropyl}$ of 0.87,[13] which is comparable to that obtained using the extrapolation procedure. For propane, the quantum yield for reaction 1 has been estimated to be 0.90 at 16 mM propane.[2] From the results in Table II the average value of ϕ_H is 0.87 at 6 mM propane, in excellent agreement.

The mercury-sensitized decomposition of propane has been the subject of numerous investigations,[2,14-18] and

"Progress in Reaction Kinetics," Vol. 1, Pergamon Press, New York, N. Y., 1961, p. 110.

(9) R. K. Brinton and E. W. R. Steacie, *Can. J. Chem.*, **33**, 1840 (1955).

(10) M. Takahasi and R. J. Cvetanovic, *ibid.*, **40**, 1037 (1962).

(11) K. Yang, *J. Am. Chem. Soc.*, **84**, 3795 (1962).

(12) K. Yang, *J. Phys. Chem.*, **67**, 562 (1963).

(13) For example, when $(C_3H_8)/(C_2{}^{14}H_4)$ is 438, $\phi_{i\text{-Pr}}/\phi_{n\text{-Pr}} = 11.4$ or 92% of the radicals are isopropyl radicals; $\phi_{C_2{}^{14}H_5}/\phi_H = 0.46$; thus 0.29 of the propyl radicals produced are from reaction 3, or $(92 - 29)/(100 - 29) = 0.89$.

(14) E. W. R. Steacie and D. J. Dewar, *J. Chem. Phys.*, **8**, 571 (1940).

(15) S. Bywater and E. W. R. Steacie, *ibid.*, **19**, 319 (1951).

(16) Y. Rousseau, G. N. C. Woodall, and H. E. Gunning, *ibid.*, **37**, 2722 (1962).

the relative radical yields determined in these studies are available for comparison with the present results. Calculations of the radical yields which are based on an analysis of the hexane products indicate that sensitization by mercury ($^3P_1$) atoms yields 93–95% isopropyl radicals.[14,15,17] However, in these studies up to 50% of the propyl radicals produced result from secondary reactions of hydrogen atoms such as reaction 3 or addition of hydrogen atoms to propylene. In either case mostly isopropyl radicals will be produced by secondary reactions of hydrogen atoms.[6,12] Such data place a lower limit on $\alpha_{i\text{-Pr}}$ of $(93 - 50)/(100 - 50) = 0.86$. The results obtained in the present study are consistent with these studies.

Recently, two quite different scavenging techniques have been utilized to measure primary radical yields in propane. One involves the use of nitric oxide as a scavenger and subsequent analysis of the various products of the NO reaction.[16,17] With this technique it has been determined that $\alpha_{i\text{-Pr}} = 0.58$. Similarly, in a study of the mercury sensitization of propane at very low partial pressures a value for $\alpha_{i\text{-Pr}} = 0.55$ has been obtained.[18] In this case the relative yields were determined by the methyl-d_3 saturation technique[19] and by analysis of the hexane fraction as well, comparable results being obtained by the two methods.

In view of these conflicting results it is important that the possibility be considered that in the use of $C_2{}^{14}H_5$ radicals as scavenger, initially formed *n*-propyl radicals might be converted to isopropyl radicals by reaction 11

$$n\text{-}C_3H_7 + C_3H_8 \longrightarrow i\text{-}C_3H_7 + C_3H_8 \quad (11)$$

That this cannot occur to any large extent is indicated by the fact that the corresponding reaction of ethyl radicals, reaction 12, is unimportant. Since large yields of labeled pentanes are produced, reaction 12 indeed

$$C_2{}^{14}H_5 + C_3H_8 \longrightarrow i\text{-}C_3H_7 + C_2{}^{14}H_6 \quad (12)$$

does not compete effectively with the scavenging reactions, 4–7. The isobutane results also support this point (see below) since abstraction of hydrogen atoms from isobutane by ethyl radicals is shown to be unimportant.

Another possible complication in the case of propane is quenching of mercury ($^3P_1$) atoms by ethylene and subsequent reactions of C_2H_4*. This is relatively more important in propane because of its low quenching cross section,[20] 1.3 Å.^{2}. At the highest ethylene concentration used ~8% of the mercury ($^3P_1$) atoms were quenched by ethylene. The excited ethylene molecules would be expected to deactivate by collisions and to decompose to form $C_2{}^{14}H_2$ and H_2.[21] The direct insertion of an excited ethylene into a carbon–hydrogen bond of propane has been suggested[21] to account for the formation of pentanes. Recently, however, this reaction has been shown to be unimportant.[22]

Butane.—The results for *n*-butane are given in Table II. The extrapolation procedure could not be used in this case since it was found that the determination of butane-C^{14} in the presence of large excesses of unlabeled butane was inaccurate. Therefore an ethylene-C^{14} concentration of less than 0.07 mole % was used so that only a small fraction of the hydrogen atoms was scavenged. Under these conditions, reaction 6 yielding labeled butane is minimal (see ref. 6) and can be neglected in calculating $\phi_{C_2{}^{14}H_5}$.

The approximate method of calculating yields of reaction 1 as described for propane can be used. Thus in a given run the fraction of hydrogen atoms which abstract can be calculated.[23]

If it is assumed that reaction 3 yields predominantly secondary butyl radicals, then from the relative yields of 3-methylpentane-C^{14} and *n*-hexane-C^{14} a minimum value for $\alpha_{sec\text{-butyl}}$ of 0.94 is obtained. Thus $\alpha_{n\text{-butyl}}$ is 0.06 and the secondary hydrogen atoms are ~24 times more reactive than the primary ones.

Isobutane.—Earlier studies have shown that the major radical formed in the sensitization of isobutane is *t*-butyl.[24] The results in Table IV are in accord with these findings since 2,2-dimethylbutane is the most important labeled product. A small yield of labeled 2-methylpentane is observed, showing that some isobutyl radicals are formed. Treatment of the data in the usual manner gave these results

$$Hg^* + i\text{-}C_4H_{10} \longrightarrow Hg + H + t\text{-}C_4H_9 \quad (97\%)$$
$$\longrightarrow Hg + H + i\text{-}C_4H_9 \quad (3\%)$$

An average value of $\phi_H = 0.81$ was obtained from three determinations.

At high conversions, since isobutene is formed by reaction 9, butyl radicals may be formed by hydrogen atom addition to isobutene. The last two runs in Table IV were carried to only 0.01% conversion (one-fifth the usual conversion). Under these conditions the fraction of hydrogen atoms scavenged by isobutene was negligible. The results are consistent with the results at 0.05% conversion. As pointed out earlier, the presence of ethylene inhibits the addition of hydrogen atoms to unsaturated products.

Isobutane was the only hydrocarbon studied containing a tertiary carbon–hydrogen bond in which the radical formed from rupture of the primary C–H bond was also detected. Therefore, it was possible by the intercept method to estimate the relative susceptibility to rupture of a tertiary C–H bond compared to a primary C–H bond. Since reaction 1 gives 97% *t*-butyl radicals, the tertiary bond is 290 times more susceptible to rupture than a primary carbon–hydrogen bond in isobutane. This must be considered as an approximate value only, since it depends on the determination of a product formed in low yield.

***n*-Pentane.**—The results given in Table III show that three different pentyl radicals are formed from *n*-pentane. Determination of their relative yields by the extrapolation method shows that the initial dissociation is

(17) G. N. C. Woodall and H. E. Gunning, *Bull. soc. chim. Belges*, **71**, 725 (1962).

(18) P. Kebarle and M. Avrahami, *Can. J. Chem.*, **41**, 335, 347 (1963).

(19) R. F. Pottie, A. G. Harrison, and F. P. Lossing, *ibid.*, **39**, 102 (1961); J. Collin and F. P. Lossing, *ibid.*, **35**, 778 (1957).

(20) B. deB. Darwent, *J. Chem. Phys.*, **18**, 1532 (1950).

(21) J. R. Majer, B. Mile, and J. C. Robb, *Trans. Faraday Soc.*, **57**, 1342, 1692 (1961).

(22) J. P. Chesick, *J. Am. Chem. Soc.*, **84**, 2448 (1962).

(23) For example, at $(C_4H_{10})/(C_2{}^{14}H_4) = 1350$ (Table II), $\phi_{C_2{}^{14}H_5}/\phi_H = 0.25$, or 75% of the hydrogen atoms abstract.

(24) B. deB. Darwent and C. A. Winkler, *J. Phys. Chem.*, **49**, 150 (1945).

$Hg^* + n\text{-}C_5H_{12}$

$\longrightarrow Hg + H + CH_3\text{–}\dot{C}H\text{–}CH_2\text{–}CH_2\text{–}CH_3$ (56%)

$\longrightarrow Hg + H + CH_3\text{–}CH_2\text{–}\dot{C}H\text{–}CH_2\text{–}CH_3$ (42%)

$\longrightarrow Hg + H + \cdot CH_2\text{–}CH_2\text{–}CH_2\text{–}CH_2\text{–}CH_3$ (2%)

Of particular interest here is the fact that the yield of 1-ethylpropyl radicals is somewhat larger than expected on the basis of the number of secondary carbon–hydrogen bonds. It appears, therefore, that small differences in C–H bond energies strongly influence the primary dissociation even though the excited mercury atom has excess energy of ~20 kcal. The quantum yield, ϕ_H, was determined to be 0.88 from an average of three determinations.

One experiment was done with unfiltered light (2537 and 1849 Å. both present). This resulted in a threefold enhancement in the rate of formation of *n*-heptane-C^{14} while the other labeled heptanes increased only 50%. This indicates that mercury ($^1P_1{}^0$) atoms must be more effective than mercury ($^3P_1$) atoms in breaking primary carbon–hydrogen bonds.

Isopentane.—Only two labeled C_7 products were observed in the sensitization of isopentane. Plots of the ratios 3,3-dimethylpentane/butane and 2,3-dimethylpentane/butane *vs.* the ratio $(i\text{-}C_5H_{12})/(C_2{}^{14}H_4)$ were linear (Fig. 2) and the intercepts (values of these ratios at infinite ethylene concentration) were 1.2 and 0.5, respectively. The values of α calculated from the intercepts were 0.76 and 0.24. Thus reaction 1 is

$Hg^* + i\text{-}C_5H_{12}$

$\longrightarrow Hg + H + CH_3\text{–}\dot{C}(CH_3)\text{–}CH_2\text{–}CH_3$ (76%)

$\longrightarrow Hg + H + CH_3\text{–}CH(CH_3)\text{–}\dot{C}H\text{–}CH_3$ (24%)

Isopentyl radicals were not detected since the corresponding product would have been masked by the large 2,3-dimethylpentane peak, but the heptane corresponding to 2-methylbutyl was formed in low yield (less than 1% of the total yield of labeled heptanes). In this instance the tertiary C–H bond is approximately six times more susceptible to attack than the secondary C–H bond. The absolute quantum yield for isopentane was calculated as described above. The average of four determinations gave $\phi_H = 0.82$.

Neopentane.—Neopentane was one of the hydrocarbons studied which was observed to dissociate in a unique way producing a single radical species, in this case neopentyl radicals. A detailed study of this substance was not made, since, if only neopentyl radicals are detected as products of reaction 1 and 3, $\alpha_{neopentyl} = 1$.

A value for ϕ_H was estimated from the data. The quantum yield of hydrogen atoms is obtained from $\phi_{C_2{}^{14}H_6}$, the sum of the yields of labeled products. These include $C_4{}^{14}H_{10}$, the analysis of which was inaccurate in the presence of a large excess of neopentane which masked the butane region. The yields for $C_4{}^{14}H_{10}$ given in Table VI are therefore minimum yields and since the maximum value of $\phi_{C_2{}^{14}H_6}$ observed in neopentane is 0.2, ϕ_H must be >0.2. This is much larger than that determined by Darwent,[25] who concluded that deactivation of excited neopentane molecules constituted the major result of sensitization since $\phi_{H_2} = 0.0045$ at 25°. The present results indicate that in the absence of scavenger the back reaction, $H + neo\text{-}C_5H_{11} \rightarrow neo\text{-}C_5H_{12}{}^*$, must be important.

(25) B. deB. Darwent and E. W. R. Steacie, *Can. J. Res.*, **27B**, 181 (1949).

Cyclopentane.—As in neopentane, only one C_7-labeled hydrocarbon was observed, in this instance, ethylcyclopentane (Table VI). The mercury-photosensitized decomposition of cyclopentane has been shown to be entirely free radical in nature and $\phi_H = 0.8$.[7]

***n*-Hexane.**—*n*-Hexane was not studied in detail since the major labeled branched octane products could not be separated on the chromatographic columns employed. Presumably, the major radicals produced are 1-methylpentyl and 1-ethylbutyl. The yield of *n*-hexyl radicals is, however, quite small in this case since only a small yield of labeled *n*-octane (~1% of the total C_8 activity) was found.

2-Methylpentane.—Three major labeled octanes were observed as products in the sensitization of 2-methylpentane. Plots of the ratios of products according to eq. I are shown in Fig. 3. Evaluation of the intercepts gave the values of α corresponding to

$Hg^* + 2\text{-methylpentane}$

$\longrightarrow Hg + H + CH_3\text{–}\dot{C}(CH_3)\text{–}CH_2\text{–}CH_2\text{–}CH_3$ (58%)

$\longrightarrow Hg + H + CH_3\text{–}CH(CH_3)\text{–}\dot{C}H\text{–}CH_2\text{–}CH_3$ (28%)

$\longrightarrow Hg + H + CH_3\text{–}CH(CH_3)\text{–}CH_2\text{–}\dot{C}H\text{–}CH_3$ (14%)

The combined yield of isohexyl and 2-methylbutyl was less than 1% of the total radical yield.

Here it is observed that the yield of 1-ethyl-2-methylpropyl is twice the yield of 1,3-dimethylbutyl although both are formed when a secondary C–H bond breaks. This is similar to the effect observed in *n*-pentane, but the presence of a branch in the molecule has enhanced the susceptibility of rupture of the secondary C–H bonds next to the isopropyl group. The tertiary hydrogen atom in this case is 4.2 times as reactive as the hydrogen atoms in the adjacent methylene group and 8.5 times as reactive as the hydrogen atoms in the other methylene group. This enhanced reactivity of the methylene group next to the branch corresponds to the effect observed by Darwent,[20] who measured the quenching cross sections of aliphatic hydrocarbons and found that the $-CH_2-$ group in isopentane contributed more to the quenching than the $-CH_2-$ groups in straight chain alkanes. The average value of ϕ_H is found to be 0.75.

2,2-Dimethylbutane.—From this hexane, three labeled octanes were expected and only two peaks were observed on the chromatogram. The 2,2-dimethylhexane was separated, but the small amount of the 3,3-dimethylhexane formed appeared under the tail of the major octane product (2,2,3-trimethylpentane) and no quantitative estimate of its yield could be obtained. The extrapolation procedure showed that reaction 1 is

$Hg^* + 2,2\text{-dimethylbutane}$

$\longrightarrow H + Hg + CH_3\text{–}C(CH_3)_2\text{–}\dot{C}H\text{–}CH_3$ (92%)

$\longrightarrow H + Hg + CH_3\text{–}C(CH_3)_2\text{–}CH_2\text{–}CH_2\cdot$ (2%)

$\longrightarrow H + Hg + \cdot CH_2\text{–}C(CH_3)_2\text{–}CH_2\text{–}CH_3$ (6%)

It is assumed here that the yield of 2,2-dimethylbutyl is three times the yield of 3,3-dimethylbutyl. The secondary hydrogen atoms in 2,2-dimethylbutane are 77 times more reactive than the primary hydrogen atoms or three times the analogous ratio in propane. Presumably, this enhancement is an effect caused by the higher degree of branching in the molecule. The average value of ϕ_H from three determinations was 0.90.

2,3-Dimethylbutane.—The primary quantum yield in the mercury-sensitized photolysis of 2,3-dimethylbutane is 0.63 and only 1,1,2-trimethylpropyl radicals are detected (Table VI).

Relative Reactivity of Carbon–Hydrogen Bonds.—From the known quenching cross section, σ_Q^2, and the values of α_i obtained for each hydrocarbon, an effective cross section for each carbon–hydrogen bond may be calculated.

$$\sigma_Q^2/(\text{C–H})_i \text{ bond} = \sigma_Q^2 \times (\alpha_i)/\text{number of (C–H)}_i \text{ bonds}$$

The values thus obtained are shown in Table VII. The observed value of σ_Q^2 per primary C–H bond is nearly constant for all hydrocarbons studied; the average is 0.024. Secondary carbon hydrogen bonds are much more reactive. The cross section per secondary C–H bond varies from 0.59 for propane to 2.76 for 2-methylpentane. The carbon–hydrogen bonds on methylene groups attached to a highly substituted carbon atom are unusually reactive. This is particularly evident for 2-methylpentane and 2,2-dimethylbutane for which σ_Q^2 (effective) is 2.76 and 2.64, respectively. Tertiary carbon–hydrogen bonds are even more reactive. There is less variation in this case and an average value of σ_Q^2 per tertiary C–H bond of 8.5 may be assigned.

TABLE VII

Hydrocarbon	σ_Q^2 (Å.^{2})[a]	σ_Q^2/C–H Bond Primary	Secondary	Tertiary
Propane	1.3	0.020	0.59	..
n-Butane	3.0	~ .03	~ .70	..
i-Butane	4.9	.015	..	4.8
n-Pentane	8.6	.029	1.21; 1.80	..
i-Pentane	12.0	...	1.45[b]	9.1
n-Hexane	16.0	.022	1.99	..
2-Methylpentane	20.0	...	1.38; 2.76	11.7
2,2-Dimethylbutane	5.7	.034	2.64[b]	..
2,3-Dimethylbutane	15.0	...	..	7.5
Average		.024	1.57	8.5

[a] Cross sections from reference 20 [b] These values are for the methylene group next to the branch in the molecule.

The average values of σ_Q^2 (effective) for primary, secondary, and tertiary carbon hydrogen bonds, 0.024, 1.57, and 8.5, are in the ratio 1:65:350, in good agreement with the relative values of σ_Q^2/C–H bond calculated by Darwent of 1:100:680 from quenching data. Thus there is a very close correspondence of relative quenching cross section obtained by the two methods for the same set of hydrocarbons. Also, there is a correlation of the unusually high reactivity of methylene groups near a branch in the molecule as reported here with the high values of σ_Q for these groups as observed by Darwent.

Disproportionation to Combination Ratios.—At the present time there is very little data available on the disproportionation to combination ratios for reactions of ethyl radicals with the various butyl, pentyl, and hexyl radicals. The results obtained in this study are summarized in Table VIII. Several determinations of k_5/k_4 were made in each case and the stated deviation is the average deviation which was usually <5%. The ratio of disproportionation to combination k_5/k_4 is given by

$$k_5/k_4 = \frac{\phi_{C_2{}^{14}H_6} - 0.12\phi_{C_4{}^{14}H_{10}}}{\phi_{RC_2{}^{14}H_5}}$$

when only one radical R is formed in the photodissociation. In several cases two radicals, for example, a secondary and a normal radical, were formed. In calculating k_5/k_4 for the secondary radicals a correction was included for the small yield of ethane formed by disproportionation of $C_2{}^{14}H_5$ with the *n*-alkyl radicals. It was assumed that $k_5/k_4 = 0.06$ for *n*-alkyl radicals. A similar relationship was used to calculate k_5/k_4 for the tertiary radicals formed from isopentane and 2-methylpentane except that in these cases $C_2{}^{14}H_6$ was formed by disproportionation reactions of $C_2{}^{14}H_5$ with both secondary and tertiary radicals. Since for the secondary radicals studied $0.20 \leqq k_5/k_4 \leqq 0.27$ (Table VIII), an average value of 0.23 was assumed for the secondary radicals produced in these compounds. Thus for *t*-pentyl radicals from isopentane

$$k_5/k_4 = \frac{\phi_{C_2H_6} - 0.12\phi_{C_4H_{10}} - 0.23\phi_{2,3\text{-dimethylpentane}}}{\phi_{3,3\text{-dimethylpentane}}}$$

TABLE VIII

$$C_2{}^{14}H_5 + R \xrightarrow{k_5} C_2{}^{14}H_6 + R(-H)$$
$$\xrightarrow{k_4} RC_2{}^{14}H_5$$

Radical (R)	k_5/k_4 Observed	Calculated A[a]	Calculated B[b]
Secondary radicals			
Isopropyl	0.21 ± 0.02	0.40	0.21
sec-Butyl	.23 ± .01	.34	.21
sec-Pentyl	.25 ± .01	.30	.26
sec-Hexyl	.27 ± .01	.27	.24
Cyclopentyl	.265 ± .005	.27	.09
1,2,2-Trimethylpropyl	.20 ± .02	.20	.15
Tertiary radicals			
t-Butyl	0.54 ± 0.01	0.60	0.51
t-Pentyl	.60 ± .01	.54	.81
1,1-Dimethylbutyl	.74 ± .03	.54	.94
1,1,2-Trimethylpropyl	.72 ± .01	.47	.46
1-Methyl-1-ethylpropyl	~0.8	.47	1.01

[a] Calculated from $k_5/k_4 = 0.067 \times$ no. of available hydrogen atoms. [b] Calculated from eq. III.

The value of k_5/k_4 for isopropyl radicals is 0.21, which is in excellent agreement with the previously determined value of 0.2.[26] The value of k_5/k_4 for secondary radicals increases from 0.21 for propane to 0.27 for *n*-hexane. The values for pentane and hexane are for mixed *sec*-pentyl and *sec*-hexyl radicals, respectively.

The only other ratio for which comparison is possible is that for *t*-butyl radicals, for which we find $k_5/k_4 = 0.54$ and Boddy and Robb report $k_5/k_4 = 0.3$.[26a] Our value

(26) P. J. Boddy and J. C. Robb, *Proc. Roy. Soc.* (London), **A249**, 547 (1959).

(26a) NOTE ADDED IN PROOF.—A recent report gives $k_5/k_4 = 0.48$ for *t*-butyl radicals, *cf.* J. A. Garcia Domingues, J. A. Kerr, and A. F. Trotman-Dickenson, *J. Chem. Soc.*, 3359 (1962).

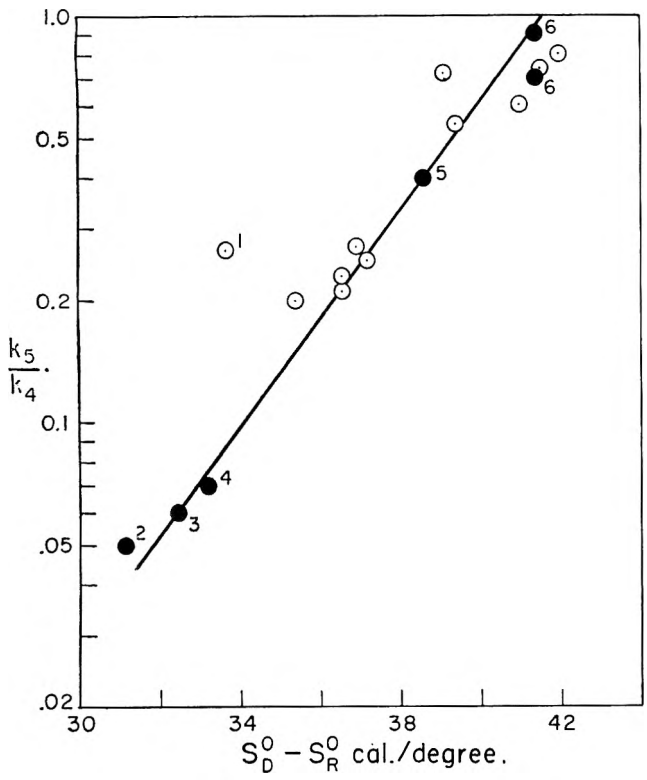

Fig. 4.—Disproportionation to combination ratios: ⊙, values of k_5/k_4 from Table VIII, (1) $C_2{}^{11}H_5$ + cyclopentyl →; ●, values of k_D/k_R, (2) CH_3 + CH_3CO, (3) CH_3 + C_2H_5, (4) C_2H_5 + C_2H_5, (5) i-C_3H_7 + sec-C_4H_9, (6) CH_3 + t-C_4H_9.

was independent of the isobutane concentration (Table IV); thus $C_2{}^{14}H_6$ was not formed by the abstraction reaction

$$C_2{}^{14}H_5 + i\text{-}C_4H_{10} \longrightarrow C_2{}^{14}H_6 + t\text{-}C_4H_9 \quad (13)$$

No explanation for this discrepancy is apparent at present. For t-pentyl radicals, k_5/k_4 is 0.60 and for the t-hexyl radicals, this ratio is 0.72 and 0.74.

It has been suggested that for closely related radicals the extent of disproportionation should be proportional to the number of β hydrogen atoms.[27] From the data reported in Table VIII, the ratio of k_5/k_4 divided by the number of available hydrogen atom varies from a low of 0.04 for isopropyl to a high of 0.10 for 1,2,2-trimethylpropyl. The average value found is 0.067. This average value was used to calculate k_5/k_4 in each case (column A, Table VIII). A comparison of column A with the experimental results shows general agreement. However, k_5/k_4 for t-butyl with nine hydrogens should be greater than k_5/k_4 for other tertiary radicals with less than nine hydrogens, whereas the observed value for t-butyl is the smallest. Similarly, k_5/k_4 for isopropyl (six hydrogens) should be large but is only 0.21. Thus this correlation does not appear to be exact when radicals of different size and structure are being considered.

Bradley[28] has pointed out that for reactions of alkyl radicals, a correlation over a wide range exists between disproportionation ratios and the difference in entropies of the products, $S°_{disp} - S°_{comb}$. To test this suggestion a plot of log k_5/k_4 *vs.* $S°_{disp} - S°_{comb}$ was made[29] (open circles, Fig. 4). Several well established ratios from the literature have also been included in Fig. 4 (solid points). These are disproportionation to combination ratios, k_D/k_C, for: methyl + ethyl, 0.06[30]; ethyl + ethyl, 0.07 = 0.14/2[31]; isopropyl + *sec*-butyl, 0.4[26]; methyl + t-butyl, 0.7[32] and 0.9[33]; and methyl + acetyl, 0.05.[34] The data shown in Fig. 4 suggest a linear relationship and the equation for the straight line as drawn is

$$R_1 + R_2 \longrightarrow R_1{-}R_2 \quad (C)$$

$$\longrightarrow R_1H + R_2(-H) \quad (D)$$

$$\log k_D/k_C = 0.131(S°_{disp} - S°_{comb}) - 5.47 \quad (III)$$

The solid points fall quite close to the straight line. Values of k_5/k_4 calculated from eq. III are given in column B of Table VIII. The observed ratios are in reasonably good agreement with the calculated ones with the exception of cyclopentyl for which the predicted value is 0.09. On the whole, however, the data clearly indicate that an empirical relationship exists between log k_D/k_C and $S°_{disp} - S°_{comb}$.

This entropy difference correlation correctly predicts a lower value of k_D/k_C for ethyl + t-butyl than for methyl + t-butyl. Since the number of available hydrogens (nine) is the same in the two cases, equal ratios would be expected on that basis. The entropy differences are 39.4 e.u. in the ethyl case and 41.4 e.u. in the methyl case, from which the calculated values, using eq. III, are 0.51 and 0.91, respectively. The observed values of k_D/k_C are 0.54 for ethyl + t-butyl and 0.9 (or 0.7) for methyl + t-butyl.

(27) J. W. Kraus and J. G. Calvert, *J. Am. Chem. Soc.*, **79**, 5921 (1957).

(28) J. N. Bradley, *J. Chem. Phys.*, **35**, 748 (1961).

(29) Entropy data were obtained from the American Petroleum Institute Research Project 44. Calculation of the entropy of the products of reaction 5 (since several isomers will be formed) involved assuming that the percentage of each isomer formed depended on the number of available hydrogens and that the yields of *cis–trans* isomers were given by the equilibrium distribution.

(30) C. A. Heller, *J. Chem. Phys.*, **28**, 1255 (1958).

(31) C. G. L. James and E. W. R. Steacie, *Proc. Roy. Soc.* (London), **A244**, 289 (1958).

(32) J. A. Kerr and A. F. Trotman-Dickenson, *J. Chem. Soc.*, 1609 (1960).

(33) G. R. McMillan, *J. Am. Chem. Soc.*, **82**, 2422 (1960).

(34) M. H. J. Wijnen, *J. Chem. Phys.*, **28**, 271 (1958).

SOME ASPECTS OF THE RADIATION CHEMISTRY OF METHANE[1]

BY L. W. SIECK AND R. H. JOHNSEN

Department of Chemistry, Florida State University, Tallahassee, Florida

Received March 12, 1963

In order to establish the relative chemical importance of initial ionization and excitation processes in the high energy radiolysis of methane, discharge tube studies under various conditions have been correlated with high energy electron bombardments using chemical and spectroscopic techniques. These studies indicate an overwhelming chemically interesting contribution from processes initiated by ionization. Investigations of the radiolysis at very low conversions indicate a dose-dependence for the yields of hydrogen and ethane which can be related to ethylene production and subsequent consumption by free radical attack. In addition, the process for polymeric liquid formation has been investigated. A general interpretation has been attempted, particularly with regard to the role of hydrogen atom abstraction processes.

Introduction

During the past decade a considerable number of papers have appeared concerning the gas phase radiolysis of methane.[2-4] The product yield has been correlated in some cases with mass spectral data and probable mechanisms for the radiolytic decomposition have been proposed involving the initial production of ions and subsequent reactions of free radicals having ions as precursors. The addition of radical scavengers has also been used in an attempt to determine the free radical contribution to the total decomposition mechanism, and some free radical schemes have been suggested.[5]

In related studies it has recently been shown that G-values for hydrogen production in saturated hydrocarbon gases depend to a large extent on the degree of conversion.[6] This has been attributed to the scavenging of hydrogen atoms by unsaturates produced during the radiolysis with concurrent depletion of the unsaturate and hydrogen yields with increasing time of irradiation. In the nitric oxide scavenged radiolysis of methane, for example, the yield of ethylene has been seen to increase markedly over the unscavenged value,[7] indicating the role of secondary reactions and suggesting that initial yields of products may well be quite different from those obtained at higher conversions.

The present work concerned itself with several aspects of the radiolysis of methane. First, a determination was achieved of the yields of major products as a function of the degree of conversion, and investigations were made to elucidate the apparently related mechanism for ethylene consumption upon prolonged radiolysis.

Another perplexing problem which had to be resolved before a complete mechanism could be proposed was the reaction sequence resulting in the production of the polymeric liquid formed and the associated stoichiometric excess of hydrogen appearing in the total volatile product yield. A study has been carried out to determine (1) the nature of the polymeric product and (2) a possible mechanism for its formation.

In order to demonstrate the relative significance of chemically important excitation and ionization processes in the high energy radiolysis, the luminescence characteristics of the methane system during radiolysis were determined both with and without rare gas sensitizers. Concurrent with these studies, related investigations were carried out to determine the product distributions and spectral properties of the spark and glow induced decomposition under conditions at which initial ionization and excitation processes could be separately studied and correlated.

Finally, a small pressure dependence for the radiolysis has been detected in the dose-independent region of conversions.

The results of these studies may be incorporated into a general mechanism for the radiolysis which accounts quantitatively for the observed product yields, both for the scavenged and unscavenged situations.

Experimental

Apparatus.—The irradiation vessel was fashioned from a brass cylinder (approximately 3-in. i.d. × 10-in. o.l.) equipped with "O" ring-sealed 0.005-in. aluminum foil windows through which the electron beam passed along an axis perpendicular to the longitudinal axis of the cell (Fig. 1). At either end of the system were placed vacuum-sealed Corning ultraviolet grade fused silica windows which were unaffected optically by radiation doses in excess of 10^{10} r. of Co^{60} γ-rays. Filling and evacuation was achieved through Whitey Teflon-seated needle valves fitted with metal tapered joints for connection to a vacuum and gas handling system. The cell contained a volume of 1250 cc. and could be evacuated to 10^{-6} mm. with no detectable leakage after a 24-hr. period. The entire apparatus was cooled during radiolysis by chilled water (8°) which was pumped through copper tubing wound around the exterior of the vessel.

An optical system was also designed for use in scattering and emission studies concurrent with radiolysis (Fig. 2). Emitted light was focused by a plano-convex quartz lens having a 55-in. focal length on the entrance slit of a Bausch and Lomb 1.5-m. grating spectrograph after single reflection at a front-surface aluminum mirror. With this arrangement, emission occurring in the region between 2300 and 7000 Å. could be detected. The spectrograph was enclosed in sufficient lead shielding to prevent complications due to X-rays produced by the electron beam.

It was found that the production of the polymeric species during radiolysis leads to the formation of a mist in the irradiation vessel, the rate of production of which could be followed by the scattering of a beam of light passed through the radiolysis system. In those experiments in which polymer accumulation was determined *in situ*, visible light (5700 Å.) was passed through the cell and the spectrograph was replaced by a photoelectric tube with an associated amplifier. The rate of polymer formation could then be determined in arbitrary units by computing the slope of the amplified photocurrent *vs.* time plot which resulted from the recording potentiometer trace.

The Pyrex discharge tube used in the spectroscopic and chemical studies was constructed from 55/50 standard taper joints and contained a total volume of 1560 cc. Corning fused-silica windows were positioned opposite each other and adjacent to the discharge region to facilitate the detection of ultraviolet spectral features. Movable electrodes machined from iron and alumi-

(1) This research was supported in part by the U. S. Atomic Energy Commission under Contract AT-(40-1)-2001, and is abstracted from a thesis presented by L. W. Sieck in partial fulfillment of the requirements for the Ph.D. degree.

(2) J. Maurin, *J. Chim. Phys.*, **59**, 15 (1962).

(3) L. Reinisch, *ibid.*, **57**, 1064 (1960).

(4) See A. Swallow, "Radiation Chemistry of Organic Compounds," Pergamon Press, New York, N. Y., 1960, for work preceding 1960.

(5) J. G. Mains and A. S. Newton, *J. Phys. Chem.*, **64**, 511 (1960).

(6) R. A. Back, *ibid.*, **64**, 124 (1960).

(7) K. Yang and P. J. Manno, *J. Am. Chem. Soc.*, **81**, 769 (1959).

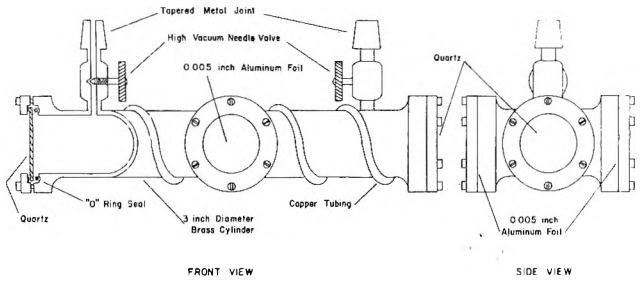

Fig. 1.—Irradiation vessel.

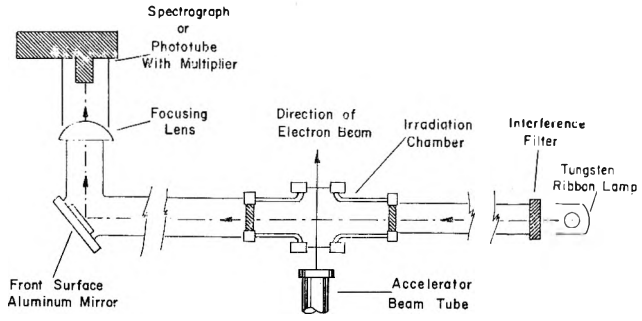

Fig. 2.—Optical system for spectroscopic and light scattering experiments.

num acted as the anode and cathode, respectively, and were supported on aluminum rods sealed at the ends of the vessel with uranium glass. The apparatus was equipped with a cold finger which was used as a trap for condensable products. An induction coil capable of maintaining a pulsed direct current of approximately 65 μa. across a potential varying between zero and 35 kv. (depending on the operating conditions desired) was connected to the electrodes, and the apparatus was aligned so that the emission from the spark or discharge region could be analyzed on the Bausch and Lomb grating spectrograph.

Materials and Gas Handling.—Matheson research grade methane was further purified by bulb to bulb distillation and the middle fraction was used in each case. The only impurity detected was ethane (<0.004%). Matheson C.P. reagent grade nitric oxide and research grade ethylene were used without further purification. Analysis of the ethylene by v.p.c. using flame ionization detection showed methane to be the only impurity present in detectable concentrations. The rare gas–methane mixture was P-10 counting gas (90% argon, 10% methane) from which the oxygen and carbon dioxide impurities had been removed by fractional distillation.

In those experiments in which mixtures of hydrocarbon gases were to be studied, the additive gas was first admitted to a pre-evacuated system containing the cell and two 1.5-l. mixing bulbs. The distilled methane was then added in small pressure increments until the desired total pressure was obtained. In every case manometric determinations of the partial pressures of component agreed to within 1% with an analysis of the resulting gas mixture by v.p.c.

Product Analysis.—C_1 to C_4 products were analyzed by v.p.c. on silica gel columns operated under various conditions of temperature and carrier (helium) flow rates. Hydrogen was determined on the same columns using nitrogen as the carrier gas and higher molecular weight products were separated on a 30% Squalene-on-firebrick column using helium. In some cases a Model 14 Time-of-flight mass spectrometer was used to determine relative yields.

Radiation Source and Dosimetry.—The irradiation source was a High Voltage Engineering Corp. 3-Mev. Van de Graaff electron accelerator capable of delivering a collimated beam of essentially monoenergetic electrons at a current which could be varied between 5 and 1000 μa. Dosimetry was determined by the radiolysis of both nitrous oxide and acetylene, although the former gave ambiguous results and the absolute G-values reported are based on the acetylene data only. The G for acetylene disappearance was taken as 79[8,9] and was corrected for the benzene formed (G = 5.1). The absolute G-values for the products reported are probably accurate to within 4%, while the relative yields are accurate to 1%.

Results

G-Values.—The energy yields for the various products are listed in Table I for the unscavenged radiolysis of methane. Also listed are the G-values for the free radical-scavenged system obtained by the addition of nitric oxide according to the method of Yang and Manno.[7] All products were determined in the dose-independent region (>0.2% conversion) at a methane pressure of 731 mm. and do not represent initial yields. The absolute values found were in good agreement with those reported by other workers both for the scavenged and the unscavenged situations. For the purposes of the tabulation it was most convenient to define a G for polymer formation in terms of a $G(-CH_4$ forming polymer) due to the uncertainty in assignment of an exact molecular weight to the polymeric species. Of particular interest is the fact that addition of a free radical scavenger has no apparent effect on the polymer yield (to be discussed in a later section), while other products are seen to decrease markedly (with the exception of C_2H_4) under conditions of presumably efficient free radical scavenging.

Low Conversion Studies.—In Fig. 3 and 4 are shown the G-values for hydrogen and ethane formation, respectively, as a function of the degree of conversion of methane. The yield of hydrogen is seen to decrease from an initial (zero conversion) value of 6.47 to a dose-independent value of 5.73 above 0.2% conversion (the yields are corrected for the amount of methane decomposed). The extrapolation was achieved using a log–log plot of the same parameters. Simultaneously, ethane production increases from an indeterminately low initial value to a constant value of 2.20. The dramatic effect of prolonged radiolysis is clearly demonstrated, and the results re-emphasize the need for examination of initial yields in hydrocarbon systems where mechanistic complications arise which might obscure the magnitude of primary processes.

Effects of Added Ethylene.—Figure 5 shows the effect of added ethylene on the major product distribution (excluding polymer) in the dose-independent region of conversions. Higher molecular weight hydrocarbons were also determined but initial slopes in every case were essentially zero and no significant effect was noted in the more important region of low ethylene concentrations. $G(H_2)$ is observed to decrease from the dose-independent value of 5.73 to a limiting value of 3.70 which is reached when unconsumed ethylene appears in the volatile product yield. $G(C_2H_6)$ rises quickly to a maximum at 3.5 mole % and then decreases without reaching a limiting value in the range of our studies. The yields of propane and n-butane also increase initially, and $G(C_3H_8)$ appears to approach a constant value concurrently with $G(H_2)$ at higher additive concentrations.

Polymeric Products.—Relative rates for polymer production in methane determined by the light scattering technique with added nitric oxide and ethylene are shown in Fig. 6. The addition of 3 mole % of ethylene increases the rate of polymer formation by a factor of 10, suggesting that reactions involving ethylene may very well play an important role in polymerization processes in methane. Nitric oxide has no apparent

(8) L. M. Dorfman and F. J. Shipko, *J. Am. Chem. Soc.*, **77**, 4723 (1955).
(9) S. C. Lind, D. C. Bardwell, and J. H. Perry, *ibid.*, **48**, 1556 (1926).

TABLE I

PRODUCTS FROM THE RADIOLYSIS OF METHANE[a]

Conditions	G-Values (number of molecules formed/100 e.v. absorbed)								
	H_2	C_2H_6	C_2H_4	C_3H_6	C_3H_8	n-C_4H_{10}	i-C_4H_{10}	C_5-C_6	Polymer
Pure CH_4	5.73	2.20	0.004	0.00	0.36	0.114	0.040	0.03	2.1
CH_4 + NO	3.52	0.16	0.704	0.04	0.03	0.00	0.00	0.00	2.1

[a] Pressure = 731 mm.; 1.9-Mev electrons.

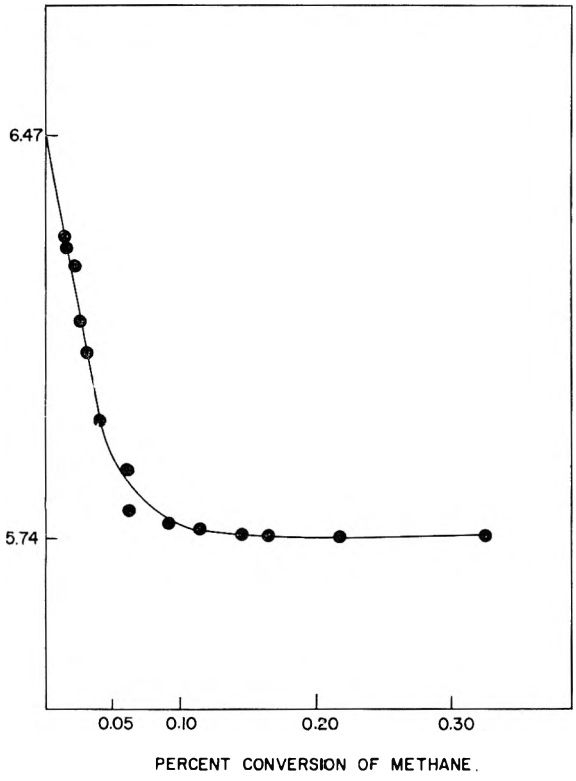

Fig. 3.—Variation in $G(H_2)$ with per cent conversion.

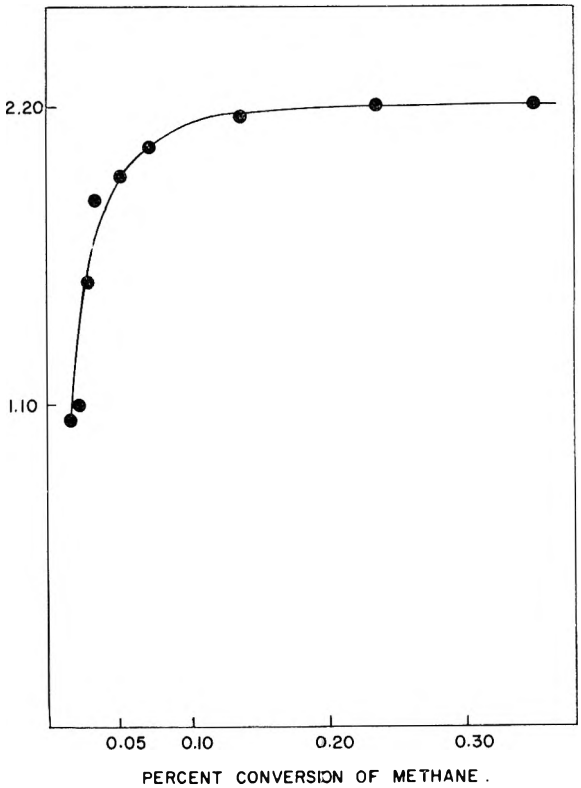

Fig. 4.—Variation in $G(C_2H_6)$ with per cent conversion.

effect on polymer production. This is indicated by the scattering experiments as well as total weight de-

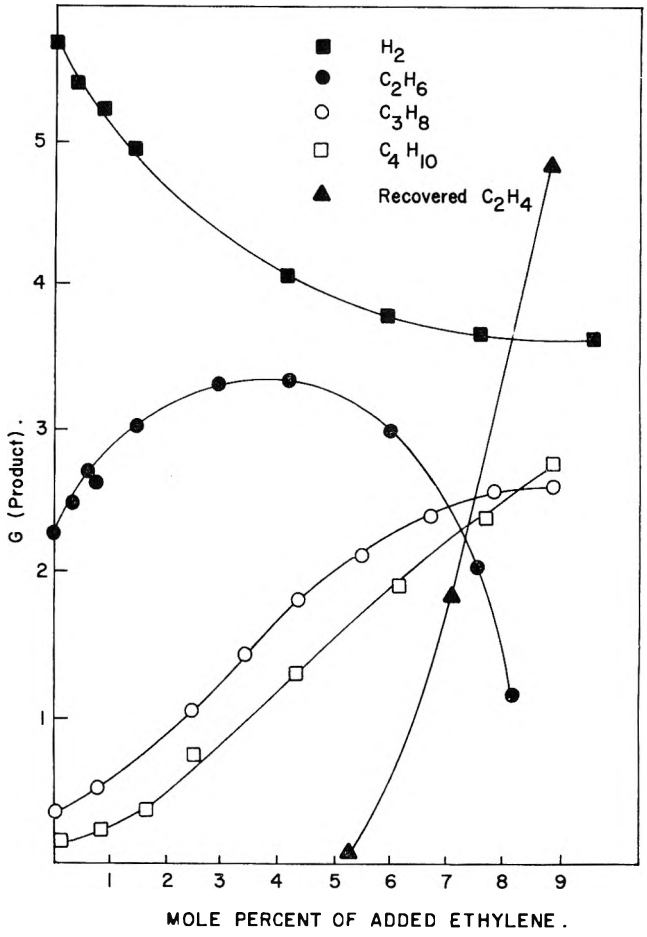

Fig. 5.—Effect of added ethylene on the volatile product distribution.

terminations of the amount of residue produced in both the scavenged and unscavenged situations. In several experiments, the polymeric residue produced in the nitric oxide scavenged system was washed from the cell with Eastman Spectro grade CCl_4. Upon evaporation of the solvent a blue, oily material was found which quickly decolorized with the concurrent appearance of a liquid polymer having essentially the same properties as that resulting from the radiolysis of pure methane. It was apparent, however, that no polymerization took place during the decolorization process. The characterization of the colored condensate is, as of this time, incomplete, although tentative assignment of this material as a high molecular weight nitroso compound seems reasonable.

The infrared spectrum of the polymer resulting from the radiolysis of pure methane indicates partial unsaturation as well as a high proportion of methyl group incorporation. Broad bands appear in the ultraviolet absorption spectrum at wave lengths shorter than 5000 Å., indicating conjugation of some of the π-bonds in addition to isolated unsaturation. The n.m.r. spectrum of this same material indicates that the molecules are highly branched and have a methyl

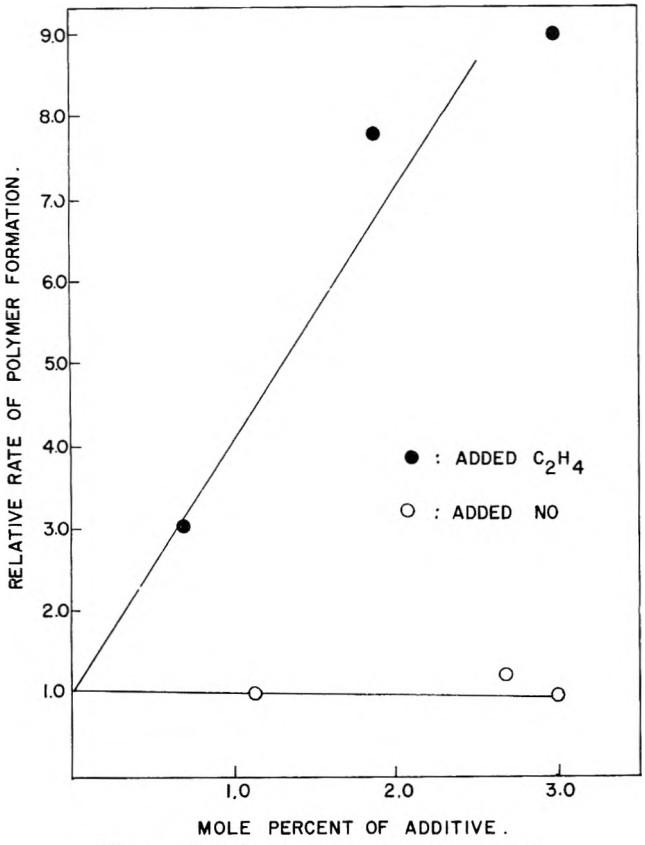

Fig. 6.—Relative rates of polymer formation.

to methylene ratio of about 2:1. This ratio decreases slightly for those samples resulting from the nitric oxide scavenged radiolysis, and high resolution studies of the methyl absorption indicate that fewer types of substitutional methyl groups exist compared to the polymer from pure methane.

Analysis by v.p.c. indicates that between 12 and 20 carbons are incorporated in the polymeric chain. The uncertainty in carbon content can be attributed to the fact that the various isomeric structures which seem to exist prohibit an accurate correlation between v.p.c. retention times and molecular weight.

Spectroscopic Studies. 2.0-Mev. Electron Bombardment. A. Methane.—The emission observed when methane was exposed to 2.0-Mev. electron radiolysis included only three bands and no lines of atomic origin in the region 2300 to 7000 Å. The dominant feature was the (0–0) transition of the $^2\Delta \rightarrow {}^2\pi$ system of the CH radical at 4312 Å. The two other bands corresponded to the $^2\Sigma^- \rightarrow {}^2\pi$ and $^2\Sigma^+ \rightarrow {}^2\pi$ systems of CH at 3890 and 3144 Å., respectively. Determinations were carried out at various pressures (70 to 900 mm.) but no features other than those described earlier were noted regardless of experimental conditions. A weak continuum arising from Cerenkov radiation was noted in the blue.

B. Argon–Methane Mixture.—The luminescence characteristics of methane in a ninefold excess of argon included the CH bands noted in pure methane in addition to line spectra which could be assigned to various transitions in excited atomic and singly ionized argon. Other lines could not be associated with any known transitions, but presumably result from radiative de-excitation in multiple-ionized argon.

C. Argon.—The purpose in determining the emission from pure argon was to establish whether or not any new features appeared which were absent in the argon–methane mixtures. In the event that additional lines were obtained, some speculation as to the mechanism of energy transfer from the rare gas could be made. That is, optical quenching of certain emissions by methane would suggest energy transfer from the excited donor state, resulting perhaps in sensitized decomposition of the acceptor (methane).

Unfortunately it was impossible to obtain pure argon. In spite of all purification procedures, emissions from trace amounts of impurities were obtained in addition to the same atomic lines noted in the rare gas–methane mixtures. These impurity bands, including the $^2\Sigma \rightarrow {}^2\pi$ transition of OH resulting from the sensitized decomposition of water (3090 Å.), the $^3\pi \rightarrow {}^3\pi$ transition of N_2, and the $^2\Sigma \rightarrow {}^2\Sigma$ bands of N_2^+, could not be eliminated from the system. Subtle alterations in the intensity distributions of the argon emissions were evident, but the absence of new features prohibited any speculation as to the nature of the energy transfer states or charge exchange states.

Spark and Glow Discharge Experiments. A. Results of Chemical Analysis.—The discharge induced decomposition of methane, both with and without argon as an additive, led to the formation of hydrogen, ethane, ethylene, acetylene, propane, and higher hydrocarbons. Since it was difficult to determine accurately the energy yields for product formation under the various discharge conditions, the yields of major volatile products (excluding hydrogen) were determined relative to the amount of acetylene produced in a given experiment. These are shown in Fig. 7. Of particular interest is the fact that ethane, ethylene, and propane increase (relative to acetylene) as the pressure in the system is lowered from one atmosphere to 10^{-2} mm. The addition of argon in a ninefold excess served to accelerate the specific rate of decomposition of methane by a factor of nine, while resulting in essentially the same product distribution.

B. Spectral Features of the System.—In the spark discharge at 760 mm. the emission from methane and the argon–methane mixture consisted of the CH bands discussed previously and the $^3\pi_g \rightarrow {}^3\pi_u$ Swan bands of C_2. In addition, several doublets were detected which could be assigned to transitions in atomic carbon. Perhaps the most significant result was the failure to observe any luminescence whatsoever from argon in the spark discharge through the rare gas–methane mixture at one atmosphere total pressure.

As the pressure in the system was decreased, new features corresponding to the hydrogen Balmer series appeared both in the methane and the argon–methane mixtures. More importantly, however, decreasing the pressure of the rare gas–methane mixture resulted in the gradual appearance of emissions resulting from the radiative de-excitation of argon and singly ionized argon. As a matter of fact, the spectral distribution at very low pressures resulting from the decomposition of the mixture in the negative glow resembled very closely that obtained from the mixture under 2.0-Mev. electron bombardment at one atmosphere.

Pressure Dependence of the Radiolysis.—A slight but interesting pressure dependence for the radiolysis was found in the dose-independent region of conversion (Fig. 8). $G(C_2H_6)$ decreased linearly with increasing

methane pressure while $G(H_2)$ showed a linear increase over the range investigated. Stoichiometric analysis indicates that 1.5 molecules of C_2H_6 are lost for every molecule of H_2 formed. $G(C_3H_8)$ was observed to be invariant within experimental error throughout the entire range of pressures.

Discussion

The Role of Ethylene in the Radiolysis of Methane.—It is evident from the added nitric oxide studies that ethylene is produced by an ionic reaction and consumed by free radical attack at higher methane conversions in the absence of a scavenger. In order to discuss the mechanism by which it is apparently destroyed upon prolonged radiolysis, several free radical reactions must be considered.

$$H\cdot + C_2H_4 \longrightarrow C_2H_5\cdot \qquad (1)$$

$$C_2H_5\cdot + H\cdot \xrightarrow{M} C_2H_6 \qquad (2)$$

Reaction 1, the addition of a hydrogen atom to the π-electron system of ethylene, has a very low activation energy and should be a very efficient process for removal of both reactants. Reference to Fig. 5 indicates that the addition of small amounts of ethylene to methane results in a pronounced depletion of the total hydrogen yield. The resultant formation of ethyl radicals, which are obvious precursors for ethane production, should, therefore, lead to an enhancement of $G(C_2H_6)$ according to the termolecular combination (2). This assumption is supported by the observed increase in $G(C_2H_6)$ at low concentrations of added ethylene (Fig. 5).

On this basis, if the postulate is made that the ethylene produced in pure methane at high conversions is quantitatively consumed by reactions involving hydrogen atom attack, then the difference between $G(C_2H_4)$ obtained in the nitric oxide scavenged radiolysis and the high conversion value should be equal to the difference between the zero conversion and high conversion G-values for hydrogen production. The addition of sufficient nitric oxide to prevent free radical attack on ethylene gives an increase in $G(C_2H_4)$ of 0.70, which is very close to the difference in hydrogen yields of 0.74 (refer to Fig. 3) and seems to support the hypothesis of hydrogen atom attack.

According to this scheme, one would expect that the yield of ethane would decrease at lower conversions due to the fact that fewer $C_2H_5\cdot$ radicals are produced which eventually react according to 2. A decrease in the yield is observed which certainly is sufficient to account for the expected drop of 0.70, and in fact, a somewhat greater decrease is suggested by the variation in $G(C_2H_6)$ at very low conversions. In spite of the fact that no accurate extrapolated value for $G(C_2H_6)$ could be obtained, the variation in $G(H_2)$ and $G(C_2H_6)$ can reasonably be explained on the basis of secondary reactions involving ethylene.

However, this argument assumes that the decrease in $G(H_2)$ due to scavenging by ethylene results from the reaction of two hydrogen atoms (per ethylene molecule consumed) which would have reacted, in the absence of ethylene scavenging, in the termolecular combination reaction 3.

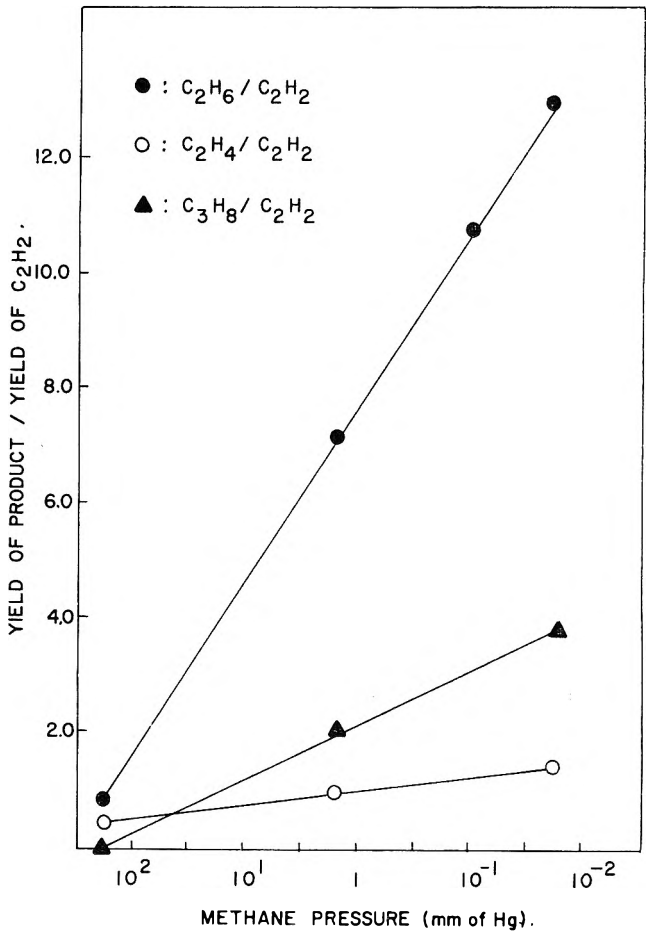

Fig. 7.—Relative product yields from the discharge at various pressures.

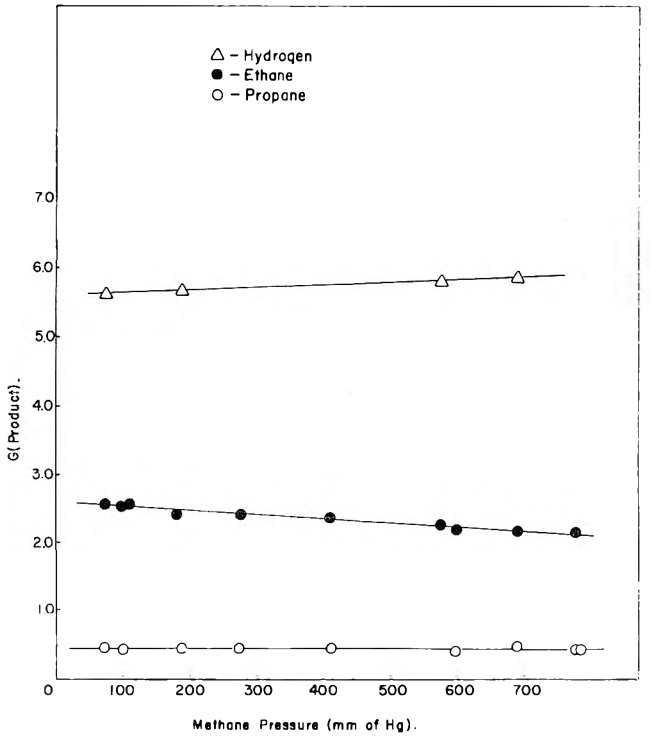

Fig. 8.—Pressure dependence of the radiolysis.

$$H\cdot + H\cdot \xrightarrow{M} H_2 \qquad (3)$$

In two recent studies involving the gas phase radiolysis of methane,[2,3] the assumption has been made that hydrogen atoms produced in the radiolysis are involved

predominantly in abstraction reactions of type 4, which occur readily in the higher alkanes.

$$H\cdot + CH_4 \longrightarrow H_2 + CH_3\cdot \qquad (4)$$

If such abstraction reactions predominated, however, the difference between the zero and high conversion $G(H_2)$ would have to be twice as great as that observed, assuming every ethylene molecule produced scavenged two hydrogen atoms. On the basis of the observed numbers, however, it would seem that hydrogen atoms react according to (3), *i.e.*, in combination processes. Additional proof for the minor role of abstraction and its implications in the over-all radiolysis will be discussed in the section dealing with the general mechanism for the radiolysis of methane.

The effect of added ethylene on other volatile products also has implications which are important for an understanding of the over-all mechanism. The increase in the propane and *n*-butane yields at higher mole per cents of additive seems explicable in terms of radical–radical combination reactions. The formation of propane, for example, can be accounted for by two well established sequences involving methyl radicals.

$$H\cdot + C_2H_4 \longrightarrow C_2H_5\cdot \qquad (1)$$

$$CH_3\cdot + C_2H_5\cdot \xrightarrow{M} C_3H_8 \qquad (5)$$

or

$$CH_3\cdot + C_2H_4 \longrightarrow C_3H_7\cdot \qquad (6)$$

$$C_3H_7\cdot + H\cdot \xrightarrow{M} C_3H_8 \qquad (7)$$

The net result of reactions 1 and 5 to produce propane, or the scavenging of methyl radicals by ethylene (6) followed by the combination reaction 7 involve the same number and types of reactive intermediates.

The enhancement of the *n*-butane formation with increased ethylene addition can also be explained in similar terms. Obvious choices for probable reaction mechanisms would include the dimerization of two ethyl radicals, or the combination of a methyl and an *n*-propyl radical resulting from (6). The over-all activation energies are about the same in each case, although the latter sequence contributes to a greater degree due to the fact that the *n*-butane yield is increasing rapidly at added ethylene concentrations where scavenging of hydrogen atoms is already complete.

The Relative Roles of Ionization and Excitation in the High Energy Radiolysis.—In the spark discharge at one atmosphere the initial decomposition of methane must be described by nonionic processes. This is based on the following arguments. (i) No emission whatsoever is obtained from argon in the 9:1 mixture although the decomposition rate per molecule of methane in the system is increased by a factor of 9. This suggests that sensitization is occurring *via* energy transfer processes involving the lowest metastable in argon (11.5 e.v.), which lies below the ionization potential of methane (13.1 e.v.). The population of higher levels in argon would have been detected by the resulting radiative transitions between the closely spaced higher levels. These transitions appear as spectral features in the visible blue in the high energy radiolysis at a pressure of one atmosphere and are therefore not quenched. The failure to observe any luminescence from argon indicates that electron energies are such that only the lowest lying rare gas states are populated, these states eventually transferring the excitation energy in a quenching process and leading to subsequent decomposition of the methane *via* a free radical mechanism. (ii) The product distribution resembles more closely that obtained from the photolysis[10] of methane with sub-ionization photons ($E < 13.1$ e.v.) which of necessity is described by the initial production of free radicals. (iii) At a pressure of one atmosphere the maximum electron energies are quite low due to the shorter mean free paths of the electrons at these higher pressures in the accelerating field.

As the pressure in the apparatus is lowered, the electrons have increasingly higher average energies due to their lower collision frequencies under these conditions in our apparatus. This is evidenced spectroscopically by the gradual appearance of transitions from higher excited states of argon and the singly ionized atoms. At very low pressures, as was discussed previously, the spectrum appears to differ only slightly from that obtained from the high energy radiolysis.

Reference to Fig. 7 indicates that, at decreasing pressures, the major product distribution is approaching that found in the high energy radiolysis experiments. At one atmosphere, where the spark discharge induced decomposition is described by excitation processes, acetylene and hydrogen are the major products. At lower pressures, where the spectroscopic investigations indicate an increasing contribution from ionic processes, the relative yield of acetylene becomes vanishingly small and other product ratios assume the high energy radiolytic values. It is apparent, therefore, that the radiation chemistry of methane must be described for the most part by the initial production of ionic species, since (i) acetylene, the chief hydrocarbon product under conditions of excitation by sub-ionization electrons,[11] is never obtained as a product in the 2.0-Mev. experiments regardless of conditions and (ii) the correlations between the spectral data, the discharge conditions, and relative product yields are unambiguous.

Polymer Production.—It has been argued that free radical action on ethylene results in a chain reaction eventually leading to polymer.[4] This assumption seems at first to be substantiated by the present studies, which show that added ethylene greatly increases the rate of formation. From the relative rates of formation in the nitric oxide scavenged radiolysis, however, it is evident that this assumption is incorrect. Additional evidence contrary to this hypothesis arises from the fact that several weighings of the polymeric residue collected at methane conversions of 5%, both with and without added nitric oxide, gave essentially identical total weights of material after evaporation of all solvent. Furthermore, under scavenging conditions, ethylene appears in significant yields ($G = 0.70$). It would seem, therefore, that a free radical mechanism cannot account for the observation of the high molecular weight material produced in this system.

In view of our findings, an alternative mechanism

(10) P. A. Leighton and A. B. Steiner, *J. Am. Chem. Soc.*, **58**, 1823 (1936).
(11) H. Wiener and M. Burton, *ibid.*, **76**, 5815 (1953).

must be proposed. An obvious choice for selection as the chain initiator would be an ionic transient, since the reactions of these species would not be affected by the addition of a thermal free radical scavenger if the propagation sequence has a very high cross section compared to the charge transfer reaction $R^+ + NO \rightarrow NO^+ + R$, which might be efficient for chain breaking due to the low ionization potential of nitric oxide (9.24 e.v.).[12]

It is apparent that a consecutive ion–molecule condensation reaction must be proposed whose over-all specific rate constant, at a nominal ion energy, approaches those observed for "normal" ion–molecule reactions under the same conditions. It is our postulate that polymer formation results from an initiation step involving hydrogen deficient fragmentary ions. Support for such a scheme has been given by Wexler and Jesse,[13] who have recently determined that ion–molecule reaction cross sections for secondary and tertiary ions resulting from the initial interactions of C^+, CH^+, and CH_2^+ with methane are very high. Therefore, assuming the same cross sections, consecutive reactions involving these ions in an environment of methane molecules affected by the polarization interaction of the synthesis carrier ions should be an extremely likely process for polymer formation. Such a theory could also explain the enhancement of polymer formation in the presence of added ethylene, since the polarizability of ethylene (4.26 Å.^{3}) is greater than that of methane (2.60 Å.^{3}),[14] suggesting that ethylene is preferentially affected by the electric field of the ionic chain carrier at high initial ethylene concentrations in the system. Likewise, the incorporation of NO in the high molecular weight species could be due to the same effect because of its high polarizability, although incorporation of the radical scavenger could also occur after neutralization of the polymeric ion by addition at a reactive site.

General Comments on a Mechanism for the Radiolysis of Methane

In view of our findings, it seems appropriate to speculate briefly on a possible general mechanism for the radiolysis, including in such a discussion the implications of the current data as well as the contributions of other investigators to the present state-of-the-art regarding this particular problem.

As a starting point for such a discussion, we have chosen those ionic fragmentation processes which are known to occur in the mass spectrometer at pressures lower than 0.1 mm. Although experimental evidence is lacking concerning the relative contribution of each of these processes at much higher pressures, it can be assumed that the individual probabilities and relative abundances are about the same at a pressure of one atmosphere. Such a conclusion seems reasonable in view of the small total number of oscillators associated with an excited methane molecule ion.

It can further be assumed that the relative yields of the primary ionic fragments do not depend to a large extent on the energy of the incident electron. This assumption seems to be borne out by recent results in this Laboratory which indicate that, although the absolute values for the ionization cross sections leading to fragmentation depend critically on the electron energy, the relative values are about the same from the threshold to 300 e.v. This range of energies certainly includes the major portion of the ionizing electron degradation spectrum obtained in the high energy electron experiments carried out in the present work.

The G-values for the various processes can then be calculated in the usual manner from the ion pair yield (W = 27.1 e.v.) and the relative abundance of the particular fragmentary ion. Such a treatment gives the following yields for the primary ionic processes after assigning equal probability for molecular and atomic hydrogen formation concurrent with CH_2^+ production; $H\cdot$, 1.9; CH_4^+, 1.7; CH_3^+, 1.46; CH_2^+, 0.3; CH^+, 0.14; C^+, 0.04; H^+, 0.06; $CH_3\cdot$, 0.06; H_2, 0.36.

Secondary Processes.—Those secondary processes under consideration in this section include all reactions which would not be inhibited by the addition of a thermal free radical scavenger. This discussion is prompted by the observation that the "scavenged" yields of products in the methane radiolysis are invariant within experimental error regardless of the nature of the scavenger employed in the various laboratories. These processes include the reactions of the fragmentary ions produced as well as probable charge neutralization processes involving synthesis ions.

The reactions of the methyl ion with methane lead to the formation of the pressure stabilized ion $C_2H_7^+$, which dissociates at lower pressures into ethyl ions and molecular hydrogen. While such dissociation processes have not been investigated at normal radiolysis pressures, it has been established that the further reactions of this ion at 1 atm. lead almost quantitatively to the production of ethyl radicals and ethylene.[15] Such processes can account for the unscavengeable yield of ethylene (G = 0.70) and a molecular hydrogen yield equal to the G for $C_2H_7^+$ (1.46).

The over-all reactions of CH_5^+ are less well understood,[13] although it might be anticipated that the further reactions of protonated forms of stable molecules (CH_5^+, $C_2H_5^+$) with methane could not compete favorably with charge neutralization at lower conversions. The most energetically favorable process following neutralization of CH_5^+ should result in the production of nonscavengeable H_2 and an equivalent yield of methyl radicals, as has been suggested by some previous investigators.

It is apparent that the polymeric liquid is formed by an ionic chain mechanism. Due to the demonstrated high reactivity of the hydrogen deficient ions C^+, CH^+, and CH_2^+ in producing chain-lengthened ions in methane,[13] it is believed that polymer production arises from the subsequent reactions of these species. If the G-values for molecular (unscavengeable) hydrogen production resulting from the previous general treatment are summed, the total yield is equal to about 3.5. This is in almost exact agreement with the hydrogen yield observed in the free radical scavenged radiolysis (G = 3.5 to 3.7, depending on whether nitric oxide or ethylene is employed). Hence, the

(12) F. H. Field and J. L. Franklin, "Electron Impact Phenomena," Academic Press Inc., New York, N. Y., 1957.

(13) S. Wexler and N. Jesse, *J. Am. Chem. Soc.*, **84**, 3425 (1962).

(14) D. H. Landolt and M. Bornstein, "Zahlenwerte und Functionen," Vol. I, Part 3, Springer-Verlag, Berlin, 1951

(15) R. W. Looney, Ph.D. Thesis, University of Wisconsin, 1960.

formation of the liquid polymer must be accompanied by the release of hydrogen atoms with a $G(H\cdot)$ equal to twice the stoichiometric excess of hydrogen appearing in the total volatile product yield. Therefore, assuming no abstraction by hot atoms, $G(H\cdot)$ resulting from the chain condensation process must be about 4.3. It will be shown in the following section that abstraction processes must play a negligible role in the over-all decomposition, a condition which has already been indicated by the low conversion studies.

Free Radical Reactions.—A discussion of this extremely important aspect of the over-all problem depends critically on the relative rates of reactions 3 and 4.

$$H\cdot + H\cdot \xrightarrow[k_r]{CH_4} H_2 \qquad (3)$$

$$H\cdot + CH_4 \xrightarrow[k_a]{} H_2 + CH_3. \qquad (4)$$

Reaction 4 has been extensively investigated[16-18] and an average value of $k_a = 6.0 \times 10^5$ cc./mole-sec. at 20° for the specific bimolecular rate constant seems to represent an upper limit, reflecting the exceptional inertness of methane at moderate temperatures to hydrogen atom attack as compared to other hydrocarbons. Reaction 3, the termolecular combination of hydrogen atoms with methane (or the cell wall) as the third body, has not been investigated specifically. Rate constants for the combination, however, have been determined in the gas phase for various other third bodies including argon, H_2, and atomic hydrogen.[19,20] From considerations of the relative efficiencies of argon, H_2, and methane as third bodies in halogen atom recombination,[21,22] a lower limit for the termolecular rate constant at 20° for reaction 3 can be approximated. The value arrived at by this method is 1.5×10^{17} cc.^{2}/mole^2-sec., which lies between the experimentally determined values for the combination in the presence of argon and that obtained with atomic hydrogen as the third body.

In making a calculation of the relative rates of reactions 3 and 4 by the steady-state method, the following values were used for the various parameters: $k_a = 6.0 \times 10^5$ cc./mole-sec.; $k_r = 1.5 \times 10^{17}$ cc.^{2}/mole^2-sec.; dose rate $= 6.4 \times 10^{18}$ e.v./sec.; reaction volume = 1200 cc.; pressure = 760 mm.; and $G(H\cdot) = 6$. Evaluation of the steady-state equation indicates that under these conditions only 20% of the hydrogen atoms react by an abstraction process. This value must represent a maximum because (i) k_a was taken to be 6.0×10^5 cc./mole-sec. and recent work by Firestone[23] indicates a very much lower value ($<1.0 \times 10^5$ cc./mole-sec.), (ii) it was assumed that the absorbed energy was deposited uniformly throughout a reaction volume of 1200 cc., therefore completely neglecting any track effects or corrections for cell geometry (which might decrease the reaction volume by a factor of 10), and (iii) a consideration of combination reactions involving hydrogen atoms and other free radical species only further reduces the contribution from abstraction.

In conclusion, it is interesting to note that if one considers the intercombination reactions of the free radical species present in the system (methyl radicals resulting from the subsequent reactions of CH_5^+; ethyl radicals and ethylene from CH_3^+; and hydrogen atoms produced in the primary ionic fragmentation and concurrently with polymer formation) the remainder of the total product yield observed in the unscavenged radiolysis in the dose-independent region of conversions can be almost quantitatively accounted for. Although such an equivalence might be fortuitous, it does satisfy those criteria imposed by the currently available data concerning this problem.

(16) J. L. Carrico and R. G. Dickenson, *J. Am. Chem. Soc.*, **57**, 1343 (1935).
(17) M. R. Berlie and D. J. LeRoy, *Can. J. Chem.*, **32**, 650 (1954).
(18) D. J. LeRoy, *Discussions Faraday Soc.*, **14**, 120 (1953).
(19) L. Farkas and H. Schasse, *Z. physik. Chem.*, **111**, 1327 (1934).
(20) R. W. Patch, *J. Chem. Phys.*, **36**, 1919 (1962).
(21) E. Rabinowitch and W. C. Wood, *Trans. Faraday Soc.*, **32**, 907 (1936).
(22) K. E. Russell and J. Simons, *Proc. Roy. Soc.* (London), **A215**, 271 (1953).
(23) R. F. Firestone, *et al.*, *J. Am. Chem. Soc.*, **84**, 2279 (1962).

THE REACTION BETWEEN COBALT(III) AND SILVER(I) PERCHLORATES IN PERCHLORIC ACID MEDIA

BY J. B. KIRWIN, F. D. PEAT, P. J. PROLL, AND L. H. SUTCLIFFE

Donnan Chemical Laboratories, University of Liverpool, Liverpool, England

Received March 28, 1963

The reaction of cobalt(III) with silver(I) in perchlorate media has been studied in detail and found to consist of a rapid equilibrium producing silver(II) and cobalt(II), followed by the decomposition of silver(II). The mechanism of the latter reaction has been reported previously.[1] The value of the equilibrium constant for the equilibrium Co(III) + Ag(I) $\rightleftharpoons$ Ag(II) + Co(II) at a temperature of 25° is 0.76 with a free energy change of +162 cal. mole^{-1}; the associated over-all enthalpy change and over-all entropy change at 25° are 12 ± 3 kcal. mole^{-1} and 38 ± 10 cal. mole^{-1} deg.$^{-1}$, respectively.

Introduction

As part of a detailed study of the silver(I) catalyzed reaction between cobalt(III) and chromium(III) in perchloric acid media, it became necessary to study separately (i) the decomposition of silver(II) perchlorate and (ii) the reaction of cobalt(III) with silver(I). The former kinetic investigation has already been reported,[1] the latter reaction is the subject of the present paper. Since the mechanism of reaction (ii) contains that of reaction (i) it is essential to summarize the results already found. These are [a] a second-order disappearance with respect to the concentration of Ag(II), [b] an inverse dependence upon the concentration of Ag(I), [c] an inverse square dependence

(1) J. B. Kirwin, F. D. Peat, P. J. Proll, and L. H. Sutcliffe, *J. Phys. Chem.*, **67**, 1617 (1963).

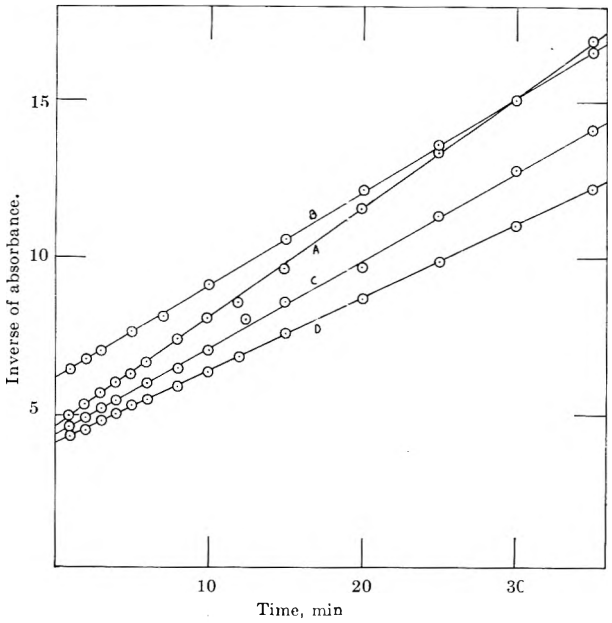

Fig. 1.—The plot of the inverse of the corrected absorbance *vs.* time: temperature, 25.0°; $[HClO_4]$ = 3.0 *M*, [Co(II)] = 7.2×10^{-2} *M*. Concentrations of Ag(I) are A = 0.288 *M*, B = 0.216 *M*, C = 0.173 *M*, and D = 0.072 *M*. Ionic strength = 3.65. [Co(III)] $\sim 7 \times 10^{-3}$ *M*.

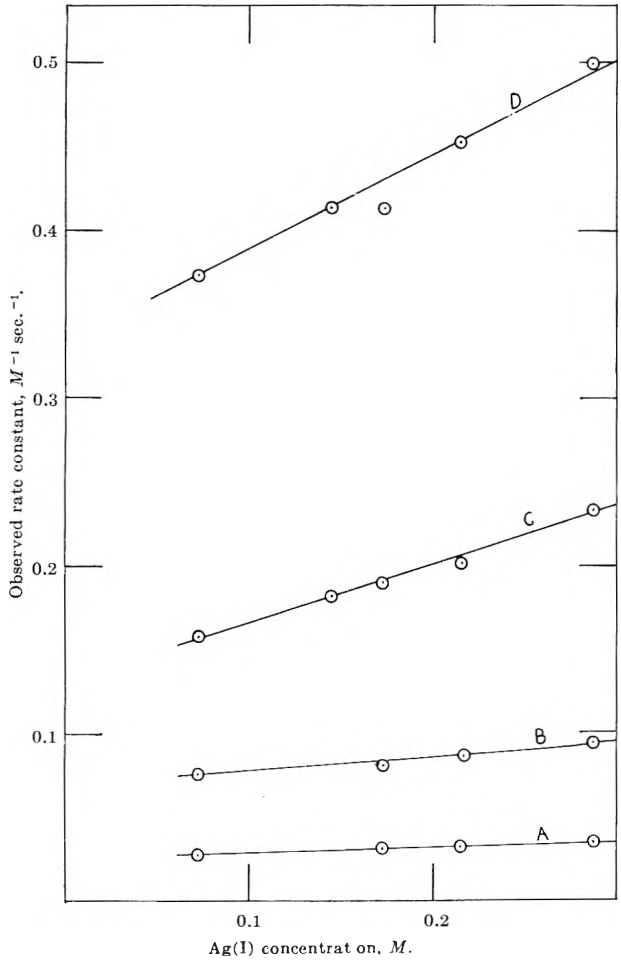

Fig. 2.—The plot of the observed rate constant *vs.* the concentration of Ag(I), at a constant ionic strength of 3.65 *M*: [Co(III)] $\sim 7 \times 10^{-3}$ *M*; [Co(II)] = 7.2×10^{-2} *M*; temperatures are A, 15.0°, B, 20.0°, C, 25.0°, and D, 30.0°.

upon the acidity, and [d] a dependence upon the perchlorate ion concentration of either power one or two, or both. The mechanism proposed to fit these observations except [d] is

$$2Ag^{2+} \underset{}{\overset{K}{\rightleftharpoons}} Ag^{+} + Ag^{3+} \qquad \text{rapid}$$

$$Ag^{3+} + H_2O \underset{}{\overset{K_1}{\rightleftharpoons}} AgO^{+} + 2H^{+} \qquad \text{rapid}$$

$$AgO^{+} \xrightarrow{k} Ag^{+} + \tfrac{1}{2}O_2 \qquad \text{rate determining}$$

from which the rate law was found

$$-\frac{d[Ag^{2+}]}{dt} = \frac{kKK_1[Ag^{2+}]^2}{[Ag^{+}][H^{+}]^2}$$

A suitable modification to this mechanism could not be found to account for the effect on the rate of the perchlorate ion concentration. The occurrence of this effect means that no inert salt is available to maintain constant ionic strength.

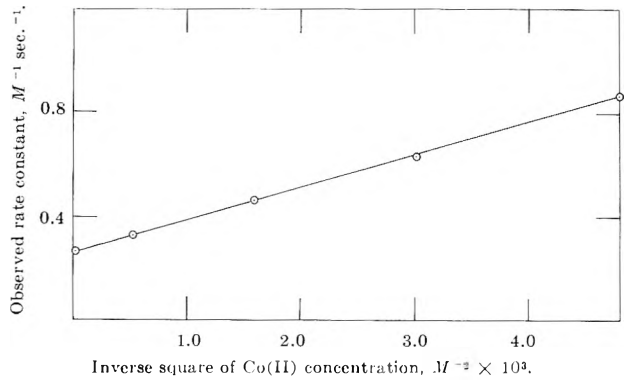

Fig. 3.—The plot of the observed rate constant *vs.* the inverse square of the concentration of cobaltous perchlorate at 25°: [Co(III)] $\sim 5 \times 10^{-3}$ *M*; [Ag(I)] = 0.575 *M*; $[HClO_4]$ = 3.75 *M*.

Experimental

Materials. Silver(I) Perchlorate.—The B. Newton Maine commercial product was used. The silver concentration was estimated by titration with thiocyanate in the usual manner.

Cobalt(II) Perchlorate.—The B. Newton Maine commercial product was used. The cobalt concentration was estimated spectrophotometrically from the known visible region absorption curve. Cobaltous perchlorate solutions used to establish the spectrum were analyzed gravimetrically.

Perchloric Acid.—The B.D.H. analytical reagent was used, the concentrations being estimated by titration with standard caustic soda or sodium bicarbonate solutions.

Cobalt(III) Perchlorate.—The cobalt(III) perchlorate solutions were prepared by ozonolysis of the cobalt(II) perchlorate in perchloric acid. The concentration of the cobalt(III) was estimated spectrophotometrically from the known visible region absorption curves.[2,3]

Apparatus and Technique.—The reaction of Co(III) and Ag(I) produces Ag(II) as an initial product. Ag(II) is a very reactive species; hence, in the present kinetic work all solutions were ozonized before use to remove trace amounts of reducing impurities.

All measurements were made using a Unicam SP500 spectrophotometer set at a wave length of 605 mμ. The temperatures of solutions were maintained to within ±0.05° using a cell block through which thermostated water flowed. An attempt was made to keep ionic strengths constant by replacing Ag(I) perchlorate and perchloric acid with sodium perchlorate and lithium perchlorate, respectively.

Results and Discussion

The visible and ultraviolet absorption spectra of Co(III),[2,3] Co(II),[2,3] and Ag(II)[1] in perchloric acid have been reported. The wave length 605 mμ, the position of an absorption maximum, was chosen for the measurement of the rate of disappearance of Co(III). At

(2) G. Hargreaves and L. H. Sutcliffe, *Trans. Faraday Soc.*, **51**, 786 (1955).
(3) L. H. Sutcliffe and J. R. Weber, *J. Inorg. Nucl. Chem.*, **12**, 281 (1960).

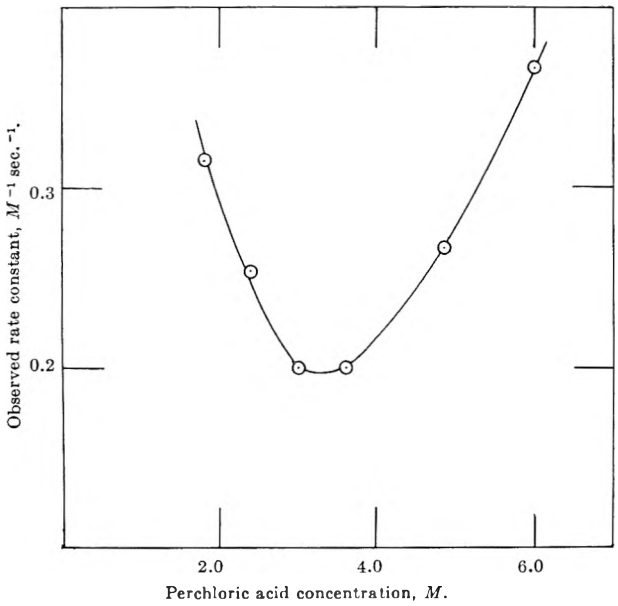

Fig. 4.—The plot of the observed rate constant against the concentration of perchloric acid at 25°. Initial concentrations of Co(II), Co(III), and Ag(I) have the constant values of 5.9×10^{-2} M, $\sim 5 \times 10^{-3}$ M and 1.15×10^{-1} M, respectively.

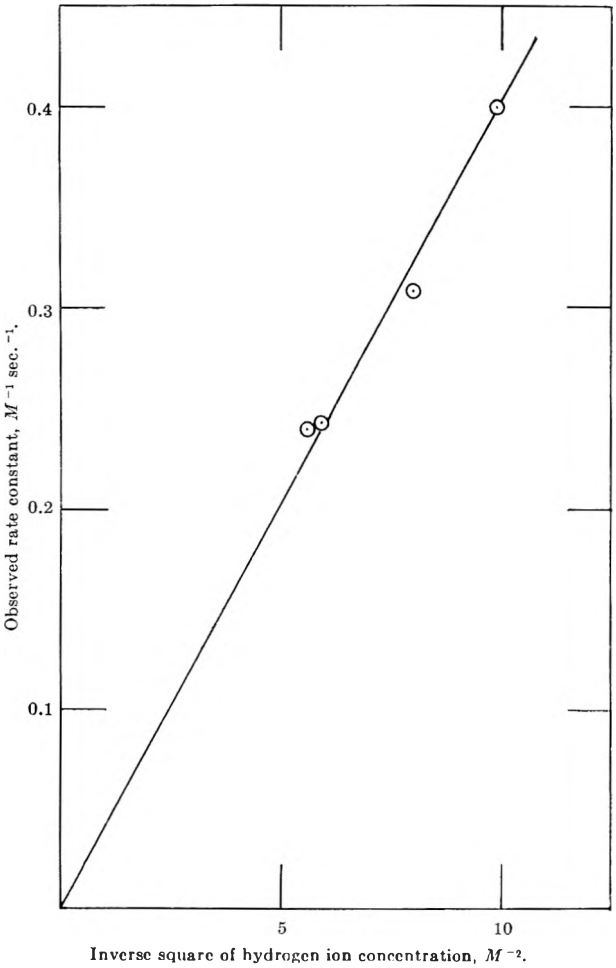

Fig. 5.—The observed rate constant plotted *vs.* the inverse square of the hydrogen ion concentration at 25°. Initial concentrations of Co(II), Co(III), and Ag(I) have the constant values of 7.2×10^{-2} M, 5.0×10^{-3} M, and 1.44×10^{-1} M, respectively. Ionic strength was held constant at 3.50 M.

this wave length a slight correction is needed for the absorption of Co(II); in all the results presented here this correction has been made. The final reaction products are Co(II) and Ag(I).

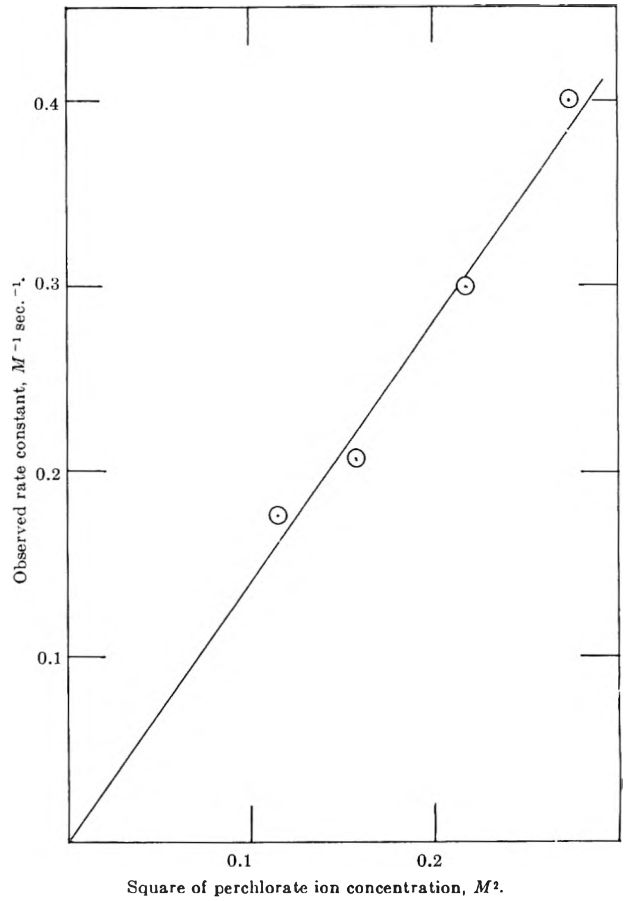

Fig. 6.—The plot of the observed rate constant *vs.* the square of the perchlorate ion concentration at 25°. Initial concentrations of Co(II), Co(III), and Ag(I) were constant at 7.2×10^{-2} M, $\sim 5 \times 10^{-3}$ M, and 1.44×10^{-1} M, respectively. The perchloric acid concentration was 2.25 M.

The rate of disappearance of Co(III) was found to be second order, as can be seen from Fig. 1, which shows the plot of the inverse of the corrected absorbance *vs.* time. The linearity is good and no deviations were found for reactions taken to 90% completion. In all the results quoted in this paper the Co(III) concentration was always less than the concentration of Ag(I).

As can also be seen from this figure, the effect of increasing the concentration of the Ag(I) is to increase the rate of reaction; this is in the opposite direction to that observed previously in the decomposition of Ag(II).[1] Plots of the observed rate constant against the concentration of Ag(I) are shown in Fig. 2, at four temperatures in the range 15 to 30°. It can be seen from this figure that the rate is linearly dependent on the concentration of Ag(I); obviously this relationship only holds when [Ag(I)] > [Co(III)]. Using the slopes of these plots an over-all heat of activation of 34 ± 4 kcal. mole^{-1} was found. This is considerably higher than the value of 11 ± 2 kcal. mole^{-1} found for the decomposition of divalent silver.[1] The rate obtained at zero Ag(I) concentration would correspond to the reduction of Co(III) by water. The latter reaction is too rapid to allow measurements to be made at low Ag(I) concentrations.

Figure 3 shows the effect of varying the cobaltous perchlorate concentration. The linearity of the plot for cobaltous concentrations less than about 0.15 M suggests that the rate expression contains the term $[Co(II)]^{-2}$.

From the results presented in Fig. 1, 2, and 3, it is apparent that the mechanism is of the form

$$\mathrm{Co(III)} + \mathrm{Ag(I)} \underset{}{\overset{K_1}{\rightleftharpoons}} \mathrm{Co(II)} + \mathrm{Ag(II)}$$

$$\mathrm{Ag(II)} \xrightarrow{k} \text{products}$$

In order to confirm that Ag(II) is produced, e.s.r. measurements were made on reaction mixtures. The characteristic signal[4] of divalent silver was observed. Further proof of the presence of Ag(II) was obtained from absorption in the visible and ultraviolet regions.

Attempts to measure the rate of the backward step of the equilibrium defined by K_2 were unsuccessful, as the reaction was found to be too rapid to study even at concentrations of Ag(II) and of Co(II) less than 10^{-4} M.

Since our results show a dependence on $[\mathrm{Co(II)}]^{-2}$, on $[\mathrm{Co(III)}]^2$, and on $[\mathrm{Ag(I)}]$, the equilibrium characterized by K_2 must be established rapidly, that is

$$[\mathrm{Ag(II)}] = \frac{K_2[\mathrm{Co(III)}][\mathrm{Ag(I)}]}{(\mathrm{Co(II)})}$$

Thus, the disappearance of Co(III) should follow a pattern similar to that already established for the decomposition of divalent silver. The rate law is then

$$-\frac{\mathrm{d}[\mathrm{Co(III)}]}{\mathrm{d}t} = \frac{-\mathrm{d}[\mathrm{Ag}^{2+}]}{\mathrm{d}t} =$$

$$\frac{kKK_1K_2^2[\mathrm{Co(III)}]^2[\mathrm{Ag(I)}]}{[\mathrm{Co(II)}]^2[\mathrm{H}^+]^2}$$

This only applies when $[\mathrm{Ag(I)}] > [\mathrm{Co(III)}]$ and $[\mathrm{Co(II)}]$ is less than about 0.15 M. The symbols k, K, K_1 have been defined in the Introduction. If the rate law is strictly comparable with that found previously for Ag(II) decomposition, then the effect of variation of acid concentration should lead to the observed rate constant passing through a minimum. There should also be an inverse square dependence upon the hydrogen ion concentration and a dependence upon the perchlorate ion concentration. It is known that the spectrum of Co(III) is not affected[3] by the changes in concentration of perchloric acid employed in the present experiments. Figure 4 shows the plot of the observed rate constant *vs.* the concentration of perchloric acid at 25°; the predicted minimum was observed.

Figure 5 shows the effect on the rate of the change in the concentration of hydrogen ions plotted as an inverse square dependence; this dependence is predicted by the preceeding mechanism. The ionic strength was kept at a constant value of 3.5 M, using lithium perchlorate to replace the perchloric acid.

Figure 6 shows the effect of the variation of perchlorate ion concentration upon the observed rate constant. The results have been plotted as a square dependence. The result is very similar to that found previously for the decomposition of Ag(II),[1] and, hence, the mechanism proposed earlier in this paper is substantiated.

The over-all heat of activation found from the results in this present paper is 34 ± 4 kcal. mole^{-1}, whereas the value obtained for the decomposition of Ag(II) is 11 ± 2 kcal. mole^{-1}. Thus, the equilibrium governed by K_2 must have an over-all enthalpy change associated with it of 12 ± 3 kcal. mole^{-1}.

K_2 was evaluated by direct comparison of the results obtained in the present paper with those obtained previously for the decomposition of Ag(II).[1] A value of 0.76 at 25.0° was obtained for an ionic strength of 3.5 M. Calculations of the free energy and over-all entropy changes associated with K_2 gave values of +162 cal. mole^{-1} and +38 ± 10 cal. mole^{-1} deg.$^{-1}$, respectively, at this ionic strength. The rather large value for the entropy change is probably a consequence of working with reaction mixtures of necessarily high ionic strength. The free energy change was also estimated from the standard oxidation–reduction potentials[5] of Ag^{2+}/Ag^+ and Co^{3+}/Co^{2+} when a value of 3.7 kcal. mole^{-1} was obtained. This value refers, of course, to zero ionic strength; hence, good agreement with the kinetic value cannot be expected.

Acknowledgment.—The authors wish to express their thanks to Mr. A. T. Bullock for making the e.s.r. measurements and to Mr. M. K. Jackson for his assistance. P. J. P. wishes to thank D. S. I. R. for the award of a fellowship during the tenure of which this work was completed.

(4) J. A. McMillan and B. Smaller, *J. Chem. Phys.*, **35**, 1698 (1961).

(5) R. Parsons, "Electrochemical Constants," Butterworths Scientific Publications, London, 1959.

VISCOELASTIC PROPERTIES OF POLYVINYL ACETATES. I. CREEP STUDIES OF FRACTIONS[1]

BY KAZUHIKO NINOMIYA AND JOHN D. FERRY

Department of Chemistry, University of Wisconsin, Madison, Wisconsin, and Japan Synthetic Rubber Company, Yokkaichi, Japan

Received April 22, 1963

Tensile creep measurements on three polyvinyl acetate fractions and shear creep measurements on five sharp fractions are reported. The range of molecular weights was from 5500 to 780,000 and the temperatures were between 19 and 143°. The temperature dependence of the creep compliance was described by the method of reduced variables. The shift factors were identical for all fractions provided that each was referred to a separate reference temperature corresponding to iso-free-volume states. The treatment implies a fractional free volume which decreases with increasing molecular weight approaching an asymptotic value. At very high molecular weight, the fractional free volume at 75° is $f_{75} = 0.0532$ (or $f_g = 0.026$) and its thermal expansion coefficient is $\alpha_f = 5.9 \times 10^{-4}$, in reasonable agreement with previous estimates. In the transition zone, the creep compliance and hence all viscoelastic properties are identical in the iso-free-volume states. In the terminal zone, the viscoelastic properties are characterized by the steady-state compliance, whose value (for the sharp fractions) is near that predicted by the Rouse theory, and the steady-flow viscosity, which is proportional to the 3.4 power of molecular weight. The viscosities of the sharp fractions agree very well with data of Long and of Fox and Nakayasu. The relaxation modulus in the terminal zone, derived from the creep compliance by approximation methods, agrees moderately well with the predictions of the Rouse theory in the molecular weight range from 10,500 to 262,000.

Introduction

The viscoelastic properties of certain polyvinyl acetate fractions and blends of fractions, investigated by tensile stress relaxation, have been reported previously.[2,3] We now present some creep measurements on polyvinyl acetate fractions. These were undertaken to extend the earlier work with (1) more direct determinations of the steady flow viscosity and steady-state compliance, which cannot be obtained from stress relaxation as reliably as from creep; (2) inclusion of fractionated samples covering a range extending to much lower molecular weights; (3) measurements in shear as well as extension, providing greater accuracy; (4) the basis for subsequent work on a large number of blends of fractions with widely different molecular weights, to be reported subsequently.

Experimental

Materials.—Three polyvinyl acetate fractions described earlier[3] as IX, X, and XI were used for tensile creep measurements. Their molecular weights were recalculated from their intrinsic viscosities, $[\eta]$, in acetone, using the relation of Matsumoto and Ōyanagi[4]

$$[\eta] = 1.08 \times 10^{-2} M^{0.72} \qquad (1)$$

and are given in Table I. Five fractions were used for shear creep measurements. These were kindly furnished by Dr. Y. Ōyanagi; they had been polymerized in ethyl acetate at 60° with α,α'-azobisisobutyronitrile as initiator, the conversion being less than 5%. They were fractionated by precipitation with *n*-heptane from very dilute methyl ethyl ketone solutions. The elaborate fractionation procedure is described elsewhere.[5] The molecular weights were also derived from intrinsic viscosities, with an empirical relation based on osmotic pressure data which deviates somewhat from eq. 1 at the lowest molecular weights. The molecular weight distribution is believed to be sharper in these samples than in samples IX, X, and XI; ultracentrifugal analysis of molecular weight distribution is in progress. The fractions were dried *in vacuo* at 80° for 1 week.

For tensile measurements, thin films were cast on mercury, leached in water, and dried as described previously.[2] For shear measurements, disk-shaped samples were molded under pressure at 150°.

TABLE I

POLYVINYL ACETATE FRACTIONS

Tensile creep		Shear creep	
Fraction	$M \times 10^{-3}$	Fraction	$M \times 10^{-3}$
IX	232	D-15	5.5
X	340	B-7	10.5
XI	480	1-A-11	112
		1-A-4	262
		12-B-2	780

Methods.—The tensile creep measurements on thin films were made with a chainomatic balance originally designed for stress relaxation studies[6] but modified for measurement of creep strain. Each creep run ordinarily was made over an interval of about 80 min., and the maximum tensile strain did not exceed 30%.

The shear creep measurements were made with the torsion pendulum of Plazek, Vrancken, and Berge,[7] modified for measurement of very small torsional deformation.[8] The optical path was increased from 14.34 to 26.25 ft. The sample disk dimensions ranged from 0.9 to 3.5 cm. in diameter and from 0.05 to 0.35 cm. in thickness. The height was measured at each temperature *in situ*, immediately after lowering the thermostat to bring the sample housing into view. The maximum shear strain including viscous flow did not exceed 0.1 and was much less than this at low temperatures.

Results

Tensile Creep.—The tensile creep compliance, $D_p(t)$, is plotted logarithmically in Fig. 1 for fraction XI at three different temperatures. Here the subscript p denotes that $D(t)$ has been multiplied by $T\rho/T_0\rho_0$, where ρ and ρ_0 are the densities at T and T_0, respectively, and T_0 is a reference temperature chosen as 348°K.; this procedure permits temperature shift factors to be determined from horizontal displacements. Similar curves were obtained for fractions IX (at 80.0, 92.2, and 104.6°) and X (at 93.0, 108.1, and 121.3°).

The results for each fraction were reduced to 75° by the method of reduced variables to give the composite curves illustrated in Fig. 2. The many individual points for all different temperatures, not shown, lay mostly

(1) Part XLII of a series on mechanical properties of substances of high molecular weight.

(2) K. Ninomiya and H. Fujita, *J. Colloid Sci.*, **12**, 204 (1957).

(3) K. Ninomiya, *ibid.*, **14**, 49 (1959).

(4) M. Matsumoto and Y. Ōyanagi, *J. Polymer Sci.*, **46**, 441 (1960).

(5) M. Matsumoto, "Kobunshi-jikkenkagaku-koza," Vol. 6, Kyoritsu-huppan, Tokyo, 1958, p. 1.

(6) K. Ninomiya, A. Kishimoto, and H. Fujita, *Kobunshi-kagaku*, **14**, 504 (1957); we are indebted to Professor Fujita for the use of this equipment at the Department of Fisheries, Maizuru, Japan.

(7) D. J. Plazek, M. N. Vrancken, and J. W. Berge, *Trans. Soc. Rheol.*, **2**, 39 (1958).

(8) K. Ninomiya, J. R. Richards, and J. D. Ferry, *J. Phys. Chem.*, **67**, 327 (1963).

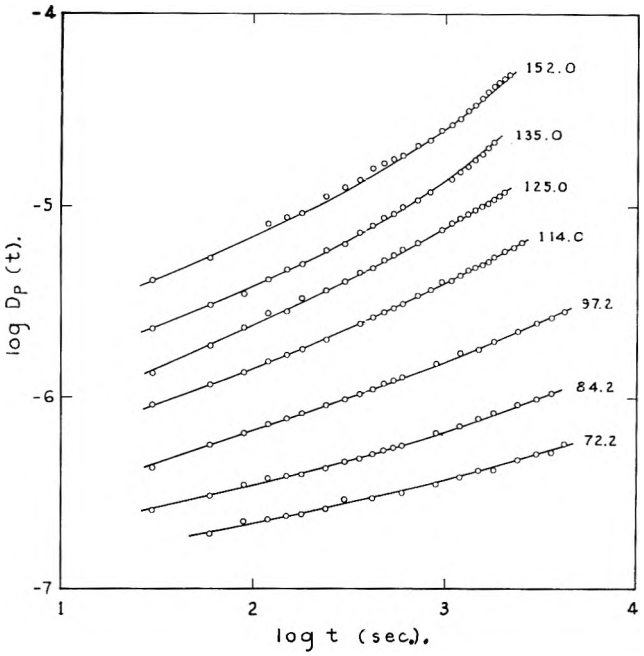

Fig. 1.—Tensile creep compliance of sample XI, plotted logarithmically at seven temperatures as indicated. The subscript p indicates multiplication by $T\rho/T_0\rho_0$.

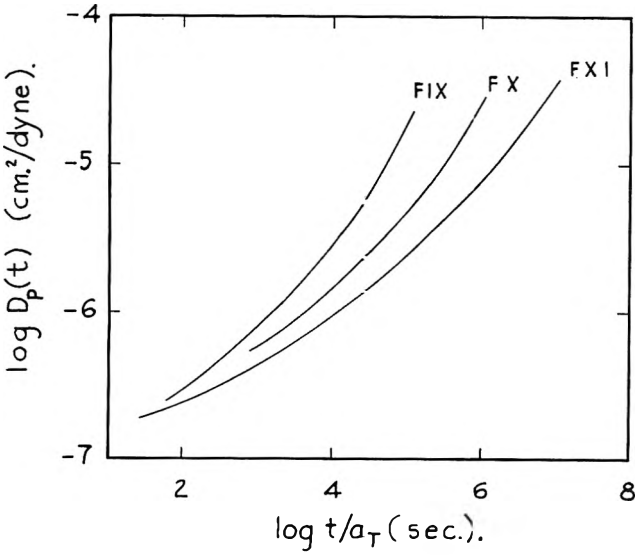

Fig. 2.—Tensile creep compliance of three samples as indicated, plotted logarithmically after reduction to 75°.

within 2% of the composite curves. The shift factors a_T used in the reduction followed the WLF equation[9]

$$\log a_T = -c_1^0(T - T_0)/(c_2^0 + T - T_0) \quad (2)$$

with $T_0 = 348$°K., $c_1^0 = 8.86$, and $c_2^0 = 101.6$. They are very close to those used for reducing earlier dynamic mechanical measurements on a polyvinyl acetate of broad molecular weight distribution.[10] The latter can be represented either by the "universal" WLF parameters with $T_0 = 349°$, $c_1^0 = 8.86$, and $c_2^0 = 101.6$, or by an alternative choice[11] equivalent to $T_0 = 348°$, $c_1^0 = 8.13$, and $c_2^0 = 89.8$.

Shear Creep.—The shear creep compliance, $J_p(t)$, is plotted logarithmically in Fig. 3 for fraction 1-A-11 at 13 different temperatures. Similar curves were obtained for fraction D-14 at 12 temperatures from 18.6 to 74.4°; for fraction B-7 at 12 temperatures from 32.3 to 74.6°; for fraction 1-A-4 at 14 temperatures from 39.1 to 102.8°; and for fraction 12-B-2 at 15 temperatures from 37.7 to 142.6°.

(9) M. L. Williams, R. F. Landel, and J. D. Ferry, *J. Am. Chem. Soc.*, **77**, 3701 (1955).

(10) M. L. Williams and J. D. Ferry, *J. Colloid Sci.*, **9**, 479 (1954).

(11) J. D. Ferry, "Viscoelastic Properties of Polymers," John Wiley and Sons, Inc., New York, N. Y., 1961, p. 219.

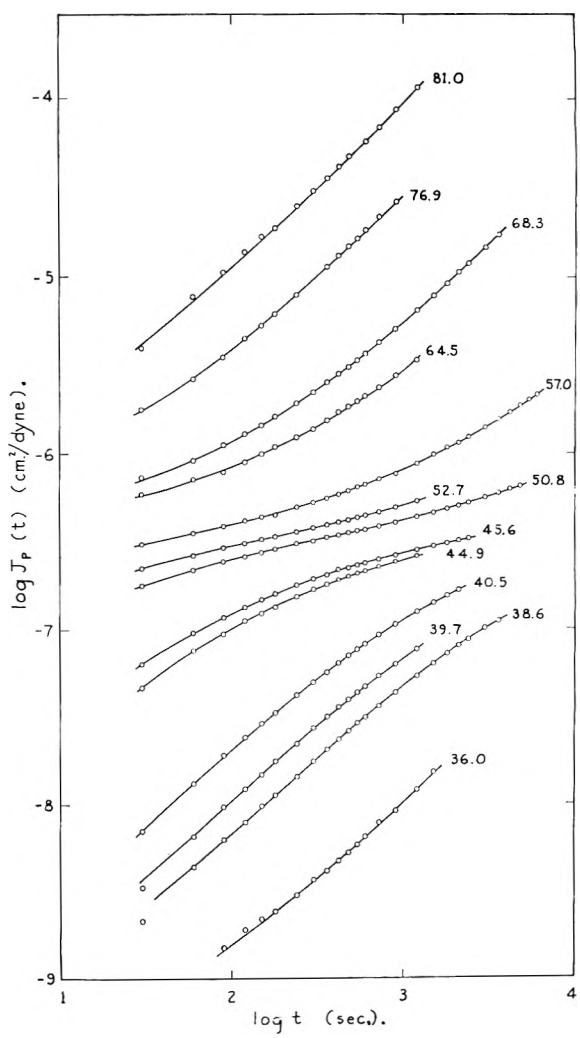

Fig. 3.—Shear creep compliance of sample 1-A-11, plotted logarithmically at 13 temperatures as indicated. The subscript p indicates multiplication by $T\rho/T_0\rho_0$.

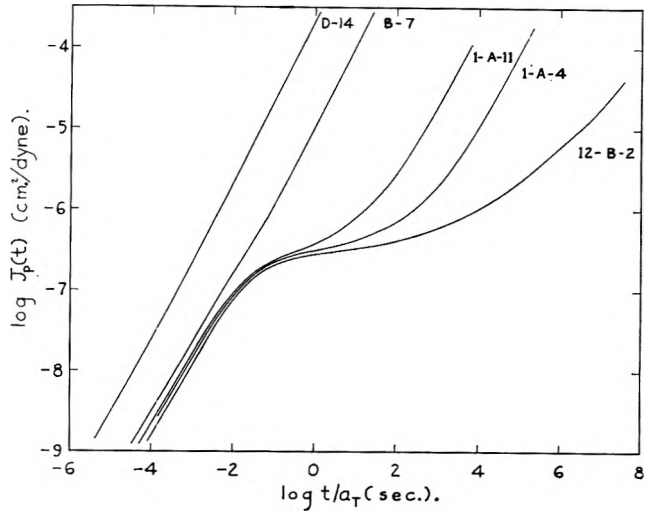

Fig. 4.—Shear creep compliance of five samples as indicated, plotted logarithmically after reduction to 75°.

The results for each fraction were again reduced to 75° by the method of reduced variables to give the composite curves illustrated in Fig. 4. Here the individual

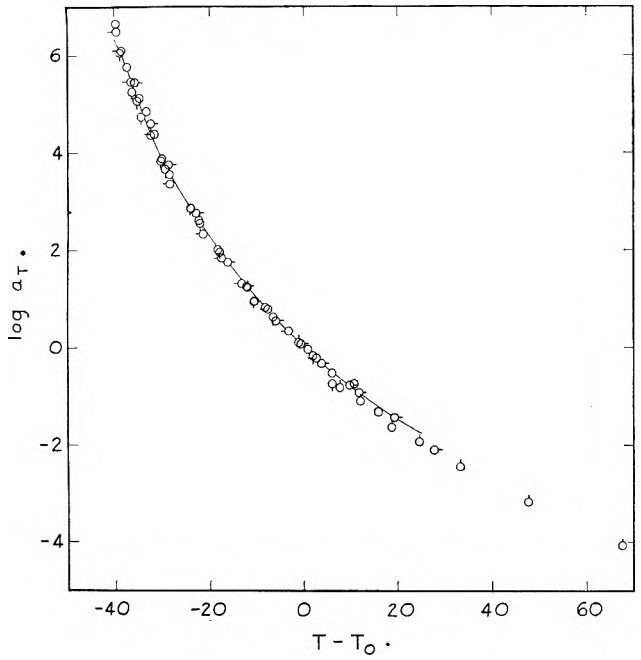

Fig. 5.—Log a_T for reduction of shear creep measurements, with each sample reduced to its own T_0 as given in Table II. No pip, sample D-14; pip left, sample B-7; down, 1-A-11; right, 1-A-4; up, 12-B-2.

points, far too numerous to display, were mostly within 1% of the composite curves. The shear measurements are not only more accurate but also extend into the transition region of retardation times. The expansion of the plateau zone with increasing molecular weight is evident; in fraction D-14, with molecular weight below the critical value for entanglement coupling, it is entirely absent, and in sample 12-B-2 it extends over 5 or 6 decades.

The shift factors a_T used in the reduction of Fig. 4, where the reference temperature is 75° throughout, were somewhat different for each fraction. (Such differences did not appear in the data of Fig. 2 because the molecular weight range is much narrower and the measurements were less precise.) Thus, curves of log a_T against T for the different fractions crossed at the point T = 348.2°, log a_T = 0 with different slopes. However, when a suitably different T_0 was chosen for each fraction, the temperature dependences of a_T for all fractions were found to be coincident. For this purpose, the small horizontal separations in the transition zone at the left of Fig. 4 were assumed attributable to the dependence of free volume on molecular weight. The fraction with the highest molecular weight, 12-B-2, was chosen as the reference with T_0 = 348.2°K. For each of the other fractions, the separation $\Delta \log t$ from 12-B-2 was measured on Fig. 4 in the transition zone, where log $J(t)$ is in the range from −8.5 to −7.5. This separation of time scale is equivalent to $\Delta \log a_T$ for the fraction concerned between 348.2°K. and a temperature of iso-free-volume with 12-B-2. The corresponding value of ΔT_0 was read from an empirical plot of log a_T against T for the fraction. The resulting reference temperatures representing iso-free-volume states are given in Table II. When log a_T based on T_0 for each fraction is plotted against $T - T_0$, values for all samples coincide as shown in Fig. 5.

A somewhat similar treatment was given previously[9] for viscosities of polyisobutylenes and polystyrenes of different molecular weights, although a separate reference temperature T_s was then chosen empirically or based on a dilatometric glass transition temperature, whereas the method used here evaluates T_0 more directly.

TABLE II

ISO-FREE-VOLUME REFERENCE TEMPERATURES AND FRACTIONAL FREE VOLUMES AT 75°

Fraction	T_0 − 273.2, °C.	f_{75}
D-14	58.0	0.0632
B-7	71.3	.0554
1-A-11	74.0	.0538
1-A-4	74.5	.0535
12-B-2	75.0	.0532

Discussion

Analysis of Temperature Dependence.—The shift factors for shear creep in Fig. 5 follow eq. 2 with the alternative parameters given above, T_0 = 348°, c_1^0 = 8.13, and c_2^0 = 89.8, as represented by the solid curve. In fitting these data, the high-temperature points for 12-B-2 are omitted because the annealing of this sample of high molecular weight to remove residual stresses was somewhat uncertain. These WLF parameters also fit extensive data on blends of these fractions, to be reported subsequently.[12] They correspond[11] to a fractional free volume of fraction 12-B-2 which at 75° is f_{75} = 0.0532, while its thermal expansion coefficient is $\alpha_f = 5.9 \times 10^{-4}$; the corresponding fractional free volume at the glass transition temperature, if 28° is chosen[13] for the latter, is 0.026. From α_f and the ΔT_0 for each fraction in an iso-free-volume state, each fractional free volume at 75° may be calculated, and these values are also listed in Table II. The free volume decreases with increasing molecular weight in the manner predicted by Fox and Flory,[14] although it is not exactly a linear function of $1/M$. This relation will be discussed further in the following paper.[12]

Viscoelastic Behavior in the Transition Zone.—Only the shear data extend into the transition zone. From the manner in which T_0 was obtained for each fraction (Table II), it follows that the creep compliance in the transition zone, where the curves are all parallel at the left side of Fig. 4, would be coincident if each fraction were at its own reference temperature T_0. Thus, the horizontal displacements at the left of Fig. 4, which reflect differences in the monomeric fraction coefficient, ζ_0, are quantitatively represented by the relation

$$\Delta \log \zeta_0 = (1/2.303)(1/f - 1/f_0) \qquad (3)$$

where f_0 is the fractional free volume of the fraction with highest molecular weight. The Doolittle concept of dependence of mobility on free volume holds here where the free volume varies with molecular weight at constant temperature.

It has been more common to study the viscoelastic behavior in the transition zone by dynamic measurements. A few measurements were made on fraction 1-A-4 with the Fitzgerald transducer apparatus[15,16] from 75 to 90°, and from the values of J' and J'' thus

(12) K. Ninomiya, J. D. Ferry, and Y. Ōyanagi, *J. Phys. Chem.*, **67**, 2297 (1963).
(13) A. Kovacs, R. A. Stratton, and J. D. Ferry, *ibid.*, **67**, 152 (1963).
(14) T. G Fox and P. J. Flory, *J. Appl. Phys.*, **21**, 581 (1950).
(15) E. R. Fitzgerald, *J. Chem. Phys.*, **27**, 1180 (1957).
(16) We are indebted to Mr. R. G. Mancke for these measurements.

obtained, the creep compliance function $J(t)$ was calculated by approximation methods.[17] The resulting curve reduced to 75° fell quite close to the creep function for this fraction in Fig. 4 from $\log t = -3.5$ to -1. At the shortest times, however, it was displaced to the left by about 0.2 on the logarithmic time scale. This discrepancy is not too disturbing because the dynamic data were measured near 75°, whereas the creep was measured near 40°; the reduction from 40 to 75° involves a large $\log a_T$ shift (about 5), so the absolute position of the transition zone on the time scale, derived from creep, may be somewhat uncertain. The relative positions in Fig. 4 are more precisely known, however.

From earlier dynamic measurements on another polyvinyl acetate sample (AYAX) with broad molecular weight distribution,[10] the creep compliance was calculated by approximation methods also; at short times ($\log t = -3.5$), the reduced curve for $\log J(t)$ against $\log t$ fell about 0.3 unit to the left of that derived from the dynamic measurements on fraction 1-A-4. This difference may reflect the presence of some components of very low molecular weight in sample AYAX.

Viscoelastic Behavior in the Terminal Zone.—In the steady state, the viscoelastic behavior is characterized by the viscosity η and the steady-state compliance J_e. These quantities were calculated for all fractions except 12-B-2 by an extrapolation procedure recently described.[18] For the latter, it was impossible to reach steady-state flow within the experimental time scale at the maximum apparatus temperature of 150°. Estimates of η and J_e for fraction 12-B-2 were made from data on binary blends of it with other fractions of lower molecular weight, to be reported subsequently.[12] The calculation of J_e for this fraction was based on a method given by Peticolas and Menefee[19] and is described elsewhere.[12] The values are listed in Table III, which includes η calculated for samples VI–XIII from earlier tensile stress relaxation data.[2] (The values of η listed for these samples are shear viscosities, obtained from tensile viscosities by dividing by 3.)

TABLE III

VISCOSITIES AND STEADY-STATE COMPLIANCES AT 75°

Fraction	log M	log η from stress relaxation,[2] poises	log η from creep, poises	log J_e from creep, cm.²/dyne
VI	5.072	8.12		
VII	5.013	8.09		
IX	5.365	9.24	9.36	−4.92
X	5.531	10.07	10.20	−4.77
XI	5.681	11.00	11.10	−4.54
XIII	5.919	12.75		
D-14	3.744		3.682	−8.07
B-7	4.041		4.988	−6.97
1-A-11	5.049		7.788	−5.60
1-A-4	5.418		9.076	−5.59[b]
12-B-2	5.892		11.47[a]	−4.87[a]

[a] Estimated from data on blends of this fraction with other fractions of lower molecular weight (see ref. 12). [b] Determination uncertain.

The viscosities from creep agree quite well with those from stress relaxation for fractions IX, X, and XI, even though the derivation from stress relaxation involves a less direct calculation and may be less reliable. The viscosities are all plotted in Fig. 6 against viscosity-average molecular weight, which is probably negligibly

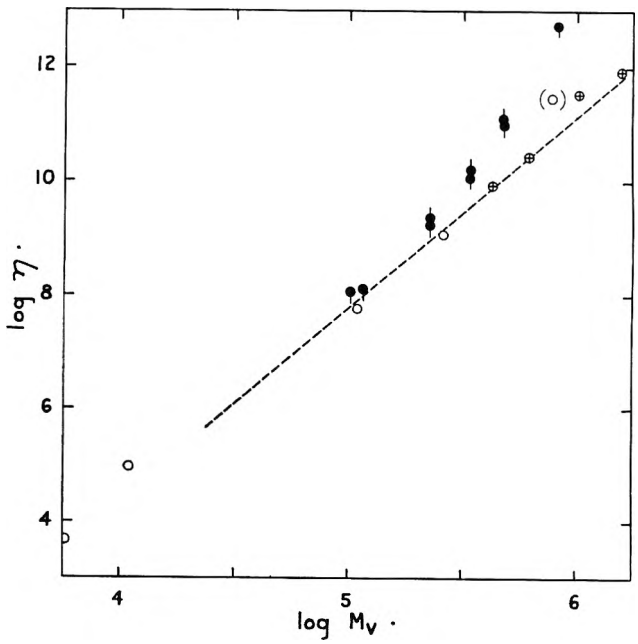

Fig. 6.—Shear viscosity plotted logarithmically against M_v. Open circles, shear measurements; black circles, calculated from tensile measurements; pip up from creep, pip down from stress relaxation.[2] Crossed circles, data of Long on linear fractions; dotted line, data of Fox and Nakayasu, with slope of 3.4.

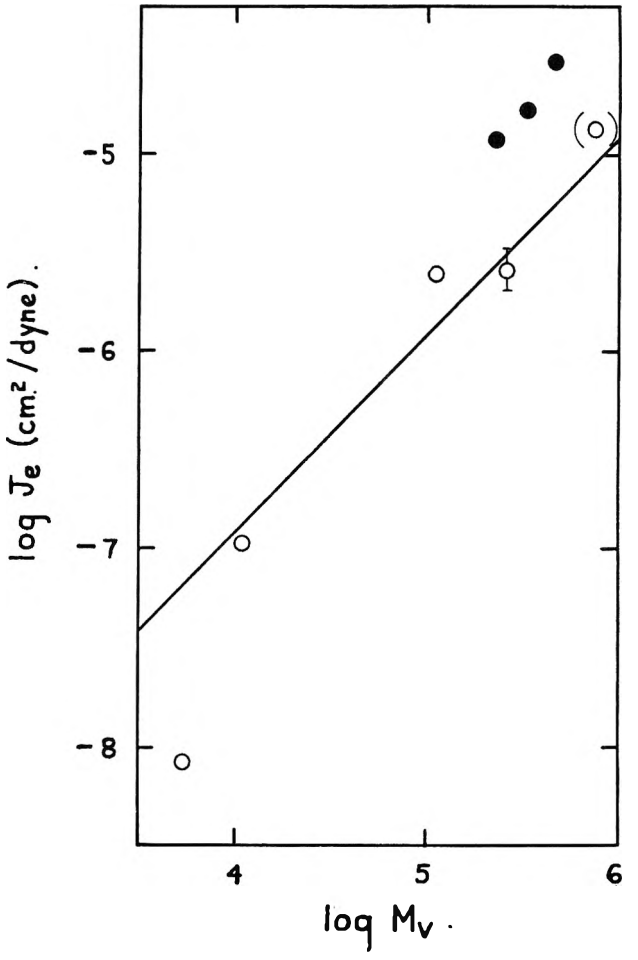

Fig. 7.—Steady-state shear compliance plotted logarithmically against M_v. Open circles, shear measurements; black circles, calculated from tensile creep measurements. The line is drawn from the theory of Rouse, eq. 4.

(17) K. Ninomiya and J. D. Ferry, *J. Colloid Sci.*, **14**, 36 (1959).
(18) K. Ninomiya, *J. Phys. Chem.*, **67**, 2152 (1963).
(19) W. L. Peticolas and E. Menefee, *J. Chem. Phys.*, **35**, 952 (1961).

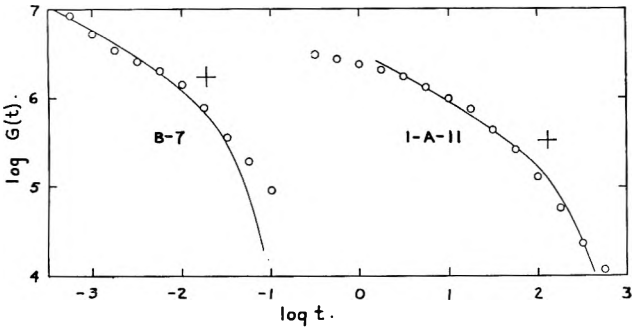

Fig. 8.—Relaxation modulus calculated from creep measurements and plotted logarithmically against time for fractions B-7 and 1-A-11. Curves are drawn from the theory of Rouse with parameters given in Table IV. Crosses denote the origin of the theoretical dimensionless function, corresponding to $t = \tau_1$ and $G(t) = \rho RT/M$.

different from the weight-average for these fractions. For the sharp fractions, the data are in gratifying agreement with measurements by Long[20] on linear polyvinyl acetate fractions and also recent data of Fox and Nakayasu,[21] which follow the familiar 3.4 power law. The viscosities of fractions IX, X, and XI are somewhat higher, a deviation conceivably associated with some branching. There are not enough points to define the break characteristic of the onset of entanglement coupling, but this will be precisely determined by the data on blends to be reported,[12] after reduction of viscosities to iso-free-volume states.

The steady-state shear compliances, covering a range of more than three decades, are plotted against molecular weight in Fig. 7. The values for IX, X, and XI, obtained from the measured tensile compliances by multiplying by 3, are somewhat higher than those for the other fractions. The difference no doubt reflects the sharper molecular weight distribution in the latter group, since J_e increases with breadth of molecular weight distribution.[22] In fact, the fractions used for the shear measurements are evidently fairly sharp, since their J_e values are not far from those predicted by the Rouse theory[22]

$$J_e = (2/5)M/\rho RT \qquad (4)$$

drawn in the figure as a solid line. Small departures from homogeneity can cause positive deviations. The negative deviation for fraction D-14 may be associated with its very low molecular weight, perhaps too small for the Rouse theory to be applicable.

It is of interest also to compare the time-dependent viscoelastic behavior in the terminal zone, before the steady state is reached, with the predictions of the Rouse[23] and Zimm[24] theories. (Here the term "Zimm theory" applies to the case of dominant hydrodynamic interaction, as in previous discussions.[25]) This is most readily done in terms of the relaxation modulus $G(t)$, which was calculated from the reduced creep data of Fig. 4 by the Leaderman–Smith approximation method.[26] Values obtained in this way for fractions B-7 and 1-A-11 are plotted as points in Fig. 8. The predictions of the theories can be expressed in dimensionless form as $G_R(t/\tau_1)$, where τ_1 is the theoretical terminal relaxation time and $G_R(t) = G(t)/(\rho RT/M)$, by analogy with the formulation of dynamic properties.[25] This function has been evaluated numerically for both theories.[27]

By matching logarithmic plots of G_R *vs.* t/τ_1 to experimental data with suitable horizontal and vertical shifts, the shapes of the time dependence can be compared and values of τ_1 and M can be obtained from the position of the origin of the theoretical plot on the experimental coordinate axes.[25] It was found that fractions B-7 and 1-A-11 fit the Rouse better than the Zimm theory; Rouse curves are drawn in Fig. 8. For 1-A-4, a fair fit was obtained by either theory; for 12-B-2, the end of the terminal zone was not well defined by the experimental data; for D-14, the calculation of $G(t)$ was not considered to be reliable.

The parameters τ_1 and M obtained from the matching procedure are given in Table IV. The value of τ_1 (in seconds) is compared with that calculated by the Rouse theory

$$\tau_1 = 6\eta M/\pi^2\rho RT \qquad (5)$$

and for the first two samples they are in excellent agreement. The molecular weights obtained from the viscoelastic data are of the correct order of magnitude, but that for B-7 (with no entanglements) is too high and the others (with entanglements present) are too low.

Table IV

Parameters Obtained from Applying Rouse Theory to Relaxation Modulus

Fraction	log τ_1 (obsd.)[a]	log τ_1 (calcd.)[b]	log M (obsd.)[c]	log M (act.)[d]
B-7	−1.73	−1.71	4.24	4.04
1-A-11	2.11	2.10	4.96	5.05
1-A-4	3.36	3.74	4.94	5.42

[a] From the position of cross on abscissa scale. [b] Calculated from eq. 5. [c] From position of cross on ordinate scale. [d] From intrinsic viscosity.

Interpretation of viscoelastic behavior in the plateau or rubbery zone requires a more detailed analysis which will be undertaken in the future.

Acknowledgment.—This work was supported in part by a grant from the National Science Foundation.

(20) V. C. Long, Ph.D. Thesis, University of Michigan, 1958.
(21) T. G Fox and H. Nakaysau, private communication.
(22) Reference 11, p. 171.
(23) P. E. Rouse, Jr., *J. Chem. Phys.*, **21**, 1272 (1953).
(24) B. H. Zimm, *ibid.*, **24**, 269 (1956).
(25) R. B. De Mallie, Jr., M. H. Birnboim, J. E. Frederick, N. W. Tschoegl, and J. D. Ferry, *J. Phys. Chem.*, **66**, 536 (1962).
(26) T. L. Smith, *Trans. Soc. Rheol.*, **2**, 131 (1959).
(27) N. W. Tschoegl, unpublished calculations.

VISCOELASTIC PROPERTIES OF POLYVINYL ACETATES. II. CREEP STUDIES OF BLENDS[1]

BY KAZUHIKO NINOMIYA,[2a] JOHN D. FERRY, AND YASUJI OYANAGI[2b]

Department of Chemistry, University of Wisconsin, Madison, Wisconsin

Received April 22, 1963

Shear creep measurements have been made on 18 binary blends of polyvinyl acetate fractions. In five blends, both component molecular weights exceeded M_c, the critical molecular weight for onset of coupling entanglements; in four, both were less than M_c; and in nine, one molecular weight was less and one greater than M_c. The temperature range was from 19 to 136°. The temperature dependence of the creep compliance was described by the method of reduced variables. The shift factors were identical for all the blends and also for the component fractions, provided that each was referred to a separate reference temperature corresponding to iso-free-volume states. From these reference temperatures and the thermal expansion coefficient of free volume obtained from the WLF equation ($\alpha_f = 5.9 \times 10^{-4}$), the fractional free volume, f, of each blend was calculated at 40°. In each blend, f was nearly equal to $v_1 f_1 + v_2 f_2$, where the subscripts refer to the two components and v is volume fraction. In terms of molecular weight, the expression $f = 0.0325 + 51.5/\bar{M}_n$ holds for nearly all the blends, where $\bar{M}_n$ is number-average molecular weight. In the transition zone of viscoelastic behavior, the creep compliances of all the blends are identical when reduced to iso-free-volume states. In the terminal zone, the viscosities and terminal relaxation times depend on the combined effects of free volume (a function of $\bar{M}_n$, governing the local friction coefficient) and molecular length (a function of $\bar{M}_w$, which includes entanglements if at least one species has $M > \bar{M}_c$). The former effect can be eliminated by reducing the viscosities to iso-free-volume states (η_{if}). For $\bar{M}_w < M_c$, η_{if} is closely proportional to $\bar{M}_w$, and for $\bar{M}_w > M_c$ it is closely proportional to $\bar{M}_w^{3.4}$ up to $\bar{M}_w = 400{,}000$. The steady-state compliances of most of the blends were close to the values calculated from the Rouse theory, $J_e = (2/5)\bar{M}_{z+1}\bar{M}_z/\bar{M}_w\rho RT$, where ρ is the density, especially when the possibility of some degree of molecular heterogeneity in the component fractions was taken into account by the method of Peticolas and Menefee. The ratio λ_2 of the terminal relaxation times of the component of higher molecular weight in the blend to their values in that pure component was obtained for each blend by applying the method of Ninomiya to the relaxation modulus, calculated from the creep compliance by approximation methods. For most of the blends, λ_2 was found to be quite close to the value calculated from the Rouse theory, $\eta_{b1}M_2/\eta_2\bar{M}_w$. The data in the terminal zone were further analyzed by the phenomenological theory of viscoelasticity in terms of two auxiliary dimensionless parameters N_{21} and D. Here $D = \lambda_1^{v_1}\lambda_2^{v_2}$, where λ_1 is the ratio of terminal relaxation times of the component of lower molecular weight in the blend to their values in that pure component. The data are all consistent with the assumption that $D = 1$ when the λ and η values are reduced to iso-free-volume states, and that otherwise $\log D = (1/2.303)(1/f - v_1/f_1 - v_2/f_2)$. The parameter N_{21} is the ratio of the contributions per unit volume of the two components to energy dissipation in steady flow. When both $M < M_c$, $N_{21} = M_2/M_1$ as predicted by the Rouse theory. When both $M > M_c$, N_{21} exceeds M_2/M_1 by a factor which ranges from 6 to 10 in our systems. When $M_1 < M_c < M_2$, N_{21} increases rapidly with v_2. In such a blend, λ_2 is far more dependent on composition than λ_1, because component 1 participates in the entanglements to a very limited extent. The plateau zones of the creep compliances of the blends also show interesting features for which an analysis will be attempted subsequently.

Introduction

In the preceding paper,[3] shear creep measurements on five polyvinyl acetate fractions ranging in molecular weight from 5500 to 780,000 were reported. The temperature dependence of the creep compliance and its molecular weight dependence in the transition zone were analyzed in terms of free volume; from analysis of the terminal zone, the viscosity and the steady-state compliance and their molecular weight dependence were obtained.

In the present paper, shear creep measurements on 18 binary blends of the above five fractions are reported. The blends include pairs in which both, only one, or neither of the components exceed in molecular weight the critical value for entanglement coupling. Their weight and number average molecular weights are in some cases very different. Nevertheless, some aspects of their viscoelastic properties can be described rather simply in terms of those of the components and furnish additional information on the role of free volume and entanglement coupling in such systems.

Experimental

Materials.—The five component fractions have been described.[3] Blends were prepared by dissolving pairs of fractions with chosen compositions in acetone at a concentration of about 3%. Each mixture was allowed to stand 2 days with occasional shaking and then was evaporated *in vacuo* at room temperature. The resulting film was leached in water for 2 days, dried *in vacuo* at room temperature, and stored over silica gel. Disk-shaped samples for torsional creep measurements were molded at 90 to 175°, higher temperatures being used for the higher molecular weights.

The volume fractions of the components were calculated from the weight fractions by assuming linear additivity of volumes, taking into account the dependence of density of polyvinyl acetate on molecular weight determined in an earlier study.[4]

The compositions and weight and number-average molecular weights, $\bar{M}_w$ and $\bar{M}_n$, of the blends are given in Table I. Each pair of components is denoted by an initial letter (series L to S, inclusive.) The component of lower molecular weight always has the subscript 1, as in previous discussions of such blends,[5,6] and the composition is given as the volume fraction v_2. The list is divided into three groups accordingly as both M_1 and M_2 are greater than M_c, neither is greater than M_c, or only M_2 is greater than M_c. The value of M_c, the critical molecular weight for onset of entanglement coupling as determined from the molecular weight dependence of viscosity, is given as 29,000 in a recent compilation[7]; from the results of the present paper it is estimated to be 22,000.

Method.—The creep measurements were made with the Plazek pendulum[8] as described previously.[3]

Results

Most of the blends were studied over a sufficiently wide temperature range to encompass both the ter-

(1) Part XLIII of a series on mechanical properties of substances of high molecular weight.

(2) (a) Japan Synthetic Rubber Company, Yokkaichi, Japan; (b) Kurashiki Rayon Company, Osaka, Japan.

(3) K. Ninomiya and J. D. Ferry, *J. Phys. Chem.*, **67**, 2292 (1963).

(4) K. Ninomiya and H. Fujita, *J. Colloid Sci.*, **12**, 204 (1957).

(5) K. Ninomiya, *ibid.*, **14**, 49 (1959).

(6) K. Ninomiya and J. D. Ferry, *ibid.*, **18**, 421 (1963).

(7) H. Markovitz, T. G Fox, and J. D. Ferry, *J. Phys. Chem.*, **66**, 1567 (1962).

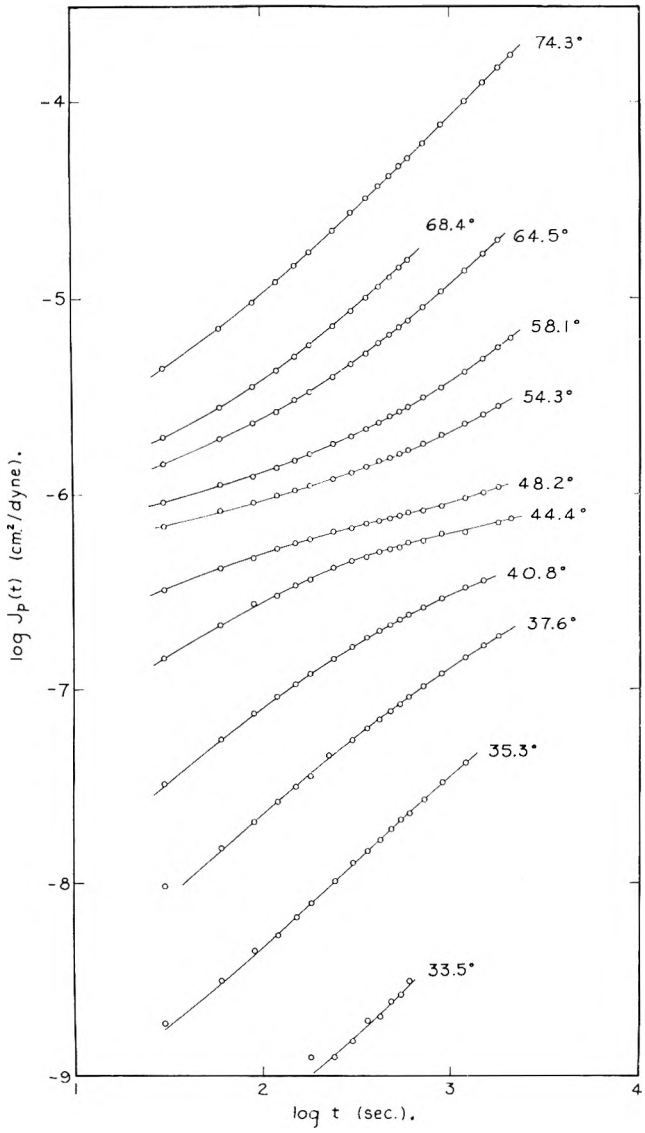

Fig. 1.—Shear creep compliance of blend Q-8, plotted logarithmically at 11 temperatures as indicated. The subscript p denotes multiplication by $T\rho/T_0\rho_0$, where T_0 = 313.2°K.

TABLE I

COMPOSITIONS AND AVERAGE MOLECULAR WEIGHTS OF BLENDS

Blend no.	Comp. 1	Comp. 2	$M_1 \times 10^{-3}$	$M_2 \times 10^{-3}$	v_2	$\bar{M}_n \times 10^{-3}$	$\bar{M}_w \times 10^{-3}$
			$M_1 > M_c, M_2 > M_c$				
L-3	1-A-11	1-A-4	112	262	0.318	137	160
L-7					.700	187	217
M-4	1-A-11	12-B-2	112	780	.396	170	389
N-4	1-A-4	12-B-2	262	780	.415	362	477
N-7					.649	460	598
			$M_1 < M_c, M_2 < M_c$				
O-2	D-14	B-7	5.5	10.5	0.184	6.04	6.4
O-4					.382	6.73	7.4
O-6					.601	7.72	8.5
O-8					.793	8.84	9.5
			$M_1 < M_c, M_2 > M_c$				
P-4	D-14	12-B-2	5.5	780	0.384	8.94	305
Q-1	D-14	1-A-11	5.5	112	.095	6.07	15.7
Q-2					.185	6.70	25.4
Q-4					.395	8.85	47.9
Q-6					.598	12.8	69.5
Q-8					.794	22.6	90.5
R-4	D-14	1-A-4	5.5	262	.386	8.89	105
R-8					.792	24.6	209
S-4	B-7	12-B-2	10.5	780	.412	17.8	330

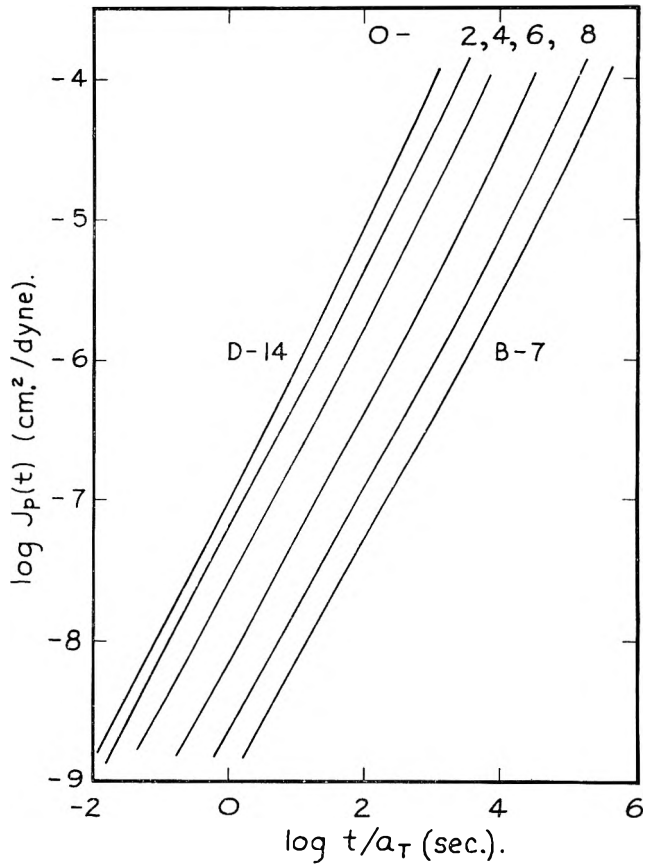

Fig. 2.—Shear creep compliance of four blends of the O series and of the component fractions, all reduced to 40° and plotted logarithmically.

minal zone and a portion of the transition zone of the viscoelastic spectrum, with the plateau zone between. In the O series, both molecular weights are below the critical level for entanglement, and the plateau zone was absent. In the L series, measurements did not extend into the transition zone.

An example of the creep compliance at various temperatures is shown for blend Q-8 in Fig. 1. Similar groups of curves were obtained for the other blends at different temperatures whose numbers and ranges are summarized in Table II.

The results for each sample were reduced by the method of reduced variables to give single composite curves. The reference temperature was chosen as 40° instead of 75° as used before[3] because many of the systems were studied primarily at lower temperatures. The shift factors a_T, obtained empirically, were different for each blend, but they are all related in a simple manner as explained below. The composite reduced creep compliances of the 18 blends are shown in Fig. 2–5. The individual points, far too numerous to reproduce, were mostly within 1% of the curves. Tabular data interpolated from large-scale graphs are available upon request to the authors.

O Series.—The molecular weights of the components of the O series, D-14 and B-7, are both below the critical value for entanglements, and no plateau zone appears in the creep compliance (Fig. 2). The creep is dominated by viscous flow, but the slopes of the logarithmic plots are slightly less than unity and exhibit inflections demonstrating a small elastic effect. The

(8) D. J. Plazek, M. N. Vrancken, and J. W. Berge, *Trans. Soc. Rheol.*, **2**, 39 (1958).

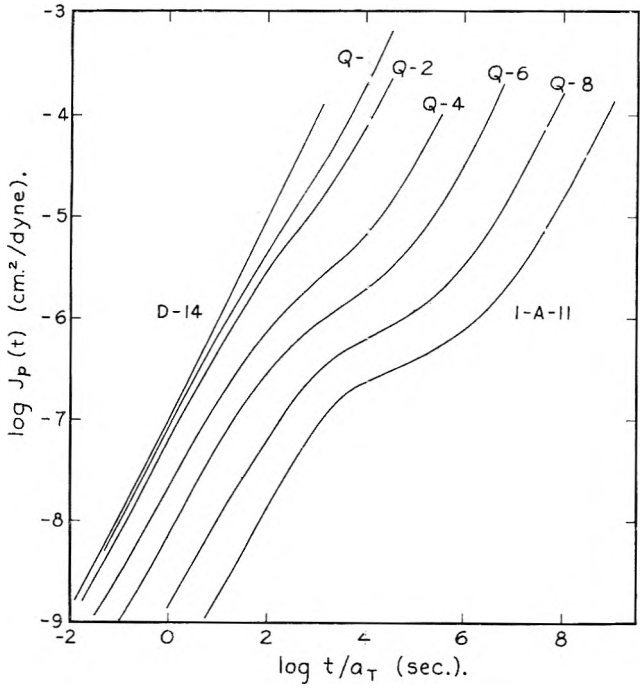

Fig. 3.—Shear creep compliance of five blends of the Q series, and of the component fractions, all reduced to 40° and plotted logarithmically.

TABLE I

TEMPERATURE RANGES, ISO-FREE-VOLUME REFERENCE TEMPERATURES, AND FRACTIONAL FREE VOLUMES AT 40°

Fraction or blend	No. of temps.	Range	$T_0 - 273.2$	f_{40}
D-14	12	18.6–74.4°	23.0	0.0425
B-7	12	32.3–74.6°	36.3	.0347
I-A-11	13	36.0–81.0°	39.0	.0331
I-A-4	14	39.1–102.8°	39.5	.0328
12-B-2	15	37.7–142.6°	40.0	.0325
L-3	8	52.3–87.0°	39.15[a]	.0330
L-7	8	53.6–90.0°	39.35[a]	.0329
M-4	12	38.1–136.5°	39.4[a]	.0329
N-4	13	37.4–131.8°	39.7[a]	.0327
N-7	6	74.7–143.5°	39.8[a]	.0326
O-2	6	23.5–45.0°	26.2	.0407
O-4	7	23.4–50.4°	27.6	.0398
O-6	6	28.3–50.7°	31.8	.0373
O-8	6	33.5–58.2°	34.2	.0359
P-4	11	28.2–99.8°	31.0	.0378
Q-1	9	22.6–54.3°	25.0	.0414
Q-2	7	22.4–51.1°	26.1	.0407
Q-4	10	24.5–63.8°	28.0	.0396
Q-6	9	29.1–68.8°	31.8	.0373
Q-8	11	33.5–74.3°	36.0	.0349
R-4	10	25.6–69.4°	28.7	.0392
R-8	9	33.9–92.5°	35.5	.0352
S-4	10	34.4–134.9°	37.0	.0343

[a] Interpolated linearly from values for components.

shift of the time scale with composition is slightly different in the transition zone (shortest times) from that in the terminal zone (longest times), and the differences will be analyzed below.

Q Series.—The 5 blends of the Q series are composed of one component (D-14) with $M < M_c$ and one (I-A-11) with $M > M_c$. With increasing proportion of the latter, the plateau zone gradually makes its appearance and broadens, while the magnitude of the compliance in the plateau region drops (Fig. 3). The shift of the time scale with composition is much greater in the terminal

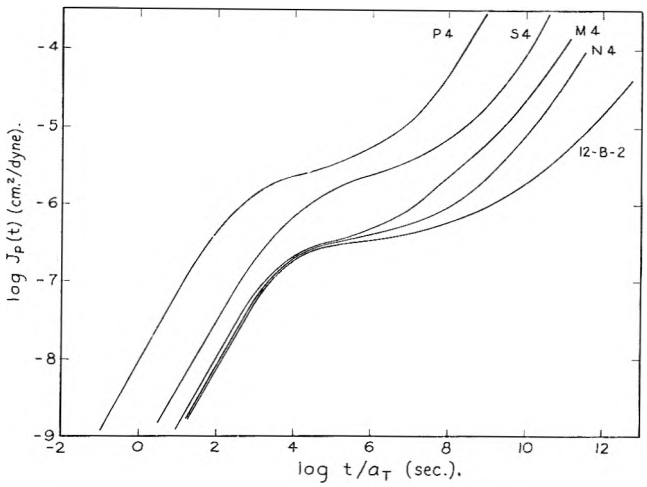

Fig. 4.—Shear creep compliance of fraction 12-B-2 and of four blends containing about 40% by volume of 12-B-2, all reduced to 40° and plotted logarithmically.

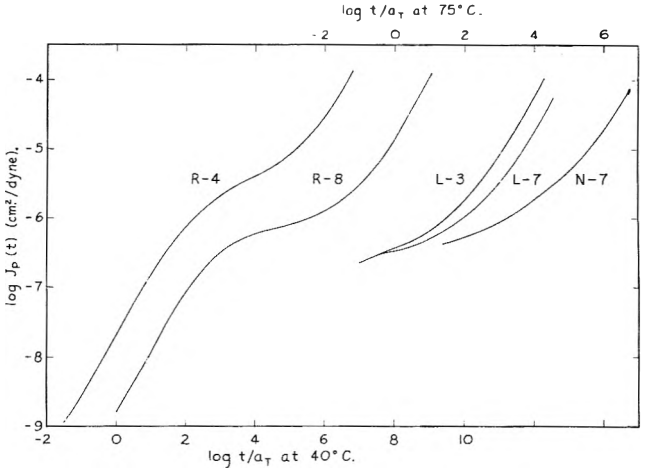

Fig. 5.—Shear creep compliance of blends L-3, L-7, and N-7 reduced to 75° and R-4 and R-8 reduced to 40°, plotted logarithmically.

than in the transition zone because of the role of entanglements in the former.

Comparison of Blends with About 40% 12-B-2.—The component of highest molecular weight, 12-B-2, is combined with others of various lower molecular weights in the same proportions (*viz.*, about 40% of 12-B-2) in the comparison shown in Fig. 4. When the component of lower molecular weight has $M_1 > M_c$, exemplified by M-4 and N-4, the creep compliance curves lie very close to that for 12-B-2 in the transition and the beginning of the plateau zone; while there are distinguishable differences, the principal effect of the component of lower molecular weight appears in the terminal zone. When $M_1 < M_c$, exemplified by S-4 and P-4, the plateau is narrowed and its level is shifted markedly upward, while both the transition and terminal zones are shifted to shorter times.

L and R Series and N-7.—The R series, in which $M_1 < M_c$ and $M_2 > M_c$, is shown in Fig. 5 together with the results for L-3, L-7, and N-7, which were studied in the terminal zone only. The latter, in which both M_1 and M_2 exceed M_c, are reduced to 75° rather than 40° because the measurements did not extend to lower temperatures. The shapes of the curves for R-4 and R-8 resemble those of P-4, Q-4, and S-4 in Fig. 4, while the others resemble those of M-4 and N-4.

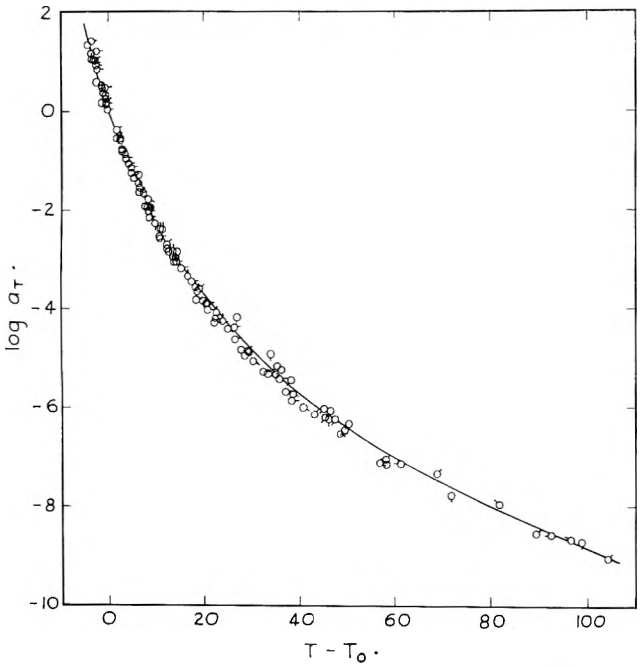

Fig. 6.—Log a_T for reduction of creep compliance, with each blend reduced to its own reference temperature as given in Table II. Pip up, blends of series O; successive 45° rotations clockwise, series P, Q, R, S, L, M, and N.

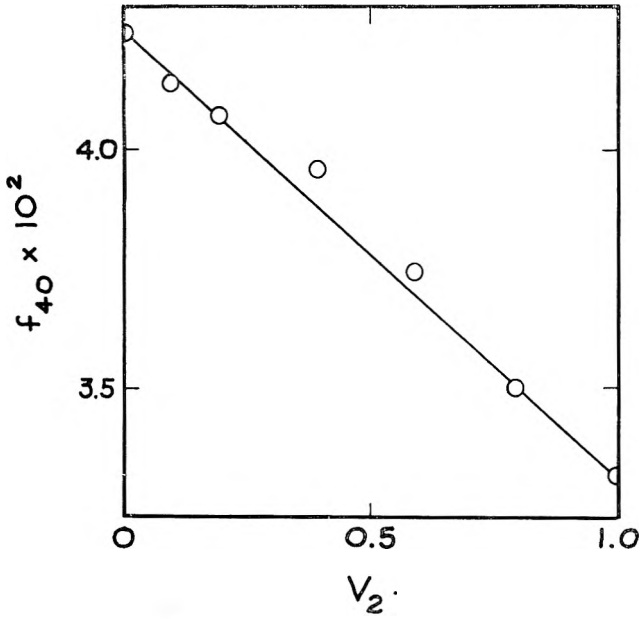

Fig. 7.—Fractional free volume at 40° for blends of Q series, from temperature dependence (Table II), plotted against volume fraction of high molecular weight component.

Analysis of Temperature Dependence.—While the reduced curves in Fig. 2–5 are all based on the same reference temperature of 40° (except for three curves in Fig. 5 based on 75°), the temperature dependence of the shift factors a_T can be analyzed more simply by choosing a separate reference temperature T_0 for each blend, as was done for the individual components in the preceding paper.[3] As before, the component of highest molecular weight (12-B-2) was taken as the standard of reference, though its T_0 was chosen as 40.0 + 273.2° instead of 75.0 + 273.2°. The separation $\Delta \log t$ in the transition zone, where $\log J(t)$ is in the range from −7.5 to −8.5, was obtained between each blend and 12-B-2 from measurements on Fig. 2–5. If the shift of the time scale (equivalent to a difference in the monomeric friction coefficient) can be attributed to the difference in free volume, it corresponds to $\Delta \log a_T$ for the blend between 40° and a (lower) temperature where the free volume of the blend is the same as that of 12-B-2 at 40°. The value of this lower temperature then was read from an individual graph of $\log a_T$ against T for the blend. The results are listed in Table II. (Where the difference in temperature was less than 1°, for blends whose components were both of high molecular weight, the creep curves in the transition zone were very close together as seen in Fig. 4; so T_0 was interpolated linearly on the basis of volume fraction between the values for the components, instead of being determined by the procedure described above.)

When $\log a_T$ referred to each individual T_0 is plotted against $T - T_0$, a single composite curve is obtained for all the blends, as shown in Fig. 6. It is practically identical with the curve which describes the similar composite plot for the individual components,[3] after reduction from 75 to 40°. It is gratifying to find that in these blends with a very wide range of molecular weight and heterogeneity the temperature dependence of viscoelastic rate processes can be described by a single parameter T_0 which in turn is related to free volume.

The solid curve in Fig. 6 corresponds to the WLF equation[9] in the form

$$\log a_T = -13.32(T - T_0)/(54.8 + T - T_0) \quad (1)$$

in which the coefficients differ from those previously given for the components[3] because the basic reference temperature here is 40°. From this we obtain for the fractional free volume $f_{40} = 0.0325$ for fraction 12-B-2 and for its thermal expansion coefficient $\alpha_f = 5.9 \times 10^{-4}$. (Thus, $f_{75} = 0.0532$ for fraction 12-B-2 as before.) For each of the blends, $f_0 = 0.0325$ at its own T_0; the fractional free volumes of the blends can all be compared at 40° by calculating $f_{40} = f_0 + \alpha_f(313.2° - T_0)$ and these are given in the last column of Table II.

Additivity of Free Volume.—For the Q series, whose components have significantly different fractional free volumes, f is plotted in Fig. 7 against volume fraction, v_2, of component 2. The points lie close to a straight line, corresponding to the additivity relation

$$f_{bl} = f_1 v_1 + f_2 v_2 \quad (2)$$

where the subscript bl refers to the blend and 1 and 2 to the respective components. A further confirmation of eq. 2 is given in Fig. 8, where the fractional free volume for each blend as determined directly from analysis of temperature dependence is plotted against the value calculated by eq. 2 from the blend components. The points all lie close to a straight line with unit slope.

In accordance with the concepts of Fox and Flory,[10,11] f_{bl} should be a linear function of reciprocal number-average molecular weight. The appropriate plot is shown in Fig. 9, and all points fall quite near a single line except for component B-7 and the blends which contain this component (O, S), all of which are somewhat low. There appears to be some anomalous feature in B-7, although it is not apparent in comparisons

(9) M. L. Williams, R. F. Landel, and J. D. Ferry, *J. Am. Chem. Soc.*, **77**, 3701 (1955).
(10) T. G Fox and P. J. Flory, *J. Appl. Phys.*, **21**, 581 (1950).
(11) T. G Fox and S. Loshack, *J. Polymer Sci.*, **15**, 371 (1955).

of any other properties. The slope of the line drawn in Fig. 9 is 51.5 g./mole; multiplied by the limiting specific volume at high molecular weight, 0.843 ml./g. at 40°, we have 43.4 ml., which may be interpreted as the excess free volume associated with a mole of (both) molecular ends.

Viscosities and Steady-State Compliances.—From the reduced creep curves in Fig. 2–5, the viscosities (η) and steady-state compliances (J_e) were calculated by an extrapolation method recently described.[12] The viscosities are probably more precise than the compliances. The logarithms of η and J_e at 40° for blends and components are listed in Table III.

TABLE III

VISCOSITIES AND STEADY-STATE COMPLIANCES

Fraction or blend	log η at 75°	log η at 40°	log η at f = 0.0325	log J_e at 40°
D-14		7.040	10.26	−8.03
B-7		9.550	10.54	−6.93
1-A-11	7.788	12.900	13.18	−5.56
1-A-4	9.076	14.237	14.39	−5.55[a]
12-B-2	11.47	16.72	16.72	−4.83
L-3	8.288	13.453	13.69	−5.11
L-7	8.824	14.009	14.20	−5.47
M-4	9.851	15.064	15.23	−4.64
N-4	10.430	15.644	15.72	−4.68
N-7	10.959	16.209	16.25	−5.0[a]
O-2		7.365	10.38	−6.72
O-4		7.804	10.40	−6.68
O-6		8.491	10.45	−6.72
O-8		9.124	10.51	−6.89
P-4	8.504	12.602	14.72	−4.24
Q-1		7.757	10.88	−4.92
Q-2		8.217	11.22	−4.85
Q-4		9.570	12.08	−5.19
Q-6		10.548	12.52	−5.35
Q-8		11.821	12.97	−5.43
R-4		10.778	13.26	− 5.2[a]
R-8	8.291	12.979	14.19	− 5.2[a]
S-4	9.441	14.179	14.87	−4.47

[a] Determination uncertain.

The viscosities of the blends with large proportions of high molecular weight components, expressed thus reduced to 40°, have been extrapolated far below the temperatures at which steady-state flow was approached experimentally and represent physically unrealizable magnitudes (10^{12}–10^{16} poises) Log η at 75° is also listed for these, therefore, to provide values within a physically measurable range. Nevertheless, the values at 40° are comparable among themselves and form the basis for comparison in iso-free-volume states as will be discussed below.

Discussion

Viscoelastic Behavior in the Transition Zone.—The shape of the creep compliance in the transition zone is the same for all fractions and blends. Its position on the time scale, which may be related to the monomeric friction coefficient[3] ζ_0 or some analogous parameter such as a segmental jumping frequency,[13] depends on the fractional free volume alone as is evident from the manner in which the T_0 values were calculated in Table II. Thus

$$\log \zeta_0 = \log \zeta_{00} + (1/2.303)(1/f - 1/f_0) \quad (3)$$

(12) K. Ninomiya, *J. Phys. Chem.*, **67**, 152 (1963).

(13) T. G Fox, S. Gratch, and S. Loshaek, in F. R. Eirich, "Rheology," Vol. I, Academic Press, New York, N. Y., 1956, p. 480.

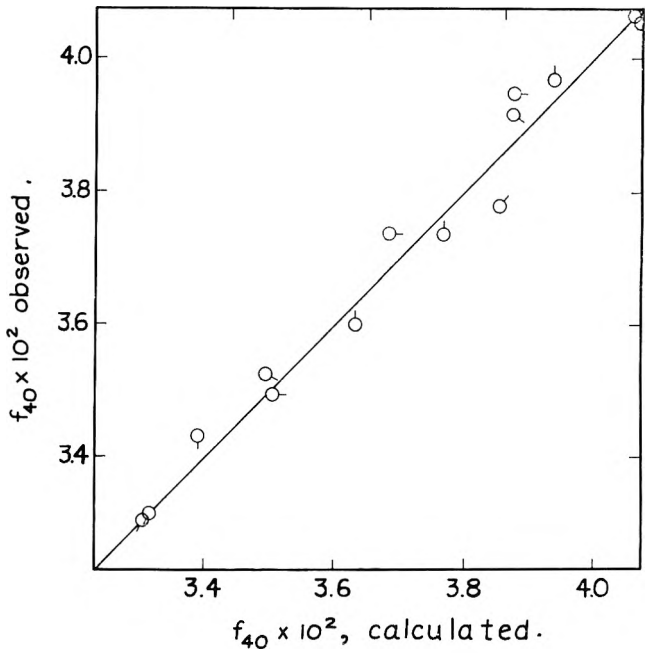

Fig. 8.—Observed fractional free volume at 40° for each blend, from temperature dependence (Table II), plotted against calculated value assuming linear additivity of free volume of components. Pip up, series O; successive 45° rotations clockwise, series P, Q, R, S, and L. Line drawn with slope of unity.

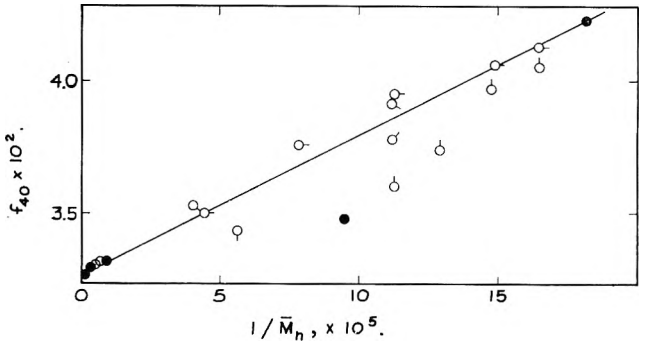

Fig. 9.—Fractional free volume at 40° from temperature dependence (Table II), plotted against reciprocal number-average molecular weight. Open circles, blends identified as in Fig. 8; black circles, components.

where ζ_{00} and f_0 refer to fraction 12-B-2 at 40°. Except for blends containing fraction B-7, f can be expressed to a good approximation by

$$f = 0.0325 + 5.9 \times 10^{-4}(T - 313.2°) + 51.5/\bar{M}_n \quad (4)$$

and from eq. 3 and 4 the position of the transition zone can be predicted over a wide range of composition and temperature.

Viscoelastic behavior in the plateau zone is more complicated and will be deferred for a later communication; dynamic measurements in the plateau zone are also in progress. The remaining discussion is devoted to the terminal zone and includes the dependence of viscosity and steady-state compliance on composition and molecular weight, the dependence of terminal relaxation times on composition, and a phenomenological analysis in terms of the relative energy dissipation by different molecular species in blends.[6]

Dependence of Viscosity on Composition in Series O and Q.—In Fig. 10, log η at 40° is plotted against v_2 for series O and Q (open circles). There is a mono-

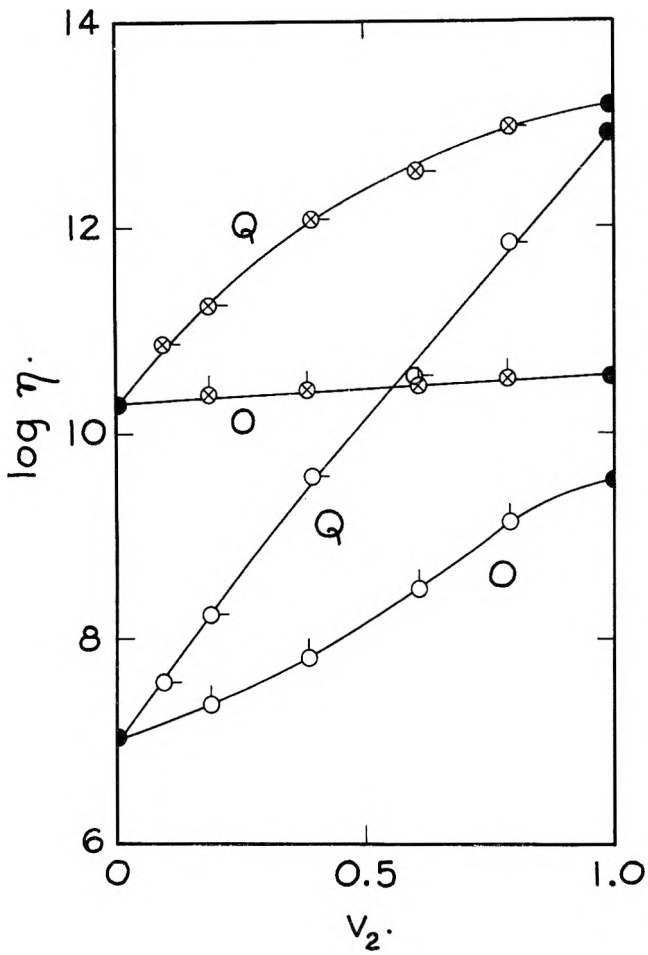

Fig. 10.—Logarithm of viscosity at 40° (open circles) and in iso-free-volume state $f = 0.0325$ (crossed circles), plotted against volume fraction of high molecular weight component in blends of series O and Q.

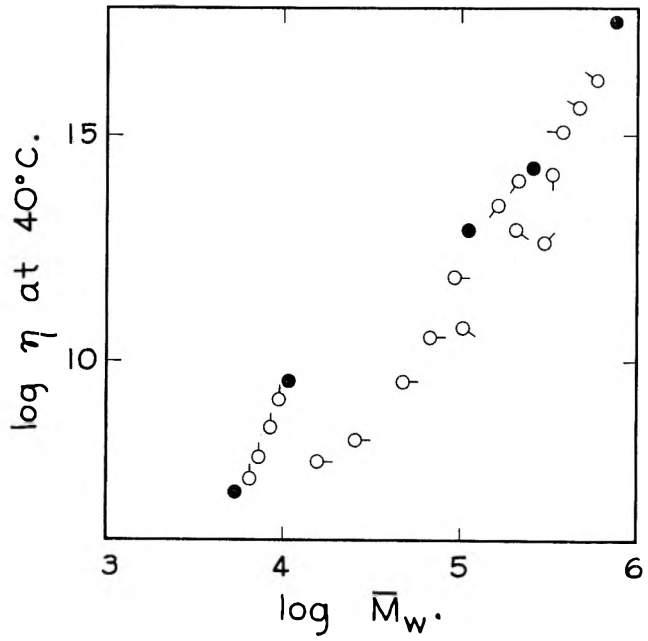

Fig. 11.—Viscosity at 40° plotted logarithmically against weight-average molecular weight. Blends and components identified as in Fig. 9, with pip left for series M and upper left for series N.

tonic increase with increasing proportion of high molecular weight component. This is partly due to progressive diminution of free volume, and it is of interest to separate out the latter contribution by calculating the viscosity which each blend would have at a fractional free volume of 0.0325, *i.e.*, in a state of iso-free-volume with fraction 12-B-2 at 40°. This has been done by adding to log η the separation $\Delta \log t$ in the transition zone from the creep curve of component 12-B-2, as in the determination of the T_0 values in Table II. The reduction term is equivalent to the last term in eq. 3, considered at constant temperature, although the values of $\Delta \log t$ used do not correspond exactly to calculations from f in Table II because the latter involve a smoothing of data in the composite curve of Fig. 6. Somewhat similar formulations have been made, less directly, in terms of the glass transition temperature.[14,15] The resulting iso-free-volume viscosity, η_{if}, is given in Table III for all the components and blends. Those for series O and Q are plotted in Fig. 10 as crossed circles. For series O, in which there are no coupling entanglements, η_{if} increases only slightly with the proportion of component 2; the values of η_{if} are exactly proportional to M, and for the blends η_{if} is nearly proportional to $\bar{M}_w$. For series Q, in which the component of higher molecular weight participates in entanglements, the viscosity η_{if} increases by three powers of 10 but still far less than before reduction to iso-free-volume. The changes in viscosity with composition here may be attributed primarily to entanglements and will be discussed further below.

Dependence of Viscosity on Weight-Average Molecular Weight.—When the viscosity at 40° is plotted logarithmically against $\bar{M}_w$ for all components and blends, considerable scatter is observed (Fig. 11), and it does not seem likely that any molecular weight average could be used to yield a single-valued function when the breadth of molecular weight distribution varies so widely as in these systems. This effect arises because the viscosity is partly determined by the free volume, which is essentially a function of $\bar{M}_n$, and partly by molecular length, in a manner which involves $\bar{M}_w$.

The effect of free volume can be removed by plotting log η_{if} from Table III. As seen in Fig. 12, all the components and blends then fall on a single line if $\bar{M}_w$ is chosen as the abscissa. It is particularly striking that below M_c the slope is unity. The proportionality of η_{if} to $\bar{M}_w$ (mentioned above in connection with Fig. 10) agrees with the prediction of the Rouse theory[16,17] for the case that the monomeric friction coefficient is independent of molecular weight. Deviations from direct proportionality of η to M as commonly observed for polymer fractions below M_c are evidently due to differences in free volume.[14]

Above the break point, the slope is 3.4 except for values of $\bar{M}_w$ above 400,000, where slight upward curvature is observed. In this region, the difference between η and η_{if} is slight, and the deviation from the 3.4 slope would be observed also for η, either at 40° (where the absolute values represent an unrealistic extrapolation) or at 75° (where the values, given in Table III, are in a realistic range). In view of the very high magnitudes of these viscosities even at the temperatures of

(14) R. B. Beevers and E. F. T. White, *Trans. Faraday Soc.*, **56**, 744 (1960).

(15) F. Bueche, C. J. Coven, and B. J. Kinzig, *J. Chem. Phys.*, **39**, 128 (1963).

(16) J. D. Ferry, "Viscoelastic Properties of Polymers," John Wiley and Sons, Inc., New York, N. Y., 1961, p. 170.

(17) E. Menefee and W. L. Peticolas, *J. Chem. Phys.*, **35**, 946 (1961).

measurement (130–144°), it is difficult to be certain that the deviation from the 3.4 slope is real. Fox and Nakayasu[18] have found the 3.4 power law applicable for polyvinyl acetate up to $M = 1.3 \times 10^6$.

There is no evidence that the viscosity depends on any other molecular weight average than $\bar{M}_w$, even though the breadth of distribution varies widely, with $\bar{M}_w/\bar{M}_n$ ratios from nearly unity up to 34. The conclusion that $\bar{M}_w$ is the appropriate average agrees with the results of Fox and Allen.[19]

The break point in Fig. 12 corresponds to $M_c = 22{,}000$. It is believed that this determination is more reliable than that from a conventional plot without reduction to iso-free-volume. It agrees with a recent estimate by Fox.[19]

Dependence of Steady-State Compliance on Composition in Series O and Q.—In Fig. 13, J_e is plotted against v_2 for series O and Q. The latter shows the familiar sharp maximum for mixtures rich in the component of low molecular weight.[20] In series O, the compliances are far smaller (tenfold larger scale), but there is still a slight maximum at intermediate compositions. The curves are calculated from the relative energy dissipation parameter N_{21} as described below.

Dependence of Steady State Compliance on Molecular Weight.—According to the Rouse theory,[21] the steady-state compliance should be given by

$$J_e = (2/5)\bar{M}_{z+1}\bar{M}_z/\bar{M}_w\rho RT \qquad (5)$$

where the molecular weight averages have their usual definitions and ρ is the density. Equation 5 presupposes that the effective friction coefficient per unit length governing the terminal relaxation times which dominate J_e is the same for both species, so that the magnitudes of the relaxation times are proportional to the square of M. This cannot be strictly true when entanglements are present, since their effect on the terminal relaxation times of an individual molecule will depend on its length as well as the properties of the average medium. However, the applicability of eq. 5 as an approximation may be tested by plotting J_e logarithmically against $\bar{M}_{z+1}\bar{M}_z/\bar{M}_w$ as in Fig. 14. Here the higher molecular weight averages are calculated assuming the component fractions to be strictly homogeneous. Most of the points lie somewhat higher than the theoretical line representing eq. 5, but the deviation is roughly constant, representing a compliance of about twice the predicted value over a very wide range of magnitudes (a factor of about 300).

It may be remarked that the Zimm theory of viscoelastic properties, *i.e.*, the normal coordinate theory in which hydrodynamic interaction dominates,[22] predicts[23] J_e to be proportional to a different combination of molecular weight averages with less weighting of the high molecular weights, $\bar{M}_z\bar{M}_w\bar{M}_n/(\overline{M^{1/2}})^2$, and would give values still smaller than those calculated from eq. 5. Thus, although the Zimm theory appears to be more successful for dilute solutions, especially in Θ solvents,[22] it is not to be preferred over the Rouse theory here. It seems probable that the higher observed values of J_e are due to some residual heterogeneity in the component fractions, relatively sharp though they are. Thus the weighting of high molecular weight components is somewhat stronger in all the blends than calculated from the molecular weights in Table I.

Peticolas and Menefee[24] have pointed out that eq. 5 can be tested on blends of polymers even if the components are not homogeneous, by comparing the steady-

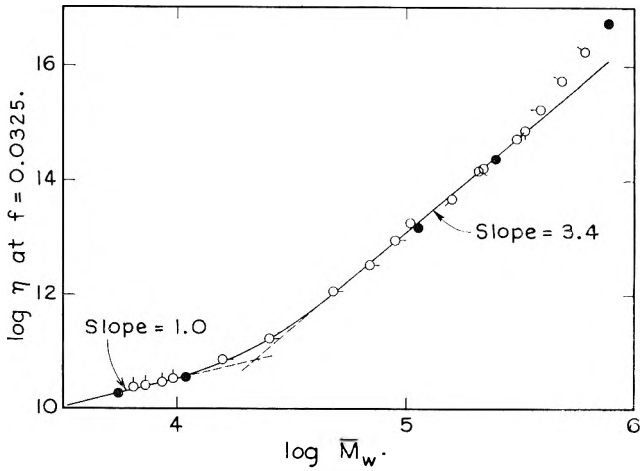

Fig. 12.—Viscosity plotted logarithmically against weight-average molecular weight after reduction to an iso-free-volume state of $f = 0.0325$. Blends and components identified as in Fig. 11.

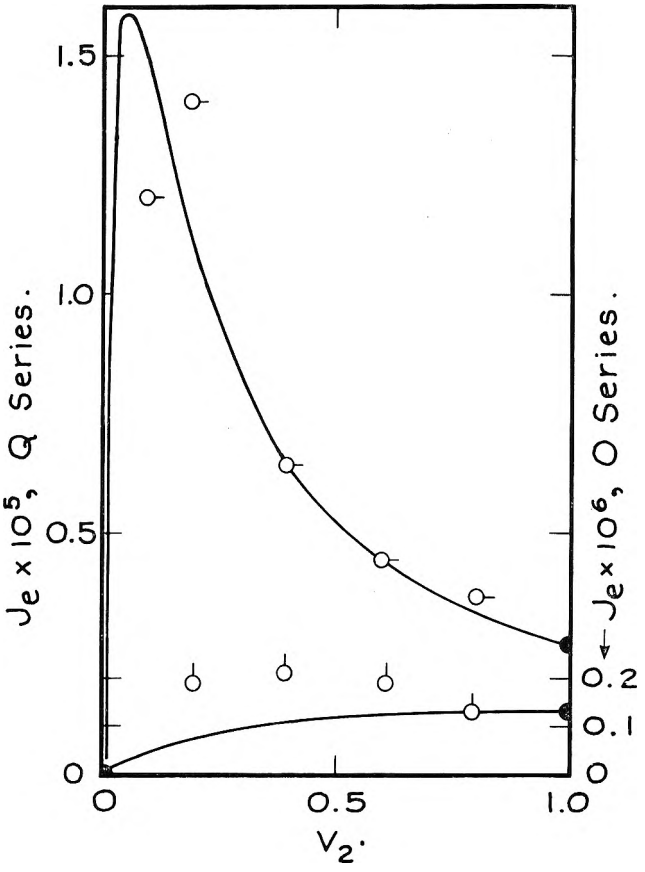

Fig. 13.—Steady-state compliance at 40°, plotted against volume fraction of high molecular weight component in blends of series O (pip up) and Q (pip right). Solid curves, calculated from eq. 13.

(18) T. G Fox and H. Nakayasu, private communication.

(19) T. G Fox and V. R. Allen, Abstracts ACS Division of Polymer Chemistry, **3**, 6 (1962), and private communication.

(20) H. Leaderman, R. G. Smith, and L. C. Williams, *J. Polymer Sci.*, **36**, 233 (1959).

(21) J. D. Ferry, M. L. Williams, and D. M. Stern, *J. Phys. Chem.*, **58**, 987 (1954).

(22) N. W. Tschoegl, *J. Chem. Phys.*, **39**, 149 (1963).

(23) S. E. Lovell and J. D. Ferry, *J. Phys. Chem.*, **65**, 2274 (1961).

(24) W. L. Peticolas and E. Menefee, *J. Chem. Phys.*, **35**, 951 (1961).

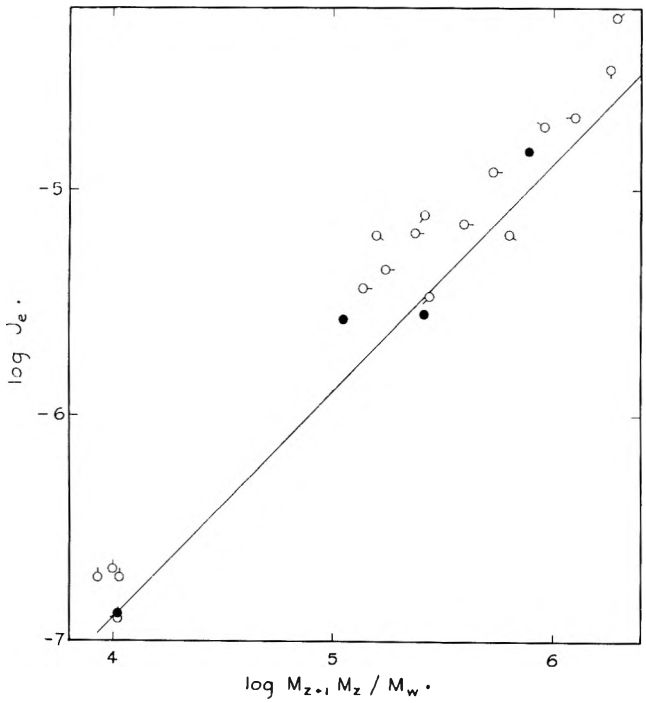

Fig. 14.—Steady-state compliance at 40°, plotted logarithmically against $M_{z+1}M_z/M_w$. Blends and components identified as in Fig. 11. Line corresponds to derivation from Rouse theory (eq. 5).

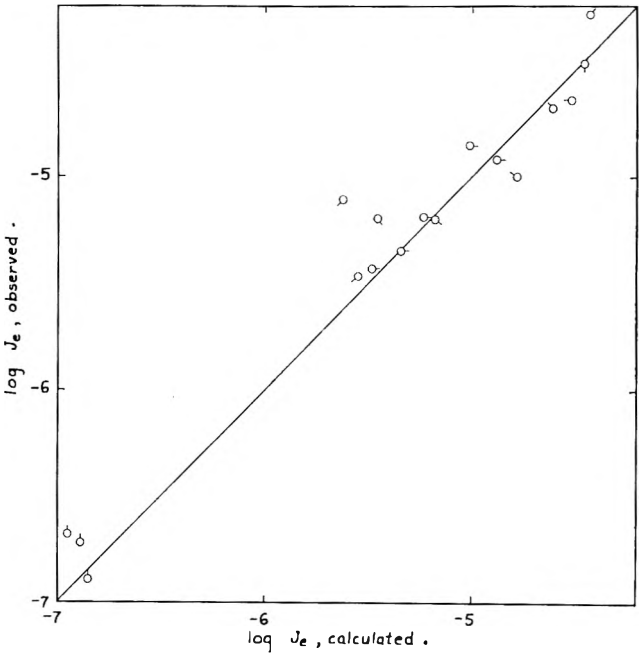

Fig. 15.—Observed steady-state compance at 40° plotted logarithmically against the value calculated from the compliances of the components by the method of Peticolas and Menefee, based on the Rouse theory (eq. 6). Blends identified as in Fig. 11.

state compliances of blends and of components. From eq. 5 it follows that for a binary blend

$$J_e = J_{e1}z_1^2/w_1 + J_{e2}z_2^2/w_2 \qquad (6)$$

where z_i is the z-fraction of the ith component, defined as $w_i\bar{M}_{wi}/\bar{M}_w$. The cited molecular weights for the fractions, based on intrinsic viscosity measurements, will certainly be very close to $\bar{M}_{wi}$. The value of J_{e2} for component 12-B-2 was actually calculated from eq. 6, since it could not be reliably measured directly,[3] by substituting J_{e1} and J_e for blends M-4, N-4, P-4, and S-4. The values of log J_{e2} thus obtained were −4.95, −4.91, −4.64, and −4.83; average −4.83 at 40°. Values of J_e were then calculated for all the blends and are compared with the observed values by a logarithmic plot in Fig. 15. The points for M-4, N-4, P-4, and S-4 do not constitute any evidence, of course, but all the points scatter on both sides of the line with unit slope, indicating moderately good agreement with the theory considering the very wide range of magnitudes.

In blends where $w_1M_1 << w_2M_2$, as in series P, R, S, and all but the first two members of Q, the term in J_{e1} is negligible. The reservation expressed above concerning the effect of entanglements on terminal relaxation time is then no cause for concern, since the molecules of component 2 are all entangled to the same degree and those of component 1 make no significant contribution to J_e.

Dependence of Terminal Relaxation Times on Composition.—In the terminal zone, the composition dependence of relaxation times is characterized[5,6] by the factor λ_i which is the ratio of a given relaxation time in the blend to its corresponding value in the pure polymer; in any binary blend, $\lambda_1 > 1$ and $\lambda_2 < 1$. If it is assumed that the contributions of the individual molecules to viscoelastic energy storage and dissipation are additive, as is inherent in the molecular theories of Rouse and others,[25] then a straightforward determination of λ_2 can be made[5] by plotting $G(t)/v_2$ logarithmically against time and measuring the horizontal separations on the logarithmic time axis for different compositions. Here $G(t)$ is the relaxation modulus, which can be calculated from the creep compliance by approximation methods.[26] If λ_2 is the same for several of the longest relaxation times of the higher molecular weight species, then $G(t)$ for the blend can be expressed by the equation

$$G(t) = v_1G_1(t/\lambda_1) + v_2G_2(t/\lambda_2) \qquad (7)$$

where G_1 and G_2 are the relaxation moduli of the respective pure components. At long times, the first term on the right contributes little, so that logarithmic curves for $G(t)$ are parallel and a composite plot results when $G(t)/v_2$ is plotted against $t/a_T\lambda_2$. Such plots are shown for the O and Q series in Fig. 16, demonstrating the constancy of λ_2 in the terminal zone both with and without entanglements. In the rubbery zone at the left of the plot for the Q series, the different compositions diverge because the term in G_1 in eq. 7 becomes important; from the divergences, λ_1 can sometimes be evaluated.

Values of log λ_2 were determined in this manner for all the blends except those five containing fraction 12-B-2; for that fraction the terminal zone of creep and hence $G(t)$ could not be reliably obtained. The position of the terminal zone of 12-B-2 was obtained by extrapolation from blends M-4 and N-4 as follows. The separation Δ log λ_2 between the $G(t)$ curves for these two blends was found to be 0.49. An alternative calculation is from the viscosities, in accordance with the equation[6]

$$\eta_{b1} = v_1\lambda_1\eta_1 + v_2\lambda_2\eta_2 \qquad (8)$$

Since in both blends $v_1\lambda_1\eta_1$ is undoubtedly small com-

(25) Reference 16, p. 290.
(26) T. L. Smith, *Trans. Soc. Rheol.*, **2**, 131 (1959).

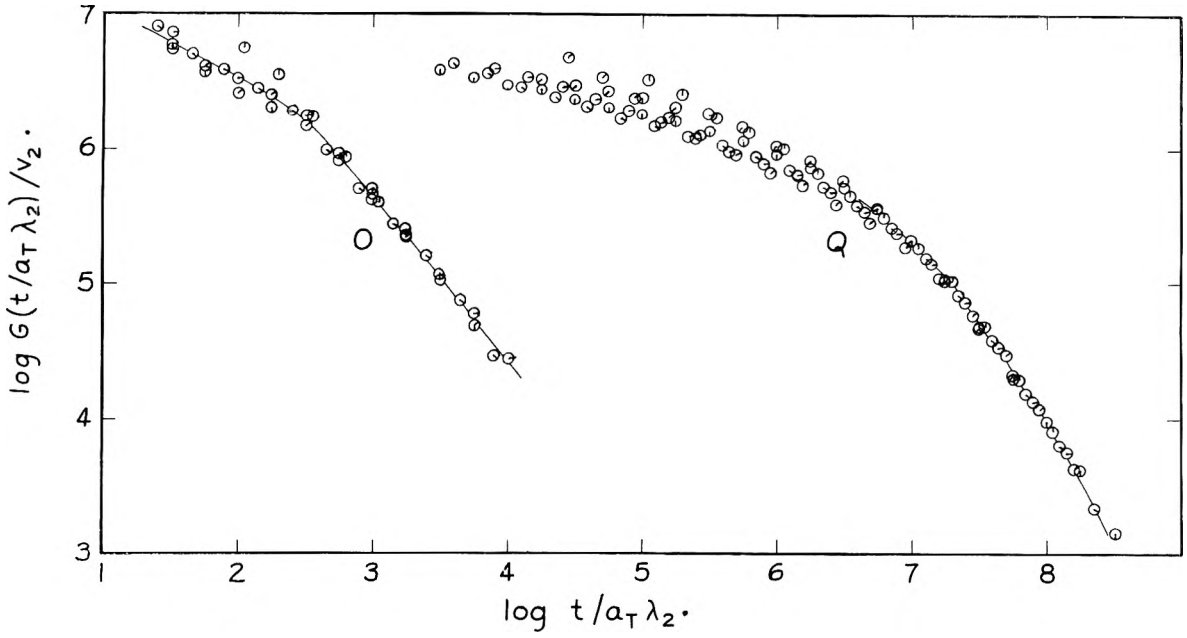

Fig. 16.—Relaxation modulus plotted logarithmically after reduction with a_T factors for temperature and with λ_2 factors for composition dependence of terminal relaxation times of high molecular weight component, for O and Q series. In each series, pip up denotes smallest v_2 in Table I; successive 45° rotations clockwise, increasing values of v_2 including $v_2 = 1.00$. Reference temperature 40°.

pared with $v_2\lambda_2\eta_2$, and v_2 is practically the same in both, we have $\Delta \log \lambda_2 \cong \Delta \log \eta_{b1} = 0.58$. The ratio $\Delta \log \lambda_2/\Delta \log M_1$ is then 1.33 or 1.57 from these respective sources. Using the mean, we extrapolate linearly on a logarithmic scale to $M_1 = 780{,}000$, *i.e.*, pure fraction 12-B-2, and obtain $\log \lambda_2 = -0.68$ for blend N-4. The extrapolation is short and the uncertainty in $\Delta \log \lambda_2/\Delta \log M_1$ is not serious. Then from measured values of $\Delta \log \lambda_2$ between N-4 and all other blends involving 12-B-2, whose $G(t)$ curves are closely parallel in the terminal zone, $\log \lambda_2$ for each blend can be calculated. At the same time, $\log \eta_2$ for fraction 12-B-2 is determined from eq. 8 to be 11.47 at 75° and 16.72 at 40°, as reported in Table III and the preceding paper.[3]

The values of $\log \lambda_2$ are listed in Table IV. It is of interest first to compare them with the predictions of the Rouse theory on the basis of the blend viscosities and weight-average molecular weights[6,27]

$$\lambda_2 = \eta_{b1}M_2/\eta_2\bar{M}_w \qquad (9)$$

Values calculated from eq. 9 are also given in Table IV and the agreement is rather good, over a wide range of magnitudes, including blends with and without entanglements. The calculation tends to exaggerate the effect of the environment slightly, giving in some cases too large a negative value of $\log \lambda_2$.

In general, the ratio λ_2 is the product of a factor due to a difference between the free volumes of component 2 and the blend, which affects the local friction coefficient, and a factor involving entanglements. The former can be separated by subtracting from $\log \lambda_2$ the time separation of the creep curves in the transition zone, in a manner analogous to the calculation of $\log \eta_{if}$ in Table III except that here the reference state is component 2 of the particular blend rather than always fraction 12-B-2. The result, $\log \lambda_{2if}$, represents the ratio of terminal relaxation times of component 2 in the blend and in the pure component, compared in a state of isofree-volume.

(27) Reference 16, p. 290.

TABLE IV

PARAMETERS DESCRIBING COMPOSITION DEPENDENCE OF RELAXATION TIMES IN TERMINAL ZONE

Blend	$\log \lambda_2$ at 40°	$\log \frac{\eta_{b1}}{\eta_2}\frac{M_2}{M_w}$	$\log \lambda_{2if}$	$\log \lambda_1$ at 40°	$\log \lambda_1/\lambda_2$
L-3	−0.35	−0.57	−0.26	0.075	0.42
L-7	−0.12	−0.11	−0.08	0.030	0.42
M-4	−1.17	−1.36	−1.00		
N-4	−0.68	−0.87	−0.60		
N-7	−0.35	−0.39	−0.31		
O-2	(−1.80)	−1.96	(−0.23)	0.15	(1.95)
O-4	−1.50	−1.55	0.11	0.47	1.97
O-6	−1.00	−0.97	−0.03	1.34	2.34
O-8	−0.40	−0.39	0.00	1.94	2.34
P-4	−3.72	−3.71	−1.60		
Q-1	−4.20	−4.29	−1.36		
Q-2	−3.85	−4.04	−1.13		
Q-4	−2.80	−2.96	−0.57		
Q-6	−2.00	−2.14	−0.31		
Q-8	−0.90	−0.93	−0.03		
R-4	−3.00	−3.06	−0.67		
R-8	−1.05	−1.15	0.01		
S-4	−2.02	−2.17	−1.33		

Log λ_{2if} is also given in Table IV. In series O, it is zero within experimental scatter, as expected since there are no entanglements in these blends. In series L and M, where both M_1 and M_2 exceed M_e, the fragmentary data are not far from direct proportionality of $\log \lambda_{2if}$ to $1 - v_2$, as observed previously for certain polystyrene blends.[6] For the Q and R series, a plot of $\log \lambda_2$ against v_2 is far from linear as shown in Fig. 17. This departure is undoubtedly associated with the fact that $M_1 < M_e < M_2$, so that λ_1/λ_2 cannot be independent of composition, as described below.

In a few cases, it was possible to determine λ_1 also, either by subtracting $v_2\lambda_2G_2(t/\lambda_2)$ from $G(t)$ as previously described[5] (L-3 and L-7), or from eq. 8 with the knowledge of λ_2 (O series). These values are included in Table IV. In the L and O series, where both M_1 and M_2, respectively, are much greater or considerably less than M_e, the ratio λ_1/λ_2 appears to be fairly inde-

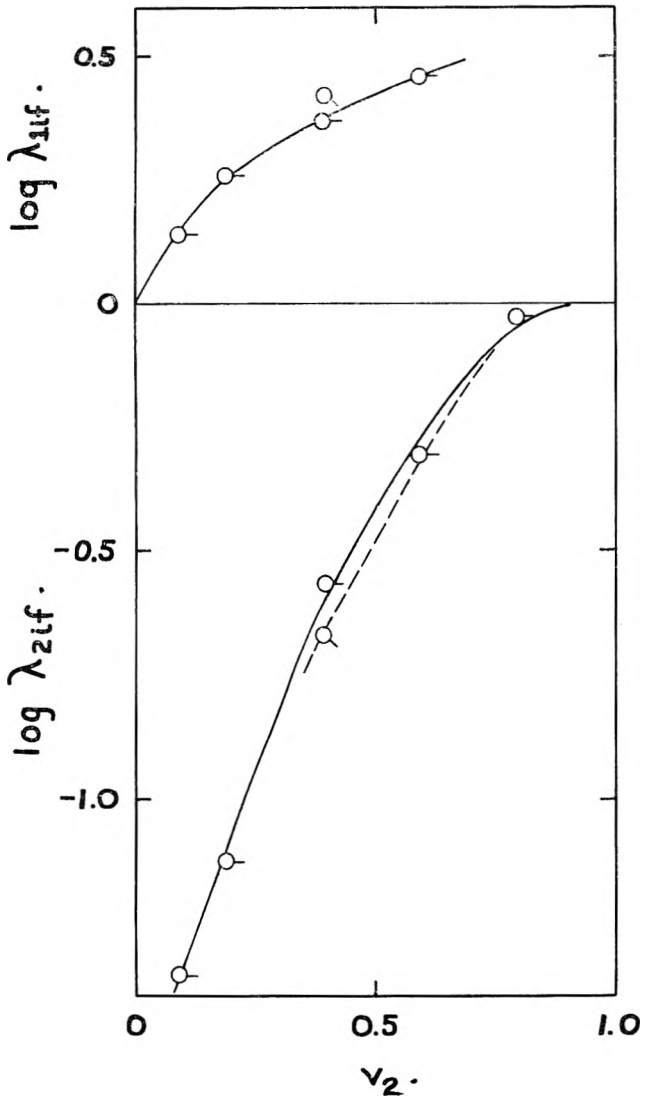

Fig. 17.—Log λ_{2if} plotted against volume fraction of component of higher molecular weight, for series Q (solid curve) and R (dashed curve); also, log λ_{1if} calculated from eq. 15.

pendent of composition, as deduced from application of the blending laws to blends of blends.[6] Moreover, the value of log λ_1/λ_2 for series O is not far from that calculated from the Rouse theory,[6] log $\eta_2 M_1/\eta_1 M_2$ = 2.34. For series L, the Rouse prediction of 0.96 is too large, as was also the case in the earlier analysis of polystyrene blends.[6]

Values of λ_1 for certain other blends were estimated by an indirect procedure as described below.

Analysis of Behavior in Terminal Zone in Terms of Auxiliary Parameters N_{21} and D.—Independently of molecular theory, the values of λ, J_e, and η can be interrelated in terms of two auxiliary parameters, N_{21} and D, as described recently.[6] This treatment is based on two relations, derivable from the principles of linear viscoelasticity,[28] eq. 8, and the analogous expression for steady-state compliance

$$J_e = (\lambda_1^2\eta_1^2 v_1 J_{e1} + \lambda_2^2\eta_2^2 v_2 J_{e2})/\eta^2 \qquad (10)$$

where the subscripts refer to components 1 and 2 and symbols without subscripts refer to the blend. The simplest definition of N_{21} is

$$N_{21} = \lambda_2\eta_2/\lambda_1\eta_1 \qquad (11)$$

(28) K. Ninomiya, *J. Colloid Sci.*, **17**, 759 (1962).

from which, together with eq. 8, it is seen to be the ratio of contributions per unit volume of the two components to energy dissipation in flow of the blend (*i.e.*, to η). The value of N_{21} is the same whether or not the λ's and η's are reduced to iso-free-volume states, since the free volume corrections in numerator and denominator cancel. The parameter N_{21} is closely related to the maximum in J_e in a plot such as Fig. 13; in fact,[6] approximately, the height of the maximum is $J_{e2}N_{21}/4$ and its location on the v_2 scale is $1/N_{21}$ (provided $J_{e2} >> J_{e1}$).

The parameter D is defined by the relation

$$D = \lambda_1^{v_1}\lambda_2^{v_2} \qquad (12)$$

and its physical significance appears to be associated with the dependence of the local friction coefficient on blend composition. In principle, both D and N_{21} can be determined from analysis of viscosities and compliances of blends in accordance with the following equations[6] which relate the values for the blends to those of the pure components

$$J_e = \frac{J_{e1}v_1 + N_{21}^2 J_{e2}v_2}{[1 + v_2(N_{21} - 1)]^2} \qquad (13)$$

$$\eta = D\eta_1^{v_1}\eta_2^{v_2}[1 + v_2(N_{21} - 1)]/N_{21}^{v_1} \qquad (14)$$

In practice, however, solution of these equations for N_{21} and D requires higher precision of the numerical data than is generally available.

In certain blends where all the components have high molecular weight, D is found to be unity.[6] We make the assumption here that $D = 1$ when all data are reduced to a state of iso-free-volume, *i.e.*, when differences in the local friction coefficient are eliminated. In this case, log λ_{1if} can be readily calculated from log λ_{2if} by eq. 12

$$\log \lambda_{1if} = -(v_2/v_1) \log \lambda_{2if} \qquad (15)$$

and then N_{21} is obtained from eq. 11. In Table V, values of log λ_{1if} and log N_{21} derived in this manner are listed for most of the blends except the O series.

TABLE V

PARAMETERS FROM PHENOMENOLOGICAL ANALYSIS OF BEHAVIOR IN TERMINAL ZONE

Blend	log λ_{1if}	log N_{21}	log η_{if} (calcd.)	log J_e (calcd.)
L-3	0.12	0.95	13.80	−5.26
L-7	.19	1.06	14.20	−5.43
M-4	.66	1.88	15.33	−4.44
N-4	.43	1.30	15.78	−4.51
N-7	.57	1.45	16.23	−4.66
P-4	1.00	3.86	14.72	−4.41
Q-1	0.14	1.42	10.94	−4.82
Q-2	.26	1.53	11.37	−4.95
Q-4	.37	1.98	12.22	−5.18
Q-6	.46	2.15	12.65	−5.35
R-4	.42	3.04	13.30	−5.14
S-4	.93	3.92	15.01	−4.46

A test of the validity of these calculations can be made by calculating J_e and η from eq. 13 and 14 and comparing with observed values. In eq. 14, D is again set equal to unity and η, η_1, and η_2 are all taken in the iso-free-volume states. The resulting calculations for log η_{if} and log J_e are listed in Table V and are plotted in Fig. 18 and 19 against the observed values. The agreement is quite good for η and is as good for J_e

as that in Fig. 15. Only one observed datum for each blend enters these calculations, namely, λ_2. The calculated J_e for series Q and series O (in the latter, taking $N_{21} = 1.9$) is plotted against v_2 in Fig. 13 together with the experimental points. The values for N_{21} can be taken with some degree of confidence, and their dependence on composition can be examined.

In the O series, not included in Table V, λ_{2if} and λ_{1if} can both be taken as unity within experimental error, so $N_{21} = (\eta_2/\eta_1)_{if} = 1.9$. This is identical with the ratio M_2/M_1, which is the Rouse theory prediction[6] for N_{21}; apparently this prediction holds when both M_1 and M_2 are less than M_c. In the L, M, and N series, where both M_1 and M_2 are greater than M_c, N_{21} appears to be relatively independent of composition and determined by the properties of the two components alone. However, it is *not* equal to M_2/M_1; it exceeds the latter ratio by a factor of 6 to 10. A similar discrepancy was found in certain polystyrene blends[6]; its significance is not clear and requires further data for elucidation.

In the Q series (and undoubtedly in P, R, and S if more information were available), where $M_1 < M_c < M_2$, it is evident that N_{21} depends markedly on composition, increasing with v_2. This is to be expected from the interpretation of N_{21} as the relative energy dissipation of the two components per unit volume. When v_2 is very small, neither component participates in entanglements, and probably $N_{21} \rightarrow M_2/M_1$ at this end of the concentration scale, as is almost fulfilled for blend Q-1 ($\log N_{21} = 1.42$, $\log M_2/M_1 = 1.31$). With increasing v_2, component 2 participates increasingly in entanglements while component 1 does so scarcely at all (see discussion of λ_1 below), so the relative energy dissipation of component 2 to component 1 increases rapidly.

We turn now to the significance of D. If $D = 1$ when iso-free-volume values of viscosity are substituted into eq. 14, it is evident from the ratio of η to η_{if} (*cf.* eq. 3) that

$$\log D = (1/2.303)(1/f - v_1/f_1 - v_2/f_2) \qquad (16)$$

and D reflects the influence of free volume on the local friction coefficient.

Finally, examining the composition dependence of λ_{1if} in the Q series, it is evident in Fig. 17 that λ_{1if} is affected by composition much less than λ_{2if}. This is to be expected since when $M_1 < M_c < M_2$ the increasing extent of entanglement with rising v_2 will prolong the terminal relaxation times of the long molecules far more than the short ones. Thus, $(\lambda_1/\lambda_2)_{if}$ cannot be independent of composition for such a pair of components.

Conclusions

Analysis of the viscoelastic properties of blends of different molecular weights is greatly facilitated by combining data in the transition and terminal zones to separate the effects of the local friction coefficient (primarily dependent on $\bar{M}_n$ through the fractional free volume) and of molecular length (primarily dependent on $\bar{M}_w$). The behavior in the transition zone is determined by the local friction coefficient alone. In the terminal zone, the behavior is somewhat more complicated. However, over very wide ranges of molecular weight and breadth of distribution, the steady-state

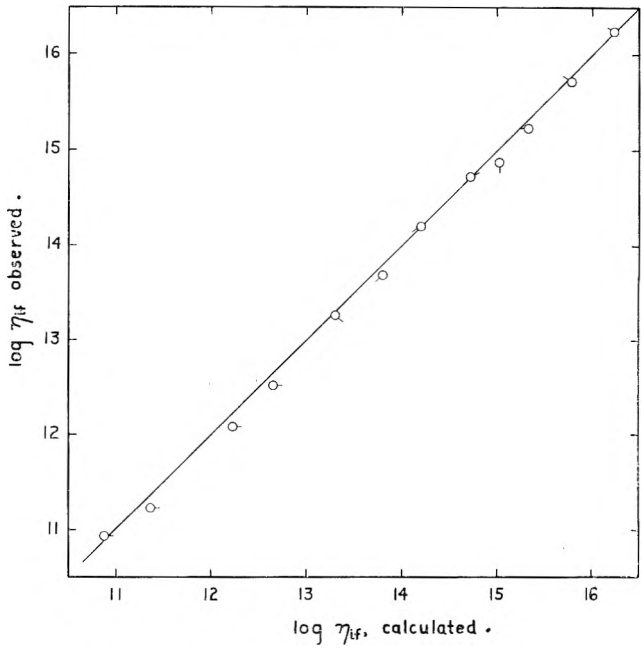

Fig. 18.—Observed blend viscosities reduced to iso-free volume, plotted logarithmically against values calculated from eq. 14 with N_{21} values in Table V. Blends identified as in Fig. 11.

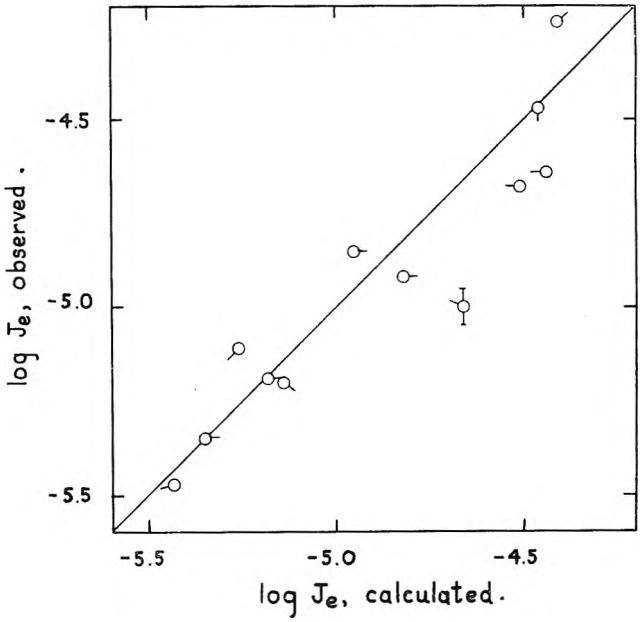

Fig. 19.—Observed steady-state compliances at 40° plotted logarithmically against values calculated from eq. 13 with N_{21} values in Table V. Blends identified as in Fig. 11.

compliance is proportional to $\bar{M}_{z+1}\bar{M}_z/\bar{M}_w$ as predicted by the Rouse theory. The Rouse theory also satisfactorily predicts the composition dependence of viscosity and terminal relaxation times provided both molecular weights are less than M_c and the dependence of the local friction coefficient on free volume is taken into account. If the molecular weight of one component or those of both components exceed M_c, the terminal relaxation times of component 2 (with higher molecular weight) are more strongly affected by entanglements than those of component 1. Nevertheless, the composition dependence of the terminal relaxation times of component 2 is rather well expressed by the Rouse theory in terms of $\bar{M}_w$ and the blend viscosity. The terminal relaxation times of com-

ponent 1 do not appear to be satisfactorily described by the molecular theory in its present form. It may be necessary to measure them by different experimental means, especially when the molecular weight of component 1 is less than M_c, to obtain sufficiently direct and precise information for a complete analysis.

Acknowledgment.—This work was supported in part by a grant from the National Science Foundation.

PRESSURE–TEMPERATURE–RESISTANCE PROPERTIES OF LANTHANUM, BISMUTH, NEPTUNIUM, PLUTONIUM, AND AMERICIUM TO 450° AND 30 KB.

By D. McWhan, P. W. Montgomery, H. D. Stromberg, and G. Jura

Department of Chemistry, and Lawrence Radiation Laboratory, University of California, Berkeley, California

Received April 23, 1963

The actinide elements neptunium, plutonium, and americium are materials of considerable interest to the high pressure investigator. The possibility of pressure-induced electronic transitions such as those in cerium and cesium is suggested by the electronic configurations of the actinides. Such transitions are usually detectable by a discontinuous change in the electrical resistance of the sample. A matter of additional interest is the known one atmosphere polymorphism of plutonium with six allotropic forms between room temperature and its melting point, of neptunium with two allotropic forms, and a suspected allotropism in americium. The program therefore involved the development of apparatus capable of developing high pressures and temperatures which could allow electrical resistance measurements to be made on milligram quantities of metal. In addition, the apparatus was to be resistant to breakage or blowout which could contaminate the laboratory, permanent equipment, and, of course, laboratory personnel.

Details of the construction of the cavity anvil are available in UCRL Report 10333. It consists of a shallow 0.5-in. diameter cavity in a hardened steel or tungsten carbide cylinder. The cylinder is supported with a steel jacket in the same fashion as the tungsten carbide inserts in the Bridgman type anvils.[1] The bottom of the cavity consists of a jam fit high-speed tool steel plug, in order to alleviate rounded corner effects in the bottom of the cavity. The piston is of the same hardened steel as the bottom plug, being kept as short as possible, to obtain maximum column strength. Originally tungsten carbide pistons, bottom plugs, and cylinders were used, but they were prone to frequent breakage. Analysis of the breaks indicated that failure occurred due to tension stresses. The use of hardened steels with their higher tensile strengths has eliminated the breakage problem. Repeated runs to 30 kb. and 450° did not result in any apparent serious deformation of the high-speed steel components.

Electrical resistance is measured by a four-lead technique using a two-channel Leeds and Northrup Speedomax recorder to record current and potential drop across the sample. Electrical contact can be made in two ways: one by spring-loaded probes located on the bottom side of the cavity plug and directly on top of the piston by copper plates inserted between the anvils and the heat blocks. With the probe method the potential contacts are made at the ends of the probes and the current is brought in through a side contact on the probe to minimize end effects. When Cu plates are used, the current and potential contacts are made on separate tabs. Iron–constantan thermocouples are located in the tips of both the top and bottom probes. Heat is supplied by an external heater. For safety and ease of transportation the cavity anvil, when assembled, is wrapped with 0.010-in. stainless steel sheet, secured with hose clamps. This is insulated from the top and bottom by asbestos sheet. This allows radioactive metals to be loaded in glove boxes and then safely transported to the pressure laboratory.

The metal sample is in the form of a fine wire or sliver mounted vertically in a disk of silver chloride which serves as the pressure transmitting medium. The silver chloride is coated with acrylic lacquer to prevent reaction with the metal. The metal should protrude very slightly (0.001 in.) on each side and be faced off with 0.001-in. platinum foil to improve electrical contact between the sample and steel. Sample lengths varied from 0.010 to 0.050 in., depending upon the amount of material available. The silver chloride disk is placed in the cavity inside an iron oxide coated pyrophyllite ring of the same height as the silver chloride. The pyrophyllite ring serves as a gasket, preventing extrusion of the silver chloride past the piston. The piston is insulated from the wall of the cylinder by coating with several coats of a mixture of iron oxide and Bisonite. The Bisonite is a phenolic resin having good high temperature properties; the iron oxide improves the mechanical strength of the coating which has a tendency to chip off on loading. There is a 0.0025 in. radial gap between the piston and cylinder wall. It should be noted that it is important that the height of the ring match the height of the silver chloride disk. If this is not done, the load will not be distributed evenly and erroneous pressures will be obtained. The radial thickness of the ring is not critical; in these experiments it was 0.032 in.

Calibration

In designing the cavity anvil, it was hoped that by keeping the sample cell and piston configuration as simple as possible there would be negligible friction so that the pressure in the cell could be calculated from the load exerted on the 0.5-in. diameter piston. The calibration was carried out using the transitions in bismuth at around 25 kb. The phase diagram for these has been carefully worked out by Bridgman[2] using a

(1) R. E. Harris, R. J. Vaisnys, H. Stromberg, and G. Jura, "Progress in Very High Pressure Research," John Wiley and Sons, Inc., New York, N. Y., 1961.

(2) P. W. Bridgman, *Phys. Rev.*, **48**, 893 (1935).

truly hydrostatic pressure chamber. Figure 1 gives the phase diagram obtained in the cavity anvil superimposed upon that of Bridgman for comparison. For the I–II transition at room temperature the average transition pressure for 15 runs was 24.1 kb. with a scatter of ±1.5 kb. The temperature uncertainty is taken as half the difference between the top and bottom thermocouples, which is generally less than 5°. The I–II transition in bismuth is taken as the standard for calibration. The II–III transition provides a useful secondary check but in practice proves to be more sluggish and irreproducible.

Single crystal silver chloride is used to transmit pressure to the sample. It has a tendency to react with the metals involved in this study and during the calibration work pyrophyllite was used in one run at room temperature to determine its suitability as a pressure medium. Experience has shown that a good measure of the hydrostatic nature of a substance is the sharpness of the bismuth transitions in the material. Figure 2 shows the results of two room temperature runs, one in silver chloride and the other in pyrophyllite. The spread of the transition in pyrophyllite ruled it out as a substitute for silver chloride. Qualitatively similar results to those of pyrophyllite were obtained when Teflon was used as the pressure transmitting medium.

One valuable feature of the cavity anvil is that it may be cycled up and down in pressure as often as desired. In this respect, the cavity anvils behave in a fashion similar to the conventional piston–cylinder apparatus, provided the pressure is above 6–8 kb.

While calibrating the cavity anvil it was found that the AgCl disk which holds the sample forms an effective thermal barrier which upon suitable arrangement of the heater insulation allows thermal gradients as high as 20° to develop between the top and bottom thermocouples. Since it has not been possible to develop more than a 3° gradient when there is no AgCl in the cavity (piston to piston) it is reasonable to assume that the whole temperature difference between the thermocouples occurs across the sample. This fact allows rough measurements to be made of the thermal e.m.f. of the sample and the effect of pressure thereon. In the case of bismuth the thermal e.m.f. was seen to go from 8 μv. in phase I to approximately zero in phase II and III. The thermal e.m.f. measured is bismuth–tungsten carbide superimposed on the tungsten carbide–copper thermal e.m.f. where the leads leave the apparatus.

Neptunium

The neptunium used in this work as prepared by a lithium reduction technique and contained 0.015 wt. % calcium and 0.0015 wt. % lithium. The material required handling in a dry nitrogen atmosphere.

The room temperature resistance–pressure curve shows no evidence of transitions between 4 and 27 kb. In all, four runs were made on two different samples. The phase diagram in Fig. 3 shows the effect of pressure on the α–β transition temperature which involves a transition from an orthorhombic to a tetragonal structure.

The very shallow slope of the extrapolated transition curve to one atmosphere gives a dP/dT of about 1.1 kb. per degree. Using the density values of Zachariasen[3] a heat of transition of 4.8 kcal./mole is obtained, which is probably no better than 50% due to difficulties in estimating the small slope, and a ±5° uncertainty in the 1-atm. transition temperature.

(3) W. H. Zachariasen, *Acta Cryst.*, **5**, 664 (1952).

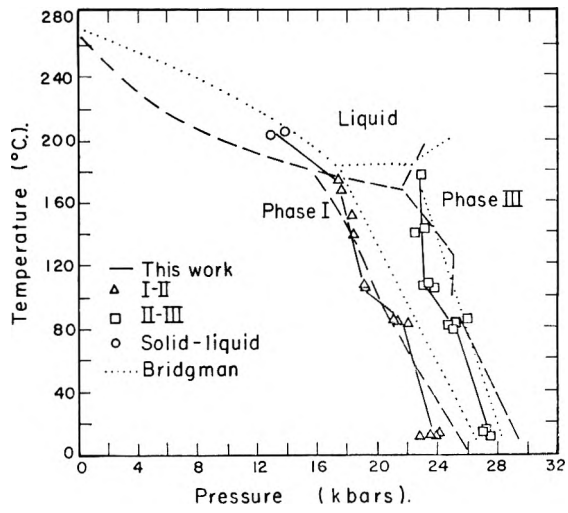

Fig. 1.—Phase diagram of bismuth as determined in cavity anvils.

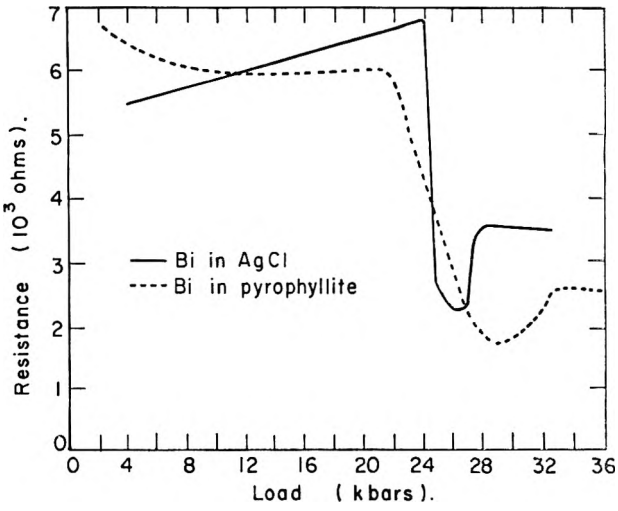

Fig. 2.—Comparison of pyrophyllite and silver chloride as pressure transmitting media in cavity anvils. The metal is bismuth.

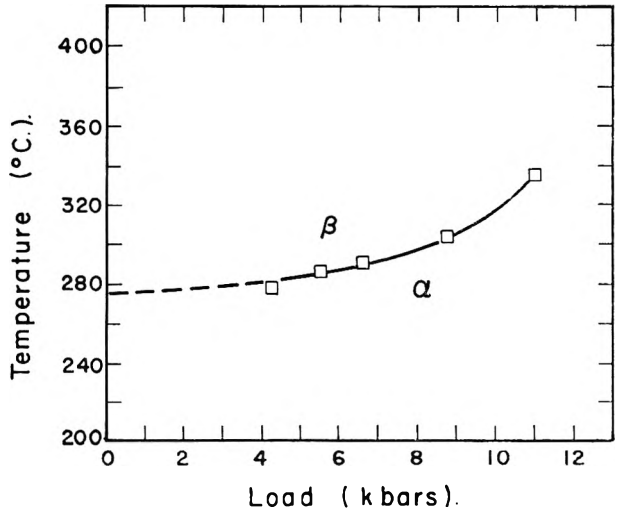

Fig. 3.—Pressure–temperature diagram of neptunium.

Plutonium

The plutonium studied was 99+% pure obtained from Los Alamos. Although there are seven polymorphic transitions between room temperature and its

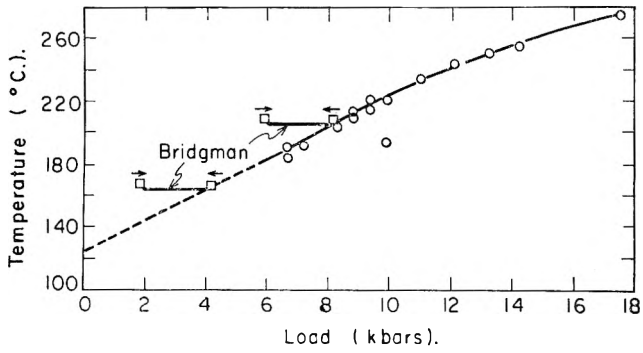

Fig. 4.—Phase diagram of plutonium.

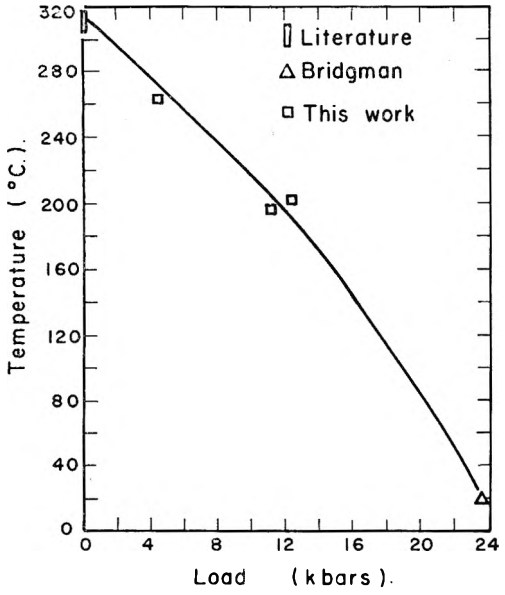

Fig. 5.—Phase diagram of lanthanum.

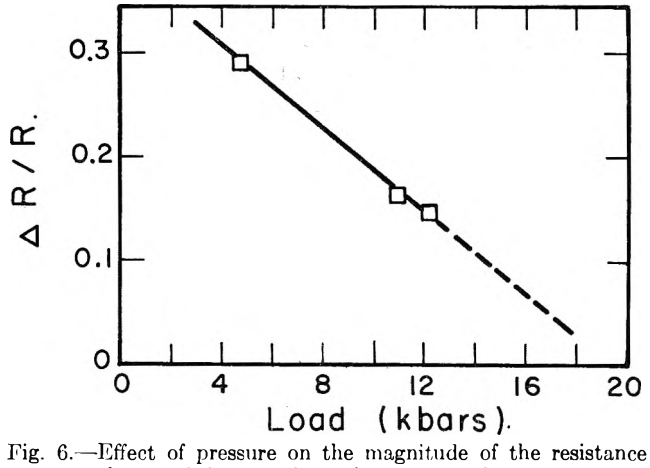

Fig. 6.—Effect of pressure on the magnitude of the resistance change of the α–β phase change in lanthanum.

melting point at 640°, only the α–β transition gave a resistance change large enough and sharp enough to establish the onset of a transition beyond doubt. Other features in the resistance temperature curves were observed but the small magnitudes involved, together with difficulties in pressure phenomena, have led us to omit these details until further work clarifies the complex situation present.

All data were taken by isobaric heating. The transitions were sharp, running over not more than 5°. The transition temperature is taken at the onset of the transition with increasing temperature. A hysteresis of 30 to 50° between the α and β transitions was observed by us as well as previous investigators at atmospheric pressure. Figure 4 shows our work together with that of Bridgman[4] which was determined by volume measurements.

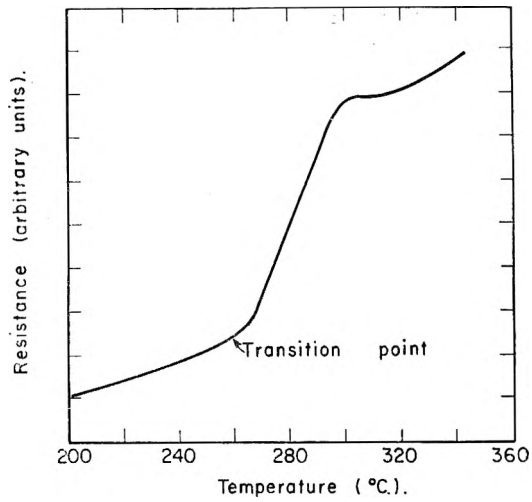

Fig. 7.—An isobaric determination of resistance *vs.* pressure for lanthanum.

Bridgman's phase diagram was obtained by the method of piston displacement at constant temperature, the general idea being to manipulate the pressure to force the material to be approximately equally divided between the two phases. Two points were obtained at each temperature: a high pressure point at which the transition would just begin to run from β to α and a low pressure point at which the transition would begin to run from α to β. The difference between these values is referred to as the "region of indifference" by Bridgman.

In this work all points were taken by heating at constant pressure. The transition is sharp, running to completion within 10° at a heating rate of 2 to 5°/min. No attempt was made to establish an equilibrium situation. In the one constant pressure run in which he cooled from β to α, Bridgman observed the same hysteresis found in this work.

The discrepancy between our work and Bridgman's is probably attributable to two impurity effects. Bridgman's material was the best available in 1945 but contained around 0.1 wt. % impurity. In addition, Bridgman encased his plutonium in a lead capsule. It is possible that alloying effects at the temperature of the α, β transition between the lead and the plutonium affected the results. Another possibility is, of course, the fact that the initial volume changes may not correspond to the initial change in resistance.

Americium and Lanthanum

Americium was of interest to us because early X-ray studies indicated that it existed in both an expanded and collapsed double hexagonal close-packed structure with the expanded form being the low temperature form. This is similar to the situation in cesium where it is believed that the collapsed structure involves an electronic transition from the 6s to the 5d level.

Americium was studied using both isothermal compressions and isobaric heatings. No reproducible feature was detected at room temperature from 4 to 36 kb. Americium proved to be very sensitive to heating. The resistance behavior became erratic and rose irreversibly

(4) P. W. Bridgman, *J. Appl. Phys.*, **30**, 214 (1959).

above 70°. On at least one occasion the resistance increased by a factor of a thousand. We could not establish whether this was due to chemical or metallurgical changes in the americium. The sample was always clean and shiny when removed from the acrylated AgCl and did not show evidence of oxide in its X-ray pattern.

At very high temperatures americium goes into a face-centered cubic phase and early in this work we decided to look at lanthanum, which undergoes a hexagonal to face centered cubic transformation at 310° (atmospheric pressure). This involves a negative volume change and was therefore believed to be the same transformation observed by Bridgman in his compressibility studies at room temperature and 24 kb. Bridgman was unable to detect this transition using resistance measurements.

The lanthanum used in this work was 99+% pure and was loaded in a nitrogen atmosphere. The phase diagram is shown in Fig. 5. Above 13 kb. the transition could not be detected in our measurements. The reason for this is shown in Fig. 6, where the relative change in resistance at the transition, $\Delta R/R$, is plotted as a function of pressure. It falls rapidly and drops below the limits of detection by 14 kb. That the transition still occurs is shown by the point at room temperature, due to Bridgman's compressibility work. Figure 7 shows the resistance–temperature curve for La at 4.4 kb.

It is interesting to note that after being heated from the α- to the β-phase, the transition could not be seen on cooling, nor could it be found on subsequent heating. This change in subsequent compression of lanthanum was observed by Bridgman[5] in isothermal compressions.

(5) P. W. Bridgman, *Proc. Acad. Arts Sci.*, **81**, 165 (1952).

AUTOMATIC AND COULOMETRIC TITRATIONS IN STUDIES OF CHEMICAL KINETICS. II. DISPROPORTIONATION, CATALYTIC, AND COMPETING REACTIONS

BY RICHARD E. COVER[1] AND LOUIS MEITES

Department of Chemistry of the Polytechnic Institute of Brooklyn, Brooklyn 1, New York

Received April 21, 1963

When an oxidation–reduction reaction is caused to occur at a constant rate, as in automatic or coulometric titration, the occurrence of a side reaction affects the titration curve obtained by any of the common techniques of end point detection. Three types of side reactions are considered: (1) disproportionation of the product of the primary reaction; (2) regeneration of the starting material by reaction of the product with a major constituent of the supporting electrolyte (*e.g.*, hydrogen ion); and (3) consumption of the reagent by reaction with a reducing or oxidizing agent that is not in equilibrium with the one nominally being titrated. For each case it is shown mathematically how the nature of the side reaction can be identified and how its rate constant can be deduced from experimental data.

Introduction

The first paper of this series[2] described the effects of several types of side reactions on the titration curves obtained when a substance A is titrated at a constant rate with a reagent T′. In the cases treated there, either A or the product A′ of the titration reaction was assumed to be in slow equilibrium with another species in the same oxidation state, and it was shown how different possibilities could be distinguished and how their rate constants could be evaluated from titration curve data. Those cases shared the characteristic that the consumption of reagent could not exceed the stoichiometric figure for reaction with the A and the other species in equilibrium with A in the original solution.

The present paper gives similar treatments of several other cases, in which the amount of reagent consumed must exceed this stoichiometric value. The procedure followed, the assumptions made, the manner in which the equations given for automatic titrations may be converted to the form appropriate for coulometric titrations, the mode of formulating the titration reactions, and the symbols employed are all given in the preceding paper.[2] It is again arbitrarily assumed that the titrant T′ is a reducing agent; cases in which the titrant is an oxidizing agent will be described by equations identical with the following except for the sign of the change of potential with time.

(1) (a) This paper is based on the dissertation submitted by Richard E. Cover to the Faculty of the Polytechnic Institute of Brooklyn in partial fulfillment of the requirements for the degree of Doctor of Philosophy in June, 1962; (b) Socony Mobil Oil Company, Brooklyn Laboratory, Research Department, Brooklyn 22, N. Y.

(2) R. E. Cover and L. Meites, *J. Phys. Chem.*, **67**, 1528 (1963).

Results and Discussion

System A.—This system may be represented by the scheme

$$A + T' \xrightarrow{k_A} A' + T$$

$$2A' \xrightarrow{k_1} A + A''$$

That is, species A is reduced to A′ by the titrant, and the A′ then disproportionates, regenerating A and also yielding the species A″, which is in a still lower oxidation state. The disproportionation is assumed to be second order or pseudo second order, and its rate constant k_1 is expressed in cm.^{3} mole^{-1} sec.$^{-1}$. The titration of uranium(VI) with chromium(II) in hydrochloric acid solutions, which exemplifies this system, will be described elsewhere.

With the aid of eq. 1–4 of the preceding paper, one may write the following rate equations for this system.

$$dC_A/dt = k_1C_{A'}^2 - k_AC_AC_{T'} \quad (1)$$

$$dC_{A'}/dt = k_AC_AC_{T'} - 2k_1C_{A'}^2 \quad (2)$$

$$dC_{A''}/dt = k_1C_{A'}^2 \quad (3)$$

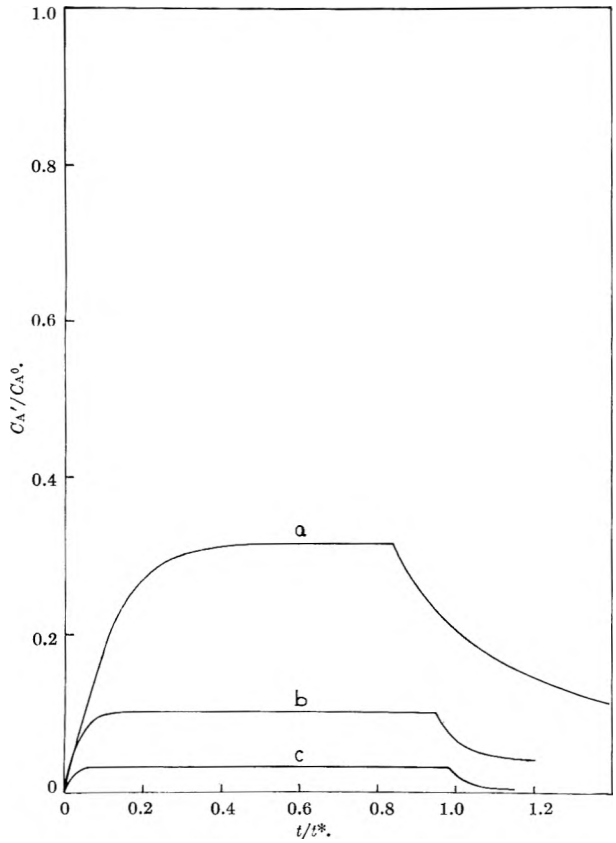

Fig. 1.—Plots of C_A'/C_A^0 for system A, showing the effect of varying ρ while holding C_A^0 constant; $n_A = 1$, $k_1 = 83.3$ cm.^{3} mole^{-1} sec.$^{-1}$, t^* = (a) 1,200, (b) 12,000, and (c) 120,000 sec.

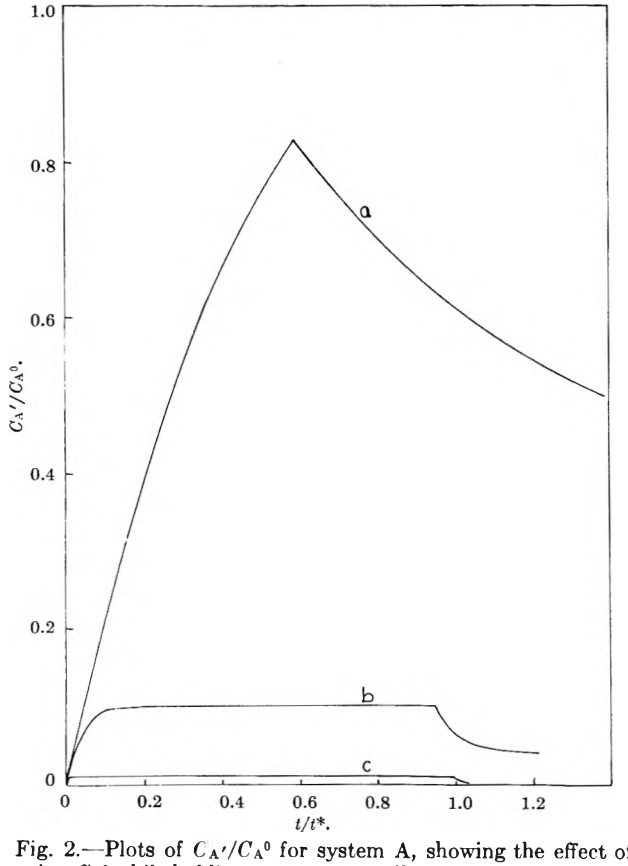

Fig. 2.—Plots of C_A'/C_A^0 for system A, showing the effect of varying C_A^0 while holding ρ constant. All parameters are identical with those for the similarly labeled curves in Fig. 1.

$$dC_T'/dt = \rho - k_A C_A C_T' \tag{4}$$

$$C_A^0 = \rho t^*/2 \tag{5}$$

where, in accordance with the definitions given previously, ρ is the constant stoichiometric rate of addition of titrant (in mole cm.$^{-3}$ sec.$^{-1}$) and t^* is the time corresponding to the A'' equivalence point, while t is the elapsed titration time (both t and t^* are expressed in seconds), C_X is the concentration (moles/cm.^{3}) of species X at time t, and C_A^0 is the initial concentration (moles/cm.^{3}) of the species titrated. It is convenient, as before, to define a time τ such that $C_A \rightarrow 0$ as $t \rightarrow \tau$.

In the interval $t \leq \tau$, the solution of eq. 2 is

$$C_{A'} = \sqrt{\frac{\rho}{2k_1}} \tanh \sqrt{2\rho k_1}\, t \tag{6}$$

while in the interval $t \geq \tau$ it is

$$C_{A'} = \frac{C_{A'_\tau}}{C_{A'_\tau} k_1 (t - \tau) + 1} \tag{7}$$

where $C_{A'_\tau}$ is the value of $C_{A'}$ at $t = \tau$.

There are several methods of evaluating the rate constant k_1 for the disproportionation. Each involves following the concentration of some component of the titration mixture as a function of time during the titration.

It is clear from eq. 6 that, if τ is sufficiently large, $C_{A'}$ will approach a constant value in the interval $t \leq \tau$; this is given by

$$C_{A'} = \sqrt{\frac{\rho}{2k_1}} \tag{8}$$

so that k_1 is easily evaluated if this steady-state value of $C_{A'}$ is measured. On the other hand, in the interval $t \geq \tau$, eq. 7 may be rearranged to give

$$\frac{1}{C_{A'}} = k_1(t - \tau) + \frac{1}{C_{A'_\tau}} \tag{9}$$

so that a plot of $1/C_{A'}$ *vs.* t in this interval should be linear and have a slope equal to k_1.

It is also possible to evaluate k_1 from a plot of C_A *vs.* t during the interval where $C_{A'}$ has the steady-state value given by eq. 8; here, since $t \leq \tau$ and consequently $C_{T'} = 0$, it can be shown that

$$C_A = C_A^0 - \frac{C_{A'} + \rho t}{2} \tag{10}$$

Combining eq. 8 and 10 gives

$$C_A = C_A^0 - \frac{1}{2}\sqrt{\frac{\rho}{2k_1}} - \frac{\rho t}{2} \tag{11}$$

so that k_1 is readily evaluated from the intercept of a plot of C_A *vs.* t during the steady state.

Similarly, when $t \leq \tau$

$$C_{A''} = \frac{\rho t - C_{A'}}{2} \tag{12}$$

which when combined with eq. 8 yields the steady-state expression

$$C_{A''} = \frac{\rho t}{2} - \frac{1}{2}\sqrt{\frac{\rho}{2k_1}} \tag{13}$$

Thus the value of k_1 may also be obtained from the intercept of a plot of $C_{A''}$ *vs.* t during the steady state.

Finally, one may evaluate k_1 from data on either C_T or $C_{T'}$ during the interval $t \geq \tau$. Here

$$C_T = 2C_A^0 - C_{A'} \quad (14)$$

and

$$C_{T'} = \rho t + C_{A''} - 2C_A^0 \quad (15)$$

and the values of $C_{A'}$ obtained from either of these equations can be used to evaluate k_1 with the aid of eq. 9.

We have defined τ in such a way that $C_A > 0$ while $C_{T'} = 0$ if $t < \tau$, whereas $C_A = 0$ and $C_{T'} > 0$ if $t > \tau$. If the end point is obtained from the customary linear extrapolation of a plot of C_A, $C_{A''}$, C_T, or $C_{T'}$ *vs.* t, it must always precede the A'' equivalence point. This will also be true if the titration is performed potentiometrically and if A is one of the potential-controlling species, for τ, which is the time when $C_A \rightarrow 0$, must necessarily occur in the interval $t^*/2 \leq \tau \leq t^*$. No matter how the end point is detected, the relative error of the titration will be decreased by increasing t^*.

From eq. 5 and the definition $\rho = NV'/nv$, it is clear that, in principle, t^* can be varied by changing either ρ or C_A^0 (variations of ρ can be accomplished by varying either N the normality or V' the volume rate of addition of the titrant, or v the volume of solution being titrated). No appreciable qualitative differences in the shapes of concentration–time plots for species A, A'', or T result from adopting one or the other of these techniques of varying t^*. However, the manner in which t^* is varied has a radical effect on the concentration–time plot for A', as is shown by the curves in Fig. 1 and 2. All these curves represent the effects of varying t^* under otherwise identical conditions. Figure 1 shows that varying t^* by a factor of 100 by varying ρ while holding C_A^0 constant produces only a tenfold change in the concentration of A' at the steady state; Fig. 2 shows that the same variation of t^* produces a very much larger change in the steady-state concentration of A' when it is accomplished by varying C_A^0 while holding ρ constant. Moreover, the variations of $C_{A'}$ with time are also much more pronounced if t^* is decreased by decreasing C_A^0 than if it is decreased by decreasing ρ. From these considerations it is evident that the rate constant k_1 is best evaluated from data obtained when both C_A^0 and t^* are small.

From all of the foregoing equations it is clear that absolute values of the concentration of at least one species are needed to permit the evaluation of k_1: values of quantities (*e.g.*, absorbance, diffusion current, etc.) proportional to concentration will not suffice. In general, the proportionality constants needed in applications of eq. 10–15 should be readily available from measurements on pure solutions of A, A'', T, or T'. But that required in eq. 8 and 9 may be experimentally inaccessible if the disproportionation of A' is rapid under all feasible conditions.

The potentiometric titration curves shown in Fig. 3–5 are largely self-explanatory. Each figure represents the titration of a single system for various values of t^*. The shapes of these curves, and the manners in which they change as t^* is varied, are highly characteristic of the system and of the potential-determining couple.

System B.—This system may be represented by the scheme shown on the following page.

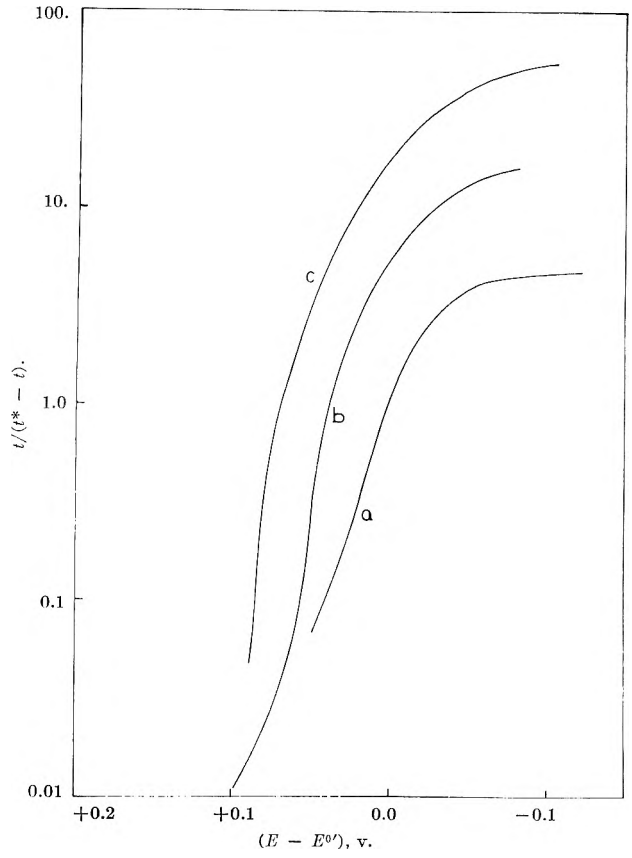

Fig. 3.—Plots of $(E - E^{0\prime})$ *vs.* log $t/(t^* - t)$ for system A. The A–A' couple is assumed to be potential-determining; $n_A = 1$, $k_1 = 83.3$ cm.^{3} mole^{-1} sec.$^{-1}$, $t^* =$ (a) 1,200, (b) 12,000, and (c) 120,000 sec.

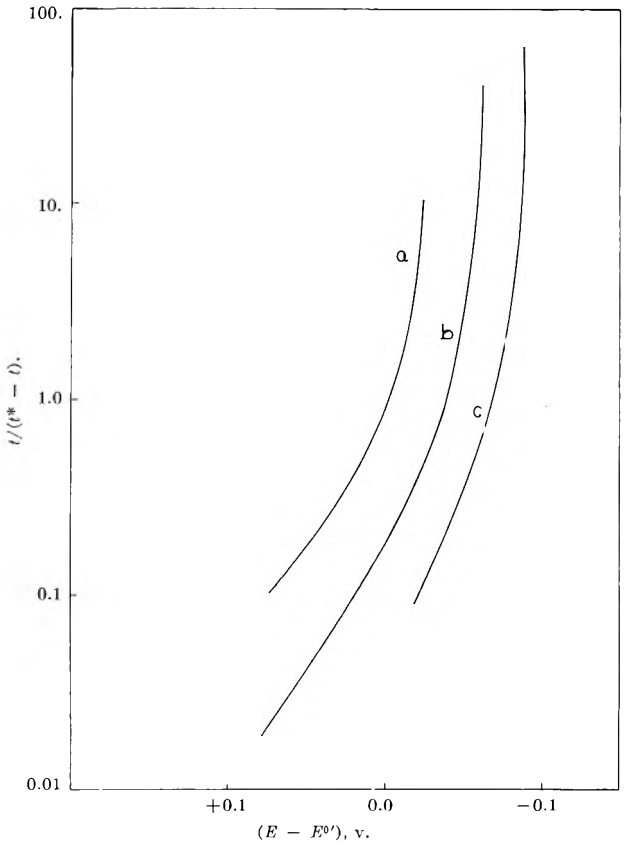

Fig. 4.—Plots of $(E - E^{0\prime})$ *vs.* log $t/(t^* - t)$ for system A. The A'–A'' couple is assumed to be potential-determining; $n_{A'} = 1$. All other parameters are identical with those for the similarly labeled curves in Fig. 3.

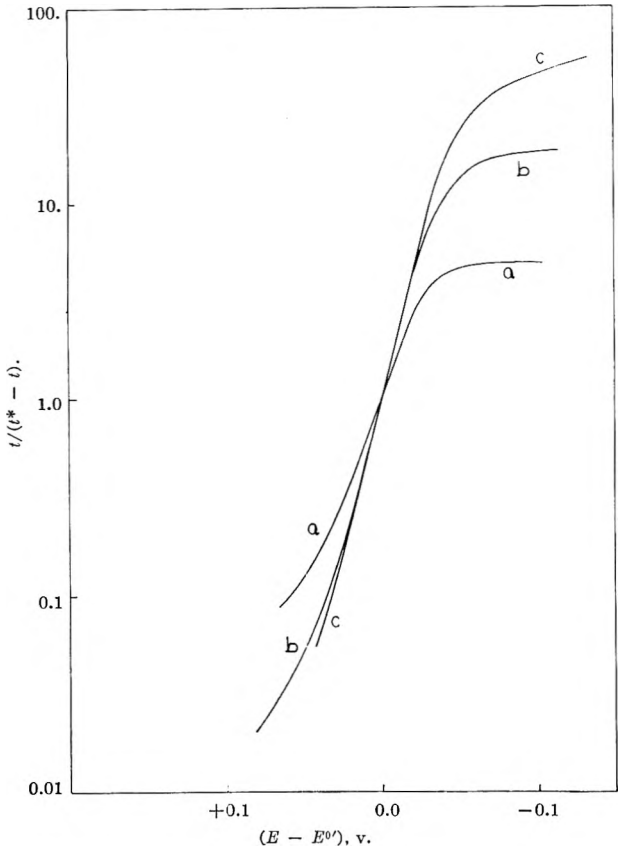

Fig. 5.—Plots of $(E - E^{0\prime})$ *vs.* log $t/(t^* - t)$ for system A. The A–A'' couple is assumed to be potential-determining; $n_{A-A''} = 2$. All other parameters are identical with those for the similarly labeled curves in Fig. 3.

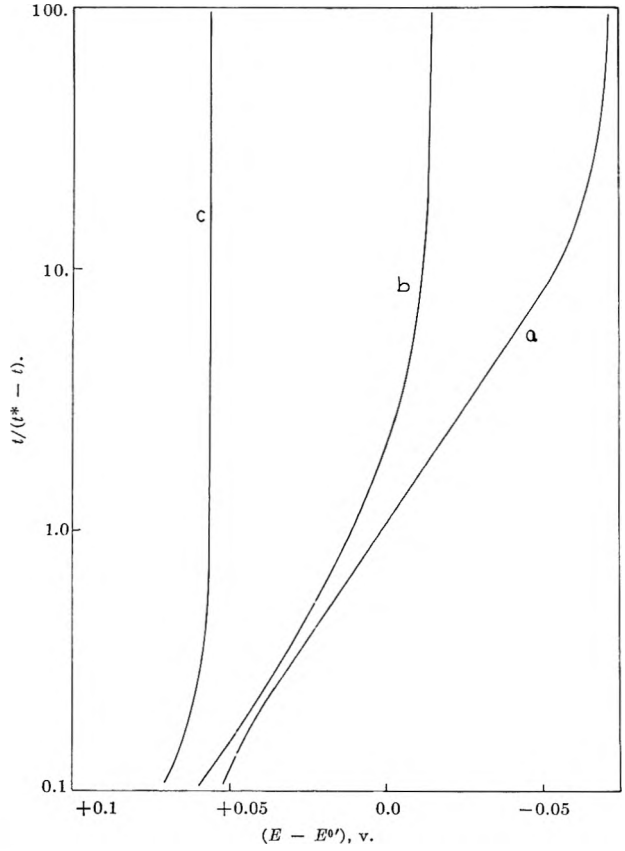

Fig. 6.—Plots of $(E - E^{0\prime})$ *vs.* log $t/(t^* - t)$ for system B. The A–A' couple is assumed to be potential-determining; $n_A = 1$, $k_2 = 1.67$ cm.^{3} mole^{-1} sec.$^{-1}$, t^* = (a) 600, (b) 6,000, and (c) 60,000 sec.

$$A + T' \xrightarrow{k_A} A' + T$$

$$A' + C \xrightarrow{k_2} A + C'$$

That is, species A is reduced to A' by the titrant, and A' is then reoxidized to A by some species C (*e.g.*, water, hydrogen ion, etc.), which is assumed to be present at a constant concentration throughout the titration.

This system is described by the rate equations

$$dC_A/dt = k_2 C_{A'} C_C - k_A C_A C_{T'} \quad (16)$$

$$dC_{C'}/dt = k_2 C_{A'} C_C \quad (17)$$

$$C_A{}^0 = \rho t^* \quad (18)$$

where k_2 is a second-order or pseudo-second-order rate constant in cm.^{3} mole^{-1} sec.$^{-1}$. These equations have the solutions

$$C_A = C_A{}^0 - \frac{\rho}{k_2 C_C}(1 - e^{-k_2 C_C t}) \quad (19)$$

$$C_{A'} = \frac{\rho}{k_2 C_C}(1 - e^{-k_2 C_C t}) \quad (20)$$

$$C_{C'} = \rho t - \frac{\rho}{k_2 C_C}(1 - e^{-k_2 C_C t}) \quad (21)$$

Obviously, for sufficiently large values of t, the exponential terms in these equations become negligible, so that

$$C_A = C_A{}^0 - \frac{\rho}{k_2 C_C} \quad (22)$$

$$C_{A'} = \frac{\rho}{k_2 C_C} \quad (23)$$

$$C_{C'} = \rho t - \frac{\rho}{k_2 C_C} \quad (24)$$

It is therefore possible to obtain the value of k_2 from the steady-state value of C_A and eq. 22, from the steady-state value of $C_{A'}$ and eq. 23, or from the intercept of a plot of $C_{C'}$ *vs.* time during the steady state.

It is also possible to evaluate the rate constant k_2 from potentiometric data if the A–A' couple is potential-determining. At the steady state the Nernst equation becomes

$$E = E^{0\prime}{}_{A,A'} + \frac{0.0591}{n_A} \log (k_2 C_C t^* - 1) \quad (25)$$

In some cases (*e.g.*, those in which C is water), the determination of the formal potential required for the direct application of eq. 25 may not be feasible. It may then be advantageous to measure the steady-state potentials in two titrations in which the values of t^* differ, but in which all of the other experimental conditions (such as the mass-transfer rates around the indicator electrode) are the same. One then has

$$k_2 = \frac{1 - Q}{C_C(t_1^* - Qt_2^*)} \quad (26)$$

where

$$\log Q = \frac{n_A}{0.0591}(E_1 - E_2) \quad (27)$$

Plots of C_A and $C_{A'}$ *vs.* time[3] for this system indicate that attempts to locate the end points of such titrations by amperometric, spectrophotometric, or similar means may be afflicted by large relative errors. As would be expected, these tend to decrease with decreasing t^* under otherwise identical conditions. Typical potentiometric titration curves, shown in Fig. 6 and 7, have shapes and manners of variation with t^* that, as usual, are highly characteristic of the system and the potential-determining couple.

System C.—This is the simplest possible two-couple system, in which two different species that are not in equilibrium with each other react with the titrant according to the equations

$$A + T' \underset{k_A}{\overset{k_{-A}}{\rightleftharpoons}} A' + T$$

$$D + T' \underset{k_D}{\overset{k_{-D}}{\rightleftharpoons}} D' + T$$

where A, D, and T are the oxidized and A′, D′, and T′ the reduced forms of the couples, and k_A, k_{-A}, k_D, and k_{-D} are second-order or pseudo-second-order rate constants (mole^{-1} cm.^{3} sec.$^{-1}$). Assuming, as before,[2] that both forward reactions are very fast and that both equilibria lie far to the right—in effect, that $k_A = k_{-D} = 0$ while $k_A = k_D = \infty$—one has, in the interval when $C_A \neq 0$ and $C_D \neq 0$

$$\rho = k_A C_A C_{T'} + k_D C_D C_{T'} = NV'/nv \quad (28)$$

If the reaction represented by the equation

$$A + D' \longrightarrow A' + D$$

is assumed to occur at a finite rate, one obtains some rather complicated differential equations that do not appear to possess analytical solutions. If, on the other hand, one assumes that this reaction is immeasurably fast in the forward direction but does not occur in the reverse direction, one obtains the trivial conclusion that the reduction of A reaches completion before that of D begins. In the following it is assumed that this reaction does not take place in either direction.

These assumptions lead to the rate equations

$$\frac{dC_A}{dt} = -\rho\left(\frac{k_A C_A}{k_A C_A + k_D C_D}\right) \quad (29)$$

$$\frac{dC_D}{dt} = -\rho\left(\frac{k_D C_D}{k_A C_A + k_D C_D}\right) \quad (30)$$

$$C_A^0 + C_D^0 = \rho t^* \quad (31)$$

whose solutions are

$$\rho t = \rho t^* - C_A - C_D^0(C_A/C_A^0)^{k_D/k_A}$$

$$= \rho t^* - C_D - C_A^0(C_D/C_D^0)^{k_A/k_D} \quad (32)$$

from which it is clear that the variations of C_A and C_D are governed by the ratio, rather than by the absolute values, of the rate constants k_A and k_D. It should be possible to evaluate this ratio from data obtained in a titration in which, for example, C_A^0, t^*, and the value of C_A at some time t are known, using eq. 33.

(3) R. E. Cover, Ph. D. Dissertation, Polytechnic Institute of Brooklyn, 1962. Fig. XXVI and XXVII.

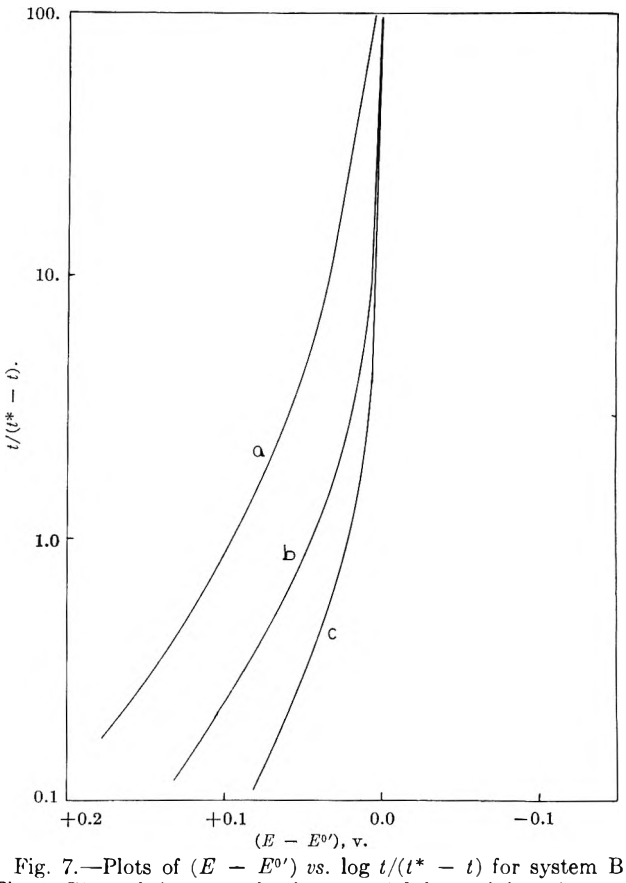

Fig. 7.—Plots of $(E - E^{0'})$ *vs.* log $t/(t^* - t)$ for system B. The A–C′ couple is assumed to be potential-determining; $(\gamma n_A - \beta' n_{C'}) = 1$. All other parameters are identical with those for the similarly labeled curves in Fig. 6.

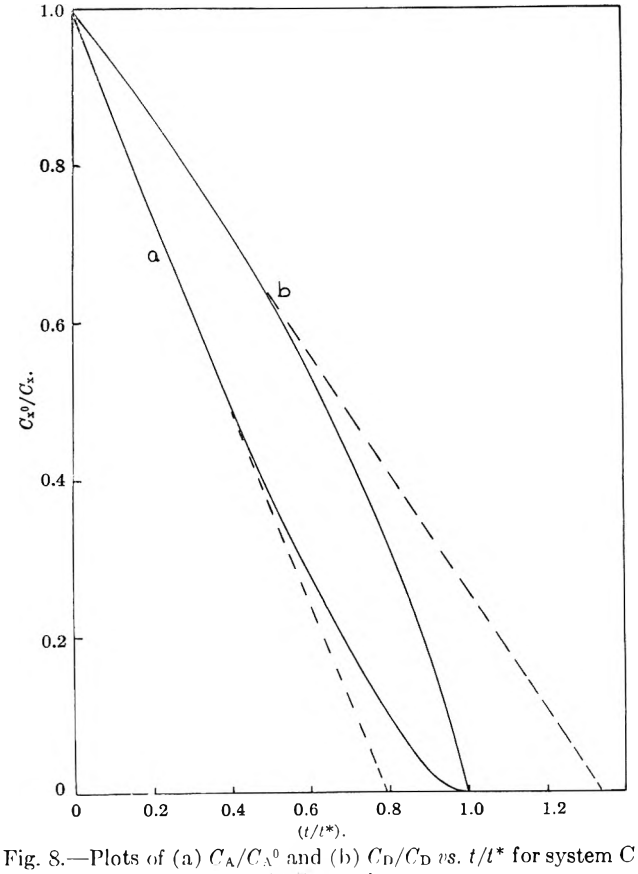

Fig. 8.—Plots of (a) C_A/C_A^0 and (b) C_D/C_D *vs.* t/t^* for system C; $k_A/k_D = 2$.

$$\frac{k_D}{k_A} = \frac{\log\{[\rho(t^* - t) - C_A]/[\rho t^* - C_A^0]\}}{\log(C_A/C_A^0)} \quad (33)$$

An entirely similar equation can be deduced for the case in which a value of C_D is known at some time during the titration, using eq. 32.

Figure 8 shows the calculated concentration–time curves for species A and D with $k_A/k_D = 2$, and demonstrates that substantial errors may be incurred by conventional techniques of end point location. It may be remarked that this system may be expected to be exemplified by many titrations of solutions containing two complexes of a single transition element that are in very slow equilibrium. It is obviously equivalent to the well known technique of determining a ratio of rate constants for two independent reactions by observing the ratio in which their products are formed in a mixture.

Acknowledgment.—R. E. C. wishes to express his gratitude to the Socony Mobil Oil Company for awarding him the Socony Mobil Incentive Fellowship during the period 1959–1962.

THE INFERENCE OF ADSORPTION FROM DIFFERENTIAL DOUBLE LAYER CAPACITANCE MEASUREMENTS. II. DEPENDENCE OF SURFACE CHARGE DENSITY ON ORGANIC NONELECTROLYTE SURFACE EXCESS[1,2]

BY ROBERT S. HANSEN, DENNIS J. KELSH, AND D. H. GRANTHAM

Institute for Atomic Research and Department of Chemistry, Iowa State University, Ames, Iowa

Received April 24, 1963

Dependences of boundary tension and capacitance at the mercury–aqueous 0.1 N $HClO_4$ interface on polarization and organic solute concentration were determined for the solutes *n*-amyl alcohol and phenol. The surface charge density at fixed polarization varied linearly with surface excess in the case of *n*-amyl alcohol, but contained both linear and cubic terms in surface excess in the case of phenol, suggesting a change in phenol orientation with increasing coverage. Near the electrocapillary maximum the differential capacitance varied linearly with coverage in both cases. The theory of inference of adsorption from capacitance measurements is further discussed. It is pointed out that the inference based on double integration of nonstatic capacitance curves introduces (by integrating across desorption peaks) serious errors where solutes are strongly adsorbed at small concentrations. Criteria for estimating the errors thus introduced are suggested. An earlier treatment proposed by this Laboratory,[3] based on the assumption of linear variation of surface charge density with coverage, appears adequately justified for inference of fractional surface coverages near the electrocapillary maximum, but must be considered approximate for evaluation of molar areas at full coverage in cases where linear variation of charge with coverage has not been demonstrated.

Introduction

This Laboratory has recommended[3] a method for inference of amount of adsorption from differential double layer capacitance measurements claimed to be especially suited for systems exhibiting monomolecular adsorption. The method stems from earlier work by Frumkin[4] and is indicated in outline by eq. 1–4.

If

$$\frac{\theta}{1-\theta} = B_0 a e^{2\alpha\theta} \quad (V = 0) \qquad (1)$$

then

$$\frac{\theta}{1-\theta} = B_0 a e^{2\alpha\theta} e^{-(S\Phi/RT)} \quad (\text{V general}) \qquad (2)$$

where

$$\Phi = \int_0^V [Q_w - C'(V - V_N)]\, dV \qquad (3)$$

and parameters may be established by observing the dependence of the quantity θ_{app} on V and a, where

$$\theta_{app} = \frac{C_w - C}{C_w - C'} = \theta\left[1 - (S/RT) \times \frac{1-\theta}{1-2\alpha\theta(1-\theta)} \frac{\{Q_w - C'(V - V_N)\}^2}{C_w - C'}\right] \qquad (4)$$

In these equations, θ is the fractional surface coverage, a the solute activity, Q_w the interfacial charge density with the base solution at polarization V, C_w and C the differential capacitances per unit area in absence and in presence of adsorbate, C' the capacitance when $\theta = 1$, V_N the electrocapillary maximum potential when $\theta = 1$, S the molar area of adsorbate when $\theta = 1$, B_0 and α are adjustable constants.

Since our work appeared, an article by Parsons[5] has criticized the assumption of linear variation of capacitance with coverage and conclusions derived from this assumption. It should be noted that our previous treatment assumed linear variation of charge density with coverage, and, as should be evident from the form of eq. 4 derived on the basis of this assumption, this does not imply a linear variation of capacitance with coverage in general. An article by Breiter and Delahay[6] has compared surface excesses inferred from capacitance curves (treating data in a manner somewhat similar to ours) and electrocapillary curves, for the system mercury–1 M $NaClO_4$–amyl alcohol, and found results obtained by the two methods to be in good gen-

(1) Based in part on a dissertation submitted by Dennis J. Kelsh to the Graduate College, Iowa State University, in partial fulfillment of the requirements for the degree of Doctor of Philosophy, 1962.

(2) Contribution No. 1293; work was performed in the Ames Laboratory of the U. S. Atomic Energy Commission.

(3) R. S. Hansen, R. E. Minturn, and D. A. Hickson, *J. Phys. Chem.*, **60**, 1185 (1956); **61**, 953 (1957).

(4) A. Frumkin, *Z. Physik*, **35**, 792 (1926).

(5) R. Parsons, *Trans. Faraday Soc.*, **55**, 999 (1959).

(6) M. Breiter and P. Delahay, *J. Am. Chem. Soc.*, **81**, 2938 (1959).

eral agreement. Breiter and Delahay emphasize the importance of using static (zero frequency) capacitances for the inference of adsorption. This point is well taken; Frumkin and Melik-Gaikazyan[7,8] have demonstrated both theoretically and experimentally that differential capacities may be expected to be highly frequency dependent at potentials near the desorption peaks in capacity–polarization curves.

The present work is an investigation of the dependence of surface charge on adsorbate surface coverage in the systems mercury–0.1 *M* $HClO_4$–*n*-amyl alcohol and mercury–0.1 *M* $HClO_4$–phenol. We shall also extend the theory presented in our earlier papers, and discuss its applicability critically with respect to the findings of Parsons,[5] Breiter and Delahay,[6] and the present investigation.

Theoretical

We shall be concerned with the dependence of interfacial properties on polarizing potential and activity of an adsorbable organic solute in a solution containing electrolytes whose chemical potentials are kept constant, the system being at constant temperature. Then

$$-\mathrm{d}\gamma = Q\,\mathrm{d}V + RT\Gamma\,\mathrm{d}\ln a \qquad (5)$$

where γ is the interfacial tension, Q the charge per unit area on the electrode side of the double layer, V the potential of the polarizable electrode (mercury in the present work) with respect to a reference electrode (we shall refer V to the electrocapillary maximum potential at $a = 0$), Γ is the surface excess of the adsorbable component per unit area, and a is its activity.

From eq. 5 we obtain

$$\left(\frac{\partial \ln a}{\partial V}\right)_\Gamma = -\frac{1}{RT}\left(\frac{\partial Q}{\partial \Gamma}\right)_V \qquad (6)$$

Hence if we define $F(a)$ by

$$F(a) = \Gamma(a,\ V = 0) \qquad (7)$$

we have

$$\Gamma(a,\ V) = F(ae^{-(S\Phi/RT)}) \qquad (8)$$

where

$$\Phi = -\frac{1}{S}\int_0^V \left(\frac{\partial Q}{\partial \Gamma}\right)_V \mathrm{d}V \qquad (9)$$

Equations 6–9 are of purely thermodynamic origin; no assumptions as to adsorption model are implicit in them. For subsequent model discussions we define S as the molar area of the adsorbate in a complete monolayer, but evidently eq. 8 with Φ defined by eq. 9 is valid for any choice of S.

If a certain value, say Γ_0, of the surface excess occurs at an activity a_0 when $V = 0$ and at an activity a' at a polarization V', then from eq. 8

$$(S\psi/RT) = \ln a' - \ln a_0\ (\Gamma = \Gamma_0) \qquad (10)$$

In this way the function $(S\Phi/RT)$ can be evaluated experimentally. It is convenient to suppose $(S\Phi/RT) = f(\Gamma, V)$ for the purpose of model discussions.

We define the spreading pressure π by

$$\pi(a, V) = \gamma(0, V) - \gamma(a, V) \qquad (11)$$

and obtain by use of eq. 5

$$\mathrm{d}\pi = (Q - Q_w)\,\mathrm{d}V + RT\Gamma\,\mathrm{d}\ln a \qquad (12)$$

where Q_w is the surface charge density at polarization V when $a = 0$. From eq. 12 we find

$$\left(\frac{\partial \ln a}{\partial V}\right)_\pi = \frac{Q_w - Q}{\Gamma RT} \qquad (13)$$

Hence if we define $G(a)$ by

$$G(a) = \pi(a,\ V = 0)$$

we have

$$\pi(a,\ V) = G(ae^{-(S\psi/RT)}) \qquad (14)$$

where

$$\psi = \frac{1}{S}\int_0^V \frac{Q_w - Q}{\Gamma}\,\mathrm{d}V \qquad (15)$$

If a certain value, say π_0, of the spreading pressure occurs at an activity a_0 when $V = 0$ and at an activity a' at polarization V', then from eq. 14

$$(S\psi'/RT) = \ln a' - \ln a_0\ (\pi = \pi_0) \qquad (16)$$

In this way the function $(S\psi/RT)$ can be evaluated experimentally. Most conveniently, we obtain $(S\psi/RT)$ as a function of π and V by plotting experimental values obtained at a given value of π against V and repeating for as many values of π as desired; for the purpose of model discussions, however, it is most useful to obtain the function $(S\psi/RT) = g(\Gamma, V)$. Equations 11–16 are also purely thermodynamic in character and contain no assumptions as to adsorption model.

If and only if Q varies linearly with Γ at fixed V, Φ and ψ will be equal and independent of Γ. If the linear dependence of Q on Γ is limited to a range $0 \leqslant \Gamma \leqslant \Gamma_0$, Φ and ψ will be equal and independent of Γ in this range. Finally, if Φ or ψ can be shown to be independent of Γ for some range of Γ, say $0 < \Gamma < \Gamma_0$, then Φ and ψ are equal in this range and Q must vary linearly with Γ at fixed V in this range.

If Q varies linearly with Γ, ψ depends on V only and, where G' and G'' are the first and second derivatives of $G(a\ e^{-(S\psi/RT)})$ after its argument we obtain from eq. 12 and 14

$$Q - Q_w = \left(\frac{\partial \pi}{\partial V}\right)_a = -\frac{Sa}{RT}e^{-S\psi/RT}\frac{\mathrm{d}\psi}{\mathrm{d}V}G' \qquad (17)$$

$$C - C_w = \left(\frac{\partial^2 \pi}{\partial V^2}\right)_a = -\frac{Sa}{RT}e^{-S\psi/RT}\frac{\mathrm{d}^2\psi}{\mathrm{d}V^2}G' + \left[\frac{Sa}{RT}e^{-S\psi/RT}\right]^2\left[G'' + \frac{G'}{a}e^{S\psi/RT}\right]\left(\frac{\mathrm{d}\psi}{\mathrm{d}V}\right)^2 \qquad (18)$$

$$\Gamma = \left(\frac{\partial \pi}{RT\,\partial \ln a}\right)_V = \frac{a}{RT}e^{-S\psi/RT}G' \qquad (19)$$

From eq. 18 and 19

$$C_w - C = S\Gamma\frac{\mathrm{d}^2\psi}{\mathrm{d}V^2} - \left(S\Gamma\frac{\mathrm{d}\psi}{\mathrm{d}V}\right)^2 \times \left[\frac{G''}{(G')^2} + \frac{1}{aG'}e^{S\psi/RT}\right] \qquad (20)$$

(7) A. Frumkin and V. I. Melik-Gaikazyan, *Dokl. Akad. Nauk SSSR*, **77**, 855 (1951).

(8) V. I. Melik-Gaikazyan, *Zh. Fiz. Khim.*, **26**, 560 (1952).

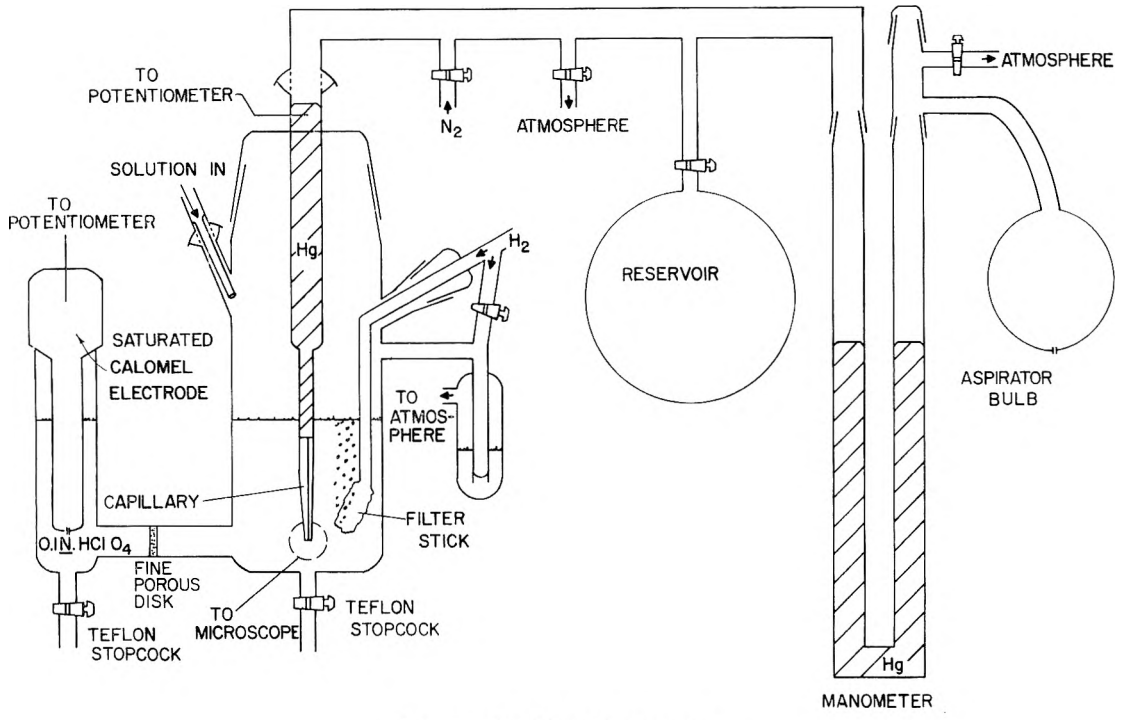

Fig. 1.—Capillary electrometer.

Equation 19 shows that Γ also depends only on $ae^{-(S\psi/RT)}$; where Γ' is its derivative after this argument

$$\Gamma' = \frac{1}{RT}\left(G' + ae^{-(S\psi/RT)}\,G''\right) \qquad (21)$$

From eq. 18–21

$$C_w - C = \Gamma S\frac{d^2\psi}{dV^2} - \frac{a\Gamma'}{RT}e^{-(S\psi/RT)}\left(S\frac{d\psi}{dV}\right)^2 \qquad (22a)$$

or

$$C_w - C = \Gamma S\frac{d^2\psi}{dV^2} - \left(S\frac{d\psi}{dV}\right)^2\frac{d\Gamma}{RT\,d\ln\left(ae^{-(S\psi/RT)}\right)} \qquad (22b)$$

Suppose that Q is linear in Γ at fixed V for $0 \leqslant \Gamma \leqslant \Gamma_0$, $-V' \leqslant V \leqslant V''$. V' and V'' are positive, so that the range of V includes the electrocapillary maximum for the base solution, and Γ_0 is a fixed number (independent of V). Let Q_0 be the value of Q when $\Gamma = \Gamma_0$, $C_0 = dQ_0/dV$. Then

$$Q = Q_w + (Q_0 - Q_w)\frac{\Gamma}{\Gamma_0} \qquad (23)$$

$$\frac{d\psi}{dV} = \frac{1}{S}\frac{Q_w - Q}{\Gamma} = \frac{Q_w - Q_0}{S\Gamma_0} \qquad (24)$$

$$\frac{d^2\psi}{dV^2} = \frac{C_w - C_0}{S\Gamma_0} \qquad (25)$$

Substituting these results in eq. 20 and 22 we obtain

$$C_w - C = \frac{\Gamma}{\Gamma_0}(C_w - C_0) - \left[\frac{\Gamma}{\Gamma_0}(Q_w - Q_0)\right]^2\left[\frac{G''}{(G')^2} + \frac{1}{aG'}e^{S\psi/RT}\right] \qquad (26)$$

$$C_w - C = \frac{\Gamma}{\Gamma_0}(C_w - C_0) - \frac{a\Gamma'}{RT}e^{-S\psi/RT}\left(\frac{Q_w - Q_0}{\Gamma_0}\right)^2 \qquad (27a)$$

$$C_w - C = \frac{\Gamma}{\Gamma_0}(C_w - C_0) - \left(\frac{Q_w - Q_0}{\Gamma_0}\right)^2\frac{d\Gamma}{RT\,d\ln\left[ae^{-S\psi/RT}\right]} \qquad (27b)$$

Equations 26–27 are generalizations of eq. 10 of ref. 5, and eq. 18 is similar in content to Parsons'[5] eq. 8; Parsons has not assumed linear variation of charge with coverage, so his analogs of $d\psi/dV$ and $d^2\psi/dV^2$ are partial derivatives.

It should be noted that, if Q varies linearly with Γ at fixed V, C will *not* be linear in Γ in general. This is clear from eq. 22–23; more generally

$$C = \left(\frac{\partial Q}{\partial V}\right)_a = \left(\frac{\partial Q}{\partial V}\right)_\Gamma + \left(\frac{\partial Q}{\partial \Gamma}\right)_V\left(\frac{\partial \Gamma}{\partial V}\right)_a \qquad (28)$$

The term $(\partial Q/\partial V)_\Gamma$ is linear in Γ if Q is linear in Γ, but the term $(\partial Q/\partial \Gamma)_V(\partial \Gamma/\partial V)_a$ is not and is the term responsible for the well known desorption peaks in capacitance–polarization curves obtained with solutions containing adsorbable nonelectrolytes. In the neighborhood of the electrocapillary maximum $(dQ/d\Gamma)_V$ (approximately proportional to V) and $(d\Gamma/dV)_a$ are both small, the second term in eq. 28 is hence substantially negligible, and in this region linearity of Q in Γ implies linearity of C in Γ.

Experimental

The capillary electrometer used in this research incorporates several ideas presented by previous workers[9–11] and is shown schematically in Fig. 1. Because the design and operation of a capillary electrometer are not described fully in any of the generally accessible modern literature, we feel that a description of our

(9) S. R. Craxford, Dissertation, Oxford, 1936.
(10) L. A. Hansen and J. W. Williams, *J. Phys. Chem.*, **39**, 439 (1935).
(11) F. O. Koenig, *Z. physik. Chem.*, **A54**, 454 (1931).

apparatus is warranted although the general principles of operation have been known for more than 80 years.

The tapering capillary was formed from precision bore Pyrex capillary tubing of internal diameter 0.0025 ± 0.005 in. This tubing was drawn out in a gas flame to the extent that the original outside diameter of 5 mm. became approximately 2 mm. at the narrowest constriction. The tubing was cut just above this point of minimum diameter, producing a tapering capillary with an internal diameter of approximately 0.03 mm. at the tip.

The mercury reservoir directly above the capillary was approximately 27 cm. in height. A tungsten wire sealed through the glass near the top served as lead to the polarizing source. All ball joints and standard tapers attached or leading to the cell proper were greaseless. The large ball joint connecting the mercury reservoir to the manometer system was lubricated lightly with Apiezon N, which was also used on the three stopcocks attached to the manometer system.

A Leeds and Northrup K-2 potentiometer monitored the voltage supplied by three 2-v. cells of a wet-cell storage battery which were wired in parallel. The potential of the mercury electrode was measured in reference to a saturated calomel electrode in contact with the 0.10 *N* perchloric acid solution. The porous plug separating the cell proper from the compartment containing the reference electrode minimized the transfer of chloride ion to the solution.

The gas pressure above the mercury reservoir was increased by addition of tank nitrogen controlled by a standard regulator valve or decreased by venting nitrogen to the atmosphere through a stopcock and tapering vent prepared from 1-mm. i.d. capillary tubing. A 1-l. ballast reservoir further increased the ease with which the pressure could be adjusted to a high degree of precision. The system was designed in such a way as to allow the operator to increase pressure *via* the nitrogen tank or decrease it by venting nitrogen to the atmosphere while simultaneously observing the level of the mercury in the capillary through a microscope.

The manometer was constructed of large bore (20 mm. i.d.) tubing to eliminate the need for any correction for capillary depression effect. An opaque white background was provided, and each meniscus was illuminated from the side by a small flashlight. Movable brass cylinders around each arm of the manometer served to eliminate interfering glare from above. A Gaertner cathetometer was used to measure pressures with a reproducibility of 0.05 mm. The aspirator bulb attached to the atmosphere side of the manometer ensured complete wetting of the capillary walls. The bulb was used to oscillate the mercury in the capillary before and after each measurement to make sure that the position of the meniscus in the capillary was truly the equlibrium position.

A Gaertner scale micrometer microscope, M 105 A, with objective of 48-mm. effective focal length and a magnification of 23 diameters, was used to observe the meniscus in the capillary. The focal distance was large enough to permit the meniscus and the tip of the capillary to be viewed simultaneously, thus allowing the tip to serve as a convenient reference point. During measurement, the meniscus was always brought to a point about 0.20 mm. from the tip as seen through the eyepiece scale of the microscope. The capillary was illuminated from behind by a small electric bulb placed behind a white translucent background. A flat piece of glass fused to the front side of the electrometer cell allowed the capillary to be viewed through optically plane glass.

After cleaning the cell components in a hot bath of 3–1 sulfuric–nitric acid, followed by rinsing with conductivity water, the cell was assembled and the capillary was allowed to soak in conductivity water for a day or two before any interfacial tension measurements were made. We found, as had Craxford previously,[9] that the capillary radius tends to increase significantly in size with soaking until it reaches a constant value.

The radius of the capillary at the null point was determined by standardization against a solution of known surface tension. Smolders' value[12] of 426.2 ± 0.2 dynes/cm. for the interfacial tension of mercury–0.05 *M* sodium sulfate at the electrocapillary maximum at 25.0 ± 0.3° was used for this purpose.

The electrometer was thermostated only by the air-conditioning of the building. Measurements were made at a temperature of 26.5 ± 0.9°; such a temperature fluctuation generates errors of the order of 0.2 dyne/cm. in the interfacial tension.

Differential double layer capacitances were measured by a substitution technique with an impedance bridge whose schematic design is shown in Fig. 2. A Leeds and Northrup shielded ratio box, catalog number 1553, served as the central connecting terminal. A shielded stepdown transformer is incorporated in this box. Shielded binding posts made connection to the various external pieces of equipment. All electrical connections were made with high quality shielded cables.

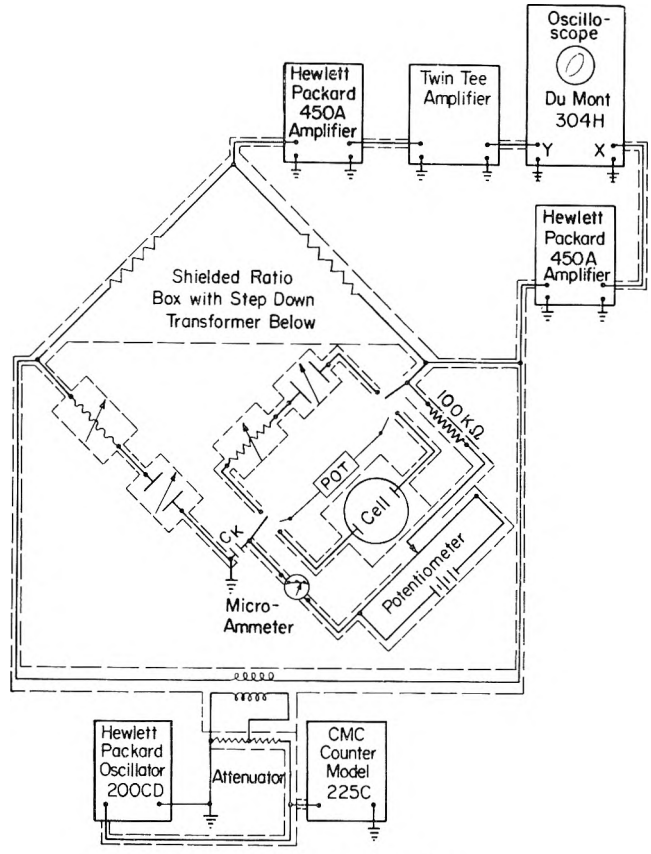

Fig. 2.—Impedance bridge.

The input signal to the transformer in the ratio box was supplied by a Hewlett-Packard Model 200 CD wide range oscillator. The signal from the oscillator was attenuated by use of a simple potential divider constructed from precision resistors. This permitted operation of the oscillator at a high output level where best frequency stability was observed while allowing use of a low level signal for the operation of the bridge.

The measuring arm of the bridge consisted of a Freed Transformer Co. Model 1350 decade capacitor and a noninductively wound Leeds and Northrup decade resistance, catalog no. 4764, in series connection. The lowest capacitance range was covered by a continuously variable air capacitor with a maximum value of 100 $\mu\mu$f. Four decades in units of 0.001, 0.01, 0.1, and 1 μf. extended the range of the decade capacitor to 11 μf. The decade resistance had six units variable in increments of 0.01, 0.1, 1, 10, 100, and 1000 ohms, respectively, and covered the range from 0.01 to 11,000 ohms. Contact resistances were negligible in both of these circuit elements and the reproducibility in settings consequently was limited only by other factors in the measurement.

A second pair of elements like the above was used in the substitution procedure to be described later. The connections to this cell analog were made as nearly identical with those to the cell proper as could be achieved.

The null detector for the bridge was based on a DuMont Type 304-H cathode ray oscilloscope with both x and y input terminals. The output signal from the bridge was of such low level that amplification was necessary prior to display on the oscilloscope screen. The bridge output was first amplified by a Hewlett-Packard wide band amplifier, Model 450 A, operating at a gain of 100 to 1. This signal in turn was amplified by a twin-tee narrow band amplifier designed and constructed in this Laboratory. Pairs of tees used in the measurement were constructed for use at nominal frequencies of 100, 500, 5000, and 10,000 c.p.s. The filtered, amplified signal from the twin tee produced the y displacement on the cathode ray oscilloscope screen.

To gain some additional sensitivity in the measurements, a

(12) C. A. Smolders, *Rec. trav. chim.*, **80** 635 (1961).

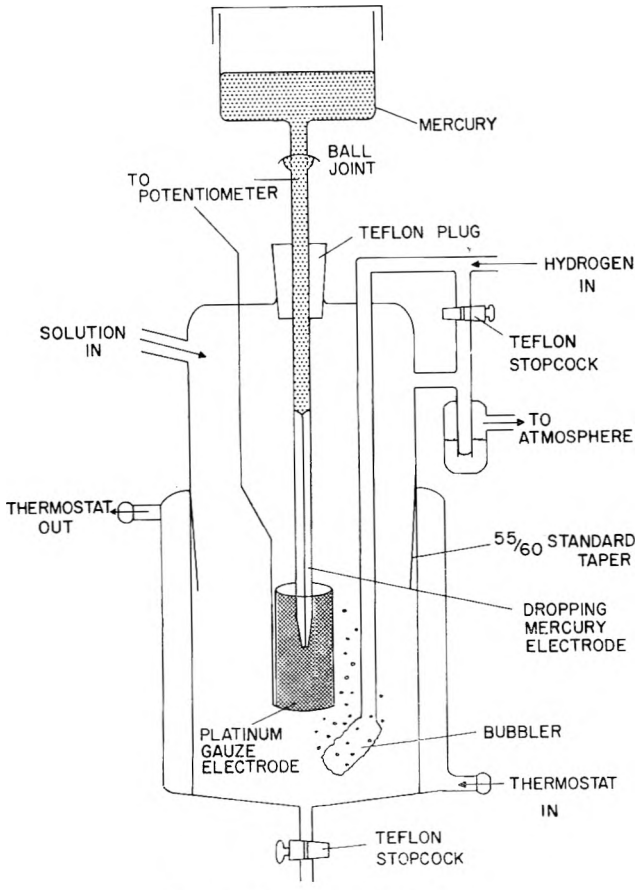

Fig. 3.—Impedance bridge cell.

phase sensitive technique was used. A second Hewlett-Packard Model 450 A wide band amplifier was connected to the bridge so that the input signal to the bridge could be amplified and used to produce the x deflection on the oscilloscope screen. Thus, a series of Lissajous figures showed the amplitude of the output signal from the bridge and the phase of this signal with respect to the input. A horizonal straight line indicated a balance condition. The x-axis of the cathode ray oscilloscope was calibrated and used to measure the input signal to the bridge.

The mercury electrode was polarized by means of a Leeds and Northrup student potentiometer. To eliminate effectively the path available for the alternating current flow parallel to the path through the double layer and solution, a 100,000 ohm resistor was placed in series with this polarizing source. A Rubicon Type B high precision potentiometer, shown as POT in Fig. 2, was used to measure the polarization of the mercury surface in reference to the standard hydrogen electrode. The Rubicon potentiometer (but of course not the polarizing potentiometer) was switched out of the circuit during capacity measurements, thus removing any alternate path for the a.c. current flow. C_k was a 60 μf. condenser which essentially eliminated the direct current path from the electrodes through the oscillator transformers. C_k was in series with the cell capacitance, but its small contribution to the impedance was corrected for by substitution.

Six-volt storage batteries supplied current to the potentiometers. The Rubicon potentiometer slide wire was calibrated against an Eppley Laboratories standard cell, catalog no. 100. A Rubicon galvanometer, catalog no. 3411, with a sensitivity of 1.5 μv./mm. was used in the calibration. The potentiometer was completely enclosed in a grounded metal box for shielding.

A Simpson microammeter with a full scale deflection of 25×10^{-6} amp. was connected in series with the cell and potentiometer to detect and measure any direct current in the system. Capacitance measurements were not made whenever this current exceeded 0.5 μa.

A schematic diagram of the cell used in the capacitance measurements is shown in Fig. 3. The container for the solution was formed from a 55/60 Pyrex double walled standard taper, outer. The ring seal at the bottom completed a thermostating jacket through which water from a constant temperature source could be circulated. The temperature of a solution in the cell was maintained at 25 $\pm$ 0.15°.

A 55/60 Pyrex standard taper, inner, closed the cell against the atmosphere and served as a support for the various components of the cell. A gas dispersing tube was connected to this support by a ring seal, and a Teflon-plug stopcock directed the incoming gas through this tube when closed, or, when open, forced the gas to by-pass the tube while maintaining an atmosphere of hydrogen above the solution. The platinum gauze reference electrode was also connected to the support by a firm platinum wire sealed through a glass sheath, which in turn was ring-sealed to the support.

The dropping mercury electrode was inserted through a Teflon plug, the outside of which had been machined to fit tightly the 12/30 Pyrex standard taper, outer, which was attached to the top of the cell support. The electrode was fed by a reservoir of large cylindrical cross section in order that flow of mercury through the capillary during the course of a day would not significantly change the height of mercury above the electrode tip, and hence would cause no change in the volume flow rate of the mercury. A greaseless ball joint connected this reservoir to the electrode in order to facilitate removal of the electrode from the cell when necessary.

The dropping mercury electrode was formed from the same precision bore capillary tubing used in the construction of the capillary electrometer. A central segment of this tubing about 2 in. in length was heated over a wide gas flame and, when soft, was pulled to give an extension about 2 in. in length. The diameter of the capillary, both inner and outer, decreased as a result. A head of about 40 cm. of mercury applied to the capillary was necessary to produce a flow rate of approximately 10^{-4} g./sec. A drop of mercury was formed and fell from the tip in 60 to 100 sec.

Desicote, a Beckman product which forms a hydrophobic surface layer when applied to clean air-dry glass, was drawn into the tube by capillary action and, after rising some 3 or 4 cm. up the tube, was forced out with nitrogen. After rinsing the capillary interior with acetone, Desicote was again applied in the same manner, and after rinsing again with acetone the capillary was dried by forcing nitrogen through the tubing for several hours. We found that this procedure markedly reduced the frequency dependence of the capacitance measured in solutions containing no organic solutes; this result suggests that solution creeping between mercury and capillary walls may lead to an apparent dispersion of the double layer capacitance.

The procedure for measurement involved setting a capacitance value on the variable arm of the bridge and observing the variation of the Lissajous figure depicting the state of bridge balance. If the resistance of the variable arm of the bridge is adjusted properly, the Lissajous figure passes through a horizontal straight line configuration. At this instant, the size of the droplet is such that its double layer capacitance and its resistance are just the proper values necessary to balance the bridge. If the surface area of the drop at this instant is known, then one can easily calculate the capacitance per unit area of electrode surface. By determining the volume flow rate of the mercury through the capillary, and assuming a spherical shape for the mercury droplet at the instance of balance, the age of the drop can be used as a measure of the surface area. The relationship

$$\log A = 2/3 \log (0.7843 Z t)$$

can be shown to represent the area of a spherical mercury droplet at time t and flow rate Z when the density of mercury is taken as 13.56 g./cm.^{3}. Thus, to determine the surface area, the age of the droplet t was measured with a stopwatch, and flow rate Z was measured by weighing the mercury expended from the electrode over a period of several hours. This mercury was washed well with conductivity water and acetone and then dried thoroughly prior to weighing. All times were measured with a reproducibility of 0.2 sec. in 70 sec.

A substitution technique was used to eliminate effects due to asymmetries in the bridge network and in the electrical leads and the capacitor C_k. The cell was replaced by a series combination of a decade resistance with a decade capacitance. This cell-analog combination became the adjustable arm of the bridge in the calibration procedure. The resistance and the capacitance which initially balanced the cell impedance were in turn balanced by adjusting the resistance and capacitance in the analog. By using identical shielded electrical leads for connecting both the

cell and the analog to the bridge terminals, the identity of the impedance of the analog with that of the cell was ensured.

Materials.—Goldsmith Brothers triply distilled mercury was further purified by washing with 5% nitric acid, rinsing with conductivity water, drying, and finally by vacuum distillation. The mercury was added to the electrode reservoir through a pinhole filter which removed any dust which might have collected on the surface.

The conductivity water used in making up solutions was prepared by redistilling tap distilled water through an all fused silica continuous double distillation column obtained from Englehard Industries, Inc. The first stage of this column contained enough sulfuric acid to make the concentration of the solution there approximately 1 *M* when the column was in operation. This acid reacted with any long chain amines present in the tap distilled water; with this procedure, the surface tension of the product of the double distillation as measured with a commercial Cenco-DuNoüy tensiometer was always within 0.2 dyne/cm. of the literature value.

The electrolytic solution was 0.10 *N* perchloric acid. Preelectrolysis was carried out for several hours on a number of solutions studied early in the investigation. It was thought that this would ensure the removal of any ions which might have interfered in the measurement of the double layer capacity; however, repeating these runs using solutions which had not been subjected to this treatment showed that the preelectrolysis had no measurable effect on the results obtained, indicating that any interfering ions had already been removed in preceding purification steps, and hence the pre-electrolysis was discontinued.

Carefully purified hydrogen was used to outgas the solutions and, in conjunction with the platinized platinum gauze, served as the reversible reference electrode for the capacitance measurements. The hydrogen entered the cell through a fritted glass filter stick which dispersed the gas in a stream of fine bubbles, and left the cell through a water bubbler. Provision was made for by-passing the hydrogen stream above the solution when measurements were being taken; thus the cell was continuously flushed and was under a positive pressure of hydrogen at all times.

When measurements were being made on a solution containing a volatile component, *e.g.*, *n*-amyl alcohol, phenol, etc., the hydrogen was bubbled through a solution of the same concentration as that being studied prior to its admittance to the cell. The bubbler was used in the cell for only 30–60 min. in such cases, and the gas pressure was always adjusted to such a level that only enough hydrogen to maintain a positive pressure inside the cell was admitted. To check on any possible change in concentration over the course of a run, the first point taken was always repeated at the end of the run. In every case, the readings were identical within normal experimental error.

Mallinckrodt A.R. grade phenol was fractionally frozen and distilled in a single stage glass still The corrected boiling point of the product was 181.4 ± 0.1°. A concentrated aqueous solution was prepared and standardized by bromination; all phenol solutions subsequently were made up from this solution. Eastman *n*-amyl alcohol was distilled through a 30 plate Oldershaw column at a reflux ratio of ten to one; the boiling point of the product was 137.8 ± 0.1° at STP.

Results

Electrocapillary data for solutions of *n*-amyl alcohol and phenol are shown in Fig. 4 and 5, respectively. The mercury electrode potential is expressed in volts relative to the electrocapillary maximum for the base solution, 0.1 *M* $HClO_4$. For each concentration, experimental points were obtained at 25-mv. intervals over the polarization range.

Figure 6 shows typical dependence of capacitance on frequency at the mercury–base solution + *n*-amyl alcohol interface. Frequency dependence of capacitance in the neighborhood of the desorption peaks is pronounced, as is to be expected.[6-8] Generally, some dispersion of capacitance occurred even at polarizations substantially removed from desorption peaks. The capacitance of the mercury–base solution system varied about 8% near the capacitance "hump," less than 4% elsewhere as the frequency varied from 100 to 10,000

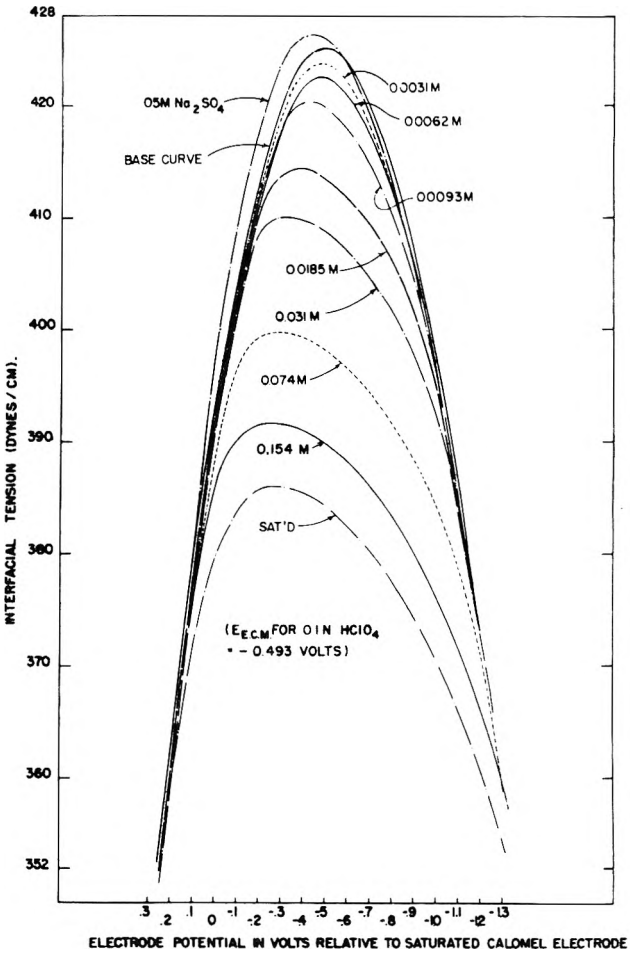

Fig. 4.—Electrocapillary curves: interface mercury–0.1 *N* $HClO_4$ + indicated *n*-amyl alcohol concentration and interface mercury–0.05 *M* Na_2SO_4 (standardization).

c.p.s. It is suspected that variations in capacitance with frequency observed in the base solution system and in systems with adsorbable solutes at polarizations well removed from the desorption peaks result from imperfect electrode design, although a theory attributing them to interfacial properties has been advanced.[13,14]

Figure 7 shows the dependence of static differential capacitance on phenol concentration and polarizing potential at the mercury–base solution + phenol interface. The static differential capacitance was obtained at each polarization and concentration by plotting capacitances measured at frequencies of 100, 500, 4910, and 9050 c.p.s. against square root of frequency and extrapolating to zero frequency. For each concentration, static capacitances thus were obtained at 50-mv. intervals over the range of polarizations. Electrocapillary maxima, as obtained from the previously obtained electrocapillary curves, are shown on each curve. The charge density at a given concentration and polarization can be obtained by integrating the capacitance curve for that concentration from the electrocapillary maximum potential to the polarization of interest; Fig. 8 shows the dependence of charge density on polarization and phenol concentration obtained by integrating static capacitance curves in this manner. The interfacial tension at a given concentration and polarization can be obtained by integrating the charge

(13) J. O'M. Bockris, W. Mehl, B. E. Conway, and L. Young, *J. Chem. Phys.*, **25**, 776 (1956).

(14) J. O'M. Bockris and B. E. Conway, *ibid.*, **28**, 707 (1958)

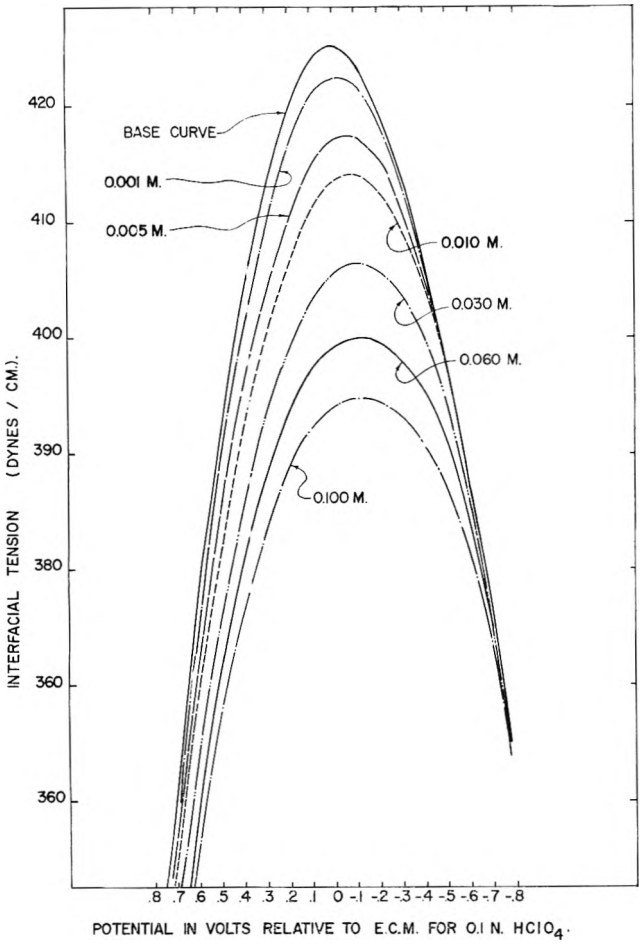

Fig. 5.—Electrocapillary curves: interface mercury–0.1 N $HClO_4$ + indicated phenol concentration.

density curve for that concentration from the electrocapillary maximum potential to the polarization potential and subtracting the result from the interfacial tension for that concentration at the electrocapillary maximum; electrocapillary curves thus obtained agreed with those determined directly within experimental error.

Figures 9 and 10 show isotherms for the adsorption of n-amyl alcohol and phenol at their respective mercury–base solution interfaces at various polarizations. These were obtained graphically by a method based on the equation

$$\Gamma = \frac{1}{RT}\left(\frac{\partial \pi}{\partial \ln c}\right)_V \qquad (29)$$

Because the dependence of π on c (molar concentration of adsorbate) at fixed V was rather closely approximated by a Volmer type isotherm over a large part of the concentration range, it was convenient to represent the dependence of π on c by a Volmer term plus a correction term, obtaining Γ by analytical differentiation of the Volmer term and graphical differentiation of the correction term. Thus

$$\ln \frac{c}{\pi} = \alpha + \beta\pi + \Delta \ln \frac{c}{\pi} \quad (V \text{ fixed}) \qquad (30)$$

implies

$$\frac{1}{\Gamma} = \frac{RT}{\pi} + \beta RT + RT\left[\frac{\partial\left(\Delta \ln \frac{c}{\pi}\right)}{\partial \pi}\right]_V \qquad (31)$$

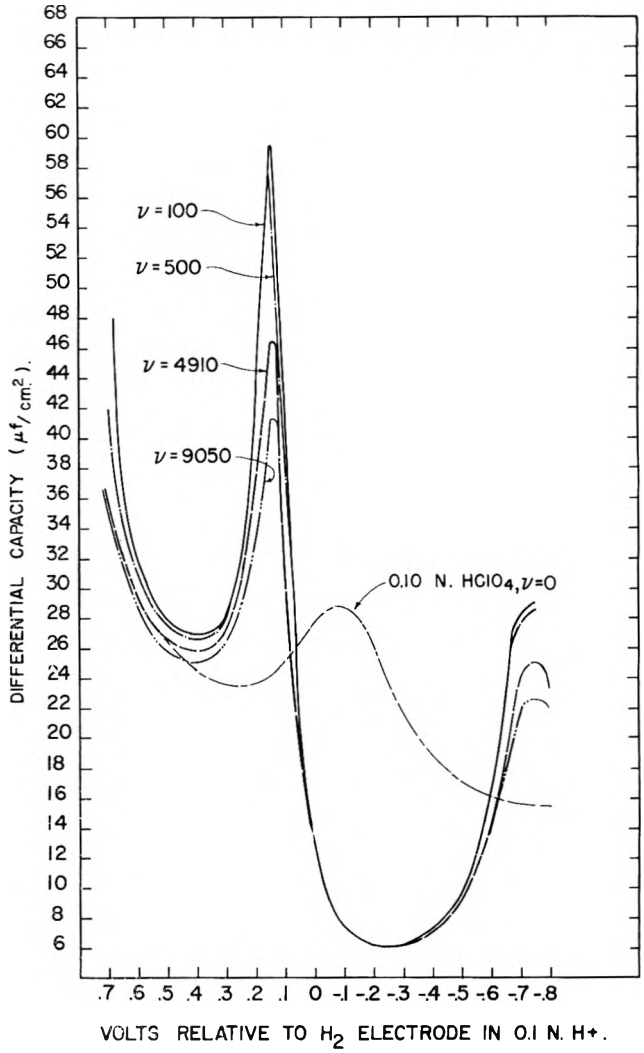

Fig. 6.—Frequency dependence of differential capacitance at the interface mercury–0.1 N $HClO_4$ + 0.031 M n-amyl alcohol.

This method is, of course, exact in principle; in practice constants α and β could be chosen so that the correction term was very small except at very small spreading pressures, and evaluation of Γ was convenient and highly objective except at very small spreading pressures. Most of the data in Fig. 9 and 10 were obtained in this way. An alternate method based on the Langmuir isotherm is outlined by eq. 32 and 33

$$\pi = \Gamma_m RT \ln (1 + bc) + \Delta\pi \quad (V \text{ constant}) \qquad (32)$$

$$\Gamma = \frac{\Gamma_m bc}{1 + bc} + \frac{1}{RT}\left(\frac{\partial\, \Delta\pi}{\partial \ln c}\right)_V \qquad (33)$$

For suitable choices of the parameters Γ_m and b, the Langmuir term, $\Gamma_m RT \ln (1 + bc)$ represented π well for small c, but deviated significantly at moderate c and markedly at large c, so that this method was less satisfactory than that outlined by eq. 30 and 31 over most of the concentration range. The method 2 curve for $V = 0.175$ in Fig. 10 was obtained by application of eq. 32 and 33.

Figure 11 shows the dependence of $(S\psi/RT)$ on π and V at the mercury–base solution + n-amyl alcohol interface. Evidently $(S\psi/RT)$ is substantially independent of π (and so also of Γ) at this interface. Similar plots showed that $(S\psi/RT)$ varied systematically with π at fixed V at the mercury–base solution +

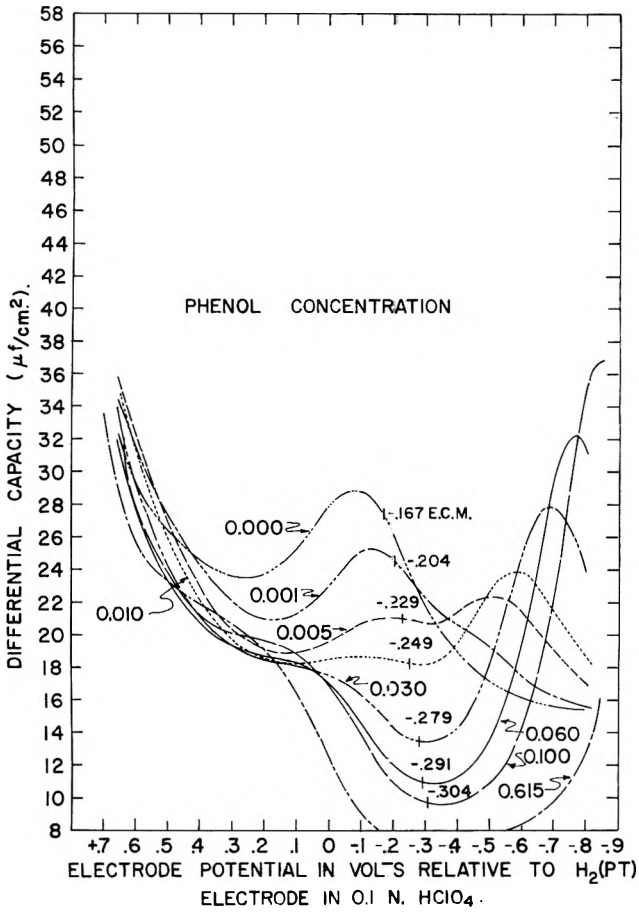

Fig. 7.—Dependence of zero frequency differential capacitance on polarization, interface mercury–0.1 N $HClO_4$ + indicated phenol concentration. Electrocapillary maximum potential for each concentration is indicated.

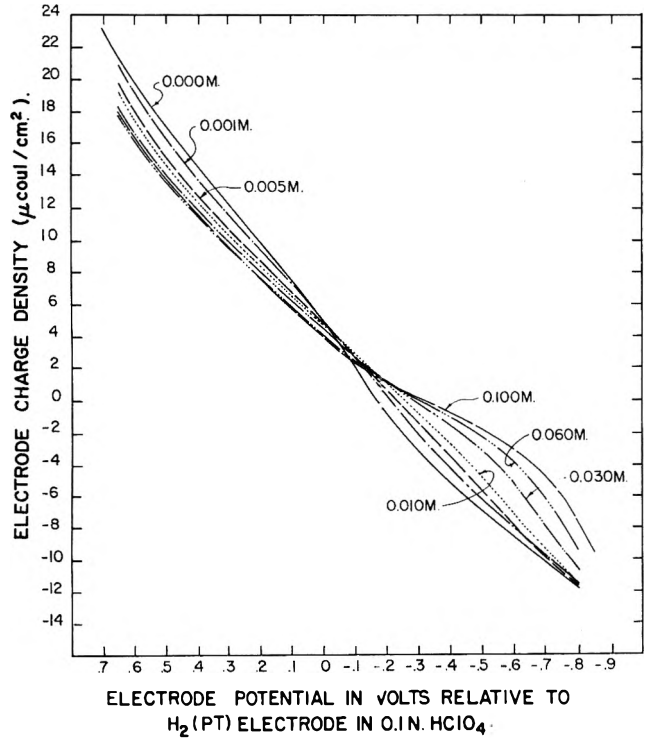

Fig. 8.—Dependence of interfacial charge density on polarization, interface mercury–0.1 N $HClO_4$ + indicated phenol concentration.

phenol interface; for interpretation of this behavior in terms of a model the dependence of $(S\psi/RT)$ on Γ and V therefore was investigated. Within experimental

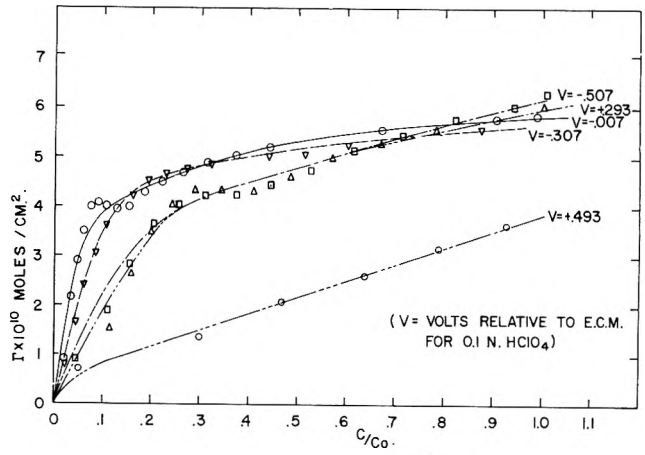

Fig. 9.—Isotherms for the adsorption of n-amyl alcohol at the mercury–0.1 N $HClO_4$ interface at various polarizations. (C_0 is saturation concentration of n-amyl alcohol in 0.1 N $HClO_4$, taken as 0.222 M.)

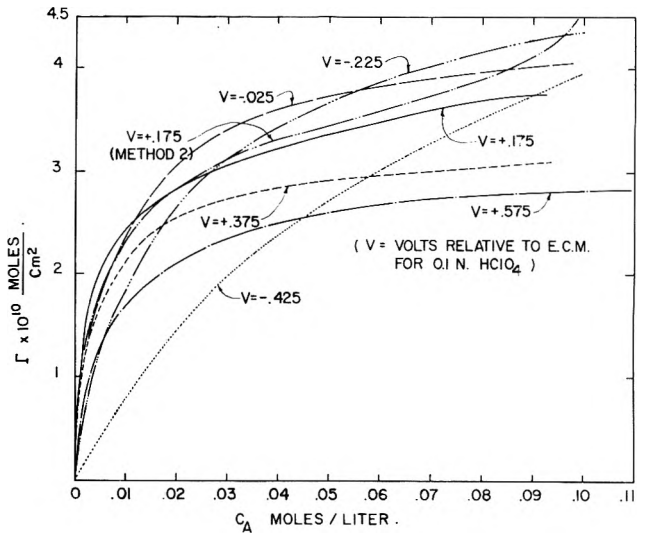

Fig. 10.—Isotherms for the adsorption of phenol at the mercury–0.1 N $HClO_4$ interface at various polarizations.

error this dependence was represented by

$$(S\psi/RT) = F_1(V) + \Gamma^2 F_2(V) \qquad (34)$$

This result is shown graphically in Fig. 12. To good approximation, $F_1(V) = 6.57\ V^2 - 3.02\ V$, $F_2(V) = 1.28 \times 10^{19} V$ for the phenol system, V being expressed in volts relative to the base solution electrocapillary maximum.

Discussion

Dependence of spreading pressure on concentration and polarization at the interface mercury–0.1 N $HClO_4$ + n-amyl alcohol found in this work agrees generally with that obtained by Breiter and Delahay[6]; these workers used a 1 M $NaClO_4$ + 0.001 M $HClO_4$ base solution so their results are not quantitatively comparable to ours. Derived adsorption isotherms also are generally in accord with those inferred from capacitance results in our earlier work,[3] and this result also confirms findings of Breiter and Delahay.

Isotherms for the adsorption of phenol at the mercury–0.1 N $HClO_4$ interface shown in Fig. 10 agree generally with those found by Blomgren, Bockris, and Jesch[15] using a 0.1 N HCl base solution. Although

(15) E. Blomgren, J. O'M. Bockris, and C. Jesch, *J. Phys. Chem.*, **65**, 2000 (1961).

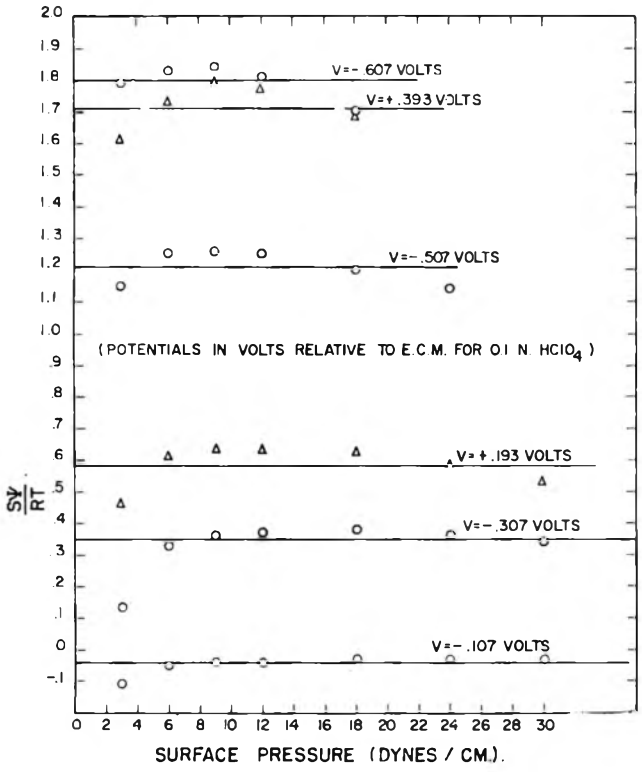

Fig. 11.—Dependence of $S\psi/RT$ (see eq. 14–17 of text) on polarization and spreading pressure, interface mercury–0.1 N $HClO_4$ + n-amyl alcohol.

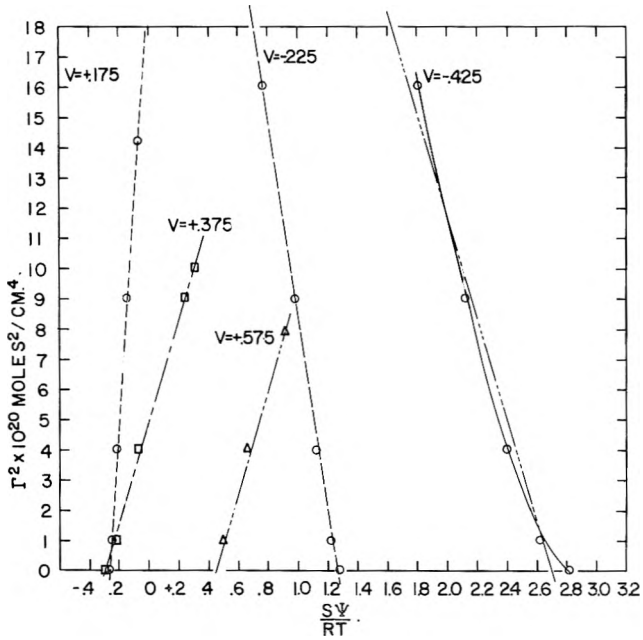

Fig. 12.—Dependence of $S\psi/RT$ (see eq. 14–17 of text) on polarization and surface excess, interface mercury–0.1 N $HClO_4$ + phenol.

capacitance results obtained in our earlier work are in general agreement with those found here at comparable concentrations, adsorption isotherms shown in Fig. 10 accord very poorly with those which would be calculated from a Frumkin isotherm using parameters previously reported. This stems basically from the fact, apparent from Fig. 10, that the phenol data cannot be represented by a Frumkin isotherm, and our earlier work, limited to three concentrations ranging from 0.1 to 0.2 M in phenol, was insufficiently extensive to make this fact obvious. By choosing parameters in the Frumkin equation to represent data at these three concentrations, an isotherm equation was obtained which grossly underestimates the adsorption at substantially lower concentrations.

Figure 11, which demonstrates that the quantity $(S\psi/RT)$ is independent of surface excess when the adsorbate is n-amyl alcohol, therefore also shows that the surface charge is linear in Γ at fixed V for all V and Γ investigated. This result justifies the basic assumption in our earlier work[3] for this system. Figure 12 shows, however, that when the adsorbate is phenol the quantity $(S\psi/RT)$ varies linearly with Γ^2 at fixed V, and that the surface charge is therefore not linear in Γ at fixed V in this system. From eq. 34, 13, and 16 we find

$$Q_w - Q = RT\Gamma[F_1'(V) + \Gamma^2 F_2'(V)] - 2\Gamma^3 RTF_2(V)\frac{\partial^2\left(\frac{S\psi}{RT}\right)}{\partial\pi\,\partial V} \quad (35)$$

in which $F_1' = dF_1/dV$, $F_2' = dF_2/dV$. The last term on the right proved to be negligible at all concentrations and polarizations studied. Hence to good approximation

$$Q_w - Q = RT\Gamma(F_1'(V) + \Gamma^2 F_2'(V)] \quad (36)$$

and

$$C_w - C = \Gamma RT\,[F_1''(V) + \Gamma^2 F_2''(V)] + RT[F_1'(V) + 3\Gamma^2 F_2'(V)]\left(\frac{\partial\Gamma}{\partial V}\right)_a \quad (37)$$

From eq. 36, if Γ is small in first order, Q will be linear in Γ to terms of second order in Γ, but this linearity does not extend to large values of Γ. Our earlier treatment therefore is not justified for the phenol system at all polarizations and surface excesses. Near the electrocapillary maximum the second term in eq. 37 becomes negligible, and since $F_2(V)$ was found experimentally to be linear in V, $F_2''(V) = 0$, so the capacitance must be linear in Γ for all Γ near the electrocapillary maximum for both the n-amyl alcohol and phenol-containing systems.

Linear dependence of Q on Γ at fixed V was first assumed by Frumkin[4] in the form

$$Q = (1 - \theta)C_w V + \theta C'(V - V_N) \quad (38)$$

(quantities as defined following eq. 4). Capacitances were assumed independent of polarizations; this assumption is unnecessary but is consistent with the degree of approximation in the discussion to follow. Frumkin's assumption is most easily pictured as supposing the double layer to consist of a water-filled condenser and an organic-filled condenser connected in parallel. This implies that a zero net charge at intermediate values of θ corresponds to nonzero charges, equal but opposite in sign, on the organic-filled and water-filled condensers,[16] and this implication is not entirely attractive physically. Instead of eq. 38 we might also suppose

$$Q = [(1 - \theta)C_w + \theta C'][V - \theta V_N] \quad (39)$$

(16) This point was called to the attention of R. S. H. by J. Th. G. Overbeek in a discussion in September, 1959.

i.e., that both capacitance and electrocapillary maximum potential varied linearly with coverage. Equation 39 implies a quadratic dependence of Q on θ, and therefore does not agree with results obtained with either *n*-amyl alcohol or phenol adsorbates. We shall therefore retain Frumkin's model, rewrite eq. 38 in the form

$$\frac{C_w V - Q}{\theta} = (C_w - C')V + C'V_N \qquad (40)$$

and compare this with the result obtained for phenol, eq. 36, using the experimental values $F_1'(V) = 13.14V - 3.02, F_2'(V) = 1.28 \times 10^{19}$. We have

$$\frac{Q_w - Q}{\Gamma} = RT(13.14V - 3.02 + 1.28 \times 10^{19}\Gamma^2) \qquad (41)$$

Comparison of eq. 40 and 41 suggests that the term in Q not linear in Γ in the phenol system is associated with a variation in V_N with coverage, probably due to a change in orientation of the phenol molecules as coverage increases. A model leading to a dependence of V_N on Γ of approximately the form suggested by comparison of eq. 40 and 41 is one in which adsorbed molecules are distributed at random on fixed sites, and each molecule has one orientation if it has zero or one neighbor, a different orientation if it has two or more neighbors. This could be considered a "quasi-lattice" representation for a monolayer without fixed adsorption sites, which is physically more likely in the cases here studied. The adsorption isotherms for phenol shown in Fig. 10 show some evidence of reaching limiting surface excesses at high concentrations, but these limits are certainly not well defined over the range of concentrations studied, and vary markedly from polarization to polarization. This may again reflect a change in orientation with increasing coverage.

It is of course possible to obtain adsorption isotherms from capacitance data by doubly integrating capacitance–polarization curves to obtain electrocapillary curves and differentiating the function $\gamma(a, V)$ thus obtained after $RT \ln a$. As mentioned in the Results section, electrocapillary curves obtained by double integration of our capacitance–polarization curves agreed within experimental error with those obtained directly, *provided* static capacitance (obtained by extrapolating observed capacitance data to zero frequency) was used. This result was also noted for the adsorbate *n*-amyl alcohol by Breiter and Delahay.[6] Two constants of integration result from double integration of the capacitance curves. It is attractive to base evaluation of surface excess on eq. 12 and to fix these two constants by setting $\pi = 0$, $Q = Q_w$ at some potential well beyond one of the desorption peaks (*i.e.*, at a polarization such that desorption can be supposed complete with negligible error). *This procedure guarantees that isotherms calculated between desorption peaks (the only polarization region where appreciable adsorption occurs) have been based on two integrations over a desorption peak, and the area under this peak is known to be highly frequency dependent in many cases.* Unless zero-frequency capacitance values are used in these integrations, isotherms derived from them not only have no special "thermodynamic" justification, but are also likely to be seriously in error. A recently published treatment of the adsorption of thiourea at the mercury–electrolyte interface by Schapink, *et al.*,[17] and further treatment of these data by Parsons[18] and Devanathan[19] are open to criticism in this respect. Two criteria can be suggested for testing whether or not capacitance data obtained at other than zero frequency can be safely substituted for zero frequency capacitances in thermodynamic treatments. In the first place, if desorption peaks on both sides of the electrocapillary maximum have been documented, the integral

$$I = \int_{-\infty}^{\infty} (C_w - C)\,dV \qquad (42)$$

(the infinite limits, of course, cannot be realized in practice, but the integral should cover the range of polarizations over which C_w and C differ appreciably) should be zero. If $I \neq 0$, some error must surely be introduced into quantities derived from treating such capacitances as thermodynamic. Let V', V'' be the points of intersection of the curves $C(V)$, $C_w(V)$, and let $I' = \int_{V'}^{V''} (C_w - C)\,dV$ (*i.e.*, I' is the area between C_w and C between desorption peaks); the error referred to is probably of the order I/I'. In the second place, diffusion places a lower bound on the time required for re-equilibration of adsorption following polarization change. The fractional error in capacitance $\Delta C/C$ due to diffusional time lag in nonzero frequency capacitance measurements can be shown from the theory of Frumkin and Melik-Gaikazyan[7] to be $(\partial\Gamma/\partial C)_V\sqrt{2\pi\nu/D}$ to first order for low frequencies, in which D is the diffusion coefficient, ν the frequency in c.p.s. Where $c_{1/2}$ (moles/liter) is the concentration required for adsorption of half a monolayer at the desorption peak potential and Γ_m (moles/cm.^{2}) the full monolayer surface excess, we may suppose $(\partial\Gamma/\partial C)_V \sim {}^1/_4 \times 10^3\Gamma_m/c_{1/2}$. Taking $\Gamma_m \sim 5 \times 10^{-10}$ mole/cm.^{2}, $D \sim 10^{-5}$ cm.^{2}/mole, we find $(\Delta C/C) \sim 1 \times 10^{-4}\nu^{1/2}/c_{1/2}$. For $\gamma = 1000$ c.p.s., $(\Delta C/C)$ would hence exceed 10% if $c_{1/2} < 0.03\ M$, if only diffusion limited re-equilibration, and the error would be more serious if other rate processes were limiting.

We turn finally to the method of inference of adsorption parameters used by Hansen, Minturn, and Hickson[3] and its justification in terms of the present work. The parameters B_0 and α of eq. 1 and C' of eq. 4 were obtained from the dependence of capacitance on concentration at the electrocapillary maximum potential of the base solution assuming (a) linear dependence of capacitance on coverage at the electrocapillary maximum and (b) possibility of adequately representing adsorption by the Frumkin eq. 1. Assumption (a) has been shown to be well justified for the adsorbates *n*-amyl alcohol and phenol in the present work. Validity of assumption (b) can hence be tested in these cases (and presumably more generally) from capacitance measurements alone; with an additional adjustable parameter the Frumkin isotherm is more versatile than the Langmuir isotherm, but as previously mentioned it is inadequate for representation of adsorption

(17) F. W. Schapink, M. Oudeman, K. W. Leu, and J. N. Helle, *Trans. Faraday Soc.*, **56**, 415 (1960).

(18) R. Parsons, *Proc. Roy. Soc.* (London), **A261**, 79 (1961).

(19) M. A. V. Devanathan, *ibid.*, **A264**, 133 (1961).

of phenol at the mercury–base solution interface. The parameter V_N of eq. 3 then was established to best represent the capacitance data near the polarization of maximum adsorption for given solute activity. From eq. 5 we obtain

$$\left(\frac{\partial\Gamma}{\partial V}\right)_a = \frac{1}{RT}\left(\frac{\partial Q}{\partial \ln a}\right)_V = \frac{1}{RT}\left(\frac{\partial Q}{\partial \Gamma}\right)_V\left(\frac{\partial \Gamma}{\partial \ln a}\right)_V \tag{43}$$

i.e., $(\partial\Gamma/\partial V)_a = 0$ when $(\partial Q/\partial\Gamma)_V = 0$. If Q is linear in Γ the potential at which $(\partial\Gamma/\partial V)_a = 0$ should be independent of Γ (and so of a), and if Frumkin's assumption as indicated by eq. 38 were valid, the potential of maximum adsorption should be $V_{max} = -C'V_N/C_w - C'$ (independent of a). In our earlier work it was noted that such constancy of V_{max} was not always observed; in the present work Q was found to be linear in Γ for *n*-amyl alcohol but not strictly so for phenol. Finally, the parameter S was established by (essentially) fitting the curvature of plots of θ_{app} against polarization in the neighborhood of the plot maxima. From eq. 43 we have

$$\frac{\partial^2\Gamma}{\partial V^2} = \frac{1}{RT}\frac{\partial^2 Q}{\partial V\,\partial \ln a} = \frac{1}{RT}\left(\frac{\partial C}{\partial \ln a}\right)_V \tag{44}$$

and so

$$\frac{\partial^2\theta}{\partial V^2} = \frac{S}{RT}\left(\frac{\partial C}{\partial \ln a}\right)_V \tag{45}$$

Equation 45 implies a relation between curvature of a plot of θ_{app} against V and molar area at full coverage, but does not furnish a basis for calculation of molar area from capacitance data alone. This is because $\partial^2\theta_{app}/\partial V^2$ differs strongly from $\partial^2\theta/\partial V^2$ even near the electrocapillary maximum where to good approximation $\theta = \theta_{app}$. It therefore appears impractical to avoid a model in calculation of molar area if double integration of capacitance curves is to be avoided. Choice of molar area to provide representation of curvature of plots of θ_{app} against V near their maxima must be considered to give only an approximation to this parameter if dependence of Q on Γ is not known to be linear, and results obtained with phenol in the present work show that such linearity cannot be assumed safely.

SECONDARY REACTIONS IN CONTROLLED POTENTIAL COULOMETRY. III. PRECEDING AND SIMULTANEOUS CHEMICAL REACTIONS

BY ALLEN J. BARD AND EMANUEL SOLON

Department of Chemistry, The University of Texas, Austin 12, Texas

Received April 24, 1963

Controlled potential coulometric experiments, in which the electroactive species, C, is consumed before and during the electrolysis by a first- or second-order chemical reaction, or in which C is produced by a reversible chemical reaction preceding the electrode reaction, are considered. A mathematical treatment of the effect of these upon n_{app}, the apparent number of faradays per mole of electroactive material, and upon current–time behavior, is given. The use of controlled potential coulometric data for the estimation of the rate constants of the chemical reactions is described and several examples are given.

Introduction

Secondary chemical reactions during controlled potential coulometric electrolyses generally lead to variations in n_{app}, the apparent number of faradays per mole of electroactive substance consumed, and variations in the current–time behavior. Previous communications treated cases involving reactions of the product of the primary electrode reaction leading to consumption or regeneration of the electroactive species[1] or leading to secondary electrode reactions.[2] This paper discusses cases in which the electroactive species is consumed before and during the electrode reaction in a chemical reaction, and in which the electroactive species is produced by a reversible chemical reaction. The use of controlled potential coulometric data for the determination of the number of electrons involved in the electrode reactions and for the estimation of the rate constants of chemical reactions is described.

Classification.—The primary electrode reaction is represented as

$$C \pm ne^- \longrightarrow R$$

where C is the electroactive material and R is the product of the electrode reaction. In the reactions below R, X, Y, and Z represent electrolytically inert materials at the applied potential.

Case I. C Undergoes a Pseudo First-Order Chemical Reaction.—

$$C\ (+\ Z) \longrightarrow X$$

Case II. C Undergoes a Second-Order Chemical Reaction.—

$$\text{(a)}\quad C + Z \longrightarrow X$$

$$\text{(b)}\quad 2C \longrightarrow X$$

Case III. C is Produced by a Preceding, Reversible First-Order Reaction.—

$$Y \rightleftharpoons C$$

Variations of these cases can be treated by suitable modification of the procedure outlined below.

Mathematical Treatment

General Considerations.—The assumptions and conditions of this treatment are the same as those previously described.[1,2] The current, i, taken as a positive quantity, is related to the rate of consumption of C by

$$i = -nFV[\mathrm{d}(C)/\mathrm{d}t]_{\text{elec. rxn.}} \tag{1}$$

(1) D. H. Geske and A. J. Bard, *J. Phys. Chem.*, **63**, 1057 (1959).
(2) A. J. Bard and J. S. Mayell, *ibid.*, **66**, 2173 (1962).

where F is the faraday, V is the total volume of solution, and (C) is the concentration of species C. The rate of concentration change under limiting current conditions (it is assumed that the applied potential is such that the electrode reaction occurs without activation polarization) is

$$[\mathrm{d}(C)/\mathrm{d}t]_{\text{elec. rxn.}} = -p(C) \qquad (2)$$

where p is a constant, dependent upon prevailing mass transfer conditions, electrode area, solution volume, and cell geometry.[1] Combination of (1) and (2) yields

$$i = nFVp(C) \qquad (3)$$

The apparent number of faradays per mole of electroactive material, n_{app}, is determined experimentally and is defined as

$$n_{app} = \frac{\int_0^t i\,\mathrm{d}t}{FV[(C_i) - (C)]} \qquad (4)$$

where (C_i) is the initial concentration of C. At the completion of electrolysis

$$n^0_{app} = \frac{\int_0^\infty i\,\mathrm{d}t}{FV(C_i)} \qquad (5)$$

where the symbol n^0_{app} refers to evaluation of n_{app} at the completion of the electrolysis, where (C) approaches zero. Similar superscript notation is used below for (Z). Note that for case III, since all of substance Y is eventually electrolyzed, the denominators of (4) and (5) contain the additional terms $+FV[(Y_i) - (Y)]$ and $+FV(Y_i)$, respectively.

Case I.—The electroactive species C is consumed before and during electrolysis by a first- or pseudo-first-order reaction

$$\mathrm{C}(+\mathrm{Z}) \xrightarrow{k} \mathrm{X} \qquad (6)$$

where Z is present in large excess, and $k' = k(Z)$. C and Z are mixed at time $t = 0$, and the electrolysis is started at $t = t_1$. The system is described by the equations

$$\mathrm{d}(C)/\mathrm{d}t = -k'(C) \quad 0 < t < t_1 \qquad (7)$$

$$\mathrm{d}(C)/\mathrm{d}t = -p(C) - k'(C) \quad t > t_1 \qquad (8)$$

At t_1, from (7) and the initial condition $(C) = (C_i)$ at $t = 0$

$$(C)_{t_1} = (C_i)\exp(-k't) \qquad (9)$$

where $(C)_{t_1}$ is the concentration of C at t_1. Solving (8), using (9) as a boundary condition

$$(C) = (C_i)\exp[-k't - p(t - t_1)] \qquad (10)$$

Combination of (3), (5), and (10) yields

$$n^0_{app} = npe^{pt_1}\int_{t_1}^\infty e^{-(p+k')t}\,\mathrm{d}t \qquad (11)$$

and

$$n^0_{app}/n = \exp(-k't_1)/(1 + \gamma') \qquad (12)$$

where $\gamma' = k'/p$. Plotting $\log(n^0_{app}/n)$ *vs.* t_1, as shown in Fig. 1, allows the determination of k' and p from the slope and intercept of the line, respectively.

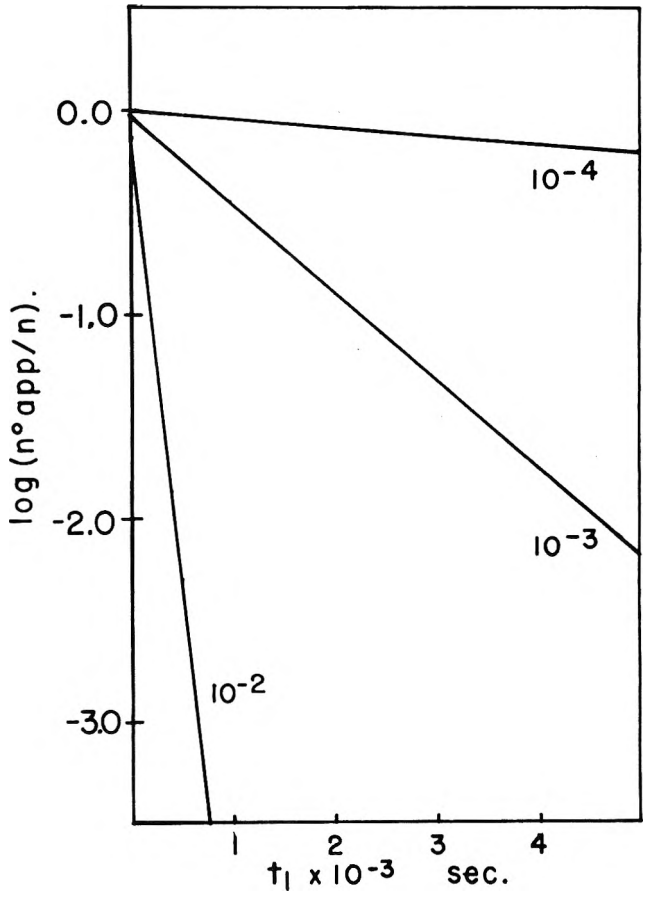

Fig. 1.—Case I: Variation of $\log n^0_{app}/n$ with t_1 for different values of k' shown on curves, calculated for $p = 0.03$ sec.$^{-1}$.

Case II.—The electroactive species C is consumed before and during the electrolysis by a second-order reaction.

(a) $$\mathrm{C} + \mathrm{Z} \xrightarrow{k} \mathrm{X}$$

C and Z are mixed at $t = 0$, and the electrolysis is started at $t = t_1$. The system is described by the equations

$$\mathrm{d}(C)/\mathrm{d}t = -k(C)(Z) \quad 0 < t < t_1 \qquad (13)$$

$$\mathrm{d}(C)/\mathrm{d}t = -p(C) - k(C)(Z) \quad t > t_1 \qquad (14)$$

$$\mathrm{d}(Z)/\mathrm{d}t = -k(C)(Z) \quad t > 0 \qquad (15)$$

At t_1, from (13), (15), and the initial conditions $(C) = (C_i)$ and $(Z) = (Z_i)$ at $t = 0$,[3]

$$(C)_{t_1} = \frac{(C_i)[(Z_i) - (C_i)]}{(Z_i)e^{[(Z_i)-(C_i)]kt_1} - (C_i)} \qquad (16)$$

$$(Z)_{t_1} = \frac{(Z_i)[(C_i) - (Z_i)]}{(C_i)e^{[(C_i)-(Z_i)]kt_1} - (Z_i)} \qquad (17)$$

Dividing (14) by (15) yields

$$\mathrm{d}(C)/\mathrm{d}(Z) = 1 + 1/[\gamma(Z)] \qquad (18)$$

where $\gamma = k/p$. Solution of (18) for (C), using the boundary condition $(C) = (C)_{t_1}$ and $(Z) = (Z)_{t_1}$ at $t = t_1$, yields, for $t > t_1$

$$(C) = (C)_{t_1} + (Z) - (Z)_{t_1} + \gamma^{-1}\ln[(Z)/(Z)_{t_1}] \qquad (19)$$

(3) See *e.g.* equivalent forms in A. A. Frost and R. G. Pearson, "Kinetics and Mechanism," John Wiley & Sons, Inc., New York, N. Y., 1953, Chapter 2

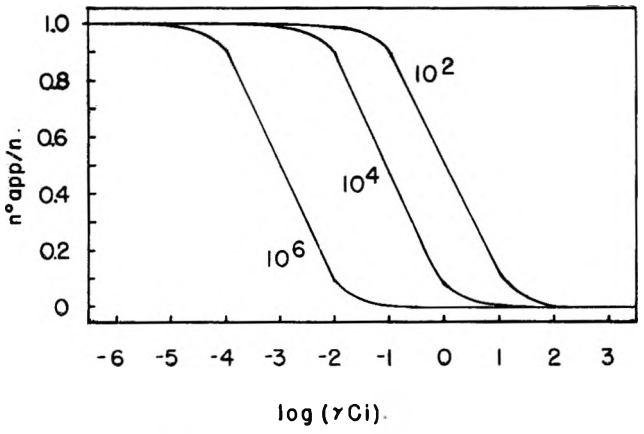

Fig. 2.—Case II(a): Variation of n^0_{app}/n with $\gamma(C_i)$ for different values of t_1 shown on curves, calculated for $(Z_i)/(C_i) = 1.0$.

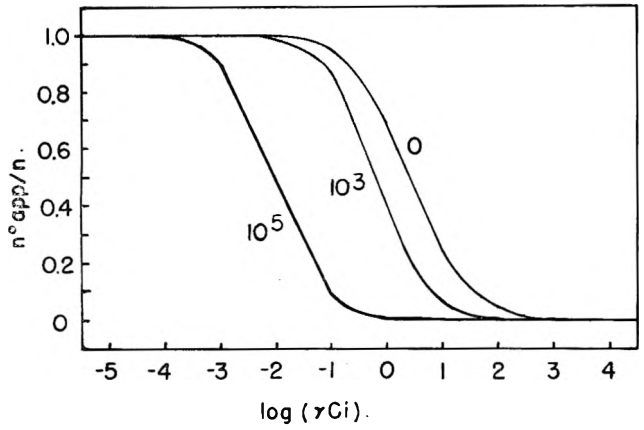

Fig. 3.—Case II(b): Variation of n^0_{app}/n with $\gamma(C_i)$ for different values of t_1 shown on curves.

From (3) and (15)

$$\int_{t_1}^{\infty} i\,dt = nFpV \int_{t_1}^{\infty} (C)dt = \frac{nFV}{\gamma} \int_{(Z)^0}^{(Z)t_1} d(Z)/(Z) \quad (20)$$

Combining (5) and (20) yields

$$n^0_{app}/n = [\gamma(C_i)]^{-1} \ln [(Z)_{t_1}/(Z)^0] \quad (21)$$

An implicit relation for $(Z)^0$ is obtained from (19)

$$(Z)^0 = (Z)_{t_1} - (C)_{t_1} + \gamma^{-1} \ln [(Z)_{t_1}/(Z)^0] \quad (22)$$

An explicit relation for γ is obtained by combining (21) and (22)

$$\gamma = \frac{n}{n^0_{app}(C_i)} \ln \left[\frac{(Z)_{t_1}}{(Z)_{t_1} - (C)_{t_1} + n^0_{app}(C_i)/n} \right] \quad (23)$$

n^0_{app}/n can be evaluated by appropriate combination of (16), (17), and (23).

For the special case $(C_i) = (Z_i)$

$$(C)_{t_1} = (Z)_{t_1} = (C_i)/[1 + (C_i)kt_1] \quad (24)$$

and from (23) and (24)

$$\gamma = \frac{n}{n^0_{app}(C_i)} \ln \left[\frac{n/n^0_{app}}{1 + (C_i)kt_1} \right] \quad (25)$$

Variation of n^0_{app}/n with (C_i), (Z_i), γ, and t_1 is shown in Fig. 2 and Table I.

TABLE I

VARIATION OF n^0_{app}/n WITH $(Z_i)/(C_i)$, t_1, AND $\gamma(C_i)$

[n^0_{app}/n depends only upon the product $\gamma(C_i)$ at a given t_1]

t_1 (sec.)	n^0_{app}/n for $\gamma(C_i)$ of 0.01	0.10	1.00	10.0
	$(Z_i)/(C_i) = 1.0$			
0	0.990	0.913	0.567	0.175
10	.990	.912	.564	.169
10^2	.989	.904	.533	.133
10^3	.980	.836	.352	.053
10^4	.901	.477	.084	.009
10^5	.498	.090	.010	.000
	$(Z_i)/(C_i) = 5.0$			
0	0.953	0.674	0.179	0.021
10	.952	.671	.171	.014
10^2	.948	.643	.115	.000
10^3	.907	.426	.003	.000
10^4	.592	.010	.000	.000
10^5	.014	.000	.000	.000
	$(Z_i)/(C_i) = 17.0$			
0	0.855	0.375	0.057	0.006
10	.854	.369	.048	.001
10^2	.841	.318	.011	.000
10^3	.723	.074	.000	.000
10^4	.166	.000	.000	.000

(b) $$2C \xrightarrow{k} X \quad (26)$$

The solution is prepared at $t = 0$, and electrolysis is started at t_1. The system is described by the equations

$$d(C)/dt = -k(C)^2 \qquad 0 < t < t_1 \quad (27)$$

$$d(C)/dt = -k(C)^2 - p(C) \qquad t > t_1 \quad (28)$$

Up to t_1, $(C)_{t_1}$ is given by (24). An equation for (C) is obtained from (28) and (24)

$$(C) = (C_i)/\{[\gamma(C_i) + 1 + (C_i)kt_1]\, e^{p(t-t_1)} - \gamma(C_i)\} \quad (29)$$

n^0_{app}/n is evaluated from (3), (5), and (29)

$$\frac{n^0_{app}}{n} = \frac{p}{(C_i)} \int_{(C)_{t_1}}^{0} (C)dt = \frac{p}{(C_i)} \int_0^{(C)_{t_1}} \frac{d(C)}{k(C) + p} \quad (30)$$

and, using (24)

$$\frac{n^0_{app}}{n} = \frac{1}{\gamma(C_i)} \ln \left[1 + \frac{\gamma(C_i)}{1 + (C_i)kt_1} \right] \quad (31)$$

Variation of n^0_{app}/n with $\gamma(C_i)$ and t_1 is shown in Fig. 3.

Case III.—The electroactive species C is formed by a reversible reaction

$$Y \underset{k_b}{\overset{k_f}{\rightleftharpoons}} C \quad (32)$$

The system is described by the equations

$$d(C)/dt = -p(C) + k_f(Y) - k_b(C) \quad (33)$$

$$d(Y)/dt = -k_f(Y) + k_b(C) \quad (34)$$

Equations 33 and 34 are solved conveniently by using the LaPlace transform method, with the initial condition $(C) = (C_i)$ and $(Y) = (Y_i)$ at $t = 0$. The results are

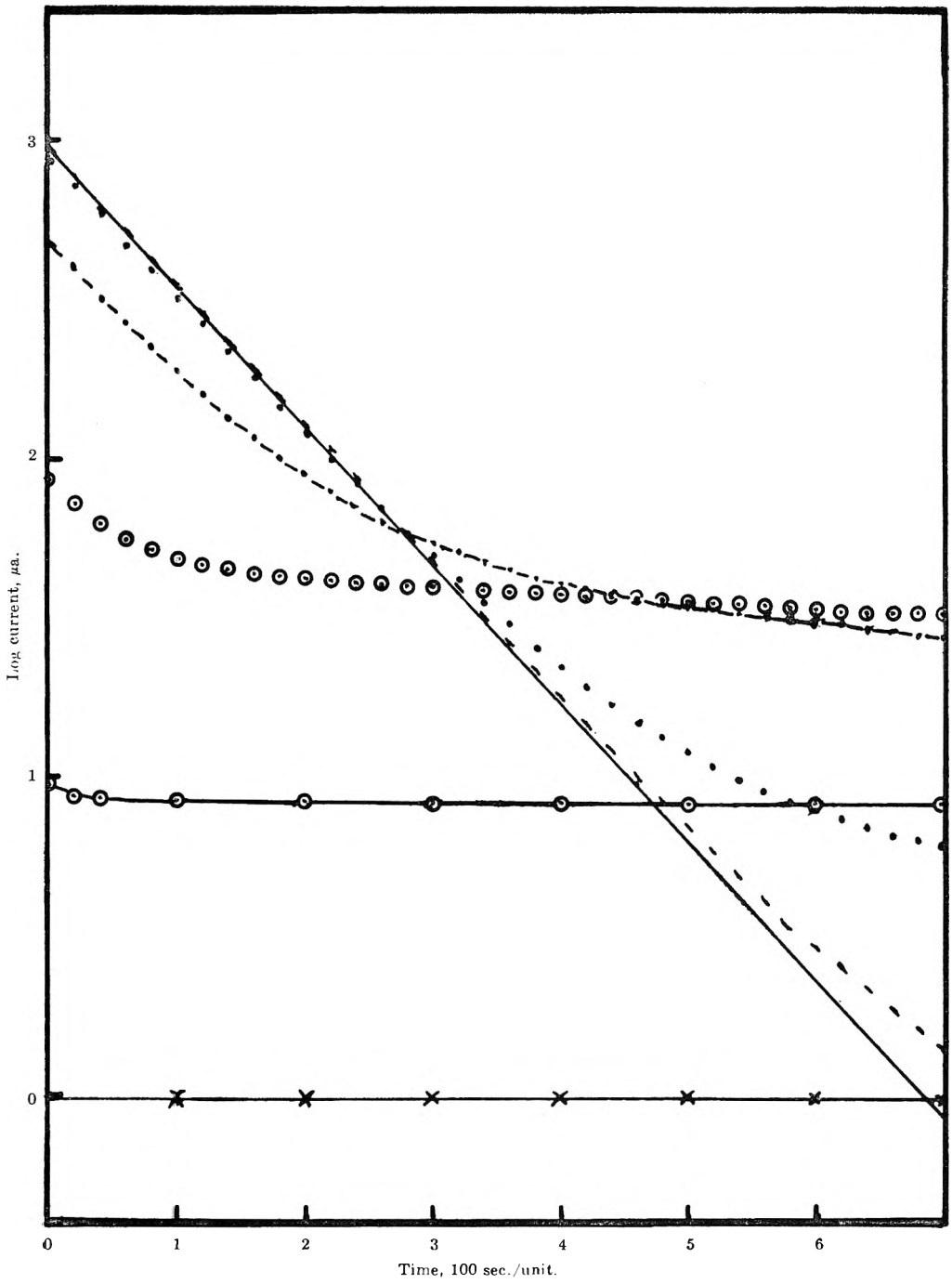

Fig. 4.—Case III: Log i *vs.* t for different values of $K = k_f/k_b$, calculated for $(C_i) + (Y_i) = 10^{-4}$ M, $p = 0.01$ sec.$^{-1}$, and $k_f = 10^{-3}$ sec.$^{-1}$: ×——×, $K = 0.001$; ⊙——⊙, $K = 0.01$; ⊙, $K = 0.1$; —·—, $K = 1.0$; •••, $K = 10.0$; – – –, $K = 100.0$; ——, $K = \infty$.

$$(C_i)/(Y_i) = k_f/k_b = K \quad (35)$$

$$(C) = (C_i)e^{-Lt}\{\cosh(Gt) + [(k_b + k_f - p)/2G]\sinh(Gt)\} \quad (36)$$

where L and G are given by

$$L = 0.5(p + k_b + k_f) \quad (37)$$

$$G = (L^2 - k_f p)^{1/2} \quad (38)$$

Note that under all circumstances, since the total amount of electroactive species, $(Y_i) + (C_i)$, is eventually electrolyzed, $n^0_{app} = n$. The presence of a preceding chemical reaction will only affect the current–time behavior, causing curvature of log i *vs.* t plots, or variation of the "apparent-p" for the electrolysis. The current–time equation is obtained by combining (3) and (36). Log i–t curves for several values of k_f and k_b are shown in Fig. 4 and 5.

Discussion

For those cases in which C is converted to a nonelectroactive species by a chemical reaction (cases I and II) n^0_{app} varies with t_1, k, p, (C_i), and (Z_i). When the concentration of Z is initially about twenty or more times the initial concentration of C, the reaction is essentially pseudo-first order, and can be treated as case I, with n^0_{app} being independent of the (C_i). Taking p as adjustable between 10^{-1} and 10^{-4} sec.$^{-1}$, and assuming usual values for the other variables, k' in the range of 10^{-1} to 10^{-5} sec.$^{-1}$ will lead to nonintegral values of n^0_{app}. In common with other coulometric determinations in which the current decays to background level, relatively little rate constant information

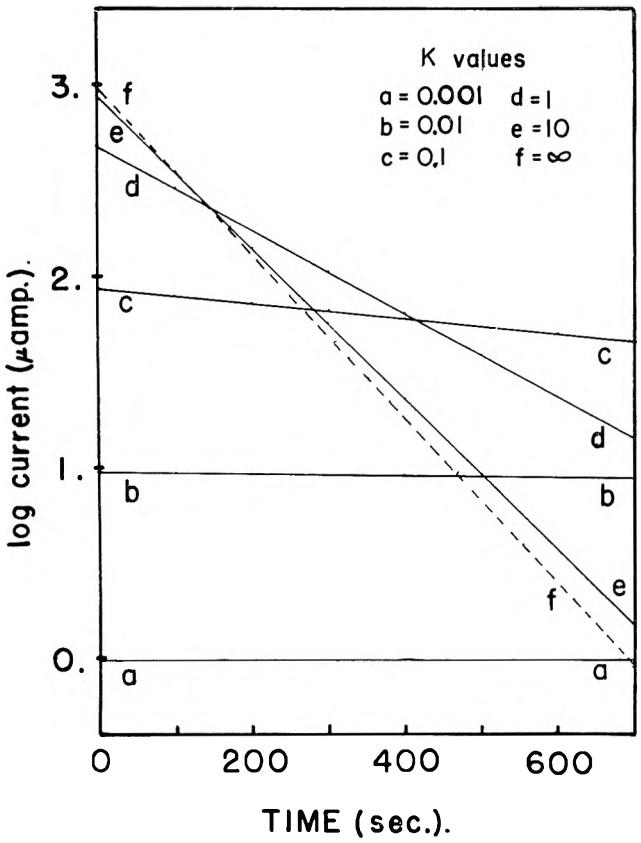

Fig. 5.—Case III: Log i *vs.* t for different values of $K = k_f/k_b$, calculated for $(C_i) + (Y_i) = 10^{-4}$ M, $p = 0.01$ sec.$^{-1}$, and $k_f = 10$ sec.$^{-1}$

can be obtained from log i–t curves. For case III, generation of C by a preceding chemical reaction, on the other hand, rate constant data can only be obtained from log i–t curves, since in all cases $n^0_{app} = n$. Reactions of this type are indicated when integral, constant, n^0_{app} values are obtained under a variety of experimental conditions, and log i–t curves show appreciable curvature, or have slopes which are smaller than usual. Both k_f and k_b determine the shape of the log i–t curves. When $k_f > 100\ k_b$, 99% of the total species is initially present in the electroactive forms, and the i–t behavior differs only very slightly from the uncomplicated behavior. When k_f/k_b is small, then the current may take a long time to decay to the background level, even for k_f values which are large compared to p (Fig. 5). In general, a preceding reaction with a K in the range of 100 to 0.01 can be investigated.

Reaction schemes corresponding to the preceding cases are probably fairly common in controlled potential coulometry. Cases I and II occur whenever the electroactive species can react with the solvent, supporting electrolyte, oxygen, etc. Analytical coulometric data can be corrected for the effect of side reactions by techniques suggested in these studies. The reaction of α,α-diphenylpicrylhydrazyl (DPPH) with bromide ion during the electroreduction of DPPH in an acetonitrile solution of tetrabutylammonium bromide was studied coulometrically by this technique.[4] Reactions of the type described in case III might have been responsible for the curvature in log i–t curves obtained during the coulometric determination of tin.[5] A recent communication on the coulometry of the uranium(VI)–uranium(IV) system in a tripolyphosphate medium indicated that the electrolysis time for the reoxidation of U(IV) was much longer than that for the reduction of U(VI).[6] This difference in electrolysis times under essentially identical cell conditions may be due to a slow chemical reaction step during the anodic oxidation.

Acknowledgment.—The authors are grateful to the National Science Foundation for support of this work (Grant No. G 14478).

(4) E. Solon and A. J. Bard, to be submitted for publication.
(5) A. J. Bard, *Anal. Chim. Acta*, **22**, 577 (1960).
(6) H. E. Zittel and L. B. Dunlap, *Anal. Chem.*, **35**, 125 (1963).

SALT EFFECTS ON THE ACTIVITY COEFFICIENTS OF HYDROCHLORIC ACID AND IONIZED α-NAPHTHOIC ACID AND ON THE DISSOCIATION CONSTANT OF α-NAPHTHOIC ACID IN 50 WEIGHT PER CENT DIOXANE–WATER[1a]

BY ARTHUR F. BUTLER AND ERNEST GRUNWALD[1b]

Chemistry Department, Florida State University, Tallahassee, Florida

Received April 25, 1963

Activity coefficients are reported for millimolal hydrochloric and ionized α-naphthoic acid (H,Cl and H,A) in 50 wt. % dioxane–water in the presence of 0.04–0.6 m NaCl, $NaClO_4$, $(CH_3)_4NCl$, and sodium β-naphthalenesulfonate (NaNs) at 25°. The observed salt effects indicate that salt-induced medium effects make only a relatively small contribution to $\gamma_{H\gamma Cl}$ and $\gamma_{H\gamma A}$ and are masked by other interactions. There are significant specific differences between the salt effects of NaCl and $NaClO_4$ on the one hand, and those of $(CH_3)_4NCl$ and NaNs on the other, in such a direction as to suggest stabilizing interactions with the large organic ions. In particular, there is evidence for specific attractive interactions between the two naphthyl anions A^- and Ns^-. The values of $\gamma_{H\gamma A}$ are based on measurements of the solubility[2] and acid dissociation constant of α-naphthoic acid in these salt solutions.

We wish to report a study of salt effects on the activity coefficients of hydrochloric acid ($\gamma_{H\gamma Cl}$) and ionized α-naphthoic acid ($\gamma_{H\gamma A}$) and on the acid dissociation constant of α-naphthoic acid, in a solvent consisting of 50.00 wt. % dioxane–50.00 wt. % water at 25°. The dielectric constant of this solvent is 35.85.[3]

(1) (a) Work supported by Office of Naval Research; reproduction in whole or in part is permitted for any purpose of the United States government; (b) Bell Telephone Laboratories, Inc., Murry Hill, N. J.
(2) E. Grunwald and A. F. Butler, *J. Am. Chem. Soc.*, **82**, 5647 (1960).
(3) F. E. Critchfield, J. A. Gibson, and J. L. Hall, *ibid.*, **75**, 1991 (1953).

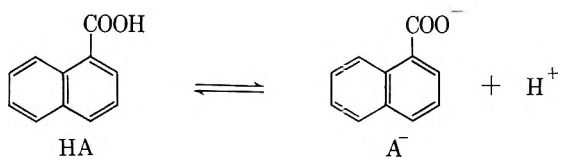

The salts were NaCl, $NaClO_4$, $(CH_3)_4NCl$, and sodium β-naphthalenesulfonate (NaNs). The concentrations of the substrates were small compared to the salt concentrations, which ranged from 0.04 to 0.6 m.

The fact that the solvent consists of two components introduces the possibility of special interactions, such as salt-induced medium effects that are typical of mixed solvents. A simplified model of the salt-induced medium effect is that the selective solvation of the added salt changes the effective solvent composition for the substrate.[4] It has already been shown that salt-induced medium effects make relatively large contributions to the observed salt effects on activity coefficients and first-order reaction-rate constants of nonelectrolytes in 50% dioxane–water,[2,5] and we now wish to evaluate the relative importance of these effects in the interaction of electrolytes. One qualitative consequence of a large salt-induced medium effect would be that specific interactions are important even between ions of like charge, so that Brönsted's principle of the specific interaction of ions[6] would fail. We are also interested in finding out whether salts with large organic ions, such as $(CH_3)_4N^+$ or Ns^-, interact with electrolytes by specific additional mechanisms analogous to those involved in their interaction with nonelectrolytes.[2,7]

Our results indicate that the salt-induced medium effects make only a relatively small contribution to the observed salt effects and are masked by other interactions. There are, however, significant specific differences between the salt effects of NaCl and $NaClO_4$ on the one hand, and those of $(CH_3)_4NCl$ and NaNs on the other. In particular, there is evidence for a specific attractive interaction between α-naphthoate ion and β-naphthalenesulfonate ion.

Experimental

Method of Measurement.—Activity coefficients of HCl were measured using a cell without liquid junction, as shown in eq. 1.

glass electrode/HCl(m_3), MX(m_4),

in 50 wt. % dioxane–water/AgCl–Ag (1)

AgCl–Ag was a silver mirror–electrolytic AgCl electrode.[8a] The glass electrode was of the type (Beckman No. 1190-42) that has been shown to give accurate results in measurements involving the hydrogen ion activity in aqueous–organic solvents[8b] and was stored in 50 wt. % dioxane–water between experiments. In the experments without added MX ($m_4 = 0$), m_3 varied from 0.001 to 0.45 m. Otherwise m_3 was about 0.002 m and m_4 varied from 0.04 to 0.6, 0.3, 0.2, and 0.2 m, respectively, for NaCl, $NaClO_4$, $(CH_3)_4NCl$, and NaNs.

K_A values for α-naphthoic acid were measured by a modification of cell 1 in which the solutes: HA(m'_3), NaA(m''_3), and NaCl(m_3''') were substituted for HCl(m_3). Values of m'_3 ranged from 0.001 to 0.005, values of m''_3 were less than 0.003, and values of m_3''' were about 0.002 except in those experiments in which MX was NaCl.

Solutions were prepared from purified reagents[2] by standard gravimetric and volumetric methods. The effect of each salt was measured in at least two independent series. All concentrations are expressed in moles/kg. of dioxane–water mixture.

Calculations.—Molal activity coefficients, γ, for HCl were calculated from the measured e.m.f., E, according to eq. 2.

$$\ln \gamma_H\gamma_{Cl} = [(E^* - E)F/RT] - \ln m_H m_{Cl} \quad (2)$$

The quasi-standard e.m.f., E^*, was deduced from experiments on cell 1 without added MX and with $m_3 < 0.005$ and was checked frequently throughout the course of these experiments. Values of $\gamma_H\gamma_{Cl}$ at these dilutions were close to the limiting-law values and were actually calculated from eq. 3, in which the coefficient, 7.732, is the appropriate Debye–Hückel limiting slope. Equation 3 actually fits the e.m.f. data for HCl within experimental error up to concentrations well over 0.01 m.

$$\ln \gamma_H\gamma_{Cl} = \frac{-7.732 m_3^{1/2}}{1 + 2.474 m_3^{1/2}};\ m_3 < 0.005,\ m_4 = 0 \quad (3)$$

Since in the experiments with added salt, m_3 is small in an absolute sense and very small relative to m_4, we may neglect the contribution of HCl(m_3) relative to that of MX(m_4) in the interpretation of $\gamma_H\gamma_{Cl}$. For the same reason we may neglect, in the K_A determinations, the effects of HA(m'_3), NaA(m''_3), and NaCl(m_3''') relative to that of MX(m_4). Since the value of $\gamma_H\gamma_{Cl}$ for a given salt solution is therefore the same, whether the substrate be dilute HCl or a dilute buffer consisting of HA, NaA, and NaCl, we may combine activity coefficients obtained in the former case with e.m.f. data for the latter case to calculate m_H according to eq. 2. The value of K_A for the given salt solution is then given by eq. 4, in which m_A/m_{HA} is equal to m''_3/m'_3.

$$K_A = \frac{m_H m_A}{m_{HA}} \quad (4)$$

It will be noted that K_A is a quotient involving molal concentrations. K_A is related to the thermodynamic constant, K_A°, by eq. 5, in which the γ's are molal activity coefficients.

$$K_A = K_A^\circ \gamma_{HA}/\gamma_H\gamma_A \quad (5)$$

K_A° was obtained by a differential potentiometric method,[9] using dilute solutions of the substrates without added salt, in 45, 50, and 55 wt. % dioxane–water. Activity coefficients could be estimated with sufficient accuracy under these conditions of low ionic strength from Debye–Hückel expressions analogous to 3, assuming a value of 5 Å. for the "distance-of-closest-approach" parameter.

Results

In most of our salt effect studies, we are measuring the activity coefficient of the substrate (component 3) in the presence of salt (component 4) at essentially zero substrate concentration. We find it convenient to represent our results as power-series functions of the salt molality,[10] as illustrated in eq. 6 and 7. In these equations, and in the rest of this section, we shall use symbols with commas (such as Na, Cl or H, Cl) to denote electrolytes, and symbols without commas (such as HA) to denote nonelectrolytes.

$$(\log \gamma_H\gamma_{Cl})_{\substack{m_3=0 \\ Na,Cl}} = -2Sm_4^{1/2} + B_{H,Cl:Na,Cl}m_4 + C_{H,Cl:Na,Cl}m_4^{3/2} + D_{H,Cl:Na,Cl}m_4^2 + \ldots \quad (6)$$

$$(\log \gamma_{HA})_{\substack{m_3=0 \\ Na,Cl}} = k_{HA:Na,Cl}m_4 + l_{HA:Na,Cl}m_4^2 + \ldots \quad (7)$$

(4) J. O'M. Bockris and H. Egan, *Trans Faraday Soc.*, **44**, 151 (1948); *Experientia*, **3**, 453 (1947); E. Grunwald, in "Electrolytes–International Symposium," B. Pesce, Ed., Pergamon Press Ltd., London, 1962.

(5) E. F. J. Duynstee, E. Grunwald, and M. L. Kaplan, *J. Am. Chem. Soc.*, **82**, 5654 (1960).

(6) J. N. Brönsted, *ibid.*, **44**, 877 (1922); **45**, 2898 (1923).

(7) R. L. Bergen, Jr., and F. A. Long, *J. Phys. Chem.*, **60**, 1131 (1956).

(8) (a) E. L. Purlee and E. Grunwald, *ib d.*, **59**, 1112 (1955); (b) E. L. Purlee and E. Grunwald, *J. Am. Chem. Soc.* **79**, 1366 (1957); A. L. Bacarella, E. Grunwald, H. P. Marshall, and E. L. Purlee, *J. Phys. Chem.*, **62**, 856 (1958).

(9) A. L. Bacarella, E. Grunwald, H. P. Marshall, and E. L. Purlee, *J. Org. Chem.*, **20**, 747 (1955).

(10) G. Scatchard and S. S. Prentiss, *J. Am. Chem. Soc.*, **56**, 1486 (1934); **56**, 2320 (1934).

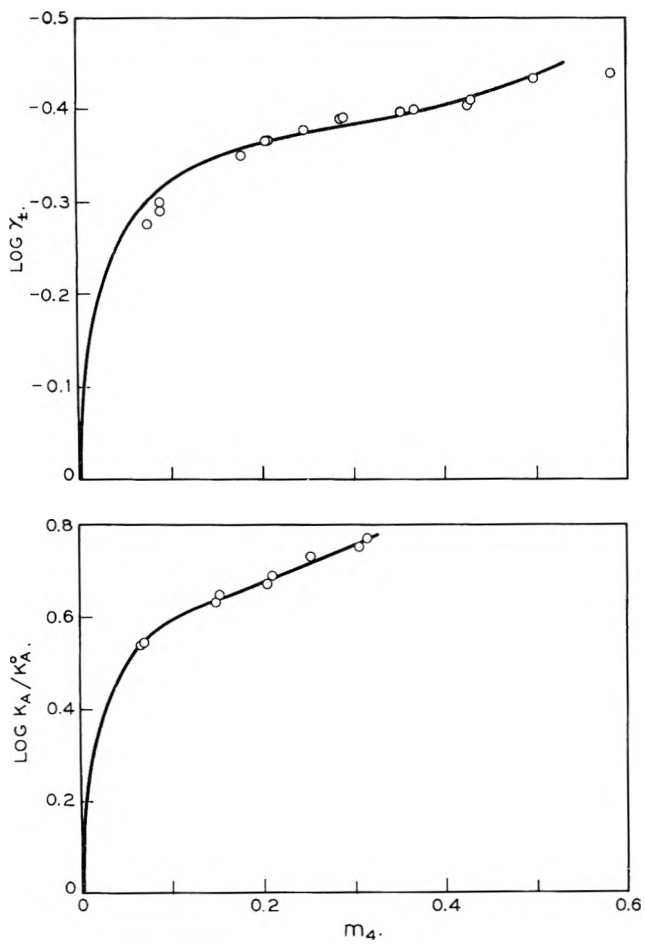

Fig. 1.—Salt effect of sodium chloride on the activity coefficient of hydrochloric acid (top) and on the acid dissociation constant of α-naphthoic acid in 50 wt. % dioxane–water at 25°. The solid lines are calculated from the parameters in Table I. The substrate concentrations are very small compared with that of sodium chloride.

The power series for electrolyte substrates involves successive powers of $m_4^{1/2}$, that for nonelectrolyte substrates involves successive powers of m_4.[10] The coefficient of the leading term in eq. 6 can be predicted from the Debye–Hückel limiting law and has the value $S = 1.679$ for 50 wt. % dioxane–water at 25°. All other coefficients in eq. 6 and 7 are obtained by adjustment to the data.

It follows from eq. 5, 6, and 7 that the salt effects on log K_A at zero concentration of substrates are represented similarly by power series of the form 8, in which the coefficients have a significance as shown in eq. 9.

$$(\log K_A)_{Na,Cl} = \log K_A^\circ + 2Sm_4^{1/2} - b_{Na,Cl}m_4 - c_{Na,Cl}m_4^{3/2} - d_{Na,Cl}m_4^2 \ldots \quad (8)$$

$$\left.\begin{aligned} b_{Na,Cl} &= B_{H,A:Na,Cl} - k_{HA:Na,Cl} \\ c_{Na,Cl} &= C_{H,A:Na,Cl} \\ d_{Na,Cl} &= D_{H,A:Na,Cl} - l_{HA:Na,Cl} \end{aligned}\right\} \quad (9)$$

Coefficients k and l for the salt effects on the activity coefficient of α-naphthoic acid in 50 wt. % dioxane–water have been reported previously.[2]

In applying eq. 6 and 8 to represent the salt effects on $\gamma_H\gamma_{Cl}$ and on K_A, we felt that our data were sufficiently extensive and accurate to warrant the use of two adjustable parameters, but not of three or more. We decided, somewhat arbitrarily, to let these parameters be the coefficients of m_4 and m_4^2. That is, we let the coefficients of $m_4^{5/2}$, as well as those of $m_4^{4/2}$, m_4^3, . . . , be zero. This decision was partly based on an analogy to a previous study of the activity coefficients of sodium chloride in 50 wt. % dioxane–water,[11] in which it was found that the complete series, involving all powers of $m^{1/2}$ up to $m^{5/2}$, did not fit any better than an abbreviated series involving only $m^{1/2}$, m, and m^2. As a matter of fact, the fit of the present data to the abbreviated series is satisfactory, the worst of the fits being shown in Fig. 1.

The standard deviation of 49 values of $\gamma_\pm$ for HCl in our salt effect experiments from the respective power series function was 2.4%, that of 35 K_A values was 1.2%.

Values of the parameters that give best fit to our data are listed in Table I. The table also lists activity coefficients calculated from these parameters for $m_4 = 0.2$.

Table II summarizes our measurements of K_A° for α-naphthoic acid, and certain derived functions that are of interest in connection with the salt-induced medium effect.

TABLE I

SALT-EFFECT PARAMETERS AND ACTIVITY COEFFICIENTS FOR THE SUBSTRATES H,Cl, HA, AND H,A IN 50 WT. % DIOXANE–WATER AT 25°

Salt	HCl	NaCl	$NaClO_4$	$(CH_3)_4NCl$	NaNs
$B_{H,Cl:salt}$	5.17	4.45	4.76	4.45	4.43
$D_{H,Cl:salt}$	−4.81	−2.90	−4.01	−4.81	−4.05
b_{salt}	...	−5.19	−4.60	−5.40	−4.38
d_{salt}	...	5.24	4.46	7.33	4.05
$k_{HA:salt}$[a]	0.12	−0.10	0.31	−0.19	−0.25
$B_{H,A:salt}$	...	5.10	4.91	5.22	4.13
$D_{H,A:salt}$	...	−5.24	−4.46	−7.33	−4.05
$\gamma_H\gamma_{Cl}$ (0.2 *m*)	0.218	0.187	0.195	0.157	0.167
$\gamma_H\gamma_A$ (0.2 *m*)	...	.203	.200	.177	.145
γ_{Cl}/γ_A (0.2 *m*)	...	.92	.97	.88	1.15

[a] From ref. 2; $l_{HA:salt} = 0.00$

TABLE II

ACID DISSOCIATION OF α-NAPHTHOIC ACID IN DIOXANE–WATER MIXTURES AT 25°

Dioxane (wt. %)	Z_1	$K_A^\circ \times 10^5$ (molal concn.)
45	0.8567	1.10 ± 0.04
50[a]	.8302	.532 ± .007
55	.8000	.220 ± .001
[a] In 50 wt. % dioxane–water		
$-2.303RT$ d log K_A°/dZ_1		−16.7 kcal.
dF_m°/dZ_1 for HA (ref. 2)		10.9 kcal.
dF_m°/dZ_1 for $H^+ + A^-$		− 5.8 kcal.

Discussion

As far as we know, this is the first investigation of salt effects on the activity coefficients of electrolytes for a variety of structural types in a binary solvent. Although the accuracy of the data is only moderate, a few conclusions concerning the relative importance of various interactions can be reached. It will be sufficient to compare activity coefficients at a single salt concentration that is high enough for specific effects to be appreciable. We have therefore tabulated $\gamma_H\gamma_{Cl}$, $\gamma_H\gamma_A$, and γ_{Cl}/γ_A at $m_4 = 0.2$ (Table I). Although the accuracy of these values is not uniform, we estimate that differences in excess of 5% are significant, with a statistical probability of at least 0.67. Thus we obtain the salt-effect sequences

(11) E. Grunwald and A. L. Bacarella, *J. Am. Chem. Soc.*, **80**, 3840 (1958).

For $\gamma_H\gamma_{Cl}$, HCl > NaCl ≷ $NaClO_4$ > $(CH_3)_4NCl$ ≷ NaNs

For $\gamma_H\gamma_A$, NaCl ≷ $NaClO_4$ > $(CH_3)_4NCl$ > NaNs

For γ_{Cl}/γ_A, NaCl ≷ $NaClO_4$ = $(CH_3)_4NCl$ < NaNs

It is seen in the first two series that the organic ion salts interact so as to reduce the activity coefficient relative to the inorganic salts, in spite of their somewhat larger size. This stabilizing interaction is especially strong between H,A and Na,Ns, and here the high value obtained for γ_{Cl}/γ_A shows that the additional interaction involves specifically the α-naphthoate ion and the β-naphthalenesulfonate ion. The effect is probably the result of an attraction between the naphthalene rings that is strong enough to overcome the electrical repulsion between these ions.

Our chief aim in undertaking this study was to look for salt-induced medium effects. In first approximation, the salt-induced medium effect on log γ_3 can be represented as an additive term proportional to m_4, as in eq. 10.

$$\log \gamma_3 = \log \gamma_3' + s_{34}m_4 \qquad (10)$$

Theory and experimental results for nonelectrolytes in the system dioxane–water[2,5] both indicate that s_{34} is given by an equation of the form

$$s_{3,4} = A + B\left(\frac{dF_{3m}^\circ}{dZ_1}\right)\left(\frac{dF_{4m}^\circ}{dZ_1}\right) \qquad (11)$$

where F_{im}° is the standard partial molal free energy (on the m-scale) of the ith component, Z_1 is the mole fraction of water in the binary solvent, and the subscripts 3 and 4 denote the substrate and salt, respectively. A and B are parameters, the value of B being about 0.004 according to the previous results[2,5] for nonelectrolyte substrates, if F_m° is expressed in kcal. In the present case, values of dF_m°/dZ_1 in 50 wt. % dioxane–water are −10.7, −5.8, −16.6, −6.8, −16.3, and −7.3 kcal., respectively, for H,Cl, H,A, Na,Cl, Na,ClO_4, $(CH_3)_4N$,-Cl, and Na,Ns (ref. 2 and Table II). Hence, at m_4 = 0.2, this mechanism acting along should increase $\gamma_H\gamma_{Cl}$ in the presence of sodium chloride by about 21% relative to the value in the presence of sodium perchlorate, and there should be a similar increase of 11% in $\gamma_H\gamma_A$, assuming that B is again 0.004. Nothing of the sort has been observed.

Acknowledgment.—It is a pleasure to thank Dr. E. L. Purlee for helpful advice about the e.m.f. measurements.

A VARIATIONAL PRINCIPLE FOR THE POISSON–BOLTZMANN EQUATION. ACTIVITY COEFFICIENT OF A SALT IN A CHARGED MICROCAPILLARY[1]

BY LAWRENCE DRESNER

Neutron Physics Division, Oak Ridge National Laboratory, Oak Ridge, Tennessee

Received April 29, 1963

A functional which is a minimum for solutions of the Poisson–Boltzmann equation is given. The minimum of this functional is shown to be related to the electrostatic contribution to the free energy of the system. Using a simple trial function, an illustrative problem of interest in water desalination is worked.

Introduction

The Poisson–Boltzmann equation has been used to describe many phenomena in electrochemistry,[2a-c] solution chemistry,[3] colloid chemistry,[4] and the chemistry of polyelectrolytes[5a,b] and ion-exchange materials.[6a,b] Because of the complexity created by its nonlinearity, only a few exact solutions to the Poisson–Boltzmann equation are known.[2a,b,5a,b,7] In general, the powerful methods of solution developed for linear partial differential equations, such as separation of variables, expansion in orthogonal functions, use of Fourier and other transformations, etc., cannot be applied to the Poisson–Boltzmann equation.[8a] However, one of the well known approximate methods of solution developed for linear problems, the variational method, can be applied to the nonlinear Poisson–Boltzmann equation.[8b] In this paper, a functional will be exhibited that is a minimum for solutions of the Poisson–Boltzmann equation and whose minimum value is related to the electrostatic part of the free energy of the system. With the help of this functional and a simple trial function, the following illustrative example will be worked: the electrostatic contribution to the mean activity coefficient of 1:1 electrolyte invading a small, surface-charged microcapillary will be estimated.

The Poisson–Boltzmann Equation.—The Poisson–Boltzmann equation describing the equilibrium of a mixture of N types of ions and a solvent in a volume V depends on two assumptions:

(i) The concentration c_i [ions cm.$^{-3}$] of the ith type

(1) Work performed for the Office of Saline Water, U. S. Department of the Interior, Oak Ridge National Laboratory, Oak Ridge, Tennessee, operated by Union Carbide Corporation for the U. S. Atomic Energy Commission.

(2) (a) G. Gouy, *J. Phys.*, [4] **9**, 357 (1910); *Ann. Physik*, [9] **7**, 129 (1917); (b) D. L. Chapman, *Phil. Mag.*, [6] **25**, 475 (1913); (c) O. Stern, *Z. Elektrochem.*, **30**, 508 (1924).

(3) P. Debye and E. Hückel, *Physik Z.*, **24**, 185, 305 (1923).

(4) E. J. W. Verwey and J. T. G. Overbeek, "Theory of Stability of Lyophobic Colloids," Elsevier Publishing Co., Inc., New York, N. Y., 1948.

(5) (a) R. N. Fuoss, A. Katchalsky, and S. Lifson, *Proc. Natl. Acad. Sci. U. S.*, **37**, 579 (1951); (b) T. Alfrey, P. W. Berg, and H. Morawetz, *J. Polymer Sci.*, **7**, 543 (1951).

(6) (a) L. Lazare, B. T. Sundheim, and H. P. Gregor, *J. Phys. Chem.*, **60**, 641 (1956); (b) L. Dresner and K. A. Kraus *ibid.*, **67**, 990 (1963).

(7) The solution independently found by Fuoss, *et al.*,[5a] and by Alfrey, *et al.*,[5b] has also been given by H. Lemke [*J. Math.*, **142**, 118 (1913)] and by G. W. Walker [*Proc. Roy. Soc.* (London), **A41**, 410 (1915)]. It is a special case of a very general two-dimensional solution to the equation $\Delta^2 u = e^u$ stated by J. Liouville [*J. Math.*, (1) **18**, 71 (1853)].

(8) (a) Interestingly enough, in a certain special case conformal mapping is applicable. See M. v. Laue, "Jahrbuch der Radioaktivität und Elektronik," Band 15, Heft 3, 206, 1918; (b) the possible use of the variational method in the Debye–Hückel case was mentioned in a footnote by S. Levine, *J. Chem. Phys.*, **7**, 836 (1939).

of ion depends on the electrical potential ϕ through the Boltzmann factor, *i.e.*

$$c_i \alpha e^{-z_i e\phi/kT} \tag{1}$$

where z_i is the valence of these ions, e is the charge of the proton, k is Boltzmann's constant, and T is the absolute temperature.

(ii) The discrete nature of the ionic charge can be neglected and the electrical potential ϕ related to the ionic concentrations by Poisson's law

$$\nabla^2\phi = (-1/\epsilon)\sum_{i=1}^{N} z_i e c_i \tag{2}$$

Here ϵ is the dielectric constant.[9]

The Poisson–Boltzmann equation is obtained by substituting a suitably normalized form of (1) into (2). Writing (1) as

$$c_i = n_i e^{-z_i e\phi/kT} \Big/ \int_V e^{-z_i e\phi/kT}\, \mathrm{d}^3r \tag{3}$$

where n_i denotes the total number of ions of type i in V, we find the result

$$\nabla^2\phi = (-1/\epsilon)\sum_{i=1}^{N} z_i e n_i e^{-z_i e\phi/kT} \Big/ \int_V e^{-z_i e\phi/kT}\, \mathrm{d}^3r \tag{4}$$

Equation 4 is the Poisson–Boltzmann equation. If the volume V is all space, eq. 4 is valid everywhere. If the volume V is finite by virtue of the ions being confined in a container, eq. 4 is valid inside V, while Laplace's equation $\nabla^2\phi = 0$ is valid outside. As is usual in electrostatics, ϕ and the normal component of the electric displacement are continuous across S, the surface of V, except when there are surface charges on S, etc.

The Variational Principle.—Let us now consider the functional

$$H[\phi] = \frac{1}{2}\int_\infty \epsilon(\nabla\phi)^2\mathrm{d}^3r + kT\sum_{i=1}^{N} n_i \ln V^{-1}\int_V e^{-z_i e\phi/kT}\, \mathrm{d}^3r \tag{5}$$

where a subscript ∞ denotes an integration over all space. If ϕ is allowed to vary over all functions which vanish at least as rapidly as $1/r$ at ∞, then H will vary over a semiinfinite range of values bounded from below and attain its minimum when $\phi = \phi^*$, a solution of the Poisson–Boltzmann eq. 4.

This statement is proved as follows. Let $\phi = \phi^* + \chi$. Then, first

$$\frac{1}{2}\int_\infty \epsilon(\nabla\phi)^2\mathrm{d}^3r = \frac{1}{2}\int_\infty \epsilon(\nabla\phi^*)^2\mathrm{d}^3r + \frac{1}{2}\int_\infty \epsilon(\nabla\chi)^2\mathrm{d}^3r + \int_\infty \epsilon\nabla\phi^*\cdot\nabla\chi\, \mathrm{d}^3r \tag{6a}$$

$$= \frac{1}{2}\int_\infty \epsilon(\nabla\phi^*)^2\mathrm{d}^3r + \frac{1}{2}\int_\infty \epsilon(\nabla\chi)^2\mathrm{d}^3r - \int_\infty \epsilon\chi\nabla^2\phi^*\mathrm{d}^3r \tag{6b}$$

Here the second equality has been obtained from the first by use of Green's theorem and the fact that $\chi\nabla\phi^*$ vanishes at least as rapidly as $1/r^3$ at ∞.

(9) The units are rationalized m.k.s. units. In these units, the dielectric constant of free space is 8.85×10^{-12} f./m.

Secondly

$$\ln\int_V e^{-z_i e\phi/kT}\, \mathrm{d}^3r = \ln\int_V e^{-z_i e\phi^*/kT}\, e^{-z_i e\chi/kT}\, \mathrm{d}^3r \tag{7a}$$

$$= \ln\int f(y)\, e^y \mathrm{d}y \tag{7b}$$

where $y = -z_i e\chi/kT$ and $f(y)\,\mathrm{d}y$ is defined as the integral of $e^{-z_i e\phi^*/kT}$ over that part of the volume V in which y lies in the interval $\mathrm{d}y$. According to a theorem of Hardy, *et al.*[10]

$$\int f(y)e^y\mathrm{d}y \Big/ \int f(y)\,\mathrm{d}y \geqq \exp\left\{\int yf(y)\mathrm{d}y \Big/ \int f(y)\mathrm{d}y\right\} \tag{8}$$

Substitution of (8) into (7b) allows the latter to be written

$$\ln V^{-1}\int_V e^{-z_i e\phi/kT}\, \mathrm{d}^3r \geqq \ln V^{-1}\int_V e^{-z_i e\phi^*/kT}\, \mathrm{d}^3r - \frac{z_i e}{kT}\cdot\frac{\int_V \chi e^{-z_i e\phi^*/kT}\, \mathrm{d}^3r}{\int_V e^{-z_i e\phi^*/kT}\, \mathrm{d}^3r} \tag{9}$$

If we now multiply (9) by kTn_i and sum over i and then add the result to (6b), we get

$$H[\phi] \geqq H[\phi^*] + \frac{1}{2}\int_\infty \epsilon(\nabla\chi)^2\mathrm{d}^3r - \int_V \epsilon\chi\left[\nabla^2\phi^* + (1/\epsilon)\sum_{i=1}^{N} z_i e n_i e^{-z_i e\phi^*/kT} \Big/ \int_V e^{-z_i e\phi^*/kT}\, \mathrm{d}^3r\right]\mathrm{d}^3r \tag{10}$$

The bracketed expression in the last integral vanishes because ϕ^* satisfies (4). Since the second term on the right-hand side is never negative, $H[\phi]$ is always $\geqq H[\phi^*]$.

Relation to the Free Energy.—The minimum value $H[\phi^*]$ of the functional H is related to the electrostatic part of the free energy of the system. Starting from (5), one can easily show by an application of Green's theorem that

$$H[\phi^*] = -\frac{1}{2}\int_\infty \epsilon\phi\nabla^2\phi^*\mathrm{d}^3r + kT\sum_{i=1}^{N} n_i \ln V^{-1}\int_V e^{-z_i e\phi^*/kT}\, \mathrm{d}^3r \tag{11}$$

Using (3) and (4) we can rewrite the first term on the right-hand side as

$$-\frac{1}{2}\int_\infty \epsilon\phi^*\nabla^2\phi^*\, \mathrm{d}^3r = \frac{1}{2}\int_V \sum_{i=1}^{N} z_i e c_i\phi^*\, \mathrm{d}^3r \tag{12}$$

The summands in the second term on the right-hand side (11) can be rewritten as follows.

$$n_i \ln V^{-1}\int_V e^{-z_i e\phi^*/kT}\, \mathrm{d}^3r = n_i \ln (n_i/V) - n_i[z_i e\phi^*/kT + \ln c_i] \tag{13a}$$

$$= n_i \ln (n_i/V) - \int_V c_i[z_i e\phi^*/kT + \ln c_i]\mathrm{d}^3r \tag{13b}$$

(10) G. H. Hardy, J. E. Littlewood, and G. Pólya, "Inequalities," Cambridge University Press, London and New York, N. Y., 1934, Theorem 184.

The first equality follows from use of eq. 3; the second follows from the observation that according to eq. 3 the bracketed term in eq. 13a is actually independent of position. Combining (12) and (13b) with (11), we find that

$$-H[\phi^*] = \sum_{i=1}^{N} [-kTn_i \ln (n_i/V) + kT \int_V c_i \ln c_i \mathrm{d}^3r + \frac{1}{2} \int_V z_i e\phi^* c_i \mathrm{d}^3r] \quad (14)$$

Marcus[11] has shown that the right-hand side of (14) is the electrostatic contribution to the free energy of the system.

With $-H[\phi^*]$ now identified as the electrostatic free energy, it is possible to find expressions for the activity coefficients of the various ions in the mixture. Let us begin by finding the derivative of H with respect to n_i. A short calculation shows that

$$\frac{\partial H[\phi^*]}{\partial n_i} = -\int_\infty e\nabla^2\phi^* (\partial\phi^*/\partial n_i) \mathrm{d}^3r - \sum_{j=1}^{N} z_j e n_j \int_V e^{-z_j e\phi^*/kT} (\partial\phi^*/\partial n_i)\mathrm{d}^3r \Big/ \int_V e^{-z_i e\phi^*/kT} \mathrm{d}^3r + kT \ln V^{-1} \int_V e^{-z_i e\phi^*/kT} \mathrm{d}^3r \quad (15a)$$

Here $\partial\phi^*/\partial n_i$ is given by

$$\frac{\partial\phi^*}{\partial n_i} = \lim_{\Delta n_i \to 0} \left[\frac{\phi^*(n_1, n_2, \ldots, n_i + \Delta n_i, \ldots n_N) - \phi^*(n_1, n_2, \ldots, n_i, \ldots, n_N)}{\Delta n_i} \right] \quad (15b)$$

where $\phi^*(n_1, n_2, \ldots, n_N)$ is the solution of (4) corresponding to the ionic population $n_1, n_2, \ldots, n_N$. Since ϕ^* satisfies Laplace's equation outside of V and eq. 4 inside of V, the first two terms in (15a) drop out, and the derivative $\partial H/\partial n_i$ is given by the last term in eq. 15a. From this fact, it follows that the electrostatic contribution to the chemical potential of the ith ionic type is

$$\mu_i^{el} = -kT \ln V^{-1} \int_V e^{-z_i e\phi^*/kT} \mathrm{d}^3r \quad (16a)$$

This means that the quantity

$$\gamma_i = V \Big/ \int_V e^{-z_i e\phi^*/kT} \mathrm{d}^3r \quad (16b)$$

is the electrostatic contribution to the activity coefficient of the ith type of ions. This result has also been obtained by Marcus.[11]

Illustrative Example.—The electrostatic contributions to the ionic activity coefficients and/or the free energy can be numerically evaluated with the help of the functional 5 in the following way. An n-parameter family of trial functions is chosen, and the functional H is evaluated in terms of these as yet undetermined parameters. The parameters are then chosen so that the value of the functional is a minimum. This specifies a "best" member of the n-parameter family. With this "best" trial function approximate values of the various physical quantities of interest can be evaluated. It is important to note that the physical quantity represented by the functional itself is more accurately approximated than any other; if the error in the trial function is of order η, then the error in the approximate value of the functional is of order η^2. In general, the better the "best" trial function is able to approximate the behavior of the true solution, the more accurate will be the approximate values of the various physical quantities.

(11) R. A. Marcus, *J. Chem. Phys.*, **23**, 1057 (1955).

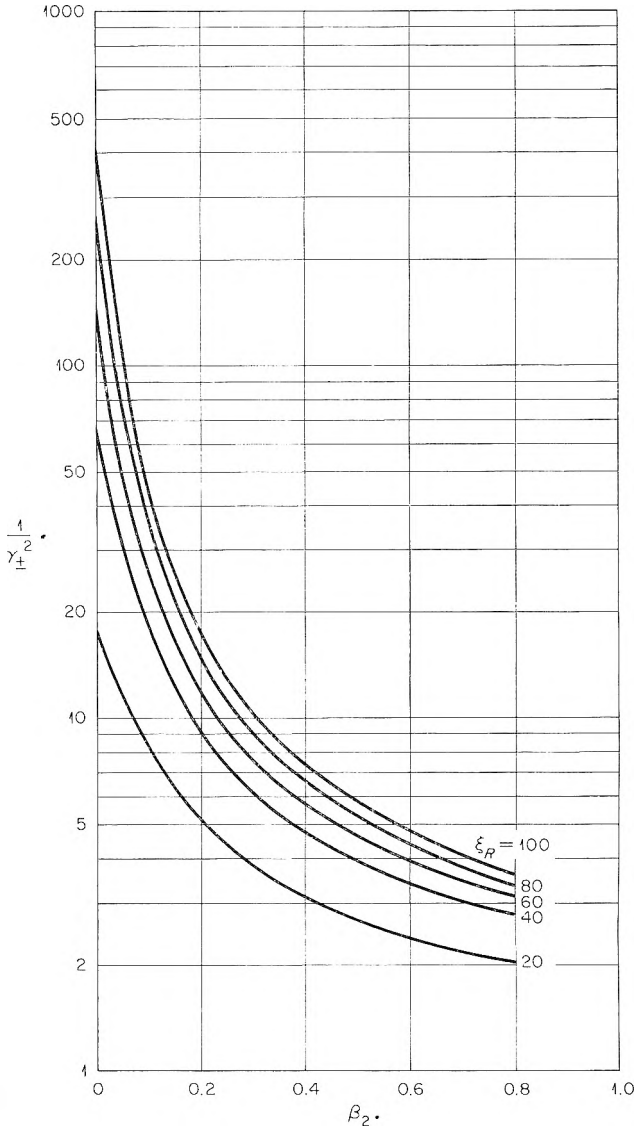

Fig. 1.—The reciprocal mean squared activity coefficient $1/\gamma_\pm^2$ of a 1:1 electrolyte in a surface-charged capillary plotted against the dimensionless salt concentration β_2 for various dimensionless radii ξ_R.

Let us consider a cylindrical capillary of radius R and length $L \gg R$ on whose inner surface a fixed electric charge is distributed with surface density σ. Let the interior of the capillary be filled with a solution in thermodynamic equilibrium with an infinite external solution of a 1:1 electrolyte. We wish to estimate $\gamma_\pm$, the electrostatic contribution to the mean activity coefficient of the electrolyte in the microcapillary.

When the electrolyte concentration is vanishingly small compared to the average fixed charge concentration $2\sigma/R$ in the capillary, $\gamma_\pm$ can be calculated ex-

actly using Liouville's solution to the equation $\nabla^2 u = e^u$.[7] This has been done by Dresner and Kraus,[6b] who found the results

$$1/\gamma_\pm^2 = 1 + \xi_R^4/(192 + 24\xi_R^2) \quad (17a)$$

where

$$\xi_R = \kappa R \quad (17b)$$

and

$$\kappa^2 = 2e|\sigma|/kT\epsilon R \quad (17c)$$

The value of the electrical potential corresponding to these results is

$$\phi^* = (kT/z_1e) \ln [1 + (\xi_R^2 - \xi^2)/8]^2 \qquad r \leq R \quad (17d)$$

$$\phi^* = 0 \qquad r \geq R \quad (17e)$$

where $\xi = \kappa r$, r is the radius vector ($0 \leq r \leq R$), and z_1 is the valence of the ions of opposite charge to the fixed charge σ (counter-ions).

When the electrolyte concentration is not vanishingly small, $\gamma_\pm$ can be estimated variationally by use of the trial function

$$\phi = (kT/z_1e) \ln [1 + b(\xi_R^2 - \xi^2)]^c \qquad r \leq R \quad (18a)$$

$$\phi = 0 \qquad r \geq R \quad (18b)$$

where b and c are as yet undetermined constants. If we introduce the notation β_1 for the ratio of n_1, the number of counter-ions in V, to $2\pi RL|\sigma|/e$, the number of monovalent "fixed" ions in V, and the notation β_2 for the ratio of n_2, the number of co-ions in V, to $2\pi RL|\sigma|/e$, then a straightforward calculation yields the result

$$H[\phi] = V(kT/e)^2\kappa^2\epsilon \left\{2bc^2\left[1 - \frac{\log (1 + b\xi_R^2)}{b\xi_R^2}\right] + \ln\left[\frac{(1 + b\xi_R^2)^{1-c} - 1}{b\xi_R^2(1 - c)}\right] + \beta_2 \ln\left[\frac{(1 + b\xi_R^2)^{1-c} - 1}{b\xi_R^2(1 - c)}\right]\left[\frac{(1 + b\xi_R^2)^{1+c} - 1}{b\xi_R^2(1 + c)}\right]\right\} \quad (19)$$

Here use has been made of the condition of charge neutrality in the form $1 + \beta_2 = \beta_1$. The coefficient of β_2 in eq. 19 is the value of $\ln (1/\gamma_\pm^2) = \ln (1/\gamma_1\gamma_2)$ defined by eq. 16b that corresponds to the trial function (18).

Shown in Fig. 1 are values of the reciprocal mean activity coefficient $1/\gamma_\pm^2$ calculated with the trial function 18, the constants b and c having been chosen (by trial and error) to minimize the value of H given in (19). The $\beta_2 = 0$ values are the same as those given by (17a), since for $\beta_2 = 0$, the values $b = {}^1/_8$ and $c = 2$, which make (17) and (18) identical, will minimize H.

The ease with which these estimates have been obtained demonstrates the power of the variational method; on the other hand, a disadvantage of the present calculation is that it gives no clue to the magnitude of the error involved. Nevertheless, it is the author's feeling that the precipitous drop in $1/\gamma_\pm^2$ with increasing β_2 near $\beta_2 = 0$ is realistically described because the trial function 18 is exact at $\beta_2 = 0$ and because it can accommodate itself through two independent constants to changes in β_2.

The capillary system discussed in this section has been used by Dresner and Kraus[6b] as a model of a suggested salt filter composed of a porous bed of ion-exchange active particles. Their studies of the thermodynamic equilibria of such salt filters in contact with electrolyte solutions were based on the $\beta_2 = 0$ mean activity coefficient $\gamma_\pm$ given by (17). Since in their work β_2 was always ≤ 0.01, the curves of Fig. 1 indicate that their results do not stand in need of correction.

HETEROGENEITY INDEX DURING DEAD-END POLYMERIZATION

By A. V. Tobolsky, R. H. Gobran, R. Böhme, and R. Schaffhauser

Frick Chemical Laboratory, Princeton University, Princeton, New Jersey

Received April 29, 1963

Expressions are developed for determining the cumulative number and weight average degrees of polymerization throughout a free radical polymerization.

Introduction

It can be shown[1] that in the absence of retardation of the termination reaction, radical-initiated polymerization may cease short of complete conversion even when the initiator does not undergo wasteful side reactions. This phenomenon, termed "dead-end polymerization," is due to the fact that the initiator may be depleted before the polymerization has gone to completion.

The theory of this type of polymerization has been checked[2] quantitatively for the polymerization of styrene using 2,2′-azobisisobutyronitrile (azo-1) as the initiator. It was found that in the absence of the Tromsdorff–Norrish effect,[3,4] the actual amount of conversion agreed quite well with the predicted value. The effect of chain transfer to monomer was neglected in the above study since only the amount of conversion was considered.

In the present treatment, the effect of chain transfer to monomer is considered and expressions are developed for calculating the cumulative values of $\bar{P}_n$ and $\bar{P}_w$ (the number and weight average degrees of polymerization) at any time during the polymerization.

Theoretical

In a free radical polymerization where the growing radicals do not undergo transfer reactions with solvent

(1) A. V. Tobolsky, *J. Am. Chem. Soc.*, **80**, 5927 (1958).

(2) A. V. Tobolsky, C. E. Rogers, and R. D. Brickman, *ibid.*, **82**, 1277 (1960).

(3) E. Tromsdorff, H. Kohle, and P. Lagolly, *Makromol. Chem.*, **1**, 169 (1948).

(4) R. G. W. Norrish and R. R. Smith, *Nature*, **150**, 336 (1942).

or initiator and thermal polymerization is negligible, the number average degree of polymerization ($\bar{P}_n$) of the polymer former at any instant is given by the relation[5]

$$\frac{1}{\bar{P}_n} = C_{Tm} + \frac{R_p k_t}{[M]^2 k_p^2} \quad (1)$$

In expression 1, [M] is the monomer concentration, k_t is the rate constant for the termination reaction, k_p is the rate constant for the propagation reaction, and C_{Tm} is the transfer constant to monomer.

The rate of polymerization (neglecting thermal polymerization) is given by

$$R_p = \frac{k_p f^{1/2} k_d^{1/2} [cat]^{1/2} [M]}{k_t^{1/2}} \quad (2)$$

where f is the initiator efficiency, k_d is the rate constant for catalyst decomposition, and [cat] is the catalyst concentration.

Substituting this expression for R_p in eq. 1, one obtains

$$\bar{P}_n \text{ (instantaneous)} = \frac{[M]k_p}{[M]k_p C_{Tm} + k_t^{1/2} f^{1/2} k_d^{1/2} [cat]^{1/2}} \quad (3)$$

The cumulative $\bar{P}_n$ at any time (t) during the polymerization is equal to the ratio of the total amount of polymer formed to the total number of chains present. Thus

$$\bar{P}_n \text{ (cumulative)} = \frac{[M]_0 - [M]_t}{f([cat]_0 - [cat]_t) + C_{Tm}([M]_0 - [M]_t)} \quad (4)$$

where subscripts 0 and t refer to time zero and t, respectively.

The ratio of $\bar{P}_{wi}$ to $\bar{P}_{ni}$ for the polymer which is formed in a very narrow range of conversion in vinyl polymerization can be obtained from the coupling distribution[6]

$$\frac{\bar{P}_{wi}}{\bar{P}_{ni}} = \frac{1 + 4p + p^2}{(1 + p)^2} \quad (5)$$

where p is a parameter which specifies the actual distribution encountered and whose value lies between zero and unity. Although p may change slightly as the polymerization proceeds, its value is quite close to unity if the number average degree of polymerization is at all appreciable. Taking p equal to unity as an approximation, one obtains

$$\bar{P}_{wi} = 1.5\bar{P}_{ni} \quad (6)$$

for the polymer formed at any instant.[7]

The cumulative weight average degree of polymerization is the product of the instantaneous fractional

(5) A. V. Tobolsky and R. B. Mesrobian, "Organic Peroxides," Interscience Publishers, Inc., New York, N. Y., 1954, pp. 138, 139.

(6) A. V. Tobolsky, "Properties and Structure of Polymers," John Wiley and Sons, Inc., New York, N. Y., 1960, Appendix F.

(7) For the case where transfer is the only chain termination reaction, $\bar{P}_{wi} = 2\bar{P}_{ni}$. Therefore in expression 6, etc., the factor 1.5 may be replaced by a weighted factor

$$y = \frac{1.5K_d([cat]_0 - [cat]) + 2C_{Tm}([M]_0 - [M])}{K_d([cat]_0 - [cat]) + C_{Tm}([M]_0 - [M])} \quad (6a)$$

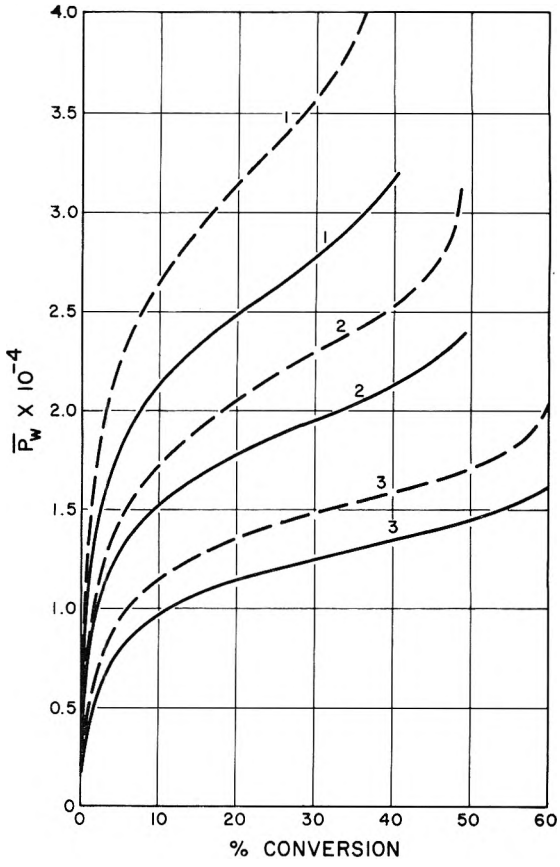

Fig. 1.—Calculated weight average degree of polymerization during a styrene polymerization at 60° for varying concentrations of initiator (1, 0.0009 mole/l.; 2, 0.0016 mole/l.; 3, 0.0030 mole/l.) including (solid lines) and omitting (broken lines) transfer to monomer.

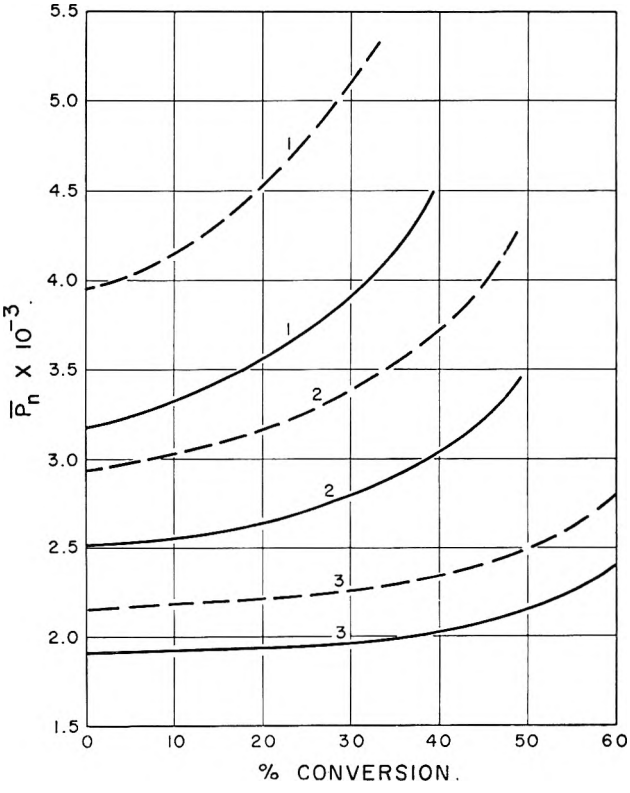

Fig. 2.—Calculated number average degree of polymerization during a styrene polymerization at 60° for varying concentrations of initiator (1, 0.0009 mole/l.; 2, 0.0016 mole/l.; 3, 0.0030 mole/l.) including (solid lines) and omitting (broken lines) transfer to monomer.

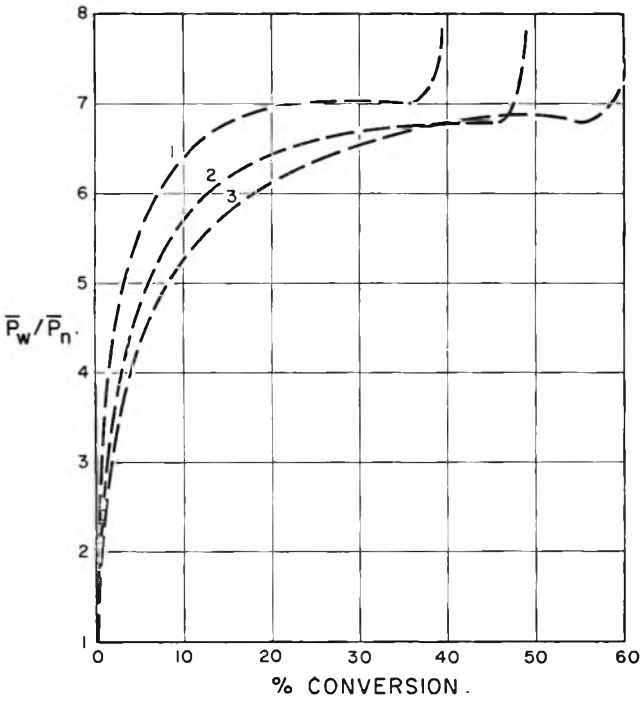

Fig. 3.—Calculated variation of the heterogeneity index during a styrene polymerization at 60° for varying concentrations of initiator (1, 0.0009 mole/l.; 2, 0.0016 mole/l.; 3, 0.0030 mole/l.) omitting transfer to monomer.

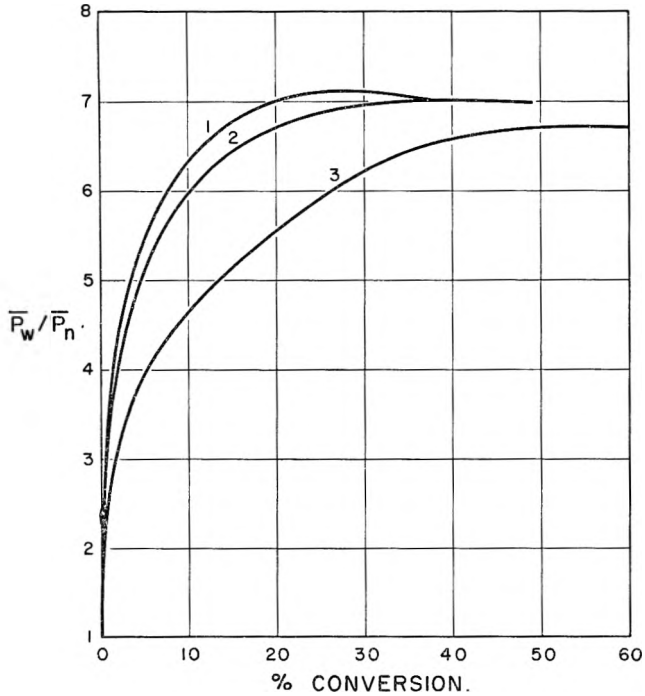

Fig. 4.—Calculated variation of the heterogeneity index during a styrene polymerization at 60° for varying concentrations of initiator (1, 0.0009 mole/l.; 2, 0.0016 mole/l.; 3, 0.0030 mole/l.) including transfer to monomer.

increase of polymer (W_i) and the $\bar{P}_{wi}$ of this fraction summed over all times

$$\bar{P}_w(\text{cumulative}) = \sum_i W_i \bar{P}_{wi} \qquad (7)$$

where $W_i = \dfrac{-d[M]}{[M]_0 - [M]}$ and $\bar{P}_{wi} = 1.5\bar{P}_{ni}$

$\bar{P}_{ni}$ is defined by the differential form of eq. 4

$$\bar{P}_{ni} = \frac{d[M]/dt}{f\dfrac{d[cat]}{dt} + C_{Tm}\dfrac{d[M]}{dt}} \qquad (8)$$

$$\therefore \bar{P}_{wi} = \frac{1.5d[M]/dt}{f\dfrac{d[cat]}{dt} + C_{Tm}\dfrac{d[M]}{dt}} \qquad (9)$$

or

$$\bar{P}_w(\text{cumulative}) = \int_{[M]}^{[M]_0} \frac{+d[M]}{([M]_0 - [M])} \left[\frac{1.5d[M]/dt}{f\dfrac{d[cat]}{dt} + C_{Tm}\dfrac{d[M]}{dt}}\right] \qquad (10)$$

Substituting the appropriate expressions for the rate of change in monomer and catalyst (found in ref. 1) and rearranging, one obtains an expression which can be integrated by increments

$$\bar{P}_w = \int_0^x \frac{1.5\,dx}{\left[\dfrac{f^{1/2}k_d^{1/2}k_t^{1/2}[cat]_0^{1/2}\exp -k_d t/2}{k_p[M]_0(1-x)} + C_{Tm}\right]x} \qquad (11)$$

where $x = ([M]_0 - [M])/[M]_0$, and 1.5 may be replaced by y, equation in footnote 7, for a more accurate treatment.

If the kinetic constants for a particular monomer–initiator system are known at a given temperature, the cumulative $\bar{P}_n$ and $\bar{P}_w$ at any time during the polymerization can be calculated from eq. 4 and 11.

Results and Discussion

Polymerization of Styrene.—Equations 4 and 11 were applied to the case of styrene initiated by azo-1, the kinetic constants used being listed in Table I. The variations of $\bar{P}_n$ and $\bar{P}_w$ with degree of conversion were calculated for three catalyst concentrations at a temperature of 60° and are shown in Fig. 1 and 2. The influence of chain transfer to monomer is shown by the calculation of $\bar{P}_n$ and $\bar{P}_w$ with and without the inclusion of chain transfer. The ratios of $\bar{P}_w$ to $\bar{P}_n$ (the heterogeneity index, H.I.) throughout the polymerization were determined as a function of per cent conversion and are shown in Fig. 3 and 4.

Table I

Rate Constants for the Polymerization of Styrene by Azo-1 at 60°

	Reference
$f = 0.60$	*a*
$k_d = 9.7 \times 10^{-6}$/sec.	*b*
$k_p/k_t^{1/2} = 0.0341$	*c*
$C_{Tm} = 6 \times 10^{-5}$	*d*
$[M]_0 = 8.03$	

[a] J. P. Van Hook and A. V. Tobolsky, *J. Polymer Sci.*, **33**, 429 (1958). [b] J. P. Van Hook and A. V. Tobolsky, *J. Am. Chem. Soc.*, **80**, 779 (1958). [c] See ref. 2. [d] D. H. Johnson and A. V. Tobolsky, *J. Am. Chem. Soc.*, **74**, 938 (1952).

The main interest in calculating $\bar{P}_n$ and $\bar{P}_w$ is to observe their variation as the polymerization proceeds. Initially, $\bar{P}_n$ remains practically constant while $\bar{P}_w$ increases. In the later stages of polymerization, the

rate of increase of $\bar{P}_n$ is accelerated while that of $\bar{P}_w$ becomes relatively constant.

From the figures representing $\bar{P}_n$, $\bar{P}_w$, and H.I., it is evident that a small amount of chain transfer to monomer has an important effect on $\bar{P}_n$ and $\bar{P}_w$, but that the H.I. remains relatively unaffected. Although the general shapes of the $\bar{P}_n$ and $\bar{P}_w$ *vs.* per cent conversion curves are not altered by chain transfer, its inclusion lowers them considerably. This effect is most apparent at low catalyst concentrations.

To observe the effect of temperature on the variation of $\bar{P}_n$ and $\bar{P}_w$, a few calculations were made for polymerization of styrene at 100°. While larger rates of increase in both $\bar{P}_n$ and $\bar{P}_w$ were indicated, a limiting value for H.I. of 5.0 was found. These considerations are merely qualitative, however, since styrene undergoes appreciable thermal polymerization at this temperature,[8] the effect of which was assumed to be negligible in these calculations.

Polymerization of Isoprene.—The kinetic constants for the bulk polymerization of isoprene at various temperatures have been determined recently using the dead-end polymerization theory.[9] Using these kinetic constants (Table II) and applying the expressions developed in this paper, the cumulative number and weight average degrees of polymerization were computed for isoprene at 80° assuming no chain transfer to monomer. The calculated values for $\bar{P}_n$, $\bar{P}_w$, and H.I. are listed in Table III.

(8) R. F. Boundy and R. F. Boyer, Ed. "Styrene, Its Polymers, Copolymers and Derivatives," Reinhold Publ. Corp., New York, N. Y., 1952, p. 218.

(9) R. H. Gobran, M. B. Berenbaum, and A. V. Tobolsky, *J. Polymer Sci.*, **46**, 431 (1960).

TABLE II

RATE CONSTANTS[a] FOR THE POLYMERIZATION OF ISOPRENE BY AZO-1 AT 80°

$f = 0.60$
$k_d = 1.0 \times 10^{-4}$/sec.
$k_p/k_t^{1/2} = 1.1 \times 10^{-2}$
$M_0 = 10$

[a] See ref. 9.

TABLE III

HETEROGENEITY INDEX IN THE POLYMERIZATION OF ISOPRENE

Fractional conv.	Cum. $\bar{P}_w$	Cum. $\bar{P}_n$	H.I.
0.02	97.5	58.4	1.67
.06	184.8	60.1	3.07
.10	238.5	62.2	3.83
.14	281.0	69.3	4.05
.18	320.5	75.5	4.25
.22	363.3	82.3	4.41
.24	389.1	86.4	4.50
.26	421.4	91.2	4.62
.28	468.9	96.7	4.75

The technique suggested in this study might well be used to prepare polymers of desired molecular weight and molecular weight distribution. However, one should bear in mind that at the onset of diffusion controlled termination[3,4] these theoretical calculations become inaccurate; hence, a polymerization should be quenched before this effect becomes dominant.

Acknowledgment.—The partial support of the Army Research Office (Durham) and the Goodyear Tire and Rubber Company is gratefully acknowledged.

VOLUME CHANGES ON MIXING SOLUTIONS OF SODIUM CHLORIDE, HYDROCHLORIC ACID, SODIUM PERCHLORATE, AND PERCHLORIC ACID AT CONSTANT IONIC STRENGTH. A TEST OF YOUNG'S RULE[1]

BY HENRY E. WIRTH, RICHARD E. LINDSTROM, AND JOSEPH N. JOHNSON

Department of Chemistry, Syracuse University, Syracuse 10, New York

Received May 1, 1963

The volume changes on mixing two solutions of equal ionic strength were determined for the six possible combinations of the four electrolytes, NaCl, HCl, $NaClO_4$, and $HClO_4$, at two concentrations, 1.000 and 4.1724 *m*. A dilatometer capable of measuring volume changes to $\pm 1 \times 10^{-4}$ ml. in a total volume of 100–300 ml. was used. It was found that the volume change on mixing two heteroionic electrolytes (NaCl and $HClO_4$, or $NaClO_4$ and HCl) could be calculated from the volume changes observed in homoionic solutions. In the most unfavorable case the mean apparent volume calculated by Young's rule is in error by 0.6 ml. (2%), and the corresponding density is in error by only 0.2%.

The mean apparent molal volume of a mixture of electrolytes (Φ) is defined by

$$\Phi = \frac{V - 55.51\bar{v}_1^\circ}{m_2 + m_3} \qquad (1)$$

where V is the volume of solution containing 1000 g. of water, $\bar{v}_1^\circ$ is the molar volume of pure water, and m_2 and m_3 are the molalities of the two electrolytes. Young and Smith[2] have shown that their mixture rule

$$\Phi = \frac{m_2\phi_2 + m_3\phi_3}{m_2 + m_3} \qquad (2)$$

accurately represents data for KCl–NaCl,[3] KBr–NaCl,[3] and $NaClO_4$–$HClO_4$[4] mixtures. In eq. 2, ϕ_2 is the apparent molal volume of one of the electrolytes in a solution containing only water and this electrolyte at an ionic strength μ_w corresponding to $m_2 + m_3$, and ϕ_3 is the apparent molal volume of the other electrolyte in a binary solution at this same ionic strength. A

(1) Presented in part at the 144th National Meeting of the American Chemical Society, Los Angeles, Calif., April, 1963.

(2) T. F. Young and M. B. Smith, *J. Phys. Chem.*, **58**, 716 (1954).

(3) H. E. Wirth, *J. Am. Chem. Soc.*, **59**, 2549 (1937).

(4) H. E. Wirth and F. N. Collier, Jr., *ibid.*, **72**, 5292 (1950).

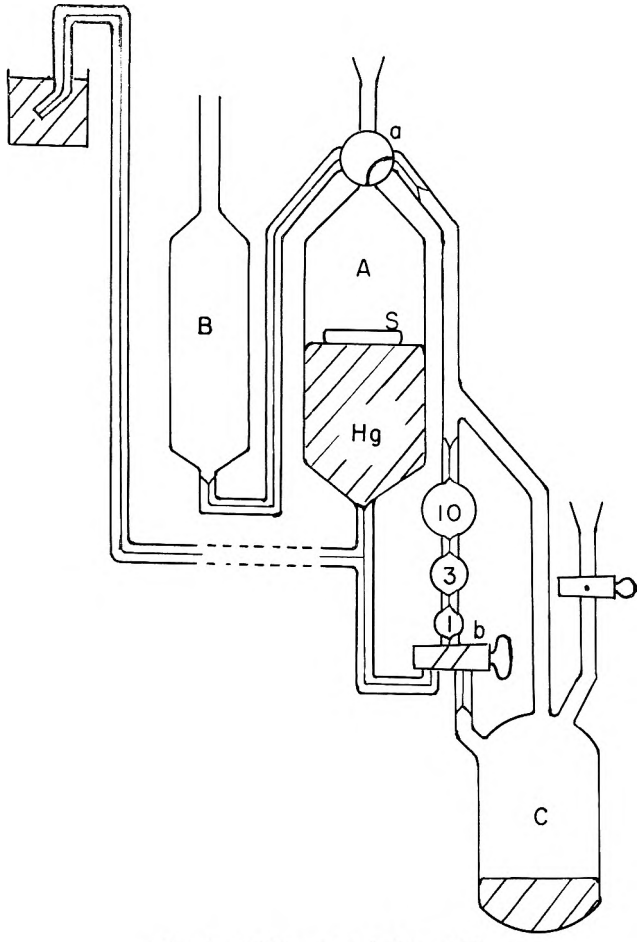

Fig. 1.—Dilatometer (schematic).

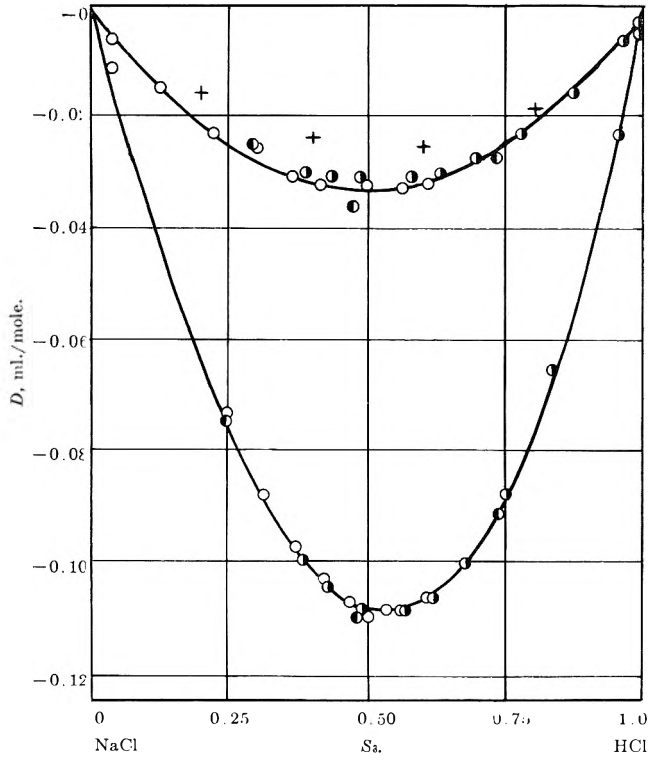

Fig. 2.—Volume change on mixing equimolal solutions of NaCl and HCl: upper curve, 1.000 m; lower curve 4.172 m.

small correction term D has to be added to eq. 2 to give complete agreement for NaCl–HCl[5] mixtures. The suggested form of D is $S_2S_3\mu_wK$, where $S_2 = m_2/(m_2 + m_3)$ and $S_3 = m_3/(m_2 + m_3)$.

(5) H. E. Wirth, *J. Am. Chem. Soc.*, **62**, 1128 (1940).

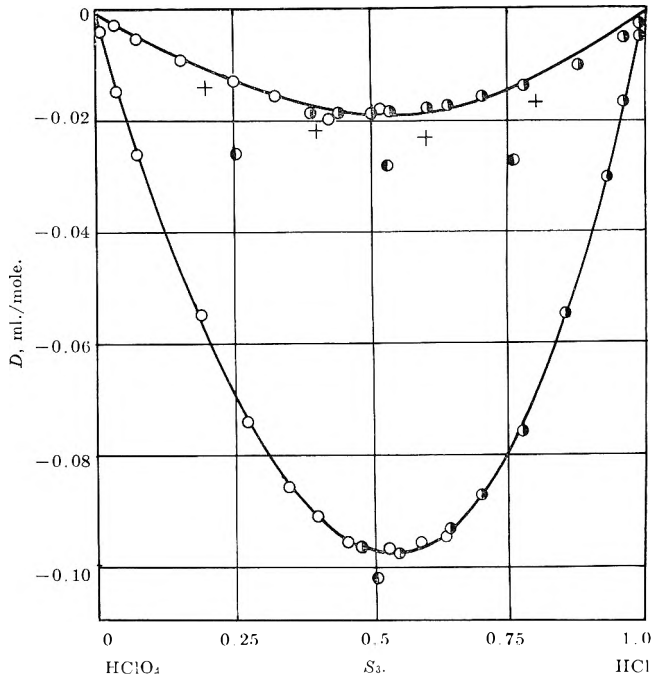

Fig. 3.—Volume changes on mixing equimolal solutions of $HClO_4$ and HCl: upper curve, 1.000 m; lower curve, 4.172 m.

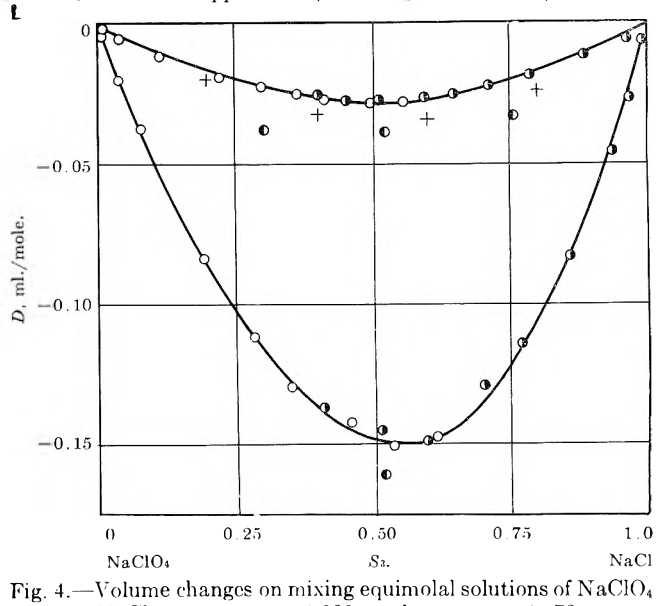

Fig. 4.—Volume changes on mixing equimolal solutions of $NaClO_4$ and NaCl: upper curve, 1.000 m; lower curve 4.172 m.

One consequence of Young's unmodified rule is that there should be no change in volume on mixing solutions of equal ionic strength. Since such information can be obtained from the data in the literature only by interpolation it was felt desirable to make a direct test of this prediction.

Experimental

Materials and Apparatus.—Stock solutions of NaCl, HCl, $NaClO_4$, and $HClO_4$ were prepared from C.P. chemicals. The concentrations of the salt solutions were determined by evaporating weighed portions to dryness and heating at 350–400°. The acid solutions were analyzed by weight titration methods previously described[5] using constant boiling HCl as the reference standard. Solutions exactly 1.000 and 4.1725 m were prepared by weight dilution of the stock solutions.

Volume changes on mixing solutions of equal ionic strength were determined using a dilatometer (Fig. 1) similar to that described by Geffcken, Kruis, and Solana.[6] About 100 ml. of one

(6) W. Geffcken, A. Kruis and L. Solana, *Z. physik. Chem.* (Leipzig), **B35**, 317 (1937).

solution was introduced from bulb E into A (volume 350 ml.) through the four-way stopcock a. The amount introduced was determined by weighing the mercury displaced through the capillary tube at the left of the apparatus. A second solution filled the bulb C and all connecting tubing. Stopcock b was opened to the position shown and mercury from A displaced the second solution into the first through a. The bulbs permitted the addition of 1, 4, or 14 ml. of the second solution and were calibrated by weighing the mercury required to fill them to reference marks on the connecting capillary tubing. After addition of the second solution, the solution in A was thoroughly mixed by the magnetic stirrer S. Any volume change was reflected by an increase or decrease in weight of mercury in a weighing bottle around the capillary tip. Weight changes were determined to ±1 mg., corresponding to a volume change of $\pm 1 \times 10^{-4}$ ml. Stopcock b was turned to permit the mercury in the bulbs to flow into the bottom of C, and more of the second solution could be added. The pressure at the capillary tip was adjusted in order to keep the pressure on the solution in A constant. The apparatus was immersed in a thermostat at a temperature of 25° maintained constant to ±0.0005°.

The volume of the first solution $V_2 = n_1\bar{v}_1^\circ + n_2\phi_2$, where n_1 is the number of moles of water, n_2 is the number of moles of electrolyte, and ϕ_2 is its apparent molal volume in this solution. The volume of the second solution $V_3 = n_1'\bar{v}_1^\circ + n_3\phi_3$. The total volume V is $V_2 + V_3 + \Delta v$, where Δv is the observed change in volume on mixing.

By definition, the mean apparent molal volume $\Phi = (V - n_1''\bar{v}_1^\circ)/(n_2 + n_3)$, where $n_1'' = n_1 + n_1'$. Substituting, $\Phi = (n_2\phi_2 + n_3\phi_3)/(n_2 + n_3) + \Delta v/(n_2 + n_3)$. The first term is Young's rule, and $D = \Delta v/(n_2 + n_3)$.

Values of ϕ_2 and ϕ_3 were determined by direct density measurements using the sinker method.[4] A few values of D were obtained by direct density determination on mixed solutions.

Results and Discussion

Results obtained are given in Fig. 2 through 7. In these figures open circles (○) designate points obtained by adding solution 1 to solution 2, while points labeled ◑ were obtained by adding solution 2 to solution 1. Overlap of these points near a mole fraction of 0.5 indicates the reproducibility of the experimental procedure. Points labeled ◐ were obtained by direct density measurements and are generally in good agreement with the dilatometer values, although they are much more sensitive to experimental error. Points marked + are calculated for a 1 *m* solution from the values in 4.17 *m* solution, assuming D is linearly dependent on μ_w.

Tables I and II give the constants for the equations which represent the experimental results in 1.0 and 4.17 *m* solutions for the six possible mixtures. The results in 4.17 *m* solution had to be represented by the relation $D = kS_2S_3 + k'S_2^2S_3$, since in all cases D was not symmetric around a mole fraction of 0.5. In the $NaClO_4$–$HClO_4$ mixture the maximum value of D was at mole fraction 0.61 of $HClO_4$. In 1.0 *m* solution the data could be adequately represented by the expression $D = kS_2S_3$, although there were some indications that the curves are not completely symmetrical.

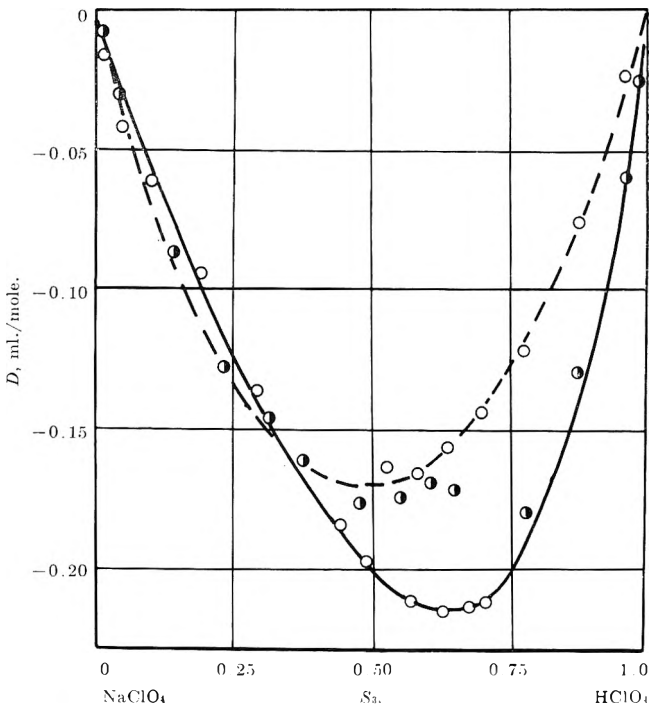

Fig. 5.—Volume changes on mixing equimolal solutions of $NaClO_4$ and $HClO_4$: dashed curve, 1.000 *m*; solid curve 4.172 *m*.

TABLE I

RESULTS FOR 1 *m* SOLUTION

$D = kS_2S_3$

Electrolyte pair				
Y_2	Y_3	k	Av. dev., ml./mole	$D_{0.5}$, ml./mole
HCl	$HClO_4$	−0.0744	±0.0008	−0.0186
NaCl	HCl	− .1290	± .0009	−0.0323
$NaClO_4$	$HClO_4$	− .0686	± .0005	−0.0172
NaCl	$NaClO_4$	− .1087	± .0004	−0.0272
			$\Sigma\square$ =	−0.0953
$NaClO_4$	HCl	− .8150	± .0016	−0.2038
NaCl	$HClO_4$	+ .4251	± .0017	+0.1063
			ΣX =	−0.0975
			Difference =	0.3101

$1/2(\phi_{NaClO_4} + \phi_{HCl} - \phi_{NaCl} - \phi_{HClO_4}) = 1/2R = 0.307$

TABLE II

RESULTS FOR 4.17 *m* SOLUTION

$D = kS_2S_3 + k'S_2^2S_3$

Y_2	Y_3	k	k'	Av. dev., ml./mole	$D_{0.5}$, ml./mole
HCl	$HClO_4$	−0.3270	−0.1250	±0.0007	−0.0974
NaCl	HCl	− .5071	+ .1466	± .0004	−0.1085
$NaClO_4$	$HClO_4$	− .1228	+ .0813	± .0008	−0.0205
NaCl	$NaClO_4$	− .4805	− .2256	± .0012	−0.1483
				$\Sigma\square$ =	−0.3747
$NaClO_4$	HCl	−2.7810	+ .3859	± .0019	−0.6470
NaCl	$HClO_4$	+1.4907	− .6944	± .0027	+0.2859
				ΣX =	−0.3611
				Difference =	0.9329

$1/2(\phi_{NaClO_4} + \phi_{HCl} - \phi_{NaCl} - \phi_{HClO_4}) = 1/2R = 0.922$

TABLE III

CONSTANTS FOR THE EQUATIONS: $k = \alpha\mu_w + \beta\mu_w^2$ AND $k' = \gamma\mu_w^2$

Electrolyte pair				
Y_2	Y_3	α	β	γ
HCl	$HClO_4$	−0.0731	−0.0013	−0.0072
NaCl	HCl	− .1314	+ .0024	+ .0084
$NaClO_4$	$HClO_4$	− .0809	+ .0123	+ .0047
NaCl	$NaClO_4$	− .1067	− .0020	− .0130
$NaClO_4$	HCl	− .8618	+ .0468	+ .0222
NaCl	$HClO_4$	+ .4465	− .0214	− .0399

While this work is primarily concerned with the deviations from Young's rule, it should be emphasized that these deviations are small, and that the rule gives a remarkably good first approximation. For example, the maximum contraction observed on mixing 500 ml. of a 1 *m* solution with 500 ml. of another 1 *m* solution containing a common ion is 0.03 ml., or about 0.1% error in the value of the mean apparent molal volume.

TABLE IV

CONSTANTS FOR THE EQUATION:

$$\phi = a + b\mu_w^{1/2} + c\mu_w + d\mu_w^{3/2} + e\mu_w^2$$

Electrolyte	a	b	c	d	e	Av. dev. $\phi_{obsd} - \phi_{calcd.}$, ml./mole
NaCl	16.6516	1.72081	0.00831	0.15844	−0.05266	±0.010
HCl	17.8479	1.78964	−1.11531	.56722	− .10709	± .021
$HClO_4$	44.2441	0.87571	−0.74702	.18627	− .02715	± .010
$NaClO_4$	42.9242	1.94690	− .43780	.39198	− .09914	± .008

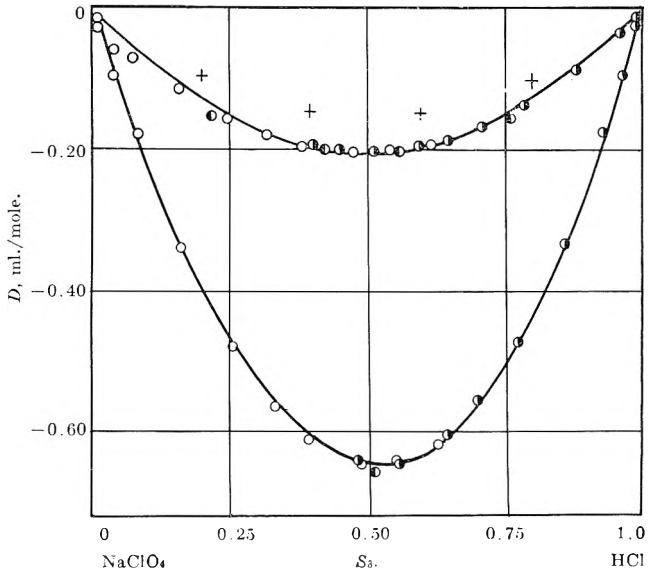

Fig. 6.—Volume changes on mixing equimolal solutions of $NaClO_4$ and HCl: upper curve, 1.000 m; lower curve, 4.172 m.

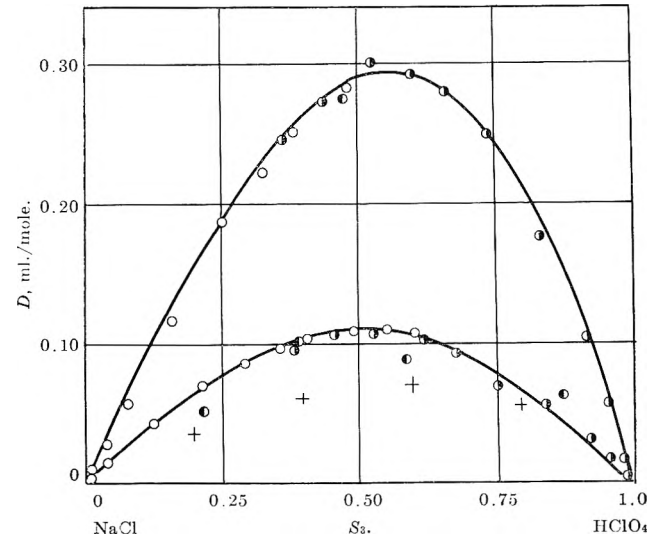

Fig. 7.—Volume changes on mixing equimolal solutions of NaCl and $HClO_4$: upper curve, 4.124 m; lower curve, 1.000 m.

Only in heteroionic solutions or at high concentrations are the deviations larger than the errors in the equations representing the apparent molal volumes of pure salts (Table IV).

If we consider the array

$$\begin{array}{ccc} NaClO_4 & \longleftrightarrow & HClO_4 \\ \uparrow\downarrow & \nearrow\swarrow & \uparrow\downarrow \\ NaCl & \longleftrightarrow & HCl \end{array}$$

similar to that used by Young, Wu, and Krawetz[7] in discussing results on the heats of mixing of homoionic and heteroionic solutions, it was found that in 1 m solution (Table I) the sum of the deviations ($D_{0.5}$) on mixing the four pairs of homoionic solutions to give 50–50 mixtures ($\Sigma\square$) was equal to the sum of the deviations on mixing the two pairs of heteroionic solutions (ΣX) within the experimental error. In 4.17 m solution ($\Sigma\square - \Sigma X$) = −0.0135 ml./mole (Table II). This difference is considered to be outside the experimental error and could be due to different degrees of ionization of the perchloric acid in the presence of various salts.

Except at infinite dilution the apparent molal volumes of electrolytes are not additive functions of the apparent ionic volumes. For the set of four electrolytes, NaCl, HCl, $NaClO_4$, and $HClO_4$, the net departure from additivity (R) is given by $R = \phi_{NaClO_4} + \phi_{HCl} - \phi_{NaCl} - \phi_{HClO_4}$, and for purposes of calculation can be attributed to one of the electrolytes, *i.e.*, $HClO_4$. At a given ionic strength, the apparent molal volumes of the electrolytes are then given by $\phi_{NaCl} = \phi_{Na} + \phi_{Cl}$, $\phi_{HCl} = \phi_H + \phi_{Cl}$, $\phi_{NaClO_4} = \phi_{Na} + \phi_{ClO_4}$, and $\phi_{HClO_4} = \phi_H + \phi_{ClO_4} - R$, where ϕ_H, ϕ_{Na}, ϕ_{Cl}, and ϕ_{ClO_4} are the apparent ionic volumes of the ions. The mean apparent molal volume of a mixture containing equal concentrations of all four ions as calculated by the unmodified Young's rule for the electrolyte pair HCl–$NaClO_4$ is $1/2(\phi_H + \phi_{Cl} + \phi_{Na} + \phi_{ClO_4})$ and is $1/2(\phi_{Na} + \phi_{Cl} + \phi_H + \phi_{ClO_4} - R)$ for the pair NaCl–$HClO_4$. The difference between these two calculated values is $0.5R$ and is equal to the algebraic difference between the observed D values for the 50–50 mixtures for HCl–$NaClO_4$ and NaCl–$HClO_4$ (Tables I and II).

On the basis of these relationships it is possible to design a synthetic equation which will represent the mean apparent molal volumes for all possible combinations of the four electrolytes, using the constants obtained experimentally for the four homoionic pairs. In 4.17 m solution this equation is

$$\begin{aligned}\Phi = {} & S_{Na}(\phi_{Na} + S_{Cl}S_{ClO_4}k_{Na} + S^2_{Cl}S_{ClO_4}k'_{Na}) + \\ & S_H(\phi_H - S_{ClO_4}R + S_{Cl}S_{ClO_4}k_H + S^2_{Cl}S_{ClO_4}k'_H) + \\ & S_{Cl}(\phi_{Cl} + S_{Na}S_Hk_{Cl} + S^2_{Na}S_Hk'_{Cl}) + \\ & S_{ClO_4}(\phi_{ClO_4} + S_{Na}S_Hk_{ClO_4} + S^2_{Na}S_Hk'_{ClO_4}) \quad (3)\end{aligned}$$

where $S_{Na} = m_{Na}/(m_{Na} + m_H)$, $S_{Cl} = m_{Cl}/(m_{Cl} + m_{ClO_4})$, etc., and k_{Na} and k'_{Na} are observed values of k and k' for the pair NaCl–$NaClO_4$ with sodium as the common cation, k_{Cl} and k'_{Cl} are for the pair NaCl–HCl with chloride as the common anion, etc.

If this equation is rearranged to represent NaCl–$HClO_4$ mixtures by setting $S_{Na} = S_{Cl} = S_{NaCl}$ and $S_H = S_{ClO_4} = S_{HClO_4}$, it becomes

(7) T. F. Young, Y. C. Wu, and A. A. Krawetz, *Discussions Faraday Soc.*, **24**, 78 (1957).

$$\Phi = S_{NaCl}\phi_{NaCl} + S_{HClO_4}\phi_{HClO_4} + S_{NaCl}S_{HClO_4}(k_H + k_{ClO_4} + R) + S^2_{NaCl}S_{HClO_4}(k_{Na} + k_{Cl} - k_H - k_{ClO_4} + k'_{Na} + k'_{Cl}) + S^2_{NaCl}S^2_{HClO_4}(k'_H + k'_{ClO_4} - k'_{Na} - k'_{Cl}) \quad (4)$$

The value of D calculated from eq. 4 agrees with the observed data for this mixture (Fig. 4) with an average deviation of ±0.0047 ml./mole In a 50–50 mixture

$$D_{0.5} = +0.25R + 0.125\Sigma k + 0.0625\Sigma k'$$

Rearranged to represent $NaClO_4$–HCl mixtures by setting $S_{Na} = S_{ClO_4} = S_{NaClO_4}$ and $S_H = S_{Cl} = S_{HCl}$ eq. 3 becomes

$$\Phi = S_{NaClO_4}\phi_{NaClO_4} + S_{HCl}\phi_{HC} + S_{NaClO_4}S_{HCl}(k_H + k_{Cl} + k'_H - R) + S^2_{NaClO_4}S_{HCl}(k_{Na} + k_{ClO_4} - k_H - k_{Cl} - k'_H + k'_{ClO_4}) + S^2_{NaClO_4}S^2_{HCl}(k'_{Na} + k'_{Cl} - k'_H - k'_{ClO_4}) \quad (5)$$

For this system the average deviation ($D_{calcd} - D_{obsd}$) is ±0.0044 ml./mole in 4.17 m solution. This is only twice the deviation found with the empirical equation (Table II). In a 50–50 mixture

$$D_{0.5} = -0.25R + 0.125\Sigma k + 0.0625\Sigma k'$$

The sum of these two $D_{0.5}$ values (ΣX) is $0.25\Sigma k + 0.125\Sigma k'$ and is equal to $\Sigma\square$. The difference is $0.5R$.

In one molal solution the synthetic equation represents the data for NaCl–$HClO_4$ mixtures with an average deviation of +0.0017 ml./mole, and the data for $NaClO_4$–HCl mixtures with an average deviation of ±0.0016 ml./mole. The synthetic equations which contain only the arbitrary constants derived from data on homoionic systems represent the results on heteroionic systems as well as does the empirical equation. The mixing of four ions therefore involves no interactions not already taken into account in mixtures containing three ions.

Comparison with Previous Results.—In order to compare the results obtained here with data in the literature, it is necessary to make some assumption as to the dependence of k and k' on the ionic strength. It was assumed that $k = \alpha\mu_w + \beta\mu_w^2$ and $k' = \gamma\mu_w^2$. The values of α, β, and γ are given in Table III.

The apparent molal volumes of the pure salts were represented by equations of the form $\phi = a + b\mu_w^{1/2} + c\mu_w + d\mu_w^{3/2} + e\mu_w^2$. The constants given in Table IV for the electrolytes investigated are based on the original data for HCl,[5] NaCl,[5] $HClO_4$,[4] and $NaClO_4$[4] solutions, except that the data of Redlich and Bigeleisen[8] were used for dilute HCl solutions. It should be emphasized that these equations are valid only for interpolation between 0.04 and 4 m. Values of ϕ° are best obtained by extrapolation of equations involving volume concentrations and the theoretical limiting slope.[9]

Values of Φ were calculated from the original data on HCl–NaCl[5] and $NaClO_4$–$HClO_4$[4] mixtures, and compared with those calculated from the equation

$$\Phi = S_2\phi_2 + S_3\phi_3 + S_2S_3(\alpha\mu_w + \beta\mu_w^2) + S_2^2S_3\gamma\mu_w^2 \quad (6)$$

(8) O. Redlich and J. Bigeleisen, *J. Am. Chem. Soc.*, **64**, 758 (1942); *cf.* also ref. 1, p. 721.

(9) O. Redlich, *J. Phys. Chem.*, **67**, 496 (1963).

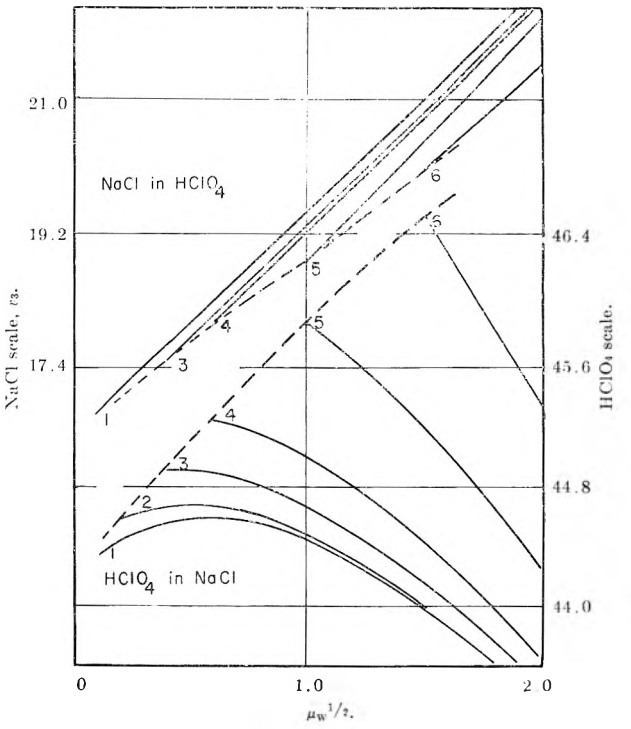

Fig. 8.—Partial molal volumes of NaCl in $HClO_4$ solution and $HClO_4$ in NaCl solution as a function of the ionic strength: curve 1, $\bar{v}_3$ of the electrolyte in pure water; curves 2 to 6, $\bar{v}_3$ of one electrolyte in 0.04, 0.16, 0.36, 1.0, and 2.25 m solutions of the other electrolyte; dashed curves are the partial molal volumes of one electrolyte in a solution containing only the other electrolyte (note that the $HClO_4$ scale is twice that for NaCl).

The average deviation was found to be ±0.012 ml./mole (max. dev. 0.054) for HCl–NaCl mixtures, and ±0.015 ml./mole (max. dev. 0.087) for $NaClO_4$–$HClO_4$ mixtures.

Partial Molal Volumes.—If eq. 1 and 6 are combined, and solved for V, differentiation with respect to m_2 or m_3 gives the partial molal volumes $\bar{v}_2$ and $\bar{v}_3$

$$\bar{v}_2 = \phi_2 + \frac{m_2}{2\mu_w^{1/2}}\left(\frac{d\phi_2}{d\mu_w^{1/2}}\right) + \frac{m_3}{2\mu_w^{1/2}}\left(\frac{d\phi_3}{d\mu_w^{1/2}}\right) + m_3\alpha + 2m_2m_3(\beta + \gamma) + m_3^2\beta \quad (7)$$

and

$$\bar{v}_3 = \phi_3 + \frac{m_2}{2\mu_w^{1/2}}\left(\frac{d\phi_2}{d\mu_w^{1/2}}\right) + \frac{m_3}{2\mu_w^{1/2}}\left(\frac{d\phi_3}{d\mu_w^{1/2}}\right) + m_2\alpha + 2m_2m_3\beta + m_2^2(\beta + \gamma) \quad (8)$$

These equations are valid only for uni-univalent electrolytes. The values obtained are in agreement with those previously calculated for NaCl–HCl and $NaClO_4$–$HClO_4$ mixtures with an average deviation of ±0.025 ml./mole, except for the NaCl in 4 m solution. It is felt that the equation for HCl (Table IV) yields the incorrect slope in 4 m solution, since no experimental points at concentrations greater than 4 m were used in obtaining the equation.

These equations were also used to calculate the partial molal volumes of the four other combinations of electrolytes. The results for the pair NaCl–$HClO_4$ are given in Fig. 8. In this combination the two slopes ($d\phi/d\mu_w^{1/2}$) differ by the largest amount, and the deviation terms are also larger than for any of the electrolyte pairs investigated.

The original observation[3] that the partial molal

volume of a salt depends only on the total ionic strength of the solution is valid only if $d\phi_2/d\mu_w^{1/2} = d\phi_3/d\mu_w^{1/2}$, and α, β, and γ are negligible. In this case eq. 8 reduces to: $\bar{v}_3 = \phi_3 + (\mu^{1/2}/2)(d\phi_3/d\mu_w^{1/2})$, and $\bar{v}_3$ is independent of the value of m_2. In some cases the correction terms partially compensate for the difference in slopes for one member of the pair of electrolytes. For example, in 1*m* solution the partial molal volume of NaCl is 19.49 ml. in pure NaCl and 19.30 ml. in pure $NaClO_4$ solution, while the partial molal volume of $NaClO_4$ is 45.65 ml. in pure $NaClO_4$ and 45.61 in pure NaCl solution. In 4.17 *m* solution the corresponding values for NaCl are 22.52 and 21.82 ml.; for $NaClO_4$, they are 48.34 and 47.92 ml.

Choice of Variable.—Before beginning this work, the possibility was considered that there would be smaller deviations from Young's rule if molar rather than molal concentrations were used. Preliminary experiments using direct density measurements indicated that the volume contractions on mixing two solutions of equal molarity were of the same order of magnitude as in mixing solutions of equal molality. Since such contractions do occur, the resulting solution no longer has the same molarity as the components and further corrections would be required. For practical reasons, molal concentrations were used.

With the aid of eq. 6 it is possible to calculate by an iterative procedure the deviations between the value of Φ at a given volume concentration and that calculated from Young's rule using volume concentrations. For example, in a 50–50 mixture of NaCl and HCl, where the total molarity is 3.8317, the calculated deviation is −0.110 ml./mole, or almost exactly the same as for 4.1724 *m* solutions. (A molarity of 3.8317 corresponds to *m* = 4.1724 in pure NaCl and *m* = 4.1586 in pure HCl.)

For a $NaClO_4$–$HClO_4$ mixture at a molarity of 3.4841 (corresponding to 4.1724 *m* $NaClO_4$ and 4.1268 *m* $HClO_4$), the deviation is −0.027 ml./mole for a 50–50 mixture, which is a third larger than for equimolal solutions, but the deviations were more nearly symmetrical about a mole fraction of 0.5 (maximum near 0.57 mole fraction of $HClO_4$).

Calculation of Density.—The density of a solution containing any possible combination of the four electrolytes, NaCl, HCl, $NaClO_4$, and $HClO_4$, can be obtained at 25° in the range 0–4 *m* by use of the equation

$$d = \frac{1000 + (m_2M_2 + m_3M_3 + \ldots)}{1002.93 + (m_2 + m_3 + \ldots)\Phi}$$

If Φ is evaluated by Young's unmodified rule, using eq. 2 and the constants in Table IV, the maximum error in the density in a most unfavorable case (a 50–50 mixture of $NaClO_4$–HCl in 4 *m* solution) would be about 2 parts per 1000. If eq. 6 with the constants in Tables III and IV is used to evaluate Φ, then the maximum error would be of the order of 2 parts in 10,000 (0.02%).

Acknowledgment.—The authors wish to thank Mr. Jeffrey Greenhouse for preparing the computer program for many of the calculations. This work was supported in part by the National Science Foundation, Grant G-14623.

ADSORPTION FROM SOLUTION. III. DERIVATIVES OF PYRIDINE, ANILINE, AND PYRROLE ON ALUMINA

BY L. R. SNYDER

Union Oil Company of California, Union Research Center, Brea, California

Received May 3, 1963

Linear isotherm free energies of adsorption from *n*-pentane onto 3.6% H_2O–Al_2O_3 are reported for 66 nitrogen compounds related to pyridine, aniline, or pyrrole. A previously developed theoretical model permits the calculation of the nitrogen group adsorption energy for each adsorbate, free from the "normal" contributions to total adsorption energy by other adsorbate groups. It is concluded that the nitrogen group in the pyridines and anilines adsorbs with n-electron transfer to an adsorbent site, while the pyrrole nitrogen group adsorbs with proton transfer to the alumina surface. The localization or anchoring of strongly adsorbing adsorbate groups on the adsorbent surface is also discussed.

Introduction

Recent communications[1–3] have drawn attention to certain regularities in the adsorption on alumina of the substituted pyridines and related aza aromatics. The contribution of the nitrogen atom in these adsorbates to total adsorption energy is markedly sensitive to the steric environment about the nitrogen atom, adsorption energy decreasing with increased crowding of the nitrogen. This observation has led Klemm[2] to postulate that the nitrogen atom(s) in the less crowded aza aromatics serves as an "anchoring" group (a concept first introduced by Zechmeister[4]), with the remainder of the adsorbate only loosely attached to the adsorbent surface. The sensitivity of the nitrogen atom adsorption energy to crowding by adjacent substituent groups is regarded by Klemm as resulting from the interference by such groups to a preferred tilted or edgewise configuration of the adsorbate relative to the plane of the adsorbent surface (presumably for optimum interaction of nitrogen and surface site). Klemm also has proposed that the interaction between nitrogen and adsorbent is the result of charge-transfer complex formation involving the nitrogen n electrons, on the basis of spectral evidence for the greater polarizability of the nitrogen n electrons and by analogy with the previously postulated[5] π-complexation of aromatic hydrocarbons adsorbed on alumina.

A previous study of the variation of adsorption energy

(1) L. R. Snyder, *J. Chromatog.*, **6**, 22 (1961).
(2) L. H. Klemm, E. P. Antoniades, G. Capp, E. Chiang, and E. Y. K. Mak, *ibid.*, **6**, 420 (1961).
(3) L. R. Snyder, *ibid.*, **8**, 319 (1962).
(4) L. Zechmeister, *Discussions Faraday Soc.*, **7**, 54 (1949).

on alumina with adsorbate structure[3] appears to verify the concept of an anchoring group in adsorbates possessing sufficiently strongly adsorbing groups. It was shown that adsorbates with no strongly adsorbing groups have adsorption energies which are the simple sum of adsorbate group contributions (*i.e.*, no anchoring). In the case of adsorbates with one or more strongly adsorbing groups, anchoring or "localization" of the strongest adsorbate group k occurs, and the resultant "delocalization" of remaining adsorbate groups (from a "normal" semilocalized or localized state) decreases their individual contributions to adsorbate adsorption energy. Reduction in adsorption energy of the delocalized groups i becomes appreciable at a threshold value of the adsorption energy of k (corresponding to the onset of localization of k), increases with further increase in the adsorption energy of k, and finally levels off at a constant factor when the adsorption energy of k has increased to about four times the threshold value (corresponding to complete localization of k). This localization or anchoring behavior is typical both of the anilines and pyridines, as well as of other anchoring groups k (*e.g.*, nitro, acetyl, etc.).

While the anchoring group postulate of Klemm and Zechmeister thus appears in agreement with the adsorption of the aza aromatics and other strongly adsorbing compounds, the configuration of the "anchored" adsorbate is more equivocal. Solvent variations tudies[3,6] suggest that the aza-aromatics and other compounds are adsorbed parallel (flat) to the adsorbent surface, rather than tilted or perpendicular. Similarly, analysis of the adsorption energies of certain of the aza-aromatics[3] leads to the same conclusion, flat adsorption; all similar groups i in the adsorbed aza aromatics contribute an equal increment to the total adsorption energy (although this increment is smaller in localized adsorbates). This cannot be reconciled with significant tilting of the adsorbate, since nonlocalizing groups i would not then be equidistant from the adsorbent surface as their equal (for similar groups) adsorption energies seem to require. Klemm's postulate of a vertical adsorbate configuration appears to be based on the interference of substituent groups around the nitrogen with the adsorbent surface in this position. Actually, the sensitivity of the nitrogen adsorption energy to crowding by adjacent groups cannot be used *per se* to conclude anything about the adsorbate configuration, since both flat and perpendicular situations can be visualized in which steric hindrance to adsorption is possible. Many *molecular* complexes and adducts of pyridine show similar steric effects (n-complexes with iodine,[7] adducts with trimethylamines,[8] even proton salts[9]).

The existence of analogous n-complexes of pyridine with other electron acceptors[7,8] supports an n-complex structure for the adsorbed pyridine derivatives, as do the apparently related inductive[3,7] and steric effects in these different systems. Arguments of a similar nature have been advanced as evidence for π-complex formation in the adsorption of the aromatic hydrocarbons, however, while two preceding papers in this series[10,11] have shown the latter theory to be incorrect. It is, therefore, unclear that the analogous arguments on behalf of an *n*-complex structure for the adsorbed aza aromatics are valid.

In addition to the uncertainties with respect to both configuration and bond type in the adsorbed pyridine derivatives, similar questions are suggested with respect to the related aniline and pyrrole derivatives. The adsorption energy of the nitrogen group in uncrowded members of these three series of compounds is approximately constant (3.8–4.1 kcal./mole for adsorption from pentane onto 3.7% H_2O–Al_2O_3),[3] suggesting the same type of adsorption bonding for the nitrogen in each of these aza aromatic types. A similar adsorption mechanism for the pyridines and pyrroles, however, would appear to rule out an n-complex mechanism, in view of the greatly differing basicities of pyridine and pyrrole; n-complex formation should be promoted by basicity of the nitrogen atom.[7] Previous papers in this series and elsewhere[1,6] have demonstrated the practicality of acquiring adsorption energy data at low surface coverages (in the linear isotherm region) in various solvent systems and of extrapolating such data to a common solvent basis. This permits the acquisition of adsorption energies for numerous related adsorbates in a single standard state and prepares the way for a precise analysis of the relationships between adsorption affinity and adsorbate structure. The initial intention of the present study was the review and further acquisition of quantitative energy data for adsorption on alumina of a wide range of pyridine, aniline, and pyrrole derivatives. In addition to clarifying the nature of the configuration and bonding type in the adsorbed aza aromatics, it was hoped that this investigation would provide additional insight into the related problem of adsorbate localization on alumina, as well as furnish further verification of previously proposed concepts in the general area of adsorption from solution.

Experimental

All of the presently reported data were derived from chromatographic retention volume measurements carried out as previously,[6] with a few exceptions involving the determination of inconveniently large (>100 ml./g.) retention volumes. In the latter cases, solute was partially eluted through a column by passage of a large volume V of the eluent under study, the column dissected into several equal segments, and solute in each of the segments determined (by extraction into a very strong eluent and measurement in the usual manner). The point on the column dividing the solute band into halves could then be determined by interpolation, and a corresponding R^0 value determined straightforwardly. All retention volume measurements were carried out in the linear isotherm region, with adsorbent loading by sample never exceeding 5×10^{-5} g./g.

Values of the linear equivalent retention volume R^0 (ml./g.) were corrected to a pentane solvent basis (R_p) by means of the previously used relationship

$$R_p = R^0 10^{\alpha\epsilon^0 A_s} \qquad (1)$$

α is the adsorbent activity function,[1] ϵ^0 is the eluent strength function,[1] and A_s is the solute surface volume ($\Sigma\delta_i$).[1,6] The eluent strength–adsorbent activity product $\alpha\epsilon^0$ for the pure solvents was calculated from previously tabulated parameters[1,6]: 0.000 for *n*-pentane, 0.118 for CCl_4, 0.209 for benzene, 0.275 for

(5) L. H. Klemm, D. Reed, L. A. Miller, and B. T. Ho, *J. Org. Chem.*, **24**, 1468 (1959).
(6) L. R. Snyder, *J. Chromatog.*, **8**, 178 (1962).
(7) J. N. Chaudhuri and S. Basu, *Trans. Faraday Soc.*, **55**, 898 (1959).
(8) H. C. Brown and G. K. Barbaras, *J. Am. Chem. Soc.*, **69**, 1137 (1947).
(9) A. Streitwieser, Jr., "Molecular Orbital Theory for Organic Chemists," John Wiley and Sons, Inc., New York, N. Y., 1961, pp. 419–424.
(10) L. R. Snyder, *J. Phys. Chem.*, **67**, 234 (1963).
(11) L. R. Snyder, *ibid.*, **67**, 240 (1963).

CH_2Cl_2, and 0.411 for dioxane. The corresponding values for the various binary solvents used were evaluated as previously[6,10] from experimental R^0 values of several solutes in both a pure solvent of known $\alpha\epsilon^0$ and the binary solvent to be studied, using eq. 1. Experimental values found were 0.085 for 10% volume CH_2Cl_2/pentane, 0.160 for 25% volume CH_2Cl_2/pentane, 0.216 for 50% volume CH_2Cl_2/pentane, and 0.361 for 50% volume dioxane/pentane. The solute surface volumes A_s were calculated as previously[6] for all but the pyrrole derivatives. Studies reported in the following section show that the contribution of the pyrrole type –NH– group to the total solute A_s value is 2.5 units larger than previously predicted from the area of this group.

Free energy of adsorption data from pentane ΔF_p were calculated from the relationship

$$\Delta F_p = -(\log R_p/V_a)/2.31RT \qquad (2)$$

V_a is the previously defined[1,10] adsorbent surface volume. For the present adsorbent, chromatographically standardized[1] 3.6% H_2O–Al_2O_3 (Alcoa F-20) prepared and tested as previously,[1,10] V_a was assumed equal to 0.017.[1]

Previously reported retention volume data for adsorption of several solutes on alumina of similar chromatographic activities (3.7–5.0% H_2O–Al_2O_3) were used in some instances. These data were corrected to a 3.6% H_2O–Al_2O_3 basis as described previously[1]

$$\log R_1 = \log V_1 + (\alpha_1/\alpha_2) \log (R_2/V_2) \qquad (3)$$

Here, R_1 and R_2 are retention volumes corresponding to adsorbents 1 and 2, V_1 and V_2 are the respective adsorbent surface volumes V_a, and α_1 and α_2 are the respective adsorbent activities α. The accuracy of this extrapolation of retention volume values from one adsorbent to another can be estimated from duplicate determinations of ΔF_p values using the present 3.6% H_2O–Al_2O_3 for twelve ΔF_p values calculable as above from previously reported retention volume data for 3.7% H_2O–Al_2O_3. The standard deviation of these twelve corrected (eq. 3) pairs of data was ±0.14 kcal./mole.

The accuracy of eq. 1 in the present study was estimated from multiple determinations of ΔF_p on the same solute using two or more solvents. For 36 different solutes involving an average of 3.7 different solvents each, the standard deviation of individual values of ΔF_p for each solute from the average was ±0.17 kcal./mole.

Eluent Variation Studies

Measurement of R^0 for a particular solute–adsorbent combination with two or more different eluents permits the experimental evaluation of A_s for the adsorbate from eq. 1. The value of A_s associated with various possible configurations of the adsorbate relative to the adsorbent surface can also be calculated, so that comparison of experimental and calculated A_s values offers the possibility of determining the actual configuration of the adsorbate.[6] As already discussed, previous eluent variation studies tentatively suggest a flat configuration for the adsorbed aza aromatics. Inasmuch as the confidence associated with an experimental A_s value increases with the range in $\alpha\epsilon^0$ values covered and the number of eluents studied, and since previous R^0 data for both the aza aromatics and reference hydrocarbons are largely confined to only two eluent systems (benzene, CCl_4) differing in ϵ^0 by but 0.13 unit, additional experimental confirmation of this conclusion is desirable.

For nine adsorbates of interest as regards configuration in the adsorbed state, R^0 values were obtained for at least six of the seven solvent systems of Table I, and values of A_s were derived by a least squares application of eq. 1. The derived ΔF_p values for these nine adsorbates are summarized in Table I. Since ϵ^0 varies from 0.00 to 0.42 for these seven solvents, an accurate determination of A_s and of adsorbate configuration is hence available. The two aromatic hydrocarbons, 1,2,4,5-dibenzpyrene and benzcoronene, had experimental A_s values (13.6 and 15.7) in close agreement with calculated values (15.0 and 17.0), as expected. The experimental A_s values for the two pyridine derivatives, quinoline (8.0) and acridine (9.8), were in almost exact agreement with calculated values (8.0 and 10.0) for the flat configuration. An edgewise configuration for these pyridine derivatives would have given A_s values only slightly larger than half that for flat adsorption. The standard deviation of experimental ΔF_p values for these two adsorbates in the seven solvents of Table I is only ±0.09 kcal./mole, well within the experimental uncertainty of these measurements. The data of Table I thus lend considerable support to the flat adsorption of the pyridine derivatives.

As indicated in the Experimental section, the experimental A_s values of pyrrole, indole, carbazole, and the two benzcarbazoles (8.1, 10.4, 12.4, 14.3, and 13.3) were consistently higher than the calculated values (5.5, 7.5, 9.5, 11.5, and 11.5) for flat adsorption. The average difference in these calculated and experimental A_s values is both experimentally significant and constant (2.6 ± 0.4 std. dev.). Since the flat configuration gives the largest theoretical A_s value, an explanation other than configuration must be invoked. Previous studies of the adsorption of various solutes on both silica[12] and Florisil[13] have shown that strongly adsorbing groups *generally* exhibit larger contributions to A_s on these adsorbents than predicted from their areas, and that this effect is linked to some sort of anchoring or localization phenomena.[12] Furthermore, the effect is particularly pronounced in the case of the pyrrole nitrogen group. In the case of experimental and calculated A_s values for 9-methylcarbazole (10.0 *vs.* 10.5), the effect vanishes, suggesting a key role of the hydrogen in this anomalously large A_s effect. Assuming that the –NH– group in pyrrole and its derivatives for some reason contributes an unusually large increment (3 units) to A_s, the experimental data of Table I for the pyrroles support flat adsorption for this series of compounds as well.

Absorbate Localization

Previous studies[1,3,10] of adsorption on alumina show that the adsorption energies of compounds with no strongly adsorbing groups can be expressed as the simple sum of contributions F_i from each adsorbate group i

$$-\Delta F_p = \sum^{i} F_i \qquad (4)$$

In the case of adsorbates with one or more strongly adsorbing groups, a localization term must be added to (4)

$$-\Delta F_p = \sum^{i} F_i - f(F_k) \sum^{i \neq k} F_i \qquad (5)$$

The function $f(F_k)$ varies from zero for small values of F_k to 0.45 for sufficiently large values, where localization is presumed complete. The original derivation of (5) was qualitative rather than rigorous, although it appears to give as good a description of relevant experimental data[3] as is possible at the present time.

(12) L. R. Snyder, *J. Chromatog.*, **11**, 195 (1963).
(13) L. R. Snyder, *ibid.*, in press.

TABLE I

LINEAR ISOTHERM ADSORPTION ENERGIES FROM PENTANE OF SEVERAL UNSUBSTITUTED MONOAZA AROMATICS, 3.6% H_2O–Al_2O_3, 24°

	Solute	A_s[a]	$-\Delta F_p$, kcal./mole: P[b]	10% M[c]	CCl_4	25% M[d]	Benzene	50% M[e]	CH_2Cl_2	Average	F_N	d_{a_1-x} (Å.)
	1,2,4,5-Dibenzpyrene	15	5.88	6.23	6.63	6.41	6.34	6.46	6.51			
	Benzcoronene	17		7.32	7.50	7.48	7.68	7.56	7.66			
1	Pyridine	6								5.57[f]	4.19	0.2
2	Isoquinoline	8								6.29[f]	4.30	0.2
3	1,2(3,4-Pyridino)-3,4-benz-5-phenylpyrene, $C_{29}NH_{17}$	16½			8.26	8.83	8.67	8.90	9.24	8.78	4.39	0.2
4	Quinoline	8	5.65	5.57	5.49	5.69	5.66	5.57	5.57	5.60	3.61	0.7
5	β-Naphthoquinoline	10								6.03[f]	3.43	0.7
6	Phenanthridine	10								6.27[f]	3.67	0.7
7	1-Azapyrene	11								6.46	3.56	0.7
8	Acridine	10	6.00	5.95	5.87[g]	6.11	6.23[g]	6.04	5.90	6.01	3.41	0.7
9	7,8-Benzoquinoline	10		5.08	5.05[g]	5.22				5.12	2.00	2.0
10	3,4-Benzacridine	12			5.19[g]	5.23	5.43[g]			5.28	0.59	2.0, 0.7
11	N-Benzylidene-aniline	11				5.30		5.13		5.22	2.07	2.0, 0.7
12	Pyrrole	8	5.17[g]	4.96	5.41	5.12		5.14	5.12	5.15	4.05	
13	Indole	10	6.19[h]	5.72	6.25[f]	5.98	5.85	5.85	5.81	5.95	4.24	
14	Carbazole	12	6.74[h]	6.62	6.87	6.68	6.55[f]	6.68	6.60	6.68	4.36	
15	1,2-Benzcarbazole	14		8.12	7.99	7.05	7.86	7.95	7.91	7.81	4.88	
16	2,3-Benzcarbazole	14		7.19	8.03	7.01	7.43	7.22	7.91	7.47	4.54	
17	9-Methylcarbazole	10½	4.36	4.36	4.58	4.41				4.43	1.18	

[a] Calculated (see ref. 6 and present discussion of A_s for pyrrole derivatives). [b] *n*-Pentane. [c] Methylene chloride/pentane, 10% volume. [d] Methylene chloride/pentane, 25% volume. [e] Methylene chloride/pentane, 50% volume. [f] Average of values for 3.7% H_2O–AlO_3 (corrected to 3.6% H_2O–Al_2O_3). [g] Averages of presently determined values for 3.6% H_2O–Al_2O_3 and previously reported values for 3.7% H_2O–Al_2O_3 (cor.). [h] Previously reported value for 4.8% H_2O–Al_2O_3 (cor.).

TABLE II

ADSORBATE LOCALIZATION IN SOME AMINO-SUBSTITUTED AROMATICS, 3.6% H_2O–Al_2O_3, 24°

Solute	$-\Delta F_p$, kcal./mole: 50% M[a]	Benzene	CH_2Cl_2	Dioxane	Average ΔF_p	Reference adsorbate	$f(F_k)$	d,[c] $\bar{d}$,[d] Å.
Aniline					5.55[b]			
1,2-Diaminobenzene					8.17[e]	Aniline	0.37	2.9
1,3-Diaminobenzene					7.83[e]	Aniline	.45	4.9
1,4-Diaminobenzene					7.79[e]	Aniline	.46	5.7
1,2-Diaminonaphthalene				8.30	8.30	[f]	.51	2.9
1,5-Diaminonaphthalene					8.43[e]	[f]	.48	6.2
1,8-Diaminonaphthalene				7.63	7.63	[f]	.64	2.4
2,3-Diaminonaphthalene				8.46	8.46	[f]	.47	2.9
2-Aminonaphthalene	6.27	6.32	6.14		6.24	Aniline	.37	5.8
2-Aminoanthracene	7.53	7.36	6.65		7.18	[f]	.14	8.1
2-Aminochrysene	8.08	8.19	7.97		8.08	[f]	.16	8.7

[a] Methylene chloride/pentane, 50% volume. [b] See Table IV. [c] Distance between two nitrogen atoms. [d] Average of distances between nitrogen and additional carbon atoms relative to reference adsorbate. [e] Extrapolated from data for 3.7% H_2O–Al_2O_3 (see ref. 3). [f] 2-Aminonaphthalene.

Certain theoretical limitations on (5) require elaboration. The original derivation assumes that the adsorption of nondelocalized adsorbates, where (4) holds, involves more or less equal interaction of each adsorbent site with several adjacent adsorbate groups. Localization then involves the strengthening of this interaction with one adsorbate group and its weakening for remaining groups. Where two equivalent strong groups k are involved, eq. 5 assumes delocalization of one group and localization of the other. If the two equivalent strong groups are separated from one another by a distance d, localization of one group should have a decreasing effect upon localization of the other as d increases. The effect should be particularly pronounced as d approaches the average distance separating sites on the adsorbent surface. Previously reported data[3] on the adsorption of the α, ω-disubstituted alkanes verify a dependence of the localization effect upon d, but the effect is partially obscured by steric interaction of the two substituent groups at small values of d.

In Table II, adsorption energies are summarized for several of the diamino aromatics, as a further test of the dependence of $f(F_k)$ on d. F_i for the aromatic carbon atom can be calculated from previously reported data (0.276 kcal./mole), and F_i for the amino group is then equal to $-\Delta F_p$ for aniline less (6 × 0.276) or 4.16 kcal./mole. This latter calculation lumps any delocalization energy loss of the phenyl ring into the final value of F_i for the amino group for convenience,[14] as previously.[3] The localization function $f(F_k)$ for the various diamino aromatics of Table II can be calculated from the free energy increment produced by substituting an amino group into a suitable reference compound or its equivalent (the diamino aromatic minus one amino group) and dividing by the energy of an undelocalized amino group as in aniline (4.17); 1.00 minus this figure is $f(F_k)$. In addition to calcu-

(14) A similar convention is followed throughout the present paper in ignoring the delocalization of the 5- or 6-membered ring which the localizing group k is attached to or forms part of.

lated values of $f(F_k)$ for the diamino aromatics, Table II lists the distance separating the two amino groups. With the exception of the very high value of $f(F_k)$ for 1,8-diaminonaphthalene (0.64), which will be discussed later, the values of $f(F_k)$ for the remaining diamino aromatics are within experimental error of one another (0.46 ± 0.04 std. dev.) and are completely independent of d. This implies that the strong sites on the alumina surface are separated by more than 6.2 Å., the largest value of d for the diamino aromatics. A preceding study of the adsorption of the aromatics hydrocarbons on alumina[11] suggests the existence on the alumina surface of strong sites with an average spacing of 11 Å. (assuming aromatic carbon atoms as adsorbing units), in agreement with the minimum spacing of sites on which amino groups can be strongly adsorbed. While it is reasonable to assume that the strong sites indicated in the adsorption of both the hydrocarbons and aromatic amines may be the same, it is apparent that the interaction of these sites, relative to the remainder of the adsorbent surface, with strong (amino) and with weak (aromatic carbon) adsorbate groups is vastly different. In the former case, the strong sites appear highly selective, giving an adsorption energy with the amino group about twice that of the surrounding surface. In the latter case, the energy advantage in the adsorption of an aromatic carbon on one of these sites appears relatively slight, as indicated by the applicability of eq. 4 for the aromatic hydrocarbons, regardless of d (to a first approximation[10,11]).

As a result of this apparent difference in the attachment of strong and weak adsorbate groups to strong adsorbent sites, it is obvious that the related delocalization processes leading to the energy difference given by (5) must also differ. The localization energy loss involved in the adsorption of a benzene derivative substituted by two or more strongly adsorbing groups arises from the inability of one adsorbent strong site to satisfy all of the strong groups. The corresponding energy loss involved in a benz-derivative of a monosubstituted benzene (relative to the monosubstituted benzene) arises from some disruption of the normal attachment of the hydrocarbon nucleus to the general adsorbent surface (and not to a strong site). The empirical applicability of eq. 5 to the delocalization of *both* weak and strong adsorbate groups must therefore be regarded as fortuitous.

Data are offered in Table II on the delocalization of clusters of 4–8 aromatic carbon groups separated from the localized amino group by various *average* distances $\bar{d}$. The localization function is seen to drop to less than half its normal value when $\bar{d}$ exceeds 8 Å. These data permit an approximate calculation of $f(F_k)$ for adsorbates with very large aromatic nuclei.

Absorption Energy–Adsorbate Structure Relationships

The analysis of adsorption energy as a function of adsorbate structure first requires the separation of "primary" or "normal" contributions to ΔF_p, following which attention may be focused on the residual, more interesting "secondary" or "anomalous" effects. In the general class of adsorbates presently under consideration, these residual, secondary contributions to adsorption energy must be further distinguished as arising from steric or ring transmitted electronic effects. Thus, while Klemm[2] has focused attention on certain steric requirements in the adsorption of the pyridine derivatives, Chaudhuri and Basu[7] have emphasized electronic factors in their discussion of the n-complexation of the pyridines with iodine. A previous discussion of the adsorption of the pyridine derivatives[3] stresses the importance of both steric and electronic effects in the adsorption of the pyridines.

Table I summarizes best ΔF_p values for the various unsubstituted benz-derivatives of pyridine and pyrrole. F_i values (F_N) for the nitrogen group in each of these adsorbates can be calculated through eq. 5 and are given in Table I. In each case $f(F_k)$ was derived from Table II (first and second columns) of ref. 3 in a fashion consistent with the treatment in that paper and with the treatment on localization in the preceding section of the present paper. Only the calculation of F_N for the large solute 3 of Table I requires further comment. For each aromatic carbon group in this adsorbate $f(F_k)$ was calculated as a function of the distance separating it from the localized nitrogen group, using the data for the monoamino aromatics of Table II as a guide. For a separation distance of less than 6 Å., $f(F_k)$ was taken as 0.45. The phenyl group at the 5-position of solute 3 is sterically equivalent to the phenyl group in 9-phenylanthracene, which is severely crowded. A preceding theoretical treatment of the latter adsorbate for adsorption on a mole active alumina indicates a contribution F_i to total adsorbate adsorption energy of about 0.3 kcal./mole, in agreement with experiment. The contribution of the phenyl group to ΔF_p for solute 3 of Table I should be less than 0.3 kcal./mole, in view of the lower adsorbent activity, and was actually assumed equal zero in the calculation of F_N for this compound.

The pyridine derivatives of Table I are grouped according to similar crowding of the nitrogen atom by adjacent adsorbate groups. As recognized previously,[3] and confirmed in the data of Table I, the value of F_N within each of these similar groups of adsorbates is constant within experimental error (pyridine types, F_N equals 4.29 ± 0.08 kcal./mole; quinoline types, F_N equals 3.57 ± 0.08 kcal./mole) and decreases as the crowding of the nitrogen atom increases. The constancy of F_N within a series of pyridine derivatives where steric effects are constant represents additional confirmation of the flat configuration for the adsorbed pyridines. Significant tilting of the molecule should result in a decreasing contribution of additional carbon atoms to ΔF_p, as previously discussed, with F_N of the nitrogen group appearing to decrease with increasing adsorbate size. No such effect is indicated in the data of Table I.

The constancy of F_N within a group of pyridines of similar nitrogen geometry also suggests that electronic effects within the unsubstituted benzpyridines are negligible. Chaudhuri and Basu[7] have postulated that electronic effects *are* important in this series of compounds, while elementary quantum theory predicts no first-order electronic effect.[8] The experimental data of Chaudhuri and Basu[7] appear inconclusive in this regard, although confirming the importance of *steric* effects in the iodine complexation of the pyridines.

The pyrrole derivatives of Table I contrast sharply with the pyridines in the susceptibility of F_N to steric crowding. As the pyrrole –NH– group becomes more crowded, a small but consistent *increase* in F_N is ap-

TABLE III

LINEAR ISOTHERM ADSORPTION ENERGIES FROM PENTANE OF SUBSTITUTED PYRIDINES, QUINOLINES, ANILINES, INDOLES, AND ACETANILIDES; 3.6% H_2O–Al_2O_3, 24°

		$-\Delta F_p$, kcal./mole							
	Solute	CCl_4	25% M[a]	Benzene	50% M[b]	CH_2Cl_2	Average	$-\Delta\Delta F_p$[c]	σ[d]
18	3,4-Dimethylpyridine						−6.48[e]	+0.81	−0.239
19	4-Methylpyridine						−6.05[e]	+ .45	− .170
20	4-Ethylpyridine						−6.19[b]	+ .60	− .151
21	3-Aminopyridine						−6.84[f]	− .82	− .161, +0.92[f]
22	3-Methylpyridine						−5.99[e]	+ .39	− .069
	Pyridine						−5.57	.00	.000
23	4-Chloropyridine		−5.36		−5.43		−5.40	− .27	+ .227
24	3-Acetylpyridine				−6.79	−6.58	−6.69	− .66	+ .306
25	3-Formylpyridine				−6.43	−6.12	−6.27	− .89	+ .355
26	3-Chloropyridine	−4.76	−5.05		−5.00		−4.94	− .73	+ .373
27	3-Bromopyridine		−5.06			−4.98	−5.02	− .71	+ .391
28	4-Cyanopyridine			−5.26	−5.61	−5.42	−5.43	−1.68	+ .628
29	3-Cyanopyridine			−5.82	−5.86	−5.55	−5.74	−1.37	+ .678
30	3,5-Dichloropyridine	−4.19	−4.39				−4.29	−1.47	+ .746
31	6-Methoxyquinoline						−6.69	+0.25	− .164
32	6-Methylquinoline						−5.83[e]	+ .20	− .084
33	7-Methylquinoline						−6.10[g]	+ .38	
	Quinoline						−5.60	.00	.000
34	6-Chloroquinoline						−5.61[g]	− .09	+ .170
35	6-Bromoquinoline						−5.58[g]	− .18	+ .191
36	6-Nitroquinoline						−6.45[g]	− .45	+ .512
37	*p*-Methylaniline		−6.02		−5.89		−5.95	+ .37	− .170
38	Aniline	−5.65	−5.61	−5.51	−5.44		−5.55	.00	.000
39	*p*-Fluoroaniline		−5.69		−5.65		−5.67	+ .05	+ .062
40	*p*-Chloroaniline	−5.55	−5.82		−5.65		−5.67	− .01	+ .227
41	*m*-Chloroaniline		−5.73		−5.61		−5.67	− .01	+ .373
42	*m*-Nitroaniline						−6.69[g]	− .17	+ .710
43	*p*-Nitroaniline						−6.98[g]	+ .03	+ .778
44	3-Methylindole		−5.95	−5.95	−5.87		−5.92	− .06	− .120
45	Indole						−5.95	− .00	− .000
46	3-Acetylindole					−8.49 −8.97[h] −9.04[i]	−8.83	+1.10	+ .411
	Acetanilide		−7.10		−7.33	−7.00	−7.16	0.00	.000
	m-Nitroacetanilide					−8.27 −8.25[h]	−8.10	− .36	+ .710
	p-Nitroacetanilide					−8.25 −8.33[h]	−8.29	− .17	+ .778

[a] Methylene chloride/pentane, 25% volume. [b] Methylene chloride/pentane, 50% volume. [c] Calculated from eq. 5 and F_i values given in ref. 3. [d] Calculated as described in text. [e] Value for 5.0% H_2O–Al_2O_3 (cor. to 3.6% H_2O–Al_2O_3). [f] Value for 3.7% H_2O–Al_2O_3 (cor.). [g] Average of values for 3.6% and 3.7% (cor.) H_2O–Al_2O_3. [h] Dioxane/pentane solvent, 50% volume. [i] Dioxane solvent. [j] Value for $-NH_3^+$ group.

parent. Thus, F_N increases in the sequence pyrrole, indole, carbazole, and F_N is greater for 1,2-benzcarbazole than for the 2,3-isomer. The F_N values of the latter pair of compounds should be contrasted with the values expected or found for the analogous pyridine derivatives: 1,2-benzacridine, F_N equals 3.4 kcal./mole; 3,4-benzacridine, F_N equals 0.6 kcal./mole.

Table III summarizes a number of adsorption energy data for the non-*ortho*-substituted pyridines, quinolines, anilines, indoles, and acetanilides, in order to evaluate the response of the nitrogen atom in each of these adsorbates to ring transmitted electronic effects, free of steric complications. Values of the Hammett σ-constant[15] with each substituent are also listed in Table III. These σ-values are for the most part those summarized by Jaffé[16] and require no comment in the case of the monosubstituted pyridines, anilines, and acetanilides. The σ-values of disubstituted derivatives are taken as the sum of individual substituent values.[16] The σ-values for the 6-position of quinoline are either the corresponding naphthalene σ-values summarized by Jaffé[16] or quinoline σ-values from the work of Illuminati and Marino.[17] The σ-values for the 3-substituted indole derivatives are taken as the average of *m*- and *p*-values, inasmuch as this position is *meta* to the nitrogen group in one direction, and *para* in the other.

Through the use of eq. 5 and previously summarized values of F_i,[3] values of ΔF_p for each of the solutes of Table III can be calculated. This calculation ignores the electronic interaction of the substituent group(s) with the nitrogen group, and the differences $\Delta\Delta F_p$ in experimental and calculated values of ΔF_p then measures the electronic effect of the substitutent on the adsorption energy of the nitrogen atom.

Table IV and Fig. 1 summarize the Hammett σ–ρ correlation[15] of values of $\Delta\Delta F_p$ for these various adsorbate types with substituent. The substituted

(15) L. P. Hammett, "Physical Organic Chemistry," McGraw-Hill Book Co., Inc., New York, N. Y., 1940, pp. 186–193.

(16) H. H. Jaffé, *Chem. Rev.*, **53**, 191 (1953).

(17) G. Illuminati and G. Marino, *J. Am. Chem. Soc.*, **80**, 1422 (1958).

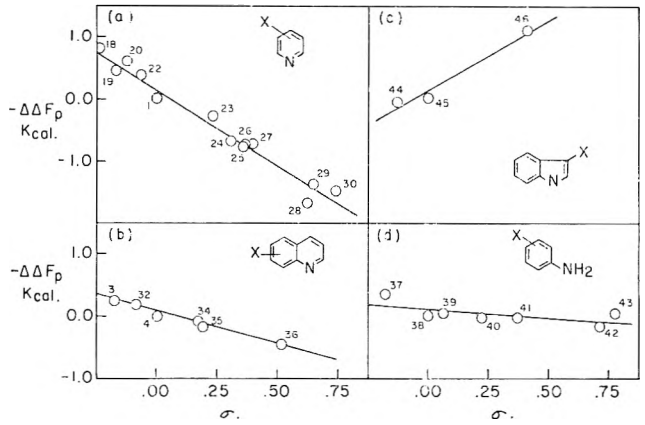

Fig. 1.—Effect of non-*ortho* substituents on adsorption energy.

pyridines ($\rho = -2.42$) show a pronounced dependence of the nitrogen atom adsorption energy on the electron density of the ring, electron-donating substituents *strongly* increasing adsorption energy. This provides quantitative support for electron transfer from adsorbate to adsorbent in the adsorption of the pyridine derivatives. The correlation of Table III and Fig. 1(a) for the pyridines does not include the point for the 3-amino derivative, which deviates badly from the correlation. This deviation is reasonably ascribed to partial charge transfer in the amino group itself upon adsorption. The σ-value for the 3-amino group is -0.161, while that for a 3-amino substituent bearing a full positive charge can be estimated at about 0.9.[16] The experimental value of $\Delta\Delta F_p$ for 3-aminopyridine corresponds to a σ-value of about $+0.4$, suggesting that the amino group bears about one-half of a formal charge.

TABLE IV

NONSTERIC SUBSTITUENT EFFECTS IN THE ADSORPTION ENERGIES OF PYRIDINE, QUINOLINE, ANILINE, INDOLE, AND ACETANILIDE

Adsorbate	$-\Delta\Delta F_p$[a]	ρ	Std. dev.[b]	n
Pyridine	+0.15	−2.42	±0.14	13
Quinoline	+ .11	−1.04	± .06	6
Aniline	+ .11	−0.27	± .12	7
Indole	+ .12	+2.31	± .09	3
Acetanilide	− .01	−0.34	± .09	3

[a] Best value of $(-\Delta\Delta F_p)$ for unsubstituted derivative. [b] Of experimental data.

The correlation of $\Delta\Delta F_p$ values with σ for the 6-substituted quinolines confirms the increase in nitrogen adsorption energy with electron-donating substituents ($\rho = -1.04$), but the response to substituent electronic effects is less than half that expected by analogy with previous σ–ρ correlations in solution. While some slight lowering of ρ between the substituted quinolines and pyridines would have been expected because of the lowered nitrogen adsorption energy in quinoline relative to pyridine, the actual experimental value for the substituted quinolines must be viewed as surprising. Possibly the polarization of the adsorbate double bonds by the adsorbent results in reduced transmission of electrical effects through these various ring systems.

The $\Delta\Delta F_p$–ρ correlation for the substituted anilines shows practically no response ($\rho = -0.27$) of the nitrogen adsorption energy to substituent induced electronic effects, as may be better appreciated from Fig. 1(d). This is surprising, since the basicity constants of the substituted pyridines and anilines in water show ρ-values, respectively, of -5.7[18] and -2.73.[15] That is, ρ for the adsorption of the anilines should have been about half that of the pyridines (~ -1.2). This suggests a difference in the charge on the pyridine and aniline nitrogens, which is however contradicted by the anomalous σ-value of the 3-amino group in pyridine. An alternative explanation for the very small ρ-value in the adsorption of the anilines may be that the transmission of electrical effects from a substituent group through an aromatic ring is basically different for adsorbed molecules relative to molecules in solution (where the Hammett theory is customarily applied), as suggested for the quinolines.

Table IV and Fig. 1(c) summarize the dependence upon σ of $\Delta\Delta F_p$ for the 3-substituted indoles. The large positive value of ρ (+2.31) associated with these data suggests the presence of a sizeable *negative* charge on the adsorbed indole nitrogen atom and contrasts sharply with the positive charge indicated on the adsorbed pyridine and aniline nitrogens. The simplest interpretation of this dependence of F_N for the indole nitrogen upon substituent effects is that the pyrrole –NH– group functions as an acid toward alumina upon adsorption, with either hydrogen bonding or partial proton transfer from the pyrrole nitrogen occurring. The extreme reduction in F_N for the pyrrole nitrogen upon replacement of the hydrogen by methyl supports this view, although the effect is complicated by concomitant steric effects. Comparison of this effect with similar situations[3] (*e.g.*, $-NH_2 \rightarrow -N(CH_3)_2$, $-CHO \rightarrow -COCH_3$) shows a normal reduction in adsorption energy of the unsubstituted group upon methyl substitution of no more than 45%. The corresponding reduction for the pyrrole nitrogen is over 70%.

The final correlation of Table IV summarizes the dependence of adsorption energy with the substituted acetanilides on the substituent σ-constant. It was initially hoped that the acidic anilides might furnish an exocyclic analog of the pyrroles corresponding to the anilines *vs.* pyridines, and that comparison of the ρ-values for the pyrroles and anilides might check the anomalous behavior of ρ for the anilines. While the ρ-value for the acetanilides happens to be small, in agreement with the aniline situation, eluent variation studies indicate that acetanilide has a *normal* A_s value (9), which casts some doubt on the similarity of adsorption mechanism in the anilides and pyrroles.

Having established the magnitude of the nonsteric contribution of a substituent to F_N in the nitrogen compound types under study, it is possible to correct for this nonsteric factor in the case of *ortho*-substituted derivatives and hence to derive the quantitative contribution of the steric factor to F_N. Charton[19] has studied the σ-values of the *ortho* and *para* substituents in benzene derivatives where the reaction center is insulated from direct steric interaction with *ortho* substituents, and finds the σ-values for the two positions approximately equal. Taft[20] has presented an analysis of the contributions of electronic and steric effects in *ortho* substitution which leads to the same conclusion (see Table XII of reference 20). Consequently, the F_N

(18) H. H. Jaffé and G. O. Doak, *J. Am. Chem. Soc.*, **77**, 4441 (1955).
(19) M. Charton, *Can. J. Chem.*, **38**, 2493 (1960).
(20) R. W. Taft, Jr., "Steric Effects in Organic Chemistry," M. Newman, Ed., John Wiley and Sons, Inc., London, 1956, p. 619.

values of the *ortho*-substituted nitrogen compounds of Table V can be calculated from eq. 5 and then corrected for electronic effects transmitted through the ring by subtracting the difference in F_N values for the corresponding *para* isomer relative to the parent unsubstituted nitrogen derivative. Table V summarizes these corrected values F_N^* of the nitrogen group adsorption energies on a no-ring charge basis.

The absence of significant electronic contributions to F_N in the unsubstituted aza aromatics has already been noted,[8] so thar $F_N = F_N^*$ for these compounds. Consequently, the F_N and F_N^* values of Tables I and V provide a comprehensive, quantitative description of the purely steric interaction of the adsorbed nitrogen atom with adjacent adsorbate groups.

Assumption of n-electron charge transfer between the nitrogen atom and the adsorbent surface presumably requires a reasonably strong, highly directional bond between the nitrogen and an adsorbent aluminum atom. In the analogous case of the pyridine–iodine complex,[21] the nitrogen–iodine bond is in the plane of the pyridine ring and has a length (2.16 Å.) close to that calculated[22] (2.03 Å.) for a covalent bond. Assumption of a similar optimum configuration for the nitrogen–aluminum bond in the adsorbed aza aromatics (covalent bond in the plane of the adsorbate ring) permits the calculation of the van der Waals distance d_{Al-X} between an adsorbate substituent group X and the aluminum atom, which is a measure of the interference of X to the formation of a charge-transfer complex involving nitrogen and aluminum. The calculation of d_{Al-X} requires estimates of the covalen bond length[22] between aluminum and nitrogen and values of the van der Waals radii[23] of the various atoms involved.

These values of d_{Al-X} in Tables I and V represent the distance between van der Waals spheres around each atom; since they are negative in every case, the implied penetration of van der Waals radii means a significant steric interaction of the atoms Al and X. This distance d_{Al-X} should therefore correlate with F_N^*, although these calculated values of d_{Al-X} do not imply significant interpenetration of atomic van der Waals radii. More energetically favorable processes for relieving the large strain energies that such penetration would involve are available: bending of bond angles, lengthening of the Al–N bond, etc.

Figure 2 provides a plot of F_N^* *vs.* d_{Al-X} for the 2-substituted pyridines. The substituent X is variously a methyl, a benzo or naphtho ring system, an amino, or a chloro group. A single smooth curve falls on top of all of these data, confirming the cancellation of electronic effects in our treatment and demonstrating the dependence of nitrogen adsorption energy on the distance between adjacent adsorbate groups and the aluminum atom electron acceptor on the adsorbent surface. Figure 3 shows a similar plot for the disubstituted pyridines, where the group Y is either a methyl or a benzo substituent. Again, a single curve falls through all of these data. The dashed curve in Fig. 3 is the superposition of the curve from Fig. 2 on top of these data. Additive steric effects in the adsorbates of

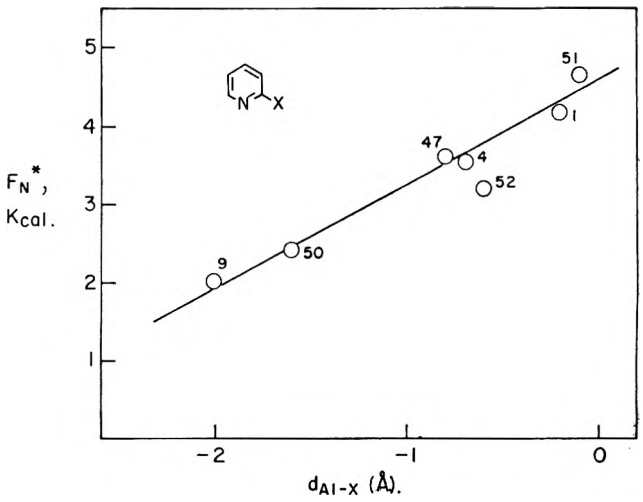

Fig. 2.—Nitrogen adsorption energy as a function of steric interaction of *ortho* groups in the pyridine derivatives.

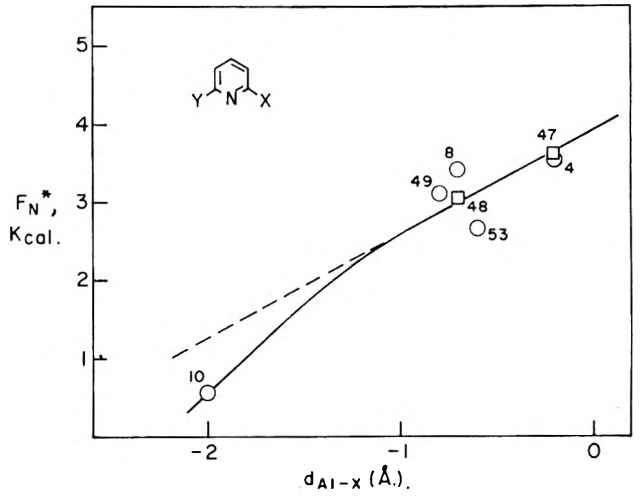

Fig. 3.—Nitrogen adsorption energy as a function of steric interaction of buttressed *ortho* groups in the pyridine derivatives: O, Y = benzo; □, Y = methyl.

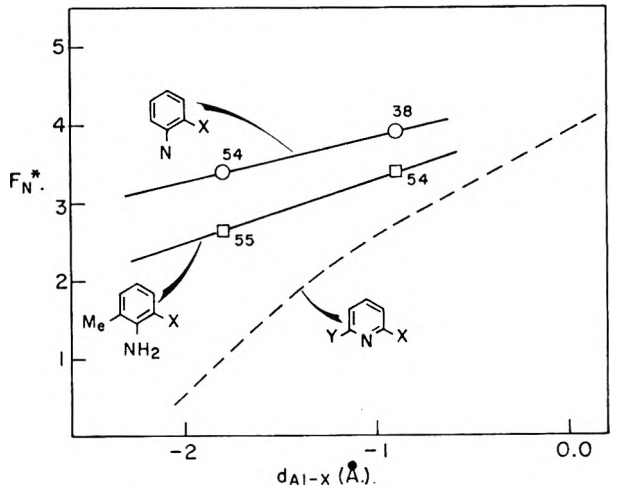

Fig. 4.—Nitrogen adsorption energy as a function of steric interaction of *ortho* groups in the aniline derivatives.

Fig. 3 would have resulted in the adherence of these data to the dashed curve. The deviations at small d_{Al-X} values can be ascribed to a buttressing effect of the group Y in the more highly hindered situations, preventing the relief of strain energies by bending of the C–N–Al bond in the plane of the adsorbate.

Figure 4 shows an analogous plot of the *ortho*-substituted aniline data, with the curve for the disubstituted

(21) O. Hansel and H. Hope, *Acta Chem. Scand.*, **15**, 407 (1961).

(22) G. E. K. Branch and M. Calvin, "The Theory of Organic Chemistry," Prentice-Hall, Inc., New York, N. Y., 1941, pp. 106–112.

(23) L. Pauling, "The Nature of the Chemical Bond," Cornell University Press, Ithaca, N. Y., 1940, p. 189.

TABLE V

STERIC EFFECTS IN THE ADSORPTION OF *ortho*-SUBSTITUTED NITROGEN COMPOUNDS FROM PENTANE; 3.6% H_2O–Al_2O_3, 24°

	Solute	$-\Delta F_p$, kcal./mole: 10% M[a]	25% M[b]	50% M[c]	Benzene	Average	Cor.[d]	F_N*	d_{Al-X}, Å.
47	2-Methylpyridine					−5.46[e]	−4.98	3.60	−0.8
48	2,6-Dimethylpyridine					−5.38[e]	−4.42	3.04	−0.8
49	2-Methylquinoline					−5.60[e]	−5.12	3.10	−0.8, −0.7
50	8-Methylquinoline					−4.79[e]	−4.56	2.40	−1.6
51	2-Aminopyridine					−7.29[e]	−4.56	4.64	−0.1
52	2-Chloropyridine	−4.44	−4.38			−4.41	−4.58	3.20	−0.6
53	2-Chloroquinoline		−4.62			−4.62	−4.79	2.67	−0.6, −0.7
54	2-Methylaniline		−5.52	−5.41		−5.46	−5.06	3.40	−1.8
55	2,6-Dimethylaniline	−4.98	−5.17	−5.09		−5.08	−4.28	2.62	−1.8
	2-Methylindole		−5.89	−5.80	−5.95	−5.88	−5.91	4.20	

[a] Methylene chloride/pentane, 10% volume. [b] Methylene chloride/pentane, 25% volume. [c] Methylene chloride/pentane, 50% volume. [d] Corrected for electronic effects of *ortho* substituent. [e] Value for 5.0% H_2O–Al_2O_3 (cor. to 3.6%).

pyridines (from Fig. 3) superimposed. The aniline $F_N^* - d_{Al-X}$ curve would be expected to have a smaller slope than the corresponding pyridine curve because of the greater possibility for relieving steric strain through distortion of bond angles, similar to the situation for the buttressed and unbuttressed 7,8-benzoquinolines. Similarly, F_N for benzylideneaniline (Table I) is greater (2.07) than F_N for the apparently sterically equivalent 3,4-benzacridine (0.59) because of the greater flexibility of the former. The previously cited large $f(F_k)$ value of 1,8-diaminonaphthalene, which is equivalent to a lower value of F_N in this compound, is now seen to be the result of a very small d_{Al-X} value between the nonlocalizing amino group and the aluminum site for the alternate amino group.

The correlations of Fig. 2 and 3, based on interaction of crowding groups X with a point site, conclusively show that the adsorption energies of the crowded pyridine derivatives can be reconciled with flat adsorption. Klemm's postulate[2] of vertical adsorption is therefore left without any unique evidence in its behalf.

The one F_N^* value of Table V for an *ortho*-substituted indole (56) corroborates the insensitivity of F_N in the pyrroles to steric strain and argues for a basically different mechanism of adsorption.

Discussion

The nature of the interaction between the adsorbed pyridines, anilines, and pyrroles and the adsorbent surface can now be set forth in some detail. A flat configuration of the adsorbed molecule is indicated in every case, both on the basis of eluent variation studies and the applicability of eq. 5 to solutes where nitrogen geometry is similar. The large substituent effect in the substituted pyridines strongly suggests the development of a fractional positive charge on the adsorbed nitrogen atom, supporting the n-complex theory of Klemm.[2] Similarly, the anomalously high σ-value for the amino group in 3-aminopyridine leads to a similar conclusion for the nitrogen in aniline derivatives, in spite of the absence of a significant substituent effect on aniline adsorption energy. The steric response of the nitrogen adsorption energy to *ortho* groups in both the pyridines and anilines is basically similar, and the adsorption energies of the nitrogen group in pyridine (4.29 kcal.) and in aniline (3.90 kcal.) are within experimental error equal. It is reasonable to conclude that the adsorption mechanism in these two compound types is essentially the same.

The correlation of F_N^* for the anilines and pyridines with the distance between hindering groups X and an aluminum atom which forms a chemical bond with the n-electrons of the nitrogen confirms the importance of the n-electrons in the bonding of both nitrogen types to the alumina surface. The presently reported data are incompatible with a model which presumes π-electron interaction of the nitrogen atom, for example.

The close similarity of the pyridine and aniline derivatives upon adsorption contrasts sharply with the dependence of the pyrrole adsorption energies upon substituent effects. For the pyrrole nitrogen group, F_N increases with decreasing electron density of the pyrrole ring, implying the presence on the adsorbed pyrrole nitrogen group of a *negative* charge. While steric crowding of the nitrogen in the pyridines and anilines markedly decreases F_N^*, similar crowding of the pyrrole nitrogen group has essentially no effect, actually appearing to increase F_N^* slightly. Both the steric and electronic effects in the adsorption of the pyrroles are compatible with an adsorption mechanism involving partial proton transfer from the pyrrole nitrogen to an adsorbent surface oxygen atom. The natural tilting of the N–H bond out of the plane of the pyrrole ring combines with the greater bond length associated with an N···H···O bond (~2.8 Å.) relative to an N–Al bond (1.9 Å.) to greatly reduce the theoretical steric requirements for the adsorption of the pyrrole –NH– group. Significant increase in the N–H bond length upon adsorption would also serve to alleviate the intramolecular strain between the nitrogen hydrogen and adjacent hydrogen atoms, and hence explain the slight *increase* in F_N for the more crowded pyrroles. A final, less easily interpreted distinction exists with respect to the adsorption of the pyrroles, in the anomalously high A_s values. A similar effect has been noted in the adsorption of all strong groups on certain other adsorbents[12,13] and appears related to peculiarities in the way strongly adsorbing solute groups localize on strong adsorbent sites. These two experimental phenomena presently are believed to be closely related, and a future communication will discuss them in detail.

In view of the differing mechanisms of adsorption of the pyridines and pyrroles, it is attractive to consider the anomalous dependence of $\Delta\Delta F_p$ on σ for the anilines to arise from the amino group behaving as an n-electron donor in some situations (basic anilines) and a proton donor in others (nonbasic anilines such as nitroaniline). The plot of Fig. 1(d) does not confirm this conjecture, since a well defined minimum in the curve

would have been expected. Possibly the experimental uncertainty in the latter data does not permit a firm conclusion in this regard.

Acknowledgment.—The author is grateful to his associate, Dr. J. F. Fogo, for editing the original manuscript and for many helpful discussions, and to Mr. F. O. Wood for assistance in the experimental work. The gift of sample number 3 (Table III) by Dr. F. A. Vingiello of the Virginia Polytechnic Institute is gratefully acknowledged.

SELF-DIFFUSION OF LIQUID ZINC

BY NORMAN H. NACHTRIEB, ESTHER FRAGA, AND CHRISTOPHER WAHL

The Institute for the Study of Metals, The University of Chicago, Chicago 37, Illinois

Received May 4, 1963

Self-diffusion in liquid zinc has been measured by the open capillary technique over the temperature range 450 to 600°. The results are described by the equation $D_{Zn} = 8.2 \times 10^{-4} \exp(-5090/RT)$. Satisfactory agreement with the Cohen–Turnbull free volume theory is found, and the diffusing particle appears to be the Zn^{+2} ion.

Introduction

The diffusive movements of atoms in the liquid state are often described in terms of the activated state theory, more by reason of analogy with the corresponding process in crystalline solids than for any cogent experimental or theoretical evidence to support it. In its application to the hole theory of liquids, the activated state theory assumes that a local energy fluctuation creates a void of atomic dimensions, analogous to a vacancy in a crystal, and a neighboring atom jumps into the gap in the elementary diffusive process. Aside from the fact that no very satisfactory theory of liquids exists, the activated state theory is *ad hoc* in character and provides no clue to the calculation of its parameters (*viz.*, energy) even for solids of high structural symmetry. At the other extreme from the hole theory, diffusion in liquids may be considered as a highly cooperative process, in which a very large number of particles execute concerted displacements on a scale which is small compared with atomic dimensions. If this were the case, the distribution of atom configurations contributing to the activated state would be so enormous that the concept of a transition state would be meaningless: the entire liquid would be in the activated state. Although such a "swarm" model of diffusion in liquids may well be closer to physical reality than the hole theory, a recent version of the latter by Cohen and Turnbull[1] has given results which are in good agreement with experimental work on both van der Waals liquids and liquid metals. The present study of self-diffusion in liquid zinc is in satisfactory agreement with their theory.

Experimental

The procedure used was the first employed by Anderson and Saddington.[2] Glass or Vycor capillaries were filled with Zn^{65} and slowly rotated in a bath of liquid zinc of ordinary isotopic composition. At the end of the diffusion period the capillaries were withdrawn and their contents analyzed for the remaining Zn^{65} by conventional counting techniques.

The greatest difficulty encountered was the devising of a satisfactory method of filling the capillaries with Zn^{65} metal in such a manner that traces of gas left at the closed bottom end would not expand and force the metal out during melting. This was satisfactorily accomplished in the following manner. A 1.00-mm. bore Pyrex or Vycor heavy wall capillary tubing, selected for uniformity of bore section by observing the length of a contained mercury thread, was ground to a square end on a carborundum wheel and sealed to a piece of Pyrex or Vycor rod of the same diameter. This was a delicate operation, since it was necessary to preserve the diameter of the bore unchanged to the very bottom of the tube at the seal. This done, the capillary tube was sealed at its other end to a Pyrex or Vycor tube of normal wall thickness for attachment to a vacuum line. Zn^{65} metal was earlier prepared by the following exchange reaction in a sealed tube above the melting point of zinc (419°). $Zn^{65}Cl_2 + Zn^{64} \rightarrow Zn^{65} + Zn^{64}Cl_2$. The globule of radioactive zinc so obtained was swaged to rod form and drawn into 0.038-in. diameter wire, which would just fit into the capillary tubes. With the wire in the capillary a vacuum of 10^{-6} mm. was produced in the tube and the zinc thoroughly outgassed by gentle heating to the melting point. Tapping during this operation compacted the metal so that it filled the capillary with no voids. After the metal had solidified, the capillary was sawed to a length of about 3 cm. and a conical tip was ground on the open end. Capillary lengths were measured with a traveling microscope to ±0.0001 cm., following which the rod was bent to a U-shape and attached with a coupling to a length of 1/8-in. drill rod to provide for stirring. The zinc bath consisted of 345 g. of resublimed metal ("Super Purity," obtained from the New Jersey Zinc Co.), and was contained in a 2.8-cm. i.d. × 35-cm. Vycor tube whose upper end bore a 34/45 taper quartz joint. This tube was closed by a Pyrex head which consisted of a complementary taper joint, a side arm for attachment to the vacuum line, and a heavy wall axial tube to accept the 1/8-in. drill rod. A square section neoprene "O" ring lubricated with Octoil-S gave a vacuum tight (10^{-6} mm.) rotating seal when the shaft was driven by a small 1 r.p.m. motor. The zinc bath was heated by means of a cylindrical furnace having two independent sets of helically wound nichrome heating coils. Temperatures were maintained constant to within ±1° by modulation of the energy input with one set of windings, as sensed by four series-connected chromel–alumel thermocouples and a Leeds & Northrup Micromax recording potentiometer. A massive silver core surrounding the Vycor tube maintained an axial temperature gradient of 0.5°/in. over the 4 in. length of the zinc bath; the upper end was slightly higher in temperature to avoid convection within the rotating capillary. Temperature was measured by means of a Leeds & Northrup Type K potentiometer and a calibrated chromel–alumel thermocouple located in a hole drilled into the wall of the silver furnace core.

Each diffusion run was carried out under 0.5 atm. of hydrogen or helium after the system was evacuated. Stirring was begun immediately after the capillary was immersed below the surface of the zinc bath. At the conclusion of a run, any excess of metal adhering to the capillary was removed. Several runs were discarded because the capillary was found to be incompletely filled; presumably, gas was liberated from the metal in the capillary during melting, resulting in partial expulsion. Runs attempted at 700° were invariably failures for this cause.

The mass of zinc contained in the capillaries after each run was determined by weighing the tubes on a microbalance before and after removal of the metal with dilute hydrochloric acid. A fine platinum wire in contact with the metal thread greatly accelerated dissolution. Much effort went into the selection of a suit-

(1) M. H. Cohen and D. Turnbull, *J. Chem. Phys.*, **31**, 1164 (1959).
(2) J. S. Anderson and K. Saddington, *J. Chem. Soc.*, S381 (1949).

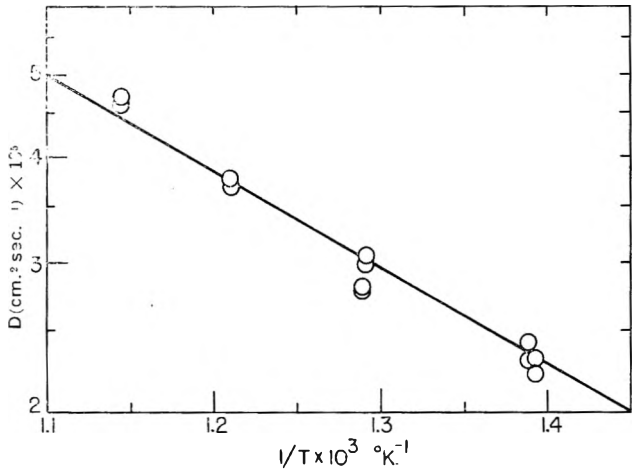

Fig. 1.—Self-diffusion in liquid zinc (log D *vs.* $1/T$).

able technique for determining the specific activity of the resulting zinc solution. Finally selected was the precipitation of $ZnNH_4PO_4$ with diammonium hydrogen phosphate in a solution buffered to pH 7. The precipitate was filtered on 1-in. diameter circles of No. 42 Whatman paper which had been cemented to 0.25-in. tall rings cut from Pyrex tubing. With practice it was possible to obtain a reproducibly uniform layer of the precipitate and to limit the counting error arising from variable absorption to ±0.7%. For each analysis a determination of the activity of the original zinc wire was simultaneously made as a control of the procedure. Aliquot portions (generally 0.1 of the mass of zinc in the capillary) were calculated to make the quantity of metal in the precipitate 0.0300 ± 0.0030 g. A 10-mil aluminum absorber foil was interposed between the precipitate and the methane proportional flow counter to absorb the low energy β^+ and electron capture radiation from the Zn^{65}, whose self-absorption in the precipitate was responsible for early difficulties in obtaining reproducible counting measurements. No systematic attempt was made to test for convection within the capillary by varying the capillary radius and length, the diffusion time, or the speed of capillary rotation, since these factors have been studied in similar investigations in this and other laboratories. The conditions chosen and the internal consistency of the results give us confidence that convection does not seriously affect our results.

Calculations and Results

For the infinite open capillary geometry the average tracer concentration is given by the series

$$C_{av} = \frac{8C_0}{(\pi)^2} \sum_{n=0}^{\infty} \frac{1}{(2n+1)^2} \exp - \frac{(2n+1)^2\pi^2 Dt}{4L^2} \quad (1)$$

where C_0 is the initial tracer concentration, L is the capillary length, and the remaining symbols have their usual meaning. Two or three terms were necessary for the evaluation of D, according to the magnitude of C_{av}/C_0. No correction was made for the "end effect" of the capillary. Table I summarizes the data. The agreement in D is better than 4% at each temperature, and the average values are believed to be accurate to within 6%.

The temperature dependence of D_{Zn} is shown in Fig. 1, in which log D is seen to be a linear function of $1/T$ to within the precision of the measurements. The corresponding empirical equation is

$$D_{Zn} = 8.2 \times 10^{-4} \exp(-5090/RT) \quad (2)$$

Discussion

Although the experimental results show an exponential dependence of D upon temperature, it does not follow that the process must be regarded as thermally activated in the conventional sense. In our present state of knowledge of diffusion in liquids it seems preferable to regard eq. 2 as a convenient empirical representation of the data, rather than to conclude that an energy barrier of the order of 5100 cal. must be surmounted by an atom which attempts a diffusive jump.

Table I

Self-Diffusion Coefficients of Liquid Zinc

T, °C.	C_{av}/C_0[a]	L, cm.	$t \times 10^4$ cm.	$D \times 10^5$ cm.² sec.⁻¹[a]
445	0.69750	2.9810	2.880	2.22
	.69150			2.31
447	.67000	2.8931	3.108	2.30
	.66201			2.42
501	.53408	3.0787	5.406	2.99
	.53904			3.06
503	.65773	3.0653	3.084	2.80
	.65886			2.79
553	.56015	2.7069	3.024	3.68
	.55504			3.77
600	.55262	2.9012	2.880	4.60
	.54700			4.71

[a] Duplicate values of C_{av}/C_0 and D correspond to two chemical- and radio-assays on aliquots of metal from the same diffusion run.

A more promising approach is provided by the Cohen–Turnbull theory, which avoids the concept of a simply activated state and instead attempts to describe the diffusive movements of particles in dense fluids in terms of their escape from a cage of surrounding particles by the redistribution of the free volume. Its advantage over the activated state model is that it relates the coefficient of diffusion to measureable and calculable properties of the liquid, while the elementary jump distance emerges as a parameter. According to their point of view, the particle moves with gas kinetic velocity u in a cage of average volume $\bar{v}_m$. It may make a diffusive displacement through a distance a^* only when an isoenergetic redistribution of the free volume occurs to open up a void greater than a critical volume v^*, and a second particle moves in to occupy the site of the first particle. The free volume v_f is a function of both temperature and pressure and is related to them through the coefficients of thermal expansion α and of compressibility β by

$$v_f = \alpha\bar{v}_m(T - T_0) - \beta\bar{v}_m\Delta P \quad (3)$$

A simple statistical mechanical calculation gives the probability of finding a void whose volume exceeds a critical value v^* and leads to the following expression for the diffusion coefficient

$$D = ga^*u \exp -(\gamma v^*/v_f) \quad (4)$$

In eq. 4 g is the *a priori* geometric jump factor which has the value $1/6$, and γ is a parameter lying between 0.5 and 1 which is introduced to correct for the overlap of free volume. Also a^* (or $v^* = 1/6\pi a^{*3}$) is a parameter—the critical displacement length (volume) of the particle. Cohen and Turnbull have observed that v^* closely approximates the van der Waals volume of molecular liquids and the cationic volume in liquid metals. The Cohen–Turnbull theory is thus seen to be a version of the hole theory, in which voids of molecular or ionic volume or larger are required for diffusion, as distinct from models in which cooperative infinitesimal displacements of many particles occur. The essential difference between the Cohen–Turnbull theory and the activated state theory is the former's emphasis on the

isoenergetic redistribution of the available free volume as the origin of voids.

Table II lists the values of the mean displacement a^* calculated from eq. 4 with average values of D and with $\gamma = 1$. The free volume was obtained from eq. 3, with $T_0 = 0$, $\alpha = 1.34 \times 10^{-4}$ deg.$^{-1}$, and $\bar{v}_m = 16.48 \times 10^{-24}$ cm.^{3}; the latter values for the mean coefficient of thermal expansion and the mean atomic volume of liquid zinc in the temperature range of the measurements were calculated from density data in Smithells.[3]

TABLE II

VALUES FOR COHEN–TURNBULL EQUATION (LIQUID ZINC)

T, °K.	$D \times 10^5$ cm.^{2} sec.$^{-1}$	u, 10^{-4} cm. sec.$^{-1}$	$v_f \times 10^{24}$ cm.^{3}	$\gamma^* \times 10^8$ cm.
720	2.31	5.24	1.590	0.90
775	2.91	5.44	1.711	.89
826	3.72	5.61	1.824	.86
873	4.66	5.77	1.928	.82

With γ arbitrarily set equal to unity in these calculations, the particle radius ($r^* = (^3/_4\pi v^*)^{1/3}$ and one-half the mean displacement a^* are equal. Their value ranges from 0.82×10^{-8} to 0.90×10^{-8} cm. and is reasonably close to the ionic radius of Zn^{+2} (0.74×10^{-8} cm.).[4] Its apparent dependence upon temperature may not be correct, since the coefficient of expansion (and consequently the free volume) probably increases with temperature. The interesting conclusion is that the diffusing particle appears to be the ion core in zinc metal, in agreement with the observations of Cohen and Turnbull and of other workers[5-7] who have shown that the Stokes–Einstein relation is followed by liquid metals when the ion radius is used. Equally important is the fact that the results are satisfactorily interpreted in terms of a simple free volume theory which avoids the drawbacks of the activated state approach.

Acknowledgments.—The authors wish to express their thanks to the Air Force Office of Scientific Research for partial support of this work under Grant AFOSR 62–231.

(3) C. J. Smithells, "Metals Reference Book," Vol. 2, Butterworths Scientific Publications, London, 1955, p. 640.

(4) L. Pauling, "The Nature of the Chemical Bond," Cornell University Press, New York N. Y., 1945, p. 346.

(5) R. E. Hoffman, *J. Chem. Phys.*, **20**, 1567 (1959).

(6) N. H. Nachtrieb and J. Petit, *ibid.*, **24**, 746 (1956).

(7) R. E. Meyer and N. H. Nachtrieb, *ibid.*, **23**, 1851 (1955).

DIFFUSION CONTROLLED BUILDUP OF SURFACE ACTIVE MATERIAL AT THE AIR–WATER INTERFACE DURING EVAPORATION

BY F. L. JACKSON AND F. P. KRAUSE

Miami Valley Laboratories, The Procter & Gamble Company, Cincinnati, Ohio

Received May 6, 1963

The buildup of sodium dodecyl sulfate (SDS) at the air–water interface during evaporation of the water was followed using S^{35}-tagged surfactant and a counter for counting the surface activity of solutions in the inverted position, that is, with the air-exposed surface at the bottom. Buildup of SDS was found to be essentially linear with time of evaporation, the slope depending upon evaporation rate. The amount of SDS accumulating in the air–water interfacial region was substantial, being by a factor of six greater than the initial concentration after 25 min. of evaporation at the rate of 1.68×10^{-4} g./sec./cm.^{2} at 60°. A mathematical formula was derived which allowed calculation of diffusion coefficients from the rate of surfactant buildup at the air–water interface. Comparison of calculated diffusion coefficients with bulk solution diffusion coefficients, obtained by the self-diffusion open-end capillary method, led to the conclusion that the rate of buildup of SDS at the air–water interface during evaporation is essentially diffusion controlled.

Introduction

Many investigators have used radiotracer techniques to determine the excess surface concentration of surfactants under equilibrium conditions. Reference to these works is given in Nilsson's[1] article.

The present work is concerned with determination of excess concentration of surfactants at the air–water interface under nonequilibrium conditions when evaporation of the solute is allowed to proceed continuously. Mathematical analysis of the system and of the experimental data enabled conclusions to be drawn regarding the basic factors responsible for surfactant buildup at the air–water interface during evaporation.

Within the authors' knowledge, there have been no studies published previously which describe the effect of evaporation of water on the concentration of surfactants at the air–water interface of a detergent solution. However, it may be of interest to cite briefly some related studies concerned with the mechanism responsible for changes in interfacial tension, of solutions containing surface active material, immediately after the formation of the air–water interface. Over a short time period evaporation is negligible. Flengas and Rideal[2] concluded, as a result of their study of the surface aging of C^{14}-tagged sodium stearate solutions, that the process is very slow and is diffusion-controlled. Defay and Hommelen,[3,4] using the vibrating jet technique, found that normal alcohols (C_6–C_{10}) and decanoic acid exhibit a surface tension lowering with time that is essentially diffusion-controlled. Azelaic acid, however, produced a slower change in surface tension with time than was explicable on the basis of diffusion, leading to the conclusion that an energy barrier exists in this system. Defay and Hommelen[4] concluded that their data (with the exception of azelaic acid) and those of Dervichian[5] for aqueous solutions of undecylic acid, those of Kalousek and Blahnik[6] for cosine solution at water–mercury interface, and those of Saraga[7] for lauric acid aqueous

(1) G. Nilsson, *J. Phys. Chem.*, **61**, 1135 (1957).

(2) S. N. Flengas and E. Rideal, *Trans. Faraday Soc.*, **53**, 339 (1959).

(3) R. Defay and J. R. Hommelen, *J. Colloid Sci.*, **13**, 553 (1958).

(4) R. Defay and J. R. Hommelen, *ibid.*, **14**, 411 (1959).

(5) D. G. Dervichian, *Kolloid-Z.*, **146**, 96 (1956).

(6) M. Kalousek and R. Blahnik, *Trav. chim. Tchecoslov.*, **20**, 782 (1955).

(7) L. Ter Minassian-Saraga, Thesis Paris, 1956.

solutions are consistent in indicating that the diffusion mechanism controls changes in surface tension with time. On the other hand, Ward and Tordai,[8] using data of Addison[9] for normal alcohols in aqueous solutions, found calculated diffusion coefficients to be smaller than accepted diffusion coefficients. On this basis, Ward and Tordai concluded that an energy barrier existed at the surface.

The effect of evaporation on surface tension at the air–water interface was the subject of papers by Schwarz and Wood[10] and by Hommelen.[11] Schwarz and Wood described an experimental setup designed to eliminate evaporation during the measurement of radiotagged-surfactant concentration at the air–water interface. Hommelen discussed the avoidance of errors, due to the evaporation of the solute, in the determination of the surface tension of solutions of long chain alcohols in water. Neither of the works by Schwarz and Wood nor Hommelen considered the buildup of surfactant at the air–water interface or the factors which control such a buildup.

Theoretical

The derivation of a formula which allows calculation of diffusion coefficients from the rate of increase of surfactant concentration at the air–water interface as a function of time is based on the model indicated.

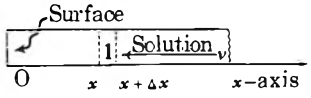

In this model the solution moves toward the surface with the velocity v. Consider a solution element **1** whose sides are taken to be of unit area. The amount of solute moving across the plane at x during the short time Δt is dependent upon Fick's first law of diffusion and the movement of the solution

$$Q_x = -D\left(\frac{\partial c}{\partial x}\right)_x \Delta t - c_x v \Delta t$$

where Q_x is the amount of solute moving across the plane at x; D is the diffusion coefficient of the solute, in cm.^{2} sec.$^{-1}$, assumed to be constant; c_x is the concentration of solute at x; and v is the evaporation rate in terms of relative movement between the surface and the solution, in cm. sec.$^{-1}$.

Similarly at $x + \Delta x$

$$Q_{x+\Delta x} = -D\left(\frac{\partial c}{\partial x}\right)_{x+\Delta x} \Delta t - c_{x+\Delta x} v \Delta t$$

The difference, $Q_{x+\Delta x} - Q_x$, is equal to the change of concentration $-\Delta c$ in **1**, whose volume is Δx, that is

$$Q_{x+\Delta x} - Q_x = -\Delta c \Delta x$$

The negative sign indicates that the change in concentration is opposite to that of Q. Substitution and algebraic rearrangement gives

$$\frac{\Delta c}{\Delta t} = \frac{D\left(\frac{\partial c}{\partial x}\right)_{x+\Delta x} - \left(\frac{\partial c}{\partial x}\right)_x}{\Delta x} + v\frac{c_{x+\Delta x} - c_x}{\Delta x}$$

which, on taking the limit with $\Delta t \to 0$ and $\Delta x \to 0$, becomes the differential equation

$$\frac{\partial c}{\partial t} = D\frac{\partial^2 c}{\partial x^2} + v\frac{\partial c}{\partial x} \qquad \text{(I)}$$

It will be noted that eq. I is Fick's second law of diffusion plus a variable factor which takes into account the movement of internal elements of solution toward the surface reference point as a consequence of evaporation of the solution.

Initial and Boundary Conditions.—The initial conditions of the system described by (I) are given as

$$\left.\begin{aligned} c(x,0) &= c_0,\ x > 0 \\ c(x,0) &= 0,\ x < 0 \end{aligned}\right\} \qquad \text{(Ii)}$$

which simply state that at positive values of x the concentration found initially is equal to the original molarity of the solution; for negative values of x the concentration is zero.

The first boundary condition

$$vc(0,t) = -D\left(\frac{\partial c}{\partial x}\right)_{x=0} \qquad \text{(Ib}_1\text{)}$$

expresses the fact that the rate of solute deposition at the surface ($x = 0$), resulting from evaporation, must equal the diffusional flux of solute away from the surface. Suppose the evaporation is discontinued for the short period Δt, but not the movement of the solution, then the solution volume $v\Delta t$ cm.^{3} crosses the surface plane and with it $c(0,t)v\Delta t$ g. of solute. When evaporation proceeds, this amount of solute is left behind at the surface. Hence the rate of solute deposition is $c(0,t)v$ which, when set equal to the diffusional flux at the surface, gives eq. Ib$_1$.

The secondary boundary condition

$$\lim_{x \to \infty} c(x,t) = c_0,\ t \text{ finite} \qquad \text{(Ib}_2\text{)}$$

is intuitively true. It can be deduced rigorously from the fact that the solute excess at time t

$$\int_0^\infty [c(x,t) - c_0]\mathrm{d}x$$

is equal to the amount of solute that would have crossed the surface plane in the absence of evaporation, $c_0 vt$. In other words, the integral must converge for finite times, a necessary consequence of which is that the integrand vanishes as $x \to \infty$, and eq. Ib$_2$ follows.

Surface Activity.—The absorption of β rays is well approximated by the formula $A_x = A_0 e^{-kx}$, where A_0 is the activity in the absence of an absorber, A_x the activity observed through the absorber of thickness x, and k the absorption coefficient.[12] The activity of a solution element x cm. from the surface and dx cm. thick is $anc(x,t)\mathrm{d}x$ where a is the specific activity of the solute in c. g.$^{-1}$; n is the disintegration rate in 1 c. of radioactive material; and c is the concentration in g. ml.$^{-1}$. Of this activity, only the fraction G is emitted in the direction of the counter, therefore

$$\mathrm{d}A_x(t) = anGc(x,t)e^{-kx-w}\mathrm{d}x$$

where the constant w allows for the absorption in the

(8) A. F. H. Ward and L. Tordai, *J. Chem. Phys.*, **14**, 453 (1946).
(9) C. C. Addison, *J. Chem Soc.*, **252**, 477 (1944).
(10) W. J. Schwarz and D. C. Wood, *J. Colloid Sci.*, **13**, 616 (1958).
(11) J. R. Hommelen, *ibid.*, **14**, 385 (1959).

(12) The value of k is calculated from the mass absorption coefficient μ, usually reported in cm.^{2} mg.$^{-1}$, by $k = 10^3\mu\sigma$, where σ is the density of the absorber: G. Friedlander and J. Kennedy, "Introduction to Radiochemistry," John Wiley and Sons, Inc., New York, N. Y., 1949.

air path and the tube window. Integration of $dA_x(t)$ and setting $K = anGe^{-w}$, gives eq. II.

$$A = K \int_0^\infty c\epsilon^{-kx}\,dx \qquad (II)$$

The surface activity of the unevaporated solution, A_b, is obtained from eq. II by setting $c(x,t) = c_0$ and integrating

$$A_b = A_{(0)} = \frac{Kc_0}{k} \qquad (1)$$

Solution of the Problem.—The diffusion problem (eq. I, Ii, Ib_1, and Ib_2) was solved by means of the Laplace transformation

$$L_c(x,p) = \int_0^\infty e^{-pz}c(x,z)dz,\ z = Dt$$

The substitution of t by z/D merely serves to simplify the expressions. By established procedures, for which reference should be made to textbooks,[13] the Laplace transform of c in terms of x and the parameter p is found to be

$$L_c(x,p) = \frac{c_0}{p} + \frac{2c_0bq}{p^2}\,e^{-qx} \qquad (2)$$

where

$$b = \frac{v}{2D}$$

$$q = b + \sqrt{b^2 + p}$$

The straightforward continuation would be to obtain c from eq. 2 by inversion of the transform, then A from c by eq. II. This, however, leads to very cumbersome expressions. To avoid them, the order of integration was changed. Application of eq. II to eq. 2 yields the Laplace transform of A

$$L_A(p) = \frac{Kc_0}{kp} + \frac{2Kc_0bq}{p^2(k+q)}$$

and inversion of $L_A(p)$, which can be carried out with the aid of tables,[14] gives the surface activity A.

$$A(t) = \frac{Kc_0}{k} + \frac{2Kc_0k(b+k)^2}{m^2}\,\mathrm{erf}\,(b\sqrt{Dt}) + \frac{2Kc_0b^2k}{m}\left[Dt + \int_0^{Dt}\mathrm{erf}\,(b\sqrt{z})dz\right]^{15} + \frac{2Kc_0bk(b+k)}{m^2}\{e^{mDt}[1 - \mathrm{erf}\,(b+k)\sqrt{Dt}] - 1\} \qquad (3)$$

where

$$\mathrm{erf}\,(b\sqrt{Dt}) = \frac{2}{\sqrt{\pi}}\int_0^{b\sqrt{Dt}} e^{-y^2}\,dy,$$

$$m = k^2 + 2kb$$

(13) See for instance N. V. Churchill, "Operational Calculus," McGraw-Hill Book Co., Inc., New York, N. Y., 1953.

(14) A. Erdelyi, Editor, "Tables of Integral Transforms," McGraw-Hill Book Co., Inc., New York, N. Y., 1954 (notably item 22, Vol. I, p. 235).

(15) $\int_0^{Dt}\mathrm{erf}\,(b\sqrt{z})dz = \left(Dt - \frac{1}{2b^2}\right)\mathrm{erf}\,(b\sqrt{Dt}) + \frac{1}{b}\sqrt{\frac{Dt}{\pi}}\,e^{-b^2Dt}$

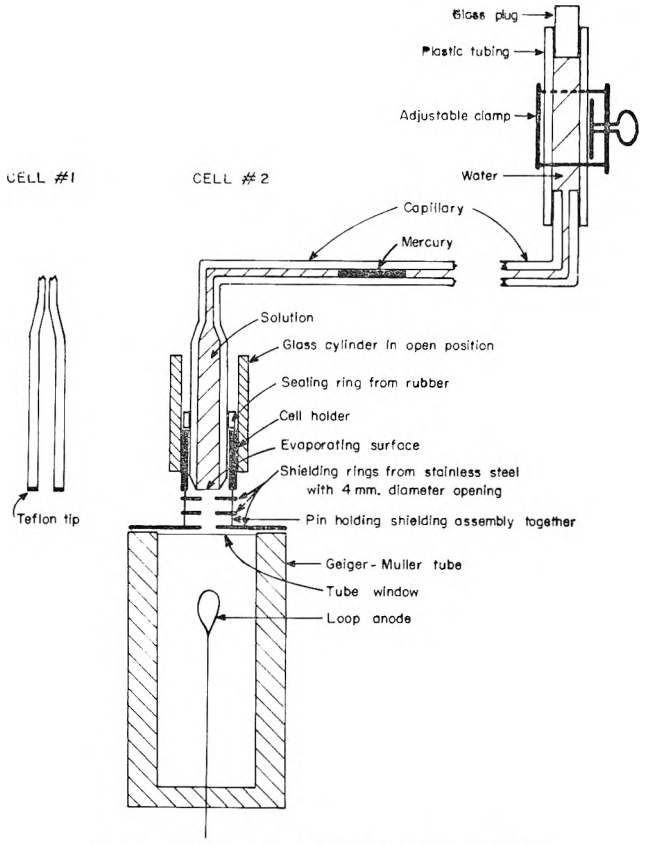

Fig. 1.—Surface counter for inverted solutions.

Equation 3 can be verified as follows. Equation II, which has the form of a Laplace transformation, is used to transform eq. I with respect to x in the same way as eq. I is transformed with respect to t (or z) in the usual Laplace transformation. The concentration at the surface, $c(0,t)$, needed for the lower integration limit, is given by eq. 5 later. This transformation leads to the ordinary differential equation

$$\frac{dA}{dt} = mDA - KkDc(0,x)$$

which must be satisfied by eq. 3 as it indeed is.

Calculation of Diffusion Coefficients.—Direct calculation of diffusion coefficients from eq. 3 is obviously impractical. Fortunately, for sufficiently long evaporation times, the diffusion coefficients can be calculated conveniently from the slope of the asymptote of eq. 3

$$S = \lim_{t\to\infty}\frac{dA}{dt} = \frac{Kc_0v^2}{v + kD}$$

which, on substituting K from eq. 1 and rearrangement, becomes

$$D = \frac{A_b}{S}v^2 - \frac{v}{k} \qquad (4)$$

an expression that relates D in simple terms with experimentally measurable quantities.

The slope of the surface activity curve approximates rapidly the slope of the asymptote. Theoretically, the approximation becomes good at the critical time $t_c = b^{-2}D^{-1}$, that is, when the exponents in the dominant exponential terms of A become -1. Typical critical

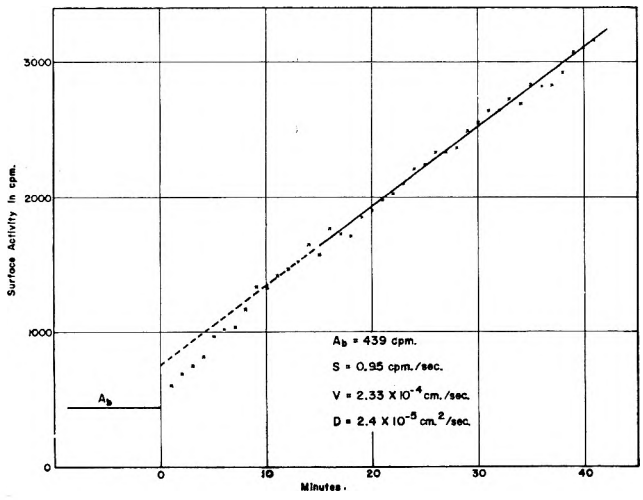

Fig. 2.—Surface activity of 0.1% $H_2S^{35}O_4$ solution during evaporation at 60°; cell 1 (diameter 3.7 mm.); high rate of evaporation.

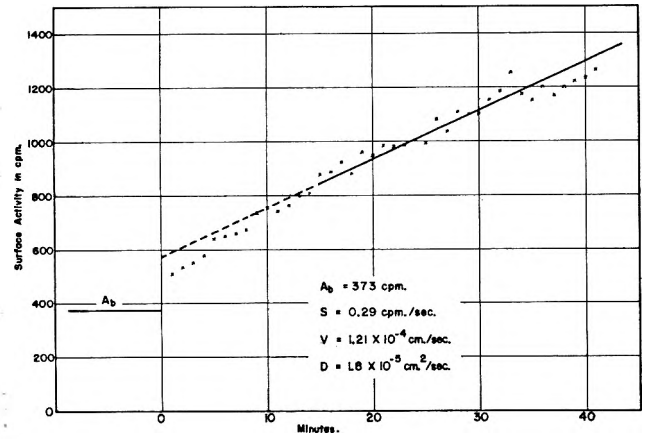

Fig. 3.—Surface activity of 0.1% $H_2S^{35}O_4$ solution during evaporation at 60°; cell 1 (diameter 3.7 mm.); reduced rate of evaporation.

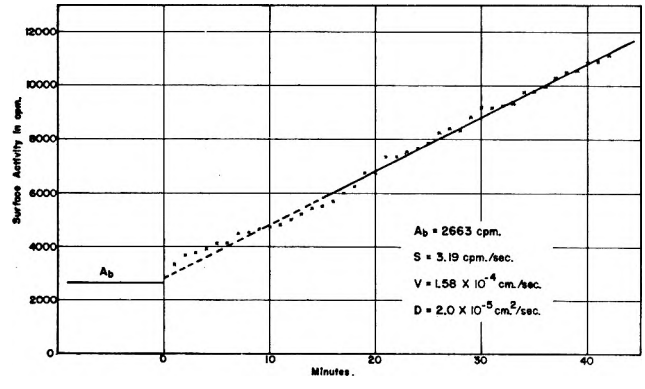

Fig. 4.—Surface activity of 0.1% $H_2S^{35}O_4$ solution during evaporation at 60°; cell 2 (diameter 6.1 mm.).

times are 10–20 min., which are easily exceeded in practice. The surface activity curve in Fig. 6, which was calculated from a set of typical constants, illustrates how good the approximation is not only at t_c but even earlier.

Solute Concentrations.—The formula for the solute concentration at the surface is obtained from eq. 2 by setting $x = 0$ and interpreting the transform in t.

$$c(0,t) = c_0 + 2c\,\mathrm{erf}(b\sqrt{Dt}) + 2cb\left[Dt + \int_0^{Dt} \mathrm{erf}(b\sqrt{z})dz\right]^{15} \quad (5)$$

The concentration is highest at the surface. Away from the surface it falls off to c_0 approximately proportionately with e^{-bz} for sufficiently long evaporation times.

Experimental

The apparatus for counting solution surfaces during evaporation is shown in Fig. 1. The solutions were held in the inverted position in round glass cells 3.7 and 6.1 mm. in diameter and about 5 cm. long (cells 1 and 2). A horizontal capillary connected the upper end of the cell with a plastic reservoir from which, by means of an adjustable clamp, solvent could be forced manually into the cell to replace evaporated solvent. A mercury plug in the capillary served to measure the solvent flow, from which the evaporation rate was computed.

The shielding assembly consisted of three stainless steel rings with aligned central openings 4 mm. in diameter and rested on the window frame of a Geiger–Müller tube. The assembly collimated the radiation emanating from the solution and thereby blocked out any stray radiation from the cell rim. A tightly fitting movable glass sleeve on the outside of the assembly permitted closure of the evaporation space and discontinuation of evaporation.

The end of the large cell was tapered from the outside to a sharp edge in order to facilitate shielding, which was adequate for the large cell. However, this provision proved to be inadequate for the small cell. The end of the small cell was, therefore, ground flat and covered with a matching piece of Teflon sheet 0.5 mm. thick, which, since Teflon is not wetted by detergent solution, prevented the deposition of radioactive solute at the cell rim and thus made shielding unnecessary.

The surface counter was mounted inside an air temperature box so that only the water reservoir remained outside. Inside the box a small fan provided as vigorous an air circulation as was possible to attain without causing noticeable vibration. The humidity inside the box was kept from rising by admitting some outside air to the box. During evaporation tests the air temperature in the box was 60 ± 0.5°.

The cell, the capillary, and the reservoir were filled outside the box while in an upright position, inverted and put in place with the cell rim 1.5–2 mm. above the upper shielding ring and approximately 16 mm. above the tube window. After the sleeve was closed and the meniscus of the solution adjusted so as to be level with the cell rim, the base count, *i.e.*, the surface activity of the unevaporated solution, was taken at room temperature. This was necessary because evaporation could not be completely prevented at 60° and the base counts taken at that temperature were too high, notably with the small cell. The base count at 60°, A_b, was obtained from the count taken at room temperature by multiplication with 1.06. The correction factor was computed from the air-density change, the length of the air path, and the mass absorption coefficient of the S^{35}-radiation. A similar correction factor was obtained experimentally with an 8 mm. diameter cell. Because the diffusion coefficient is not computed from the surface activity but from its rate of increase, the slow evaporation in the closed system is, except for its effect on the base count, of little consequence to the evaporation experiment.

The evaporation was usually begun 10 min. after the air temperature in the box had reached 60°. Counts were taken continuously for 1-min. periods and meniscus adjustments made every 0.5 or 1 min., depending on the rate of evaporation. The delays of resetting the scaler, about 2.5 sec./min. counting time, were allowed for in the computations. The displacement of the mercury plug was read every 10 min. Total evaporation time was usually 40 min.

Low evaporation rates were obtained by raising the sleeve only to the level of the second shielding ring.

The evaporation rates were constant during the tests except for the first few minutes of evaporation when they were about 20% higher. Assuming, as a first approximation, that the rate of evaporation is proportional to the vapor pressure of the solvent, the surface temperature of the rapidly evaporating solutions is estimated at 55°.

The sulfuric acid-S^{35} was used as received from Oak Ridge after removal of the bulk of HCl by evaporation and appropriate dilution with inactive sulfuric acid. The sodium dodecyl sulfate-S^{35} (SDS) was at least 95% pure, the remainder being 1–2% each of Na_2SO_4 and NaCl with up to 1% water.

Results

Typical surface activity curves for evaporating solutions are shown in Fig. 2–5. The first three are those of 0.1% sulfuric acid solutions tested at different evaporation rates and in different cells. The fourth belongs to a 0.5% sodium dodecyl sulfate solution. The base counts, A_b, are indicated by short horizontal lines preceding the beginning of the evaporation. All curves rise with increasing evaporation times.

The diffusion coefficients are computed as follows. A straight line is drawn through the points of the curve disregarding those for the first 15 min. of evaporation. In the anomalous case of the SDS curve a tangent is drawn instead at the 15-min. point. The slope of the straight lines or the tangent, S is expressed in terms of activity increase per second, that is, in counts/min./sec. From S, the base count A_b, the evaporation rate v in terms of the solution advancement in the cell, in cm./sec., and the absorption coefficient of the radiation k in cm.$^{-1}$, the diffusion coefficient is calculated by means of the formula

$$D = \frac{A_b}{S} v^2 - \frac{v}{k} \text{ [cm.}^2\text{/sec.]}$$

whose derivation was given in the Theoretical section.

The diffusion coefficients for the curves are listed in Table I along with the figures from which they were computed. For comparison, diffusion coefficients determined by the open-ended capillary method are also listed.

TABLE I

DATA FOR THE COMPUTATION OF DIFFUSION COEFFICIENTS BY THE EVAPORATION METHOD AND STANDARD DIFFUSION COEFFICIENTS

Solution	Figure	A_b, c.p.m.	S, c.p.m./sec.	$v \times 10^4$, cm./sec.	$k(S^{35}$ in $H_2O)$, cm.$^{-1}$	$D \times 10^5$, in cm.^{2}/sec. Evaporation method	Standard method
0.1% H_2SO_4	2	439	0.95	2.33	230	2.4	2.2
.1% H_2SO_4	3	373	0.29	1.21	230	1.8	2.2
.1% H_2SO_4	4	2663	3.19	1.58	230	2.0	2.2
.5% SDS	5	109	0.30	1.68	230	0.95	0.82

Discussion

It is seen that the diffusion coefficients estimated from the surface activity increase during evaporation do not differ by more than 10–20% from their standard values. This is a satisfactory agreement, for the very nature of the evaporation experiment is such that disturbing factors like vibration, impact of air currents, and surface cooling cannot be adequately controlled or eliminated.

For high evaporation rates the cell diameter has no effect on the diffusion coefficient as long as it is not larger than 6 mm. When it was increased to 8 mm., the diffusion coefficients became too large, presumably because the solution in a wide cell is more easily disturbed than in a narrow cell.

To test the diffusion coefficient formula experimentally, the diffusion coefficients of sulfuric acid were determined at different evaporation rates (Fig. 2 and 3). The formula requires that the slope of the surface activity curve should increase almost with the square of the evaporation rate. The experimental agreement with this requirement is fair.

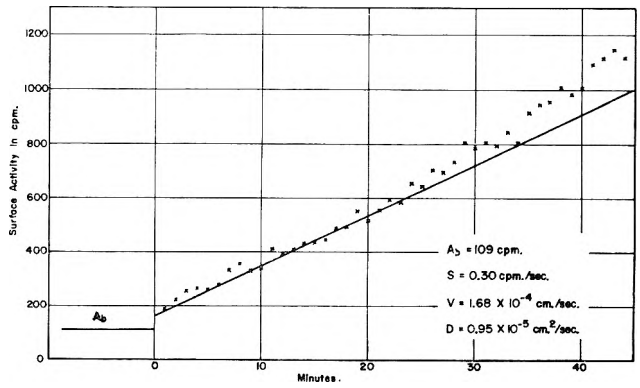

Fig. 5.—Surface activity of 0.5% sodium dodecyl sulfate (S^{35}) solution during evaporation at 60°; cell 2 (diameter 6.1 mm.).

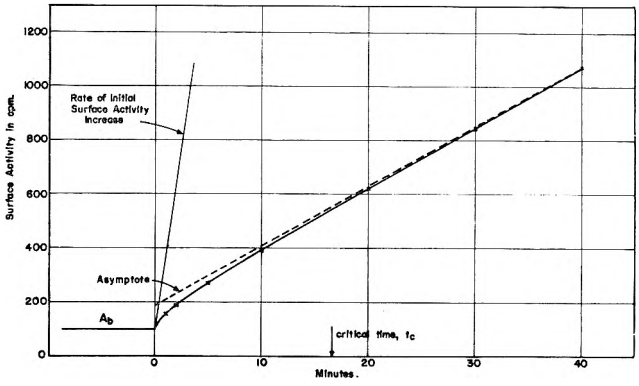

Fig. 6.—Theoretical surface activity curve eq. 3: $c_0 = 10^{-3}$ g./cm.^{3}; $K = 2.3 \times 10^7$ c.p.m. cm.^{2}/g.; $\mu = 2.30$ cm.$^{-1}$; $A_b = 100$ c.p.m.; $v = 2 \times 10^{-4}$ cm./sec.; $D = 10^{-5}$ cm.^{2}/sec.

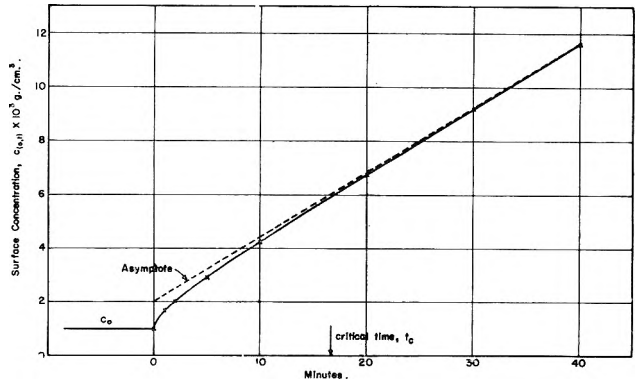

Fig. 7.—Theoretical surface concentration curve eq. 5: $c_0 = 10^{-3}$ g./cm.^{3}; $v = 2 \times 10^{-4}$ cm./sec.; $D = 10^{-5}$ cm.^{2}/sec.

The theory also requires a virtually[1] constant surface activity increase for solutes with constant diffusion coefficients. This is actually observed with sulfuric acid solutions. It is interesting that the detergent SDS, whose diffusion coefficient decreases with increasing concentration above 0.5%, should give an upward curving surface activity curve, thus reflecting the diffusion coefficient decrease.

From the agreement between experiment and theory with respect to the surface activity, it follows that the surface concentration of the solute, too, should be as given by the theory (eq. 5). Figures 6 and 7 show that there is a close parallelism between the calculated surface activity and the calculated surface concentration, the latter merely increasing somewhat more steeply than the former.

Conclusions

From the agreement between the conventional diffusion coefficients and those estimated by the evaporation procedure follows that the solute buildup at the surface of evaporating solutions is diffusion controlled. This holds equally for electrolytes and surface active compounds. When the radioactive source is a weak β emitter, the surface activity increase approximates the surface concentration increase. After a short initial transition period, both increase continuously and virtually linearly with the time of evaporation. Away from the surface the concentration falls off approximately exponentially from its highest value at the surface to the bulk concentration.

THE CONFIGURATION OF AN ADSORBED POLYMERIC DISPERSANT BY INFRARED STUDIES

BY B. J. FONTANA

California Research Corporation, Richmond, California

Received May 6, 1963

The fraction of attached ester segments of an alkyl methacrylate–polyglycol methacrylate copolymer molecule adsorbed onto silica was determined directly by infrared spectrometry. The exclusion of ester segments from attachment to the surface because of preferential adsorption of the polyglycol ether segments is demonstrated. It is suggested that the resultant polymer configuration is thus more extended away from the surface and that this accounts for the enhanced colloid stabilization properties reported for such polar-substituted polymers.

Introduction

The steric mechanism of stabilization of colloids requires the adsorption on the particles of a surfactant film of a thickness sufficient to increase the distance of closest approach and thus decrease the van der Waals energy of attraction to below the thermal energy. Such an effect has been demonstrated experimentally by van der Waarden[1] and others and treated theoretically by Mackor and van der Waals and by Vold.[2] Adsorbed macromolecules would be expected to possibly function well in this respect. Heller and Pugh[3] have postulated such a mechanism for aqueous gold sols stabilized by high molecular weight polyethylene glycols. With regard to hydrocarbon media, it has been found that appropriate modification of alkyl methacrylates can result in outstanding dispersants for use in automotive lubricating oils.[4] The introduction of a relatively small fraction of polar substituents into the polymer molecule results in a great enhancement of the dispersance.

In a previous study[5] it has been shown that polylauryl methacrylate, PLMA, adsorbed on silica, is attached to the surface through about 40% of the segments. In this case then, a relatively flat adsorbed film results, estimated to be ~30 Å. thick. Incorporating about 17 mole % N-vinyl-2-pyrrolidone into PLMA as a copolymer, PAM–VP, increased the adsorption at total surface coverage and gave a thicker film (~200 Å. as determined from sedimentation measurements).[5] The PAM–VP was shown to adsorb *via* both the ester and pyrrolidone carbonyl groups. The enhanced dispersant property of the PAM–VP[4] then is apparently due to the thicker adsorbed film, and it appears reasonable to assume that the thicker film results from the preferential adsorption of the smaller number of more strongly polar pyrrolidone groups. The latter behavior is in accord with the predictions of the recent statistical analysis of polymer adsorption by Silberberg.[6] It was not possible to demonstrate this effect in the previous studies because of the overlapping of the pertinent infrared bands. In the present study the effect has been quantitatively determined for an alkyl methacrylate–polyglycol methacrylate copolymer, PAM–PG. The latter belongs to a class of outstanding dispersants used as ashless detergents in engine oils and specifically designed to be efficient hydrogen bonding detergents.[7]

Experimental

PAM–PG was prepared by direct copolymerization of the alkyl methacrylate and polyethylene glycol tridecyl ether methacrylate with 2,2′-azobis(2-methylpropionitrile) initiator in refluxing benzene. The alkyl groups were of mixed length averaging 14 carbon atoms. The polyethylene glycol residue $[CH_2CH_2O]_n$ was 1600 average molecular weight and was capped with a 13-carbon alkyl. The present sample was a narrow fraction obtained by solvent precipitation. The mole ratio of alkyl methacrylate to polyethylene glycol in this fraction was 20:1 as determined by both infrared and elemental analysis. The copolymer molecular weight was ~310,000 as determined from intrinsic viscosity (29 in isooctane, 86 in benzene at 25°).

The measurement of the adsorption isotherms and of the infrared spectra of the adsorbed species on silica is described in a previous publication.[5] The details of the determination of the pertinent extinction coefficients and calculations of the fraction of adsorbed ester segments, p, are also given therein. The carbonyl extinction coefficient, ϵ_w, for free polymer PAM–PG in *n*-dodecane solution was 1120 as compared to 1465 for PLMA (and 1180 and 1510, respectively, in decalin). This ratio (0.773 ± 0.009) is accounted for by the difference in equivalent weights. Hence, the ϵ_w value used for adsorbed carbonyl was corrected accordingly

$$\epsilon_w \text{ (PAM–PG)} = 1650 \times 0.773 = 1275$$

The infrared frequencies for the free and adsorbed carbonyl had exactly the same values as previously observed for PLMA.

Results and Discussion

In comparing the behavior of the polyglycol substituted polymer with the simple polyalkyl methacrylate, it should be noted that both have identical methacrylate "backbones." The basic structural formula of PAM–PG is given on the following page.

(1) M. van der Waarden, *J. Colloid Sci.*, **5**, 317 (1950); **6**, 443 (1951).

(2) E. L. Mackor, *ibid.*, **6**, 492 (1951); E. L. Mackor and J. H. van der Waals, *ibid.*, **7**, 535 (1952); M. J. Vold, *ibid.*, **16**, 1 (1961).

(3) W. Heller and T. L. Pugh, *J. Polymer Sci.*, **47**, 203 (1960).

(4) A. L. Lyman and F. W. Kavanagh, *Proc. Am. Petrol. Inst., Sect. III*, **39**, 296 (1959).

(5) B. J. Fontana and J. R. Thomas, *J. Phys. Chem.*, **65**, 480 (1961).

(6) A. Silberberg, *ibid.*, **66**, 1872 (1962).

(7) W. T. Stewart, F. A. Stuart, and J. A. Miller, Division of Petroleum Chemistry, American Chemical Society, Preprints, Vol. 7, No. 4, 1962, p. B-19.

TABLE I

DETERMINATION OF THE FRACTION OF ADSORBED ESTER SEGMENTS

Polymer (solvent)	Adsorbed polymer mg./g. silica, σ	Fraction of surface covered, θ	Mg. polymer/cm.^{2}[a] — Adsorbed segments — From CO data	From OH data	Total adsorbed polymer	Fraction of adsorbed carbonyl groups,[b] p
PAM–PG (*n*-dodecane)	586	0.69	0.040	0.151	0.486	0.08 (0.31)
	283	.33	.026	.098	.276	.094 (.35)
PAM–PG (decalin)	652	.95	.017	.156	.508	.033 (.31)
	500	.73	.029	.150	.517	.06 (.29)
	301	.44	.024	.110	.293	.082 (.38)
	178	.26	.019	.084	.180	.106 (.47)
PLMA (both)	...	0.16–0.96	...	...	...	.40 (.46)

[a] Weight per unit area in the spectrometer beam, see ref. 5. [b] Based on CO data; values in parentheses are the "apparent p" based on OH data, see text. PLMA data are from ref. 5.

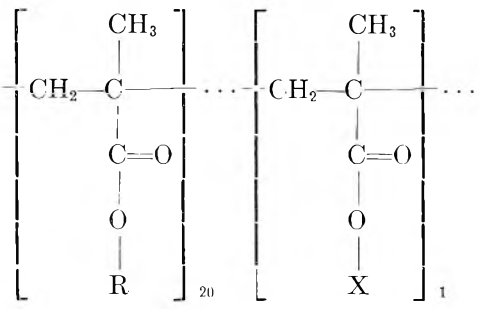

where $R = C_{14}H_{29}$, and $X = [CH_2CH_2O]_{36}C_{13}H_{27}$.

The results obtained for PAM–PG are given in Table I. Comparison of these data should be made with those of ref. 5. The pertinent values in the latter have been averaged and summarized in the last line of Table I.

Substitution of the long polyglycol chains into the alkyl methacrylate polymer results in a 2.4- to 2.6-fold increase in the amount of polymer adsorbed at total coverage, σ_0 (Table II). Accompanying this effect is a fourfold or greater decrease in p, the fraction of the total number of ester carbonyl groups in an adsorbed polymer molecule which are directly attached to the silica surface hydroxyls *via* hydrogen bonds. The increase in σ_0 and decrease in p must be interdependent if the effects are interpreted as being due to preferential adsorption of the polyethylene oxide groups to the exclusion of the ester carbonyl groups. Correlatively, the change in σ_0 should be smaller than that in p, as found, if the polyethylene oxide groups are also adsorbed at the interface. The large increase in σ_0 brought about by introduction of a small fraction of more polar segments has been demonstrated elsewhere with partially hydrolyzed polymethyl methacrylate[8] and polyvinyl acetate.[9]

The fraction θ of the surface covered is here the ratio of the amount of adsorbed polymer σ to the amount adsorbed σ_0 at the plateau of the adsorption isotherm at high polymer concentrations. The results in Table I show a trend in the values of p decreasing with increasing coverage θ. No such effect was apparent with PLMA.[5] This is not unreasonable in view of the apparent configurations of the adsorbed polymers. The PLMA is relatively flat and extended parallel to the surface with 40% of the ester segments attached, while the PAM–PG is relatively extended away from the surface with only 10% or less of the ester segments attached. In the latter case, of course, some of the preferentially adsorbed but less populous polyglycol segments are also attached to the surface.

TABLE II

INTRINSIC VISCOSITY AND ADSORPTION

Polymer	$[\eta]$ at 25° — Dodecane	Decalin	Inverse ratio	σ_0 at 25° — Dodecane	Decalin	Ratio
PAM–PG	24	56	2.3	855	685	1.3
PLMA	74	95	1.3	329	282	1.2

The data also show (Table II) more definitively than previously for PLMA[5] that the state of the polymer in the solvent phase (voluminosity as indicated by the intrinsic viscosity) has only a weak, if any, effect on the configuration at the surface. The decrease in σ_0 in going from dodecane to decalin as solvent is about the same for PLMA and PAM–PG. This suggests that competition with the solvent for surface sites is mainly involved.

The spectral data for bound hydroxyl at the surface cannot be used as before[5] to calculate a supplementary value for the fraction of attached ester segments if, as suggested, the polyglycol segments are also involved in the attachment to the silica surface hydroxyls. That the latter is, indeed, the case can be shown by calculating the apparent adsorbed carbonyl from the bound hydroxyl peak intensity enhancement on the same basis as previously (that is, assuming for the purpose of this calculation, that H-bonding by carbonyl oxygen only is contributing to the observed effect on the OH peak). These values (in parentheses in Table I) are seen to be about fourfold greater than the "true" value obtained from the carbonyl data. This can only mean that a notable fraction of the polyethylene oxide groups are attached to the surface *via* H-bonding of the ether oxygen to surface hydroxyl. No additional significance should be attached to the apparent p values since the quantitative effect of ether oxygen on the hydroxyl extinction is not known.

The preferential adsorption observed here of the polyethylene oxide groups requires, of course, that ether oxygen form a stronger H-bond than ester carbonyl oxygen. The available data in homogeneous systems[10,11] support this view. Conflicting enthalpy data have apparently been resolved in recent work by Joesten and Drago.[12] The OH stretching frequency shift (decrease)

(8) S. Ellerstein and R. Ullman, *J. Polymer Sci.*, **55**, 123 (1961).

(9) J. Koral, R. Ullman, and F. R. Eirich, *J. Phys. Chem.*, **62**, 451 (1958).

(10) G. C. Pimentel and A. L. McClellan, "The Hydrogen Bond," Freeman and Company, San Francisco and London, 1960, pp. 86, 91, and 362.

(11) R. F. Blanks and J. M. Pravsnitz, *J. Chem. Phys.*, **38**, 1500 (1963); this recent study of H-bonding with propanol of polybutyl methacrylate and polypropylene oxide is especially pertinent.

(12) M. D. Joesten and R. S. Drago, *J. Am. Chem. Soc.*, **84**, 3817 (1962).

is invariably greater for H-bonding with ethers (for example, by over 100 cm.$^{-1}$ with phenol as the H-donor). The latter is taken to mean that ethers are more powerful electron donors than esters with respect to H-bond formation.[13] The present results appear to concur with this view. The broad bound OH peak observed at about 3420 cm.$^{-1}$ with PLMA shifts only about 17 cm.$^{-1}$ lower with PAM–PG; however, the peak broadens considerably (80 to 105 cm.$^{-1}$ at the half-intensity width) on the low frequency side.

(13) W. Gordy, *J. Chem. Phys.*, **7**, 93 (1939); **9**, 215 (1941).

The data presented here, support the view that increased film thickness occurs with polymeric dispersants because of the preferential adsorption of the more polar segments. This results in a configuration more extended away from the surface than with a monophyletic polymer. This is in accord with the consequent enhancement of the effectiveness as colloidal dispersants.

Acknowledgment.—The author is obligated to Dr. J. R. Thomas for past contributions in our Laboratory to the study of colloid stabilization.

PROTON MAGNETIC RESONANCE SPECTRA OF VINYLSILANES

BY ROBERT SUMMITT,[1] JOHN J. EISCH,[2] JAMES T. TRAINOR,[3] AND MAX T. ROGERS[4]

Corning Glass Works, Corning, New York, Kedzie Chemical Laboratory, Michigan State University, East Lansing, Michigan, and the Department of Chemistry, University of Michigan, Ann Arbor, Michigan

Received May 11, 1963

The proton magnetic resonance spectra of a series of vinylsilanes, $R_3SiCH{=}CH_2$ (where R = chloro, alkyl, or a substituted phenyl group), have been analyzed to obtain the spin coupling constants and chemical shift parameters for the vinylic protons. The small variation in the coupling constant sum, ΣJ_{ij}, supports the view that the silicon atom effectively shields the vinyl group from inductive electronic effects exerted by the substituent R. On the other hand, the approximate correlation noted between the electronic nature of R and the *trans* proton chemical shift is consistent with a variable d_π–p_π resonance effect between the silicon atom and the vinyl group. Possible reasons for the failure of β-*cis* and α-protons to show a similar trend are discussed.

Introduction

Considerable attention has focused on the question of bond overlap between the π-cloud of vinyl and propargyl groups and available d-orbitals of elements from the second or higher rows of the periodic table (d_π–p_π overlap).[5-7] Studies of acid and base strengths[8] and the addition of hydrogen halides to vinylsilanes[9] have been interpreted in terms of such d_π–p_π bonding, and measurements of dipole moments[10] and infrared[11-13] and proton magnetic resonance (p.m.r.)[14,15] spectra have been used to investigate this problem.

P.m.r. spectra of a few vinylsilanes, $R_nSi(CH{=}CH_2)_{4-n}$ where R = CH_3 or C_6H_5, have been analyzed and the results discussed with reference to possible d_π–p_π bonding.[14,15] We have synthesized a series of vinylsilanes, $R_3SiCH{=}CH_2$, in which the group R can be varied to achieve differences in the electronic environment at the silicon atom.[13] Examination of the infrared spectra of these compounds has revealed a correlation between the CH_2 "wag" frequency of the vinyl group and the electron-withdrawing power of the substituent R.[13] The p.m.r. spectra of these vinylsilanes have now been obtained and analyzed to learn whether they reflect a similar sensitivity to the electronic nature of R. This paper presents the results and discusses the vinylic spin coupling constants and chemical shift parameters in relation to possible substituent effects.

(1) Research and Development Division, Corning Glass Works, Corning, N. Y.

(2) Department of Chemistry, Catholic University of America, Washington, D. C.

(3) Research Laboratories, Raybestos Division, Raybestos-Manhattan, Inc., Stratford, Conn.

(4) Kedzie Chemical Laboratory, Michigan State University, East Lansing, Mich.

(5) P. D. George, M. Prober, and J. R. Elliot, *Chem. Rev.*, **56**, 1065 (1956).

(6) C. Eaborn, "Organosilicon Compounds," Academic Press, Inc., New York, N. Y., 1960, pp. 91–103.

(7) D. Seyferth, "Progress in Inorganic Chemistry," Vol. 3, F. A. Cotton, Ed., Interscience Publishers, New York, N. Y., 1962, p. 129 ff.

(8) R. A. Benkeser and H. R. Krysiak, *J. Am. Chem. Soc.*, **75**, 2421 (1953).

(9) L. H. Sommer, D. L. Bailey, G. M. Goldberg, C. E. Buck, T. S. Bye, J. F. Evans, and F. C. Whitmore, *ibid.*, **76**, 1613 (1954).

(10) H. Soffer with T. DeVries, *ibid.*, **73**, 5817 (1951).

(11) W. J. Potts and R. A. Nyquist, *Spectrochim. Acta*, **15**, 679 (1959).

(12) H. Buchert and W. Zeil, *ibid.*, **18**, 1043 (1962).

(13) J. J. Eisch and J. T. Trainor, *J. Org. Chem.*, **28**, 487 (1963).

(14) R. T. Hobgood, Jr., J. H. Goldstein, and G. S. Reddy, *J. Chem. Phys.*, **35**, 2038 (1961).

(15) R. T. Hobgood, Jr., and J. H. Goldstein, *Spectrochim. Acta*, **19**, 321 (1963).

Experimental

The preparation and purification of the vinylsilanes employed in this study (Table I) have been given elsewhere.[13]

P.m.r. spectra of the vinylsilanes listed in Table I were recorded on a Varian A-60 analytical spectrometer at 25°. Chemical shifts of spectral lines were measured relative to tetramethylsilane (TMS) as an internal standard (*ca.* 5% concentration) using a 500-c.p.s. sweep width. These measurements and the chemical shifts relative to TMS computed from them are accurate to ±1 c.p.s. Higher resolution spectra of the vinylic region were recorded using a 100-c.p.s. sweep width. Reproducibility in the measurement of relative chemical shifts of these lines was ±0.05 c.p.s., and relative chemical shifts and spin coupling constants appear to be accurate to about ±0.3 c.p.s. All samples were 15% concentration by weight in carbon tetrachloride, because small concentration shifts were noticed.[16]

Results

With one exception, spectra in the vinylic region were of the ABC type.[17] The spectra of $(C_6H_5)_3SiCH{=}CH_2$, $(C_6H_5)_2ClSiCH{=}CH_2$, and $(C_6H_5CH_2)_3SiCH{=}CH_2$ are reproduced in Fig. 1. These examples serve to illustrate the forms of the spectra and the assignment used in computation. The spectra of $(C_6H_5)_3$-

(16) Strictly speaking, one would prefer data from spectra at several concentrations which could be extrapolated to obtain the chemical shifts at infinite dilution. However, the observed solvent effects were small (for affected lines, differences of less than 0.5 c.p.s. between a dilute sample, *e.g.*, 5%, and pure liquid $(CH_3)_3SiCH{=}CH_2$), and since these effects are not understood well, no effort was made to obtain these data.

(17) H. J. Bernstein, J. A. Pople, and W. G. Schneider, *Can. J. Chem.*, **35**, 65 (1957).

Table I

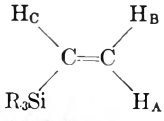

Compound	Chemical shifts[a] $-\nu_0\delta_A$	$-\nu_0\delta_B$	$-\nu_0\delta_C$	Coupling constants[b] J_{gem}	J_{trans}	J_{cis}	ΣJ_{ij}[c]
$(C_6H_5CH_2)_3SiCH=CH_2$	332.2	355.9	356.8	3.1	21.0	15.1	39.10
$(C_6H_5)_2ClSiCH=CH_2$	353.9	370.7	384.2	3.2	20.1	13.9	37.83
$(CH_3)_3SiCH=CH_2$	336.5	351.5	364.9	3.6	20.2	15.0	38.53
$(C_6H_5)_3SiCH=CH_2$	345.0	374.1	397.7	3.6	20.4	14.5	38.40
$(p\text{-}FC_6H_4)_3SiCH=CH_2$	343.5	375.9	394.2	3.4	20.5	14.5	38.33
$(p\text{-}CH_3C_6H_4)_3SiCH=CH_2$	341.9	370.9	395.1	3.7	20.1	14.4	38.25
$(p\text{-}CH_3OC_6H_4)_3SiCH=CH_2$	344.3	373.5	396.9	3.8	20.3	14.3	38.40
$(p\text{-}CF_3C_6H_4)_3SiCH=CH_2$	347.0	380.0	395.2	3.0	20.1	14.2	37.30
$Cl_3SiCH=CH_2$	374.8[d]						

[a] Relative to tetramethylsilane (5%) as internal standard, in c.p.s. at 60 Mc. Error in calculated values ±1 c.p.s. Error in chemical shift differences, *i.e.*, $\nu_0\delta_A - \nu_0\delta_B$, etc., ±0.3 c.p.s. [b] Calculated coupling constants in c.p.s. Error, ±0.3 c.p.s. [c] Sum of the repeated spacings observed in the spectra. [d] Only one line observed, with Si^{29} side bands.

$SiCH=CH_2$, $(p\text{-}CH_3C_6H_4)_3SiCH=CH_2$, and $(p\text{-}CH_3OC_6H_4)_3SiCH=CH_2$ were remarkably similar, differing only by slight chemical shifts of the entire spectrum and partial overlap by the phenyl proton resonances. Those of $(C_6H_5)_2ClSiCH=CH_2$, $(CH_3)_3SiCH=CH_2$, $(C_6H_5CH_2)_3SiCH=CH_2$, and $Cl_3SiCH=CH_2$ showed the greatest multiplet collapse.

Hobgood, Goldstein, and Reddy[14] examined $Cl_3SiCH—CH_2$ at 40 Mc. and reported its spectrum to consist of a single slightly broadened line at −248 c.p.s. (−372, converted to 60 Mc.), with a suggestion of structure. Our spectrum of this substance at 60 Mc. showed a single sharp line at −374.8 c.p.s., with no suggestion of structure save for the side bands presumably due to the Si^{29} isotope (spin $^1/_2$, natural abundance 4.7%). The separation of these side bands was 4.0 c.p.s. The chemical shift of the signal is almost exactly the same as that of Cl_3SiH.[18] It is puzzling that all three protons apparently are magnetically equivalent to both the external field and the Si^{29} nucleus.

Chemical shifts and coupling constants were calculated from the spectra by the method of Castellano and Waugh.[19] This is an exact method in which parameters are computed directly from measured frequencies rather than by the numerical fitting of the observed spectra by successive approximations. The details of the computation can be found in ref. 19. For most of the vinylsilanes assignment of lines to the A, B, and C quartets was unambiguous. In the remaining cases assignment was made by comparison with simpler spectra (see Fig. 1) and with the spectra of other vinyl derivatives, making use of the fact that $J_{trans} > J_{cis} > J_{gem}$.[20-22] Calculated values for chemical shifts and coupling constants, together with experimental values for the coupling constant sum, are listed in Table I. These were computed from the eigenvalues of the Hamiltonian matrix, obtained as differences between observed line frequencies. Although these latter were measureable to ±0.05 c.p.s., the resulting error in derived eigenvalues was large enough to produce small discrepancies between calculated and observed values for the coupling constant sums.

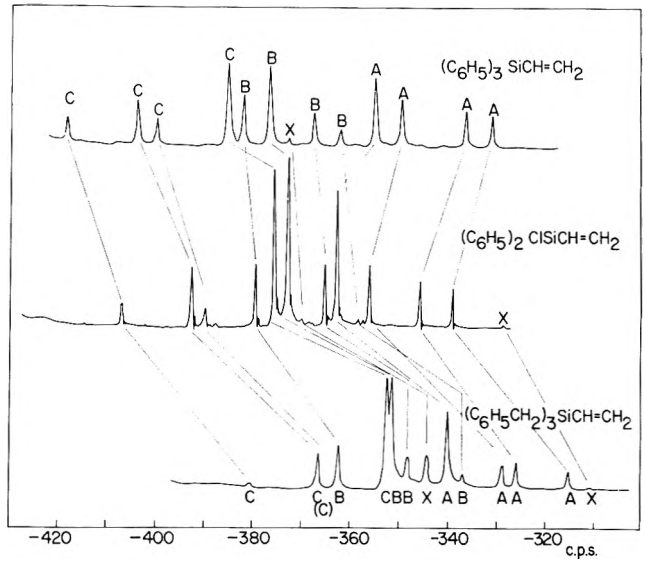

Fig. 1.—Vinyl region of the high resolution p.m.r. spectra of $(C_6H_5)_3SiCH=CH_2$, $(C_6H_5)_2ClSiCH=CH_2$, and $(C_6H_5CH_2)_3SiCH=CH_2$. Scale is in c.p.s. relative to tetramethylsilane at 60 Mc. Letters A, B, and C indicate nucleus to which transition has been "assigned," and X indicates combination transition.

Analyses have been given previously for trimethylvinylsilane[14] and triphenylvinylsilane,[15] using a numerical method of fitting the spectra. The agreement with the present results is quite satisfactory, in that the values calculated for ΣJ_{ij} are identical, and both sets differ from the experimental value by less than 1%.

In all cases studied here the signs of J_{cis}, J_{trans}, and J_{gem} were the same and presumably all positive.

Discussion

The experimental values of the coupling constant sum lie in the narrow range between 37.3 and 39.1 c.p.s. This seems surprising at first sight. Waugh and Castellano[23] have noted that a rough correlation exists between this quantity and the electronegativity of the vinyl substituent. While electronegativities here do not span a tremendous range, one might expect, for example, different electronegativities for the triphenylsilyl and the diphenylchlorosilyl groups. If the differences in the electronegativities of the

(18) D. E. Webster, *J. Chem. Soc.*, 5132 (1960).
(19) S. Castellano and J. S. Waugh, *J. Chem. Phys.*, **34**, 295 (1961).
(20) N. Banwell and N. Sheppard, *Mol. Phys.*, **3**, 351 (1960).
(21) W. Brügel, Th. Ankel, and F. Kruckeberg, *Z. Elektrochem.*, **64**, 1121 (1960).
(22) J. A. Pople, W. G. Schneider, and H. J. Bernstein, "High Resolution Nuclear Magnetic Resonance," McGraw-Hill Book Co., Inc., New York, N. Y., 1960.
(23) J. S. Waugh and S. Castellano, *J. Chem. Phys.*, **35**, 1900 (1961).

chlorine and phenyl groups are transmitted through the silicon atom as an inductive effect, these variations in the group electronegativity should be apparent in ΣJ_{ij}. For a comparison, the values for styrene and vinyl chloride are 29.5 and 20.7 c.p.s.,[20] respectively. However, a situation similar to that of the vinylsilanes has been noted[18] in the chemical shifts of the single proton in trisubstituted silanes, R_3SiH, where substituent effects would probably be transmitted through the single σ-bond, and the observed differences in the chemical shift would reflect the different inductive effects of the substituents. In two series of compounds where three methyl groups were successively replaced by chlorine and by phenyl groups, the proton chemical shift of R_3SiH was found to move downfield by approximately one-third the downfield shift observed in the corresponding methane series, R_3CH. Clearly the inductive electronic effect of substituents bonded directly to silicon is attenuated markedly in comparison with that observed for carbon analogs. A greater attenuation of such purely inductive effects should be expected at atoms one or two bonds further removed from the silicon atom. Consequently, the small variation in ΣJ_{ij} for the vinylsilanes is consonant with the view that silicon shields the vinyl protons from the *inductive* electronic effect of the substituent R.

Banwell and Sheppard[20] have shown that an approximately linear relationship exists between J_{trans} and the substituent's electronegativity (χ), while J_{gem} and J_{cis} are similarly related to it. If their plot of J_{trans} *vs.* χ is extended to the value $\chi_{Si} = 1.8$, the value $J_{trans} = 19.8$ c.p.s. is obtained; values calculated from the spectra of the vinylsilanes lie between 20.1 and 21.0 c.p.s. From this and the previous considerations it is apparent that the values of vinyl proton spin coupling constants in vinylsilanes are in agreement with the interpretation of Banwell and Sheppard: namely, that the variation in vinylic coupling constants from one compound to another is primarily a function of inductive effects with relatively minor contributions by other factors.

Values of J_{gem} for the vinylsilanes vary between 3.0 and 3.8 c.p.s. The geminal coupling in the HCH group has been related theoretically to the HCH bond angle.[24] By utilizing the curve obtained by Gutowsky and coworkers[24] one obtains values of the bond angle H_ACH_B (notation of Table I) of 119–120° in the vinylsilanes, in good agreement with the value reported[25] from microwave spectroscopy for $H_3SiCH{=}CH_2$ itself. In view of the known dependence of J_{gem} on the electronegativity of the substituent, however, this agreement is probably fortuitous.

Chemical shifts of the vinylic protons in the vinylsilanes have two noteworthy features: first, the resonance of the *trans* proton is at a lower field than that of the *cis* proton; and second, the chemical shifts, $\nu_0\delta_{cis}-\nu_0\delta_{trans}$ and $\nu_0\delta_{trans}-\nu_0\delta_{gem}$, are approximately equal (except in $(C_6H_5CH_2)_3SiCH{=}CH_2$). These characteristics contrast sharply with those of typical vinylic shifts in which the *trans* proton occurs at highest field and the chemical shift difference, $\nu_0\delta_{cis}-\nu_0\delta_{trans}$, is 5 to 50 times greater than $\nu_0\delta_{trans} - \nu_0\delta_{gem}$.[20-22] Closer examination of the p.m.r. spectra of vinylsilanes shows that the resonances of both β-protons are at lower field and, in general, the center of gravity in these spectra is at a lower field than in most vinyl spectra.

Banwell and Sheppard[20] have noted a correlation between the internal chemical shift of the α-proton and the mean shift of the β-protons (their quantity $\Delta_2 = \delta_A - (\delta_B + \delta_C)/2$, where δ is the chemical shift in p.p.m.) and σ_R the resonance contribution to the Hammett σ-constants.[26,27] This correlation appears to reflect the extent to which the electrons are supplied to or removed from the vinyl group by resonance (I).

$$R{-}CH{=}CH_2 \longleftrightarrow R{-}\overset{-}{C}H{-}\overset{+}{C}H_2 \longleftrightarrow R{=}CH{-}\overset{+}{C}H_2 \qquad (I)$$

Such a description as I implies that the electron density at the two β-protons would be affected equally and their chemical shifts should move in unison as the nature of the vinyl substituent changes, which is the observed result for most vinyl compounds. However, when the vinyl substituent is changed to an atom of the second (or higher) period, as in the vinylsilanes studied here and the series $(CH_2{=}CH)_nM$, where M = As, Pb, Sb, Bi, etc.,[21] the resonance of the β-proton *trans* to the substituent suffers a much larger downfield shift than the β-*cis* proton, and the *trans* proton resonance now occurs at *lower* field than the *cis*. The β-protons clearly do not shift in unison if second or higher row substituents are considered.

A comparison between the β-*trans* proton chemical shifts and the σ-parameters for two series of vinylsilanes, $(R{-}C_6H_5)_3SiCH{=}CH_2$ and $R_3SiCH{=}CH_2$ (Table II), reveals the following points of interest. First, with the exception of tris-*p*-anisylvinylsilane, the triarylvinylsilanes, $(RC_6H_4)_3SiCH{=}CH_2$, tend to display increasingly deshielded β-*trans* proton resonances as the σ_p-value of the *para* substituent becomes more positive. This implies the operation of the electron-withdrawing power of the *para*-substituted phenyl group through the Si–C–C chain upon the β-*trans* proton. Secondly, with the exception of chlorodiphenylvinylsilane (the only entry with nonidentical Si substituents and, hence subject to conformational considerations), the vinylsilanes of the type $R_3SiCH{=}CH_2$ tend to exhibit increasingly deshielded β-*trans* proton resonances as the group R withdraws electrons more strongly from silicon by the inductive effect (increasing value of σ^*).[28] Since the small variation in the value of ΣJ_{ij} for the series of vinylsilanes does not suggest any significant inductive electronic effect, this trend in chemical shifts is ascribed to a variable contribution in the d_π–p_π resonance effect (II). Elec-

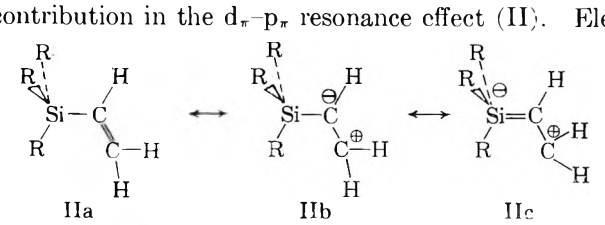

IIa IIb IIc

(24) H. S. Gutowsky, M. Karplus, and D. M. Grant, *J. Chem. Phys.*, **31**, 1278 (1959).

(25) J. M. O'Reilly and L. Pierce, *ibid.*, **34**, 1176 (1961).

(26) R. W. Taft, Jr., *J. Am. Chem. Soc.*, **79**, 1045 (1957).

(27) R. W. Taft, Jr., "Steric Effects in Organic Chemistry," M. S. Newman, Ed., John Wiley and Sons, Inc., New York, N. Y., 1956, pp. 594–597.

(28) Similar to the findings in the infrared study of vinylsilanes,[18] σ_p-values may correlate better with the observed chemical shifts of the β-*trans* protons than the σ^*-values. Unfortunately, not all the requisite σ_p-values are available for examination (Table II). However, with both types of vinylsilanes it is apparent that the $\nu_0\delta_{trans}$–σ correlations are not cleanly linear in any event.

Table II

Comparison of β-*trans* Proton Chemical Shifts with σ-Parameters

p-Substituted phenylvinylsilanes, $(R—C_6H_4)_3Si—CH=CH_2$				Trisubstituted vinylsilanes, $R_3Si—CH=CH_2$				
R	$-\nu_0\delta_{trans}$[b]	σ_p	$\sigma_p - \sigma'$[a]	R	$-\nu_0\delta_{trans}$[b]	σ^*[c]	$\sigma_p - \sigma'$[a]	σ_p
CH_3	370.9	−0.170	−0.13	CH_3	351.5	0.00	−0.13	−0.17
CH_3O	373.5	− .268	− .50	$C_6H_5CH_2$	355.9	.22	?	?
H	374.1	+ .000	.00	$CH_2=CH$[d]	364.4	.1–0.5[e]	?	?
				$(C_6H_5)_2Cl$[f]	370.7	1.38		
F	375.9	+ .062	− .44	C_6H_5	374.1	0.6	0.00	0.00
CF_3	380.0	+ .551	+ .14	Cl	374.8	2.94	− .24	+ .23

[a] $\sigma_p - \sigma' = \sigma_R$, resonance contribution of the substituent. *Cf.* ref. 26. [b] Chemical shift in c.p.s. at 60 Mc. relative to tetramethylsilane. [c] σ^* = net polar contribution of the substituent. *Cf.* ref. 27, p. 587. [d] Reference 15. [e] Values estimated to be from 0.1 to 0.5 (ref. 18). [f] Weighted average of σ^* of $2C_6H_5$ + 1Cl atom. (May be subject to conformational variations.)

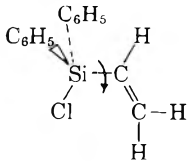

tron withdrawal by R would be expected to enhance the importance of canonical forms IIb and IIc and hence to cause increased deshielding of the β-*trans* proton in both series of vinylsilanes. It seems unlikely that the downfield shift of the *trans* proton could arise entirely from a neighbor anisotropy effect.

On the other hand, no equally satisfactory correlation can be discerned between the chemical shifts of the β-*cis* and α-protons and any reasonable σ-parameters (Tables III and IV). The failure of $\nu_0\delta_{cis}$ and $\nu_0\delta_{gem}$ to parallel any definite trend in the electronic character of the substituent R is open to at least two interpretations. In the first place, *trans*-delocalization of the π-cloud toward silicon (IIIa) (and hence, selective deshielding) may be favored preferentially over *cis*-delocalization (IIIb). Such preferential *trans*-delocalization would be consistent with the hypothesis of the minimum bending of molecular orbitals.[29] The smaller curvature of the hypothetical molecular orbital encompassing the silicon atom and the β-*trans* proton (IIIa) would presumably make it more important in the ground state than IIIb. However, an alternative explanation may lie in the greater sensitivity of the β-*cis* and α-protons to anisotropic effects arising from the neighboring groups on silicon (IIa). The projection of the β-*trans*-proton away from such R groups on silicon would make it less susceptible to these field effects.

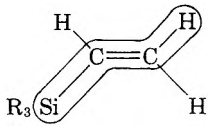

IIIa

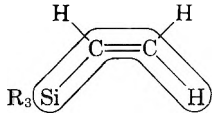

IIIb

(29) (a) H. Eyring, G. H. Stewart, and R. F. Smith, *Proc. Natl. Acad. Sci. U.S.*, **44**, 259 (1958); (b) G. H. Stewart and H. Eyring, *J. Chem. Educ.*, **35**, 550 (1958).

Table III

Comparison of β-*cis* Proton Chemical Shifts with σ-Parameters

p-Substituted phenylvinylsilanes, $(R—C_6H_4)_3Si—CH=CH_2$				Trisubstituted vinylsilanes, $R_3Si—CH=CH_2$		
R	$-\nu_0\delta_{cis}$[a]	σ_p	$\sigma_p - \sigma'$	R	$-\nu_0\delta_{cis}$[a]	σ^*
CH_3	341.9	−0.17	−0.13	$C_6H_5CH_2$	332.2	0.22
F	343.5	+0.06	−0.44	CH_3	336.5	0.00
CH_3O	344.3	−0.27	−0.50	C_6H_5	345.0	0.60
H	345.0	0.00	0.00	$CH_2=CH$[b]	346.2	0.1–0.5
CF_3	347.0	+0.55	+0.14	Cl	374.8	2.94

[a] Chemical shift in c.p.s. at 60 Mc. relative to tetramethylsilane. [b] Reference 15.

Table IV

Comparison of α-Proton Chemical Shifts with σ-Parameters

p-Substituted phenylvinylsilanes, $(R—C_6H_4)_3Si—CH=CH_2$				Trisubstituted vinylsilanes, $R_3Si—CH=CH_2$		
R	$-\nu_0\delta_{gem}$[a]	σ_p	$\rho_p - \sigma'$	R	$-\nu_0\delta_{gem}$[a]	σ^*
F	394.2	+0.06	−0.44	$C_6H_5CH_2$	356.8	+0.22
CH_3	395.1	−0.17	−0.13	CH_3	364.9	0.0
CF_3	395.2	+0.55	+0.14	$CH_2=CH$[b]	366.8	+0.1–0.5
CH_3O	396.9	−0.27	−0.50	Cl	374.8	2.94
H	397.7	0.00	0.00	C_6H_5	397.7	0.60

[a] Chemical shift in c.p.s. at 60 Mc. relative to tetramethylsilane. [b] Reference 15.

Acknowledgment.—We gratefully acknowledge a grant from the Atomic Energy Commission which supported part of this work.

COAGULATION OF SILVER HALIDE SUSPENSIONS IN THE PRESENCE OF GELATIN

BY EDGAR B. GUTOFF, PETER H. ROTH, AND ALBERT E. STEIGMANN

Emulsion Development Laboratory, Polaroid Corporation, Waltham, Massachusetts

Received May 14, 1963

Silver halide suspensions formed in the presence of gelatin are the main product of the photographic industry. This paper reports studies of some of the conditions affecting the agglomeration and coagulation of these suspensions at the time of their formation. We have corroborated and extended the work of earlier investigators showing that coagulation is reduced by diluting the reagents, having ammonia present, raising the operating temperature, using more gelatin (up to a limit), and using less iodide in bromoiodide systems. In addition, it was found that the effect of ammonia is mainly due to its pH effect, that the iodide content of the agglomerate in a bromoiodide system is less than the average value, that the protective power of a gelatin decreases with increasing reactivity toward silver ions and is relatively independent of the gelatin isoelectric point and viscosity, and that coagulation is reduced at higher levels of agitation. A mechanism of coagulation is suggested for this type of system which takes into account the role of gelatin and explains the observed phenomena in terms of the electrical charge on the particles and on the adsorbed gelatin.

Introduction

The formation of silver halide crystals by mixing a silver nitrate solution with an alkali metal halide solution in the presence of gelatin is the first step in the production of photographic emulsions. Under certain conditions the silver halide crystals can agglomerate to form large clusters which make the "emulsion" unfit for photographic use. This paper is a study of the conditions affecting the agglomeration process.

This agglomeration process is familiar to workers in the field. In a 1930 handbook on photography, Jahr[1] mentions that sedimentation occurs if the silver and halide solutions are too concentrated or if not enough gelatin is present. It was generally known[2] that ammonia, which is used to form ammoniacal silver nitrate for the preparation of some types of emulsions, peptizes the silver halide suspension, and that relatively high gelatin and iodide concentrations in the halide solution lead to agglomerates which were called "pepper." Glafkides, in his recent text,[3] notes that agglomeration is reduced by working at higher temperatures, by diluting the silver nitrate solution, by increasing the gelatin content (in the range of 1–3%), and in mixed bromoiodide systems, by reducing the iodide content.

Photographic emulsions normally contain relatively large crystals, on the order of 1 μ in diameter. The microcrystals formed during the precipitation stage are allowed to grow or ripen to the desired size by holding the suspension at elevated temperatures, with or without the addition of more reagents. However, agglomeration, if it occurs, takes place during or immediately after the precipitation stage.[4,5] If the agglomeration is limited to very small clumps, it may be an important mechanism in the crystal growth process.[6]

Zharkov and Dobroserdova[7,8] noted a tendency toward agglomeration when approximately stoichiometric quantities of silver and halide were used, and also that agglomeration is most extensive in pure silver iodide emulsions.[9]

The silver halide suspensions normally are prepared by the single jet technique, that is, by adding the silver nitrate solution to the halide solution containing gelatin and excess halide.[3] However, less agglomeration occurs when one uses the double jet technique,[3,10] in which the halide and silver solutions are added simultaneously to a gelatin solution and in which it is possible to keep the excess halide concentration constant at all times.

According to the Derjaguin–Landau–Verwey–Overbeek theory,[11,12] the stability of suspended particles is due to the charge repulsion of the electrical double layers, while the coagulating tendency is caused by London–van der Waals attractive forces. When the effective charge on the particles is sufficiently reduced, coagulation occurs. This charge reduction may take place by compression of the double layer caused by added electrolyte, with higher valency counterions having a greater effect. Tezak, *et al.*,[13] approached the question differently. They explained the effects of higher valency coagulating ions by assuming ion pair formation between the coagulating counterion and the stabilizing ion in the double layer, with a consequent reduction in the surface charge. Mirnik[14] developed this same theory further. Packter[15] reconciled and combined these two approaches and estimated that in extreme cases the surface potential may be reduced by ion pair formation to 40% of its original value.

In general, silver halides have been studied only in dilute solutions and in the absence of gelatin. The school of Tezak, and then Matijevic, have made the most complete study.[13,15–27] They have accumulated these findings:

(1) R. Jahr in A. Hay, Ed., "Handbuch der wissen u. angew. Photographie," Vol. IV, Julius Springer, Vienna, 1930, pp. 217–226.

(2) A. Steigmann, *Phot. Korr.*, **67**, 97 (1931).

(3) P. Glafkides, "Photographic Chemistry," Vol. I, Fountain Press, London, 1958, pp. 298–303.

(4) A. Hirata, *Nippon Shashin Gakkai Kaishi*, **23**, 71 (1960); *Chem. Abstr.*, **55**, 14135*d* (1960).

(5) V. N. Zharkov and E. P. Dobroserdova, *Zh. Nauchn. i Prikl. Fotogr. i Kinematogr.*, **1**, 250 (1956).

(6) A. deCugnac and H. Chateau, *Sci. Ind. Phot.*, **33**, 121 (1962).

(7) V. N. Zharkov and E. P. Dobroserdova, *Zh. Nauchn. i Prikl. Fotogr. i Kinematogr.*, **1**, 170 (1956).

(8) V. N. Zharkov and E. P. Dobroserdova, *ibid.*, **1**, 337 (1956).

(9) V. N. Zharkov, E. P. Dobroserdova, and L. N. Panfilova, *ibid.*, **2**, 103 (1957).

(10) H. Ammann-Brass in H. Sauvenier, Ed., Scientific Photography, Proc. of the International Colloquium at Liege, 1959, Pergamon, New York, N. Y., 1962, pp. 276–290.

(11) B. Derjaguin and L. Landau, *Acta Physicochim. URSS*, **14**, 633 (1941).

(12) E. J. W. Verwey and J. T. Overbeek, "Theory of the Stability of Lyophobic Colloids," Elsevier Publishing Co., New York, N. Y., 1948.

(13) B. Tezak, *et al.*, *J. Phys. Chem.*, **57**, 301 (1953).

(14) M. Mirnik, *Nature*, **190**, 689 (1961).

(15) A. Packter, *Z. physik. Chem.* (Leipzig), **214**, 63 (1960).

(16) B. Tezak, E. Matijevic, and K. Schulz, *J. Phys. Chem.*, **55**, 1557 (1951).

(17) B. Tezak, E. Matijevic, and K. Schulz, *ibid.*, **55**, 1567 (1951).

(a) The coagulation concentration for a precipitating counterion is relatively independent of the silver ion concentration (pAg), almost down to the isoionic point.[17,19]

(b) The coagulation value of higher valency counterions, up to a charge of six, follows the expression of Tezak[18] in that the log of the coagulating concentration decreases linearly with increasing valency.[20,21] Thus the coagulation concentration drops from about 2×10^{-1} N for monovalent cations to about 9×10^{-8} N for hexavalent cations in a given system.

(c) Larger ions of the same valency have a slightly greater coagulating effect.[18]

(d) The concentration of the silver sol has very little effect on the coagulation value of an added electrolyte.[17]

(e) Using mixed electrolytes for coagulation, one can get additive, superadditive, and antagonistic effects.[22] Some of the deviations from additivity can be explained by ionic association or by hydrolysis of the hydrated ions.

(f) Small amounts—say 0.5–1%—of gelatin strongly retard the coagulation of silver halides. However, the gelatin has very little effect on the isoelectric maxima, where neither silver nor halide is in appreciable excess and the sol is uncharged.[13,23] Much of the above work has been summarized by Matijevic in a German paper.[24]

(g) At elevated temperatures the general picture is the same, but the stable sol region is narrower.[25] Furthermore, the isoionic point of the sol, which normally is on the excess silver side of the equivalence point due to the greater adsorption of the halide ion, shifts towards the equivalence point because of the more nearly equal adsorption of silver ions.[25]

(h) Negatively charged silver iodide is least stable against multivalent positive coagulating ions, and negatively charged silver chloride is most stable. The reverse is true for monovalent coagulating ions.[17]

(i) The coagulating effect is greater, the more insoluble the salt formed by the coagulating ion and the stabilizing ion.[26,27] That work was done using salts of different organic acids to coagulate positive silver halide sols.

(j) Large simple organic cations, such as amines and materials having a quaternary nitrogen, have a much stronger coagulating action than would be expected from their valence. Monovalent materials behave as simple tri- or tetravalent ions, and like them can reverse the charge and stabilize a negative sol.[28,29] Tamaki has shown that divalent organic cations have an even greater effect and that the sol concentration is important.[30] The strong coagulating and charge reversal action is due to the adsorption of these materials onto the silver halide.[28,31] Materials with more alkyl groups on the nitrogen,[32] with larger head groups,[28] and with greater chain lengths (up to a limit)[33] have a greater coagulating and charge reversal action. Above the critical micelle concentration these materials completely protect the sol.[28] Mathai and Ottewill[34] showed that nonionic surfactants also are strongly adsorbed, and tend to protect the sol, therefore requiring larger quantities of electrolyte for coagulation.

Ottewill, *et al.*,[35–38] have developed a theory for the coagulation by large organic ions, and along with Pravdic and Mirnik,[29] have shown the strong effect of these ions on the ζ potential of the system.

Barr and Dickinson[39] found that the ζ-potential of a silver bromide sol is a function of particle size. The isoelectric pAg of a 1 μ sol is 5.15, of a 1000 μ sol 4.17, and the largest particles resisted positive charging by either excess silver ions or cationic compounds such as quaternary salts. Gelatin above its isoelectric pH is anionic and increases the isoionic pAg of the sol,[39,40] while below the isoelectric pH it is cationic and decreases the isoionic pAg of the sol. Herz and Helling[40] also showed that raising the pH of a pure aqueous bromide or bromoiodide sol increases the isoionic pAg, probably because of the adsorption of hydroxyl ions, as demonstrated by Nicolae and Labau.[41]

The studies reviewed above are helpful in understanding the more complex photographic emulsion containing concentrated silver halide suspensions in the presence of gelatin. Our experimental program to increase this understanding now will be described.

Experimental

Measurement of Agglomeration.—To measure the extent of agglomeration, two methods were used. One consists of examining a drop of the silver halide suspension under a 400 power microscope. This method can be used to rank different degrees of agglomeration approximately, but does not give a quantitative value.

In the other method the volume of settled agglomerates is measured in a graduate. The suspension is first filtered through a silk screen having an average pore diameter of 150 μ, and the coarse agglomerates retained on the screen are then gently washed three times with 500-ml. portions of distilled water at 35°. The agglomerates not peptized by the washing are transferred to a 25-ml. (or larger if needed) graduated cylinder and allowed to settle for 5 min. The volume is read directly, and these volume measurements are reproducible to within about 1 ml. There are disadvantages of this technique. (a) The measured agglomeration depends greatly on the settled density of the material. Thus, in the complete absence of gelatin there will be complete and total agglomeration, and yet the volume of the agglomerates is low due to the high settled density. However, the packed density should not vary too greatly with gelatin present. (b) Small agglomerates will pass through the screen. (c) Some fraction of the agglomerates will be peptized during washing.

In spite of these disadvantages, this measure of the volume of agglomerates can be a useful tool in studying these systems.

Turbidity measurements did not prove to be useful in these concentrated systems containing up to 10% of gelatin.

(18) B. Tezak, E. Matijevic, and K. Schulz, *J. Phys. Chem.*, **59**, 769 (1955).
(19) M. Mirnik, F. Flajsman, K. F. Schulz, and B. Tezak, *ibid.*, **60**, 1473 (1956).
(20) E. Matijevic and M. Kerker, *ibid.*, **62**, 1271 (1958).
(21) E. Matijevic, D. Broadhurst, and M. Kerker, *ibid.*, **63**, 1552 (1959).
(22) B. Tezak, *et al.*, *Proc. Intern. Congr. Surface Activity, 2nd, London*, **3**, 607 (1957).
(23) B. Tezak and S. Kratohvil-Babic, *Arhiv Kem.*, **24**, 67 (1952).
(24) E. Matijevic, *Chimia* (Aarau), **9**, 257 (1955).
(25) G. Dezelic and B. Tezak, *Croat. Chem. Acta*, **30**, 119 (1958).
(26) J. Herak and B. Tezak, *Arhiv Kem.* **27**, 49 (1955).
(27) J. Herak and B. Tezak, *ibid.*, **26**, 1 (1954).
(28) E. Matijevic and R. H. Ottewill, *J. Colloid Sci.*, **13**, 242 (1958).
(29) V. Pravdic and M. Mirnik, *Croat. Chem. Acta*, **32**, 1 (1960).
(30) K. Tamaki, *Kolloid-Z.*, **177**, 45 (1961).
(31) R. W. Horne, E. Matijevic, R. H. Ottewill, and J. W. Weymouth, *ibid.*, **161**, 50 (1958).
(32) K. Tamaki, *ibid.*, **170**, 113 (1960).
(33) B. Tamamushi and K. Tamaki, *ibid.*, **163**, 122 (1959).
(34) K. G. Mathai and R. H. Ottewill, *ibid.*, **185**, 55 (1962).
(35) R. H. Ottewill, M. C. Rastogi, and A. Watanabe, *Trans. Faraday Soc.*, **56**, 854 (1960).
(36) R. H. Ottewill and M. C. Rastogi, *ibid.*, **56**, 866 (1960).
(37) R. H. Ottewill and M. C. Rastogi, *ibid.*, **56**, 880 (1960).
(38) R. H. Ottewill and A. Watanabe, *Kolloid-Z.*, **170**, 132 (1960).
(39) J. Barr and H. O. Dickinson, *J. Phot. Sci.*, **9**, 222 (1961).
(40) A. H. Herz and J. O. Helling, *J. Colloid Sci.*, **16**, 199 (1961).
(41) M. Nicolae and V. Labau, *J. Phot. Sci.*, **10**, 170 (1962).

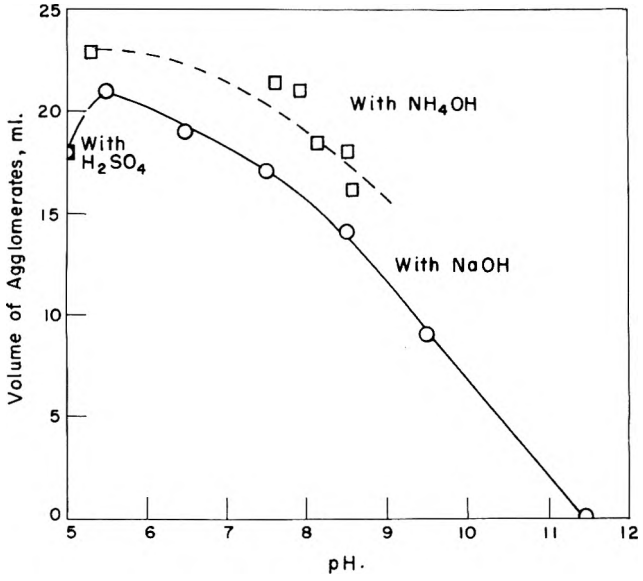

Fig. 1.—Effect of pH on the volume of agglomerates at 50°.

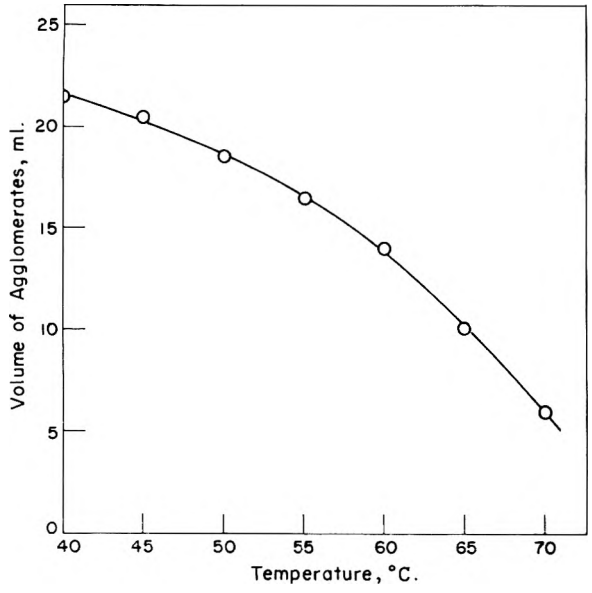

Fig. 2.—Effect of temperature on the volume of agglomerates, using a formulation containing ammonia.

Basic Formulation.—A published bromoiodide formulation[42] was slightly modified and, in order to obtain measureable quantities of agglomerates, the water content was greatly reduced. In many cases some of the remaining water was replaced by ammonium hydroxide. Because agglomeration takes place during or immediately after the nucleation stage,[4,5] as mentioned in the Introduction, only one rapid addition of silver nitrate was used. The halide content, at 470 mole % of the total silver, and the iodide content, at 10 mole % of the total silver, is therefore much higher than in any complete emulsion formulation. Measurements were made 5 min. after the silver nitrate addition. The basic formulation is

Solution A	Water plus ammonium hydroxide	225 ml.
	Ammonium bromide	40 g.
	Potassium iodide	1.5 g.
	Gelatin	8 g.
Solution B	Water	50 ml.
	Silver nitrate	15 g.
	Solution B is preheated to 40°	

Solution A in an 1800-ml. beaker is brought to temperature, normally 50°, and then the ammonium hydroxide, if used, is added. After 2 min., solution B is dumped in while agitating the mixture. After 5 min., the silver halide suspension is cooled to 35° and the volume of agglomerate is determined. If the measurement of agglomeration is done visually with the microscope, the cooling may be omitted.

(42) A. Steigmann, *Congr. Chim. Ind. 15e Bruxelles*, 65 (1935); *Sci. Ind. Phot.*, **7**, 120 (1936).

Results

pH and Ammonia Concentration.—Figure 1 illustrates the reduction of agglomeration on increasing the pH from 5.0 to 11.5 using both ammonium and sodium hydroxides. With ammonium hydroxide the total volume was kept constant, but with sodium hydroxide considerable dilution took place. For a pH of 11.5, 210 ml. of 2 *N* caustic was used. A succinyl-derivatized limed bone gelatin[43] with an isoelectric point below pH 5.0 was used. In one test the ammonium bromide was replaced by an equivalent amount of potassium bromide, and at a pH of 11.5, volume of agglomerates increased from 0 to 6.5 ml.

Temperature.—When using the basic formulation with 30 ml. of 2 *N* ammonium hydroxide to give a pH of about 8.2, increasing the temperature from 40 to 70° greatly reduced the volume of agglomerates, as shown in Fig. 2.

Agitation and Addition Rates.—Reducing the degree of agitation increased the volume of agglomerates, as shown in Table I. Microscope studies showed that it made no noticeable difference whether the silver nitrate is dumped rapidly or added over a period of 15 sec.

TABLE I

EFFECT OF AGITATION ON AGGLOMERATION

Standard formulation with 30 ml. of 2 *N* ammonium hydroxide

R.p.m. of paddle	No. of baffles	Amount of agglomerate, ml.
180	4	18.0
180	1	18.5
90	4	25.0
90	1	26.5

TABLE II

EFFECT OF GELATIN CONCENTRATION ON AGGLOMERATION

Neutral, more dilute formulation

	Wt. % of halide solution	
Gelatin	Concn. range	Optimum concn.
Succinyl-derivatized limed bone	0.09–7.0	2.0–4.0
Limed bone	0.09–7.0	4
Acid pig	0.09–10.0	7

Concentration of Reagents.—A full factorial design of 81 experiments was run using the same basic formulation containing 30 ml. of 2 *N* ammonium hydroxide and keeping the total volume constant. Each of the following factors was varied over the listed three levels, and the middle level is that of the basic formulation.

Final total silver concentration, moles/l.	0.147	−0.293	−0.586
Weight ratio of gelatin to silver metal	0.42	−0.84	−1.68
Volume ratio of silver nitrate phase to bromide phase	0.075	−0.218	−0.433
Mole ratio of bromide to silver	2.31	−4.62	−9.24

The results of this series were analyzed statistically to determine significance. The data show these results.

(a) The volume of agglomerates is directly related

(43) H. C. Yutzy and G. F. Frame, U. S. Patent 2,614,928 (Oct. 21, 1952).

to the total quantity of silver nitrate added, as shown in Fig. 3a.

(b) Diluting the silver phase with water from the bromide phase greatly reduces agglomeration, as shown in Fig. 3b. This has been confirmed by other experiments which show that, to eliminate agglomeration, it is more effective to dilute the silver nitrate phase than to add the same volume of water to the bromide phase.

(c) The ratio of the halide ion concentration in its phase to the silver ion concentration in its phase appears to play an important role, as shown in Fig. 3c. Despite the scatter of the data, one can see agglomeration is at a maximum when the bromide ion concentration is just slightly less than the silver concentration, and falls off more rapidly on the dilute silver side than on the dilute bromide side.

(d) The mole ratio of bromide to silver and the total bromide concentration were also statistically highly significant, but this is probably due to the strong effects of factors already described in (a) and (c).

(e) The effects of gel to silver ratio and its interactions, such as total gel concentration and gel to bromide ion concentration, were not statistically significant. In other tests, however, using visual examination under the microscope to determine agglomeration it was found that agglomeration was reduced with increasing gelatin concentrations. Above an optimum concentration the agglomeration slowly increased. The data are presented in Table II for an ammonia-free formulation that was made more dilute in order to have only slight amounts of agglomeration.

(f) The agglomerates tended to be coarser at higher silver nitrate concentrations.

Increasing the iodide content up to double its standard value gave increased agglomeration as observed under the microscope. Decreasing the iodide content to zero lowered the volume of agglomerates from about 23 to 9.5 ml. In these cases a neutral formulation was used.

Additional Silver Nitrate Solution.—In this test an ammonia-free, all bromide formulation was used. Silver nitrate of the same concentration as the basic formulation was used, but the amounts were 0.25, 0.50, 1.0, and 2.0 times that of the basic formulation. The volumes of agglomerates were 3.5, 6.9, 9.5, and 16.5 ml. The volumes of agglomerates did not increase as rapidly as did the volumes of silver nitrate used, showing that the silver nitrate in the later stages of the dump addition gives rise to a lesser volume of agglomerates than the first stages.

Composition of the Agglomerate.—In one test where the iodide content of the system was 10.2 mole % based on silver, the washed agglomerate had only 6.5 mole % iodide based on silver, and the nonagglomerated suspension passing through the silk screen analyzed 9.3 mole % iodide based on silver. A silver analysis showed that the agglomerate was 98% silver halide, and a semimicro Kjeldahl analysis showed that the adsorbed gelatin content could not be over 1% based on silver.

Effect of Different Gelatins.—The effect of different gelatins on agglomeration was tested in several ways. Using the basic formulation with 30 ml. of 2 *N* ammonium hydroxide at 50° and measuring the volume of agglomerate gave the results presented in Table III.

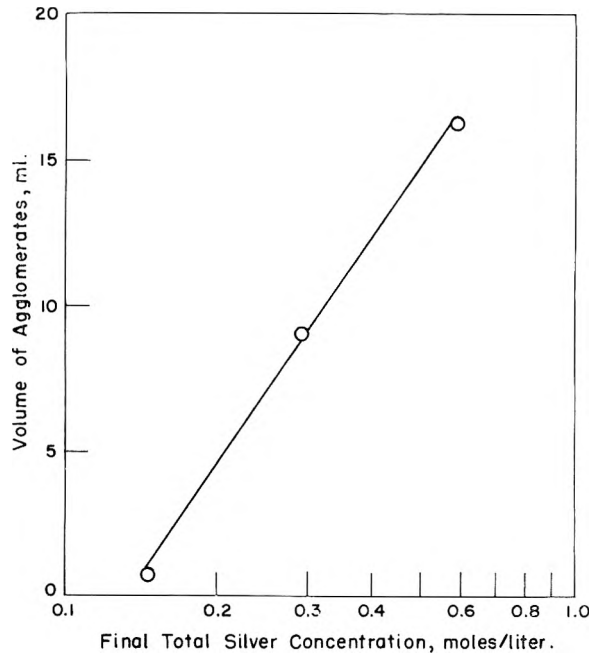

Fig. 3a.—Effect of total quantity of silver on agglomeration using a formulation containing ammonia. Each point is the average of 27 results.

TABLE III

ACTION OF DIFFERENT GELATINS ON AGGLOMERATION

Basic formulation at 50° with 30 ml. of 2 *N* ammonium hydroxide

Gelatin	Isoelectric pH	Viscosity of 10% soln. at 40°, cp.	Volume of agglomerate, ml.
Acid pig			
As is	9.3	15.8	22.0
Succinyl derivatized	4.7	21.0	17.0
Ammonia degraded	6.0	5.9	5.0
Succinyl derivatized limed ossein			
As is	4.2	22.5	18.0
Acid degraded		4.5	15.0
Limed ossein			
As is	5.0	15.6	19.5
Phthaloyl derivatized	4.0	18.0	17.5
Acid degraded		3.5	13.5
Limed calf hide	5.1	15.6	17.5

Similar experiments were performed in more dilute systems where much less agglomeration results, and the gelatins were ranked by microscopic examination. In both neutral and ammonia systems, it was found that: (a) an acid pig gelatin with an isoelectric pH of 9.0 and a limed ossein gelatin with an isoelectric pH of 5.0 both have about the same agglomerating tendencies; (b) derivatized gelatins—namely gelatin derivatives made with phthalic anhydride or benzene sulfonyl chloride—have greater agglomeration tendencies and give more agglomeration at higher degrees of derivatization; (c) an alkali-degraded gelatin which inhibited silver halide crystal growth gave very large quantities of agglomerates. The size of the individual agglomerates was small when using this gelatin in a formulation with ammonia.

Gelatin in the Silver Nitrate.—An ammonia-free, all bromide formulation was used, with a deionized

Table IV

Effect of Surfactants on Agglomeration

Surfactant	Ionic charge	Concn., *M*	Impurities	Volume of agglomerates	Type of agglomerates
Control				19.0	
Igepon T-77 [sodium N-methyl-N-oleoyl taurate]	Minus	0.003	NaCl	16.0	Sudsy
Ethoquad 0/12 [oleylmethyldi(hydroxyethyl)quaternary ammonium chloride]	Plus	.002	2-Propanol	13.0	Rapid settling
Igepal CO-530 [nonylphenoxypolyoxyetherethanol]	Zero	.003		53.0	Sticky

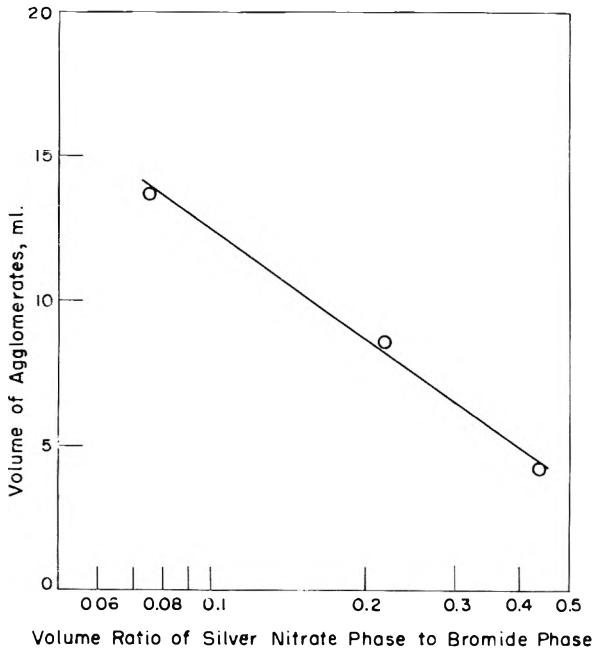

Fig. 3b.—Effect of the distribution of water between the silver nitrate phase and the bromide phase. Each point is the average of 27 results.

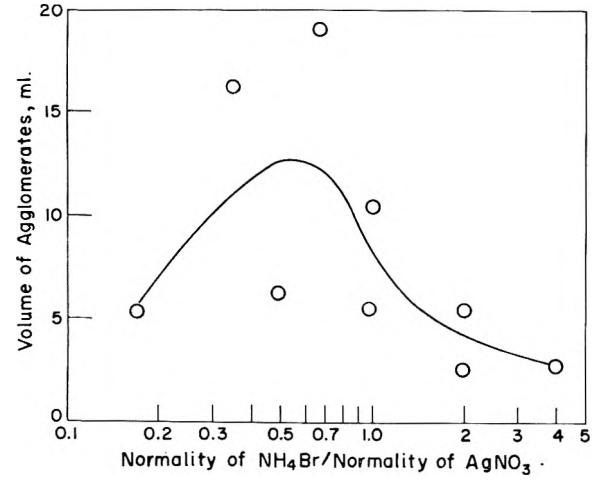

Fig. 3c.—Effect of the ratio of bromide concentration to silver nitrate concentration. Each point is the average of 9 results.

limed ossein gelatin in order to eliminate the formation of a precipitate between impurities (such as chloride or sulfate) in the gelatin and the silver. The volume of each phase was kept constant. The results are given here in tabular form.

Grams of gelatin in bromide phase	8	4	4
Grams of gelatin in silver phase	0	0	4
Amount of agglomeration by microscope	Little	Much	Very little

Effect of Additives. A. Surfactants.—Anionic, nonionic, and cationic surfactants were added to the halide phase of the standard formulation, and the ammonia was used. The results are presented in Table IV.

In a neutral formulation, by microscopic examination neither 0.02 *M* sorbital (a nonionic material) nor the same weight of Nekal BA-75 (a sodium alkyl naphthalenesulfonate) had a noticeable effect on agglomeration.

B. Electrolytes.—Several anionic heteropoly salts were added to the silver to try to reduce agglomeration by rapidly reversing the charge of the positive silver halide salts formed in the silver nitrate stream. A neutral formulation was used, with 50 g. of potassium bromide in place of the ammonium bromide and with 6 g. of a limed ossein gelatin. The silver nitrate was diluted to give just a slight amount of agglomeration. Ammonium 9-phosphotungstate, $(NH_4)_6P_2W_{18}O_{62}$, ammonium nickel-3-molybdeno-3-tungstate, $(NH_4)_4NiMo_3W_3O_{21}$, and 12-silicotungstic acid, $H_4SiW_{12}O_{40}$, were used. A precipitate formed when the nickel molybdenotungstate was added to the silver nitrate. At over-all concentrations of 10^{-4} *M* none of the salts helped. The effects of silicotungstic acid are shown in Table V.

Table V

Over-all concentration of $H_4SiW_{12}O_{40}$, *M*	Amount of agglomeration by microscope
Zero (control)	Slight amount
10^{-8}	About same as control
10^{-7}	More than control
10^{-6}	More than control
10^{-5}	More than control
10^{-4}	About same as control
10^{-3}	More than control

A test was run which confirmed published results[18] that this heteropoly salt will discharge and coagulate a positive silver bromide sol between 10^{-5} and 10^{-6} *N* and will reverse the charge and stabilize the sol at concentrations above 10^{-5} *N*.

The silicotungstic acid did not reduce the coagulation of a negative silver bromide or bromoiodide sol in gelatin-free systems and systems diluted 100-fold. It did not matter whether the acid was added to the silver phase or to the bromide phase.

Gelatin Tests.—To test the suggestion of Matijevic[44] that the agglomerating effect of different gelatins might be related to their ability to react with silver ions, several gelatins were titrated with silver nitrate. The results are tabulated in Table VI. The data show that the derivatized gelatins give rise to higher pAg values than the nonderivatized gelatins. This means they tie up more silver ions than do the nonderivatized gelatins.

Discussion

Coagulation of a sol takes place when the charge on the particles, and therefore the electrostatic forces of

(44) E. Matijevic, personal communication, Oct. 10, 1962.

TABLE VI

TITRATIONS OF GELATINS WITH SILVER NITRATE

Samples of 100 ml. of gelatin solution were used. Meter readings of pAg are given for the water blank. For gelatins, the differences from the water value at the same titer are given.

Vol. 0.01 *N* $AgNO_3$ using 1.5% gelatins, ml.	Water blank	—Regular gelatins— Acid pig	Limed bone	—Derivatized gelatins— Acid pig	Limed bone
0	6.95	+1.50	+0.14	−0.76	+0.37
5	3.83	+0.41	+ .87	+1.07	+1.22
10	3.58	+ .22	+ .43	+0.64	+0.75
20	3.33	+ .11	+ .26	+ .34	+ .42
Using 2.5% gelatins					
0		+0.37	+0.62	+1.70	+1.28
5		+1.11	−1.59	+2.00	+2.00
10		+0.72	−1.04	+1.48	+1.45
20		+ .41	−0.58	+0.93	+0.91
Using 3.0% gelatins					
0		+0.20	−0.05	+1.16	+0.79
5		+ .79	−1.62	+1.75	+1.98
10		+ .44	−1.08	+1.28	+1.48
20		+ .25	−0.59	+0.76	+0.91

repulsion, are reduced almost to zero. In gelatin–silver halide photographic emulsions the silver halide particles are formed where the silver nitrate jet enters the halide solution, in a region of high silver concentration, and therefore are initially positively charged. The halide concentration varies from zero in the silver nitrate jet to full strength in the bulk solution, while the silver concentration is full strength in the jet and almost zero in the bulk solution. The postively charged silver halide particles formed in the vicinity of the jet must migrate to the bulk solution with its high excess halide concentration, and so the original positive charge on the particles must decrease to zero and then be reversed before the suspension is stabilized. We feel that coagulation takes place only during this period before the particles reach the bulk solution and are stabilized.

The gelatin in the system plays an important role in the prevention of agglomeration. It stabilizes the silver halide suspension, for without gelatin complete coagulation takes place. For example, the ammonium ion concentration in the basic formulation used here is much higher than the 0.2 *N* monovalent cation concentration that is sufficient to coagulate a silver halide sol.[18]

However, gelatin also can exert a coagulating effect. Gelatin at concentrations under 0.3% flocculates silver halide sols.[45] It is thought that the polar groupings of the gelatin are adsorbed to the polar surface of the silver halide, leaving the predominantly hydrocarbon groups facing outwards. Aqueous suspensions of these particles with organophilic surfaces would coagulate.[45] On further additions of gelatin, the hydrocarbon groups of the gelatin would be attracted to the hydrocarbon surface, leaving the charged polar groups facing outward and thereby stabilizing the particles. This same reasoning is used to explain the stability of negative silver halide sols in higher concentrations of cationic surfactants.[28] On the other hand, Pouradier and Roman[46] believe that the added gelatin, not having sufficient space on the surface, is just partly adsorbed with part of the molecule, including some of the polar groups extending outward. This also explains the increased adsorption at higher molecular weights.

We think that at least part of the agglomeration is due to the coagulating action of the low concentrations of gelatin in the vicinity of the silver nitrate jet. As evidence, we have noted in the results that a demineralized gelatin added to the silver nitrate appears to reduce agglomeration. The over-all process of stabilization might well be a result both of the charge reversal by the excess halide and of the adsorption of additional gelatin in the bulk solution.

The decrease in agglomeration with increasing gelatin content shown in Table II agrees with previous photographic emulsion experience.[3] The higher gelatin concentrations reduce the time interval during which the silver halide particles in the neighborhood of the silver nitrate jet are exposed to the low coagulating quantities of gelatin migrating toward the jet. The slight decrease in the protective action of the gelatin at still higher concentrations noted in the same table has also been reported previously.[2] This may well be due to the increased viscosities of the more concentrated gelatin solutions reducing the effectiveness of agitation and also reducing the diffusivities of the various components. Because of these opposing effects the degree of agglomeration goes through a maximum with increasing gelatin content. However, the effect of gelatin viscosity is not great compared to the other gelatin properties and hardly affects the over-all protective power of the gelatin, as seen in Table III.

Gelatin, like all proteins, is amphoteric with both anionic carboxylic groups and cationic amino groups. Under alkaline conditions above the isoelectric pH more of the carboxylic groups are ionized and therefore the gelatin carries a net negative charge. Below the isoelectric pH the protonated amino groups give the gelatin a net positive charge. Gelatin, at low concentrations, has its greatest coagulating action on dilute silver bromide sols at or near the isoelectric point[45] which is the pH where the net charge on the gelatin molecule is zero. At high and low values of pH there is less agglomeration.[45] On negative quartz suspensions, Kragh and Langston[47] found that the coagulating action of small amounts of gelatin is greatest when the pH is just slightly below the isoelectric pH, about 4.8 for gelatin of isoelectric pH of 5.0 and about 6.0 for gelatin of isoelectric pH of 8.4. The small net positive charge with both gelatins is about the same.[47] At the pH of the greatest agglomerate formation the adsorption of the gelatin is at a maximum. That the electrophoretic mobility of the quartz suspension in aqueous gelatin is not at a minimum at the optimum pH for flocculation demonstrates that the net charge on the particles plus adsorbed gelatin is not the major factor in agglomeration. The authors suggest that the main effect of pH is on the configuration of the adsorbed molecules and believe coagulation is caused by gelatin molecules bridging the gap between particles.[47] However, the explanation presented earlier that coagulation takes place at low gelatin coverages when the surface is organophilic, and is retarded when the surface is highly polar, seems more reasonable. At or near the iso-

(45) S. E. Sheppard, R. H. Lambert, and D. Swinehart, *J. Chem. Phys.*, **13**, 372 (1945).

(46) J. Pouradier and J. Roman, *Sci. Ind. Phot.*, **23**, 4 (1952).

(47) A. M. Kragh and W. B. Langston, *J. Colloid Sci.*, **17**, 101 (1962).

electric pH the ionization of the gelatin molecule would be at a minimum and so the surface would be least hydrated and most organophilic. The gelatin coatings of two particles then would attract each other. As the pH diverges from the isoelectric point the gelatin coating would become more and more charged. Therefore, the coated particles would tend to repel each other, irrespective of the net charge on the complete gelatin–particle system. Also the polar gelatin would now be more highly hydrated and this too would aid dispersion.[45]

This discussion adequately explains the pH behavior observed here. The volume of agglomerates decreases as the pH rises above 5.3, as shown in Fig. 1. The isoelectric point of this gelatin is under pH 5.0. One point indicates that agglomeration may also decrease as the pH is lowered; but this could not be confirmed with this derivitized gelatin which, by itself, flocculates at lower values of pH.

The action of both ammonium and of sodium hydroxides on agglomeration, as shown in Fig. 1, seems to be mainly of pH. The slight displacement of one curve from the other is due to slight differences in experimental conditions, for these differences persist even when no alkali is added (at a pH of about 5.3). The complexing and solubilizing action of ammonia on silver does not seem to be important, although one test at a pH of 11.5 indicates that ammonium bromide may give less agglomeration than potassium bromide.

The isoelectric point of the gelatin does not seem to be of major importance in differentiating between the protective action of different gelatins, as shown in Table III. The one gelatin which gives markedly less agglomeration had been degraded by ammonia. Microscopic examination of the dispersion formed using this gelatin in a neutral formulation showed only slightly less agglomeration than when using other gelatins. The agglomerates were smaller in size, however, and so in the test reported in Table III many clumps probably passed through the 150 μ opening in the silk screen used in filtering out the agglomerates.

As a class, the derivatized gelatins give rise to more agglomeration than the nonderivatized gelatins. From Table V one may note that the derivatized gelatins react more with silver than do the nonderivatized gelatins. Herak and Tezak,[26,27] in studying the effect of monovalent organic anions on coagulation, have shown that those that form more insoluble silver salts more readily coagulate a positive silver halide sol. These reactive gelatins undoubtedly are adsorbed onto the surface of the silver halide particles to a greater extent. The agglomerating tendencies therefore would be stronger, just as higher molecular weight gelatins are more strongly adsorbed and more readily agglomerate silver halide sols.[45]

Increased agitation rates reduce agglomeration, as shown in Table I. This may be a result of several factors: reduction of the time interval between particle formation and stabilization; reduction of the time interval that two particles are in the neighborhood of each other; and irreversible peptization of the agglomerates coagulated by the gelatin, as has been noted in the case of quartz suspensions.[47] Adding the silver nitrate at a slightly lower rate, over 15 sec. instead of a rapid dump, did not noticeably affect agglomeration. The addition rate would not be expected to have much effect on the length of the period of instability. Diluting the system reduced agglomeration by decreasing the probability of particles approaching each other before they are stabilized in the bulk solution.

The silver ion concentration in the neighborhood of the particles must drop from its initial value in the vicinity of the silver nitrate jet almost to zero before the particles are stabilized. Therefore decreasing the silver nitrate concentration is very effective in reducing the period of instability and also agglomeration. Decreasing the bromide ion concentration, however, has two counteracting effects. One is that of greater dilution, which would be expected to decrease agglomeration by increasing the particle separation. The other effect of bromide dilution is to increase the time interval before the particle reaches a high enough bromide concentration to give it a stable negative charge. These counteracting tendencies probably account for the maximum in Fig. 3c, where the volume of agglomerates is plotted against the ratio of bromide ion to silver ion concentrations. The greater effectiveness of diluting the silver is demonstrated in Fig. 3b.

Figure 3a, showing that agglomeration increases with the amount of silver nitrate added, indicates that agglomeration occurs throughout the whole dump addition. It was also shown in the Results, however, that a greater volume of agglomerates is formed in the earlier stages of the dump addition, probably because of the greater dilution of the system towards the end of the addition. This does not contradict Fig. 3c, which indicates that under certain conditions dilution of the bromide can reduce agglomeration, while under other conditions it can increase agglomeration.

In a bromoiodide system the heavier and larger iodide ions would diffuse more slowly to the region of the silver nitrate jet. This could explain the observation that the agglomerate contains less iodide than the over-all system, as shown in the Results. Only when the particles reach the bulk solution would the full iodide concentration be available to the growing particles. It is also possible that silver iodide may have a lower rate of nucleation than the silver bromide, but this has not been determined. On the other hand, it is possible that silver iodide does form first but that the size of the particles and agglomerates is small enough to pass through the 150 μ screen.

Our observation that higher iodide contents cause increased agglomeration confirms the findings reported in the literature[2,3] and is in agreement with a published study showing that pure silver iodide emulsions have more agglomeration than bromide or chloride emulsions.[5,7–9] Tezak, *et al.*, have shown that negative silver iodide sols without gelatin are slightly less stable towards multivalent coagulating ions, and slightly more stable toward monovalent coagulating ions than negative sols of pure bromide or chloride. Bromide and iodide sols are equally stable toward cationic surfactants[28] and both are less stable than the chloride. The positive silver iodide sol is the most stable toward the sulfate ion.[27] These results do not help in explaining the higher agglomerating tendencies of iodide in bromoiodide systems containing gelatin. Perhaps mixed crystals are less stable than pure crystals because of distortions of the lattice. Perhaps the adsorption of

gelatin and its coagulating action is different on silver bromide and silver iodide sols. The amount of gelatin irreversibly adsorbed onto silver bromide is less than 1%[45,46] and is less than our analytical techniques could measure.

Increasing the temperature of the system has multiple effects. First, it reduces the viscosity of the system, and this, as explained earlier, should reduce the agglomeration by facilitating the movement of the initially formed positive particles to the bulk solution where they become stabilized. Second, the adsorption of gelatin should be reduced at higher temperatures, and this should reduce agglomeration. Third, the solubility of silver salts of gelatin are increased, which should again reduce the adsorption and therefore the agglomeration. Fourth, the solubility of the silver halides is increased and so the silver ion concentration does not have to be reduced to the same extent to stabilize the particles with the bromide ions. Fifth, relative to the bromide ions, the silver ions are more readily adsorbed than at lower temperatures, as evidenced by the shift of the isoionic pAg from the silver excess region towards the equivalence point.[25]

Added polyvalent anions—the heteropoly acids and salts—did not reduce agglomeration. However, Mathai and Ottewill[34] have shown that in the presence of nonionic surfactants the effect of coagulating electrolytes is greatly reduced, and above a minimum concentration (the critical micelle concentration for surfactants) is nil. It would appear that the adsorbed gelatin reduces the effect of added electrolyte. However, in the absence of gelatin, where coagulation was much greater, and in the presence and absence of gelatin using solutions diluted 100-fold, the heteropoly salts still did not reduce agglomeration noticeably. We suggest that in the presence of gelatin, the gelatin reduces the effect of added electrolyte, while in the absence of gelatin the over-all system is unstable because the over-all electrolyte concentration makes the particles coagulate.

Added surfactants, as shown in Table IV, did not reduce agglomeration materially, and in one case increased it. The cationic surfactant did reduce the volume of agglomerates, but the agglomerates settle rapidly and probably had a much higher packed density. One would expect a cationic surfactant to tend to flocculate particles protected by an anionic gelatin. The anionic surfactant had little effect, for it would not act much differently than the anionic gelatin. The nonionic material greatly increased the volume of agglomerate. We suspect that it could have been preferentially adsorbed and yet, because of its lack of charge, it may not have protected the particles sufficiently.

Conclusions

To summarize, we have confirmed earlier work that agglomeration of silver halide emulsions may be reduced by: (a) diluting the silver nitrate; (b) working at a pH above neutrality as by using ammonia; (c) working at higher temperatures; (d) increasing the gelatin content (up to a certain point); and (e) reducing the iodide content in bromoiodide systems.

We have also found that: (a) the isoelectric point and viscosity of the gelatin have little effect on agglomeration during the precipitation stage; (b) increased agitation reduces agglomeration; (c) the iodide content of the agglomerate in a bromoiodide system was less than the average value; and (d) the agglomeration tendency of gelatins increases with increasing reactivity toward silver nitrate.

Acknowledgment.—The exploratory work of Jerome Reid is gratefully acknowledged. Much of the experimental program was carried out by Richard Varney and George Whitehouse. Analyses were done by Peter Kliem. The heteropoly salts were kindly supplied by Prof. Matijevic of Clarkson College.

HEAT CAPACITIES AND THERMODYNAMIC PROPERTIES OF GLOBULAR MOLECULES. V. 3-AZABICYCLO[3,2,2]NONANE FROM 5 TO 350°K.

BY CAROLYN M. BARBER AND EDGAR F. WESTRUM, JR.[1]

Department of Chemistry, University of Michigan, Ann Arbor, Michigan

Received May 14, 1963

The heat capacity of the globular molecule 3-azabicyclo[3,2,2]nonane was determined by adiabatic calorimetry from 5 to 350°K. A transition to the plastically crystalline ("rotator") state was found at 297.78°K. with an associated transitional entropy increment of 11.63 cal./mole-°K. At 298.15°K. the entropy ($S°$), the enthalpy function $[(H° - H°_0)/T]$, and the Gibbs free energy function $[(G° - H°_0)/T]$ are 56.14, 33.39, and −22.75 cal./mole-°K., respectively.

Introduction

In conjunction with a series of studies on the thermodynamics of the transitions involved in the formation and fusion of the "plastically crystalline" or "rotator" phase,[2-5] the family of molecules of which bicyclo[2,2,2]octane is the prototype has proven interesting for study. Previously, triethylenediamine (1,4-diazabicyclo[2,2,2]octane) has been studied over the low[3] and intermediate[6] temperature ranges, and low temperature data on norbornylane have received preliminary mention by Guthrie and McCullough.[7] Another member of the family, 3-azabicyclo[3,2,2]nonane ($C_8H_{15}N$, hereafter AZBN), offers further interesting possibilities for investigation of the nature of the plastically crystalline phase, for the transition producing this phase occurs

(1) To whom correspondence concerning this work should be addressed.
(2) S. S. Chang and E. F. Westrum, Jr., *J. Phys. Chem.*, **64**, 1547 (1960).
(3) S. S. Chang and E. F. Westrum, Jr., *ibid.*, **64**, 1551 (1960).
(4) S. S. Chang and E. F. Westrum, Jr., *ibid.*, **66**, 524 (1962).
(5) D. H. Payne and E. F. Westrum, Jr., *ibid.*, **66**, 748 (1962).
(6) J. C. Trowbridge and E. F. Westrum, Jr., *ibid.*, **67**, 2381 (1963).
(7) G. B. Guthrie and J. P. McCullough, *J. Phys. Chem. Solids*, **18**, 53 (1961).

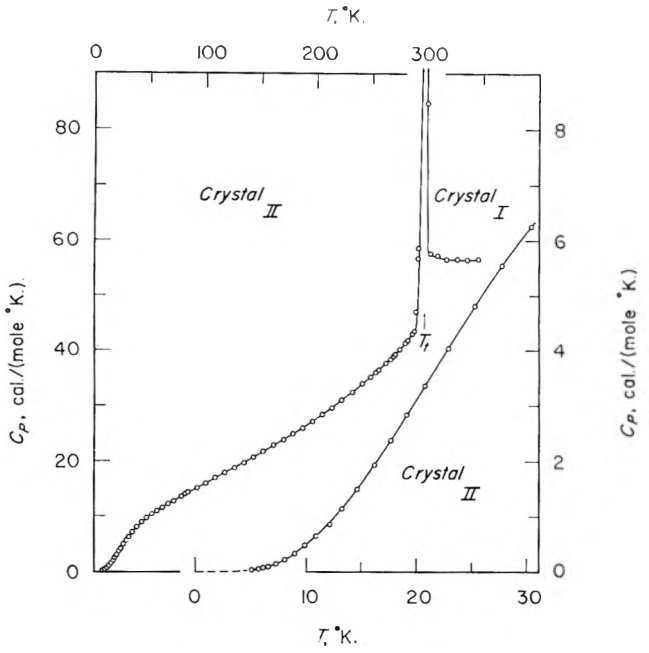

Fig. 1.—Heat capacity of 3-azabicyclo[3,2,2]nonane.

at almost exactly 25°. AZBN is assumed to be a relatively new composition of matter since no references describing its preparation or properties have been found in the chemical literature. It has, however, recently been made commercially available by Eastman Chemical Products, Inc., and is stated to melt at approximately 180°.[8]

Experimental

Preparation and Characterization of Sample.—A reputedly 98% pure sample of the AZBN obtained from the Eastman Chemical Products, Inc. (Kingsport, Tennessee), was subsequently purified by several consecutive sublimations under high vacuum in a simple sublimation apparatus contained within the nitrogen atmosphere of a drybox. The resultant transparent crystals, apparently stable in dry air, become translucent in ambient air, possibly as a consequence of the reported tendency of these hygroscopic crystals to adsorb water and carbon dioxide rapidly. For this reason handling of the sublimed crystals was minimized and the calorimeter was loaded with AZBN (43.087 g. *in vacuo*) in the drybox to prevent contamination of the sample. Duplicate microchemical analysis indicate the composition to be 12.14 ± 0.07% hydrogen, 76.71 ± 0.08% carbon, 11.15 ± 0.03% nitrogen (theoretical: 12.07% H, 76.74% C, and 11.19% N).

Cryostat and Calorimeter.—The Mark II adiabatic cryostat, a gold-plated copper calorimeter (laboratory designation W-28) and a calibrated platinum resistance thermometer (laboratory designation A-5) were used in measuring the heat capacity of this sample. The cryostat[9] and the adiabatic technique employed[10] have been previously described. Helium gas at 9.6 cm. pressure at 300°K. provided thermal contact between the calorimeter and sample. A sample density of 1.14 g./cm.^{3} was assumed for the buoyancy correction. The heat capacity of the calorimeter–heater–thermometer assembly was determined in a separate series of measurements with small adjustments applied as needed for slight differences in the quantities of helium, thermal conductivity grease, and solder between the runs with and without sample. The heat capacity of the sample decreased from 90% of the total observed at 15°K. to a minimum of 55% at 110°K.; above this temperature (except in the transition) it steadily increases to about 75% at 350°K.

Manual shield control was used below 100°K. Above this temperature, three separate channels of recording electronic circuitry provided with proportional, rate, and reset control actions gave control of the temperature of the adiabatic shield to within approximately a millidegree, thereby reducing the energy exchanged between the calorimeter and surroundings to an amount negligible in comparison with other sources of error. All measurements of temperature, time, potential, resistance, and mass refer to calibrations or standards of the National Bureau of Standards.

Results and Discussion

Heat Capacity.—The experimental data on the heat capacity of AZBN are presented in Table I in chronological order of the determinations so that the approximate temperature increments used usually may be estimated from the adjacent mean temperatures. A small adjustment for curvature has been applied to correct for the finite temperature increments used in the measurements. Precision reflected by probable errors decreasing from 5% at 5°, to 1% at 12°, to 0.1% at 20°K., and to less than 0.1% at higher temperatures is considered to characterize these data. The heat capacity data are depicted graphically in Fig. 1. These data are based on the molecular weight of 125.216 g., the defined thermochemical calorie of 4.184 abs. j., and an ice point of 273.15°K. The values of heat capacity at selected temperatures derived from a computer least-squares fitted smooth curve through the experimental data points are presented in Table II. These values accord well with those from a large-scale plot of the data.

The Thermodynamic Functions.—The thermodynamic functions (also presented in Table II) were obtained by exact integration of an analytical expression through the experimental points by means of an IBM digital computer program.[11]

These functions are considered to have a probable error of less than 0.1% above 100°K. An additional digit beyond those significant often is included in order to provide internal consistency and to permit interpolation within the table.

The heat capacity was extrapolated below 5°K. by means of the Debye T^3 limiting relationship.

Solid–Solid Transition.—A very sharp, presumably first-order transition was discovered at 297.78°K. with apparent heat capacities as high as 5600 cal./mole-°K. The very slow rate of attainment of equilibrium occasioned corrections for drifts extending over periods as long as 12 to 14 hr. and rendered the small transitional temperature increments uncertain. Since it was not possible to determine heat capacity in the transition region with high accuracy, a number of enthalpy-type runs of various magnitudes were taken over the transition region to provide direct experimental values of enthalpy increments rather than heat capacity values. The results of these determinations are summarized in Table III. It was noted from cooling curves made in the cryostat that an undercooling of about 7° was typical for this transition.

To evaluate the transitional enthalpy and entropy, it is necessary to obtain an estimate of the "normal" lattice-vibrational heat capacity for this substance over the transition region. In this instance it appears appropriate to extrapolate the heat capacity of the crystal II phase to the transition temperature and like-

(8) Technical Data Report No. X-119, Eastman Chemical Products, Inc., Kingsport, Tennessee, May, 1962.

(9) E. F. Westrum, Jr., *J. Chem. Educ.*, **39**, 443 (1962).

(10) E. F. Westrum, Jr., J. B. Hatcher, and D. W. Osborne, *J. Chem. Phys.*, **21**, 419 (1953).

(11) B. H. Justice, "Calculation of Heat Capacities and Derived Thermodynamic Functions from Thermal Data with a Digital Computer," Appendix to Ph.D. dissertation, University of Michigan; U. S. Atomic Energy Commission Report TID-12722, 1961.

TABLE I

HEAT CAPACITY OF 3-AZABICYCLO[3,2,2]NONANE

[Units: cal., mole, °K.]

T[a]	C_p[b]	T	C_p	T	C_p
Series I		14.68	1.505	125.57	18.79
		16.23	1.950	134.23	19.78
253.28	36.04	17.68	2.396	142.88	20.73
262.09	37.78	19.10	2.845	151.79	21.75
270.92	39.38	20.75	3.378	160.88	22.81
279.77	41.41	22.84	4.059	169.64	23.85
Trans. runs A		25.25	4.818	178.33	24.91
		27.69	5.559	187.03	25.98
Series II		30.29	6.281	195.85	27.15
		33.60	7.143	204.88	28.39
Trans. runs B		37.64	8.066	213.92	29.68
317.30	56.83	41.99	8.909	223.09	31.05
326.47	56.55	46.35	9.648	232.29	32.51
335.82	56.48	50.82	10.329	241.28	34.03
345.37	56.57	55.39	10.950	248.66	35.25
		60.20	11.594	225.94	36.51
Series III		65.36	12.232	269.16	38.99
		70.59	12.803	Trans. runs C	
5.20	0.036	76.07	13.415		
5.73	.052	82.06	14.122	Series V	
6.18	.070				
6.67	.091	Series IV		266.28	38.43
7.33	.140			274.94	40.32
8.14	.215	76.40	13.442	ΔHt run D	
9.02	.330	83.92	14.343		
9.95	.478	91.21	15.14	Series VI	
10.99	.645	99.47	15.96		
12.20	.868	108.00	16.90	ΔHt run E	
13.31	1.143	116.72	17.87		

T[a]	ΔT[c]	C_p	T	ΔT	C_p
Transition runs A			297.50	0.099	2584
			297.59	.074	3444
287.96	7.934	45.05	297.67	.081	3320
294.29	4.967	101.0	297.73	.049	5219
296.87	0.899	644	297.78	.045	5649
297.40	.476	1231	297.82	.051	5002
297.63	.313	1885	297.91	.116	2254
297.85	.430	1364	298.09	.242	1032
298.52	1.332	628	299.44	2.465	84.69
303.85	10.667	61.66	302.33	3.316	57.64
Transition runs B			308.36	8.758	57.21
291.45	2.740	58.81	Transition runs C		
293.88	2.155	99.61	281.88	7.730	41.83
295.39	0.946	161.0	286.79	2.048	43.20
296.10	.507	317	288.93	2.240	47.04
296.70	.762	651	291.03	1.946	56.86
297.17	.185	1362	301.05	18.095	243.0
297.36	.190	1331			

[a] T is the mean temperature of the individual heat capacity determinations. [b] C_p is the heat capacity of the crystal at the essentially constant pressure (<10 cm.) of conduction helium plus the saturation sublimation pressure of the sample. [c] ΔT is the actual temperature increment used in the heat capacity measurement.

wise to extrapolate the heat capacity of the crystal I phase down to this temperature. The selected curves are also indicated in Fig. 1. On this basis the apparent enthalpy of transition is 3461 cal./mole, and the corresponding entropy increment of transition is 11.63 cal./mole-°K.

The approximate value of the entropy at 298.15°K. is 56.14 cal./mole-°K. Since this temperature lies within the region of high heat capacity, it is inherently less reliable than is usual for a reference temperature value.

TABLE II

THERMODYNAMIC PROPERTIES OF 3-AZABICYCLO[3,2,2]NONANE

[Units: cal., mole, °K.]

($C_8H_{15}N$, 1 mole = 125.216 g.)

T, °K.	C_p	$S°$	$H° - H°_0$	$-(G° - H°_0)/T$
5	0.030	0.010	0.04	0.002
10	.451	.120	.95	.026
15	1.592	.498	5.79	.112
20	3.135	1.162	17.53	.286
25	4.741	2.035	37.24	.546
30	6.205	3.032	64.68	.876
35	7.470	4.086	98.95	1.259
40	8.539	5.155	139.05	1.679
45	9.443	6.214	184.06	2.124
50	10.22	7.251	233.27	2.585
60	11.56	9.236	342.36	3.530
70	12.75	11.108	463.96	4.480
80	13.89	12.885	597.19	5.420
90	15.00	14.586	741.66	6.345
100	16.08	16.222	897.10	7.251
110	17.15	17.805	1063.3	8.139
120	18.21	19.343	1240.1	9.009
130	19.30	20.843	1427.6	9.862
140	20.41	22.314	1626.1	10.699
150	21.54	23.760	1835.8	11.522
160	22.71	25.188	2057.0	12.331
170	23.89	26.600	2290.0	13.129
180	25.11	28.000	2535.0	13.916
190	26.37	29.391	2792.3	14.694
200	27.70	30.777	3062.6	15.464
210	29.10	32.16	3346.6	16.23
220	30.59	33.55	3645.0	16.98
230	32.15	34.94	3958.6	17.73
240	33.77	36.35	4288.1	18.48
250	35.46	37.76	4634.3	19.22
260	37.25	39.18	4997.7	19.96
270	39.18	40.63	5379.7	20.70
280	41.37	42.09	5782.2	21.44
292.00	(70)	(44.00)	(6333.2)	(22.31)
310	57.13	58.73	10724.8	24.13
320	56.73	60.54	11293.9	25.24
330	56.52	62.28	11860.0	26.34
340	56.49	63.96	12424.9	27.42
350	56.66	65.60	12990.5	28.49
273.15	39.83	41.08	5504	20.93
298.15	(643)	(56.14)	(9957)	(22.74)

TABLE III

SUMMARY OF ENTHALPY INCREMENTS OVER THE TRANSITION REGION

[Units: cal., mole, °K.]

Designation	No. of runs	$T_{initial}$	T_{final}	$H°_{310} - H°_{280}$
A[a]	8	283.99	309.18	4948.0
B[a]	18	290.08	312.74	4942.0
C	5	278.01	310.10	4937.6
D	1	279.20	309.55	4947.0
E	1	279.91	311.02	4943.2
			Average[a]	4943.6

[a] Runs A and B were corrected for drift during the extended afterdrifts required for equilibrium.

Further measurements in an intermediate temperature adiabatic calorimeter are in progress and the

discussion of the transition and its apparently large activation energy will be deferred until the thermodynamics of the fusion process have been ascertained.

Acknowledgment.—The financial assistance of the Division of Research of the Atomic Energy Commission is recognized with gratitude. C. B. thanks the National Science Foundation for an Undergraduate Summer Research Participation Award. The cooperation of Peter Castle and Ray Radebaugh in the calorimetric measurements is acknowledged with thanks.

HEAT CAPACITIES AND THERMODYNAMIC PROPERTIES OF GLOBULAR MOLECULES. VI. SUCCINONITRILE[1]

BY CLAUS A. WULFF[2] AND EDGAR F. WESTRUM, JR.[3]

Department of Chemistry, University of Michigan, Ann Arbor, Michigan

Received May 20, 1963

The heat capacity of succinonitrile has been determined by adiabatic calorimetry between 5 and 350°K. Crystal II is stable below 233°K., at which temperature it undergoes an isothermal transition to solid crystal I with enthalpy and entropy increments of transition of 1482 cal./mole and 6.35 cal./mole-°K. The latter value is in accord with a statistically calculated value of 6.39 cal./mole-°K. Crystal I melts at 331.30°K. at 1 atm. and under its own vapor pressure at 331.16°K. with enthalpy and entropy increments of fusion of 885 cal./mole and 2.68 cal./mole-°K. An analysis of the heat capacity of crystal II permitted evaluation of the spectroscopically unobserved torsional frequency as 136 ± 6 $cm.^{-1}$. The standard entropy of the vapor at 298.15°K. was computed by a third-law path as 79.04 cal./mole-°K. and spectroscopically as 79.09 cal./mole-°K.; the agreement constitutes a third-law verification. Thermodynamic functions were evaluated for the condensed phases by integration of the heat capacity data and are, for crystal I at 298.15°K., in units of cal./mole-°K.: $C_p = 34.80$, $S° = 45.79$, $(H° - H°_0)/T = 24.35$, and $-(F° - H°_0)/T = 21.44$.

Introduction

Characterization of the plastically crystalline state[4] is a topic of current solid-state chemical interest. The distinguishing macroscopic features of compounds exhibiting plastic crystal behavior are: a relatively high melting point, preceded by a transition to the plastically crystalline phase; a high vapor pressure (the triple point is often above one atmosphere); and a low entropy of fusion which is usually less than 5 cal./mole-°K. The appearance of the plastic crystal state has been attributed to the onset of molecular "rotation"[4] in the solid and can be expected for "globular" molecules, *i.e.*, molecules of high symmetry such as methane. The previous papers in this series have reported results for such "globular" systems. In this paper the results for a less symmetrical substance, succinonitrile [$NC-(CH_2)_2CN$], are presented.

Comparison of the available data for succinonitrile with the criteria presented previously does not establish conclusively the existence of a plastically crystalline phase. Of the dinitriles in the series $NC(CH_2)_nCN$, $n = 1$ to 6, only malonitrile ($n = 1$) and succinonitrile ($n = 2$) are solids at room temperature, indicating that their melting points are anomalously high. The sublimation pressure[5] is low, however, and the liquid is stable for a 200° range. The entropy of melting, ΔSm, can be estimated from the enthalpy of melting, ΔHm, and the melting temperature, Tm. The earliest determination of ΔHm,[6] by a measurement of the cryoscopic constant, gave 940 cal./mole and $Tm = 330$°K., leading to $\Delta Sm = 2.85$ cal./mole-°K. This value is well below the arbitrary limit given by Timmermans and indicates that succinonitrile exhibits plastically crystalline behavior prior to melting. Subsequent determinations of ΔHm,[7] also by freezing point lowering, led to $\Delta Sm = 8.5$ cal./mole-°K. This value is in accord with entropies of fusion for related mono- and dinitriles[8] and has been accepted by handbooks such as that of Beilstein. A still more recent determination is tabulated by Timmermans[5] as $\Delta Hm = 990$ cal./mole and $\Delta Sm = 3.0$ cal./mole-°K. Measurements of the dielectric constant[9] and the infrared spectrum[10] as a function of temperature indicate a transition between 228 and 235°K. Existence of the transition was further confirmed by single crystal X-ray diffraction methods[11] and the structure of the crystal I phase established. Surprisingly, thermal analyses by van de Vloed[7] did not detect the substantial thermal effect associated with the transition.

To clarify the conflicting data on the plastically crystalline nature and to delineate the thermal properties of the substance and its transformation, the low temperature heat capacity of succinonitrile was investigated.

Experimental

Sample and Calorimetric Apparatus.—The calorimetric sample was purified by two successive vacuum sublimations of Coleman and Bell succinonitrile. Duplicate quantitative microanalyses gave the following results: C, 60.01; H, 5.04; and N, 35.04. The theoretical composition is: C, 59.99; H, 5.03; and N, 34.98. Further evidence of its purity is presented in the fractional fusion data. The calorimeter was loaded in an anhydrous nitrogen atmosphere with a molten sample weighing 88.3200 g. (*in vacuo*), and after brief evacuation, 135 mm. of helium gas at 300°K. were added to enhance thermal contact with the sample.

The Mark II cryostat,[12] a gold-plated copper calorimeter (laboratory designation W-28) with six internal vanes, and a calibrated capsule-type platinum-resistance thermometer (labora-

(1) This work was supported in part by the Division of Research of the United States Atomic Energy Commission.

(2) Institute of Science and Technology Fellow.

(3) To whom correspondence concerning this paper should be addressed.

(4) J. Timmermans, *J. Phys. Chem. Solids*, **18**, 1 (1961).

(5) A. L. Woodman, W. J. Murbach, and M. H. Kaufman, *J. Phys. Chem.*, **64**, 658 (1960).

(6) G. Bruni and A. Manuelli, *Z. Elektrochem.*, **11**, 860 (1905).

(7) A. van de Vloed, *Bull. soc. chim. Belges*, **48**, 229 (1939).

(8) J. Timmermans, "Les Constantes Physiques des Composés Organiques Cristallisés," Masson et Cie., Paris, 1953.

(9) A. H. White and S. O. Morgan, *J. Chem. Phys.*, **5**, 655 (1937).

(10) W. E. Fitzgerald and G. J. Janz, *J. Mol. Spectry.*, **1**, 49 (1957).

(11) C. R. Peters and C. E. Nordman, personal communication.

(12) E. F. Westrum, Jr., *J. Chem. Educ.*, **39**, 443 (1962).

TABLE I

THE HEAT CAPACITY OF SUCCINONITRILE

[Units: cal., mole, °K.]

$\bar{T}$	C_p	$\bar{T}$	C_p	$\bar{T}$	C_p
Series I		335.32	126	79.64	13.19
		338.80	38.48	86.52	13.99
187.93	22.80	343.18	38.56	93.61	14.70
196.41	23.48	347.63	38.73		
205.46	24.37			Series VIII	
		Series V			
Series II				96.84	15.01
		ΔHt run B		103.93	15.66
121.76	17.25	Enthalpy run C		110.76	16.28
128.35	17.82	ΔHm run D		117.84	16.91
136.50	18.51			Enthalpy run E	
144.83	19.20	Series VII		ΔHt run F	
153.02	19.82			Enthalpy run G	
		5.00	0.026		
Series III		5.42	.053	Series IX	
		6.00	.067		
155.22	20.05	6.80	.097	341.14	38.56
163.90	20.76	7.71	.16		
172.42	21.48	8.67	.26	Series X	
180.75	22.18	9.66	.36		
		10.71	.48	227.82	26.53
Series IV		11.81	.621	229.70	26.74
		13.16	.821	235.95	32.28
205.74	24.40	14.60	1.081		
215.07	25.32	16.22	1.398	Series XI	
224.35	26.22	18.01	1.780		
241.38	32.40	20.09	2.253	161.36	20.56
249.51	32.62	22.51	2.837	169.64	21.26
258.44	32.97	25.23	3.515	178.44	21.97
267.78	33.35	28.15	4.241	187.74	22.81
277.12	33.74	30.73	4.883		
286.36	34.16	33.51	5.558	Series XII	
295.48	34.64	37.15	6.396		
304.41	35.15	41.34	7.294	326.42	36.94
		46.13	8.251	328.32	40.05
Series V		47.09	8.439	329.60	71.5
		50.85	9.123	334.05	38.32
303.97	35.12	55.11	9.837	337.44	38.40
313.20	35.71	60.18	10.64	340.82	38.55
322.49	36.38	65.83	11.47	344.19	38.67
328.79	94.9	72.56	12.33	347.55	38.75
330.87	1320				

$\bar{T}$	ΔT	C_p	$\bar{T}$	ΔT	C_p
Transition runs A			233.223	0.068	3520
			233.280	.036	16100
231.056	4.293	62.0	233.309	.021	12700
233.213	0.107	2710	234.045	1.451	212
233.274	.081	3580			
233.303	.060	4820	Melting runs J		
233.345	.102	2850			
236.387	6.113	61.0	330.27	0.599	237
			330.67	.215	680
Transition runs H			330.83	.105	1400
			330.92	.062	2300
231.360	1.446	27.06	330.97	.045	4150
232.446	0.753	37.19	331.67	1.359	133
233.008	.372	639			

tory designation A-5) were used in the heat capacity measurements. The quasi-adiabatic technique used has been previously described.[13] The heat capacity of the calorimeter–heater–thermometer assembly was determined by a separate series of measurements with small adjustments applied as needed for the slight differences in the quantities of helium, thermal conductivity grease, and solder between the runs with sample and without.

(13) E. F. Westrum, Jr., J. B. Hatcher, and D. W. Osborne, *J. Chem. Phys.*, **21**, 419 (1953).

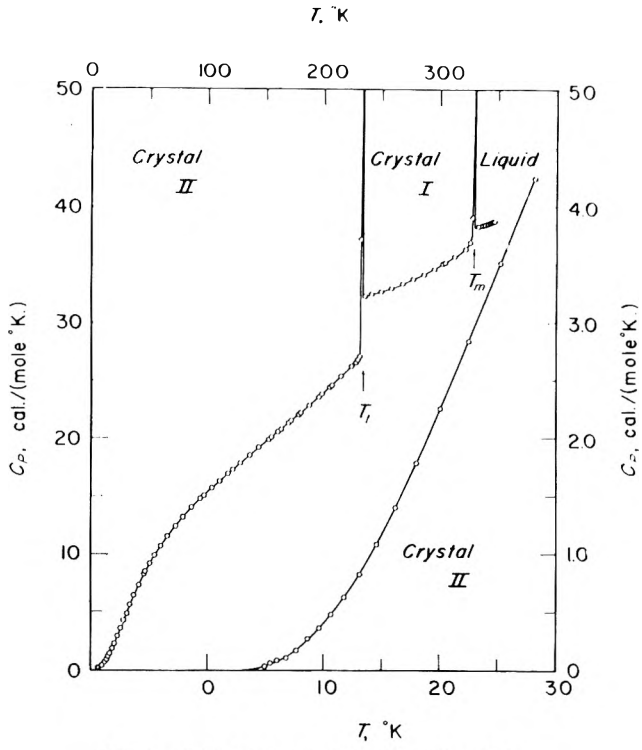

Fig. 1.—The heat capacity of succinonitrile.

The heat capacity of the sample amounted to 95% of the total heat capacity at 10°K., a minimum of 80% at 120°K., and 86% at 350°K. Manual shield control was used below 50°K. Above this temperature three separate channels of recording electronic circuitry provided with proportional, rate, and reset control actions gave control of the temperature of the adiabatic shield to within approximately a millidegree and thereby reduced the energy exchanged between the calorimeter and surroundings so that it is negligible in comparison with other sources of error. All measurements of temperature, time, potential, resistance, and mass are referred to calibrations or standards of the National Bureau of Standards.

Results and Discussion

Heat Capacity.—The experimentally determined heat capacity is depicted in Fig. 1 and presented in Table I in chronological order so that temperature increments across individual runs in a series may be estimated from the adjacent mean temperatures. Since the nature of the phase transition may be deduced from the temperature dependence of the heat capacity in the anomalous regions, apparent heat capacities observed during transition and fusion have been included. The data are stated in terms of the defined thermochemical calorie exactly equal to 4.1840 j., an ice point of 273.15°K., and a molecular mass of 80.092 g. An analytically determined curvature correction has been applied to the measured values of $\Delta H/\Delta T$. The vapor pressure is sufficiently low that no error is introduced by equating C_p with C_s. Corrections for vaporization are also negligibly small. These data are considered to be characterized by a probable error of about 3% near 6°K., decreasing to 1% at 10°K. and to less than 0.08% above 25°K. Values of the smoothed heat capacity obtained from a digital computer fit accord well with those read from a large-scale plot and are presented in Table II.

A test of the experimental heat capacities is provided by the enthalpy-type runs over the crystal I and crystal II heat capacity regions as given in Table III. The agreement of these determinations with the integral

TABLE II

THERMODYNAMIC PROPERTIES FOR SUCCINONITRILE

[Units: cal., mole, °K.]

T	C_p	$S°$	$H° - H°_0$	$(H° - H°_0)/T$	$-(F° - H°_0)/T$
			Crystal II		
5	0.047	0.016	0.058	0.012	0.004
10	.382	.127	.955	.096	.032
15	1.154	.414	4.629	.309	.106
20	2.235	.889	13.011	.651	.239
25	3.455	1.518	27.205	1.088	.430
30	4.705	2.258	47.607	1.587	.671
35	5.899	3.074	74.153	2.119	.956
40	7.010	3.936	106.46	2.662	1.274
45	8.034	4.821	144.11	3.202	1.619
50	8.973	5.717	186.7	3.733	1.984
60	10.619	7.503	284.9	4.748	2.755
70	12.02	9.247	398.2	5.689	3.559
80	13.23	10.933	524.6	6.558	4.376
90	14.32	12.556	662.5	7.361	5.195
100	15.31	14.116	810.7	8.107	6.010
110	16.23	15.619	968.4	8.804	6.815
120	17.10	17.069	1135.1	9.460	7.610
130	17.95	18.472	1310.4	10.080	8.392
140	18.78	19.832	1494.0	10.672	9.160
150	19.61	21.156	1686.0	11.240	9.916
160	20.44	22.45	1886	11.79	10.66
170	21.28	23.71	2095	12.32	11.39
180	22.12	24.95	2312	12.84	12.11
190	22.97	26.17	2537	13.35	12.82
200	23.86	27.37	2771	13.86	13.52
210	24.80	28.56	3015	14.35	14.20
220	25.78	29.74	3267	14.85	14.89
225	26.28	30.31	3375	15.10	15.21
			Crystal I		
235	32.26	37.87	5155	21.94	15.93
240	32.38	38.55	5317	22.15	16.39
250	32.66	39.87	5642	22.57	17.31
260	33.00	41.16	5970	22.96	18.20
270	33.39	42.41	6302	23.34	19.07
273.15	33.53	42.80	6407	23.46	19.35
280	33.84	43.64	6638	23.71	19.93
290	34.35	44.83	6979	24.07	20.77
298.15	34.80	45.79	7261	24.35	21.44
300	34.91	46.01	7325	24.42	21.59
310	35.53	47.16	7677	24.77	22.40
320	36.20	48.30	8036	25.11	23.19
325	36.56	48.86	8218	25.29	23.58
			Liquid		
335	38.37	52.67	9477	28.29	24.38
340	38.52	53.24	9670	28.44	24.80
350	38.81	54.36	10056	28.73	25.63

of the heat capacity is excellent and confirms both the validity of the measurement and calculational aspects of the determinations.

Thermodynamic Functions.—The molal values of the entropy, enthalpy increment, enthalpy function, and free energy function are also listed in Table II at selected temperatures. These values have been obtained by integration of a least-squares-fit polynomial through the data points by means of a high-speed digital computer. Below 5°K. the heat capacity data were extrapolated by means of the Debye limiting law. Nuclear spin and isotope mixing contributions have not been included in the entropy and free energy functions.

TABLE III

ENTHALPY INCREMENTS AND ENTHALPY OF TRANSITION

[Units: cal., mole, °K.]

Designation	Number of runs	T_1	T_2	$H_{T_2} - H_{T_1}$	$\int_{T_1}^{T_2} C_p\,dT$
			Crystal II		
Run C	1	121.64	227.87	2312.1	2312.5
			Crystal I		
Run E	1	238.68	329.94	3161.5	3160.6
Run G	1	243.50	324.99	2787.9	2787.4
			II → I Transition		
					ΔHt
Runs A	6	228.909	239.444	1796.4	1480.4[a]
Run B	1	225.808	238.675	1855.7	1481.9
Run F	1	227.872	243.504	1957.0	1482.4
Runs H	7	232.069	234.77	1565.3	1481.9[a]
				Average:	1481.7 ± 0.6

[a] Corrected for quasi-adiabatic drifts.

The estimated probable error in the thermodynamic functions is less than 0.1% above 100°K.

Transition.—Succinonitrile undergoes an essentially isothermal transition between 227 and 233°K. The low-temperature phase, crystal II, is monoclinic, $P2_1/a$, with unit cell parameters $a = 9.11$ Å., $b = 8.60$ Å., $c = 5.87$ Å., and $\beta = 100°36'$; the high-temperature phase, crystal I, is body-centered cubic with a density of 1.034 g./cc. at 25° (pycnometric) and 1.023 at 45°.[14] The X-ray diffraction patterns indicate crystal II to be completely ordered, whereas crystal I is highly disordered. This disorder is ascribed in part to the onset of rotation about the principal axis passing through the length of the molecule.[14] Similar anomalies in the heat capacities of the corresponding dibromo- and dichloroethanes have been attributed to the onset of molecular motion of this type.[15] The X-ray diffraction data[11] indicate the presence only of an equimolal mixture of the enantiomorphic forms of the *gauche* isomers in an ordered array in the crystal II phase, whereas the infrared data show that the crystal I phase consists of a temperature-dependent equilibrium mixture of *gauche* and *trans* isomers.[10]

In the course of the heat capacity measurements four series of runs were made through the transition region with the enthalpy increments shown in Table III. Although most of the enthalpy of transition, ΔHt, is concentrated between 233 and 234°K., the apparent heat capacity is anomalously high above 227°K. (but not above 234°K.). From large-scale plots, the best representations of the equilibrium heat capacities were extrapolated into the transition region and integrated to evaluate lattice contributions to the enthalpy increments (exclusive of ΔHt). Integrations of the excess heat capacities were then performed to evaluate the ΔHt-values tabulated in Table III. The temperature increments in runs A and H were sufficiently small to allow evaluation of the entropy of transition, ΔSt (corrected for contributions between 227°K. and T_1). The temperature of transition, T_t, was taken as the temperature of maximum apparent heat capacity. The average values for ΔSt and T_t are 6.349 ± 0.002

(14) C. Finback, *Arch. Math. Naturvidenskab*, **B42**, No. 1, 71 (1938); *cf. Chem. Abstr.*, **34**, 12 (1940).

(15) K. S. Pitzer, *J. Am. Chem. Soc.*, **62**, 331 (1940).

cal./mole-°K. and 233.31 ± 0.02° K., respectively, where the uncertainties are the probable errors of the mean values.

The entropy of transition reflects a disordering process concomitant with the phase change. Three factors influence this process, namely: (a) the change in crystal symmetry, (b) the onset of hindered internal molecular rotation, or of over-all (*i.e.*, rigid) rotation about a single axis, and (c) the volume change. The magnitudes of these contributions will each be estimated below.

A. Crystal Symmetry.—Guthrie and McCullough[16] have had some success in correlating transitional entropy increments with the number of orientations allowable by alignment of molecular and crystal symmetry elements. Considering this viewpoint, the following may be envisioned for succinonitrile. The body-centered cubic structure contains a central molecule and eight others at the cube corners. Comparison of the longest interatomic distance in the molecule with the intermolecular distance indicates the absence of free over-all rotation about three axes. The existence of some degree of order can be inferred from the appearance of a diffraction pattern. It is plausible to assume that the principal rotation axis along the length of the molecule will align with one of the four cube diagonals of the unit cell. The entropy increment for this amount of disorder is $\Delta S = R \ln 4 = 2.755$ cal./mole-°K.

B. Molecular Rotation.—For the *trans* configuration of succinonitrile the axis aligned with a unit cell cube diagonal is a two fold rotation–reflection axis of the molecule. If rotational freedom is allowed about this axis (but not about either of the other principal axes), two configurations are apparent, separated by a 180° rigid rotation of the molecule. For a *gauche* configuration the same rearrangement also gives rise to two different configurations. Thus for either isomer two additional configurations are available and contribute $\Delta S = R \ln 2 = 1.377$ cal./mole-°K. to the entropy.

The infrared spectra[10] indicate a *gauche–trans* equilibrium in crystal I (with the *gauche* of lower energy by 360 cal./mole in contrast to the presence of only *gauche* forms in crystal II, the totally ordered phase. If X_g and X_t are the mole fractions of the *gauche* and *trans* isomers, respectively, the onset of this geometrical isomerism contributes an entropy of mixing term

$$X_g/X_t = 2 \exp(360/RT) = 4.348$$

$$X_t = 0.1870 \quad X_g = 0.8130$$

$$\Delta S = -R(X_t \ln X_t + X_g \ln X_g - X_g \ln 2) = 2.077 \text{ cal./mole-°K.}$$

C. Volume Change.—Resolution of the entropy associated with the volume increment from that of the rotation–reorientation process is inherently difficult. Examination of the entropies of order–order transitions in silicon dioxide polymorphs reveals such contributions to be small. Recognition of the effect is provided by estimating the contribution as $\Delta S = R \ln (V_2/V_1)$ and utilizing previously mentioned values for the density of crystal I and lattice parameters for crystal II. Whether total or free volumes are invoked, approximately the same entropy increment, about 0.15 cal./mole-°K., results.

Table IV indicates excellent accord between observed and summarized calculated contributions for the entropy of transition.

TABLE IV
ANALYSES OF ENTROPY OF TRANSITION
[Units: cal./mole-°K.]

Factors	ΔSt_i
Alignment of axes	2.755
Rigid rotation of molecule	1.377
Entropy of mixing isomers	2.077 ± 0.04
Volume change on transition	0.15 ± 0.05
Calcd.:	6.36 ± 0.09
Observed:	6.35 ± 0.03

Melting.—In the course of the heat capacity measurements, three series of runs were made through the region. The process was observed to be isothermal with evidence of premelting above 327°K. From large-scale plots, normal heat capacities were extrapolated into the region to determine enthalpy increments exclusive of ΔHm. The excess heat capacities were integrated to evaluate ΔHm, and the small temperature increments in series V, runs J, permitted evaluation of ΔSm. The results are presented in Table V, with the ΔHm value for fusion run C corrected for a contribution of 31.43 cal./mole below T_1.

TABLE V
ENTHALPY AND ENTROPY OF MELTING
[Units: cal., mole-°K.]

Designation	Number of runs	T_1	T_2	$H_{T_2} - H_{T_1}$	ΔHm	ΔSm
Series V	4	326.802	333.983	1141.6	885.1	2.676
Run D	1	329.933	334.019	1008.7	885.1	
Runs J	9	325.437	332.353	1158.0	885.1	2.678
				Averages:	885.1	2.677

The amount of liquid-soluble solid-insoluble impurity can be estimated from a plot of the apparent melting temperature, T, against the reciprocal of the fraction melted, $1/F$. This quantity is tabulated in Table VI for the six experimental points nearest complete melting in runs J and is a linear function of the T-values. The temperature corresponding to $1/F = 1$ is the triple point of the calorimetric sample, T_1, and is 330.99°K. The temperature corresponding to $1/F = 0$ is the triple point of the pure substance, T_0, and is 331.16°K. The mole fraction of impurity is given by

$$\Delta X = \Delta Hm(T_0 - T_1)/RT_0^2 = 0.0007$$

Extrapolation of the sublimation pressure measurements to the triple point temperature indicates a triple point pressure of *ca.* 10^{-4} atm. The normal melting point, Tm, can be approximated by

$$Tm = T_0 + \Delta Vm/\Delta Sm(1 - P_{He})$$

where $\Delta Vm = 3.71$ cm.^{3}, $\Delta Sm = 2.68$ cal./mole-°K., and $P_{He} = 135/760$ atm. is the pressure of gas inside the calorimeter. To this approximation Tm is 331.30°-

(16) G. B. Guthrie and J. P. McCullough, *J. Phys. Chem. Solids*, **18**, 53 (1961).

K., a value in accord with the latest tabulated result[8] of 331.30–331.35°K.

TABLE VI

FRACTIONAL MELTING DATA ON SUCCINONITRILE

[Units: cal., mole-°K.]

T	ΔT	C_p	ΔH_{excess}	$1/F$	T_{final}
330.27	0.599	237	149.8	5.908	330.566
330.67	.215	682	288.5	3.068	330.781
330.83	.105	1393	431.1	2.053	330.886
330.92	.062	2297	570.7	1.551	330.948
330.97	.045	4150	757.2	1.169	330.993
331.67	1.359	132	885.1		332.353

Triple point temperature of sample: 330.99

Triple point of pure succinonitrile: 331.16

The low value of ΔSm indicates that succinonitrile is a plastic crystal below fusion. The sum of ΔSt and ΔSm is 9.03 cal./mole-°K. and is comparable to ΔSm for malonitrile 7.9, glutaronitrile 9.4, and acetonitrile 9.3.

Heat Capacity of the Liquid.—The heat capacity data points for the liquid region were fitted (by least squares) to the straight line

$$C_p = 28.583 + 0.02922T$$

with a root-mean-square deviation of 0.08%.

Analysis of the Heat Capacity of Crystal II.—The heat capacity is composed of contributions attributable to the lattice vibrations, the internal vibrations, the hindered rotation (torsion at low temperatures), and the expansion of the lattice. To the harmonic oscillator approximation the lattice vibrational contribution can be given by a Debye function, the internal vibrations by Einstein functions for each of the normal vibrations, the torsional contribution by an additional Einstein function, and the expansion contribution by an empirical relation[17]

$$C_p - C_v = (aC_{lattice} - bC_{internal})^2T$$

The heat capacity of crystal II can be fitted, with a mean deviation of ±0.4%, between 30 and 140°K. by the following parameters: $\theta_D = 148$°K., $\theta_E = 200$°K., $a = 0.0070$, $b = 0.0024$, and characteristic Einstein parameters corresponding to the observed normal vibrational frequencies.[10] The θ_E corresponds to the spectroscopically unobserved frequency for the torsional oscillation. The frequency (derived by a method fully discussed elsewhere[18]), 136 ± 6 cm.$^{-1}$, is of the same magnitude as those for the corresponding ethylene dibromide and dichloride.[15]

The Entropy of Gaseous Succinonitrile Vapor.—Two routes are available for the evaluation of the entropy of the vapor, and agreement would constitute a third-law test for this substance. Such a verification is important for succinonitrile in view of the fact that crystal II has been assumed to be perfectly ordered in calculating the entropy of transition. The third-law entropy of the vapor can be computed from the thermal data plus the enthalpy of sublimation and the sublimation pressure.[5] The third-law calculation for 298.15°K. is presented in Table VII.

TABLE VII

THE THIRD-LAW ENTROPY OF GASEOUS SUCCINONITRILE AT 298.15°K.

[Units: cal./mole-°K.]

T range, °K.	Contribution	ΔS_i
0 – 5	Debye extrapolation	0.02
5 –233.31	Numerical integration crystal (II)	31.23
233.31	Transition 1482/233.31	6.35
233.31–298.15	Numerical integration crystal (I)	8.19
298.15	Entropy of crystal I:	45.79 ± 0.03
298.15	Sublimation 16,730/298.15	56.11
298.15	Compression to 1 atm.	−22.86
298.15	Ideal gas correction	0.00
298.15	Entropy of the gas:	79.04 ± 0.10

The second value of the vapor phase entropy can be computed from molecular and spectroscopic data. Translational, over-all rotational, and vibrational contributions were computed using the frequency assignments of Fitzgerald and Janz,[10] a gram formula weight of 80.092, and moment of inertia products of 1.758×10^{-113} g.^{3} cm.^{6} and 1.059×10^{-113} g.^{3} cm.^{6} for the *gauche* and *trans* isomers, respectively. The vapor phase consists of an equilibrium mixture of the two forms with the *trans* of lower energy by 1000 cal./mole.[10] The internal rotational contribution was determined from the tabulated values of Scott and McCullough[19] for the thermodynamic functions for substances possessing rotational isomerism. The barriers chosen, in the notation of Scott and McCullough, were 1000 and 2000 cal./mole. These are consistent with the observed energy difference between the *trans* and *gauche* forms and with barriers observed in other substituted ethanes. The reduced moment of inertia was taken[20] as 9.403×10^{-39} g. cm.^{2}. In addition to these contributions, an entropy of mixing must be accounted for.

$$X_t/X_g = {}^1/_2 \exp(1000/RT)$$

$$X_t = 0.7301 \quad X_g = 0.2699$$

$$S = -R(X_t \ln X_t + X_g \ln X_g - X_g \ln 2) = 1.53 \text{ cal./mole-°K.}$$

The contributions to the spectroscopic entropy are tabulated for the equilibrium *gauche–trans* mixture in Table VIII.

TABLE VIII

SPECTROSCOPIC ENTROPY OF GASEOUS SUCCINONITRILE AT 298.15°K.[a]

[Units: cal./mole-°K.]

Contribution	ΔS_i
Translation and rotation	63.97
Vibration	8.52
Internal rotation	5.07
Entropy of mixing isomers	1.53
Entropy of the gas:	79.09 ± 0.10

[a] The values are for the equilibrium mixture of isomers.

The agreement between the third-law and the spectroscopic entropies is an indication of the absence of

(17) R. C. Lord, Jr., J. E. Ahlberg, and D. H. Andrews, *J. Chem. Phys.*, **5**, 649 (1937).

(18) C. A. Wulff, *ibid.*, **39**, 1227 (1963).

(19) D. W. Scott and J. P. McCullough, Bureau of Mines Report, RI 5930, 1962.

(20) G. J. Janz, personal communication.

residual disorder in crystal II and justifies assumptions made in the entropy of transition calculation.

Summary

From the evidence presented, we conclude that the transition from crystal II to crystal I is from an ordered phase to a plastically crystalline phase. The analysis of the entropy and transition shows that some freedom of molecular rotational reorientation must be allowed to account for the observed entropy increment. This conclusion is supported by the low value for the entropy of melting, which indicates crystal I to be highly disordered. Comparison of the measured enthalpy of melting with this value obtained by van de Vloed[7] from freezing point depressions indicates that care must be taken in the interpretation of data obtained by that method. If relatively large amounts of the second component are used, the formation of a solid solution could lead to a crystal structure other than that of the plastic crystal phase and a resulting enthalpy of melting corresponding to the melting of an ordered phase. The existence of an ordered phase by solid solution formation is supported by the accord between the entropy of melting, from freezing point depressions, 8.5 cal./mole-°K., and the sum of the observed entropies of transition and melting, 9.0 cal./mole-°K. The postulated molecular rotational reorientation in crystal I is supported by dielectric dispersion data of Clemett and Davies[21] who conclude that rotation in the solid involves the entire molecule and is a cooperative phenomenon involving adjacent molecules.

Future studies suggested by this research concern the heat capacities of malo- and glutaronitriles which contain one less and one more CH_2 group, respectively. Malonitrile is a solid at room temperature having the mechanical properties associated with a plastic crystal. Glutaronitrile exists in two solid modifications, a metastable phase (formed by rapid cooling to −60°) which undergoes an irreversible transition to a stable form at −40°.[22] The dimorphism has also been noted by van de Vloed[7] who reported melting temperatures and entropies of melting derived from cryoscopic constants. Thermal measurements on glutaronitrile are presently in progress.

Acknowledgment.—The authors thank Professor C. E. Nordman for making accessible unpublished X-ray diffraction data and Professor G. J. Janz of Rensselaer Polytechnic Institute for unpublished preliminary results on the gas phase thermodynamic functions of succinonitrile and Dr. Elfreda Chang for assistance in the evaluation of the data. C. A. W. acknowledges the support of the Institute of Science and Technology of the University of Michigan in the form of a postdoctoral fellowship. The partial financial support of the U. S. Atomic Energy Commission Division of Research is greatly appreciated.

(21) C. Clemett and M. Davies, *J. Chem. Phys.*, **32**, 316 (1960).

(22) I. Matusbara, *ibid.*, **35**, 373 (1961).

HEAT CAPACITIES AND THERMODYNAMIC PROPERTIES OF GLOBULAR MOLECULES. VII. TRANSITION AND FUSION OF TRIETHYLENEDIAMINE[1]

BY JOHN C. TROWBRIDGE AND EDGAR F. WESTRUM, JR.[2]

Department of Chemistry, University of Michigan, Ann Arbor, Michigan

Received May 23, 1963

The heat capacity of 1,4-diazabicyclo[2,2,2]octane has been determined from 300 to 450°K. by adiabatic calorimetry. A sharp transition at 351.08°K. associated with the transformation to the plastically crystalline phase involves an entropy increment of 7.19 cal./(mole °K.). The triple point occurs at 433.1°K. with an entropy increment 4.10 cal./(mole °K.) and thus confirms the classification of this substance as a plastic crystal. Thermodynamic functions have been computed from the primary thermal data.

Introduction

In a previous paper of this series[3] the low temperature heat capacity of triethylenediamine, 1,4-diazabicyclo-[2,2,2]octane, was reported, revealing the onset of a transition just beyond the high temperature limit (350°K.) of the cryostat. This investigation concerns studies on the same material at higher temperatures and presents evidence concerning the nature of the "rotator" or as designated by Timmermans[4] the "plastically-crystalline" phase.

Experimental

Preparation of Sample.—The triethylenediamine sample used in this investigation was that previously used in the low temperature measurements.[3] Because of the hygroscopicity of the sample, the calorimeter was loaded in the anhydrous nitrogen atmosphere of a drybox. Although crystals used for the calorimetry were in the form of transparent hexagonal platelets approximately 1 cm. in diameter, they were fused in the process of these measurements. The fractional melting experiments reported later in this paper give a further indication of the high purity of this material. Microchemical analysis of the triethylenediamine sample indicated the following composition: C, 64.39; H, 10.81; and N, 24.75 (calcd.: C, 64.24; H, 10.78; and N, 24.96, for $C_6H_{12}N_2$).

Silver Calorimeter.—The calorimeter used in this study (laboratory designation W-22) is machined from two solid silver cylinders and shown in Fig. 1. It is provided with an entrant, axial well (G) containing the 250-ohm Karma wire heater and Leeds and Northrup capsule-type resistance thermometer (H). The thermometer is gripped in a threaded beryllium–copper collet arrangement tightened by being forced into the slightly conical bore of the heater sleeve. The heater sleeve is itself conical and is held in a mating hole within the well of the calorimeter by means of a fine screw thread. The thermal equilibration spool (I) ensures that the leads achieve the surface temperature of the calorimeter. Six vertical radial vanes machined as an integral piece of the thermometer well portion facilitated thermal equili-

(1) This work was supported in part by the Division of Research of the United States Atomic Energy Commission. Submitted by J. C. T. in partial fulfillment of the requirements for the Ph.D. degree of the Horace H. Rackham School of Graduate Studies of the University of Michigan.

(2) To whom correspondence concerning this paper should be directed.

(3) S. S. Chang and E. F. Westrum, Jr., *J. Phys. Chem.*, **64**, 1551 (1960).

(4) J. Timmermans, *J. chim. phys.*, **35** 331 (1938); *Ind. chim. Belge*, **16**, 178 (1951); *cf. J. Phys. Chem. Solids*, **18**, 53 (1961).

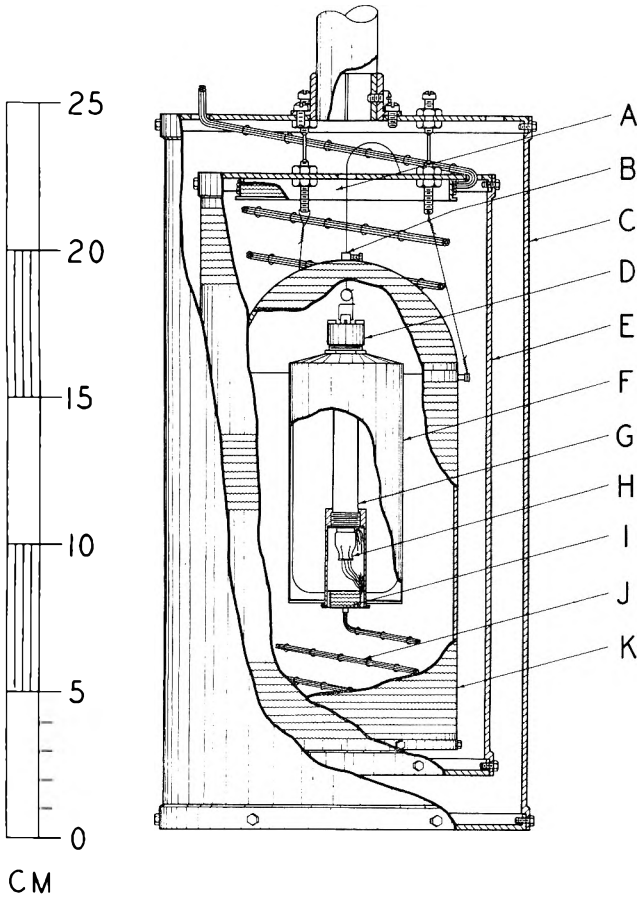

Fig. 1.—Cross-sectional diagram of Mark IV intermediate temperature thermostat: (A) guard shield ring; (B) calorimeter suspension collar; (C) primary radiation shield; (D) calorimeter closure assembly; (E) guard shield; (F) calorimeter assembly; (G) thermometer–heater well; (H) thermometer; (I) thermal equilibration spool; (J) lead bundle; (K) adiabatic shield.

bration. All seams of the calorimeter are force-fitted and sealed vacuum-tight by silver alloy brazing.

For expeditious loading and unloading of this calorimeter, a vacuum-tight closure (D), operable at room temperature and not involving weight adjustments of solder, etc., is desirable. To meet these requirements, a gold gasket is forced by screw threads against a circular knife edge to provide a suitable seal to a 1-cm. diameter inlet tube. A suitable jig within a cylinder which can be evacuated to 10^{-6} mm. is used to close this seal in the presence of vacuum or low pressures of inert gases for thermal conduction.

Further details concerning the demountable thermometer–heater assembly, the nature of the seal for the sample space, and the mechanism for closing this seal under vacuum may be found elsewhere.[5]

Intermediate Temperature Thermostat.—The Mark IV adiabatic thermostat depicted in Fig. 1 in schematic cross section is designed for the study of thermal properties of substances and systems over the temperature range 250 to 550°K. The calorimeter (F) is suspended by a fine alloy wire from the collar (B) on adiabatic shield (K) which consists of a hemispherical top spun from 1.3-mm. copper silver-alloy brazed to a cylindrical middle section. The open lower end of the adiabatic shield is closed with a closely fitting copper plate held in place by six machine screws. All exterior surfaces of the adiabatic shield are wound with Fiberglas-insulated wire. The bundle of lead wires (J) is tempered by the guard shield ring (A) and is laid in a helical groove along the exterior of the adiabatic shield. Those wires which lead to the calorimeter and the heater windings make good thermal contact with the adiabatic shield by being firmly cemented to the respective copper members with Formvar. The adiabatic shield is suspended by three alloy wires from the guard shield (E) which is also provided with heater and control thermocouples on portions of each of its three sections. The ends from the cylindrical section may be withdrawn by removing small machine screws. The top end is rigidly supported from the top plate of the radiation shield (C) which is fixed to a 2.0-cm. diameter stainless steel tube with 0.25-mm. wall supporting the entire assembly within the cylindrical brass can evacuated by high-speed vacuum pumps. Another radiation shield not shown in Fig. 1 surrounds the shield (C) and reduces somewhat the electrical power required to maintain the highest temperatures. A liquid nitrogen tank (not shown) was used for achieving lower temperatures.

In operation, the temperature differential between the adiabatic shield and calorimeter is maintained at less than ±0.001°, and the guard shield is held about 1° below the calorimeter temperature. Adiabaticity is maintained by a three-channel automatic shield control device described elsewhere.[6] Separate channels are used to control the main and bottom portions of the adiabatic shield and the guard shield.

Calorimetric Procedure.—The technique of the calorimetric measurements was in general similar to that described in the cryogenic studies previously reported,[7] with the exception that a Rubicon double, thermal-free potentiometer, together with a photoelectric galvanometer, was used for the microvolt potential measurements. All potential resistance, mass, and time measurements were referred to standards or devices calibrated by the National Bureau of Standards. A platinum resistance thermometer (laboratory designation A-7), also calibrated by the National Bureau of Standards, was used to define the temperature scale. The calorimeter was loaded in an anhydrous nitrogen atmosphere with 70.3256 g. (*in vacuo*) of triethylenediamine. The calorimeter was heated during the loading process to fuse the sample and permit a greater quantity to be used. After filling, the calorimeter was evacuated and filled with purified helium at 10 cm. pressure at 300°K. to provide better thermal contact between sample and calorimeter. The heat capacity of the empty calorimeter–heater–thermometer assembly was determined in a separate series of measurements and represented approximately 24% of the total normal observed heat capacities. The calorimetric system was calibrated with a Calorimetry Conference sample of synthetic sapphire.[8]

Results

Heat Capacity.—The experimental heat capacity determinations are presented in Table I in chronological order, in terms of the thermochemical calorie defined as exactly 4.1840 abs. j. The ice point is taken as 273.15°K. and the molecular weight of triethylenediamine as 112.172 g. Corrections to the observed values of $\Delta H/\Delta T$ were applied to adjust for the analytically determined curvature correction, when applicable, and for the sublimation (or vaporization) of the sample at higher temperatures. These corrections have magnitudes of approximately 0.01 and 0.03% as maximum values, respectively. The basic logic of the vaporization correction is patterned after that devised by Hoge[9] but was adapted for digital computer application.[5] The approximate temperature increments used in the measurements usually can be inferred from the adjacent mean temperatures in Table I. These data are considered to have a probable error of approximately 0.08% over the entire range on the basis of the statistical analysis of the deviations from the smoothed curve calibration runs with synthetic sapphire and on several separate series of runs on the heater–thermom-

(5) J. C. Trowbridge, "Thermodynamic Functions and Phase Transitions including Fusion for Perchloric Acid, Pentaerythrityl Fluoride and Triethylenediamine," Doctoral Dissertation, University of Michigan, University Microfilms.

(6) H. G. Carlson, "Thermodynamic Properties of Methyl Alcohol, 2-Methyl-2,5-dimethylthiophene and 2-Methylfuran," Doctoral Thesis, University of Michigan, Ann Arbor, Michigan, 1963; U. S. Atomic Energy Commission Report TID-15153, 1962.

(7) E. F. Westrum, Jr., J. B. Hatcher, and D. W. Osborne, *J. Chem. Phys.*, **21**, 419 (1953).

(8) G. T. Furukawa, T. B. Douglas, R. E. McCoskey, and D. C. Ginnings, *J. Res. Natl. Bur. Std.*, **57**, 67 (1956).

(9) H. J. Hoge, *ibid.*, **36**, 111 (1946).

eter–calorimeter assembly. The smoothed heat capacities at saturation obtained by a digital computer fit of the experimental data (which accords excellently with values read from curves on large-scale plots) are presented in Table II.

TABLE I

HEAT CAPACITY OF TRIETHYLENEDIAMINE

[Units: cal., mole, °K.]

$\bar{T}$	C_s	$\bar{T}$	C_s	$\bar{T}$	C_s
Series I		397.65	53.95	Series V	
		407.03	54.83		
302.43	37.06	416.34	55.81	354.02	49.86
311.66	38.74	423.61	56.33	357.49	50.54
321.34	40.65	428.66	56.56	365.80	51.26
331.10	42.86	429.60	56.96	376.83	52.20
340.79	45.50	430.54	56.76		
Transition runs A		431.64	57.91	Series VI	
358.51	50.58	432.44	64.55		
368.74	51.46	Fusion runs D		Fusion runs J	
378.97	52.23	434.59	57.37		
389.42	53.16	436.25	57.24	Series VII	
400.02	54.20	438.94	57.78		
410.64	55.19			433.66	57.23
421.28	56.35	Series III		434.19	57.26
Fusion runs B				434.54	57.26
427.62	57.51	344.76	46.38	435.07	57.47
		348.09	47.74	438.21	57.70
Series II		349.94	47.88	441.91	57.96
		Transition runs E		443.80	58.19
320.03	40.09	Enthalpy run F		445.83	58.36
326.63	41.62	ΔHf run G		448.01	58.64
334.36	43.62				
341.64	45.64	Series IV		Series VIII	
347.60	47.83				
Transition runs C		299.89	36.44	Transition runs K	
355.29	50.16	303.33	37.14	383.49	52.70
358.30	50.31	308.09	37.94		
359.55	50.40	311.43	38.66	Series IX	
363.97	51.00	319.33	40.23		
372.45	51.67	328.56	42 09	Fusion runs L	
381.18	52.46	338.18	44.82		
389.34	53.19	ΔHt run H			

Transition runs			Fusion runs		
$\bar{T}$	ΔT	C_s[a]	$\bar{T}$	ΔT	C_s[a]
	Runs A			Runs B	
348.34	5.433	(97.22)	429.82	6.414	(104.3)
351.06	0.058	13400	433.01	0.018	454
351.13	.131	7030	433.71	1.405	(524.5)
352.21	2.279	(288.1)			
	Runs C			Runs D	
350.58	0.970	301	432.79	0.207	175
351.09	.102	15800	433.61	1.416	(1291)
351.16	.156	3010			
352.04	1.762	(157.5)		Runs J	
	Runs E		432.38	1.212	(515.8)
			432.99	0.015	52500
350.69	0.528	97.8	434.48	2.973	(202.2)
351.86	1.826	(1413)		Runs L	
	Runs K			(*Cf.* Table III)	
350.67	0.300	82.1			
364.44	27.23	(98.10)			

[a] Values in parentheses involve finite temperature increments in regions of high curvature.

Enthalpy of II → I Transition.—The sharp and seemingly first-order transition at 351.08°K. is characterized by apparent heat capacities as high as 15,800 cal./(mole°K.) and thermal equilibrium within an hour after energy input. If the lattice contributions to the heat capacity (as depicted by the dashed curve in Fig. 2) are deducted from the apparent heat capacity, a transitional enthalpy increment of 2524 cal./mole and a corresponding entropy increment of 7.19 cal./(mole °K.) are obtained. These probably represent minimal values since a maximum value of lattice heat capacity probably has been taken.

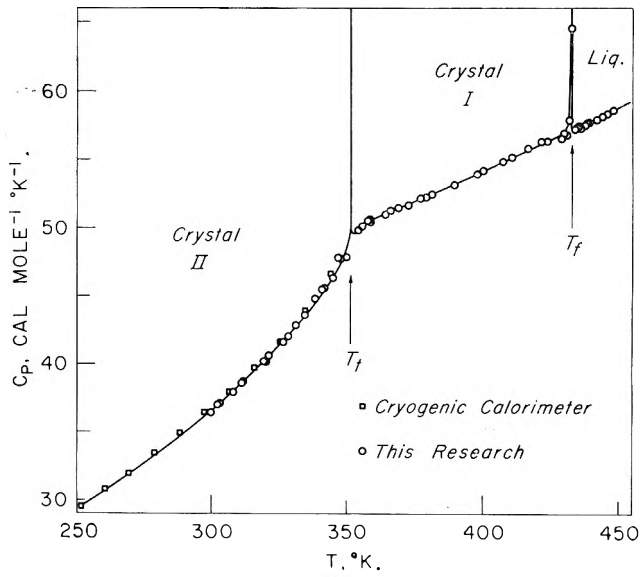

Fig. 2.—Heat capacity of triethylenediamine: □, data from cryogenic adiabatic calorimeter of Chang and Westrum[3]; ○, from this research.

TABLE II

THERMODYNAMIC FUNCTIONS OF TRIETHYLENEDIAMINE

($C_6H_{12}N_2$: 1 mole = 112.172 g.; units: cal., mole, °K.)

T	C_s	$S°$	$H° - H°_0$	$-(G° - H°_0)/T$
		Crystal II		
298.15[a]	36.49	37.67	5524.8	19.14
300	36.80	37.90	5592.6	19.25
320	40.35	40.38	6363.1	20.50
340	45.13	42.96	7214.7	21.74
351.08	(48.80)	44.43	7723.3	22.43
		Crystal I		
351.08	(49.90)	51.61	10244	22.43
360	50.62	52.90	10707	23.16
380	52.34	55.69	11737	24.80
400	54.17	58.42	12802	26.42
420	56.04	61.11	13904	28.00
432.98	(56.90)	62.84	14636	29.04
		Liquid		
432.98	(57.16)	66.95	16412	29.04
440	57.83	67.86	16817	29.64
450	58.79	69.17	17400	30.50

[a] From Chang and Westrum.[3]

Fusion Transition and Purity of the Sample.—Fusion occurs at 432.98°K. with an enthalpy increment of 1776 cal./mole and an entropy increment of 4.10 cal./(mole °K.) upon subtraction of the lattice contributions. Molal heat capacities as high as 58,000 cal./(mole °K.) were observed in the fusion region and thermal equilibrium was readily attained within 1 hr.

The near absence of premelting permitted application of the method of Tunnicliff and Stone[10] for the determinations of sample purity using the data listed in Table III. The linearity of the melting temperature *vs.* reciprocal fraction melted ($1/F$) implies absence of

(10) D. D. Tunnicliff and H. Stone, *Anal. Chem.*, **27**, 73 (1955).

solid solution formation and indicates 0.003 mole % liquid-soluble solid-insoluble impurity in this sample. Extrapolation of this plot also furnishes the true triple point temperature of this sample and that of the pure substance as 432.98 and 432.99°K., respectively.

TABLE III

FRACTIONAL FUSION OF TRIETHYLENEDIAMINE

[Units: cal., mole, °K.]

$\bar{T}$	ΔT	C_s	ΔH_{excess}	$1/F$	T_{final}
		Fusion runs L			
430.46	4.953	69.13	60.9	29.153	432.909
432.94	0.054	7530	468.5	3.791	432.964
432.97	.009	42530	856.7	2.074	432.973
432.98	.007	58230	1294.2	1.373	432.980
432.98	.002	1690	1749.1	1.016	432.982
433.54	1.048	70.37	1776.7		434.030
Triple point: this sample				(1.000)	(432.98)
pure compound				(0.000)	(432.99)

Thermodynamic Functions.—Molal values of the heat capacity at saturation (C_s), the entropy at saturation ($S_s°$), the enthalpy increment ($H° - H°_0$), and the free energy function $[(G° - H°_0)/T]$ have been computed by numerical quadrature of the heat capacity plus values associated with phase transitions and are tabulated at selected temperatures in Table II. The normal heat capacity values and the thermodynamic functions are considered to have a probable error of less than 0.1%. In order to make the tables internally consistent and to permit interpolation, the tabulated values occasionally include more digits than are justified by the probable error. The entropy and free energy functions do not include contributions from nuclear spin and isotope mixing and are hence practical values for chemical thermodynamic purposes.

As a further test of the precision of the calorimetry and the trend of the heat capacity curve in the transition regions, enthalpy increments, each entirely spanning the respective transition regions or a portion of the crystal I region (solid phase stable immediately below the melting point), were made and compared with heat capacity-type determinations as shown in Table IV. Excellent agreement was obtained for transitions and enthalpies over heat capacity regions. The listed enthalpy changes in these regions are a direct summation of the energies used while entropy increments have been integrated from heat capacity data except in regions of extremely high heat capacities where the process is assumed to be isothermal.

Discussion

The pseudo-rotational transition observed at 351.08°K. is found at a temperature approximately 4° higher than previously reported by Farkas, *et al.*[11,12] The higher temperature is attributed to the careful purification of the sample and its handling in the anhydrous nitrogen atmosphere of the drybox to prevent contamination by moisture and carbon dioxide. The fractional melting studies attest to the results achieved.

The crystal II phase of triethylenediamine stable below 351.08°K. has been subjected to room temperature X-ray analysis by Wada, *et al.*,[13] who also made

TABLE IV

ENTHALPY AND ENTROPY INCREMENTS FOR TRIETHYLENEDIAMINE

[Units: cal., mole, °K.]

Designation	No. of runs	T_{final}	$T_{initial}$	$H°_{355} - H°_{345}$	$S°_{355} - S°_{345}$
			Transition		
Series II (C)	7	357.66	338.18	3011.1	8.569
Runs A	4	353.35	345.62	(3008.3)[a]	(8.561)[a]
Series III (E)	5			3010.9	8.568
Run H	1	354.29	342.96	3010.6	8.568
Runs K	2	378.06	350.54	3010.9	8.568
			Average	3010.9	8.568
			Fusion		
				$H°_{440} - H°_{430}$	$S°_{440} - S°_{430}$
Series II (D)	9	440.81	429.98	2348.4	5.423
Runs B	4	440.84	426.61	(2352.9)[a]	(5.433)[a]
Run G	1	435.97	429.34	2350.1	5.428
Runs J	3	439.97	431.78	2348.2	5.423
Runs L	6	434.03	427.99	2349.8	5.427
			Average	2349.1	5.425
			Crystal I		
				$H°_{430} - H°_{355}$	
Series I	7	426.60	353.36	4010.4	
Series II	16	431.09	352.91	4009.8	
Run F	1	429.38	352.77	4014.3	
			Average	4011.5	
Numerical quadrature of smoothed curve:				4013.1	

[a] Rejected from average by Chauvenet's criterion.

differential thermal studies on the transition first reported by Farkas, *et al.*,[12] and on fusion. The structure of crystal I is not yet available. These data, combined with the information obtained from this research, still are not adequate to account for the magnitude of the entropy increment of the solid–solid transition. According to Guthrie and McCullough,[14] molecular orientations that are energetically favorable usually will be among those for which the approximate symmetry elements of the molecule are aligned with the symmetry elements of the lattice. Thus, for favorable orientations the effective point symmetry of the molecule will be a sub-point group of the crystal symmetry at the lattice site, and the number of possible distinguishable orientations can be estimated from symmetry considerations. Using this theory an entropy term of only $R \ln 8$ [*i.e.*, 4.13 cal./(mole °K.)] might be anticipated for triethylenediamine, whereas a value of 7.19 cal./(mole °K.) was found experimentally. The calculated value would arise from assuming a molecular symmetry of D_{3h} and finding the most likely distinguishable orientations of the molecule at an O_h lattice site. With this assignment the threefold molecular axis could be aligned with each of the four threefold axes of the cubic lattice in two different ways differing by a 60° rotation about the molecular axis.

Hendrickson[15] concludes from molecular orbital calculations that the bicyclo[2,2,2]octane molecule would be energetically most favorably arranged in a slightly twisted conformation allowing the hydrogen atoms on the ethylene groups to be situated at positions of mini-

(11) A. Farkas, G. A. Mills, W. E. Erner, and J. B. Maerker, *Ind. Eng. Chem.*, **51**, 1299 (1959).

(12) A. Farkas, G. A. Mills, W. E. Erner, and J. B. Maerker, *J. Chem. Eng. Data*, **4**, 334 (1959).

(13) T. Wada, E. Kishida, Y. Tomiie, H. Suga, S. Seki, and I. Nitta, *Bull. Chem. Soc. Japan*, **33**, 1317 (1960).

(14) G. B. Guthrie and J. P. McCullough, *J. Phys. Chem. Solids*, **18**, 53 (1961).

(15) J. B. Hendrickson, *Chem. Eng. News*, **39**, 47, 40 (1961).

mum potential energy rather than at the less favorable D_{3h} configuration. This twisting reduces the molecular symmetry to D_3 which leads to several interesting ramifications.

Wada, *et al.*,[13] reported the space group of the crystal II phase to be C^2_{6h}, which if true would preclude the twisted form in this phase region, but twisting could take place at the transition temperature and exist in the crystal I transition entropy increment. This would increase the transitional entropy contribution to R ln 16 [*i.e.*, 5.51 cal./(mole °K.)] since both a right-handed and left-handed twist would be equally probable. However, X-ray analysis distinguishes conclusively only with difficulty between C^2_{6h} and C^6_6, the latter of which is the space group for D_3 molecular symmetry in this case.

If the true molecular symmetry is D_3 at room temperature, right-handed and left-handed forms may exist in the crystal II phase without producing much strain. Since no thermal anomalies have been observed below room temperature,[3] it is possible that a residual entropy may exist at extremely low temperatures in the amount R ln 2. Availability of spectral data would permit an independent evaluation of the entropy and resolution of any ambiguity.

The entropy values reported by Wada, *et al.*,[13] for the crystal II → I transition and fusion do not agree with those of this research. They reported the increments to be 6.62 cal./(mole °K.) at 353.0°K. and 3.3 cal./(mole °K.) at 434.3°K., respectively, in contrast to corresponding increments from this study of 7.19 cal./(mole °K.) at 351.09°K. and 4.10 cal./(mole °K.) at 432.98°K., respectively. Their values are based on sublimation and vapor pressure data. Experience has shown that discord between such data and the more accurate calorimetric values often obtains[16] unless pressure data of high excellence are used.

Entropies of transition of other homologous bicyclic compounds have also been reported. Bicyclo[2,2,1]-heptane[14] and 3-azabicyclo[3,2,2]nonane[17] have been studied thermally yielding transitional entropies of 7.53 cal./(mole °K.) at 131.7°K. and 11.63 cal./(mole °K.) at 297.78°K., respectively. Both compounds would be expected to have identical C_{2v} molecular symmetry and are presumed to be in the plastically crystalline region above their transitions. Therefore, symmetry considerations alone will not account for the magnitudes of the anomalies. Work presently underway in this Laboratory to investigate the fusion thermal effects of 3-azabicyclo[3,2,2]nonane may provide some insight into the mechanism of the solid-state transition. Recent unpublished studies by Kolesov, *et al.*,[18] on *exo*-2-cyanobicyclo[2,2,1]heptane give an enthalpy of transition of 7.97 cal./(mole °K.) at 237.7°K. and an entropy of melting of 2.34 cal./(mole °K.) at 300.27°K. The authors consider that the family of which bicyclooctane is the prototype and triethylenediamine a member provide unusually fertile opportunities to study plastically crystalline behavior in terms of availability, opportunities to modify the symmetry and ligands. More studies by X-ray diffraction and infrared and Raman spectroscopy of crystals I and II would be obvious desiderata.

Acknowledgment.—The authors thank Dr. G. T. Furukawa for helpful advice concerning the design of the automatic shield control apparatus and the closure on the W-22 calorimeter, and Drs. G. A. Mills and A. Farkas and Houdry Process Corporation for the triethylenediamine sample. The generous assistance of H. G. Carlson in the construction of the calorimeter and of Dr. B. H. Justice in the numerical analysis of the data is recognized. The authors are indebted to the United States Atomic Energy Commission for facilities and funds, and J. C. T. is grateful to the Monsanto Chemical Company for a research fellowship.

(16) *E.g.*, *cf.* data on transition hexafluorides reported by E. F. Westrum, Jr., summarily in *J. Chem. Educ.*, **39**, 443 (1962).

(17) C. M. Barber and E. F. Westrum, Jr., *J. Phys. Chem.*, **67**, 2373 (1963).

(18) V. P. Kolesov, E. A. Seregin, and S. M. Skuratov, Luginin Thermochemistry Laboratory, Moscow State University, personal communication.

$NbB_{1.963}$: THE HEAT CAPACITY AND THERMODYNAMIC PROPERTIES FROM 5 TO 350°K.

BY EDGAR F. WESTRUM, JR.,

Department of Chemistry, University of Michigan, Ann Arbor, Michigan

AND GERALD A. CLAY

Arthur D. Little, Inc., Cambridge, Massachusetts

Received May 28, 1963

The heat capacity of a zone-melted nonstoichiometric $NbB_{1.963}$ has been measured by adiabatic cryogenic calorimetry and found to have a normal sigmoid temperature dependence without transitions or thermal anomalies. Values of the heat capacity at constant pressure (C_p), the entropy ($S°$), the enthalpy function ($H° - H°_0$), and the Gibbs free energy function ($-[G° - H°_0]/T$) are 11.42, 8.91, 5.433, and 3.478 cal./(g.f.m. °K.), respectively, at 298.15°K.

Introduction

Increasing demand for thermodynamic data on carbides, borides, and related compositions of the group IV elements as a consequence of technological developments in nuclear reactors, missiles, and other high temperature applications of refractory materials has prompted the present endeavor to procure reliable thermodynamic data in the cryogenic range on one of these materials, nonstoichiometric $NbB_{1.963}$, by adiabatic calorimetry.

Experimental

Cryostat and Calorimeter.—Measurements were made in the Mark III adiabatic cryostat previously described.[1] The gold-plated copper calorimeter (laboratory designation W-35) with a capacity of 100 cm.^{3} was constructed for measurement on the long rod-like, zone-refined cylinders of sample. In most essential details it is similar to one (W-9) previously described[2] with the exceptions that only a double vane is employed and that the thermometer well has been extended to support the cover. The sample space has a diameter of 3.6 cm. and an internal length of 10.4 cm. The heat capacity of the calorimeter–heater–thermometer assembly was determined in a separate series of measurements in which identical amounts of indium–tin (Cerroseal) solder for sealing the calorimeter and Apiezon-T grease for thermal contact with the heater–thermometer assembly were used. At 15°K. the heat capacity of the sample represented about 25% of the total; this increased to about 50% at 80°K. and to 75% at 350°K., and hence was a reasonably favorable fraction over most of the range. The mass of the calorimetric sample was 182.334 g. *in vacuo*. Buoyancy corrections were made on the basis of the density of 6.9 g./cm.^{3}. A pressure of 3.35 cm. of helium at 300°K. was used to facilitate thermal equilibrium in the sample space.

Temperatures determined with a capsule-type, strain-free, platinum-resistance thermometer (laboratory designation A-3) contained within an entrant well in the calorimeter are considered to accord with the thermodynamic temperature scale within 0.03°K. from 10 to 90°K. and within 0.04°K. from 90 to 350°K. Temperature increments, of course, may be determined with more precision than absolute temperatures and are probably correct to a few tenths of a millidegree after correction for quasi-adiabatic drift. All measurements of resistance, potential, temperature, time, and mass are referred to calibrations made by the National Bureau of Standards.

Preparation and Characterization of the Sample.—The raw material for this preparation was obtained from the United States Borax and Chemical Corporation in the form of a powder containing 82.56% Nb, 16.72% B, 0.47% O, and traces of C, N, and metallic impurities. This corresponds to a composition of $NbB_{1.741}$. In order to improve the stoichiometry and to reduce the level of impurities, the powdered NbB_2 was prepared for zone-refining by sintering into rods about 1 cm. in diameter by 18 cm. long, using a split mold of boron nitride and heating by direct passage of current through the sample. To compensate for boron losses during melting, 14% excess boron (based on the theoretical content of boron in NbB_2) was added to the powder before sintering. This treatment was followed by zone-melting in an atmosphere of 5% hydrogen in argon using the vertical, floating-zone technique with induction heating. The zone-refining apparatus was similar in principle to that described by Wernick, *et al.*,[3] except that the high frequency heating coil rather than the sample was moved. Power was furnished by a 10-kw., 450-kc. radiofrequency supply equipped with a manually operated thyratron output control. It was found desirable to do the melting at about 1 atm. pressure to minimize evaporation of boron from the molten zone, to move the molten zone about 25 cm./hr., and to eliminate minor arcing difficulties by the addition of 5% hydrogen to the atmosphere.

The zone-refined product was obtained in the form of macrocrystalline rods about 6 to 8 mm. in diameter, which were established to be single phase by metallographic examinations and X-ray diffractional examination of several representative samples. Chemical analysis for Nb and B gave the results in Table I.

TABLE I

Sample no.	435-2	473-1	477-2	527-2	531-3
Wt. %, Nb	81.51	82.01	81.41	80.93	80.51
Wt. %, B	18.45	18.22	18.69	18.79	18.71
Total	99.96	100.23	100.10	99.72	99.22
B/Nb ratio	1.945	1.909	1.973	1.995	1.997

This represents an average composition of $NbB_{1.963}$. Analyses for nonmetallic impurities indicate (in p.p.m.): 142 C, 66 O, and 45 N. Quantitative spectrographic analyses show: 0.13% Ti, 0.001% Fe, and less than 0.001% Si by weight. Carbide, oxide, nitride, and metallic impurities are present in amounts too small to require correction of the heat capacity data.

Results and Discussion

Heat Capacities and Thermal Properties.—The experimental heat capacities are presented in chronological order at the mean temperatures of the determinations in Table II. These data are presented in terms of the defined thermochemical calorie equal to 4.1840 j., an ice point of 273.15°K., and a gram formula mass (g.f.m.) of 114.15 for $NbB_{1.963}$. These data have been corrected for curvature, *i.e.*, for the difference between the measured $\Delta H/\Delta T$ and the derivative $(\partial H/\partial T)_p$. The approximate values of ΔT used in the determinations usually can be estimated from the increments between adjacent mean temperatures shown in Table II. These heat capacity values are considered to have a probable error decreasing from less than 5% at 5°K., to 1% at 10°K., and to less than 0.1% above 50°K., but are further subject to the purity of the sample as noted earlier.

TABLE II

HEAT CAPACITY OF $NbB_{1.963}$

[Units: cal., g.f.m., °K.]

T	C_p	T	C_p	T	C_p
Series I		Series III		203.03	8.058
				211.65	8.423
7.74	0.0057	38.46	0.2408	220.48	8.781
8.94	.0066	42.23	.3411	229.49	9.136
		46.81	.4923	238.23	9.469
Series II		49.22	.5838	247.12	9.796
		53.94	.7805	256.05	10.103
8.64	0.0061	59.15	1.0240	265.06	10.406
10.09	.0082	64.98	1.3184	273.19	10.669
11.74	.0097	71.67	1.661	282.10	10.949
12.96	.0115	79.63	2.082	290.82	11.211
14.14	.0132	87.98	2.530	299.72	11.467
15.46	.0157	95.92	2.929	309.17	11.728
16.85	.0193	104.09	3.339	318.83	11.981
18.28	.0229	112.42	3.759	328.42	12.221
19.76	.0284	120.72	4.177	337.71	12.436
21.39	.0335	129.29	4.607	346.05	12.635
23.19	.0420	138.05	5.042		
25.05	.0518	147.04	5.481	Series IV	
27.04	.0666	151.78	5.715		
29.25	.0868	160.23	6.121	313.40	11.832
31.85	.1176	169.10	6.540	322.59	12.069
34.75	.1637	178.07	6.954	331.91	12.307
37.92	.2282	186.83	7.346	341.21	12.515
		195.44	7.727	347.74	12.652

The heat capacities and thermodynamic functions at selected temperatures, as presented in Table III, are obtained from the heat capacity data by a least-squares-fitted curve through the experimental points (carefully compared with a large-scale plot of the data) and the integration thereof. Both the fitting and the quadrature are performed by high-speed digital computers using programs previously described.[4]

The thermodynamic functions are considered to have a precision indicated by a probable error of less than 0.1% above 100°K. An additional digit beyond those

(1) E. F. Westrum, Jr., *J. Chem. Educ.*, **39**, 443 (1962).

(2) S. S. Chang and E. F. Westrum, Jr., *J. Chem. Phys.*, **36**, 2420 (1962).

(3) J. H. Wernick, D. Dorsi, and J. J. Byrnes, *J. Electrochem. Soc.*, **106**, 245 (1959).

(4) B. H. Justice, Appendix to Ph.D. Dissertation, University of Michigan, 1961; USAEC Report TID-12722, 1961.

TABLE III

THERMODYNAMIC PROPERTIES OF $NbB_{1.963}$

[$NbB_{1.963}$: g.f.m. = 114.15. UNITS: cal., g.f.m., °K.]

T	C_p	$S°$	$H° - H°_0$	$-(G° - H°_0)/T$
5	0.0044	0.0011	0.004	0.0003
10	.0074	.0055	.036	.0019
15	.0152	.0098	.090	.0037
20	.0283	.0158	.197	.0060
25	.0516	.0243	.390	.0087
30	.0950	.0372	.746	.0123
35	.1681	.0569	1.390	.0172
40	.2788	.0861	2.491	.0239
45	.4292	.1273	4.244	.0330
50	.6145	.1818	6.841	.0450
60	1.066	.3323	15.16	.0796
70	1.578	.5347	28.36	.1296
80	2.104	.7798	46.77	.1951
90	2.624	1.0578	70.42	.2753
100	3.135	1.3607	99.22	.3685
110	3.640	1.683	133.11	.4732
120	4.143	2.022	172.03	.5881
130	4.642	2.373	215.96	.7118
140	5.137	2.735	264.85	.8433
150	5.626	3.106	318.68	.9818
160	6.108	3.484	377.35	1.1263
170	6.580	3.869	440.80	1.2763
180	7.042	4.258	508.91	1.4312
190	7.492	4.651	581.59	1.5903
200	7.929	5.047	658.70	1.7533
210	8.352	5.444	740.12	1.920
220	8.762	5.842	825.70	2.089
230	9.155	6.240	915.30	2.261
240	9.533	6.638	1008.8	2.435
250	9.894	7.034	1105.9	2.611
260	10.239	7.429	1206.6	2.788
270	10.569	7.822	1310.6	2.968
280	10.884	8.212	1417.9	3.148
290	11.186	8.599	1528.3	3.329
300	11.473	8.983	1641.6	3.511
310	11.748	9.364	1757.7	3.694
320	12.008	9.741	1876.5	3.877
330	12.256	10.113	1997.8	4.060
340	12.491	10.484	2121.6	4.244
350	12.719	10.849	2247.6	4.427
273.15	10.67	7.94	1344	3.024
298.15	11.42	8.91	1620	3.478

significant often is given in Table III for internal consistency and to permit interpolation and differentiation. The entropies and Gibbs free energy function have not been adjusted for nuclear spin and isotopic mixing contributions and are hence practical values for use in chemical thermodynamic calculations.

The heat capacity of NbB_2 has been estimated previously by Kaufman[5] by adaptation of a method devised by Tauer, Weiss, *et al.*,[6] in which the heat capacity of an element is represented as

$$C_p = C_v\,[\theta/T](1 + 10^{-4}T) + \gamma T$$

Here the heat capacities are those at constant pressure and volume, θ is an average Debye characteristic temperature chosen to provide the best fit to the heat capacity over the range $\theta/6 \leq T \leq \theta$, $C_v\,[\theta/T]$ is the Debye heat capacity,[7] γT is the electronic contribution, and the term in parenthesis approximates the $C_p - C_v$ correction arising from anharmonicity in the lattice and internal vibrational terms. The 298°K. values of C_p and S for $NbB_{1.963}$ are 3.84 and 2.99 cal./(g. atom °K.) and accord well with the corresponding experimental values of 3.81 and 2.97.

Enthalpy increments were determined by Mezaki, *et al.*,[8] from 468 to 1102°K. with respect to 299°K. on NbB_2 and yield an extrapolated result at 298.15°K. of 11.81 cal./(g.f.m. °K.) in fair accord with the 11.42 obtained in this study. The temperature dependence of their values at higher temperatures also accords reasonably well with the trend of these data.

Acknowledgment.—This work was supported in part by the United States Air Force Aeronautical Systems Division under Contract AF 33(657)-8635 with Manlabs, Inc. The advice and assistance of George Feick in the preparation of the sample, cooperation of Jim Huntzicker and Carolyn Barber in the operation of the calorimetric cryostat, and counsel and advice from Dr. Larry Kaufman are gratefully acknowledged.

(5) L. Kaufman, Data Sheet No. 42 (October, 1962) and Semi-Annual Report No. 1 (October, 1962), Contract AF 33(657)-8635.

(6) K. J. Tauer and R. J. Weiss, *J. Phys. Chem. Solids*, **4**, 135 (1958); J. A. Hoffman, A. Pasken, K. J. Tauer, and R. J. Weiss, *ibid.*, **1**, 45 (1956).

(7) J. Beattie, *J. Math. Phys.*, **6**, 1 (1926).

(8) R. Mezaki, E. W. Tilleux, D. W. Barnes, and J. L. Margrave, in "Thermodynamics of Nuclear Materials," International Atomic Energy Agency, Vienna, 1962, p. 775.

FLUORINE BOMB CALORIMETRY. VII. THE HEAT OF FORMATION OF CADMIUM DIFLUORIDE[1-3]

BY EDGARS RUDZITIS, HAROLD M. FEDER, AND WARD N. HUBBARD

Chemical Engineering Division, Argonne National Laboratory, Argonne, Illinois

Received May 15, 1963

The energy of formation of cadmium difluoride was measured by direct combination of the elements in a bomb calorimeter. The standard enthalpy and Gibbs energy of formation are $\Delta H_f^\circ_{298.15} = -167.39 \pm 0.23$ and $\Delta G_f^\circ_{298.15} = -155.4 \pm 0.3$ kcal. mole^{-1}, respectively.

Introduction

The heat of formation of cadmium fluoride has not been determined previously by calorimetry. Thus, the primary purpose of the present work was to determine this quantity by direct combination of the elements in a calorimeter. Such a determination was expected to afford an interesting comparison with heat of formation values derived from equilibrium measurements.

Because this work constituted part of a continuing program in fluorine bomb calorimetry, it also served a further purpose: namely, to extend the applicability of combustions in fluorine to a wider range of substances. In previous researches of this series neither the burning substances nor their fluorination products accumulated as liquids in the combustion zone. Cadmium and its fluoride, however, were observed to liquefy during combustion. After a number of trials, it was found that a pressed and slightly sintered dish of cadmium fluoride had sufficient mechanical strength and thermal shock stability to serve as an acceptable noncontaminating support material. (This technique parallels that of Huber and Holley,[4] who successfully employed sintered disks of oxides to support samples of the corresponding metals during combustions in oxygen.) In subsequent work, the technique of using sintered dishes of metal fluorides to support the corresponding metal during its combustion in fluorine was successfully extended to magnesium, aluminum, and zinc. The results of these studies will be reported in forthcoming publications.

Experimental

Materials. A. Cd.—Preliminary experiments showed that more complete combustion was obtained with cadmium filings than with massive cadmium. Reagent grade stick cadmium (Baker) was converted to filings in a helium-filled drybox. A few particles of steel from the file were removed with a magnet. Cadmium was found to undergo a limited surface reaction with fluorine at room temperature. The filings were therefore pretreated with fluorine; typically, a weight increase of 0.127% resulted. Chemical and spectrochemical analyses showed that the treated filings contained 220 ± 20 p.p.m. of oxygen[5] and trace amounts of carbon, hydrogen, silicon, lead, and copper. By difference, the filings contained 99.85% cadmium. With the assumption that fluorine and oxygen were present as CdF_2 and CdO, the filings contained 99.40 mole % of elemental cadmium.

B. F_2.—A special grade of high purity fluorine, obtained from General Chemical Co., was used. By mercury titration analysis,[6] it contained 99.9% fluorine. After the titration, the residual gases were collected and analyzed by mass spectrometry. The relative amounts of the impurities found were: O_2, 35; N_2, 60; CO_2, 2; H_2O, 1; CF_4, 1; SiF_4, 1. During the precombustion period (about 1 hr.) the oxygen content of the fluorine increased to 0.10 ± 0.007%, presumably because of reaction with impurities adsorbed on the bomb walls.[7] No significant change in the amounts of other impurities was observed.

C. CdF_2.—Cadmium fluoride (A. D. Mackay Co.) was spectrochemically pure and monophasic by X-ray analysis. Chemical analysis yielded the following composition: Cd, 74.48; F, 25.22; O, 0.11% (theor.: Cd, 74.74; F, 25.26%). When this cadmium fluoride was used as a support during the combustion of cadmium in fluorine, oxygen was evolved. Attempts to remove the oxide by fluorination at 600–700° were unsuccessful. After several exposures to the higher temperatures prevailing during actual combustions the oxygen content was reduced, but significant quantities of oxygen were still evolved during the combustion. It was later found that the oxide content of cadmium fluoride could be eliminated by autoclaving the powder overnight with anhydrous HF at 240°.

Calorimetric System.—The calorimetric system (ANL-R1) has been previously described.[8] The nickel bomb (laboratory designation Ni-4) was modified, as shown in Fig. 1, to provide a greater area of thermal contact between the base and support dish. A combination of aluminum and Teflon gaskets improved the sealing of the bomb.

Calibration.—The energy equivalent of the calorimetric system, ε(calor.), was determined by calibration combustions of benzoic acid (N.B.S. certified sample 39h) in oxygen under prescribed conditions. The benzoic acid pellet was ignited by passage of a current through a short length of fine (0.001-in. diameter) platinum wire.[9] The electrical energy input to the wire, as indicated by a current integrating device, was negligible. Calibration experiments were performed both before and after the cadmium combustions. ε(calor.), determined by the average of a series of ten combustions, was 3603.2 ± 0.5 cal. deg.$^{-1}$. For the last two calorimetric combustions (performed a year later with a slightly modified bomb), ε(calor.) was 3586.9 cal. deg.$^{-1}$.

Procedure.—Cadmium filings, pretreated as described, were evenly distributed over the center portion of a cadmium fluoride dish. These dishes, prepared from the material purified as described earlier, were cold pressed in a special die at 2500 p.s.i. and sintered in fluorine at 600° for 48 hr. The bomb was assembled, evacuated, filled with fluorine to a pressure of 6 atm. (about 150% excess), and placed in the calorimeter. The sample was ignited by passage of an electric current through a 0.003-in. diameter 0.5 in. long cadmium fuse wire. Electrical connections to the terminals were made *via* cadmium metal strips.

The interior surfaces of the bomb were thoroughly prefluorinated during preliminary experiments. After each calorimetric combustion, the interior surfaces were blown clean from small amounts of fluoride powder. No significant changes in weight of any of the bomb parts occurred during the calorimetric series.

Analyses.—After each combustion some of the cadmium metal

(1) This work was performed under the auspices of the U. S. Atomic Energy Commission.

(2) Presented in part at the 17th Annual Calorimetry Conference, Berkeley, California, August, 1962.

(3) For the previous paper in this series see: J. L. Settle, H. M. Feder, and W. N. Hubbard, *J. Phys. Chem.*, **67**, 1892 (1963).

(4) E. J. Huber, Jr., C. O. Mathews, and C. E. Holley, Jr., *J. Am. Chem. Soc.*, **77**, 6493 (1955); see also E. J. Huber, Jr., E. L. Head, and C. E. Holley, Jr., *J. Phys. Chem.*, **61**, 1021 (1957), for reference to other papers in that series.

(5) B. D. Holt and H. T. Goodspeed, *Anal. Chem.*, **34**, 374 (1962).

(6) G. T. Armstrong and R. S. Jessup, *J. Res. Natl. Bur. Std.*, **64A**, 49 (1960).

(7) S. S. Wise, J. L. Margrave, H. M. Feder, and W. N. Hubbard, *ibid.*, **67**, 815 (1963).

(8) E. Greenberg, J. L. Settle, H. M. Feder, and W. N. Hubbard, *J. Phys. Chem.*, **65**, 1168 (1961).

(9) J. Coops, R. S. Jessup, and K. van Nes, "Experimental Thermochemistry," Vol. I, F. D. Rossini, Ed., Interscience Publishers, Inc., New York, N. Y., 1956, Chapter 3.

TABLE I

RESULTS OF CADMIUM COMBUSTION EXPERIMENTS[a]

1	Mass, g.	2.38678	2.01297	1.97671	1.72233	2.01222	1.95371	1.77095	1.78832
2	Δt_c, de.[b]	0.98829	0.82956	0.81358	0.71168	0.82871	0.80496	0.73086	0.73707
3	ε(calor.)$(-\Delta t_c)$, cal.	−3561.2	−2989.2	−2931.7	−2564.4	−2986.2	−2900.6	−2621.5	−2643.8
4	ΔE (contents),[c] cal.	−7.5[d]	−3.6	−3.3	−3.1	−3.6	−3.7	−3.7	−3.6
5	$\Delta E_{ignition}$, cal.	0.1	0.1	0.1	0.1	0.1	0.1	0.1	0.1
6	ΔE (gas), cal.	−0.4	−0.4	−0.4	−0.3	−0.4	−0.4	−0.3	−0.3
7	ΔE (impurities), cal.	27.0	2.5	7.1	6.5[e]	2.3	3.2[e]	0.0	0.0
8	$\Delta E_c°/M$, cal. g.$^{-1}$	−1484.0	−1485.7	−1481.4	−1487.1	−1484.8	−1485.1	−1482.5	−1480.5

Mean $\Delta E_c°/M$ = −1483.9 cal. g.$^{-1}$

Std. dev. of mean = ±0.8 cal. or 0.06%

[a] The symbols employed are explained in ref. 10. [b] $\Delta t_c = t^f - t^i + \Delta t_{corr.}$. [c] ΔE (cont.) = $[\varepsilon^f(\text{cont.}) - \varepsilon^i(\text{cont.})](25 - t_i) + \varepsilon^f(\text{cont.})(-\Delta t_c)$. [d] Two support dishes were used in this experiment. [e] ΔE (impurities), estimated by assuming that the amount of oxygen liberated was proportional to the mass of sample burned.

remained unreacted. The amount of unburned metal (approx. 0.5–2.5%) was determined as follows. The solidified melt was crushed and placed in an erlenmeyer flask attached to a vacuum line. The flask was evacuated, approx. 20 ml. of concentrated HCl was added, and the mixture was agitated overnight with a magnetic stirrer. The evolved hydrogen was transferred by means of a Toepler pump through a series of cold traps and a heated (450°) palladium diaphragm (permeable to hydrogen only) into a gas buret. In trial experiments 99.8% of the hydrogen equivalent of a known mass of cadmium was recovered. The precision of this measurement was such that the uncertainty in the mass of unburned cadmium did not exceed the weighing error of 3×10^{-5} g.

After each combustion an aliquot of the bomb gas was analyzed to determine the extent of side reactions. The method already described for fluorine was used.

The reaction product was identified as cadmium fluoride by its X-ray diffraction pattern.

Results

Experimental Results.—The results of the combustion experiments are summarized in Table I. Energy quantities are expressed in terms of the defined calorie equal to exactly 4.184 absolute joules. The corrections to standard states were applied in the usual manner.[10] The entries in the table are: (1) the mass (weight *in vacuo*) of cadmium burned; (2) the observed increase in the calorimeter temperature, corrected for the heat exchanged between the calorimeter and its surroundings; (3) the energy equivalent of the calorimeter multiplied by the negative of the corrected temperature increase; (4) the correction for the difference between the energy of the real bomb process and the energy of the hypothetical isothermal bomb process at 25°; (5) the measured electrical energy input for the ignition of the fuse wire; (6) the net correction of the bomb gases to standard state; (7) the correction for the fluorination of impurities in the sample and support dish; (8) the energy change per gram of cadmium for the reaction

$$Cd(c) + F_2(g) \longrightarrow CdF_2(c) \qquad (1)$$

with the reactants and product in their respective standard states at 25°.

For the calculation of item 1 the mass of filings was corrected for its contents of CdO and CdF_2 and for the recovered unburned cadmium. For the calculations of item 4, the values used were: C_p: Cd,[11] 6.14 and CdF_2,[12] 15.8; C_v: F_2,[13] 5.50 cal. mole^{-1} deg.$^{-1}$. For the calculation of item 6, the coefficients, $(\partial E/\partial P)_T$ and μ, for fluorine[10] were taken as −1.780 cal. mole^{-1} atm.$^{-1}$ and 0.0008 atm.$^{-1}$, respectively. The internal volume of the empty bomb was 0.293 l.

The energy correction in item 7 is due to the fluorination of the oxide in the support dish as well as in the filings. The standard heat of formation of CdO[11] was taken as −60.9 kcal. mole^{-1}. The extent of this side reaction was based on the change in oxygen content of the bomb gas as measured before and after com-

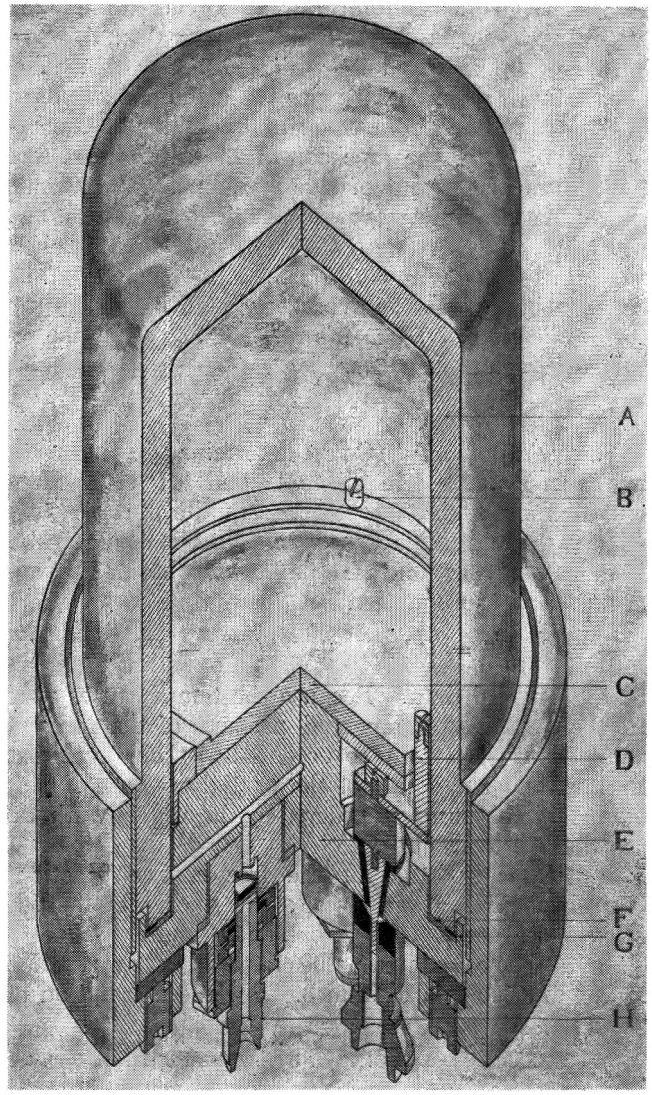

Fig. 1.—Combustion bomb (Ni-4). A, body; B, ground terminal; C, sample support dish (2-in. diameter × 3/16 in. thick); D, insulated terminal; E, bomb base; F, aluminum main gasket; G, Teflon back-up gasket; H, valve.

(10) W. N. Hubbard, "Experimental Thermochemistry," Vol. II, H. A. Skinner, Ed., Interscience Publishers, Ltd., London, 1961, Chapter 6.

(11) F. D. Rossini, D. D. Wagman, W. H. Evans, S. Levine, and I. Jaffe, "Selected Values of Chemical Thermodynamic Properties," National Bureau of Standards, Circular 500, Washington, D. C., 1952.

(12) Estimated on the basis of Kopp's law.

(13) W. H. Evans, T. R. Munson, and D. D. Wagman, *J. Res. Natl. Bur. Std.*, **55**, 147 (1955).

TABLE II

ESTIMATED HEATS OF FORMATION OF CADMIUM FLUORIDE FROM GASEOUS EQUILIBRIUM MEASUREMENTS

Method	Temp., °C.	$-\Delta H°_{298}$, kcal. mole^{-1}	$\Delta H_f°_{298}$, kcal. mole^{-1}
(3) $Cd(c) + 2HF(g) = CdF_2(c) + H_2(g)$[a]	400, 500, 600	37.76, 38.80, 38.84	-168.3 ± 1
(4) $CdCl_2(c) + 2HF(g) = CdF_2(c) + 2HCl(g)$[b]	311, 420, 513	3.04, 1.59, 0.10	$-(180)$
(5) $CdO(c) + 2HF(g) = CdF_2(c) + H_2O(g)$[c]	600, 650, 700, 750, 800	32.71, 32.98, 33.31, 33.63, 34.04	-166.2 ± 1

[a] See ref. 17. [b] See ref. 18. [c] See ref. 19.

bustion. Other changes in the bomb gas composition could be attributed to the trace impurities. The energy of combustion of the trace impurities was not significantly different from that of an equal mass of cadmium; hence, no correction was made for them.

The following standard thermal data (in kcal. mole^{-1}) were derived for the formation of $CdF_2(c)$ at 25° according to eq. 1: $\Delta E_f° = -166.79 \pm 0.23$, $\Delta H_f° = -167.39 \pm 0.23$, and $\Delta G_f° = -155.4 \pm 0.3$. The uncertainties given equal twice the combined standard deviations arising from the reproducibility of the experimental data, the precision of the calibration, and the nature and extent of side reactions. The atomic weight of cadmium[14] was taken as 112.40 g. (g.-atom)$^{-1}$. The entropies $S°_{298}$ were taken to be Cd[15] 12.4, F_2[15] 48.5, and CdF_2 20.8 ± 0.7 cal. deg.$^{-1}$ mole^{-1}. The latter estimate was the average of results obtained by the application of Latimer's method[16] to all of the reported[15] divalent fluorides.

Discussion

The value of $\Delta H_f°$ (CdF_2) determined in this work has been compared in Table II and III with values obtained by high temperature equilibrium measurements[17-19] and e.m.f. measurements,[20] respectively. The heats of reaction in Table II were obtained by application of the equation

$$-\Delta H°_{298}/T = R \ln K_p + \Sigma\Delta(F°_T - H°_{298})/T \quad (2)$$

to the original data. Because the temperatures were sufficiently high, the partial pressure of the gases at equilibrium were taken to be equal to their fugacities. In reaction 3 the effect of the partial pressure of cadmium (which was not considered by the original authors) was taken into account.

For the calculation of the free energy functions tabular data[15,21,22] were used; for cadmium fluoride $C_p = 14.5 + 4.7 \times 10^{-3} T$ cal. deg.$^{-1}$ mole^{-1} was estimated. The calculated values for the heats of reaction at 25° are listed in column 3. For the calculation of the corresponding average values of $\Delta H_f°_{298}$ (CdF_2), column 4, the following standard heats of formation were used: HF,[23] −64.9; $CdCl_2$,[11] −93.0; HCl,[11] −22.1; CdO,[11] −60.9; and H_2O,[11] −57.8. Table III exhibits a recalculation of the heat of formation of CdF_2 based on Jahn-Held and Jellinek's e.m.f. measurements,[20] supplemented by more recent data[23-26] for the auxiliary reactions. The uncertainties of the derived $\Delta H_f°$ (CdF_2) values given in Tables II and III were estimated from the scatter of the calculated heats of reactions and the uncertainties of the auxiliary data.

TABLE III

ESTIMATED HEATS OF FORMATION OF CADMIUM FLUORIDE FROM E.M.F. MEASUREMENTS

Reaction	$-\Delta F°_T$, cal. mole^{-1} at 288°K.	298°K.	308°K.
(6) $PbF_2(c) + Cd$ (8 w/o) $- Hg = CdF_2(c)$[a] $+ Pb$ (5 w/o) $- Hg$	−4287	−4389	−4495
(7) Pb (5 w/o) $- Hg + 2HF(aq)$(1 N) $= H_2(g)$[b] $+ PbF_2(c)$	−7177	−7159	−7136
(8) $Cd(s) = Cd$ (8 w/o) $- Hg$[c]	−2202	−2110	−2018
(9) $2HF(g) = 2HF(aq)$(1 N)[d]	−11888	−11676	−11160
(10) $H_2(g) + F_2(g) = 2HF(g)$[e]	−130772	−130808	−130844
(Sum) $Cd(s) + F_2(g) = CdF_2(s)$	−156322	−156142	−155650
Average $\Delta H_f°_{298}$ (CdF_2)	−168.0 ± 0.8 kcal. mole^{-1}		

[a] See ref. 20. [b] See ref. 24. [c] See ref. 25. [d] See ref. 26. [e] See ref. 23.

The values of the heat of formation of CdF_2 obtained from the e.m.f. data and reactions 3 and 5 agree with the value -167.39 ± 0.23 obtained in this work within their combined uncertainties. The value based on reaction 4 may be rejected, as previous compilers[11,27] have done, because the standard heat of reaction obtained from third law calculations shows a strong trend. Such a trend is usually symptomatic of a systematic error, which in this case may be due to the solid state interaction[28] of CdF_2 and $CdCl_2$.

Acknowledgment.—The authors wish to acknowledge the technical assistance of Rosemary Terry. The performance of special analyses by B. D. Holt, R. V. Schablaske, and R. J. Meyers are gratefully acknowledged.

(14) A. E. Cameron and E. Wichers, *J. Am. Chem. Soc.*, **84**, 4175 (1962).
(15) K. K. Kelley and E. G. King, U. S. Bureau of Mines, Bull. 592 (1961).
(16) G. N. Lewis, M. Randall, K. S. Pitzer, and L. Brewer, "Thermodynamics," 2nd Ed., McGraw-Hill Book Co., Inc., New York, N. Y., 1961, p. 517.
(17) K. Jellinek and A. Rudat, *Z. anorg. allgem. Chem.*, **175**, 281 (1928).
(18) K. Jellinek and R. Koop, *Z. physik. Chem.*, **A145**, 305 (1929).
(19) L. Domange, *Ann. Chim.*, [11], **7**, 225 (1937).
(20) W. Jaan-Held and K. Jellinek, *Z. Elektrochem.*, **42**, 401 (1936).
(21) JANAF Thermochemical Tables, Dow Chemical Company, Midland, Michigan, 1962.
(22) K. K. Kelley, U. S. Bureau of Mines, Bull. 584 (1960).
(23) H. M. Feder, W. N. Hubbard, S. S. Wise, and J. L. Margrave, *J. Phys. Chem.*, **67**, 1148 (1963).
(24) H. H. Broene and T. De Vries, *J. Am. Chem. Soc.*, **69**, 1644 (1947).
(25) "Selected Values of Thermodynamic Properties of Metals and Alloys," R. Hultgren, Ed., University of California, Berkeley, California.
(26) J. C. Brosheer, F. A. Lenfesty, and K. L. Elmore, *Ind. Eng. Chem.*, **39**, 423 (1947).
(27) G. T. Armstrong and L. A. Krieger, Chapter 8, Preliminary Report on the Thermodynamic Properties of Selected Light Elements and Some Related Compounds, National Bureau of Standards Report 7192 (1961).
(28) I. G. Ryss, "The Chemistry of Fluorine and Its Inorganic Compounds," State Publishing House for Scientific, Technical, and Chemical Literature, Moscow, 1956 (AEC-tr-3927), Chapter XXV.

THE OXIDATION OF METHYL RADICALS AT LIQUID HELIUM TEMPERATURE

BY JOHN L. ROEBBER[1]

Texaco Research Center, Beacon, New York

Received May 18, 1963

Infrared spectrometry has been used to follow the photooxidation of azomethane and methyl iodide in solid oxygen at liquid helium temperatures. Ethane, formaldehyde, and ozone are the main azomethane products. Formaldehyde and ozone, but no ethane, are the main methyl iodide products. Ethane arises from the recombination of two methyl radicals formed in the same matrix cage. Ozone may be produced by the photolysis of an unidentified intermediate trapped in the oxygen matrix. The mechanism by which formaldehyde is formed is not clear. The unidentified species responsible for the 11.10-μ band of an azomethane photodecomposition product may be decomposed by the 6000–3100-Å. light used to photolyze the azomethane. The 11.10-μ band of this species, whose behavior upon warm-up is characteristic of a free radical, shows an isotope shift of 17 cm.$^{-1}$ when an O^{18} matrix is used.

Spurred by the needs of workers concerned with oxidation studies, a number of investigations have recently been made of the reactions of the methyl radical with oxygen.[2-15] There is still considerable uncertainty as to the mechanism which is operative. There is general agreement that the first step in the reaction sequence is the formation of an excited methylperoxyl radical.[6,7,9]

$$CH_3 + O_2 \rightleftarrows CH_3O_2^* \qquad (1)$$

The third-order kinetics of the reaction between the methyl radical and oxygen in the usual pressure region suggests the establishment of an equilibrium between the excited radical, $CH_3O_2^*$, and its dissociation products in eq. 1. However, there is little agreement as to the subsequent reactions of the methylperoxyl radical.

Reported herein are the results of a study of the oxidation of methyl radicals by solid oxygen at liquid helium temperatures. This work was undertaken to obtain direct evidence of the oxidation mechanism by trapping unstable intermediates in a solid oxygen matrix.

Experimental

The experimental techniques were identical with those of ref. 16 except as noted. Photolysis of azomethane was conducted with a high pressure mercury arc, General Electric B-H6. An elliptical spun aluminum reflector was used to focus the light from the arc onto the sample. A 3.1-cm. Pyrex cell containing an aqueous solution of $CuSO_4 \cdot 5H_2O$ at a concentration of 80 g./l. was used to reduce the heating of the sample. This filter transmits between 6000 and 3100 Å. Methyl iodide was photolyzed with a Hanovia 100-w. mercury arc equipped with a filter consisting of a 1-cm. path of an aqueous solution containing 500 g./l. of $NiSO_4 \cdot 6H_2O$. This filter transmits between 3450 and 2250 Å.

Azomethane was prepared by the reduction of dimethylhydrazine with mercuric oxide according to the method of Renaud and Leitch.[17] Fisher reagent methyl iodide (b.p. 41–43°) was purified by passage through silica gel. Monomeric formaldehyde vapor, obtained by heating Matheson Co. 91% pure paraformaldehyde under vacuum, was purified by vacuum distillation through a trap immersed in Dry Ice. Eastman White Label formic acid was dried over anhydrous copper sulfate and purified by vacuum distillation. Dimethyl peroxide was prepared according to the procedures of Hanst and Calvert.[8] Linde oxygen, dried by passage through a liquid nitrogen trap, was used as the matrix material. All other compounds were obtained from commercial sources and used without purification except for removal of any gases not condensable in liquid nitrogen.

Infrared spectra were obtained using a Perkin-Elmer Model 21 double beam spectrometer equipped with a NaCl prism. Wave length accuracy is estimated to be 0.02 μ. Some spectra were recorded using a modified optical wedge giving a 4× scale expansion.[18] The uncertainty in optical density measurements is estimated to be less than 0.01 optical density units.

Identification of products was made by comparisons to reference spectra run on pure compounds in solid oxygen at helium temperatures. Conditions of resolution, per cent absorption, etc., were as near as possible to those existing after photolysis. Measurements of concentrations of products relative to the concentration of azomethane were made by adding a known amount of carbon tetrachloride to the pure compound whose reference spectra were being run. The carbon tetrachloride bands had previously been compared to the azomethane bands. In cases when overlap of bands was not a problem, azomethane was added directly to the compound whose reference spectra were being run.

Visible-ultraviolet spectra were obtained with a Cary Model 14 M spectrophotometer.

Results

Photolysis of Azomethane in Oxygen.—The major new infrared bands which appear when azomethane is photolyzed in oxygen are listed in Table I. The assigned identities of the photolysis products are shown in the last column of Table I. The identification of ethane was verified by an experiment in which ethane was suspended in oxygen. The most intense bands observed are listed in Table II. The bands at 6.80 and 12.15 μ listed in Table I agree in both position and relative intensity with the two strongest ethane bands. Strong azomethane bands obscure the other ethane bands in the experiment listed in Table I. Under higher resolution, product bands can be distinguished from the parent azomethane bands at 3.35, 3.40, 3.46, and 7.27 μ as shown in Fig. 1. From the intensity of the 6.80 and 12.15-μ bands, the ratio of ethane produced to azomethane decomposed by photolysis is 0.5.

The identification of ozone as a product was also checked in separate experiments. Ozone was produced

(1) Department of Chemistry, Northeastern University, Boston 15, Massachusetts.

(2) (a) A. D. Walsh, *Trans. Faraday Soc.*, **43**, 297 (1947); (b) J. E. Raley, L. M. Porter, F. F. Rust, and W. E. Vaughan, *J. Am. Chem. Soc.*, **73**, 15 (1951).

(3) E. R. Bell, J. H. Raley, F. F. Rust, F. H. Seubold, and W. E. Vaughan, *Discussions Faraday Soc.*, **10**, 242 (1951).

(4) F. B. Marcotte and W. A. Noyes, Jr., *J. Am. Chem. Soc.*, **74**, 783 (1952).

(5) G. R. Hoey and K. O. Kutschke, *Can. J. Chem.*, **33**, 496 (1955).

(6) D. E. Hoare and A. D. Walsh, *Trans. Faraday Soc.*, **53**, 1102 (1957).

(7) M. I. Christie, *Proc. Roy. Soc.* (London), **A244**, 411 (1958).

(8) P. L. Hanst and J. G. Calvert, *J. Phys. Chem.*, **63**, 71 (1959).

(9) W. C. Sleppy and J. G. Calvert, *J. Am. Chem. Soc.*, **81**, 769 (1959).

(10) R. L. Strong and K. O. Kutsche, *Can. J. Chem.*, **37**, 1456 (1959).

(11) F. Wenger and K. O. Kutschke, *ibid.*, **37**, 1546 (1959).

(12) M. Shahin and K. O. Kutschke, *ibid.*, **39**, 73 (1961).

(13) M. Shahin and K. O. Kutschke, *J. Phys. Chem.*, **65**, 189 (1961).

(14) N. R. Subbaratnam and J. G. Calvert, *J. Am. Chem. Soc.*, **84**, 1113 (1962).

(15) D. F. Dever and J. G. Calvert, *ibid.*, **84**, 1362 (1962).

(16) J. L. Roebber, *J. Chem. Phys.*, **37**, 1974 (1962).

(17) R. Renaud and L. C. Leitch, *Can. J. Chem.*, **32**, 545 (1954).

(18) S. A. Francis and A. H. Ellison, *J. Opt. Soc. Am.*, **49**, 131 (1959).

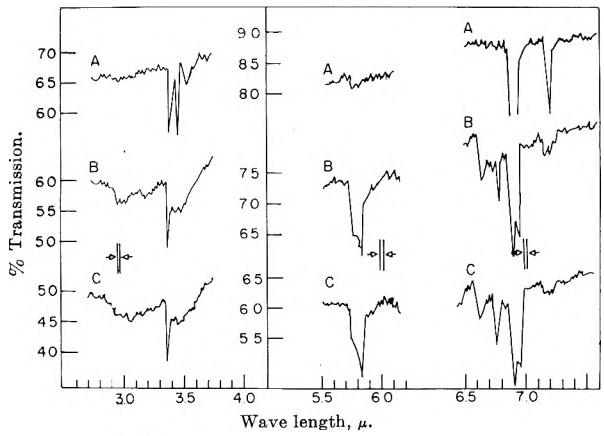

Fig. 1.—Photooxidation of azomethane in solid oxygen (tracings of spectra recorded during expt. 4, M/R = 217, T = 8°K.): a, before photolysis; b, photolysis (48 min.); c, after warm-up.

TABLE I

OPTICAL DENSITIES OF INFRARED BANDS BY PHOTOLYSIS OF $CH_3N_2CH_3$ IN SOLID OXYGEN[a]

Wave length, μ	Photolysis time 0 min.	24 min.	48 min.	Warm-up	Identity
3.14	...	0.003	0.005	0.002	Polymeric water?
4.28	...	.007	.012	.012	CO_2
4.68	...	.001	.002	.002	CO
5.76	...	.007	.022	.026	H_2CO
5.82	...	.010	.026	.039	?
6.66	...	.005	.009	.012	H_2CO
6.80	...	.016	.022	.018	C_2H_6
7.23	0.040	.022	.019	.015	$CH_3N_2CH_3$
8.47	...	.010	.013	.011	?
9.00	0.012	.019	.021	.012	$CH_3N_2CH_3$ + products
9.63	...	...	...	.042	O_3
9.66[b]	...	.025	.049	...	O_3
10.22	...	.013	.020	.053	?
11.10	...	.024	.033	.013	?
12.15	...	.015	.024	.022	C_2H_6
12.90	...	.002	.002	.006	?
14.28	...	.003	.005	.006	O_3

[a] Experiment 7, M/R = 200, T = 6°K., 4× scale expansion. [b] In some experiments this band appeared as a doublet.

directly in the oxygen matrix by using 3400–2250-Å. ultraviolet light.[19] The three bands produced are listed in Table II. The 9.66-μ band was observed to shift on warm-up to 9.63 μ. The good agreement between the position, intensity, and shift on warm-up of the 9.66 and 14.28-μ bands listed in Table I leaves little doubt that ozone is a product of the photolysis of azomethane in oxygen.

In the gas phase photooxidation of azomethane at room temperature, methanol and formaldehyde are major while formic acid and methyl hydroperoxide are minor products.[8-15] Dimethyl peroxide is another possible minor product.[8] Spectra of all of these compounds, except methyl hydroperoxide, were obtained in solid oxygen. The positions and intensities of their strongest bands are listed in Table II. It can be seen from the results for methanol that the strongest band of any methanol formed in the photooxidation of azomethane in solid oxygen might be hidden by the strong ozone band. However, large changes take place in the spectrum of methanol on warm-up due to the formation of hydrogen bonds. In particular, a strong band

(19) Blank experiments showed that ozone cannot be produced from the oxygen matrix by the 6000–3100-Å. light used to decompose the azomethane.

TABLE II

OPTICAL DENSITIES OF INFRARED BANDS OF REFERENCE COMPOUNDS IN SOLID OXYGEN[a]

Compound	M/R	Wave length, μ	Spray-on	Warm-up
C_2H_6	200	3.35	0.090	0.094
		3.40	Shoulder	Shoulder
		3.46	.034	.032
		6.80	.068	.068
		7.27	.017	.020
		12.15	.064	.062
O_3	Unknown	4.75	0.002	0.002
		9.63	...	.064
		9.66[b]	.060	...
		14.28	.005	.006
CH_3OH	200	3.38	0.012	0.010
		7.48	.011	...
		9.54	...	.033
		9.65	...	.050
		9.69	.113	...
H_2CO	200	3.50	0.008	Not run
		3.58	.009	
		5.75	.048	
		6.66	.014	
		8.54	.004	
HCOOH	260	5.67	0.056	0.015
		5.76	.019	...
		5.77	...	.038
		5.82	...	.041
		8.50	.014	.014
		9.06	.075	...
		9.09	...	.022
CH_3OOCH_3	260	6.77	0.025	Not run
		7.00	.021	
		9.62	.048	
		9.68	.064	

[a] T = 6°K., 4× scale expansion. [b] In some experiments this band appeared as a doublet.

appears at 9.54 μ. No band appears on warm-up at 9.54 μ from the azomethane photooxidation products. This indicates that the ratio of methanol formed to azomethane decomposed is less than 0.01. Hence methanol is not an important product in the solid phase.

The large bands in the carbonyl region at 5.76 and 5.82 μ easily visible in Fig. 1 suggest that formaldehyde or formic acid, or both, are photooxidation products in solid oxygen. As shown by Table II, formaldehyde does indeed have a strong band at 5.75 μ. The formaldehyde band at 6.66 μ also agrees well in position and relative intensity with a photooxidation product band listed in Table I. The weaker formaldehyde band at 3.58 μ was not observed in the experiment listed in Table I nor in the experiment shown in Fig. 1. In one experiment, a very small band was observed at 3.58 μ. The weak formaldehyde bands at 3.50 and 8.54 would be obscured by the other bands. It seems likely that the 5.76 and 6.66-μ bands of Table I are due to formaldehyde. However, the failure to observe the 3.58-μ band consistently makes this identification less certain than that of ethane and ozone.

Monomeric formic acid also has a band at 5.76 μ in solid oxygen as can be seen from Table II. However, the two strongest monomeric formic acid bands, 9.06 and 5.67 μ, are not present in any spectra of the photooxidation products of azomethane in solid oxygen. From the intensity of the 5.67-μ band, the ratio of

monomeric formic acid produced to azomethane decomposed is less than 0.003. Hence monomeric formic acid is not an important product in solid oxygen.

Table II shows that warm-up greatly changes the spectrum of formic acid due to polymer formation. The 5.82-μ band due to polymeric formic acid does agree with a product band listed in Table I. There are also very small product bands in the 8.95–9.10-μ region not individually listed in Table I. However, the product band at 9.08 μ is much too weak to permit polymeric formic acid to be the species responsible for the large product band at 5.82 μ.

In the gas phase methyl hydroperoxide shows strong bands at 12.2, 9.8, and 7.5 μ with weaker bands at 3.4 and 2.8 μ.[8] While the strong bands at 12.2 and 9.8 μ might be overlapped by other product bands, the complete absence of any band at 7.5 μ in the azomethane photodecomposition products makes it unlikely that methyl hydroperoxide is present.

The four strongest dimethyl peroxide bands are listed in Table II. The very large ozone band at 9.66 μ might hide small dimethyl peroxide bands at 9.68 and 9.62 μ. While dimethyl peroxide can be ruled out as a major product, it could be a minor product.

The bands in the 3.0-μ region shown in Fig. 1 make the presence of polymeric water seem likely in view of matrix studies of water.[20] Other absorptions for which the assignment to a species has been supported by matrix studies are CO_2 at 4.28 μ and CO at 4.68 μ.[16,21,22a]

The visible-ultraviolet region from 6500–2800 Å. was examined. Except for slightly increased scattering, no change could be detected after photolysis of azomethane. Upon warm-up, the scattering increased greatly, but no new bands appeared.

Photolysis of Methyl Iodide in Oxygen.—The principal new bands which appear when methyl iodide is photolyzed in oxygen are listed in Table III. The observation of bands at 3.50, 3.58, 5.77, and 6.67 μ makes the identification of formaldehyde as a product quite certain in this case. The absence of any band in the 9.0-μ region rules out monomeric and polymeric formic acid as the cause of the 5.81-μ band.

TABLE III

OPTICAL DENSITIES OF INFRARED BANDS PRODUCED BY PHOTOLYSIS OF CH_3I IN SOLID OXYGEN[a]

Wave length, μ	Photolysis time 0 min.	Photolysis time 60 min.	Identity
2.72	...	0.014	H_2O?
2.95	...	.028	Polymeric water?
3.50	0.006	.019	$CH_3I + H_2CO$
3.58	...	.016	H_2CO
4.28	...	.075	CO_2
4.68	...	.013	CO
5.77	...	.033	H_2CO
5.81	...	.061	?
6.25	.041	.088	$O_2 + H_2O$
6.67	...	.022	H_2CO
7.18	...	.015	?
8.02	.141	.082	CH_3I
9.65	...	.054	O_3

[a] Experiment 2, $M/R = 400$, $T = 5$°K.

(20) M. Van Thiel, E. D. Becker, and G. C. Pimentel, *J. Chem. Phys.*, **27**, 486 (1957).

(21) H. W. Brown and G. C. Pimentel, *ibid.*, **29**, 883 (1958).

(22) (a) Photolysis of formaldehyde suspended in O_2 (M/R = 200) also produces bands in the 3.0-μ region and at 4.28 and 4.68 μ; (b) this band might be due to I_2. The weakness of the band and the large light scattering of the matrix makes identification impossible.

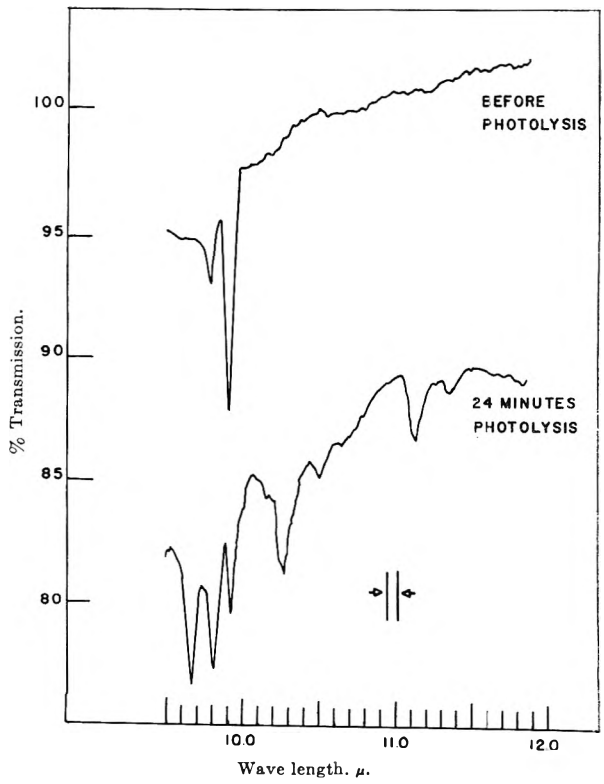

Fig. 2.—Photooxidation of azomethane in solid oxygen enriched with O^{18} (tracings of spectra recorded during expt. 9, M/R = 220, O^{16}/O^{18} = 2.9, T = 6°K.).

There are several striking differences between the spectra of the methyl iodide and azomethane photooxidation products. The large ethane bands at 6.80 and 12.15 μ are not present in the methyl iodide case. Furthermore azomethane photooxidation product bands at 11.10, 10.22, 9.00, and 8.47 μ are not found among the methyl iodide product bands.

Examination of the visible-ultraviolet region from 6500–2100 Å. revealed only one new feature produced on photolysis. This was a small, broad band extending from about 4000 to 5000 Å. with a maximum at 4600 Å.[22b]

Photolysis of Azomethane in Oxygen Enriched with O^{18}.—In order to aid in the identification of the prominent product bands at 11.10 and 10.22 μ, the photooxidation of azomethane was carried out in an oxygen matrix enriched with O^{18}. Mass spectrometric analysis of the oxygen showed the O^{16} to O^{18} ratio to be 2.7. The prominent new bands in the 10–12-μ region are listed in Table IV. A second experiment, shown in Fig. 2, was carried out using oxygen recovered from the experiment of Table IV. The O^{16} to O^{18} ratio was checked before this experiment and found to be 2.9. The new bands at 11.32 and 10.45 μ so clearly evident in Fig. 2 prove that the species responsible for the 11.10 and 10.22-μ bands contain oxygen. The average ratio of the optical densities of the 11.10 to the 11.32-μ peak in these two runs is 3.0. The average ratio of the 10.22 to the 10.45 μ peak is 2.8.

The band at 9.80 μ shown in Fig. 2 is due to $O^{16}O^{16}O^{18}$. This isotope shift of 15 cm.$^{-1}$ is in good agreement with the shift predicted by Pierce on the basis of the potential constants of ozone determined from microwave data.[23] The peak due to $O^{16}O^{18}O^{16}$, predicted to be

(23) L. Pierce, *J. Chem. Phys.*, **24**, 131 (1956).

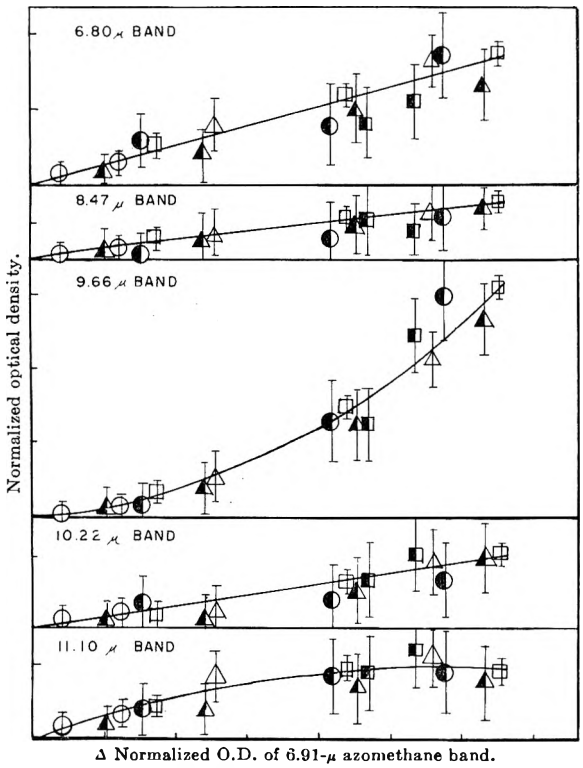

Fig. 3.—Increase in normalized optical density of the product bands as a function of the decrease in the normalized optical density of the 6.91-μ azomethane band: ○, expt. 1; △, expt. 3; □, expt. 4; ◐, expt. 5; ▲, expt. 6; ■, expt. 7. Normalized optical densities are obtained by dividing the optical density of the band by the optical density of the 6.91-μ band before photolysis [O.D. (6.91 μ): expt. 1, 0.50; expt. 3, 0.23; expt. 4, 0.47; expt. 5, 0.09; expt. 6, 0.22; expt. 7, 0.20].

TABLE IV

OPTICAL DENSITIES[a] OF INFRARED BANDS PRODUCED BY PHOTOLYSIS OF $CH_3N_2CH_3$ IN SOLID OXYGEN ENRICHED WITH O^{18}

Wavelength, μ	Frequency, cm.$^{-1}$	Photolysis time: 0 min.	42 min.	Warm-up
10.22	979	..	0.0025	0.0090
10.45	957	..	...	.0030
11.10	901	..	.0075	...
11.32	884	..	.0025	...

[a] Experiment 8, $M/R = 200$, $T = 6°$K., 4× scale expansion, $O^{16}/O^{18} = 2.7$.

at 10.00 μ, is obscured by an azomethane peak at 9.92 μ.

The 8.47-μ band showed no isotope shift. The evidence regarding the 9.0-μ band is unclear due to possible impurity bands.

Discussion

Mechanism of Formation of Ethane, Formaldehyde, and Ozone. (a) **Ethane.**—Kutschke, *et al.*, have demonstrated that the only primary process in the gas phase photolysis of azomethane in the presence of oxygen is[5,11]

$$CH_3N_2CH_3 + h\nu \longrightarrow 2CH_3 + N_2 \qquad (I)$$

with a quantum yield near unity. In the absence of evidence to the contrary, it will be assumed that primary process (1) also takes place in solid oxygen. Since two methyl radicals are inevitably formed together in a single matrix cage according to primary process (1), a high yield of ethane would be expected to be produced by the reaction

$$CH_3 + CH_3 \longrightarrow C_2H_6 \qquad (2)$$

taking place within the matrix cage.[24] Equations 1 and 2 predict that there should be a linear relation between the amount of ethane produced and the azomethane decomposed. Figure 3 shows that this prediction is confirmed. The large amount of ethane produced, about 50% of the azomethane decomposed, is also entirely consistent with the occurrence of reaction 2 within a matrix cage.

In analogy with the gas phase results for the photooxidation of methyl iodide, the primary process in solid oxygen will be assumed to be[25]

$$CH_3I + h\nu \longrightarrow CH_3 + I \qquad (II)$$

The absence of ethane shows that reaction 2 is indeed a cage reaction.

(b) **Ozone.**—Calvert and his co-workers have obtained indirect evidence by a number of independent methods that a small steady state concentration of ozone is built up during the gas phase photooxidation of azomethane.[26] Hanst and Calvert have favored reaction 3 to explain ozone formation.[8] More recent gas

$$CH_3O_2^* + O_2 \longrightarrow CH_3O + O_3 \qquad (3)$$

phase work has made reaction 3 seem very unlikely.[26] If reaction 3 were of importance in the formation of ozone in solid oxygen, a linear relation would be expected between the growth of the ozone bands and the decrease in the azomethane bands because of the very short lifetime of the excited methylperoxyl radical. It can be seen from Fig. 3 that the greater the extent of azomethane decomposition, the faster is the growth of ozone. This shows the unimportance of reaction 3 in solid oxygen and suggests that ozone is produced by the photolysis of some azomethane photooxidation product such as, for example, trapped methylperoxyl radicals.

$$CH_3O_2 + h\nu \longrightarrow CH_3O + O \qquad (III)$$

$$O + O_2 \longrightarrow O_3 \qquad (4)$$

(c) **Formaldehyde.**—Many reactions have been postulated to account for the presence of formaldehyde as a photooxidation product in the gas phase.[2-15]

$$CH_3O_2^* \longrightarrow H_2CO + OH \qquad (5)$$

$$CH_3O_2^* + M \longrightarrow CH_3O_2 + M \qquad (6)$$

$$2CH_3O_2 \longrightarrow H_2CO + CH_3OH + O_2 \qquad (7)$$

$$2CH_3O_2 \longrightarrow CH_3OOH + CH_2O_2 \text{ (or } CH_2O + O) \qquad (8)$$

$$2CH_3O_2 \longrightarrow 2H_2CO + H_2O + O_2 \qquad (9)$$

$$2CH_3O_2 \longrightarrow 2CH_3O + O_2 \qquad (10)$$

$$2CH_3O \longrightarrow H_2CO + CH_3OH \qquad (11)$$

(24) Rebbert and Ausloos [R. E. Rebbert and P. Ausloos, *J. Phys. Chem.*, **66**, 2253 (1962)] have found evidence for the formation of small amounts of ethane by a molecular elimination from azomethane in the gas phase photolysis. Toby and Weiss [S. Toby and B. H. Weiss, *ibid.*, **66**, 2681 (1962)] have postulated an additional ethane forming step at temperatures above 50° and pressures above 50 mm. This reaction, which takes place to a very small extent, is probably $2CH_3N_2 \rightarrow C_2H_6 + 2N_2$.

(25) R. B. Martin and W. A. Noyes, Jr., *J. Am. Chem. Soc.*, **75**, 4183 (1953).

(26) See ref. 15 for summary of this evidence and references to earlier work.

$$CH_3O_2 + CH_3O \longrightarrow CH_3OOH + H_2CO \quad (12)$$

$$CH_3O_2 + CH_3 \longrightarrow CH_4 + CH_2O_2 \text{ (or } CH_2O + O) \quad (13)$$

$$CH_3 + CH_3O \longrightarrow CH_4 + H_2CO \quad (14)$$

Reactions 7 and 10 followed by 11 predict the formation of as much methanol as formaldehyde. The failure to find even one-fourth as much methanol as formaldehyde rules them out as important reactions in solid oxygen. The failure to detect methyl hydroperoxide as a product makes reactions 8 and 12 unlikely. Although methane was not found as a product, the weakness of its bands might have enabled it to escape detection. Hence reactions 5 and 6 followed by 9, 13, or 14 remain as possibilities.

Formaldehyde might also be produced by the photolysis of some trapped azomethane photooxidation product. This possibility cannot be tested by plotting the increase in the formaldehyde band at 5.76 μ *vs.* the decrease in azomethane bands because of overlapping by the 5.82-μ band. Plots of the 6.66-μ formaldehyde band do show curvature, but the experimental error is so large as to render these plots untrustworthy. In view of the large number of unidentified bands present, particularly the band in the carbonyl region at 5.82 μ, extensive speculation concerning the mechanism of formaldehyde formation is unjustified.

The Unidentified Bands. (a) **The 5.82-μ Band.**—The growth curve of this band cannot be determined with certainty due to overlapping by the 5.76-μ band.

(b) **The 8.47-μ Band.**—The linear growth of this band is shown in Fig. 3. It seems to be a band of a product formed directly from azomethane or by rapid reactions between azomethane photooxidation products.

(c) **The 10.22 and 11.10-μ Bands.**—The growth curves of the 10.22 and 11.10-μ bands are shown in Fig. 3. Although the experimental error is large, the growth curve of the 11.10-μ band is probably concave downward. This implies that the species responsible for this band is destroyed as photolysis proceeds. The marked decrease on warm-up of the 11.10-μ band is behavior characteristic of a very reactive intermediate. The 10.22-μ band, on the other hand, shows linear growth during photolysis but nearly doubles on warm-up. The 11.10-μ species may react on warm-up to produce the 10.22-μ species. It is important, therefore, to consider what can be deduced about the identity of these species from the spectroscopic evidence.

Other than data on their wave lengths and behavior on warm-up, the spectroscopic evidence consists of the intensity and wave length of the bands produced when an O^{18}-enriched matrix is used. The isotope shift shown by both the 11.10 and 10.22-μ bands proves these bands to be due to vibrations involving oxygen atoms. A fundamental stretching vibration about the O–O bond absorbs in the 11–12-μ region.[14,27,28] That neither the 11.10 nor the 10.22-μ band is due to an O–O vibration can be deduced from the number and intensity of the isotope bands. Compounds containing the O–O linkage would be isotopically substituted in the four different ways listed in Table V Assuming that substitution of O^{16} by O^{18} would not change the intensity of the band, four bands would be produced by these four species with relative intensities in the same ratio as their relative abundances, also listed in Table V. Only two bands are observed. If the R and R′ groups are identical or do not affect the position of the O–O band, only three bands would be produced. The $RO^{18}O^{18}R'$ species band might not be observed since its relative intensity is so small. The ratio of the two bands predicted to be observed would be 1.35. However, the actual ratio is 3.0 for the 11.10-μ band and 2.8 for the 10.22-μ band. Hence, it is evident that an O–O vibration can be responsible for neither the 11.10 nor the 10.22-μ band.

TABLE V

RELATIVE ABUNDANCES OF ISOTOPICALLY SUBSTITUTED PEROXIDE COMPOUNDS[a]

Species	Relative abundance
$RO^{16}O^{16}R'$	7.3
$RO^{16}O^{18}R'$	2.7
$RO^{18}O^{16}R'$	2.7
$RO^{18}O^{18}R'$	1.0

[a] $O^{16}/O^{18} = 2.7$.

Since the behavior of the 11.10-μ species on warm-up is characteristic of a free radical, perhaps this band should be assigned to the methoxyl radical. The 17-cm.$^{-1}$ isotope shift and the observation of only two bands with an intensity ratio of three to one are consistent with this assignment.[29,30] However, the methoxyl radical would be expected to absorb at about the same place as methanol, 9.69 μ. In order to have a band at 11.10-μ, the methoxyl radical, treated as a diatomic molecule, would have to have a C–O stretching constant of 3.7×10^5 dynes cm.$^{-1}$. This is a large decrease over the C–O stretching constant, 4.86×10^5 dynes cm.$^{-1}$, of methanol, also treated as a diatomic molecule. The stretching force constant for the O–H bond in the hydroxyl radical, 7.12×10^5 dynes cm.$^{-1}$, differs little from the value for water, 7.66×10^5 dynes cm.$^{-1}$.[31] The C–O bond energy computed from the thermochemical data of Gray and Williams is 89 ± 3 kcal. mole^{-1} for the methoxyl radical and 77 kcal. mole^{-1} for methanol.[32] The O–H bond energy is 101.2 kcal. mole^{-1} for the hydroxyl radical and 110.6 kcal. mole^{-1} for water.[32] Hence, the C–O stretching force constant might actually be somewhat larger for the methoxyl radical than for methanol.

Style and Ward observed that methyl nitrite, when illuminated with a hydrogen arc through a thin quartz window, emitted a number of narrow bands between 3200–4200 Å.[33] These bands, assigned to the methoxyl radical, fall into three progressions with ω = approximately 1010 cm.$^{-1}$. If this assignment is correct, the methoxyl radical is eliminated as a possible cause of the 11.10-μ (900 cm.$^{-1}$) band.

The methylperoxyl radical might be responsible for the 11.10-μ band. The same argument used before to

(27) G. J. Minkoff, *Proc. Roy. Soc.* (London), **A224**, 176 (1954).

(28) P. A. Giguere, *Can. J. Chem.*, **30**, 821 (1952).

(29) If CH_3O is treated as a diatomic molecule, a shift of 25 cm.$^{-1}$ is predicted when O^{16} is replaced by O^{18}.

(30) The ratio of the intensity of the unshifted to the shifted methoxyl radical band should be the same as the ratio of O^{16} to O^{18}, *i.e.*, 2.7.

(31) G. Herzberg, "Spectra of Diatomic Molecules," D. Van Nostrand Co., New York, N. Y., 1950.

(32) P. Gray and A. Williams, *Chem. Rev.*, **59**, 239 (1959).

(33) D. W. G. Style and J. C. Ward, *Trans. Faraday Soc.*, **49**, 999 (1953).

rule out O–O stretching vibrations as possible causes of the 11.10-μ band also applies to the methylperoxyl radical. If the methylperoxyl radical possesses a characteristic C–O stretching band at 11.10 μ and if the shift in frequency between the C–O bands of the $CH_3O^{16}O^{16}$ and $CH_3O^{16}O^{18}$ species and also between the C–O bands of the $CH_3O^{18}O^{16}$ and $CH_3O^{18}O^{18}$ species is less than the resolving power of the spectrophotometer, only two bands would be produced with an intensity ratio of 2.7, in agreement with the observed ratio of 3.0. Since similar masses and force constants are involved in the C–O and O–O vibrations of the methylperoxyl radical, at first glance, extensive coupling between these vibrations would be expected to take place. However, it has been shown that for a chain of nearly equally heavy mass points connected by springs, there will be no transfer of vibrational energy from one bond to the next if the angle between the bonds is 90°.[34] There is every reason to believe the angle between the C–O and O–O bonds in the methylperoxyl radical to be close to 90°. Walsh's bond angle correlation diagrams predict that the methylperoxyl radical will have about the same bond angle as hydrogen peroxide and dimethyl peroxide.[35] Hydrogen peroxide has a HOO angle of 102 ± 2° and dimethyl peroxide has a COO angle of 105 ± 3°.[36,37]

The results of a valence force calculation of the interaction between the C–O and O–O vibrations and the isotope effect on the position of the C–O band are presented in Table VI. The force constants, bond lengths, and bond angles used in this calculation are also listed in Table VI. The COO bending constant is the value Kohlrausch obtained for dimethyl ether treated as a triatomic molecule.[38] Since the methylperoxyl radical is expected to have a three electron bond in addition to a single bond, the O–O stretching force constant was chosen to lie between the constants for hydrogen peroxide, 3.84×10^5 dynes cm.$^{-1}$, and ozone, 5.7×10^5 dynes cm.$^{-1}$.[23,36] Badger's rule was used to calculate the O–O bond distance from this force constant.[39] The C–O stretching force constant was chosen to give a band in the 11-μ region. The C–O bond distance was read off the bond length *vs.* force constant chart given by Ewing, Thompson, and Pimentel for this force constant.[40] The results in Table VI show clearly that the methylperoxyl radical would have a characteristic C–O stretching vibration. Moreover, the splitting of 0.01 μ between the C–O bands for the $CH_3O^{16}O^{16}$ and $CH_3O^{16}O^{18}$ species, and between the $CH_3O^{18}O^{16}$ and $CH_3O^{18}O^{18}$ species, is much less than the calculated spectral resolution of 0.04 μ. Therefore, the methylperoxyl radical could give two bands with an intensity ratio of about 3. On warm-up, methylperoxyl radicals might dimerize to form $CH_3OOOOCH_3$. Since $CH_3OOOOCH_3$ would also be expected to have a C–O bond angle close to 100°, the band at 10.22 μ might be due to characteristic C–O vibrations. While $CH_3COOOOCH_3$ would not be stable at room temperature, it might exist at 35°K.

TABLE VI

VALENCE FORCE TREATMENT ON CH_3O_2 REGARDED AS A NONLINEAR TRIATOMIC MOLECULE[a]

Species	O–O stretching, cm.$^{-1}$	O–O stretching, μ	C–O stretching, cm.$^{-1}$	C–O stretching, μ	COO bending cm.$^{-1}$	COO bending μ
$CH_3O^{16}O^{16}$	1043.16	9.587	907.6	11.018	317.4	31.51
$CH_3O^{16}O^{18}$	1016.1	9.842	906.4	11.032	309.9	31.33
$CH_3O^{18}O^{16}$	1012.4	9.877	882.0	11.338	314.5	31.80
$CH_3O^{18}O^{18}$	984.4	10.158	880.9	11.352	307.1	32.56

[a] $k_{CO} = 3.7 \times 10^5$ dynes cm.$^{-1}$, $k_{OO} = 5.0 \times 10^5$ dynes cm.$^{-1}$, O–O bond distance = 1.40 Å., $\delta_{COO}/r^\circ_{CO}r^\circ_{OO} = 0.30 \times 10^5$ dynes cm.$^{-1}$, C–O bond distance = 1.44 Å., COO = 100°.

There are a number of objections to assigning the 11.10-μ band to the methylperoxyl radical, nevertheless. Just as was the case for the methoxyl radical, a C–O force constant of 3.7×10^5 dynes cm.$^{-1}$ is considerably smaller than would have been expected for the methylperoxyl radical. No spectroscopic observations have been made on the HO_2 radical from which, by analogy, an estimate of the C–O force constant could be made. From thermochemical data, the heat of atomization of CH_3O_2 is 438 ± 5 kcal. mole^{-1}.[15,32] Assuming that the C–H bond energy retains its normal value of 98.8 kcal. mole^{-1}, the sum of the C–O and O–O bond energies must be 142 ± 5 kcal. mole^{-1}. Unfortunately, there is no method of independently determining the O–O and C–O bond energies. If the O–O bond energy is assumed to be equal to that of a bond and one-half, 34 + 17 = 51 kcal. mole^{-1}, the C–O bond energy is 91 ± 5 kcal. mole^{-1}, which is about equal to a normal C–O bond energy of 84 kcal. mole^{-1}. While this estimate for the O–O bond energy may be somewhat too small, it is hard to believe that the O–O bond energy could be high enough to lower the C–O bond energy significantly below 84 kcal. mole^{-1}.

A second objection to assigning the 11.10-μ band to the methylperoxyl radical is the absence of this band from the spectra of the methyl iodide photooxidation products. If methylperoxyl radicals are produced and trapped in the photooxidation of azomethane, they should also be found among the methyl iodide products. A possible explanation for this absence may lie in the shorter wave length of the light used to photolyze methyl iodide. The filter used during the methyl iodide photolyses transmitted down to 2250 Å., whereas no light shorter than 3100 Å. was used to photolyze azomethane. More effective photolysis by light below 3100 Å. might keep the concentration of the 11.10-μ species too low to detect.[41]

A third objection is failure to detect visible or ultraviolet bands after photooxidation of azomethane. According to the orbital diagram for HAB molecules given by Walsh, HO_2 should have low-lying optical transitions.[35] Low-lying transitions would, therefore, be expected for CH_3O_2. Walsh's diagrams also predict HNO to have transitions very similar to those of HO_2. Dalby has found HNO to absorb from 5900–

(34) G. Herzberg, "Infrared and Raman Spectra of Polyatomic Molecules," D. Van Nostrand Co., New York, N. Y., 1945.

(35) A. D. Walsh, *J. Chem. Soc.*, 2288 (1953).

(36) O. Bain and P. A. Giguere, *Can. J. Chem.*, **33**, 527 (1955).

(37) M. T. Rogers and T. W. Campbell, *J. Am. Chem. Soc.*, **74**, 4742 (1952).

(38) K. W. F. Kohlrausch, "Ramanspektren, Hand-und Jahrbuch der Chemischen Physik," Vol. 9, A. Euken and K. L. Wolf, Ed., Becker and Erler, Leipzig, 1943; Edwards Bros., Ann Arbor, Mich., 1945.

(39) R. M. Bader, *J. Chem. Phys.*, **2**, 128 (1934).

(40) G. E. Ewing, W. E. Thompson, and G. C. Pimentel, *ibid.*, **32**, 927 (1960).

(41) A referee has suggested the following alternative explanation for the absence of the 11.10-μ band. There is considerable evidence that methyl radicals produced by the photolysis of CH_3I have excess energy (see especially ref. 25, but also 7. A "hot" methyl radical, particularly if some of the excess energy were vibrational, might not stop at the methyl peroxyl stage on reacting with oxygen, *i.e.*, $CH_3^* + O_2 \rightarrow CH_3O_2^{**} \rightarrow CH_2O + OH$.

7600 Å. with the strongest band being the zero–zero band at 7590 Å.[42] The strongest CH_3O_2 band might absorb at wave lengths longer than 6500 Å., and, therefore, not be detected. In addition, broad, weak bands could easily be missed. For example, the 3570–2750 Å. formaldehyde bands were not observed even though, from the infrared evidence, formaldehyde must have been present in fairly large concentration. All of these objections make it seem unlikely that the 11.10-μ species is the methylperoxyl radical, but they do not conclusively rule it out.

It is probably fruitless to speculate further concerning the identity of the 11.10-μ species. Additional evidence is needed. Use of C^{13} would determine if the 11.10-μ band is indeed due to a C–O vibration. A grating instrument would have sufficient resolution to see if four bands are produced in an O^{18}-enriched matrix. In addition, the low-lying optical transition predicted for CH_3O_2 should be looked for more thoroughly.

(42) F. W. Dalby, *Can. J. Phys.*, **36**, 1336 (1958).

Conclusions

The large ethane yield shows the importance of the cage effect even in solid oxygen. Ozone is formed by the photolysis of some azomethane photooxidation product. The light used to photolyze azomethane may decompose the 11.10-μ species. The isotope effect shown by both the 10.22 and 11.10-μ species proves that they contain oxygen but also that neither band is due to an O–O stretching vibration. It seems unlikely that the 11.10-μ band can be assigned to the methoxyl or methylperoxyl radical. Further experiments are needed before positive assignment can be made. While this work illustrates the difficulties inherent in the identification of a product based on one infrared band, it also shows the potentialities of the matrix isolation technique for shedding new light on old problems.

Acknowledgments.—The author is grateful to Dr. L. C. Roess for his interest and encouragement, to Dr. S. A. Francis and Professor R. M. Hammaker for many helpful discussions, and to Mr. F. J. Lopez for his help with the experimental work.

KINETICS OF THE REACTION BETWEEN ANTIMONY(III) AND FERRICYANIDE IN ALKALINE MEDIA

BY LOUIS MEITES AND RICHARD H. SCHLOSSEL[1]

Department of Chemistry of the Polytechnic Institute of Brooklyn, Brooklyn, New York

Received May 18, 1963

The rates of oxidation of antimony(III) by ferricyanide in sodium hydroxide media have been measured by following the polarographic diffusion current of ferricyanide in solutions containing excess antimony(III) and also, with the aid of a simple device that causes the potential applied by a polarograph to alternate between two preset values, by following the diffusion current of antimony(III) in solutions containing excess ferricyanide. Over wide ranges of the concentrations of the reactants, the data can be described by rate laws deduced from a mechanism involving the reactions of the species $(HO)_2Sb–O–Sb(OH)_2$ and $Sb(OH)_6^{-3}$ with ferricyanide and the existence of the former as the predominating species of antimony(III) under the conditions employed.

Introduction

In developing a new technique of amperometric titration intended to permit the location of the end point when the reaction is slow or incomplete, the reaction between antimony(III) and ferricyanide was selected for study because of the favorable polarographic characteristics of the reactants and products. The results of a detailed investigation of its kinetics are described here.

Experimental

Ferrocyanide ion and antimony(V) are polarographically inert in strongly alkaline solutions; ferricyanide ion gives a cathodic wave rising from zero applied e.m.f.; and antimony(III) gives both an anodic wave ($E_{1/2}$ = *ca.* −0.40 v. *vs.* s.c.e. in 0.25 *M* hydroxide) reflecting its oxidation to the +5 state and a cathodic wave ($E_{1/2}$ = *ca.* −1.1 v. *vs.* s.c.e. in 0.25 *M* hydroxide) reflecting its reduction to the elemental state.[2–4] From these data it is apparent that, in a reaction mixture containing both ferricyanide and antimony(III), the diffusion current of ferricyanide can readily be measured at an appropriate potential in the vicinity of −0.7 v. *vs.* s.c.e., whereas the anodic diffusion current of the antimony cannot be measured directly because it occurs only at potentials where ferricyanide is reduced.

The rate of the reaction in the presence of excess antimony(III) was followed by recording a current–time curve in the conventional manner at −0.66 v. *vs.* a silver–silver chloride–saturated potassium chloride electrode.[5] Appropriate volumes of water and standard solutions of sodium hydroxide, potassium ferricyanide, and antimony(III) chloride (in a hydrochloric acid solution whose acidity was taken into account in computing the hydroxyl ion concentration of the reaction mixture) were mixed in the solution compartment of a modified H-cell[6] that contained a little chloroform to prevent reduction of ferricyanide by mercury accumulated from the dropping electrode. Due precautions were taken to avoid air-oxidation of the antimony(III), whose half-wave potential shows it to be a powerful reducing agent under these conditions. Reaction times were obtained from the recorder chart, whose rate of motion had been accurately measured. The sensitivity of the polarograph was readjusted periodically so that the pen deflection never fell below 50% of full scale. The recording was continued until no further decrease of current could be detected, and the residual current was taken to be the current that flowed after the reaction was complete. Data obtained with the same capillary on the diffusion currents of ferricyanide at various concentrations in antimony-free 0.25 *F* sodium hydroxide were used in computing ferricyanide concentrations from the recorded diffusion currents.

To permit the measurement of the diffusion current of antimony(III) in the presence of a large excess of ferricyanide, a

(1) This paper is based on a thesis submitted by Richard H. Schlossel to the faculty of the Polytechnic Institute of Brooklyn in partial fulfillment of the requirements for the B.S. in Chemistry degree, June, 1962.

(2) J. J. Lingane, *Ind. Eng. Chem., Anal. Ed.*, **15**, 583 (1943).

(3) I. M. Kolthoff and R. L. Probst, *Anal. Chem.*, **21**, 753 (1949).

(4) S. Vivarelli, *Anal. Chim. Acta*, **6**, 379 (1952).

(5) L. Meites and S. A. Moros, *Anal. Chem.*, **31**, 23 (1959).

(6) L. Meites and T. Meites, *ibid.*, **23**, 1194 (1951).

synchronous motor-driven cam was so arranged as alternately to actuate and release a microswitch at intervals of approximately 30 sec. The microswitch was connected to the initial-potential circuit of the polarograph. When it was open, a potential of −0.23 v. *vs.* the silver–silver chloride electrode was applied to the dropping electrode by the span-potential circuit of the polarograph; when it was closed, a potential of −0.66 v. was applied by the span- and initial-potential circuits together. During the first interval, the sum of the diffusion currents of antimony(III) and ferricyanide was presented to the recorder; during the second, only that of ferricyanide was recorded. By employing suitable compensation and damping, the difference between these two currents could be made to occupy a large fraction of the width of the recorder chart. This difference is equal to the diffusion current of antimony after correction for the difference between the residual currents at the two potentials employed, which was easily measured when the reaction was complete. In this simple fashion useful data were obtained even when the diffusion current of antimony(III) was only 0.1–0.2% of that of ferricyanide. This technique might be called "low frequency (or large-amplitude) square-wave polarography."

All measurements were made at 25.00 ± 0.02°. Calibrated volumetric apparatus was employed throughout.

The initial concentrations of antimony(III) and ferricyanide were varied from about 0.02 to 10 m*M*; the diffusion-current data would have been afflicted by increasing uncertainties had smaller concentrations been used, while precipitation always occurred during the reaction when higher concentrations were used. One reactant was always present in at least a 10-fold, and usually a 20- to 40-fold, excess, so that its concentration could be taken as constant. The hydroxyl-ion concentration was varied from 0.14 to 0.46 *M*.

Data and Discussion

For every experiment a first-order plot of the concentration of the reactant followed was concave downwards, indicating that the apparent order with respect to that reactant was smaller than 1. As the concentrations of the reactants were varied, the order with respect to ferricyanide appeared to vary from nearly zero to nearly 1, while the order with respect to antimony(III) appeared to vary from about 1/2 to 1.

A mechanism that serves to describe all of the experimental observations involves the assumption that the predominating species of antimony(III) under these conditions is binuclear. No information bearing on this assumption is available in the literature; for whatever the analogy may be worth, however, bismuth(III) has been reported[7−12] to exist predominantly in the form of a polynuclear hydroxo complex in alkaline solutions. The binuclear hydroxo complex is assumed to be in equilibrium with a monomeric species[13]

$$Sb_2^{III} = 2Sb^{III};\ K' = \frac{[Sb^{III}]^2}{[Sb_2^{III}]} \qquad (1)$$

and also to be capable of reacting with ferricyanide. In this equation and hereafter, the symbols "Feic" and "Feoc" are used to denote ferri- and ferrocyanide ions, respectively.

$$Sb_2^{III} + Feic \xrightarrow{k_2'} Sb^{IV} + Sb^{III} + Feoc \qquad (2)$$

To account for the fact that the apparent order with respect to ferricyanide is always less than 1 and may approach 0, one must assume a further transition

$$Sb^{III} \xrightarrow{k_3'} (Sb^{III})' \qquad (3)$$

yielding a complex that can react with ferricyanide[14]

$$(Sb^{III})' + Feic \underset{(k_{-4})}{\overset{k_4}{\rightleftharpoons}} Sb^{IV} + Feoc \qquad (4)$$

while, finally

$$Sb^{IV} + Feic \xrightarrow{k_5} Sb^{V} + Feoc \qquad (5)$$

This yields the rate law

$$\frac{d[Feic]}{dt} = -2k_2'[Sb_2^{III}]\left([Feic] + \frac{k_3'[Sb^{III}]}{k_2'[Sb_2^{III}]}\right) \qquad (6)$$

whence

$$\ln\left([Feic] + \frac{k_3'[Sb^{III}]}{k_2'[Sb_2^{III}]}\right) = 2k_2'[Sb_2^{III}]t + c \qquad (7)$$

If it is assumed that essentially all of the antimony(III) in the solution is present in the binuclear form, then $[Sb_2^{III}] = C_3/2$ and $[Sb^{III}] = \sqrt{K'C_3/2}$, where C_3 is the number of moles per liter of antimony(III), and eq. 7 may conveniently be written

$$\ln([Feic] + a) = -bt + c \qquad (8)$$

where c is the constant of integration and

$$b = k_2'C_3 \qquad (9)$$

$$ab = k_3'\sqrt{2K'C_3} \qquad (10)$$

For solutions containing a constant excess of ferricyanide, however, it is more convenient to write

$$\frac{dC_3}{dt} = -\frac{k_2'[Feic]}{2}\left(C_3 + \frac{\sqrt{2K'C_3}\,k_3'}{k_2'[Feic]}\right) \qquad (11)$$

whence, as above

$$\ln(C_3^{1/2} + d) = -et + f \qquad (12)$$

where f is the constant of integration and

$$e = \frac{1}{4}k_2'[Feic] \qquad (13)$$

$$de = \frac{k_3'\sqrt{K'}}{2\sqrt{2}} \qquad (14)$$

Typical plots of the form of eq. 8 and 12 are shown in Fig. 1 to illustrate the conformity of the data to these rate equations. In every case the appropriate choice of numerical parameters served to reproduce the experimental values, within a reasonable estimate of the uncertainty of measurement, until the reaction was at least 90% complete. The experimental conditions

(7) F. Granér and L. G. Sillén, *Acta Chem. Scand.*, **1**, 631 (1947).
(8) J. Faucherre, *Bull. soc. chim. France*, 253 (1954).
(9) F. Granér, Å. Olin, and L. G. Sillén, *Acta Chem. Scand.*, **10**, 476 (1956).
(10) R. W. Holmberg, K. A. Kraus, and J. S. Johnson, *J. Am. Chem. Soc.*, **78**, 5506 (1956).
(11) Å. Olin, *Acta Chem. Scand.*, **11**, 1445 (1957).
(12) R. S. Tobias, *J. Am. Chem. Soc.*, **82**, 1070 (1960).
(13) Primes accompanying rate and equilibrium "constants" here signify that they actually vary with hydroxyl ion concentration.

(14) The essential assumption is that the product of the reaction described by eq. 1 cannot react directly with ferricyanide. In eq. 2 we have indicated that the antimony(III) species formed when the dimer is oxidized is identical with the one formed when it dissociates. With equal justice to the rate data, however, one could write

$$Sb_2^{III} + Feic \xrightarrow{k_2^{*\prime}} Sb^{IV} + (Sb^{III})' + Feoc \qquad (2^*)$$

for this yields the same rate law with $k_2^{*\prime} = k_2'/2$. This possibility is discussed further in footnote 15.

TABLE I

KINETIC PARAMETERS FOR THE REACTION BETWEEN ANTIMONY(III) AND FERRICYANIDE IN SODIUM HYDROXIDE SOLUTIONS

$10^4 C_3^{0a}$	10^4[Feic]^{0a}	[NaOH]^a	$k_2'^{b,c}$	$10^7 k_3'\sqrt{K'}^{b,c}$	k_2'/[OH$^-$]	$10^5 k_3'\sqrt{K}$/[OH$^-$]^3
6.86	0.448	0.243	0.175	3.58	0.72	2.5
10.72	.522	.275	.380	6.10	1.38	2.9
15.87	.774	.253	.290	6.80	1.15	4.2
19.85	1.206	.235	.217	5.58	0.92	4.3
51.6	5.10	.235	.189	4.31	.80	3.3
104.3	5.10	.214	.153	7.40	.72	(7.6)
0.229	9.55	.239	.195	1.49	.82	(1.1)
0.961	18.99	.229	.130	5.91	.57	4.9
1.019	41.97	.243	.126	4.24	.52	3.0
44.8	3.53	.461	.369	36.8	.80	3.8
48.5	2.52	.351	.348	14.25	.99	3.3
47.5	2.46	.145	.142	0.82	.98	2.7
44.9	1.97	.131^d	.140	0.83	1.07	3.7
					Mean: 0.87 ± 0.19	3.5 ± 0.6

[a] The first three columns give the initial concentrations, in moles/l., of antimony(III), ferricyanide, and sodium hydroxide in the reaction mixture. [b] When antimony(III) was initially present in excess, values of b and ab were obtained from a plot according to eq. 8; then the value of k_2' in the fourth column is equal to b/C_3 and the value of $k_3'\sqrt{K'}$ in the fifth column is equal to $ab/2C_3$. [c] When ferricyanide was initially present in excess, values of e and de were obtained from a plot according to eq. 12; then the value of k_2' in the fourth column is equal to $4e$/[Feic] and the value of $k_3'\sqrt{K'}$ in the fifth column is equal to $2\sqrt{2}\,de$. [d] Sodium perchlorate was added to give an ionic strength of 0.51.

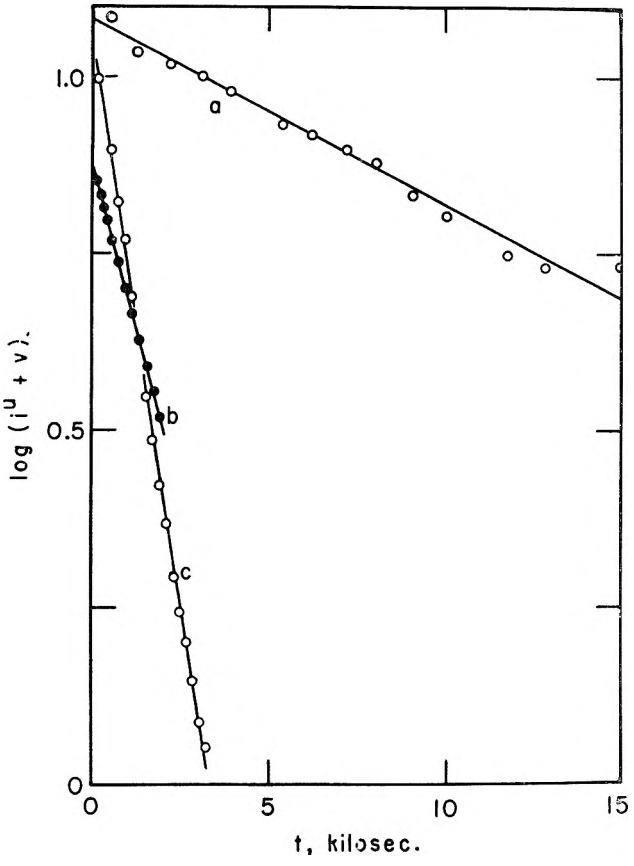

Fig. 1.—Kinetic plots, according to eq. 8 and 12, of the diffusion-current data obtained under various conditions. The quantity plotted on the vertical axis and the initial concentrations of the reactants are: (a) log ($\sqrt{i_{d_{Sb}}}$ + 0.30), C_3^0 = 0.0961 mM, [Feic]^0 = 1.900 mM, [OH$^-$] = 0.229 M; (b) log ($i_{d_{Feic}}$ + 0.294), C_3^0 = 1.985 mM, [Feic]^0 = 0.1206 mM, [OH$^-$] = 0.235 M; (c) log ($i_{d_{Feic}}$ + 0.043), C_3^0 = 4.746 mM, [Feic]^0 = 0.2463 mM, [OH$^-$] = 0.143 M.

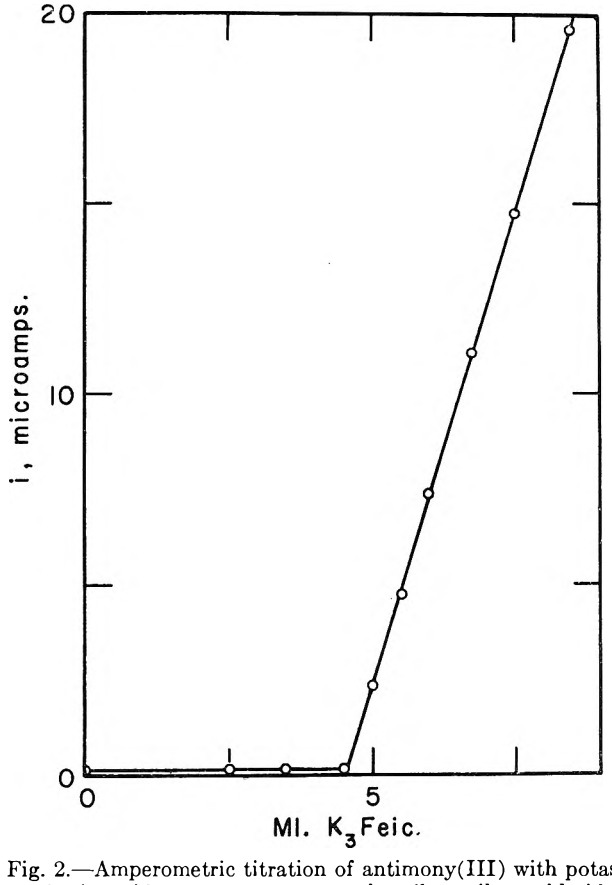

Fig. 2.—Amperometric titration of antimony(III) with potassium ferricyanide at −0.66 v. *vs.* the silver–silver chloride–saturated potassium chloride electrode. Fifty-five ml. of an air-free solution containing 3 M hydroxide was titrated with 0.1040 F reagent from a 10-ml. microburet, with deaeration after each addition; present: 2.527 mmoles of antimony(III); found: 2.512.

are summarized, and the values of the parameters obtained from plots like those in Fig. 1 are given in Table I.

From the last two columns of this table it appears that k_2' is proportional to the first power, while $k_3'\sqrt{K'}$ is proportional to the cube of the hydroxyl ion concentration. Rewriting eq. 1 and 3 to include hydroxyl ions, one has

$$Sb_2(OH)_m + nOH^- = 2Sb(OH)_{(m+n)/2};$$

$$K = \frac{[Sb(OH)_{(m+n)/2}]^2}{[Sb_2(OH)_m][OH^-]^n} \quad (15)$$

$$Sb(OH)_{(m+n)/2} + pOH^- \xrightarrow{k_3} Sb(OH)_{[p+(m+n)/2]} \quad (16)$$

Evidently

$$k_3'\sqrt{K'} = k_3K^{1/2}[OH^-]^{[p+(n/2)]} \qquad (17)$$

so that

$$p + \frac{n}{2} = 3 \qquad (18)$$

It would be difficult to believe that a cationic species of antimony(III) predominates in such strongly alkaline solutions, while no species of antimony(III) is known in which its coordination number exceeds 6. Accordingly, it appears necessary to assume $m \geq 6$ and $[p + (m + n)/2] \leq 6$, and eq. 18 then demands the equality in each case. Of course it is improbable on structural grounds that the binuclear complex should actually be $Sb_2(OH)_6$; it may therefore be assigned the kinetically identical oxo-bridged structure $(HO)_2Sb{-}O{-}Sb(OH)_2$. If the coordination number of the antimony is taken to be 6, this formula in turn would become $(HO)_2(H_2O)_3Sb{-}O{-}Sb(OH_2)_3(OH)_2$. Now eq. 10 requires either $n = p = 2$ or $n = 4$ and $p = 1$. The latter values would correspond not only to the breaking of the oxo bridge but also to the exchange of two hydroxyl ions for water molecules in the ligand field of each of the antimony atoms during the fast equilibrium described by eq. 15. On the ground so that complex a reaction would surely be slow, the alternative $n = p = 2$ seems preferable. Then, in summary, one has (omitting coordinated water for simplicity)

$$(HO)_2Sb{-}O{-}Sb(OH)_2 + 2OH^- + H_2O = 2Sb(OH)_4^-;$$

$$K = \frac{[Sb(OH)_4^-]^2}{[(HO)_2Sb{-}O{-}Sb(OH)_2][OH^-]^2}$$

$$(HO_2)Sb{-}O{-}Sb(OH)_2 + Feic + OH^- \xrightarrow{k_2} Sb^{IV} + Sb(OH)_4^- + Feoc;\ k_2 = 0.87 \pm 0.19^{15}$$

$$Sb(OH)_4^- + 2OH^- \xrightarrow{k_3} Sb(OH)_6^{-3};\quad k_3K^{1/2} = (3.5 \pm 0.6) \times 10^{-5}$$

$$Sb(OH)_6^{-3} + Feic \underset{(k_{-4})}{\overset{k_4}{\rightleftharpoons}} Sb^{IV} + Feoc$$

$$Sb^{IV} + Feic \xrightarrow{k_5} Sb^{V} + Feoc$$

The omission of the salt effect from the foregoing discussion is justified by the values shown in the last line of Table I, which indicate that the effects of ionic strength on k_2 and on $k_3K^{1/2}$ are small over the range of ionic strengths between about 0.15 and 0.5. It may be recalled that the Davies equation, as modified by Robinson and by Guggenheim and Bates, predicts only a negligible variation of an ionic activity coefficient over this same range.

The rapid increase of reaction rate with increasing concentration of hydroxyl ion should permit the amperometric titration of antimony(III) with ferricyanide to be performed conveniently and rapidly in sufficiently strongly alkaline solutions. A typical titration curve in 3 *F* sodium hydroxide is shown in Fig. 2.

(15) More explicitly, one might write

$$(HO)_2Sb{-}O{-}Sb(OH)_2 + Feic + OH^- + H_2O \longrightarrow Sb(OH)_3^+ + Sb(OH)_4^- + Feoc$$

If the antimony(III) species formed here is assumed to be identical with that formed in the following, rather than in the preceding, reaction [that is, $Sb(OH)_6^{-3}$ instead of $Sb(OH)_4^-$], the same rate law is obtained, as was mentioned in footnote 14, but then the antimony(IV) species formed here would have to have some such formula as $Sb(OH)^{+3}$. It is the implausibility of this formula that has dictated our preference for eq. 2 over eq. 2*.

THE SUBLIMATION OF INDIUM SESQUISULFIDE[1]

BY ALAN R. MILLER[2] AND ALAN W. SEARCY

Department of Mineral Technology and Lawrence Radiation Laboratory, Inorganic Materials Research Division, University of California, Berkeley, California

Received May 18, 1963

Sublimation pressures were measured for indium sesquisulfide between 950 and 1130°K. by the Knudsen effusion method, and the composition of the vapor was investigated with a mass spectrometer. The solid sublimes almost exclusively by the reaction $In_2S_3(s) = In_2S(g) + S_2(g)$ for which ΔH_{298} is calculated to be 147.4 ± 3 kcal. The equilibrium constant is given in the experimental range by the equation $-\log K = 30{,}660/T - 17.94$. The heat of formation of $In_2S(g)$ at 298°K. is calculated to be +14.6 ± 5 kcal. The free-surface sublimation rate is about 0.01 times the equilibrium rate at 1000°K.

Introduction

To engender better understanding of mechanisms of sublimation reactions and, in particular, of the conditions under which sublimation rates are low, equilibrium and kinetic studies for a variety of solids are needed. Suitable solids for study must sublime to yield vapors which have over-all compositions that are the same as those of the solid, so that kinetics of the surface steps are not obscured by the presence of condensed phase reaction products. The solids should preferably have sublimation pressures in ranges convenient for measurement at only moderately high temperatures and should be obtainable in pure forms. A material that will yield vapor molecules that have structural units distinctly different from those in the solid is de-

(1) Supported in part by a contract with the Office of Naval Research and the Advanced Research Projects Agency and in part by the U. S. Atomic Energy Commission.

(2) Aerojet-General Nucleonics, San Ramon, California.

sirable in order to increase the probability that the sublimation will show a high activation energy.

Indium sesquisulfide was chosen for investigation because it was expected to satisfy these requirements. Indium sesquisulfide can be precipitated from aqueous solutions[3] or prepared directly from the elements.[4] Its heat of formation was measured by Hahn and Burow with a bomb calorimeter.[5] They reported the standard heat of formation to be -101.6 kcal./mole.

Rooymans[6] has presented evidence that the material identified by Hahn and Klingler[3] as a low temperature α-phase is simply a poorly crystallized form of the material they had designated as a high temperature β-phase. Rooymans argued that an initial precipitate from acid solutions did not form crystals large enough to produce a sharp X-ray diffraction pattern until heated to 300°, and that "α-phase" lines of the Hahn and Klingler structure were simply the strongest lines of the poorly crystallized material.

Prior investigation of the vaporization of indium sesquisulfide has been made by Rumyantsev, Zhitenava, and Kochkin[7] who also used the Knudsen effusion method with the sample heated in a fused silica cell. They (incorrectly) assumed $In_2S_3(g)$ molecules to be the major vapor species. Rumyantsev, *et al.*, reported a distinct change in slope of their vapor pressure plot at about 800°K. which they suggest was due to a phase transition. This explanation cannot be correct because their data would require that the higher temperature condensed phase form from the lower temperature modification with a negative heat of transition. It has been shown[8,9] that the higher temperature crystallographic modification of any phase must always form from a lower temperature modification with a positive heat of transition. The equations reported by Rumyantsev, *et al.*, therefore must be in error at least in one of the temperature ranges above or below the change in slope.

The objectives of the present investigation were to establish whether or not indium sesquisulfide sublimes to a vapor of over-all composition which is the same as that of the solid (*i.e.*, sublimes congruently), to identify the major vapor species by a mass spectrometer study, to measure the equilibrium rate of sublimation of the phase by the Knudsen effusion weight loss method, and to measure the rate of sublimation from a free surface of the solid.

Experimental

Preparation and Purification of Indium Sesquisulfide.—Indium which was stated by the supplier (Indium Corporation of America) to be 99.999% pure was dissolved in HCl. The resultant solution was heated to dryness. A 0.1 *m* solution of ammonium acetate was added to the white indium chloride; HCl was also added to bring the acidity to pH 3.

Hydrogen sulfide, bubbled through the solution, precipitated yellow indium sulfide by the reaction

$$2In^{3+}(aq) + 3H_2S = In_2S_3(s) + 6H^+(aq)$$

provided that the pH was maintained between 3.4 and 1.5. In solutions of pH greater than 3.4, indium hydroxide precipitates and at pH lower than 1.5 the indium sulfide is soluble.

One-molal ammonium acetate solution was added continuously during precipitation because the precipitation reaction produces hydrogen ion and the buffering action of acetate ion is inefficient at pH 3.

The yellow precipitate was decanted and washed four times to remove most of the adsorbed ions and free sulfur. Dilute hydrochloric acid was added after each wash to keep the acidity at pH 3.

The impure sulfide (3.5 g.) was precipitated from 2 l. of solution. The precipitate was dried at 110° in air. The product was an orange powder which yielded a weak and diffuse diffraction pattern.

When heated at 350° *in vacuo* for 2 hr., the sample decreased in weight by about 7% and a dark red powder remained. This powder yielded a sharp X-ray diffraction pattern of many lines. The line spacings and intensities corresponded to the pattern of the phase identified as β-In_2S_3 by Hahn and Klingler and subsequently re-indexed by Rooymans. The yield of the sulfide was 98% based on the original indium.

The product, as analyzed by K. C. Conway of the Pacific Experiment Station of the U. S. Bureau of Mines, was 70.49% In, 28.84% S, and 0.10% SiO_2. A weight loss of 1.28% was produced by heating for 1 hr. at 500° in a stream of nitrogen. In our subsequent mass spectrometric experiments, $InCl^+$ was the principal ion detected during initial vacuum sublimation under conditions of our vapor pressure measurements.

The $InCl^+$ could have been produced by ionization of InCl or by fragmentation and ionization of $InCl_3$. If the 1.28% weight loss is ascribed to escape of InCl, the formula of the indium sulfide phase is calculated to be $InS_{1.485}$. If the weight loss is ascribed to escape of $InCl_3$, the formula of the indium sulfide phase is calculated to be $InS_{1.475}$. Probably the analysis is accurate in suggesting that the composition for congruent sublimation is slightly poorer in sulfur than is the stoichiometric compound.

The $InCl^+$ intensity in the mass spectrometer became immeasurable after a few weight per cent of solid was vaporized. Halide vapor species could not have significantly contributed to the weight losses measured in the Knudsen effusion studies, since several weight per cent of each sample was vaporized prior to the start of each series of runs.

Congruent sublimation of the indium sesquisulfide on heating was confirmed experimentally. Samples (0.5 g.) of In_2S_3 were used for weight-loss runs in experiments with lids of three different orifice diameters. Between heatings, small amounts of sample were removed for X-ray diffraction examinations. From 60 to 97% of each sample was evaporated. Although the samples changed in appearance from dark red to black as evaporation progressed, the X-ray diffraction pattern remained unchanged.

The few weak diffraction lines obtained for the pattern of the initial precipitate after it was dried at 110° corresponded in position to the strongest lines of the sharp β-In_2S_3 pattern. The material did not undergo a structural change when heated for 2 hr. at 800° and cooled at 50°/min. The conclusion of Rooymans that "α-In_2S_3" is simply an impure and poorly crystalline form of β-In_2S_3 is apparently correct.

Sublimation Pressure Studies.—A Knudsen effusion cell was machined from National Carbon Co. grade AUC graphite. Cylindrical effusion holes of approximately 1.5, 1.0, and 0.5 mm. diameter, d, as determined by a traveling microscope, were used; the length of each orifice was about twice its diameter so that the Clausing factors were each about 0.4.[10] The cell was cylindrical in shape, 1.6 cm. high and 1.4 cm. in diameter. A larger graphite crucible surrounded the cell and was in turn supported by a graphite stand.

The entire assembly was supported by the closed end of a vertical fused silica tube. The system was evacuated to a pressure of 10^{-5} mm. A vertical tube furnace, mounted on a counterweighted dolly, could be raised rapidly over the fused silica tube and sample. The time required to reach the desired temperature was always less than 1% of the heating time employed. Heating time and temperature for each run were chosen to obtain a weight loss of about 10 mg.

The temperature of the sample was measured with a millivolt potentiometer connected to a Pt–Pt 10% Rh thermocouple. The thermocouple was insulated with fused silica and inserted

(3) H. Hahn and W. Klingler, *Z. anorg Chem.*, **260**, 97 (1949).

(4) M. F. Stubbs, J. A. Schufle, A. J Thompson, and J. M. Duncan, *J. Am. Chem. Soc.*, **74**, 1441 (1952).

(5) H. Hahn and F. Burow, *Angew. Chem.*, **68**, 382 (1956).

(6) C. J. M. Rooymans, *J. Inorg. Nucl. Chem.*, **11**:1, 78 (1959).

(7) Yu. V. Rumyantsev, G. M. Zhitenava, and V. P. Kochkin, *Tr. Vost. Sibirsk. Filiala, Akad. Nauk SSSR*, **25**, 110 (1960).

(8) M. J. Buerger, *Am. Mineralogist*, **32**, 101 (1948).

(9) A. W. Searcy, *Progr. Inorg. Chem.*, **3**, 46 (1962).

(10) S. Dushman, "Scientific Foundations of Vacuum Technique," John Wiley and Sons, Inc., New York, N. Y., 1949.

into a hole in the larger crucible. The temperature of this thermocouple was calibrated in experiments in which a second Pt–Pt 10% Rh thermocouple was inserted through the crucible orifice into indium sulfide powder. The thermocouple used for effusion studies recorded a temperature 2° higher than the temperature of the sulfide powder over the entire experimental range. The two thermocouples were both calibrated against a standardized couple and were both found to read 2° low. An on–off controller, operated by a thermocouple located near the furnace windings, maintained the sample temperature within 2° of the desired value.

A lid with no hole was used to establish the weight loss through the walls or through cracks at the lid edges of the cell. This loss can be expressed as

$$-\log Y = \frac{16{,}300}{T} - 10.6 \qquad (1)$$

where Y is the number of moles of In_2S_3 lost per second and T the absolute temperature. The loss amounts to 37% of the loss through the smallest orifice, 10% of the loss through the middle-sized orifice, and 6% of that through the largest orifice. These results demonstrate the danger of the assumption that a dependence of apparent pressure on orifice area in Knudsen effusion studies necessarily reflects a low evaporation coefficient.

Free-Surface Sublimation Studies.—The approximate rate of free-surface sublimation of indium sesquisulfide at 970 and 1003°K. was calculated from the weight losses of indium sesquisulfide disks which were forced into graphite cups so that only one end surface of a disk was exposed. Disks 0.65 cm. in diameter and 0.2 cm. high were prepared by pressing to 2000 p.s.i. in National Carbon Company's AUC grade graphite. The disks were heated 5°/min. and held at 800° for 20 min. This technique yielded samples of about 94% theoretical density. Microscopic examination suggests that the porosity consisted mainly of very small pores or of closed pores. Graphite from the die was removed from one end of the disk by grinding on wet 400- and 600-mesh silicon carbide paper. The X-ray diffraction pattern obtained from a crushed cylinder then showed only the β-In_2S_3 pattern.

The disks were pushed into a graphite cup so that one end and the cylindrical surface of the disk were forced to within a maximum distance of 0.002 cm. from the graphite surface. At vaporizing temperature the gap was slightly smaller because the coefficient of thermal expansion of graphite is lower than that of indium sesquisulfide.

Temperatures were measured with a Pt–Pt 10% Rh thermocouple inserted in a hole in the graphite near the exposed surface of the disk. An optical pyrometer was used to calibrate the thermocouple at 830 and 865°. These were the lowest temperatures for which reproducible optical measurements could be made but were too high for free-surface sublimation experiments using the 0.65-cm. diameter disks. Black body cavities 0.158 cm. in diameter and 0.317, 0.476, and 0.793 cm. deep were drilled into the graphite cup. The apparent temperature of the holes, the graphite surface, and the adjacent indium sesquisulfide surface were read with an optical pyrometer. The black body holes gave identical temperatures of 830 and 868° when the apparent surface temperatures of the graphite were 826 and 860°, respectively. Apparent surface temperatures of the indium sesquisulfide were then 819 and 850°. Since the apparent temperature of the graphite surface is lower than that read in the black body cavities, light reflected from the graphite and indium sulfide surfaces cannot have made the brightness temperatures of either surface greater than the true temperature. The unknown emissivity of the indium sesquisulfide surface is expected to be lower than that of graphite which has an exceptionally high emissivity.[11] The true surface temperature must be above the apparent temperature and is probably no higher than the black body temperature. The surface temperature is known, therefore, to within ±15° at worst. For our calculations the surface temperatures were assumed to be equal to 832 and 863°. Sublimation rates were measured at 697 and 730°.

The surface of the sample, after a few milligrams had vaporized, appeared deeply etched as if along grain boundaries. The deep grooves occupied between 1 and 4% of the gross surface area. The value of the sublimation coefficient α calculated from the gross dimensions of the sample surface with surface roughness neglected would, therefore, be an upper limit to the true value of α. The value of α calculated from the assumption that the fraction of surface that is occupied by grooves can be assigned an effective α of unity should yield a lower limit to α. From these considerations, the limits of α were calculated to be $0.005 < \alpha < 0.04$.

Until better definition of the surface area for sublimation can be achieved, perhaps by utilization of surfaces of single crystals, attempts to refine measurements of α do not appear warranted.

Identification of Vapor Species.—An Inghram-type mass spectrometer, made by Nuclide Analysis Associates, was used to identify the major species from the sesquisulfide when heated in tantalum, graphite, and fused silica crucibles by radiation from tungsten filaments. Temperatures were determined with a Pt–Pt 10% Rh thermocouple embedded in the base of the crucible. A shutter 0.05 cm. wide by 1 cm. long was moved across the molecular beam in order to distinguish between molecules that effused from the cell and molecules produced by secondary reactions outside the cell.

The ions S_2^+, In^+, InS^+, In_2^+, and In_2S^+ were observed when the vapor that effused from the cell was bombarded with 60-v. electrons. When a graphite cell was used, CS_2^+ was also observed; however, moving the shutter across the beam did not affect the CS_2^+ intensity. Furthermore, the crucible lost less than 0.05 mg. (4.2×10^{-6} g.-atom of carbon) in weight, while a total of 500 mg. (1.5×10^{-3} mole) of indium sulfide was sublimed. The CS_2^+ peak is not produced, therefore, by reaction of indium sulfide with graphite inside the cell. The ion intensity ratios In^+/In_2S^+, InS^+/In_2S^+, and In_2^+/In_2S^+ remained constant over the temperature range 970 to 1250°K., indicating that these ions were all produced by interaction of the electron beam with the same parent molecule. The simplest molecule that could be the common parent of these ions is In_2S; so In^+, In_2^+, and InS^+ must all be produced mainly by fragmentation rather than by simple ionization of gaseous In, In_2, and InS.

Purely thermodynamic arguments also lead to the conclusion that the In^+ and In_2^+ ions must be produced by fragmentation of something other than the corresponding neutral species. The partial pressure of In gas that would be produced by the reaction $In_2S_3(s) = 2\,In(g) + 3/2S_2(g)$ can be calculated from the heat of formation of indium sesquisulfide[5] and from standard thermodynamic tables for the elements. The calculated pressure is several orders of magnitude lower than the pressures found from the Knudsen experiments. In_2 gas is a minor species in the saturated vapor of elemental indium and would be even less important above indium sesquisulfide since the reduced indium activity in the sesquisulfide necessarily favors dissociation of the dimer.

The intensity of the InS^+ peak was less than 1% of the intensity of the In_2S^+ peak so that even if part of the InS^+ were produced from ionization of an InS gas species, the partial pressure of that species is fixed as less than 1%. The remaining important possibility to be considered is the possibility that the In_2S^+ ion is produced by fragmentation of a more complex molecule such as In_2S_2 or In_2S_3.

The parent was established by means of experiments in which the sulfur activity in the indium sesquisulfide phase was deliberately changed. The S_2^+/In_2S^+ ratio was decreased to 0.001 at 870°K. when the sesquisulfide was saturated with the solid phase of next higher indium content; the ratio was increased to 2 by equilibration with excess sulfur. If In_2S^+ were produced by fragmentation of In_2S_3 gas, there should have been no change in the In_2S^+ intensity when the S_2^+ intensity was varied. If In_2S_2 gas were the parent, the In_2S^+ intensity should have varied inversely with the square root of the S_2^+ intensity. If In_2S gas were the parent, the In_2S^+ intensity should have varied inversely with the S_2^+ intensity so that the product of intensities of the two ions would remain constant.

The product of the In_2S^+ and S_2^+ intensities remained constant to within a factor of three while the relative intensities of the two ions was changed by more than a factor of 1000, so In_2S is identified as the parent molecule.

At the highest temperatures, $In_2S_2^+$ was observed; the maximum intensity of $In_2S_2^+$ was 0.1% of the In_2S^+ intensity. No other ions were detected in a scan to mass 1500.

(11) The assumption that the temperature of the cavities, the polished graphite surface, and the indium sesquisulfide surface were at the same temperature and that the emissivity of polished graphite is 0.77 leads to an emissivity value of 0.52 for indium sesquisulfide.

Results and Discussion

Table I summarizes the equilibrium constant calculations from the Knudsen effusion studies. The first eight runs were made with lids for which $d = 1.50$ mm., the next nine with lids for which $d = 1.04$ mm., the next three with lids for which $d = 0.475$ mm., and the last five with lids for which $d = 0.480$ mm. The data and least squares line are plotted in Fig. 1. No evidence of a change in slope such as reported by Rumyantsev, *et al.*, was found Their measurements actually agree to within the experimental scatter with ours except at the lowest temperatures. Our data can be reproduced by the equation

$$-\log K = \frac{30{,}66(}{T} - 17.94$$

In estimating the free energy functions from which the heat of sublimation at 298°K. could be calculated, the molecule In_2S was assumed to be bent with an In–S–In angle of 110°. The In–S distance was estimated to be 2.1 Å. from the known interatomic distances in SnS(g) and SiS(g)[12] and from comparison of ionic radii of Sn, Si, and In.[13] Stretching and bending constants were chosen as 3.7×10^5 and 1.75×10^4 dynes/cm., respectively. The standard entropy at 298°K. was then calculated as 76 e.u., and $-(F_T - H_{298})/T$ was calculated to be 83.92 at 900°K., 84.96 at 1000°K., 85.91 at 1100°K., and 86.78 at 1200°K.

The entropy of In_2S_3 solid at 298°K. recently has been determined by King and Weller.[14] The high temperature heat content of In_2S_3 was estimated[15] by assuming that C_p varies linearly with temperature and reaches 35 cal. deg.$^{-1}$ mole^{-1} at the melting point.[4] These data then were used to calculate free energy functions for solid In_2S_3. The values are 52.27 at 900°K., 54.50 at 1000°K., 56.62 at 1100°K., and 58.63 at 1200°K.

A second-law treatment of the data yields 146.8 kcal. for the heat of the reaction $In_2S_3(s) = In_2S(g) + S_2(g)$ at 298°K. compared to 147.4 ± 0.6 kcal. calculated by the third-law method. The absolute uncertainty of the heat is estimated to be ±3 kcal. When the third-law heat of reaction is combined with the heat of formation of solid indium sesquisulfide reported by Hahn and the heat of formation of S_2 gas (30.8 kcal.) tabulated by Stull and Sinke,[16] the heat of formation of $In_2S(g)$ is calculated to be +14.6 ± 5 kcal.

Klanberg and Spandau[17] have measured the vapor pressure of $In_2S(g)$ above melts which had the over-all composition In_2S between 986 and 1198° by the transpiration method. They found the pressure of $In_2S(g)$ to be expressed by

$$-\log P_{In_2S}(\text{atm}) = + \frac{9320.3}{T} - 5.0404 \quad (986\text{–}1198°)$$

and calculated

$$\Delta H°_{298(\text{form})}\ [In_2S(g)] = 6.5 \pm 8 \text{ kcal./mole}$$

(12) G. Herzberg, "Molecular Spectra and Molecular Structure. I. Spectra of Diatomic Molecules," D. Van Nostrand Co., New York, N. Y., 1950.

(13) L. Pauling, "The Nature of the Chemical Bond," Cornell University Press, New York, N. Y., 1960.

(14) E. G. King and W. W. Weller, U. S. Bureau of Mines R1-6040, 1962.

(15) K. K. Kelley, U. S. Bureau of Mines Bull. No. 476, 1949, p. 206.

(16) D. R. Stull and G. C. Sinke, "Thermodynamic Properties of the Elements," American Chemical Society, Washington, D. C., 1956.

(17) F. Klanberg and H. Spandau, *J. Inorg. Nucl. Chem.*, **19**, 180 (1961).

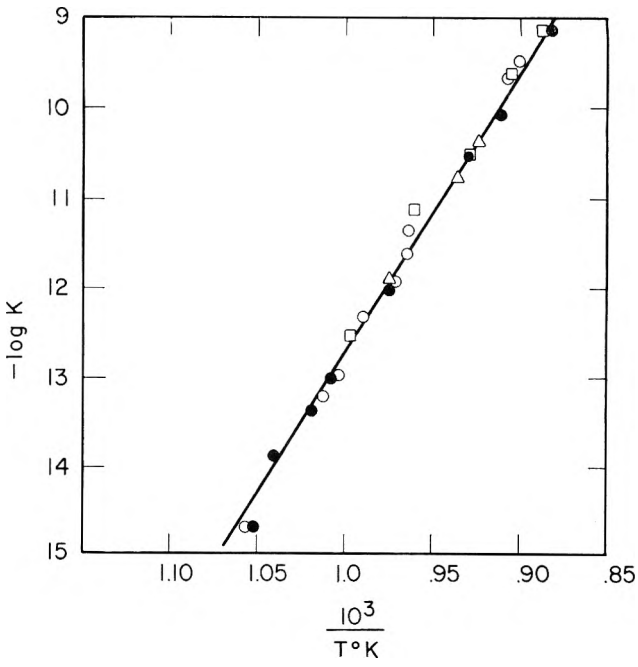

Fig. 1.—The equilibrium constant for the vaporization of indium sesquisulfide as a function of temperature for the reaction $In_2S_3(s) = In_2S(g) + S_2(g)$: ●, 1.50-mm. orifice diameter; ○, 1.04-mm. orifice diameter; △, 0.475-mm. orifice diameter; □, 0.480-mm. orifice diameter.

TABLE I

DATA FOR THE REACTION $In_2S_3(s) = In_2S(g) + S_2(g)$

Temp., °K.	Time, min.	Corrected wt. loss, mg.	$-\log K_{eq}$	$\Delta H°_{298}$
1076	117	9.1	10.530	147.2
1028	301	4.2	12.040	148.0
993	1140	5.3	13.010	147.8
962	5460	9.4	13.886	147.1
982	2547	7.8	13.377	149.1
1135	66	25.1	9.130	147.7
951	6708	4.7	14.674	148.9
1098	87	11.4	10.067	147.8
1037	1054	18.4	11.362	146.0
1011	1346	7.9	12.321	147.1
1031	994	9.0	11.936	148.1
1111	91	13.1	9.498	146.5
988	3815	8.2	13.202	147.9
997	2602	7.1	12.991	148.2
947	9946	3.9	14.697	148.4
1102	82	9.6	9.682	146.4
1037	1005	13.3	11.602	147.3
1083	1023	10.5	10.386	147.5
1070	1045	7.1	10.752	147.6
1026	3837	7.0	11.910	147.2
1127	147	6.5	9.101	146.5
1042	1031	4.8	11.131	145.8
1105	113	2.8	9.614	147.5
1003	5509	4.9	12.544	147.1
1078	366	3.4	10.517	147.4

apparently on the assumption that the activity of the condensed phases was unchanged by solution formation. Solution would reduce the partial pressure of $In_2S(g)$ by an unknown amount.

Khvorostukhina and Skobeev[18] have reported studies of the equilibrium pressures established in the reaction $H_2(g) + In_2S_3(s) = H_2S(g) + 2\ InS(s)$. Since no

(18) N. A. Khvorostukhina and I. K. Skobeev, *Tr. Vost. Sibirsk. Filiala, Akad. Nauk SSSR*, **41**, 72 (1962).

thermodynamic data are available for solid InS, the results of the dissociation study cannot be compared to the results of the present investigation.

If the slow step in the evaporation of indium sesquisulfide from a free surface is due entirely to an energy barrier, an α of 0.01 leads to an activation energy of 167 kcal./mole for the congruent sublimation at 298°K. This value is about 20 kcal. more than the equilibrium heat of sublimation.

Acknowledgments.—Dr. K. K. Kelley and Mr. K. C. Conway of the U. S. Bureau of Mines kindly provided the analysis of the solid indium sesquisulfide.

HYDROCARBON ADSORPTION STUDIES AT LOW PRESSURES ON THE SODIUM AND ACID FORMS OF SYNTHETIC MORDENITE

By P. E. Eberly, Jr.

Esso Research Laboratories, Humble Oil and Refining Company, Baton Rouge Refinery, Baton Rouge, Louisiana

Received May 22, 1963

The adsorption of benzene, cyclohexane, and *n*-hexane on both Na and H mordenite was investigated at pressures of 0.010 to 6 mm. from 90 to 260°. Na mordenite has exceptionally high adsorptive capacity for the hydrocarbons at these conditions. The saturation value of adsorption expressed in liq. cc./g. is 0.0759 and is essentially independent of the nature of the hydrocarbon and temperature. This is of the same order of magnitude as the pore volume of 0.094 cc./g. determined from the crystallographic dimensions. The heats of adsorption of benzene, cyclohexane, and *n*-hexane on Na mordenite are nearly independent of coverage and amount to 25, 18, and 21 kcal./mole, respectively. The H form exhibits a slow irreversible adsorption process occurring simultaneously with a fast reversible adsorption. The reversible adsorption is considerably less than that observed on the Na form. Heats of the reversible adsorption of benzene, cyclohexane, and *n*-hexane are 12.5, 13.5, and 16.0 kcal./mole, respectively. There is evidence to suggest that *n*-hexane molecules have access to more of the intracrystalline surface than either benzene or cyclohexane. Entropy calculations indicate that the hydrocarbons have more degrees of freedom of motion on the H form than on the Na form.

I. Introduction

In recent years, several reports have appeared in the technical literature concerning the structure,[1] synthesis,[2] and adsorptive properties of mordenite.[3-5] This mineral is a crystalline sodium aluminosilicate having the general formula $Na_8Al_8Si_{40}O_{96}\cdot 24H_2O$. As reported by Meier[1] in his structure determination, mordenite is orthorhombic with unit cell dimensions of $a = 18.13$, $b = 20.49$, and $c = 7.52$ Å. The main building blocks are four- and five-membered rings composed of SiO_4 and AlO_4^- tetrahedra. These rings are so arranged that the resulting crystal contains parallel adsorption tubes having an approximately elliptical opening with a major and minor diameter of 6.95 and 5.81 Å., respectively. A schematic diagram of a cross section of the mordenite structure is shown in Fig. 1. The points of intersection represent the silicon and aluminum atoms and the lines represent atoms of oxygen. The indicated unit cell contains two of these elliptical tubes and extends a distance of 7.52 Å. perpendicular to the plane of the page. The volume of these tubes per unit cell is $V_a = 480$ Å.^{3}. Along the walls of the tubes, other cavities occur at periodic intervals. These have openings which can also be approximated by an ellipse having a major and minor axis of 4.72 and 3.87 Å., respectively. The volume of these cavities per unit cell is $V_b = 428$ Å.^{3}.

In spite of this fairly open structure, earlier reports on the adsorption properties of mordenite indicated that the material had an effective pore opening of only about 4 Å.[3]. It adsorbed nitrogen and smaller molecules rapidly, whereas it took up methane and ethane slowly. This lack of capacity for larger molecules was attributed to stacking faults in the mordenite structure.[1] More recently, however, a synthetic form of mordenite has become commercially available which has considerable capacity for larger molecules such as *n*-heptane, cyclohexane, and benzene and, hence, is apparently more nearly free of stacking faults.[6,7] This material is obtainable in both the Na and so-called "hydrogen-form" and has a surface area of 400–500 m.^{2}/g. as measured by the B.E.T. method with nitrogen adsorption. The H form is made by replacing the sodium with ammonium ions and subsequently calcining to liberate free ammonia or by direct treatment with dilute acid. The H mordenite has been found to be an active cracking catalyst.[6]

The present investigation deals with the study of benzene, cyclohexane, and *n*-hexane adsorption on both the Na and H forms of this new mordenite preparation in the low pressure region from 0.010 to 6 mm. As is characteristic of zeolites of this type, the adsorption isotherms are very steep and saturation is nearly complete at low pressures. Use of an electromagnetic microbalance facilitated the determination of these isotherms.

II. Experimental

Apparatus.—The Cahn electromagnetic microbalance was used for the adsorption measurements. The sample was placed in a small quartz bucket which was suspended from one end of the balance beam by a quartz fiber. Under the conditions of the experiment, the balance could detect a weight change of 0.001 mg. The entire balance and quartz suspension were enclosed in a glass system which could be evacuated to a pressure on the order of 10^{-5} mm. The pumping system consisted of a three-stage oil diffusion pump backed up by a mechanical pump. The system was protected from oil vapors by a liquid nitrogen trap.

The heating system consisted of an aluminum block heater which was placed around the glass tube containing the sample bucket. Two copper–constantan thermocouples were placed

(1) W. M. Meier, *Z. Krist.*, **115**, 439 (1961).
(2) R. M. Barrer, *J. Chem. Soc.*, 2158 (1948).
(3) R. M. Barrer, *Brennstoff-Chem.*, **35**, 325 (1954).
(4) R. M. Barrer and A. B. Robins, *Trans. Faraday Soc.*, **49**, 929 (1953).
(5) R. M. Barrer and A. B. Robins, *ibid.*, **49**, 807 (1953).
(6) A. H. Keough and L. B. Sand, *J. Am. Chem. Soc.*, **83**, 3536 (1961).
(7) *Chem. Eng. News*, **40**, No. 11, 52 (1962).

about 0.25 in. below the sample bucket. One couple was connected to the control system and the other to a millivolt recorder. Good temperature control was achieved by the combination of an on–off controller connected to a stepless, proportional controller.

After closing off the adsorption system to the vacuum pumps, injections of liquid hydrocarbons were accomplished by inserting pipets of various sizes through a mercury layer to a glass frit. The volumes of these pipets were 0.0005, 0.001, 0.002, 0.003, 0.02, and 0.04 cc. Since the volume of the adsorption system was near 3 l., these pipets produced pressures in the desired range.

Procedure.—For the adsorption measurements about 20 mg. of sample was placed in the quartz bucket and heated to 370°. The sample was degassed at this temperature for 16 hr. The temperature was then lowered to the desired value and the system closed off from the pumps. Successive injections of the hydrocarbon were made until the pressure reached 6–10 mm. During this process, the weight of the sample was continuously recorded. It normally took four to five hours for the measurement of one isotherm. The system was then opened to the vacuum pumps and the rate of desorption measured at near vacuum conditions to determine the degree of reversibility of the adsorption. The sample was then heated again to 370° and degassed for 16 hr. in preparation for the next isotherm measurement.

All determinations were made above 90°. Below this temperature, the sample even under high vacuum conditions began to increase in weight at the rate of about 1 μg./min. It was not determined whether this was merely an apparent weight change due to temperature effects on the balance or a true weight change reflecting the adsorption of small amounts of mercury or water vapor. Above 90°, this effect did not occur.

To correct the weight changes for thermomolecular flow and buoyancy effects, calibration runs were made with a 19.762-mg. sample of nonadsorptive quartz chips. The corrections for cyclohexane at four different temperatures and various pressures are shown in Fig. 2. These were added to the weight measurements observed during the actual isotherm determination. In most cases, they were negligible compared to the total weight change due to adsorption.

Materials.—Specially purified samples of the Na and H forms of mordenite were obtained from the Norton Co., Worcester, Mass. Chemical analyses are shown in Table I. In preparing the H form from the Na form, nearly complete removal of the sodium was achieved.

Benzene, cyclohexane, and *n*-hexane were obtained from the Phillips Petroleum Co., and had purities of 99.9, 99.8, and 99.9 mole %, respectively. Prior to use, they were filtered through columns of silica gel.

TABLE I

COMPOSITION OF MORDENITE SAMPLES

	Na form	H form
SiO_2, wt. %	78.26	86.05
Al_2O_3, wt. %	12.57	13.87
Na_2O, wt. %	9.17	0.08
SiO_2/Al_2O_3, molar ratio	10.56	10.53

III. Results

A. Adsorption Studies on Na Form of Mordenite. Benzene Isotherms.—Large amounts of benzene were adsorbed on Na mordenite at very low pressures and high temperatures. The rate of adsorption was rapid and equilibrium was established within a few minutes after injection. Figure 3 shows a portion of three isotherms up to 1 mm. pressure obtained at 223, 241, and 260°.

The following Langmuir equation can be used to express the data.

$$x = \frac{ax_m p}{1 + ap} \qquad (1)$$

or

$$\frac{p}{x} = \frac{1}{ax_m} + \left(\frac{1}{x_m}\right) p \qquad (2)$$

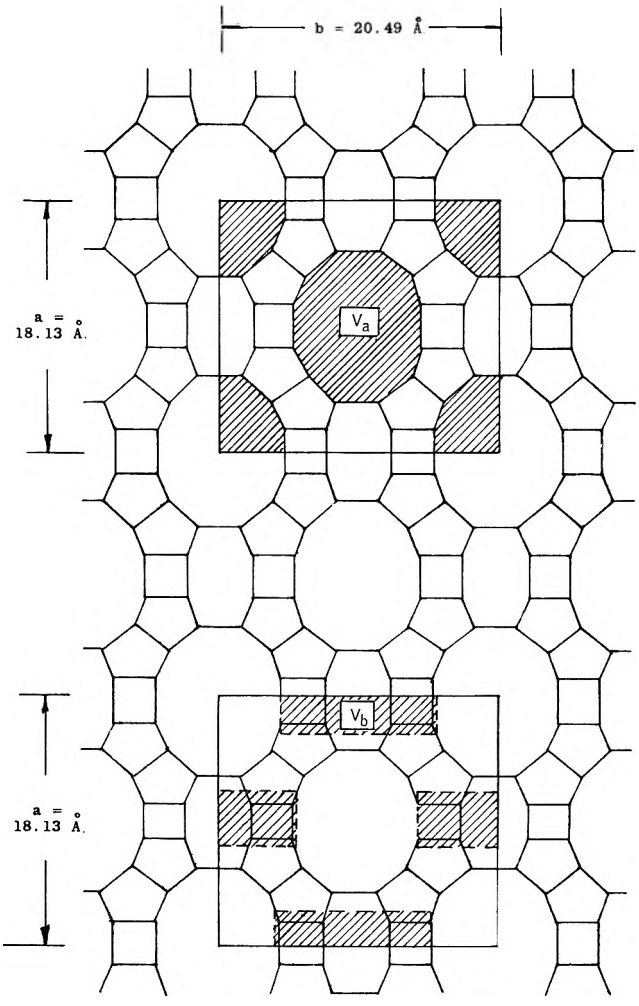

Fig. 1.—Schematic diagram of a cross section of mordenite. The points of intersection represent silicon or aluminum atoms and the lines represent oxygen atoms. The two volumes possible for adsorption are indicated by V_a and V_b.

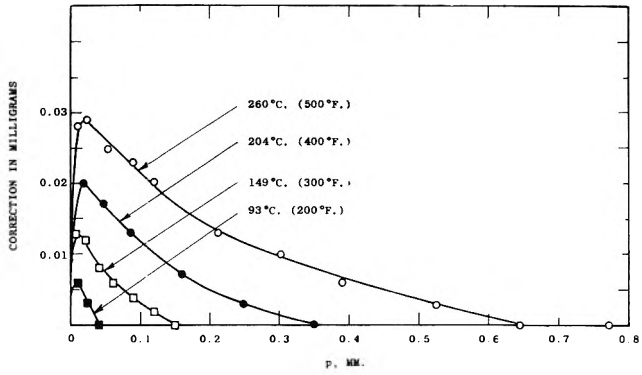

Fig. 2.—Weight corrections for cyclohexane. Data represent apparent weight losses observed with cyclohexane on a 19.762-mg. sample of quartz chips.

where p is the pressure and x is the amount of material absorbed in mmole/g. The quantity x_m represents the amount of material necessary to cover the surface with a monomolecular layer. Thus, if p/x is plotted *vs.* p, a straight line should result. The slope and intercept are equal to $1/x_m$ and $1/ax_m$, respectively. Such Langmuir plots for these benzene isotherms are shown in Fig. 4 up to 6 mm. pressure. At all three temperatures, the data are best represented by two straight lines intersecting at a pressure near 0.6 mm. Values of a and x_m are listed in Table II for both pressure regions.

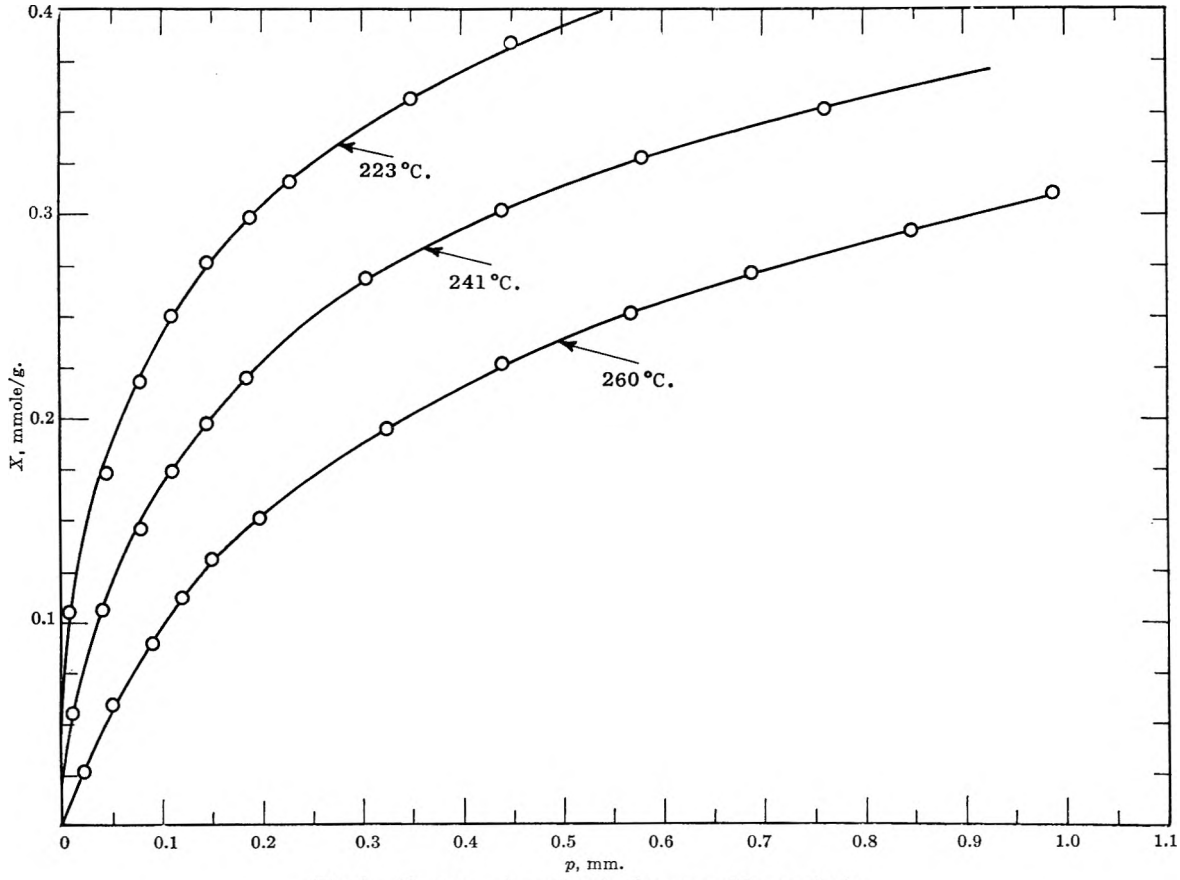

Fig. 3.—Benzene adsorption isotherms on Na mordenite.

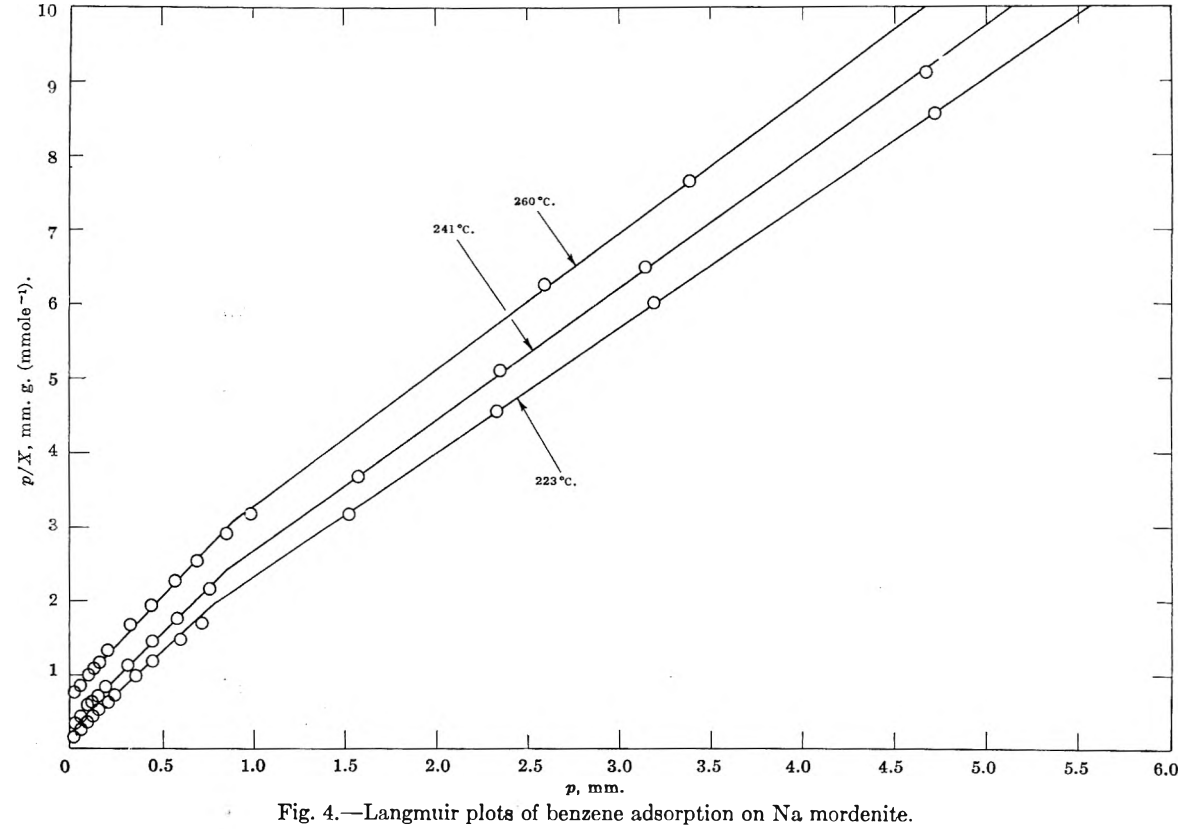

Fig. 4.—Langmuir plots of benzene adsorption on Na mordenite.

If ΔH, the heat of adsorption, is assumed to be independent of temperature, it can be evaluated for any given coverage, x, by the relationship

$$\left(\frac{\mathrm{d} \ln p}{\mathrm{d}T}\right)_x = \frac{-\Delta H}{RT^2} \qquad (3)$$

These data are listed in Table III. The heat of benzene adsorption is fairly independent of coverage varying only from 24.6 to 26.8 kcal./mole from 0.100 to 0.300 mmole/g., respectively.

To calculate the entropy changes accompanying the adsorption, use is made of eq. 4–6

TABLE II

LANGMUIR CONSTANTS FOR ADSORPTION ON SODIUM MORDENITE

Adsorbate	T, °C.	Press. range, mm.	a, mm.$^{-1}$	X_m, mmole/g.	Liq. cc./g.[a]	Molecules/ads. tube[b]
Benzene	223	0–0.7	16.69	0.4280	.....	..
	223	0.7–6	2.716	.5938	0.0750	0.91
Benzene	241	0–0.9	7.344	.4126	.....	..
	241	0.9–6	1.967	.5648	0.0757	0.86
Benzene	260	0–0.9	3.877	.3738	.....	..
	260	0.9–6	1.273	.5456	0.0800	0.84
Cyclohexane	161	0–6	2.331	.5430	0.0725	0.83
Cyclohexane	183	0–6	0.8204	.5277	.0739	.81
Cyclohexane	203	0–6	0.3652	.5510	.0808	.84
n-Hexane	162	0–0.6	15.34	.3259	.....	..
	162	0.6–6	3.198	.4468	0.0765	0.68
n-Hexane	182	0–0.6	5.958	.2945	.....	..
	182	0.6–6	2.309	.4011	0.0731	0.61
n-Hexane	204	0–0.6	2.937	.2560	.....	..
	204	0.6–6	1.352	.3736	0.0754	0.57

[a] Calculated from the orthobaric densities. [b] Having unit cell length of $c = 7.52$ Å.

TABLE III

THERMODYNAMIC DATA FOR BENZENE ADSORPTION ON SODIUM MORDENITE

X, mmole/g.	T, °C.	$-\Delta H$, kcal./mole	$-\Delta G°$, cal./mole	$-\Delta S°$, cal./deg.-mole	$S_g°$, cal./deg.-mole	$\bar{S}_s$, cal./deg.-mole
0.100	223	24.7	10,500	28.6	77.3	48.7
	241		9,980	28.6	78.3	49.7
	260		9,530	28.5	79.7	51.2
.150	223	24.6	9,940	29.5	77.3	47.8
	241		9,390	29.6	78.3	48.2
	260		8,890	29.5	79.7	50.2
.200	223	25.0	9,480	31.2	77.3	46.1
	241		8,880	31.4	78.3	46.9
	260		8,320	31.3	79.7	48.4
.250	223	25.6	9,000	33.4	77.3	43.9
	241		8,370	33.5	78.3	44.8
	260		7,720	33.6	79.7	46.2
.300	223	26.8	8,490	36.8	77.3	40.5
	241		7,810	36.9	78.3	41.3
	260		7,070	37.0	79.7	42.7

$$\Delta G° = -RT \ln \frac{P}{p} \quad (4)$$

$$\Delta G° = \Delta H° - T\Delta S° \quad (5)$$

$$\Delta S° = \frac{\Delta H°}{T} - R \ln \frac{P}{p} \quad (6)$$

where $\Delta G°$, $\Delta H°$, and $\Delta S°$ are standard free energy, enthalpy, and entropy changes in the adsorption process. P and p are the equilibrium pressures of the adsorbed phase in its standard state and the state under study. The standard state pressure, P, is taken as one atmosphere. For isothermal conditions, neglecting gas imperfections, $\Delta H = \Delta H°$.

Furthermore, the entropy change accompanying adsorption ($\Delta S°$) can be expressed by

$$\Delta S° = S_g° - \bar{S}_s \quad (7)$$

where $S_g°$ is the molar entropy of the hydrocarbon vapor at the standard pressure P of one atmosphere and $\bar{S}_s$ is the partial molar entropy of the adsorbed phase.

Such thermodynamic data for benzene adsorption on Na modenite are given in Table III. $\bar{S}_s$ and consequently the mobility of the adsorbed phase tends to decrease with coverage and increase with temperature.

The entropy of the adsorbed phase, $\bar{S}_s$, can be further analyzed in the manner originally proposed by Barrer, Bultitude, and Sutherland[8] in their study of hydrocarbon adsorption on faujasite. In this case, $\bar{S}_s$ can be represented by

$$\bar{S}_s = \bar{S}_c + \bar{S}_{th} \quad (8)$$

where $\bar{S}_c$ and $\bar{S}_{th}$ denote the partial molar configurational and thermal entropies of the adsorbed phase, respectively. If adsorption is localized, as indicated by the near agreement with the Langmuir equation, $\bar{S}_{th}$ becomes independent of θ, the fraction of surface covered. For our purposes, θ can be expressed as x/x_m. The configurational entropy, $\bar{S}_c$, is equal to

$$\bar{S}_c = R \ln \left[\frac{1-\theta}{\theta}\right] \quad (9)$$

which at $\theta = 0.5$, reduces to zero, and $\bar{S}_s$ becomes equal to $\bar{S}_{th}$.

For polyatomic hydrocarbon molecules, the thermal entropy of the adsorbed phase can be expressed as the sum of three terms

$$\bar{S}_{th} = {}_3\bar{S}_V + \bar{S}_I + \bar{S}_R \quad (10)$$

where ${}_3\bar{S}_V$ is the partial molar vibrational entropy of the adsorbed molecule as a whole; $\bar{S}_I$, the partial molar entropy associated with the *internal* vibrational and rotational degrees of freedom; and $\bar{S}_R$, the partial molar rotational entropy of the adsorbed molecule as a whole.

Following the procedure described by Barrer,[8] ${}_3\bar{S}_V$ can be estimated by the equation

$${}_3\bar{S}_V = 3R[y(\exp(y-1))^{-1} - \ln(1-\exp -y)] \quad (11)$$

where $y = h\nu/kT$

(8) R. M. Barrer, F. W. Bultitude, and J. W. Sutherland, *Trans. Faraday Soc.*, **53**, 1111 (1957).

The quantity ν is the vibrational frequency of the hydrocarbon molecule as a whole in its intracrystalline environment. This was estimated according to the procedure previously described.[8] Knowing ${}_3\bar{S}_V$, the sum of $\bar{S}_I + \bar{S}_R$ can be evaluated for the adsorbed phase.

This latter sum can be compared to a similar quantity in the gas phase, $S_{Ig} + S_{Rg}$. This is obtained by subtracting the standard translational entropy, ${}_3S_{Tg}$, from the standard entropy of the gaseous hydrocarbon.

$$ {}_3S_{Tg} = 6.864 \log M + 11.439 \log T - 2.314 \quad (12) $$

where M is the molecular weight of the hydrocarbon and T is the absolute temperature.

Summary calculations of the entropy of benzene in the adsorbed phase at $\theta = 0.5$ are included in Table IV. As can be seen, there is a considerable decrease in the internal vibrational and rotational degrees of freedom of adsorbed benzene as compared to its vapor. This difference changes little over the temperature range studied.

TABLE IV

ENTROPIES FOR HYDROCARBON ADSORPTION ON SODIUM MORDENITE

$\theta = 0.500$

Adsorbate	T, °C.	$\bar{S}_s = S_{th}$, cal./deg.-mole	${}_3\bar{S}_V$, cal./deg.-mole	${}_3S_{Tg}$, cal./deg.-mole	$S_{Ig} + S_{Rg}$, cal./deg.-mole	$\bar{S}_I + \bar{S}_R$, cal. deg.-mole	Diff., cal./deg.-mole
Benzene	223	40.5	11.1	41.5	35.8	29.4	−6.4
Benzene	241	41.4	11.2	41.7	36.6	30.2	−6.4
Benzene	260	42.7	11.2	41.9	37.8	31.4	−6.4
Cyclohexane	161	56.8	11.3	41.1	42.4	45.5	+3.1
Cyclohexane	183	58.4	11.4	41.3	44.0	47.0	+3.0
Cyclohexane	203	60.6	11.6	41.5	45.7	49.1	+3.4
n-Hexane	162	77.5	11.2	41.1	66.9	66.4	−0.5
n-Hexane	182	79.4	11.3	41.1	69.4	68.2	−1.2
n-Hexane	204	81.7	11.4	41.3	71.3	70.3	−1.0

Cyclohexane Isotherms.—The isotherms for cyclohexane were determined at 161, 183, and 203°. The constants corresponding to eq. 2 are listed in Table II. In contrast to the benzene isotherms, one straight line fitted the data over the entire pressure range from 0–6 mm.

Values of the thermodynamic quantities are given in Tables IV and V. The heat of adsorption is 18 kcal./mole, considerably less than that observed for benzene. Also, it is fairly constant over the range of coverage of 0.100–0.300 mmole/g. From the entropy analyses made in the manner previously described, the degrees of freedom of the adsorbed phase are somewhat higher than the internal vibrational and rotational degrees of freedom of cyclohexane vapor (see Table IV). Possibly, the adsorbed phase possesses some translational motion through the parallel adsorption tubes of mordenite.

***n*-Hexane Isotherms.**—The Langmuir constants for *n*-hexane adsorption on Na mordenite are listed in Table II for the 162, 182, and 204° isotherms. As previously observed for benzene, the plot of p/x *vs.* p exhibited two straight line portions with the point of intersection near 0.6 mm. pressure.

The thermodynamic data of *n*-hexane adsorption are included in Tables IV and VI. The heat of adsorption is about 21 kcal./mole and is independent of coverage. The difference between the internal vibrational and rotational degrees of freedom of the adsorbed phase and of *n*-hexane vapor is very small.

TABLE V

THERMODYNAMIC DATA FOR CYCLOHEXANE ADSORPTION ON SODIUM MORDENITE

X, mmole/g.	T, °C.	$-\Delta H$, kcal./mole	$-\Delta G°$, cal./mole	$-\Delta S°$, cal./deg.-mole	$S_g°$, cal./deg.-mole	$\bar{S}_s$, cal./deg.-mole
0.100	161	18.0	7750	23.6	83.5	59.9
	183		7150	23.8	85.3	61.5
	203		6760	23.6	87.2	63.6
.150	161	17.7	7300	23.9	83.5	59.6
	183		6670	24.2	85.3	61.1
	203		6260	24.0	87.2	63.2
.200	161	18.1	6930	25.7	83.5	57.8
	183		6280	25.9	85.3	59.4
	203		5870	25.7	87.2	61.6
.250	161	18.2	6600	26.7	83.5	56.8
	183		5930	26.9	85.3	58.4
	203		5512	26.6	87.2	60.6
.300	161	17.4	6280	25.6	83.5	57.9
	183		5580	25.9	85.3	59.4
	203		5170	25.7	87.2	61.6

TABLE VI

THERMODYNAMIC DATA FOR *n*-HEXANE ADSORPTION ON SODIUM MORDENITE

X, mmole/g.	T, °C.	$-\Delta H$, kcal./mole	$-\Delta G°$, cal./mole	$-\Delta S°$, cal./deg.-mole	$S_g°$, cal./deg.-mole	$\bar{S}_s$, cal./deg.-mole
0.100	162	20.3	8790	26.5	107.9	81.5
	182		8211	26.6	110.1	83.5
	204		7748	26.3	112.6	86.3
.125	162	20.6	8503	27.8	107.9	80.1
	182		7910	27.9	110.1	82.2
	204		7370	27.7	112.6	84.9
.150	162	21.0	8230	29.4	107.9	78.5
	182		7580	29.5	110.1	80.6
	204		7000	29.3	112.6	83.3
.175	162	21.4	7960	30.9	107.9	77.0
	182		7270	31.1	110.1	79.0
	204		6590	31.0	112.6	81.6
.200	162	20.9	7690	30.4	107.9	77.5
	182		6940	30.7	110.1	79.4
	204		6120	30.9	112.6	81.7

B. Adsorption Studies on H Form of Mordenite.—The acid or H form of mordenite exhibited an entirely different adsorptive behavior than its parent sodium analog. The adsorption equilibria were established very slowly and full equilibration did not occur even after 4 or 5 hr. There appeared to be two types of adsorption occurring on this material. The first type took place at a rapid rate and its equilibrium was established within a minute or so after injection. Superimposed on this adsorption, a slow process occurred which never really reached equilibrium. Also, the rate of this second type of adsorption did not change significantly with pressure.

Figure 5 illustrates the adsorption behavior observed with *n*-hexane vapor on H mordenite at 163° and shows a continuous record of the weight changes during the isotherm determination. The instantaneous adsorption could be easily separated from the slow adsorption by extrapolating the weight change back to the initial time of injection. During desorption of the solid at near

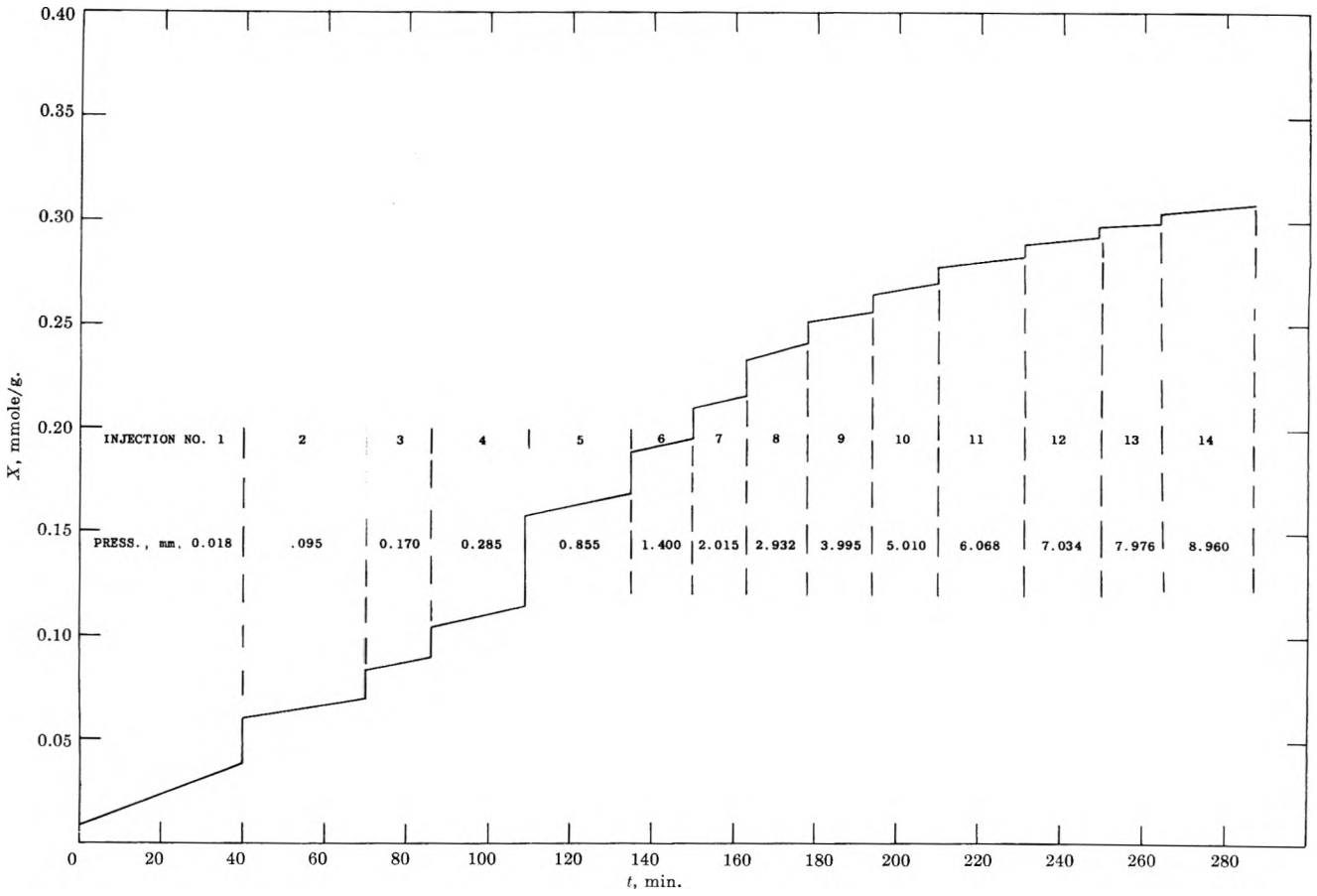

Fig. 5.—*n*-Hexane adsorption at 163° on H mordenite as a function of time.

vacuum conditions, the material associated with the instantaneous adsorption was easily removed, whereas that due to the slow process was very difficult to desorb. Removal of the latter material could only be achieved by elevating the temperature of the sample to 370° and evacuating. For this reason, we chose to separate the adsorption into an instantaneous reversible adsorption and a slow irreversible adsorption.

In general, the behavior was typical of all three hydrocarbons at the temperatures studied. Table VII lists the reversible and irreversible portions of the total adsorption for benzene, cyclohexane, and *n*-hexane at the final conditions of the experiment.

TABLE VII

HYDROCARBON ADSORPTION ON HYDROGEN MORDENITE

Adsorbate	*T*, °C.	Final press., mm.	Final time, hr.	*X*, mmole/g. Irrev.	Rev.	Total
Benzene	92	8.09	4.2	0.0736	0.3640	0.4376
Benzene	116	9.00	4.6	.0618	.3491	.4106
Benzene	138	7.56	4.9	.0860	.2787	.3647
Benzene	163	9.94	4.1	.0352	.2520	.2872
Cyclohexane	93	7.30	4.2	.0840	.2392	.3232
Cyclohexane	116	6.11	4.0	.0724	.2181	.2905
Cyclohexane	137	7.27	3.8	.0290	.2290	.2580
n-Hexane	94	5.01	4.1	.0661	.3016	.3677
n-Hexane	118	6.27	4.8	.0815	.2697	.3512
n-Hexane	137	6.82	5.5	.1133	.2355	.3488
n-Hexane	163	8.97	4.8	.1223	.1870	.3093

Such data are difficult to analyze theoretically. However, an insight into the reversible portion may be obtained by assuming the surfaces responsible for the two types of adsorption to be independent of one another. Thus, we may make an analysis of the reversible adsorption similar to that previously described for Na mordenite.

Reversible Portion of Benzene Adsorption.—The isotherm constants for the reversible portion of benzene adsorption on H mordenite are included in Table VIII. Below 0.6 mm. pressure, deviations occurred in the Langmuir plots of p/x *vs.* p. These, however, could have been due to experimental error in view of the low amount of adsorption in this region. Above this pressure, the straight line relationship was obeyed. The saturation values (x_m or liq. cc./g.) were less than half of those observed on Na mordenite and tended to decrease with increasing temperature. This indicates that successively smaller fractions of the surface are available for the reversible adsorption and, hence, more available for irreversible adsorption as the temperature is raised.

Thermodynamic data for the reversible benzene ad-

TABLE VIII

LANGMUIR CONSTANTS FOR REVERSIBLE PORTION OF ADSORPTION ON HYDROGEN MORDENITE

Adsorbate	*T*, °C.	*a*, mm.$^{-1}$	X_m, mmole/g.	Liq. cc./g.[a]
Benzene	92	1.721	0.3849	0.0375
Benzene	116	1.204	.3610	.0364
Benzene	138	0.9693	.2931	.0307
Benzene	163	0.7812	.2375	.0260
Cyclohexane	93	6.426	.2358	.0281
Cyclohexane	116	3.010	.2291	.0283
Cyclohexane	137	1.326	.2342	.0299
n-Hexane	94	81.67	.3061	.0449
n-Hexane	118	45.63	.2740	.0421
n-Hexane	138	21.84	.2410	.0387
n-Hexane	163	11.6	.1954	.0335

[a] Calculated from orthobaric densities.

sorption are listed in Tables IX and X. The heat of adsorption is 12.5 kcal./mole, and is constant with coverage. This is about half the value observed on Na mordenite. The entropy of the reversibly adsorbed benzene is higher than that on the Na form and the degrees of freedom of motion are considerably higher than those associated with the internal vibrational and rotational motion of benzene vapor. This is evidenced by the 11–13 cal./deg. mole difference between $S_{Ig} + S_{Rg}$ and $\bar{S}_I + \bar{S}_R$. Some translational motion may be possible in the adsorption tubes.

Table IX

Thermodynamic Data for Reversible Portion of Benzene Adsorption on Hydrogen Mordenite

X, mmole/g.	T, °C.	$-\Delta H$, kcal./mole	$-\Delta G°$, cal./mole	$-\Delta S°$, cal./deg.-mole	$S_g°$, cal./deg.-mole	$\bar{S}_a$, cal./deg. mole
0.100	116	12.4	6520	15.2	70.2	55.0
	138		6150	15.3	71.7	56.4
	163		5790	15.2	73.3	58.1
.125	116	12.5	6150	16.3	70.2	53.9
	138		5750	16.4	71.7	55.3
	163		5360	16.3	73.3	57.0
.150	116	12.5	5840	17.1	70.2	53.1
	138		5420	17.2	71.7	54.5
	163		5020	17.1	73.3	56.2
.175	116	12.4	5550	17.6	70.2	52.6
	138		5130	17.7	71.7	54.0
	163		4700	17.7	73.3	55.6
.200	116	12.5	5170	18.7	70.2	51.5
	138		4720	18.8	71.7	52.9
	163		4270	18.8	73.3	54.5

Table X

Entropies for Reversible Portion of Hydrocarbon Adsorption on Hydrogen Mordenite

$\theta = 0.500$

Adsorbate	T, °C.	$\bar{S}_a = S_{th}$, cal./deg.-mole	$_2\bar{S}_V$, cal./deg.-mole	$_2S_{Tg}$, cal./deg.-mole	$S_{Ig} + S_{Rg}$, cal./deg.-mole	$\bar{S}_I + \bar{S}_R$, cal./deg.-mole	Diff., cal./deg.-mole
Benzene	116	52.6	11.4	40.3	29.9	41.2	+11.3
Benzene	138	54.5	11.6	40.6	31.1	42.9	+11.8
Benzene	163	57.0	11.7	40.9	32.4	45.2	+12.8
Cyclohexane	93	58.3	11.2	40.2	37.1	47.0	+ 9.9
Cyclohexane	116	60.3	11.4	40.5	38.8	48.9	+10.1
Cyclohexane	137	62.2	11.5	40.8	40.4	50.7	+10.3
n-Hexane	94	76.1	11.1	40.2	60.4	65.0	+ 4.6
n-Hexane	118	78.8	11.3	40.6	62.5	67.5	+ 5.0
n-Hexane	138	81.1	11.4	40.9	64.4	69.8	+ 5.4

Reversible Portion of Cyclohexane Adsorption.—The isotherm constants for cyclohexane adsorption on H mordenite are listed in Table VIII and the thermodynamic data in Tables X and XI. The values of x_m or liq. cc./g. are less than half of those observed on Na mordenite. The heat of adsorption is 13.5 kcal./mole. The entropies of the reversibly adsorbed cyclohexane indicate more degrees of freedom of motion than observed on the Na form.

Reversible Portion of *n*-Hexane Adsorption.—The Langmuir constants for *n*-hexane adsorption on H mordenite are included in Table VIII. In this case, the values of liq. cc./g. adsorbed at saturation are considerably higher than those for either benzene or cyclohexane at a given temperature. Similar data on the Na form (see Table II) showed that the amount

Table XI

Thermodynamic Data for Reversible Portion of Cyclohexane Adsorption on Hydrogen Mordenite

X, mmole/g.	T, °C.	$-\Delta H$, kcal./mole	$-\Delta G°$, cal./mole	$-\Delta S°$, cal./deg.-mole	$S_g°$, cal./deg.-mole	$\bar{S}_a$, cal./deg.-mole
0.100	93	13.7	6750	19.1	77.3	58.3
	116		6330	19.0	79.3	60.3
	137		5930	19.0	81.2	62.2
.125	93	13.6	6380	19.8	77.3	57.5
	116		5950	19.8	79.3	59.5
	137		5520	19.8	81.2	61.4
.150	93	13.5	5990	20.5	77.3	56.8
	116		5550	20.4	79.3	58.9
	137		5110	20.5	81.2	60.7
.175	93	13.4	5510	21.6	77.3	55.7
	116		5060	21.5	79.3	57.8
	137		4600	21.5	81.2	59.7

adsorbed at saturation expressed in liq. cc./g. was essentially the same for the three hydrocarbons. This leads to the conclusion that *n*-hexane has access to certain portions of the surface which are inaccessible to benzene and cyclohexane. Of all three molecules, *n*-hexane has the smallest cross-sectional diameter. Conceivably, it could enter the smaller cavities which occur at periodic intervals along the main adsorption tubes. The volume of these is represented by V_b in Fig. 1.

Thermodynamic data for the reversible portion of *n*-hexane adsorption are given in Tables X and XII. The heat of adsorption is about 16 kcal./mole and is 3–4 kcal./mole higher than the corresponding heats of cyclohexane and benzene adsorption. This is also indicative of *n*-hexane adsorbing on a different surface than that available for the adsorption of the larger molecules. As seen from the difference between $S_{Ig} + S_{Rg}$ and $\bar{S}_I + \bar{S}_R$, the degrees of freedom of motion for *n*-hexane are lower relative to those of benzene and cyclohexane.

Table XII

Thermodynamic Data for Reversible Portion of *n*-Hexane Adsorption on Hydrogen Mordenite

X, mmole/g.	T, °C.	$-\Delta H$, kcal./mole	$-\Delta G°$, cal./mole	$-\Delta S°$, cal./deg.-mole	$S_g°$, cal./deg.-mole	$\bar{S}_a$, cal./deg.-mole
0.100	94	15.8	8400	22.8	100.6	77.8
	118		6850	22.9	103.1	80.2
	138		6410	22.9	105.3	82.5
.125	94	15.9	7020	24.1	100.6	76.5
	118		6470	24.1	103.1	79.0
	138		5970	24.2	105.3	81.1
.150	94	15.7	6680	24.5	100.6	76.1
	118		6117	24.5	103.1	78.6
	138		5610	24.6	105.3	80.8
.175	94	16.2	6340	26.7	100.6	74.0
	118		5730	26.6	103.1	76.5
	138		5180	26.7	105.3	78.6
.200	94	16.1	5970	27.6	100.6	73.0
	118		5340	27.6	103.1	75.5
	138		4780	27.6	105.3	77.7

IV. Discussion

One result of this investigation is the demonstration of large adsorptive capacities of Na mordenite at very low pressures (<1 mm.) and temperatures up to 260°. Use of the electromagnetic microbalance greatly facili-

tated the accurate measurement of adsorption isotherms in this region.

From the saturation values (x_m) in Table II, the volume of liquid adsorbed per gram was calculated by assuming the density of the adsorbed phase to be equal to the orthobaric density of liquid hydrocarbon at the same temperature. On this basis, the amount of liquid adsorbed was essentially independent of the nature of the hydrocarbon and the temperature. The average value was 0.0759 liq. cc./g. This is of the same order of magnitude as the pore volume associated with the main adsorption tubes (V_a) which amounts to 0.094 cc./g., as calculated from the crystallographic dimensions. The number of molecules adsorbed per tube of unit cell length (c = 7.52 Å.) at the saturation value (x_m) is 0.9, 0.8, and 0.6 for benzene, cyclohexane, and *n*-hexane, respectively.

The hydrocarbon heats of adsorption on Na mordenite are considerably higher than those observed on synthetic faujasite ("13X molecular sieve"). Barrer[8] and Eberly,[9] for example, list 15.5–16.8 kcal./mole for benzene and 10.8 kcal./mole for *n*-hexane on this material. These are about 10 kcal./mole lower than the corresponding values on Na mordenite. This effect probably reflects the narrower intracrystalline channel system in mordenite.

Removal of the sodium ions from the mordenite structure to produce the so-called hydrogen form causes marked changes in the adsorptive properties. Instead of the rapid establishment of equilibrium observed on the Na form, a slow irreversible adsorption occurs which might be designated as chemisorption. In view of its known catalytic cracking activity at comparatively low temperatures (<350°),[6,7] it is possible that a small amount of cracking is occurring producing olefins which are subsequently adsorbed on the surface. This irreversibly adsorbed material can be removed, however, by heating to 370° and evacuating.

The fraction of surface remaining for reversible adsorption also has different properties than the Na form. First of all, the fraction decreases with increasing temperature, which indicates that more of the surface is becoming active in the chemisorption or cracking activity. Secondly, for the reversible adsorption on H mordenite, there is evidence that *n*-hexane has access to more surface than available to either benzene or cyclohexane. For example, with Na mordenite, the saturation values expressed in liq. cc./g. are independent of the nature of the hydrocarbon and temperature. With H mordenite, however, the volume of *n*-hexane reversibly adsorbed at saturation is higher at any given temperature than the corresponding values for either benzene or cyclohexane. Also, the heat of adsorption of *n*-hexane is 3–4 kcal./mole greater than the adsorption heats of the other hydrocarbons. One explanation for this can be based on molecular size. Since *n*-hexane has the smallest cross-sectional diameter, it could enter those cavities which occur periodically along the walls of the main adsorption tubes. Their volume per unit cell is represented by V_b in Fig. 1. Benzene and cyclohexane are too large to enter these side cavities.

The analysis of entropy indicates that the reversibly adsorbed hydrocarbons have more degrees of freedom of motion in H mordenite. This suggests that the removal of the sodium ions effectively leaves more space for motion in the intracrystalline channel system.

Acknowledgment.—The author wishes to express his sincere appreciation to Dr. Leo Broussard and Mr. C. N. Kimberlin for their helpful advice and encouragement in this work and also to Mr. Lloyd Bourgeois for the experimental measurements.

(9) P. E. Eberly, Jr., *J. Phys. Chem.*, **65**, 68 (1961).

THE HEAT OF SUBLIMATION OF CALCIUM CHLORIDE

BY RENATO G. BAUTISTA AND JOHN L. MARGRAVE

Departments of Chemistry, University of Wisconsin, Madison, Wisconsin, and Rice University, Houston, Texas

Received May 24, 1963

The heat of sublimation of $CaCl_2$ (crystal) as measured by the Langmuir free-evaporation technique is 75.9 kcal./mole on the assumption that the predominant vapor species is $CaCl_2(g)$. The average bond energy in $CaCl_2(g)$ is, then, ~107 kcal./mole, in contrast to a reported dissociation energy for CaCl(g) of 63.6 kcal./mole from band spectra. This latter value is undoubtedly incorrect, and $D_0^0(CaCl) = 80 \pm 10$ kcal./mole is estimated from recent electron diffraction data and an ionic model.

The sublimation pressure of $CaCl_2$ has been measured for a single crystal sample by the Langmuir free-evaporation technique. The only previous work was a single experimental pressure point included by von Wartenberg and Bosse[1] in their report on the vapor pressures of several halide salts. From this pressure point, Brewer, Somayajulu, and Brackett[2] estimated the heat of sublimation to be 71.5 kcal./mole.

Experimental

Apparatus and Techniques.—A microbalance built inside a vacuum system was used to follow the weight loss of the sample. The construction and operation of the beam microbalance has been described previously in detail.[3] The change in weight of the sample was obtained in terms of a change in voltage needed to bring the magnetically controlled balance back to the zero point. The sample and the tungsten wire holder were contained inside a glass envelope and were heated in a wire-wound tube furnace. A calibrated chromel–alumel thermocouple placed inside the glass envelope and near the sample was used for temperature measurement, and the pressure in the system was kept below 10^{-6} mm.

For increased accuracy, several measurements of the rate of weight loss of the sample at each temperature were made and the time-weighted average of all the weight loss readings was calcu-

(1) H. V. Wartenberg and O. Bosse, *Z. Elektrochem.*, **28**, 384 (1922).

(2) L. Brewer, G. Somayajulu, and E. Brackett, *Chem. Rev.*, **63**, 111 (1963).

(3) (a) L. H. Dreger and J. L. Margrave, *J. Phys. Chem.*, **64**, 1323 (1960); (b) G. D. Blue, J. W. Green, R. G. Bautista, and J. L. Margrave, *ibid.*, **67**, 877 (1963).

lated and reported as one pressure point. These points were fitted to a log P *vs.* $1/T$ equation with a Fortran program on a Control Data 1604 digital computer.

Discussion of Results

$CaCl_2(g)$ was assumed to be the only important vapor species. The free energy functions for both solid and gaseous $CaCl_2$ were taken from the compilation of Brewer, Somayajulu, and Brackett.[2]

In Table I are summarized the results of the experiments. The experimental result obtained by von Wartenberg and Bosse[1] is included for comparison. The third-law treatment of these data gives $\Delta H°_{298}$ = 75.9 ± 1.0 kcal./mole. A second-law least-square plot of log P *vs.* $1/T$ gives $\Delta H_R°$ = 77.3 ± 6.4 kcal./mole at T_{av} = 973°K. When this is corrected to 298°K. using the heat content values compiled by Kelley[4] and the molecular constants given by Brewer, Somayajulu, and Brackett,[2] the second-law method gives $\Delta H°_{298}$ = 80.2 ± 6.4 kcal./mole. Since the temperature range studied was only 41°, the agreement between the second- and third-law calculations is considered reasonable, and the third-law value is more reliable.

TABLE I

SUBLIMATION PRESSURE OF CALCIUM CHLORIDE

Point	T, °K.	P_{atm}	$\Delta H°_{298}$
1	986	6.35×10^{-9}	76.1
2	965	1.36×10^{-8}	73.1[a]
3	987	6.87×10^{-9}	76.0
4	993	1.06×10^{-8}	75.7
5	973	4.47×10^{-9}	75.8
6	982	7.30×10^{-9}	75.6
7	970	4.10×10^{-9}	75.8
8	952	1.73×10^{-9}	76.1
			75.9 ± 1.0 kcal./mole
9[b]	1819	8.16×10^{-2}	71.5

[a] Given zero weight. [b] Work of H. V. Wartenberg and O. Bosse.

(4) K. K. Kelley, U. S. Bur. Mines Bull. 584, 1960.

The atomization energy of $CaCl_2(g)$ was calculated to be 213.3 kcal./mole, based on the third-law heat of sublimation and other available thermochemical data.[5] Brewer, *et al.*,[2] estimated ΔH_{atom} = 218.6 kcal./mole. The average bond energy in CaCl is, then, 107 ± 1 kcal./mole.

Gaydon[6] has recommended $D_0°$(CaCl) as 63.6 kcal./mole with reservations, indicating that the poor linear Birge-Sponer extrapolation for the ground state favors a higher value. The binding energy of CaCl and internuclear distance have also been considered by Margrave,[7] based on an ionic model. The reported internuclear distance (1.86 Å.)[8] is quite short compared to other Ca molecules and one must put an uncertainty of ±40 kcal./mole on the dissociation energy. Akishin, *et al.*,[9] have reported the Ca–Cl distance in gaseous $CaCl_2$ to be 2.51 ± 0.03 Å. from high temperature electron diffraction studies and this yields $D_0°$(CaCl) = 80 ± 10 kcal./mole on the basis of an approximate ionic model calculation. Recent work on BeF, MgF, CaF, SrF, and BaF would suggest a still higher value for CaCl.[10]

Acknowledgments.—The authors are pleased to acknowledge the financial support of the National Science Foundation and of the United States Atomic Energy Commission.

(5) (a) D. R. Stull and G. C. Sinke, "Thermodynamic Properties of the Elements," Advances in Chemistry Series, No. 18, 1956; (b) F. D. Rossini, D. D. Wagman, W. H. Evans, S. Levine, and I. Jaffe, National Bureau of Standards Circular 500, 1952; (c) JANAF Interim Thermochemical Tables, edited by D. R. Stull, The Dow Chemical Co., Midland, Mich., 1961.

(6) A. G. Gaydon, "Dissociation Energies," Chapman and Hall, Ltd., 1953.

(7) J. L. Margrave, *J. Phys. Chem.*, **58**, 258 (1954).

(8) G. Herzberg, "Spectra of Diatomic Molecules," D. Van Nostrand Co., Inc., New York, N. Y., 1950.

(9) P. Akishin, private communication.

(10) (a) G. D. Blue, J. W. Green, R. G. Bautista, and J. L. Margrave, *J. Phys. Chem.*, **67**, 877 (1963); (b) G. D. Blue, J. W. Green, T. C. Ehlert, and J. L. Margrave, *Bull. Am. Phys. Soc.*, **8**, 112 (1963); (c) M. A. Greinbaum, J. N. Foster, M. L. Arin, and M. Farber, *J. Phys. Chem.*, **67**, 36 (1963).

MECHANICALLY INDUCED MOLECULAR REORIENTATION IN MULTIMOLECULAR FILMS[1,2]

BY L. S. BARTELL AND C. L. SUTULA

Contribution No. 1315 from the Institute for Atomic Research and Department of Chemistry, Iowa State University, Ames, Iowa

Received May 24, 1963

Multimolecular films of a variety of long-chain hydrocarbons and hydrocarbon derivatives were subjected to the shearing action of rubbing with soft tissue paper. If the effective total chain length (monomers of most substances, dimers of acids) exceeded 25–30 carbon atoms, the molecules were found by electron diffraction to fall over with their horizontal component parallel to the direction of rubbing. The molecular axes pointed upward against the direction of rubbing, forming an angle of several degrees with the plane of the surface. The angle was larger for orthorhombic packing than monoclinic, larger for short chains than for long. Chains shorter than the critical length were observed to disorder instead of reorienting regularly. Impurities often, but not always, interfered seriously with reorientation. Commercial paraffin wax, for example, completely resisted reorientation during the strongest shearing actions. The mechanism of the reorientation process is discussed. Measurements also were made of the rate of evaporation of the films as a function of chain length. It was found that molecules shorter than the critical length for reorienting were significantly more volatile than molecules exhibiting reorientation. Accordingly, the possibility is not ruled out that surface layers of molecules below the "critical length" are reoriented by shear but lost by evaporation into the vacuum chamber of the electron diffraction unit. For chains just under the critical length the thickness of such a superficial layer appears to be no greater than a molecular length.

In 1938, Finch[3] observed that molecules in multimolecular films of stearic acid could be reoriented by rubbing the films with filter paper. Before rubbing, the molecular chains were stacked together with molecular axes tilted away from the normal to the surface by 37°. The azimuths of independent clumps of molecules were random. After rubbing, the molecular chains were found to have been knocked over and swung around parallel to the direction of rubbing and nearly parallel to the surface. Unlike rubbed bristles in a brush, however, they pointed upward against the direction of rubbing, forming an angle of about 5° with the plane of the surface.

Following Finch's report, Germer and Storks[4] performed a detailed study of the effect of unidirectional rubbing on Langmuir–Blodget multimolecular films of stearic acid and barium stearate deposited upon metal surfaces. Multimolecular films of stearic acid were reoriented by the applied shear, as found by Finch, whereas multimolecular films of barium stearate resisted reorientation and suffered only slight disordering.

Brummage[5] has examined the effect of shear on multimolecular films of several long-chain *n*-hydrocarbons on surfaces of stainless steel and copper. Unidirectionally applied shear was observed to reorient only a small fraction of the molecules in these films.

In the course of investigating the structures of films of various *n*-hydrocarbon derivatives as described in an earlier paper[6] (hereafter referred to as I), it was observed that different derivatives of a given hydrocarbon radical exhibited markedly different responses to shearing forces. Therefore it was decided to study multimolecular films of a variety of long-chain derivatives to seek correlations between structure and mechanically induced molecular reorientation. An advantage over previous investigations was the availability of a convenient optical method permitting the optical thickness of the films to be followed routinely as a function of the treatment, to within a few per cent of a molecular length. The optical method also made it possible to study the rate of evaporation of the films, a factor which was found to be significant.

Experimental

The films were prepared by evaporating dilute solutions of long-chain *n*-hydrocarbon derivatives on carefully polished platinum and chromium surfaces, or by spreading the fused compounds over the metal substrates, as described in I. After a determination of the optical thickness of a given film, its initial structure and molecular orientation were examined by electron diffraction. The film was then subjected to the shearing of unidirectional polishing, and its thickness and structure were re-examined at intervals as the film was polished down. For the most part, unrubbed films were of the order of 1000 Å. Rubbed films were usually examined in the range of 300 to 50 Å., and often at several thinner stages down to the order of 10 Å.

The shear was applied with controlled pressure transmitted through several layers of soft lens or facial tissue mounted on a flat steel slider. The velocity of sliding was approximately 3 cm./sec., and pressures ranging from about 5–25 $\times$ 10^4 dynes/cm.^{2} were tested. Increasing the pressure fivefold increased the response of the film but it was not clear that the effect was as great as that of increasing the number of shearing strokes fivefold. In general, only a few strokes (1 to 3) were required to reduce a film from 1000 Å. to 100 Å. in thickness. Films rapidly became increasingly resistant to loss of material as optical thicknesses approached molecular lengths. Considerable variation from compound to compound was observed.

There can be no doubt that additives and natural waxes in the polishing tissues are a source of contamination in studies of such exceedingly thin films. Vigorous rubbing of freshly cleaned slides with soft tissues left a deposit which approached a limiting value of about 20 Å. after extensive rubbing. To minimize the introduction of foreign materials into the films during polishing, the tissue paper used was pretreated with a dilute benzene solution of the film material before polishing, and was used for only one rub. When films are polished down to 10 or 20 Å., it is uncertain how much contamination has been introduced. In a parallel study[7] with C^{14}-tagged octadecylamine, however, the amine radioactivity remained proportional to the total optical thickness down to submolecular thicknesses.

Optical thicknesses were measured with a polarization spectrometer, and structures by means of electron diffraction as described in I. The purity of compounds is discussed in I along with techniques of preparation of the metal surfaces.

(1) Work was performed in the Ames Laboratory of the U. S. Atomic Energy Commission; presented at the 135th National Meeting of the American Chemical Society, Boston, Massachusetts, April 6, 1959.

(2) Based on a dissertation by C. L. Sutula to the Graduate School, Iowa State University, in partial fulfillment of the requirements for the degree of Doctor of Philosophy, 1959.

(3) G. I. Finch, *J. Chem. Soc.*, 1137 (1938).

(4) L. H. Germer and K. H. Storks, *Phys. Rev.*, **55**, 648 (1939).

(5) K. G. Brummage, *Proc. Roy. Soc.* (London), **A188**, 414 (1947).

(6) C. L. Sutula and L. S. Bartell, *J. Phys. Chem.*, **66**, 1010 (1962).

(7) L. S. Bartell and J. F. Betts, *ibid.*, **64**, 1075 (1960).

TABLE I

OBSERVED ORIENTATIONS AND CRYSTAL FORM IN FILMS OF *n*-HYDROCARBON DERIVATIVES BEFORE AND AFTER APPLYING SHEAR

Compound	Unrubbed film: α, deg.	Unrubbed film: Crystal form	Rubbed film: α, deg.	Rubbed film: Crystal form	Pattern type
Stearic acid	52	Monoclinic, C	3–8	Monoclinic, C	II
Arachidic acid	51–52	Monoclinic, C	2–3	Monoclinic, C	II
n-Heptadecanoic acid	70	Possibly triclinic	5–6	Possibly triclinic	II
Palmitic acid	51–53	Monoclinic, C	4–9	Monoclinic, C	II
Isostearic acid	45–50	Possibly triclinic	2–5	Possibly triclinic	II
Isopalmitic acid	55	Possibly triclinic	4–7	Possibly triclinic	II
Lauric acid	(?)	(?)	....	Disordered film	I
n-Octadecane	90	Orthorhombic	Random	Disordered film	I
n-Eicosane	90	Orthorhombic	Random	Disordered film	I
n-Docosane	...	Triclinic	Random	Disordered film	I
n-Triccsane	90	Orthorhombic	Random	Disordered film	I
n-Hexacosane	52	Monoclinic	4–6	Monoclinic	II
n-Heptacosane	90	Orthorhombic	12–14	Orthorhombic	II
n-Octacosane	52	Monoclinic	3–4	Monoclinic	II
n-Nonacosane	90	Orthorhombic	10–11	Orthorhombic	II
n-Triacontane	32	Monoclinic	3–6	Monoclinic	II
n-Hentriacontane	90	Orthorhombic	3–10	Orthorhombic	II
n-Dotriacontane (impure)	90	Orthorhombic	90 and 3	Orthorhombic (partially reoriented)	III
n-Octadecyl stearate	52	Monoclinic	0–6	Monoclinic	II
n-Hexadecyl stearate	52	Monoclinic	0–5	Monoclinic	II
n-Dodecyl laurate	60	Monoclinic	Random	Disordered film	I
n-Octadecyl alcohol	90	Orthorhombic	Random	Disordered film	I
n-Stearamide (impure)	70	.....	....	.....	III
Paraffin wax	90	Orthorhombic	90	Orthorhombic	III

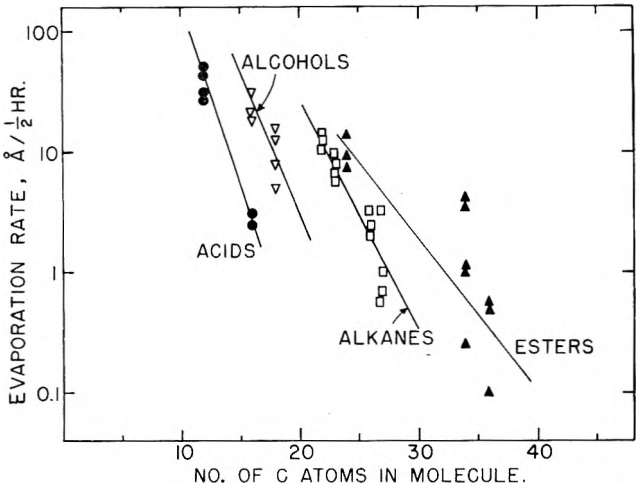

Fig. 1.—Dependence of evaporation rate on chain length of compounds in films 40–100 Å. thick.

Results

Reorientation.—Molecules of many of the substances studied underwent a profound reorientation when subjected to shear. By the time a susceptible film of a pure material had been polished down by several hundred angstrom units its reorientation, in the upper layers at least, was virtually complete. In the case of some impure natural waxes with very long chain lengths, a few light strokes often induced both disorder and some ordered reorientation. In these cases, perfection of packing in reoriented layers often improved substantially with hard polishing.

The diffraction patterns of rubbed films could be classified conveniently into three types. Type I corresponded to films which were appreciably disoriented by applied shear. Type II corresponded to films which were quite thoroughly reoriented by shear, at least in the superficial layers penetrated by the electron beam. Type III corresponded to films which were reoriented only partially or not at all by the shearing force.

The molecular orientations in multimolecular films before and after applying a unidirectional shearing force were generally readily evident from the layer lines of the diffraction patterns. The angle between the long axis of the molecules and the plane of the substrate surface is designated by α in the tabulated results. The molecules in the multimolecular films were aggregated into submicroscopic crystallites for which it was often possible to determine lattice parameters. Lattice parameters were compared whenever possible with X-ray and electron diffraction results reported for bulk crystals of the same or closely related compounds. In this way the molecular packing in the films could be related to the known polymorphic forms of the bulk crystals. The molecular packing and response of the substances to shear are indicated in Table I.

Evaporation Rates.—Rates of evaporation of films were measured in a vacuum desiccator at a pressure of about 10^{-3} torr. This pressure, while a rather poor vacuum, roughly duplicated that enountered in diffraction studies during the greater part of the exposure of the slides to a vacuum in the electron diffraction apparatus. The results for films ranging in thickness from about 100 to 40 Å. are plotted in Fig. 1 in terms of the thickness evaporated in 30-min. intervals (approximately the time required to pump and operate the diffraction apparatus). Not indicated in Fig. 1 is the observation that the rate of evaporation always dropped markedly when the film approached a thickness of one or two molecular lengths.

The scatter of data points was considerable in the runs, owing in part to the great difficulty in preparing the exceedingly thin films required with a sufficient uniformity of thickness. Nevertheless, fairly definite trends appear to be established, as shown in Fig. 1.

The evaporation rates were two or three orders of magnitude slower than the maximum rates calculated according to kinetic theory. It is judicious to regard them, then, as characteristic of particular experimental conditions and not as absolute rates relevant for any system.

Discussion

Comparison with Other Results; Effects of Impurities.—Brummage has obtained diffraction patterns of type III from rubbed multimolecular films of *n*-triacontane and *n*-tetracontane. In his work only a small proportion of the molecules reoriented, but those which did were observed to pack in aggregates with chains inclined to the surface by about 3°, pointed upward against the direction of rubbing. Brummage attributed this orientation to crystallization with 201 planes parallel to the surface. He suggested that rubbing caused local melting, followed by crystallization with random azimuths and 201 orientations, preferred for crystallographic reasons. Further rubbing, he reasoned, preferentially removed 201 crystallites unless their azimuths were against the rubbing direction.

In the present investigation the fraction of long-chain hydrocarbon molecules that reoriented was much greater than observed by Brummage, provided the compounds were pure. In fact, with rubbed films several molecular layers in thickness or thinner, the reorientation was often essentially complete, with no evidence of the 00*l* orientation remaining. It is probable that Brummage made his observations on films which were impure, as discussed in I, for the molecular packing before shear was not that characteristic of the pure compounds. An incomplete response to rubbing similar to that found by Brummage was noted in the present study with films of impure palmitic acid, impure octacosane, and impure dotriacontane. Also, commercial paraffin wax which contains a wide distribution of chain lengths and a few branched chains was found to be exceedingly immune to effects of shear. It remained in a well ordered, vertical, orthorhombic packing throughout the most vigorous rubbing treatments, retaining this orientation even when the average film thickness was decreased below one molecular length.[8]

Another fact casting doubt on Brummage's interpretation is that the angles of inclination of the orthorhombically packed molecules which tipped over in the present study were several degrees larger than the angles implied by a 201 orientation. The present patterns (type II instead of type III) made the determination of the angles much more direct than was possible in Brummage's work. Nevertheless, despite the close correlation between observed and crystallographic angles reported in paper I for unrubbed films, it must be admitted that the relationship between observed angles of molecular objects and planes of macro objects remains speculative. Perhaps rubbing caused a disproportionate accumulation of material on the leeward (downhill) slopes of surface asperities, biasing the observed slope. In any event, we are inclined to regard the mechanism of the reorientation more as a direct consequence of plastic flow under shear than as a random recrystallization from local melting, followed by preferential wiping away of crystallites.

Effect of Chain Length.—Whether a multimolecular film of a particular *n*-hydrocarbon derivative was found by electron diffraction to be disordered or reoriented orderly by shear depended largely on its chain length. In the saturated *n*-hydrocarbon series, films of compounds containing less than 24 carbon atoms were disoriented by shear. Films of *n*-hexacosane, however, were regularly reoriented by a shearing force. The critical chain length for the reorientation appears to occur in this series at 25 or 26 carbon atoms at room temperature. It is possible that the critical length depends on temperature, perhaps increasing as the temperature increases.

Films of lauric acid, which were difficult to study by electron diffraction, seemed disordered by shear, whereas films of palmitic acid were reoriented by shear. Because the *n*-aliphatic acids pack as dimers in their crystals, films of the *n*-aliphatic acids can be seen to change in their response to shear at an effective chain length only slightly greater than that of *n*-hydrocarbons. Quite analogously, in films of the long-chain esters, *n*-dodecyl laurate disordered, whereas films of *n*-hexadecyl stearate and *n*-octadecyl stearate reoriented readily. It is not implausible that a somewhat shorter length suffices in the reorientation of a uniform chain like a hydrocarbon than for a bumpy derivative like an acid dimer or ester.

The data for other types of *n*-hydrocarbon derivatives are less complete. Films of *n*-octadecyl alcohol were rapidly disordered by shear. Films of mellisyl alcohol (C_{31}), however, have been reoriented by shear.[9] It is probable that the critical length for alcohols and many α-substituted derivatives where dimerization is weak or absent, is similar to that for *n*-hydrocarbons.

It is tempting to conclude that shear-induced reorientation is a simple mechanical property related to molecular chain length. While there undoubtedly is a certain validity in this view, it is not definitely established that the electron diffraction "critical length" for reorientation is directly correlated with this property. The "critical length" for reorientation of molecules in the present study is uncomfortably close to the molecular length at which evaporation rates are 10 to 30 Å./hr. Longer molecules have trivial rates insofar as the present experiments are concerned but shorter molecules have rates which might seriously deplete a reoriented surface layer, if one were formed. Consequently, the possibility is not ruled out that surface layers of molecules below the "critical length" are reoriented by shear but lost by evaporation into the vacuum chamber of the electron diffraction unit. Lauric acid, in particular, beyond its firmly adsorbed base layer, is certainly too volatile for its reorientation to be definitively studied in the apparatus of the present work. On the other hand, for molecules just shorter than the critical length, the layer evaporated is appreciably thinner, according to Fig. 1, than the completely reoriented layers in films of longer molecules. Moreover, barium stearate, which was observed to re-

(8) The presence of impurities or inhomogeneity of chain length does not necessarily prevent reorientation. Virtually complete reorientation with striking perfection of packing was observed for several natural waxes consisting of mixtures of many compounds. Nevertheless, in these cases a greater amount of buffing was necessary to achieve complete ordering. The principal components of these films, however, had chains perhaps 20 carbons longer than those in paraffin wax.

(9) J. V. Sanders and D. Tabor, *Proc. Roy. Soc.* (London), **A204**, 525 (1951).

sist reorientation in an earlier study,[4] is essentially nonvolatile. Therefore, the "critical length" may be more than an artefact of evaporation rates.

Other significant structural features emerged from the study. As a rule the angle α was greater in reoriented films for orthorhombic packing than for monoclinic. It was also observed that, for a given type of packing, the longer molecules in a homologous series tended to lie flatter. The orientation of the short axes of the essentially crystalline arrays in the reoriented films was usually far less definite than that of the long axes. The range of angles of the a and b axes with respect to the plane of the substrate seemed to narrow as the chain length increased. Preferred orientation of the a axis of some of the shorter chains was scarcely discernible (*e.g.*, C_{26} hydrocarbon). Stearic acid, effectively longer than C_{36}, exhibited a strong tendency to orient its a axis parallel to the surface. Nevertheless, reflections observed when the beam was parallel to the chains revealed a distribution of a orientations over a range of 35°. Certain very long chain natural waxes, in films 40 Å. thick, packed with astonishingly well defined directions of short axes. Twinning was observed in these cases, however, associated with the pseudohexagonal packing often enountered with long chain compounds[5] in which the a axis may take on any of three orientations differing by 120°.

Considerations of Mechanism of Reorientation.—It is worthwhile to illustrate the stresses to which the system is subjected with a few rough order-of-magnitude calculations. Let us consider a film of intermediate thickness encountered in this work, 300 Å., with a coefficient of friction of, say, ~0.1. For a slider 5 cm. long with the lightest pressure used (5×10^4 dynes/cm.^{2}), the energy dissipated in one rubbing stroke would be $0.1 \times 5 \times 5 \times 10^4 = 2500$ ergs/cm.^{2} or 70 kcal./mole of film (800 kcal./mole of surface molecules). The work of cohesion ($2\gamma A$) of a surface of methyl groups is of the order of 50 ergs/cm.^{2}. Clearly, the input energy per stroke is sufficient to influence the molecules profoundly if fully utilized. On the other hand, the rate of input of energy is so low that the mean temperature rise calculated from the thermal conductivity is less than 10^{-4} deg./sec.[10] Therefore, melting could not occur uniformly over the entire surface of the film but only, at most, at points of adhesional contact in the friction process. Even at these localized spots the energy would be quickly dissipated.[11] The temperature rise of such contacts can be computed using various models discussed by Bowden and Tabor.[12] It is found that the most extreme choices of models and estimates of asperity sizes lead to calculated temperature rises far too low to cause local melting, if films are assumed to be uniform in thickness. This is due to the relative mildness, as frictional processes go, of the surface treatment in which the low values of the applied pressure, sliding velocity, coefficient of friction, and yield pressure of the organic materials minimize the heating. It is possible, nevertheless, that appreciable local temperature rises occur in those few spots where the tissue fibers contact the metal slide directly.

Although thermal effects seem small, the mechanical stress is considerable. According to the work of Bowden and Tabor[13] on friction, plastic deformation occurs at contacts of asperities and continues until the area of real contact reaches the area that would theoretically support the load at the pressure associated with the commencement of plastic flow. In the present problem such a flow presumably occurs in films which are not too thin, although a significant fraction of the load at low film thicknesses may be borne by tissue fiber deformation on thinly covered metal asperities. The shear rates met in the flow process are enormous despite the low sliding velocity, because the velocity gradient in the highly non-Newtonian flow must occur over a thickness of not many molecular lengths. The shear rate, assuming a shear across one molecular length, would be over 10^7 sec.$^{-1}$. This would lead to an orientation of the anisotropic molecules in the viscous medium somewhat analgous to, but more complete than that occurring in streaming birefringence experiments.[14]

These foregoing considerations make it simpler to understand the molecular reorientations in terms of an ordered plastic flow rather than Brummage's melting mechanism. Moreover, the work of Tabor, *et al.*,[15] indicates that simple melting and recrystallization do not lead spontaneously to the 201 orientation required by the melting theory. It is also clear that the reorientation is more than a simple rotation of microcrystals, since multilayers are sometimes observed to transform during reorientation from one crystal form to another, as A to C in the case of stearic acid.[4]

The most definitive generalization to be drawn from the present investigation is the dependency of the observed reorientation on the effective length of the chains and on the presence of impurities. A more detailed study of the mechanism of reorientation would be helpful in clarifying the role of evaporation, and might prove fruitful in casting light on other problems, as rheological properties of polymers.

Acknowledgments.—We are pleased to acknowledge the assistance of Mr. R. R. Roskos in measurements of rates of evaporation. We are deeply indebted to Dr. A. E. Smith and the Shell Development Co. for samples of a series of extremely pure n-hydrocarbons, and to Dr. M. Senkus and the R. J. Reynolds Tobacco Co. for a sample of pure n-hentriacontane. We should also like to acknowledge support from the American Petroleum Institute in the early phases of this investigation.

(10) This assumes all energy is degraded into heat and that the metal slide is an infinite sink.

(11) The calculated half-life of cooling is of the order of 10^{-10} sec. for a disturbed region 100 Å. thick.

(12) F. P. Bowden and D. Tabor, "The Friction and Lubrication of Solids," Oxford University Press, London, 1950.

(13) F. P. Bowden and D. Tabor, "Friction and Lubrication," Methuen and Co., Ltd., London, 1956.

(14) J. T. Edsall, "Advances in Colloid Science," Vol. I, Interscience Publishers, Inc., New York, N. Y., 1942, p. 269.

(15) J. W. Mentor and D. Tabor, *Proc. Roy. Soc.* (London), **A204**, 514 (1951); J. V. Sanders and D. Tabor, *ibid.*, **A204**, 525 (1951).

THE ROLE OF FILTRATION IN INVESTIGATING FLOCCULATION AND REDISPERSION OF COLLOIDAL DISPERSIONS

BY VICTOR K. LA MER AND THOMAS W. HEALY

Departments of Mineral Engineering and Chemistry, Columbia University, New York 27, New York

Received May 25, 1963

The state of flocculation and redispersion of colloidal systems may be followed by measurements of turbidity, rate of subsidence, sediment volume, or rate of filtration. Filtration has proven to be the most quantitative method and can now be interpreted in terms of basic theory. The adsorption process upon which the theory depends has been examined quantitatively, and its relation to Langmuir's isotherm is discussed. Evidence is presented that the terms coagulation and flocculation do not represent identical concepts or mechanisms. They should be distinguished; criteria for their distinction are given on the bases of theory and of observation.

Introduction

When high molecular weight natural or synthetic polymers are added to colloidal dispersions of solids in liquids, they frequently induce, over limited ranges of concentrations, a dramatic flocculation of the dispersion. As the concentration of the polymer is increased, the successive changes of state from dispersed to flocculated to redispersed may be followed by measurements of turbidity, rate of subsidence, or rate of filtration of the flocculated suspensions.

La Mer and co-workers,[1] in an extensive study of this subject, have found that measurements of the refiltration rate offer a means of characterizing quantitatively the state of flocculation. The technique is simple, and the data can be reproduced with surprisingly high precision under controlled conditions. For the flocculated state, the rate of refiltration through a cake approaches a maximum value, whereas for the dispersed state it is a minimum. Filtration rate measurements are of particular value in characterizing the state of flocculated systems, since they take cognizance of the presence of both the large flocs which yield large pores and the incompletely flocculated material called "haze" which obstructs the pores.

The theory of Smellie and La Mer[2] utilizes a limiting form of the Kozeny–Carman equation for filtration through a porous bed to correlate filtration rate (*i.e.*, the measure of extent of flocculation) with the concentration of added polymer. In this form of the equation only the geometry of flocs and pores are involved. The predictions of the filtration theory have been verified for many polymer–solid systems.[2-4]

Recently, Healy and La Mer[5] modified the theory by incorporating molecular parameters for the solid surface and the polymer molecule in the original adsorption equations. It was shown that the optimum polymer concentration P_m, *i.e.*, that concentration which produces the maximum filtration rate for a given system, is given by

$$P_m = (1 + b\dot{k}/\beta)^2/b \qquad (1)$$

Here β is the number of segments of an adsorbed molecule that cover surface sites, and b is the ratio of rate constants for adsorption–desorption of segments at the surface. k is given by

$$k = \frac{sS_0}{N} \qquad (2)$$

where s is the number of adsorption sites per unit area, S_0 is the specific surface area, and N is Avogadro's number.

With the aid of eq. 1 and other equations of the flocculation theory,[2-4] it is now possible to give a more detailed analysis of the reactions occurring between the polymer molecules and the dispersed colloid.

For further details the reader is referred to a recent comprehensive review of the literature pertaining to both polymer adsorption and polymer flocculation.[5]

Theory

In their initial presentation, Smellie and La Mer[2] proposed that adsorption of the polymer at the solid–liquid interface be described by an adsorption equation of the form of Langmuir's, *viz.*

$$\frac{\theta}{1 - \theta} = bP \qquad (3)$$

where θ is the fraction of surface covered, P is the residual polymer concentration (in moles of polymer/g. of solid), and b is an adsorption constant, defined as the ratio of adsorption–desorption rate constants for the reaction of the adsorbing species with the solid surface.

We have shown previously (eq. 1, ref. 3) that

$$P = P_0 - k\theta/\beta \qquad (4)$$

where P_0 is the added or initial concentration of polymer. Combining eq. 3 and 4 and rearranging

$$\frac{P}{P_0 - P} = \frac{\beta P}{k} + \frac{\beta}{kb} \qquad (5)$$

where, as before, k is defined by eq. 2. Plots of eq. 5 are linear from which values of β/k and b have been obtained for each molecular weight and time of agitation. Substitution of these values in eq. 1 gives values of P_m which have been designated as P_m (adsorption).

The filtration theory of Smellie and La Mer, and the modified theory also, yields as a final equation

$$\frac{P_0^{1/2}}{(Q - Q_0)^{1/2}} = A_m + B_m P_0 \qquad (6)$$

where Q_0 is the measured filtration rate of the dispersion in the absence of added polymer, and Q is the filtration

(1) V. K. La Mer and R. H. Smellie, Jr., *J. Colloid Sci.*, **11**, 704, 710, 720 (1956); **13**, 589 (1958); V. K. La Mer, R. H. Smellie, Jr., and P. K. Lee, *ibid.*, **12**, 230, 566 (1957). A summary of this work appears as a chapter in "Clays and Clay Minerals," Vol. 9, Pergamon Press, New York, N. Y., 1961, p. 295.

(2) R. H. Smellie, Jr., and V. K. La Mer, *J. Colloid Sci.*, **13**, 589 (1958).

(3) T. W. Healy and V. K. La Mer, *J. Phys. Chem.*, **66**, 1835 (1962).

(4) J. C. Kane, V. K. La Mer, and H. B. Linford, *ibid.*, **67**, 1977 (1963).

(5) V. K. La Mer and T. W. Healy, *Rev. Pure Appl. Chem.*, in press.

rate for added polymer. We have shown previously[3] the refiltration rate–polymer concentration curves for the present system. They exhibit the sharp maximum in refiltration rate at a polymer concentration $P_0 = P_m$, where P_m is the optimum polymer concentration for a given set of conditions. From eq. 6 it has been shown[2,3,5] that P_m is related to the constants A_m and B_m by

$$P_m = A_m/B_m \qquad (7)$$

Experimental

The vacuum filtration assembly used in this investigation was in principle the same as used by previous workers in these Laboratories.[1] A complete description is given by Healy[6] and more recently by Kane, La Mer, and Linford.[4] A new technique of mixing the polymer solution with the suspension, agitation of the suspension, and filtration was developed, such that identical suspensions did not differ in filtration rate by more than 3%. Agitation of the suspension was carried out with a magnetic stirrer assembly set at a fixed degree of intensity for all the results reported.

Fresh calcium phosphate suspensions of 3% by weight of solids in distilled water were used to obtain each individual filtration rate. The calcium phosphate (tribasic) was Fisher A.R. grade reagent and the particles had an average radius of approximately 10 μ.

We are indebted to the American Cyanamid Co. for furnishing samples of polyacrylamide having the molecular weights 0.5, 1.0, 3.0, and 5.3 million, determined by viscosity measurements.

Results

Plots of $P_0^{1/2}(Q - Q_0)^{1/8}$ *vs.* P_0 for calcium phosphate polyacrylamide which are linear in accordance with eq. 6 lead to values of P_m calculated from eq. 7 that are designated as P_m (filtration).

Three forms of presentation of the values of P_m are shown in Tables I, II, and III; *viz.*, (1) experimental, *i.e.*, P_m (exptl.), obtained directly from a graphical determination of the maximum in $(Q - Q_0)$ *vs.* P_0 plots; (2) filtration theory, *i.e.*, P_m (filt.), obtained from the ratio of intercept to slope of linear plots of eq. 6 through eq. 7; (3) adsorption, *i.e.*, P_m (ads.), obtained by substitution of β/k and b from adsorption data in eq. 1. In this case P_m, the polymer concentration that ensures maximum flocculation, is obtained with the aid of the bridging model and the flocculation theory from adsorption experiments alone.

TABLE I

P_m VALUES OBTAINED FROM Q *vs.* Q_0 PLOTS, *i.e.*, P_m (EXPERIMENTAL)

Mol. wt., millions	Time of agitation, min. 2	5	10
0.5	160 ± 40	68.0 ± 1.0	160 ± 5
1.0	31 ± 2	21.5 ± 1.0	25 ± 1
3.0	4.5 ± 0.3	7.3 ± 0.3	8.5 ± 0.2
5.3	1.1 ± 0.1	1.0 ± 0.1	2.9 ± 0.1

TABLE II

P_m (10^{10} MOLES/G.) VALUES OBTAINED FROM FILTRATION EQUATIONS, *i.e.*, P_m (FILTRATION)

Mol. wt., millions	Time of agitation, min. 2	5	10
0.5	101.5	62.6	148.8
1.0	27.3	16.0	25.5
3.0	2.9	11.8	8.5
5.3	1.3	4.74	2.6

In general, the agreement among these three sets of data is acceptable. The principal discrepancy is that the P_m results for adsorption at 3–10 times larger than the values of P_m (exptl.) and P_m (filt.). This discrepancy is probably due to the fact that the surface area per gram of solid calcium phosphate used in the present work was greater than that for the sample used by Jankovics[7] for his adsorption studies. This means that the term bk/β of eq. 1 should be replaced by $bk/x\beta$, where x is the ratio of the surface areas of the two investigations.[6,7] The exact value of x is at present unknown. With this in mind, the P_m (ads.) appears to be in satisfactory agreement with the independent filtration experiments, especially with respect to molecular weight dependence for a given time of agitation. Substitution of β/k and b values obtained from eq. 5 in eq. 1, predicts that for a molecular weight increase from 1 to 5.3 million, P_m should decrease by 94.2–95.8% depending on time of agitation; this is to be compared with the experimentally observed decrease of 88.4–96.5% again depending on the time of agitation.[6] In assessing these results it should be recognized that P_m (ads.) values have been calculated solely from a determination of the adsorption isotherm and do not involve any measurement of the filtration rate. This confirms the validity and usefulness of the basic theory.

TABLE III

P_m (10^{10} MOLES/G.) VALUES OBTAINED FROM ADSORPTION DATA, *i.e.*, P_m (ADSORPTION)

Mol. wt., millions	Time of agitation, min. 2	5	10
0.5	264.5	...	...
1.0	91.2	183.5	379
3.0	13.3	24.0	48.2
5.3	5.34	8.0	16.4

The derivation of eq. 6 for filtration rate shows that the extent of flocculation for any given concentration of added polymer depends upon the factor $\theta(1 - \theta)$. This factor is the product of the fraction of surface sites covered and the fraction uncovered. It is the mathematical representation of the bridging theory of polymer flocculation.[2,5]

Bridging occurs between solid particles whose surface is partially covered by polymer, and particles with partially uncovered surface. Segments of the polymer molecule that extend out from the surface of the solid bridge onto an uncovered surface of an adjacent particle. The Smoluchowski treatment of *rate of coagulation* leads to a rate that is proportional to n_0^2 where the dispersion contains n_0 primary particles on the other hand, the Smellie–La Mer treatment of the *rate of flocculation* leads to a rate equation that is proportional to $n_0^2\theta(1 - \theta)$. This latter rate is therefore an extension of the Smoluchowski coagulation theory to systems where *flocculation* is induced by the bridging action of polymers.

The adsorption data have been collected in schematic form in Fig. 1 to illustrate the region where maximum flocculation is observed.

The Flocculation Process.—The following model is proposed. Polymer molecules adsorb at a fraction β/τ of the total segments per molecule. The remaining segments protrude out from the interface and can attach to the uncovered surface on an adjacent solid

(6) T. W. Healy, Ph.D. dissertation, Columbia University, 1963.

(7) L. Jankovics, Ph.D. dissertation, Columbia University, 1961.

particle. A floc built up in this fashion consists of solid particles held together loosely by polymer bridges.

The requirements for flocculation are: (a) that extended segments of polymer are available; (b) that they are of sufficient length and number; (c) that an uncovered surface for bridge sites is available.

A flocculated system becomes dispersed if: (d) the surface becomes so covered that there is insufficient uncovered surface for bridging (e) if the extended segment bridges are so long as to be unable to withstand the thermal motion of individual particles in the floc; (f) the extended segments physically interfere with one another to prevent bridge formation; (g) if agitation is sufficiently intense.

Our theory of polymer flocculation[2] which employs the bridging model leads to the conclusion that maximum flocculation occurs at a coverage of surface sites by polymer at a value of θ equal to one-half. The extent to which this prediction is verified by the adsorption and filtration studies is shown schematically in Fig. 1. All isotherms are of this type. In the foregoing discussion and in Fig. 1, the assumption is made that the onset of the plateau region of the isotherm corresponds to full coverage of those surface sites that were originally available to polymer molecules.

This may be restated as follows. Initially, a polymer molecule in solution has available a certain number of surface sites. Adsorption of polymer molecules continues until an incoming molecule has available less than the critical number of sites required for attachment. This is the plateau region of the isotherm for which we have defined $\theta = 1$. The concept that for a polymer molecule to remain attached at a surface it must be attached by a critical number of segments was suggested by Healy[8] to explain the effect of intensity of agitation on the amount of polyacrylamide adsorbed on silica powders.

Coagulation *vs.* Flocculation.—On Fig. 1 we have represented the region over which maximum flocculation, as measured by the refiltration rate, is observed. It occurs around $\theta = 0.5$ as predicted by the Smellie–La Mer flocculation theory. This verification of the theory substantiates further our basic proposal that *flocculation* occurs between classes of particles represented by the numbers $(n_0\theta)$ and $[n_0(1 - \theta)]$. *Coagulation* occurs between the classes of particles represented by the numbers n_0 and n_0 in the Smoluchowski equation.

The correction factor $[\theta(1 - \theta)]$ to the simple Smoluchowski equation of coagulation is the key to our distinction between these two terms and their mechanisms. This factor appears as $[\theta^4(1 - \theta)^4]$ in the filtration form of the equation which has now been verified for five separate systems.

Based on these and other findings, we deplore the indiscriminate use of the terms coagulation and flocculation which is to be found in textbooks as representing identical or at least synonymous concepts. A clear distinction is vital to understanding the series of six papers entitled "Flocculation, Subsidence and Filtration of Colloidal Dispersion,"[1] which treat the behavior of colloidal dispersions flocculated by high polymeric molecules—often called still more loosely "coagulant aids."

We propose that coagulation be used for the general

(8) T. W. Healy, *J. Colloid Sci.*, **16**, 609 (1961).

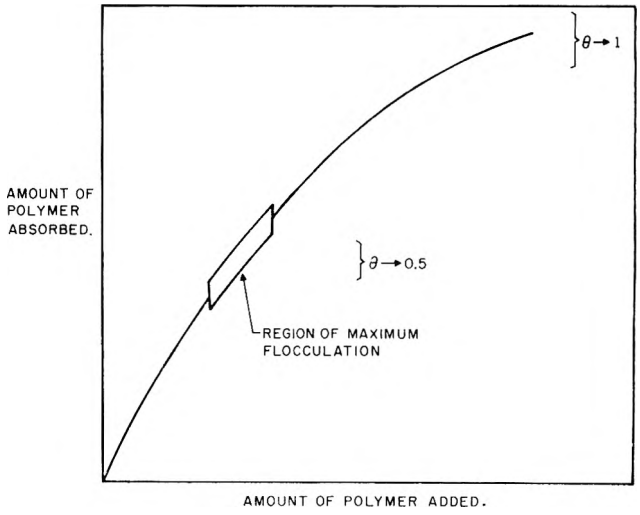

Figure 1.

kinetic process obeying the simple Smoluchowski equation independent of θ, whereby colloidal particles are united (*L. coagulare*—to be driven together) as typified by the effects of electrolytes upon gold sols. Coagulation is brought about primarily by a reduction of the repulsive potential of the electrical double layer in accordance with the ideas advanced by Derjaguin, Landau, Verwey, and Overbeek.

We propose that the term flocculation should be restricted more in accordance with original usage corresponding to the latin meaning of "floc" (*L. flocculus*—a small tuft of wool or a loosely fibrous structure).

Flocculation is usually brought about by the action of high molecular weight materials (potato starch and polyelectrolyte in general) acting as linear polymers which bridge and unite the solid particles of the dispersion into a random structure which is three dimensional, loose, and porous.

On the other hand, we have found that the action of simple neutral salts ($CaCl_2$, $Ca(OH)_2$ *on the same suspensions* generally yields a "coagulum"[1] of small sediment volume, which filters very poorly compared to the product resulting from flocculation by polyelectrolytes where the final volume is larger and exhibits a greatly enhanced rate of refiltration—as much as 200-fold in certain instances.

When a dilute colloidal dispersion is coagulated, the individual particles *sediment* as independent units obeying as a *limiting law* the well known law of Stokes, thus yielding an atmosphere of settling particles distributed according to size of particle. On the other hand, when the same dispersion is flocculated, there is a transient period in which the particles sediment more or less according to Stokes' law. As soon as the bridging becomes effective, a sharp subsidence line appears and the entire solid content of the cylinder settles by a uniform compression of the flocs to final volume which is generally larger than that for the coagulated sediment volume.

It has been shown previously (ref. 1, p. 720) that for *well flocculated dispersions of high solid content* an entirely different law of settling prevails for which we find the simple equation

$$t/(h - h_0) = \alpha + \beta t \qquad (8)$$

to be valid (t = time; h = height of subsidence line in the cylinder; α and β are constant).

Equation 8 appears to be the *limiting law* of subsidence, as opposed to Stokes' law which is the limiting law of sedimentation. In many practical cases the system settles as a compromise between eq. 8 and Stokes' law.

Attention is also directed toward the simple relation (ref. 1, p. 716) we have found for well flocculated dispersions, namely, that the square of the rate of subsidence is linearly related over a wide range of the variables to the fourth power of the filtration rate. The explanation is that the latter rate is governed by the fourth power of the radius of the pores of the filter cake (Poiseulle's law).

We also find that flocculation (or the bridging mechanism) is in general far less dependent upon the electrical charge interactions of the polymer–solid system than is the case with coagulation of hydrophobic colloids where the mechanism is given by the Derjaguin–Landau–Verwey–Overbeek (D-L-V-O) electrostatic theory. We have obtained, uniformly, our most striking examples of flocculation by employing high polymers of net negative charge, like the hydrolyzed polycarylamides, acting upon dispersed particles (clays, phosphates, silica, etc.) which are also almost invariably negatively charged.

In the five systems in which the polymer and the solid have been varied and the filtration rate studied quantitatively, we have uniformly found that these rates obey a law dependent upon $\theta^4(1-\theta)^4$, where θ is the fraction of the surface covered by polymer and $(1-\theta)$ is the uncovered fraction. We believe that conformity with the $[\theta^4(1-\theta)^4]$ law will be the unique characteristic that distinguishes flocculated systems.

We recognize that some systems will aggregate by a mechanism which is intermediate between those we have defined for flocculation and coagulation. The interaction of transition metal ion complexes with AgI sols is difficult to classify. On the basis of experiments now in progress, it appears that the coagulation produced by aluminum salts, as in water purification, will ultimately prove to be the interaction of the *linear polymer* resulting from the hydrolysis of Al(III)[9–11] with the particles of the dispersion; in other words, a form of the flocculation mechanism in which the inorganic aluminum polymer performs the bridging function.

(9) A. W. Thomas, "Colloid Chemistry," McGraw-Hill Book Co., Inc., New York, N. Y., 1934, Chapter 7; *Paper Trade J.* (Feb. 28, 1935).
(10) L. Pokras, *J. Chem. Educ.*, **33**, 152 (1956).
(11) W. Stumm and J. J. Morgan, *J. Am. Water Works Assoc.*, **54**, 971 (1962).

THERMODYNAMIC PROPERTIES OF AQUEOUS SOLUTIONS OF MIXED ELECTROLYTES: THE HYDROCHLORIC ACID–SODIUM CHLORIDE SYSTEM FROM 40 TO 0°

By J. H. Stern and A. A. Passchier

Department of Chemistry, Long Beach State College, Long Beach 4, California

Received May 25, 1963

Heats of mixing of solutions of HCl and NaCl at a total molality of 1, 2, and 3 were determined microcalorimetrically at 40, 25, 10, and 0° and fitted to an equation based on Harned's rule. The results are discussed in relation to deviations from the Bronsted–Guggenheim theory of specific interaction and are contrasted with some estimated heats based on electromotive force studies. Calculated excess free energies and entropies of mixing also are given.

I. Introduction

The thermodynamic studies of aqueous strong electrolytes have dealt mainly with the properties of solutions containing a single strong electrolyte. Although the interactions governing the equilibrium and transport properties of hydrated ionic solutions are quite complex, good theoretical support has been possible for a large body of experimental results.[1]

Mixed electrolytes present a more complicated problem, especially since there is a lack of data for testing and supplementing existing theories. This is particularly true in the case of excess heats, entropies, and free energies of mixing. These are significant criteria in examining the change in interactions which occur as a result of the mixing process in the absence of chemical reactions.

We shall define the excess free energy of mixing solutions of two electrolytes ΔF_M^E by the relation

$$\Delta F_M^E = \Delta F_M - \Delta F_M^i \qquad (1)$$

(1) H. S. Harned and B. B. Owen, "The Physical Chemistry of Electrolytic Solutions," 3d Ed., Reinhold Publishing Corp., New York, N. Y., 1958.

where ΔF_M and ΔF_M^i are the total and ideal free energy changes, respectively, when the mixture is formed from its component solutions at constant total molality, temperature, and pressure.

The excess heat of mixing ΔH_M^E is defined similarly.

$$\Delta H_M^E = \Delta H_M - \Delta H_M^i \qquad (2)$$

In this case ΔH_M^i is zero and ΔH_M^E is equal to the heat of mixing, ΔH_M. These and other excess properties of state show the same functional relationships as the fundamental variables of thermodynamics. Thus the excess entropy ΔS_M^E may be obtained from

$$\Delta S_M^E = \frac{\Delta H_M - \Delta F_M^E}{T} \qquad (3)$$

Of particular interest to this study will be the simplest type of mixture consisting of two uni-univalent strong electrolytes with a common anion. Activity coefficients of such binary ionic components in a mixed ternary solution have been calculated primarily from electrochemical cells of the type $H_2/HX(m_2)$, $MX(m_3)/AgX$,

Ag, where m_2 and m_3 are the molalities of HX and MX, respectively, or from isopiestic vapor pressure measurements.[2,3]

The activity coefficients were found to obey Harned's rule in many cases

$$\log \gamma_2 = \log \gamma_{2(0)} - \alpha_{23} m_3 \quad (4)$$

$$\log \gamma_3 = \log \gamma_{3(0)} - \alpha_{32} m_2 \quad (5)$$

where γ_2 and γ_3 are the activity coefficients of electrolytes 2 and 3 in the presence of each other. $\gamma_{2(0)}$ and $\gamma_{3(0)}$ are the activity coefficients of the pure electrolytes at molality m, where m is the total molality and is equal to the sum of m_2 and m_3. α_{23} and α_{32} are functions of the total molality m but are independent of the individual molalities m_2 and m_3. Activity coefficients calculated from eq. 4 and 5 are in many cases within experimental error of observed values. In some instances, however, it was necessary to modify these equations by adding a higher-order term.

$$\log \gamma_2 = \log \gamma_{2(0)} - \alpha_{23} m_3 - \beta_{23} m_3^2 \quad (6)$$

$$\log \gamma_3 = \log \gamma_{3(0)} - \alpha_{32} m_2 - \beta_{32} m_2^2 \quad (7)$$

Examples of such systems include NaCl–KCl,[4] HCl–KCl,[2] and HCl–NaCl.[5] The latter two have been studied over a wide temperature range by the e.m.f. method. For the HCl–NaCl system, Harned has found that eq. 4 and 5 were obeyed between 20 and 40° for total concentrations between 0.5 and 3.0 m. At lower temperatures, eq. 4 and 7 represented the data more accurately with β_{23} equal to zero over the entire range of temperatures and concentrations.

It can be shown[6] that ΔF_M^E takes the following form for mixing two uni-univalent electrolytes obeying Harned's rules

$$\Delta F_M^E = -2.303RTm_2m_3[(\alpha_{23} + \alpha_{32}) + 2(m_3\beta_{23} + m_2\beta_{32}) + {}^2/_3(\beta_{23} - \beta_{32})(m_2 - m_3)] \quad (8)$$

Both electrolytes are initially at molality m and yield a final solution of total molality m, containing m_2 and m_3 moles of each solute, respectively, per kilogram of solvent. It may be noted that Friedman, in connection with the cluster ionic solution theory,[7] gives an expression for ΔF_M^E which is essentially similar to eq. 8 and is also consistent with Harned's rule. The temperature dependence of ΔF_M^E obtained from e.m.f. measurements over a range of temperatures permits the calculation of ΔH_M from the Gibbs–Helmholtz equation

$$\Delta H_M = \left[\frac{\partial(\Delta F_M^E/T)}{\partial(1/T)}\right]_P \quad (9)$$

In practice, however, this indirect method for obtaining heats does not yield very satisfactory results and calorimetric measurements lead to results of much higher precision.

(2) H. S. Harned, *J. Phys. Chem.*, **64**, 112 (1960).
(3) R. A. Robinson and R. H. Stokes, "Electrolyte Solutions," 2nd Ed., Butterworths Scientific Publications, London, 1959, p. 440.
(4) R. A. Robinson, *J. Phys. Chem.*, **65**, 662 (1961).
(5) H. S. Harned, *ibid.*, **63**, 1299 (1959).
(6) G. N. Lewis and M. Randall, "Thermodynamics," revised by K. S. Pitzer and L. Brewer, McGraw-Hill Book Co., Inc., New York, N. Y., 1961, p. 571.
(7) H. L. Friedman, "Ionic Solution Theory," Interscience Publishers, Inc., New York, N. Y., 1962, p. 200.

By combining eq. 8 and 9 we obtain the relation for the heat of mixing

$$\Delta H_M = 2.303RT^2m_2m_3\frac{\partial}{\partial T}\left[(\alpha_{23} + \alpha_{32}) + 2(m_3\beta_{23} + m_2\beta_{32}) + \frac{2}{3}(\beta_{23} - \beta_{32})(m_2 - m_3)\right] \quad (10)$$

The heat of mixing thus leads to the fixing of a function of the temperature derivatives of the Harned coefficients. An alternate form of eq. 10 is pertinent to this study. ΔH_M may be expressed in terms of the total molality m and the solute mole fraction X_2, where $m_2 = X_2m$ and $m_3 = (1 - X_2)m$. Substitution for m_2 and m_3 gives

$$\Delta H_M = 2.303RT^2(X_2)(1 - X_2)m^2\frac{\partial}{\partial T}\left[(\alpha_{23} + \alpha_{32}) + \frac{2m}{3}(2\beta_{23} + \beta_{32}) + \frac{2mX_2}{3}(\beta_{32} - \beta_{23})\right] \quad (11)$$

at $X_2 = X_3 = 0.50$, eq. 11 reduces to

$$\Delta H_M = \frac{2.303RT^2m^2}{4}\frac{\partial}{\partial T}[(\alpha_{23} + \alpha_{32}) + m(\beta_{23} + \beta_{32})] \quad (12)$$

ΔF_M^E and ΔH_M may be examined in relation to the Bronsted–Guggenheim theory of mixed electrolytes based on Bronsted's principle of the specific interaction of ions.[8,9] This principle assumes that specific short-range interaction in solutions of constant total molality is limited to ions of opposite charge only. Ions of like charge influence each other uniformly without regard to their species. The theory leads to a very simple result for mixing two binary electrolytes with a common ion at constant total molality. No net changes in specific interaction are predicted and consequently ΔF_M^E and ΔH_M are zero for such systems.[9] Harned's eq. 4 through 7 are consistent with the theory when α_{23} equals $-\alpha_{32}$ and all higher terms are zero. Nonzero values of ΔF_M^E and ΔH_M could be considered as a measure of the deviations from the Bronsted–Guggenheim assumptions and on this basis attributed to differences in interaction between like charged ions.

Calorimetric heats of mixing at 25° of several 1 m uni-univalent electrolyte pairs have been determined by Young, Wu, and Krawetz.[10] These were parabolic and approximately symmetrical about solute mole fraction $X = 0.50$, ranging from 32 cal./mole (extrapolated) for HCl–NaCl to −49 cal./mole for LiCl–CsCl at this composition.

We have made direct determinations of ΔH_M at constant total molality of 1, 2, and 3 m solutions of HCl and NaCl between 40 and 0°. Aside from their intrinsic interest, the data will show the departure of ternary ionic mixtures from the Bronsted–Guggenheim theory over a wide range of temperatures and concentrations, and provide a basis for comparison with some estimated results from the e.m.f. data. In all preceding equations, variables with subscripts 2 and 3 refer to components HCl and NaCl, respectively.

(8) See ref. 3, p. 435.
(9) See ref. 6, pp. 345, 569.
(10) T. F. Young, Y. C. Wu, and A. A. Krawetz, *Discussions Faraday Soc.*, **24**, 37, 77 (1957).

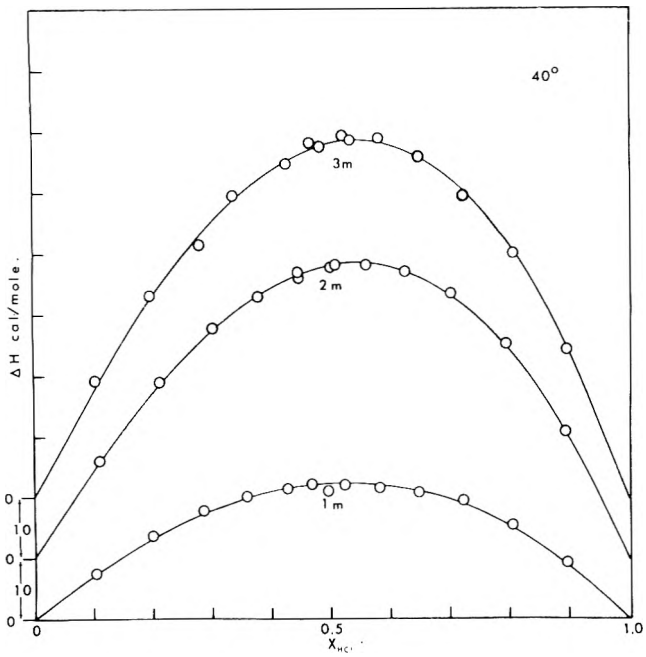

Fig. 1.—Heats of mixing (ΔH_M) as a function of the solute mole fraction of HCl (X_{HCl}) at 40°.

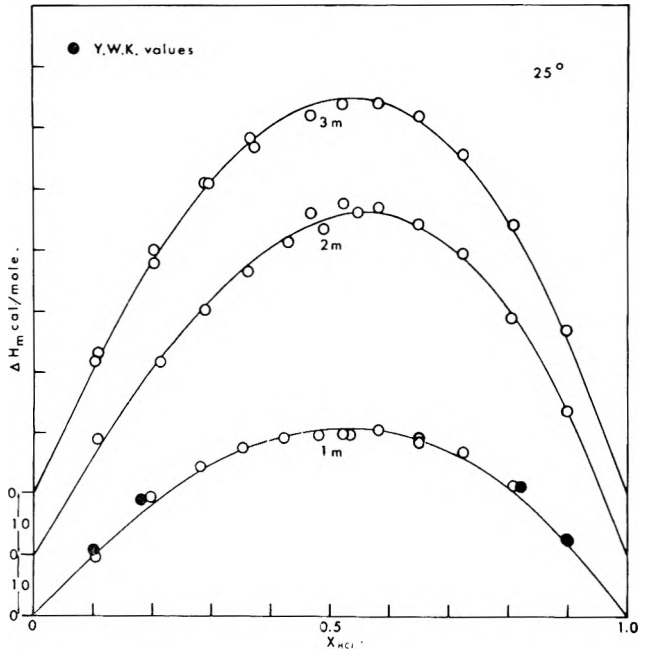

Fig. 2.—Heats of mixing (ΔH_M) as a function of the solute mole fraction of HCl (X_{HCl}) at 25°.

II. Experimental

Materials.—HCl was prepared from concentrated solution and was analyzed with NaOH standardized with KHP. NaCl was heated for several hours prior to weighing, dissolved, and diluted to the desired molalities with weighed quantities of triply distilled water. All chemicals were A.R. grade.

Calorimeter.—The twin heat-leak calorimeter and its operation have been described elsewhere,[11] except for the following change: the energy for the heater was furnished by a transistorized d.c. power supply (Power Designs 4005) instead of the mercury batteries.

The mixing sequence was initiated by crushing a glass ampoule of solution (*ca.* 5 ml.) containing one of the pure binary electrolytes submerged in a larger volume of aqueous solution (*ca.* 45 ml.) of the other electrolyte to produce a ternary solution. The details of subsequent mixing steps are described elsewhere.[10] The actually observed heats per step ranged from 0.120 to 5.84 cal. with an over-all experimental uncertainty of ±4%.

(11) J. H. Stern and A. A. Passchier, *J. Phys. Chem.*, **66**, 752 (1962).

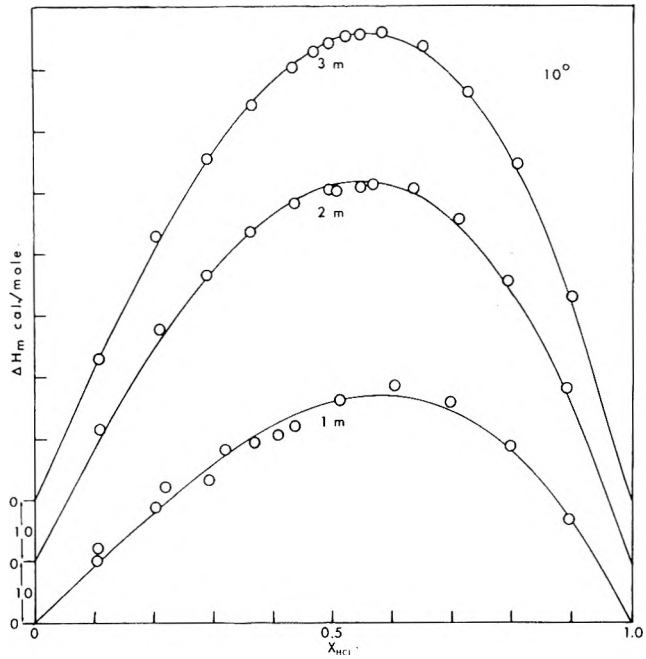

Fig. 3. Heats of mixing (ΔH_M) as a function of the solute mole fraction of HCl (X_{HCl}) at 10°.

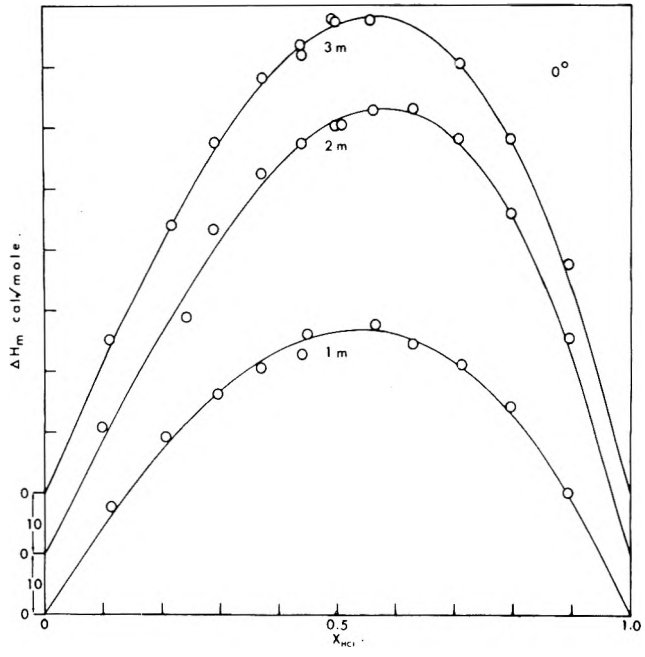

Fig. 4.—Heats of mixing (ΔH_M) as a function of the solute mole fraction of HCl (X_{HCl}) at 0°.

III. Results and Discussion

Observed values of ΔH_M as a function of the solute mole fraction X of HCl for 1.00, 2.00, and 3.00 m solutions at all temperatures are represented by symbols in Fig. 1 through 4. The data reported by Young, Wu, and Krawetz are shown in Fig. 2 and are in good agreement with our results. The curves represent the least squares fit of all data arranged in analytical equations of the type

$$\Delta H_M = 2.303RT^2m^2X_{HCl}(1 - X_{HCl})(A + BX_{HCl}) \quad (13)$$

where A and B are constants; these constants expressed in terms of eq. 11 are[12]

$$A = \frac{\partial}{\partial T}\left[(\alpha_{23} + \alpha_{32}) + \frac{2}{3} m(\beta_{23} + 2\beta_{32})\right] \quad (14)$$

$$B = \frac{\partial}{\partial T}\left[\frac{2}{3} m(\beta_{23} - \beta_{32})\right] \quad (15)$$

Table I gives values of A and B which were obtained on the IBM 1620 computer using a program devised by Mr. Richard Tapia. Table II shows values of $\partial/\partial T[(\alpha_{23} + \alpha_{32}) + m(\beta_{23} + \beta_{32})]$ of eq. 12 at $X = 0.50$.

TABLE I

SUMMARY OF PARAMETERS A AND B

m	40°	25°	10°	0°
	$A \times 10^5$			
1	17.7	26.8	25.2	46.3
2	8.73	10.4	13.5	13.8
3	4.68	6.15	6.78	7.36
	$B \times 10^5$			
1	4.49	6.64	28.4	17.1
2	4.04	6.45	6.47	14.4
3	2.20	1.85	4.57	5.52

TABLE II

SUMMARY OF

$$\frac{\partial}{\partial T}[(\alpha_{23} + \alpha_{32}) + m(\beta_{23} + \beta_{32})] \text{ AT } X = 0.50$$

m	$\frac{\partial}{\partial T}[(\alpha_{23} + \alpha_{32}) + (\beta_{23} + \beta_{32})] \times 10^4$			
	40°	25°	10°	0°
1	1.99	3.02	3.94	5.48
2	1.08	1.36	1.68	2.10
3	0.578	0.707	0.906	1.01

Several interesting statements may be made regarding the graphs and Tables I and II. All curves are approximately parabolic and are consistent with the functional form of eq. 11 with maxima generally displaced somewhat toward the HCl-rich side. This asymmetry may be attributed to the effect of the β terms. The heats and $\partial/\partial T[(\alpha_{23} + \alpha_{32}) + m(\beta_{23} + \beta_{32})]$ decrease regularly with increasing temperature for all systems. It thus appears that adherence to the Bronsted–Guggenheim theory improves with increasing temperature, that is, the differences between the short-range repulsive interactions of hydrated like-charged ions diminish. It may be observed that $\partial/\partial T[(\alpha_{23} + \alpha_{32}) + m(\beta_{23} + \beta_{32})]$ shows a decrease with increasing molality at all temperatures, which is remarkable especially since, according to eq. 12, the heats are a function of m^2.

Values of $[(\alpha_{23} + \alpha_{32}) + m(\beta_{23} + \beta_{32})]$ calculated[13] from e.m.f. results may be plotted against temperature. The slope of this plot yields the temperature derivative of this function and consequently ΔH_M *via* eq. 12. Estimates of $\partial/\partial T[(\alpha_{23} + \alpha_{32}) + m(\beta_{23} + \beta_{32})]$ are subject to a very high experimental error, so that ΔH_M may be uncertain by a factor of two for 1 m mixtures. At higher molalities the error becomes even larger.[14] Therefore no comparison has been made with Harned's data at 2 and 3 m concentrations, and we shall limit our discussion to 1 m mixtures. The calculated heats increase regularly from 17 to 37 cal./mole between 40 and 0° ($X = 0.50$) compared to our values of 22 and 47 cal./mole for the same temperature interval. Both direct and calculated results are in qualitative agreement and show that heats tend toward zero as the temperature increases. The relationship of ΔH_M to temperature is approximately linear. Extrapolation shows that ΔH_M may be expected to reach zero at 80°, while the calculated heats do so at 65° for 1 m mixtures. It is recognized that such extrapolations are speculative since we must assume constant slope over wide temperature ranges.

For the 2 and 3 m solutions, the extrapolated heats would not reach zero until well past the boiling point of water. Qualitative direct measurements with 3 m solutions at 60° indicate that heats are small and still positive. Quantitative data above 40° were not possible because of instrument limitations.

The e.m.f. data may be used to very good advantage in combination with our heats to obtain excess entropies of mixing. The value of ΔF_M^E calculated from eq. 8 has an accuracy at least an order of magnitude greater than that of ΔH_M obtained by the Gibbs–Helmholtz equation. Table III gives values of ΔS_M^E at $X = 0.50$ obtained from eq. 7, together with ΔF_M^E and ΔH_M at this composition.

TABLE III

SUMMARY OF ΔF_M^E, ΔH_M AND ΔS_M^E AT $X = 0.5$ FOR HCl–NaCl FROM 40 TO 0° AT TOTAL MOLALITIES OF 1, 2, AND 3 m

t, °C.	m	ΔF_M^E, cal./mole	ΔH_M, cal./mole	ΔS_M^E, e.u.
40	1	9.4	22	0.04
	2		48	
	3		58	
25	1	9.0	31	.07
	2	48	56	.03
	3	75	65	− .03
10	1	9.3	37	.09
	2	41	62	.08
	3	92	76	− .06
0	1	10	47	.13
	2	43	73	.11
	3	98	78	− .07

Certain trends are apparent from Table III. In all cases ΔS_M^E decreases with molality at constant temperature and also with temperature at constant molality and is considerably smaller in magnitude when compared with ΔS_M^i. This quantity equals $-2Rm$ ln 0.5 or 2.76 m e.u. at $X = 0.50$. It is possible that the excess entropies of mixing for all solutions may be due to the change in clustering between hydrated ions of unlike charge. It is very difficult to correlate the changes in microscopic configurations and properties of hydrated ions with values of the macroscopic excess functions. The interpretations of these trends may become clearer after completion of a study on HCl–KCl and other similar systems.

(12) Equation 11 is a third-order polynomial in X_{HCl}. This equation has four degrees of freedom, *i.e.*, given four independent sets of points, four parameters could be obtained. Thermodynamics, however, requires that $\Delta H_M = 0$ at $X_{HCl} = 1$ and $X_{HCl} = 0$. Two degrees of freedom remain and only two parameters thus may be determined. The temperature derivatives of the individual Harned coefficients therefore cannot be determined from eq. 11.

(13) For method of calculation, see ref. 3, p. 574.

(14) See ref. 6, p. 583.

Acknowledgments.—We wish to express our deepest appreciation to Professor Leo Brewer for fruitful discussion and encouragement of this work. The authors are grateful to the United States Army Research Office (Durham) and the Research Corporation for financial support.

KINETICS OF SOLUTION IN LIQUID METALS. SOLUTION RATE OF ZINC, SILVER, AND TIN INTO LIQUID MERCURY

BY F. W. HINZNER AND D. A. STEVENSON

Department of Materials Science, Stanford University, Stanford, California

Received May 7, 1963

The solution rates of solid polycrystalline zinc, silver, and tin into liquid mercury were studied under turbulent flow conditions (rotating solid cylinders with and without simultaneous ultrasonic fields) and at different temperatures using radioactive tracers to follow the reaction. In addition, zinc single crystals and a zinc–mercury intermediate phase were studied to gain further insight into the solution mechanism. The solution rate constant was constant when ultrasonics were applied but varied with concentration under pure rotation for all the systems studied. The variation could not be explained by the dependence of diffusion coefficients on concentration. The solution rate constants were related to Reynolds and Schmidt numbers using dimensionless correlations. The exponents on the Reynolds and Schmidt groups were found to be consistent with transport control except in the zinc–mercury system, which appeared to be mixed controlled. Experiments performed on single crystals of zinc showed a more rapid rate of solution for planes perpendicular to the basal plane than for the more densely packed basal planes. The solution rate of zinc from the γ-intermediate phase (46 wt. % Zn–54 wt. % Hg) was more rapid than from pure zinc, indicating that the formation of the intermediate phase would not act as a solution barrier for zinc. The viscosity compensated activation energy agreed, within experimental error, with the literature values for the corresponding diffusion activation energies. It was concluded that the solution rate of zinc into mercury is mixed controlled while the solution rates of tin and silver into mercury are transport controlled for the range of experimental conditions investigated.

Introduction

The kinetics of solution of solids in aqueous and organic systems have been studied quite extensively[1-6] but only recently have similar studies been made in liquid metal systems.[7-11] It is unclear whether the solution mechanisms are similar and whether the rate equations used in aqueous and organic systems describe the behavior in metallic systems. It is the purpose of this study to evaluate the applicability of existing rate equations and investigate the rate controlling steps in the solution process in simple liquid metal systems.

Solution Rate Equations.—The solution of a pure component consists of two steps in series: (1) surface solvation and (2) transport of the solvated species from the interface. The most general solution rate equation, the Berthoud equation, expresses the rate of approach to saturation as[12]

$$C = C_s\left[1 - \exp\left(-Km\,\frac{At}{V}\right)\right] \qquad (1)$$

or

$$\ln\left(1 - \frac{C}{C_s}\right) = -Km\left(\frac{At}{V}\right) \qquad (2)$$

(1) C. V. King, *Trans. N. Y. Acad. Sci.*, **10**, 262 (1948).
(2) M. Eisenberg, C. W. Tobias, and C. R. Wilke, *Chem. Eng. Progr. Symp. Ser.*, **51**, 1 (1955).
(3) D. W. van Krevelen and J. T. C. Krekels, *Rec. trav. chim.*, **67**, 512 (1958).
(4) M. Davion, *Ann. chim.* (Paris), **8**, 259 (1953).
(5) C. Wagner, *J. Phys. Colloid Chem.*, **53**, 1030 (1949).
(6) A. R. Cooper, Jr., and W. D. Kingery, *J. Phys. Chem.*, **66**, 665 (1962).
(7) J. A. R. Bennett and J. B. Lewis, *J. chim. phys.*, **55**, 83 (1958).
(8) A. G. Ward and J. W. Taylor, *J. Inst. Metals*, **85**, 145 (1956).
(9) A. G. Ward and J. W. Taylor, *ibid.*, **86**, 36 (1957).
(10) D. A. Stevenson and J. Wulff, *Trans. AIME*, **221**, 279 (1961).
(11) L. F. Epstein, *Chem. Eng. Progr. Symp. Ser.*, **53**, 67 (1957).
(12) A. Berthoud, *J. chim. phys.*, **10**, 633 (1912).

$Km = \dfrac{KsD/\delta_c}{Ks + D/\delta_c}$
C = bulk concentration
C_s = saturation concentration
Km = solution rate constant
A = area of the interface (solid–liquid)
V = volume of liquid
t = time
Ks = interface reaction constant
D = diffusion coefficient of solute (dissolving species) in the liquid
δ_c = the thickness of the effective concentration boundary layer

The equation is usually used in a limiting form for transport control ($D/\delta_c \ll Ks$) or interface control ($D/\delta_c \gg Ks$).[13]

For cases of transport control, Km reduces to D/δ_c. The equation in this form is known as the Noyes–Nernst equation[14] and has been found to apply to a broad range of experimental conditions. The solution rate constant may be evaluated by plotting $\ln(1 - C/C_s)$ *vs.* $(A/V)t$. The linear nature of this plot in aqueous systems indicates a constant value of Km. In some metal systems, however, nonlinear plots have been observed at higher values of C/C_s.[10] Inasmuch as the experimental precision of the quantity $\ln(1 - C/C_s)$ decreases as saturation is approached, an evaluation of this region requires refined analytical techniques. In order to document the nonlinear region and contribute to its explanation, a radioactive tracer technique was developed for precise determination of solution rates in liquid metal systems.

Rate Controlling Steps.—A number of criteria have been employed by previous investigators to distinguish

(13) For a general discussion of the rate equations, *cf.* (a) H. E. Buckley, "Crystal Growth," John Wiley and Sons, Inc., New York, N. Y., 1951, p. 147; (b) E. A. Moelwyn-Hughes, "The Kinetics of Reactions in Solution," Oxford University Press, London, 1947, p. 367.
(14) (a) A. A. Noyes and W. R. Whitney, *Z. physik. Chem.* (Leipzig), **23**, 689 (1892); (b) W. Nernst, *ibid.*, **47**, 52 (1904).

the cases of transport control, interface control, and mixed control. These criteria are summarized in subsequent sections.

Influence of Hydrodynamic Conditions.—Interface controlled solution rate should be independent of hydrodynamic conditions, whereas a transport or mixed control solution process should depend on hydrodynamic conditions. The relative motion of the fluid and solid influences the thickness of δ_c and this influence has been analyzed for simple geometries.[15] In complex processes such as fluid flow, heat transfer, and mass transfer, useful phenomenological relations have been developed using dimensionless groups of variables.[16] The relevant relation for the present investigation is given as

$$\frac{d_g K_m}{\nu} = \alpha\left(\frac{d_g u}{\nu}\right)^a\left(\frac{\nu}{D}\right)^{b-1} = \alpha(\mathrm{Re})^a(\mathrm{Sc})^{a-1} \quad (3)$$

where α, a, and b are dimensionless numbers, d_g is the relevant dimension, Re and Sc are the Reynolds and Schmidt numbers, and the other symbols have their usual meaning.[7,10] For transport controlled processes, the exponent on the Reynolds number varies between 0.6 and 0.8, and the exponent on the Schmidt number between -0.6 and -0.8.[1-11] The exponent on the Reynolds number would be 0.00 for interface control, and some value between 0.0 and 0.6 for mixed control.

Activation Energy.—The activation energy for the solution rate constant is determined from an Arrhenius plot. The activation energy is then compared with the activation energy for diffusion and with interfacial energies.[8,9]

Etching Effect.—The appearance of a uniformly bright surface after solution has occurred is interpreted as evidence for transport control, whereas an etched surface is considered evidence for interface or mixed control.[17]

General Aims and Approach.—The clearest interpretation may be made for solution kinetic studies which are done with high precision over wide ranges of hydrodynamic conditions and temperatures. It is also essential to obtain adequate concentration–time resolution so that a variation in Km may be observed. Many previous investigations have determined average Km values only.[2,7] The most common means of varying the hydrodynamic conditions for such studies has involved rotating solid cylinders in a static fluid and restricting the solution process either to the base of the cylinder or to the periphery. Although the hydrodynamics of flow about the base of the cylinder is understood better for the transition region from laminar to turbulent flow, the flow about the periphery has the advantage that the relative velocity of solid and liquid is constant over the entire peripheral area and the momentum boundary layer at high Reynolds numbers may be considered constant over this area. Equipment was designed as described in the Experimental section to permit variation of temperature and hydrodynamic conditions over wide limits and to be compatible with tracer analysis. The solution rate of solid metals into liquid mercury was studied over a wide range of hydrodynamic conditions by the rotation of solid samples with and without concurrent ultrasonic fields. The results were then compared with existing rate equations and the rate controlling steps implied from the experimental information.

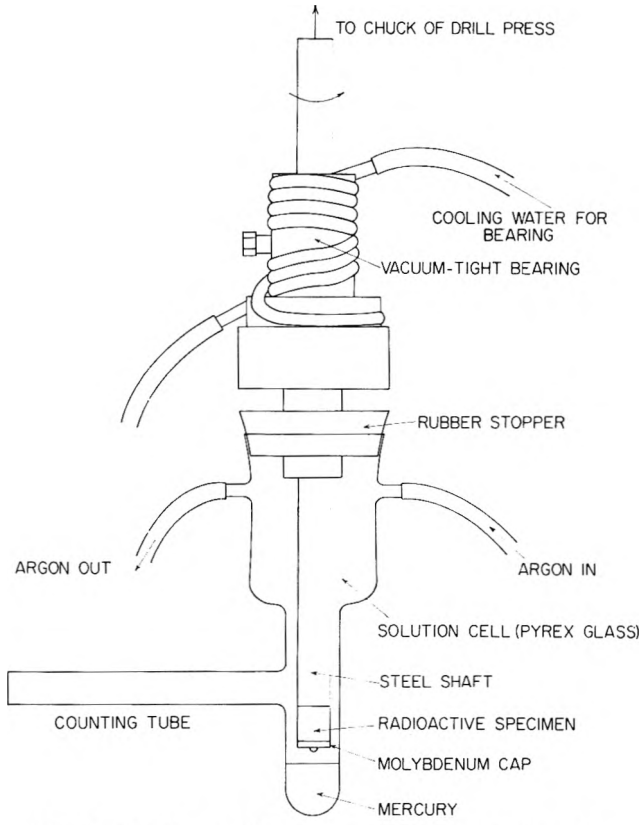

Fig. 1.—Solution cell for experiments using rotation only.

Systems Studied.—The systems zinc–mercury, silver–mercury, and tin–mercury were selected for study for the following reasons: (1) limited solubility of the solid in the liquid and consequently small changes in dimension during solution; (2) the absence of intermediate phases involving solute and solvent; and (3) a suitable isotope for the solute—a γ-emitter with energy greater than 0.5 Mev. and a half-life greater than one month. In addition to these systems, zinc single crystals and a zinc–mercury intermediate phase were studied for reasons given in the discussion.

Experimental

Apparatus and Procedure.—The solution cell used in these studies is shown in Fig. 1. Determination of the solution rate was carried out by immersing the rotating specimen into mercury for an appropriate period of time, removing the specimen, and transferring the liquid to the counting tube to measure the activity of the liquid metal. The transfer of the mercury to the counting tube was carried out in argon by detaching the cell from the drill press and tilting the entire cell. Since the amount of solute dissolved in mercury was low, the fluidity of mercury was excellent and no difficulty was encountered in effecting complete transfer to and from the counting tube. The process was repeated until saturation was achieved. The entire experiment was performed in an argon atmosphere and the temperature controlled by immersing the solution cell in a thermostatic bath regulated to $\pm 0.5°$. The rotational velocity of the specimen was varied and the rotational speed, once set, fluctuated less than 1%. A solution cell was designed to permit experiments involving simultaneous rotation and ultrasonic vibration and was essentially the same as that discussed above with added provisions for acoustical contact between the liquid and the vibrating plate of the ultrasonic transducer. The temperature during the latter

(15) L. L. Bircumshaw and A. C. Riddiford, *Quart. Rev.* (London), **6**, 157 (1952).

(16) A. S. Foust, L. A. Wenzel, C. W. Clump, L. Maus, and L. B. Andersen, "Principles of Unit Operations," John Wiley and Sons, Inc., New York, N. Y., 1960, Chapter 13.

(17) J. M. Lommel and B. Chalmers, *Trans. AIME*, **215**, 499 (1959).

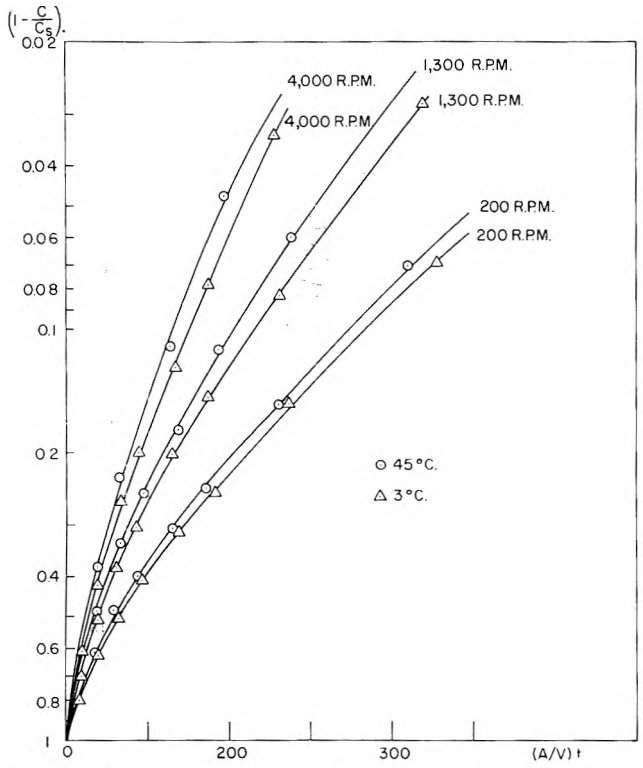

Fig. 2.—Plot of ln $(1 - C/C_s)$ as a function of $(A/V)t$, Zn–Hg system.

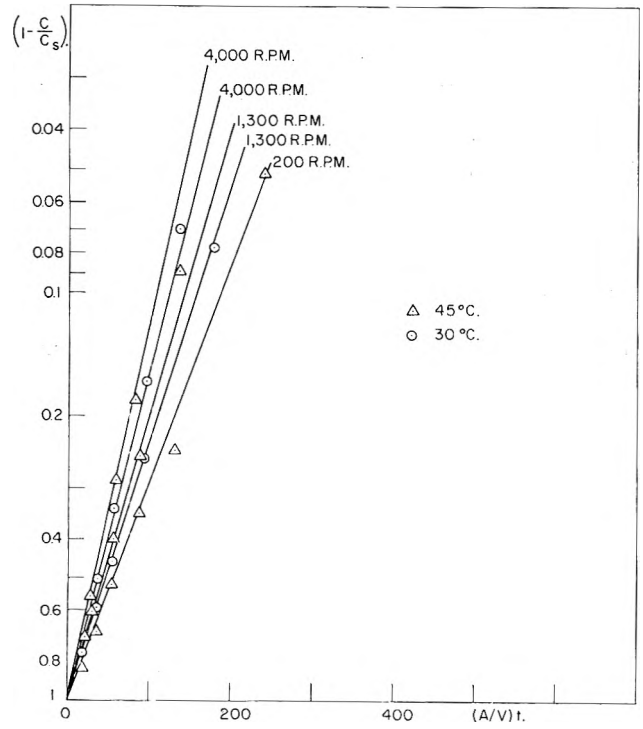

Fig. 3.—Plot of ln $(1 - C/C_s)$ as a function of $(A/V)t$, Zn–Hg system under ultrasonic vibrations.

experiments was regulated to ±1°. A 20-kc. magnetostrictive transducer driven by a 400-w. GU 400 General Ultrasonic Co. signal generator (10 kc. to 1.2 Mc.) provided the ultrasonic field.

Analytical.—The analytical system was an integral part of the solution cell. The solute concentration was determined by measuring the activity of the mercury solution. All the isotopes selected (Zn^{65}, Ag^{110}, Sn^{113}) were adequate γ-emitters to permit use of a Baird Atomics Co. Model 8100 γ-ray spectrometer. The counting tube of the solution cell containing mercury with radioactive solute was inserted in the well of the counting crystals. This method gave a counting efficiency of approximately 60%, and the geometry was reproducible since the entire volume of mercury was counted. Approximately 3000 counts were taken in each measurement corresponding to a standard deviation of 1.8%. In order to avoid high background interference, the base line was set at the minimum prior to the 1.12-Mev. peak of zinc-65. For silver and tin, the base line was set at 0.58 and 0.34 Mev., respectively

Materials.—Zinc (99.98%) and tin (99.96%) were acquired from the Baker Chemical Co., and silver (99.99%) from Western Gold and Platinum Co., Belmont, Calif. The radioactive metals were prepared by irradiation of a small specimen in the Stanford reactor and diluting and homogenizing the resulting high activity material by melting under hydrogen in a graphite crucible. Half-inch diameter cylindrical rods were chill cast and half-inch long specimens prepared. The specimen was mounted on the rotating shaft of identical diameter and the bottom face covered with a molybdenum cap. In this way only the sides of the cylinder were exposed to the mercury. The specimen was pre-amalgamated by cleaning it in hydrochloric acid, dipping it in mercury, and then washing it with distilled water in order to prevent a delay in the solution process due to a surface barrier film.

Zinc single crystals were grown by a modified Bridgeman technique to study the influence of crystallographic orientation on the solution rate. Sections of radioactive zinc single crystals were mounted on the periphery of cylindrical epoxy resin holders in such a way that either faces perpendicular or parallel to the basal plane of the zinc single crystal were exposed to the mercury.

Experimental Results

Zinc–Mercury System.—The zinc–mercury system was the most extensively studied. Solution kinetic data for this system were obtained for four different temperatures: 3, 30, 45, and 59°. At each temperature, data were obtained for three different rotations: 200, 1300, and 4000 r.p.m., a total of 12 combinations of temperatures and rotational speeds. These rotational speeds correspond to surface velocities of 12, 85, and 250 cm./sec., respectively. The zinc–mercury system was also studied under conditions of simultaneous rotation and ultrasonic fields (20 kc./sec.) in five combinations of temperature and hydrodynamic conditions. For all the systems studied, a minimum of two sets of data were obtained for each experimental condition in order to establish the reliability of the data. The tracer techniques developed allowed Km values to be obtained with a precision of 2% up to C/C_s values of 0.90. Systematic errors are not expected to exceed 2% and a maximum error of 4% is predicted for this range of relative concentration. When ultrasonic fields were applied, it was found necessary to establish conditions so that cavitation occurred; otherwise no appreciable effect was noted. In all the studies involving ultrasonics, cavitation was occurring.

Figure 2 shows a graph of ln $(1 - C/C_s)$ *vs.* $(A/V)t$, according to eq. 2, for a few typical experiments for pure rotation, while Fig. 3 gives the same curve for ultrasonic vibrations and concurrent rotation.[18] In evaluating the quantity $(A/V)t$, any changes in A or V due to solution were considered. A similar graph is given in Fig. 4 for the solution of zinc single crystals into mercury at 30° with rotational speeds of 800 and 4000 r.p.m. Figure 4 also shows the solution kinetics of an intermediate phase (46% Zn–54% Hg by weight) into mercury at a temperature of 30° with rotational speeds of 1300 and 4000 r.p.m.

Silver–Mercury and Tin–Mercury Systems.—Solution kinetic data for these systems have been obtained for two different temperatures and four different hydrodynamic conditions. Because of the low solubility of

(18) The complete experimental data in tabular form will be furnished on request.

silver in mercury, the experiments were performed at the temperatures of 59 and 85°. The rotational speeds were 800 and 4000 r.p.m. both with and without simultaneous ultrasonic fields. These speeds correspond to surface velocities of 50 and 250 cm./sec. A plot of ln $(1 - C/C_s)$ *vs.* $(A/V)t$ for the silver–mercury system for rotation only is shown in Fig. 5, and the same plot at 59° under simultaneous rotation and ultrasonic vibrations is shown in Fig. 6.

In the tin–mercury system, the experiments were done at 3 and 30° at the same velocities as in the last system and studies with simultaneous rotation and ultrasonic vibration were made at 30°. Figure 7 gives a plot of ln $(1 - C/C_s)$ *vs.* $(A/V)t$ for the tin–mercury system for rotation only, and Fig. 6 gives the same plot at 30° under concurrent rotation and ultrasonic vibrations.

Discussion

The dependence of solution rate on velocity is demonstrated by curves of ln $(1 - C/C_s)$ *vs.* $(A/V)t$, as in Fig. 2–6, the slope of these curves being equal to Km according to the Berthoud equation. These curves show that Km is not constant for cases of pure rotation, in agreement with earlier studies in the lead–nickel and lead–copper systems.[10] For rotation with concurrent ultrasonic fields, however, the linear relation between ln $(1 - C/C_s)$ and $(A/V)t$ is obeyed as seen in Fig. 3 and 6. The former behavior could be explained by a variation in D or δ_c with time (or concentration) or lack of interface equilibrium.

Reference to literature D-values for zinc and tin in liquid mercury shows that D decreases less than 5 and 10% for the respective systems over the concentration ranges in question.[19–21] This decrease is insufficient to explain the decrease in Km with increasing concentration. The possibility of δ_c changing with concentration was considered.[22] A mathematical analysis of the solution process was made assuming: that δ_c increases with time; a constant value of D over the concentration range in question; and Couette flow (linear variation of fluid velocity with distance from the solid interface) within the range of the concentration boundary layer. For systems in which the momentum boundary layer δ_u is significantly greater than δ_c, such as the present systems with Sc $\gg$ 1, this flow condition is reasonable. The solution of the resulting equation led to the relation[22]

$$\ln (1 - C/C_s) = -K'(A/V)t^{2/3} \qquad (4)$$

Although this rate law provides significant improvement in the empirical representation of the experimental information (as seen, for example, in Fig. 8), subsequent estimates of the momentum boundary layer and concentration boundary layer were made[23] and the time required for development of the concentration boundary layer calculated to be less than 1 sec. This time is such a small portion of the entire dissolution experiment that the transient behavior may be neglected; consequently, eq. 4 must be considered empirical. The main portion of the nonlinearity is probably due to lack of interface

(19) H. W. Schadler and R. E. Grace, *Trans. AIME*, **215**, 555 (1959).
(20) M. H. Nachtrieb and J. Petit, *J. Chem. Phys.*, **24**, 746 (1956).
(21) W. C. Cooper and N. H. Furman, *J. Am. Chem. Soc.*, **74**, 6183 (1952).
(22) F. Hinzner, Ph.D. Thesis, Stanford University, 1962.
(23) R. J. Donnelly and N. J. Simon, *J. Fluid Mech.*, **7**, 401 (1960).

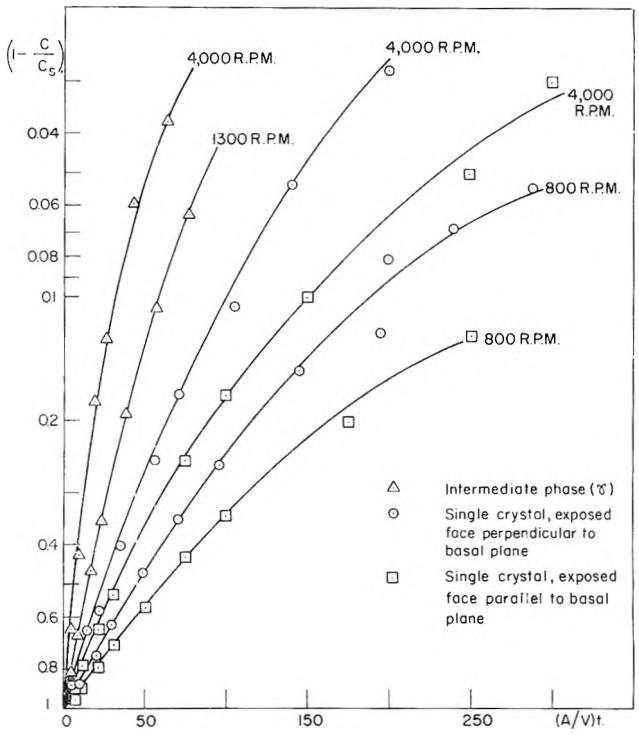

Fig. 4.—Plot of ln $(1 - C/C_s)$ as a function of $(A/V)t$, Zn single crystals–Hg and γ-intermediate phase–Hg systems (30°).

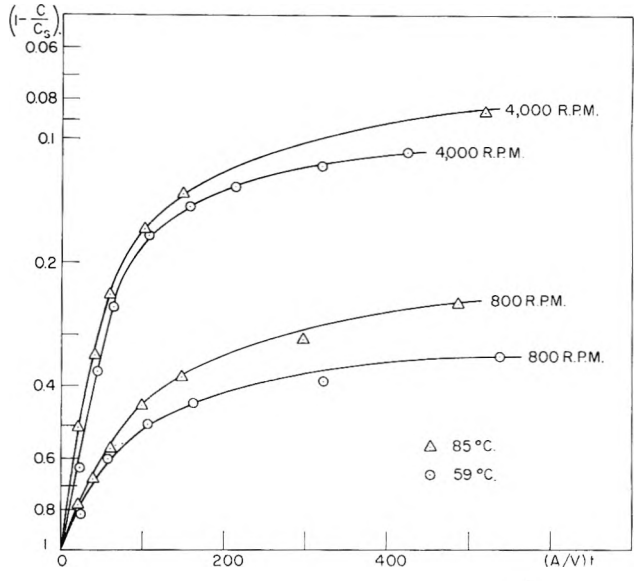

Fig. 5.—Plot of ln $(1 - C/C_s)$ as a function of $(A/V)t$, Ag–Hg system.

equilibrium. A detailed explanation of this behavior is not yet apparent and may result from a number of causes.

The zinc–mercury phase diagram shows a peritectic reaction at 43° resulting in the formation of an intermediate γ-phase.[24] Below 43° this phase is stable in the concentration range from 44 to 48 wt. % of zinc. This intermediate phase could form at temperatures below 43° by reaction of the mercury with the zinc sample. If this phase goes into solution into mercury more slowly than zinc, it could act as a barrier and decrease the solution rate. Since the flux of mass away from the interface is smaller toward the end of the solution process, the formation of the intermediate

(24) M. Hansen and K. Anderko, "Constitution of Binary Alloys," McGraw-Hill Book Co., Inc., New York, N. Y., 1958.

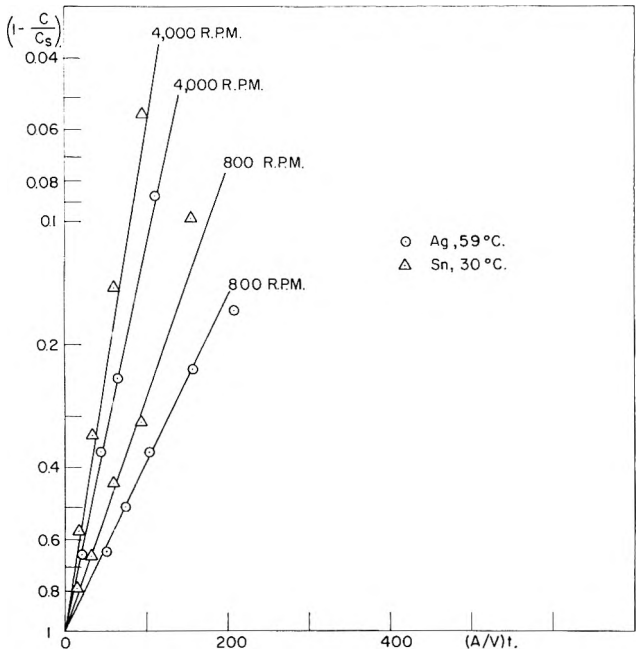

Fig. 6.—Plot of ln $(1 - C/C_s)$ as a function of $(A/V)t$, Ag–Hg and Sn–Hg systems under ultrasonic vibrations.

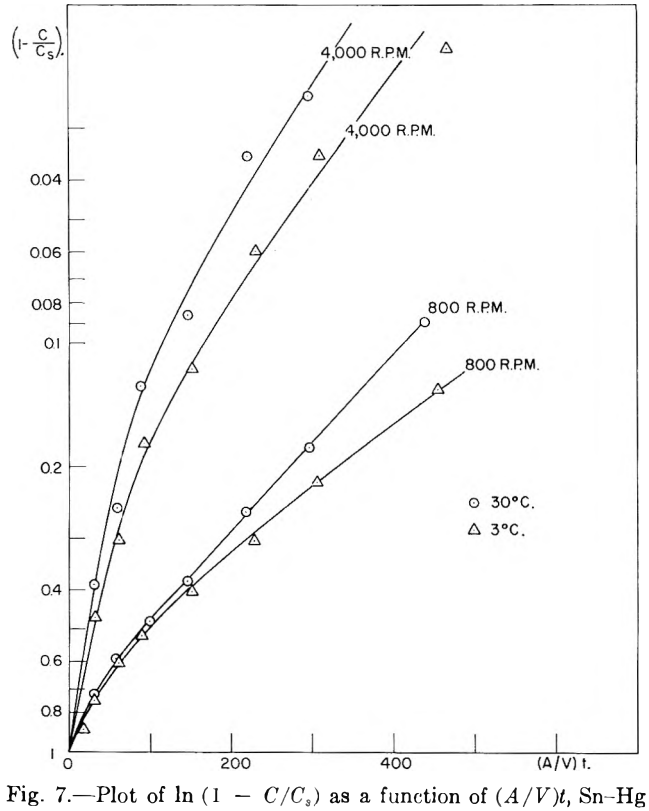

Fig. 7.—Plot of ln $(1 - C/C_s)$ as a function of $(A/V)t$, Sn–Hg system.

phase by back diffusion of mercury would more likely occur in the latter stages of solution. If this were the case, the decrease in the solution rate constant toward the end of the experiment might be explained by the formation of the intermediate phase. In order to experimentally prove or disprove this possibility, the intermediate phase was prepared and its solution rate into mercury was studied. The reaction was followed by observing the increase in activity of Zn^{65} in the liquid amalgam. The results are shown as a graph of ln $(1 - C/C_s)$ *vs.* $(A/V)t$ in Fig. 4. Comparing this result with pure zinc under the same conditions it is seen that the solution

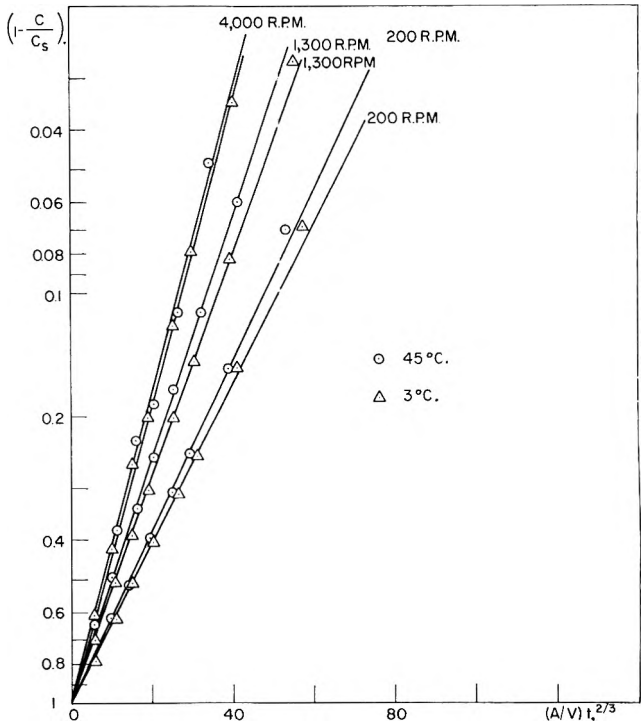

Fig. 8.—Plot of ln $(1 - C/C_s)$ as a function of $(A/V)t^{2/3}$, Zn–Hg system.

rate of the intermediate phase into mercury is faster than the solution rate of zinc into mercury. Additional studies on the diffusion of mercury into zinc indicate that the time required for conducting the entire experiment is shorter than the time necessary for the formation of the intermediate phase; hence it would go into solution as soon as it forms.[25] It is concluded that the formation of the intermediate phase does not act as a barrier for the solution reaction and does not lower the solution rate.

It is of interest to evaluate the criteria for predicting the rate controlling step as discussed in the introduction. One of the criteria is the comparison of the dimensionless exponents in eq. 3. The relevant dimension in evaluating Re for the present geometry has been shown to be the gap distance between the sample cylinder and container walls.[2] The values of K were taken from the initial slope of the ln $(1 - C/C_s)$ *vs.* $(A/V)t$ curves. The exponents a and $b - 1$ in eq. 3 were obtained by appropriate log–log plots of $d_g K_m/\nu$ *vs.* Reynolds number and Schmidt numbers, respectively. The following values for exponents are obtained: for zinc–mercury, $a = 0.20$, $1 - b = -0.60$; for tin–mercury and silver–mercury, $a = 0.62$, $1 - b = -0.60$. These may be compared with the average of 22 previous investigations for systems believed to be transport controlled, namely, $a = 0.60$; $1 - b = -0.58$.[22] The exponent of 0.20 Re in the zinc–mercury system shows that K in that system is less dependent on Re than for a normal transport controlled reaction, indicating that the reaction is mixed controlled. The exponents for the tin–mercury and silver–mercury systems comply with transport controlled kinetics.

The orientation dependence of the solution rate is seen by referring to Fig. 4, which shows a significantly slower rate for the basal planes in contrast to the faces

(25) The diffusion of mercury into zinc was studied at 298° K. using radioactive mercury, and some preliminary results show D to be of the order of 10^{-15} cm.²/sec.

perpendicular to the basal plane. This is qualitatively explained by the fact that nine nearest neighbor bonds in the solid are broken in the former case in contrast to seven or eight bonds in the latter case. This correlates with the higher heat of sublimation for the atoms in the former case.[26] The demonstrated dependence of the rate of solution both on orientation and hydrodynamic conditions further substantiates the postulated mixed control.

Arrhenius plots for the solution rate group (at a constant Reynolds number of 100,000) were made and corresponding activation energies for the systems evaluated. Previous authors have compared these activation energies directly with the activation energy for diffusion or to the interfacial energy to imply the rate controlling step.[8,9] In the former case the interpretation is not straightforward since the influence of temperature on both the diffusion coefficient and boundary layer thickness must be considered. The boundary layer thickness depends on viscosity which is temperature dependent. The analysis of the activation energy must therefore consider the simultaneous change of D and ν with temperature. The solution rate data may be represented by an equation similar to eq. 3 and may be rearranged as

$$K = (1/d_g)\alpha(\mathrm{Re})^a \nu^b D^{1-b} \qquad (5)$$

Both mass and momentum transport are thermally activated and D and ν may be expressed as

$$D = D_0 \exp[-(\Delta E_1/RT)] \qquad (6)$$

$$\nu = \nu_0 \exp(\Delta E_2/RT) \qquad (7)$$

Combining the above equations

$$K = \frac{\alpha}{d_g} (\mathrm{Re})^a \nu_0{}^b D_0{}^{(1-b)} \exp\frac{b\Delta E_2}{RT} \times \exp\left[-\frac{(1-b)\Delta E_1}{RT}\right] \qquad (8)$$

or for a constant Reynolds number and d_g

$$K = \text{const.} \exp(-\Delta E_3)/RT \qquad (9)$$

where

$$\Delta E_3 = (1-b)\Delta E_1 - b\Delta E_2 \qquad (10)$$

The over-all activation energy ΔE_3 may be evaluated for a transport controlled case from a graph of ln K *vs.* $1/T$. Knowing ΔE_3 and taking ΔE_2 from the literature,[27] ΔE_1, the activation energy for diffusion may be calculated. The value obtained for zinc in mercury was 850 cal./mole as compared with the value of 1000 cal./mole in the literature. The discrepancy may be caused by the zinc–mercury system being mixed controlled. In the tin–mercury and silver–mercury systems, similar analysis led to values of 1300 and 1600 cal./mole in contrast to literature values of 1230 and 1500 cal./mole for the activation energy for diffusion. This agreement is considered satisfactory and is further evidence for transport control.

The surface of all the specimens remained smooth after solution had occurred. This supports the conclusion that the reactions were not interface controlled and that no problem resulted from Taylor's vortices in the range of flow conditions encountered.[7]

Conclusions

The tracer technique developed in this study provides a higher degree of accuracy for determining solution rate constants than is possible with previous techniques. The use of tracers is superior in all systems for which suitable isotopes are available. The dynamic rates of solution of three metals into mercury were studied using tracers and the following conclusions were made.

The solution rate constant K, defined by the Berthoud equation, was constant when simultaneous rotation and ultrasonic fields were applied (under conditions that ultrasonic fields produced cavitation), whereas a pronounced decrease in K with increasing per cent saturation was observed for cases of pure rotation. This behavior could not be explained by the observed concentration dependence of the diffusion coefficient as published in the literature.

For single crystal faces of zinc, solution was less rapid from the basal plane faces than from faces perpendicular to the basal plane. This indicates that the more closely packed planes have the lowest energy, a fact which has additional experimental support. The solution rate of an intermediate phase (46 wt.% Zn–54 wt.% Hg) was more rapid than for pure zinc, proving that the formation of the intermediate phase does not act as a barrier for the solution process.

The dependence of the solution rate constant on velocity and temperature was analyzed using dimensionless groups and led to the following conclusions for the experimental conditions studied: the solution for polycrystalline zinc into mercury is mixed control, whereas silver and tin into mercury is transport controlled.

An approach for analyzing the temperature dependence of K' was developed which considered the temperature dependence of viscosity as well as diffusion coefficient. The analysis resulted in independent calculation of activation energies for diffusion which were in close agreement with literature values.

Acknowledgments.—Appreciation is extended to Mr. J. Viecelli who assisted in the experimental measurements, to Prof. R. Johnk for helpful discussions, to Prof. T. J. Connolly for supervising the activation of the tracers, to Prof. G. A. Parks and Mr. A. Ardell who critically reviewed the manuscript, and to the U. S. Atomic Energy Commission for sponsoring the research which was conducted under contract No. AT (04-3)-283.

(26) H. H. Uhlig, "Metal Interfaces," American Society for Metals, Cleveland, Ohio, 1952, p. 312.

(27) (a) W. E. Dunn, C. F. Bonilla, C. Ferstenberg, and B. Gross, *A.I.Ch.E. J.*, **2**, 184 (1952); (b) A. Von Schweidler, *Akad. Wiss. Wien. Math. Naturw. Kl. Sitzber.*, 104 (1895).

THE ADDITIVITY OF CARBON-13 CHEMICAL SHIFTS IN THE CH_3X, C_2H_5X, i-C_3H_7X, t-C_4H_9X SERIES

BY GEORGE B. SAVITSKY AND KEISHI NAMIKAWA

Department of Chemistry, University of California, Davis, California

Received May 27, 1963

Previous results on C^{13} chemical shifts on α- and β-carbons in the series $(CH_3)_nCH_{3-n}X$ for various X indicated that the effects of replacement of the hydrogen atoms on the α-carbon by methyl groups were nearly additive. The C^{13} chemical shifts toward lower field per methyl substitution depend very little on the nature of X in case of β-carbon but vary considerably in case of α-carbon. These literature results supplemented by further experimental measurements for X = COOH, C_6H_5 are discussed in terms of possible correlation between the absolute magnitude of the relative shifts on α-carbon and C–X bond lengths.

Introduction

As part of his extensive studies on the n.m.r. C^{13} chemical shifts, Lauterbur[1] investigated the series $(CH_3)_nCH_{3-n}X$ (X = Cl, Br, I, OH, NO_2). His plots of chemical shifts on the α- and β-carbons for each X *vs.* n showed a fairly linear relationship, indicating that the effects of replacement of the hydrogen atoms on the α-carbon by methyl groups were nearly additive, with few exceptions. More recently, Spiesecke and Schneider[2] determined chemical shifts in various CH_3X and C_2H_5X compounds, using spherical sample and reference containers, and thus obviating bulk susceptibility effects. If these more recent results are used in the RBr and RCl series, more nearly linear plots and hence better additivity relationships result for these series.

Whereas β-carbon plots consist of nearly parallel straight lines, the most striking feature of the α-carbon plots is the great variation in the slopes of best-fitting straight lines with the nature of X.

The relative chemical shifts in both plots are toward decreasing field with increasing methyl substitution and follow the normally accepted order of positive inductive effects of the alkyl groups: t-C_4H_9 > i-C_3H_7 > C_2H_5 > CH_3.

This order appears to be in line with the qualitative picture of gradual electron density withdrawal from the alkyl groups toward the electronegative X and hence to progressively lower shielding on the alkyl carbons. In compounds where possible contributions of non-bonded resonance structures (hyperconjugation) may take place, the over-all differences in the electron releasing effects of the alkyl groups for each methyl substitution could become somewhat moderated by hyperconjugation, the order of hyperconjugation effects in the alkyl series in question usually being assumed to be opposite to that of the inductive effects, although both mechanisms of electron density release lie in the same direction.

Since among the RX compounds which have been investigated only in the RNO_2 series may hyperconjugation be operative, we have determined the C^{13} chemical shifts for two other series in which hyperconjugation is also supposed to take place, namely RCOOH and RC_6H_5. This was done with the view of comparing the α-carbon plots of two groups of compounds with and without possible hyperconjugation effects in the light of any correlation between α-carbon slopes and the nature of X.

Before attempting to make any correlation of the α-carbon slopes with X we also decided to check the chemical shifts for a few points in Lauterbur's plots by using essentially the same sample cell arrangement as in the work of Spiesecke and Schneider,[2] in view of some discrepancies between their results and those of Lauterbur.[1]

Experimental

Our measurements were made with respect to aqueous 2-C^{13}-sodium acetate as standard reference, but all chemical shifts subsequently were referred to benzene. All experimental conditions and instrumental procedures were identical with those described by Spiesecke and Schneider,[2] except that no provision for spinning of the sample was made. All determinations were made on neat liquids, which were commercially available reagents and which were used without purification. Only pivalic acid, which is a solid, was measured by making a concentrated solution of it in CCl_4.

Results and Discussion

Our measurements are summarized in Table I. These results together with results previously obtained[1,2] are plotted in Fig. 1 (β-carbon chemical shifts) and Fig. 2 (α-carbon chemical shifts). It is seen from Fig. 2 that in the case of RBr and RCl series, the experimental points determined in the cell with concentric spheres (ref. 2 and present work) result in better linearity. In general, points determined in cylindrical arrangement by Lauterbur[1] tend to be displaced somewhat toward lower field except in the case of CH_3Br. The curvature in the ROH series obtained by Lauterbur, however, has been substantiated by our results except that our shifts are about 2 p.p.m. to higher field. This may be at least partially due to cumulative experimental errors resulting from referring shifts to different standards.

TABLE I

α- AND β-C^{13} CHEMICAL SHIFTS OF $(CH_3)_nCH_{3-n}X$ COMPOUNDS IN P.P.M. REFERRED TO BENZENE

Compound	α-C	β-C
CH_3COOH	109.2	
C_2H_5COOH	102.9	121.7
i-C_3H_7COOH	95.1	111.1
t-C_4H_9COOH	90.1	102.4
$CH_3C_6H_5$	108.8	
$C_2H_5C_6H_5$	101.1	114.6
i-$C_3H_7C_6H_5$	95.6	105.9
t-$C_4H_9C_6H_5$	94.2	98.1
CH_3OH	80.7	
C_2H_5OH	71.8	111.9
i-C_3H_7OH	66.1	104.7
t-C_4H_9OH	61.3	99.2
i-C_3H_7Cl	76.8	102.6
t-C_4H_9Cl	63.3	95.2
t-C_4H_9Br	67.6	92.4

(1) P. C. Lauterbur, *Ann. N. Y. Acad. Sci.*, **70**, 841 (1958).
(2) H. Spiesecke and W. G. Schneider, *J. Chem. Phys.*, **35**, 722 (1961).

It can be seen from Fig. 1 that the additivity of chemical shifts on β-carbon for each methyl substituent is very good. All plots are nearly parallel and the series RNO_2, RCOOH, RC_6H_5 do not show any exceptional behavior. Actually, only the ROH series seems to be somewhat out of line indicating deviation from additivity.

The plots shown in Fig. 2, on the other hand, present several distinctive features. The halogen series show the best linearity if one assumes that the two points for CH_3Cl and CH_3Br determined in spherical cell are more nearly correct. In the series in which hyperconjugation may be operative (X = NO_2, COOH, C_6H_5) there exists deviation from additivity in shifts from isopropyl to *t*-butyl group. This deviation is the most pronounced in the case of alkylbenzenes. Thus, the difference between the α-C^{13} chemical shifts of isopropylbenzene and *t*-butylbenzene is only 1.4 p.p.m., whereas the difference between methylbenzene and ethylbenzene is 7.7 p.p.m. One could argue that, if the normal linear trend in α-C^{13} shifts is related to electron-releasing ability of the alkyl groups, this deviation from linearity may indeed be due to hyperconjugation effects superimposed on the inductive effects. However, among the compounds studied, the alcohol series presents the greatest deviation from linearity in both plots. On the other hand, it is conceivable that in case of alcohols the difference in degree of intermolecular association *via* hydrogen bonding might account for the observed deviation from linearity in both α- and β-carbon plots. At the same time, the possibility of increased strain on the *t*-butyl group by bulky substituents such as phenyl group cannot be disregarded entirely.

TABLE II

Series	X	d_X	Reference
RF	3.9	1.38	*a*
RCl	13.5	1.78	*a,b*
RBr	17.2	1.94	*b*
RI	20.6	2.12	*b*
ROH	6.5	1.43	*a*
RNO_2	7.8	1.47	*a*
RCOOH	6.3	1.50	*a*
RC_6H_5	6.6	1.50	*a*

[a] David R. Lide, Jr., *Tetrahedron*, **17**, 125 (1962). [b] J. W. Simmons, *et al.*, *Phys. Rev.*, (2) **74**, 1246 (1948).

As to the possible correlation between the various slopes in Fig. 2 and the nature of X, it becomes immediately apparent that the slopes tend to be greater the bulkier the atom of the X group which is immediately attached to α-carbon. If for each series RX we define the quantity Δ_X which is the average chemical shift of α-C^{13} to lower field per methyl substitution, Δ_X will represent the slope of the straight line of best fit for halogen series and an average of three differences in shifts (δMe − δEt), (δEt − δi-Pr), (δi-Pr − δt-Bu) for the remaining plots which cannot be adequately represented by a straight line. Table II lists the Δ_X thus obtained and the lengths of the bonds d_X between the α-carbon and the atom of the X group immediately attached to it. The Δ_F has been determined only from two points available in the literature[2] which are also plotted in Fig. 2.

Figure 3 shows the plot of Δ_X *vs.* d_X which reveals an increase of Δ_X with increasing bond length d_X.

This trend suggests that the α-carbon-13 chemical shifts in these systems are related to the relative polarizability or deformability of the electron density in the C–X bond by induction. As one goes from R = CH_3 to

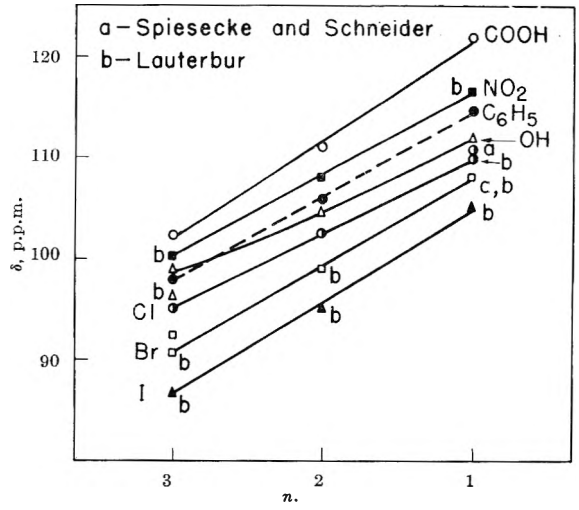

Fig. 1.—β-C^{13} chemical shifts in the series $(CH_3)_nCH_{3-n}X$.

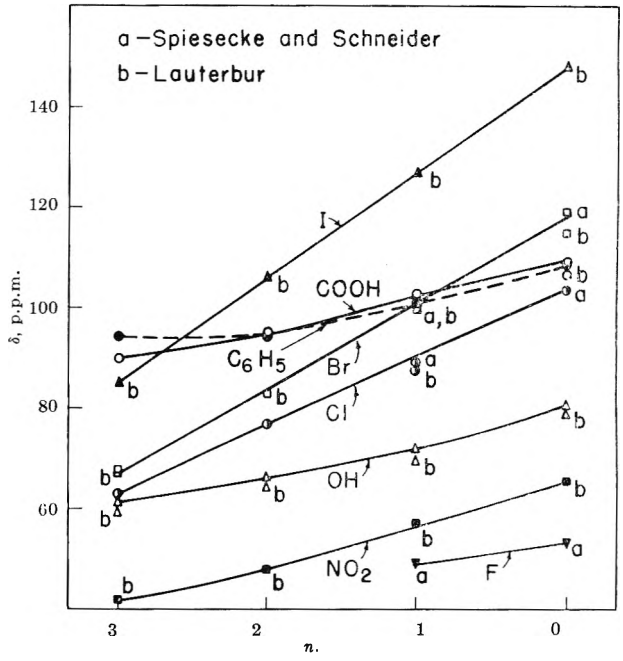

Fig. 2.—α-C^{13} chemical shifts in the series $(CH_3)_nCH_{3-n}X$.

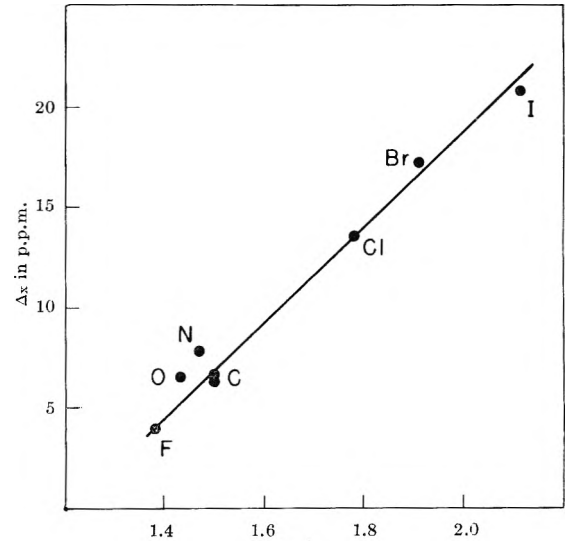

Fig. 3.—The plot of Δ_X *vs.* d_X.

$R = C_2H_5$ in each series, the extent of the shift of electron density away from the α-carbon or the actual enhancement of charge transfer toward the electronegative X which is due to the electropositive inductive effect of the additional methyl group seems to be more important in a longer than in a shorter bond. Thus, for the RI series, the relative change in electron shielding on the α-carbon per substitution of hydrogen by a methyl group is of greater magnitude than it is in the RF series, the relative changes in all other groups being intermediate. That the relative spatial displacement of the center of gravity of the negative end of the dipole moment or additional increment in charge transfer toward X in RX series with the increase in the inductive effect of R is more significant for longer C–X bonds, in going from CH_3X to C_2H_5X, for example, seems to be borne out by the dipole moment measurements of the methyl and ethyl halides listed in Table III.

TABLE III
DIPOLE MOMENTS OF METHYL AND ETHYL HALIDES

X	μ_{CH_3X}	$\mu_{C_2H_5X}$	$\mu_{CH_3X} - \mu_{C_2H_5X}$	Reference
F	1.81	1.92	0.11	*a*
Cl	1.83	2.00	.17	*b*
Br	1.75	1.99	.24	*b*
I	1.60	1.93	.33	*b*

[a] C. P. Smyth and K. B. McAlpine, *J. Chem. Phys.*, **2**, 499 (1934). [b] P. C. Mahanti, *Phil. Mag.*, (7) **20**, 274 (1935).

We see that the increments in dipole moments in going from CH_3X to C_2H_5X follow the order of increasing C–X bond lengths, which in this case is opposite to the order of electronegativities.

It is difficult to explain the relative constancy of the slopes in β-C^{13} shifts. The small differences in these slopes, however, do exist and may still be significant. Thus in the halogen series (X = Cl, Br, I) the slopes still follow the order I > Br > Cl, but then the slope for X = COOH is even greater than that for X = I. It seems, therefore, that the induced polarity of the C–X bond may have only a second-order effect on these slopes and that some other factors predominantly account for the rather significant chemical shifts of β-carbon resonance toward lower field per methyl substitution. We do not feel prepared to advance any plausible explanation for these effects. Also, the evidence presented for hyperconjugation effects cannot be regarded as conclusive.

On the other hand, if our tentative explanation of the large variation in the slopes of α-carbon plots is correct, the bond lengths between the carbon in question and substituent groups should be considered together with other factors such as electronegativities, types of hybridization, and magnetic anisotropies of various groups in future theoretical appraisals of C^{13} chemical shifts.

Acknowledgments.—The authors wish to thank Professor C. P. Nash for his helpful suggestions and Professor W. E. Thiessen for proofreading the manuscript.

HIGH-TEMPERATURE CHEMISTRY OF THE RUTHENIUM–OXYGEN SYSTEM[1]

BY WAYNE E. BELL AND M. TAGAMI

General Atomic Division of General Dynamics Corporation, John Jay Hopkins Laboratory for Pure and Applied Science, San Diego, California

Received May 28, 1963

The ruthenium–oxygen system has been studied over the temperature range 800 to 1500° and over the oxygen pressure range 0.01 to 1.0 atm. Results show that solid RuO_2 is the only stable condensed oxide under the conditions of the study. The dissociation pressure of the oxide reaches 1 atm. at 1540°. The effect of oxygen pressure on vapor pressure indicates that the important vapor species are RuO_3 and RuO_4. From the pressure data, the following heats of formation, $\Delta H°_{298}$, and standard entropies, $S°_{298}$, were obtained: -72.2 ± 2.0 kcal./mole and 12.5 ± 2.0 e.u. for $RuO_2(s)$, -18.0 ± 4.0 kcal./mole and 63.7 ± 4.0 e.u. for $RuO_3(g)$, and -46.7 ± 5.0 kcal./mole and 65.5 ± 5.0 e.u. for $RuO_4(g)$.

Introduction

As part of a systematic investigation of the high-temperature chemistry of transition element compounds, the ruthenium–oxygen system was studied. Condensed phases and vapor species were identified, dissociation and vapor pressures were measured, and thermodynamic data were calculated from the pressure data.

Prior to the start of this work, literature on the behavior of the ruthenium–oxygen system at high temperature was scant and to some extent discordant. Remy and Kohn[2a] reported a few dissociation pressure data for $RuO_2(s)$. Alcock and Hooper[2b] studied the volatility of ruthenium in oxygen as a function of temperature in the range 1200 to 1400° and as a function of oxygen pressure at 1280°. They found the vapor pressure to be proportional to $p_{O_2}^{1/2}$ and, assuming the solid phase to be ruthenium metal, deduced the vapor species to be Ru_2O. Schäfer, Gerhardt, and Tebben[3] studied the effect of oxygen pressure on vapor pressure at 800° and in the range 1465 to 2090° and found evidence for the vapor species RuO_4 and RuO_3. They observed the dissociation pressure of RuO_2 to be much less than that reported by Remy and Kohn.

Recently, Schäfer, *et al.*,[4,5] have completed an exhaustive study of the ruthenium–oxygen system at high temperature. We were pleased to receive preprints of publications covering their work and find good agreement between their results and the results of our study.

Experimental

Dissociation Pressure Studies.—Dissociation pressures were

(1) This work was supported in part by the U. S. Atomic Energy Commission under Contract AT(04-3)-164.

(2) (a) H. Remy and M. Kohn, *Z. anorg. allgem. Chem.*, **137**, 365 (1924); (b) C. B. Alcock and G. W. Hooper, *Proc. Roy. Soc.* (London), **A254**, 551 (1960).

(3) H. Schäfer, W. Gerhardt, and A. Tebben, *Angew. Chem.*, **73**, 27 (1961).

(4) H. Schäfer, G. Schneidereit, and W. Gerhardt, *Z. anorg. allgem. Chem.*, **319**, 327 (1963).

(5) H. Schäfer, A. Tebben, and W. Gerhardt, *ibid.*, **321**, 41 (1963).

measured by both static and dynamic (transpiration) methods using techniques similar to those described in a previous paper.[6] In the static method, the oxide sample was contained in a dead-end mullite reaction tube and dissociation pressures were read on a mercury manometer. A small sulfuric acid manometer was used as a sensitive indicator to show when the pressure in the mercury manometer was equal to the pressure in the reaction tube.

For the transpiration method, a mullite reaction tube was used.[7] Helium served as the carrier gas and the effluent helium–oxygen mixture was analyzed by use of a gas chromatograph. Flow rates of the carrier gas were in the range (2 to 5 ml. STP/min.) where measured oxygen pressures were found to be independent of flow rate.

Vapor Pressure Studies.—Vapor pressures were determined by the transpiration method using techniques similar to those used in previous studies.[7] Mullite reaction tubes were used, and oxygen normally served as the carrier gas. The effluent oxygen gas was collected over mercury in a known volume at reduced pressure. A correction was made for the oxygen released on the condensation of the oxide vapor.

Flow-rate studies were conducted at 802, 1303, and 1453° and the results show that at the flow rates used (0.01 to 0.10 mmole of O_2/min., depending on temperature and oxygen pressure conditions) equilibrium conditions were established and diffusion effects were not important.

To permit working at pressures of oxygen as low as 0.01 atm. at temperatures around 1500°, argon–oxygen mixtures were tried as carrier gases. However, in each case, it was found that the oxygen content of the mixture decreased appreciably (20 to 30%) in passing through the reaction tube as a result of the formation of ruthenium oxide (solid and vapor). It was simple to analyze the effluent gas mixture mass spectrometrically, but how the oxygen content of the mixture varied during the course of the experiment was quite difficult to determine.

A radiotracer method of analysis was used to determine the quantity of ruthenium transpired. The ruthenium metal used was irradiated in a TRIGA reactor to produce the radionuclide 41-day Ru^{103}. Three different metal samples having activities in the range of 1,000 to 12,000 c.p.m./mg. under our counting conditions have been used. γ-Ray spectra of the samples agreed with spectra reported for Ru^{103}. At the end of each experiment, the mullite condensing region was crushed, placed in a plastic vial, and counted in a well-type counter. Optimum counting conditions were obtained by counting the main γ-energy peak of Ru^{103} (0.50 Mev.) through a window. To minimize geometry problems, each sample was counted at least five times after being shaken between each count. Statistical counting errors were less than 2% standard deviation. For standards, samples of the radioactive metal were weighed out, mixed with crushed mullite, and counted in the same manner as the unknowns. Activities of the unknowns ranged from about 200 to 25,000 c.p.m. The background was about 20 c.p.m.

As a check on analytical procedures, two vapor-pressure measurements were made at each of the temperatures 902 (903), 1002 (1003), and 1303° using different ruthenium metal samples. Agreement among the values obtained (see column 2 of Table I) was satisfactory. It should be mentioned that the same ruthenium metal sample was used throughout the studies on the effect of oxygen pressure on vapor pressure at each temperature.

General.—The materials used were ruthenium metal sponge (Johnson, Matthey, 99.995% purity), oxygen gas (Matheson, research grade), argon gas (Liquid Carbonic), and helium gas (Liquid Carbonic). The oxygen flowed through a sulfuric acid bubbler and P_2O_5 before entering the reaction tube. The helium was purified by passage through a charcoal trap held at liquid nitrogen temperature. A 10% platinum–rhodium wound tube-furnace was used. Pt *vs.* Pt–10% Rh thermocouples were used. Temperature uncertainties are believed to range from ±2° at 800° to ±4° at 1500°.

Results and Discussion

Condensed Phase Studies.—It was found that heating of ruthenium for several days in oxygen at 950° yields an oxide having an oxygen content within 1% of the theoretical value for RuO_2. Other investigators have reported the preparation of RuO_2(s).[2a,8,9]

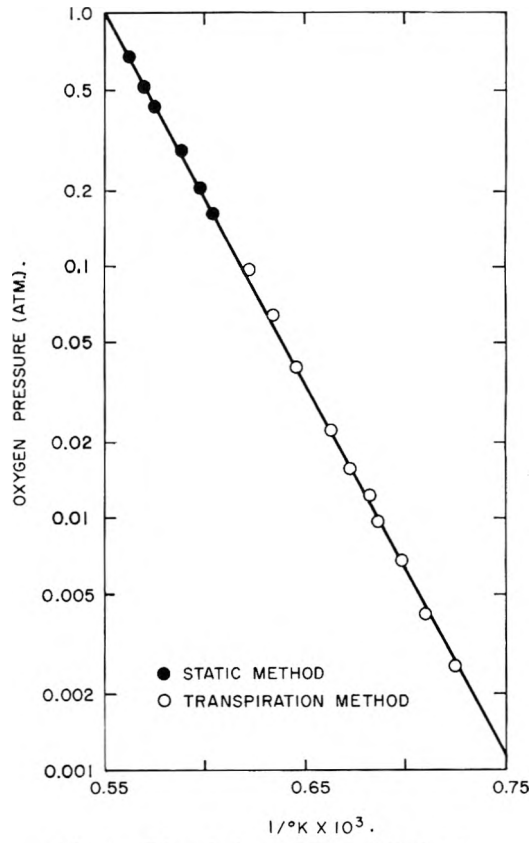

Fig. 1.—Dissociation pressure of RuO_2(s).

To test for lower oxides and also to determine oxygen solubility in the metal, a sample of the oxide contained in a dead-end mullite tube was decomposed at 1450° and at an oxygen pressure that was a few millimeters below the dissociation pressure at 1450°. The sample then was sealed off, quenched in air, and analyzed gravimetrically. The resulting material was obviously metal and contained less than 0.40 atom % oxygen.

In a further test for lower oxides, a mixture of Ru(s) and RuO_2(s) was made in which ruthenium and oxygen were in the atomic ratio 1 to 1. The mixture was sealed in a small evacuated quartz tube, annealed at 1000° for 48 hr., quenched, and then analyzed by X-ray techniques. Diffraction lines were found only for Ru(s) and RuO_2(s).

From the results of these tests and from the fact that the degree of oxidation had no effect on dissociation pressure data (see below), we conclude that RuO_2 is the only stable condensed oxide under our experimental conditions.

Dissocation Pressures.—Dissociation pressure data measured over the range 1107 to 1503° by two different methods are plotted in Fig. 1. The data are linear on the log p *vs.* $1/T$ plot within experimental error and extrapolate to 1 atm. oxygen pressure at 1540°.

From the slope of the line drawn through the points in Fig. 1, we calculate at the mean temperature of the measurements (1570°K.) $\Delta H^\circ_{1570} = -67.4 \pm 1.0$ kcal./mole and from this we obtain $\Delta S^\circ_{1570} = -37.2 \pm 0.5$ e.u. for reaction 1.

(6) W. E. Bell, M. C. Garrison, and U. Merten, *J. Phys. Chem.*, **64**, 145 (1960).

(7) W. E. Bell, U. Merten, and M. Tagami, *ibid.*, **65**, 510 (1961).

(8) F. Krauss and G. Schrader, *Z. anorg. allgem. Chem.*, **176**, 385 (1928).

(9) G. Lunde, *ibid.*, **163**, 345 (1927).

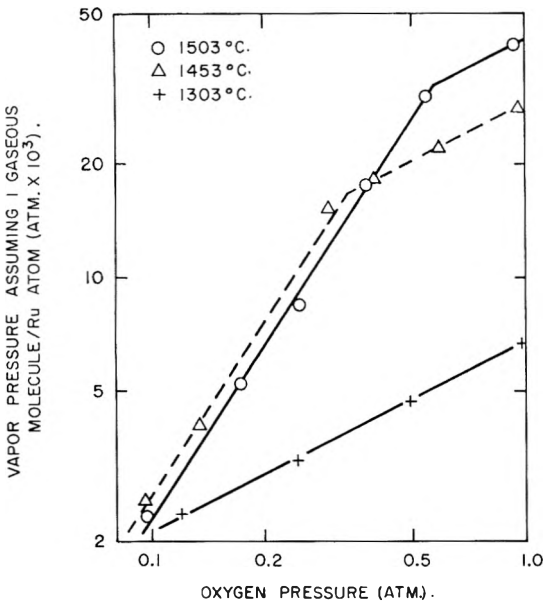

Fig. 2.—Effect of oxygen pressure on vapor pressure at 1303, 1453, and 1503°.

$$Ru(s) + O_2 = RuO_2(s) \qquad (1)$$

Using $\Delta C_p = 3.7 \pm 1.0$ cal./deg.-mole, estimated from heat capacity values for the elements and for solid metal dioxides given by Kelley,[10] we calculate (assuming ΔC_p to be constant) $\Delta H°_{298} = -72.2 \pm 2.0$ kcal./mole; $\Delta S°_{298} = -43.3 \pm 2.0$ e.u.; and log p_{O_2} (atm.) $= -16{,}002/T - 1.862 \log T + 14.89$. The heat of formation agrees with $\Delta H°_{298} = -73 \pm 1$ kcal./mole obtained calorimetrically by Shchukarev and Ryabov.[11]

Combining $\Delta S°_{298}$ with standard entropies $S°_{298}$ Ru $= 6.82 \pm 0.05$ e.u. and $S°_{298}\,O_2 = 49.01 \pm 0.01$ e.u., given by Kelley and King,[12] yields $S°_{298}\,RuO_2(s) = 12.5 \pm 2.0$ e.u. This value seems reasonable when compared with standard entropy values given by Kelley and King[12] for similar oxides: 12.68 ± 0.10, MnO_2; 13.03 ± 0.07, NbO_2; 12.04 ± 0.04, TiO_2; 12.3 ± 0.2, VO_2; 12.12 ± 0.08, ZrO_2.

A slight change in dissociation pressure with oxygen content was observed. For example, in static measurements at 1380° which were begun with a sample of oxide-coated metal particles (X-ray analysis showed that the particles were almost completely converted to the oxide), the first observed vapor pressure was 0.23 atm. On oxygen removal, the dissociation pressure rapidly decreased to 0.16 atm., at which point further removal of oxygen had no effect. This behavior can be attributed to adsorbed oxygen (or gaseous impurities) or to a small range of homogeneity in solid RuO_2.

Except for the initial effect just mentioned, the oxygen content of the sample had no apparent effect on the dissociation pressure values observed at the temperatures of study. This is another indication that solid oxides with oxygen content lower than RuO_2 are not thermodynamically stable under our conditions.

Remy and Kühn[2] reported dissociation pressure data for RuO_2 in the narrow temperature range 923 to 932°. Their pressure values exceed our values in this temperature range by more than two orders of magnitude. They observed a sharp decrease in the dissociation pressure of RuO_2 on mixing a small quantity of ruthenium metal with the oxide. They attributed this behavior to slight solubility of metal in the oxide.

Ortner, Anderson, and Campbell[13] made rough measurements of the dissociation pressure of RuO_2 in the range 1000 to 1450°. Their results, which were reported in the form of an equation, are in reasonable agreement with our results. They calculate $\Delta H°_{298} = -75$ kcal./mole for reaction 1.

Recently, Schäfer, Schneidereit, and Gerhardt[4] measured the dissociation pressure of RuO_2 using glowing-filament, thermobalance, and static techniques. They estimated $S°_{298}\,RuO_2(s) = 14.5$ e.u. using Latimer's tables[14] and calculated the third-law value $\Delta H°_{298} = -71$ kcal./mole for reaction 1. Their results indicate that the oxygen pressure reaches 1 atm. at 1580°.

Identification of Vapor Species.—Since Ru and RuO_2 are the stable condensed phases in the temperature range and in the oxygen pressure range studied, the solid–vapor equilibria to be considered are

$$xRu(s) + \frac{y}{2} O_2 = Ru_xO_y(g) \qquad (2)$$

$$xRuO_2(s) + \frac{y - 2x}{2} O_2 = Ru_xO_y(g) \qquad (3)$$

From the equilibrium constant for reaction 2, we obtain

$$\log p_{Ru_xO_y} = \frac{y}{2} \log p_{O_2} + \log K$$

A similar expression is obtained for reaction 3, and it can thus be seen that $y/2$ and $(y - 2x)/2$ can be evaluated and the vapor species identified by studying the effect of oxygen pressure on vapor pressure.

Vapor pressures measured as a function of oxygen pressure at 1303, 1453, and 1503° are shown on a log–log plot in Fig. 2. The data were plotted assuming one gaseous molecule per ruthenium atom condensed. The lines through the data were drawn with slopes of 0.5 and 1.5. Breaks occur at $p_{O_2} = 0.34$ atm. at 1453° and $p_{O_2} = 0.58$ atm. at 1503°. These values fix the dissociation pressure of $RuO_2(s)$ at the respective temperatures and may be compared with the corresponding values 0.38 and 0.65 atm. taken from the dissociation pressure curve in Fig. 1.

Figure 2 shows that the data conform to 0.5 and 1.5 powers of the oxygen pressure; thus, $y/2 = 1.5$ and $(y - 2x)/2 = 0.5$, $y = 3$ and $x = 1$. It is therefore apparent that the principal vapor species is $RuO_3(g)$ in the temperature range 1300 to 1500°.

To check for lower-oxide vapor species (RuO and RuO_2), several transpiration experiments were conducted at low partial pressures of oxygen using argon–oxygen mixtures as carrier gases. The partial pressure of oxygen in each experiment was determined by mass spectrometric analysis of the effluent gas. Two values obtained at 1453° seem reliable: $p_v = 1.1 \pm 0.1 \times 10^{-3}$ atm. at $p_{O_2} = 0.06 \pm 0.01$ atm., and $p_v = 0.20 \pm 0.04 \times 10^{-3}$ atm. at $p_{O_2} = 0.018 \pm 0.002$ atm. Within the uncertainties given, these values lie on an extrapolation

(10) K. K. Kelley, Bureau of Mines Bulletin 584 (1960).
(11) S. A. Shchukarev and A. N. Ryabov, *Russ. J. Inorg. Chem.*, **5**, 941 (1960).
(12) K. K. Kelley and E. G. King, Bureau of Mines Bulletin 592 (1961).
(13) M. H. Ortner, C. J. Anderson, and P. F. Campbell, U. S. Atomic Energy Commission, Idaho Operations Office, Report IDO-14504, May 19, 1961.
(14) W. M. Latimer, *J. Am. Chem. Soc.*, **73**, 1480 (1951).

of the 1453° curve shown in Fig. 2; thus, the two results provide no evidence for lower oxides.

It was found that vapor pressures measured in the temperature range 800 to 1100° were substantially higher than could be accounted for by $RuO_3(g)$ alone. This behavior suggested the existence of a higher oxide vapor species. This species was, of course, suspected to be $RuO_4(g)$, a familiar vapor species which in a metastable state can exist at appreciable partial pressures at room temperature.

To obtain further evidence for the existence of $RuO_4(g)$, the dependence of vapor pressure on oxygen pressure was studied at 802°. The resulting data are shown in Fig. 3 together with a curve that represents the expected dependence assuming the existence of the vapor species RuO_3 and RuO_4. The curve was derived by summing individual linear pressure-dependence curves for RuO_3 and RuO_4. The individual curves were derived by resolving the observed (total) vapor pressures at 802° (see Table I). It can be seen that the data follow the curve reasonably well.

It will be noted that the vapor pressure data were less consistent at 802° than at higher temperatures (compare Fig. 2 and 3). This behavior can be attributed to the relatively small amount of condensate (0.01 to 0.05 mg.) obtained in each experiment at 802°.

Our observations are in accord with those of Schäfer, Gerhardt, and Tebben.[3] They demonstrated the existence of gaseous RuO_3 and RuO_4 by studying the effect of oxygen pressure on vapor pressure using glowing-filament and transpiration methods.

Alcock and Hooper,[2b] in studies of the volatility of ruthenium in oxygen at 1280° using a transpiration method, observed a 0.5-power oxygen pressure dependence. They considered the solid phase to be ruthenium metal and thus deduced the vapor species to be Ru_xO. Based on presently available dissociation-pressure data, it is apparent that the solid phase was actually RuO_2 under their conditions and that their data are indicative of the vapor species Ru_xO_3.

Norman, Staley, and Bell[15] of this Laboratory have recently conducted a mass-spectrometric study of the ruthenium–oxygen system in the range 850 to 1600° and at oxygen pressures of around 10^{-5} atm. The purpose of this study was to check for the vapor species RuO_2 and RuO. They used a Knudsen cell with provision for an oxygen feed. No evidence was found for lower oxides. The species RuO_3 was readily detected, but the pressure of RuO_4 was below the range of detectability.

Temperature Dependence of Vapor Pressure.—Pressures of ruthenium oxide vapor species have been measured at 1 atm. oxygen pressure over the temperature range 802 to 1503°. The experimental data are shown in column 2 of Table I. Where possible, the vapor pressure values were taken from the pressure-dependence curves in Fig. 2 and 3. The remainder of the values represent the results of individual measurements. Slight corrections were necessary to bring the latter values to an oxygen pressure of 1 atm.

In the temperature range of the measurements (802 and 1503°) and at 1 atm. oxygen pressure, the stable solid phase is RuO_2 and the important vapor species are

(15) J. H. Norman, H. G. Staley and W. E. Bell, to be published.

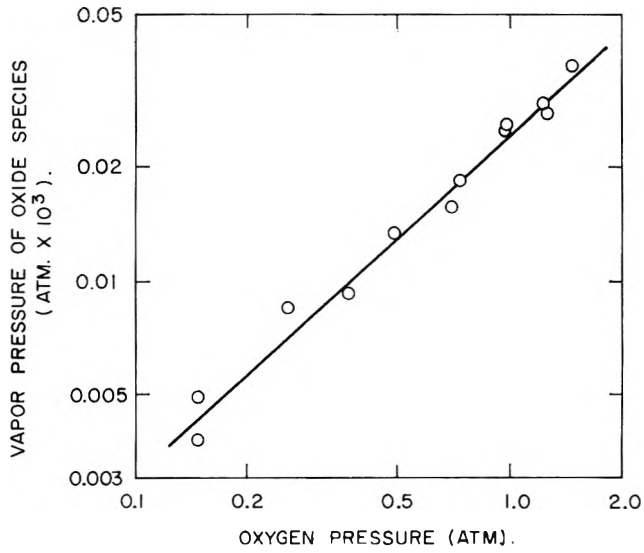

Fig. 3.—Effect of oxygen pressure on vapor pressure at 802°.

TABLE I

OBSERVED TOTAL VAPOR PRESSURES AND CALCULATED PARTIAL PRESSURES OF RuO_3 AND RuO_4 AT 1-ATM. OXYGEN PRESSURE

Temp., °C.	Observed total pressures, atm. × 10^3	Calculated individual pressures, atm. × 10^3 p_{RuO_3}	p_{RuO_4}	Calculated total pressure, atm. × 10^3, $p_{RuO_3} + p_{RuO_4}$
802	0.024[a]	0.0032	0.021	0.024
902	.078	.025	.051	.076
903	.085	.025	.052	.077
1002	.26	.136	.109	.25
1003	.27	.139	.110	.25
1103	.78	.60	.21	.81
1153	1.20	1.16	.28	1.44
1203	2.4	2.13	.36	2.5
1303	6.8[a]	6.5	.59	7.1
1303	7.7	6.5	.59	7.1
1403	18.5	17.1	.91	18.0
1453	28[a]	27	1.11	28
1503	42[a]	41	1.34	42

[a] Taken from Fig. 2 and 3.

RuO_3 and RuO_4. Therefore, the vaporization equilibria of importance are

$$RuO_2(s) + {}^1/_2O_2 = RuO_3(g) \qquad (4)$$

and

$$RuO_2(s) + O_2 = RuO_4(g) \qquad (5)$$

Both vaporization reactions are important over the entire temperature range of study; thus, each of the observed vapor pressure values given in column 2 of Table I represents the sum of individual partial pressures of RuO_3 and RuO_4.

In order to determine thermodynamic values and individual pressures of the two species, it was necessary to resolve the observed vapor pressure data. This was done with the aid of an iterative procedure in an IBM-7090 computer. The computation involved fitting the equation

$$p_{RuO_3} + p_{RuO_4} = Ae^{C/T} + Be^{D/T} \qquad (6)$$

to the data by a least-squares method. Equation 6 was derived from the usual thermodynamic relationships assuming the heat and entropy changes to be constant over the temperature range of the measurements.

The constants A, B, C, and D represent heat and entropy changes for reactions 4 and 5. In the computation, approximate values of the constants were first calculated by hand. These were fed into the computer and the iterative procedure was continued until the constants were changing only slightly with iteration number. At this point, the fit looked as good as could be expected and further iterations did not seem worthwhile.

Thermodynamic values derived from the computation are $\Delta H^\circ_{1400} = +51.2 \pm 1.0$ kcal./mole and $\Delta S^\circ_{1400} = +22.5 \pm 1.0$ e.u. for reaction 4, and $\Delta H^\circ_{1400} = +22.5 \pm 2.0$ kcal./mole and $\Delta S^\circ_{1400} = -0.2 \pm 2.0$ e.u. for reaction 5. The uncertainty given for each thermodynamic value was derived from estimated uncertainties in the vapor pressure values.

Using these thermodynamic values, the individual partial pressures of RuO_3 and RuO_4 shown in columns 3 and 4 of Table I are calculated. The calculated sums of the individual pressures are given in column 5, and it can be seen that they are in good accord with the observed pressures in column 2.

Using the heat and entropy values computed for reaction 4 and an estimated ΔC_p of -2.7 ± 1.0 cal./deg.-mole (based on heat capacity values for gaseous metal oxides given by Kelley,[10] the heat capacity for $RuO_3(g)$ was taken to be 20), we calculate $\Delta H^\circ_{298} = +54.2 \pm 2.0$ kcal./mole and $\Delta S^\circ_{298} = +26.7 \pm 2.0$ e.u. for reaction 4. ΔC_p was assumed to be constant in the calculation.

Combining ΔS°_{298}, S°_{298} $RuO_2(s) = 12.5 \pm 2.0$ e.u., calculated above, and $S^\circ_{298}O_2 = 49.01 \pm 0.01$ e.u., given by Kelley and King,[12] yields S°_{298} $RuO_3(g) = 63.7 \pm 4.0$ e.u. This value appears reasonable when compared with S°_{298} values given by Kelley and King[12] for other metal oxide gases: 55.80 ± 0.10, TiO; 57.7 ± 2.0, VO_2; and 70.1 ± 1.0, OsO_4.

By combining ΔH°_{298} and ΔS°_{298} values for reaction 4 with respective heat and entropy values given above for reaction 1, we calculate $\Delta H^\circ_{298} = -18.0 \pm 4.0$ kcal./mole and $\Delta S^\circ_{298} = -16.6 \pm 4.0$ e.u. for the formation reaction

$$Ru(s) + {}^3/_2O_2 = RuO_3(g) \qquad (7)$$

The ΔH°_{298} value for reaction 7 may be compared with $\Delta H^\circ_{298} = -12.7$ kcal./mole calculated by Schäfer, Tebben, and Gerhardt[5] from their data using a third-law method. Based on statistical considerations, they took S°_{298} $RuO_3(g)$ to be 68.3 ± 2 e.u.

Standard heats and entropies for reaction 5 are now calculated using the ΔH°_{1400} and ΔS°_{1400} values computed for the reaction. ΔC_p is estimated to be -2.7 ± 1.0 cal./deg.-mole (based on the heat capacity for $OsO_4(g)$ given by Kelley,[10] the heat capacity for $RuO_4(g)$ was taken to be 24), and it is assumed to be constant with temperature. Thus, $\Delta H^\circ_{298} = +25.5 \pm 3.0$ kcal./mole and $\Delta S^\circ_{298} = +4.0 \pm 3.0$ e.u. for reaction 5.

Combining ΔS°_{298} with standard entropy values for $RuO_2(s)$ and O_2 given above yields S°_{298} $RuO_4(g) = 65.5 \pm 5.0$ e.u. This value appears reasonable when compared with the S°_{298} values given above for other metal oxide gases.

By combining thermodynamic quantities for reactions 5 and 1, we obtain $\Delta H^\circ_{298} = -46.7 \pm 5.0$ kcal./mole and $\Delta S^\circ_{298} = -39.3 \pm 5.0$ e.u. for the formation reaction

$$Ru(s) + 2O_2 = RuO_4(g) \qquad (8)$$

Schäfer, Tebben, and Gerhardt calculated from their data by the third-law method that $\Delta H^\circ_{298} = -43.2$ kcal./mole for reaction 8. They used S°_{298} $RuO_4(g) = 69.3$ e.u., which they derived from statistical considerations.

Acknowledgments.—The authors are indebted to Drs. Ulrich Merten and J. H. Norman for suggestions and helpful discussions, and to R. E. Inyard for performing part of the experimental work.

A CORRELATION BETWEEN THE CATALYTIC ACTIVITY OF PLATINUM AND ITS ABILITY TO ADSORB HYDROGEN[1]

BY THOMAS C. FRANKLIN AND DONALD H. MCCLELLAND

Chemistry Department, Baylor University, Waco, Texas

Received May 31, 1963

A study was made of the catalytic activity of platinized platinum used for the decomposition of hydrogen peroxide and the hydrogenation of quinone. The surface area of the platinum was measured by its ability to adsorb hydrogen. It was concluded that the hydrogenation of quinone occurred on the whole surface, whereas the decomposition of the hydrogen peroxide only occurred on certain sites.

Recently, a series of studies has been made of different processes occurring on platinum electrodes using the ability of the electrode to adsorb hydrogen as a measure of the surface area of the electrode.[2]

It has been observed repeatedly that there are two surface forms of hydrogen.[3-8] As part of these studies, an examination was made of other surface processes to see which of the two sites was involved. Therefore, a comparison was made between the catalytic activity of a platinum electrode and its ability to adsorb hydrogen in the two forms. A study was made of two types of

(1) The hydrogen peroxide portion of this paper was presented at the Southwest Regional Meeting of the American Chemical Society at Tulsa, Oklahoma, in 1957.

(2) (a) T. C. Franklin and R. D. Sothern, *J. Phys. Chem.*, **58**, 951 (1954); (b) M. W. Breiter and S. Gilman, *J. Electrochem. Soc.*, **109**, 622 (1962).

(3) A. Eucken and B. Weblus, *Z. Elektrochem.*, **55**, 114 (1951).

(4) M. Breiter, C. A. Knorr, and V. Volkl, *ibid.*, **59**, 681 (1955).

(5) M. Breiter, H. Kammermaier, and C. A. Knorr, *ibid.*, **60**, 37 (1956).

(6) M. Breiter, H. Kammermaier, and C. A. Knorr, *ibid.*, **60**, 119 (1956).

(7) T. C. Franklin and S. L. Cooke, Jr., *J. Electrochem. Soc.*, **107**, 555 (1960).

(8) C. H. Presbrey, Jr., and S. Schuldiner, U. S. Naval Research Laboratory Report 5472, Washington, D. C., 1962.

catalytic processes, the catalytic decomposition of hydrogen peroxide and the catalytic hydrogenation of *p*-benzoquinone.

Both processes have been investigated previously by a number of workers. The decomposition of hydrogen peroxide[9-18] has been found to be first order with respect to hydrogen peroxide composition and first order with respect to the amount of platinum. The catalytic hydrogenation of *p*-benzoquinone also has been investigated[19-21] and has been found to be zero order with respect to the quinone.

Experimental

The electrodes were 20-gage platinum wires sealed in glass. The electrodes were chemically cleaned with aqua regia and then electrolytically cleaned by alternately generating hydrogen and oxygen on the electrodes in 2 *N* sulfuric acid. After rinsing in distilled water, the electrodes were plated in a 3% chloroplatinic acid solution containing various amounts of lead acetate. The electrodes were plated at 2–25 ma. for 60–600 sec. to obtain a wide range of catalytic activity. After plating, the electrodes were placed in 2 *N* sulfuric acid and again alternately hydrogen and oxygen were electrolytically generated on the electrode until the time for the potential to pass from the oxygen evolution potential to the hydrogen evolution potential became constant.

The cell for the hydrogen peroxide experiments was a test tube connected with a stopcock to a large nonpolarizable mercury–mercury(I) sulfate reference electrode. In the reaction cell were the platinized platinum electrode to be tested, a small rotating bright platinum electrode, and a hydrogen bubbler. The stopcock was open only during the time it took to make an electrical measurement. Hydrogen was bubbled through the solution until the potential of the platinized platinum electrode became constant. The bubbling was stopped and the system was allowed to come to equilibrium for several minutes. The potential of the electrode was determined with a student potentiometer and the amount of hydrogen on the electrode was measured by the previously described coulometric technique[7] in which the hydrogen was oxidized polarographically and the large reference electrode was used as a nonpolarizable electrode. The area under the hydrogen maxima was used as a measure of the amount of hydrogen adsorbed on the electrode.

With some of the large electrodes the currents were so large that the voltage no longer increased linearly with time and the two hydrogen maxima became hard to separate. Therefore, the normal polarographic circuit was modified with a very simple one-transistor current amplifier.

The oxidation procedure was repeated until reproducible results were obtained. In the hydrogen peroxide experiments, the solution then was flushed with oxygen until the hydrogen was removed, leaving the solution saturated with oxygen. The concentration of the hydrogen peroxide was measured voltammetrically during the decomposition using a rotating microplatinum electrode.[22,23] The residual current was determined in the oxygen-saturated solution, then a known amount of hydrogen peroxide was added to the solution. Polarograms were obtained every 3 to 4 hr. during the course of the decomposition.

In the hydrogenation experiments, *p*-benzoquinone of a certain concentration was introduced into the reaction cell and hydrogen was bubbled at a constant and reproducible rate (150–160 bubbles/min.). Prior to the introduction of the *p*-benzoquinone, the amount of hydrogen on the electrode was determined coulometrically. The cell consisted of a 1.5-ml. vessel containing the platinized platinum electrode and a hydrogen bubbler. It was connected through stopcocks and capillary tubing to a large nonpolarizable mercury–mercury(I) sulfate electrode and a Beckman reference calomel electrode. After the introduction of the *p*-benzoquinone, the electrode was introduced into the solution and the potential difference between the platinum and calomel electrodes was recorded as a function of time. The electrode remained at the potential for the *p*-benzoquinone until almost all of the quinone was gone, then returned to the potential of the hydrogen electrode. The length of time from the insertion of the electrode until the return of the potential to 0 volts was used as the time for the reaction to proceed to a specific fraction of completion. After rinsing the cell and electrode with 2 *N* sulfuric acid, the procedure was repeated using varying amounts of *p*-benzoquinone.

The *p*-benzoquinone was purified by recrystallization from petroleum ether (b.p. 80–110°) and sublimation. The purity, as

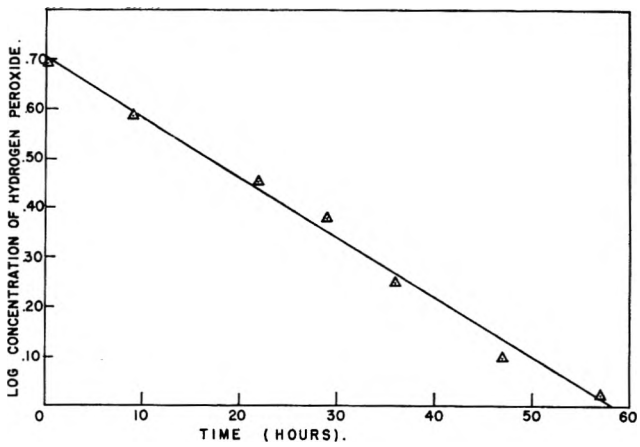

Fig. 1.—The log of the hydrogen peroxide concentration *vs.* time for the decomposition of hydrogen peroxide.

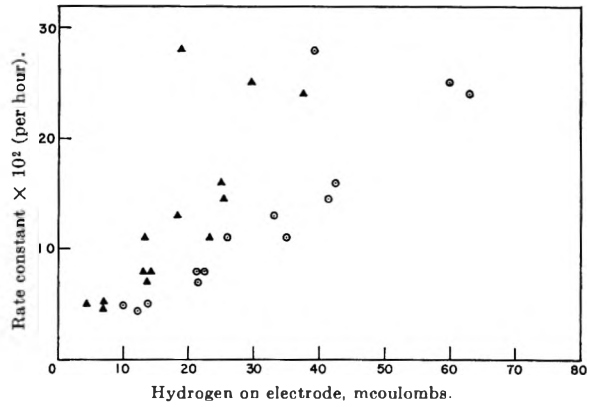

Fig. 2.—Rate constants for the heterogeneous decomposition of hydrogen peroxide on platinized platinum as a function of the amount of hydrogen.

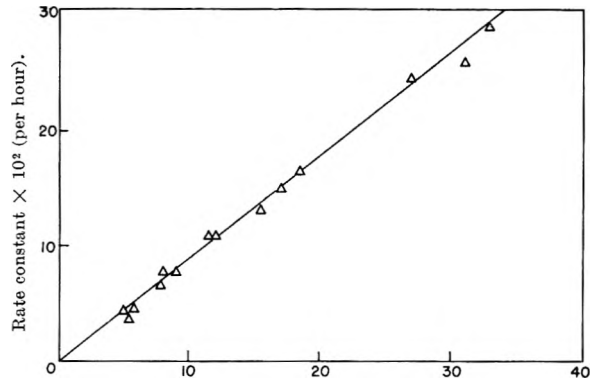

Fig. 3.—Rate constants for the heterogeneous decomposition of hydrogen peroxide on platinized platinum as a function of the amount of hydrogen adsorbed in the second form.

(9) G. Bredig, *Z. Elektrochem.*, **12**, 581 (1906).
(10) J. G. Telotov, *J. Russ. Phys. Chem. Soc.*, **39**, 1146 (1906).
(11) K. Barnmann, *Z. Elektrochem.*, **15**, 673 (1909).
(12) D. A. MacInnis, *J. Am. Chem. Soc.*, **35**, 878 (1914).
(13) G. Bianchi, G. Caprioglio, G. Davalio, F. Massa, and T. Mussini, *Chem. Ind.* (Milan), **43**, 146 (1961).
(14) J. Giner, *Z. Elektrochem.*, **64**, 491 (1960).
(15) R. Gerishcher and H. Gerishcher, *Z physik. Chem.*, **6**, 178 (1956).
(16) D. Winklemen, *Z. Elektrochem.*, **60**, 731 (1956).
(17) J. Weiss, *Trans. Faraday Soc.*, **31**, 1547 (1935).
(18) J. Lopis and J. M. Guillen, *Anales real soc. espan. fis. quim.* (Madrid), **53B**, 5 (1957).
(19) E. F. Rosenblatt, *J. Am. Chem. Soc.*, **62**, 1092 (1940).
(20) M. M. Popova and D. V. Sokolskii, *Tr. Inst. Khim. Nauk Akad. Nauk, Kozakh., SSR*, **2**, 70, 84 (1958).
(21) M. M. Popova and D. V. Sokolskii, *Zh. Fiz. Khim.*, **33**, 2573 (1959).
(22) D. Winkelmann, *Z. Elektrochem.*, **60**, 731 (1956).
(23) A. Hamamoto and T. Ansco, *Oyo Denki Kenkyusho Iho*, **9**, 206 (1957).

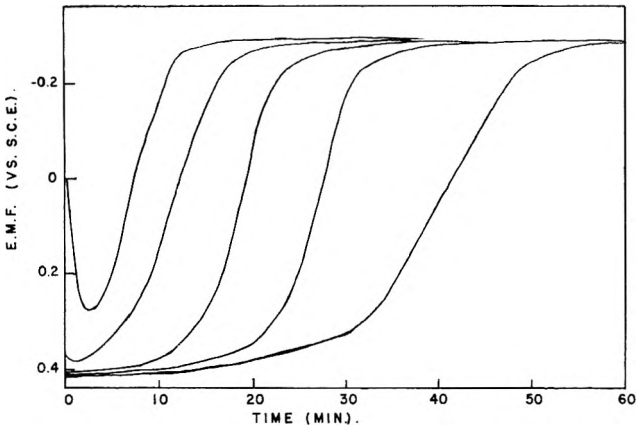

Fig. 4.—The potential of the electrode (*vs.* saturated calomel electrode) *vs.* time for varying amounts of added quinone.

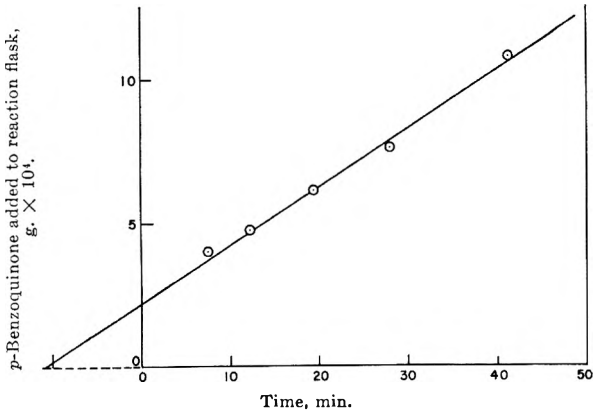

Fig. 5.—The effect of added quinone on the time necessary for the potential of the electrode to return to 0.00 v.

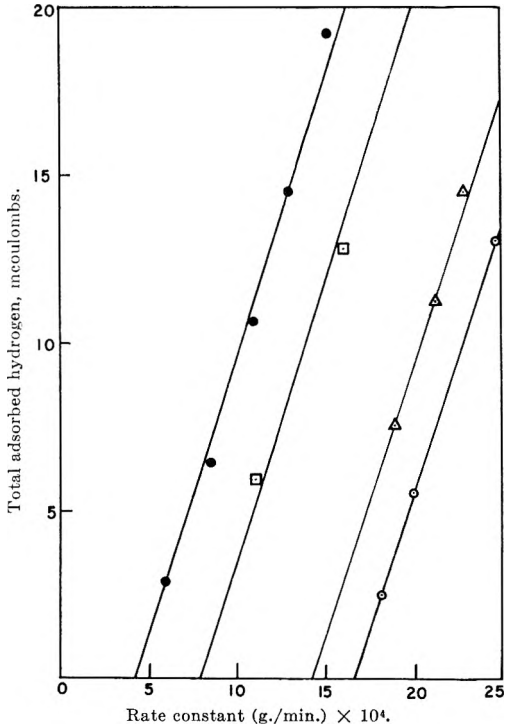

Fig. 6.—The effect of the ability of the electrode to adsorb hydrogen on the hydrogenation rate constants. The different symbols indicate different platinum base electrodes.

determined by an amperometric titration with sodium thiosulfate, was 99+%. The solutions were prepared fresh for each run since the quinone underwent a slow polymerization in the 2 *N* sulfuric acid.

All other chemicals were the best grade available commercially. The water was triply distilled, once over basic potassium permanganate. It had a maximum conductivity of 3×10^{-6} mho/cm. The commercial tank hydrogen was purified by passing it over hot copper wire, hot platinized asbestos, sodium hydroxide pellets, and finally 1–16 mesh silica gel.

All glassware was cleaned first with kerosene, then chromic acid, and, after rinsing thoroughly with triply distilled water, was soaked in the water for several hours. All connections were made with Tygon tubing. The temperature was maintained at 25 ± 0.2°.

Data and Discussion of Results

Hydrogen Peroxide Decomposition.—Figure 1 shows a plot of the log of the concentration of the hydrogen peroxide *vs.* time for a typical run. This plot shows the reaction to be first order with respect to hydrogen peroxide.

Figures 2 and 3 are plots of the rate constants for the decomposition of hydrogen peroxide *vs.* the activities of the electrode as measured by its ability to adsorb hydrogen in the various forms. It is seen that there is no relationship between the rate constant and the total ability of the electrode to adsorb hydrogen or its ability to adsorb hydrogen in the first form (the one oxidized at the lowest potentials). However, it is seen that the decomposition is first order with respect to the ability of the electrode to adsorb hydrogen in the second form.

Hydrogenation of *p*-Benzoquinone.—The potential *vs.* time curves for a particular electrode using various amounts of benzoquinone are shown in Fig. 4. In Fig. 5 it is seen that a plot of time necessary to return to zero potential (*vs.* saturated calomel electrode) against the weight of *p*-benzoquinone added to the cell is linear, indicating a reaction that is zero order with respect to quinone. The zero potential was chosen because the curve has its maximum slope in this region. This leaves a constant amount of unreacted material in each case. The only effect this has, since it is a zero-order reaction, is to cause the curve to not have a zero intercept.

Figure 6 is a plot of the zero-order rate constant (as determined from the slopes of plots similar to that in Fig. 5) against the total amount of hydrogen adsorbed on the electrode. It is seen that the reaction is first order with respect to the total amount of hydrogen in the cases where the electrode area was varied by varying the plating conditions. However, the rate was also influenced by the area of the base electrode, as is seen from the fact that one obtains four different straight lines with four different base electrodes. The four lines are parallel. If one plots the intercepts against the geometric areas of the wires used, one observes a straight line. This indicates that there is a small secondary reaction or reactions removing the quinone, but that the primary surface hydrogenation is first order with respect to the total area occupied by the hydrogen.

Conclusions

The two reactions studied here have been studied previously by several workers and have some similarities in mechanism. Vetter[24] has put forth an electron-transfer mechanism for the catalytic reduction of the quinone on the bare platinum electrode. The hydrogenation involves an anodic and cathodic reaction with the bare platinum acting as an electron acceptor and donor. Similarly, the catalytic decomposition of hy-

(24) K. J. Vetter, *Z. Elektrochem.*, **56**, 797 (1952).

drogen peroxide has been indicated to be an electrochemical reaction taking place on an oxide of platinum, an anodic reaction and a cathodic reaction; however, in this case the platinum oxide acts as an electron acceptor and donor.[14,15,17,18,25]

The data in these experiments are explainable in terms of this mechanism. The quinone is a strong enough oxidizing agent to reduce both forms of hydrogen. Therefore, the total surface takes part in the catalytic reduction of the quinone.

The hydrogen peroxide data indicate that the two forms of adsorbed hydrogen are significantly different. The decomposition of the hydrogen peroxide occurred on an oxidized electrode. The fact that the rate of decomposition is related only to the second form of hydrogen indicates that the difference in energy for bonding of hydrogen to the metal is basically a property of the metal surface and the same difference extends to the bonding of oxygen on the surface.

Acknowledgment.—We wish to acknowledge the fellowship given by Phillips Petroleum Company in support of this work. In addition, the research reported in this paper has been sponsored in part by the Geophysics Research Directorate of the Air Force Cambridge Research Laboratories, Office of Aerospace Research, under contract AF 19(604)-8414.

(25) I. A. Bagotskaya and I. E. Yablokova, *Dokl. Akad. Nauk SSSR*, **95**, 1219 (1954).

VISCOELASTIC PROPERTIES OF A SIMPLE ORGANIC GLASS

By A. V. Tobolsky and R. B. Taylor

Department of Chemistry, Princeton University, Princeton, New Jersey

Received May 31, 1963

The shear compliance of a three-dimensional glass-forming substance, Galex, composed largely of dehydroabietic acid, has been studied as a function of time and temperature by a ball indentation method, and the results are expressed in terms of a master curve of shear compliance against time at 15°. This curve has been analyzed to separate the various components of the compliance and it is found that a glassy compliance, a single retardation time, and a steady flow shear viscosity are sufficient to describe the viscoelastic behavior of the compliance over the entire time scale. This is in striking contrast to the broad distribution of retardation times exhibited by polymeric materials. The glass transition temperature has been determined by volume temperature measurements and found to be 7°. The variation of the shear viscosity and the viscoelastic shift factors as a function of temperature are also discussed.

Introduction

Although many investigations have been reported on the viscoelastic behavior of high polymer systems, very few have dealt with low molecular weight glass-forming materials. Benbow[1] has studied such systems by dynamic methods using 2-hydroxypentamethyl flavan as material and the rheological behavior of glucose[2] has also been investigated.

The material chosen for the present study was dehydroabietic acid (Galex). In molecular structure it may be represented as a roughly spherical molecule, so that the intermolecular interactions must be described as three-dimensional, similar in kind to those that exist in a molecular crystal structure. However, the regularity of a crystal structure is absent in this glass-forming material. Plastic flow by dislocations, so characteristic of crystals, is not pertinent here. In this study we were particularly interested in the viscoelastic properties of Galex in the region of transition between glass and liquid. Linear amorphous polymers such as polystyrene also undergo a glass-to-liquid transition. The interactions between segments of neighboring polymer molecules are of the same type as found in Galex. In the region of transition between glass and rubber, however, intramolecular segmental motion is of great significance. This type of molecular motion has been treated by Rouse and Bueche[3,4] as being analogous to a one dimensional array of masses coupled by springs, the entire array being immersed in a viscous fluid. This type of one dimensional motion gives rise to a very broad distribution of relaxation or retardation times.

Tobolsky[5] has calculated that the distribution of relaxation times in a three dimensional array should be very much narrower than that for a linear array and considered Galex as a substance by means of which this prediction might be verified.

Experimental

Galex is the trade name of a dehydrogenated rosin supplied by the National Rosin Oil Products Co. It is a stable nonoxidizing material. The stability is obtained by dehydrogenation of abietic acid, the principal constituent of rosin, to dehydroabietic acid, which contains the benzenoid nucleus.

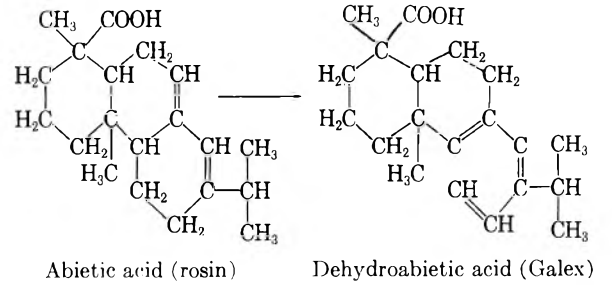

Abietic acid (rosin) Dehydroabietic acid (Galex)

The Galex, contained in shallow glass vessels, was heated in an oven at 100° until completely liquid and allowed to cool slowly to room temperature in order to minimize local stresses due to uneven contraction. This method produced short cylinders having parallel ends.

The method chosen to measure the viscoelastic behavior was a ball indentation method. By applying a force to a sphere of known diameter and measuring the indentation as a function of time, the shear compliance $J(t)$ could be calculated. The inden-

(1) J. J. Benbow, *Proc. Phys. Soc.* (London), **B67**, 120 (1954).

(2) G. S. Parks, L. E. Barton, M. E. Spaght, and J. W. Richardson, *Physics*, **5**, 193 (1934).

(3) P. E. Rouse, *J. Chem. Phys.*, **21**, 1272 (1953).

(4) F. Bueche *ibid.* **22**, 603 (1954).

(5) A. V. Tobolsky, *ibid.*, **37**, 1575 (1962).

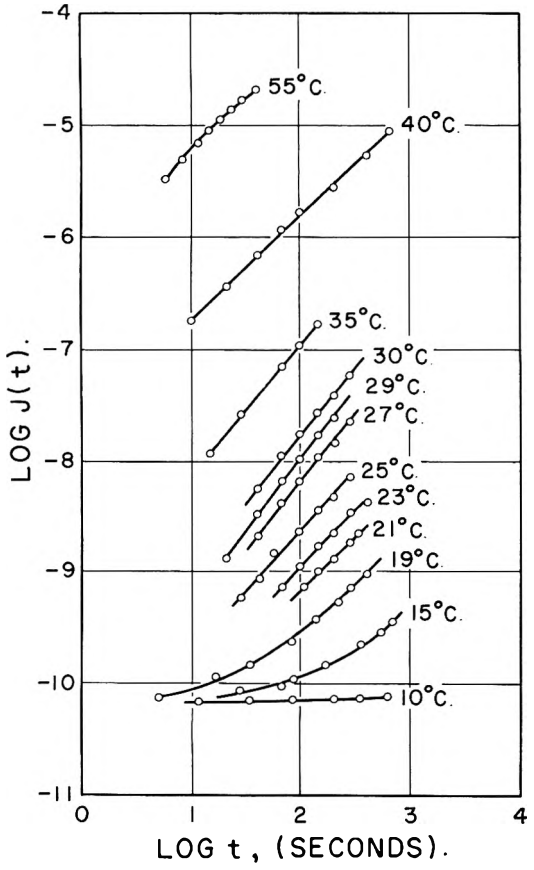

Fig. 1.—Double logarithmic plots of $J(t)$ *vs.* t at various temperatures.

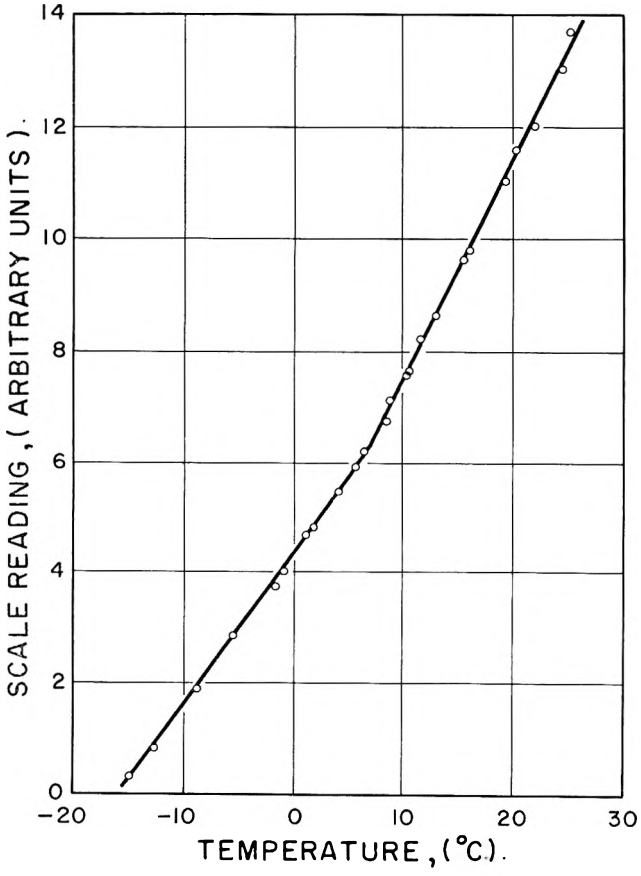

Fig. 2.—Plot of volume *vs.* temperature for Galex.

tation could be estimated to 2.5×10^{-4} cm. The sample and indentor were enclosed in an air chamber in which the temperature was controlled to ±0.1°. Measurements over periods of 40 to 1000 sec. were made at 12 temperatures between 10 and 55°.

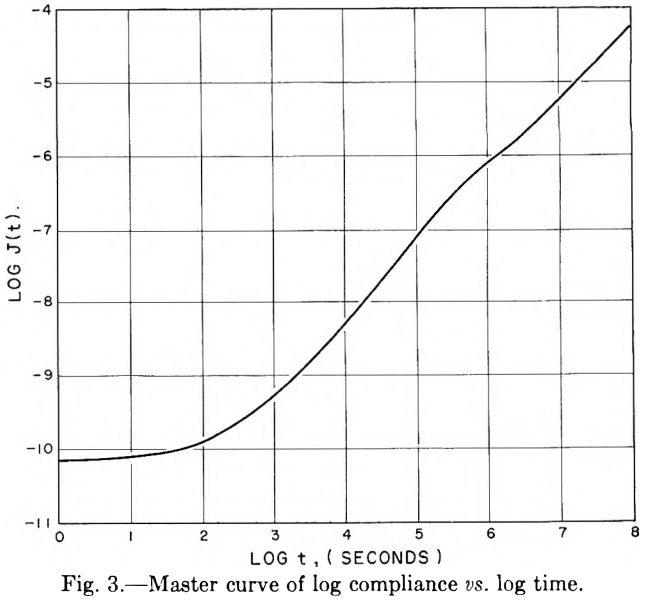

Fig. 3.—Master curve of log compliance *vs.* log time.

In all cases the indentation at the longest time was less than 10% of the diameter of the particular ball being used. For this condition the compliance is given by the equation[6,7]

$$J(t) = \frac{16}{3} \frac{R^{1/2}}{F\,(\mathrm{d}(t))^{3/2}} \qquad (1)$$

where $\mathrm{d}(t)$ is the displacement at time t resulting from a force F applied at zero time to a sphere of radius R.

This method yielded excellent reproducibility in the region $10^{-9} < J < 10^{-6}$ cm.²/dyne. In the lower compliance regions some inaccuracy was encountered due to extremely small indentations. For these cases the results quoted represent the mean of several runs at the same temperature. At regions of high compliance, the magnitude of the applied force was rendered uncertain since the effect of friction in the apparatus became appreciable. For these regions mean values were also taken. The results of these measurements plotted logarithmically are shown in Fig. 1.

Determination of the glass transition temperature was made by containing the Galex in a dilatometer under toluene and heating at a uniform rate of 1°/min., noting the scale reading on a cathetometer as a function of temperature. Figure 2 shows the results obtained on two separate runs yielding a value of 7° for the glass transition temperature.

Discussion

Assuming the validity of the time–temperature superposition principle for such a system, we reduced the curves of Fig. 1 to an arbitrary temperature of 15° and obtained the so-called "master-curve" of the shear compliance $J(t)$ as a function of time. This is shown in Fig. 3. This curve is seen to exhibit a glassy compliance at low times followed by a transition region leading to a steady-state viscosity. In contrast to most polymeric systems, there is no intermediate plateau indicating rubbery behavior.

The curve in Fig. 3 may be described by the equation

$$J(t) = J_g + \int_{-\infty}^{+\infty} L(1 - e^{-t/\tau})\, \mathrm{d} \ln \tau + \frac{t}{\eta} \qquad (2)$$

J_g is the value of the glassy compliance, τ the retardation time, L the distribution of retardation times, and t/η a term describing the steady-state viscosity prevailing at long times. The middle term is a measure of the truly viscoelastic nature of the material. In order to separate this term, the glassy compliance was esti-

(6) L. Larrick, *Phys. Rev.*, **57**, 358 (1940).
(7) H. C. Pocklington, *Proc. Cambridge Phil. Soc.*, **36**, 507 (1940).

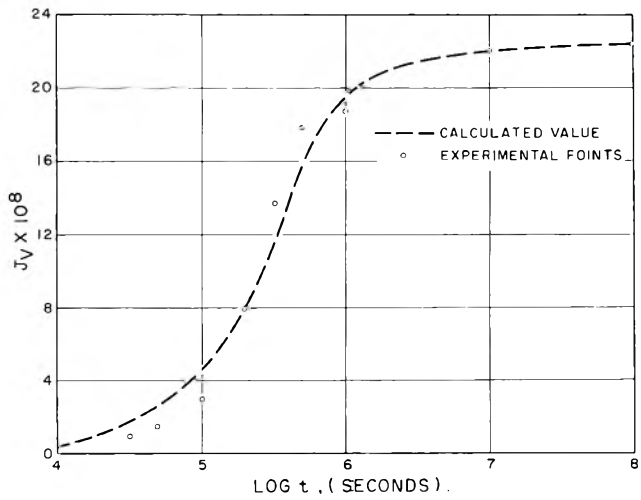

Fig. 4.—Plot of J_v *vs.* log t: Dashed curve calculated by eq. 4; experimental points obtained by eq. 3.

mated as 6.9×10^{-11} cm.²/dyne and the viscosity at 15° was calculated as described below to be 2.7×10^{12} poises. Then

$$J_v = \int_{-\infty}^{+\infty} L(1 - e^{-t/\tau})\, d \ln \tau = J(t) - J_g - \frac{t}{\eta} \quad (3)$$

was calculated for several values of t. A plot of $J(v)$ *vs.* log t is shown in Fig. 4 and illustrates the viscoelastic behavior of the material. The significance of this behavior lies in the extremely narrow time range in which viscoelastic effects are operative compared to that observed for polymeric materials, indicating a narrow distribution of retardation times.

If the behavior of the material can be approximated in terms of a single retardation time, the above integral may be replaced by

$$J_v = J_i(1 - e^{-t/\tau}) \quad (4)$$

where J_i is the limiting compliance at very long times. Equation 4 may be written

$$\log (J_i - J_v) = \log J_i - \frac{t}{2.303\tau} \quad (5)$$

Under these circumstances a plot of log $(J_i - J_v)$ *vs.* t should yield a straight line of gradient $-1/2.303\tau$. This was found to be the case and a value of $\tau = 4.8 \times 10^5$ sec. was calculated. With this value of τ, eq. 4 was plotted as the dashed curve in Fig. 4. At low values of time, meaningful values of J_v could not be obtained but over a considerable part of the time scale eq. 4 seems to predict the viscoelastic behavior reasonably well.

Equation 2 may be rewritten by substituting $J_i \cdot (1 - e^{-t/\tau})$ for the integral and using the experimental obtained values of J_g and J_i. This yields the equation

$$J(t) = 6.9 \times 10^{-11} + 2.24 \times 10^{-7}(1 - e^{-t/\tau}) + \frac{t}{\eta}$$

where τ and η are temperature dependent.

The temperature dependence of such viscoelastic processes may be described by two methods. First, the variation of the shift factors K with temperature may be described by an equation of the Arrhenius form as shown in Fig. 5. This yields a high value (67 kcal./mole) for the apparent activation energy of the

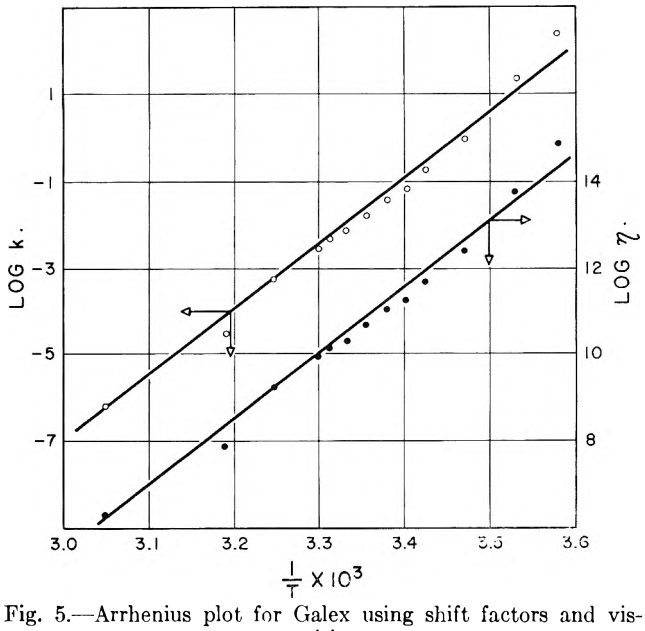

Fig. 5.—Arrhenius plot for Galex using shift factors and viscosities.

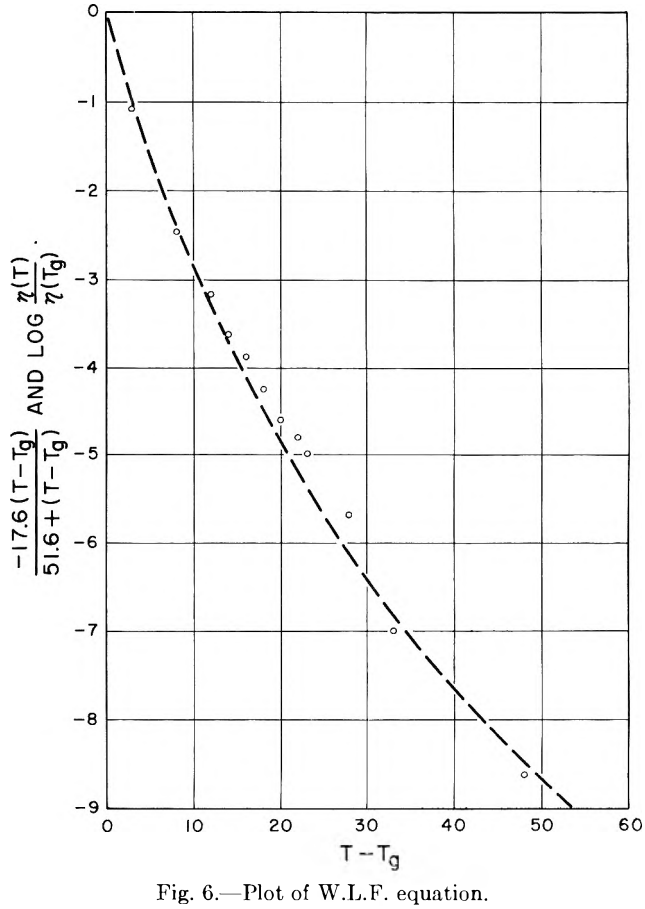

Fig. 6.—Plot of W.L.F. equation.

process. A similar plot for the variation of viscosity with temperature yields substantially the same value. In both of these plots some curvature may be detected. It has been shown[8] that a considerable increase in apparent activation energy should occur as the glass transition temperature is approached owing to the rapid decrease in free volume.

A more modern treatment of the temperature dependence is embodied in the W.L.F. equation which may be written in the form

(8) J. Bischoff, E. Catsiff, and A. V. Tobolsky, *J. Am. Chem. Soc.*, **74**, 3378 (1952).

$$\log \frac{\eta(T)}{\eta(T_g)} = -\frac{17.6(T - T_g)}{51.6 + (T - T_g)} \qquad (6)$$

This is a semiempirical equation, the constants in which have been found to render the equation applicable for many polymer systems.

In order to test the fit of the present data to eq. 6 the following procedure was adopted. From a plot of log K *vs.* $(T - T_g)$, the K-value at 7° was obtained by extrapolation. Making use of the equations

$$\frac{K(T)}{K(T_g)} = \frac{\eta(T)}{\eta(T_g)} = \frac{\tau(T)}{\tau(T_g)} \qquad (7)$$

values of the viscosity and retardation time were obtained at several temperatures using the value of η_{55} as determined from $J_{(t)} = t/\eta$ for the steady flow region,

TABLE I

Temp., °C.	K	η, poises	τ, sec.
7	2.98×10^{2}	8×10^{14}	1.46×10^{8}
10	2.52×10^{1}	6.76×10^{13}	1.20×10^{7}
15	1	2.68×10^{12}	4.8×10^{5}
19	2×10^{-1}	5.36×10^{11}	9.6×10^{4}
21	7.15×10^{-2}	1.98×10^{11}	3.42×10^{4}
23	3.97×10^{-2}	1.06×10^{11}	1.9×10^{4}
25	1.8×10^{-2}	4.82×10^{10}	8.65×10^{3}
27	7.52×10^{-3}	2.01×10^{10}	3.59×10^{3}
29	5.0×10^{-3}	1.34×10^{10}	2.40×10^{3}
30	3.14×10^{-3}	8.42×10^{9}	1.50×10^{3}
35	6.3×10^{-4}	1.65×10^{9}	3.01×10^{2}
40	3.0×10^{-5}	8.0×10^{7}	1.44×10^{1}
55	7.46×10^{-7}	2.0×10^{6}	3.58×10^{-1}

and $\tau_{15} = 4.8 \times 10^{5}$ sec. evaluated as described above. The values of K, η, and τ are listed for the various temperatures in Table I. A plot of $[-17.6(T - T_g)]/[51.6 + (T - T_g)]$ *vs.* $(T - T_g)$ is shown as the dashed line in Fig. 6. Values of $\eta(T)/\eta(T_g)$ calculated from Table I are also plotted as a function of $T - T_g$ and the experimental points are seen to be in good agreement with the theoretical line. From the volume temperature study, the coefficients of expansion α_l and α_g for the liquid and glassy states were calculated. Equation 6 may be written, from the free volume theory, as

$$\log \frac{\eta(T)}{\eta(T_g)} = -\frac{1}{2.303 f_g} \frac{T - T_g}{f_g/(\alpha_l - \alpha_g) + (T - T_g)}$$

f_g being the fractional free volume at the glass transition temperature. Thus $^1/_{2.303} f_g = 17.6$ and $f_g = 0.025$. Experimentally $\alpha_l - \alpha_g = 3.3 \times 10^{-4}$ deg.$^{-1}$. From the second constant in eq. 6, f_g is determined as 0.017. Considering the relatively poor precision with which $\alpha_l - \alpha_g$ can be measured, the agreement between the predicted and experimental values of f_g can be considered as satisfactory.

This investigation by transient rather than dynamic measurements reinforces and confirms the conclusions of previous investigations on low molecular weight glass-forming materials, namely, that a single retardation time is sufficient to represent the process. In this investigation, moreover, the W.L.F. equation is found to predict the temperature variation over the complete temperature range studied.

ACTIVITY COEFFICIENTS IN CALCIUM PERCHLORATE–HYDROCHLORIC ACID MIXTURES IN WATER AT 25°

BY JEAN M. STOKES AND R. H. STOKES

Department of Physical Chemistry, University of New England, Armidale, N.S.W., Australia

Received June 4, 1963

By measuring the change in potential of the hydrogen–silver, silver chloride cell as calcium perchlorate is added at constant hydrochloric acid molality, the activity coefficient of calcium perchlorate at vanishingly low concentration in hydrochloric acid solutions is evaluated. That of hydrochloric acid at a low concentration in calcium perchlorate solutions is obtained from a separate experiment.

Introduction

In connection with other work in this Laboratory, the question arose: what is the activity coefficient of a 2:1 electrolyte at vanishingly low concentration in a hydrochloric acid solution of 1 *m* or higher concentration? Two such systems, in which the 2:1 electrolytes were barium and strontium chlorides, have been studied by Harned and collaborators,[1] but the concentrations of the two electrolytes were not such as to make a reasonably accurate estimation of the required activity coefficient possible. A recent paper by Argersinger, Leifer, and Davidson[2] deals with the system cadmium chloride–hydrochloric acid using both cadmium and hydrogen electrodes in combination with a silver–silver chloride electrode, but this system is not typical because of strong complex formation. No divalent metal free from chloro-complexing difficulties appeared likely to operate as a reversible electrode toward its ions at high hydrochloric acid concentrations, so the method described below was adopted. This method depends on a rather direct exploitation of the well known "cross-differentiation identity"

$$\nu_1 \left(\frac{\partial \log \gamma_1}{\partial m_2}\right)_{m_1} = \nu_2 \left(\frac{\partial \log \gamma_2}{\partial m_1}\right)_{m_2} \qquad (1)$$

The cell used is

$$(\mathrm{Pt})\mathrm{H_2}|\mathrm{HCl},\ m_1|\mathrm{AgCl}\text{–}\mathrm{Ag}$$

The 2:1 electrolyte is progressively added in such a way as to maintain a constant hydrochloric acid molality. The initial rate of change of the e.m.f. gives the left-hand side of eq. 1 as $m_2 \rightarrow 0$; integration of the

(1) H. S. Harned and T. R. Paxton, *J. Phys. Chem.*, **57**, 531 (1953); H. S. Harned and R. Gary, *J. Am. Chem. Soc.*, **76**, 5924 (1954); **77**, 1994 (1955).

(2) W. J. Argersinger, I. Leifer, and A. W. Davidson, *J. Phys. Chem.*, **66**, 1321 (1962).

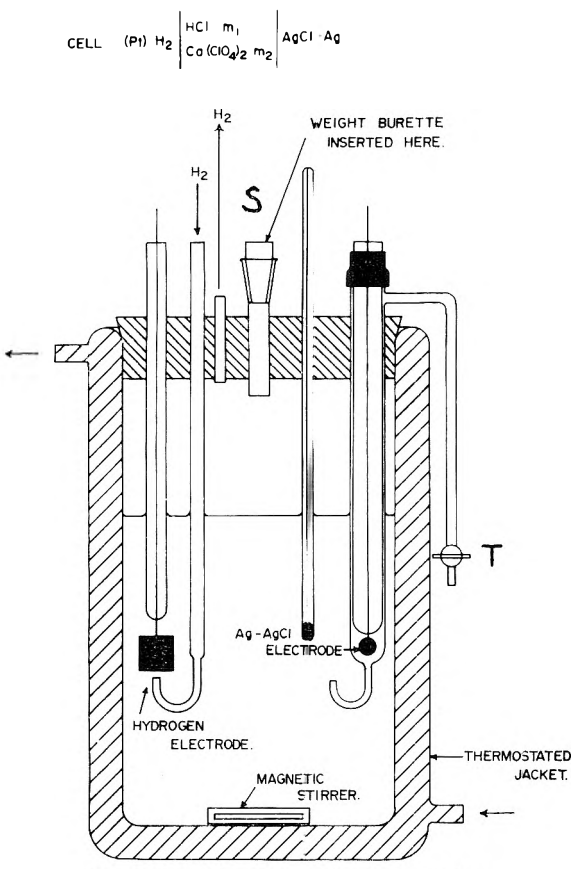

Fig. 1a.—The cell vessel and electrodes.

right-hand side with respect to m_1 then gives log $\gamma_{(0)2}$, the required activity coefficient of the 2:1 electrolyte at vanishing concentration.

Experimental

Hydrochloric acid was analytical reagent quality material, suitably diluted and analyzed conductometrically with the help of the data of Stokes.[3] Calcium perchlorate was prepared as a stock solution of known concentration as follows. Analytical reagent quality perchloric acid (chloride content less than 0.0001%) was diluted to about 40% by weight and analyzed by weight titration against carbonate-free sodium hydroxide, prepared from amalgam and analyzed as in ref. 3. To a known weight of this perchloric acid a very small excess over the calculated amount of A.R. calcium carbonate was added, with precautions to avoid loss in spray. The solution was boiled free of carbon dioxide and weighed, and the composition calculated from the original perchloric acid content. The hydrogen electrodes were conventional and were supplied with electrolytic hydrogen presaturated at 25° in a solution near the composition of that in the cell. The silver–silver chloride electrodes were of the thermal-electrolytic type. The cell is shown in Fig. 1a; it contained in practice two hydrogen electrodes of which for clarity only one is shown. Agreement between these was within 0.02 mv. Since silver chloride is appreciably soluble in hydrochloric acid above a few tenths molal, it was necessary to isolate the silver–silver chloride electrode from the bulk of the solution to prevent contamination of the hydrogen electrodes by reduced silver, which was formed in a few minutes in 1 *M* hydrochloric acid when the silver–silver chloride electrode was in the bulk solution, and which resulted in a rapid drift of the e.m.f. The silver–silver chloride electrode was therefore placed inside a tube with a bent capillary tip and with provision for drawing off solution by the tap to replace the solution round the silver–silver chloride electrode by fresh cell solution.

For each run, a solution was prepared by mixing suitable weights of the hydrochloric acid and calcium perchlorate stocks and diluting as required. This solution (solution A) contained hydrochloric acid at molality m_1, and a known weight percentage of calcium perchlorate. A solution of hydrochloric acid alone (solution B) of the same molality m_1 was then prepared.

(3) R. H. Stokes, *J. Phys. Chem.*, **65**, 1242 (1931).

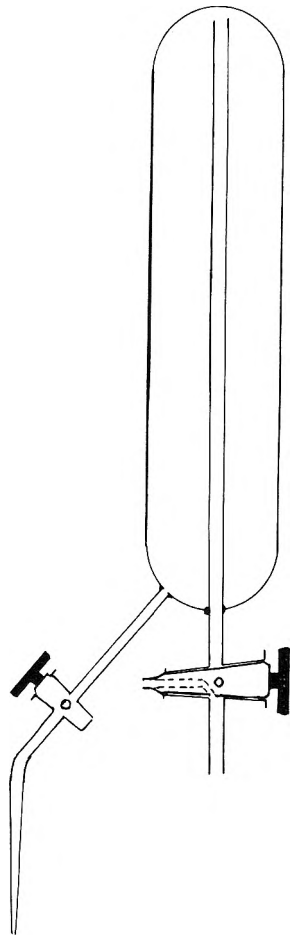

Fig. 1b.—Weight-buret. Presaturated hydrogen is passed through the solution, while the buret is inverted, to remove dissolved oxygen. The three-way tap is connected to the hydrogen supply during delivery of solution; the position shown is for flushing out air from the hydrogen delivery tube.

The electrodes were rinsed in solution B, and the guard tube containing the silver–silver chloride electrode was completely filled with solution B. The hydrogen pre-saturator (a vessel jacketed with thermostated water, similar to the cell vessel) was also filled with this solution. About 200 g. of solution B was then weighed into the clean dry cell vessel, and when the temperature had reached 25° the hydrogen flow and the stirrer were started. Complete removal of dissolved oxygen took about 1 hr., but in most cases the cell was left overnght with a slow hydrogen flow.

The potential of the cell, at this stage containing only hydrochloric acid of molality m_1, was measured on a Tinsley vernier potentiometer. A few milliliters of the cell solution was then bled off *via* tap T through the silver–silver chloride electrode guard tube into a weighing bottle, to check that the solution round the electrode was still of the cell composition. If any small change in potential occurred, this operation was repeated until the potential was constant.

Meanwhile, about 60 ml. of solution A had been freed from dissolved oxygen in a weight-buret of the design shown in Fig. 1b. The flow of hydrogen into the cell was increased and the stopper S removed; a few grams of solution A was then introduced into the cell against the flow of emerging hydrogen. Stopper S was replaced and the solution thoroughly stirred; then a few grams of the cell solution was bled off through T, and as soon as the temperature was back to 25° the new potential was measured. The bleeding was repeated until the potential was constant within 0.01 mv.; usually no more than three bleedings sufficed. Equilibrium readings could be obtained within 20 min. of the addition of solution A, provided that oxygen was completely excluded from the solution in the weight-buret, but even a trace of oxygen would increase this time to 1 hr. The additions of solution A and the bleeding operations were continued until the change from the original cell potential was a few millivolts. At this stage the stopper carrying the whole electrode assembly was removed from the cell, without disturbing

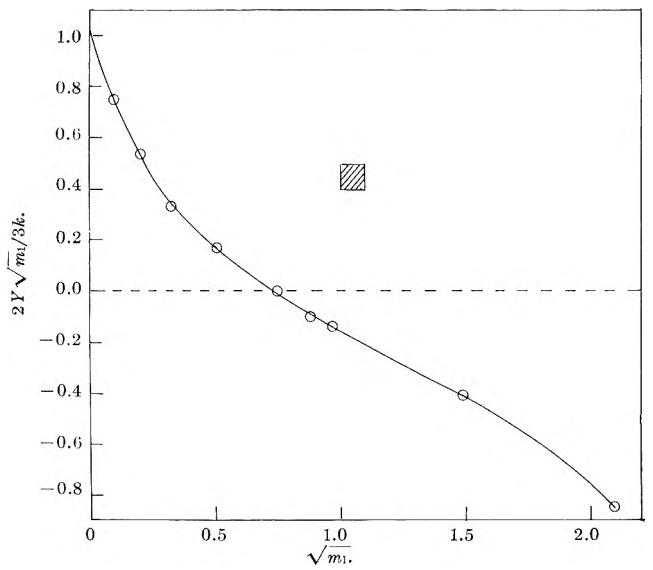

Fig. 2.—Integration of eq. 6 to give log $\gamma_{(0)2}$. Hatched area represents 1% in γ.

the electrodes, and the cell and electrodes were rinsed with solution B and the cell refilled with it. The reading, after removal of dissolved oxygen and bleeding through T, provided a check on the constancy of the electrode behavior during the run; the drift after correcting for changes in barometer reading during the run did not exceed 0.02 mv.

In this way, since the same electrodes were used throughout a run, the *changes* in cell e.m.f. with the addition of calcium perchlorate were, we believe, obtained with a higher order of accuracy than could be expected by setting up a new cell for each composition of the mixture. Bias potentials were certainly present in some of the silver–silver chloride electrodes, for the observed e.m.f. values in solution B often differed by a few tenths of a millivolt from the best literature values for the hydrochloric acid cell, but these bias potentials were proved to remain constant during the run. The molality of calcium perchlorate m_2 in each solution is calculated at each stage from the initial weight of solution B in the cell, the weights of solution A added, and the weights of cell solutions withdrawn *via* T. This rather laborious piece of bookkeeping is the most tedious feature of the experiment. As a check on the arithmetic, it is desirable to calculate both m_1 and m_2 at each stage; m_1 should of course remain constant.

Runs were made with nine different hydrochloric acid molalities from $m_1 = 0.01$ to $m_1 = 4$. In addition, one run was made with 0.01 *M* HCl as solution B, in which the addition of calcium perchlorate was continued until the calcium perchlorate molality was 1.1. From this run, the activity coefficient of hydrochloric acid at near-vanishing concentrations in calcium perchlorate was obtained. The results are assembled in Table I.

Theoretical

Computation of the Activity Coefficient of Calcium Perchlorate at Trace Concentration in Hydrochloric Acid.—The potential of the cell

$$(\mathrm{Pt})\ \mathrm{H_2}\ \Big|\ \begin{matrix}\mathrm{HCl} & m_1\\ \mathrm{Ca(ClO_4)_2} & m_2\end{matrix}\ \Big|\ \mathrm{AgCl\text{–}Ag}$$

is, with the convention that E represents the excess positive potential of the right-hand electrode over the left-hand electrode

$$E = E^0 - 2k \log (m_1\gamma) \qquad (2)$$

where $k = 2.303RT/F$, and E° is the standard potential. Differentiation with respect to m_2 at constant m_1 yields

$$2k \left(\frac{\partial \log \gamma_1}{\partial m_2}\right)_{m_1} = -\left(\frac{\partial E}{\partial m_2}\right)_{m_1} \qquad (3)$$

and hence by eq. 1

$$3k \left(\frac{\partial \log \gamma_2}{\partial m_1}\right)_{m_2} = -\left(\frac{\partial E}{\partial m_2}\right)_{m_1} \qquad (4)$$

where γ_2 is the mean activity coefficient of the 2:1 electrolyte 2. In particular, as $m_2 \to 0$, we have

$$3k \frac{\mathrm{d} \log \gamma_{(0)2}}{\mathrm{d}m_1} = -\lim_{m_2 \to 0}\left(\frac{\partial E}{\partial m_2}\right)_{m_1} = -Y \qquad (5)$$

where $\gamma_{(0)2}$ is the activity coefficient of 2 at vanishing concentration in 1. The right-hand side of (5) was evaluated in several ways from the data of Table I. It was thought undesirable to use any theoretical function as a guide to obtaining the required initial slope; therefore, graphs were prepared of $(\Delta E/m_2)$ or of $(m_2/\Delta E)$ *vs.* either m_2 or ΔE; in every case at least one of these graphs was sufficiently linear to permit an evaluation of Y from the intercept at $m_2 = 0$ (or $\Delta E = 0$).

We now integrate (5) at constant $m_2 = 0$ with respect to m_1 (see Fig. 2), obtaining

$$\log \gamma_{(0)2} = -\frac{1}{3R}\int_{m_1=0}^{m_1} Y \mathrm{d}m_1$$

$$= -\frac{2}{3k}\int_{m_1=0}^{m_1} (Y\sqrt{m_1})\mathrm{d}\sqrt{m_1} \qquad (6)$$

the second form being chosen since the integrand remains finite as $m_1 \to 0$. The integrand at the lower limit may be evaluated from the Debye–Hückel limiting law

$$\log \gamma_2 = -2A\sqrt{m_1 + 3m_2} \qquad (7)$$

where $A = 0.5107$ mole$^{-1/2}$ kg.$^{1/2}$ at 25°.

$$\frac{\mathrm{d} \log \gamma_{(0)2}}{\mathrm{d}m_1} = -Am_1^{-1/2} \qquad (8)$$

$$\lim_{m_1 \to 0} (Y\sqrt{m_1}) = 3kA \qquad (9)$$

Table Ia includes the values of Y and the integrand in eq. 6. The integrated values of log $\gamma_{(0)2}$ at round concentrations, obtained by a tabular integration of data read off at close intervals from Fig. 3, are given in Table II. The estimated precision of the $\gamma_{(0)2}$ values is about ±1%.

Table III gives the activity coefficient of hydrochloric acid at vanishing concentration in calcium perchlorate solutions, $\gamma_{(0)1}$. These were obtained from a large-scale graph of the data of Table Ib; in order to allow for the fact that the actual hydrochloric acid molality was not zero but 0.01075, the log γ values read from the curve were lowered by the amount 0.01075 (log $\gamma_{1(0)}$ − log $\gamma_{(1)})/I \approx 0.0006$, where I is the total ionic strength and log $\gamma_{1(0)}$ is the activity coefficient of hydrochloric acid alone at ionic strength I. The precision of these data is considerably higher than those for the calcium perchlorate, since they are much closer to the directly measured experimental quantity; it is estimated at ±0.0005 in log γ_1.

Discussion

Figure 3 compares the trace-activity coefficients with those of the single electrolytes; the log γ scale for

TABLE IA

THE CELL $(Pt)H_2|HCl\ m_1|AgCl-Ag$ AT 25°
$Ca(ClO_4)_2\ m_2|$

$\Delta E = E - E_{(m_2=0)}$, m_1 = constant; $Y = \lim_{m_2 \to 0} \left(\frac{\partial E}{\partial m_2}\right)_{m_1}$;

$k = 2.303\ RT/F$

m_1	m_2	ΔE, mv.	$2Y\sqrt{m_1}/3k$
0.009754	0.000540	0.35	
.009754	.001607	.91	
.009754	.002525	1.39	0.75
.009754	.004197	1.92	
.04118	.00321	0.72	
.04118	.00538	1.14	
.04118	.00939	1.85	537
.04118	.01376	2.44	
.04118	.02232	3.53	
.10323	.00617	0.545	
.10323	.01211	1.03	
.10323	.02191	1.72	.331
.10323	.03605	2.51	
.10323	.05542	3.33	
.2532	.01948	0.51	
.2532	.03316	.79	.168
.2532	.05276	1.06	
.5532	.0244	0.03	
.5532	.0434	.10	− .002
.7702	.0216	− .20	
.7702	.0763	− .84	− .103
.7702	.1948	−2.39	
.9360	.0130	− .16	
.9360	.0464	− .59	− .140
.9360	.0787	−1.00	
2.214	.0289	−0.72	
2.214	.0664	−1.61	− .412
2.214	.1268	−3.12	
4.372	.0367	−1.29	
4.372	.0762	−2.58	− .848
4.372	.1285	−4.19	

TABLE IB

$m_1 = 0.010754$

m_2	ΔE, mv.	$-\log \gamma_1$
0.0	0.0	(0.0450)
.03685	7.99	.1125
.1142	11.57	.1428
.2132	12.67	.1520
.3397	12.01	.1465
.4503	10.72	.1356
.7161	5.85	.0944
1.1063	−3.31	.0170

hydrochloric acid is made twice that for calcium perchlorate, as the electrical (Debye–Hückel) component of log γ should be approximately twice as great for the 2:1 electrolyte. It should be remembered that the values for calcium perchlorate as a single electrolyte, being computed from isopiestic vapor pressure measurements, involve some uncertainty due to the difficulty of extrapolation from 0.1 M to zero. The cross-over of the log $\gamma_{2(0)}$ and log $\gamma_{(0)2}$ curves would be eliminated if the former curve were bodily displaced downward by about 0.01 in log γ. It is clear that with the possible exception of this region below the cross-over, the replacement at constant ionic strength of calcium perchlorate by hydrochloric acid raises the activity coefficient of calcium perchlorate, and at all concentrations the replacement of hydrochloric acid by calcium perchlorate at constant ionic strength lowers the activity coefficient of hydrochloric acid. There is a very pronounced difference between log $\gamma_{(0)2}$ and 2 log $\gamma_{(0)1}$ above 0.1 ionic strength, though up to that limit the curves are close together, in accordance with the prediction of Guggenheim's theory[4] of mixed electrolytes.

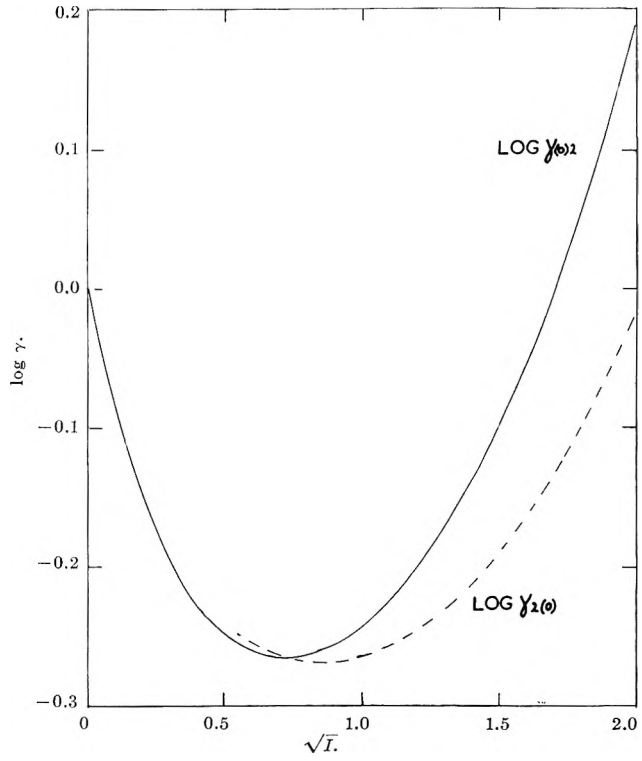

Fig. 3a.—Activity coefficients of calcium perchlorate at vanishing concentrations in hydrochloric acid ($\gamma_{(0)2}$) with those of calcium perchlorate in water at the same ionic strength ($\gamma_{2(0)}$).

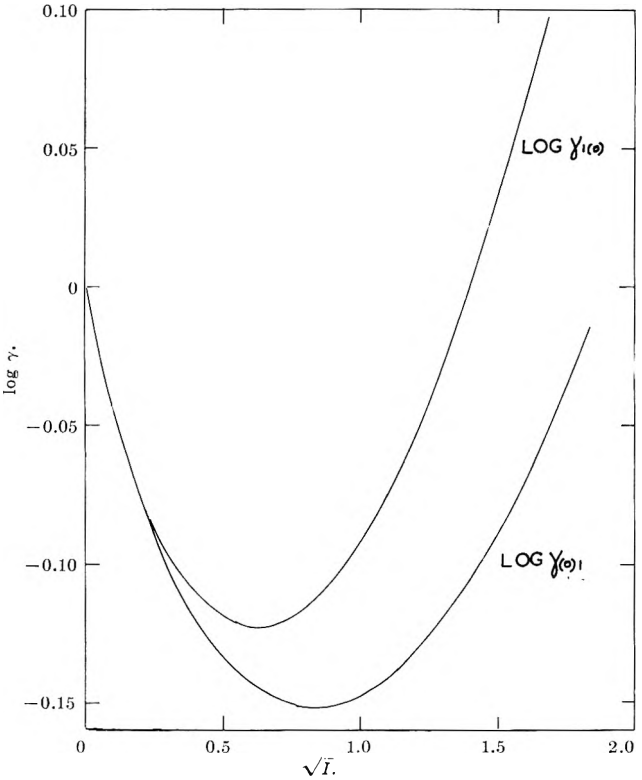

Fig. 3b.—Activity coefficients of hydrochloric acid at vanishing concentration in calcium perchlorate solutions ($\gamma_{(0)1}$) compared with those of hydrochloric acid in water at the same ionic strength ($\gamma_{1(0)}$).

TABLE II

ACTIVITY COEFFICIENT OF CALCIUM PERCHLORATE AT VANISHING CONCENTRATION IN HYDROCHLORIC ACID SOLUTIONS AND IN ITS AQUEOUS SOLUTIONS

$\gamma_{(0)2}$ = activity coefficient at vanishing concentration; $\gamma_{2(0)}$ = activity coefficient in aqueous solution[a]; ionic strength $I = m_1$ in hydrochloric acid solutions and $3m_2$ in aqueous calcium perchlorate solutions.

I	log $\gamma_{(0)2}$	log $\gamma_{2(0)}$
0.01	−0.088	.....
.04	− .152	.....
.1	− .203	.....
.25	− .249	−0.238
.5	− .265	− .264
.7	− .262	− .268
1.0	− .243	− .264
2.0	− .131	− .210
3.0	+ .017	− .123
4.0	+ .191	− .016

[a] R. A. Robinson and R. H. Stokes, "Electrolyte Solutions," Butterworths, London, 1959, Appendix 8.10.

As far as we have been able to determine, this is the first investigation of mixed electrolytes of two different valency types with no common ion; the pattern of behavior is generally similar to that found by Harned and collaborators[1] for the systems hydrochloric acid–strontium chloride and hydrochloric acid–barium chloride. There is, however, evidence that in the present case the activity coefficient of hydrochloric acid in mixtures of constant ionic strength cannot be represented adequately by the linear form of Harned's rule

$$\log \gamma_1 = \log \gamma_{1(0)} - \alpha_1 I_2$$

where I_2 is the component of the ionic strength due to electrolyte 2. This conclusion is reached by comparing values of $(\log \gamma_{(0)1} - \log \gamma_{1(0)})/I$ (Table III) with values of $(\log \gamma_1 - \log \gamma_{1(0)})/I_2$ computed from the data of Table Ia; the latter are numerically smaller.

(4) E. A. Guggenheim, "Thermodynamics—an Advanced Treatise," 4th Ed., North-Holland Publishing Company, Amsterdam, 1959, pp. 357, 358.

TABLE III

ACTIVITY COEFFICIENT OF HYDROCHLORIC ACID AT VANISHING CONCENTRATION IN CALCIUM PERCHLORATE SOLUTIONS AND IN ITS AQUEOUS SOLUTIONS

$\gamma_{(0)1}$ = activity coefficient at vanishing concentration; $\gamma_{1(0)}$ = activity coefficient in aqueous solutions[a]; ionic strength $I = m_1 = 3m_2$.

I	log $\gamma_{(0)1}$	log $\gamma_{1(0)}$	$(\log \gamma_{1(0)} - \log_{(0)1})/I$
0.1	−0.1070	−0.0991	0.079
.3	− .1393	− .1215	.059
.6	− .1525	− .1175	.0583
1.0	− .1475	− .0921	.0554
1.4	− .1345	− .0575	.0550
2.0	− .1034	+ .0037	.0535
3.0	− .0395	+ .1192	.0529
3.3	− .0194	+ .1560	.0531

[a] See ref. *a* in Table II.

IONIC AND FREE RADICAL PROCESSES IN LIQUID MIXTURES CONTAINING HYDROCARBONS[1]

BY JOHN ROBERTS AND WILLIAM H. HAMILL

Department of Chemistry and Radiation Laboratory, University of Notre Dame, Notre Dame, Indiana

Received June 5, 1963

Yields of HCl from γ-irradiation of cyclo-C_6H_{12} solutions containing CCl_4, $CHFCl_2$, $CFCl_3$, CF_2Cl_2, $C_2F_4Cl_2$, and C_2H_5Cl have been measured over a range of concentration. $G(H_2)$ for cyclo-C_6H_{12}–cyclo-C_6H_{10} with 0.03 M I_2, $G(CH_4)$ for n-butane–cyclo-C_6H_{12}, and both $G(H_2)$ and $G(CH_4)$ for n-C_6H_{14}–CH_3I have also been examined, all at *ca.* 20°. Mixtures of C_2H_5I in 80% alkane–20% alkene and also in methyltetrahydrofuran were irradiated at −196° and analyzed subsequent to thawing for $G(H_2)$, $G(C_2H_4)$, and $G(C_2H_6)$. All results are considered in relation to ionic processes in irradiated organic glasses.[2]

This work extends a series of studies on ionic reactions in liquid solutions of cyclohexane[3] and benzene[4] which are supported by direct observations of ionic species in organic glasses.[2,5] We shall also freely use information gained from mass spectrometry, both qualitatively and quantitatively. In particular, this work has been influenced by recently available data for appearance potentials of dissociative electron attachment processes of various halides.[6]

Experimental

Materials.—Fisher certified reagent grade cyclohexane and *n*-hexane were passed through a 50-cm. silica gel column and used without further purification. Phillips research grade 3-methylpentane was used as received. Eastman spectral grade cyclohexene and Phillips pure grade 2-methylpentene-1 were treated with Na–K and used without further purification. The purification and handling of 2-methyltetrahydrofuran has been described.[2] Fisher certified reagent grade methyl and ethyl iodides were fractionally distilled. Carbon tetrachloride (Fisher certified reagent), benzyl acetate (Eastman White Label), and triphenylmethane (Eastman) were used without additional purification.

Propane (99.5%), ethyl chloride (99.5%), trichlorofluoromethane (99.9%), dichlorodifluoromethane (98.1%), dichlorofluoromethane (99.0%), and 1,2-dichlorotetrafluoroethane, all Matheson Company chemicals, were collected in a storage bulb after several trap-to-trap distillations.

Sample Preparation.—Pyrex cells used for γ-irradiations were 16 mm. o.d., approximately 15 cm. long, and were equipped with side arm and breakseal. Solids were weighed, liquids pipetted, and gases measured by PVT. Ten-milliliter samples were outgassed by trap-to-trap distillation using suitable refrigerants. Irradiations were performed in the Hochanadel–Ghormley Co^{60} source,[7] and dose rates were established by Fricke dosimetry.

Analysis.—Gaseous products were separated using a micro-

(1) This article is based on a thesis submitted by J. Roberts in partial fulfillment of the requirements for the Ph.D. degree at the University of Notre Dame. The Radiation Laboratory is operated under AEC contract AT(11-1)-38.

(2) M. R. Ronayne, J. P. Guarino, and W. H. Hamill, *J. Am. Chem. Soc.*, **84**, 4230 (1962).

(3) L. J. Forrestal and W. H. Hamill, *ibid.*, **83**, 1535 (1961).

(4) W. Van Dusen, Jr., and W. H. Hamill, *ibid.*, **84**, 3648 (1962).

(5) J. P. Guarino, M. R. Ronayne, and W. H. Hamill, *Radiation Res.*, **17**, 379 (1962).

(6) W. M. Hickam and D. Berg, *J. Chem. Phys.*, **29**, 517 (1958).

(7) M. Burton, J. A. Ghormley, and C. Hochanadel, *Nucleonics*, **13**, 74 (1955).

still,[4] measured on a modified Saunders-Taylor apparatus, and analyzed by mass spectrometry.

Acids were separated from the organic samples by washing with CO_2-free distilled water. Acid yields were measured using standardized base (0.01 *N* NaOH) with bromocresol purple. Indicator standards were made with the same amount of water used to extract the acid.

For low temperature runs, the sample was allowed to melt in the dark immediately after irradiation and then treated by usual methods.

Results

In all runs for which G(HCl) was measured, solutions were 0.04 *M* in triphenylmethane which served to convert Cl atoms to HCl. A small amount of water was added to convert HCl to H^+ and prevent back reaction. Doses approximated 10^{19} e.v./g.

Values of G(HCl) *vs.* mole % RCl (all in cyclohexane, except as noted) appear in Fig. 1 for CCl_4, Fig. 2 for $CHFCl_2$, Fig. 3 for $CFCl_3$, Fig. 4 for CF_2Cl_2, Fig. 5 for $C_2F_4Cl_2$, and Fig. 6 for C_2H_5Cl.

The results for cyclohexane–carbon tetrachloride are very similar to those for cyclohexane–chloroform[3] and show important differences from benzene–carbon tetrachloride.[4] The latter, however, exhibits a similarity to the results in Fig. 3. For two runs, $G(H_2)$ was 1.52 and 0.48 at 5.6 and 11.1 mole % carbon tetrachloride.

In a single experiment with 5.8 mole % benzene in cyclohexane, also 0.03 *M* in iodine, G(HI) was 1.55. The question concerned was formation of C_6H_7 and its reaction with iodine.[4]

The possibility that cyclohexadiene or a somewhat similar compound is the missing product responsible for lack of material balance[2] suggested that it might be detected by post-irradiative addition of iodine. In two runs pure cyclohexane was irradiated with a dose of 1.5×10^{19} e.v./g. and iodine subsequently added *in vacuo*. The sample then was opened and analyzed; G(HI) was 0.42 and 0.41. Under comparable conditions, excepting irradiation, a solution of 1,3-cyclohexadiene showed only *ca.* 5% reaction.

Another series of experiments was designed to test for possible effects of charge exchange and electron attachment on the yields of gaseous products. In the first of these, Fig. 8, the 0–100 mole % range of cyclohexene in cyclohexane was covered. Excepting three runs in pure cyclohexane ($G(H_2)$ = 5.47), all samples contained 0.03 *M* iodine. Yields do not reflect, therefore, the effect of cyclohexene as H-atom scavenger. Charge exchange is allowed, since the ionization potentials are $I(C_6H_{12})$ = 9.88 and $I(C_6H_{10})$ = 8.95 e.v.[8]

Mixtures of *n*-butane and cyclohexane were also examined briefly for positive charge exchange. Values of $G(CH_4)$ in butane containing 0, 10, and 20 vol. % cyclohexane were 0.20, 0.09, and 0.03.

Yield of hydrogen and methane from *n*-hexane–methyl iodide containing 0.03 *M* iodine (to prevent a chain reaction) might be expected to resemble those in cyclohexane–methyl iodide–iodine.[3] In fact, they are very similar (Fig. 7) both in respect to the decrease in $G(H_2)$ and the constancy of $G(CH_4)$ with increasing mole % methyl iodide; $G(H_2)$ = 5.38 and $G(CH_4)$ = 0.15 in pure *n*-hexane.

Some systems were irradiated at −196° and subsequently analyzed for gaseous products. Results for ethyl iodide in 80 vol. % 3-methylpentane–20 vol. %

(8) K. Watanabe, *J. Chem. Phys.*, **26**, 542 (1957).

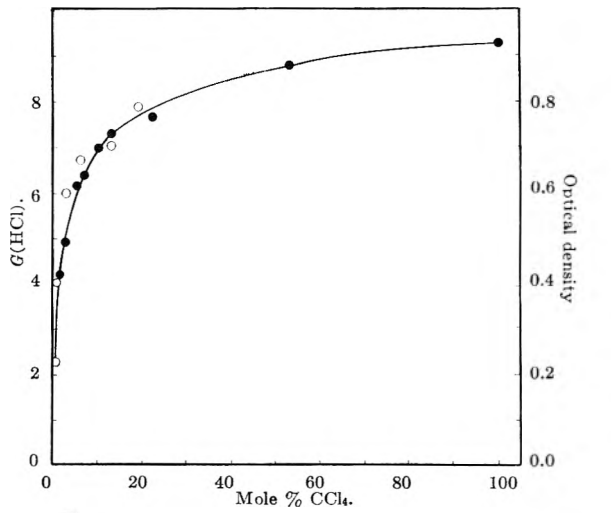

Fig. 1.—G(HCl) for CCl_4 in cyclo-C_6H_{12} (●); optical density of a cationic species from CCl_4 in 3-methylpentane at −196° (○).

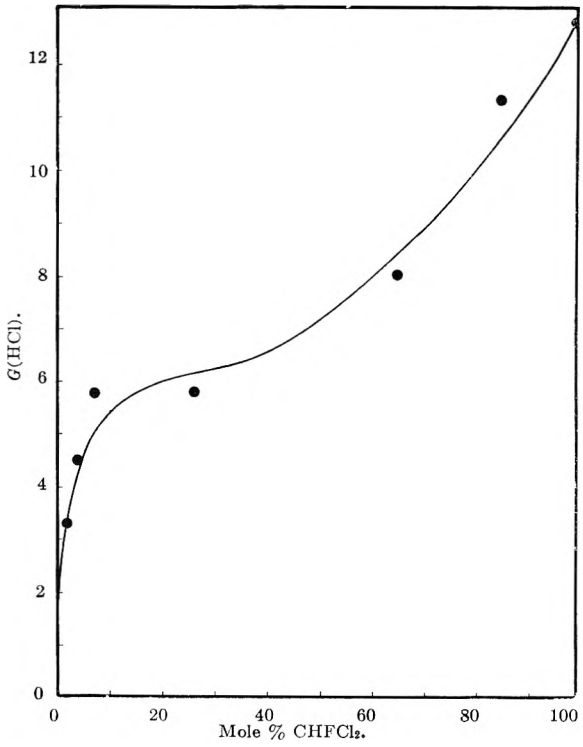

Fig. 2.—G(HCl) for $CHFCl_2$ in cyclo-C_6H_{12}.

2-methylpentene-1 appear in Table I. The sum of $G(H_2)$ and $G(C_2H_4)$ is remarkably constant while $G(C_2H_6)$ increases rather slowly after the initial abrupt rise. The increments in $G(C_2H_6)$ and $G(C_2H_4)$ are in fact practically equal above 0.1% ethyl iodide.

TABLE I

γ-IRRADIATION OF ETHYL IODIDE IN 3-METHYLPENTANE–2-METHYLPENTENE-1 GLASSES AT 77°K.

Mole % C_2H_5I	$G(H_2)$	$G(C_2H_6)$	$G(C_2H_4)$
0.0	1.84	0.34	0.17
.10	1.79	1.24	.27
.16	1.82	1.20	.26
.31	1.57	1.31	.41
.47	1.62	1.37	.41
.78	1.55	1.48	.47
1.16	1.48	1.58	.54

In contrast, ethyl iodide does not depress $G(H_2)$ in 2-methyltetrahydrofuran (Table II). The latter is

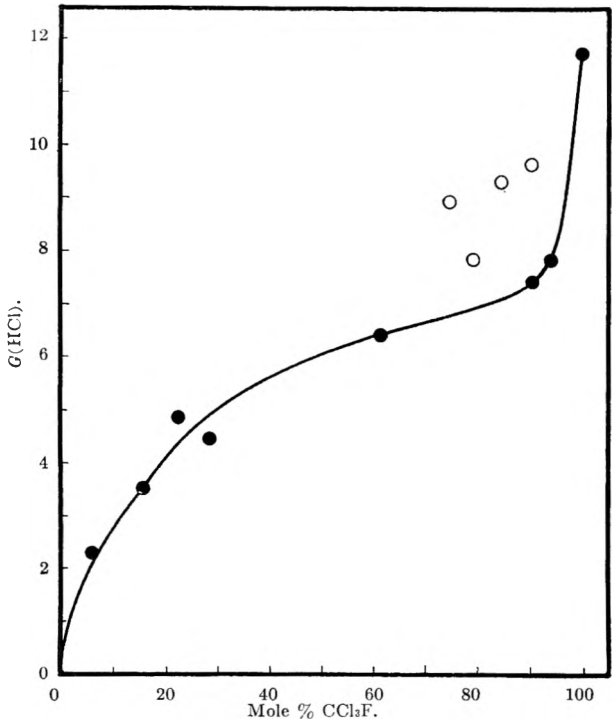

Fig. 3.—G(HCl) for CCl_3F in cyclo-C_6H_{12} (●) and in C_3H_8 (○).

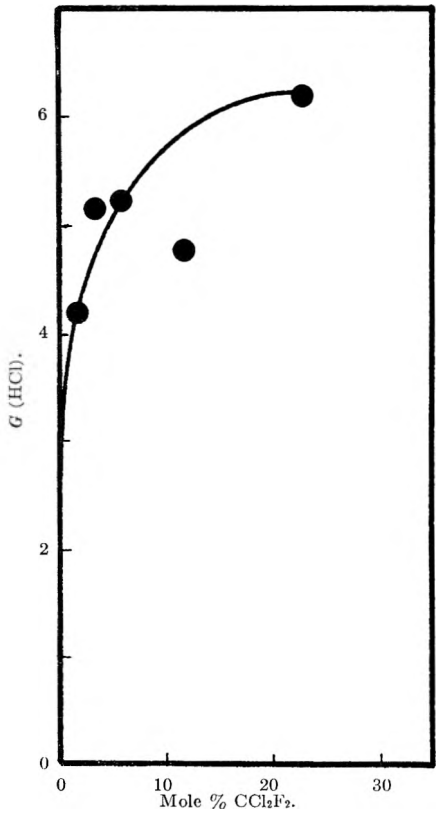

Fig. 4.—G(HCl) for CCl_2F_2 in cyclo-C_6H_{12}.

TABLE II

γ-IRRADIATION OF ETHYL IODIDE IN METHYLTETRAHYDROFURAN GLASS AT 77°K.

Mole % C_2H_5I	$G(H_2)$	$G(C_2H_6)$	$G(C_2H_4)$
0.00	2.40	..	0.10
.07	2.48	1.05	..
.12	2.51	1.22	.41
.19	2.30	1.49	.32
.37	2.40	2.13	.35
.62	2.51	2.50	.36

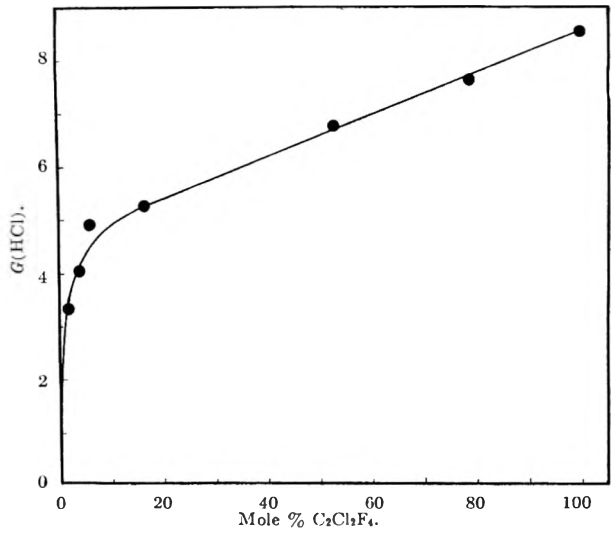

Fig. 5.—G(HCl) for $C_2Cl_2F_4$ in cyclo-C_6H_{12}.

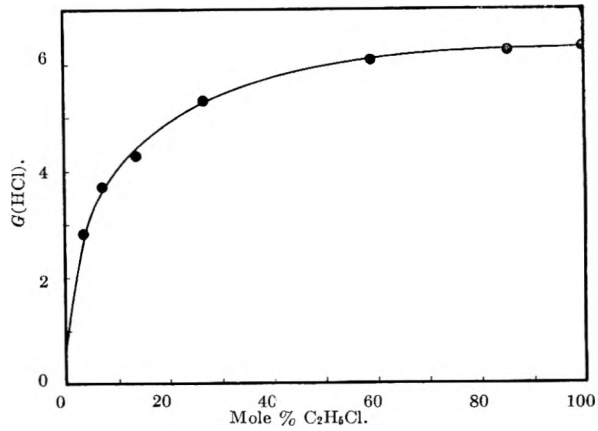

Fig. 6.—G(HCl) for C_2H_5Cl in cyclo-C_6H_{12}.

known to be a good scavenger for H-atoms.[4] Yields of ethane and ethylene do not appear to be related.

Discussion

The dependence of G(HCl) upon composition in carbon tetrachloride–cyclohexane in Fig. 1 resembles the analogous system chloroform–cyclohexane.[3] There is an important advantage in knowing the appearance potential (AP) for

$$CCl_4 + e^- \longrightarrow Cl^- + CCl_3 \qquad (1)$$

which lies between 0 and 0.05 e.v. as well as a second process forming Cl^- at 0.4 e.v.[9] There is no comparable information for chloroform. The combined energy range over which reaction 1 occurs is 1.0 e.v. It might be expected that in a radiation chemical system, low appearance potential and large energy range over which electron attachment can occur would favor the efficiency of attachment, and of the associated chemical changes, at low solute concentrations. The extent to which electron impact measurements in collision-free space can be translated to condensed media remains to be established. The AP of CCl_3^+/CCl_4 is 11.65 e.v. and breaks in the total positive ionization curve appear at 12.6 and 13.5 e.v., which are attributed to excited states of CCl_3^+.[9] Direct observation of CCl_3^+/CCl_3F shows two breaks at energy increments of 1.53 ± 0.35 and 2.73 ± 0.35 e.v. The ionization potential (IP) of CCl_3 has been reported

(9) R. E. Fox and R. K. Curran, *J. Chem. Phys.*, **34**, 1595 (1961).

to be 8.78[10] and also $\geq 7.92 = 0.35$ e.v.[11] The ion CCl_4^+/CCl_4 cannot be detected in a mass spectrometer.

Spectrophotometric measurements in γ-irradiated 3-methylpentane glasses at $-196°$ demonstrate substantially complete electron attachment by only *ca.* 0.2 mole % carbon tetrachloride.[2,5] The anionic species cannot be established, but the mechanism is probably reaction 1, *viz.*, resonant dissociative attachment. An absorption band in this glass at $\lambda_{max} = 4800$ Å., originally attributed to an anion,[5] has now been shown to behave as a cationic color center.[12] Its optical density increases with solute concentration and only approaches a limiting value at *ca.* 10 mole % of carbon tetrachloride, as shown in Fig. 1.

We suggest that the initial rapid rise in G(HCl), Fig. 1, is due to reaction 1 with subsequent ion neutralization and H-abstraction by Cl, as well as to reaction 2, while the subsequent slower rise in G(HCl) may

$$H + CCl_4 \longrightarrow HCl + CCl_3 \qquad (2)$$

be related to the cationic species observed in the hydrocarbon glass. If this species results from positive charge exchange with the primary hydrocarbon cation, the latter would have to be electronically excited because of the disparity in ground state ionization potentials. Such excitation is invariably indicated by mass spectrometric measurements.[13]

The results for G(HCl) from tetrafluorodichloroethane in Fig. 5 resemble those of Fig. 1. Since AP = 0.2 e.v. for $Cl/C_2F_4Cl_2$ and the energy range for attachment is 2.8 e.v., we interpret contribution to G(HCl) from dissociative electron attachment as in the preceding case. We find it surprising that G(HCl) from difluorodichloromethane in Fig 4 should rise so rapidly, since AP = 0.5 e.v. and the range is 0.4 e.v. for Cl^-/CF_2Cl_2. In the case of fluorodichloromethane, Fig. 2, the inefficiency is again consistent with AP = 0.9 e.v. for $Cl^-/CHFCl_2$ and a range 0.0 e.v.

In the system cyclohexane–fluorotrichloromethane, the efficiency of G(HCl) formation in the lower concentration range is poor, while AP Cl^-/CCl_3F is 0.1 e.v. and the range is 0.10 e.v. In general we observe a better correlation of G(HCl) with the energy range than with the appearance potential. This system exhibits a marked decrease of G(HCl) as cyclohexane is added to the halide; a similar effect has been observed in benzene–carbon tetrachloride and was tentatively ascribed to positive charge exchange.[4] Since $CFCl_3^+$ has negligible abundance in the mass spectrum and $CFCl_2^+$ is by far the most abundant ion, then $CFCl_2^+$ would be required to participate if positive charge exchange is responsible. Evidence of excitation of $CFCl_2^+$ at *ca.* 10.2 e.v. has been reported.[11] Charge exchange with C_6H_{12} (IP = 9.88 e.v.) can therefore occur. This effect does not appear in mixtures with propane (IP = 11.08 e.v.) as shown in Fig. 3. It should be recalled that a similar conclusion was reached for observations with carbon tetrachloride at $-196°$.

There is no information from mass spectrometry for

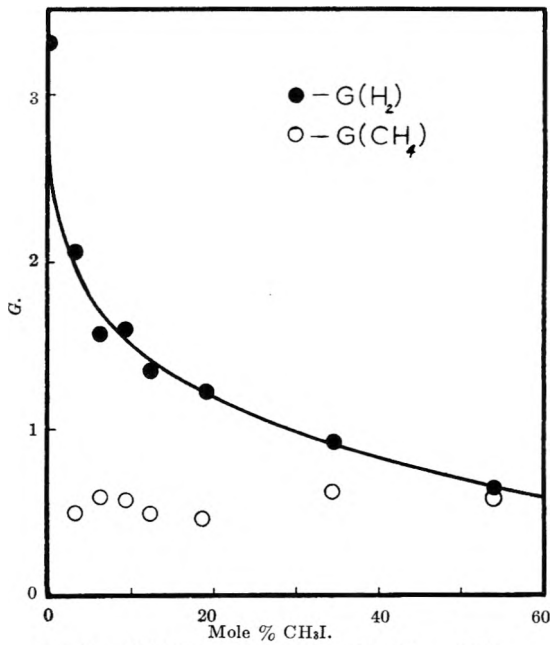

Fig. 7.—$G(H_2)$ and $G(CH_4)$ for CH_3I in n-C_6H_{14}.

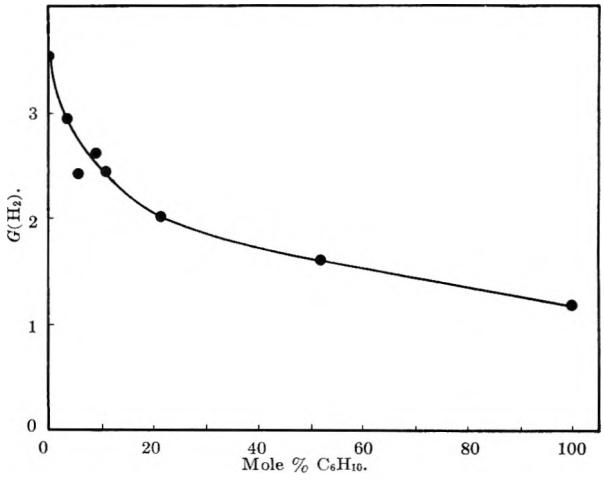

Fig. 8.—$G(H_2)$ for cyclo-C_6H_{10} in cyclo-C_6H_{12}; solutions also contain 0.03 M I_2.

C_2H_5Cl but AP = 9 e.v. for Cl^-/CH_3Cl by ion pair formation has been reported.[14] Failure to observe AP $\sim$ 0 for Cl^-/CH_3Cl by simple resonant attachment which is allowed by thermochemistry was apparently due to the very small cross section of the process. It has recently been found that there is some Cl^- formation at low electron energy.[13] The moderately small efficiency of ethyl chloride in Fig. 6 can be so understood. Although $C_2H_5Cl^+$ is the most abundant ion in the mass spectrum of ethyl chloride and IP ($C_2H_5Cl^+$) = 10.89 e.v., there is no evidence of charge exchange. Either G(HCl) happens to be the same for processes arising from the two cations or ion–molecule reactions intervene and render charge exchange impossible. The high pressure spectrum of ethyl chloride has not been reported but various ions of the type R_2Cl^+ have been observed.[15,16] The potential energy of an ion of this type would be much too small to undergo charge exchange with C_6H_{12}.

The results for $G(H_2)$ and $G(CH_4)$ from n-hexane–methyl iodide in Fig. 7 closely resemble those for cyclo-

(10) J. B. Farmer, I. H. S. Henderson, F. P. Lossing, and D. G. H. Marsden, *J. Chem. Phys.*, **24**, 348 (1956).
(11) R. K. Curran, *ibid.*, **34**, 2007 (1961).
(12) J. P. Guarino and W. H. Hamill, unpublished results.
(13) C. E. Melton and W. H. Hamill, unpublished results.
(14) V. Dibeler and R. Reese, *J. Res. Natl. Bur. Std.*, **54**, 127 (1955).
(15) L. P. Theard and W. H. Hamill, *J. Am. Chem. Soc.*, **84**, 1134 (1962).
(16) A. J. Lorquet and W. H. Hamill, *J. Phys. Chem.*, **67**, 1709 (1963).

hexane–methyl iodide[2] and are similarly interpreted. There is recent evidence[17] which supports the interpretation that the constant $G(CH_4) \cong 0.6$, although 0.03 M iodine is present, arises from the diffusion controlled reaction

$$CH_3I + H \longrightarrow (CH_3 + HI) \longrightarrow CH_4 + I$$

The initial sharp decrease in $G(H_2)$ is due in part to the preceding reaction and in part, we assume, to electron attachment. It has been demonstrated that ethyl iodide removes electrons very efficiently in γ-irradiated alkane glass[2] and it has recently been shown that organic iodides produce I^- under similar conditions.[18] We conclude that

$$CH_3I + e^- \longrightarrow CH_3 + I^-$$

occurs at least as efficiently in liquid solution at room temperature. If we estimate that the liquid state IP with the electron *in vacuo* is *ca.* 2 e.v. less than that for the gaseous state,[19] and if the polarization energy for I^- is about the same, then IP (C_6H_{12}, liq.) $\cong$ 6 e.v. and the heat of reaction for

$$C_6H_{12}^+ \text{ (soln.)} + I^- \text{ (soln.)} = C_6H_{12}^* \text{ (soln.)} + I \text{ (soln.)}$$

is diminished by an additional 3.1 e.v. for the electron affinity of iodine, or *ca.* 3 e.v. net. We conclude that the charge neutralization above induces no further chemical change.

Recent observations of irradiated organic glasses provide clear evidence for charge exchange processes which approach limiting yields at *ca.* 10 mole % of the solute, provided the solvent molecular cation does not undergo an efficient ion–molecule reaction.[12] Methyl iodide is one of the solutes which produces a cationic species in a 3-methylpentane glass.[18] In the present instance since IP (C_6H_{12}) = 9.88 and IP (CH_3I) = 9.35 e.v.,[8] it is possible that the $G(H_2)$ dependence is due in part to the reaction

$$C_6H_{12}^+ + CH_3I \longrightarrow C_6H_{12} + CH_3I^+$$

Similarly, in the system cyclohexane–cyclohexene, for which the values of IP are 9.88 and 8.95 e.v., respectively,[8] we may expect charge exchange since it has been observed for cyclohexene in 3-methylpentane glass.[12] Since 0.03 M iodine effectively suppresses the contribution of thermal H-atoms to $G(H_2)$, the observed decrease in $G(H_2)$ with added cyclohexene presumably represents the consequence of the reaction

$$C_6H_{12}^+ + C_6H_{10} \longrightarrow C_6H_{12} + C_6H_{10}^+$$

Comparison of the results in Fig. 6 and 7 demonstrates that methyl iodide causes the more rapid decrease in $G(H_2)$. This is consistent with observations of rather more efficient formation of solute anions than of solute cations in rigid organic media.

There is no direct evidence from low temperature measurements for positive charge exchange between alkanes, although it is well known from mass spectrometry. It is quite likely, however, that the marked decrease in $G(CH_4)$ from *n*-butane (IP = 10.63 e.v.) by added cyclohexane is another example of this effect.

This work is not directly concerned with the radiation chemistry of pure cyclohexane but the observation that $G(HI) \sim 0.4$ for post-irradiative addition of iodine demonstrates that there is a significant yield of some organic product not previously identified. Oxidation by iodine of 1,3-cyclohexadiene to benzene suggested itself but was ruled out. We cannot reconcile this result with the work of Dyne and Stone,[20] who obtained a material balance for irradiated cyclohexane but found only cyclohexene, bicyclohexyl, and cyclohexylhexene-1 as primary hydrogen-deficient products.

In hydrocarbon glasses containing 20% olefin, electron attachment by ethyl iodide is relatively very efficient,[2] while its reduction by H-atoms should be comparatively unimportant. The chemical yields (Table I) are consistent with these spectrophotometric observations. It is probable that 0.03 M iodine alone depresses $G(H_2)$ in *n*-hexane from 5.38 to 3.29 in large part through electron attachment, as with hydrogen iodide in cyclohexane.[21]

Methyl tetrahydrofuran exhibits self-scavenging of H-atoms,[2] and this is supported by the results of Table II. Ethyl iodide is relatively less efficient as an electron scavenger in this medium than in hydrocarbon, based upon observations with glasses at −196°.[2,5] Values of $G(C_2H_6)$ in Table II are consistent with the interpretation that ethyl radicals from dissociative electron attachment are the principal precursors of ethane. Positive charge exchange to solute has not been achieved in this solvent.[12]

(17) S. Toma and W. H. Hamill, unpublished results.
(18) E. P. Bertin and W. H. Hamill, unpublished results.
(19) D. R. Kearns and M. Calvin, *J. Chem. Phys.*, **34**, 2026 (1961).
(20) P. J. Dyne and A. Stone, *Can. J. Chem.*, **39**, 2381 (1961).
(21) J. R. Nash and W. H. Hamill, *J. Phys. Chem.*, **66**, 1097 (1962).

THE EFFECT OF PRESSURE ON THE EQUILIBRATION OF α- AND γ-METHYLALLYL AZIDE[1]

BY W. J. LE NOBLE

Department of Chemistry, State University of New York at Stony Brook, Stony Brook, New York

Received June 7, 1963

The interconversion of α- and γ-methylallyl azide in methylene chloride has been studied as a function of pressure over a range of 6700 atm. The reaction, which presumably goes through a nonpolar, cyclic transition state, has an activation volume of −9.5 cm.³/mole if approached from the α-direction, −7.9 cm.³/mole if approached from the pure γ-isomer. The ratio of densities of the azides calculated from these numbers agrees well with the directly observed value. Thus, a volume diminution of about 10 ml./mole is one of the consequences of the formation of a cyclic transition state.

In the past 10 years equipment has become commercially available by means of which high pressures (~10,000 atm.) can routinely be generated and contained for prolonged periods of time. This fact has enabled chemists to turn to the application of pressure as a tool in elucidating reaction mechanisms.[2] It is now known that very important (if not the most important) changes in rate occur when pressure is applied to a system in which ionization or neutralization of charge is involved in the rate-determining step.[3] Another important feature often postulated in mechanistic studies is the opening or closure of a ring. Several authors[4a-e] have estimated the corresponding part of ΔV^* on the basis of known densities of stable linear and cyclic molecules; however, there appear to be no literature reports of studies undertaken with the specific objective of determining the effect of pressure on reactions in which ring opening or closure is involved in the transition state and in which furthermore charge separation or neutralization is at most minor.

It was recently reported by Gagneux, Winstein, and Young[5] that α- and γ-methylallyl azide rapidly form an equilibrium mixture of the two. They measured both the rate and equilibrium constants of this reaction. It was noted that these quantities were remarkably insensitive to changes in solvent as well as to methyl substitution. For instance, the rate of equilibration in ethanol is only four times as great as in *n*-pentane, and in either solvent the rate of equilibration of α,α- and γ,γ-dimethylallyl azide is only three times as large as that of the butenyl azides. These observations are indicative of very little charge separation in the transition state. Although the exact geometry of the transition state is not known, it seems very likely that a six-membered ring is involved. For these reasons the isomerization seemed an excellent model for this study.

Experimental

Preparation of α- and γ-Methylallyl Azides.[6]—A sample of 18 g. of *trans*-crotyl chloride (commercial material purified by fractional distillation) was added to a filtered solution of sodium azide in a mixture of 1.5 l. of acetone and 0.5 l. of water. After 24 hr., this mixture was shaken with 2 l. of water and 2 l. of ether. The ether phase was washed three times with 1 l. of water, then dried over sodium sulfate. Vacuum distillation by means of a Vigreux column with a Dry Ice reflux condenser yielded a residue the infrared spectrum of which had a strong band at 2040 cm.$^{-1}$. This mixture was stored at Dry Ice temperature. Samples were separated into the pure isomers by preparative gas chromatography as needed. The separation was accomplished by means of an Aerograph instrument, which was fitted with a 3-ft. Silicone-90 column held at room temperature. The α- and γ-isomers had retention times of 30 and 60 min., respectively, when the pressure of the carrier gas was 10 p.s.i. Up to 50 mg. of the mixture could thus be separated in a single operation. A convenient analytical procedure depends on the fact that the α-isomer has a strong, sharp peak at 10.67 μ in the infrared spectrum (characteristic of vinyl compounds)[7] and the γ-isomer at 10.30 μ (characteristic of *trans* olefins). A smooth curve constructed from experimental optical density ratios *vs.* composition of known mixtures provided a routine and rapid method of analysis of unknown mixtures; the ratio of isomers in a mixture could thus be estimated easily to 3% accuracy over most of the range.

Apparatus.—The apparatus has been described earlier.[8] The container used was type E described in the same paper; this type is particularly suited for very small samples (0.1 ml. or less).

During the generation of pressure there is a considerable temperature rise, so that care must be exercised in rate studies to keep the effect of temperature changes from masking the effect of pressure. Precooling of the reaction mixture, reasonably slow generation of pressure, and choice of the temperature such that the reaction is not too rapid (when compared with the rate of heat exchange through the walls of the pressure vessel) were used to minimize the problem, but it still was necessary to make a correction for the reaction taking place during the initial phase.

Procedures.—A 0.3-ml. test tube, fitted with a small piece of rubber tubing as described earlier,[8] was charged with 0.1 ml. of a 4% solution of the isomer of interest in methylene chloride. This solution was frozen in liquid nitrogen. The remainder of the vessel then was filled with mercury, care being taken to leave a small air bubble between the mercury and the frozen solution to allow for expansion of the latter as it warmed up. The Teflon stopper was put in place and the vessel was inverted and stored under liquid nitrogen. After the reaction had proceeded for the allotted time, the tubes were again frozen until just before analysis. It was found that temperature equilibrium inside the pressure vessel was reached in about 10 min. Therefore, kinetic runs at every pressure used included samples withdrawn after 15 min.; the results of these experiments determined the correction to be applied to longer runs. The thermostat was set at 20.0°. The ratio of densities of the isomers was determined by means of a dilatometric study of the rate of isomerization of pure γ-methylallyl azide; a sensitive, long-stem thermometer was used as the dilatometer. The thermometer was calibrated, the top was cracked off, and the mercury removed. The weight of the mercury and the calibrated scale thus provided a very accurate means of measuring changes in density requiring only 0.1 ml. of liquid.

Results and Discussion

The data apply to reaction 1.

(1) Presented at the 144th National Meeting of the American Chemical Society, Los Angeles, California, April, 1963.

(2) See, *e.g.*, S. D. Hamann, "Physico-Chemical Effects of Pressure," Academic Press, Inc., New York, N. Y., 1957, Chapters VIII and IX.

(3) H. G. David and S. D. Hamann, *Trans. Faraday Soc.*, **50**, 1188 (1954).

(4) (a) C. Walling and J. Peisach, *J. Am. Chem. Soc.*, **81**, 5819 (1959); (b) W. J. le Noble, *ibid.*, **82**, 5253 (1960); (c) K. R. Brower, *ibid.*, **83**, 4370 (1961); (d) A. R. Osborn and E. Whaley, *Trans. Faraday Soc.*, **58**, 2144 (1962); (e) C. Walling and M. Naiman, *J. Am. Chem. Soc.*, **84**, 2628 (1962).

(5) A. Gagneux, S. Winstein, and W. G. Young, *ibid.*, **82**, 5956 (1960).

(6) The author is indebted to Professor S. Winstein for providing a number of unpublished details of this preparation.

(7) L. J. Bellamy, "The Infrared Spectra of Complex Molecules," John Wiley and Sons, Inc., New York, N. Y., 1954, Chapter II.

(8) W. le Noble, *J. Am. Chem. Soc.*, **85**, 1470 (1963).

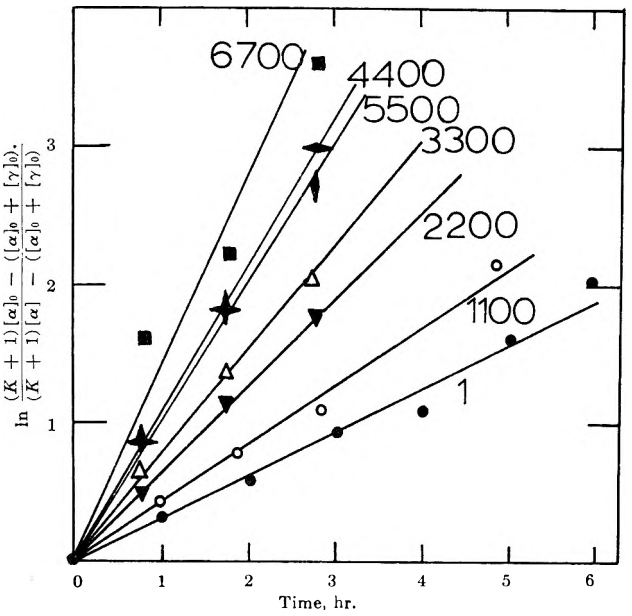

Fig. 1.—First-order plot of the equilibration of α-methylallyl azide in methylene chloride solution at 20° at various pressures.

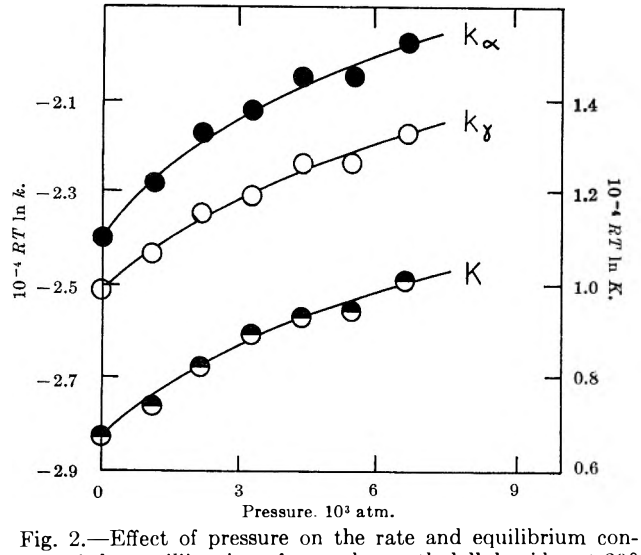

Fig. 2.—Effect of pressure on the rate and equilibrium constants of the equilibration of α- and γ-methylallyl azides at 20° in methylene chloride solution; R = 82 cm.^{3} atm. mole^{-1} °K^{-1}.

$$CH_2{=}CH{-}\underset{\alpha}{\underset{|}{CH}}(CH_3){-}N_3 \underset{k_\gamma}{\overset{k_\alpha}{\rightleftarrows}} \underset{\gamma}{CH_3{-}CH{=}CH{-}CH_2{-}N_3} \quad (1)$$

This reaction is first order, as shown by Gagneux, Winstein, and Young[5] and by the present work; Fig. 1 shows the first-order plots of the reaction of the α-isomer at various pressures. The equilibrium constants were determined by allowing samples of either isomer as well as of mixtures already equilibrated at atmospheric pressure to remain under pressure for relatively long periods of time; at each pressure, all these solutions had identical infrared spectra. The constants thus obtained agreed well with the values calculated from the relative rates at which the pure α- and γ-isomers approached equilibrium (see below). Starting with pure α-methylallyl azide, the following rate expression applies

$$\ln K/\{(1 + K)([\alpha]_t/[\alpha]_0) - 1\} = (k_\gamma + k_\gamma)t$$

Starting with pure γ-isomer, the rate law is

$$\ln 1/\{(1 + K)([\gamma]_t/[\gamma]_0) - K\} = (k_\alpha + k_\gamma)t$$

If the right-hand members of these expressions are set equal and the resulting equation is solved for K, one obtains

$$K = N_\gamma/N_\alpha$$

where N_γ is the mole fraction of γ-isomer in a mixture that started as pure α-isomer and similarly N_α is the mole fraction of α-isomer in a mixture that started as pure γ-isomer. Hence, by allowing samples of pure α- and γ-isomers to react under the same conditions for the same length of time, it was possible to determine the equilibrium constant also without actually allowing them to reach equilibrium. Thus, each run yielded a value of K as well as k_α and k_γ. In the rate experiments under pressure, slightly more complicated rate equations were used: those that would obtain if the starting samples of α-isomer were contaminated with some of the γ-azide and *vice versa*. The degree of contamination assumed was that actually found after the heat of compression had been completely dissipated at a given pressure.

The results of the measurements of rate and equilibrium constants are shown in Table I.

TABLE I

THE RATE OF EQUILIBRATION AND THE EQUILIBRIUM CONSTANT OF α- AND γ-METHYLALLYL AZIDE AS A FUNCTION OF PRESSURE

Pressure, atm.	K^a	K^b	$(k_\alpha + k_\gamma) \times 10^4$, sec.$^{-1c}$
1	1.80 ± 0.10 (5)	1.77 ± 0.06	0.83 ± 0.06 (13)
1100	1.90 ± .20 (5)	1.86 ± .06	1.19 ± .10 (8)
2200	2.00 ± .10 (3)	2.00 ± . 06	1.83 ± .06 (4)
3300	2.12 ± .10 (3)	2.11 ± .06	2.17 ± .09 (4)
4400	2.20 ± .05 (3)	2.18 ± .06	2.97 ± .20 (4)
5500	2.21 ± .05 (3)	2.20 ± .06	2.94 ± .20 (5)
6700		2.33 ± .06	3.94 ± .40 (3)

[a] The values of K listed in this column were obtained by the kinetic method described in the text and are shown here with the average error and the number of determinations. [b] The values of K listed in this column were determined from the identical spectra obtained from solutions of α- and γ-isomers kept at high pressure, as well as of mixtures pre-equilibrated at 1 atm. and then stored at high pressure; the average error is estimated to be ±0.06. Only the values listed in this column were used in the calculations. [c] The deviations listed here are also average errors and the number of measurements is shown in parentheses. The decrease in precision reflects the effect of heats of compression.

When $RT \ln K$ and $RT \ln k$ are plotted *vs.* p (see Fig. 2), the slopes of the resulting curves are equal to $-\Delta V$ and $-\Delta V^*$, respectively. The curves represent the least squares expressions

$$-RT \ln k_\alpha = 236{,}000 - 9.5p + 0.56 \times 10^{-3}p^2$$

$$-RT \ln k_\gamma = 250{,}000 - 7.9p + 0.47 \times 10^{-3}p^2$$

$$-RT \ln K = -13{,}700 - 1.48p + 0.077 \times 10^{-3}p^2$$

Thus, at 0 atm., $\Delta V^*\alpha = -9.5$ cm.^{3}/mole, $\Delta V^*\gamma = -7.9$ cm.^{3}/mole, and $\Delta V = -1.5$ cm.^{3}/mole. There appears to be some disagreement on the reliability of ΔV terms so obtained.[9] For this reason, it is of interest to note that the ratio of densities d_γ/d_α = 1.015 when calculated from the density (0.91 at 20°)

(9) (a) S. W. Benson and J. A. Berson, *J. Am. Chem. Soc.*, **84**, 152 (1962); (b) C. Walling and D. D. Tanner, *ibid.*, **85**, 612 (1963).

of the equilibrium mixture and from ΔV (as determined by the pressure dependence of K); this value agrees closely with that obtained from the dilatometric experiment, 1.018. It is believed, therefore, that the ΔV^* terms are accurate to about 1 cm.^{3}/mole.

In the study of a mechanism of a reaction, there are several questions which knowledge of pressure effects on the rate constant may help to answer; among these are the extent of charge separation or neutralization, of charge dispersal or concentration, of homolytic bond formation or cleavage, and the effect of conformational changes such as the assumption of cyclic or extended shapes. Unfortunately, the latter type of change cannot be studied in the absence of all others by means of high pressure techniques, since a mere conformational change cannot provide all the activation needed for reactions occurring at convenient rates at room temperature. Thus, attempts to determine the effect of cyclization on ΔV^* should be limited to reactions in which the other effects can be estimated. As remarked earlier, the transition state in the isomerization of the butenyl azides is not much more polar than the reactant. Furthermore, it seems safe to assume that homolytic bond cleavage cannot be much more extensive than bond formation, since it would be difficult to explain the stability of the isomers to nitrogen formation if the N_3^- group were free at any time. The conclusion is that if ring formation is a feature in the formation of the transition state, the corresponding diminution in volume is not greater than 8–10 cm.^{3}/mole; this value agrees quite well with those reported in ref. 4c and 4e.

ELECTRICAL CONDUCTANCES OF AQUEOUS SOLUTIONS AT HIGH TEMPERATURE AND PRESSURE. I. THE CONDUCTANCES OF POTASSIUM SULFATE–WATER SOLUTIONS FROM 25 TO 800° AND AT PRESSURES UP TO 4000 BARS[1]

BY ARVIN S. QUIST, E. U. FRANCK,[2a] H. R. JOLLEY,[2b] AND WILLIAM L. MARSHALL

Reactor Chemistry Division, Oak Ridge National Laboratory, Oak Ridge, Tennessee

Received June 7, 1963

The electrical conductances of 0.0005032, 0.002199, and 0.004986 *m* K_2SO_4 solutions in H_2O have been measured at temperatures from 25 to 800° and at pressures from 1 to 4000 bars. Electrical conductance was observed at solution densities as low as 0.2 g./cm.^{3}. At constant temperature the equivalent conductances increased rapidly with increasing density and reached maximum values at densities between 0.5 and 0.7 g./cm.^{3}. Although at densities below 0.8 g./cm.^{3} considerable ion association and hydrolysis appear to occur, K_2SO_4 is found to behave as a relatively strong electrolyte between 0.8 and 1.0 g./cm.^{3} solution density. This is in accordance with the behavior of monovalent salts in supercritical water as observed earlier. Thermodynamic dissociation constants for the equilibrium $KSO_4^- \rightleftharpoons K^+ + SO_4^{-2}$ have been estimated at 100, 200, and 300°.

Introduction

The ability of water to act as an electrolytic solvent is not restricted to temperatures below the critical point, but extends well into the region of supercritical temperatures if it is compressed to high enough densities. This is indicated by the electrical conductance of ordinary electrolytes in supercritical water. At present, information on conductances of electrolytes in water at elevated temperatures is somewhat limited. The first comprehensive studies up to 306° and at saturation vapor pressures were performed by A. A. Noyes and co-workers.[3] Precise conductance measurements of NaCl in water between 378 and 393° and at pressures up to 300 bars were reported by Fogo, Benson, and Copeland.[4] More recently, apparatus was developed by one of the authors for making conductance measurements in aqueous solutions at pressures up to 2500 bars and temperatures up to 750°.[5a] By the use of this equipment, extensive measurements were made of the conductances of many 1–1 electrolytes as a function of temperature, pressure, and concentration from which dissociation constants, entropy changes, and heats of dissociation were calculated and compared to each other.[5] Also from these previous data, the relative behavior of the ion product of water was evaluated at extreme conditions of temperature and pressure. A general review of investigations in this field has been published elsewhere.[5c]

At this Laboratory an improved apparatus has been developed which again extends the range of accessible temperatures and pressures. Since the influence of corrosion has been reduced, more accurate measurements may be obtained, particularly with acidic solutions. Since in the earlier high temperature measurements only uni-univalent electrolytes were studied, a program has been initiated to investigate electrolytes containing polyvalent ions. In a study on the behavior of sulfate salts, the electrical conductances of K_2SO_4 dissolved in H_2O at three concentrations have been measured at temperatures from 25 to 800° and at pressures from 1 to 4000 bars. Sufficient data have

(1) This paper is based on work performed at the Oak Ridge National Laboratory, which is operated by Union Carbide Corporation for the U. S. Atomic Energy Commission.

(2) (a) Research participant, 1960, Institut für Physikalische Chemie und Electrochemie, Karlsruhe Technische Hochschule, Karlsruhe, Germany; (b) Summer participant, 1961 and 1962, Department of Chemistry, Loyola University, New Orleans, Louisiana.

(3) A. A. Noyes, *et al.*, "The Electrical Conductivity of Aqueous Solutions," Publication No. 63, Carnegie Institution of Washington, Washington, D. C., 1907.

(4) J. K. Fogo, S. W. Benson, and C. S. Copeland, *J. Chem. Phys.*, **22**, 209, 212 (1954).

(5) (a) E. U. Franck, *Z. physik Chem.* (Frankfurt), **8**, 92 (1956); (b) *ibid.*, **8**, 107, 192 (1956); (c) *Angew. Chem.*, **73**, 309 (1961).

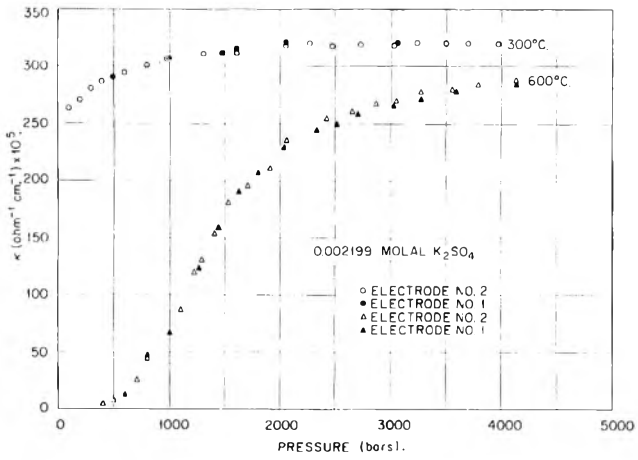

Fig. 1.—Specific conductances of 0.002199 m K_2SO_4 solutions as a function of pressure at 300 and 600° (two experimental runs at each temperature).

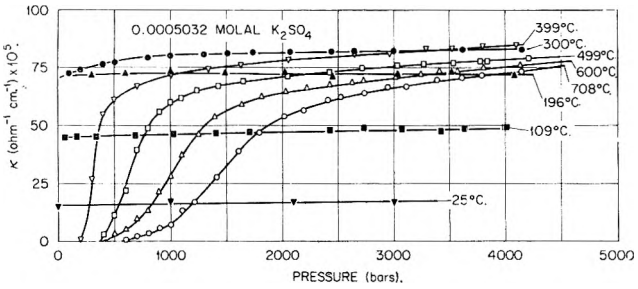

Fig. 2.—Specific conductances of 0.0005032 m K_2SO_4 solutions as a function of pressure at several temperatures.

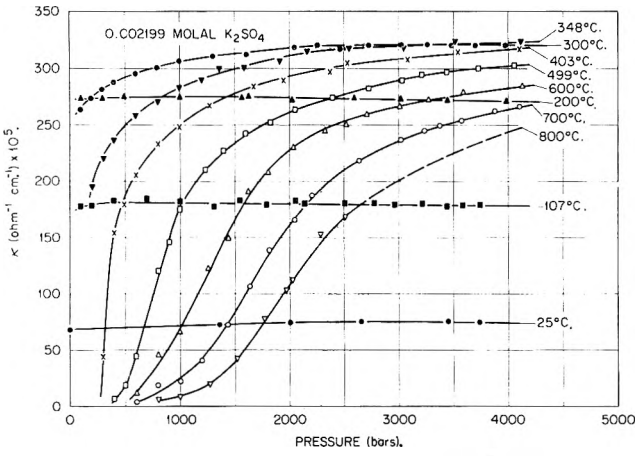

Fig. 3.—Specific conductances of 0.002199 m K_2SO_4 solutions as a function of pressure of several temperatures.

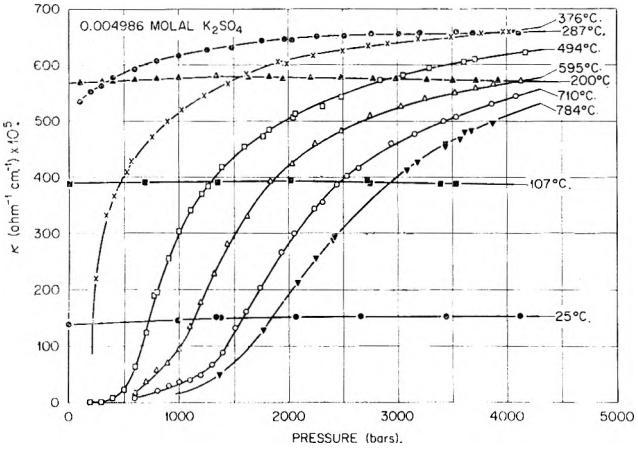

Fig. 4.—Specific conductances of 0.004986 m K_2SO_4 solutions as a function of pressure at several temperatures.

been collected to show that K_2SO_4 at high temperatures in H_2O solutions at moderately high densities behaves as a relatively strong electrolyte, but as the density decreases, association and hydrolysis probably occur extensively. The evaluation of the respective thermodynamic dissociation and association constants requires additional data on H_2SO_4 and $KHSO_4$ solutions. It appears, however, that the dissociation constant for the equilibrium $KSO_4^- \rightleftharpoons K^+ + SO_4^{-2}$ can be estimated at high densities and relatively low temperatures.

Experimental

Apparatus.—The conductance cell and associated equipment have been described previously.[6] The conductance cell is a small cylindrical autoclave, approximately 2 in. in diameter, constructed from a special nickel alloy [Udimet 700] having very high mechanical strength at elevated temperatures. The cell is completely lined with platinum–iridium which serves as one electrode. The central second electrode is also made from a platinum–iridium alloy and is insulated by a tube of sintered nonporous aluminum oxide. The pressurizing system was modified by replacing the hand operated pressure generator with an air-driven diaphragm pump [Sprague Engineering Corp., Gardena, Calif.] and an intensifier [Harwood Engineering Co., Inc., Walpole, Mass., Model B-2.5]. The oil used in the intensifier was isolated from the electrolyte solution by using two separator units. Each unit consisted of a high-pressure thick-walled cylinder containing a close-fit floating piston and a high-pressure connection at both ends. The first separator unit, in series with the second, isolated the oil from pure water; the second separator unit isolated the electrolyte solution from the water. Thus two barriers were provided between the electrolyte solution and the oil. Both separator units were maintained in vertical positions, with water in the bottom section of the first unit and electrolyte solution in the bottom of the second unit. At the start of each experiment, the pistons were positioned at the top of their respective separator units. As a consequence of the relative arrangement of the liquids in each unit, if the floating pistons slowly fell during the experiment the electrolyte solution would not be diluted nor would there be opportunity for water to be introduced into the intensifier (and thus cause corrosion) when the pressure was reduced.

Materials.—The conductivity water used to prepare all solutions was obtained by passing distilled water through a cation–anion exchange resin [Illinois Water Treatment Co., Rockford, Ill., Research Model De-Ionizer] and then redistilling it twice from a fused-quartz distillation unit [Heraeus; Hanau am Main, Germany]. The resulting specific conductance of the water was about 1×10^{-7} ohm^{-1} cm.$^{-1}$ at 25°. Single crystals of potassium chloride [Harshaw Chemical Co.] were used to prepare the solutions for the determination of the cell constants. The potassium sulfate solutions were prepared gravimetrically, using calibrated weights, from Mallinckrodt analytical reagent salt dried at 120° prior to use.

Cell Constant.—Three different inner electrode assemblies were used throughout this series of measurements. The cell constants, as determined at 25.00 ± 0.01° by using 0.01 Demal KCl solutions were 0.305, 0.239, and 0.290 cm.$^{-1}$ for electrodes 1, 2, and 3, respectively. The effects of changes of temperature and pressure on the cell constant were minimized by the design of the cell. The maximum change in cell constant was found to be only 0.25%, and consequently no corrections were made to the experimental data.

Solvent Conductance.—The correction for the conductance of water and of impurities from the all-metal system was determined by making many measurements over the entire range of temperature and pressure with conductivity water in the conductance cell. These measurements were made after the system had been rinsed many times with conductivity water and after several runs had been made at 500° with conductivity water in the cell. The corrections for the background conductance of water and impurities from the system varied from about 2 to 10% of the total conductance of 0.0005 molal K_2SO_4 to 0.5 to 2% of the total conductance in the case of 0.005 molal K_2SO_4.

Effect of Frequency.—Many conductance measurements were

(6) E. U. Franck, J. E. Savolainen, and W. L. Marshall, *Rev. Sci. Instr.*, **33**, 115 (1962).

made over the entire range of temperature, pressure, and concentration at frequencies of 0.5, 1, 2, 4, 10, and 20 kc./sec. These values were then plotted as a function of (frequency)$^{-1/2}$ and extrapolated to infinite frequency The values obtained at infinite frequency differed from those measured at 2 kc./sec. by a small amount, varying from 0.5 to 2%, depending upon the conductance of the solution. Frequent platinization of the inner electrode (which becomes gray above about 500°) minimized the effect of frequency.

Accuracy of Measurements.—The cell temperature and the temperature gradients along the cell were determined by means of three calibrated Pt:Pt–10% Rh thermocouples placed at the top, middle, and bottom of the cell. The absolute accuracy of the calibration of the thermocouples was estimated to be ±0.6°. The pressure gages [a Heise gage was used for pressures to 1000 bars, and a Baldwin–Lima–Hamilton strain gage was used at higher pressures] were calibrated by a dead weight piston gage, with a resulting accuracy in pressure measurements estimated to be better than 0.5%. The accuracy of the Wayne–Kerr B-211 bridge with its associated audio oscillator and wave-form analyzer is stated by the manufacturer to be better than ±0.5%. The accuracy of the smoothed values of the specific conductance of the solutions, corrected for solvent conductance and frequency effect, is estimated to be within ±1–2% at the higher concentrations and densities.

Procedure.—The conductance cell and the high-pressure tubing leading from the separator unit to the cell were rinsed thoroughly with the solution prior to each run. The system was then pressurized so that when the cell reached the desired temperature, the pressure on the solution was in the range of 2000 to 3000 bars. The conductance cell was held at constant temperature (within ±1°) while conductance measurements were made at a series of pressures, first by raising the pressure to 4000 bars, then by decreasing the pressure stepwise to the lowest values, and finally by increasing the pressure to near the original value. Measured conductances were the same, within experimental error, whether measured on increasing or on decreasing the pressure. An indication of the reproducibility of the measurements of the conductance of potassium sulfate solutions is shown in Fig. 1, at temperatures of 300 and 600°, where the results of two series of measurements, using two different electrodes and electrode holder assemblies, are plotted.

Other than when the conductance was measured over the range of frequencies of 0.5–20 kc./sec., all measurements were made at 2 kc./sec. Experimentally determined values of conductance were first converted to resistances and a correction made for the effect of lead resistance (2.6 ohms). A correction was then applied to obtain the value of the resistance at infinite frequency. By using the appropriate value of the cell constant, specific conductances were obtained, which were then corrected for the conductance of water. For each set of measurements at constant temperature the specific conductances were plotted against pressure, and from the smoothed plot, values of specific conductance at various integral pressures were obtained. The equivalent conductances were then calculated at integral pressures using the equation

$$\Lambda = \frac{1000K}{2md} \qquad (1)$$

where Λ is the equivalent conductance, K is the specific conductance, m is the molality, and d is the density in g/cm.^{3}. The densities of the solutions were assumed to be the same as those of pure water. Values of the density of pure water have been determined by Kennedy, *et al.*,[7-10] to 1000° and to 1400 bars. An earlier paper[11] gives values of the density to 2500 bars and to 1000°, but these are less accurate than the later data. By the use of these data, extrapolations were made to higher densities from the nearly straight-line relationship between temperature and pressure at constant density. Table I contains values of the pressure required to give various densities at several temperatures. These densities were used to obtain molarities in addition to values of Λ.

The equivalent conductances were then plotted against densities and from these graphs the values of equivalent conductance at integral densities were obtained. The values at integral densities were then plotted as a function of temperature to obtain values of equivalent conductance at integral densities and temperatures.

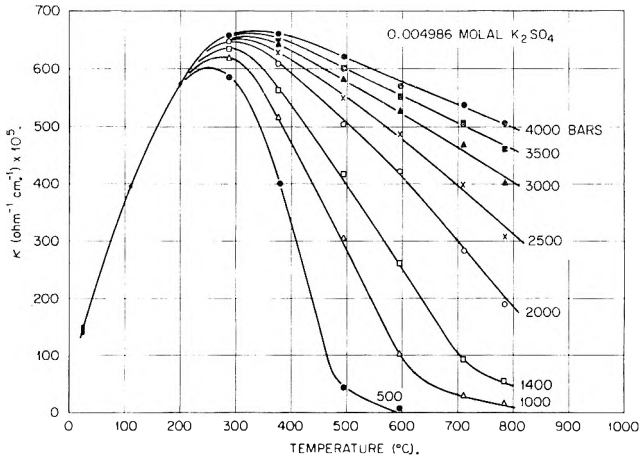

Fig. 5.—Specific conductances of 0.004986 m K_2SO_4 solutions as a function of temperature at several pressures.

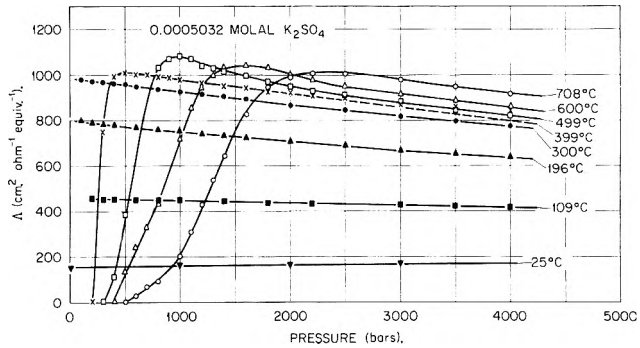

Fig. 6.—Equivalent conductances of 0.0005032 m K_2SO_4 solutions as a function of pressure at several temperatures.

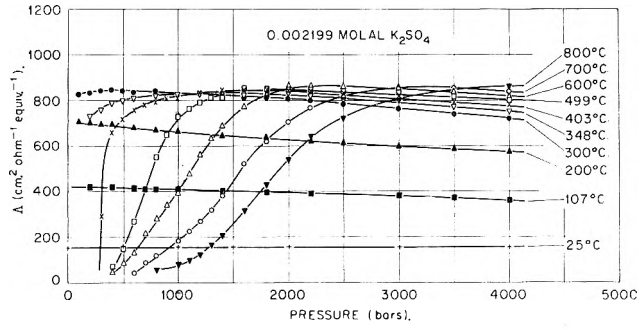

Fig. 7.—Equivalent conductances of 0.002199 m K_2SO_4 solutions as a function of pressure at several temperatures.

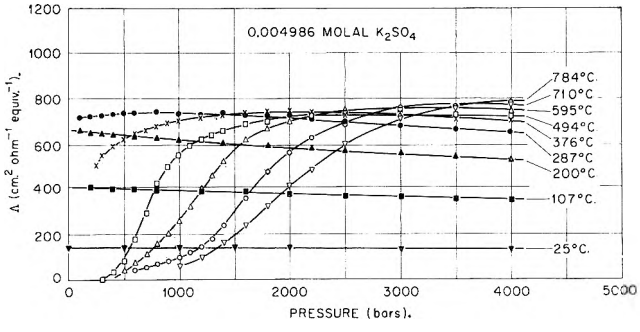

Fig. 8.—Equivalent conductances of 0.004986 m K_2SO_4 solutions of a function of pressure at several temperatures.

Results and Discussion

Figures 2, 3, and 4 show values for the specific conductances of the three potassium sulfate solutions

(7) W. T. Holser and G. C. Kennedy, *Am. J. Sci.*, **257**, 71 (1959).
(8) W. T. Holser and G. C. Kennedy, *ibid.*, **256**, 744 (1958).
(9) G. C. Kennedy, W. L. Knight, and W. T. Holser, *ibid.*, **256**, 590 (1958).
(10) G. C. Kennedy, *ibid.*, **255**, 724 (1957).
(11) G. C. Kennedy *ibid.*, **248**, 540 (1950).

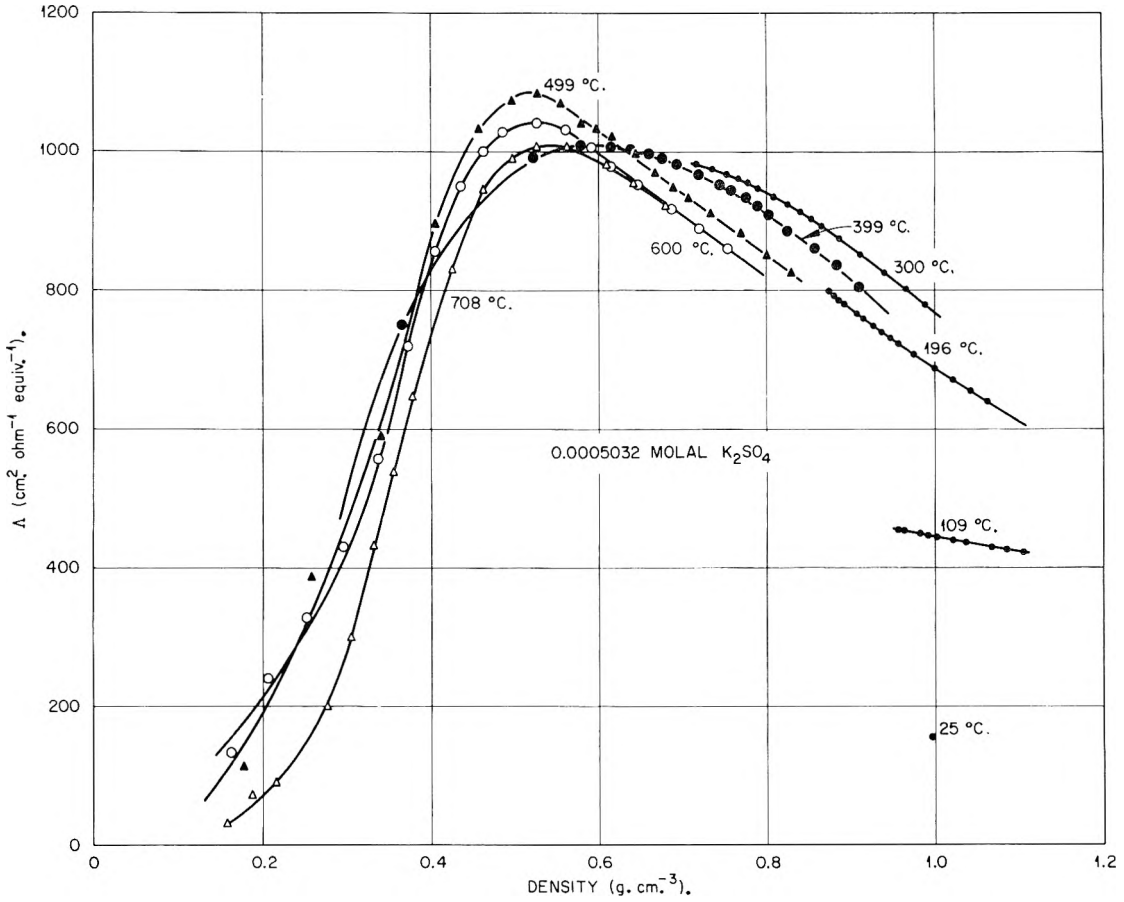

Fig. 9.—Equivalent conductances of 0.0005032 *m* K_2SO_4 solutions as a function of density of the solution at several temperatures.

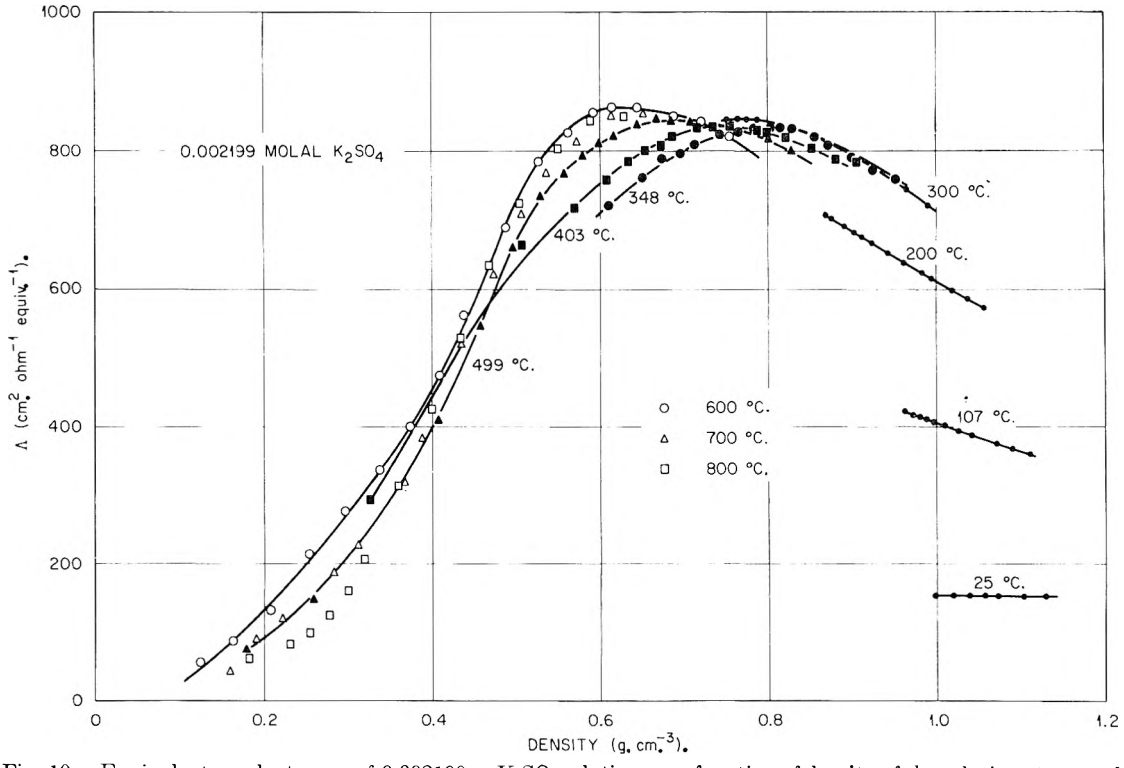

Fig. 10.—Equivalent conductances of 0.002199 *m* K_2SO_4 solutions as a function of density of the solution at several temperatures.

(corrected for solvent conductance, lead resistance, and frequency effect) plotted against pressure at the temperatures at which measurements were made. The changes in specific conductance of these solutions as a function of temperature at various constant pressures, taken from the smoothed curves of Fig. 4, are shown in Fig. 5. The series of curves obtained when the equivalent conductances of these solutions are plotted against pressure at the various temperatures are given in Fig. 6, 7, and 8. When equivalent con-

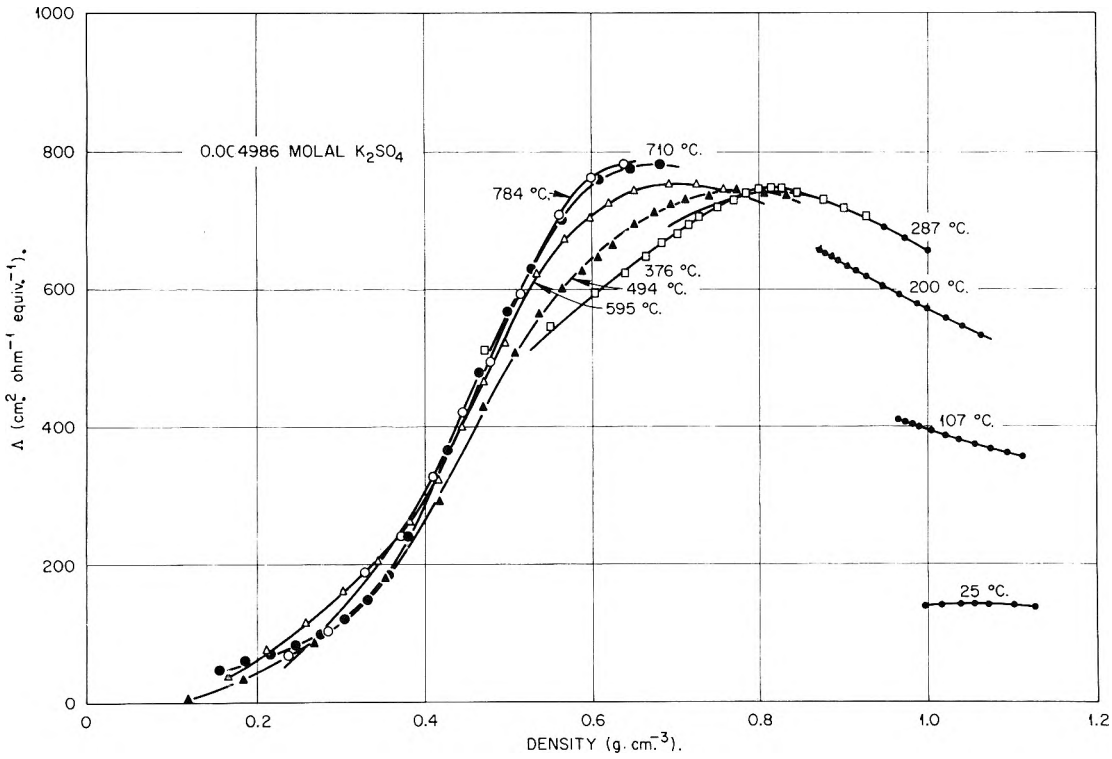

Fig. 11.—Equivalent conductances of 0.004986 *m* K_2SO_4 solutions as a function of density of the solution at several temperatures.

TABLE I

THE PRESSURE OF H_2O IN BARS AT INTEGRAL VALUES OF TEMPERATURE AND DENSITY[a]

	Density, g./cm.³										
Temp., °C.	0.1	0.2	0.3	0.4	0.5	0.6	0.7	0.8	0.9	1.0	1.1
0										1	2800
100										1000	3700
200									545	2580	
300								720	2250	4150	
400	200	260	290	410	380	560	1050	2120	3940	5720	
500	270	430	550	690	910	1310	2120	3500	5610	7300	
600	340	580	805	1080	1460	2070	3170	4870	7250		
700	410	730	1060	1440	1960	2820	4170	6240			
800	450	870	1305	1800	2500	3570	5260	7600			

[a] Interpolated and extrapolated from values of Kennedy, *et al.* (ref. 7–10).

ductances are plotted as a function of density, curves such as given by Fig. 9, 10, and 11 are obtained for the three potassium sulfate solutions. A three dimensional representation of the effect of density and temperature on the equivalent conductance of 0.0005032 *m* potassium sulfate is presented in Fig. 12. From these data the maximum value (1070 cm.² ohm^{-1} equiv.$^{-1}$) of the equivalent conductance of potassium sulfate was found to occur at a density of 0.52 g./cm.³ at 499°. Tables II, III, and IV give the equivalent conductances at integral temperatures and densities as obtained from plots of equivalent conductance *vs.* temperature at constant density. Noyes, *et al.*,[3] measured the conductance of aqueous K_2SO_4 solutions along the liquid–vapor equilibrium curve at temperatures up to 306°. The present experimental results are in excellent agreement (within experimental error) with those obtained by Noyes.

When the equivalent conductances of the potassium sulfate solutions are plotted against (molarity)$^{1/2}$, straight lines result at densities of 0.70 g./cm.³ and above. However, when the slopes of these lines are compared with the theoretical limiting law slopes for a 1:2 electrolyte[12] good agreement is observed only at a density of 1.0 g./cm.³ and temperatures of 100, 200, and 300°. In order to calculate the limiting law slopes for potassium sulfate, it was assumed that the transport numbers of the potassium and the sulfate ions remained the same (0.43 and 0.57, respectively) at temperatures above

TABLE II

THE EQUIVALENT CONDUCTANCES (CM.² OHM^{-1} EQUIV.$^{-1}$) OF 0.0005032 *m* K_2SO_4 SOLUTIONS AT INTEGRAL TEMPERATURES AND DENSITIES

Temp.,	Density, g./cm.³								
°C.	0.2	0.3	0.4	0.5	0.6	0.7	0.8	0.9	1.0
100									405
200								770	680
300							942	857	770
400	180	500	850	990	1015	973	903	830	
500	190	470	860	1045	1020	942	863		
600	190	410	835	1050	1015	913	822		
700	165	320	745	1010	980	882			
800	100	240	610	950	920				

$$S = \alpha\Lambda_0 + \beta \qquad (2)$$

(12) H. S. Harned and B. B. Owen, "The Physical Chemistry of Electrolytic Solutions," 3rd Ed., Reinhold Publishing Co., New York, N. Y., 1958, p. 178.

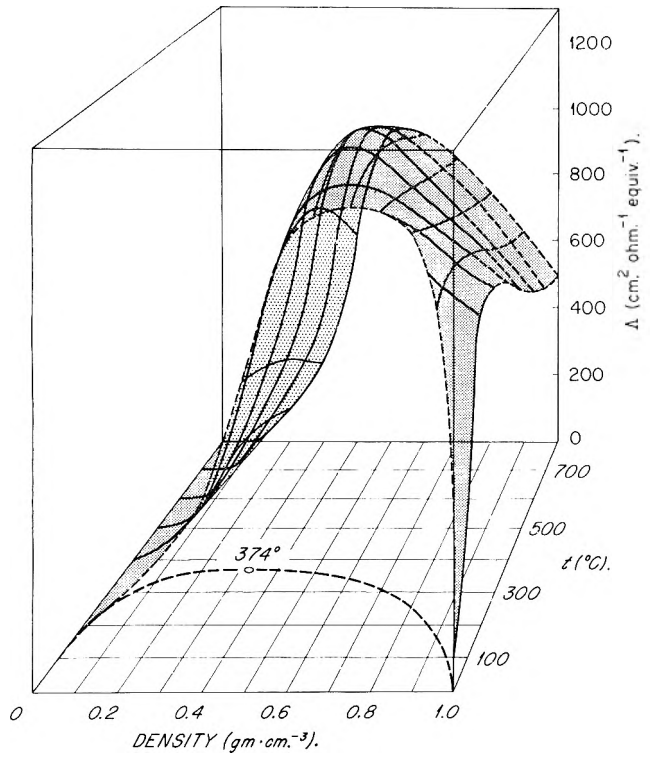

Fig. 12.—Equivalent conductances of 0.0005032 *m* K_2SO_4 solutions as a function of density and temperature.

TABLE III

THE EQUIVALENT CONDUCTANCES (CM.² OHM⁻¹ EQUIV.⁻¹) OF 0.002199 *m* K_2SO_4 SOLUTIONS AT INTEGRAL TEMPERATURES AND DENSITIES

Temp., °C.	Density, g./cm.³ 0.2	0.3	0.4	0.5	0.6	0.7	0.8	0.9	1.0
100									382
200								695	610
300							841	790	712
400	85	250	420	635	750	822	828	780	
500	110	255	445	685	820	844	813		
600	115	240	455	720	860	848	782		
700	95	220	440	720	855	832			
800	50	160	400	700	830				

TABLE IV

THE EQUIVALENT CONDUCTANCES (CM.² OHM⁻¹ EQUIV.⁻¹) OF 0.004986 *m* K_2SO_4 SOLUTIONS AT INTEGRAL TEMPERATURES AND DENSITIES

Temp., °C.	Density, g./cm.³ 0.2	0.3	0.4	0.5	0.6	0.7	0.8	0.9	1.0
100									362
200								636	570
300							732	718	663
400	25	140	235	440	600	696	748	715	
500	55	145	268	500	655	732	740		
600	70	150	290	540	707	760	735		
700	60	140	300	560	752	778			
800	25	120	290	560	770				

100° as those reported for 100° and 1 atm. pressure.[13] The values of viscosity and dielectric constant used in the calculation of S were those estimated by Franck.[5b]

The limiting law slopes obtained from the plots of Λ *vs.* (molarity)$^{1/2}$ at a density of 1.0 g./cm.³ were found to be 800, 1700, and 2000 cm.² ohm^{-1} equiv.$^{-1}$ (*moles*/l.)$^{-1/2}$ at 100, 200, and 300°, respectively. These are in good agreement with calculated values of 820, 1550, and 1900 cm.² ohm^{-1} equiv.$^{-1}$ (moles/l.)$^{-1/2}$. At densities of 0.70 to 0.90 g./cm.³, the measured slopes were usually much greater than the calculated slopes. In addition the measured slopes decreased with increasing temperature at constant density, whereas the calculated slopes increase with increasing temperature. At a density of 0.60 g./cm.³, straight-line relationships were obtained only at the higher temperatures, whereas at lower densities they could no longer be obtained at any temperature from plots of Λ *vs.* (molarity)$^{1/2}$.

The equivalent conductance of potassium sulfate at infinite dilution, Λ_0, was obtained by a variation of the method of Owen.[14] The Fuoss–Onsager conductance equation[15] contains three unknown quantities, Λ_0, E, and J

$$\Lambda = \Lambda_0 - Sc^{1/2} + Ec \log c + Jc \qquad (3)$$

In the present case with three concentrations of potassium sulfate solutions there are three equations. These equations can be solved simultaneously to give values of Λ_0 which have been "forced" from the data. These values of Λ_0 are given in Table V.

TABLE V

VALUES OF Λ_0 FOR K_2SO_4 IN H_2O SOLUTION[a]

Temp., °C.	Density, g./cm.³ 0.3	0.4	0.5	0.6	0.7	0.8	0.9	1.0
100								426
200							844	741
300						1021	921	821
400	779	1254	1303	1247	1099	968	879	
500	711	1252	1367	1190	1028	912		
600	608	1199	1348	1150	979	871		
700	447	1042	1278	1105	946			
800	354	822	1184	1027				

[a] See explanation in text.

Limiting equivalent conductances were not calculated below densities of 0.30 g./cm.³, since it was evident that the values obtained by the above method would be much too low. Comparison of the values of Λ_0 for K_2SO_4 in Table V with values of Λ_0 for KCl as reported by Franck[5b] reveals that the values of Λ_0 for K_2SO_4 are greater than those of KCl at temperatures of 300° or less. At higher temperatures the Λ_0 values for KCl exceed those of K_2SO_4. Since the method of Owen gives accurate values of Λ_0 only when the degree of association between ions is small (dissociation constants greater than approximately 5×10^{-3}),[14] and since the decrease in the ratio of the limiting equivalent conductivity of K_2SO_4 to that of KCl indicates that this method begins to give unreliable results for K_2SO_4 at temperatures of 300° and above, this indicates that perhaps significant association and hydrolysis of K_2SO_4 is occurring.

Using Franck's values for the viscosity of water at elevated temperatures and pressures[5b] and values of Λ_0 from Table V, the Walden product, $\Lambda_0\eta_0$, was calculated for each Λ_0 reported in Table V. The results of these calculations are shown in Fig. 13, where $\Lambda_0\eta_0$ is plotted against density at several temperatures. The rapid decrease of the Walden product below 0.5 g./cm.³ probably indicates that measurements were not carried out at low enough concentrations to obtain reliable values of Λ_0 from the Owen method.

(13) R. A. Robinson and R. H. Stokes, "Electrolyte Solutions," 2nd Ed., Butterworths Scientific Publications, London, 1959, p. 465.

(14) B. B. Owen, *J. Am. Chem. Soc.*, **61**, 1393 (1939).

(15) R. M. Fuoss and L. Onsager, *J. Phys. Chem.*, **36**, 2689 (1932); **61**, 668 (1957).

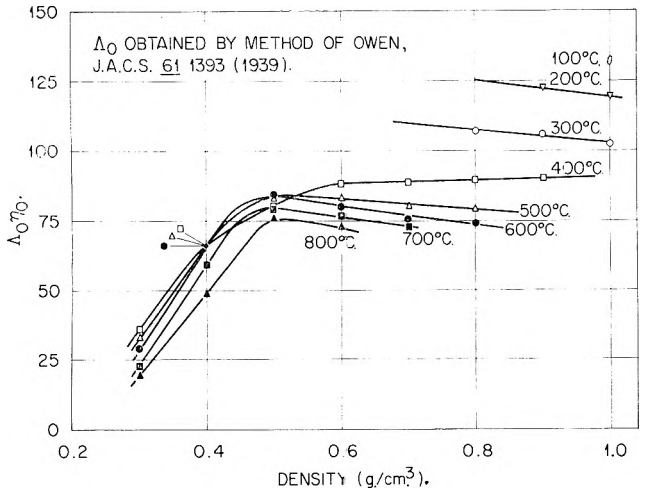

Fig. 13.—The Walden product, $\Lambda_0\eta_0$, *vs.* density for aqueous K_2SO_4 solutions.

The values of Λ_0 at temperatures above 300°, other than those given in Table V, could be obtained by a method reported previously by Franck.[5b] In this method, $\Lambda_0\eta_0$ is assumed to be constant above a selected temperature, and values of Λ_0 are calculated at higher temperatures by using estimated values for the viscosity of water.

Another procedure would be to extrapolate the linear portion of the curves in Fig 13, between densities of 1.0 and 0.5, to the lowest densities and to use these curves to obtain Λ_0 values. Thus Λ_0 values at densities between 0.5 and 1.0 at the higher temperatures would be identical with those given in Table V but differ markedly at densities below 0.5. The fact that the estimated viscosity values can only be of limited accuracy should not be ignored. Experimental data are not yet available for viscosities of water in this region of temperature and pressure.

Proceeding from the range of complete dissociation into the region of concentrations where an appreciable degree of association begins, probably the first reaction of importance would be

$$KSO_4^- \rightleftharpoons K^+ + SO_4^{-2} \qquad (4)$$

Equilibrium constants in molar units for this reaction

$$K_c = \frac{[K^+][SO_4^{-2}]}{[KSO_4^-]} \qquad (5)$$

were calculated from the conductance data according to the method of Davies.[16,17] The limiting equivalent conductance of the KSO_4^- ion was assumed to be 0.6 that of the sulfate ion.[17] The thermodynamic equilibrium constants, K^0 values, were obtained from plots of log K_c + log $f_{SO_4^{-2}}$ *vs.* I, extrapolated to infinite dilution

$$\log f_{SO_4^{-2}} = -\frac{4A\sqrt{I}}{1+\sqrt{I}} \qquad (6)$$

where I is the ionic strength, $f_{SO_4^{-2}}$ is the activity coefficient of the SO_4^{-2} ion, and $4A$ is the theoretical, Debye–Hückel limiting slope. The values of K^0 so obtained are shown in Table VI. The value at 25° has been reported to be 0.11.[17] Above 300° the values for K_c obtained by the above procedure are negative. Since the values of K_c obtained by this method are strongly dependent upon values of Λ_0 assigned to K_2SO_4, this result, and the observation that the dissociation constant at 300° was greater than at 200°, indicates that the values of Λ_0 above 200°, as reported in Table V, may be somewhat in error.

TABLE VI

VALUES OF K^0 FOR THE DISSOCIATION EQUILIBRIUM $KSO_4^- \rightleftharpoons K^+ + SO_4^{-2}$

Temp., °C.,	Density g./cm.^{3}		
	0.8	0.9	1.0
100			0.05
200		0.010	.011
300	0.032	.036	.045

Determinations of the dissociation constant of KSO_4^- at higher temperatures and lower densities depend also upon knowledge of values of K_1 and K_2 for H_2SO_4 in order to correct for hydrolysis of the sulfate ion. Experiments designed to produce values of K_1 and K_2 for H_2SO_4 over the range of temperature and pressure reported here are in progress at this Laboratory.

Acknowledgments.—We are indebted to J. E. Savolainen, Oak Ridge National Laboratory, for his help in the preliminary runs of this investigation. We wish to thank Professor R. M. Fuoss, Yale University, for several helpful discussions on this work.

(16) E. C. Righellato and C. W. Davies, *Trans. Faraday Soc.*, **26**, 592 (1930).

(17) I. L. Jenkins and C. B. Monk, *J. Am. Chem. Soc.*, **72**, 2695 (1950).

THE MAGNESIUM–MAGNESIUM CHLORIDE SYSTEM. A CHRONOPOTENTIOMETRIC STUDY[1]

By J. D. Van Norman and J. J. Egan

Brookhaven National Laboratory, Upton, New York

Received June 10, 1963

The mode of dissolution of magnesium in molten magnesium chloride contacted with Mg–Pb alloys was studied at 750° using anodic chronopotentiometry. Relative amounts of magnesium dissolved in its chloride were determined as a function of magnesium activity in the alloy. According to the law of mass action a linear dependence of magnesium solubility on a_{Mg} indicates Mg_2^{2+} ion as the reaction product and a parabolic dependence indicates Mg^+ ion. It was found that the amount of magnesium dissolved in its chloride was directly proportional to the magnesium activity in the metal phase, *i.e.*, a linear dependence, indicating Mg_2^{2+} ion formation. Due to the corrosive nature of the Mg–$MgCl_2$ system, a special apparatus was used so that only the inert metals tantalum and molybdenum came in contact with the melt. Purification procedures for materials and conditions for proper equilibration and measurement were established and are reported. The basic equation of chronopotentiometry, $i\tau^{1/2} = nF\pi^{1/2}D^{1/2}C/2$, was found to hold and at given magnesium activities the product $i\tau^{1/2}$ did not vary with the current, indicating the validity of the analytical technique. The diffusion coefficient of the Mg_2^{2+} ion was calculated and found to be 5.3×10^{-6} cm.²/sec. at 750°.

Introduction

It is well known that many metals will dissolve to some extent in their own molten halide salts. A variety of techniques has been employed to study such systems in an effort to determine the form of the excess metal in the salt. Investigations include solubility studies,[2] electrical conductivity measurements,[3,4] e.m.f. measurements,[5] magnetic susceptibility,[6] polarographic,[7] and spectral studies,[8] for a number of metal–metal halide systems.

The Mg–$MgCl_2$ system has been studied by Zhurin,[9] Rogers, *et al.*,[10] and Bukun and Ukshe.[11] These investigators measured the solubility of magnesium in its chloride at various temperatures and in the latter two investigations the change of solubility of magnesium as a function of magnesium activity was determined. Still discrepancies remain, *i.e.*, the solubilities determined by Zhurin and by Bukun and Ukshe were two to three times as great as those determined by Rogers, *et al.*, and furthermore, the mode of dissolution of magnesium in its molten chloride was not definitely established. It was, therefore, believed useful to make further studies on this system.

Two possible modes of dissolution of magnesium in its chloride are

$$Mg + Mg^{2+} \longrightarrow 2Mg^+ \qquad (1)$$

or

$$Mg + Mg^{2+} \longrightarrow Mg_2^{2+} \qquad (2)$$

where the reaction product of either reaction is termed a subhalide ion. Since the solubility of excess magnesium in its chloride is low, less than 1 mole %, the activity of the subhalide ion formed can be assumed to be proportional to its concentration. It, therefore, follows from the law of mass action that the solubility of magnesium in its chloride would be proportional to the square root of the activity a_{Mg} of magnesium in the case of reaction 1, but directly proportional to a_{Mg} in the case of reaction 2. The same conclusion would hold if reactions 1 and 2 were formulated in terms of molecular species. Thus, by varying the activity of magnesium, a_{Mg}, using a suitable alloy, and measuring the relative solubilities of magnesium, the mode of dissolution of magnesium in its chloride may be ascertained. Although one is unable to distinguish between reaction 2 and the possibility of Mg dissolving in the melt as Mg atoms by this experiment, evidence accumulated on other subhalide systems indicates that the latter mechanism is unlikely.

An *in situ* analysis for dissolved magnesium has the advantage of measuring the solubility under the actual condition of equilibrium as opposed to the previous investigations where samples were quenched and later chemically analyzed for excess magnesium content. Egan[7] has utilized the technique of anodic polarography to determine relative amounts of excess lead dissolved in its chloride, but because of the corrosive nature of the Mg–$MgCl_2$ system, a microelectrode did not appear feasible. Instead, anodic chronopotentiometry was found to be a suitable method for determining relative amounts of excess magnesium dissolved in molten magnesium chloride at 750°. Topol and Osteryoung[12] have utilized anodic chronopotentiometry in their study of the Bi–$BiBr_3$ system.

From the basic equation of chronopotentiometry

$$i\tau^{1/2} = nF\pi^{1/2}D^{1/2}C/2 \qquad (3)$$

where i is the current density in amp./cm.², τ the transition time in seconds, n the number of electrons transferred per ion, D the diffusion coefficient in cm.²/sec., and C the concentration in moles/cm.³, it follows that the product $i\tau^{1/2}$ is proportional to concentration and may be used to determine relative solubilities. Denoting this product at $a_{Mg} = 1$ by $(i\tau^{1/2})_0$, it follows that in the case of reaction 1

$$\frac{i\tau^{1/2}}{(i\tau^{1/2})_0} = a_{Mg}^{1/2} \qquad (4)$$

(1) This work was done under the auspices of the U. S. Atomic Energy Commission.

(2) (a) J. D. Corbett and S. von Winbush, *J. Am. Chem. Soc.*, **77**, 3964 (1955); (b) E. A. Ukshe and N. G. Bukun, *Russ. Chem. Rev.*, **30**, 90 (1961).

(3) H. R. Bronstein and M. A. Bredig, *J. Phys. Chem.*, **65**, 1220 (1961).

(4) G. W. Mellors and S. Senderoff, *ibid.*, **64**, 294 (1960).

(5) L. E. Topol, S. J. Yosim, and R. A. Osteryoung, *ibid.*, **65**, 1511 (1961).

(6) N. H. Nachtrieb, *ibid.*, **66**, 1163 (1962).

(7) J. J. Egan, *ibid.*, **65**, 2222 (1961).

(8) C. R. Boston and G. P. Smith, *ibid.*, **66**, 1178 (1962).

(9) A. I. Zhurin, *Metallurg.* **10**, No. iv, 87 (1935).

(10) P. S. Rogers, J. W. Tomlinson, and F. D. Richardson, "Physical Chemistry of Process Metallurgy," Interscience Publishers, Inc., New York, N. Y., 1961, p. 909.

(11) N. G. Bukun and E. A. Ukshe, *Russ. J. Inorg. Chem.*, **6**, 465 (1961).

(12) L. E. Topol and R. A. Osteryoung, *J. Phys. Chem.*, **66**, 1587 (1962).

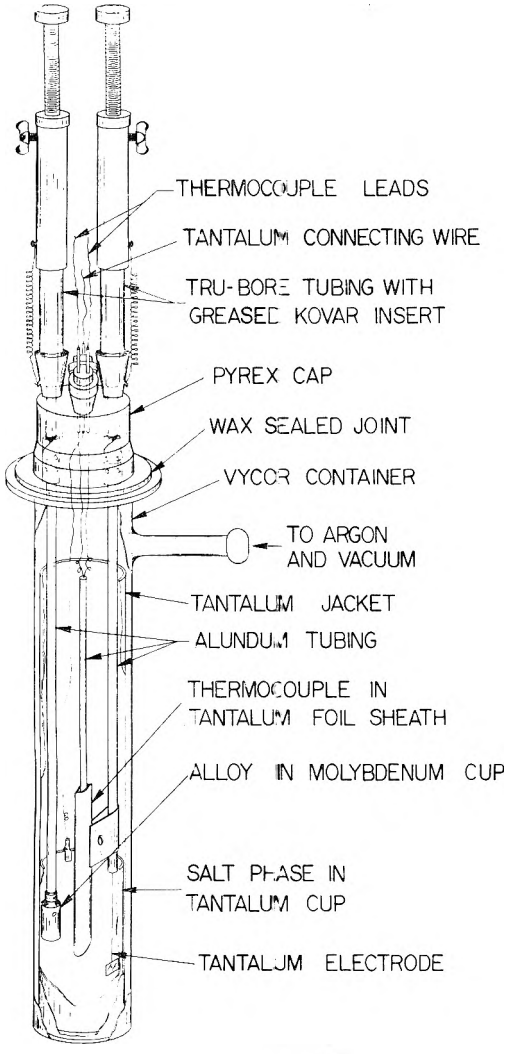

Fig. 1.—Chronopotentiometric cell used for the study of the Mg–$MgCl_2$ system.

whereas in the case of reaction 2

$$\frac{i\tau^{1/2}}{(i\tau^{1/2})_0} = a_{Mg} \qquad (5)$$

A plot of $i\tau^{1/2}/(i\tau^{1/2})_0$ *vs.* activity of magnesium, a_{Mg}, would yield a parabola for reaction 1 and a straight line for reaction 2.

Experimental

The magnesium chloride used in this investigation was a by-product of the production of titanium and was initially anhydrous. It was further purified by passing dry HCl gas through the powder for 24 hr. at less than 100° and for 6 hr. more while the temperature of the salt was raised above its melting point, 708°. The salt thus obtained was filtered through fine quartz frits and stored under dry argon until used. Spectrographic grade magnesium metal was in the form of one-quarter-inch rods. The surface of the rods was filed to remove the oxide film and the metal used directly. The lead metal used in the Mg–Pb alloys was filtered in the molten state through a coarse Pyrex frit to remove the insoluble oxide.

The chronopotentiometric cell used is shown in Fig. 1. The salt phase, $MgCl_2$, was contained in a large tantalum cup and the alloys were contained in a small molybdenum cup; a hole in the side of the small cup, below the surface of the salt, furnished contact of the alloy with the salt phase. The indicator electrode was a small tantalum foil of known area suspended in the salt from a thin tantalum wire. The temperature was measured with a Chromel–Alumel thermocouple protected with a tantalum sheath and immersed in the salt phase. The indicator electrode, the small molybdenum cup, and the thermocouple were attached with Alundum tubing to movable Kovar inserts in the Pyrex cap, to permit vertical positioning of these components. Electrical contact was made to the Kovar inserts from the electrodes with small tantalum wires inside the Alundum tubing. The large tantalum cup and the entire electrode assembly were contained in a tantalum jacket to protect the outer Vycor container from attack by magnesium vapor. The cell was contained in a resistance furnace maintained at the proper temperature. All metal components in contact with the metal–salt system were cleaned by induction heating in a fast pumping, high vacuum system.

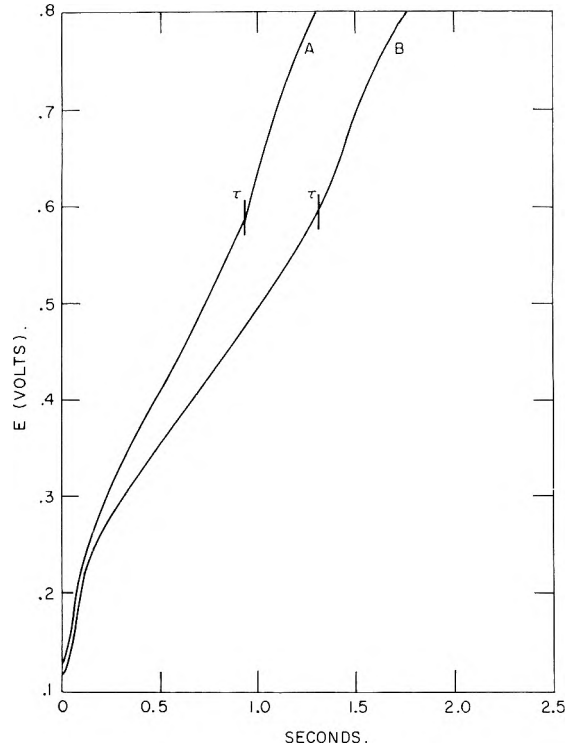

Fig. 2.—Typical anodic chronopotentiograms obtained in the Mg–$MgCl_2$ system.

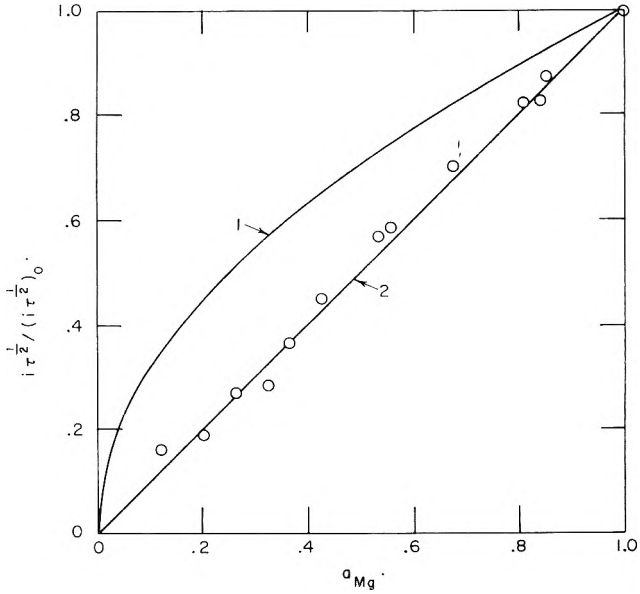

Fig. 3.—A plot of $i\tau^{1/2}/(i\tau^{1/2})_0$ *vs.* a_{Mg}: curve 1 corresponds to the formation of Mg^+; curve 2 corresponds to the formation of Mg_2^{2+}.

Anodic chronopotentiograms were obtained by passing a known constant current between the tantalum indicator electrode and the large tantalum cup, which served as the counter electrode while measuring the potential between the indicator electrode and the molybdenum cup, the reference electrode, as a function of time. The constant current was furnished by an all-electronic current regulator designed by the Instrumentation Division of Brookhaven National Laboratory and the potential–time curves were recorded on a Leeds and Northrup High Speed

Speedomax G recorder which had a pen speed of 0.25 sec. full scale and chart speed of 2 in./sec.

Transition times for the chronopotentiograms obtained were read from the chart recordings with an estimated accuracy of ±0.025 sec. The alloy–salt systems were equilibrated for at least 12 hr. before chronopotentiometric measurements were made. Measurements taken at times greater than 12 hr. (up to 18 hr.) always gave the same results, ensuring true equilibration between salt and alloys.

Results and Conclusions

Anodic chronopotentiograms for the oxidation of the subhalide ion in magnesium chloride were obtained for a series of Mg–Pb alloy compositions at 750°. Figure 2 shows typical anodic chronopotentiograms obtained. Transition times were measured from the current onset to the potential break where the potential shifted rapidly to the more positive value of the limiting reaction. In practice, the potential at this potential break was measured for several anodic chronopotentiograms and subsequent transition times for that composition were measured to this point. It was found that at a given alloy composition the product $i\tau^{1/2}$ was indeed a constant for varying current densities, indicating the validity of the analytical technique. The final $i\tau^{1/2}$ for each composition was an average of twelve or more measurements at various current densities.

When anodic chronopotentiograms were taken of magnesium chloride equilibrated with pure lead, $a_{Mg} \cong 0$, a potential holdup was noted. A "residual" $i\tau^{1/2}$ was calculated by measuring the time necessary to achieve the predetermined potential when a constant current was passed. This background is probably due to oxidizable impurities in the salt. The various $i\tau^{1/2}$ values were corrected for this residual product as shown in Table I. Figure 3 shows the plot of $i\tau^{1/2}/(i\tau^{1/2})_0$ *vs.* a_{Mg}. Activities of magnesium in Mg–Pb alloys determined by Schmal and Sieben[13] and by Lantratov[14] were used. Curve 1 is the plot expected for the formation of Mg^+ ion, reaction 1, while curve 2 corresponds to the theoretical plot for reaction 2, the formation of Mg_2^{2+} ions. The experimental points fall on the straight line, curve 2, confirming that magnesium dissolves in its chloride to form Mg_2^{2+} ions. Strangely, Bukun and Ukshe hypothesize the formation of Mg^+ ions (MgCl), although a plot of their data shows the three experimental points they obtained on a straight line.

(13) N. Schmal and P. Sieben, "Physical Chemistry of Metallic Solutions and Intermetallic Compounds," National Physical Laboratory Symposium, No. 9, Paper 2K, England, 1958.

(14) M. F. Lantratov, *Russ. J. Inorg. Chem.*, **4**, 636 (1959).

Table I

x_{Mg}	a_{Mg}	$i\tau^{1/2} \times 10^2$ amp. sec.$^{1/2}$/cm.^{2}	$i\tau^{1/2} \times 10^2$ corrected amp. sec.$^{1/2}$/cm.^{2}	$\frac{i\tau^{1/2}}{(i\tau^{1/2})_0}$
1.000	1.000	2.22	1.60[a]	1.000
.901	0.850	2.01	1.39	0.868
.897	.842	1.94	1.32	.825
.875	.810	1.93	1.31	.820
.801	.672	1.74	1.12	.700
.751	.552	1.56	0.94	.587
.741	.534	1.54	.92	.575
.699	.424	1.35	.73	.456
.677	.367	1.20	.58	.362
.663	.325	1.07	.45	.282
.631	.261	1.05	.43	.269
.591	.200	0.92	.30	.188
.448	.118	.88	.26	.162
.000	.000	.62[b]	.00	.000

[a] Value of $(i\tau^{1/2})_0$. [b] Residual $i\tau^{1/2}$.

Cooled samples were analyzed for dissolved magnesium by measuring the hydrogen evolved when the samples were dissolved in water. The solubility of magnesium in its chloride at 750° found in this manner was 17% lower than the extrapolated value obtained from the data of Rogers, *et al.*, whereas the values of Zhurin as well as Bukun and Ukshe were much higher, by a factor of 2 or 3. It is felt by the authors that the values of Rogers and co-workers are the most accurate. Using their extrapolated value for the solubility of Mg in $MgCl_2$ at 750° of 0.23 mole %, the diffusion coefficient of the Mg_2^{2+} ion was calculated using eq. 3 and was found to be 5.3×10^{-6} cm.^{2}/sec. This is similar to diffusion coefficients of other ions in fused salts.

Acknowledgments.—The authors wish to express their gratitude to John Bracker for preparing the $MgCl_2$ and to Dr. R. Wiswall for encouragement and helpful discussions.

APPEARANCE POTENTIALS AND MASS SPECTRA OF FLUORINATED ETHYLENES. I. DECOMPOSITION MECHANISMS AND THEIR ENERGETICS[1]

BY CHAVA LIFSHITZ[2] AND F. A. LONG

Department of Chemistry, Cornell University, Ithaca, New York

Received June 11, 1963

Appearance potentials and mass spectra have been determined for a group of fluorinated olefins. The reactions of the positive ions are similar to those of the hydrocarbon analogs in that there are frequent losses of H_2 or HF to form acetylene ions. Rearrangement processes, involving atom migration, occur more frequently in the more highly fluorinated compounds. For the most part the relative rates of the unimolecular decomposition processes vary with the energy demands, but frequency factors are occasionally quite low for rearrangements and for four-center processes leading to acetylenic ions. The observed appearance potentials agree fairly well with values calculated from heats of formation of the species involved, but there are some exceptions. Ionization efficiency curves for some of the fragments from CF_2CFH and C_2F_4 show unusual features. Decomposition mechanisms are derived for all the olefins.

Introduction

The mass spectra of fluorocarbons are of interest both for themselves and for comparison with the spectra of their hydrocarbon analogs. Comparison reveals that the positive ions of the two series of compounds undergo somewhat different sorts of chemical reactions. There tend to be larger amounts of rearrangements occurring with the fluorocarbons and the rearrangements are of different types. As one example,[3] the species CF_3^+ is usually observed in high yield from fluorocarbons which themselves do not contain the CF_3 group; in contrast CH_3^+ is not a common rearrangement product. The energetics of the fluorocarbon decompositions are also of interest both because they yield data of thermochemical importance and because they permit significant comparisons with theory to be made. In contrast to the perfluoro paraffins, the mass spectra of the fluorinated olefins show considerable intensity of the parent ion peaks[3,4]; as a consequence, it is possible to measure the ionization potential of the molecules by electron impact.

When data for the decomposition of hydrocarbon ions are analyzed by the statistical theory of mass spectra,[5] it is commonly observed that the breaking of a C–H bond occurs with a frequency factor which is smaller by several orders of magnitude than that for the breaking of a skeletal C–C bond.[5,6] This comparison suffers from the fact that the two sorts of bonds do not occupy equivalent positions in the molecule with, as a consequence, different structures for the activated complexes.[7] By studying a partly fluorinated hydrocarbon or by comparing hydrocarbon–fluorocarbon analogs, one can obtain systems where the fluorines and hydrogens occupy equivalent positions, permitting reactions for breakage of C–H and C–F bonds to be compared more directly. Both for these comparisons and for development of the decomposition patterns for the parent positive ions it is essential to have the energetics of the decomposition processes, *i.e.*, appearance potentials are needed for all of the fragments produced in significant yield. Data are presented here for both the mass spectra and the appearance potentials for the following compounds: C_2H_4, CH_2CHF, CH_2CF_2, CHF-CF_2, C_2F_4.

Experimental Procedure and Results

All the fluorinated ethylenes studied were shown by vapor phase chromatography to be better than 99.8% pure. The compounds CH_2CHF and CH_2CF_2 were kindly furnished by Allied Chemical Co.; CF_2CFH was purchased from Penninsular Chem. Research, Inc., and C_2F_4 was synthesized from CF_2BrCF_2Br by debromination with zinc in dioxane. Samples of CF_2CFH and C_2F_4, purified by gas chromatography, were also kindly furnished by A. Fainberg, Pennsalt Chemicals Corp. Argon, neon, and ethylene were the best grade available from Matheson and were used without further purification.

The data were taken on a Consolidated Engineering Corp. mass spectrometer, Model 21–401, which had been modified as described previously.[8] Table I gives the spectra (in terms of percentage yields of the various ions) of several fluoroethylenes. These were obtained with 75-v. electrons, 10-μa. current, and an accelerating voltage of 210 v. The values are rounded off to the nearest 0.1%, and peaks below this value are usually omitted. Doubly charged ions are not included. The agreement with previously published results on C_2H_4, CH_2CF_2, and C_2F_4 is good, except for a frequent smaller degree of decomposition than observed by other workers. This is especially apparent for C_2F_4, where $C_2F_3^+$ is the highest peak in the present spectrum,

TABLE I

MASS SPECTRA OF FLUOROETHYLENES

Species	CH_2CH_2	CH_2CHF	CH_2CF_2	$CHFCF_2$	CF_2CF_2
CH_2^+	0.9	0.6	2.6		
CH_3^+	0.1	0.2			
C_2H^+	4.1	1.8			
$C_2H_2^+$	24.7	9.9	1.1		
$C_2H_3^+$	26.8	11.4			
$C_2H_4^+$	41.3$_p$				
CF^+		2.8	13.1	15.2	28.6
CFH^+		0.9		5.7	
CFH_2^+		0.1	12.4		
C_2FH^+		10.4	9.2	1.8	
$C_2FH_2^+$		24.9	16.7		
$C_2FH_3^+$		34.5$_p$			
CF_2^+			0.9	1.7	10.6
CF_2H^+			0.3	16.0	
$C_2F_2^+$				1.0	0.3
$C_2F_2H^+$			4.8	29.7	
$C_2F_2H_2^+$			35.4$_p$		
CF_3^+					1.3
$C_2F_3^+$				0.4	37.3
$C_2F_3H^+$				26.2$_p$	
$C_2F_4^+$					20.4$_p$

(1) This work was supported by the Advanced Research Projects Agency through the Materials Science Center.

(2) Department of Chemistry, Hebrew University of Jerusalem, Israel.

(3) J. R. Majer, "Advances in Fluorine Chemistry," Vol. 2, M. Stacey, J. C. Tatlow, and A. G. Sharpe, Ed., Academic Press, New York, N. Y., pp. 55–103.

(4) F. L. Mohler, V. H. Dibeler, and R. M. Reese, *J. Res. Natl. Bur. Std.*, **49**, 343 (1952).

(5) H. M. Rosenstock, N. B. Wallenstein, A. L. Wahrhaftig, and H. Eyring, *Proc. Natl. Acad. Sci. U.S.*, **38**, 637 (1952).

(6) L. Friedman, F. A. Long, and M. Wolfsberg, *J. Chem. Phys.*, **30**, 1605 (1959).

(7) M. Wolfsberg, *ibid.*, **36**, 1072 (1962).

(8) A. B. King and F. A. Long, *ibid.*, **29**, 374 (1958).

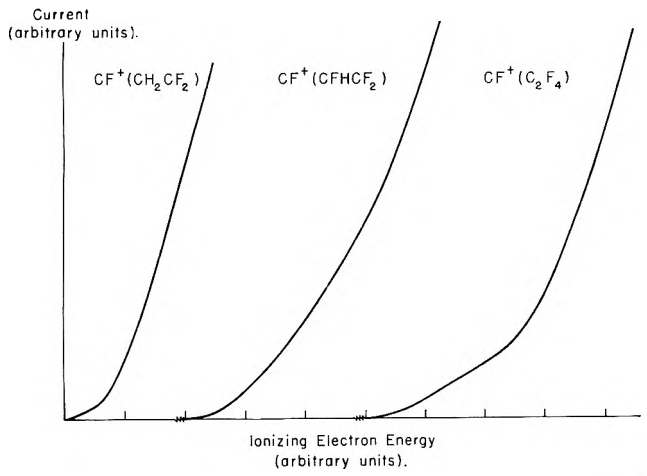

Fig. 1.—Ionization efficiency curves of CF^+ from three fluorinated ethylenes.

whereas CF^+ is the highest in the spectrum of Dibeler and coworkers.[4]

Appearance potentials were determined by the vanishing current method, using argon or neon as calibrating gas, in the same way as has been discussed previously.[8,9] Table II summarizes the appearance potentials for the main peaks of the fluoroethylenes. The values are averages of from three to five runs for each species. The standard deviations are in the order of from 0.05 to 0.1 e.v. for the more abundant ions.

TABLE II

APPEARANCE POTENTIALS FOR FLUOROETHYLENES IN VOLTS

Species	CH_2CH_2	CH_2CHF	CH_2CF_2	$CHFCF_2$	CF_2CF_2
CH_2^+	19.0		17.8		
$C_2H_2^+$	13.2	13.73	19.78		
$C_2H_3^+$	14.06	14.38			
$C_2H_4^+$	10.66				
CF^+		15.43	15.23	15.2	14.06
CFH^+				15.38	
CFH_2^+			15.08		
C_2FH^+		14.04	14.44	20.0	
$C_2FH_2^+$		14.02	14.80		
$C_2FH_3^+$		10.45			
CF_2^+				19.28	15.13
CF_2H^+				14.22	
$C_2F_2^+$				14.83	
$C_2F_2H^+$			16.67	16.13	
$C_2F_2H_2^+$			10.45		
CF_3^+					13.54
$C_2F_3^+$					16.00
$C_2F_3H^+$				10.33	
$C_2F_4^+$					10.12

Values for some of the ionization potentials and appearance potentials given in Table II have been reported previously. Table III gives a comparison of the earlier results with the present ones; agreement is quite good. The present electron impact ionization potentials are all 0.1–0.2 v. higher than the photoionization values, except for C_2F_4 where the photoionization and the electron impact values are the same. A similar behavior has been observed for partially fluorinated benzenes.[3]

The semilog slope matching technique[10,11] for determining appearance potentials was tried on several of the ions and the values obtained by this method usually agreed very well with those given in Table II. However, it was not possible to match the semilog curves of CF^+ from either C_2F_4 or $CHFCF_2$ nor that of CF_3^+ from C_2F_4 with the respective calibrating Ar^+ curves. Ionization efficiency curves for CF^+ from different olefins are shown in Fig. 1. These were drawn so that the slopes of the linear parts are equal in all three cases. The CF^+ curve from CH_2CF_2 illustrates the expected behavior, the CF^+ curve from C_2F_4 shows a break, while the CF^+ curve from $CFHCF_2$ shows a long tail.

(9) R. R. Bernecker and F. A. Long, *J. Phys. Chem.*, **65**, 1565 (1961).
(10) R. E. Honig, *J. Chem. Phys.*, **16**, 105 (1948).
(11) S. N. Foner and R. L. Hudson, *ibid.*, **25**, 602 (1956).

TABLE III

IONIZATIONS POTENTIAL OF MOLECLUES

Molecule	IP, e.v.	Method	Ref.
C_2H_4	10.51	Spectroscopy	*a*
C_2H_4	10.58	Electron impact	*b*
C_2H_4	10.66	Electron impact	*c*
CH_2CHF	10.36	Photoionization	*d*
CH_2CHF	10.31	Photoionization	*e*
CH_2CHF	10.45	Electron impact	*c*
CH_2CF_2	10.33	Photoionization	*d*
CH_2CF_2	10.30	Photoionization	*e*
CH_2CF_2	10.45	Electron impact	*c*
$CHFCF_2$	10.14	Photoionization	*e*
$CHFCF_2$	10.33	Electron impact	*c*
C_2F_4	10.12	Photoionization	*e*
C_2F_4	9.3	Electron impact	*f*
C_2F_4	10.12	Electron impact	*c*

APPEARANCE POTENTIALS OF FRAGMENTS

Ion	Parent molecule	Present AP, e.v.	Previous AP, e.v.	Ref.
CH_2^+	C_2H_4	19.0	19.3	*g*
$C_2H_2^+$	C_2H_4	13.2	13.5	*g*
C_2H_3	C_2H_4	14.06	14.06	*g*
CF_2^+	C_2F_4	15.13	15.2	*f*

[a] W. C. Price and W. T. Tutte, *Proc. Roy. Soc.* (London), **A174**, 207 (1940). [b] See ref. 9. [c] Present study; results from Table II. [d] F. M. Matsunaga and K. Watanabe, private communication. [e] See ref. 13. [f] J. L. Margrave, *J. Chem. Phys.*, **31**, 1432 (1959). [g] See ref. 20.

The appearance potentials of the ions showing "abnormal" ionization efficiency curves, namely CF^+, $CF_3^+(C_2F_4)$, and $CF^+(CHFCF_2)$ were determined in the following way: the pressure of the gas studied and that of the argon were matched so that the *first* parts of the ionization efficiency curves for the ion and for Ar^+ coincided (contrary to the usual procedure of matching the linear parts[8]). The values thus obtained are the ones given in Table II. Appearance potentials for these CF^+ and CF_3^+ ions are uncertain to a greater extent than is shown by the experimental spread because of the abnormal shapes of the ionization efficiency curves.

A 60° sector mass spectrometer was used to look for negative ions in the C_2F_4 spectrum. The only detected species was F^-. The ionization efficiency curve of F^- indicated that an ion-pair process was occurring with an appearance potential of 14 ± 1 e.v., where the energy scale was calibrated by means of O^- from the ion-pair process in CO. Independent experiments on the negative ions from C_2F_4 were carried out by Morrison and Dorman,[12] who have verified the occurrence of an ion-pair process forming F^-, the observed appearance potential being 14.3 e.v. They also observed three resonance capture processes forming F^- at 2.7, 5.8, and 11.2 e.v. Two other negative ions were reported by them, F_2^- and C_2F^-, both in very small yield.

Mass spectral patterns of C_2F_4 and $CHFCF_2$ were determined at low electron voltages as a function of the ionizing voltage (Fig. 2 and 3). In Fig. 2 ($V_e - I^z$) is the ionizing voltage minus the ionization potential of the parent; in the case of $CHFCF_2$ the ionizing voltage was not calibrated. The ionization efficiency curves obtained for the fluoroolefins may be classified according to three types as previously explained.[8] The parent ions (not shown in Fig. 2 and 3) all belong to the type I curve, CF_3^+ (from C_2F_4) and CF_2H^+ (from $CFHCF_2$) belong to type II, while all the other fragments give type III behavior.

Discussion

The 75-v. Spectra.—As one goes from ethylene to perfluoroethylene (Table I), successively substituting the hydrogens by fluorines, the general features are: a gradual decrease in yields of acetylene ions ($C_2H_2^+$, C_2HF^+, or $C_2F_2^+$); an increase in the yields of the rearrangement products CH_3^+, CH_2F^+, and CF_3^+; an

(12) Personal communication from J. D. Morrison.

increase in the yield of CF^+. The compounds CH_2CF_2 and $CHFCF_2$ show low yields of the ion of the parent-minus-one-hydrogen-atom; a similar behavior has been observed in $C_6F_4H_2$ and C_6F_5H.[3] There is also a gradual decrease in parent ion yield with increase in fluorine content and an increase in the yields of methylene ions, *e.g.*, CH_2^+, CHF^+, and CF_2^+.

Ionization and Appearance Potentials.—The ionization potentials of the ethylenes decrease upon successive fluorination (Tables II and III). This has previously been explained[13] as being the resultant of two opposing effects of the fluorine atom—an inductive effect which tends to increase the ionization potential of the molecule and a slightly larger resonance effect which stabilizes the molecular ion and thus tends to decrease the ionization potential. If this explanation for the trend in ionization potentials is correct then the structure of the molecule-ion in its ground state is planar with some double-bond character in the C–C bond.

The ionization potentials measured by photoionization are the *adiabatic* ionization potentials, while the ones measured by electron impact need not be and may more nearly reflect vertical "Franck–Condon" ionizations. The ionization potential of C_2F_4 is the same according to either photoionization or the present electron impact measurement (Table III), which suggests that the spatial configurations of the C_2F_4 molecule and molecule-ion are the same at the minima of their potential curves. Usually electron impact measurements of ionization potentials give slightly higher values than photoionization and this is the case for the other members of the ethylene series.

The ions of lowest appearance potentials for the hydrogenated end of the ethylene series (Table II) are the acetylene ions, formed from the parent by the split-off of H_2 or HF. For the more fluorinated members, the rearrangement ions CF_2H^+, CF_3^+, as well as CF^+ lead to the lowest appearance potentials. The energy demand for the production of the CX_2^+ ions (CH_2^+, CHF^+, and CF_2^+) decreases with fluorine content. On the other hand, the energy which is needed for the production of parent-minus-one species increases with fluorine content; this again is similar to the trend observed for fluorobenzenes.[3] The next section illustrates these features further.

Mechanisms for Production of Mass Spectra of Fluoroethylenes.—The proposed mechanisms for the breakdown of the ethylenes are based solely on energetic considerations. No metastable transitions have been observed and for these molecules isotopic labeling cannot add any further information.

The acetylene ions $C_2X_2^+$, where X is either H or F, usually have lower appearance potentials than the parent-minus-one ions, so that they must be formed by a direct H_2 or HF split from the parent. The ions CX_3^+ have also lower appearance potentials than the parent-minus-one ions, so that they too appear to be formed by a direct rearrangement from the parent, a proposal which is confirmed by the low energy patterns (Fig. 2 and 3). The choice between a single-step and a two-step mechanism for the formation of CX^+ or CX_2^+ from the parent ion is based on similar considerations, supplemented by comparisons with available thermochemi-

(13) R. Bralsford, P. V. Harris, and W. C. Price, *Proc. Roy. Soc.* (London), **A258**, 459 (1960).

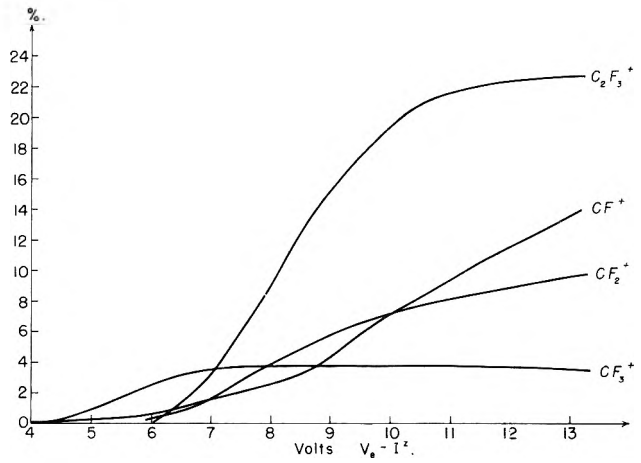

Fig. 2.—Dependence of fragment-ion yields on ionizing electron energy in C_2F_4.

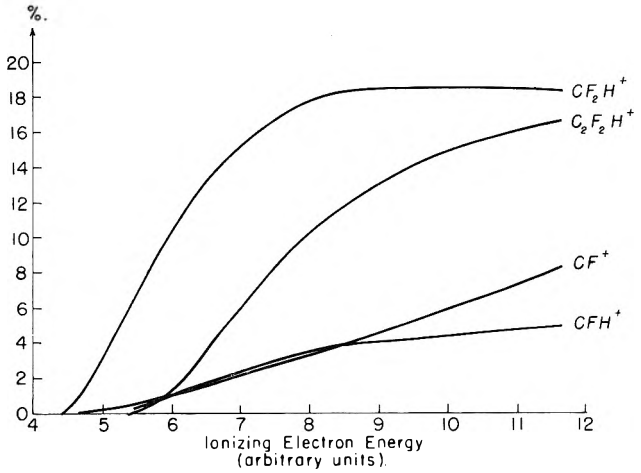

Fig. 3.—Dependence of fragment-ion yields on ionizing electron energy in $CHFCF_2$.

cal data on the fragments. Table IV summarizes some thermochemical calculations for processes which may lead to the observed CX_2^+ and other ions; the results are compared with the experimental energies. A few calculations are included for fragments which are actually absent from the spectrum. For instance, CH_3^+ (C_2H_4) comprises only 0.1% of the spectrum at 75 v. and its appearance potential could not be measured, although it can be calculated. The calculation is of interest for comparison since with the highly fluorinated ethylenes there is abundant rearrangement to form CX_3^+ ions.

The heats of formation of hydrocarbons and their positive ions, used in the calculations of Table IV, are from a recent compilation.[9] The heats of formation of C_2F_4,[14] CH_2CF_2,[14] $CHFCH_2$,[15] $CFHCF_2$,[15] CF,[16] and CF_2[17] are from the recent literature. Other heats of formation come from the compilation of Rossini, *et al.*[18] The recently measured IP (CH_2) = 10.39[19] was utilized for calculations involving the CH_2 radical.

(14) C. A. Neugebauer and J. L. Margrave, *J. Phys. Chem.*, **60**, 1318 (1956).

(15) P. G. Maslov and Yo P. Maslov, *Khim. i Tekhnol. Topliva i Masel*, **3**, 50 (1958); *Chem. Abstr.*, **53**, 1910 (1959).

(16) E. B. Andrews and R. F. Barrow, *Nature*, **165**, 890 (1950); *Proc. Roy. Soc.* (London), **A64**, 681 (1951).

(17) L. Brewer, J. L. Margrave, R. F. Porter, and K. Wieland, *J. Phys. Chem.*, **65**, 1913 (1961).

(18) F. D. Rossini, D. D. Wagman, W. H. Evans, W. H. Levine, and I. Jaffe, Natl. Bur. Std. Circ. No. 500, U. S. Govt. Printing Office, Washington, D. C., 1952.

(19) G. Herzberg, *Can. J. Phys.*, **39**, 1511 (1961).

TABLE IV

	Process	Thermochemical cycle	Calcd., AP, e.v.	Obsd. AP, e.v.
1.	$C_2H_4 \rightarrow C_2H_2^+ + H_2$	$C_2H_4 \rightarrow C_2H_2 + H_2 \rightarrow C_2H_2^+ + H_2$	13.21	13.2
2.	$C_2H_4 \rightarrow CH_2^+ + CH_2$	$C_2H_4 \rightarrow 2CH_3 - 2H \rightarrow 2CH_2^+ \rightarrow CH_2^+ + CH_2$	16.36	19.0
3.	$C_2H_3 \rightarrow CH_2^+ + CH + H$	$C_2H_3 \rightarrow CH_2^+ + CH + H$	22.28	19.0
4.	$C_2H_4 \rightarrow CH_3^+ + CH$	$C_2H_4 \rightarrow CH_3 + CH \rightarrow CH_3^+ + CH$	16.85	..
5.	$CH_2CHF \rightarrow C_2H_2^+ + HF$	$CH_2CHF \rightarrow C_2H_2 + HF \rightarrow C_2H_2^+ + HF$	12.19	13.73
6.	$CH_2CHF \rightarrow C_2H_2^+ + H + F$	$CH_2CHF \rightarrow C_2H_2 + H + F \rightarrow C_2H_2^+ + H + F$	18.05	13.73
7.	$CH_2CHF \rightarrow C_2H_3^+ + F$	$CH_2CHF \rightarrow C_2H_4 - H + F \rightarrow^a C_2H_3^+ + F$	14.38	14.38
8.	$CH_2CHF \rightarrow CH_2F^+ + CH$	$CH_2CHF \rightarrow CH_2CF_2 + H - F \rightarrow^a CH_2F^+ + CF + H - F \rightarrow CH_2F^+ + CH$	15.87	..
9.	$CH_2CF_2 \rightarrow CH_2^+ + CF_2$	$CH_2CF_2 \rightarrow CH_2^+ + CF_2$	16.3	17.8
10.	$CH_2CF_2 \rightarrow CH_2^+ + CF + F$	$CH_2CF_2 \rightarrow CH_2^+ + CF + F$	21.81	17.8
11.	$CH_2CF_2 \rightarrow CH + CHF_2^+$	$CH_2CF_2 \rightarrow CHFCF_2 + H - F \rightarrow^a CHF_2^+ + CF + H - F \rightarrow^a CHF_2^+ + CH$	15.69	..
12.	$CHFCF_2 \rightarrow CH + CF_3^+$	$CHFCF_2 \rightarrow C_2F_4 + H - F \rightarrow^a CF_3^+ + CF + H - F \rightarrow^a CF_3^+ + CH$	14.88	..
13.	$CHFCF_2 \rightarrow C_2F_3^+ + H$	$CHFCF_2 \rightarrow C_2F_4 + H - F \rightarrow^a C_2F_3^+ + H$	15.67	..

[a] The energy changes involved in these transitions are from Table II.

C_2H_4.—The two principal decomposition products, $C_2H_2^+$ and $C_2H_3^+$, are attributed to direct decompositions (Fig. 4), as suggested previously.[20] The observed appearance potential for $C_2H_2^+$ is in excellent agreement with the calculated value for a direct four-center process. Almost no CH_3^+ is observed and this is consistent with a high calculated appearance potential for its formation (Table IV). The yield of CH_2^+ is small, and the observed appearance potential suggests that it results from a direct decomposition (Table IV), but the agreement between observed and calculated is not good. The formation of CH_2^+ with excess kinetic energy is not likely to be the reason for the observed discrepancy, since the major component of this peak was observed to be "a normal one" with small kinetic energy.[20b] The yield of $C_2H_2^+$ is lower than that of $C_2H_3^+$ even though the energy requirement is less; this is qualitatively in agreement with statistical theory in that the four-center elimination process implies a rigid transition state which should in turn lead to a small frequency factor for the process.

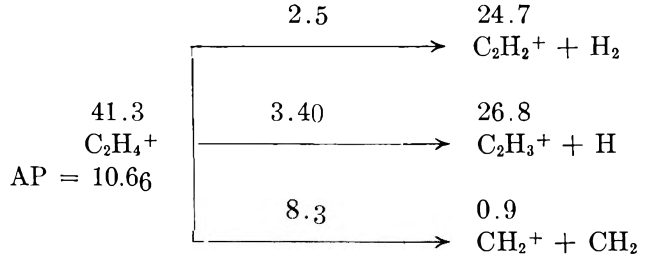

Fig. 4.—Proposed mechanism for origin of C_2H_4 spectrum. The numbers over the arrows are derived from the appearance potentials and give the activation energy in volts for going from reactant ion to products. The numbers over the ion formulas give the observed per cent yields from Table I.

CH_2CHF.—Five direct decomposition processes are proposed for this species (Fig. 5). Four-center elimination reactions are involved in the production of the acetylene ions, $C_2H_2^+$ and C_2HF^+, while rearrangement is probably involved in the production of CF^+. The formation of $C_2H_2^+$ along with the neutral species HF involves about 1.5 v. excess activation energy, in striking contrast to the minimum energy requirements for the production of the same ion from $C_2H_4^+$. Since a similar need for excess energy enters in the splitting of HCl from $C_2H_3Cl^+$ to give $C_2H_2^+$, it appears that the introduction of a halogen atom substantially modifies the character of the activated complex. Further indication of some unusual features of the transition states comes from the observation that production of C_2HF^+ slightly exceeds that of $C_2H_2^+$ even though the energy requirement for the former is 0.3 v. higher. It is conceivable that the production of $C_2H_2^+$ involves formation of F^- ion and indeed the energy requirement for formation from CH_2CHF of $C_2H_2^+ + H + F^-$ is very close to the observed appearance potential but there are difficulties. The process cannot go by initial decomposition to $C_2H_3^+ + F^-$ since this would give a much lower appearance potential for $C_2H_3^+$ than is observed. The other alternative is simultaneous formation of the three products, a most unusual sort of reaction.

Formation of CF^+ must involve a rearrangement with simultaneous production of CH_3 at least at the threshold, since a two-step process for its production necessarily requires improbably low values for the heat of formation of CF^+, much lower than reported by previous workers.[21,22]

The simple bond rupture processes whereby CH_2CHF^+ loses either an H or an F atom give relatively larger amounts of decomposition in terms of the energy requirements than do the rearrangement or four center processes. This is the expected result; so is the fact that production of the lower energy species $C_2H_2F^+$ is larger than that of $C_2H_3^+$. However, this last result does indicate that the frequency factors for breaking C–H and C–F bonds in CH_2CHF^+ are rather similar, a somewhat unexpected result in view of the anomalously low factor for breaking C–H bonds in saturated hydrocarbon ions.

CH_2CF_2.—Neutral radicals are assumed to be formed along with the positive ions, since no negative ions were observed for CH_2CF_2.[23] For this species, yields from four-center processes to give acetylenic ions are diminished relative to the more hydrogenated olefins (Fig. 6). So also are yields of simple decompositions to give parent-minus-one species, *e.g.*, $C_2H_2F^+$ and $C_2HF_2^+$. Rearrangements to give CH_2F^+ plus CF and to give CF^+ plus CH_2F are, however, much more probable, evidently due to lower energy demands. Further-

(20) (a) F. W. Field and J. L. Franklin, "Electron Impact Phenomena," Academic Press, New York, N. Y., 1957, pp. 249, 252 (best values); (b) P. Kusch, A. Hustrulid, and J. T. Tate, *Phys. Rev.*, **52**, 843 (1937).

(21) R. I. Reed and W. Snedden, *Trans. Faraday Soc.*, **54**, 301 (1958).

(22) J. W. C. Johns and R. F. Barrow, *Proc. Roy. Soc.*, (London), **A71**, 476 (1958).

(23) R. M. Reese, V. H. Dibeler, and F. L. Mohler, *J. Res. Natl. Bur. Std.*, **51**, 367 (1956).

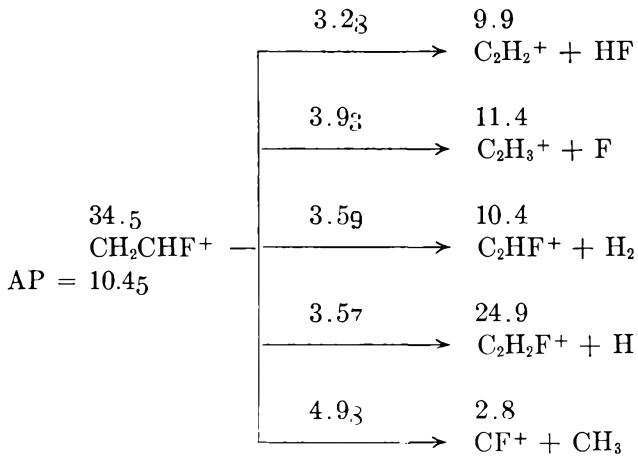

Fig. 5.—Mechanism for CH_2CHF spectrum.

more, the yields from the rearrangement processes which give CH_2F^+ and CF^+ are both higher than for that to give C_2HF^+ plus HF even though the energy requirement is smaller for this last process. This can be reconciled with statistical theory if one makes the plausible assumption that the transition state $H_2C{-}CF$ (with F) is less rigid than the one which leads to loss of the species HF. Qualitatively, the yields of the other principal products are also consistent with expectation from theory if one assumes that at high energies considerable CF^+ is produced by secondary processes. This is possible but does not appear very likely. Rearrangement to give CHF_2^+ plus CH apparently fails to occur because of a high energy requirement (Table IV).

As Table IV shows, formation of CH_2^+ must, at least near its threshold, be a primary product. However, the observed appearance potential indicates that considerable excess energy is involved, just as was found for production of CH_2^+ from C_2H_4. In both cases, the thermochemically calculated activation energy is close to 6 v. and it is possible that decomposition processes with such high energy requirements will not occur at sufficient rates to give measurable yields in a conventional mass spectrometer, for energies near the threshold.[7] Detailed calculations are now in progress to investigate this point and to see what amount of excess energy may be needed to produce measurable decomposition.

$CHFCF_2$.—By far the most probable process for decomposition of $CHFCF_2^+$ is loss of an F atom to give $C_2F_2H^+$ (Fig. 7). This occurs in large yield even though the energy requirement is 5.8 v., the largest observed for any of the primary processes. It is at least partly understandable that the products CF_2H^+, CF^+, and $C_2F_2^+$ are formed in lower yields since they all result from rearrangement or four-center processes. The energy terms favoring the rearrangements are, however, rather large, almost 2 v. for the case of CF_2H^+. Furthermore CF^+ is produced in virtually the same yield as is CF_2H^+ even though the threshold energy to form CF^+ is 1 v. higher. This apparent discrepancy can perhaps be explained by assuming that at higher energies most of the CF^+ actually results from a secondary decomposition. The observed shapes of the ionization efficiency curves are consistent with this. At the lowest energies CF_2H^+ is actually produced in larger yield than is CF^+. Furthermore the ionization

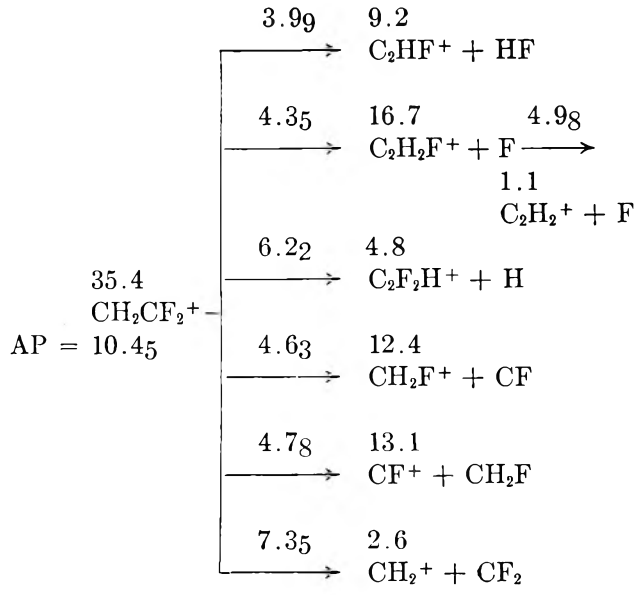

Fig. 6.—Mechanism for CH_2CF_2 spectrum.

curve for CF^+ has an abnormally long "tail" (Fig. 1) suggesting the contribution of more than one process, the higher energy one probably being $C_2F_2H^+ \rightarrow CF^+ + CFH$.

It is more difficult to understand the low yield of CFH^+ since this apparently involves only a simple C–C bond break and, at least for hydrocarbons, such breaks do not usually involve abnormally low frequency factors.

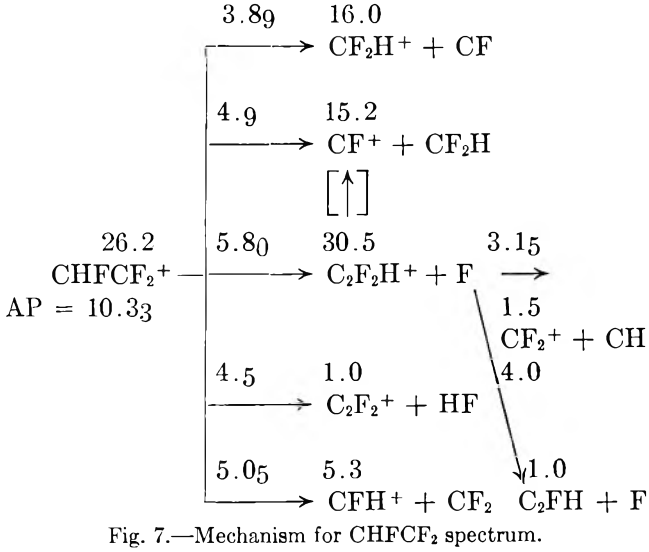

Fig. 7.—Mechanism for $CHFCF_2$ spectrum.

Yields of acetylenic ions are low from $CHFCF_2$ and only $C_2F_2^+$, at 1% yield, appears to result from a primary process. The lack of primary production of C_2FH^+ in this case (as well as of $C_2F_2^+$ from C_2F_4), can, however, be explained as due to the small energy gain which results from formation of F_2. The relevant bond energies are: $D(F_2) = 1.64$; $D(HF) = 5.8$; $D(H_2) = 4.52$ e.v.

A point of considerable interest is the lack of formation of $C_2F_3^+$. Using a heat of formation for this species obtained from its appearance potential in C_2F_4, one calculates (Table IV, no. 13) for its production from $CHFCF_2^+$ an activation energy of 5.3, *i.e.*, lower than that for the high yield species $C_2F_2H^+$. The absence of $C_2F_3^+$ cannot easily be rationalized by invoking fre-

quency factors, since, for decompositions of $CH_2CF_2^+$ and CH_2CHF^+, the intrinsic probabilities of H and F loss appear to be about equal, *i.e.*, there are no obvious differences in frequency factors. It is, of course, possible that the assumed heat of formation of $C_2F_3^+$ is wrong. Wolfsberg's recent calculations[7] suggest that for a molecule of 12 oscillators such as ethylene processes with true thermochemical activation energies of up to 4 v. will still occur normally in a mass spectrometer and hence give appearance potentials in agreement with theory.[7] However, for processes with energy requirements as large as 6 v., observation in a mass spectrometer may require the presence of excess energy in the parent species so that appearance potentials would not reflect the thermochemistry. For the present studies this suggests that the appearance potentials for $C_2F_2H^+$ from CH_2CF_2 and $CHFCF_2$, and also for $C_2F_3^+$ from C_2F_4, may be considerably higher than thermochemically required. This point merits further study both for these cases and for the previously mentioned case of CH_2^+ from C_2H_4 and CH_2CF_2.

C_2F_4.—The spectrum for this species results from a simple C–F bond split, a C–C double bond break, and two rearrangement processes leading to the species CF^+ and CF_3^+ (Fig. 8). No acetylenic ion product is observed. Production of $C_2F_3^+$ is the process of highest yield even though the required activation energy is also the largest observed. As usual, the low yields for the rearrangement processes can formally be explained as due to the requirement of a more rigid cyclic transition state for this formation. However, this explanation will not do for the low yield of CF_2^+ which requires only a simple bond split and whose yield therefore remains anomalously low.

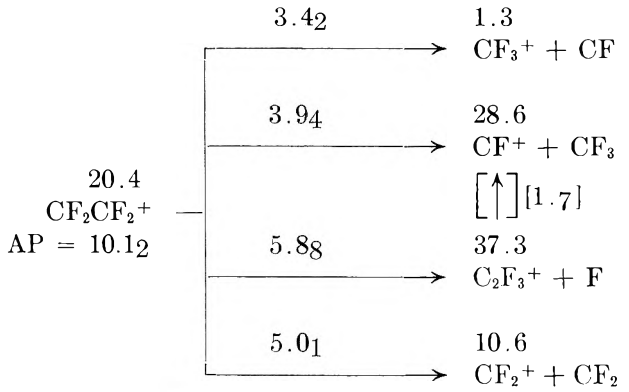

Fig. 8.—Mechanism for CF_2CF_2 spectrum.

There is an apparent anomaly for the rearrangements in that CF_3^+, which is formed at a lower threshold energy, is found at 70 v. in much lower yield than CF^+. However, the latter can also be formed by a secondary decomposition of $C_2F_3^+$, and at low energies CF_3^+ is indeed formed in higher yield than is CF^+. The ionization efficiency curves for the ions from C_2F_4 are decidedly unusual and have been discussed in detail in another publication.[24] However, the curve for CF^+ is consistent with a large secondary production of this species from $C_2F_3^+$.

A less likely but conceivable interpretation is that there is an ion-pair process involved in the low energy formation of CF^+.

$$C_2F_4 \longrightarrow CF^+ + CF_2 + F^-$$

This is consistent with the appearance of F^- ions at about 14 v. The higher yield production of CF^+, in this view, could perhaps be due to the process

$$C_2F_4 \longrightarrow CF^+ + CF_2 + F$$

In addition to problems with the rearrangement processes, the anomalous yields of $C_2F_3^+$ and CF_2^+ suggest that simple statistical theory may not be adequate to explain their yields. If the appearance potential for $C_2F_3^+$ formation is found to be in accord with thermochemistry, its formation at the thermochemical threshold will probably have to be explained by decomposition from an excited state of the parent ion which does not cross the lower electronic state. In view of the fact that we are dealing with a relatively small molecule, in which the spacing between the various electronic levels is quite large, this may very well be the case; calculations on this point are in progress.

Summary Remarks.—The over-all trends in going from the fully hydrogenated ethylene to the perfluoroolefins seem reasonable and at least roughly consistent with the changes in stabilities of the various product types. None of the results leads to inescapable contradictions with the statistical theory for mass spectra. Thus for similar energy requirements, rearrangement and four-center products usually have lower yields than do simple rupture processes, and for a given type of reaction, processes with lower energy requirements usually lead to higher yields. There are, however, a number of unusual results indicating that a more quantitative analysis may show disagreement between observation and prediction from simple theory. A point of particular interest is that several of the processes have such large energy requirements as to indicate that considerable excess energy may be needed to obtain decomposition rates high enough to give a measurable yield.

Acknowledgments.—We wish to thank Drs. J. D. Morrison, F. H. Dorman, and V. H. Dibeler for valuable discussions and for measurements of appearance potentials of negative ions from C_2F_4.

(24) C. Lifshitz and F. A. Long, submitted for publication.

SOLVENT EFFECTS ON THE MEASUREMENT OF CHEMICAL SHIFTS IN NUCLEAR MAGNETIC RESONANCE SPECTRA

BY N. LUMBROSO, T. K. WU, AND B. P. DAILEY

Department of Chemistry, Columbia University, New York 27, New York

Received June 13, 1963

Experimental studies of the van der Waals shift of nonpolar gases and the polar shifts of polar molecules have been carried out. The observed values for the former are compared with the calculated values obtained from the theoretical model proposed by Howard, Linder, and Emerson, and those of the latter with the results from Buckingham's reaction field theory. In both cases, the experimental values of the solvent shifts are greater than the theoretical ones. However, the theories account roughly for the observed trend. In general, some solvents may introduce an error as great as 30% in the measurement of internal chemical shift, but with nonpolar solvents and proper theoretical treatment, the solvent errors may be greatly reduced.

I. Introduction

In order to make a valid theoretical interpretation of the nuclear magnetic resonance spectra of a series of molecules, it is necessary that the observed or corrected chemical shifts be those characteristic of the isolated molecules. Ideally, this means that all such measurements should be made using infinitely dilute gas samples. Unfortunately, it has proved possible so far to obtain gas phase chemical shift data for only a limited number of compounds.

Buckingham, Schaefer, and Schneider[1] made a careful theoretical and experimental study of solvent shifts for the simple solutes CH_4 and CH_3CN. For more complicated molecules, it has been suggested that solvent effects can be eliminated by extrapolating to infinite dilution in a suitable solvent[2] (there has been some disagreement as to which solvent is most suitable) or that valid relative chemical shifts can be obtained by taking the difference of comparable resonances measured within the same molecule[3] as, for example, in ethyl derivatives by taking the difference between the methyl and methylene chemical shifts. The theoretical results obtained by Buckingham seem to indicate that significant solvent effects persist at infinite dilution in all solvents and that in some cases these may be different for different positions in the molecule.

In this investigation, measurements of the chemical shifts of some ethyl derivatives have been carried out in a series of polar and nonpolar solvents (see Table I). The solutes were polar and nonpolar molecules chosen to avoid any instances of known specific association with the solvents. Gas phase chemical shift data were available for most of these solutes from the work of Spiesecke and Schneider.[4] Gas phase and solvent studies were made of several nonpolar solutes to gain further light on van der Waals chemical shifts.

II. Theory

The contribution to the molecular screening constant due to the solvent, $\sigma_{solvent}$, is equal to the observed screening constant σ minus the screening constant for the isolated molecule σ_{gas}. The contributions to $\sigma_{solvent}$ which are specifically evaluated in this study are

$$\sigma_{solvent} = \sigma_b + \sigma_w + \sigma_E \quad (1)$$

where σ_b is the bulk susceptibility shift, σ_w is the van der Waals shift, and σ_E is the polar effect first discussed by Buckingham. No evidence was obtained for the presence of a term due to the magnetic anisotropy of the solvent, although such an effect might become large for certain solvents.

All of the observed chemical shifts were corrected for bulk susceptibility shifts using the expression

$$\sigma_{solvent}\,(cor.) = \sigma_w + \sigma_E = \sigma_{solvent}\,(obsd.) + \frac{2\pi}{3}(\Delta\chi_v) \quad (2)$$

where $\Delta\chi_v$ is the difference in χ_v, the volume magnetic susceptibility, of the solvent and the benzene reference. The values of χ_v were taken from Smith.[5] Because of the substantial experimental uncertainty in some of these values, the individual corrected solvent shifts may reflect a corresponding uncertainty of the order of ± 2 c.p.s.

The van der Waals shift should be made up of terms due both to long range and short range interactions. The long-range term, according to Raynes, Buckingham, and Bernstein,[6] should be proportional to

$$\sigma_w = -B\bar{F}^2 \quad (3)$$

with

$$\bar{F}^2 = \frac{3\alpha_2 I_2}{r^6}$$

where I_2 is the ionization potential of the solvent and α_2 is its static polarizability. The short range terms would be of opposite sign. The distance r above, between the perturbing solvent molecule and the proton, is somewhat difficult to define and measure precisely.

The theoretical treatment of Raynes, Buckingham, and Bernstein is basically a semiempirical statistical method. It considers the two-body interactions only: the Lennard-Jones (6–12) and the Stockmayer intermolecular potentials are used for the calculations of the average contributions to chemical shift of van der Waals and electric field effects, respectively. This method has been applied successfully in the cases of gases and gaseous solutions. Unfortunately, the systems under investigation here are either gases in liquid solvents or liquid solutions to which their method can no longer be easily applied. The calculations of Howard,

(1) A. D. Buckingham, T. Schaefer, and W. G. Schneider, *J. Chem. Phys.*, **32**, 1227 (1960).
(2) A. A. Bothner-By and R. E. Glick, *ibid.*, **26**, 1651 (1957).
(3) J. R. Cavanaugh and B. P. Dailey, *ibid.*, **34**, 1099 (1961).
(4) H. Spiesecke and W. G. Schneider *ibid.*, **35**, 722 (1961).
(5) G. W. Smith, "Compilation of Diamagnetic Susceptibilities of Organic Compounds," GMR-317, General Motors Corp., Detroit, Mich.
(6) W. T. Raynes, A. D. Buckingham, and H. J. Bernstein, *J. Chem. Phys.*, **36**, 3181 (1962).

TABLE I

CHEMICAL SHIFTS FROM GAS TO SOLVENT, C.P.S. (P.P.M.)

	Cyclohexane		Dioxane		CCl_4		Acetone		Nitromethane	
	CH_3	CH_2	CH_3	CH_2	CH_3	CH_2	CH_3	CH_2	CH_3	CH_2
Methane	−14.2 (−0.237)		−21.3 (−0.355)		−24.2 (−0.403)		−10.4 (−0.173)		−12.2 (−0.203)	
Ethane	−10.4 (−0.173)		−13.7 (−0.228)		−18.6 (−0.310)		−6.4 (−0.107)		−8.0 (−0.133)	
Ethylene	−12.1 (−0.202)		−20.5 (−0.346)		−22.3 (−0.372)		−13.6 (−0.227)		−16.1 (−0.268)	
Cyclopropane	−13.9 (−0.232)		−18.9 (−0.315)		−22.8 (−0.380)		−12.7 (−0.212)		−14.7 (−0.245)	
TMS	−13.9 (−0.232)				−21.5 (−0.358)					
Neopentane	−11.7 (−0.195)				−17.5 (−0.292)					
CH_3CN	−17.7 (−0.295)		−31.0 (−0.517)		−36.3 (−0.605)		−31.1 (−0.518)		−30.0 (−0.500)	
CH_3CH_2Br	−11.8 (−0.197)	−12.7 (−0.212)	−17.4 (−0.290)	−26.3 (−0.438)	−23.5 (−0.392)	−25.3 (−0.422)	−11.6 (−0.193)	−23.6 (−0.392)	−14.0 (−0.233)	−25.0 (−0.417)
CH_3CH_2I	−9.6 (−0.160)	−8.9 (−0.148)	−17.8 (−0.297)	−23.1 (−0.385)	−22.8 (−0.380)	−20.9 (−0.348)	−16.4 (−0.273)	−23.9 (−0.398)	−15.6 (−0.260)	−23.8 (−0.397)
CH_3CH_2CN	−9.8 (−0.163)	−17.7 (−0.295)	−14.4 (−0.240)	−29.3 (−0.488)	−24.9 (−0.415)	−32.5 (−0.542)	−9.2 (−0.153)	−28.9 (−0.482)	−11.2 (−0.187)	−27.3 (−0.455)
$(CH_3CH_2)_2O$	−8.2 (−0.137)	−6.1 (−0.102)	−12.1 (−0.202)	−12.1 (−0.202)	−19.3 (−0.322)	−17.3 (−0.295)	+0.5 (+0.008)	+5.5 (+0.092)	−8.3 (−0.138)	−10.4 (−0.173)
$(CH_3CH_2)_3N$	−7.6 (−0.127)	−5.7 (−0.095)	−11.0 (−0.183)	−10.5 (−0.175)			−4.2 (−0.070)	−3.7 (−0.062)	−5.5 (−0.092)	−6.6 (−0.110)

Linder, and Emerson[7] relate the chemical shift to van der Waals dispersive forces derived from the free energy of interaction of an oscillating dipole with its surrounding medium. This model seems to approximate more closely our systems, and their equation is

$$\sigma_w = {}^3/_4\phi hg\left[\frac{\nu_1\nu_2}{\nu_1 + \nu_2}\right] \qquad (4)$$

where ϕ is a proportionality constant, h is Planck's constant, and

$$g = \frac{2n^2 - 2}{2n^2 + 1}\frac{1}{r^3}$$

with n being the refractive index of the solvent and r the radius of the solute sphere; ν is the mean absorption frequency and can be calculated from the relations

$$\nu = I/h \qquad (5)$$

where I is the ionization potential or from

$$\nu = -\left(\frac{4m_ec^2}{hN\alpha}\right)\chi_M \qquad (6)$$

where α is the polarizability and χ_M is the molar diamagnetic susceptibility; m_e is the mass of the electron and c is the velocity of light.

The polar chemical shift term σ_E arises from the action of an electric field E acting along the axis of the C–H bond to attract electrons from the proton. The resulting chemical shift is to lower field. Buckingham[1] obtained the equation

$$\sigma_E = -2 \times 10^{-12}E_z - 10^{-18}E^2 \qquad (7)$$

where E_z is the component of the field along the C–H bond. In the Buckingham–Onsager model, when a polar molecule is dissolved it polarizes the surrounding solvent molecules giving rise to an electric field, the reaction field R at the solute. The polar solvent shift σ_E may be approximately calculated from the relation

$$\sigma_E = -2 \times 10^{-12}\left[\frac{2(\epsilon - 1)(n^2 - 1)}{3(2\epsilon + n^2)}\right]\left(\frac{\mu \cos d}{\alpha}\right) - 10^{-18}\left[\frac{2(\epsilon - 1)(n^2 - 1)}{3(2\epsilon + n^2)}\right]^2\left(\frac{\mu^2}{\alpha^2}\right) \qquad (8)$$

where μ is the permanent dipole moment of the solute, α is the polarizability of the solute, which is

(7) B. B. Howard, B. Linder, and M. J. Emerson, *J. Chem. Phys.*, **36**, 485 (1962).

TABLE II

VALUES OF PARAMETERS USED IN THE CALCULATIONS OF CHEMICAL SHIFTS

	Refractive[a] index, $n^{25}D$	Ionization[b] potential, $I \times 10^{12}$, ergs	Molecular radius cubed, $r^3 \times 10^{24}$, cm.^{3}	Dipole moment,[c] μ, D.	Dielectric constant,[d] ϵ
Methane		20.80	15.1		
Ethane		18.56	21.8		
Ethylene		16.70	18.2		
Cyclopropane		16.39	23.2		
CH_3CN	1.33934	19.90	20.74	3.5	
CH_3CH_2Br	1.42196	16.48	29.58	2.01	
CH_3CH_2I	1.51052	14.95	31.96	1.87	
CH_3CH_2CN	1.36132	18.98	27.88	3.6	
$(CH_3CH_2)_2O$	1.34995	15.27	41.46	1.16	
$(CH_3CH_2)_3N$	1.40090	12.02	54.97	0.8	
Cyclohexane	1.42354	15.83			2.023
Dioxane	1.42025	15.25			2.208
CCl_4	1.45759	18.37			2.230
Acetone	1.35609	15.52			20.74
CH_3NO_2	1.37995	18.17			35.87

[a] J. Timmermans, "Physico-Chemical Constants of Pure Organic Compounds," Elsevier Publishing Co., Inc., New York, N. Y., 1955. [b] R. W. Kiser, "Table of Ionization Potentials," U. S. Atomic Energy Commission, Kansas State University, 1960. [c] L. G. Wesson, "Table of Electric Dipole Moments," The Technology Press, M.I.T., 1948. [d] H. H. Landott and R. Börnstein, "Zahlenwert und Funktionen," Springer-Verlag, Berlin, 1951, a Band, 6 Teil.

$$\left[\frac{(n^2-1)}{(n^2+2)}\right] r^3$$

r is the radius of solute sphere, n the refractive index of pure solute, ϵ the dielectric constant of solvent, and d the angle between $\vec{\mu}$ and the C–H bond.

The form of this equation usually used in calculations is actually a special case appropriate to a solute having a value of the refractive index equal to 1.5814. All of the solvents in this study had appreciably smaller values of n, which means that the values of σ_E calculated using the approximate equation would be somewhat too large. Values of the reaction field shift were calculated for each solvent–solute pair in this study using the parameters shown in Table II. The radius r of the solute sphere was evaluated as follows. Ignoring the detailed structure of the molecule, one can obtain r^3 from the relation

$$r^3 = \frac{3}{4\pi}\frac{M}{\rho N} \qquad (9)$$

where M is the molecular weight of the solute, ρ is the density of the solute, and N is Avogadro's number.

The models used for the calculations of the reaction field solvent shifts are the following. For the molecules of CH_3CH_2X type, the methylene protons make a constant angle with the molecular dipole moment which is assumed to be along the C–X bond. The average value of the cosine of the angle between the dipole moment and the methyl protons is evaluated with the assumption that the latter are freely rotating about the C–C bond. For the cases of diethyl ether and triethylamine, the sterically favorable configuration is chosen.

III. Experimental Results

The solutes chosen for this study were polar compounds for which gas phase chemical shift data were available. They were selected to have a range of dipole moments and of angles between the dipole moment and the C–H bond. The solvents were chosen to represent a range of values of $(\epsilon - 1)/(2\epsilon + 2.5)$. The measurements were made on Varian HR60 and A60 spectrometers, using benzene as an external reference, by the modulation side band method. The audio modulation frequency was counted directly using a Hewlett Packard Model 521A frequency counter equipped with a 10-kc. crystal-controlled time base and a 10-sec. gate. The accuracy of the measurements was ±0.2 c.p.s.

The samples were placed in 3-mm. i.d. cylindrical tubes containing a capillary filled with benzene and were sealed. The capillary was fixed so that it could not move inside the sample tube. The compounds were obtained from commercial sources and were redistilled. The solvents were of the purest commercial grade, and no further purification was carried out.

Measurements were made, for the most part, on the pure compound and on 15, 10, and 5% solutions (concentration by volume) in the different solvents and the results extrapolated to infinite dilution. In all cases the extrapolation line was linear within experimental accuracy. Results are given in Table III.

Studies were also made to six additional nonpolar molecules containing C–H bonds to investigate possible variations in the van der Waals shifts.

The effect of solvent on the chemical shift of various nonpolar gases was studied. Samples were prepared by condensing known volumes of the gas directly from the vacuum line into 3-mm. i.d. n.m.r. sample tubes which contained the solvent at liquid nitrogen temperature. Due to the lack of precise solubility data for the systems under investigation, the concentrations of the solutions were estimated in terms of the pressures of the gases inside the tubes. When the pressure was calculated, the volume occupied by the solvent was neglected. For each system at least three samples were prepared at pressures of 5, 10, and 15 atm. A sealed capillary containing benzene was placed into each sample tube to serve as external reference. From solubility data for ethane in CCl_4, the mole fraction of the dissolved ethane was calculated to be less than 0.03 at a pressure of 5 atm. and a temperature of 25°. The chemical shift values for a nonpolar gas in solution at various concentrations were found to vary from 1 to 2 c.p.s. No extrapolation to infinite dilution was performed because of the uncertainties involved in the concentration calculation, and the value of the chemical shift for the most dilute sample was taken to be that at infinite dilution.

TABLE III

POLAR CHEMICAL SHIFTS IN VARIOUS SOLVENTS, C.P.S.

Solvent	CH_{3obsd}	CH_{2obsd}	CH_{3cor}	CH_{2cor}	$CH_{3cor} - CH_{3gas}$	$CH_{2cor} - CH_{2gas}$
Acetonitrile						
Cyclohexane	298.4		300.4		−17.7	
Dioxane	287.7		287.1		−31.0	
CCl_4	271.6		281.8		−36.3	
Acetone	306.0		287.0		−31.1	
CH_3NO_2	316.4		288.0		−30.0	
	$CH_{3gas} = 318.1$					
Ethyl bromide						
Cyclohexane	308.2	208.0	310.2	210.0	−11.8	−12.7
Dioxane	305.2	197.0	304.6	196.4	−17.4	−26.3
CCl_4	288.3	187.2	298.5	197.4	−23.5	−25.3
Acetone	329.4	218.2	310.4	199.2	−11.6	−23.5
CH_3NO_2	335.6	225.2	308.0	197.7	−14.0	−25.0
	$CH_{3gas} = 322.0$					
	$CH_{2gas} = 222.7$					
Ethyl iodide						
Cyclohexane	298.8	221.0	300.8	223.0	− 9.6	− 8.9
Dioxane	293.2	209.4	292.6	208.8	−17.8	−23.1
CCl_4	277.4	200.8	287.6	211.0	−22.8	−20.9
Acetone	313.0	227.0	294.0	208.0	−16.4	−23.9
CH_3NO_2	322.4	235.7	294.8	208.1	−15.6	−23.8
	$CH_{3gas} = 310.4$					
	$CH_{2gas} = 231.9$					
Ethyl cyanide						
Cyclohexane	333.6	273.0	335.6	275.0	− 9.8	−17.7
Dioxane	331.6	264.0	331.0	263.4	−14.4	−29.3
CCl_4	310.3	250.0	320.5	260.2	−24.9	−32.5
Acetone	355.2	282.8	336.2	263.8	− 9.2	−28.9
CH_3NO_2	361.8	293.0	334.2	265.4	−11.2	−27.3
	$CH_{3gas} = 345.4$					
	$CH_{2gas} = 292.7$					
Triethylamine						
Cyclohexane	346.5	258.7	348.5	260.7	− 7.6	− 5.7
Dioxane	345.7	256.5	345.1	255.9	−11.0	−10.5
CCl_4						
Acetone	370.9	281.7	351.9	262.7	− 4.2	− 3.7
CH_3NO_2	378.2	287.4	350.6	259.8	− 5.5	− 6.6
	$CH_{3gas} = 356.1$					
	$CH_{2gas} = 266.4$					
Ethyl ether						
Cyclohexane	338.7	204.2	340.7	206.2	− 8.2	− 6.2
Dioxane	337.4	200.8	336.8	200.2	−12.1	−12.1
CCl_4	319.4	184.8	329.6	195.0	−19.3	−17.3
Acetone	368.4	236.8	349.4	217.8	+ 0.5	+ 5.5
CH_3NO_2	368.2	229.5	340.6	201.9	− 8.3	−10.4
	$CH_{3gas} = 348.9$					
	$CH_{2gas} = 212.3$					

IV. Discussion

1. van der Waals Chemical Shifts.—Gas to solvent chemical shifts for six nonpolar molecules have been measured in a range of solvents. The data are presented in Table IV. Since the solutes are nonpolar, the chemical shifts after correction for bulk suscepti-

TABLE IV

VAN DER WAALS SOLVENT SHIFTS, C.P.S. (P.P.M.)

Solute	Cyclohexane	Dioxane	CCl_4	Acetone	Nitromethane
Methane					
Exptl.	−14.2	−21.3	−24.2	−10.4	−12.2
	(−0.237)	(−0.355)	(−0.403)	(−0.173)	(−0.203)
Calcd.	−10.9	−10.6	−12.5	−9.5	−10.9
	(−0.181)	(−0.177)	(−0.208)	(−0.158)	(−0.181)
Ethane					
Exptl.	−10.4	−13.7	−18.6	−6.4	−8.0
	(−0.173)	(−0.228)	(−0.310)	(−0.107)	(−0.133)
Calcd.	−7.2	−7.0	−8.2	−6.3	−7.2
	(−0.119)	(−0.116)	(−0.136)	(−0.104)	(−0.119)
Ethylene					
Exptl.	−12.1	−20.5	−22.3	−13.6	−16.1
	(−0.202)	(−0.342)	(−0.372)	(−0.227)	(−0.268)
Calcd.	−8.2	−8.0	−9.3	−7.2	−8.1
	(−0.136)	(−0.133)	(−0.155)	(−0.1200)	(−0.135)
Cyclopropane					
Exptl.	−13.9	−18.9	−22.8	−12.7	−14.7
	(−0.232)	(−0.315)	(−0.380)	(−0.212)	(−0.245)
Calcd.	−6.3	−6.2	−7.2	−5.5	−6.3
	(−0.106)	(−0.103)	(−0.120)	(−0.892)	(−0.105)
CH_3CN					
Calcd.	−7.8	−7.6	−8.9	−6.8	−7.8
	(−0.130)	(−0.126)	(−0.148)	(−0.113)	(−0.129)
CH_3CH_2Br					
Calcd.	−5.0	−4.9	−5.7	−4.4	−4.9
	(−0.083)	(−0.081)	(−0.094)	(−0.073)	(−0.082)
CH_3CH_2I					
Calcd.	−4.4	−4.3	−5.0	−3.8	−4.3
	(−0.073)	(−0.072)	(−0.083)	(−0.064)	(−0.072)
CH_3CH_2CN					
Calcd.	−5.7	−5.5	−6.5	−4.9	−5.6
	(−0.094)	(−0.092)	(−0.108)	(−0.082)	(−0.094)
$(CH_3CH_2)_2O$					
Calcd.	−3.4	−3.3	−3.9	−3.0	−3.4
	(−0.057)	(−0.056)	(−0.065)	(−0.050)	(−0.057)
$(CH_3CH_2)_3N$					
Calcd.	−2.3	−2.2	−2.6	−2.0	−2.2
	(−0.038)	(−0.037)	(−0.043)	(−0.033)	(−0.037)

bility shifts may reasonably be assigned as van der Waals shifts. Perhaps the most striking feature of these measurements and of similar published data are the large van der Waals shifts observed for the halogenated solvents, in this case CCl_4. In this series of measurements there is also a reasonably consistent trend to minimum van der Waals shifts with acetone as a solvent. Similarly, maximum shifts were usually observed with all solvents for methane as a solute, and minimum shifts when the solute was ethane.

It is interesting to note that the chemical shifts calculated using eq. 7 obtained by Howard, Linder, and Emerson given in Table V reproduce at least one of these qualitative trends. However, the calculated shifts are much too small and the agreement would be much improved through the use of a value of the constant ϕ equal to 2 or larger. The detailed agreement of calculated and observed chemical shifts is poor. Of course, the uncertainties in the bulk susceptibility data lead to fairly sizable errors in the observed van der Waals shifts.

2. Polar Chemical Shifts.—In the lower half of Table IV, gas–solution solvent chemical shifts are given for a variety of polar solutes (mostly ethyl derivatives) and for a group of solvents of varying polarity. In order to focus attention on the polar contribution to the chemical shift, it is desirable to subtract from these values the appropriate van der Waals chemical shifts. In Table VI are given values obtained by subtracting the van der Waals shift observed for unsubstituted ethane. However, the calculations presented in Table V suggest that the true van der Waals shifts for the substituted ethanes are somewhat smaller even than in ethane itself.

One of the striking features of the polar shifts presented in Table V is the occurrence of positive (upfield) shifts, especially for diethyl ether and triethylamine. For the most part, these shifts are small and might result from an overestimate of the van der Waals effect. However, there are several instances where the methylene shifts are more positive than the methyl shifts, which requires another explanation. It is possible to obtain positive calculated polar shifts for diethyl ether and triethylamine by assuming them to be in a rather sterically favorable configuration, in which the molecular dipole moment has a component along the C–H bond with its positive end in the direction of the H atom.

TABLE V

REACTION FIELD SOLVENT SHIFTS, C.P.S. (P.P.M.)

Solute	Cyclohexane		Dioxane		CCl_4		Acetone		Nitromethane	
	CH_3	CH_2	CH_3	CH_2	CH_3	CH_2	CH_3	CH_2	CH_3	CH_2
CH_3CN										
Exptl.	−3.5		−9.7		−12.1		−20.7		−17.8	
	(−0.058)		(−0.162)		(−0.202)		(−0.345)		(−0.297)	
Calcd.	−3.33		−3.74		−3.68		−10.07		−10.57	
	(−0.0555)		(−0.0623)		(−0.0630)		(−0.1679)		(−0.1761)	
CH_3CH_2Br										
Exptl.	−1.4	−2.3	−3.7	−12.6	−4.9	−6.7	−5.2	−17.2	−6.0	−17.0
	(−0.023)	(−0.038)	(−0.062)	(−0.210)	(−0.082)	(−0.112)	(−0.087)	(−0.287)	(−0.100)	(−0.283)
Calcd.	−.47	−1.29	−.53	−1.44	−.53	−1.46	−1.52	−3.72	−1.60	−3.89
	(−.0078)	(−0.0215)	(−.0088)	(−0.240)	(−.0089)	(−0.243)	(−0.0253)	(−0.0620)	(−0.0265)	(−0.0649)
CH_3CH_2I										
Exptl.	+0.8	+1.5	−4.1	−9.4	−4.2	−2.4	−10.0	−17.5	−7.6	−15.8
	(+.013)	(+0.025)	(−0.068)	(−0.157)	(−0.070)	(−0.040)	(−0.167)	(−0.292)	(−0.127)	(−0.263)
Calcd.	−.40	−1.15	−.46	−1.26	−.46	−1.28	−1.35	−3.36	−1.42	−3.52
	(−.0067)	(−0.0188)	(−.0076)	(−0.0210)	(−.0077)	(−0.0213)	(−0.0225)	(−0.0560)	(−0.0237)	(0.0587)
CH_3CH_2CN										
Exptl.	+0.6	−7.3	−0.7	−15.6	−6.3	−13.9	−2.8	−22.5	−3.2	−19.3
	(+.010)	(−0.122)	(−.012)	(−0.260)	(−0.105)	(−0.232)	(−0.047)	(−0.375)	(−0.053)	(−0.322)
Calcd.	−.97	−2.50	−1.10	−2.81	−1.12	−2.84	−3.39	−7.42	−3.58	−7.78
	(−.0161)	(−0.0417)	(−0.0183)	(−0.0468)	(−0.0186)	(−0.0473)	(−0.0565)	(−0.1237)	(−0.0597)	(−0.1296)
$(CH_3CH_2)_2O$										
Exptl.	+2.2	+4.3	+1.6	+1.6	−0.7	+1.3	+6.9	+11.9	−0.3	−2.4
	(+0.037)	(+0.072)	(+0.027)	(+0.027)	(−.012)	(+0.022)	(+0.115)	(+0.198)	(−.005)	(−0.040)
Calcd.	−.22	+.90	−.25	+1.01	−.25	+1.02	−.56	+2.56	−.58	+2.67
	(−.0037)	(+.0150)	(−.0041)	(+0.0168)	(−.0041)	(+0.0170)	(−.0093)	(+0.0426)	(−.0097)	(+0.0445)
$(CH_3CH_2)_3N$										
Exptl.	+2.8	+4.7	+2.7	+3.2			+2.2	+2.7	+2.5	+1.4
	(+0.047)	(+0.078)	(+0.045)	(+0.053)			(+0.037)	(+0.045)	(+0.042)	(+0.023)
Calcd.	−.05	+.46	−.06	+.51			−.13	+1.25	−.13	+1.28
	(−.0009)	(+.0076)	(−.0010)	(+.0085)			(−.0022)	(+0.0205)	(−.0022)	(+0.0213)

TABLE VI

ERRORS IN MEASUREMENTS OF INTERNAL SHIFTS

$\delta_{CH_2} - \delta_{CH_3}$ c.p.s. (p.p.m.)[a]

	Cyclohexane	Dioxane	CCl_4	Acetone	Nitromethane
CH_2CH_2Br	−0.9	−8.9	−1.8	−11.9	−11.0
	(−0.015)	(−0.148)	(−0.030)	(−0.198)	(−0.193)
CH_3CH_2I	+0.7	−5.3	+1.9	−7.5	−8.2
	(+0.012)	(−0.088)	(+0.032)	(−0.125)	(−0.137)
CH_3CH_2CN	−7.9	−14.9	−7.6	−19.7	−16.1
	(−0.132)	(−0.248)	(−0.127)	(−0.328)	(−0.268)
$(CH_3CH_2)_2O$	+2.1	0.0	+2.0	+5.0	−2.1
	(+0.035)	(0.0)	(+0.033)	(+0.083)	(−0.035)
$(CH_3CH_2)_3N$	+1.9	+0.5		+0.5	−1.1
	(+0.032)	(+0.008)		(+0.008)	(−0.018)

[a] Value observed in gas phase taken as correct value.

For the ethyl halides, the observed negative σ_E values increase from methyl to methylene in the same general fashion as do the calculated σ_E values. This lends some support to the functional form of Buckingham's reaction field equation Similarly, many of the positive σ_E values observed for diethyl ether and triethylamine increase from methyl to methylene.

These trends have numerous exceptions, especially where the observed polar shifts are rather small. Perhaps these fluctuations may be ascribed to errors in the bulk susceptibility and van der Waals shifts. However, there is one discrepancy between calculated and observed polar shifts which seems significant and important. The combination of a highly polar solute with a highly polar solvent produces polar shifts that are substantially larger than the calculated values. Here it no longer appears possible to treat the solvent as a homogeneous medium characterized only by its dielectric constant. The data suggest strongly that aligned dipole solute–solvent pairs are being formed.

The practical consequences of this study for the measurement of chemical shifts which may be interpreted as properties of the isolated molecule are somewhat discouraging. In many systems the solvent effects are rather large; in some solvents the measurement of the internal chemical shift may be in error by more than 30%. The use of a nonpolar solvent, however, reduces this error to less than 15%.

The theoretical treatments so far available for the calculation of van der Waals and polar shifts may permit the reduction of the solvent error by a factor of two. Solvent errors will still be quite appreciable, however, for combinations of highly polar solutes with polar solvents.

THE STRUCTURE OF THIOPHENE IN THE GAS PHASE AS DETERMINED BY ELECTRON DIFFRACTION[1]

BY R. A. BONHAM AND F. A. MOMANY

Department of Chemistry, Indiana University, Bloomington, Indiana

Received June 17, 1963

The molecular structure of thiophene was determined by the sector-microphotometer method of electron diffraction. Techniques were developed to obtain the experimental data missing as a result of the presence of the beam trap and a limited maximum scattering angle. These techniques should prove useful in the case of the missing small angle scattering intensity; however, it appears that the use of a damping factor is still necessary to reduce the effects of integral termination errors owing to the lack of large angle scattering data. The parameters characterizing the structure of thiophene have been found to be r_g(S–C) = 1.714, r_g(C–C$_1$) = 1.370, r_g(C–C$_2$) = 1.419, r_g(C–H) = 1.092, l_{S-C} = 0.049, l_{C-C_1} (assumed) = 0.044, l_{C-C_2} (assumed) = 0.046, l_{C-H} = 0.070 Å.; ∠ C–S–C = 92.2° and ∠ S–C–C = 111.4°. The structure is planar to better than 0.1 Å. and the longer C–C bond is the one directly opposite the sulfur atom.

A determination of the molecular structure of thiophene by electron diffraction can serve as a valuable calibration of the experimental apparatus used. Accurate structural parameters obtained by microwave techniques exist for this molecule[2a] and thus provide a comparison with the present results. An earlier electron diffraction study was carried out in 1939 by use of the visual method. However, it is felt that the precision of present day methods should lead to substantially more reliable parameter values than those reported in the previous work.[2b] The structural data for thiophene were collected at the same time that data on several other molecules were obtained,[3-5] and it was felt that this work would not only help to establish a check on the structural parameters obtained in these other studies, but also to serve as a test molecule for the investigation of new techniques in the analysis of diffraction data. The structure of thiophene plays a particularly important role as a comparison structure for the analysis of the new molecule 1,2,5-thiadiazole.[3] It is the purpose of this work to report on the results of the structural analysis of thiophene and the results of the new techniques that were employed in the analysis of the structural data.

Experimental

Procedure.—A sample of reagent grade thiophene was purified by distillation immediately prior to taking the diffraction photographs. The purity was checked by boiling point and index of refraction measurements. These measurements indicated that the sample used was better than 98% pure. Electron diffraction photographs were obtained with an r^3 sector using the sector-electron diffraction camera in Professor L. S. Bartell's laboratory at Iowa State University. Specimen pressures of 20 to 80 mm. with exposure times of 1 to 4 sec. were used at a temperature of 298°K. The electron beam current was 0.3 μ and the accelerating voltage was 40 kv. Four research grade plates at each of two camera distances were obtained. The photographic plates were scanned with a microphotometer located in Professor L. O. Brockway's laboratory at the University of Michigan.

The microphotometer traces of the electron diffraction photographs were read at 0.25-mm. intervals with the aid of a Bausch and Lomb 7-power measuring magnifier. The photographic emulsion was calibrated by a procedure due to Bartell and Brockway.[6]

The index of resolution for the short camera distance data (10.66 cm.) was found to be 1.00 and the index of resolution for the long camera distance (21.35 cm.) was found to be 0.75. The low value of the index of resolution for the long camera distance is probably due to delocalized gas scattering and for this reason, the short camera distance data ($20 < q < 90$) was felt to be more reliable than the data for the longer camera distance ($10 < q < 60$).

Structure Analysis.—Three different techniques were employed in the analysis of the experimental data. The first approach utilizes a scheme described elsewhere.[7] Bond lengths and vibrational amplitudes[8] were all obtained by analysis of the data using least squares procedures. Corrections to the data for electron–electron scattering, asymmetry of vibration for bonded distances, and Fourier integral termination errors were applied. Corrections for the failure of the Born approximation were made by characterizing the radial distribution curve, corrected for asymmetry effects, with a model which included corrections for failure of the Born approximation.[9] It was found necessary to use a damping factor of the form e^{-aq^2} where $a = 0.0009$, in order to prevent the introduction of errors into the analysis due to the fact that the analytical representations of the phases $\eta_l(q)$ are given incorrectly past $q = 180$. The calculated experimental radial distribution function made use of experimental intensity data, $I_0(q)$, at integral values of q ($q = 40 \sin \theta/\lambda$) over the range $q = 12$ to $q = 90$. Data for the region $q = 0$ to $q = 12$ were calculated using several theoretical models and corresponding radial distribution functions were obtained. The background function, $B(q)$, was corrected by use of Karle's nonnegative area criterion.[10] The radial distribution function was then analyzed by a least squares procedure and a new theoretical model was computed on the basis of the results of this analysis. This process was repeated until the results became consistent with those from the previous cycle. The final values for the molecular parameters obtained with this procedure were also checked by the use of the correlation method with the experimental intensity curve. In this way, the planarity of the ring was tested and it was found that the ring atoms were planar to within better than ±0.1 Å.

The second procedure for analyzing the intensity data is similar to the first in all respects except for the handling of the missing experimental data in the region $0 < q < 15$. The technique employed here is an analytical scheme due to Karle[11] which attempts to reconstruct the missing data in the small angle scattering region by making use of the nonnegative area criterion and imposing the added restriction of a smooth background. A radial distribution curve is obtained from the intensity curve, with electron–

(1) (a) Contribution Number 1151 from the Chemical Laboratories of Indiana University; (b) the authors wish to thank the National Science Foundation and the U. S. Atomic Energy Commission for financial support of this work.

(2) (a) B. Bak, D. Christersen, L. Hansen-Nygaard, and J. Rastrup-Anderson, *J. Mol. Spectry.*, **7**, 58 (1961); (b) V. Schomaker and L. Pauling, *J. Am. Chem. Soc.*, **61**, 1769 (1939).

(3) R. A. Bonham and F. A. Momany, *ibid.*, **83**, 4475 (1961).

(4) T. Ukaji and R. A. Bonham, *ibid.*, **84**, 3627 (1962).

(5) T. Ukaji and R. A. Bonham, *ibid.*, **84**, 3631 (1962).

(6) L. S. Bartell and L. O. Brockway, *J. Appl. Phys.*, **24**, 656 (1953).

(7) R. A. Bonham and L. S. Bartell, *J. Chem. Phys.*, **31**, 709 (1959).

(8) The term vibrational amplitude as used in this paper corresponds closely to the term l_m defined by several authors in previous publications. See for instance: K. Kuchitsu and L. S. Bartell, *ibid.*, **35**, 1945 (1961); R. A. Bonham and J. L. Peacher, *ibid.*, **38**, 2319 (1963).

(9) R. A. Bonham and T. Ukaji, *ibid.*, **36**, 72 (1962). Note that the second exponential term of eq. 6 should read $e^{-0.06980Z}$. a ($\pi/2$) is missing in front of eq. 13. Also in eq. 13, there is a Δ in front of the b_{ij} in the $X \pm$ term, and the expression for A should read: $A = 0.5 \text{ arc tan } [(2\Delta C_{ij})/l_{ij}^2] + \Delta a_{ij}$.

(10) I. L. Karle and J. Karle, *ibid.*, **17**, 1052 (1949).

(11) J. Karle, private communication.

electron scattering corrections and a trial background, without any added theoretical data. The positive areas of this radial distribution curve, in the region where interatomic distances should occur, are then reinverted and the resulting intensity curve in the region $0 < q < 15$ is then used to replace the missing data in this region. A gaussian damping factor is used in this procedure so that termination errors from the missing data at $q > 90$ would not affect the results. The procedure may then be iterated until no important changes in the generated intensity data are observed. In general, convergence is very slow, so an additional modification to the procedure was made. The $\lim_{q\to 0} M(q)$ can be shown to be approximately $\sum_{i,j} M_{ij}Z_iZ_j / \sum(Z_k^2 + Z_k)$, where M_{ij} is a multiplicity factor and the Z values are the atomic numbers. This quantity is independent of the structure of the molecule and depends only on a knowledge of the molecular formula. The corresponding experimental quantity $M(0)^{\text{expt}}$ can be shown to be given approximately as the first moment of the positive part of the radial distribution function $f^+(r)$ or $\int_{r_{\min}}^{r_{\max}} dr\, rf^+(r)$. The convergence rate of the data generation procedure can then be greatly accelerated by multiplying the generated missing data by the ratio $M(0)/M(0)^{\text{expt}}$ at the end of each cycle. In this way, the missing data can be constructed in three to four iterations of the procedure.

It was found that this technique was a helpful check on assessing the reliability of bond length determinations from minor peaks in the radial distribution curve. For instance, if the major contribution to a particular bond length occurred in the range of missing data, the use of a theoretical model will often give this peak a normal area in the radial distribution curve, while the generation of missing data technique will usually give an area that is considerably smaller than that predicted by theory. In this case, care must be exercised in the interpretation of the peak in question. A notable example of this effect occurred in the case of the 2.1-Å. nonbonded C–H distance in *t*-butyl chloride,[12] where the generation of missing data technique for the region $0 < q < 15$ gave almost no peak for this distance in the radial distribution curve. It is of interest to note that the earlier work of Bastiansen,[13] which employed a graphical technique for obtaining the missing data and is similar in many ways to the analytical method described here, also showed a near absence of the same peak from the radial distribution curve. It should be noted, however, that such effects may be largely eliminated by obtaining experimental data into $q = 5$ or less for most molecules.

It is also important to point out that this foregoing procedure fulfills an additional function in that it provides a guide for the drawing of the background function in the region of small q. If a trial background is drawn which is not compatible, at the point where the generated $M(s)$ function joins the experimental data, with the background indicated by the generated $M(s)$ data, then the resulting $f(r)$ function will have slowly varying anomalous positive and negative fluctuations. The shape of the $f(r)$ function can thus be used as a guide to obtain the proper background function for small values of q.

The analytical procedure just described was also employed to generate the missing data at large scattering angles. However, the rate of convergence and dependence on the background made the process impractical for routine data analysis. It was also discovered that in most cases where the missing data extended over the region $0 < q < 15$, it was possible to successfully reproduce the missing data. When the range of missing data was extended to $q = 20$, it was discovered that the procedure often failed to converge.

The other technique utilized in this work was the use of a sharpened radial distribution function obtained from the experimental intensity data without the use of the missing data in the region $0 < q < 12$. Distances were obtained by correlating this sharpened function with a theoretically computed function using data over the same range in q. The results of this analysis are reported in Table I. The use of an antidamping factor has the advantage that changes in the l_{ij} and r_{ij} values of ± 0.002 Å. make detectable differences in the correlation between the experimental and theoretical curves. Also the procedure places no reliance on a theoretical model for the missing data in the

(12) F. A. Momany, M. L. Druelinger, and R. A. Bonham, *J. Am. Chem. Soc.*, in press.

(13) O. Bastiansen and L. Smedvik, *Acta Chem. Scand.* **7**, 653 (1963).

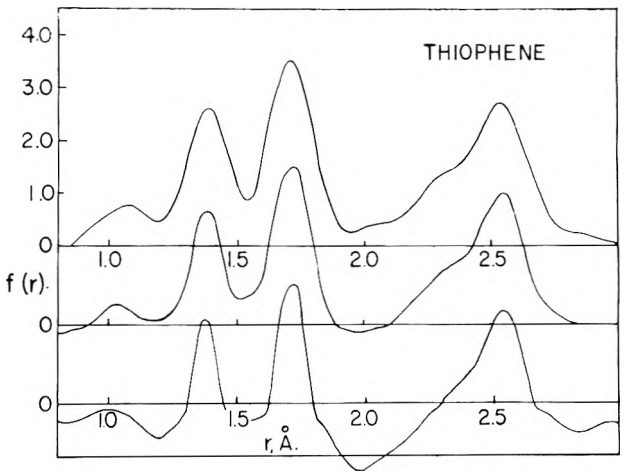

Fig. 1.—Radial distribution curves for thiophene: the upper curve is $f(r)$ with theoretical data added; the middle curve is $f(r)$ with the generated data added; and the lower curve is $f(r)$ without any data added in the missing region of the $M_c(q)$ curve. The ordinate scale refers to the absolute value of $f(r)$.

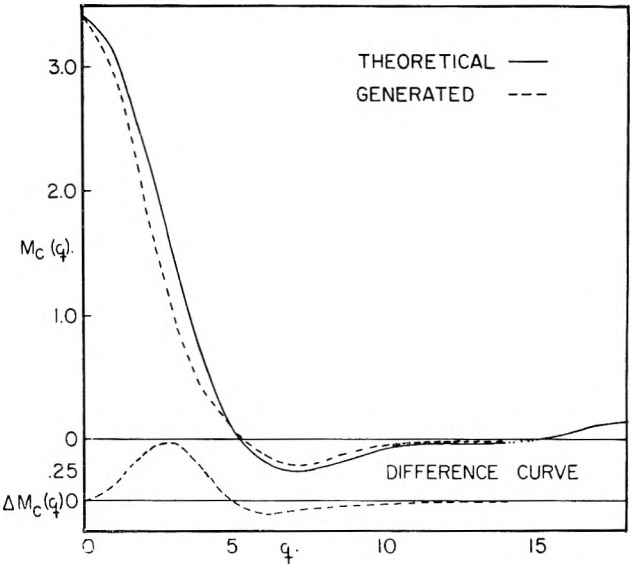

Fig. 2.—Generated and theoretical $M_c(q)$ functions over the region of missing data $0 \leq q \leq 15$. The generated data is the result of six iterations and the line beyond $q = 15$ represents experimental data: the ordinate scale refers to the absolute value of $M(q) = (I_0(q)/B(q) - 1)$ corrected for electron–electron scattering. The ordinate scale refers to the absolute value of $M(q)$.

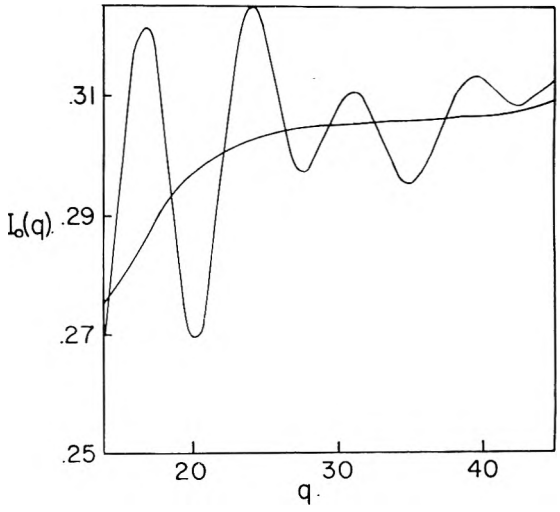

Fig. 3.—Long-camera-distance intensity data, $I_0(q)$, and the background function, $B(q)$ (smooth curve): the ordinate values refer to an arbitrary relative intensity scale.

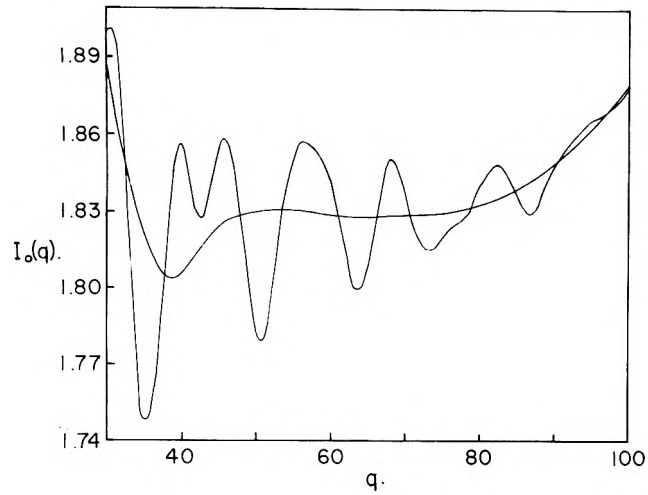

Fig. 4.—Short-camera-distance intensity data, $I_0(q)$, and the background function, $B(q)$ (smooth curve): the ordinate values refer to an arbitrary relative intensity scale.

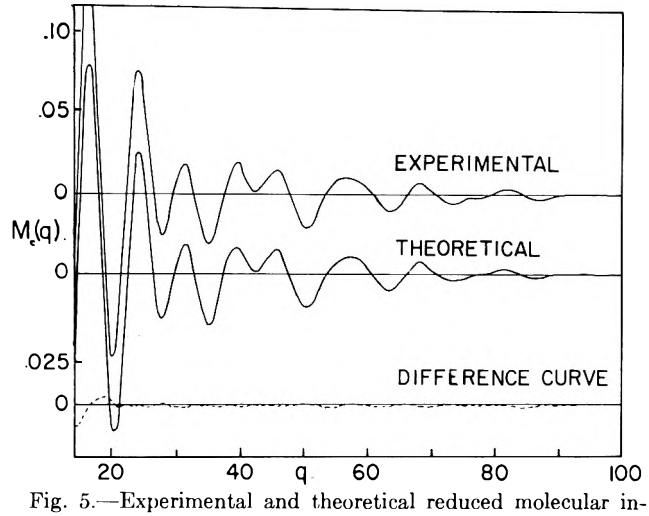

Fig. 5.—Experimental and theoretical reduced molecular intensity curves and their difference: the ordinate scale refers to the absolute value of $M(q)$.

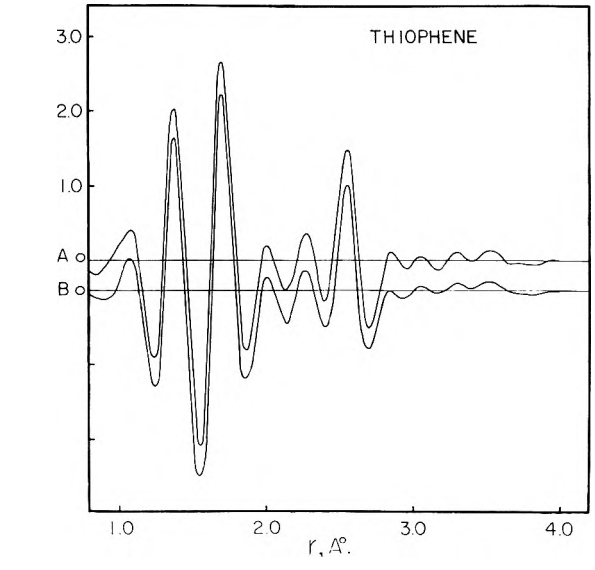

Fig. 6.—Sharpened radial distribution function: the upper curve is experimental and the lower curve is theoretical. The ordinate scale refers to the absolute value of the modified $f(r)$ function.

region $0 < q < 12$ and overlapping peaks are resolved to a greater extent. An excellent detailed discussion of the theory and use of damping and antidamping factors has been given previously by Waser and Schomaker.[14]

Results

Table I shows a comparison of the final least squares analysis of the radial distribution curve for thiophene with the results obtained by Bak[2a] using microwave techniques. Also included are the observed distances found from the sharpened radial distribution function. The approximate standard deviations of the least squares parameters were calculated from equations 12a and 12b of ref. 7. These estimates are admittedly somewhat crude in the case of badly overlapping peaks, but seem to furnish realistic estimates in other cases.[15] To obtain a total estimate of the precision for the various measured values, it was necessary to include a scale factor error of two parts per thousand.

TABLE I

STRUCTURAL PARAMETERS DERIVED FROM RADIAL DISTRIBUTION CURVES AND CALCULATED PRECISIONS

	$r_g(o)$	δr	l	δl	r_s[a]	$r_m(1)$[c]	δr
C–H	1.092	0.008	0.070	0.010	1.078[b]	1.08	0.01
					1.081		
S–C	1.714	.004	.049	.005	1.714	1.71	.01
C_1–C_2	1.370	.006	.044[d]	...	1.370	1.39Ave.	.01
C_2–C_3	1.419	.007	.046[d]	...	1.423	...	...
∠C-S-C =	92.2 ± 0.2°				92° 10′		
∠S-C-C =	111.4 ± 0.2°				111° 28′		

[a] See ref. 1. [b] The shorter distance is the C–H nearest the sulfur, and the longer C–H distance is farthest from the sulfur. [c] Results from the sharpened radial distribution function. [d] Assumed values.

Figure 1 shows the comparison of radial distribution curves obtained with assumed theoretical data in the region $0 < q < 15$, with the missing data generated from the experimental data according to the procedure described in the last section and the radial distribution curve without the use of any data over the range $0 < q < 15$. In Fig. 2, the $M(s)$ function obtained by generation of the missing data as well as the $M(s)$ function for the best theoretical model in the region $0 \leq q \leq 15$ are shown. Note that the differences between the two curves are quite small. In Fig. 3 and 4, the intensity data, $I_0(q)$, are shown with the experimental background functions used to obtain the best radial distribution function. It should be noted that in Fig. 3 and 4 not all of the overlap region has been shown and that the short distance data extend out to $q = 100$ although in the actual analysis only the data out to $q = 90$ were used. The agreement between theory and experiment is shown in Fig. 5. Note that the difference curve indicates an average deviation between the theory and experiment that is somewhat better than 5% of the theoretical $M(s)$ curve.

The sharpened radial distribution functions for both the best theoretical model and the experimental data are shown in Fig. 6.

The structure of thiophene is of interest chemically because of the effect a sulfur atom has on a conjugated system when it is used to replace an ethylene group. It is clear from the study of thiophene by Bak[2a] and also from this study that the introduction of a sulfur atom into a benzene ring by replacing an ethylene group decreases the aromaticity. This can be readily seen in the unequal C–C distances of 1.42 and 1.37 Å. reported

(14) J. Waser and V. Schomaker, *Rev. Mod. Phys.*, **25**, 671 (1953).

(15) Compare, for instance, the errors given by a more sophisticated treatment [O. Bastiansen, L. Hedberg, and K. Hedberg, *J. Chem. Phys.*, **27**, 1311 (1957)] with those given by the formulas used here for a somewhat similar case [L. S. Bartell and R. A. Bonham, *ibid.*, **31**, 400 (1959)].

in this work. These values may be compared with the C–C bond length values 1.337 and 1.483 Å.[16] for the nonaromatic molecule butadiene and the completely aromatic benzene system where the C–C distances are probably all equal to 1.397 Å.[17]

(16) A. Almenningen, O. Bastiansen, and M. Traetteberg, *Acta Chem. Scand.*, **12**, 1221 (1958).

(17) (a) I. L. Karle, *J. Chem. Phys.*, **20**, 35 (1952); (b) A. Almenningen, O. Bastiansen, and L. Fernholt, *Kgl. Norske Videnskab. Selskabs Skrifter* (1958).

Acknowledgments.—The authors wish to thank Professor L. S. Bartell for the use of his electron diffraction unit and Professor L. O. Brockway for the use of his microphotometer. We also wish to thank the Indiana University Research Computing Center for use of their equipment, Mrs. Connie Williams for her help in the preparation of the manuscript, and Mr. A. J. Atkinson for help in reading traces.

ELECTRONIC SPECTRA OF SOME BIS-(CYCLOPENTADIENYL)-METAL COMPOUNDS

BY JAMES C. W. CHIEN

The Hercules Research Center, Wilmington, Delaware

Received June 26, 1963

The electronic spectra of $(C_5H_5)_2TiCl_2$, $(C_5H_5)_2TiBr_2$, $(C_5H_5)_2TiI_2$, and $(C_5H_5)_2VCl_2$ are described. The absorptions are assigned to electronic transitions based on a LCAO-MO treatment. The metal–ligand bondings involve two bonding molecular orbitals per ligand; they are strongest in the chloride and weakest in the iodide. Two new forbidden bands have been found in the spectrum of $(C_5H_5)_2Fe$. The band positions agree with Yamazaki's SCF calculations.

Introduction

The electronic structure of bis-(cyclopentadienyl)-iron has been a subject of continuing interest. Earlier treatments[1,2] showed that the metal and the ligands are bonded by $d\pi$–$p\pi$ bonds. Linnett[3] theorized that there are three equivalent bonding orbitals between iron and each cyclopentadienyl ring. The molecular orbital energy levels were calculated approximately by Dunitz and Orgel.[4] Recently results of more sophisticated calculations have appeared.[5–7] Using slightly different sets of basic functions but similar methods of calculation, these authors arrived at molecular orbital energy levels which differ in both the absolute values and the order of stabilities.

The purpose of this communication is to present the electronic spectra of $(C_5H_5)_2TiX_2$, where X = Cl, Br, I, and to report weak new absorption bands in the spectrum of $(C_5H_5)_2Fe$. The absorption bands have been assigned to appropriate electronic transitions. The relative merits of the $(C_5H_5)_2Fe$ molecular orbital calculations are briefly discussed.

Experimental

The compounds used in this work were prepared by Dr. W. P. Long of these Laboratories. Bis-(cyclopentadienyl)-titanium and -vanadium dihalides were prepared by the method of Wilkinson and Birmingham.[8] $(C_5H_5)_2Fe$ was prepared according to the procedure of Kealy and Pauson.[9] Analyses of all compounds were correct with the exception of $(C_5H_5)_2TiI_2$, which appeared to be contaminated with $(C_5H_5)_2Ti(OH)I$.

The electronic spectra were obtained in the absence of oxygen. A Cary Model 14 spectrophotometer was used in this work.

(1) W. Moffitt, *J. Am. Chem. Soc.*, **76**, 3386 (1954).

(2) A. D. Liehr and C. J. Ballhausen, *Acta Chem. Scand.*, **11**, 207 (1957).

(3) J. W. Linnett, *Trans. Faraday Soc.*, **52**, 904 (1956).

(4) J. D. Dunitz and L. E. Orgel, *J. Chem. Phys.*, **23**, 954 (1955).

(5) M. Yamazaki, *ibid.*, **24**, 1260 (1956).

(6) E. M. Shustorovich and M. E. Dyatkina, *Dokl. Akad. Nauk SSSR*, **128**, 1234 (1959); *Zh. Strukt. Khim.*, **3**, 345 (1962).

(7) J. P. Dahl and C. J. Ballhausen, *Mat. Fys. Medd. Dan. Vid. Selsk.*, **33**, 1 (1961).

(8) G. Wilkinson and J. M. Birmingham, *J. Am. Chem. Soc.*, **76**, 4281 (1954).

(9) T. J. Kealy and P. L. Pauson, *Nature*, **168**, 1039 (1951).

Results and Discussion

Electronic Spectra of Bis-(cyclopentadienyl)-titanium and -vanadium Dihalides—In their study of $(C_5H_5)_2Fe$, Kaplan, Kester, and Katz[10] found absorption at 32.6 kK. in carbon tetrachloride. This absorption is absent in hexane, ethanol, and methanol. Brand and Snedden[11] showed that the 32.6-kK. absorption is obtained in all halogenated solvents, and they attributed this absorption to the dissociative charge-transfer process.

$$(C_5H_5)_2Fe + CCl_4 \overset{h\nu}{\rightleftharpoons} (C_5H_5)_2Fe^+ + Cl^- + CCl_3 \quad (1)$$

The possibility of dissociative charge-transfer absorption of $(C_5H_5)_2TiCl_2$ in methylene chloride was investigated by determining its spectra in methylene chloride, tetrahydrofuran, and diethyl ether (Fig. 1). The first two were found to be identical. Apparently, dissociative charge-transfer processes of the type mentioned are unimportant for $(C_5H_5)_2TiCl_2$. A slight decrease in short wave length absorption intensities was observed in diethyl ether. In addition, there exists a long wave length tail which gives a pinkish tint to the diethyl ether solution. The nature of the long wave length tail absorption in diethyl ether is not understood.

Another point which concerned us is the possibility of dimerization. Long[12] furnished spectroscopic evidence for complex formation between $(C_5H_5)_2TiCl_2$ and aluminum chloride and alkylaluminum chloride. Chien[13] also postulated these complexes as the active species in the low pressure polymerization of ethylene. We have determined the molecular weight of $(C_5H_5)_2TiCl_2$ in ethylene dichloride and found it to be 250, 252. Furthermore, the methylene chloride solutions of $(C_5H_5)_2TiCl_2$ follow Beer's law from 10^{-2} to 10^{-5} *M*.

(10) L. Kaplan, W. L. Kester, and J. J. Katz, *J. Am. Chem. Soc.*, **74**, 5531 (1952).

(11) J. C. D. Brand and W. Snedden, *Trans. Faraday Soc.*, **53**, 894 (1957).

(12) W. P. Long, *J. Am. Chem. Soc.*, **81**, 5312 (1959).

(13) J. C. W. Chien, *ibid.*, **81**, 86 (1959).

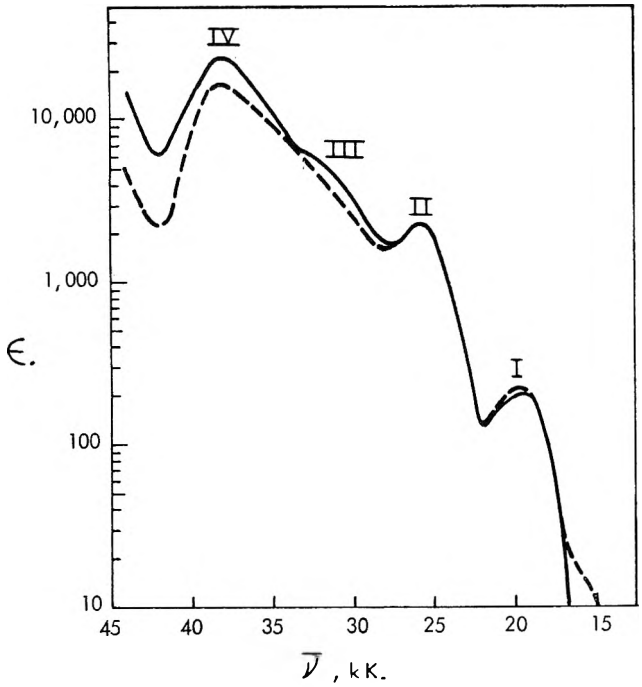

Fig. 1.—Electronic spectrum of $(C_5H_5)_2TiCl_2$ in solvents: ———, methylene chloride and tetrahydrofuran; – – – –, diethyl ether.

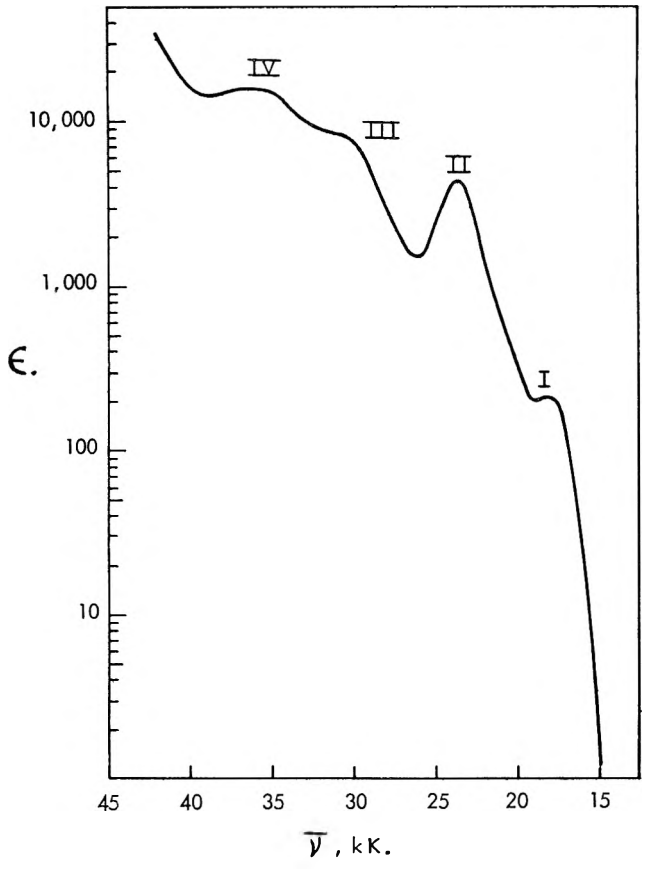

Fig. 2.—Electronic spectrum of $(C_5H_5)_2TiBr_2$ in methylene chloride.

It is, therefore, established that $(C_5H_5)_2TiCl_2$ is monomeric in these solvents.

The electronic spectra of $(C_5H_5)_2TiCl_2$, $(C_5H_5)_2TiBr_2$, $(C_5H_5)_2TiI_2$, and $(C_5H_5)_2VCl_2$ are shown in Fig. 1–4.

Electronic Structure of Bis-(cyclopentadienyl)-titanium and -vanadium Dihalides.—These compounds are

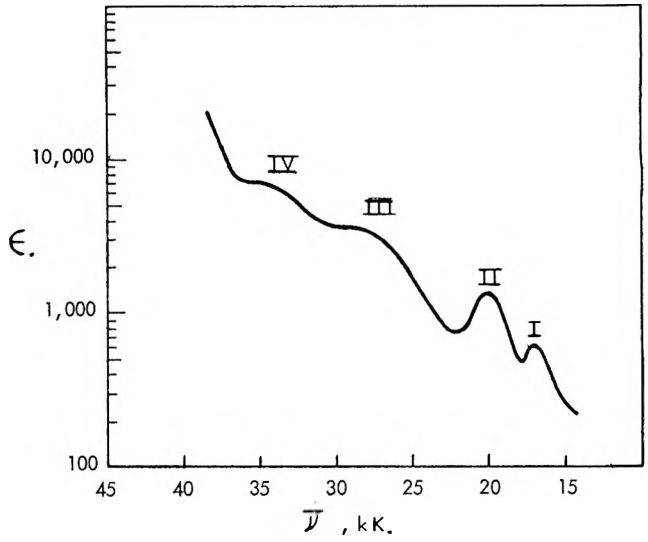

Fig. 3.—Electronic spectrum of $(C_5H_5)_2TiI_2$ in methylene chloride.

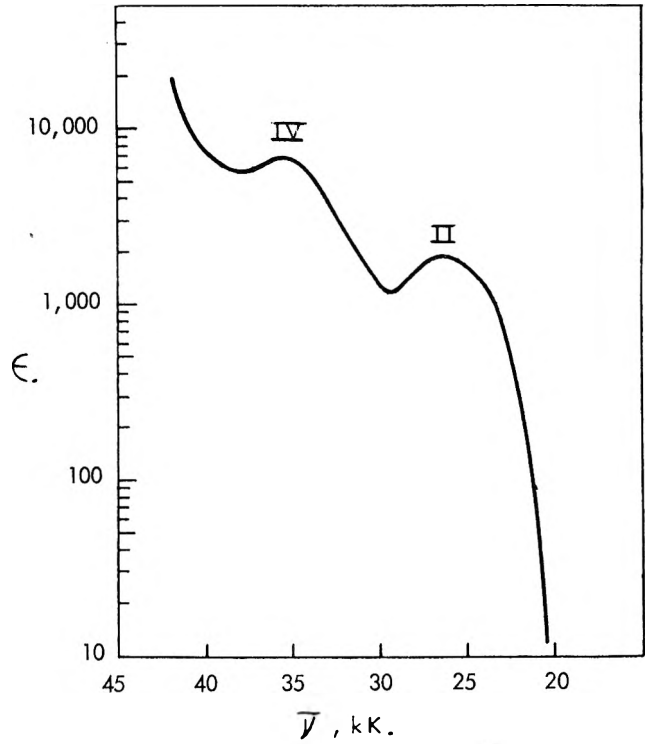

Fig. 4.—Electronic spectrum of $(C_5H_5)_2VCl_2$ in methylene chloride.

assumed to have C_{2v} symmetry in the following qualitative molecular orbital discussions. The group orbitals of interest belonging to the two cyclopentadienyl groups may be represented by

$$c(a_1) = (2)^{-1/2}\,[c_A(a) + c_B(a)] \quad (2)$$

$$c(b_2) = (2)^{-1/2}\,[c_A(a) - c_B(a)] \quad (3)$$

$$c(a_2) = c(b_2') = (2)^{-1/2}\,[c_A(e_1) - c_B(e_1)] \quad (4)$$

$$c(b_1) = c(a_1') = (2)^{-1/2}\,[c_A(e_1) + c_B(e_1)] \quad (5)$$

where c refers to cyclopentadienyl orbitals; the two rings are differentiated by subscripts A and B. The group orbital belonging to the two halogen atoms may be similarly represented by

$$Cl(a_1) = (2)^{-1/2}\,[Cl_C(2p\sigma) + Cl_D(2p\sigma)] \quad (6)$$

$$Cl(b_1) = (2)^{-1/2}\,[Cl_C(2p\sigma) - Cl_D(2p\sigma)] \quad (7)$$

$$Cl(b_2) = (2)^{-1/2}[Cl_C(2p\pi) + Cl_D(2p\pi)] \quad (8)$$

$$Cl(a_2) = (2)^{-1/2}[Cl_C(2p\pi) - Cl_D(2p\pi)] \quad (9)$$

$$Cl(a_1') = (2)^{-1/2}[Cl_C(2p\pi') + Cl_D(2p\pi')] \quad (10)$$

$$Cl(b_1') = (2)^{-1/2}[Cl_C(2p\pi') - Cl_D(2p\pi')] \quad (11)$$

The ligand orbitals are then formed by combining group orbitals of the same symmetry. The 3d, 4s, and 4p orbitals of the metal are now introduced to form the molecular orbitals of the compound. In Fig. 5, lines connecting various orbits of appropriate symmetries are omitted to avoid cluttering the figure. The primes denote the orbitals and do not have symmetry significance. There are eight bonding orbitals. Of the six primarily nonbonding orbitals ($a_1^{*\prime}$) is stabilized by combination with the metal (a_1) orbitals. (a_1^*) and (b_1^*) are primarily the lone pair orbitals of the halogen atoms. ($b_1^{*\prime}$) and (b_2^*) are nearly degenerate in energies; they are both bonding between one pair of the ligands but otherwise antibonding. The highest occupied molecular orbitals (a_2^*) is antibonding among all the ligands. With the exception of ($a_1^{*\prime}$), the other starred molecular orbitals have no bonding characteristic between the metal and the ligands. In $(C_5H_5)_2VCl_2$ (a_1^{**}) is also occupied. The compound is paramagnetic. The electron spin resonance spectra of $(C_5H_5)_2VCl_2$ and related compounds have been reported.[14]

In the molecular orbital scheme above, the halogens and the cyclopentadienyls contributed toward the eight bonding molecular orbitals of the molecule. In contrast, the theory of Ballhausen and Dahl[15] called for three electron-pair bonds to each of the cyclopentadienyl ligands, and the other ligands were bonded to the metal by one electron-pair bonds. The present scheme is consistent with the chemistry of these compounds. Thus, $(C_5H_5)TiCl_3$ can be readily prepared by the reaction of $(C_5H_5)_2TiCl_2$ and $TiCl_4$.[16]

Band Assignments.—The dipolar vector in C_{2v} symmetry encompasses the $A_1(\|)$, $B_2(\perp)$, and $B_1(\perp)$ representations. The possible transitions are

$$(\text{core})\,(b_1^{*1})^2(b_2^*)^2(a_2^*)^2\,A_1$$

$$\longrightarrow (\text{core})(b_2^*)^1(b_1^{*\prime})^2(a_2^*)^1(a_1^{**})^1\,A_2 \quad (12)$$

$$\longrightarrow (\text{core})(b_2^*)^2(b_1^{*\prime})^2(a_2^*)^1(b_2^{**})^1\,B_1 \quad (13)$$

$$\longrightarrow (\text{core})(b_2^*)^2(b_1^{*\prime})^1(a_2^*)^2(a_1^{**})^1\,B_1 \quad (14)$$

$$\longrightarrow (\text{core})(b_2^{*1})^2(b_1^{*\prime})^1(a_2^*)^2(b_2^{**})^1\,A_2 \quad (15)$$

$$\longrightarrow (\text{core})\,(b_2^*)^1(b_1^{*\prime})^2(a_2^*)^2(a_1^{**})^1\,B_2 \quad (16)$$

$$\longrightarrow (\text{core})\,(b_2^*)^1(b_1^{*\prime})^2(a_2^*)^2(b_2^{**})^1\,A_1 \quad (17)$$

Transitions 12 and 15 are symmetry forbidden, while the remainder are allowed transitions.

The longest wave length absorptions in $(C_5H_5)_2TiX_2$, band I, are found between 14.5 and 19.5 kK. They have extinction coefficients of about 200 [with the exception of $(C_5H_5)_2TiI_2$]. These absorptions are attributed to the forbidden transition 12. The higher extinction coefficient in the case of $(C_5H_5)_2TiI_2$ may be due to impurities or orbital mixings. As the (a_1^{**}) orbital is occupied in $(C_5H_5)_2VCl_2$, band I is absent in this compound.

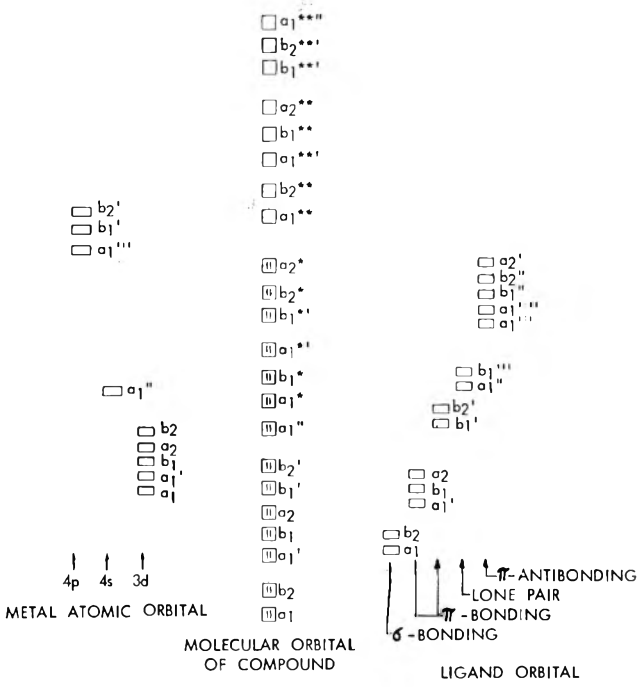

Fig. 5.—Schematic diagram of ligand orbitals involved in the metal–ligand bondings.

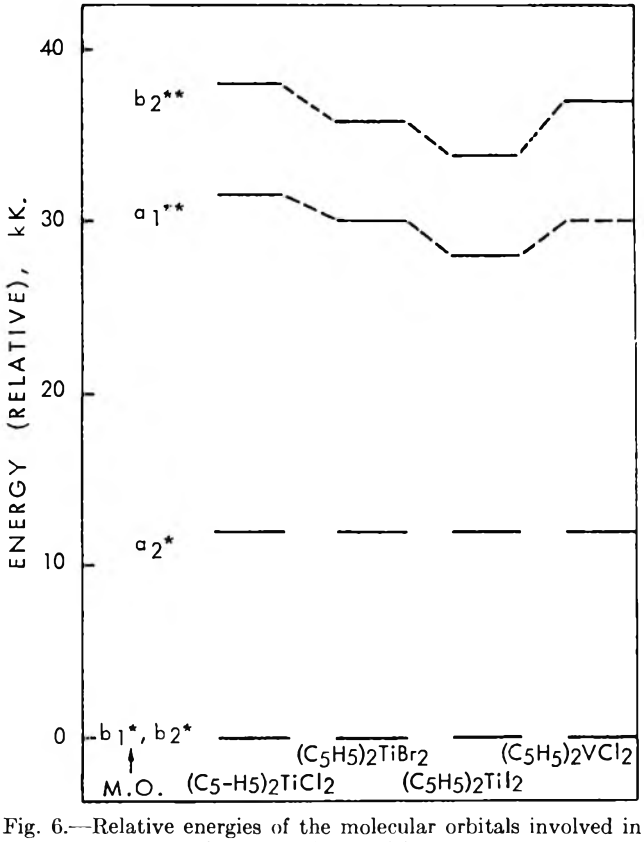

Fig. 6.—Relative energies of the molecular orbitals involved in the electronic transitions.

Band II appears between 20 and 26 kK. in all four compounds; the extinction coefficients are 5000–4000. This band is assigned to transition 13.

Band III is found between 27.5 and 31.5 kK. It is absent in $(C_5H_5)_2VCl_2$. This is attributed to transitions 14 and 16. The remaining band IV is assigned to transitions 15 and 17. From these transitions the relative energies of the molecular orbitals involved are

(14) J. C. W. Chien, *J. Am. Chem. Soc.*, **83**, 3767 (1961).
(15) C. J. Ballhausen and J. P. Dahl, *Acta Chem. Scand.*, **15**, 1333 (1961).
(16) R. D. Gorsich, *J. Am. Chem. Soc.*, **80**, 4744 (1958); C. C. Sloan and W. A. Barber, *ibid.*, **81**, 1364 (1959).

TABLE I

BAND ASSIGNMENTS FOR THE ELECTRONIC SPECTRUM OF $(C_5H_5)_2Fe$

Assignments	Intensity	Band position, kK. Obsd.	Calcd.
$^1A_{1g} \rightarrow (core)(a_{1g}')^2(e_{2g}^{\pm})^3(a_{1g}^*)^1\ ^1E_{2g}$	Symmetry and parity forbidden	0.56	0.65
$^1A_{1g} \rightarrow (core)(a_{1g}')^2(e_{2g}^{\pm})^3(a_{1u}^*)^1\ ^1E_{2u}$	Symmetry and parity forbidden	16.5	16.1
$^1A_{1g} \rightarrow (core)(a_{1g}')^1(e_{2g}^{\pm})^4(a_{1u}^*)^1\ ^1A_{1u}$	Symmetry forbidden	23.0	21.7
$^1A_{1g} \rightarrow (core)(a_{1g}')^2(e_{2g}^{\pm})^3(e^*_{1u}{}^{\pm})^1\ ^1E_{2u}$	Symmetry forbidden	31.0	31.3
$^1A_{1g} \rightarrow (core)(a_{1g}')^2(e_{2g}^{\pm})^3(e^*_{1u}{}^{\pm})^1\ ^1E_{1u}$	Allowed	38.0	37.0

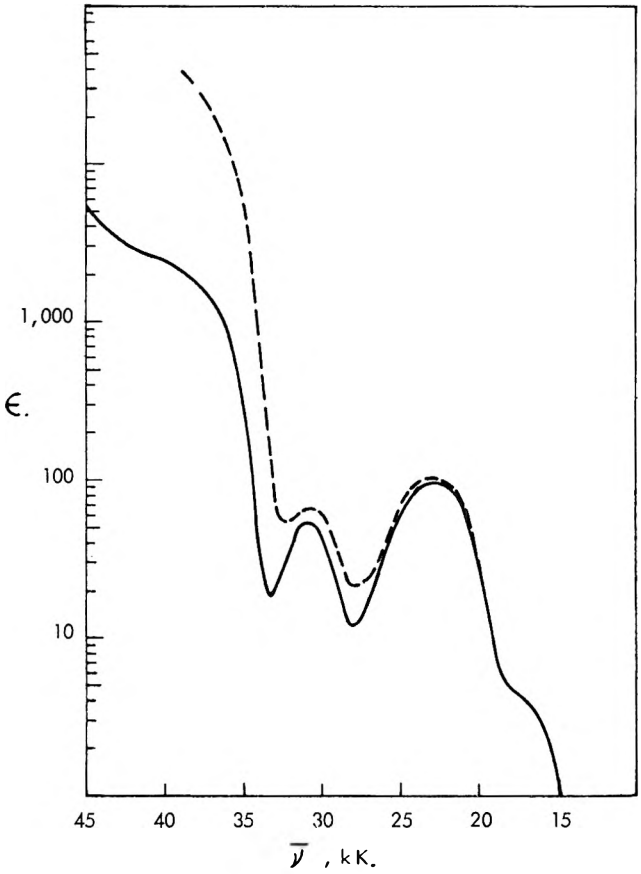

Fig. 7.—Electronic spectrum of $(C_5H_5)_2Fe$ in solvents: ———, ethanol–diethyl ether; – – – –, methylene chloride.

deduced and shown in Fig. 6. If the energies of the nonbonding molecular orbitals are assumed to be the same for the various halides, then the antibonding molecular orbitals decrease in energies in the series Cl, Br, I. It is concluded that the metal–ligand bonding orbitals have decreasing stability in the order Cl > Br > I.

Other experimental results support these band assignments. In particular, when $(C_5H_5)_2VCl_2$ is air-oxidized, presumably to $(C_5H_5)_2VOCl$, its electronic spectrum has, in addition to the absorption bands II and IV, new absorptions at 17.4 and 32.9 kK. corresponding to bands I and III, respectively. The spectrum is not included here because of the uncertainties in the composition and the concentration of the oxidation product.

Electronic Spectrum of Bis-(cyclopentadienyl)-iron.—Figure 7 contains the previously unreported spectra of $(C_5H_5)_2Fe$ in two solvents. The weak absorption at 0.56 kK. (ϵ 0.04) is not shown. These spectra are compared with the spectrum in ethanol. The spectra in ethanol and in diethyl ether are identical. In the CH_2Cl_2, the absorption intensity at 32 kK. is almost the same as those in nonhalogenated solvents. However, absorptions at wave lengths shorter than 32 kK. become very intense. This observation is consistent with the dissociative charge transfer absorption postulated by Brand and Snedden.[11] The shorter wave length observed here may be attributed to the less stable chloromethyl radical which is produced from methylene chloride.

Let us consider the electronic transitions in $(C_5H_5)_2Fe$ by assuming the ground state electronic structure to be $(a_{1g})^2(a_{1u})^2(e_{1g}^{\pm})^4(a_{1g}')^2(e_{1u}^{\pm})^4(e_{2g}^{\pm})^4\ ^1A_{1g}$ where the orbital notation is that of Linnett[3] and Shustorovich and Dyatkina.[6] By drawing appropriate correspondence between the molecular orbitals in $(C_5H_5)_2TiX_2$ and in $(C_5H_5)_2Fe$, and taking into account that the dipolar vectors in D_{5d} point group have $A_{2u}(\|)$ and $E_{1u}(\perp)$ representations, we arrive at the band assignments summarized in Table I. The calculated band position is that derived from the molecular orbital energy levels calculated by Yamazaki.[5]

Because of the close-lying positions of the $e_{1u}^{\pm}$ and the $e_{2g}^{\pm}$ orbitals, those transitions involving the $e_{2g}^{\pm}$ orbital are probably also accompanied by the other. The results are not appreciably altered.

The results showed that band assignments in the electronic spectrum of $(C_5H_5)_2Fe$ can be made which agree with the calculations of Yamazaki[5] and which are qualitatively compatible with the results of Dunitz and Orgel.[4] Both these treatments found that there is no appreciable admixing between the $e_{1u}^{\pm}$ orbitals of the ligands and the pe_{1u} orbitals of Fe and that the metal–ligand bondings involve essentially two bonding molecular orbitals per ligand. Similarly, the metal–ligand bondings in $(C_5H_5)_2MX_2$ involved two bonding molecular orbitals per ligand (*vide supra*).

A point of interest is the calculated charge density distribution in $(C_5H_5)_2Fe$. Shustorovich and Dyatkina[6] found a positive charge of 0.7 on Fe and argued that electrophilic substitution reactions of $(C_5H_5)_2Fe$ supported the results. Dahl and Ballhausen[7] found a negative charge of 0.7 on Fe and cited nucleophilic substitution reactions for support. They attributed the differences to the use by them of Watson's more contracted SCF iron atomic orbitals.[17] We question the merits of these comparisons. For instance, benzene derivatives containing either electron-donating groups or electron-withdrawing groups (such as the nitro group) undergo electrophilic substitution reactions. The donor–acceptor properties of these groups can be deduced only by comparing the relative rates of reactions of the substituted and unsubstituted benzenes. For the case in point, the comparison would have to be between the ligand without the metal and the or-

(17) R. E. Watson, *Phys. Rev.*, **119**, 1934 (1960).

ganometallic compound. Whereas this comparison is not possible when the ligand is cyclopentadienyl, it is possible when the ligand is benzene (such as dibenzenechromium).

The electronic spectra of other organometallic compounds and their complexes with aluminum halides will be the subject of another communication.

Acknowledgment.—The author is grateful to Drs. D. C. Lincoln and H. G. Tennent of these Laboratories for stimulating discussions.

ACRIDINE: A LOW TEMPERATURE INVESTIGATION OF ITS ENIGMATIC SPECTRAL CHARACTERISTICS[1a]

BY S. JULES LADNER[1b] AND RALPH S. BECKER

Department of Chemistry, University of Houston, Houston, Texas

Received May 11, 1963

The fluorescence spectrum of acridine, the N-heterocyclic analog of anthracene, is presented. The positions of the band maxima do not agree with those previously reported. Justification of the assignment of this emission as the intrinsic $\pi \leftarrow \pi^*$ fluorescence of acridine is given. This shows that acridine does not exhibit a lowest lying singlet excited state of n,π^* character. Evidence is presented which suggests the possibility that a three component complex, ethanol–acridine–solvent impurity, exists involving two different kinds of weak interactions. The complexes are discussed with regard to their bearing on the problem of acridine's intrinsic fluorescence.

Introduction

The existence of an intrinsic fluorescence for acridine, the N-heterocyclic analog of anthracene, has always been a subject of some uncertainty. Bertrand[2a] reported fluorescence from both acridine and its N-hydrochloride salt. Later, Harrell[2b] presented the fluorescence of acridine obtained from a solution in methylcyclohexane–ether, frozen at 77°K., presumably verifying the π,π^* nature of the lowest singlet excited state of acridine. Nevertheless, it has been suggested that acridine may not exhibit an intrinsic fluorescence. According to Bowen and Sahu,[3] acridine is nonfluorescent in most organic liquids, and any fluorescence which is observed is due to water impurity. Recently, McGlynn and co-workers,[4,5] in a study of photoconductivity, observed no fluorescence for crystalline acridine or for its solutions in benzene. They suggested that acridine may not possess a π,π^* lowest singlet excited state but rather an n,π^* lowest singlet excited state. The fluorescence obtained by Harrell[2b] was attributed to the reversal of the n,π^* and next lowest π,π^* singlet excited state by the presence of water as an impurity. Presumably, this would be similar to the situation in chlorophyll reported by Fernandez and Becker.[6] The quantum yield of fluorescence of $\sim 10^{-3}$ for acridine, reported by Sangster and Irvine[7] was also attributed to the presence of impurities.

The present study involves a careful investigation of the electronic spectral properties of acridine. This work consists primarily of low temperature (77°K.) electronic absorption and emission measurements on acridine, the acridine–ethanol hydrogen bonded system, and the acridine hydrochloride salt. Special attention has been given to the elimination of water and other impurities from the solvents and chemicals employed in this work.

Data will be presented which will establish the fact that acridine has an inherent fluorescence. This will be ascertained by consideration of the new experimental data coupled with correlative considerations among the different solvent systems noted in the previous paragraph. Also, comparisons of the results of our work with those of other investigations will be considered. In addition, evidence is presented for the formation of unusual complexes at low temperature. Though this phenomenon is interesting in its own regard, the precise nature of the complex has not been established. However, the phenomenon has been studied to the extent of establishing the existence of these complexes and the circumstances under which they arise. Comment will be made concerning their nature and also their bearing on the confusion which has existed with regard to the acridine fluorescence.

Experimental

The emission and most of the absorption spectra were obtained at liquid nitrogen temperature (77°K.) in either of two solvent systems which form clear glasses at this temperature: (1) EPA or (2) EI.[8] The isopentane (Phillips instrument grade) and the ether (Baker's A.R. grade), for the majority of the work, were purified by fractional distillation over calcium hydride. In addition, the isopentane was chromatographed by passing it through an activated silica gel column after distillation. Specially purified ether was prepared in the following manner. A 25% by volume middle-cut from the distillation described above was redistilled over sodium shavings. From the second distillation, only a 25% by volume middle portion was taken and it was used immediately. The pure, absolute ethanol (U.S.I.) was used without further purification.

The low temperature absorption spectra were recorded on a Baush and Lomb Spectronic 505 or on a Beckman Model DK-1 spectrophotometer. The technique employed the use of a Pyrex dewar with an unsilvered portion to admit the light beam. A Beckman Model DU was used to perform a Beer's law study of acridine.

Emission spectra were photographed on Kodak 103a-B and

(1) (a) Partially supported by a grant from the Department of Health, Education, and Welfare, No. 3133 BBC, held by Ralph S. Becker; (b) National Science Foundation Cooperative Graduate Fellow, June, 1960, to June, 1963. Part of a thesis to be submitted for partial fulfillment of the requirements for the Ph.D. degree, University of Houston.

(2) (a) D. Bertrand, *Bull. Soc. Chim.*, **12**, 1019 (1945); (b) R. W. Harrell, *Dissertation Abstr.*, **21**, 2476 (1961).

(3) E. J. Bowen and J. Sahu, *J. Chem. Soc.*, 3716 (1958); E. J. Bowen, N. J. Holder, and G. B. Woodger, *J. Phys. Chem.*, **66**, 2491 (1962).

(4) S. P. McGlynn, *J. Chem. Phys.*, **37**, 1825 (1962).

(5) M. Kleinerman, L. Azarraga, and S. P. McGlynn, "The Photoconductive and Emission Spectroscopic Properties of Organic Molecular Materials" in "Luminescence of Organic and Inorganic Materials," ed. by H. P. Kallman and G. M. Spruch, John Wiley and Sons, Inc., New York, N. Y., 1962, p. 196.

(6) J. Fernandez and R. S. Becker, *J. Chem. Phys.*, **31**, 467 (1959).

(7) R. C. Sangster and J. W. Irvine, Jr., *ibid.*, **24**, 670 (1956).

(8) D. R. Scott and J. B. Allison, *J. Phys. Chem.*, **66**, 561 (1962).

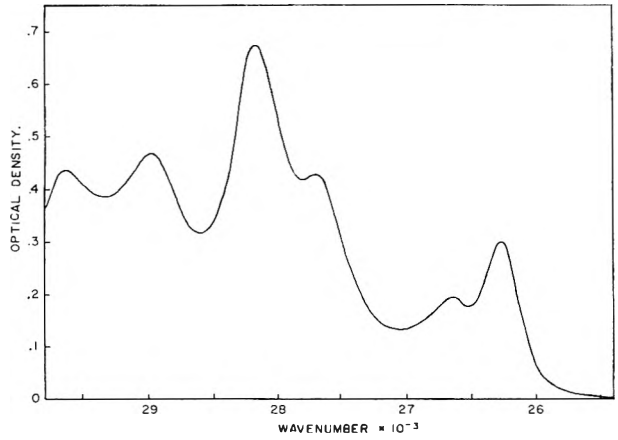

Fig. 1.—Absorption spectrum of acridine in EI (doubly distilled fresh ether) at 77°K.

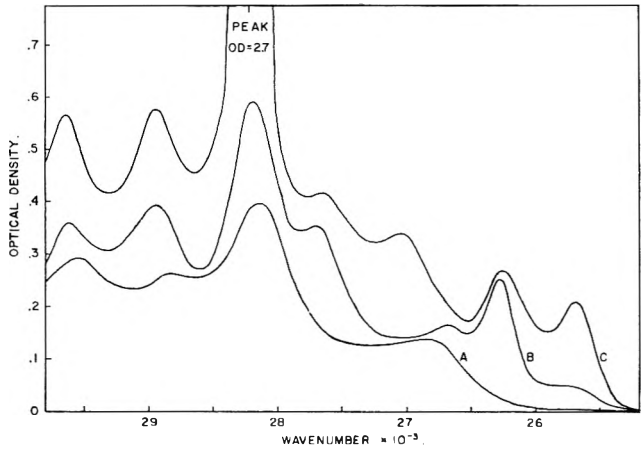

Fig. 2.—Absorption spectra of acridine in EI as a function of solvent age: A, room temperature, no dependence on solvent age; B, 77°K., ether 40 hr. old; C, 77°K., ether 96 hr. old; all concentrations are equal.

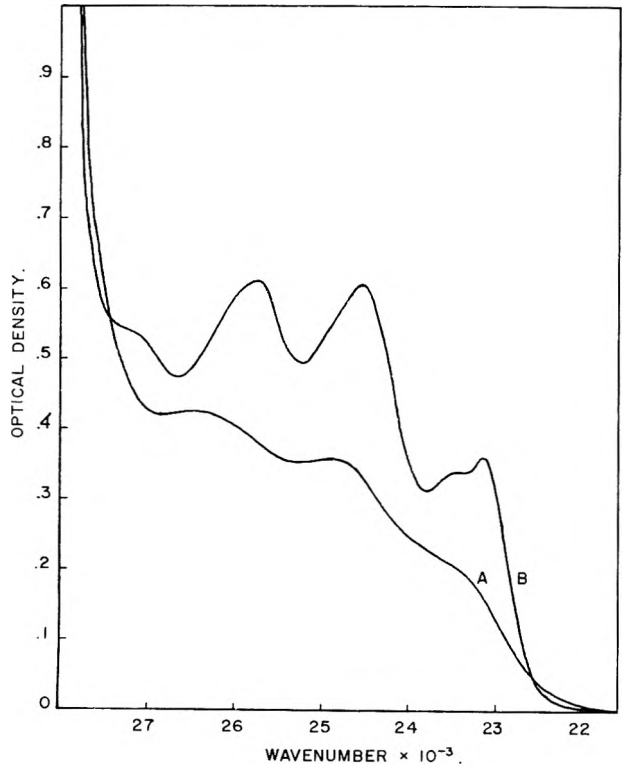

Fig. 3.—Absorption spectra of acridine hydrochloride in EPA (old solvent): A, room temperature; B, 77°K.; concentrations are equal.

103a-F spectroscopic plates employing a Hilger medium glass single prism spectrograph. A slit width of 0.1 mm. was used for all measurements. Exciting light was supplied by a Osram HBO, 100-watt, high pressure mercury lamp. Wave length selection was controlled by the use of a Baush and Lomb grating monochromator, and, in all cases, a band pass of 20 mμ was used. Spectral curves were obtained from the photographic plates by tracing them on an Applied Research Laboratories microphotometer.

Acridine was obtained from Matheson Coleman and Bell. It was purified by double sublimation under vacuum at temperatures of approximately 80°. The sublimations were carried out without the use of a cold finger to ensure that there would be no recondensation of any water which might have been present in the acridine. A sample of purified acridine was subjected to a gas chromatographic analysis which resulted in only one peak, inferring a very high degree of purity. This is further substantiated by the fact that a sample of zone refined anthracene gave one small impurity peak. All solutions of acridine were prepared immediately before use. Concentrations of approximately 10^{-4} M were employed for all absorption measurements, and concentrations ranging from 10^{-3} to 10^{-4} M were used for the emission work.

Acridine hydrochloride was prepared by passing anhydrous hydrogen chloride gas (Matheson Coleman and Bell) through a freshly prepared solution of acridine in EPA for a few seconds.

Results

Absorption Measurements.—Absorption measurements were made at various wave lengths within the first electronic absorption band system of acridine in isooctane with concentrations ranging from 10^{-3} to 10^{-5} M. Within this concentration range, it was found that Beer's law was obeyed.

The electronic absorption spectrum of acridine in EI (doubly distilled ether) frozen at 77°K., covering the spectral region from 25,000 to 30,000 cm.$^{-1}$, is presented in Fig. 1. This spectrum agrees regarding relative intensities and frequencies of absorption bands with that obtained by Wittwer and Zanker[9] except where these authors omitted the spectrum on the long wave length side of the lowest energy absorption band. The positions of the first few absorption band maxima are compiled in the first row of Table I. Figure 2 shows the variation of the absorption spectrum of acridine in EI with respect to the age of the solvent. The positions of the absorption band maxima of curve C are presented in the second row of Table I. It is important to note that: (1) the room temperature absorption spectrum is unaffected by the age of the solvent and (2) the new bands which appear in the low temperature spectrum with increasing solvent age are completely temperature dependent. They appear at low temperature with old ether and disappear as the temperature is raised or when highly purified fresh ether is used. To determine whether or not the presence of water could be responsible for these new bands, a small amount was added to a solution which had previously exhibited an intermediate intensity of the new absorption bands. This did not result in any change in the absorption spectrum.

The electronic absorption spectrum of the acridine–ethanol hydrogen bonded system in EPA (ether 96 hr. old) in the spectral region 25,000 to 29,400 cm.$^{-1}$ was obtained at 77°K. The positions of the band maxima are shown in the third row of Table I.

The electronic absorption spectrum of acridine hydrochloride in EPA (old) over the spectral region 22,000 to 27,800 cm.$^{-1}$ is shown in Fig. 3. Curve A represents

(9) A. Wittwer and V. Zanker, *Z. physik. Chem.* (Frankfurt), **22**, 417 (1959).

TABLE I

POSITIONS OF ABSORPTION BAND MAXIMA OF ACRIDINE, THE ETHANOL HYDROGEN-BONDED SYSTEM, AND ACRIDINE HYDROCHLORIDE OBTAINED FROM GLASSY SOLUTIONS AT 77°K.

Solvent system	Absorption band position, cm.$^{-1}$ 1′	1	2	3′	3	4	5 (max.)
			Acridine				
EI (freshly purified)	....	26,281	26,680		27,693		28,193
EI (96 hr. old)	25,686	26,267		27,078	27,675		28,225
EPA (old)	25,667	26,082		27,056	27,465		28,249
			Acridine-HCl				
EPA (old)	23,142	23,400			24,533	25,700	

TABLE II

POSITIONS OF THE FLUORESCENT BAND MAXIMA OF ACRIDINE, THE ETHANOL HYDROGEN-BONDED SYSTEM, AND ACRIDINE HYDROCHLORIDE OBTAINED FROM GLASSY SOLUTIONS AT 77°K.

Solvent system	Excitation wave length, mμ	Fluorescent band position, cm.$^{-1}$ 1	2	3	3′	4	(5)	6
				Acridine				
Methylcyclohexane–ether[a]	...	25,126	24,631	23,818		22,386		20,939
EI (freshly purified)	300	25,680	25,290	24,225		22,880		
EI (old)	300	25,570	25,070	24,155		22,830		(21,560)
EI (old)	395			23,755	23,390	22,473	22,050	21,100
EPA (old)	300		25,000	24,025		22,620		21,380
EPA (old)	395			23,835	(23,510)	22,500		21,250
				Acridine-HCl				
EPA (old)	400		22,340	21,350		20,030		19,055
EPA (old)	435		22,225	21,230		19,710		19,070

[a] Taken from R. W. Harrell.[2b]

the room temperature absorption, and curve B represents the spectrum obtained from the rigid glass at 77°K. Curve B is very similar to the low temperature spectrum of the acridine cation reported by Wittwer and Zanker,[9] except for the long wave length maximum at 23,142 cm.$^{-1}$. The positions of the absorption band maxima are collected in the fourth row of Table I.

Emission Measurements.—The fluorescent emission spectrum obtained from a 10^{-4} *M* solution of acridine in EI (doubly distilled ether) mixture, frozen at 77°K., is represented in Fig 4. This measurement was made immediately following the purification of the solvents and corresponds to the sample whose absorption spectrum is presented in Fig. 1. The low temperature emission is considered to be moderately strong in view of the short time required to photograph the emission at narrow slit widths. It is interesting to note that the intensity of the fluorescence was decreased 50- to 100-fold at room temperature. The positions of the principal band maxima are given in the second row of Table II. Figure 5 exhibits the variation of the fluorescence spectrum of acridine in EI (old ether) with respect to two different excitation conditions. The upper curve was obtained by exciting at 300 mμ, while the lower curve employed 395 mμ exciting light. Both spectra were recorded on the same photographic plate, using an approximately 2×10^{-4} *M* solution. The positions of the band maxima are compiled in the third and fourth rows of Table II.

The fluorescence spectra of the acridine–ethanol hydrogen bonded system were obtained from a 10^{-3} *M* solution in EPA (old) at 77°K. by exciting at 300 and 395 mμ. Both spectra were taken on the same photographic plate. The positions of the band maxima are shown in the fifth and sixth rows of Table II. Lastly, the fluorescence spectra of acridine hydrochloride in EPA (old solvent) were obtained at 77°K. from a 10^{-3} *M* solution by exciting at 400 and 435 mμ. A single photographic plate was employed for both spectra. The positions of the band maxima are shown in the seventh and eighth rows of Table II.

In all the cases mentioned above, the extreme long wave length excitation condition was such that the band-pass overlapped the long wave length half of the leading absorption band of the corresponding low temperature absorption spectrum.

We wish to point out that even though the differences involved between the emission spectra obtained at different excitation conditions are small in some cases, they are always reproducible. This fact establishes their existence.

Discussion

Zanker[10] assigned the first two long wave length transitions of acridine in alcohol, following Platt's nomenclature,[11,12] as corresponding to excitation to the ^1L_a and the ^1L_b states. In addition, the fluorescence spectra were given. The absorption maximum at 26,281 cm.$^{-1}$ (Fig. 1) was assigned as the 0–0 ^1L_a transition and the one at 28,193 cm.$^{-1}$ as the 0–0 of the ^1L_b transition. The lowest energy transtion, ^1L_a, tends to undergo more or less strong red shifts when the molecule is hydrogen bonded, protonated, or the temperature lowered. This feature will form the basis for the majority of the discussion which follows.

From a comparison between the spectral curves in Fig. 2, it is obvious that the modification of the absorption spectrum is due to the formation of a new specie at low temperature whose concentration is dependent on

(10) V. Zanker, *Z. physik. Chem.* (Frankfurt), **2**, 52 (1954).
(11) J. R. Platt, *J. Chem. Phys.*, **17**, 484 (1949).
(12) H. B. Klevens and J. R. Platt, *ibid.*, **17**, 470 (1949).

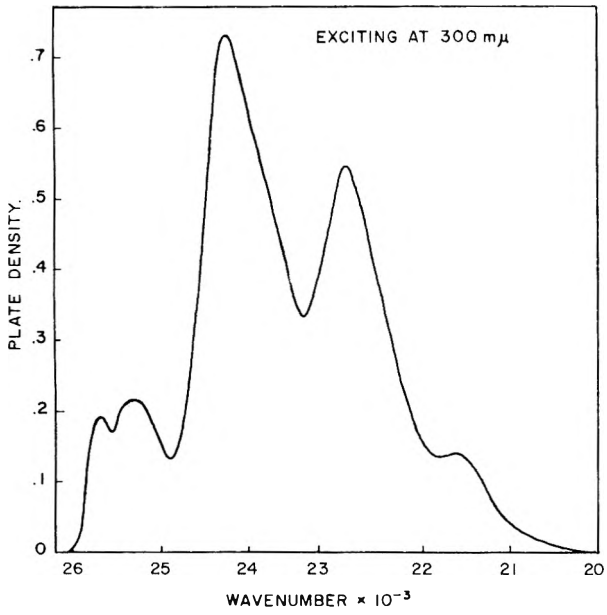

Fig. 4.—Fluorescent emission spectrum of acridine in EI (doubly distilled fresh ether) at 77°K.

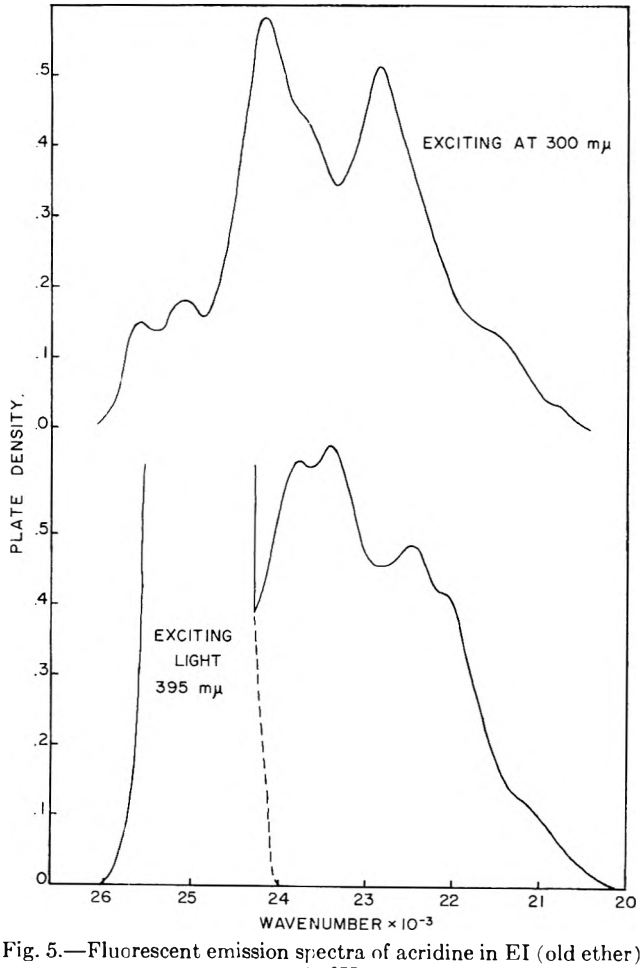

Fig. 5.—Fluorescent emission spectra of acridine in EI (old ether) at 77°K.

the age of the solvent. The absorption spectrum of this specie has the following features relative to acridine: (1) the ^1L_a transition has undergone a red shift; (2) the ^1L_b transition has undergone little or no shift; (3) the transition probability for the ^1L_b transition has increased by at least a factor of two, with a notable increase in the 0–0 band in the 28,200 cm.$^{-1}$ region. These features suggest that some of the acridine molecules have formed a complex with a solvent impurity at low temperature. The concentration of the impurity must increase as the solvent ages, since the intensity of the new absorption bands increases in that manner. As was noted in the Results section, this low-temperature complex does not involve the water molecule. In addition, a room temperature Beer's law study eliminated the possibility of dimer formation. Even though this was not done at low temperature, the fact that the spectral modifications are completely dependent upon the age of the solvent eliminates dimer formation as the cause of the change (see Fig. 1 and 2). Although we are still uncertain of the exact nature of this complex, the most likely possibility is an acridine–peroxide complex. The peroxide is formed from the ether simply by time and/or photoxidation.

The absorption spectrum of the acridine–ethanol hydrogen bonded system suggests that this system also undergoes additional complex formation at low temperature. We believe that the second and fourth band maxima at 26,082 and 27,465 cm.$^{-1}$, respectively, correspond to the hydrogen bonded specie, while the first and third bands at 25,667 and 27,056 cm.$^{-1}$, respectively, result from an additional complex specie (Table I). In this case the additional complex also depends on an impurity and may or may not involve the hydrogen bonded acridine molecule. Our analysis of the spectrum is consistent with Rammensee and Zanker,[13] who list 26,000 cm.$^{-1}$ for the position of the leading absorption band of acridine in ethanol at −180°. Similarly, the spectrum of the hydrochloride salt, Fig. 3, shows a leading absorption maximum at 23,142 cm.$^{-1}$ which is attributed as before to a complex specie which forms at low temperature. We feel that in this case it is certain that the new specie involves the hydrochloride salt and an impurity rather than acridine itself. This becomes obvious when one considers that the band occurs on the long wave length side of a band shifted approximately 3000 cm.$^{-1}$ to the red, which shift results specifically upon salt formation.

The fluorescence spectra appropriate to each case were also recorded. Acridine in EI (old) is shown in Fig. 5. Band positions for the other cases are given in Table II and Fig. 6. In each of the three cases, the first fluorescence probably corresponds to acridine, acridine–ethanol, or the hydrochloride. The second fluorescences, resulting from selective excitation into the leading absorption bands, we attribute to the complex species. The differences between each pair of fluorescence spectra as well as the relationships between those of the different cases are shown in Fig. 6. As we have stated previously, even though the differences are small between some cases, they are completely reproducible.

The case of the acridine–ethanol hydrogen bonded system is complicated in that it is difficult to decide what specie is responsible for the shifted absorption and emission. The fact that the leading absorption band at 25,667 cm.$^{-1}$ coincides with that for acridine in EI, 25,686 cm.$^{-1}$, suggests that the acridine–impurity complex, rather than a three-component acridine–ethanol–impurity specie, is responsible. However, the fact that a three-component system does exist in the case of acridine hydrochloride certainly insinuates the possibility of the latter. Nevertheless, we can say that in

(13) Von H. Rammensee and V. Zanker, *Z. Angew. Phys.*, **12**, 237 (1960).

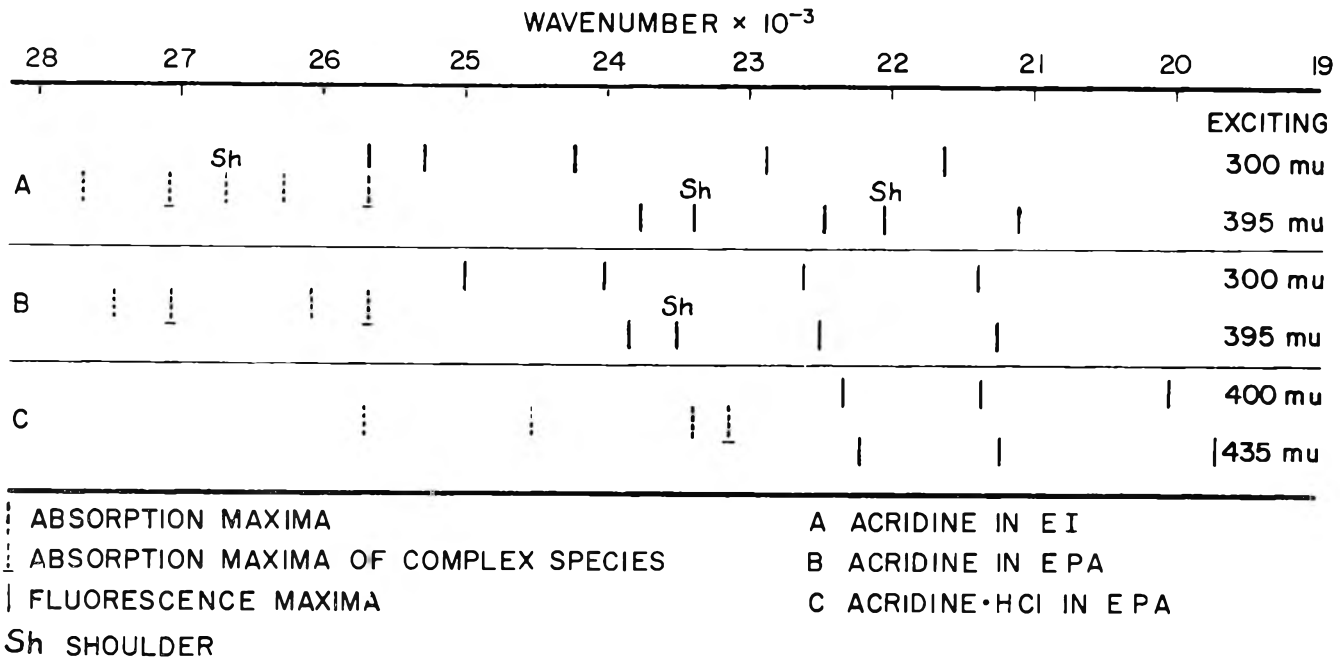

Fig. 6.—Correlation diagram of the low-temperature absorption and emission spectra of acridine and complexes.

the case of the hydrochloride salt the interaction with the solvent impurity does not occur *via* a hydrogen bonding mechanism, since the nitrogen nonbonding electrons of acridine are already involved in the bonding between acridine and the HCl molecule. This fact implies the possibility that the interaction between the solvent impurity with acridine and, possibly, with the acridine–ethanol hydrogen bonded system is also some nonhydrogen-bonding type interaction. This could, of course, lead to some interesting considerations. We would comment that a three-component system involving two different interactions does not seem unusual in the light of recent work by Allison.[14] He reported that "acridine acetate" (acridine in the presence of acetic acid) forms complexes with certain donor-type compounds. He suggests that acridine's electron affinity is greatly altered by its interaction *via* the nitrogen atom with acetic acid. The over-all picture of the relationships between the absorption spectra and fluorescence spectra for the different cases can be seen more clearly by referring to the correlation diagram given in Fig. 6.

We believe that the moderately strong emission spectrum presented in Fig. 4 represents the inherent fluorescent emission of the acridine molecule. The fluorescence obtained differs from that given by Harrell[2b] in that it lies approximately 500 cm.$^{-1}$ farther to the blue (see Table II). However, the general features of both emission spectra are the same. The difference in solvents could hardly be responsible for the energy separation, since we employed ether–isopentane and Harrell used methylcyclohexane–ether. We will make no further comment on this difference except to say that of the two emissions, our origin lies closest to the corresponding true low temperature absorption origin.

To justify the premise that the emission we have obtained is truly intrinsic to acridine, we first wish to mention the high degree of purity of the sample and solvents as earlier described. The low temperature absorption spectrum employing the purified solvents (Fig. 1) was recorded immediately after purification. In this spectrum the absorption bands belonging to the acridine–impurity complex did not appear. Immediately following the absorption measurement, the fluorescence spectrum shown in Fig. 4 was recorded. Though more clearly resolved, the intensity of this fluorescence was observed to be equivalent to that obtained from solutions of equal concentration in old solvents when exciting at 300 mμ. The two leading bands at 25,680 and 25,290 cm.$^{-1}$ in the fluorescence spectrum obtained using fresh solvents are shifted slightly blue of those in the spectrum obtained with old solvents. This is easily explained by the fact that the leading absorption band of the complex specie, which forms in the solutions made with old solvents, lies on top of the 25,680 cm.$^{-1}$ leading fluorescent band (Fig. 6 or compare curve C of Fig. 2 with Fig. 4). The result is strong re-absorption and consequential modification of the two leading fluorescent bands.

Other strong evidence in favor of identifying the fluorescence of Fig. 4 as the intrinsic fluorescence of acridine results from a comparison of shifts of the absorption bands with the shifts of the emission bands as the solvent is changed from EI to EPA. The fluorescent emission of the acridine–ethanol hydrogen bonded specie has band maxima at 24,025 and 22,620 cm.$^{-1}$ which agree with those given by Kochemirovskii and Reznikova.[15] The general features of the fluorescence match those of the fluorescence spectrum shown in Fig. 4 except for two points: (1) the first band seems to be missing in the case of the hydrogen-bonded acridine and (2) the remaining bands are red shifted by approximately 200 cm.$^{-1}$ (see Fig. 6). The missing band is probably due to re-absorption by the leading absorption band of the impurity complex specie as mentioned above. In absorption, the two leading bands at 26,281 and 27,693 cm.$^{-1}$ of acridine are also red shifted approximately 200 cm.$^{-1}$ to 26,082 and 27,465 cm.$^{-1}$ for the acridine–ethanol hydrogen-bonded system. This equality of the absorption band shifts with the shifts of

(14) A. C. Allison, *Nature*, **195**, 994 (1962).

(15) A. S. Kochemirovskii and I. I. Reznikova, *Opt. and Spectry.*, **8**, 206 (1960).

the emission bands certainly implies that the fluorescence spectrum (Fig. 4) belongs to acridine (Fig. 1). Moreover, the above argument also implies that the acridine was free from hydrogen bonded water, since, if that were not the case, the addition of ethanol would not be expected to result in further red shifts in the absorption and emission spectra.

Finally, we wish to note the mirror image relationship which exists between the fluorescence (Fig. 4) and the portion of the absorption spectrum (Fig. 1) corresponding to the longest wave length transition. This relationship is more easily seen by referring to the absorption spectrum for acridine hydrochloride (Fig. 3) in which more of this transition is exposed. The mirror image relationship would not be expected to exist if emission occurred from a lower lying n,π^* state. Thus, the possibility of fluorescence from an n,π^* state to the red of the ^1L_a state can be eliminated.

The only basis for expecting acridine not to exhibit a fluorescent emission would be that conversion of the excited molecule to a triplet state or internal conversion were so highly probable that the normal fluorescence could not compete. Under the circumstance, one might expect to see a reasonable intensity of phosphorescence. However, such is not the case, since experiment has shown the acridine phosphorescence to be very weak.[2b] Nevertheless, the argument could be kept intact if a reason for high conversion to a triplet state could be provided, accompanied by a strong internal conversion mode out of the triplet. Such a reason would exist if acridine exhibited a lowest singlet excited state of n, π^* character. This usually results in complete conversion to the triplet state. However, recent experimental work by Coppens, Gillet, Nasielski, and Donckt[16] places the n,π^* state at 360 mμ, well above the 0–0 vibrational level of the ^1L_a state of acridine. Also, this investigation points to the fact that no n,π^* state is below a π,π^* one. In addition, Bennett[17] performed lifetime measurements on the emission of acridine in a water solution and observed two exponential decays of 3.8×10^{-9} sec. and 4.3×10^{-8} sec. He attributed, *via* chemical evidence, the longer lifetime to the acridine cation and the shorter one to the acridine molecule. Thus, both the negative arguments and the positive results of Bennett give strong indication that an intrinsic fluorescence should exist for acridine. This is, of course, in agreement with the results of this investigation.

(16) G. Coppens, C. Gillet, J. Nasielski, and E. V. Donckt, *Spectrochim. Acta*, **18**, 1441 (1962).

(17) R. G. Bennett, *Rev. Sci. Instr.*, **31**, 1275 (1960).

Conclusion

The acridine molecule has a moderately strong inherent fluorescence. We feel that substantial evidence has been provided to justify its identification as such. It has been shown that the intrinsic fluorescence of acridine can be associated with the longest wave length ($\pi \rightarrow \pi^*$) electronic transition. This and more specifically the mirror image relationship allows us to conclude that acridine does not exhibit a lowest lying n,π^* electronic excited state.

The extreme sensitivity of acridine to solvent impurities, mentioned above, has been clearly illustrated in this study by the observed formation of complexes at low temperature between acridine and a solvent impurity other than water. Both the shifted absorption spectra and fluorescence spectra of these complexes have been presented. Such data in the case of acridine hydrochloride strongly suggest that these complexes are not formed *via* hydrogen bonding type interaction. The acridine hydrochloride case further suggests that for the solutions of acridine in EPA at 77°K., the observed complex specie involves the acridine–ethanol hydrogen-bonded system. This would mean that the three-component complex (acridine, ethanol, and solvent impurity) results from two different weak interactions. Parallel type complexes have been reported earlier. The complexes appear to involve peroxides.

Acknowledgments.—We wish to thank Dr. R. W. Harrell of E. I. Dupont for first suggesting that a further study of acridine would be interesting and for helpful discussions concerning it.

NOTES

CONFORMATIONS OF ACETANILIDE AND N-METHYLACETANILIDE[1]

By H. Bradford Thompson and Karen M. Hallberg

Alfred Nobel Science Laboratories, Gustavus Adolphus College, St. Peter, Minnesota

Received April 16, 1963

The question of the stable conformation(s) in acetanilides has interested several investigators.[2,3] There is evidence that one planar or nearly planar structure predominates.[3] By comparison of the electric dipole moment of acetanilide with *p*-bromoacetanilide, the relative position of the carbonyl and the aromatic ring should be indicated readily. Results of this study and of a similar investigation for methylacetanilide are reported in Table I.

Table I

Electric Dipole Moments

Compound	M.p., °C.	Electric moments: S^a	This study	Smith[b]
Acetanilide	114°	102.5	3.88	3.65
p-Bromoacetanilide	167.5–167.8	136.2	4.47	4.36
N-Methylacetanilide	104.0–104.4	87.2	3.57	
p-Bromo-N-methylacetanilide	97.5–97.8	36.8	2.32	
Bromobenzene		15.0	1.48	

[a] Slope for $(\epsilon - n^2)/(\epsilon + 2)(n^2 + 2)$ *vs.* molar concentration. See ref. 7 and 8. [b] See ref. 2.

The acetanilide case has been studied using electric dipole moments by Smith,[2] whose data are included

(1) The aid of the National Science Foundation through a basic research grant and through an undergraduate research participation program supporting K. M. H. is gratefully acknowledged. We wish to thank Dr. Columba Curran, who, as referee for this paper, made a number of helpful suggestions.

(2) J. W. Smith, *J. Chem. Soc.*, 4700 (1961).

(3) R. A. Russell and H. W. Thompson, *Spectrochim. Acta*, **8**, 138 (1956).

for comparison in Table I. Smith chose to analyze the results in terms of group moments for the carbonyl (from acetone) and amine (from aniline) groups. From these and the observed moments for acetanilide and related compounds he deduces the angle of rotation about the N–CO bond. Several assumptions are necessary in this approach: the geometry about the nitrogen must be the same in amine and amide; the moment associated with the lone pair on the amine nitrogen must be retained in the amide; and the resonance structure II must make a very limited contribution. Alternatively, we have chosen to assume that the moment

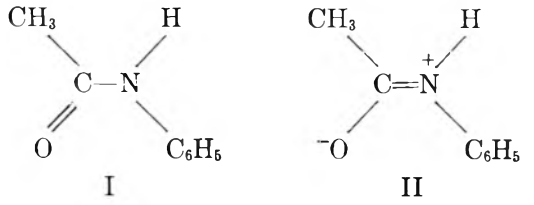

of *p*-bromoacetanilide differs from that of acetanilide by the vector addition of 1.49 D. in the direction of the C–Br bond. We have assumed the acetanilide moment to be at an angle of about 130° from the N–CO bond, and nearly parallel to the C=O bond, as shown in Fig. 1a. This angle may be deduced from the bond moments employed by Kotera, Shibata, and Sone.[4] Since the C=O moment is certainly the largest contributor in acetanilide, this orientation is probably not greatly in error. The moment according to Smith would be at a significantly smaller angle and would not lie in the OCN plane. However, even this moment would not qualitatively alter the argument to follow.

If acetanilide has the planar structure commonly assumed for the amide group,[5] or if (like formamide[6]) it is only slightly nonplanar, then the moment of *p*-bromoacetanilide should be predicted by one of the two vector drawings in Fig. 1a; the structure with the ring *cis* to the oxygen best matches the data. This is the conformation found by Brown and Corbridge to be stable in the solid.[7] Since the solid structure involved intermolecular hydrogen bonding, it was not obvious that the same conformation would be most stable in solution. Brown and Corbridge found a dihedral angle of 37° between the plane of the ring and that of the acetyl; this appears to arise from steric repulsion and may well be retained in solution. However, unlike the rotation about the OC–N bond assumed by Smith, the rotation in the crystal is about the C_6H_5–N bond; that is, a tilting of the ring. This would have little effect on the electric moment.

The difference between Smith's moments and those reported here may be due to the choice of solvent. Smith used benzene; we chose dioxane, since monosubstituted amides may form hydrogen-bonded dimers in benzene. Hydrogen bonding to the solvent seemed preferable, since this should vary little between the compounds being compared. Smith's data would lead to the same conclusion as ours when similarly analyzed.

The reverse situation clearly holds in N-methyl-

(4) A. Kotera, S. Shibata, and K. Sone, *J. Am. Chem. Soc.*, **77**, 6183 (1955); the exact direction predicted would depend on the conformation: 125° for the hydrogen *trans* to the carbonyl, 137° for the ring *trans*.

(5) L. Pauling, "The Nature of the Chemical Bond," 3rd Ed., Cornell University Press, Ithaca, N. Y., 1960, p. 281.

(6) C. C. Costain and J. M. Dowling, *J. Chem. Phys.*, **32**, 158 (1960).

(7) C. J. Brown and D. E. C. Corbridge, *Acta Cryst.*, **7**, 711 (1954).

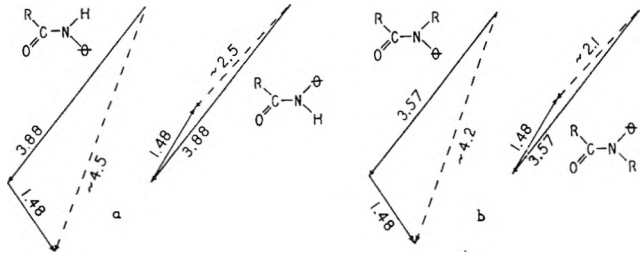

Fig. 1.—Vector addition of component electric moments: a, *p*-bromoacetanilide; b, *p*-bromo-N-methylacetanilide. Solid arrows are component moments; broken arrows are predicted molecular moments.

acetanilide. From Fig. 1b, our experimental moment of 2.32 D. corresponds to the structure with ring and oxygen *trans*. This result appears surprising at first; however, infrared studies[3] on monosubstituted formamides and acetamides have indicated that the tendency of an N-methyl group to take up the position *cis* to the oxygen is stronger than that of an N-phenyl.

Experimental

Electric moments were determined in dioxane solution by Guggenheim's method.[8] Procedure and solvent purification have been described previously.[9]

Commercial acetanilide and *p*-bromoacetanilide were recrystallized from benzene. N-Methylacetanilide was prepared by addition of acetyl chloride to chilled methylaniline in benzene. The unchanged acetyl chloride was distilled off, the crystalline product dissolved by heating, and the solution filtered and cooled. A sample of the solid product was recrystallized repeatedly from benzene and used for the electric moment measurement. A portion of the remainder was brominated by the procedure of Ashley and Berg[10] and the product recrystallized from petroleum ether. Each solid was dried for several hours in a vacuum oven before solutions were prepared. Melting points of the samples used are included in Table I.

Commercial bromobenzene was distilled twice in a small fractionating column and the product dried over $CaCl_2$; b.p. 155.3–155.5° (740 mm.), $n^{25}D$ 1.5575, d^{25}_4 1.4909.

(8) E. A. Guggenheim, *Trans. Faraday Soc.*, **45**, 714 (1949).

(9) H. B. Thompson, L. Eberson, and J. V. Dahlen, *J. Phys. Chem.*, **66**, 1634 (1962).

(10) J. N. Ashley and S. Berg, *J. Chem. Soc.*, 3089 (1957).

ACID–BASE REACTIONS IN FUSED SALTS. THE DICHROMATE–BROMATE REACTION[1]

BY F. R. DUKE AND JAMES SCHLEGEL

Institute for Atomic Research and Department of Chemistry Iowa State University, Ames, Iowa

Received April 29, 1963

Some equilibrium studies of Lewis acids and bases in fused alkali nitrates have been made in which $Cr_2O_7^{-2}$ was used as an acid, and others in which BrO_3^- was used as a base. In the first case, $Cr_2O_7^{-2}$ was allowed to react with nitrate to form NO_2^+.[2] In the second case, a heavy metal ion was added with BrO_3^- and the decomposition of the metal–bromate complex was studied.[3] When a divalent metal ion reacts with bromate, the metal–bromate complex, $MBrO_3^+$, is formed and slowly decomposes. This was postulated on the basis that the rate of decomposition varies with metal ion used. However, if one uses $Cr_2O_7^{-2}$ as an acid, no complex is formed, and BrO_2^+ is the probable equilibrium product with bromate present. Thus, a direct com-

(1) Contribution No. 1279; work was performed in the Ames Laboratory of the U. S. Atomic Energy Commission.

(2) F. R. Duke and M. Iverson, *J. Phys. Chem.*, **62**, 417 (1958).

(3) F. R. Duke and W. W. Lawrence, *J. Am. Chem. Soc.*, **83**, 1271 (1961).

parison of the relative acidities of BrO_2^+ and NO_2^+ in fused KNO_3–$NaNO_3$ could be made provided no oxides of nitrogen are formed during the course of the $Cr_2O_7^{-2}$ + BrO_3^- reaction. This turned out to be the case. The reactions involved are

$$Cr_2O_7^{-2} + BrO_3^- \overset{K}{\rightleftharpoons} BrO_2^+ + 2CrO_4^{-2}$$

$$BrO_2^+ \overset{k}{\longrightarrow} \text{products } (Br_2 + O_2)$$

Experimental

Materials and Apparatus.—A.C.S. reagent grade chemicals were used. All determinations were performed using a system similar to that described by Duke and Lawrence.[3]

Procedure.—$K_2Cr_2O_7$ was added to a solution of $Ba(NO_3)_2$ and $NaBrO_3$ in fused KNO_3–$NaNO_3$ solvent. The rate of reaction was studied by collecting evolved bromine in a sulfit solution and titrating with standard $AgNO_3$ using eosin as an indicator. The reaction was allowed to go to near completion. The rate of appearance of bromine was determined, and from this the rate of disappearance of total bromate (*i.e.*, $T_{Br} = BrO_3^- + BrO_2^+$) may be calculated. The concentrations of dichromate and barium ions were always in excess of bromate; however, barium ion concentration was varied from run to run to enable separation of the equilibrium constant from the rate constant. In all cases concentrations are expressed in molality units.

Results and Discussion

Preliminary runs allowed selection of proper temperature and concentration ranges for convenient study. The Ba^{+2}, because it precipitates the chromate ion but not the dichromate ion, controls the concentration of chromate through the solubility product. The experimental data gave a first-order plot in disappearance of total bromate, indicating decomposition of bromyl ion by some first-order mechanism to bromine and oxygen. Varying the rate of the sweep gas, nitrogen, had no effect on the rate of the reaction; therefore, there appears to be no gaseous intermediate as found in the nitrate reaction.[2]

Upon substitution $[BrO_3^-] = T_{Br} - [BrO_2^+]$ into the equilibrium expression and replacing BrO_2^+ in $-dT_{Br}/dt = k[BrO_2^+]$ one obtains an expression

$$-\frac{dT_{Br}}{dt} = \frac{kK[Cr_2O_7^{-2}]}{K[Cr_2O_7^{-2}] + [CrO_4^-]^2} T_{Br}$$

Using the solubility product for $BaCrO_4$, K_{sp}, one obtains

$$-\frac{dT_{Br}}{dt} = \frac{kK[Cr_2O_7^-][Ba^{+2}]^2}{K[Cr_2O_7^{-2}][Ba^{+2}]^2 + K_{sp}^2} T_{Br}$$

Since $[Cr_2O_7^{-2}]$ and $[Ba^{+2}]$ are in excess

$$k' = \frac{kK[Cr_2O_7^{-2}][Ba^{+2}]^2}{K[Cr_2O_7^{-2}][Ba^+]^2 + K_{sp}^2}$$

the pseudo rate constant, remains constant for a given run.

The reciprocal of k' is

$$1/k' = 1/k + \frac{K_{sp}^2}{kK[Cr_2O_7^{-2}]} \frac{1}{[Ba^{+2}]^2}$$

A plot of $1/k'$ *vs.* $1/[Ba^{+2}]^2$ gives a straight line from which k and K are evaluated.

The reaction was studied at 230, 250, and 260°. The pseudo-first-order rate constants obtained from ln T_{Br} *vs.* time plots are listed in Table I. Solubility data of $BaCrO_4$ in $NaNO_3$–KNO_3 solvent are listed in Table II. The solubility appeared to be independent of the relative amounts of potassium ion and sodium ion present but varied with temperature to give a straight line when the log of the solubility was plotted against reciprocal temperature. Table III lists the temperature dependence of the equilibrium constant and the rate constant to give the ΔH of reaction as 65 kcal. and activation energy as 55 kcal., respectively. Also both constants varied with cation ratio of the solvent. The values obtained for variation in solvent are listed in Table IV.

TABLE I

VARIATION OF RECIPROCAL PSEUDO RATE CONSTANT WITH BARIUM ION CONCENTRATION $[Cr_2O_7^{-2}] = 0.1\ m$

T, °C.	$1/k'$	$[Ba^{+2}]$
230	10.5	0.10
	50.8	.025
	76.	.020
250	5.13	.070
	6.65	.050
	12.7	.030
	17.	.025
260	2.2	.10
	4.1	.05
	8.5	.03
	14.	.02

TABLE II

SOLUBILITY OF $BaCrO_4$ IN EQUIMOLAR MIXTURE OF KNO_3 AND $NaNO_3$

T, °K.	Solubility, m
532	2.0×10^{-3}
522	1.8×10^{-3}
512	1.6×10^{-3}

TABLE III

EQUILIBRIUM AND RATE CONSTANTS AS A FUNCTION OF TEMPERATURE

T, °K.	k, min.$^{-1}$	K, mole^{-1}
503	0.13	1.05×10^{-8}
523	.33	3.50×10^{-8}
533	.58	4.80×10^{-8}

TABLE IV

VARIATION IN RATE AND EQUILIBRIUM CONSTANTS WITH SOLVENT COMPOSITION AT 250°

Cation ratio (K/Na)	k, min.$^{-1}$	K, mole^{-1}
60/40	0.30	3.2×10^{-8}
50/50	.33	3.5×10^{-8}
38/62	.38	4.8×10^{-8}

THERMOPOTENTIAL MEASUREMENTS FOR MOLTEN CADMIUM CHLORIDE, CADMIUM BROMIDE, AND LEAD CHLORIDE

BY JACOB GREENBERG, DONALD E. WEBER, AND LAWRENCE H. TEALLER

Lewis Research Center, National Aeronautics and Space Administration, Cleveland, Ohio

Received May 1, 1963

In order to obtain some information concerning the possible use of molten salts as thermoelectric materials, the thermopotentials developed when molten $CdCl_2$, $CdBr_2$, and $PbCl_2$ are subjected to a thermal gradient were measured. These fused salts were pipetted into a Vycor U-tube, the two arms of which were heated to two different temperatures. The open-circuit voltage,

which was recorded as a function of the temperature difference at the electrodes, was directly proportional to this temperature difference and appeared to be independent of the average temperature for the range and the temperature differences observed. It can be shown that the thermopotential is a function of the reduced heats of transfer and the transport numbers of the species involved. By using this relation, it is possible to estimate the entropy of transport for the salts.

Experimental

A piece of 8-mm. i.d. Vycor tubing was bent to form a U-tube approximately 13 cm. in length with side arms that were 7 cm. long. The tube then was uniformly wrapped with nichrome ribbon and covered with Alundum cement. One side arm was then wound again with the nichrome and another layer of Alundum cement applied. The cell was heated by the use of two Variacs connected to the nichrome windings. After the cell had been heated to some temperature above the melting point, the salt was pipetted into it. Two platinum–platinum-13% rhodium thermocouples with 5-mm. platinum disks welded to the tips then were inserted into predetermined positions in the melt. The Variac settings were adjusted for an approximate temperature gradient, and the cell was allowed to reach a steady-state condition for several hours. Reagent grade salts were melted, washed with the appropriate halide gas, and filtered through Pyrex glass wool before being pipetted into the cell.

Each datum point represents at least five readings taken at 20-min. intervals. The data were considered significant if the temperatures did not vary by more than 0.1% and if the open-circuit voltage did not vary by more than 1%. The voltage readings were made from the platinum leads of the thermocouples by means of a K-3 Leeds and Northrup potentiometer with an electronic galvanometer.

Results

The open-circuit voltage observed was directly proportional to the temperature difference at the electrodes and appeared to be independent of the average temperature for the temperature differences and range observed. The higher temperature electrode had a negative polarity. The plot of the thermopotentials observed against the temperature gradient, shown in Fig. 1, indicates a linear relation, which extrapolates to zero voltage at zero temperature change for the cadmium systems. At higher values of ΔT, the potentials observed for the lead chloride system showed positive deviations from linearity. The slope of the $PbCl_2$ system was estimated from the first three points closest to the origin. These results are summarized in Table I. The primary sources of error were the failure of the systems to reach steady-state temperatures under the experimental conditions and the possibility of reactions at the electrodes.

TABLE I

THERMOPOTENTIAL DATA FOR MOLTEN $CdCl_2$, $CdBr_2$, AND $PbCl_2$

Salt	Range of av. temp., °C.	Seebeck coefficient, $S = \frac{E_{DC}}{\Delta T} = \frac{\Delta\Phi}{\Delta T}$, mv./°C.	% deviation in S
$CdCl_2$	617–751	0.600	±0.96
$CdBr_2$	594–701	.846	± .25
$PbCl_2$	529–594	.349	± .43

The general equation for the potential of a thermocell has been given by deGroot[1] and has been interpreted for molten salt systems by Sundheim.[2] This equation is

$$F\frac{\Delta\Phi}{\Delta T} = -\sum_k \left(\frac{t_k}{z_k}\right)\frac{Q_k^{**}}{T} - \Delta S - \frac{Q_{el}^{**}}{T} \quad (1)$$

F = 1 faraday
$\Delta\Phi$ = open-circuit voltage
t_k = transference number of species k
z_k = algebraic valence
Q_k^{**} = reduced heat of transport, $T(S_k^* - S_k)$
S_k^* = entropy of transport of species k
S_k = partial entropy of species k
ΔS = change in entropy due to heterogeneous electrode reaction when 1 faraday of electricity has passed through cell
Q_{el}^{**} = reduced heat of transport of electrons in electrodes

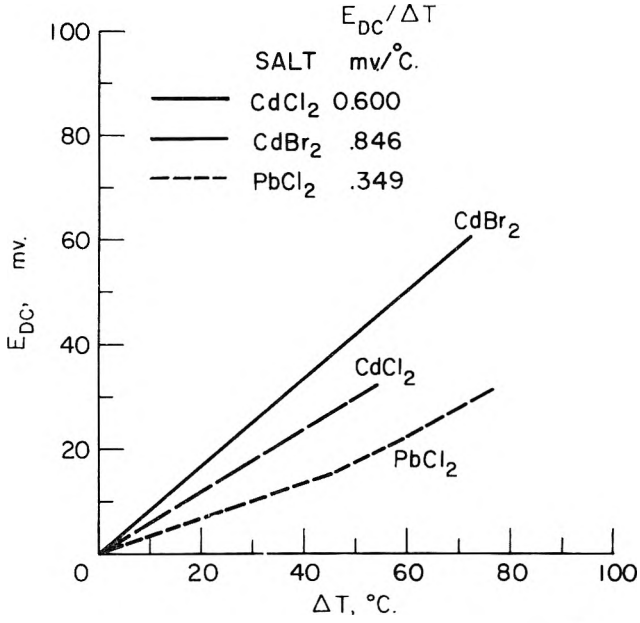

Fig. 1.—Plot of thermopotentials of fused $CdCl_2$, $CdBr_2$, and $PbCl_2$.

Since Q_{el}^{**}/T will be at least an order of magnitude lower than the other values, we can consider its effect as being negligible. The value of ΔS is defined as the change in entropy due to the heterogeneous electrode reaction when 1 faraday of electricity has passed through the cell. In our case, this value would represent the change in entropy due to the decomposition of the salt into its elemental components. In essence, ΔS refers to the difference in entropy of the ions as they exist in the liquid phase and at the electrode. This contribution will not be zero at vanishing ΔT if the decomposition products are present at the electrodes. The presence of two platinum electrodes immersed in a molten salt constitutes a decomposition cell. Electrolysis of the salt will occur when, in the process of determining the potential of the cell, the e.m.f. applied by the potentiometer is either above or below that of the salt itself. When the e.m.f. of the potentiometer is above that of the thermopotential of molten $PbCl_2$, for example, lead will be deposited at one electrode and chlorine released at the other. In the case where the voltage applied is below that of the salt system, the release of decomposition products will be reversed and therefore tend to cancel the previous deposits. In the event that there remains an excess of electrolysis products, these are soluble in the melt and will have a tendency to diffuse from the electrodes. The presence of these products is easily detected since their accumulation at the electrodes will create a back e.m.f. This effect will lower the readings observed and eventually

(1) H. Holtan, P. Mazur, and S. R. deGroot, *Physica*, **19**, 1109 (1953).
(2) B. R. Sundheim and J. Rosenstreich, *J. Phys. Chem.*, **63**, 419 (1959).

TABLE II

TRANSFERENCE NUMBERS AND ENTROPIES FOR $CdCl_2$, $CdBr_2$, AND $PbCl_2$

Salt	$F\frac{\Delta\Phi}{\Delta T}$, e.u.[a]	$t_{X^-}/2$	$t_{M^{+2}}/2$	S_{salt}, e.u.	S_{salt}^*, e.u.	$\frac{Q_{M^{+2}}^{**}}{T}$, e.u.	$\frac{Q_{X^-}^{**}}{T}$, e.u.
$CdCl_2$	13.9	0.307	0.193	~63[b]	~−4[c]	−67[d]	0[d]
$CdBr_2$	19.6	.206	.294				
$PbCl_2$	8.09	.373	.127				

[a] e. u. = entropy unit (cal. deg. $^{-1}$ mole $^{-1}$). [b] Taken as an approximate value for these salts at 900°K. The total entropy of $PbCl_2$ can be calculated from literature values to be 63.2 e.v. at 900°K. Since there are no data in the literature for cadmium salts, this value is used in preference to values based on Kopp's rule, which are slightly lower. (See K. K. Kelley, Bur. of Mines Bulletin 476, 1949, and F. D. Rossini, "Selected Values of Chemical Thermodynamic Properties," NBS.) [c] As calculated from slope in Fig. 2 and 3. [d] As calculated from intercepts in Fig. 2 and 3.

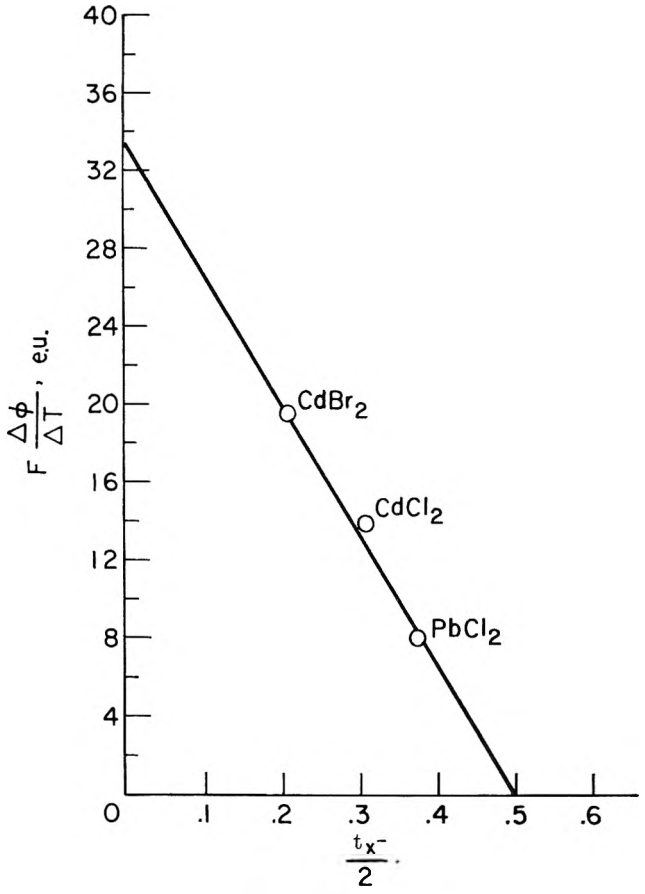

Fig. 2.—Plot of $F(\Delta\Phi/\Delta T)$ against $t_{X^-}/2$. Slope = $[S^*_{salt} - S_{salt}] \cong -67$ e.u.

lead to a reversal of polarity with a resultant e.m.f. equal to the decomposition voltage at zero ΔT. This was not found to be the case for the lead and cadmium systems. Therefore we assume that the electrolysis of the salt produced while balancing the potentiometer will not lead to any significant electrode reaction in our system and that ΔS for the electrode reactions can be considered as negligible.

We may now express the Seebeck coefficient in the general equation as

$$F\frac{\Delta\Phi}{\Delta T} = -\sum_k \left(\frac{t_k}{z_k}\right)\frac{Q_k^{**}}{T} \qquad (2)$$

In the case of lead chloride, this equation becomes

$$F\frac{\Delta\Phi}{\Delta T} = -\left[\frac{t_{Pb^{+2}}}{2}\left(\frac{Q_{Pb^{+2}}^{**}}{T}\right) - t_{Cl^-}\left(\frac{Q_{Cl^-}^{**}}{T}\right)\right]$$

and, in the general case, where $M^{+2} = Cd^{+2}$, $X^- = Cl^-$, Br^-, and $t_{M^{+2}} + t_{X^-} = 1$

$$F\frac{\Delta\Phi}{\Delta T} = \frac{t_{X^-}}{2}[S_{salt}^* - S_{salt}] - \frac{Q_{M^{+2}}^{**}}{2T}$$

$$F\frac{\Delta\Phi}{\Delta T} = -\frac{t_{M^{+2}}}{2}[S_{salt}^* - S_{salt}] + \frac{Q_{X^-}^{**}}{T}$$

The absolute entropies (S_{salt}) for the systems involved are of the same magnitude. It is not unreasonable to assume that, for salts with similar conduction processes, the values of the entropies of transport would also be similar. Thus, if we were to plot the values of $F(\Delta\Phi/\Delta T)$ observed for the cadmium and lead systems against the transport numbers of these salts, the slope of the plot should be linear.

In order to define a transference number in a pure molten salt, an arbitrary reference frame has to be established. The mass average velocity has already been used as a reference by Sundheim[3,4] and gives a value for the transference number of the chloride ion in lead chloride that is in excellent agreement with that determined experimentally.[5] In this reference system the transference numbers for the salt $C_{\nu^+}A_{\nu^-}$ are defined as

$$t^+ = \frac{\nu^+ m^+}{\nu^+ m^+ + \nu^- m^-} \qquad t^- = \frac{\nu^- m^-}{\nu^+ m^+ + \nu^- m^-} \qquad (3)$$

where ν^+, ν^- = algebraic valence, m^+, m^- = atomic mass.

The plots of $F(\Delta\Phi/\Delta T)$ against transference number are given in Fig. 2 and 3. The data are summarized in Table II.

It is of interest to note that the entire value for the reduced heat of transport is associated with the cation. If the total current is carried by the anion ($t_{X^-} = 1$, $t_{M^{+2}} = 0$), then the value of the Seebeck coefficient is zero. In other words, as the value of $t_{M^{+2}}$ increases, so does the value of the thermopotential. The entropy of transport obtained is equivalent in sign and magnitude to the entropy of activation for conductance in alkali halides[6] and other salt systems.[7] We may infer from this that the conduction mechanism in molten ionic salts is primarily a function of the cation.

The equation of deGroot based on irreversible thermodynamics for the thermopotential of a molten salt is exactly analogous to the equation for the thermo-

(3) B. Sundheim, *J. Phys. Chem.*, **60**, 138 (1956).
(4) C. Sinistri, *ibid.*, **66**, 1600 (1952).
(5) G. J. Janz, C. Solomons, and H. J. Gardner, *Chem. Rev.*, **58**, 461 (1958).
(6) I. S. Yaffe and E. R. Van Artsdalen, *J. Phys. Chem.*, **60**, 1125 (1956).
(7) K. Delimarskii and B. F. Markov, "Electrochemistry of Fused Salts," Sigma Press, Washington, D. C., 1961.

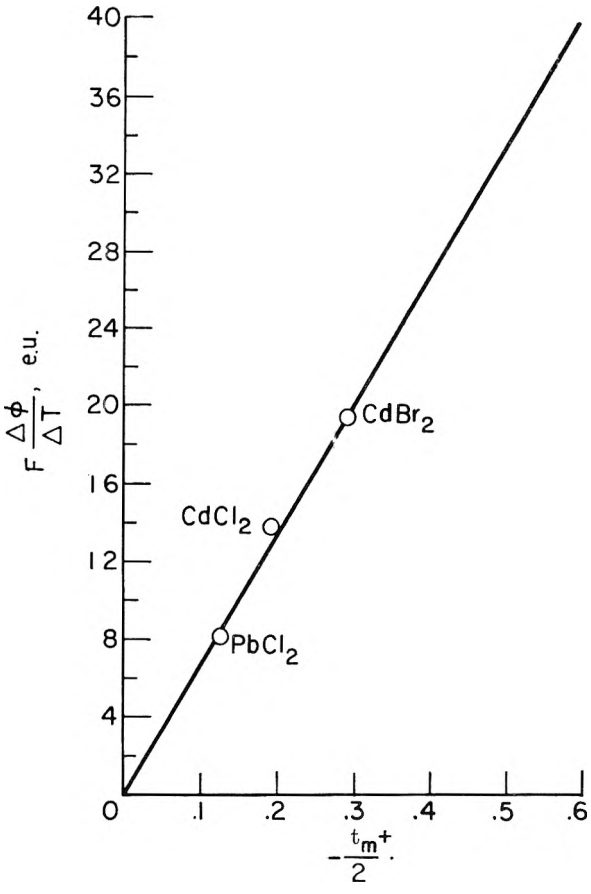

Fig. 3.—Plot of $F(\Delta\Phi/\Delta T)$ against $-t_{M^{+2}}/2$. Slope = $[S^*_{salt} - S_{salt}] \cong -6.7$ e.u.

potential in ionic crystals.[8] This latter equation is based on the models of Frenkel and Schottky for lattice disorder and permits a more detailed analysis of the system. Since the structure of a fused salt corresponds to that of the crystal, the conduction process in the melt can be considered to be a function of ions moving through vacancies. Only those ions with sufficient kinetic energy to overcome the coulombic forces at their lattice position will participate. The negative polarity at the hot junction of the thermocell can be considered to be established by the immigration of cations to the cooler junction. Once in the lower temperature zone, they lose the energy necessary for their return. The thermopotential, as well as the conductivity of these systems, is a function of the number of mobile ions present and their ability to move through the liquid. If we assume that, at about 25° above the melting point, the number of vacancies is much greater than the number of mobile ions, then the thermopotential is solely a function of the number of mobile species present. In this case the slope of the plot of $\Delta\Phi$ against ΔT (Seebeck coefficient) will vary in the same manner as the rate of formation of mobile cations.

If we take the slope of the last three points in Fig. 2 for the $PbCl_2$ system, the value of $F(\Delta\Phi/\Delta T)$ is 9.31. This is a 15% change over the value of 8.09 given in Table II. When the value of 9.31 is used to calculate $Q_{M^{+2}}{}^{**}/T$ in eq. 2, the value obtained is 68.6 e.u. (equal to $S_{Pb^{+2}}{}^* - S_{Pb^{+2}}$]. If $S_{Pb^{+2}}{}^*$ is relatively the same (−4 e.u.), this represents about a 3% change in $S_{Pb^{+2}}$. Thus, a 3% change in the rate of formation of mobile lead ions leads to a change of approximately 15% in the value of the Seebeck coefficient for lead chloride.

Acknowledgment.—We wish to express our appreciation to Dr. A. E. Potter for his valuable assistance.

(8) R. E. Howard and A. B. Lidiard, *Phil. Mag.*, **2**, 1462 (1957).

THE THERMODYNAMICS OF ASSOCIATION OF THE TRISETHYLENEDIAMINEPLATINUM-(IV) ION WITH VARIOUS ANIONS

BY DONALD C. GIEDT AND C. J. NYMAN

Department of Chemistry, Washington State University, Pullman, Washington

Received May 20, 1963

The previously reported[1] stability constants for the 1:1 outer-sphere ion pairs formed by trisethylenediamineplatinum(IV) with various anions were 11 for Cl^-, 8 for Br^-, 3.3×10^3 for SO_4^{-2}, *ca.* 0.8 for NO_3^-, and 0 for ClO_4^-. These values supported King, Espensen, and Visco's[2] claim that the stability constants for outer-sphere complexes reported by earlier workers were too high. Evans and Nancollas[3] plotted values of ΔS of formation for the ion pairs *vs.* ΔS of hydration values for the anion and found that these plots for the $[Co(NH_3)_6]^{+3}$, $[Co(en)_3]^{+3}$, and Fe^{+3}(aq.) cations were parallel lines. By means of an entropy cycle they interpreted this close linear relationship to mean that the magnitudes of the entropies of association for ion pairs of the same cation but different anions were dependent upon the differences between the entropy of hydration of the anion and the entropy of hydration of the ion pair.

The present work was undertaken to study the effect of temperature on the stability of the outer-sphere ion pairs and to establish values for the thermodynamic functions $\Delta H°$, $\Delta F°$, and $\Delta S°$ for the formation reactions of $[Pt(en)_3]^{+4}$ with various anions.

Experimental

Solutions.—All stock solutions were prepared as previously reported.[1] It was necessary to deoxygenate the water used in the preparation of the iodide and thiocyanate solutions by sweeping it for 30 min. with a stream of nitrogen prior to use.

The solutions prepared for the $[Pt(en)_3^{+4}, Cl^-]$ ion pair study contained 1.017×10^{-3} *M* $[Pt(en)_3]^{+4}$ and 1.003×10^{-3} *M* $[H^+]$, with a chloride concentration varying from 0.005 to 0.1 *M*. The solutions prepared for the other anions studied contained 1.016×10^{-3} *M* $[Pt(en)_3]^{+4}$, 1.208×10^{-3} *M* $[H^+]$, and 1.208×10^{-3} *M* $[ClO_4^-]$. The concentrations of the complexing anions in these solutions varied from 0.001 to 0.05 *M*. The acidities of all final solutions were maintained at pH 3 or less to suppress acid dissociation of the $[Pt(en)_3]^{+4}$. The ionic strength varied depending on the composition of the solution.

Procedure.—A Cary Model 14 recording spectrophotometer was used to measure the absorbance of the solutions in matched 1-cm. quartz cells. The apparent molar extinction coefficients *D* were measured at 2600 Å. for the Cl^- and Br^- anions and at 2700 Å. for the I^- and SCN^- anions and at temperatures of 10°, 25°, and 40°. A constant temperature in the cell compartment of the spectrophotometer was maintained by circulating water of (10.0 ± 0.2°), (25.0 ± 0.2°), or (40.0 ± 0.2°) as required.

Results and Discussion

The spectrophotometric data were evaluated by the same method as employed by Bale, Davies, and Monk[4] and later by Nyman and Plane.[1] Activity coefficients

(1) C. J. Nyman and R. A. Plane, *J. Am. Chem. Soc.*, **82**, 5787 (1960).

(2) E. L. King, J. H. Espensen, and R. E. Visco, *J. Phys. Chem.*, **63**, 755 (1959).

(3) M. G. Evans and G. H. Nancollas, *Trans. Faraday Soc.*, **49**, 363 (1953).

(4) W. D. Bale, E. W. Davies, and C. B. Monk, *ibid.*, **52**, 816 (1956).

TABLE I

STABILITY CONSTANTS AND THERMODYNAMIC FUNCTION VALUES FOR ION PAIRS FORMED BY $[Pt(en_3)]^{4+}$ WITH VARIOUS ANIONS

		Stability constant K_1^0					
Anion	Method	10°	25°	40°	$\Delta H°$, kcal./mole	$\Delta F°$ at 25°, kcal./mole	$\Delta S°$ at 25°, e.u.
Cl^-	Least squares	14.9 ± 0.9	17.4 ± 0.6	19.6 ± 0.9	1.6	−1.69	11.0
	Individual points	14.9 ± .9	16.8 ± .8	19.6 ± .9	±0.5	±0.25	±2.1
Br^-	Least squares	13.9 ± .3	15.2 ± .3	17.8 ± .3	1.3	−1.61	9.7
	Individual points	13.8 ± .3	15.1 ± .4	17.7 ± .4	±0.2	±0.15	±1.0
I^-	Least squares	12.8 ± .4	14.0 ± .5	15.9 ± .4	1.3	−1.56	9.6
	Individual points	12.8 ± .4	13.4 ± .7	15.2 ± .5	±0.2	±0.25	±1.2
SCN^-	Least squares	0	0	0	...	...	...

were calculated from the Davies form of the modified Debye–Hückel equation[5]

$$-\log f_i = AZ_i^2(I^{1/2}/(1 + I^{1/2}) - CI] \quad (1)$$

where A is a constant dependent upon the dielectric constant and the absolute temperature, Z_i is the charge on the ion, I is the ionic strength of the solution, and C is an arbitrary constant. A value of 0.2 was used for C in this study.

Values for K_1^0 were calculated by the "slope–intercept" method and by the "individual points" method. The best straight line used in the former method was determined by a least squares treatment. The K_1^0 values obtained by each method are listed in Table I and are in close agreement. The discrepancy between the K_1^0 values at 25° for the $[Pt(en)_3^{+4}, Cl^-]$ and $[Pt(en)_3^{+4}, Br^-]$ ion pairs reported in this paper and those reported by Nyman and Plane[1] for the same ion pairs can be attributed to the earlier workers inclusion of data from solutions containing anion concentrations greater than 0.1 M. At these higher concentrations the activity coefficients calculated are not as reliable as might be desired.

Two trends are evident from the K_1^0 values for the halide series of anions listed in Table I. The K_1^0 values decrease with increasing size of the associating anion and they increase with increasing temperature. For the $[Pt(en)_3^{+4}, SCN^-]$ ion pair the K_1^0 values were found to be equal to or very close to zero for the entire temperature range studied. This tendency can be attributed to the relatively small charge and large size of the SCN^- anion and also to a probable unfavorable entropy change. One would expect a loss of rotational entropy for the SCN^- anion on association.

The values of the thermodynamic functions calculated for the ion-pair formation are also included in Table I. These were evaluated through the usual thermodynamic relationships.

The $\Delta H°$ values reported for the ion pairs formed between the $[Pt(en)_3]^{+4}$ and the halides are small. It is doubtful that the reported data can be interpreted to mean anything more than that $\Delta H°$ is positive and in the range of 1 to 2 kcal./mole for the reactions studied.

The entropies of association of the ion pairs studied were found to be positive, which is typical for ion-pair formation.[6] They are, however, of nearly the same magnitude, showing only a slight tendency to decrease with increasing anion size. These trends can be better understood by reference to an entropy cycle for the reaction

$$[Pt(en)_3]^{+4} + X^- = [Pt(en)_3^{+4}, X^-] \quad (2)$$

$$\begin{array}{ccc} [Pt(en)_3]^4(g) + X^-(g) & \xrightarrow{\Delta S_3°} & [Pt(en)_3^{+4}, X^-](g) \\ \uparrow \Delta S_1° & \uparrow \Delta S_2° & \downarrow \Delta S_4° \\ [Pt(en)_3]^{+4}(aq.) + X^-(aq.) & \xrightarrow{\Delta S_5°} & [Pt(en)_3^{+4}, X^-](aq.) \end{array}$$

From the entropy cycle it can be shown that

$$\Delta S_5° = \Delta S_1° + \Delta S_2° + \Delta S_3° + \Delta S_4° \quad (3)$$

where $\Delta S_1°$ and $\Delta S_2°$ are the negative entropies of hydration of the $[Pt(en)_3]^{+4}$ and X^-, respectively, and $\Delta S_4°$ is the entropy of hydration of the ion pair. $\Delta S_3°$ and $\Delta S_5°$ are the entropies of association in the gaseous and aqueous states, respectively. By the methods of Latimer[7] it can be shown that changes in $\Delta S_3°$ are small and can be neglected. Since $\Delta S_2°$ decreases with increasing anion size, then the entropy of hydration of the ion pair must increase with increasing size of the associating anion. This finding is consistent with the earlier results of Evans and Nancollas.[3]

Acknowledgment.—The authors are indebted to the Washington State University Research Committee for financial support. This work is based on the M.S. thesis submitted to Washington State University by D. C. G., 1963.

(5) C. W. Davies, *J. Chem. Soc.*, 2093 (1938).

(6) J. Lewis and R. G. Wilkins, "Modern Coordination Chemistry," Interscience Publishers Inc., New York, N. Y., 1960, p. 20.

(7) W. H. Latimer, *Chem. Rev.*, **18**, 349 (1936).

PHOTOREDUCTION OF HEXAFLUOROBIACETYL BY HYDROCARBONS IN THE GASEOUS PHASE AND IN SOLUTION

BY I. M. WHITTEMORE AND M. SZWARC

Department of Chemistry, State University College of Forestry at Syracuse University, Syracuse 10, New York

Received May 21, 1963

Photolysis of hexafluorobiacetyl[1] (HFBA) vapor at 25 and 150° produces CO and C_2F_6 in a 2:1 molar ratio, and if the reaction is continued, all the diketone may be decomposed. Surprisingly, in the presence of aliphatic hydrocarbons, *e.g.*, neopentane or isobutane, only a small amount of CO is formed. For example, at 65° a mixture of HFBA and 2,3-dimethylbutane in 1:150 molar ratio was photolyzed until 84% of the diketone was decomposed (determined by the change

(1) Preparation described by L. O. Moore and J. W. Clark, U. S. Patent 3,055,913 (1962).

in the optical density at λ_{max} 420 mμ). Nevertheless, only 0.5% of CO and approximately an equivalent amount of CF_3H were found in the products. Similar results were obtained in liquid hydrocarbons, *e.g.*, a 0.06 *M* solution of HFBA in liquid 2,3-dimethylbutane, after being photolyzed at 25° for 9 min., showed a decrease in the optical density at λ_{max} 420 mμ from 1.14 to 0.19 (the optical path being 1 cm.). Again, analysis of the products gave only 0.8% of CO and an equivalent amount of CF_3H, and neither CF_3·CHO nor CF_3·CO·CF_3 were detected. It is obvious that under these conditions CF_3CO or CF_3 and CO are not the main products of the primary reaction.

The infrared spectra of the products obtained in the presence of hydrocarbons showed the absence of the very strong band at 14.25 μ, which is characteristic of HFBA. The 5.58 μ carbonyl band was observed, although its intensity was reduced to about one-half of its initial value. A new band which appeared at 2.75 μ demonstrates the presence of an OH group. Significantly, an additional band at 3.75 μ, indicating the presence of an OD group, was observed when liquid 2-methylpropane-d_2 was used as solvent. The formation of an OH group was confirmed by a positive Zerevitinoff test.

When the bleached solution was exposed to air, some HFBA was re-formed; the increase in the optical density at 420 mμ showed its concentration to be a few per cent only of the initial value. The average molecular weight of typical products was 550, and their total mass exceeded that of the initial ketone.

It appears that HFBA undergoes photoreduction in the presence of a hydrocarbon. The excited molecule abstracts a hydrogen forming a ketyl radical CF_3·COH·CO·CF_3 and a solvent radical. The interaction of these radicals then produces a complex mixture containing such species as $CF_3C(R)OH{\cdot}CO{\cdot}CF_3$, CF_3CH-OH·CO·CF_3, etc. The presence of the latter compound is indicated by its facile oxidation to HFBA. The complexity of the products arises from the fact that HFBA may react with the resulting alcohols, forming ketals.

It would appear that this is the first reported example of a bimolecular gas phase photoreduction of a ketone. Unimolecular rearrangement processes leading to similar products are known,[2] and, of course, many examples of photoreduction of ketones in solution are described in the literature.[3] Our results raise the question of how important photoreduction may be in the gaseous photolysis of other ketones, and, in fact, some peculiar observations mentioned in a few papers might be due to this phenomenon.[4]

All the irradiations were carried out in Pyrex vessels using unfiltered light from a G.E. A-H6 high pressure mercury lamp. All solution mixtures were thoroughly degassed before being irradiated.

The referee of this Note wonders whether the formation of the hydroxylic product in the gas phase photolysis of hexafluorobiacetyl could be due to the two reactions

$$CF_3 + CF_3{\cdot}CO{\cdot}CO{\cdot}CF_3 \longrightarrow (CF_3)_2{\cdot}(CO\cdot){\cdot}CO{\cdot}CF_3$$

$$(CF_3)_2{\cdot}(CO\cdot){\cdot}CO{\cdot}CF_3 + HR \longrightarrow (CF_3)_2{\cdot}COH{\cdot}CO{\cdot}CF_3$$

The answer is definitely negative. This suggestion requires formation of equivalent quantities of CO and of the hydroxylic product. This obviously is not the case. For example, it was stated at the beginning of this Note that 84% of diketone was decomposed while only 0.5% of CO was formed. Even this small quantity of CO cannot be attributed to the reaction proposed by the referee since, as was stated above, approximately an equivalent amount of CF_3H was formed with CO.

Acknowledgments.—We wish to thank Dr. Leonard Moore of the Research and Development Department of Union Carbide Chemicals for a gift of hexafluorobiacetyl, and we also wish to thank Wright-Patterson Air Force Base for financial support of this work through Grant AF-33(657)-10855.

(2) P. Ausloos and R. E. Rebbert, *J. Am. Chem. Soc.*, **83**, 4897 (1961).

(3) (a) A. Schönberg and A. Mustafa, *Chem. Rev.*, **40**, 181 (1947); (b) C. R. Masson, V. Boekelheide, W. A. Noyes, Jr., in A. Weissberger, Ed., "Techniques of Organic Chemistry," Vol. II, 2nd Ed., Interscience Publishers, Inc., New York, N. Y., 1956, p. 257; (c) G. S. Hammond, W. P. Baker, W. R. Moore, *J. Am. Chem. Soc.*, **83**, 2795 (1961).

(4) (a) W. A. Noyes, Jr., W. A. Mulac, and M. S. Matheson, *J. Chem. Phys.*, **36**, 880 (1962); (b) D. S. Weir, *ibid.*, **36**, 1113 (1962).

ELECTRON-BEAM INITIATED POLYMERIZATION OF AN ORGANIC VAPOR ADSORBED ON A METAL SURFACE

BY P. WHITE[1]

Standard Telecommunication Laboratories Limited, London Road, Harlow, Essex, England

Received April 26, 1963

Interest has recently developed in the formation of thin polymer layers by radiation treatment of monomer vapors adsorbed or condensed onto solid surfaces, and several papers have presented details and mechanisms of reactions.[2-5] In general, these papers have one thing in common, that the data have been obtained for the formation of polymer on previously deposited polymer, and in no case has any discussion included the first layer of polymer film; *i.e.*, when the monomer gas is adsorbed on a surface other than that of polymer. Some experimental results on the formation of polymer layers have been described by White and North,[6] and interpretation of these results have some bearing on the question of what happens in the formation of an initial polymer layer on a metal surface.

White and North[6] used a 3-kv. electron beam to make a number of very rapid, but precisely timed, vertical scans across the surface of a freshly deposited lead film in the presence of a monomer gas, butadiene. The polymer layers formed on the surface of the film were detected by a simplified electron-beam scanning microscope described by DaSilva and White.[7] These experiments indicated whether or not a polymer film had been formed and also yielded qualitative data on the thickness of the deposit. It was then possible to correlate the signal from the scanning microscope with the writing time defined as the period of time the electron beam irradiated any one spot on the surface.

Undoubtedly, before the electron beam scanned the metal, at least one monolayer of organic vapor was

(1) This work was performed while the author was employed by International Business Machines Corporation, Thomas J. Watson Research Center, Yorktown Heights, N. Y.

(2) R. W. Christy, *J. Appl. Phys.*, **31**, 1680 (1960).

(3) I. Haller and P. White, *J. Phys. Chem.*, **67**, 1784 (1963).

(4) V. A. Kargin and V. A. Kabanov, *J. Polymer Sci.*, **52**, 71 (1961).

(5) D. M. White, *J. Am. Chem. Soc.*, **82**, 5678 (1960).

(6) P. White and D. W. North, *IBM J. Res. Develop.*, in press.

(7) E. M. DaSilva and P. White, Proceedings of the 8th National Vacuum Symposium, Pergamon Press, London, 1960, p. 830.

adsorbed on the metal surface. The first step in the polymer formation must be polymerization of the gas already adsorbed on the metal surface, subsequent layers being formed by adsorption of further gas prior to polymerization. Experimental measurements with a gas pressure of 5×10^{-5} torr and a beam current of 5 μa. indicated that at all writing times down to 1×10^{-2} sec. the polymer film thickness decreased continuously with decrease in writing speed. This showed that at least more than one layer of polymer must have been deposited, since a deviation from the smooth dependence of signal height on writing time would be anticipated when less than a monolayer was present on the surface. Also, the dependence of film thickness, at a constant writing speed, on both pressure and current density was consistent with the kinetics previously deduced for formation of polymer on polymer.[3] Both these facts indicate that the polymer film formed at writing times down to 1×10^{-2} sec. was composed of more than one layer. It appears therefore that under the conditions of the experiment, 1×10^{-2} sec. must represent an upper limit of the time required for complete polymerization of the gas already adsorbed on the metal surface.

Consider now what may be inferred from this conclusion. A beam current of 5×10^{-6} amp. is equivalent to 3×10^{13} electrons striking the surface per second. Assuming a cross section area of 5×10^{-16} cm.^{2} for butadiene, there would be about 10^{13} molecules adsorbed in a close packed monolayer with an area equivalent to that of the electron beam (about 5×10^{-3} cm.^{2}). During the interval of time necessary to form the polymer layer, 3×10^{11} electrons would have collided with the surface. It seems, therefore, that one electron is sufficient to cause polymerization of about 30 adsorbed molecules. This compares with approximately 100 electrons/molecule required for polymer formation on a polymer surface, with a similar current and electron energy of about 0.3 kv. Preliminary experiments indicated very little or no dependence of the rate of polymer formation on electron energy.[3] The very large difference in the number of electrons required to form a single layer of polymer in the two cases must therefore be related to the difference in degree of bonding of the adsorbed gas to the underlying material and the consequence of this on the electron distribution in the adsorbed molecule. This is not unusual, since in a number of cases it has been shown that the absorption spectra of molecules are appreciably altered when they are chemisorbed on surfaces.

It seems, therefore, that the monomer molecules adsorbed on a metal surface are in an energy state from which they can very easily enter into a chain reaction and form polymer molecules containing initially up to 30 monomer units. This initial layer must then form the base from which the polymer film grows by the mechanism already described.[3]

SCALING AND THE VIRIAL THEOREM

By G. Hunter, D. G. Rush, and H. O. Pritchard

Chemistry Department, University of Manchester, Manchester 13, England

Received May 3, 1963

In some recent LCAO calculations on H_2^+, de Carlo and Griffing[1] found that the virial theorem ($2T +$ $V = 0$) was best obeyed for their 3-term wave function at $R = 2$ a.u. when the scale parameter Z was 1.2, whereas a much higher Z of 1.45 gave the best energy (see Tables V and IX of ref. 1). Dr. Griffing asked us if we could investigate this apparent anomaly further, and in so doing, we have found that the situation is somewhat complicated by the fact that, for severely truncated basis sets, the calculated equilibrium bond length is quite sensitive to the scale parameter. There is no anomaly, however, because neither $(E + T)$ nor $(E + T + R\ dE/dR)$ ever become zero when Z is around 1.2.

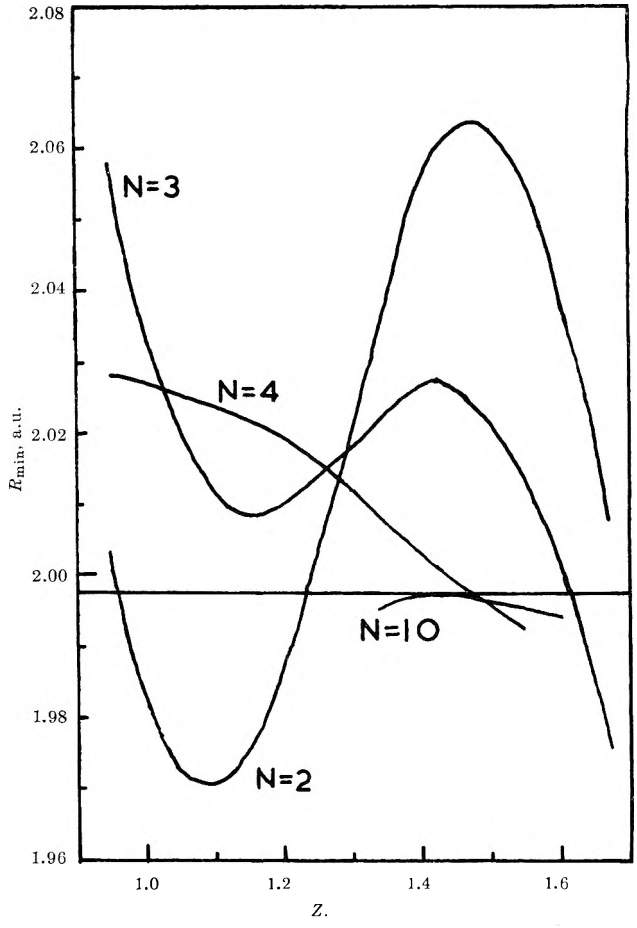

Fig. 1.—Variation of R_{min} with Z for H_2^+.

Pritchard and Sumner[2] investigated the energy of H_2^+ at $R = 2$ a.u. for nine values of the scale parameter Z. Since all the integrals involved are actually functions of RZ, it is a simple matter to reinterpret these so that we can choose a fixed value of Z and calculate the energy for nine different values of R. The minimum in the potential curve for each Z was then located by interpolation or extrapolation of the differences between our calculated energies and the exact energy function derived from the results of Bates, Ledsham, and Stewart.[3] The values of R_{min} for 2, 3, 4, and 10 basis functions are shown in Fig. 1; for 10 functions with $Z = 1.415$, $R_{min} = 1.997$ a.u., and coincides with the value given by the exact solution.

Figure 2 shows the variation of the virial function $(E + T)$ with scale parameter for internuclear separations $R = R_{min}$. In the range accessible to us, these

(1) V. de Carlo and V. Griffing, *J. Phys. Chem.*, **66**, 845 (1962), and personal communication.

(2) H. O. Pritchard and F. H. Sumner, *ibid.*, **67**, 641 (1961).

(3) D. R. Bates, K. Ledsham, and A. L. Stewart, *Phil. Trans. Roy. Soc. London*, **A146**, 215 (1953).

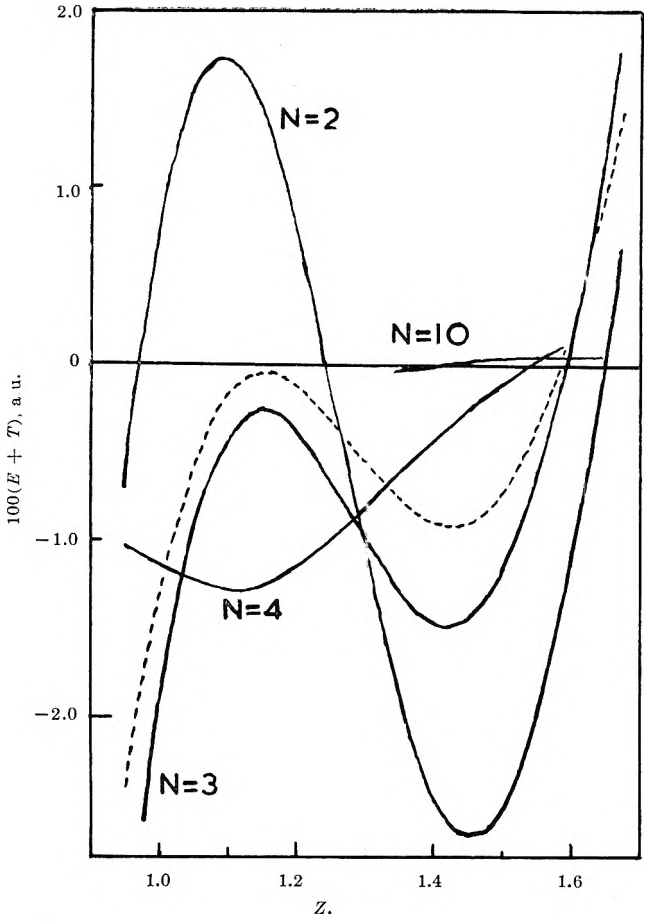

Fig. 2.—Variation of the virial function $(E + T)$ with Z for $R = R_{min}$, solid lines; variation of the virial function $(E - T + R\ dE/dR)$ with Z for $R = 2$ a.u. and $N = 3$, dotted line.

curves are of a cubic type, and the points at which they cross the axis correspond to extremes in the energy function. For an expansion length of $N = 2$, there are three extremes, a maximum at about $Z = 1.25$ (*cf.* Table I of ref. 2) and two minima at $Z = 1.65$ and 0.97. For other expansion lengths, there is only one real root in $(E + T)$, corresponding to minima in the energy at $Z = 1.59$, 1.55, and 1.415 for $N = 3$, 4, and 10, respectively.

Since the three basis functions used by de Carlo and Griffing[1] are equivalent to the first three members of the basis set used by Pritchard and Sumner,[2] the two sets of results should agree. Table IX of ref. 1 shows the agreement between the energies for $N = 3$, but our extrapolated best scale parameter of $Z = 1.59$ does not agree with their value of 1.45; however, our higher value is confirmed by some unpublished calculations by Sovers.[4] On the other hand, we do confirm a very small numerical magnitude for $(E + T)$ near $Z = 1.2$ (*cf.* Fig. 2), but (E + T) never becomes zero in this region, which is the necessary condition for an energy minimum.[5] Maxima and minima in $(E + T)$ only correspond to inflections in the energy-scale parameter curve. Our results for $N = 10$ show that the best energy obtainable is 0.602607 a.u. at $R = 1.997$ a.u. Thus, it is only when we have a reasonable expansion length that both the energy and R_{min} converge simultaneously to the correct values.

The relevant formulas for the potential and kinetic energies, which were not given in ref. 2, are, in a.u.

$$V = 2\sum_{i=1}^{N}\sum_{j=1}^{N} c_i c_j (2 + 2\xi_{ii})^{-1/2}(2 + 2\xi_{jj})^{-1/2} \times [(\xi_{ij} + \omega_{ij})/R - (L_{ij} + J_{ij} + K_{ij} + K_{ji})]$$

$$T = 2\sum_{i=1}^{N}\sum_{j=1}^{N} c_i c_j (2 + 2\xi_{ii})^{-1/2}(2 + 2\xi_{jj})^{-1/2} \times [\epsilon_j'(\xi_{ij} + \omega_{ij}) + Zn_j (L_{ij} + K_{ji})]$$

(4) O. Sovers, personal communication.
(5) P.-O. Löwdin, *J. Mol. Spectry.*, **3**, 46 (1959).

A MODIFIED DEBYE THEORY OF SALTING OF NONELECTROLYTES IN ELECTROLYTE SOLUTIONS

BY M. GIVON, Y. MARCUS, AND M. SHILOH

Radiochemistry Department, Soreq Research Establishment, Israel Atomic Energy Commission, Rehovoth, Israel

Received May 17, 1963

Consider a system of three components: water, an electrolyte, and a nonelectrolyte.

The Debye theory gives the activity coefficient of the nonelectrolyte as[1]

$$f_3 = 1\Big/\left(1 - \frac{4\pi N_0}{1000}(J_+C_+ + J_-C_-)\right) \quad (1)$$

where N_0 is Avogadro's number, $C_\pm$ are the concentrations of the respective ions of the electrolyte in moles per liter, and $J_\pm$ are functions described below. We shall confine ourselves to the case $C_+ = C_- = C_2$; extension to other cases, or to mixtures of electrolytes (with ΣJC instead of the binary sum), is obvious. The functions J may be written approximately as

$$J_\pm = \bar{R}^4 z^2/b_\pm \quad (2)$$

where $\bar{R}$ is a characteristic length discussed below, z is the charge of the ions in terms of the electronic charge e, and $b_\pm$ are the radii of the ions.

Debye has shown that $\bar{R}^4$ may be calculated from

$$\bar{R}^4 = N_0 e^2[v_3(\partial D/\partial n_1)_{n_3} - v_1(\partial D/\partial n_3)_{n_1}]/8\pi RTv_1D^2 \quad (3)$$

where R is the gas constant, T the absolute temperature, v_i the molal volume per molecule i ($v_i = V_i/N_0$), D the dielectric constant of the solution, and n_i the number of molecules i per cm.^{3}. It is the difference in the brackets which determines whether there will be salting-in or salting out. We shall depart here from Debye's treatment,[1] by considering in a different manner the dependence of the dielectric constant on the composition.

At moderate concentration of electrolyte it is usually found that[2]

$$D = D_1 - \delta_2 C_2 - \delta_3 C_3 \quad (4)$$

where D_1 is the dielectric constant of pure water, δ_2 is the molar dielectric decrement of the electrolyte, and δ_3 that of the nonelectrolyte. Considering the derivative $(\partial D/\partial n_1)_{n_3}$ in eq. 3, it may be written as $(\partial D/\partial C_2)\cdot(\partial C_2/\partial n_1)$, where the first factor, if C_3 is sufficiently small, may be equated with $-\delta_2$ from eq. 4. The second factor is

$$(\partial C_2/\partial n_1) = -1000\ v_1/(V_2^\phi + h_2V_1) \quad (5)$$

(1) P. Debye, *Z. physik. Chem.*, **130**, 56 (1927).
(2) P. Debye and J. McAulay, *Physik. Z.*, **26**, 22 (1925).

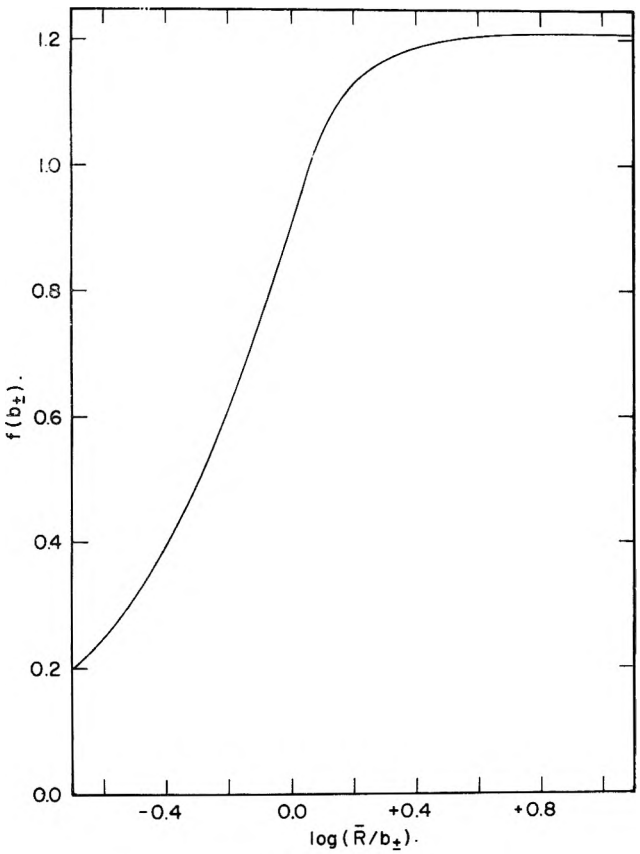

Figure 1.

where V_2^ϕ is the apparent molal volume of the electrolyte in solution and h_2 the hydration number of the electrolyte. Only "free" water molecules are counted in n_1. The derivative $(\partial D/\partial n_3)_{n_1}$ in eq. 3 is simply obtained from eq. 4, remembering that $C_3 = 1000\, n_3/N_0$

$$(\partial D/\partial n_3)_{n_1} = (\partial D/\partial C_3)(\partial C_3/\partial n_3) = -1000\delta_3/N_0 \quad (6)$$

Equation 3 may now be rewritten as

$$\bar{R}^4 = 1000e^2\left(\frac{V_3}{V_2^\phi + h_2V_1}\delta_2 + \delta_3\right)/8\pi RTD^2 \quad (7)$$

The dielectric constant of the solution in eq. 7 may be approximated for small C_3, using eq. 4, by $D^2 = D_1^2/(1 + 2C_2\delta_2/D_1)$. Using this, and eq. 7, 3, 2, and 1, the activity coefficient of the nonelectrolyte becomes

$$f_3 = 1/[1 - N_0z^2e^2(1 + 2C_2\delta_2/D_1) \times \left(\frac{V_3}{V_2^\phi + h_2V_1}\delta_2 + \delta_3\right)\left(\frac{1}{b_+} + \frac{1}{b_-}\right) C_2/2RTD_1^2] \quad (8)$$

The salting coefficient $k_s = \lim_{C_3 \to 0} \mathrm{d} \log f_3/\mathrm{d}\, C_2$ may be calculated by expanding $\log f_3$ from eq. 8 and noting that at the limit for the derivative $V_2^\phi + h_2V_1 = V_2^0 + h_2^0V_1$, the superscript zero denoting infinite dilution

$$k_s = 0.4343N_0z^2e^2\left(\frac{V_3}{V_2^0 + h_2^0V_1}\delta_2 + \delta_3\right)\times \left(\frac{1}{b_+} + \frac{1}{b_-}\right)\Big/2RTD_1^2 = 0.0197z^2 \times \left(\frac{V_3}{V_2^0 + 18\,h_2^0}\delta_2 + \delta_3\right)\left(\frac{1}{b_+'} + \frac{1}{b_-'}\right) \quad (9)$$

the last expression pertaining to 25° with $b_\pm'$ in Å.

It should be noted that eq. 2 is only a first approximation. A better approximation is to write (treating $\bar{R}^4$ as positive for obtaining the fourth root)

$$J_\pm = \bar{R}^3 f(b_\pm)$$
$$f(b_\pm) = 1.21 - 0.32(\bar{R}/b_\pm)^{-3} + \ldots \text{ for } \bar{R} > b_\pm$$
$$f(b_\pm) = (\bar{R}/b_\pm) - 0.10(\bar{R}/b_\pm)^4 + \ldots \text{ for } \bar{R} < b_\pm \quad (10)$$

The function $f(b_\pm)$ is plotted against log $\bar{R}/b_\pm$ in Fig. 1. Instead of eq. 9 the formula for k_s becomes

$$k_s = 0.0126z^2\left(\frac{V_3}{V_2^0 + 18\,h_2^0}\delta_2 + \delta_3\right)^{3/4} \times (f(b_+) + f(b_-)) \quad (11)$$

In order to calculate $f(b_\pm)$, values of $\bar{R}$ are taken as $1.57(V_3S_2/(V_2^0 + h_2^0V_1) + \delta_3)^{1/4}$ Å.

The parameter b in Debye's theory is an integration limit for the volume at the disposal of the nonelectrolyte, hence, the hydrated radii should apply. These have been tabulated,[3-5] but no agreement exists on their values. Fortunately, k_s is not too sensitive to the value of b, as Fig. 1 shows, and an error of not more that 20% will usually result if $f(b_+) + f(b_-)$ is set equal to 2.0, since $\bar{R}$ is usually slightly larger than most b values.

In order to calculate k_s, it is necessary to obtain numerical values for the quantities in eq. 11. Values of V_3 may be calculated simply from M_3/d_3 for the pure nonelectrolyte. Values of V_2^0 have been tabulated for many electrolytes (*e.g.*, ref. 6) as also have hydration numbers h_2^0 (*e.g.*, ref. 4–6). The value of δ_3 may be calculated according to Butler,[7] who showed that $\delta_3 = V_3(D_1 - D_3)/1000$, and values of D_3, the dielectric constant of the pure nonelectrolyte, are available. Data of the dielectric decrement of electrolytes, δ_2, have been published and were found to be roughly additive[8,9] for the ions (Table I).

Values of δ_2 for electrolytes which have not been studied experimentally may be calculated approximately.

From all these preceeding considerations, we obtain approximately, for aqueous solutions at 25°

$$k_s = 0.025z^{3/2}V_3^{1/4}\left(\frac{\delta_2}{V_2^0 + 18h_2^0} + \frac{D_1 - D_3}{1000}\right)^{3/4} \quad (12)$$

The checking of previous theories of salting out with experimental data has always resulted in finding qualitative agreement, but quantitative disagreement.[8,12] One of the main advantages of McDevit and Long's[10] theory as stated by the authors, is that it allows for salting in, namely for those electrolytes, whose intrinsic volume V_2 (volume of hypothetical supercooled liquid

(3) E. R. Nightingale, Jr., *J. Phys. Chem.*, **63**, 1381 (1959).
(4) C. B. Monk, "Electrolytic Dissociation," Academic Press, London 1961, p. 271.
(5) J. Padova, *J. Chem. Phys.*, in press.
(6) H. S. Harned and B. B. Owen, "Physical Chemistry of Electrolyte Solutions," 3rd Ed., Reinhold Publishing Corp., New York, N. Y., 1958.
(7) J. A. V. Butler, *J. Phys. Chem.*, **33**, 1015 (1929).
(8) J. B. Hasted, D. M. Ritson, and C. H. Collie, *J. Chem. Phys.*, **16**, 1 (1948).
(9) F. E. Harris and C. T. O'Konski, *J. Phys. Chem.*, **61**, 310 (1957).
(10) W. F. McDevit and P. A. Long, *J. Am. Chem. Soc.*, **74**, 1773 (1952).

TABLE I

IONIC DIELECTRIC DECREMENTS

	H^+	Li^+	Na^+	K^+	Mg^{2+}	Ca^{2+}	Ba^{2+}	La^{2+}	Al^{3+}	F^-	Cl^-	Br^-	I^-	OH^-	NO_3^-	ClO_4^-	SO_4^{2-}
17[a]		11	8	8	24		22	35		5	3		7	13			14
[b]		14	10	7	28	27	21		30	3	0	0	0		1	2	18

[a] See ref. 8. [b] See ref. 9.

salt[5,10]) is smaller than their partial molal volume at infinite dilution $\bar{V}_2^0$. This salting property is, however, independent of the nonelectrolyte, as their[10] equation shows

$$k_s = \frac{\bar{V}_3^0(V_2 - \bar{V}_2^0)}{2.303\beta_1 RT} \qquad (13)$$

(β_1 is the compressibility of water). Although the results for benzene[10] confirm the qualitative aspects of eq. 13, many other results do not, since the same electrolyte is found to be able to salt some nonelectrolytes in, and some out (*e.g.*, hydrocyanic acid and acetone, ref. 6, Fig. 12–10–4, p. 538, also Table 12–10–1A and 12–10–2A, p. 736–737, for other nonelectrolytes). Furthermore, eq. 13 is sensitive to the exact value of V_2, which is not always known with sufficient precision, and since theory[5] requires $V_2 - \bar{V}_2^0 > 0$, the cases reported where this difference is negative are possibly based on incorrect V_2 values.

Along with the Debye theory, eq. 12 predicts the salting coefficient to increase with the charge on the ions and to be a function of the dielectric decrement of the nonelectrolyte δ_3. Salting in will occur if δ_3 is negative (*e.g.*, as for hydrocyanic acid), provided it is sufficiently large. Equation 13 predicts also that k_s will increase with the molar volume V_3 of the nonelectrolyte, and decrease with that of the electrolyte. This result does not appear explicitly in Debye's theory, but is included in that of McDevit and Long.[10] Finally, the present treatment predicts k_s to increase with the dielectric decrement of the electrolyte. This feature has not appeared in previous derivations of the salting effect.

Calculations have been made for the salting behavior of electrolytes in water toward benzene. Table II shows the results for those electrolytes where data of $\bar{V}_2^0$, h_2^0, δ_2, and k_s are available,[6,9-11] using eq. 12.

TABLE II

SALTING OUT OF BENZENE[a]

Electrolyte	$V_2^0 + 18h_2^0$, ml.	δ_2	k_s (calcd.), M^{-1}	k_s (obsd.), M^{-1}
LiCl	107.5	14	0.22	0.14
NaCl	125.0	10	.18	.20
NaBr	114.0	11	.20	.16
NaI	107.2	12	.22	.10
$NaNO_3$	100.2	10	.20	.12
$NaClO_4$	114.7	11	.20	.10
KCl	117.1	7	.17	.17
KBr	106.1	8	.18	.10
HCl	144.9	20	.23	.05
$HClO_4$	134.6	19	.23	− .01

[a] Benzene, V_3 = 89.4 ml., D_3 = 2.25; water, D_1 = 78.5.

The calculated values are seen to be quite near the observed ones (considerably nearer than those of McDevit and Long[10]). The calculated values for hydrochloric and perchloric acids are relatively too high, the theory not being able to account for the very low salting out or in properties of acids.

(11) J. H. Saylor, A. I. Whitten, I. Claiborne, and P. M. Gross, *ibid.*, **74**, 1778 (1952).

For another type of nonelectrolyte, mercury(II) halides, the experimental value for the salting coefficient by sodium perchlorate was found to be[12] k_s = 0.14 M^{-1}. The calculated values from eq. 12, using V_3 = 49 ml. for $HgCl_2$, 59 ml. for $HgBr_2$, and 72 ml. for HgI_2, are k_s(calcd.) = 0.123, 0.142, and 0.164 M^{-1}, respectively; *i.e.*, very near the experimental value.

(12) Y. Marcus, *Acta Chem. Scand.*, **11**, 329 (1957).

THE APPARENT PARTIAL SPECIFIC VOLUMES OF PROTEINS IN SOLUTIONS OF GUANIDINE HYDROCHLORIDE

BY F. J. REITHEL AND J. D. SAKURA

Department of Chemistry, University of Oregon, Eugene, Oregon

Received May 20, 1963

During the past few years there has been a wider usage of sedimentation equilibrium in the ultracentrifuge due to the work of van Holde and Baldwin[1] and that of Yphantis.[2] The methods of calculation require reliable values for the apparent partial specific volume, ϕ, of the sedimenting species. In this Laboratory experimentation has been going forward on the determination of protein molecular weights in 6 *M* guanidine hydrochloride.[3] This solvent was chosen because of its wide applicability in dissociating proteins. Few data have been published pertaining to ϕ for proteins in three-component systems and it became necessary to examine possible variations of this quantity with respect to a number of factors.

Experimental

The density gradient technique of Linderstrøm–Lang[4] was used in this investigation. Gradients in the solvent mixture dodecane–*o*-dichlorobenzene were produced as described by Miller and Gasek.[5] In general, the techniques employed were those detailed by Schachman[6] and Miller and Gasek. One set of apparatus was assembled in an aquarium bath maintained at 25° with a regulation of ±0.005°. Another set was assembled in a water bath in the cold room and the temperature maintained at 4° with a regulation of ±0.005°.

Ribonuclease A was prepared[7,8] from Sigma Type III ribonuclease, Lot R-22B-70. The column purification demonstrated only a very small impurity in the commercial sample. The β-lactoglobulin was a sample obtained from Dr. S. Timasheff, Eastern Regional Research Laboratory. The glutamic acid dehydrogenase used was obtained as a 2% solution in 50% glycerol as prepared by Boehringer (Calbiochem).

All solvents used were purified. The guanidine hydrochloride was purified as follows. It was dissolved in a minimum volume of absolute methanol using a 45° water bath and magnetic stirring. This solution was filtered through a jacketed funnel containing a

(1) K. E. van Holde and R. L. Baldwin, *J. Phys. Chem.*, **62**, 734 (1958).

(2) D. A. Yphantis, *Ann. N. Y. Acad. Sci.*, **88**, 586 (1960).

(3) F. J. Reithel, Abstracts, Fifth International Congress of Biochemistry, Moscow, USSR, August, 1961, p. 47.

(4) K. Linderstrøm–Lang and H. Lanz, Jr., *Compt. rend. trav. Lab. Carlsberg, Ser. chim.*, **21**, 315 (1935).

(5) G. L. Miller and J. McG. Gasek, *Anal. Biochem.*, **1**, 78 (1960).

(6) H. K. Schachman in "Methods in Enzymology," Vol. IV, S. P. Colowick and N. O. Kaplan, Ed., Academic Press, New York, N. Y., 1957, p. 32.

(7) C. H. W. Hirs, ref. 6 Vol. I, S. D. Colowick and N. O. Kaplan, Ed., Academic Press, New York, N. Y., 1955, p. 113.

(8) G. Taborsky, *J. Biol. Chem.*, **234**, 2652 (1959).

pad of powdered cellulose. Crystallization was allowed to proceed overnight at −5°. The mother liquor was poured off, the crystals were drained, and finally pressed dry between sheets of filter paper. This process was repeated until the methanol solution showed no yellow color. Three crystallizations were usually found to be necessary. The final product was freed of methanol by warming for a few hours in a vacuum oven at 40° and was finally dried in a vacuum desiccator.

The moisture content of dry protein samples was determined by heating at 110° in a vacuum oven until constant weight was attained. In the case of ribonuclease and β-lactoglobulin weight fractions of protein in the solutions could be calculated directly. In the case of glutamic acid dehydrogenase this was not possible. Spectrophotometric readings were used to estimate protein content: in buffer $A^{279m\mu} = 0.971$ (1 mg./ml.); in 6 M guanidine hydrochloride $A^{279m\mu} = 0.820$.

Calculations of apparent specific volume employed the equation

$$\phi = \frac{1}{\rho_0} - \frac{1}{n}\left(\frac{1}{\rho_0} - \frac{1}{\rho}\right)$$

where n = weight fraction of protein, ρ_0 = density of solvent or dialyzate, and ρ = density of the protein solution.

Results and Discussion

Comparison of ϕ in Buffers and in 6 M Guanidine Hydrochloride.—At a concentration of 2% ribonuclease in 6 M guanidine hydrochloride the value of ϕ at 25° was 0.709 ± 0.002 ml./g.; at 4° it was 0.700. Thus $\Delta\phi$ per degree is 4.3×10^{-4}. A recent careful determination[9] of ϕ for ribonuclease in phosphate buffer at 25° yielded the value 0.709 ± 0.002. The temperature coefficient above is similar to that found by others.[10,11]

β-Lactoglobulin at a concentration of 2% in 6 M guanidine hydrochloride had a ϕ value of 0.756 at 25° and 0.738 at 4°. $\Delta\phi$ per degree was 8.6×10^{-4}. The value of ϕ, in buffer, frequently quoted,[12] 0.7514 at 20°, was redetermined. At a concentration of 2% in 0.05 M phosphate buffer at 25° the value of ϕ was 0.752.

The partial specific volume of glutamic acid dehydrogenase in buffer (temperature not given) has been estimated pycnometrically[13] as 0.75. We were not able to obtain preparations of the enzyme which could be dissolved in any buffer at a concentration of 2% and which would remain perfectly clear during overnight dialysis. We were successful in obtaining satisfactory 2% solutions in 50% glycerol. At 25° ϕ was 0.745. To these glycerol solutions was added solid guanidine hydrochloride to obtain a 6 M solution. Such a solution was then dialyzed for 5 days at 4° against 6 M guanidine hydrochloride. It was necessary to add the solid reagent because the behavior of this protein at lower concentrations of the reagent is unpredictable. The resultant concentrations of protein were about 1%. The value of ϕ at 25° was 0.752 and at 4° it was 0.739. $\Delta\phi$ per degree was 6.2×10^{-4}.

The Relation of Changes in ϕ to Dissociation and Unfolding.—Ribonuclease was used in this investigation because it can be obtained in a state of reasonable purity in reasonable quantity and because it cannot dissociate in guanidine hydrochloride.

(9) A. M. Clarke, D. W. Kupke, and J. W. Beams, *J. Phys. Chem.*, **67**, 929 (1963).
(10) D. J. Cox and V. N. Schumaker, *J. Am. Chem. Soc.*, **83**, 2433 (1961).
(11) D. N. Holcomb and K. E. van Holde, *J. Phys. Chem.*, **66**, 1999 (1962).
(12) K. O. Pedersen, *Biochem. J.*, **30**, 961 (1936).
(13) J. A. Olson and C. B. Anfinsen, *J. Biol. Chem.*, **197**, 67 (1952).

In contrast, β-lactoglobulin is known to dissociate in high concentrations of hydrogen ion.[14] The value of ϕ for a 2% solution of β-lactoglobulin in 0.01 M HCl at 25° is 0.764. A solution similar to this but 6 M in guanidine hydrochloride as well yielded a ϕ value at 25° of 0.764 and at 4° of 0.748. $\Delta\phi$ per degree was 7.6×10^{-4}. Preliminary results have indicated that the molecular weight of β-lactoglobulin in guanidine hydrochloride[3] is near 36,000 but the optical rotation has a large negative value. In this reagent some type of unfolding but no dissociation occurs. Addition of hydrogen ion does effect a dissociation with a concomitant drop in molecular weight. The change in ϕ observed seems to be related to the conformation of the charged protein rather than the dissociation process.

In the case of glutamic acid dehydrogenase, the molecular weight in guanidine hydrochloride[3] appears to be of the order of 100,000 and preliminary results indicated dissociation. However, as noted earlier, such dissociation did not cause a change in ϕ as long as the solution was kept at 4°. When such solutions were allowed to stand at room temperature for several hours, or if the dialyses were carried out at room temperature, two changes were noted. First, boundaries formed in a synthetic boundary cell in the ultracentrifuge were very asymmetric. Second, ϕ values were low and varied with the history of treatment. Values between 0.682 and 0.725 were observed at 25°. Some type of refolding may be responsible since β-lactoglobulin solutions (in guanidine hydrochloride) behaved similarly.

The results of this investigation indicate that the apparent specific volume of a protein, dissociable or not, in 6 M guanidine hydrochloride differs very little from that in buffer. This is in agreement with those[15] who have found ϕ to vary but little with salt concentration, but it is perhaps at variance with the values reported for proteins in urea.[16] It is possible that the low values found were due to experimentation at room temperature.

Acknowledgment.—This research was supported by Grant G-18736 from the National Science Foundation.

(14) R. Townend, L. Weinberger, and S. N. Timasheff, *J. Am. Chem. Soc.*, **82**, 3175 (1960).
(15) J. B. Ifft and J. Vinograd, *J. Phys. Chem.*, **66**, 1990 (1962).
(16) P. A. Charlwood, *J. Am. Chem. Soc.*, **79**, 776 (1957).

THE SOLVATION OF POLAR GROUPS. II. A PHASE STUDY OF THE DIMETHYL SULFOXIDE–*p*-CHLOROBENZONITRILE SYSTEM

BY C. D. RITCHIE AND ARDEN PRATT[1]

Department of Chemistry, State University of New York at Buffalo, Buffalo 14, New York

Received May 25, 1963

In the first paper of this series,[2] we reported the results of a study of integrated intensities of the infrared bands of a series of nitriles in binary solvent systems. The results were interpreted in terms of 1:1 complex formation of the polar nitrile group with the polar solvent component.

(1) NSF Faculty Fellow, 1962–1963.
(2) C. D. Ritchie, B. A. Bierl, and R. J. Honour, *J. Am. Chem. Soc.*, **84**, 4687 (1962).

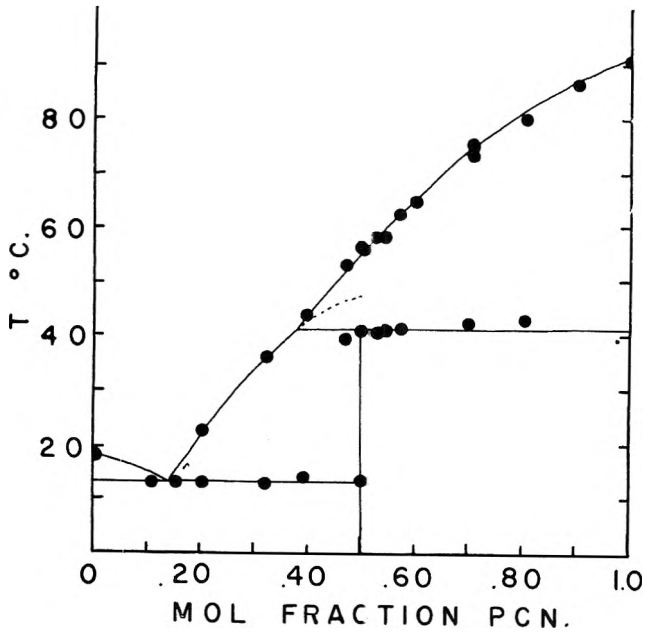

Fig. 1.—Phase diagram for the system: *p*-chlorobenzonitrile (PCN)–dimethylsulfoxide.

Although we felt that this interpretation was well supported by the data, and moreover, was in excellent agreement with the results of other studies,[3,4] we recognized the desirability of more concrete evidence for the existence of the postulated complexes. In order to provide this evidence, we have carried out a phase study of the *p*-chlorobenzonitrile–dimethylsulfoxide system.

Experimental

The dimethyl sulfoxide used was Baker's A.R. grade material and was purified by fractional freezing prior to each experiment. The *p*-chlorobenzonitrile was Eastman White Label material.

Cooling curves of various mixtures of the two materials were obtained with a Beckmann-type freezing point apparatus. The apparatus was fitted with an enclosed glass stirrer and a temperature measuring device and was immersed in an ice–salt bath. The container was insulated so that a suitably slow cooling rate was obtained.

The temperature measuring device was in most instances a Sargeant thermistor and bridge attached to a 10-mv. potentiometer. Due to the somewhat limited range of the thermistor, the higher temperatures were measured with a mercury thermometer, and the cooling curve was plotted manually.

In a few cases, supercooling occurred at the first temperature break on the cooling curve, but such supercooling rarely exceeded 0.2°. In the majority of cases, no supercooling was observable.

Additional confirmation of the freezing point of the 70 mole % *p*-chlorobenzonitrile mixture was obtained by capillary melting point observation of the solid formed on freezing. The first liquid was apparent at 45°, and the material was completely liquid at about 75°.

Results and Discussion

The phase diagram constructed from the cooling curves[5] is shown in Fig. 1. This diagram is of the same general nature as the freezing point diagram for the chloroform–benzonitrile system which has been reported by Murray and Schneider.[6] The diagram shown in Fig. 1 is, however, more complete than a simple freezing point diagram. The eutectic for the phases; dimethyl sulfoxide:complex (solid), liquid has been observed for all mixtures up to 50 mole % *p*-chlorobenzonitrile, but is not observable for higher concentrations. The incongruent melting point of the complex has been observed for mixtures of 80 to 47 mole % *p*-chlorobenzonitrile.

The diagram clearly shows the occurrence of a complex at 50 mole %, with an incongruent melting point of 41.5°, and a probable metastable melting point of 47°. Comparison of this diagram with that of the chloroform–benzonitrile system indicates that the stability of the dimethyl sulfoxide–nitrile complex is comparable to that of the chloroform–nitrile complex.[7]

We feel that this phase study provides exceptionally strong support of our earlier hypotheses.

The implication is clear that physical and chemical properties of solutes in such aprotic solvents as dimethyl sulfoxide will be strongly affected by specific solvent–solute interactions.

(3) C. D. Ritchie and E. S. Lewis, *J. Am Chem Soc.*, **84**, 591 (1962).

(4) R. W. Taft, Jr., E. Price, I. R. Fox, I. C. Lewis, K. K. Andersen, and G. T. Davis, *ibid.*, **85**, 709 (1963).

(5) B. J. Mair, Q. R. Glasgow, and F. D. Rossini, *J. Res. Natl. Bur. Std.*, **26**, 591 (1941).

(6) F. E. Murray and W. G. Schneider, *Can. J. Chem.*, **33**, 797 (1955).

(7) J. E. Ricci, "The Phase Rule and Heterogeneous Equilibrium," D. Van Nostrand Co., Inc., New York, N. Y., 1951, pp. 128–129.

THE HEATS OF FUSION OF SOME RARE EARTH METAL HALIDES

BY A. S. DWORKIN AND M. A. BREDIG

Chemistry Division, Oak Ridge National Laboratory,[1] Oak Ridge, Tennessee

Received May 27, 1963

We have previously measured and reported the heats of fusion of a number of lighter rare earth chlorides and iodides.[2] The present report extends these measurements to other rare earth halides with a variety of crystal structures. These data are of interest in connection with our continuing program of the interpretation of phase equilibria and electrical conductance measurements in metal–metal halide systems.

The copper block drop calorimeter used for the measurements and the experimental procedure were previously described in detail.[3]

The rare earth halides were prepared by the reaction of the rare earth oxide with a large excess of the corresponding ammonium halide. Upon completion of the reaction, the excess ammonium halide was sublimed at temperatures up to 500°. The rare earth halide was then sublimed under high vacuum and subsequently handled in an inert atmosphere. No insoluble matter or alkalinity was found on dissolving the halides in water or in alcohol. Spectrographic analysis indicated an absence of foreign metals and less than 0.5% of other rare earth ions.

Table I lists the heat and entropy of fusion, the heat content of the solid salts at their melting points, and the heat capacities of the solid and liquid in the vicinity of the melting temperature. The heat contents were measured with a precision of 0.1–0.2% and an estimated over-all accuracy of 0.5%. The heats of fusion are believed to be accurate to at least ±1–2% and the heat capacities to about ±5%.

$LaBr_3$, $PrBr_3$, and $GdCl_3$ (which have the UCl_3 type structure[4]) and $NdBr_3$ with the $PuBr_3$ type structure[4] have similar entropies of fusion to those found[2]

(1) Operated by the Union Carbide Corporation for the U. S. Atomic Energy Commission, Oak Ridge, Tennessee.

(2) A. S. Dworkin and M. A. Bredig, *J. Phys. Chem.*, **67**, 697 (1963).

(3) A. S. Dworkin and M. A. Bredig, *ibid.*, **64**, 269 (1960).

(4) W. H. Zachariasen, *Acta Cryst.*, **1**, 265 (1948).

TABLE I

HEAT CAPACITY AND HEAT AND ENTROPY OF FUSION OF SOME RARE EARTH METAL HALIDES

	T_m, °K.	C_p solid, cal. mole^{-1} deg.$^{-1}$	C_p liq., cal. mole^{-1} deg.$^{-1}$	H_{Tm} (solid) $- H_{298}$, kcal. mole^{-1}	ΔH_m, kcal. mole^{-1}	ΔS_m, e.u. mole^{-1}
$LaBr_3$	1061	33.0	34.5	20.3	13.0	12.3
$PrBr_3$	966	31.5	37.0	18.0	11.3	11.7
$NdBr_3$	955	31.0	35.5	17.6	10.8	11.3
$GdBr_3$	1058	32.1	32.3	19.6	8.7	8.2
$GdCl_3$	875	29.1	33.7	14.8	9.6	11.0
$HoCl_3$	993	29.0	35.3	17.4	7.0	7.1
$ErCl_3$	1049	32.0	33.7	19.2	7.8	7.4

for the chlorides of La, Pr, and Nd (UCl_3 type) and the iodides of Ce and Pr ($PuBr_3$ type). On the other hand, $HoCl_3$ and $ErCl_3$ ($YCl_3 = AlCl_3$ type[5]) and $GdBr_3$ whose structure is not reported have unusually low entropies of fusion. $AlCl_3$ has a much higher entropy of fusion (18.2 e.u.), because melting involves transformation to a liquid that unlike the crystal is not ionic but molecular in structure. The low entropy of fusion of $HoCl_3$, $ErCl_3$, and $GdBr_3$, in which the ionic radius $r_{M^{3+}}$ is greater than $r_{Al^{3+}}$, is in agreement with the fact that their melts are ionic like the crystals and like the melts of the lower rare earth trichlorides, $LaCl_3$, etc. The especially low value of ΔS_{fusion} may, however, suggest looking, *e.g.*, by X-ray diffraction, for a slightly different ionic structure of the melts, possibly including increased ion association to $(MCl)^{2+}$ or the like.

Acknowledgment.—We are indebted to R. B. Quincy for the preparation of the salts used in this work.

(5) D. H. Templeton and G. F. Carter, *J. Phys. Chem.*, **58**, 940 (1954).

EFFECTS OF IMPURITIES ON THE LUMINESCENCE OF RARE EARTH CHELATES[1]

BY M. L. BHAUMIK AND I. R. TANNENBAUM

Electro-Optical Systems, Inc., Pasadena, California

Received June 8, 1963

Recently there has been a great deal of interest in the study of luminescence of rare earth chelates, primarily because of their possible use as laser materials. It has been observed during the progress of our experimental investigations that the luminescence processes in rare earth chelates, especially those parameters which govern laser operation, *viz.*, the lifetime of the excited states, the spectral characteristics, the quantum efficiencies, etc., are strongly dependent on the impurities present and vary considerably with the degree of purification. These impurities usually are introduced during the synthesis of the chelates, and great care must be taken to remove them in order to obtain reliable and consistent results. The effects of the impurities are illustrated in the study of the luminescence in europium trisbenzoylacetonate (EuBA), europium trisdibenzoylmethide (EuDBM), and terbium trisacetylacetonate (TbAA) chelates.

The extreme sensitivity of the luminescence of the chelates on the impurities can be understood in the light of the origin of these emissions. The transitions giving rise to the line emission in rare earth atoms normally are forbidden by Laporte's rule, but become allowed due to the mixing of energy levels produced by the surrounding perturbation field. Thus the fluorescence in the rare earth atom is determined to a great extent by its microscopic environment.

The chelates were prepared according to the method of Whan, *et al.*[2] The results of the analysis of the samples are shown in Table I.

TABLE I

CHEMICAL ANALYSIS OF THE EUROPIUM CHELATES

Sample	Weight percentages C	H	M_2O_3
$Eu(BA)_3$			
Theoretical	56.70	4.25	27.80
Observed (pure)	55.61	4.78	29.30
Observed (impure)	...	..	25.01
$Eu(DMB)_3$			
Theoretical	65.80	4.02	21.40
Observed (pure)	...	..	21.80
Observed (impure)	67.04	4.85	18.06

The emission spectra of EuBA and EuDBM consist of an intense group of lines at about 613 mμ and other weaker lines. The intense lines can be identified as the transition $^5D_0$–$^7F_2$ in europium. The peak positions due to this transition are listed in Table II; both EuBA and EuDBM show four lines before purification and only two after purification. Similar results are indicated in other transitions as well. From group theoretical considerations[3] only two lines are expected in the above transition. The increased number of lines in the impure chelates may be a collection of lines arising out of different species of chelates or the impurity may, somehow, distort the symmetry of the perturbation field. In the latter case only one line is expected in the transition $^5D_0$–$^7F_0$ occurring at about 5801 Å. Actually, more than one line is observed in this transition indicating that the impure chelates consist of different species. This is also supported by the measurement of decay times. While the decay curves for the pure chelates are smooth exponential functions, those of the impure chelates seem to consist of components having different decay times.

TABLE II

PEAK POSITIONS OF LINES DUE TO TRANSITION $^5D_0$–$^7F_2$ IN EUROPIUM CHELATES

Benzoyl acetonate $\lambda_{77°K.}$, Å.		Dibenzoyl methide $\lambda_{77°K.}$, Å.	
Pure	6125	Pure	6130
	6132		6136
Impure	6111	Impure	6111
	6128		6122
	6140		6133
	6165		6143

The average lifetimes of EuDBM microcrystals before purification were measured to be about 550 and 350 μsec. at 77 and 300°K., while the corresponding values after purification are 505 and 105 μsec., respectively. Terbium acetylacetonate (TbAA), also in the microcrystal form, was found to have a lifetime of 550 and 730 μsec. at 77°K. before and after purification, respectively.

The efficiency of the rare earth emission after excita-

(1) Work supported in part by Rome Air Development Center under Contract AF 30(602)-2914.

(2) R. E. Whan and G. A. Crosby, *J. Mol. Spectry.*, **8**, 315 (1962).

(3) M. L. Bhaumik, *ibid.*, to be published.

tion in the ultraviolet would depend upon various factors. In impure chelates, the impurities themselves may absorb the exciting light without transferring the energy to the rare earth ion; instead, the energy is dissipated to the lattice by nonradiative processes and thus lowering the measured luminescence efficiency. The impurities may also enhance the nonradiative quenching in the ligand molecules before the transference of energy. Also, the energy may be lost at the rare earth ion site due to difference in lattice coupling produced by the impurities. Experimental observation in the difference of luminescence efficiency before and after purification has been quite remarkable.

The results of the present investigation, therefore, show that the luminescence processes in the rare earth chelate is very sensitive to the presence of impurities. In order to obtain consistency in results, each sample should be studied only after careful purification and satisfactory chemical analysis.

A REVALUATION OF THE QUANTUM EFFICIENCY OF THE URANYL OXALATE SYSTEM

BY C. A. DISCHER, P. F. SMITH, I LIPPMAN, AND R. TURSE

Pharmaceutical Chemistry Laboratories, Rutgers, The State University, Newark 4, New Jersey

Received May 29 1963

In preparation for projected investigations of the decomposition mechanism of some photosensitive compounds of pharmaceutical interest, it was necessary to establish a suitable irradiation apparatus. In order to evaluate the operating characteristics of the instrumentation developed, uranyl oxalate solutions were irradiated and the quantum efficiencies determined. Values of the quantum efficiency of this photoreaction have been reported for various wave lengths by Leighton and Forbes,[1] who also have shown that the photolysis products do not interfere in the analysis for the undecomposed oxalate and do not absorb light at the wave lengths used for excitation. Forbes and Heidt[2] have shown that the quantum efficiency varies with the wave length of the light used to irradiate the uranyl oxalate, but that dilution has no effect on the quantum efficiency.

Experimental

Instrumentation.—A Bausch and Lomb grating monochromator, Model No. 33-86-45-49, was used as the light source. The emergent monochromatic beam was passed from the exit lens into a light-tight reaction box, secured to the monochromator. A light shield, a reaction cell, and a thermopile were properly aligned within this box. The light shield, serving as a mask with an accurately known rectangular opening, was so positioned in front of the irradiation cell that the thermopile could effectively sample a known cross section of the light beam passing through the sample. The irradiation cell employed had quartz windows, a volume of 3.0+ ml., and was jacketed for thermostating. The light intensity was measured with an Eppley astronomical thermopile having an output of 0.0453 μv./μw./cm.^{2}. The signal from the thermopile was amplified by a Liston-Becker Model 14 breaker-amplifier. A record of the amplified signal was produced with an Esterline-Angus Model AW automatic recording d.c. milliammeter. The 117 v. a.c. required for the operation of the lamp of the monochromator and the breaker-amplifier was stabilized by a Sorenson Model 1000-S electronic voltage regulator. A heat exchanger coil was built into the reaction box; a temperature of 25 ± 0.05° was maintained during irradiation.

Irradiation Procedures.—A calibrated syringe was used to measure exactly 3.00 ml. of a 0.0500 *M* uranyl oxalate solution into the reaction cell. Samples were irradiated for varying periods of time at 365.5 and 435.8 mμ, respectively. The intensity of the incident beam and the intensity of the beam after passing through the sample were recorded at regular intervals during irradiation.

Analytical Procedures.—The oxalate concentration was determined by a micropotentiometric titration. An Alga micrometer syringe was used to measure a 0.050-ml. sample of oxalate solution, original or irradiated, into a 5-ml. beaker. The sample was diluted with 3.0 ml. of water and 0.3 ml. of 6 *N* sulfuric acid. The beaker was placed in a depression in a heated stage and maintained at 65° during the titration. Magnetic stirring was provided. A second Alga micrometer syringe was used as a buret for addition of the titrant, 0.0340 *M* cerum(IV) sulfate. The end point was detected potentiometrically, using a platinum–tungsten electrode system with a Beckman Model H-2 pH meter. The titration was performed in red light. Control samples, kept in the dark in the reaction box during each run, showed no measurable decomposition.

TABLE I

Wave length, mμ	Fraction of oxalate decomposed	Molecules decomposed × 10^{18}	Photons absorbed × 10^{18}	Quantum efficiency
365.5	0.0592	5.18	10.58	0.490
365.5	.0498	4.32	8.93	.483
365.5	.0661	5.74	11.88	.483
365.5	.0519	4.50	9.09	.495
365.5	.0227	1.97	3.98	.495
365.5	.0263	2.28	4.59	.497
365.5	.0474	4.11	8.47	.486
365.5	.0200	1.73	3.54	.490
435.8	.0242	2.10	3.64	.576
435.8	.0208	1.79	3.10	.577
435.8	.0172	1.48	2.61	.567
435.8	.0215	1.85	3.27	.566
435.8	.0207	1.78	3.08	.578

Discussion and Results

The quantum efficiencies obtained are given in Table I. At 365.5 mμ, these values have a range 0.483–0.497, with a mean of 0.492 and a standard deviation of the mean of 0.002. Leighton and Forbes[1] report a series of 14 values, in the range 0.445–0.530 at this wave length, with a mean value of 0.490 and a standard deviation of the mean of 0.007 (our calculations). At 435.8 mμ, the mean value of the results reported in Table I is 0.573, with a standard deviation of the mean of 0.002. These values compare with 0.584 and 0.016, respectively, calculated using the experimental results reported for 435.8 mμ by Leighton and Forbes.

(1) W. G. Leighton and G. S. Forbes, *J. Am. Chem. Soc.*, **52**, 3139 (1930).
(2) G. S. Forbes and L. J. Heidt, *ibid.*, **56**, 2363 (1934).

THE PHOTOLYSIS OF GLYCIDALDEHYDE IN THE VAPOR PHASE

BY F. C. GOODSPEED AND F. E. BLACET

Contribution Number 1593 from the Department of Chemistry, University of California, Los Angeles 24, California

Received June 5, 1963

Glycidaldehyde, 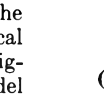 , herein referred to as GDA, is the simplest of the epoxy aldehydes. The presence of a second active functional group in the molecules has made the photochemical study of this aldehyde of particular interest.

Experimental

The GDA used in this study was kindly donated by the Shell Development Co.; f.p. −61.8°; b.p., 112–113° (760 mm.);

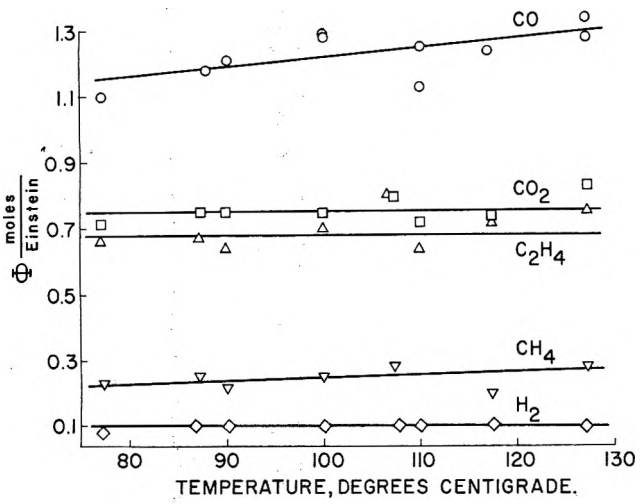

Fig. 1.—Quantum yields, Φ, of major photolysis products of pure GDA obtained at λ 3130 over the temperature range 77–127° (GDA pressures varied from 27 to 36 mm.).

refractive index, $n^{20}D$ 1.4200. Vapor phase chromatography indicated that the original sample was 99.5% pure, containing trace amounts of water, acetaldehyde, acetic acid, and a fourth unidentified substance, possibly a hydroxy aldehyde. The major impurities, water and acetaldehyde, were removed by use of a drying agent and repeated bulb-to-bulb distillation *in vacuo* from ice baths.

The photolysis cell of fused silica, 30 mm. in diameter and 200 mm. in length, was incorporated in a typical vacuum train and was inclosed in an air thermostat. The radiation source was a Hanovia Type A, medium pressure Hg arc used with a crystalline quartz monochromator. Light absorption by the GDA was monitored by using a photocell in conjunction with an amplifying microgalvanometer. Light intensity was determined by the use of an acetone internal actinometer.

Photolysis products were identified and quantitatively determined by vapor phase chromatography and by mass spectrometry.

Results

The gas phase ultraviolet absorption spectrum of GDA resembles that of propionaldehyde[1] with the following major differences. No absorption band structures are evident. The longer wave-length electronic absorption region has a maximum at 2950 Å. and an ϵ_{max} of 16.6 l. cm.$^{-1}$ mole^{-1}. The corresponding values for propionaldehyde are 2900 Å. and 21.0 l. cm.$^{-1}$ mole^{-1}. Like other aliphatic aldehydes, GDA has a second strong electronic absorption region which lies below 2500 Å.

Figure 1 gives quantum yields, Φ, for the major photolysis products of pure GDA obtained at λ 3130 Å. over the temperature range 77 to 127°. In addition to carbon monoxide, carbon dioxide, methane, ethylene, and hydrogen given in the figure, acetaldehyde was found with an average Φ of 0.05, and both propylene and formaldehyde were detected in trace amounts by mass spectrometry.

Infrared spectra of the liquid residues from several runs at λ 3130 Å. showed a band maximum at 1832 cm.$^{-1}$ which is not given by pure liquid GDA. This band is interpreted as being due to propiolactone, in view of the work of Linnell and Noyes,[2] who report an infrared band maximum at 1835 ± 5 cm.$^{-1}$ for the liquid phase of this compound.

Table I gives a comparison of quantum yields of major products obtained at λ 3130 Å. for pure GDA with quantum yields obtained in the presence of 2,3-dimethylbutane and of cyclohexene. Table I also gives exploratory results obtained at λ 2654 Å., both for pure GDA and for mixtures with acetone in which acetone was the dominant absorbing substance.

During the course of the runs, small translucent polymer-like droplets appeared on the cell walls and in the gas lines. These did not evaporate at 100° and under a vacuum maintained by liquid nitrogen.

TABLE I

RESULTS OF EXPLORATORY PHOTOLYSES OF GDA IN MIXTURES WITH OTHER COMPOUNDS AT λ 3130 and at λ 2654 Å.

	λ 3130			λ 2654		
Run	A[a]	B[b]	C[c]	D[a]	E[d]	F[d]
GDA pressure, mm.	27.0	25.5	37.0	16	15	15
Temp., °C.	77	77	77	120	120	120
Φ_{CO}	1.10	1.34	1.01	1.6	[e]	[e]
Φ_{CH_4}	0.23	0.21	0.18	0.5	[e]	[e]
Φ_{CO_2}	0.71	0.2	0.1	0.8	0.25	0.5
$\Phi_{C_2H_4}$	0.66	0.2	0.1	0.8	0.5	0.5

[a] Pure GDA. [b] 2,3-Dimethylbutane (59.5 mm.) added. [c] Cyclohexene (37.0 mm.) added. [d] Acetone (70 mm.) added. [e] Not determined.

Discussion

These results indicate that upon the absorption of light, GDA molecules can disperse the energy by several primary chemical paths, the more important of which may be represented as follows.

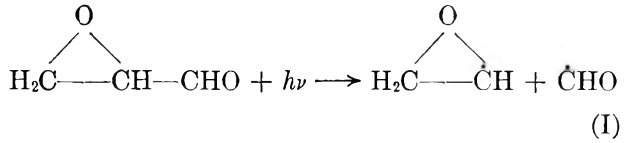

(I)

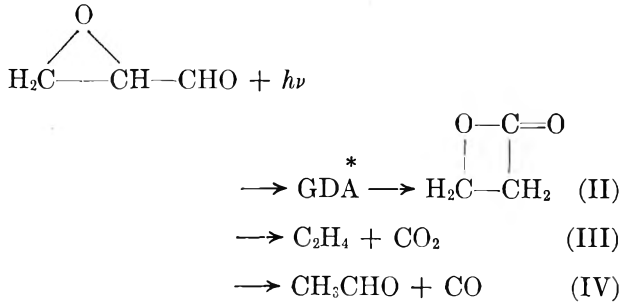

The quantum yields of carbon dioxide and ethylene given in Fig. 1 show that at λ 3130 about 75% of the absorbed energy initiates process III. In this, GDA* may have assumed the structure of activated propiolactone, some small amount of which presumably stabilized giving process II and thus accounting for the propiolactone found in the condensate. The 0.05 average for Φ_{CH_3CHO} suggests that process IV may account for about 5% of the absorbed energy, but the evidence is not conclusive since acetaldehyde could be formed in radical reactions subsequent to primary process I. Both III and IV were postulated by Linnell and Noyes[2] as photodissociation reactions of liquid propiolactone.

The temperature independence of Φ_{CO_2} and $\Phi_{C_2H_4}$ indicates that III involves concerted intramolecular rearrangement and dissociation. Since this reaction appears to be the only source of carbon dioxide, Φ_{CO_2} is a measure of ϕ_{III}. The consistent slightly smaller

(1) F. E. Blacet, *J. Phys. Colloid Chem.*, **52**, 534 (1948).
(2) R. H. Linnell and W. A. Noyes, Jr., *J. Am. Chem. Soc.*, **72**, 3863 (1950).

quantum yields of ethylene compared to carbon dioxide may be due to polymerization of the ethylene subsequent to its formation, as well as to the creation of trace amounts of propylene.

Primary process I is consistent with the generally accepted primary photolysis of the aliphatic aldehydes into radicals.[3] A variety of secondary reactions may follow I, among which the following seem pertinent.

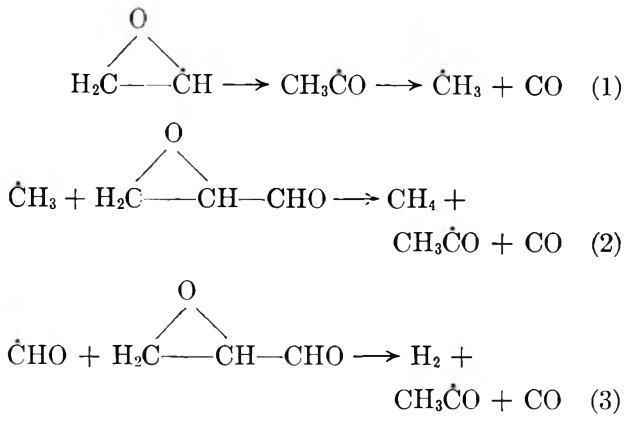

If reaction 3 is the principal consumer of formyl radicals, Φ_{H_2} should be a measure of ϕ_1 and should be temperature independent. The results given in Fig. 1 bear out this postulate and indicate that about 10% of the absorbed energy at λ 3130 Å. initiates process I. From this 10% must come carbon monoxide quantum yields greater than one, indicating the involvement of cyclic reactions. Reactions 1 and 2 constitute one such chain. These reactions, however, are inadequate to explain all that takes place since they lead to Φ_{CO} equal to $2\Phi_{CH_4}$ instead of the observed value of more than $4\Phi_{CH_4}$. To obtain a material balance, in some way carbon monoxide must become separated from substances which ultimately become condensate or polymer.

The trace of propylene found may be accounted for by a reaction of $\dot{C}H_3$ with ethylene and the resulting propyl radical extracting a hydrogen atom in a manner analogous to reaction 2. The trace of formaldehyde, likewise, may have come from similar steps involving the formyl radical.

The limited results given in Table I show that at λ 3130 Å. substantial amounts of either 2,3-dimethylbutane or cyclohexene have little effect on Φ_{CO} and Φ_{CH_4}. This indicates that the activation state leading to primary process I is of short duration and that the radicals formed in this and subsequent reactions are at most only slightly trapped by cyclohexene. On the other hand, the drastic reductions of Φ_{CO_2} and $\Phi_{C_2H_4}$ brought about by the presence of these optically transparent gases indicate that GDA* in process III has a sufficiently long life so that it may undergo substantial collisional deactivation under the experimental conditions employed. Stabilization could be to either propiolactone or to the original glycidaldehyde.

An exploratory experiment with pure GDA at wave length 2654 Å. (run D, Table I) gave quantum yields of the major products consistent with the mechanisms postulated herewith for λ 3130 Å. Additional exploration with mixtures of GDA and acetone in such proportion that the acetone absorbed about 90% of the radiant energy (runs E and F) gave surprisingly high quantum yields of carbon dioxide and ethylene. This suggests that acetone may photosensitize the decomposition of glycidaldehyde in a manner analogous to primary process III.

(3) E. W. R. Steacie, "Atomic and Free Radical Reactions," 2nd Ed., Reinhold Publishing Corp., New York, N. Y., 1954, Chapter V.

COMMUNICATIONS TO THE EDITOR

A LEAST SQUARES SOLUTION FOR THE VAN LAAR CONSTANTS OF A BINARY MIXTURE

Sir:

This note describes a statistical method for calculating the constants of a binary van Laar equation from equilibrium data at constant temperature. When the total pressure is not given, it is necessary to use a tedious trial and error technique to solve for the constants. Furthermore, if more then two equilibrium compositions are known, then a series of different constants can be calculated, which have to be averaged in some manner. The method outlined below overcomes both problems by eliminating trial and error procedures and using all available data to calculate the values of the constants which give the best fit to the data.

The van Laar equation for a two-component system takes the form

$$\ln \gamma_A = \frac{A}{\left[1 + \left(\frac{X_A}{X_B}\right)\left(\frac{A}{B}\right)\right]^2} \qquad (1a)$$

and

$$\ln \gamma_B = \frac{B}{\left[1 + \left(\frac{X_B}{X_A}\right)\left(\frac{B}{A}\right)\right]^2} \qquad (1b)$$

where γ_A and γ_B are activity coefficients, X_A and X_B are mole fractions, and A and B are the unknown constants which are to be determined. Equations 1a and 1b can be combined with the equilibrium relationships

$$P_A X_A \gamma_A = Y_A \pi \qquad (2a)$$

and

$$P_B X_B \gamma_B = Y_B \pi \qquad (2b)$$

where P_A and P_B are the vapor pressures, to yield

$$\ln\left[\frac{\alpha_{AB} P_A}{P_B}\right] = \frac{B}{\left[1 + \left(\frac{X_B}{X_A}\right)\left(\frac{B}{A}\right)\right]} - \frac{A}{\left[1 + \left(\frac{X_A}{X_B}\right)\left(\frac{A}{B}\right)\right]} \qquad (3)$$

where $\alpha_{AB} = (Y_A X_B)/(Y_B X_A)$. This result can be put in the form

$$\ln\left[\left(\frac{P_A}{P_B}\right)\alpha_{AB}\right] = B \times \frac{\left[\left(\frac{X_A}{X_B}\right)^2 - \frac{B}{A}\right]}{\left[\left(\frac{X_A}{X_B}\right)^2 + \frac{B}{A}\right]^2} \qquad (4)$$

Equation 4 can be solved for A and B using a least squares technique. This is done by assuming successive values for B/A and then solving for the associated least squares value of B in the regression equation

$$S = Bt \qquad (5)$$

where S is the left-hand side of (4), and t is the factor in (4) which multiplies B. The regression results for B and the assumed values of B/A are then plotted against R^2, the fraction of explained variance. Where this function is a maximum, the values of B and B/A are "best" in the least squares sense. Alternatively, the results can be plotted against the residual sum of squares which passes through a minimum where B and B/A are optimal.

Consider the following example taken from Krelschmer, *et al.*,[1] for an ethyl alcohol–isooctane system at 25°.

TABLE I

(P_A/P_B = 1.14286)

	X_A	Y_A	α_{AB}	X_A/X_B
1	0.0565	0.4441	0.0749	0.0598
2	.1182	.4762	.1473	.1338
3	.1700	.4910	.2132	.2048
4	.2748	.5073	.3688	.3793
5	.3773	.5153	.5699	.6051
6	.5416	.5285	1.0535	1.1834
7	.7225	.5501	2.1356	2.6101
8	.8511	.5994	3.8232	5.7114

From plots of the data in Table II, the optimum value of B/A was found to be 0.675 from which was found A = 1.600 and B = 0.640. The above calculations were carried out on an IBM 7090 regression program.

TABLE II

LEAST SQUARES SOLUTION FOR THE VAN LAAR CONSTANTS

	B/A, assumed	B, calcd.	R^2
1	0.2	0.4030	0.8759
2	.3	.4941	.9368
3	.4	.5787	.9687
4	.5	.6575	.9847
5	.6	.7315	.9916
6	.7	.8018	.9928
7	.8	.8689	.9904
8	.9	.9336	.9857
9	1.0	.9962	.9797

(1) C. B. Krelschmer, J. Nowakowska, and R. Wiebe, *J. Am. Chem. Soc.*, **70**, 1785 (1948).

PRODUCTS RESEARCH DIVISION LEON MIR
ESSO RESEARCH AND ENGINEERING COMPANY
LINDEN, NEW JERSEY FRANK E. STEIDLER

RECEIVED AUGUST 12, 1963

THERMAL FORMATION OF FERRITES FROM AMORPHOUS PRECIPITATES

Sir:

It is well known that spinel type ferrites are produced from mixtures of oxides, hydroxides, or salts of Fe^{3+} and a variety of bivalent metals in the desired proportions. The reaction may be carried out by heating the dry mixture for some hours at a temperature around 1000°.

Alternatively, the desired metals may be coprecipitated as oxides, hydroxides, or carbonates which are then converted to a ferrite structure by heating. This conversion may be preceded by a drying operation or may be carried out by heating the precipitate in the reaction liquid. This last method is described in a paper by Sato, Sugihara, and Saito.[1] The present communication is concerned with related work carried out in 1959 in the A.E.I. Research Laboratory, Harlow.[2]

A solution of metal sulfates in the ratios to yield $Ni_{0.5}Zn_{0.5}Fe_2O_4$ was allowed to react at 60° with the stoichiometric equivalent of sodium carbonate solution containing a smaller proportion of sodium hydroxide (to ensure complete precipitation of the zinc and nickel). After reaction, a bulky flocculent precipitate was obtained; in numerous repetitions of the experiment the pH of the liquid after reaction was 9.0 or slightly higher. Carbon dioxide was evolved on boiling, but it is not expected that this had a large effect on the pH.

In this present work, spinel formation was judged by increase in density and development of ferrimagnetism; X-ray diffraction was not applied. It was found that heating in the reaction liquid for 30 min. at 100° caused dehydration of the gelatinous precipitate; this became darker in color, assumed a fine powdery texture, increased greatly in apparent density, and developed noticeable ferrimagnetism. Higher temperatures (using an autoclave) up to 210° increased the effect, so that after 30 min. at 210° the material began to resemble powder mechanically mixed and reacted

TABLE I

Temp. of treatment, °C.	Degree of magnetism, g. Heated in reaction solution	Degree of magnetism, g. Heated after washing and drying	Apparent density, g./cc. Heated in reaction solution	Apparent density, g./cc. Heated after washing and drying
100	0.04	Nil	3.17	2.92
120	0.11	Nil	—	—
135	0.57	Nil	—	—
150	2.34[a]	Nil	3.82	—
210	3.41	Nil	4.18	3.18
400	—	0.05	—	3.40
500	—	1.56	—	4.35
600	—	1.90	—	4.52
900	—	2.68	—	5.05–5.10

[a] The corresponding value when this material was heated for 0.5 hr. at 150° in water was 0.98.

(1) C. Sato, M. Sugihara, and M. Saito, *J. Chem. Soc. Japan, Ind. Chem. Sect.*, **65**, 52 (1962).

(2) F. G. Stickland, British Patent 914,773 (1960).

dry at much higher temperatures. Very considerable dilution of the reaction solution before the heat treatment had only limited effect on the transformation.

Table I gives some idea of the results obtained: the degree of magnetism was assessed empirically by measuring the force required to separate a standard magnet from a small receptacle filled with ferrite.

Similar results were obtained from electrolytically produced mixed hydroxides. It has since been shown that the transformation to a spinel with magnetic properties can be carried out under the described conditions with wet precipitates yielding $FeFe_2O_4$, $Ni_{0.6}Zn_{0.4}Fe_2O_4$, and $Ni_{0.45}Zn_{0.45}Mn_{0.1}Fe_2O_4$.

This work agrees with the comparable work of the Japanese scientists, but goes beyond it in its description of the much more powerful effects to be obtained by use of higher temperatures in an autoclave.

CHEMISTRY AND MATERIALS SECTION F. G. STICKLAND
AEI RESEARCH LABORATORY
TEMPLE FIELDS, HARLOW
ESSEX, ENGLAND

RECEIVED AUGUST 15, 1963

DIFFERENCES IN THE MOBILITIES OF LIKE CHARGE IONS IN MOLTEN SYSTEMS

Sir:

We wish to report on some preliminary results, which we have obtained on ionic mobilities of cationic traces in alkaline earth halide melts and in the eutectics $NaNO_3$–KNO_3 and $NaNO_3$–KNO_3–$LiNO_3$.

During the course of counter-current electromigration experiments similar to the ones described previously,[1] it was found that in $SrBr_2$ at 770–800° the cationic migration of the specie containing the strontium ion was appreciably faster than that containing calcium or magnesium ions, while the specie containing barium migrated faster in relation to strontium. In $CaBr_2$ at the same temperature, the species containing strontium and barium migrated faster, and the ones containing magnesium migrated slower than calcium. These phenomena were found to hold for concentrations of traces of about 100 p.p.m. Direct measurements of these mobilities are made at present on films of alumina powder.[2]

Ionic mobility measurements of cationic traces in nitrate eutectics have been made on films of alumina powder under a flow of dry N_2 and the results are reported in Table I.[3] These and other systems are being further investigated with relation to temperature, composition, and effect of the supporting media on the migration.

These preliminary results together with previous literature data on counter-current electromigration experiments in the systems $SrBr_2$–$BaBr_2$, $CaBr_2$–KBr, and CaBr–LiBr,[1] electrophoresis and electromigration experiments of alkali and alkaline earth ions in $NaNO_3$,[4,5] of metal ionic traces in KCl–LiCl,[6] transport number measurements on the systems $AgNO_3$–KNO_3[7] and molten metal oxides–SiO_2,[8] and liquid junction potential measurements on the system $AgNO_3$–$CsNO_3$,[9] show the great dependence of the ionic mobilities on the composition and temperature of the system. Equalization of the mobilities of like charge ions in ionic melts, while occurring in many systems, is not a general phenomenon as stated by Laity and Moynihan.[10]

They report that data for at least ten different systems are consistent with the hypothesis that the mobilities of like-charged ions in fused salt mixtures are equal within about 10 to 15% at all concentrations.[11]

Many of the systems discussed by Laity and Moynihan[10] were studied by measurement of the liquid junction potential. No conclusion regarding the relative mobilities of cations can be drawn from zero values of the liquid junction potentials[15] as was done by Murgulescu and Marchidan,[16] since the assumption of constant mobilities over the concentration range of the cell necessary for integrating the equation relating transport numbers and liquid junction potentials is not valid, as can be seen from mobility measurements on the systems $AgNO_3$–KNO_3[7] and $NaNO_3$–KNO_3.[14]

The observation of anionic migration for traces of certain metals strongly suggests that such ions form "complexes" in the melts. These "complexes," being equilibrium phenomena, will depend on the composition and temperature of the system. For binary mixtures, having one ion in common and of approximately equal molar composition, the relative mobility of two ionic species depends on the state of aggregation[14] of the system. As the temperature increases, the aggregates disappear, and the ions can compete for other species in the melt to form "complexes" which will determine the migration velocity. Lantelme and Chemla have shown how the variations in the self-diffusion coefficients and ionic mobilities for the system $NaNO_3$–KNO_3 are consistent with this explanation. The apparent activation energy for ionic mobility therefore will depend strongly on the state in which a given specie is to be found and, while it is possible that the ionic mobilities become the same at a given composition for one temperature, they are most likely not to be the same at another temperature due to differences in the activation energies.

We also wish to point out that the observed mobilities of alkaline earth ions in solution in an alkaline earth bromide (Ca, Sr) at 770–800° and in $NaNO_3$–KNO_3 at 270° increase linearly as a function of their simple ionic radius, while the observed mobilities of the alkali

(1) F. Mènes, G. Dirian, and E. Roth, *J. chim. phys.*, **60**, 245 (1963).
(2) S. Forcheri and C. Monfrini, *J. Phys. Chem.*, **67**, 1566 (1963).
(3) R. A. Bailey and A. Steger, *J. Chromatog.*, **11**, 122 (1963).
(4) H. J. Arnikar, *Compt. rend.*, **244**, 2241 (1957).
(5) H. J. Arnikar, *Ann. phys.* (Paris), **4**, 1291 (1959).
(6) G. Alberti, G. Grassini, and R. Trucco, *J. Electroanal. Chem.*, **3**, 283 (1962).
(7) F. R. Duke and B. Owens, *J. Electrochem. Soc.*, **105**, 476 (1958).
(8) V. I. Malkin, S. F. Khokhlov, and L. A. Shvartsman, *Intern. J. Appl. Rad. Isotopes*, **2**, 19 (1957); V. I. Malkin, *Zh. Fiz. Khim.*, **35**, 336 (1961).
(9) J. A. A. Ketelaar and A. Dammers de Klerk, paper no. 88 presented at the 13th C.I.T.C.E. Meeting, Rome, 1962.
(10) R. W. Laity and C. T. Moynihan, *J. Phys. Chem.*, **67**, 723 (1963).
(11) In addition to the systems discussed by Laity and Moynihan, equalization of the ionic mobilities occurs also at certain compositions and temperatures for the systems $LiNO_3$–$NaNO_3$, $LiNO_3$–KNO_3,[12] LiBr–NaBr, LiBr–KBr,[13] and $NaNO_3$–KNO_3.[14]
(12) F. Lantelme and M. Chemla, *J. chim. phys.*, **60**, 250 (1963).
(13) J. Perie, M. Chemla, and M. Gignoux, *Bull. soc. chim. France*, 1249 (1961).
(14) F. Lantelme and M. Chemla, *Bull. soc. chim. France*, 2202 (1963).
(15) R. W. Laity, *J. Am. Chem. Soc.*, **79**, 1849 (1957); R. W. Laity, in "Reference Electrodes: Theory and Practice," ed. by D. J. G. Ives and G. J. Janz, Academic Press, New York, N. Y., 1961, pp. 548 ff.
(16) I. G. Murgulescu and D. I. Marchidan, *Zh. Fiz. Khim.*, **34**, 2534 (1960).

TABLE I

Ion	Electrolyte composition	Temp., °C.	E, v./cm.	$u \times 10^{4a}$	Remarks
Li(I)	$NaKNO_3$ eutectic	270 ± 3	5	+2.03 ± 0.18	Present work
Na(I)	$NaKNO_3$ eutectic	270 ± 3	5	+1.77 ± .07	Present work
Rb(I)	$NaKNO_3$ eutectic	270 ± 3	5	+1.47 ± .07	Present work
Cs(I)	$NaKNO_3$ eutectic	270 ± 3	5	+1.37 ± .04	Present work
Ca(II)	$NaKNO_3$ eutectic	270 ± 3	5	+0.45 ± .05	Present work
Sr(II)	$NaKNO_3$ eutectic	270 ± 3	6	+0.55 ± .08	Present work
Ba(II)	$NaKNO_3$ eutectic	270 ± 3	6	+0.79 ± .05	Present work
Cd(II)	$LiNaKNO_3$ eutectic[d]	200	7.5	+0.35	Present work
Cd(II)	$LiNaKNO_3$ eutectic[d] + 0.8 M KCl	200	7.1	−0.44	Present work
Cd(II)	$LiKNO_3$ eutectic	255	10	+0.56	Ref. 3[b]
Cd(II)	KSCN	210	10	[c]	Ref. 3[b]
Cr(III)	$LiKNO_3$ eutectic	255	10	+0.42	Ref. 3[b]
Cr(III)	KSCN	210	10	−0.16	Ref. 3[b]

[a] Ionic mobilities are given in cm.^{2} v.$^{-1}$ sec.$^{-1}$; + values for cathodic displacement and − for anodic. [b] Ionic mobilities were calculated from the displacement data given by the authors. [c] An insoluble precipitate was formed. [d] 0.1 M $Cd(NO_3)_2$ in melt investigated.

ions in the $NaNO_3$–KNO_3 eutectic at 270° decrease linearly with the increase in the ionic radius. The behavior of the mobilities of the alkaline earth ions is contrary to Stokes' law on mobilities according to which the mobilities should decrease as the radius increases. It is likely that the smaller ions have a greater tendency toward the formation of "complexes" or toward aggregation. Increasing the temperature will have the tendency to dissociate these species. The mobility of the smaller cation should therefore have a larger activation energy leading to an eventual reversal of the mobilities. Measurements are actively pursued on this point at present.[17]

Acknowledgment.—The authors wish to acknowledge helpful discussions with Dr. M. Chemla and G. Dirian. They also want to thank Dr. Chemla for having made available a preprint of the paper on the mobilities in the system $NaNO_3$–KNO_3.

(17) Some indication of a similar effect has been found in the $LiNaKNO_3$ ternary eutectic containing 1 M KCl. In electromigration experiments on powder alumina strips at low temperature (160°), two ill-defined bands of anionic migration are observed for Cl^- (Cl^{36}). These are most probably due to free Cl^- and to an ionic association containing Cl. As the temperature increases, this second band disappears, and at 240° we are left with only one band corresponding to the normal migration of Cl^-.

(18) Author to whom correspondence should be addressed.

SERVICES DES ISOTOPES STABLES
CENTRE D'ETUDES NUCLÉAIRES DE SACLAY
FRANCE
A. BERLIN[18]
F. MÉNÈS

DIPARTIMENTO MATERIALI
CHIMICA ALTE TEMPERATURE
C.C.R. EURATOM
ISPRA-VARESE, ITALY
S. FORCHERI
C. MONFRINI

RECEIVED AUGUST 22, 1963

ANOMALOUS BEHAVIOR OF THE ELECTRICAL CONDUCTIVITY OF MOLTEN BISMUTH HALIDES[1]

Sir:

We wish to call attention to the seemingly anomalous electrical conductivity of molten BiI_3, $BiBr_3$, and $BiCl_3$. Both the specific and molar conductance of these salts, when plotted against temperature, pass through a maximum 125–250° above their melting points. Positive temperature coefficients of conductance ($1/\kappa\ d\kappa/dT$) are typical of most fused salts but negative coefficients have been found in fused HgI_2, $InCl_3$, and $InBr_3$.[2] However, the bismuth halides are the only pure fused salts in which both positive and negative temperature coefficients have been observed. Even though this behavior was unexpected, it is possible that this "anomaly" may be observed in other molten salts if the electrical conductivity is measured at sufficiently high temperatures.

The preparation of reagents and the apparatus used in this work have been described elsewhere.[3,4] The conductivity cells were constructed of heavy walled (>2 mm.) quartz tubing. The specific conductivities of $BiCl_3$, $BiBr_3$, and BiI_3 as a function of temperature are shown in Fig. 1. Maxima in the specific conductances were observed at 425° for both $BiCl_3$ and $BiBr_3$ and at 525° for BiI_3. The corresponding molar conductivity maxima are found at 460° and at 610°. The sharpness of the maximum decreased with increasing molecular weight of the halide.

The factors contributing to the maxima observed in fused bismuth halides may be similar to those responsible for the maxima observed in many solutions near the critical temperature. It was found that the conductivities of many solutions of electrolytes dissolved in aqueous or nonaqueous solvents reached a maximum at about 100° below the critical temperature of the solvent and then continued to decrease with temperature until the critical temperature was reached.[5]

(1) This work was supported by the U. S. Atomic Energy Commission.

(2) I. K. Delimarskii and B. F. Markov, "Electrochemistry of Fused Salts," Sigma Press, Washington, D. C., 1961, pp. 12, 15.

(3) (a) L. F. Grantham and S. J. Yosim, *J. Chem. Phys.*, **38**, 1671 (1963); (b) S. J. Yosim, L. D. Ransom, R. A. Sallach, and L. E. Topol, *J. Phys. Chem.*, **66**, 28 (1962).

(4) S. J. Yosim, A. J. Darnell, W. G. Gehman, and S. W. Mayer, *ibid.*, **63**, 230 (1959).

(5) C. A. Kraus, *Phys. Rev.*, **18**, 40, 89 (1904).

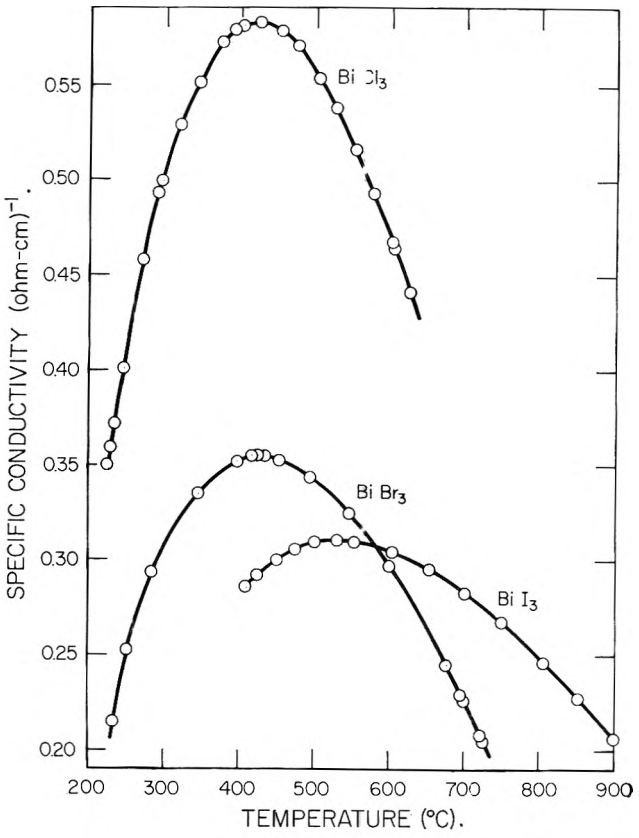

Figure 1.

This decrease in conductivity is associated with the decrease in density and dielectric constant of the solutions as the temperature is increased. It is reasonable to expect the conductivity of fused salts to reach a maximum as the critical temperature is approached, since the ions present would tend to associate to form nonconducting species at sufficiently decreased densities. (In the limiting case of an ionic gas at low pressures, the ions are known to be completely associated.) However, the temperature of the maxima observed in these measurements is still relatively low compared to the critical temperature of the salt (~900° for $BiCl_3$ and $BiBr_3$).[6]

Recently,[7] negative temperature coefficients were found in the electrical conductivities of nonaqueous solutions containing cupric perchlorate dihydrate as the temperature was varied from 15 to 40°. This unusual behavior was explained on the basis of Falkenhagen's[8] treatment of the Onsager conductivity equation. Differentiation of this equation with respect to temperature shows that the equivalent conductivity is the *difference* of two terms. The first term, which is a function of the fluidity, increases with temperature; the second term, which is a function of the concentration and of the inverse of the solvent dielectric constant, also increases with temperature. For solutions having a high concentration of electrolyte in a low dielectric medium, the second term may become larger than the first as the temperature is increased; hence the conductivity would pass through a maximum. However, this approach assumes a nonionic solvent and is probably not applicable to fused salts.

(6) D. Cubicciotti and J. W. Johnson, private communication.

(7) P. T. Armitage and C. M. French, *J. Chem. Soc.*, 743 (1963).

(8) H. Falkenhagen, "Electrolytes," Clarendon Press, Oxford, 1934, p. 201.

Some solid semiconductor systems such as arsenic-doped germanium also exhibit maxima in the electrical conductivity as a function of temperature.[9] Two opposing effects are responsible for these observations. As the temperature increases the number of carriers increases but the mobility of each carrier decreases. Eventually, a temperature is reached at which the latter effect overshadows the former; hence the conductivity passes through a maximum and then decreases with increasing temperature. A slight decomposition of BiI_3 occurs at high temperatures; these decomposition products may act as dopants. However, it is questionable whether doped fused salts should be compared with solid semiconductors due to the many orders of magnitude difference in dopant concentration.

This apparently anomalous behavior in the electrical conductivity of molten bismuth halides may not be an unusual phenomenon; the electrical conductivity of other molten salts should be measured over a wider range of temperature and pressure to see if this behavior is unique to bismuth halide systems.

(9) P. P. Debye and E. M. Conwell, *Phys. Rev.*, **93**, 693 (1954).

ATOMICS INTERNATIONAL
A DIVISION OF NORTH AMERICAN AVIATION, INC.
CANOGA PARK, CALIFORNIA
L. F. GRANTHAM
S. J. YOSIM

RECEIVED AUGUST 27, 1963

SPECTROPHOTOMETRIC STUDY OF MOLTEN LITHIUM METAL–LITHIUM CHLORIDE SOLUTIONS

Sir:

Spectrophotometric and visual observations of lithium metal–lithium chloride systems have recently been made both above and below the melting point of lithium chloride. This exceedingly corrosive solution[1] was contained for these studies in newly developed captive liquid cells[2] made from molybdenum. These cylindrical all-metal windowless cells are designed to permit transmission of light through a portion of a liquid contained therein. Molybdenum was chosen as the material of construction for these cells because of its compatibility with lithium[3] over the temperature range of interest. Similar preliminary results were obtained with the use of copper captive liquid cells, which are not, however, inert to lithium.[3]

Purified LiCl and lithium metal (approximately 1.5 mole %) were placed in the cell in an inert-atmosphere box and the samples were transferred to a high-temperature cell assembly[4] without exposure to the atmosphere for subsequent melting. All spectrophotometric measurements were made with a Cary recording spectrophotometer, Model 14M. At the end of an experimental observation the sample was cooled and transferred, again without any known exposure to the atmosphere, to a vacuum-tight apparatus[5] where it was treated with water *in vacuo* and any liberated gas was collected.

(1) A. S. Dworkin, H. R. Bronstein, and M. A. Bredig, *J. Phys. Chem.*, **66**, 572 (1962).

(2) J. P. Young, *Anal. Chem.*, in press.

(3) R. N. Lyon, "Liquid Metals Handbook," 2nd Ed., U. S. Government Printing Office, Washington, D. C., 1952, pp. 158–161.

(4) J. P. Young and J. C. White, *Anal. Chem.*, **31**, 1892 (1959).

(5) G. Goldberg, to be submitted for publication.

The gas was analyzed chromatographically and the aqueous solution was analyzed for hydroxide ion concentration and total lithium. From these analyses, the amount of lithium metal in the sample is determined from the hydrogen gas liberated; an estimate of the amount of lithium that was lost through unwanted hydrolysis can be determined from the excess hydroxide ion present over the stoichiometric equivalent of the hydrogen gas; the weight of sample is determined from the total lithium concentration after correction for hydroxide and lithium metal.

The lithium–lithium chloride mixtures melted as visually opaque liquids, although light of wave lengths greater than 1400 mμ was transmitted. The solubility of lithium in lithium chloride, *ca.* 0.5 mole % at 640°,[1] was probably exceeded in the above melt as the molten sample initially contained approximately 1.5 mole % lithium. The windowless cells which contained these melts are obviously not sealed cells, and the distillation of lithium to cooler regions of the cell assembly provided a means for continuous reduction of the lithium metal concentration. An interesting point, however, is that after the melt had decolorized, a small amount of lithium (*ca.* 0.04 mole %) was found to be present in the sample.

During the color transformation of the melt from opaque to colorless, the melt acquired a magenta color, and over the wave length range of 2.0 μ to 260 mμ, the solution at a temperature of 650° exhibited a fairly broad absorption peak at 550 mμ. The colorless melt exhibited a cut-off at *ca.* 260 mμ. It was not possible to determine accurately the concentration of lithium metal in the magenta-colored melt due to the distillation of this metal; determinations of lithium in opaque and colorless melts were made, however, to obtain limits for a concentration range of the magenta solution. The concentration of lithium in an opaque solution was found to be 1 mole %. Similar solutions, which were maintained at 650° for several hours to permit the melt to decolorize completely, were found to contain *ca.* 0.04 mole % lithium.

Based on the color exhibited by the more concentrated solution and assuming adherence to Beer's law, the 0.04 mole % lithium–lithium chloride solution should not have been colorless. A plausible explanation of this discrepancy is the existence of both a colored and colorless species in the melt, or a conversion of a portion of the colored species to a colorless one. Consideration of the nature of the light-absorbing species in this and other alkali metal–alkali metal halide solutions will be a subject of continued study.

The absorption peak that was observed at 550 mμ for lithium–lithium chloride solutions does not correlate with the data of Mollwo[6] for melts of sodium and potassium in their respective chlorides, bromides, and iodides. In this latter study, Mollwo found the solution absorbance peak to be unaffected by anion and to be displaced toward lower energy by approximately 200 mμ from the wave length of the $ns^1 \rightarrow np^1$ transition of the alkali metal vapor. In this work the solution absorption peak at 550 mμ is displaced toward higher energy by 120 mμ from the wave length of the $ns^1 \rightarrow np^1$ transition of lithium vapor. Considering the available data, one must assume a different colored species in the lithium–lithium chloride system than that which has been proposed for the analogous sodium or potassium systems,[7] *i.e.*, the solute species is the alkali metal atom with an expanded outer electronic orbital.

Some interesting visual observations were made on the colors of the solid and liquid lithium–lithium chloride systems. The opaque liquid froze to a light straw-colored solid, and it was adequately demonstrated that this color transition was completely reversible and occurred at or very near the melting point of the salt, 614°. Attempts to measure the absorption spectrum of the solid were not successful, but it was possible to show that the peak at 550 mμ was absent. The F-center absorption maximum for lithium chloride is reported to be at a wave length of *ca.* 399 mμ[8] and a straw-colored crystal might well have an absorption in this region. The complete lack of color (visually) in the solidified colorless melts which were found to contain 0.04 mole % lithium is puzzling, however. It must be assumed from these observations that the lithium found in these crystals was not present in a defect structure.

(6) E. Mollwo, *Nachr. Akad. Wiss. Gottingen II. Math. Physik Kl.*, **1**, 203 (1935).

(7) E. A. Ukshe and N. G. Bukun, *Russ. Chem. Rev.* (English Transl.), **30**, 90 (1961).

(8) A. J. Dekker, "Solid State Physics," Prentice-Hall, 1957, p. 378.

(9) Operated by Union Carbide Corporation for the U. S. Atomic Energy Commission.

ANALYTICAL CHEMISTRY DIVISION J. P. YOUNG
OAK RIDGE NATIONAL LABORATORY[9]
OAK RIDGE, TENNESSEE

RECEIVED SEPTEMBER 3, 1963

OXYGEN ADSORPTION RELATED TO THE UNPAIRED d-ELECTRONS IN TRANSITION METALS

Sir:

The behavior of oxide-free platinum electrodes immersed in 1 *N* sulfuric acid solution saturated with oxygen is different from that of electrodes on which oxides are present.[1] The uptake of oxygen by oxide-free electrodes—so-called bare electrodes—follows a dissociative adsorption isotherm.[2] The rest potentials established under these conditions depend on oxygen partial pressure. The variation of rest potentials with partial pressure of oxygen, however, does not obey the Nernst equation. From experimental adsorption isotherms, maximum coverage of oxygen on bare electrodes has been determined. In this communication, preliminary data on the maximum coverage of oxygen on palladium, platinum, rhodium, iridium, and gold electrodes at room temperature are presented. The maximum coverage of oxygen is correlated to an electronic property of these metals.

Electrodes in the form of wires with known total area of about 1 cm.^{2} were sealed in ground Pyrex tubes which fit a specially designed[2] closed cell consisting of three compartments, one each for the test electrode, reference electrode, and the counter electrode. Closed stopcocks separated the compartments and prevented the mixing of solution and gases between compartments during measurements. The solutions

(1) F. P. Bowden, *Proc. Roy. Soc.* (London), **A125**, 446 (1929).

(2) M. L. B. Rao, M. A. V. Devanathan, A. Damjanovic, and J. O'M. Bockris, to be published.

were prepared from conductivity water and analytical grade sulfuric acid. Either purified oxygen or nitrogen, or a known mixture of both, was bubbled through the test electrode compartment. At the beginning of the experiment, any oxides present on the test electrode were reduced by passing a cathodic pulse across the electrode–solution interface. After this, the solution was quickly changed to prevent traces of hydrogen (evolved during the cathodic pulse) from interfering with the oxygen adsorption process. The fresh solution was equilibrated with oxygen at a known partial pressure. The electrode then assumes a steady (rest) potential and has a definite coverage of oxygen. The amount of adsorbed oxygen on the electrode was analyzed by cathodic pulse reduction. At constant current density of 50 ma. cm.$^{-2}$, the reduction was sufficiently rapid to render negligible any additional adsorption of oxygen from solution during the measurements.[2] The number of coulombs used in the reduction was read off from the potential–time transient displayed on the oscilloscope. From capacity measurement data, obtained from initial slope of the transients, the roughness factors were determined for the electrodes. Column a of Table I gives the value of quantity of change, Q, required to reduce adsorbed oxygen. These values are obtained from the slopes of the corresponding isotherms plotted as $p_{O_2}^{1/2}/Q_p$ *vs.* $p_{O_2}^{1/2}$, unless stated otherwise, where p is the partial pressure of oxygen. Assuming, for simplicity, closest packing of atoms in the surface, a layer of adsorbed oxygen atoms with one oxygen atom attached to each surface metal atom corresponds to a coverage of about 500 μC. cm.$^{-2}$ (column b). Column c of Table I shows the relative coverage, θ, for the metals studied. It appears that the maximum coverage on these metals is proportional to the number of unpaired d-electrons per atom, which they possess (column d), to the limit of a full monolayer (*e.g.*, Ru). These results strongly suggest that the unpaired d-electrons directly participate in the bonding of oxygen atoms adsorbed on these noble metals in the oxygen-saturated solutions.

TABLE I

DATA ON OXYGEN ADSORPTION ON DIFFERENT NOBLE METALS

Metal	(a) Observed oxygen coverage[a] (μC. cm.$^{-2}$)	(b) Calculated oxygen coverage of a monolayer (μC. cm.$^{-2}$)	(c) Fraction of surface covered by by oxygen, (θ)	(d) No. of unpaired d-electrons per atom
Pd	110[b]	510	0.22	0.55
Pt	110[b]	500	0.22[b]	0.55–0.6
Pt	135	500	0.27	0.55–0.6
Rh	480	530	0.90	1.7[c]
Ir	440	525	0.84	1.7[c]
Ru	500[b]	530	0.95	2.2[d]
Au	<15[b]		<0.03	0

[a] Roughness factors of the electrodes are the major source of error in the present measurements (estimated to be ±15%). [b] Saturation coverage at 1 atm. of oxygen. [c] Number of unpaired d-electrons per atom for cobalt, *i.e.*, the metal in the same subgroup in the periodic table for which magnetic susceptibility has been determined. [d] Number of unpaired d-electrons per atom for iron, *i.e.*, the metal in the same subgroup in the periodic table for which magnetic susceptibility has been determined.

Thus, in the case of platinum, an oxygen atom shares two electrons with approximately four platinum atoms, each of which contributes on the average all of its 0.55 unpaired d-electrons, and the maximum relative coverage $\theta = 0.27$ results. On rhodium, as well as on iridium, with about 1.7 unpaired d-electrons per atom, according to the present model, a relative coverage of about 0.85, or 450 μC. cm.$^{-2}$, is expected (*cf.* Table I). Ruthenium, with more than two unpaired d-electrons per atom, shows (in the solutions saturated under one atmosphere pressure of oxygen) a coverage which is close to a monolayer. Gold, with no unpaired d-electrons available, indicates little adsorption.

Further work, particularly on alloys, is in progress and may have important bearings on the study of bonding of adsorbed oxygen onto transition metals and, in general, on the mechanism of heterogeneous catalysis on these electro-catalysts.

Acknowledgment.–This work is supported by United States Army Electronics Research and Development Laboratory, Fort Monmouth, New Jersey, under Contract No. DA 36-039-SC-88921.

THE ELECTROCHEMISTRY LABORATORY
THE UNIVERSITY OF PENNSYLVANIA
PHILADELPHIA 4, PENNSYLVANIA
M. L. B. RAO
A. DAMJANOVIC
J. O'M. BOCKRIS

RECEIVED SEPTEMBER 12, 1963

NUCLEAR MAGNETIC RESONANCE SPECTROSCOPY. LONG-RANGE PHOSPHORUS-31–HYDROGEN-1 SPIN–SPIN COUPLING

Sir:

The contributions to spin–spin coupling involving nuclei of elements other than first row members of the periodic table (heavy nuclei) have recently received considerable attention.[1-3] Although reports of long-range spin–spin coupling between similar nuclei (H–H and F–F) separated by four or more bonds have appeared in the literature, relatively few cases have been detected where the nuclei have differed and cases involving heavy nuclei are limited. Roberts[4,5] and Cross[6] have observed coupling between protons and flourine through four, five, and six bonds and pointed out the importance of the stereochemical relationship of the nuclei. A long-range P^{31}–H^1 coupling (four bonds) reported for diethyl phenylphosphate and diethyl phenylphosphonite[7] is questionable because of the presence of a magnetically asymmetric center which results in a complex ABC_3 pattern.[8,9] Fine splitting has been calculated and observed for the methyl resonance of the ethoxy groups in the diethylacetals of acetaldehyde and acetophenone which contain similar ABC_3 systems[10,11] and no long-range coupling possi-

(1) S. Manatt, G. Juvinall, and D. Elleman, *J. Am. Chem. Soc.*, **85**, 2664 (1963).
(2) G. Whitesides, J. Beauchamp, and J. D. Roberts, *ibid.*, **85**, 2665 (1963).
(3) J. Hatton, W. Schneider, and W. Siebrand, *J. Chem. Phys.*, **39**, 1330 (1963).
(4) D. Davis, R. Lutz, and J. D. Roberts, *J. Am. Chem. Soc.*, **83**, 247 (1961).
(5) M. Takahashi, D. Davis, and J. D. Roberts, *ibid.*, **84**, 2935 (1962).
(6) A. Cross and P. Landis, *ibid.*, **84**, 1736 (1962).
(7) T. Siddall and C. Prohaska, *ibid.*, **84**, 3467 (1962).
(8) H. Finegold, *ibid.*, **82**, 2641 (1960).
(9) J. S. Waugh and F. A. Cotton, *J. Phys. Chem.*, **65**, 562 (1961).
(10) D. Davis, personal communication.
(11) F. Kaplan and J. D. Roberts, *J. Am. Chem. Soc.*, **83**, 4666 (1961).

TABLE I

NUCLEAR MAGNETIC RESONANCE DATA[a]

	Compounds	Source	δ_{CH_3}[b]	J, three bonds	J, four bonds
1	Ph_3PNCH_3	*c*	180.8	24.7	
2	$[Ph_3PNHCH_3]^+Br^-$	*c*	166.5	13.8	
3	$[Ph_3PN(CH_3)_2]^+Br^-$	*c*	184.5	10.4	
4	$Ph_3PNC(CH_3)_3$	*c*	71.3		1.21
5	$[Ph_3PNHC(CH_3)_3]^+I^-$	*c*	81.5		0.58
6	$[Ph_3PNCH_3C(CH_3)_3]^+I^-$	*c*	85.0		*g*
			187.1	10.4	
7	$Ph_3PNN(CH_3)_2$	*d*	192.5		*g*
8	$[Ph_3PNHN(CH_3)_2]^+Br^-$	*d*	166.6		*g*
9	$[Ph_3PNCH_3N(CH_3)_2]^+I^-$	*d*	150.9		*g*
			187.0	8.8	
10	$[Ph_3PNCH_3NCH_3Ph]^+I^-$	*d*	187.8		*g*
			193.6	7.8	
11	$(EtO)_2P(O)NHC(CH_3)_3$[e]	*e*	72.6		0.73[h]
12	$(EtO)_2P(O)NHN(CH_3)_2$[i]	*e*	148.5		*g*
13	$ROP(S)(OCH_3)NHC(CH_3)_3$[j]	*f*	82.0		0.77

[a] Spectra were obtained on carbon tetrachloride or deuteriochloroform solutions on a Varian Associates Model A-60 spectrometer. [b] Chemical shifts are in c.p.s. from tetramethylsilane. [c] H. Zimmer and G. Singh, *J. Org. Chem.*, **28**, 483 (1963). [d] H. Zimmer and G. Singh, to be published. [e] We are indebted to W. S. Wadsworth and W. Emmons of Rohm and Haas Co. [f] We are indebted to E. H. Blair of the Dow Chemical Co. [g] Coupling between phosphorus and the protons was not observed; this set an upper limit of $J_{PH} \leq 0.4$ c.p.s. for these compounds. [h] The spacing did not change in a 100 Mc./sec. spectrum. This conclusively shows the splitting is due to spin–spin coupling. We are indebted to D. Hollis of Varian Associates for obtaining the 100 Mc./sec. spectrum. [i] Second-order splitting of 0.60 c.p.s. was observed in the methyl resonance of the ethoxy groups. [j] R = 2,4,5-trichlorophenyl.

bilities. Cotton and Schunn[12] have observed a P–C–C–C–H coupling of ~2 c.p.s. in the sodium and zinc salts of diethoxyphosphonylacetylmethane and the spectrum of the product obtained from the ring opening of dimethylketene dimer wih trimethyl phosphite[13] indicates *cis* and *trans* P—O—C=C—C—H coupling.

(12) F. A. Cotton and R. A. Schunn, *J. Am. Chem. Soc.*, **85**, 2394 (1963).
(13) W. G. Bentrude and E. R. Witt, *ibid.*, **85**, 2523 (1963).

Further investigations in the area have been limited by the availability of suitable compounds and the simplicity of their spectra.

Examination of the nuclear magnetic resonance (n.m.r.) spectra of several phosphorus-containing compounds now reveals the existence of long-range P^{31}–H^1 coupling through four bonds. The results are summarized in Table I. Compounds which exhibit coupling (**4**, **5**, **11**, and **13**) contain the P–N–C–C–H system. Protonation and methylation of **4** to yield **5** and **6** results in a decrease in coupling. Alteration of electron density and/or variation of bond angles may account for this change. Quaternization leads to similar dedecrease in coupling through three bonds (**1**, **2**, and **3**).

Long-range coupling is not observed in compounds containing the P–N–N–C–H system (**7**–**10** and **12**). In contrast, the presence of an intermediate nitrogen atom resulted in a larger F–F coupling through four bonds.[14] Bond angles were decreased, placing the flourines into a closer relationship in space, and coupling through space as well as through bonding electrons was postulated. The main contribution to long-range P^3–H^1 coupling through the agency of bonding electrons would be the Fermi contact interaction; however, one may not exclude the possibility of coupling through space. Additional systems are under investigation to ascertain the requirements of long-range P^{31}–H^1 coupling.

Acknowledgments.—The authors gratefully acknowledge financial support by the Office of Ordnance Research, U. S. Army, through grants DA-33-008-DRD-1971 and DA-ARO-D-31-124-6122. The purchase of the nuclear magnetic resonance spectrometer used in these studies was assisted by a grant from the National Science Foundation.

(14) L. Petrakis and C. H. Sederholm, *J. Chem. Phys.*, **35**, 1243 (1961).

DEPARTMENT OF CHEMISTRY
UNIVERSITY OF CINCINNATI
CINCINNATI 21, OHIO

FRED KAPLAN
GURDIAL SINGH
HANS ZIMMER

RECEIVED OCTOBER 5, 1963